

NISTIR 8271 DRAFT SUPPLEMENT

Face Recognition Vendor Test (FRVT) Part 2: Identification

Patrick Grother
Mei Ngan
Kayee Hanaoka
*Information Access Division
Information Technology Laboratory*

This document is a draft supplement of [NIST Interagency Report 8271](#)

2023/07/05



NISTIR 8271 DRAFT SUPPLEMENT

Face Recognition Vendor Test (FRVT) Part 2: Identification

Patrick Grother
Mei Ngan
Kayee Hanaoka
*Information Access Division
Information Technology Laboratory*

This document is a draft supplement of [NIST Interagency Report 8271](#)

November 2022



U.S. Department of Commerce
Gina M. Raimondo, Secretary

National Institute of Standards and Technology
Laurie E. Locascio, NIST Director and Undersecretary of Commerce for Standards and Technology

RELEASE NOTES

2023-07-05: The 1:N track of the FRVT remains open.

- ▷ This document corrects mugshot-mugshot results for algorithms submitted to FRVT 2023-02 to 2023-06. The prior report's FNIR values were uniformly approximately 0.003 higher due to a bug introduced into a script by changes to the FRVT API.

2023-07-03: The 1:N track of the FRVT remains open.

- ▷ This document is the twenty third draft update to [NIST Interagency Report 8271](#). It contains results for eight first-time participants: Advance.AI, AFIS and Biometrics Consulting, Inspur (Beijing) Electronic Information Industry, Know U Tech, Omnidarde, Serendipity, useB, and Verigram.
- ▷ The document also includes results for algorithms for four returning developers: Hangzhou Allu Network Information Technology, Megvii/Face++, Paravision, and Qnap Security.

2023-04-20: The 1:N track of the FRVT is closed until 2023-05-01.

- ▷ This document is the twenty third draft update to [NIST Interagency Report 8271](#). It contains results for one first-time participant: Armatura LLC.
- ▷ The document also includes results for algorithms for two returning developers: HyperVerge, Maxvision.

2023-03-29: The 1:N track of the FRVT remains open.

- ▷ This document is the twenty third draft update to [NIST Interagency Report 8271](#). It contains results for one first-time participant: Recognito.
- ▷ The document also includes results for algorithms for one returning developer: AllGoVision Technologies.

2023-03-14: The 1:N track of the FRVT remains open.

- ▷ This document is the twenty second draft update to [NIST Interagency Report 8271](#). It contains results for no first-time participants.
- ▷ The document also includes results for algorithms from nine returning developers: Cloudwalk - Moon-time Smart Technology, Line Corporation, Intema-LGL Group Neurotechnology, NEC, Paravision, Samsung S1, Veridas Digital Authentication Solutions, and Thales Group

2023-02-06: The 1:N track of the FRVT remains open.

- ▷ This document is the twenty first draft update to [NIST Interagency Report 8271](#). It contains results for no first-time participants.
- ▷ The document also includes results for algorithms from seven returning developers: Dermalog, DiluSense Technology, Hangzhou Allu Network Information Technology, Idemia, Innovatrics, Rank One Computing, and Sensetime Group.

2022-12-15: The 1:N track of the FRVT remains open.

- ▷ This document is the twentieth draft update to [NIST Interagency Report 8271](#). It contains results for one first-time participant: First Credit Bureau Kazakhstan.
- ▷ The document also includes results for algorithms from five returning developers: Gorilla Technology, Pangiam, Qnap Security, SQLsoft, Vixvizon (formerly known as Imagus).

2022-11-09: The 1:N track of the FRVT remains open.

- ▷ This document is the nineteenth draft update to [NIST Interagency Report 8271](#). It contains results for four first-time participant: Mukh, Turing Technology VIP, Verijelas and Verihubs Inteligensia
- ▷ The document also includes results for algorithms from two returning developers: Maxvision and Samsung S1.

2022-09-23: The 1:N track of the FRVT remains open.

- ▷ This document is the eighteenth draft update to [NIST Interagency Report 8271](#). It contains results for two first-time participants: Intema-LGL Group and T4iSB.
- ▷ The document also includes results for algorithms from two returning developers: Cloudwalk - Moon-time Smart Technology, Dermalog, Griaule, Hangzhuo Allu Network Information Technology, Intellivision, Line Corporation, NEC, Sensetime Group, Realnetworks Inc and Vietnam Posts and Telecommunications Group.

2022-07-28: The 1:N track of the FRVT remains open.

- ▷ This document is the seventeenth draft update to [NIST Interagency Report 8271](#). It contains results for one first-time participant: Maxvision.
- ▷ The document also includes results for algorithms from two returning developers: Rank One Computing, and Viettel Group.
- ▷ We have replaced the probe set used in the visa-border benchmark. It was previously comprised of 80 000 images; it now has size 1 212 892 - see amended entries in Table 1. False negative identification rates have increased.
- ▷ We have added images to the probe set used in the visa-kiosk benchmark. It was previously comprised of 21 016 mates and the same number of non-mates; it now has 31 579 mates and 45 460 non-mates - see amended and entries in Table 1. False negative identification rates are improved (reduced) slightly.

2022-06-08: The 1:N track of the FRVT remains open.

- ▷ This document is the seventeenth draft update to [NIST Interagency Report 8271](#). It includes results for algorithms submitted by three first-time participants: Digidata, DiluSense Technology, and Vietnam Posts and Telecommunications Group.
- ▷ The document also includes results for algorithms from five returning developers: Canon Inc, Imagus Technology, Neurotechnology, Thales, and Samsung S1.

2022-04-28: The 1:N track of the FRVT remains open.

- ▷ This document is the sixteenth draft update to [NIST Interagency Report 8271](#). It includes results for algorithms submitted by one first-time participants: Hangzhuo Allu Network Information Technology.
- ▷ The document also includes results for algorithms from three returning developers: HyperVerge Inc, Qnap Security, and Realnetworks Inc.
- ▷ The [1:N results page](#) has been updated.

2022-03-30: The 1:N track of the FRVT remains open.

- ▷ This document is the sixteenth draft update to [NIST Interagency Report 8271](#). It includes results for algorithms submitted by two first-time participants: Intellivision, and Pangiam.
- ▷ The document also includes results for algorithms from three returning developers: Fujitsu Research and Development Center, Idemia, and Gorilla Technology.
- ▷ The [1:N results page](#) has been updated.

2022-02-23: The 1:N track of the FRVT remains open.

- ▷ This document is the fifteenth draft update to [NIST Interagency Report 8271](#). It includes results for algorithms submitted by four first-time participants: Cloudwalk - Moontime Smart Technology, Decatur Industries Inc, NotionTag Technologies Private Limited, and Reveal Media Ltd.
- ▷ The document also includes results for algorithms from three returning developers: Cognitec Systems GmbH, Sensetime Group, and Viettel Group
- ▷ The [1:N results page](#) has been updated.

2022-01-20: The 1:N track of the FRVT remains open.

- ▷ This document is the fourteenth draft update to [NIST Interagency Report 8271](#). It includes results for algorithms recently submitted by two first-time participants: Daon and SQIsoft.
- ▷ The document also includes results for algorithms from five returning developers: Cyberlink Corp, NEC, Neurotechnology, Paravision, and Rank One Computing.
- ▷ The [1:N results page](#) has been updated.

2021-12-16: The 1:N track of the FRVT remains open.

- ▷ This document is the thirteenth draft update to [NIST Interagency Report 8271](#). It includes results for algorithms from six returning developers: Dahua Technology, Imagus Technology, Line Corporation, N-Tech Lab, Qnap Security, and Realnetworks Inc.
- ▷ The [1:N results page](#) has been updated.

2021-11-22: The 1:N track of the FRVT remains open.

- ▷ This document is the twelfth draft update to [NIST Interagency Report 8271](#). It includes results for algorithms recently submitted by three first-time participants Clearview AI, Griaule, and Mantra Softech India.
- ▷ This document and the [1:N results page](#) also include results for algorithms from six returning developers: Acer Incorporated, Canon, Dermalog, Samsung S1, VisionLabs, and Veridas Digital Authentication.

2021-10-28: The 1:N track of the FRVT remains open.

- ▷ This document is the eleventh draft update to [NIST Interagency Report 8271](#). It includes results for algorithms recently submitted by three first-time participants (20Face, Fujitsu Research and Development Center, and Vision-Box), and five returning participants (Alchera, Gorilla Technology, Tevian, Thales-Cogent, and Visidon). Visidon
- ▷ Both the main [1:N results page](#) and the small-gallery [paperless travel page](#) have been updated.

2021-09-21: The 1:N track of the FRVT remains open. Three news items:

- ▷ This document is the tenth draft update to [NIST Interagency Report 8271](#). It includes results for algorithms recently submitted by six first-time developers: Cubox, Fincore, HyperVerge, Qnap Security, Staqu Technologies, and Tripleize (Aize, 3-ize).
- ▷ It includes results also for four returning developers: Cognitec Systems, Incode Technologies, Innovatrics, Neurotechnology, and Rank One Computing.

2021-08-02: The 1:N track of the FRVT remains open. Three news items:

- ▷ This document is the ninth draft update to [NIST Interagency Report 8271](#). It includes results for algorithms recently submitted by eight participants: Cyberlink Corp, NEC Corp, N-Tech Lab, Realnetworks Inc., Sensetime Group, Veridas Digital, Viettel Group, and Vigilant Solutions.

- ▷ Algorithms submitted since July 24 will be included in the next update scheduled for September 9, 2021.
- ▷ A new report, NIST Interagency Report 8381 - FRVT Part 7: Identification for Paperless Travel and Immigration, has been released [[PDF](#), [webpage](#)]. It documents the use of FRVT 1:N algorithms in positive access control and immigration status update travel applications where the enrolled population size is as low as 420 people for aircraft boarding, and 42 000 for an airport security line. These population sizes are much smaller than those used in the main [1:N evaluation](#). Going forward, we will update the report and webpage with results for new algorithms.

2021-07-07: The 1:N track of the FRVT remains open. One update:

- ▷ This document is the eighth draft update to [NIST Interagency Report 8271](#). It include results for an algorithm from one participant: Kakao Enterprises.

2021-06-22: The 1:N track of the FRVT remains open. Three updates:

- ▷ This is the seventh draft of the update to [NIST Interagency Report 8271](#). It includes results for algorithms from three new participants: Line Corporation, Rendip, and Samsung S1 Corp.
- ▷ We have also added results for algorithms from five returning developers: Imagus Technology, Kneron, Tevian, Visidon, and Xforward AI Technology.
- ▷ The algorithm-specific report cards (examples: [1](#), [2](#), and [3](#)) now include figures showing how low threshold values can be used to reduce candidate list lengths for human review, while (usually) elevating miss rates (FNIR) only modestly. The reports also feature some minor additions and clarifications.

2021-03-26: The 1:N track of the FRVT remains open. Three updates:

- ▷ This is the sixth draft of the update to [NIST Interagency Report 8271](#). It includes results for algorithms from three returning developers: Neurotechnology, Guangzhou Pixel Solutions, and Tech5 SA.
- ▷ We have added results on the webpage and in the report for a new ageing dataset in which border crossing photos are searched against a gallery of border crossing photos collected between 10 and 15 years prior to the mated search photos. See section [2](#) for a description of the images. Table [1](#) has a new entry describing the experiment.
- ▷ We will mostly discontinue running the mugshot ageing test, reserving it for algorithms that show high accuracy on the new border-crossing set.

2021-03-26: Regarding the fifth draft of the update to [NIST Interagency Report 8271](#):

- ▷ In addition have added results for first algorithms from two new participants: Viettel Group and Veridas Digital Authentication Solutions.
- ▷ We have added results for algorithms from two returning developers: Idemia and Cognitec Systems.
- ▷ In addition to the report, the [results page](#) and its hyperlinked [report cards](#) have been updated.

2021-02-08: Regarding the fourth draft of the update to [NIST Interagency Report 8271](#):

- ▷ We have added results for eight algorithms submitted by eight developers: Cyberlink, Dermalog, Imagus, Paravision, Sensetime, Trueface, Vigilant Solutions, and X-Forward AI. With the exception of Trueface, all of these developers have participated previously.
- ▷ We anticipate updating this report again in the first week of March 2021.
- ▷ The main [results page](#) has been revised with tabs for the investigative and lights-out identification tables, and a new tab dedicated to speed and resource consumption.
- ▷ The report cards (example [here](#)) hyperlinked from the [results page](#) have been revised to improve content and format.

2020-12-14: Regarding third draft of the update to [NIST Interagency Report 8271](#):

- ▷ We have added results for fifteen algorithms submitted by thirteen developers. The four first-time participants are: Acer, Akurat Satu Indonesia, Canon, and Xforward AI Technology. The ten returning developers are: AllGoVision, Cyberlink Corp, Dahua Technology, Deepglint, Guangzhou Pixel Solutions, IIT Vision, Innovatrics, Rank One Computing, Scanovate, Sensetime Group, Synesis, and VisionLabs.
- ▷ We have added two new datasets to the evaluation: First a set of “visa-border” photos, representing search of an airport immigration lane photo against a database of closely ISO standard portraits; second a “visa-kiosk” set representing search of a photo collected in a registered traveller kiosk against the same ISO portrait gallery. The images are described in section 2.1.
- ▷ As in previous reports, we include results for searching mugshots against a mugshot gallery containing a single image of each of 12 million people. However we have suspending running searches against a gallery in which multiple lifetime photos per person are present, because this is computationally expensive. We retain a $N = 3$ million search test dedicated to ageing in which mugshots taken up to 18 years after the first photograph are searched - see Table 8.
- ▷ Tables containing computational resource information, Table 2 . . . , now include duration of the finalization step, in which search algorithms can, at their option, build fast-search data structures.
- ▷ We have linked revised per-algorithm PDF report cards from the main [results page](#).
- ▷ We have regenerated all figures and tables to drop algorithms submitted before June 2018. Results for prior algorithms appear in [archived editions](#) of this report.
- ▷ Going forward, we anticipate producing more frequent updates to this report. Developers may submit one algorithm to this evaluation every four calendar months.

2020-03-24: Regarding the second draft of the update to [NIST Interagency Report 8271](#):

- ▷ Adds results for three algorithms from three developers, Dermalog, Innovatrics, and Synesis.
- ▷ Adds Table 8 on ageing showing the increase in false negative rates with time elapsed between two photos. Some of the results were contained in graphs in prior editions of this report, but the table adds results for some newly submitted algorithms.
- ▷ Adjusts frontal mugshot results (for recent and lifetime consolidated galleries) to include the effect of removing some images that should not have been included in image test sets. These images were mostly profile views, images of tattoos containing faces, images of faces on tee shirts, and images of photographs on walls behind the intended subject. This affects many tables and reduces false negative identification rates for all algorithms. The reduction is larger for “recent” enrollments than for “lifetime consolidated” ones with the consequence that accuracy on recent images is now superior.

2020-02-26: Regarding the first draft of the update to [NIST Interagency Report 8271](#):

- ▷ Adds results for 38 algorithms from 31 different developers, eleven of whom are entirely new to the 1:N track of FRVT. These are Allgovision, Cyberlink, Deepsea Tencent, Farbar F8, Imperial College London, Intsys MSU, Kedacom, Kneron, Pixelall, and Scanovate.

DISCLAIMER

Specific hardware and software products identified in this report were used in order to perform the evaluations described in this document. In no case does identification of any commercial product, trade name, or vendor, imply recommendation or endorsement by the National Institute of Standards and Technology, nor does it imply that the products and equipment identified are necessarily the best available for the purpose.

INSTITUTIONAL REVIEW BOARD

The National Institute of Standards and Technology's Research Protections Office reviewed the protocol for this project and determined it is not human subjects research as defined in Department of Commerce Regulations, 15 CFR 27, also known as the Common Rule for the Protection of Human Subjects (45 CFR 46, Subpart A).

ACKNOWLEDGMENTS

The authors are grateful for the support and collaboration of the the Department of Homeland Security's Science & Technology Directorate (S&T), Office of Biometric Identity Management (OBIM), and Customs and Border Protection (CBP).

Additionally, the authors are grateful to staff in the NIST Biometrics Research Laboratory for infrastructure supporting rapid evaluation of algorithms.

Executive Summary

This document is a draft revision of the September 2019 report [NIST Interagency Report 8271](#). That report gave extensive documentation of face recognition applied to mugshots. This report extends that by adding more two more challenging datasets containing images with serious departures from canonical frontal image standards. The report also adds results for algorithms submitted to NIST since in 2019 and 2020. The algorithms, which implement one-to-many identification of faces appearing in two-dimensional images, are prototypes from the research and development laboratories of mostly commercial suppliers, and are submitted to NIST as compiled black-box libraries implementing a NIST-specified C++ test interface. The report therefore does not describe how algorithms operate. The report lists accuracy results alongside developer names and will therefore be useful for comparison of face recognition algorithms and assessment of absolute capability. The report is accompanied by a [webpage](#) with sortable results.

The evaluation uses six datasets: frontal mugshots, profile view mugshots, desktop webcam photos, visa-like immigration application photos, immigration lane photos, and registered traveler kiosk photos. These datasets are sequestered at NIST, meaning that developers do not have access to them for training or testing. This aspect is important because face recognition algorithms are very often deployed without the developer having access to the customers image data. A possible exception to this would be in a cloud-based application where the operational image data is uploaded to a cloud operated by a face recognition developer.

The major result in NIST IR 8271 was that massive gains in accuracy have been achieved in the years 2013 to 2018 and these far exceed improvements made in the prior period, 2010 to 2013. While the industry gains were broad - at least 30 developers' algorithms outperformed the most accurate algorithm from late 2013, there remains a wide range of capability. While this report shows accuracy gains only over the period 2018-2020, the most accurate algorithm reported here is substantially more accurate than anything reported in NIST IR 8271. This is evidence that face recognition development continues apace, and that FRVT reports are but a snapshot of contemporary capability.

From discussion with developers, the accuracy gains stem from the adoption of deep convolutional neural networks. As such, face recognition has undergone an industrial revolution, with algorithms increasingly tolerant of poorly illuminated and other low quality images, and poorly posed subjects. One related result is that a few algorithms correctly match side-view photographs to galleries of frontal photos, with search accuracy approaching that of the best c. 2010 algorithms operating on purely frontal images. The capability to recognize under a 90-degree change in viewpoint - pose invariance - has been a long-sought milestone in face recognition research.

With good quality portrait photos, the most accurate algorithms will find matching entries, when present, in galleries containing 12 million individuals, with rank one miss rates of approaching 0.1%. The remaining errors are in large part attributable to long-run ageing, facial injury and poor image quality. Given this impressive achievement - close to perfect recognition - an advocate might claim that cooperative face recognition is a solved problem, a statement that can be refuted with the following context and caveats:

- ▷ **Mugshots vs. less constrained captures:** The low error rates reported here are attained using mostly excellent cooperative live-capture mugshot images collected with an attendant present. Recognition in other circumstances, particularly those without a dedicated photographic environment and human or automated quality control checks, will lead to declines in accuracy. This is documented here for side-view images, poorer quality webcam images, and, particularly, for newly introduced ATM-style kiosk photos that were not originally intended for automated face recognition. In this case, recognition error rates are much higher, often in excess of 20% even with the more accurate algorithms which variously remain intolerant of face cropping (at image edge) and of large downward head pitch.
- ▷ **Algorithm accuracy spectrum:** Recognition accuracy is very strongly dependent on the algorithm and, more

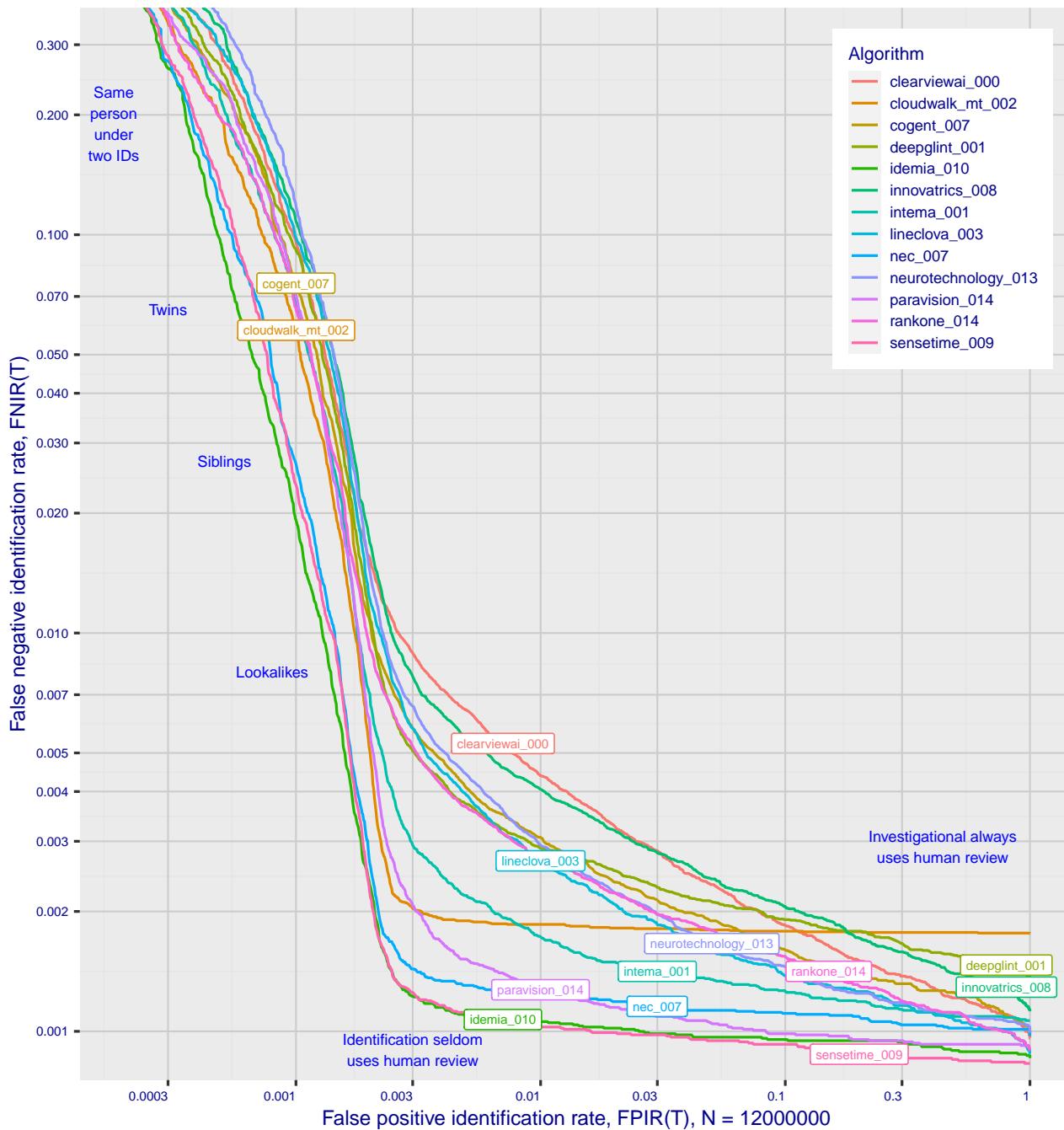


Figure 1: Identification miss rates across the false positive range. $N = 12$ million individuals are enrolled with one recent image.

generally, on the developer of the algorithm. False negative error rates in a particular scenario range from a few tenths of one percent to beyond fifty percent. This is tabulated exhaustively later: For example Table 13 shows accuracy across datasets. Figure 1 here compares algorithms on mugshot searches in a consolidated gallery of 12 million subjects and 12 million photos. Many algorithms do not achieve the low error rates noted above, and while many of those may still be useful and valuable to end-users, only the most accurate excel on poor quality images and those collected long after the initial enrollment sample.

▷ **Versioning:** While results for up to ten algorithms from each developer are reported here, the intra-provider

accuracy variations are usually smaller than the inter-provider variations. That said different versions give an order of magnitude fewer misses. Some developers demonstrate speed-accuracy tradeoffs¹. See Figs. 18, 19.

- ▷ **Low similarity scores:** In thousands of mugshot cases the correct gallery image is returned at rank 1 but its similarity score is nevertheless low, below some operationally required score threshold. This is not so important when face recognition is used for “lead generation” in investigational applications because human reviewers are specifically required to review potentially long candidate lists and the threshold is effectively 0. In applications where search volumes are higher and labor is not available to review the results from searches, a higher threshold must be applied. This reduces the length of candidate lists and false positive identification rates at the expense of increased false negative miss rates. The tradeoff between the two error rates is reported extensively later.
- ▷ **Population size:** As the number of enrolled subjects grows, some mates are displaced from rank one, decreasing accuracy. As tabulated later for N up to 12 million, false negative rates generally rise slowly with population size. This enables use of face recognition in very large populations. However in most positive and negative identification applications², a score threshold is set to limit the rate at which non-mate searches produce false positives. This has the consequence that some mated searches will report the mate below threshold, i.e. a miss, even if it is at rank 1. The utility of this is that many non-mated searches will return no candidate identities at all. As the error-tradeoff characteristic shows, investigational miss rates on the right side are very low but then rise steadily (in the center region) as threshold is increased to support “lights-out” applications, and ultimately rise quickly (left side) as discussed below. Thus, if we demand that just one in one thousand non-mate searches produce any false positives, the most accurate algorithms there (Sensetime-004 and NEC-3) would fail on between 3 and 5% of mated searches. Even though the graph shows results for the most accurate algorithms, all but two would fail to find the mate in more than 8% of mated searches. While the two most accurate algorithms produce a relatively flat error tradeoff until the threshold is raised to limit false positives to about 1 in 400 non-mated searches³.

Thereafter, as the threshold is raised to further reduce false positives, miss rates rise rapidly. This means that low false positive identification rates are inaccessible with these algorithms, a result that does not apply for ten-finger identification algorithms. The rapid rise occurs because the lower mate scores are mixed with very high non-mate scores, the low scores from poor image quality and ageing, the high non-mates from the presence of lookalikes persons (doppelgangers), twins (discussed next) and, ultimately, the presence of a few unconsolidated subjects i.e. persons present under multiple IDs.

- ▷ **False negatives from ageing:** A large source of error in long-run applications where subjects are not re-enrolled on a set schedule is ageing. Changes in facial appearance increase with the time elapsed between photographs. These will depress similarity scores and eventually cause false negatives. All faces age and while this usually proceeds in a graceful and progressive manner, drug use can accelerate this [28]. Elective surgery may be effective in delaying it although this has not been formally quantified with face recognition. As ageing is essentially unavoidable, it can only be mitigated by scheduled re-capture, as in passport re-issuance. To quantify ageing effects, we used the more accurate algorithms to enroll the earliest image of 3.1 million adults and then search

¹For example, NEC-0 prepares templates much faster than NEC-2 but gives twenty times more misses. Dermalog-5 executes a template search much more quickly than Dermalog-6 but is also much less accurate.

²In a positive identification application such as a registered traveler system, a user is making an implicit claim to be enrolled in the system - most users will be. In a negative application, such as with deportees, the implicit claim is that the subject is not enrolled - most will not be.

³The gallery size here is 12 million people, one image per person. Given 331 201 non-mated searches, an exhaustive implementation of one-too-many search would execute almost 4 trillion comparisons. At a false positive identification rate of 0.0025 the number of false positives is, to first order, 828 corresponding to single-comparison false match rate of $828 / 4 \text{ trillion} = 2.1 \times 10^{-10}$ i.e. about 1 in 5 billion. Strictly this FMR computation is meaningful only for algorithms that implement 1:N search using N 1:1 comparisons, which is not always the case.

with 10.3 million newer photos taken up to 18 years after the the initial enrollment photo. Figure 2 puts ageing into context by contrasting it with the increase in false negatives that occurs when the number of individuals in an enrollment database becomes larger and the chance of a false positive increases such that higher thresholds may become necessary⁴.

The Figure shows, from top to bottom, increases in false negative identification rates (FNIR) with the algorithm being tested. This applies to increases due to N on the left side, and increases due to ageing on the right side. The relative spacing of the dots shows that for all algorithms the dependency of FNIR on N (up to 12 million) is considerably less than on ΔT (up to 18 years). The figure additionally shows the most accurate nine algorithms for each year in which they were submitted, limiting to only one per developer.

In the inset table, accuracy is seen to degrade progressively with time, as mate scores decline and non-mates displace mates from rank 1 position. More accurate algorithms tend to be less sensitive to ageing. The more accurate algorithms give fewer errors after 18 years of ageing than middle tier algorithms give after four. Note also we do not quantify an ageing rate - more formal methods [2] borrowed from the longitudinal analysis literature have been published for doing so (given suitable repeated measures data).

See Figures 148, 181 and 197.

⁴Some algorithms implement strategies to automatically adjust scores to account for increased population size. This relieves the system owner of having to increase thresholds as N increases.

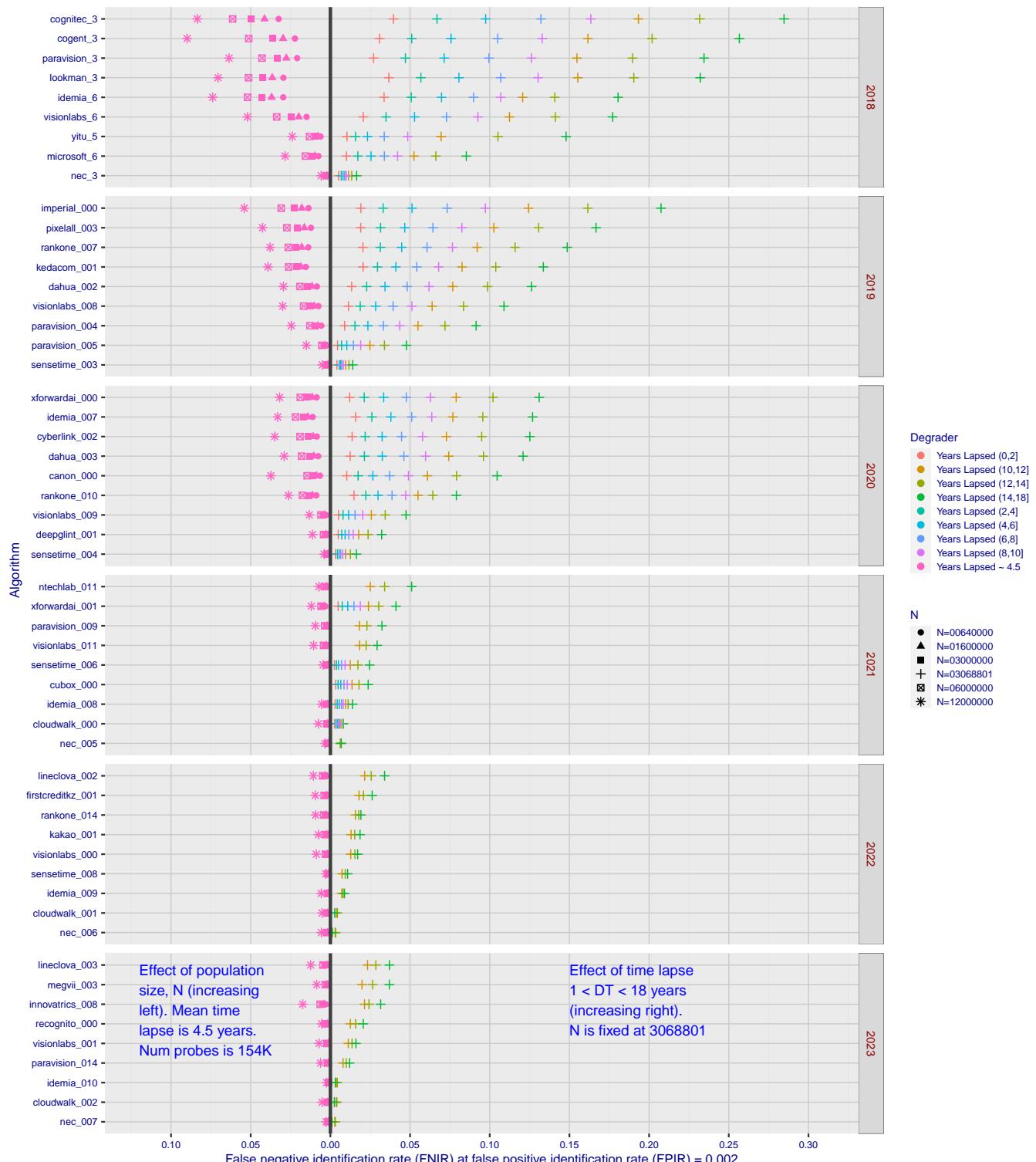


Figure 2: Identification miss rates as a function of enrolled population size, N , and time-lapse, ΔT .

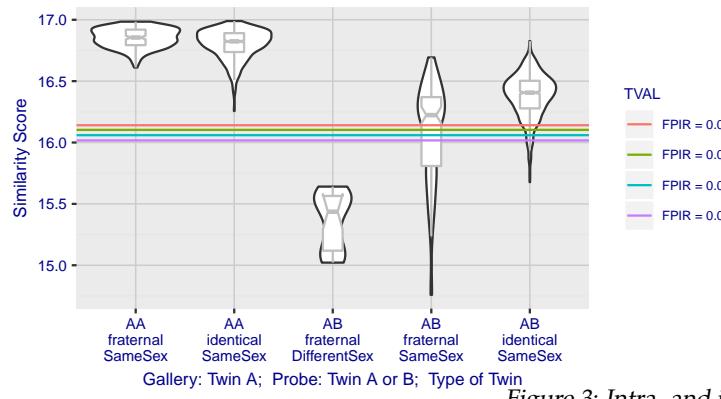


Figure 3: Intra- and inter-twin scores

▷ **False positives from twins:** By enrolling 640 000 mugshots, adding photos of one twin, and then searching photos of those subjects and their twin the inset figure shows, for one typical algorithm, the similarity is generally greater when searching twins against themselves (A) than when searching twins against their sibling (B) but very often still above even stringent thresholds i.e. those corresponding to one in one thousand searches producing a false positive. Thus twins will very often produce a high-scoring non-match on a candidate list and a false alarm in an online identification system. The plot of Fig. 3 shows that fraternal twins are sometimes correctly rejected at those thresholds - including most different sex twins (at center). Figure ?? shows substantially similar behavior for all algorithms tested. In an investigative search, a twin would typically appear at rank 1, or rank 2 if their sibling happened to also be the gallery. Twins (and triplets etc.) constituted 3.3% of all live births [17] in recent years⁵, and because that number is higher today than when the individuals in current adult databases were born, the false positives that arise from twins are now, and will increasingly be, an operational problem. Relative to the United States, twins are born with considerable regional variation. For example they are much less common in East Asia, and much more common in Sub-Saharan Africa [21].

The presence of twins in the mugshot database is inevitable given its size, around 12.3 million people. As this is not an insignificant sample of the domestic United States population, people with other familial ties will be present also. The data was collected over an extended period and because location information is not available, we are unable to estimate the proportion of the domestic population that is present in the dataset. However, if we assume twins are neither more or less disposed to arrest than the general population, we can estimate that hundreds of thousands of individuals in the dataset are twins. This will affect false positive rates because we randomly set aside 331 201 individuals for nonmate searches, and some proportion of those will be twins with siblings in the gallery.

▷ **Database integrity:** An operational error rate should be added to all false negative rates in this report reflecting the proportion of images in a real database that are un-matchable. Such anomalies arise from images that: do not contain a face; include multiple persons; cannot be decoded; are rotated by 90° or 180°; depict a face on clothing; and others introduced by a long tail of various clerical errors. While the mugshot trials in this report have been constructed to minimize such effects, they are a real problem in actual operations.

This report is being updated continuously as new algorithms are submitted to FRVT, and run on new datasets. Participation in the [one-to-many identification track](#) is independent of participation in the [one-to-one verification track](#) of FRVT.

⁵See the CDC's National Vital Statistics Report for 2017: https://www.cdc.gov/nchs/data/nvsr/nvsr67/nvsr67_08-508.pdf

Scope and Context

Audience: This report is intended for developers, integrators, end users, policy makers and others who have some familiarity with biometrics applications. The methods and metrics documented here will be of interest to organizations engaged in tests of face recognition algorithms. Some of these have been incorporated in the ISO/IEC 19795 Part 1 Biometric Testing and Reporting Framework standard, now nearing publication.

Prior benchmarks: Automated face recognition accuracy has improved massively in the two decades since initial commercialization of the various technologies. NIST has tracked that improvement through its conduct of regular independent, free, open, and public evaluations. These have fostered improvements in the state of the art. This report serves as an update to the [NIST Interagency Report 8271](#) on performance of face identification algorithms, published in September 2019.

Demographics: In December 2019, NIST published a first report on demographic dependencies in face recognition, [NIST Interagency Report 8280](#) that documented age, sex and race differentials in one-to-one and one-to-many false positive and false negative rates.

Scope: NIST IR 8271 documented recognition results for four databases containing in excess of 30.2 million still photographs of 14.4 million individuals. That constituted the largest public and independent evaluation of face recognition ever conducted. It includes results for accuracy, speed, investigative vs. identification applications, scalability to large populations, use of multiple images per person, images of cooperative and non-cooperative subjects.

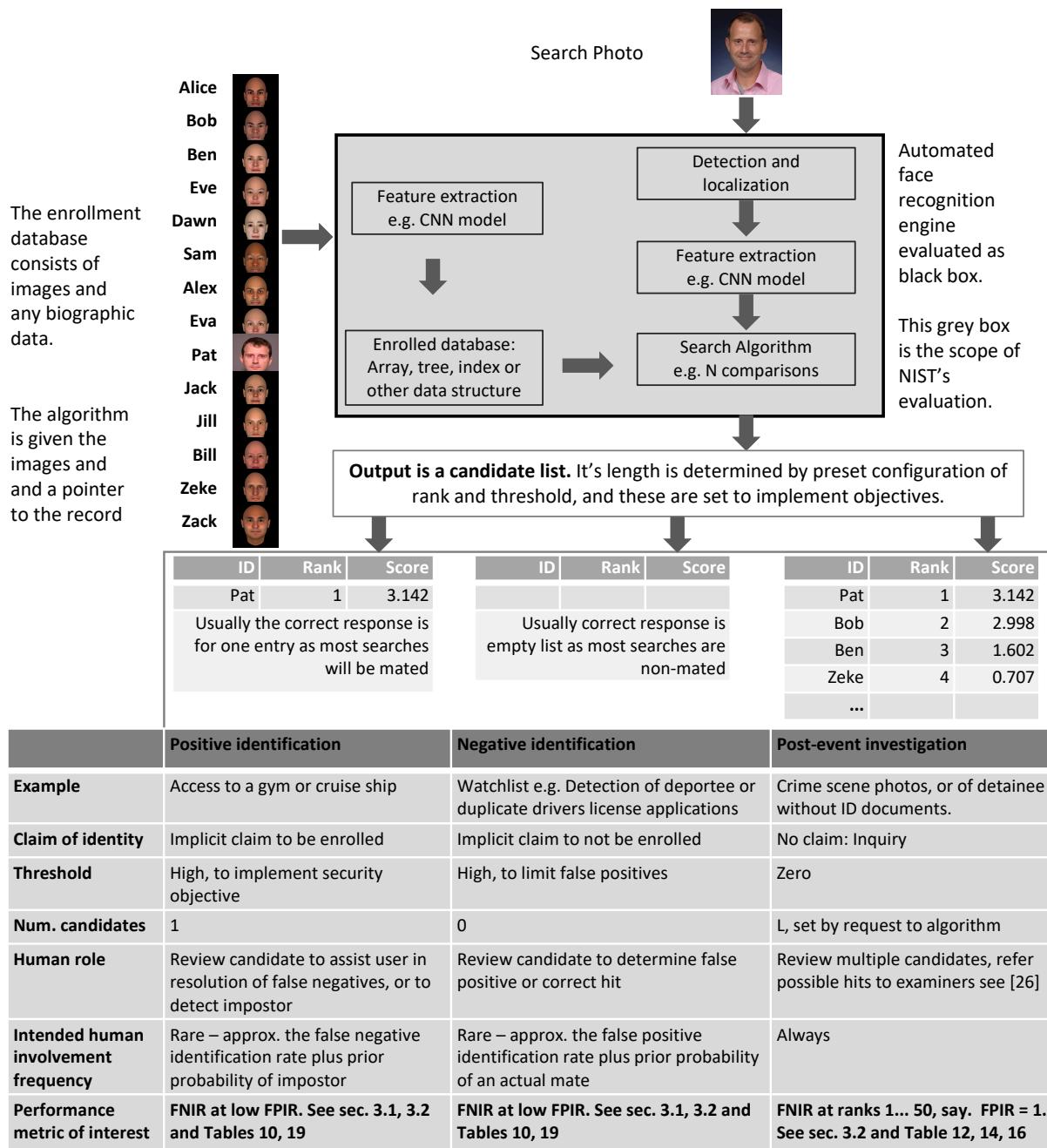
The report also includes results for ageing, recognition of twins, and recognition of profile-view images against frontal galleries. It otherwise does not address causes of recognition failure, neither image-specific problems nor subject-specific factors including demographics. Separate reports on demographic dependencies in face recognition will be published in the future. Additionally out of scope are: performance of live [human-in-the-loop transactional systems](#) like automated border control gates; human recognition accuracy as used in forensic applications; and recognition of persons in video sequences (which NIST evaluated separately [9]). Some of those applications share core matching technologies that *are* tested in this report.

Images: Five kinds of images are employed; these are either compared with images of the same kind, or against others from different capture environments as follows. The primary dataset is a set of law enforcement mugshot images (Fig. 5) which are enrolled and then searched with three kinds of images: other mugshots (i.e. within-domain); profile-view photographs (90 degree cross-view); and lower quality webcam images (Fig. 6) collected in similar detention operations (cross-domain). Additionally we compare high quality visa-like photos collected in immigration offices, with: medium quality border crossing images collected in primary immigration lanes; poor quality images collected in ATM-like registered traveller kiosks.

Participation and industry coverage: The report includes performance figures for prototype algorithms from the research laboratories of commercial developers and a few universities. This represents a substantial majority of the face recognition industry, but only a tiny minority of the academic community. Participation was open worldwide. While there is no charge for participation, developers incur some software engineering expense in implementing their algorithms behind the NIST application programming interface (API). The test is a black-box test where the function of the algorithm, and the intellectual property associated with it, is hidden inside pre-compiled libraries.

Recent technology development: Most face recognition research with deep convolutional neural networks (CNNs) has been aimed at achieving invariance to pose, illumination and expression variations that characterize photojournalism and social media images. The initial research [18, 22] employed large numbers of images of relatively few ($\sim 10^4$) individuals to learn invariance. Inevitably much larger populations ($\sim 10^7$) were employed for training [11, 20] but the benchmark, Labeled Faces in the Wild with (essentially) an equal error rate metric [12], represents an easy task,

one-to-one verification at very high false match rates. While a larger scale identification benchmark duly followed, Megaface [15], its primary metric, rank one hit rate, contrasts with the high threshold discrimination task required in most large-population applications of face recognition, namely credential de-duplication, and background checks. There, identification in galleries containing up to 10^8 individuals must be performed using a) very few images per individual and b) stringent thresholds to afford very low false positive identification rates. This track of FRVT was launched to measure the capability of the new technologies, including in these two cases. FRVT has included open-set identification tests since 2002, reporting both false negative and positive identification rates [7].



Performance metrics for applications: This report documents the performance of one-to-many face recognition algorithms. The word "performance" here refers to recognition accuracy and computational resource usage, as measured

by executing those algorithms on massive sequestered datasets.

This report includes extensive tabulation of recognition error rates germane to the main use-cases for face search technology. The Figure below, inspired by the Figure 1 in [23] differentiates different applications of the technolgy. The last row directs readers to the main tables relevant to those applications, respectively threshold-based and rank-based metrics that are special cases of the metrics given in section 3. The terms negative identification and positive identification are taken from the ISO/IEC 2382-37:2017 standardized biometrics vocabulary.

The algorithms are specifically configured for these applications by setting thresholds and candidate list lengths. Both rank-based metrics and threshold-based metrics include tradeoffs. In investigation, overall accuracy will be reduced if labor is only available to review a few candidates from the automated system. Note that when a fixed number of candidates are returned, the false positive identification rate of the automated face recognition engine will be 100%, because a probe image of anyone not enrolled will still return candidates. In identification applications where false positives must be limited to satisfy reviewer labor availability or a security objective, higher false negative rates are implied. This report includes extensive quantification of this threshold-based tradeoff.

See Sec. 3

Template diversity: The FRVT is designed to evaluate black-box technologies with the consequence that the templates that hold features extracted from face images are entirely proprietary opaque binary data that embed considerable intellectual property of the developer. Despite migration to CNN-based technologies there is no consensus on the optimal feature vector dimension. This is evidenced by template sizes ranging from below 100 bytes to more than four kilobytes. This diversity of approaches, suggests there is no prospect of a standard template something that would require a common feature set to be extracted from faces. Interoperability in automated face recognition remains solidly based on images and documentary standards for those, in particular the ICAO portrait [27] specification deriving from the ISO/IEC 19794-5 Token frontal [24] standard, which are similar to certain ANSI/NIST Type 10 [26] formats.

Training: The algorithms submitted to NIST have been developed using image datasets that developers do not disclose. The development will often include application of machine learning techniques and will additionally involve iterative training and testing cycles. NIST itself does not perform any training and does not refine or alter the algorithm in any way. Thus the model, data files, and libraries that define an algorithm are fixed for the duration of the tests. This reflects typical operational reality where recognition software, once installed, is fixed and constant until upgraded. This situation persists because on-site training of algorithms on customer data is atypical essentially because training is not a turnkey process.

Automated search and human review: Virtually all applications using automated face search require human review of the outputs at some frequency: Always for investigational applications; rarely in positive identification applications, after rejection (false or otherwise); and rarely in negative identification applications, after an alarm (false or otherwise). The human role is usually to compare a reference image with the query image or the live-subject if present, to render either a definitive decision on “exclusion” (different subjects), or “identification” (same subject), or a declaration that one or both images have “no value” and that no decision can be made. Note that automated face recognition algorithms are not built to do exclusion - low scores from a face comparison arise from different faces *and* poor quality images of the same face.

Human reviewers make recognition errors [5, 19, 25] and are sensitive to image acquisition and quality. Accurate human review is supported by high resolution - as specified in the Type 50, 51 acquisition profiles of the ANSI/NIST Type 10 record [26], and by multiple non-frontal views as specified in the same standard. These often afford views of the ear. Organizations involved in image collection should consider supporting human adjudication by collecting high-resolution frontal and non-frontal views, preparing low resolution versions for automated face recognition [24], and retaining both for any subsequent resolution of candidate matches. Along these lines, the ISO/IEC Joint Technical

Committee 1 subcommittee 37 on biometrics has just initiated projects on image quality assessment and face-aware capture.

Release Notes

FRVT Activities: Since February 2017, NIST has been evaluating one-to-one verification algorithms on an ongoing basis. NIST then restarted FRVT's one-to-many track in February 2018, inviting participants to send up to prototype algorithms. Both tracks allows developers to submit updated algorithms to NIST at any time but no more frequently than four calendar months. This more closely aligns development and evaluation schedules. Results are posted to the web within a few weeks of submission. Details and full report are linked from the [Ongoing FRVT site](#).

FRVT Reports: The results of the FRVT appear in the series NIST Interagency Reports tabulated below. The reports were developed separately and released on different schedules. In prior years NIST has mostly reported FRVT results as a single report; this had the disadvantage that results from completed sub-studies were not published until all other studies were complete.

Date	Link	Title	No.
2014-03-20	PDF	FRVT Performance of Automated Age Estimation Algorithms	7995
2015-04-20	PDF	Face Recognition Vendor Test (FRVT) Performance of Automated Gender Classification Algorithms	8052
2014-05-21	PDF	FRVT Performance of face identification algorithms	8009
2017-03-07	PDF	Face In Video Evaluation (FIVE) Face Recognition of Non-Cooperative Subjects	8173
2017-11-23	PDF	The 2017 IARPA Face Recognition Prize Challenge (FRPC)	8197
2018-11-27	PDF	Face Recognition Vendor Test - Part 2: Identification	8271
2019-09-11	PDF	Face Recognition Vendor Test - Part 2: Identification	8271
2019-12-11	PDF	Face Recognition Vendor Test - Part 3: Demographic Effects	8280
2020-01-03	WWW	Face Recognition Vendor Test (FRVT) - Part 1 Verification	Draft

Details appear on pages linked from <https://www.nist.gov/programs-projects/face-projects>.

Appendices: This report is accompanied by appendices which present exhaustive results on a per-algorithm basis. These are machine-generated and are included because the authors believe that visualization of such data is broadly informative and vital to understanding the context of the report.

Typesetting: Virtually all of the tabulated content in this report was produced automatically. This involved the use of scripting tools to generate directly type-settable L^AT_EX content. This improves timeliness, flexibility, maintainability, and reduces transcription errors.

Graphics: Many of the Figures in this report were produced using the **ggplot2** package running under **R**, the capabilities of which extend beyond those evident in this document.

Contents

Release Notes	1
Disclaimer	6
Institutional Review Board	6
Acknowledgments	6
Executive Summary	7
Scope and Context	13
Release Notes	17
1 Introduction	19
2 Evaluation datasets	20
3 Performance metrics	26
4 Results	42
Appendices	87
A Accuracy on large-population FRVT 2018 mugshots	87
B Effect of time-lapse: Accuracy after face ageing	220
C Effect of enrolling multiple images	370
D Accuracy with poor quality webcam images	377
E Accuracy for profile-view to frontal recognition	387
F Search duration	391
G Gallery Insertion Timing	425

1 Introduction

One-to-many identification represents the largest market for face recognition technology. Algorithms are used across the world in a diverse range of biometric applications: detection of duplicates in databases, detection of fraudulent applications for credentials such as passports and driving licenses, token-less access control, surveillance, social media tagging, lookalike discovery, criminal investigation, and forensic clustering.

This report contains a breadth of performance measurements relevant to many applications. Performance here refers to accuracy and resource consumption. In most applications, the core accuracy of a facial recognition algorithm is the most important performance variable. Resource consumption will be important also as it drives the amount of hardware, power, and cooling necessary to accommodate high volume workflows. Algorithms consume processing time, they require computer memory, and their static template data requires storage space. This report documents these variables.

1.1 Open-set searches

FRVT tested open-set identification algorithms. Real-world applications are almost always “open-set”, meaning that some searches have an enrolled mate, but some do not. For example, some subjects have truly not been issued a visa or drivers license before; some law enforcement searches are from first-time arrestees⁶. In an “open-set” application, algorithms make no prior assumption about whether or not to return a high-scoring result, and for a mated search, the ideal behaviour is that the search produces the correct mate at high score and first rank. For a non-mate search, the ideal behavior is that the search produces zero high-scoring candidates.

Many academic benchmarks execute only closed-set searches. The proportion of mates found in the rank one position is the default accuracy metric. This hit rate metric ignores the score with which a mate is found; weak hits count as much as strong hits. This ignores the real-world imperative that in many applications it is necessary to elevate a threshold to reduce the number of false positives.

⁶Operationally closed-set applications are rare because it is usually not the case that all searches have an enrolled mate. One counter-example, however, is a cruise ship in which all passengers are enrolled and all searches should produce exactly one identity. Another example is forensic identification of dental records from an aircraft crash.

2 Evaluation datasets

This report documents accuracy for four kinds of images - mugshots, webcam, profiles and wild - as described in the following sections.

2.1 Immigration-related images

This report includes benchmark tests sharing a common enrollment of high quality frontal portrait images collected while subject make applications for various immigration benefits. We then search that with two kinds of images, webcam images collected during in-bound immigration and also images collected from registered travelers using a ATM-style kiosk. These are described below and depicted in Figure 4.



Figure 4: Example photos.

- ▷ **Application reference photos:** The images are collected in an attended interview setting using dedicated capture equipment and lighting. The images, at size 300x300 pixels, are smaller than normally indicated by ISO. The images are all high-quality frontal portraits collected in immigration offices and with a white background. As such, potential quality related drivers of high false match rates (such as blur) can be expected to be absent. The images are encoded as ISO/IEC 10918-1 i.e. JPEG. Older images had a compression ration of about 16:1, while newer images, since 2010, are more lightly compressed at 4:1. When these images are provided as input into the algorithm, they are labeled with the type "iso". This report enrols 1 600 000 application images, one per person.
- ▷ **Border crossing photos:** Most images are have width 320 and height 240 pixels. They are JPEG compressed at 16:1 i.e. filesize just below 15KB. The images present challenges for face recognition in that subjects often exhibit non-zero yaw and pitch (associated with the rotational degrees of freedom of the camera mount), low contrast (due to varying and intense background lights), and poor spatial resolution (due to inexpensive cameras). There are often subjects standing in the background, usually at very low resolution (see Figure 4b). In such cases, algorithms should detect all faces and determine which is the largest and most centered. When these images are provided as input into the algorithm, they are labeled with the type "wild".
- ▷ **Kiosk photos:** These photos were collected from subjects whose attention was focused on interaction with an immigration kiosk. They images were not intended for use with automated face recognition. The camera is situated above a display which the user touches, and is triggered either without directing the subject to look at it, or without waiting for the subject to comply. The images are therefore characterized by pitch-down pose, sometimes exceeding 45 degrees, as in Figure 4c. Yaw-angle variation is mild, with most images close to frontal. The images

have width 320 pixels and height 240 pixels and therefore tall individuals are sometimes cropped. This is often just above the eyes and can occur at the nose or mouth. Conversely, short individuals are sometimes cropped such that only the top part of the face is visible. In a quite small number of cases, there other subjects standing just behind the primary subject such that algorithms should detect all faces and determine which is the largest and most centered. Background ceiling lighting is often visible and this sometimes leads to under-exposure of the face. When these images are provided as input into the algorithm, they are labeled with the type "wild".

2.2 Law enforcement images

The main mugshot dataset used is referred to as the FRVT 2018 set. This set was collected over the period 2002 to 2017 in routine United States law enforcement operations. This set yields three subsets

- ▷ **Mugshots:** Mugshots comprise about 86% of the database. They have reasonable compliance with the ANSI/NIST ITL1-2011 Type 10 standard's subject acquisition profiles levels 10-20 for frontal images [26]. The most common departure from the standard's requirements is the presence of mild pose variations around frontal - the images of Figure 5 are typical. The images vary in size, with many being 480x600 pixels with JPEG compression applied to produce filesizes of between 18 and 36KB with many images outside this range, implying that about 0.5 bits are being encoded per pixel. When these images are provided as input into the algorithm, they are labeled with the type "mugshot".

Example images appear in Fig. 5

[NIST Interagency Report 8238](#) includes a comparison of this set of mugshots with the smaller and easier sets of mugshots used in tests run in 2010 and 2014.

- ▷ **Profile images:** Profile-view images have been collected in law enforcement for more than 100 years, as human capability is improved with orthogonal information. The profile images used in this report were collected during the same session as the frontal mugshot photograph, in the same standardized photographic setup. These would not therefore be used with automated face recognition. A small subset, 200 000 images, were set aside for testing. When these images are provided as input into the algorithm, they are labeled with the type "wild".

Example images appear in Fig. 7

- ▷ **Webcam images:** The remaining 14% of the images were collected using an inexpensive webcam attached to a flexible operator-directed mount. These images are all of size 240x240 pixels, that are in considerable violation of most quality-related clauses of all face recognition standards. As evident in the figure, the most common defects are non-frontal pose (associated with the rotational degrees of freedom of the camera mount), low contrast (due to varying and intense background lights), and poor spatial resolution (due to inexpensive camera optics) - see examples in Fig 6. The images are overly JPEG compressed, to between 4 and 7KB, implying that only 0.5 to 1 bits are being encoded per color pixel. When these images are provided as input into the algorithm, they are labeled with the type "wild".

Example images appear in Fig. 6

These are drawn from NIST Special Database 32 which may be downloaded [here](#).

These images were partitioned in galleries and probesets for the various experiment listed in Table 1.

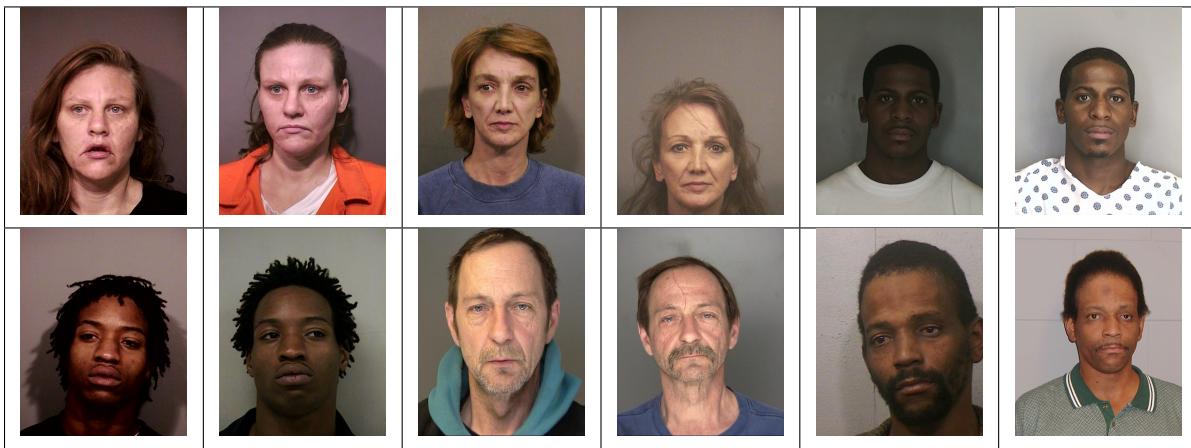


Figure 5: Six mated mugshot pairs representative of the FRVT-2014 (LEO) and FRVT-2018 datasets. The images are collected live, i.e. not scanned from paper. Image source: NIST Special Database 32 the Multiple Encounter Deceased Subjects dataset.



Figure 6: Twelve webcam images representative of probes against the FRVT-2018 mugshot gallery. The first eight images are four mated pairs. Such images present challenges to recognition including pose, non-uniform illumination, low contrast, compression, cropping, and low spatial sampling rate. Image source: NIST Special Database 32 the Multiple Encounter Deceased Subjects dataset.



Figure 7: **[Profile views]** The three images are a frontal enrollment, subsequent frontal probe, and same-session ninety degree profile view. While collection of both frontal and profile views has been typical in law enforcement for more than a century, the recognition of profile to frontal views has essentially been impossible. However, reasonably high accuracy results is now possible - see section E.

Image				
Encounter	1	...	$K_i - 1$	K_i
Capture Time	T_1	...	$T_{K_i - 1}$	T_{K_i}
Role RECENT	Not used	Not used	Enrolled	Search
Role LIFETIME	Enrolled	Enrolled	Enrolled	Search

Figure 8: Depiction of the “recent” and “lifetime” enrollment types. Image source: NIST Special Database 32

2.3 Enrollment strategies

Many operational applications include collection and enrollment of biometric data from subjects on more than one occasion. This might be done on a regular basis, as might occur in credential (re-)issuance, or irregularly, as might happen in a criminal recidivist situation [4]. The number of images per person will depend on the application area. In civil identity credentialing (e.g. passports, driver’s licenses), the images will be acquired approximately uniformly over time (e.g. ten years for a passport). While the distribution of dates for such images of a person might be assumed uniform, a number of factors might undermine this assumption⁷. In criminal applications, the number of images would depend on the number of arrests. The distribution of dates for arrest records for a person (i.e. the recidivism distribution) has been modeled using the exponential distribution but is recognized to be more complicated⁸.

In any case, the 2010 NIST evaluation of face recognition showed that considerable accuracy benefits accrue with retention and use of *all* historical images [6].

To this end, the FRVT API document provides $K \geq 1$ images of an individual to the enrollment software. The software is tasked with producing a single proprietary undocumented “black-box” template⁹ from the K images. This affords the algorithm an ability to generate a *model* of the individual, rather than to simply extract features from each image on a sequential basis.

As depicted in Figure 8, the i -th individual in the FRVT 2018 dataset has K_i images. These are labelled as x_k for $k = 1 \dots K_i$ in chronological order of capture date. To measure the utility of having multiple enrollment images, this report evaluates three kinds of enrollment:

- ▷ **Recent:** Only the second most recent image, $x_{K_i - 1}$ is enrolled. This strategy of enrollment mimics the operational policy of retaining the imagery from the most recent encounter. This might be done operationally to ameliorate the effects of face ageing. Obviously retaining only the most recent image should only be done if the identity of the person is trusted to be correct. For example, in an access control situation retention of the most recent successful *authentication* image would be hazardous if it could be a false positive.
- ▷ **Lifetime-consolidated:** All but the most recent image are enrolled, $x_1 \dots x_{K_i - 1}$. This subject-centric strategy might be adopted if quality variations exist where an older image might be more suitable for matching, despite the ageing effect.

⁷For example, a person might skip applying for a passport for one cycle, letting it expire. In addition, a person might submit identical images (from the same photography session) to consecutive passport applications at five year intervals.

⁸A number of distributions have been considered to model recidivism, see for example [3].

⁹There are no formal face template standards. Template standards only exist for fingerprint minutiae - see ISO/IEC 19794-2:2011.

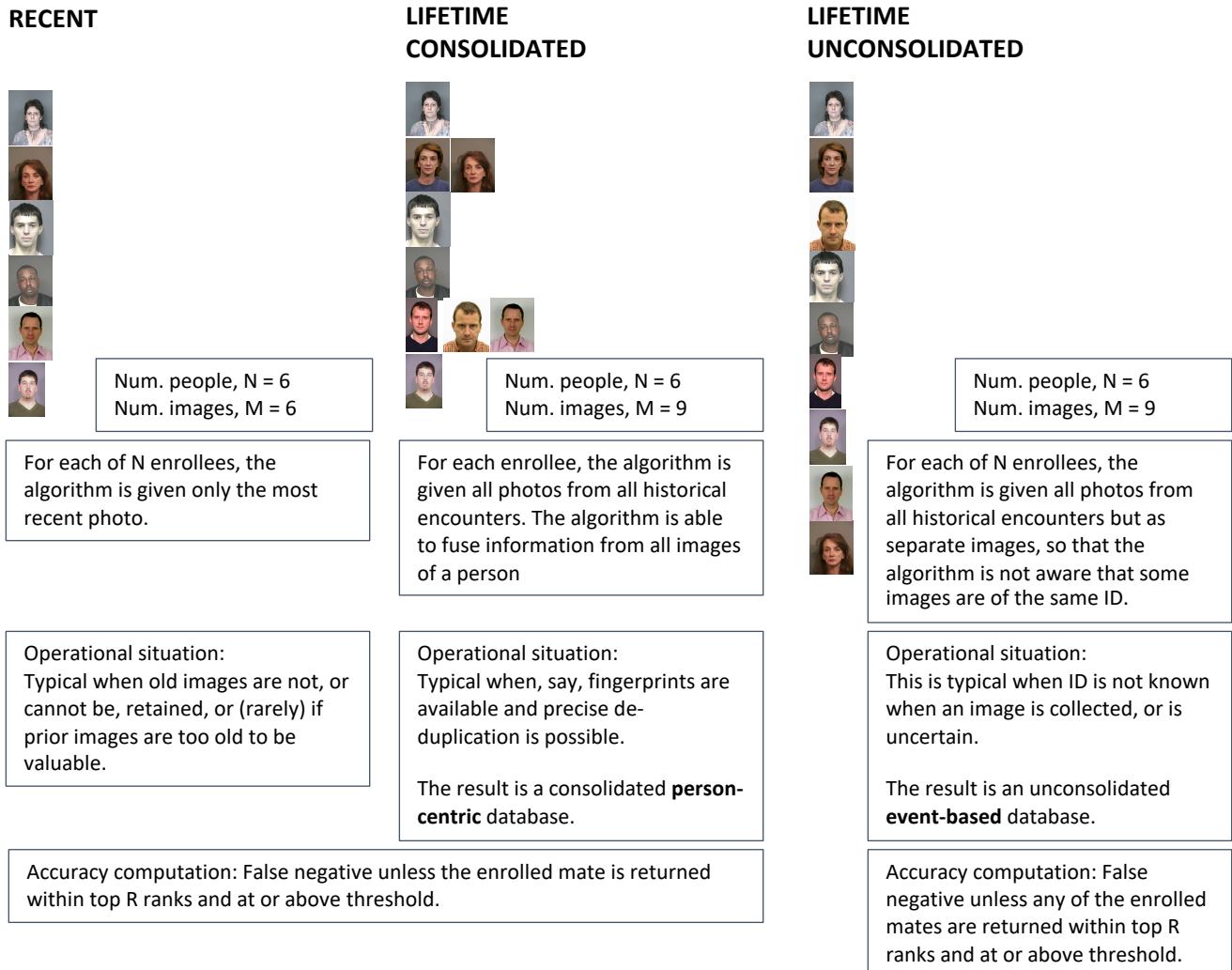


Figure 9: Enrollment strategies. The figure shows the three kinds of enrollment databases examined in this report. Image source: NIST Special Database 32

	ENROLLMENT				SEARCH			
	TYPE SEE SECTION 2.3	POPULATION FILTER	N-SUBJECTS	N-IMAGES	MATE N-SUBJECTS	NON-MATE N-IMAGES	N-SUBJECTS	N-IMAGES
Mugshot trials from enrollment of single images								
1	RECENT	NATURAL	640 000	640 000	154 549	154 549	331 254	331 254
2	RECENT	NATURAL	1 600 000	1 600 000				
3	RECENT	NATURAL	3 000 000	3 000 000				
4	RECENT	NATURAL	6 000 000	6 000 000				
5	RECENT	NATURAL	12 000 000	12 000 000				
Cross-domain								
13	MUGSHOTS AS ON ROW 2				82 106 WEBCAM	82 106 WEBCAM	331 254 WEBCAM	331 254 WEBCAM
Cross-view								
14	MUGSHOTS AS ON ROW 2				100 000 PROFILE	100 000 PROFILE	100 000 PROFILE	100 000 PROFILE
Mugshot ageing								
17	OLDEST	NATURAL	3 068 801	3 068 801	2 853 221	10 951 064	0	0
Border crossing ageing								
18	OLDEST	NATURAL	1 600 000	1 600 000	903 655	1 922 393	1 393 076	1 680 000
Visa-border								
19	PRIOR	NATURAL	1 600 000 VISA	1 600 000 VISA	577 444 BORDER	1 212 892 BORDER	79 769 BORDER	80 000 BORDER
20	VISA AS ON ROW 18				14 004 BORDER	31 579 BORDER	42 474 BORDER	45 460 BORDER

Table 1: Enrollment and search sets. Each row summarizes one identification trial. Unless stated otherwise, all entries refer to mugshot images. The term “natural” means that subjects were selected without heed to demographics, i.e. in the distribution native to this dataset. The probe images were collected in a different calendar year to the enrollment image. Missing values in rows 2-12 are the same as in row 1.

▷ **Lifetime-unconsolidated:** Again all but the most recent image are enrolled $x_1 \dots x_{K_i-1}$ but now separately, with different identifiers, such that the algorithm is not aware that the images are from the same face. This kind of event- or encounter-centric enrollment is very common when operational constraints preclude reliable consolidation of the historical encounters into a single identity. This aspect also prevents the recognition algorithm from a) building a holistic model of identity (as is common in speaker recognition systems) and b) implementing fusion, for example template-level fusion of feature vectors, or post-search score-level fusion. The result is that searches will typically yield more than one image of a person in the top ranks. This has consequences for appropriate metrics, as detailed in section 3.2.1

NIST first evaluated this kind of enrollment in mid 2018, and the results tables include some comparison of accuracy available from all three enrollment styles.

In all cases, the most recent image, x_{K_i} , is reserved as the search image. For the 1.6 million subject enrollment partition of the FRVT 2018 data, $1 \leq K_i \leq 33$ with $K_i = 1$ in 80.1% of the individuals, $K_i = 2$ in 13.4%, $K_i = 3$ in 3.7%, $K_i = 4$ in 1.4%, $K_i = 5$ in 0.6%, $K_i = 6$ in 0.3%, and $K_i > 6$ is 0.2% for everyone else. This distribution is substantially dependent on United States recidivism rates.

We did not evaluate the case of retaining only the highest quality image, since automated quality assessment is out of scope for this report. We do not anticipate that such strategies will prove beneficial when the quality assessment apparatus is imperfect and unvalidated.

3 Performance metrics

This section gives specific definitions for accuracy and timing metrics. Tests of open-set biometric algorithms must quantify frequency of two error conditions:

- ▷ **False positives:** Type I errors occur when search data from a person who has never been seen before is incorrectly associated with one or more enrollees' data.
- ▷ **Misses:** Type II errors arise when a search of an enrolled person's biometric does not return the correct identity.

Many practitioners prefer to talk about "hit rates" instead of "miss rates" - the first is simply one minus the other as detailed below. Sections 3.1 and 3.2 define metrics for the Type I and Type II performance variables.

Additionally, because recognition algorithms sometimes fail to produce a template from an image, or fail to execute a one-to-many search, the occurrence of such events must be recorded. Further because algorithms might elect to not produce a template from, for example, a poor quality image, these failure rates must be combined with the recognition error rates to support algorithm comparison. This is addressed in section 3.5.

Finally, section 3.7 discusses measurement of computation duration, and section 3.8 addresses the uncertainty associated with various measurements. Template size measurement is included with the results.

3.1 Quantifying false positives

It is typical for a search to be conducted into an enrolled population of N identities, and for the algorithm to be configured to return the closest L candidate identities. These candidates are ranked by their score, in descending order, with all scores required to be greater than or equal to zero. A human analyst might examine either all L candidates, or just the top $R \leq L$ identities, or only those with score greater than threshold, T . The workload associated with such examination is discussed later, in 3.6.

False alarm performance is quantified in two related ways. These express how many searches produces false positives, and then, how many false positives are produced in a search.

False positive identification rate: The first quantity, FPIR, is the proportion of non-mate searches that produce an adverse outcome:

$$\text{FPIR}(N, T) = \frac{\text{Num. non-mate searches where one or more enrolled candidates are returned with score at or above threshold}}{\text{Num. non-mate searches attempted.}} \quad (1)$$

Under this definition, FPIR can be computed from the highest non-mate candidate produced in a search - it is not necessary to consider candidates at rank 2 and above. FPIR is the primary measure of Type I errors in this report.

Selectivity: However, note that in any given search, several non-mate may be returned above threshold. In order to quantify such events, a second quantity, selectivity (SEL), is defined as the *number* of non-mates returned on a candidate list, averaged over all searches.

$$\text{SEL}(N, T) = \frac{\text{Num. non-mate enrolled candidates returned with score at or above threshold}}{\text{Num. non-mate searches attempted.}} \quad (2)$$

where $0 \leq \text{SEL}(N, T) \leq L$. Both of these metrics are useful operationally. FPIR is useful for targeting how often an

adverse false positive outcome can occur, while SEL as a number is related to workload associated with adjudicating candidate lists. The relationship between the two quantities is complicated - it depends on whether an algorithm concentrates the false alarms in the results of a few searches or whether it disburses them across many. This was detailed in FRVT 2014, NISTIR 8009. It has not yet been detailed in FRVT 2018.

3.2 Quantifying hits and misses

If L candidates are returned in a search, a shorter candidate list can be prepared by taking the top $R \leq L$ candidates for which the score is above some threshold, $T \geq 0$. This reduction of the candidate list is done because thresholds may be applied, and only short lists might be reviewed (according to policy or labor availability, for example). It is useful then to state accuracy in terms of R and T , so we define a “miss rate” with the general name **false negative identification rate** (FNIR), as follows:

$$\text{FNIR}(N, R, T) = \frac{\text{Num. mate searches with enrolled mate found outside top } R \text{ ranks or score below threshold}}{\text{Num. mate searches attempted.}} \quad (3)$$

This formulation is simple for evaluation in that it does not distinguish between causes of misses. Thus a mate that is not reported on a candidate list is treated the same as a miss arising from face finding failure, algorithm intolerance of poor quality, or software crashes. Thus if the algorithm fails to produce a candidate list, either because the search failed, or because a search template was not made, the result is regarded as a miss, adding to FNIR.

Hit rates, and true positive identification rates: While FNIR states the “miss rate” as how often the correct candidate is either not above threshold or not at good rank, many communities prefer to talk of “hit rates”. This is simply the **true positive identification rate**(TPIR) which is the complement of FNIR giving a positive statement of how often mated searches are successful:

$$\text{TPIR}(N, R, T) = 1 - \text{FNIR}(N, R, T) \quad (4)$$

This report does not report true positive “hit” rates, preferring false negative miss rates for two reasons. First, costs rise linearly with error rates. For example, if we double FNIR in an access control system, then we double user inconvenience and delay. If we express that as decrease of TPIR from, say 98.5% to 97%, then we mentally have to invert the scale to see a doubling in costs. More subtly, readers don’t perceive differences in numbers near 100% well, becoming inured to the “high nineties” effect where numbers close to 100 are perceived indifferently.

Reliability is a corresponding term, typically being identical to TPIR, and often cited in automated (fingerprint) identification system (AFIS) evaluations.

An important special case is the **cumulative match characteristic**(CMC) which summarizes accuracy of mated-searches only. It ignores similarity scores by relaxing the threshold requirement, and just reports the fraction of mated searches returning the mate at rank R or better.

$$\text{CMC}(N, R) = 1 - \text{FNIR}(N, R, 0) \quad (5)$$

We primarily cite the complement of this quantity, $\text{FNIR}(N, R, 0)$, the fraction of mates *not* in the top R ranks.

The **rank one hit rate** is the fraction of mated searches yielding the correct candidate at best rank, i.e. $\text{CMC}(N, 1)$. While this quantity is the most common summary indicator of an algorithm’s efficacy, it is not dependent on similarity scores, so it does not distinguish between strong (high scoring) and weak hits. It also ignores that an adjudicating reviewer is often willing to look at many candidates.

3.2.1 False negative rates for unconsolidated galleries

As detailed in section 2.3 a common type of gallery, here referred to as the lifetime unconsolidate type, is populated with all images of an individual without any association between them. That is, the gallery construction algorithm is not provided with any ID labels that would support processing of a person's images jointly. This contrasts with the lifetime consolidate type where an algorithm may explicitly fuse features from multiple images of a person, or select a best image. In such cases, where the number of enrolled images is a random variable, we define two false negative rates as follows.

The first demands that the algorithm place any of the K_i mates in the top $R \geq 1$ ranks. The proportion of searches for which this does not occur forms a false negative identification rate:

$$\text{FNIR}_{\text{any}}(N, R, T) = 1 - \frac{\text{Num. mate searches where any enrolled mate is found in the top } R \text{ ranks and at-or-above threshold}}{\text{Num. mate searches attempted.}} \quad (6)$$

The second demands that the algorithm place all K_i mates in the top $R \geq K_i$ ranks. The proportion of searches for which this does not occur forms a false negative identification rate:

$$\text{FNIR}_{\text{all}}(N, R, T) = 1 - \frac{\text{Num. mate searches where all enrolled mates are found in the top } R \text{ ranks and at-or-above threshold}}{\text{Num. mate searches attempted.}} \quad (7)$$

Placing all mates in the top ranks is a more difficult task than correctly retrieving any image, so it holds that: $\text{FNIR}_{\text{all}} \geq \text{FNIR}_{\text{any}}$. This is evident in the results presented for November 2018 algorithms in Tables starting at ??.

The information retrieval community might prefer to compute and plot *precision* and *recall*; this is a valid approach, but we advance the two metrics above because they relate to our normal definition of consolidated FNIR, and they cover the two extreme use-cases of wanting any hit vs. all hits.

3.3 DET interpretation

In biometrics, a false negative occurs when an algorithm fails to match two samples of one person – a Type II error. Correspondingly, a false positive occurs when samples from two persons are improperly associated – a Type I error.

Matches are declared by a biometric system when the native comparison score from the recognition algorithm meets some threshold. Comparison scores can be either similarity scores, in which case higher values indicate that the samples are more likely to come from the same person, or dissimilarity scores, in which case higher values indicate different people. Similarity scores are traditionally computed by fingerprint and face recognition algorithms, while dissimilarities are used in iris recognition. In some cases, the dissimilarity score is a distance possessing metric properties. In any case, scores can be either mate scores, coming from a comparison of one person's samples, or nonmate scores, coming from comparison of different persons' samples.

The words "genuine" or "authentic" are synonyms for mate, and the word "impostor" is used as a synonym for non-mate. The words "mate" and "nonmate" are traditionally used in identification applications (such as law enforcement search, or background checks) while genuine and impostor are used in verification applications (such as access control).

An error tradeoff characteristic represents the tradeoff between Type II and Type I classification errors. For identification this plots false negative vs. false positive identification rates i.e. FNIR vs. FPIR parametrically with T. Such plots

are often called detection error tradeoff (DET) characteristics or receiver operating characteristic (ROC). These serve the same function – to show error tradeoff – but differ, for example, in plotting the complement of an error rate (e.g. $TPIR = 1 - FNIR$) and in transforming the axes, most commonly using logarithms, to show multiple decades of FPIR. More rarely, the function might be the inverse of the Gaussian cumulative distribution function.

The slides of Figures 10 through 15 discuss presentation and interpretation of DETs used in this document for reporting face identification accuracy. Further detail is provided in formal biometrics testing standards, see the various parts of ISO/IEC 19795 Biometrics Testing and Reporting. More terms, including and beyond those to do with accuracy, appear in ISO/IEC 2382-37 Information technology – Vocabulary – Part 37: Harmonized biometric vocabulary.

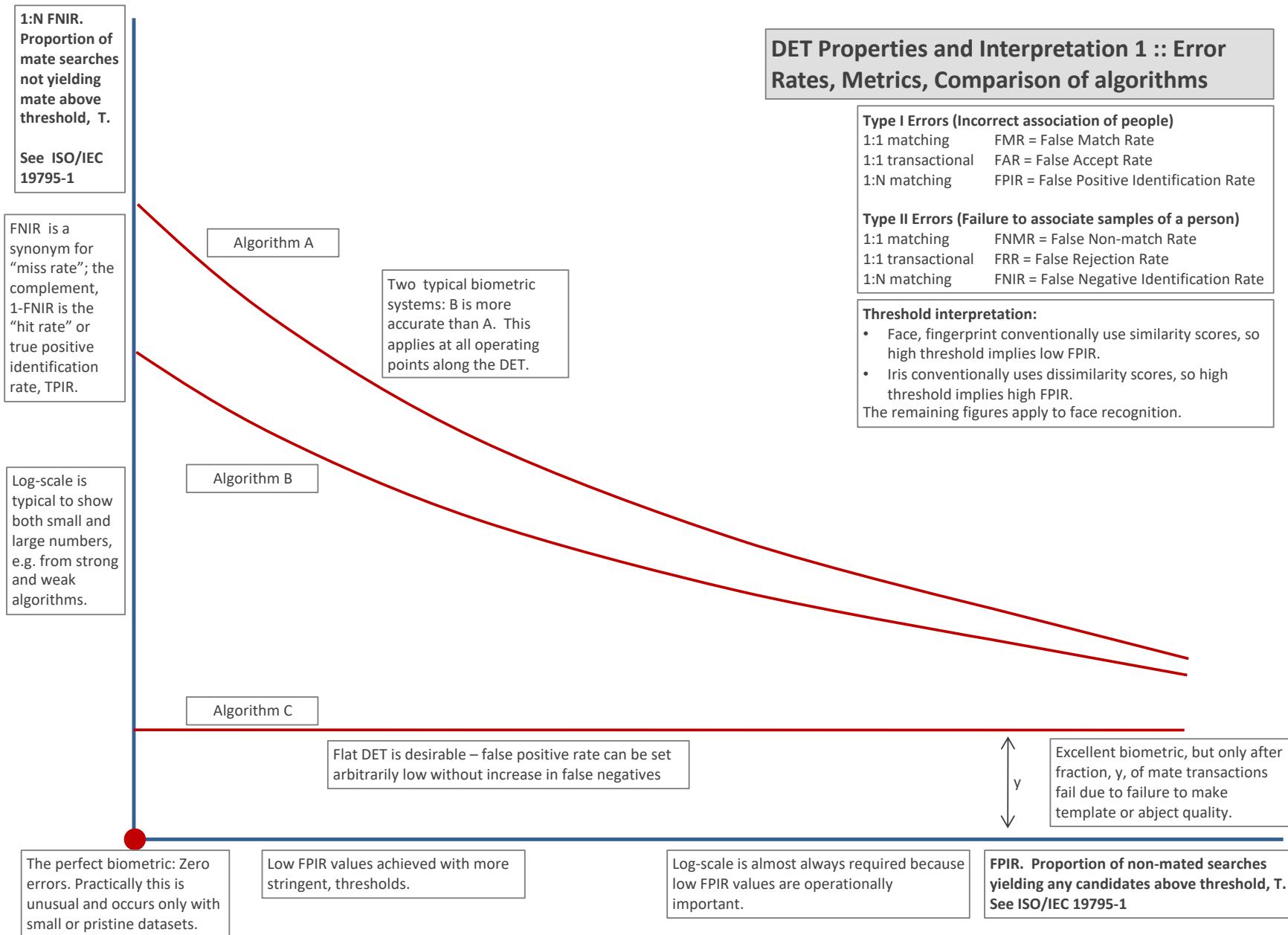


Figure 10: DET as the primary performance reporting mechanism.

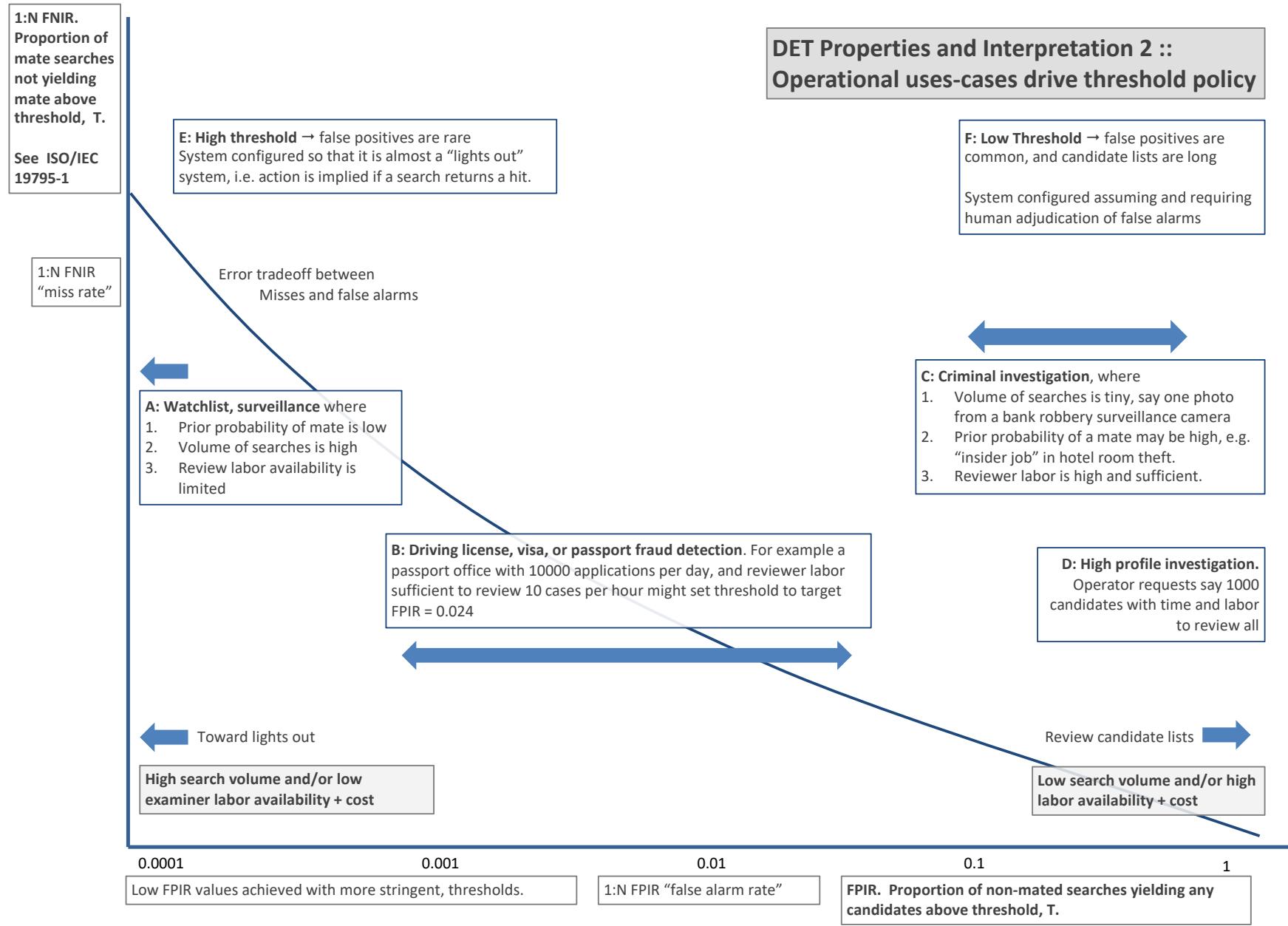
2023/07/05
16:19:47FNIR(N, R, T) = False neg. identification rate
FPIR(N, T) = False pos. identification rate
N = Num. enrolled subjects
R = Num. candidates examined
T = ThresholdT = 0 → Investigation
T > 0 → Identification

Figure 11: DET as the primary performance reporting mechanism.

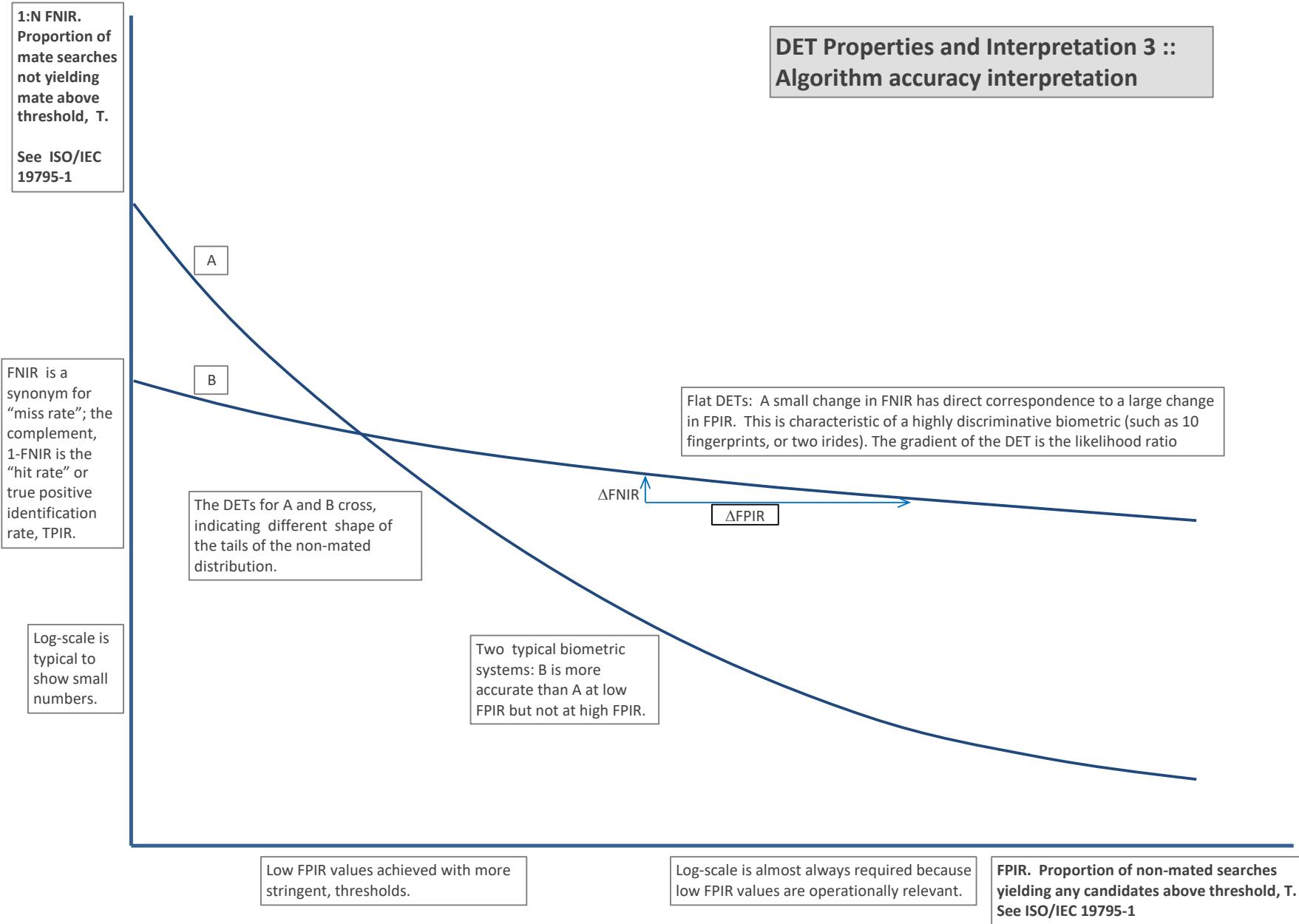
2023/07/05
16:19:47FNIR(N, R, T) = False neg. identification rate
FPIR(N, T) = False pos. identification rateN = Num. enrolled subjects
R = Num. candidates examinedT = Threshold
T = 0 → Investigation
T > 0 → Identification

Figure 12: DET as the primary performance reporting mechanism.

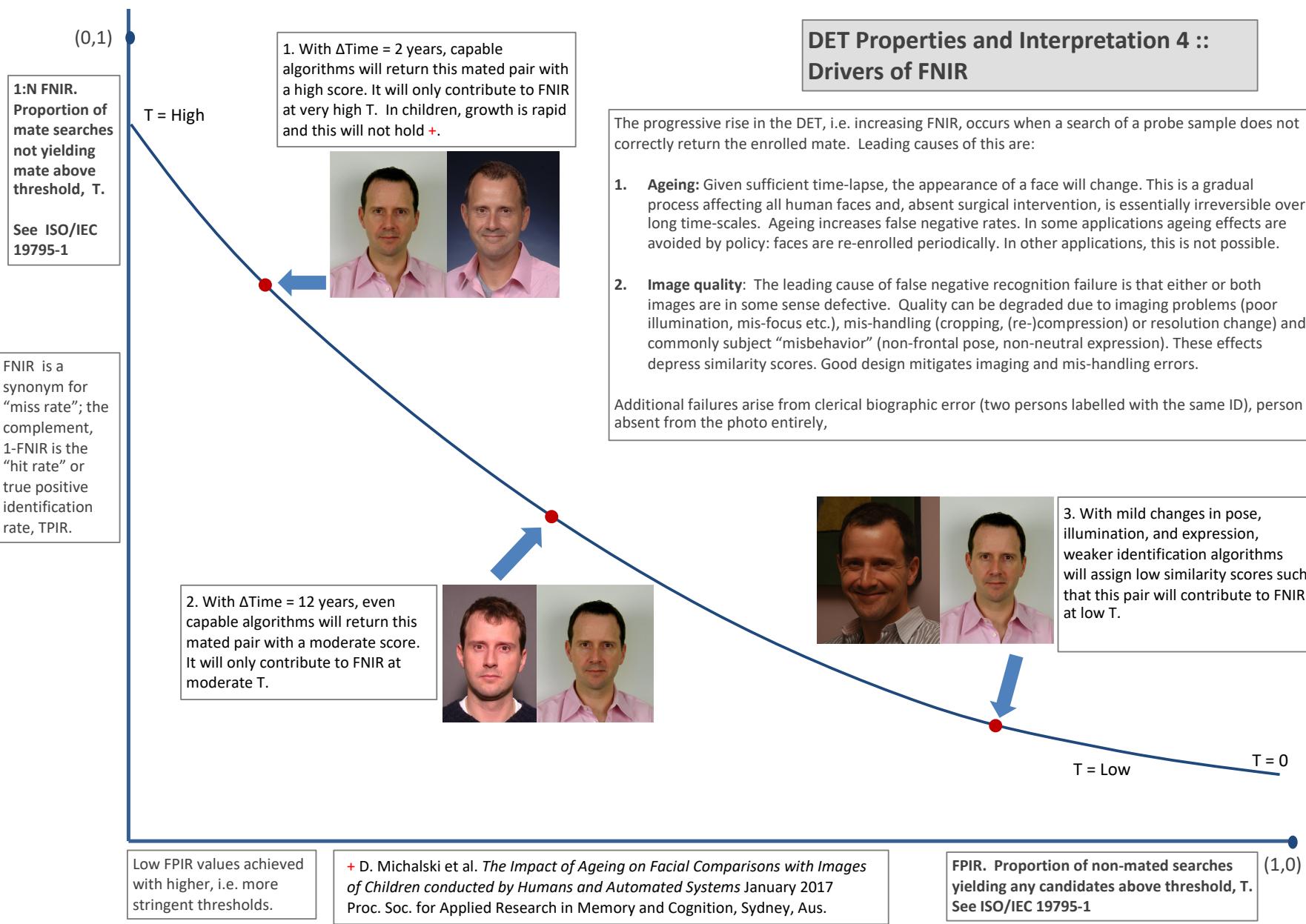


Figure 13: DET as the primary performance reporting mechanism.

2023/07/05
16:19:47

FNIR(N, K, T)
FPIR(N, T)

False neg. identification rate
False pos. identification rate

N = Num. enrolled subjects
R = Num. candidates examined

T = Threshold

$T = 0 \rightarrow$ Investigation
 $T > 0 \rightarrow$ Identification

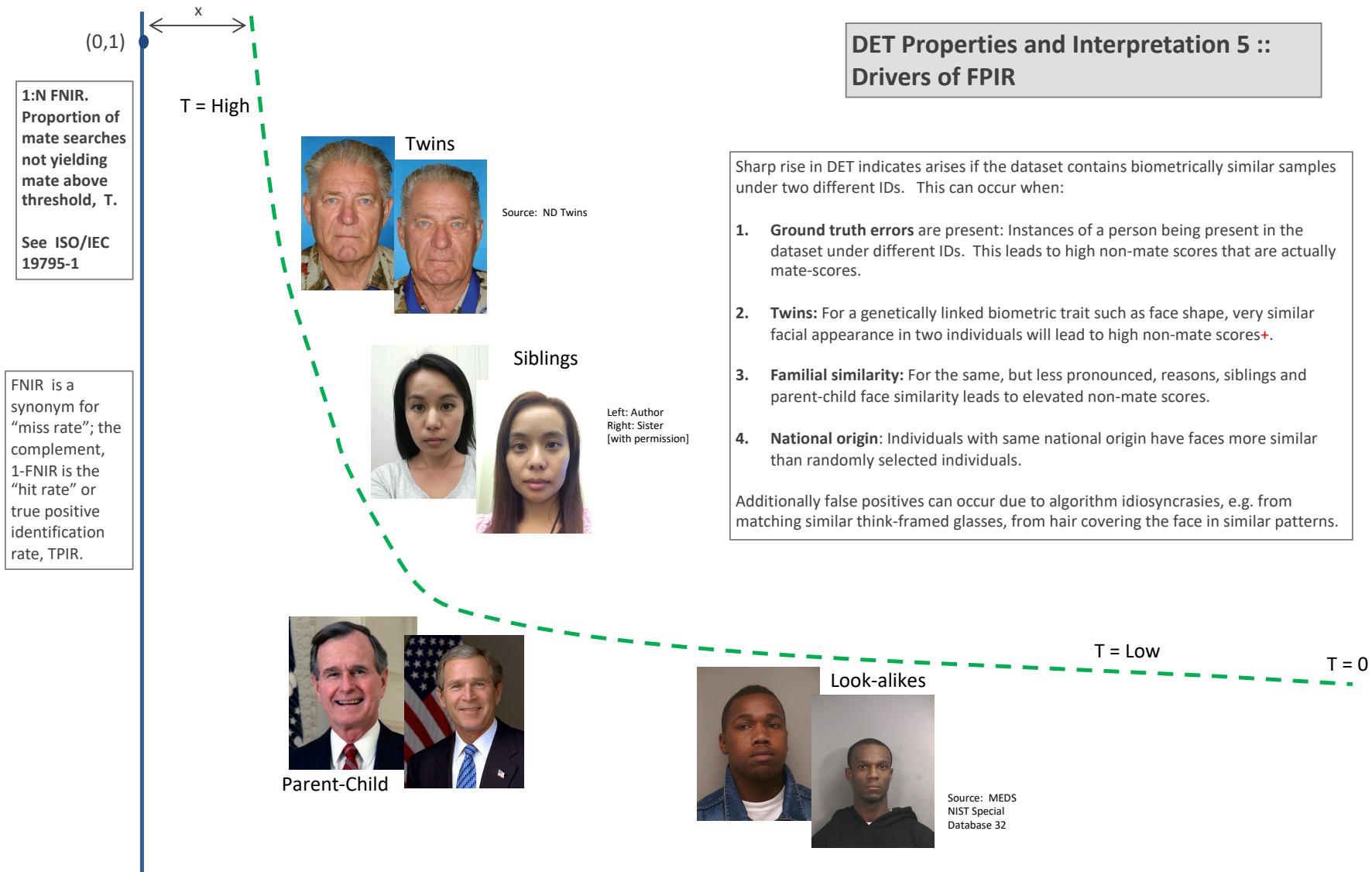


Figure 14: DET as the primary performance reporting mechanism.

2023/07/05
16:19:47

$\text{FNIR}(N, R, T) =$
False neg. identification rate
 $\text{FPIR}(N, T) =$
False pos. identification rate

$N =$ Num. enrolled subjects
 $R =$ Num. candidates examined

$T =$ Threshold

$T = 0 \rightarrow$ Investigation
 $T > 0 \rightarrow$ Identification

1:N FNIR.
Proportion of mate searches not yielding mate above threshold, T .
See ISO/IEC 19795-1

Algorithm X,
Condition 1

Algorithm X,
Condition 2

If system X is used with images of different properties, say from different imaging systems, or from different populations, generally both FNIR and FPIR will change. The dotted line joins points of the same threshold. Horizontal (vertical) lines indicate change in FPIR (FNIR) only. Two cases concerning population size are shown below (A and B), for the blue curves.

FNIR is a synonym for "miss rate"; the complement, 1-FNIR is the "hit rate" or true positive identification rate, TPIR.

Log-scale is typical to show small numbers.

Algorithm Y,
Condition 1

Algorithm Y,
Condition 2

If DETs are computed for two categories (men and women) or (cameras A and B) or (indoor vs. outdoor), generally the Type I and Type II errors will differ and the line of constant threshold will be neither horizontal nor vertical.

The ideal situation in most applications is that a fixed threshold yields a fixed FPIR so that system owners see no change in false alarms across populations or conditions.

Low FPIR values achieved with higher, i.e. more stringent, thresholds.

Log-scale is often required because low FPIR values are operationally relevant.

FPIR. Proportion of non-mated searches yielding any candidates above threshold, T . See ISO/IEC 19795-1

Figure 15: DET as the primary performance reporting mechanism.

DET Properties and Interpretation 7 :: Effect of enrolled population size.

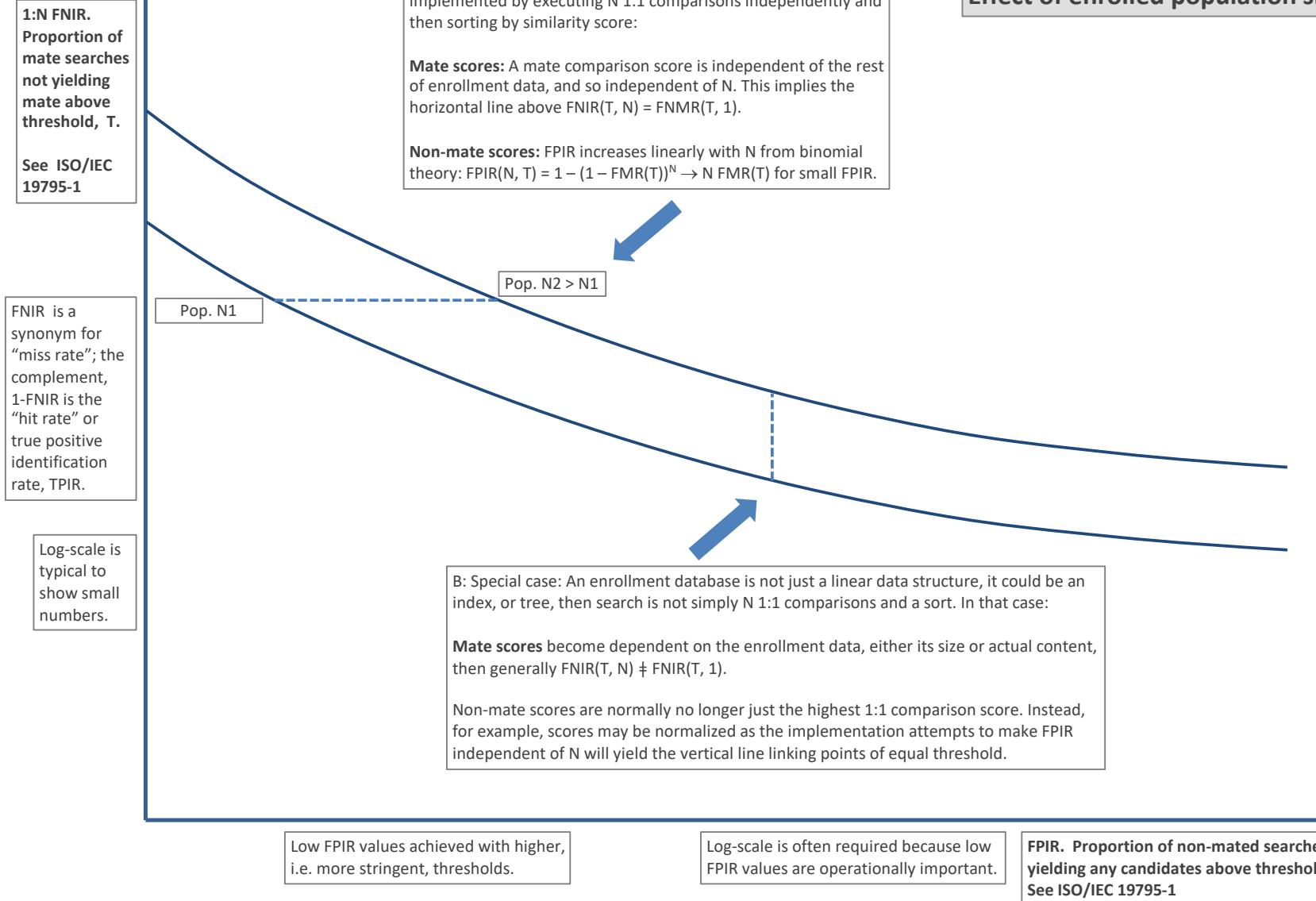


Figure 16: DET as the primary performance reporting mechanism.

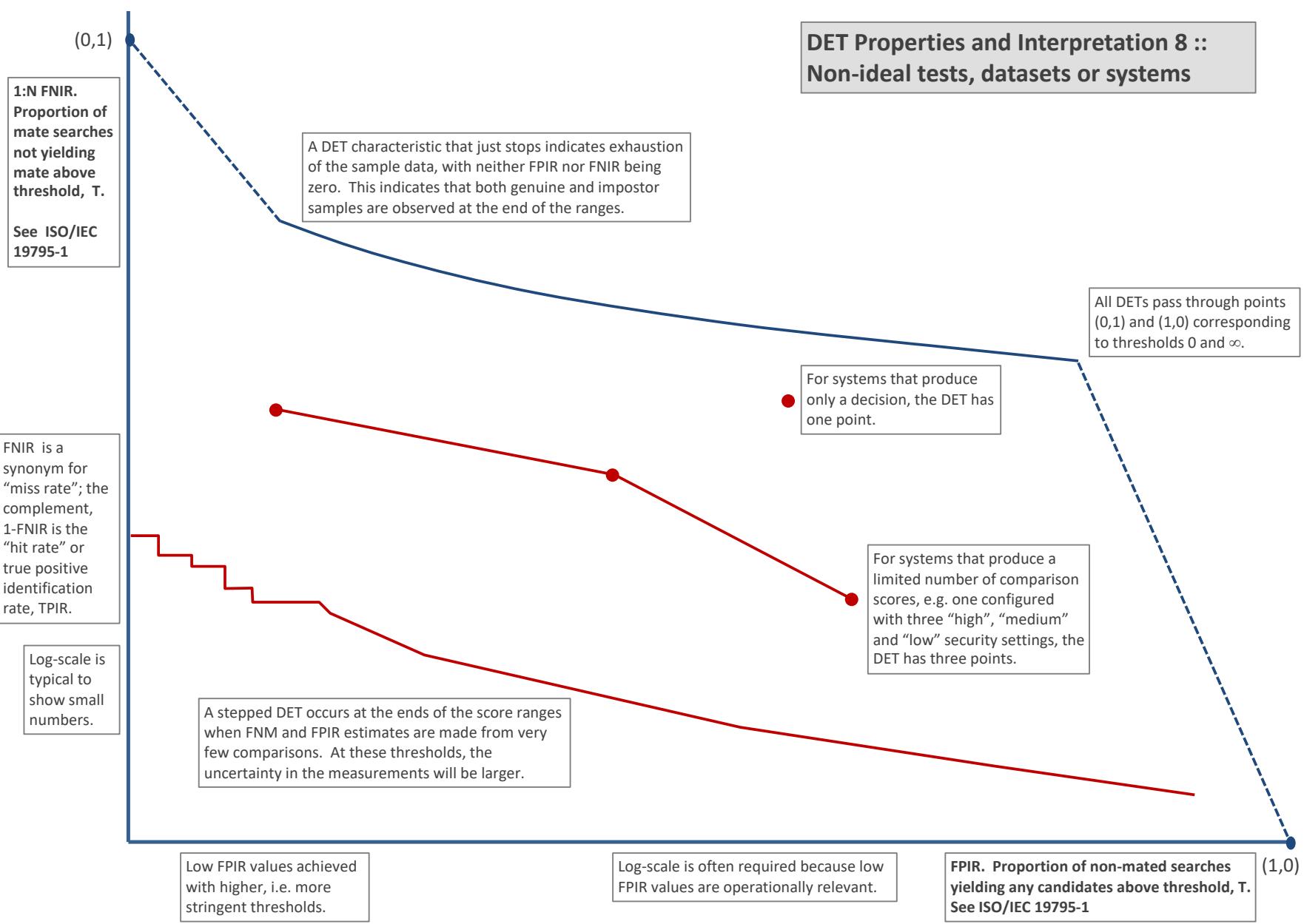


Figure 17: DET as the primary performance reporting mechanism.

3.4 Best practice testing requires execution of searches with and without mates

FRVT embeds 1:N searches of two kinds: Those for which there is an enrolled mate, and those for which there is not. The respective numbers for these types of searches appear in Table 1. However, it is common to conduct only mated searches¹⁰. The cumulative match characteristic is computed from candidate lists produced in mated searches. Even if the CMC is the only metric of interest, the actual trials executed in a test should nevertheless include searches for which no mate exists. As detailed in Table 1 the FRVT reserved disjoint populations of subjects for executing true non-mate searches.

3.5 Failure to extract features

During enrollment some algorithms fail to convert a face image to a template. The proportion of failures is the failure-to-enroll rate, denoted by FTE. Similarly, some search images are not converted to templates. The corresponding proportion is termed failure-to-extract, denoted by FTX.

We do not report FTX because we assume that the same underlying algorithm is used for template generation for enrollment and search.

Failure to extract rates are incorporated into FNIR and FPIR measurements as follows.

- ▷ **Enrollment templates:** Any failed enrollment is regarded as producing a zero length template. Algorithms are required by the API [10] to transparently process zero length templates. The effect of template generation failure on search accuracy depends on whether subsequent searches are mated, or non-mated: Mated searches will fail giving elevated FNIR; non-mated searches will not produce false positives so, to first order, FPIR will be reduced by a factor of $1 - \text{FTE}$.
- ▷ **Search templates and 1:N search:** In cases where the algorithm fails to produce a search template from input imagery, the result is taken to be a candidate list whose entries have no hypothesized identities and zero score. The effect of template generation failure on search accuracy depends on whether searches are mated, or non-mated: Mated searches will fail giving elevated FNIR; Non-mated searches will not produce false positives, so FPIR will be reduced. Thus given a measurement of false negative and positive rates made over only those where failures-to-extract did not occur, those rates - call them FNIR^\dagger and FPIR^\dagger - could be adjusted by an explicit measurement of FTX as follows

$$\text{FNIR} = \text{FTX} + (1 - \text{FTX})\text{FNIR}^\dagger \quad (8)$$

$$\text{FPIR} = (1 - \text{FTX})\text{FPIR}^\dagger \quad (9)$$

This approach is the correct treatment for positive-identification applications such as access control where cooperative users are enrolled and make attempts at recognition. This approach is not appropriate to negative identification applications, such as visa fraud detection, in which hostile individuals may attempt to evade detection by submitting poor quality samples. In those cases, template generation failures should be investigated as though a false alarm had occurred.

¹⁰For example, the [Megaface benchmark](#). This is bad practice for several reasons: First, if a developer knows, or can reasonably assume, that a mate always exists, then unrealistic gaming of the test is possible. A second reason is that it does not put FPIR on equal footing with FNIR and that matters because in most applications, not all searches have mates - not everyone has been previously enrolled in a driving license issuance or a criminal justice system - so addressing between-class separation becomes necessary.

3.6 Fixed length candidate lists, threshold independent workload

Suppose an automated face identification algorithm returns L candidates, and a human reviewer is retained to examine up to R candidates, where $R \leq L$ might be set by policy, preference or labor availability. For now, assume also that the reviewer is not provided with, or ignores, similarity scores, and thresholds are not applied. Given the algorithm typically places mates at low (good) ranks, the number of candidates a reviewer can be expected to review can be derived as follows. Note that the reviewer will:

- ▷ Always inspect the first ranked image Frac. reviewed = 1
- ▷ Then inspect those candidates where mate not confirmed at rank 1 Frac. reviewed = 1-CMC(1)
- ▷ Then inspect those candidates where mate not confirmed at rank 1 or 2 Frac. reviewed = 1-CMC(2)

etc. Thus if the reviewer will stop after a maximum of R candidates, the expected number of candidate reviews is

$$M(R) = 1 + (1 - CMC(1)) + (1 - CMC(2)) + \dots + (1 - CMC(R - 1)) \quad (10)$$

$$= R - \sum_{r=1}^{R-1} CMC(r) \quad (11)$$

A recognition algorithm that front-loads the cumulative match characteristic will offer reduced workload for the reviewer. This workload is defined only over the searches for which a mate exists. In the cases where there truly is no mate, the reviewer would review all R candidates. Thus, if the proportion of searches for which a mate does exist is β , which in the law enforcement context would be the recidivism rate [3], the full expression for workload becomes:

$$M(R) = \beta \left(R - \sum_{r=1}^{R-1} CMC(r) \right) + (1 - \beta)R \quad (12)$$

$$= R - \beta \sum_{r=1}^{R-1} CMC(r) \quad (13)$$

3.7 Timing measurement

Algorithms were submitted to NIST as implementations of the application programming interface(API) specified by NIST in the Evaluation Plan [10]. The API includes functions for initialization, template generation, finalization, search, gallery insert, and gallery delete. Two template generation functions are required, one for the preparation of an enrollment template, and one for a search template.

In NIST's test harness, all functions were wrapped by calls to the C++ std::chrono::high_resolution_clock which on the dedicated timing machine counts 1ns clock ticks. Precision is somewhat worse than that however.

3.8 Uncertainty estimation

3.8.1 Random error

This study leverages operational datasets for measurement of recognition error rates. This affords several advantages. First, large numbers of searches are conducted (see Table 1) giving precision to the measurements. Moreover, for the two mugshot datasets, these do not involve reuse of individuals so binomial statistics can be expected to apply to recognition error counts. In that case, an observed count of a particular recognition outcome (i.e. a false negative or false positive) in M trials will sustain 95% confidence that the actual error rate is no larger than some value.

As an example, the minimum number of mugshot searches conducted in this report is $M = 154\,549$, and for an observed FNIR around 0.002, the measurement supports a conclusion that the actual FNIR is no higher than 0.00228 at 99% confidence level. On the false positive side, we tabulate FNIR at FPIR values as low as 0.001. Given estimates based on 331 254 non-mate trials, the actual FPIR values will be below 0.00115 at 99% confidence. In conclusion, large scale evaluation, without reuse of subjects, supports tight uncertainty bounds on the measured error rates.

3.8.2 Systematic error

The FRVT 2018 dataset includes anomalies discovered as a result of inspecting images involved in recognition failures from the most accurate algorithms. Two kinds of failure occur: False negatives (which, for the purpose here, include failures to make templates) and false positives.

False negative errors: We reviewed 600 false negative pairs for which either or both of the leading two algorithms did not put the correct mate in the top 50 candidates. Given 154 549 searches, this number represents 0.39% of the total, resulting in $\text{FNIR} \sim 0.0039$. Of the 600 pairs:

- ▷ **A: Poor quality:** About 20% of the pairs included images of very low quality, often greyscale, low resolution, blurred, low contrast, partially cropped, interlaced, or noisy scans of paper images. Additionally, in a few cases, the face is injured or occluded by bandages or heavy cosmetics.
- ▷ **B: Ground truth identity label bugs:** About 15% of the pairs are not actually mated. We only assigned this outcome when a pair is clearly not mated.
- ▷ **C: Profile views:** About 35% included an image of a profile (side) view of the face, or, more rarely, an image that was rotated 90 degrees in-plane (roll).
- ▷ **D: Tattoos:** About 30% included an image of a tattoo that contained a face image. These arise from mis-labelling in the parent dataset metadata.
- ▷ **E: Ageing:** There is considerable time-lapse between the two captures.

All these estimates are approximate. Of these, the tattoo and mislabelled images can never be matched. These constitute an accuracy floor in the sample implying that FNIR cannot be below 0.0018¹¹. The profile-views, low-quality images, and images with considerable ageing can, in principle, be successfully matched - indeed some algorithms do so - so are not part of the accuracy floor.

¹¹This value is the sum of two partial false negative rates: $\text{FNIR}_B = 0.15 * 0.0039$ plus $\text{FNIR}_D = 0.3 * 0.0039$

For the microsoft-4 algorithm the lowest miss rate from (recent entry in Table 29) is $\text{FNIR}(640\,000, 50, 0) = 0.0018$. This is close to the value estimated from the inspection of misses. It is below the 0.0039 figure because the algorithm does match some profile and poor quality images, that the yitu-2 algorithm does not.

For many tables (e.g. Table 29), the FNIR values obtained for the FRVT-2018 mugshots could be corrected by reducing them by 0.0018. The best values would then be indistinct from zero. The results in this report *were not* adjusted to account for this systematic error.

False positive errors: As shown in Figure 1 and discussed in Figure 14 many of the DET characteristics in this report exhibit a pronounced turn upward at low false positive rates. The shape can be caused by identity labelling errors in the ground truth of a dataset, specifically persons present in the database under two IDs such that some proportion of non-mate pairs are actually mated. To look for such possibilities, we merged the highest 1000 non-mate pairs produced by three different algorithms which resulted in 1839 unique pairs. This constitutes 0.56% of all non-mate searches. We assert that it is *very* difficult for human reviewers to assign the pairs into the following three categories: twins; doppelgangers; or ground-truth errors (instances of the same person under two IDs). Given this difficulty we made no attempt to correct any possible ground truth errors except by removing 57 pairs in the following categories:

- ▷ **A: Profile views:** Thirteen pairs included one or two profile-view images. As described in Figure 310, these can cause false positives.
- ▷ **B: Same-session photographs:** For twelve pairs, the images were identical or trivially altered (e.g. cropped) versions of the same photo. These were present under a different ID likely due to some clerical or procedural mistake.
- ▷ **C: Tattoos of faces:** There were fourteen instances of tattoo photographs that contained faces causing false matches.
- ▷ **D: T-shirt faces:** There were six instances of T-shirt photographs (of Bob Marley and Che Guevara) being detected instead of the face and causing false positives.
- ▷ **E: Background faces:** There were twelve instances of one subject appearing in the background of two otherwise correct portrait photos.

Note we did not remove any images where there was a chance that the pair was actually a different person.

In any case, the results in this report have not been adjusted for this systematic error.

4 Results

This section gives extensive results for algorithms submitted to FRVT 2018. Three page “report cards” for each algorithm are contained in a [separate supplement](#). Performance metrics were described in section 3. The main results are summarized in tabular form with more exhaustive data included as DET, CMC and related graphs in appendices as follows:

- ▷ The three tables 2-4 list algorithms alongside full developer names, acceptance date, size of the provided configuration data, template size and generation time, and search duration data.
 - The **template generation duration** is most important to applications that require fast response. For example, an eGate taking more than two seconds to produce a template might be unacceptable. Note that GPUs may be of utility in expediting this operation for some algorithms, though at additional expense. Two additional factors should be considered¹²¹³.
 - The **search duration** is the time taken for a search of a search template into a gallery of N enrollment templates. This performance variable, together with the volume of searches, is influential on the amount of hardware needed to sustain an operational deployment. This is measured here with the algorithm running on a single core of a contemporary CPU. Search is most simply implemented as N computations of a distance metric followed by a sort operation to find the closest enrollments. However, considerable optimization of this process is possible, up to and including fast-search algorithms that, by various means, avoid computation of all N distances.
 - The **template size** is the size of the extracted feature vector (or vectors) and any needed header information. Large template sizes may be influential on bus or network bandwidth, storage requirements, and on search duration. While the template itself is an opaque data blob, the feature dimensionality might be estimated by assuming a four-bytes-per-float encoding. There is a wide range of encodings. For the more accurate algorithm, sizes range from 256 bytes to about 2KB bytes, indicating essentially no consensus on face modeling and template design.
 - The **template size multiplier** column shows how, given k input images, the size of the template grows. Most implementations internally extract features from each image and concatenate them, and implement some score-level fusion logic during search. Other implementations, including many of the most accurate algorithms, produce templates whose size does not grow with k . This could be achieved via selection of the best quality image - but this is not optimal in handling ageing where the oldest image could be the best quality. Another mechanism would be feature-level fusion where information is fused from all k inputs. In any case, as a black-box test, the fusion scheme is proprietary and unknown.
 - The size of the **configuration data** is the total size of all files resident in a vendor-provided directory that contains arbitrary read-only files such as parameters, recognition models (e.g caffe). Generally a large value for this quantity may prohibit the use of the algorithm on a resource-constrained device.

¹²The FRVT 2018 API prohibited threading, so some gains from parallelism may be available on multiple-cores or multiple processors, if the feature extraction code could be distributed across them.

¹³Note also that factors of two or more may be realizable by exploiting modern vector processing instructions on CPUs. It is not clear in our measurements whether all developers exploited Intel’s AVX2 instructions, for example. Our machine was so equipped, but we insisted that the same compiled library should also run on older machines lacking that instruction. The more sophisticated implementations may have detected AVX2 presence and branched accordingly. The less sophisticated may be defaulted to the reduced instruction set. Readers should see the FRVT 2018 API document for the specific chip details.

▷ Tables 29-30 report core rank-based accuracy for mugshot images. The population size is limited to $N = 1.6$ million identities because this is the largest gallery size on which all algorithms were executed. Notable observations from these tables are as follows:

- **Accuracy gains since 2018:** NIST Interagency Report 8238 documented massive gains over those reported in the FRVT 2014 report, NIST Interagency Report 8009. Further gains are documented in this report. Comparing the most accurate algorithm in November 2018, NEC-3, the value of $\text{FNIR}(N, L, T)$ reduced from 0.0031 to 0.0024 for the Sensetime-004 algorithm with $N = 12$ million recent images. The tables show broader gains: many developers have made advances since 2018 with between two and five-fold reduction in errors.
- **Wide range in accuracy:** The rank-1 miss rates vary from $\text{FNIR}(N, 1, 0) = 0.0012$ for sensetime-004 up to about 0.5 for the very fast but inaccurate microfocus-x algorithms. Among the developers who are superior to NEC in 2013, the range is from 0.002 to 0.035 for camvi-3. This large accuracy range is consistent with the buyer-beware maxim, and indicates that face recognition software is far from being commoditized.

▷ Tables 34-35 report threshold-based error rates, $\text{FNIR}(N, L, T)$, for $N = 1.6$ million for mugshot-mugshot accuracy on FRVT 2014, FRVT 2018, and also (in pink) mugshot-webcam accuracy using FRVT 2018 enrollments. Notable observations from these tables are as follows:

- **Order of magnitude accuracy gains since 2014:** As with rank-based results, the gains in accuracy are substantial, though somewhat reduced. At $\text{FPIR} = 0.01$, the best improvement over NEC in 2014 is a 27 fold reduction in FNIR using the NEC_2 algorithm. At $\text{FPIR} = 0.001$, the largest gain is a six-fold reduction in FNIR via the NEC_3 algorithm.
- **Broad gains across the industry:** About 19 companies realize accuracy better than the NEC benchmark from 2014. This is somewhat lower than the 28 developers who succeeded on the rank-1 metric. This may be due to the ubiquity of, and emphasis on, the rank-1 metric in many published algorithm development papers.
- **Webcam images:** Searches of webcam images give $\text{FNIR}(N, T)$ values around 2 to 3 times higher than mugshot searches. Notably the leading developers with mugshots are approximately the same with poorer quality webcams. But some developers e.g. Camvi, Megvii, TongYi, and Neurotechnology do improve their relative rankings on webcams, perhaps indicating their algorithms were tailored to less constrained images.

▷ Tables 21, 25, 26 and show, respectively, high-threshold, rank 1, and rank 50 FNIR values for all algorithms performing searches into five different gallery sizes, $N = 640\,000$, $N = 1\,600\,000$, $N = 3\,000\,000$, $N = 6\,000\,000$ and $12\,000\,000$. The $\text{FPIR} = 0.001$ table is included to inform high-volume duplicate detection applications. The Rank-1 table is included as a primary accuracy indicator. The Rank-50 table is included to inform agencies who routinely produce 50 candidates for human-review. The notable results are:

- **Slow growth in rank-based miss rates:** $\text{FNIR}(N, R)$ generally grows as a power law, aN^b . From the straight lines of many graphs of Figure 20 this is clearly a reasonable model for most, but not all, algorithms. The coefficient a can be interpreted as FNIR in a gallery of size 1. The more important coefficient b indicates scalability, and often, $b \ll 1$, implies very benign growth in FNIR. The coefficients of the models appear in the Tables 25 and 26.
- **Slow growth in threshold-based miss rates:** $\text{FNIR}(N, T)$ also generally grows as a power law, aN^b except at the high threshold values corresponding to low FPIR values. This is visible in the plots of Figure 84 which

show straight lines except for $FPIR = 0.001$, which increase more rapidly with N above 3 000 000. Each trace in those figures shows $FNIR(N, T)$ at fixed $FPIR$ with both N and T varying. Thus at large N , it is usually necessary to elevate T to maintain fixed $FPIR$. This causes increased $FNIR$. Why that would no-longer obey a power-law is not known. However, if we expect large galleries to contain individuals with familial relations to the non-mate search images - in the most extreme case, twins - then suppression of false positives becomes more difficult. This is discussed in the Figures starting at Fig. 10

▷ Figure ?? shows false positives from twins against their enrolled siblings, broken out by type of twin: fraternal or identical. The Figure is based on the enrollment of 104 single images on one of a pair of twins, and then the search of 2354 second images. Note that the dataset is heavily skewed towards identical twins which is not representative of the true population. There is also a skew towards same sex fraternal twin pairs compared to different sex fraternal twin pairs again not representative of the true population.

The notable results are:

- For all algorithms tested, the 1087 mated searches (Twin A vs. Twin A) produce scores almost always above typical operational thresholds, with (not shown) matches at rank 1. The images are of good quality, so this is the result expected from the rest of this report.
- For the 1066 identical twin searches (AB), almost all produce the twin at rank 1, with a few producing the mate at further down the candidate lists rank and low score.
- For the 169 fraternal searches (AB) from same sex pairs, most algorithms give a large number of very high scores, implying false positives at all thresholds. However, there are long tails containing lower scores that are correctly below threshold. In general, scores that are higher in this distribution are all rank 1 whereas the lower scores have much higher ranks.
- (Not shown) Of the 169, there are 24 fraternal searches (AB) involving different sex twins. Here most algorithms correctly report scores well below the lowest threshold, and usually not on the candidate list at all.

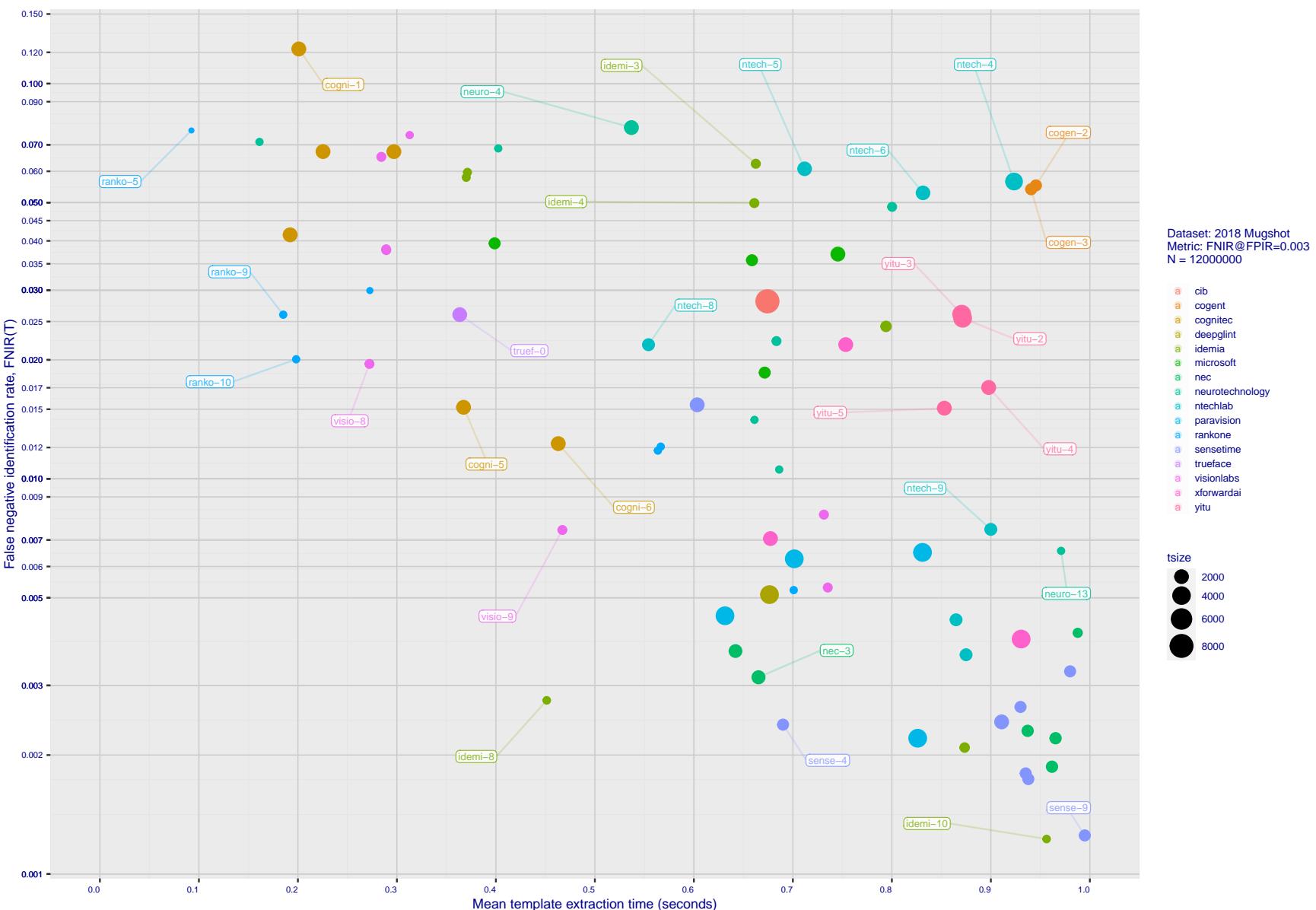
2023/07/05
16:19:47

Figure 18: [Mugshot Dataset] Speed-accuracy tradeoff. For developers of the more accurate algorithms the plot shows the tradeoff of high-threshold recognition miss-rates, $\text{FNIR}(N, N, T)$ for $\text{FPIR}(N, T) = 0.003$, and template generation time. Developers are coded by color. Template size is encoded by the size of the circle. Some labels are quite distant from the respective point, to avoid superposing text. Without any other influences, the assumption would be that taking time to localize the face, and extract features, would lead to better accuracy. The most notable result, for NEC, is that their slower algorithms are much more accurate than the version that extract features in fewer than 90 milliseconds.

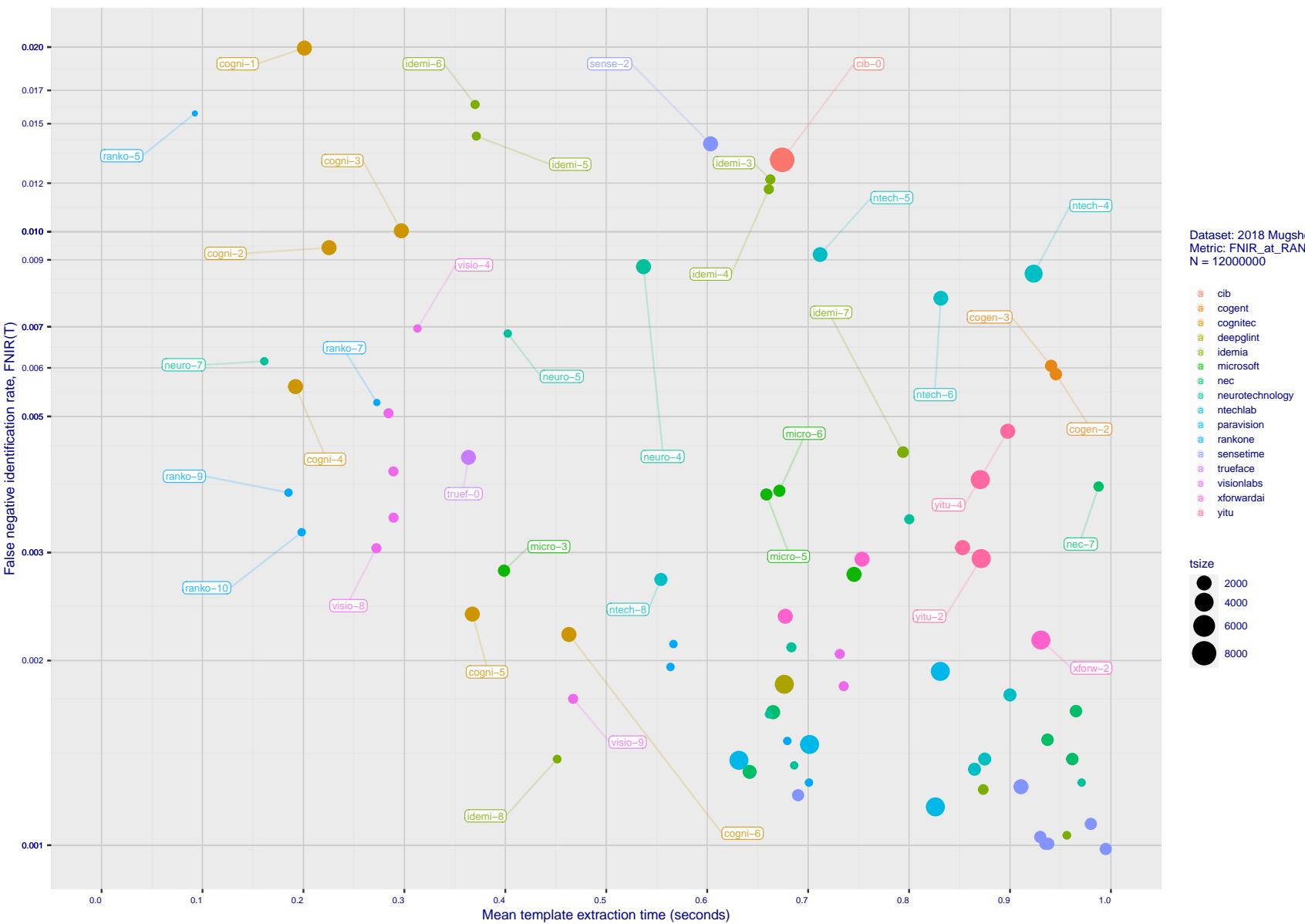
2023/07/05
16:19:47

Figure 19: [Mugshot Dataset] Speed-accuracy tradeoff. For developers of the more accurate algorithms the plot shows the tradeoff of rank-one recognition miss-rates, FNIR($N, 1, 0$), and template generation time. Developers are coded by color. Template size is encoded by the size of the circle. Some labels are quite distant from the respective point, to avoid superposing text. Without any other influences, the assumption would be that taking time to localize the face, and extract features, would lead to better accuracy. This occurs for NEC with their slower algorithm being much accurate than the version that extract features in fewer than 90 milliseconds.

	DEVELOPER	DEVELOPER	SHORT	SEQ.	VALIDATION	CONFIG ¹	LIB ¹	TEMPLATE GENERATION			FINALIZE ²	SEARCH DURATION ³ MILLISEC														
								LOCATION	NAME	NUM.	DATE	DATA (MB)	DATA (MB)	SIZE (B)	MULT ³	TIME (MS) ⁴	TIME (S)	L=1	L=50	L=50	L=50	POWER LAW				
N	1.6M	N	1.6M	N	3M	N	6M	N	12M	(μs)																
1	20Face	NL	20face	000	2021-10-01	112	319	130	2048	-	20	184	83	9	(261)	5679	(271)	6341	-	-	-	-				
2	3Divi	RU	3divi	5	2018-10-26	186	51	263	4096	k	199	638	22	28	(112)	538	(114)	537	(110)	1377	(104)	2614	(98)	5530	203	0.07N ^{1.1}
3	3Divi	RU	3divi	6	2018-10-26	187	51	55	528	k	200	640	36	5	(17)	33	(15)	33	-	-	-	-	-	-	-	
4	AFIS and Biometrics Consulting	US	afisbiometrics	000	2023-06-07	533	34	29	265	-	205	650	4	2	(201)	1718	(195)	1563	(172)	3063	(173)	6541	(174)	13588	157	0.46N ^{1.1}
5	Acer Incorporated	TW	acer	000	2020-08-12	35	67	37	512	-	26	198	24	4	(71)	295	(71)	295	(63)	623	(96)	2302	(90)	4915	233	0.00N ^{1.3}
6	Acer Incorporated	TW	acer	001	2021-11-08	42	610	128	2048	-	10	92	80	9	(99)	444	(122)	575	-	-	-	-	-	-	-	
7	Advance.AI	SG	advance	000	2023-05-30	271	825	144	2048	-	175	573	113	12	(219)	2268	(227)	2271	(196)	4338	(194)	8690	(195)	17842	85	1.15N ^{1.0}
8	Akurat Satu Indonesia	ID	ptakuratsatu	000	2020-10-23	0	572	57	538	-	286	929	291	28633	(8)	18	(6)	16	(6)	17	(5)	17	(4)	17	3	6827.74N ^{0.1}
9	Alchera Inc	KR	alchera	2	2018-10-30	7	14	134	2048	k	12	114	26	63	(232)	2923	(238)	2929	-	-	-	-	-	-	-	
10	Alchera Inc	KR	alchera	3	2018-10-30	251	14	179	2048	k	163	531	264	63	(233)	2955	(239)	2956	(211)	6546	(213)	15013	(215)	35262	230	0.10N ^{1.2}
11	Alchera Inc	KR	alchera	004	2021-09-17	476	24	114	2048	-	257	786	245	35	(268)	5801	(278)	6851	-	-	-	-	-	-	-	
12	Alivia / Innovation Sys	RU	isystems	3	2018-10-30	350	784	177	2048	1	267	825	188	16	(83)	385	(92)	389	(86)	979	(85)	1822	(139)	9348	237	0.00N ^{1.3}
13	AllGoVision	IN	allgovision	000	2019-07-30	168	150	124	2048	k	94	404	118	12	(238)	3226	(243)	3193	(208)	6129	(208)	12449	(207)	25835	110	1.40N ^{1.0}
14	AllGoVision	IN	allgovision	001	2020-07-14	283	126	140	2048	-	253	777	126	13	(237)	3174	(242)	3183	(207)	6073	(206)	12284	(206)	25701	107	1.42N ^{1.0}
15	AllGoVision	IN	allgovision	002	2023-03-13	284	797	160	2048	-	122	459	137	13	(160)	3112	(247)	3454	-	-	-	-	-	-	-	
16	Anke Investments	CN	anke	0	2018-10-30	779	27	248	2072	k	108	429	181	16	(126)	675	(141)	748	(117)	1483	(115)	2968	(112)	6148	158	0.21N ^{1.1}
17	Anke Investments	CN	anke	1	2018-10-30	779	27	247	2072	k	109	430	175	15	(131)	707	(144)	769	-	-	-	-	-	-	-	
18	Anke Investments	CN	anke	002	2019-06-27	341	401	241	2056	k	191	623	143	13	(122)	624	(132)	682	(105)	1306	(99)	2403	(99)	5082	97	0.30N ^{1.0}
19	Armatura LLC	US	armatura	000	2023-04-13	0	935	288	6144	-	208	655	265	66	(269)	6211	(267)	6138	(227)	11533	(224)	23189	(222)	46629	61	3.59N ^{1.0}
20	Aware	US	aware	5	2018-10-30	368	27	258	3100	k	259	792	240	34	(235)	95	(28)	98	(27)	203	(24)	371	(15)	252	16	4.13N ^{0.7}
21	Aware	US	aware	6	2018-10-30	368	27	7	124	k	258	789	6	2	(42)	158	(40)	162	-	-	-	-	-	-	-	
22	Ayonix	JP	ayonix	1	2018-10-29	74	2	85	1036	k	12	107	10	11	(68)	279	(67)	279	-	-	-	-	-	-	-	
23	Ayonix	JP	ayonix	2	2018-10-30	74	2	84	1036	1	6	11	156	14	(67)	279	(66)	276	(50)	535	(51)	1087	(49)	2284	124	0.11N ^{1.0}
24	Camvi Technologies	US	camvitech	4	2018-10-30	233	220	68	1024	1	223	686	231	19	(33)	313	(14)	32	(12)	38	(11)	40	(7)	48	4	8492.66N ^{0.1}
25	Camvi Technologies	US	camvitech	5	2018-10-30	257	220	71	1024	1	247	751	236	31	(16)	31	(12)	30	-	-	-	-	-	-	-	
26	Canon Inc	CN	cib	000	2020-10-19	426	127	295	8196	-	88	396	274	113	(239)	3316	(248)	3604	(213)	6738	(211)	13495	(208)	27114	38	2.33N ^{1.0}
27	Canon Inc	JP	canon	001	2021-10-27	1139	91	266	4096	-	130	480	212	21	(260)	5489	(276)	6789	(236)	12741	(231)	25650	(228)	51922	67	3.82N ^{1.0}
28	Canon Inc	JP	canon	002	2022-04-26	1231	111	289	6200	-	173	565	261	58	(272)	6767	(274)	6416	(230)	12178	(228)	24806	(226)	49653	83	3.28N ^{1.0}
29	Clearview AI Inc	US	clearviewai	000	2021-11-12	358	316	271	4096	-	87	393	233	30	(123)	639	(128)	657	(95)	1134	(88)	1939	(81)	3889	22	1.59N ^{0.9}
30	Cloudwalk - Hengrui AI Technology	CN	hr	000	2021-02-10	501	392	153	2048	-	230	701	167	15	(93)	420	(65)	276	(52)	539	(61)	1268	(71)	3177	207	0.03N ^{1.1}
31	Cloudwalk Moontime Smart Technology	CN	cloudwalk	000	2022-01-31	716	573	135	2048	-	277	869	99	10	(97)	440	(88)	371	(54)	547	(49)	1065	(63)	2902	27	0.53N ^{0.9}
32	Cloudwalk Moontime Smart Technology	CN	cloudwalk	001	2022-07-27	797	574	136	2048	-	161	529	14	16	(62)	273	(82)	349	(65)	658	(71)	1492	(69)	3026	162	0.10N ^{1.1}
33	Cloudwalk Moontime Smart Technology	CN	cloudwalk	002	2023-02-24	431	514	190	2048	-	162	531	164	14	(137)	767	(147)	826	(119)	1586	(122)	3311	(111)	6070	114	0.35N ^{1.0}
34	Cognitec Systems GmbH	DE	cognitec	2	2018-10-30	463	26	222	2052	k	31	225	222	27	(203)	1733	(208)	1763	(186)	3660	(181)	7279	(175)	13895	103	0.83N ^{1.0}
35	Cognitec Systems GmbH	DE	cognitec	3	2018-10-30	465	26	217	2052	k	49	297	182	16	(202)	1719	(209)	1791	(184)	3638	(180)	7277	(182)	14904	137	0.66N ^{1.0}
36	Cognitec Systems GmbH	DE	cognitec	004	2021-03-08	384	60	219	2052	-	23	192	14	13	(197)	1673	(204)	1727	(169)	2904	(161)	5801	(160)	11707	31	1.15N ^{1.0}
37	Cognitec Systems GmbH	DE	cognitec	005	2021-07-30	460	61	216	2052	-	74	367	86	9	(192)	1556	(194)	1551	(167)	2916	(174)	6561	(164)	13958	167	0.38N ^{1.1}
38	Cognitec Systems GmbH	DE	cognitec	006	2022-02-10	689	61	220	2052	-	125	463	96	10	(163)	1006	(164)	1002	(139)	2097	(136)	4312	(128)	7624	154	0.30N ^{1.1}
39	Cubox	KR	cubox	000	2021-08-24	529	298	173	2048	-	110	440	95	10	(240)	3410	(250)	4076	(215)	7605	(214)	15871	-	-	156	1.16N ^{1.1}
40	Cyberlink Corp	TW	cyberlink	000	2019-06-12	217	93	229	2052	1	207	654	232	30	(128)	696	(135)	701	(111)	1379	(105)	2639	(114)	6214	129	0.28N ^{1.0}
41	Cyberlink Corp	TW	cyberlink	001	2019-10-07	459	102	227	2052	1	104	423	228	28	(129)	694	(134)	700	(109)	1350	(105)	5524	(164)	12031	234	0.00N ^{1.3}
42	Cyberlink Corp	TW	cyberlink	002	2020-07-31	333	109	284	4140	-	239	724	875	1875	(183)	1353	(244)	3198	(209)	6138	(205)	12205	(171)	13106	20	16.71N ^{0.8}
43	Cyberlink Corp	TW	cyberlink	003	2021-01-05	333	100	292	6212	-	77	370	245	35	(154)	886	(188)	723	(114)	1415	(113)	2886	(99)	5643	187	0.12N ^{1.1}
44	Cyberlink Corp	TW	cyberlink	004	2021-07-16	371	100	290	6212	-	84	386	216	23	(156)	924	(111)	504	(84)	923	(68)	1448	(73)	3350	26	0.73N ^{0.9}
45	Cyberlink Corp	TW	cyberlink	005	2022-01-07	371	100	291	6212	-	242	733	238	30	(106)	501	(107)	498	(101)	1193	(106)	2672	(102)	5693	229	0.03N ^{1.2}
46	DAON	IE	daon	000	2021-12-23	274	2	24																		

	DEVELOPER FULL NAME	DEVELOPER LOCATION	SHORT NAME	SEQ. NUM.	VALIDATION DATE	CONFIG ¹ DATA (MB)	LIB ¹ DATA (MB)	TEMPLATE GENERATION			FINALIZE ² TIME (S)	SEARCH DURATION ³ MILLISEC						POWER LAW (μ s)		
								SIZE (B)	MULT ³	TIME (MS) ⁴		L=1 N=1.6M	L=50 N=1.6M	L=50 N=3M	L=50 N=6M	L=50 N=12M				
53	Deepglint	CN	deepglint	001	2019-11-15	448	265	262	4096	-	217	676	242	35	(127) 677	(191) 1495	(128) 1724	(108) 2747	(115) 6246	¹⁷ 25.27N ^{0.8}
54	Dermalog	DE	dermalog	5	2018-10-26	0	440	10	128	1	169	528	278	3155	(1) 0	(1) 0	(1) 0	(1) 0	(1) 0	⁵ 66.21N ^{0.2}
55	Dermalog	DE	dermalog	6	2018-10-26	0	453	15	256	1	148	507	8	2	(38) 142	(37) 144	(32) 269	(31) 531	(30) 1294	¹⁴⁰ 0.05N ^{1.0}
56	Dermalog	DE	dermalog	007	2020-02-12	0	424	8	128	1	97	410	1	1	(28) 98	(26) 96	(29) 218	(27) 429	(27) 1013	¹⁹³ 0.01N ^{1.1}
57	Dermalog	DE	dermalog	008	2021-01-25	0	531	41	512	-	25	198	28	4	(53) 227	(57) 246	(46) 462	(46) 924	(43) 1849	⁴⁷ 0.15N ^{1.0}
58	Dermalog	DE	dermalog	009	2021-11-09	0	318	43	512	-	19	180	19	3	(54) 227	(56) 246	(44) 461	(45) 923	(42) 1846	⁴² 0.16N ^{1.0}
59	Dermalog	DE	dermalog	010	2022-07-25	0	514	49	512	-	59	322	24	3	(55) 241	(50) 210	(39) 394	(41) 789	(36) 1580	⁴⁵ 0.13N ^{1.0}
60	Dermalog	DE	dermalog	011	2022-12-12	0	272	9	128	-	36	248	2	1	(22) 87	(21) 88	(18) 165	(18) 331	(18) 664	⁵⁸ 0.05N ^{1.0}
61	Digidata	IN	digidata	000	2022-06-03	248	33	169	2048	-	57	320	277	2444	(2) 0	(47) 198	-	-	-	-
62	DiluSense Technology	CN	dilusense	000	2022-05-26	311	56	210	2048	-	29	219	221	26	(210) 1904	(192) 1498	(174) 3116	(167) 6126	(166) 12046	¹²⁵ 0.61N ^{1.0}
63	DiluSense Technology	CN	dilusense	001	2022-12-24	599	5	273	4096	-	275	860	247	38	(234) 3026	(240) 3042	(204) 4738	(200) 9473	(202) 19026	²³ 5.36N ^{0.9}
64	FarBar Inc	TW	f8	001	2019-10-03	266	19	16	2048	k	26	810	183	14	-	-	-	-	-	
65	Fincore Ltd	UK	fincore	000	2021-08-18	250	224	178	2048	-	112	443	79	(159) 971	(119) 560	-	-	-	-	
66	First Credit Bureau Kazakhstan	KZ	firstcreditkz	001	2022-11-22	548	24	30	288	-	144	495	7	2	(20) 46	(18) 38	(16) 72	(16) 150	(16) 297	⁷⁴ 0.02N ^{1.0}
67	Fujitsu Research and Development Center	CN	fujitsulab	000	2021-10-12	497	337	82	1032	-	186	613	36	5	(208) 1864	(200) 1657	(175) 3140	(170) 6320	(169) 12723	⁹⁶ 0.78N ^{1.0}
68	Fujitsu Research and Development Center	CN	fujitsulab	001	2022-03-15	675	386	81	1032	-	168	535	78	9	(207) 1854	(205) 1740	(179) 3324	(177) 6730	(184) 14943	¹⁶⁴ 0.45N ^{1.1}
69	Gorilla Technology	TW	gorilla	2	2018-10-29	91	1252	95	1132	k	64	338	219	24	(39) 145	(38) 146	(33) 293	(32) 612	(34) 1509	¹⁹⁰ 0.02N ^{1.1}
70	Gorilla Technology	TW	gorilla	3	2018-10-26	94	1252	250	2156	k	171	559	280	12020	-	(219) 2047	-	-	-	-
71	Gorilla Technology	TW	gorilla	004	2020-01-06	182	1244	251	2192	k	88	388	249	41	(70) 286	(70) 285	(100) 1191	(100) 2416	(94) 5036	²³³ 0.00N ^{1.3}
72	Gorilla Technology	TW	gorilla	005	2021-02-22	306	1420	293	6288	-	503	303	268	78	(167) 1070	(149) 799	(118) 1514	(141) 4454	(132) 8820	²¹⁸ 0.05N ^{1.2}
73	Gorilla Technology	TW	gorilla	006	2021-09-30	377	691	298	8336	-	103	422	273	99	(189) 1504	(197) 1612	(149) 2422	(140) 4422	(140) 9363	⁹⁵ 0.59N ^{1.0}
74	Gorilla Technology	TW	gorilla	007	2022-02-16	392	322	294	6290	-	55	315	272	89	(135) 765	(140) 745	(113) 1408	(111) 2823	(105) 5764	⁶⁸ 0.42N ^{1.0}
75	Gorilla Technology	TW	gorilla	008	2022-10-31	321	290	288	4242	-	152	521	259	54	(108) 513	(160) 972	(129) 1699	(102) 2469	(120) 6768	¹³⁴ 0.30N ^{1.0}
76	Griaule	US	griaule	000	2021-11-01	0	584	221	2052	-	347	247	56	8	(235) 4868	(268) 6150	(226) 11473	(223) 22952	(220) 46070	³⁹ 3.89N ^{1.0}
77	Griaule	US	griaule	001	2022-07-26	0	615	215	2052	-	220	684	111	12	(266) 6010	(229) 11627	(226) 24207	(211) 46343	(216) 8394	³⁹ 3.02N ^{1.0}
78	Guangzhou Pixel Solutions Co Ltd	CN	pixelall	002	2019-07-01	0	165	250	2560	k	22	190	171	15	(182) 1296	(184) 1334	(156) 2526	(151) 5136	(155) 11045	¹²⁶ 0.52N ^{1.0}
79	Guangzhou Pixel Solutions Co Ltd	CN	pixelall	003	2019-11-05	0	690	252	2560	k	231	703	215	22	(179) 1273	(180) 1307	(153) 2474	(152) 5198	(156) 11141	¹⁴¹ 0.46N ^{1.0}
80	Guangzhou Pixel Solutions Co Ltd	CN	pixelall	004	2020-07-02	0	538	25	2560	k	116	449	197	17	(178) 1259	(179) 1300	(152) 2465	(157) 5492	(157) 11443	¹⁶⁵ 0.34N ^{1.1}
81	Guangzhou Pixel Solutions Co Ltd	CN	pixelall	005	2021-03-23	0	717	254	2560	-	272	840	105	11	(195) 1606	(193) 1528	(158) 2609	(148) 4926	(161) 11770	⁸¹ 0.73N ^{1.0}
82	Hangzhou Allu Network Information Technology	CN	hzailu	000	2022-03-18	855	97	69	1024	-	121	457	106	11	(229) 2609	(226) 2251	(199) 4612	(203) 10075	(194) 17156	¹¹³ 1.01N ^{1.0}
83	Hangzhou Allu Network Information Technology	CN	hzailu	001	2022-08-18	273	162	151	2048	-	81	377	114	12	(252) 4537	(256) 4511	(220) 8462	(221) 19463	(218) 42527	¹⁷⁸ 0.92N ^{1.1}
84	Hangzhou Allu Network Information Technology	CN	hzailu	002	2023-01-12	302	293	138	2048	-	170	555	119	12	(248) 4481	(255) 4509	(218) 8413	(217) 16568	(216) 39517	¹³⁸ 1.59N ^{1.0}
85	Hangzhou Allu Network Information Technology	CN	hzailu	003	2023-05-22	1434	293	261	4096	-	216	675	217	24	(276) 10145	(282) 9351	(242) 17922	(239) 40619	(234) 83432	¹⁵⁰ 3.03N ^{1.0}
86	Hikvision Research Institute	CN	hikvision	5	2018-10-29	593	9	99	1408	1	181	607	179	16	(155) 883	(154) 895	(135) 1908	(128) 3792	(141) 9387	²⁰⁴ 0.10N ^{1.1}
87	Hikvision Research Institute	CN	hikvision	6	2018-10-29	593	9	108	1408	1	181	598	183	16	(149) 871	(157) 877	-	-	-	-
88	HyperVerge Inc	IN	hyperverge	001	2021-08-11	1791	212	70	1024	-	140	490	34	5	(130) 703	(131) 681	(108) 1346	(107) 2681	(101) 5680	¹⁰⁶ 0.32N ^{1.0}
89	HyperVerge Inc	IN	hyperverge	002	2022-04-13	1140	1118	72	1024	-	114	440	79	9	(104) 484	(112) 518	(93) 1099	(99) 1690	(45) 1953	¹⁸ 6.15N ^{0.8}
90	HyperVerge Inc	IN	hyperverge	003	2023-04-04	2089	1118	188	2048	-	118	452	128	13	(136) 766	(135) 921	(134) 1900	(119) 3198	(110) 6065	⁷¹ 0.48N ^{1.0}
91	Idemia	FR	idemia	5	2018-10-29	417	48	36	352	1	79	371	38	5	(35) 137	(35) 138	(41) 437	(38) 724	(37) 1630	²²⁷ 0.01N ^{1.2}
92	Idemia	FR	idemia	6	2018-10-29	417	48	35	352	1	78	370	32	4	(36) 137	(34) 138	(42) 442	(42) 827	(38) 1646	²²⁹ 0.01N ^{1.2}
93	Idemia	FR	idemia	007	2020-01-17	738	113	67	860	1	260	794	154	14	(40) 151	(39) 152	(67) 683	(70) 1481	(67) 3022	²³⁹ 0.00N ^{1.4}
94	Idemia	FR	idemia	008	2021-03-15	378	65	33	300	-	37	251	20	3	(34) 137	(33) 131	(30) 247	(29) 501	(28) 1013	⁷² 0.07N ^{1.0}
95	Idemia	FR	idemia	009	2022-03-01	735	68	64	636	-	156	521	48	7	(51) 211	(52) 221	(47) 473	(50) 1070	(50) 2352	²⁰⁸ 0.02N ^{1.1}
96	Idemia	FR	idemia	010	2023-01-11	942	71	34	300	-	229	701	12	2	(50) 197	(48) 200	(37) 380	(39) 766	(35) 1561	¹⁰¹ 0.09N ^{1.0}
97	Imagus Technology Pty Ltd	AU	imagus	005	2021-01-15	222	311	153	2048	-	143	491	152	14	(74) 302	(75) 313	(64) 651	(64) 1361	(54) 2461	²⁰² 0.03N ^{1.1}
98	Imagus Technology Pty Ltd	AU	imagus	006	2021-05-27	248	369	207	2048	-	145	505	89	9	(75) 303	(58) 324	(48) 499	(62) 1273	(58) 2727	²²⁴ 0.01N ^{1.2}
99	Imagus Technology Pty Ltd	AU	imagus	007	2021-11-16	248	366	123	2048	-	297	32200	69	9	(73) 301	(56) 238	(43) 442	(44) 881	(41) 1765	³² 0.16N ^{1.0}
100	Imagus Technology Pty Ltd	AU	imagus	008	2022-05-26	204	335	191	2048	-	43	284	195	17	(117) 560	(104) 441	-	-	-	-
101	Imperial College London	GB	imperial	000	2019-08-28	461	15	147	2048	1	177	577	124	13	(79) 360	(91) 379	(123) 1626	(132) 4057	(153) 10291	²⁴² 0.00N ^{1.5}
102	Incode Technologies Inc	US	in																	

	DEVELOPER FULL NAME	DEVELOPER LOCATION	SHORT NAME	SEQ. NUM.	VALIDATION DATE	CONFIG ¹ DATA (MB)	LIB ¹ DATA (MB)	TEMPLATE GENERATION			FINALIZE ² TIME (S)	SEARCH DURATION ⁵ MILLISEC								
								SIZE (B)	MULT ³	TIME (MS) ⁴		L=1 N=1.6M	L=50 N=1.6M	L=50 N=3M	L=50 N=6M	L=50 N=12M	POWER LAW (μ s)			
105	Incode Technologies Inc	US	incode	005	2021-07-29	259	21	168	2048	-	44	285	94	10	(95) 427	(105) 454	(82) 890	(86) 1843	(77) 3640	181 0.07 N 1.1
106	Innovatrics	SK	innovatrics	4	2018-10-30	0	400	89	1076	k	90	399	282	10902	(7) 8	(4) 6	(4) 11	(2) 9	(3) 13	10 668.38 N 0.2
107	Innovatrics	SK	innovatrics	005	2019-09-30	0	455	56	538	1	268	827	284	11897	(6) 8	(3) 8	(3) 9	(3) 9	(2) 9	1 4055.65 N 0.1
108	Innovatrics	SK	innovatrics	007	2021-08-16	175	58	58	538	-	176	577	158	14	(32) 105	(30) 100	(24) 188	(26) 378	(25) 788	29 0.09 N 1.0
109	Innovatrics	SK	innovatrics	008	2023-01-12	609	102	283	4136	-	204	647	25	42	(144) 823	(150) 864	(121) 1610	(121) 3271	(123) 6943	86 0.43 N 1.0
110	Inspur (Beijing) Electronic Information Industry Co	CN	inspur	000	2023-05-30	356	88	171	2048	-	283	898	189	16	(241) 3574	(245) 3248	(212) 6610	(210) 13468	(209) 27332	147 1.04 N 1.0
111	Intellivision	IN	intellivision	001	2022-03-08	62	130	236	2056	-	60	325	209	20	(84) 388	(287) 18764	-	-	-	-
112	Intellivision	IN	intellivision	002	2022-07-28	114	128	237	2056	-	50	301	132	13	(279) 20542	(288) 18784	-	-	-	-
113	Intema-LGL Group	LU	intema	000	2022-08-24	1042	20	48	512	-	194	629	289	13809	(15) 27	(16) 35	(13) 39	(13) 46	(8) 51	8 3478.46 N 0.2
114	Intema-LGL Group	LU	intema	001	2023-02-22	723	20	46	512	-	262	802	280	4808	(11) 23	(9) 24	(9) 31	(8) 38	(11) 54	12 567.10 N 0.3
115	IrexAI	US	irex	000	2021-02-09	724	46	257	3080	-	164	532	209	19	(150) 873	(123) 600	(94) 1120	(103) 2477	(108) 5863	172 0.13 N 1.1
116	Kakao Enterprise	KR	kakao	000	2021-06-23	404	124	218	2052	-	91	399	58	8	(151) 876	(52) 215	(49) 510	(48) 971	(46) 1955	175 0.05 N 1.1
117	Kakao Enterprise	KR	kakao	001	2022-06-08	615	102	162	2048	-	152	509	199	18	(103) 469	(99) 418	(85) 977	(78) 1661	(82) 3898	155 0.13 N 1.1
118	Kedacom International Pte	SG	kedacom	001	2019-09-16	239	36	35	292	1	149	507	9	2	(134) 764	(145) 760	(136) 1940	(116) 2983	(118) 6623	132 0.31 N 1.0
119	Kneron	US	kneron	000	2020-03-03	366	13	200	2048	k	157	523	131	13	(228) 2535	(235) 2506	(205) 4752	(202) 9696	(204) 20926	133 0.95 N 1.0
120	Kneron	US	kneron	001	2021-06-10	270	69	121	2048	-	48	291	76	9	(256) 3141	(237) 2642	-	-	-	-
121	Know U Tech LLC	US	knowutech	000	2023-06-05	789	34	66	781	-	271	831	37	5	(242) 3773	(246) 3411	(210) 6413	(209) 12847	(210) 27685	108 1.50 N 1.0
122	Line Corporation	JP	line	000	2021-06-02	138	397	181	2048	-	56	317	63	8	(254) 4637	(261) 5418	(223) 10144	-	-	35 3.65 N 1.0
123	Line Corporation	JP	line	001	2021-11-21	471	396	125	2048	-	132	485	64	8	(205) 1815	(214) 1934	(188) 3647	(188) 7675	-	143 0.64 N 1.0
124	Line Corporation	JP	lineclova	002	2022-07-29	560	72	199	2048	-	105	425	136	13	(60) 262	(77) 321	(60) 604	(72) 1534	(68) 3023	187 0.05 N 1.1
125	Line Corporation	JP	lineclova	003	2023-01-19	574	397	207	2048	-	100	412	49	7	(41) 156	(46) 195	(89) 1018	(89) 1956	(75) 3405	195 0.05 N 1.1
126	Lomonosov Moscow State University	RU	intsysmsu	000	2019-08-19	375	168	198	2048	1	187	614	138	13	(96) 430	(102) 431	(80) 860	(80) 1730	(97) 5353	213 0.03 N 1.1
127	Lookman Electroplast Industries	IN	lookman	3	2018-10-28	203	24	31	292	1	63	336	18	3	(133) 739	(139) 745	(112) 1394	(110) 2817	(128) 8286	186 0.13 N 1.1
128	Lookman Electroplast Industries	IN	lookman	4	2018-10-28	184	24	60	548	1	58	320	31	4	(160) 981	(163) 998	-	-	-	-
129	Lookman Electroplast Industries	IN	lookman	005	2019-09-16	239	36	59	548	1	146	506	27	4	(162) 1005	(165) 1008	(157) 2597	(156) 5446	(134) 8939	184 0.19 N 1.1
130	Mantra Softech India	IN	mantra	000	2021-10-28	460	61	226	2052	-	99	412	93	10	(155) 916	(156) 910	(127) 1714	(125) 3411	(122) 6841	43 0.57 N 1.0
131	Maxvision	CN	maxvision	000	2022-06-17	167	60	117	2048	-	13	139	296	1	(258) 5044	(175) 1195	(143) 2163	(138) 4380	(133) 8914	94 0.55 N 1.0
132	Maxvision	CN	maxvision	001	2022-10-28	228	63	149	2048	-	68	351	135	13	(173) 1173	(170) 1061	(145) 2233	(135) 4311	(137) 9084	131 0.42 N 1.0
133	Maxvision	CN	maxvision	002	2023-04-12	391	63	115	2048	-	192	626	178	15	(174) 1180	(168) 1052	(144) 2213	(133) 4234	(138) 9310	144 0.37 N 1.0
134	Megvii/Face++	CN	megvii	1	2018-10-28	1703	41	270	4096	1	195	631	239	32	(114) 552	(120) 561	(103) 1222	(108) 2321	(109) 5968	194 0.08 N 1.1
135	Megvii/Face++	CN	megvii	2	2018-10-28	1735	42	260	4096	1	196	635	237	31	(115) 553	(117) 558	-	-	-	-
136	Megvii/Face++	CN	megvii	003	2023-05-11	1335	43	213	2049	-	294	1263	185	16	(212) 1972	(210) 1854	(168) 2942	(178) 6803	(177) 14061	149 0.52 N 1.0
137	MicroFocus	GB	microfocus	5	2018-10-29	94	26	21	256	k	39	262	13	2	(46) 182	(44) 186	(36) 354	(37) 708	(32) 1425	63 0.11 N 1.0
138	MicroFocus	GB	microfocus	6	2018-10-29	94	26	19	256	k	40	262	15	2	(47) 183	(48) 186	-	-	-	-
139	Microsoft	US	microsoft	5	2018-10-29	381	155	74	1024	1	210	658	109	11	(194) 1606	(201) 1673	(173) 3076	(169) 6302	(173) 13160	93 0.79 N 1.0
140	Microsoft	US	microsoft	6	2018-10-29	478	155	73	1024	1	214	671	170	15	(197) 1642	(199) 1618	(187) 3710	(171) 6401	(170) 12892	119 0.68 N 1.0
141	Mukh Technologies	US	mukh	002	2022-09-16	693	442	186	2048	-	254	780	279	4261	(4) 5	(20) 282	(17) 137	(17) 319	(17) 612	56 0.05 N 1.0
142	N-Tech Lab	RU	ntech	5	2018-10-30	1685	113	111	1940	k	236	711	266	55	(58) 243	(60) 246	(51) 538	(52) 1100	(61) 2867	209 0.02 N 1.1
143	N-Tech Lab	RU	ntech	6	2018-10-30	1686	117	112	1940	k	270	831	262	63	(57) 243	(59) 246	(53) 546	(53) 1104	(62) 2873	211 0.02 N 1.1
144	N-Tech Lab	RU	ntechlab	007	2019-06-25	2450	51	259	3348	k	261	795	267	73	(86) 393	(101) 427	(74) 780	(84) 1768	(76) 3499	130 0.16 N 1.0
145	N-Tech Lab	RU	ntechlab	008	2020-01-06	1111	51	98	1300	k	169	554	246	36	(45) 179	(41) 184	(35) 341	(36) 683	(31) 1395	57 0.11 N 1.0
146	N-Tech Lab	RU	ntechlab	009	2021-03-01	1208	42	97	1300	-	296	1936	244	35	(49) 193	(49) 184	(34) 336	(35) 676	(31) 1704	163 0.05 N 1.1
147	N-Tech Lab	RU	ntechlab	010	2021-06-24	351	213	95	1280	-	244	738	40	6	(125) 666	(103) 435	(75) 821	(76) 1645	(72) 3337	84 0.22 N 1.0
148	N-Tech Lab	RU	ntechlab	011	2021-12-07	679	208	94	1280	-	245	739	43	6	(145) 827	(106) 483	(83) 912	(87) 1869	(92) 5003	189 0.07 N 1.1
149	NEC	JP	nec	2	2018-10-30	705	35	107	1616	k	202	642	205	18	(88) 405	(96) 409	(91) 1072	(92) 1755	(87) 4255	199 0.06 N 1.1
150	NEC	JP	nec	3	2018-10-30	774	110	108	1712	k	212	665	210	21	(5) 7	(3) 7	(3) 14	(10) 40	(12) 82	219 0.00 N 1.2
151	NEC	JP	nec	004	2021-07-19	971	63	92	1104	-	203	647	44	7	(102) 468	(83) 351	(66) 662	(63) 1330	(57) 2685	65 0.20 N 1.0
152	NEC	JP	nec	005	2021-12-13	922	88	91	1104	-	188	615	45	7	(90) 407	(113) 551	(88) 1017	(91) 2091	(85) 4242	79 0.28 N 1.0
153	NEC	JP	nec	006	2022-08-10	701	54	90	1104	-	209	656	73	9	(177) 358	(95) 409	(73) 765	(73) 1543	(80) 3878	169 0.10 N 1.1
154	NEC	JP	nec	007	2023-03-03	632	56	65	560	-	201	641	41	6	(52) 216	(51) 214	(40) 423	(43) 853	(40) 1720	192 0.03 N 1.1
155	NEC	JP	nec	008	2023-07-03	1380	50	5	-	-	1	-	297	-	-	-	-	-	-	
156	Neurotechnology	LT	neurotech	5	2018-10-30	266	53	17	256	k	93	402	14	2						

	DEVELOPER	DEVELOPER	SHORT	SEQ.	VALIDATION	CONFIG ¹	LIB ¹	TEMPLATE GENERATION			FINALIZE ²	SEARCH DURATION ³ MILLSEC					
								LOCATION	NAME	NUM.	DATE	DATA (MB)	DATA (MB)	SIZE (B)	MULT ³	TIME (MS) ⁴	TIME (S)
								N=1.6M	N=1.6M	N=1.6M	N=3M	N=6M	N=12M	(μs)			
157	Neurotechnology	LT	neurotech	6	2018-10-30	564	53	16 ²⁵⁶	k	240 ⁷²⁶	11 ²	(147) ⁸³⁹	(149) ⁸⁴²	-	-	-	-
158	Neurotechnology	LT	neurotech	007	2019-10-03	57	51	20 ²⁵⁶	k	14 ¹⁶¹	10 ²	(169) ¹¹¹⁸	(171) ¹¹¹⁰	(141) ²¹⁴³	(139) ⁴³⁹⁷	(136) ⁹⁰⁴⁵	92 ^{0.55N^{1.0}}
159	Neurotechnology	LT	neurotechnology	008	2021-03-22	355	49	53 ⁵¹⁴	-	96 ⁴⁰⁵	30 ⁴	(168) ¹¹⁰⁰	(174) ¹¹⁴⁹	(146) ²²⁶⁶	(144) ⁴⁵⁷³	(145) ⁹⁵⁸⁶	100 ^{0.55N^{1.0}}
160	Neurotechnology	LT	neurotechnology	009	2021-09-01	246	82	52 ⁵¹³	-	63 ³⁴¹	16 ³	(157) ⁹⁴¹	(167) ¹⁰⁴⁹	(138) ¹⁹⁷⁷	(134) ⁴²⁷⁰	(129) ⁸⁷⁵⁶	151 ^{0.32N^{1.1}}
161	Neurotechnology	LT	neurotechnology	010	2022-01-07	247	83	22 ²⁵⁶	-	21 ⁶⁶¹	3 ²	(161) ⁹⁸⁸	(161) ⁹⁸⁴	(132) ¹⁸⁹⁷	(131) ³⁹⁷⁷	(127) ⁸⁰⁴⁸	136 ^{0.36N^{1.0}}
162	Neurotechnology	LT	neurotechnology	012	2022-06-07	247	84	18 ²⁵⁶	-	75 ³⁶⁸	17 ³	(166) ¹⁰³⁶	(159) ⁹⁴⁵	(129) ¹⁸²⁸	(127) ³⁷⁸⁷	(126) ⁷⁸³⁸	142 ^{0.32N^{1.0}}
163	Neurotechnology	LT	neurotechnology	013	2023-02-03	364	87	14 ²⁵⁶	-	12 ⁴⁷¹	5 ²	(257) ⁴⁹³⁵	(258) ⁴⁸¹²	(225) ¹⁰⁴⁶¹	(234) ³⁰⁵³⁴	(233) ⁷³⁴¹⁷	236 ^{0.03N^{1.3}}
164	Newland Computer Co Ltd	CN	newland	2	2018-10-30	96	27	17 ²⁰⁴⁸	-	27 ⁸⁵⁵	172 ¹⁵	(241) ⁸⁷⁴¹	(281) ⁸⁸⁵⁴	(241) ¹⁷⁸⁹²	(238) ³⁹³⁵⁶	-	191 ^{1.32N^{1.1}}
165	Nobilis	US	nobilis	1	2018-10-30	114	176	18 ²⁰⁴⁸	1	2 ²⁰⁶	168 ¹⁵	(180) ¹²⁷³	(178) ¹²⁷²	-	-	-	-
166	Nobilis	US	nobilis	2	2018-10-30	153	176	28 ⁶¹⁴⁴	1	154 ⁵¹⁷	252 ⁴³	(227) ²⁵¹³	(230) ²⁵²²	(206) ⁵⁶⁴⁹	(207) ¹²⁴³²	(219) ⁴⁴²⁶²	231 ^{0.04N^{1.3}}
167	NotionTag Technologies Private Limited	IN	notiontag	000	2022-01-14	265	945	24 ²¹²⁰	-	11 ⁴⁵³	97 ¹⁰	(273) ⁸⁶¹⁹	(280) ⁸⁷⁰⁵	(240) ¹⁶⁶⁵²	(237) ³⁸⁷⁹⁴	(235) ⁹⁰⁶⁰⁷	197 ^{1.15N^{1.1}}
168	Omnigarde Ltd	US	omnigarde	000	2023-05-22	417	34	54 ⁵¹⁷	-	23 ⁷⁰⁵	22 ³	(213) ¹⁹⁸³	(213) ¹⁹³³	(181) ³⁴³⁰	(179) ⁷²²⁴	(187) ¹⁵⁵⁹⁷	121 ^{0.75N^{1.0}}
169	Pangiam	US	pangiam	000	2022-02-22	453	23	18 ²⁰⁴⁸	-	19 ⁶³⁶	196 ¹⁷	(64) ²⁷⁶	(76) ³¹⁹	(58) ⁶⁰¹	(59) ¹²¹⁰	(53) ²⁴⁴³	64 ^{0.18N^{1.0}}
170	Pangiam	US	pangiam	001	2022-11-17	991	36	14 ²⁰⁴⁸	-	17 ⁵⁷⁷	150 ¹⁴	(67) ²⁷⁵	(69) ³⁷⁸	(72) ⁷²⁴	(67) ¹⁴³⁶	(78) ³⁶⁷⁶	170 ^{0.08N^{1.1}}
171	Paravision (EverAI)	US	everai	2	2018-10-30	224	304	12 ²⁰⁴⁸	1	73 ³⁶⁶	234 ³⁰	(66) ²⁷⁸	(69) ²⁸³	-	-	-	-
172	Paravision (EverAI)	US	everai	3	2018-10-30	438	304	20 ²⁰⁴⁸	1	23 ⁷¹⁷	22 ²⁸	(67) ²⁷⁸	(68) ²⁸¹	(55) ⁵⁷²	(54) ¹¹⁴⁶	(48) ²²⁷⁸	120 ^{0.12N^{1.0}}
173	Paravision (EverAI)	US	everai-paravision	004	2019-06-19	527	128	26 ⁴⁰⁹⁶	1	21 ⁶⁷²	255 ⁴⁵	(116) ⁵⁵⁹	(118) ⁵⁵⁹	(159) ²⁶¹¹	(172) ⁶⁴⁴⁵	(129) ¹⁴⁵¹⁹	240 ^{0.00N^{1.5}}
174	Paravision (EverAI)	US	paravision	005	2019-12-11	543	154	27 ⁴⁰⁹⁶	1	26 ⁸³⁰	257 ⁴⁸	(118) ⁵⁶¹	(121) ⁵⁶⁴	(90) ¹⁰⁵⁶	(94) ²²⁹⁹	(91) ⁴⁹⁶⁶	159 ^{0.16N^{1.1}}
175	Paravision (EverAI)	US	paravision	007	2021-02-01	529	235	26 ⁴⁰⁹⁶	-	89 ³⁹⁷	258 ⁴⁸	(139) ⁷⁸⁶	(116) ⁵⁵⁸	(92) ¹⁰⁸⁶	(92) ²¹¹¹	(86) ⁴²⁵⁴	24 ^{1.11N^{0.9}}
176	Paravision	US	paravision	009	2021-12-14	672	300	27 ⁴¹⁰⁰	-	61 ³³¹	269 ⁸²	(249) ⁴⁴⁹⁵	(251) ⁴²³⁰	(217) ⁸⁰³⁷	(216) ¹⁶⁵³²	(211) ³¹⁴²²	123 ^{1.62N^{1.0}}
177	Paravision	US	paravision	012	2023-02-07	762	182	27 ⁴¹⁰⁰	-	98 ⁴¹¹	270 ⁸⁵	(244) ⁴³¹³	(257) ⁴⁵³⁴	(221) ⁸⁶⁵¹	(218) ¹⁶⁵⁸²	(213) ³²¹¹⁴	37 ^{2.87N^{1.0}}
178	Paravision	US	paravision	014	2023-06-08	1501	182	27 ⁴¹⁰⁰	-	29 ²¹⁰¹	271 ⁸⁶	(250) ⁴⁵²⁴	(251) ⁴⁴⁵⁴	(216) ⁷⁹⁹³	(215) ¹⁶¹⁶⁹	(212) ³¹⁶⁹¹	104 ^{1.88N^{1.0}}
179	Qnap Security	TW	qnap	000	2021-07-28	182	15	19 ²⁰⁴⁸	-	92 ⁴⁰¹	81 ⁹	(185) ¹⁴²⁷	(207) ¹⁷⁶³	-	-	-	-
180	Qnap Security	TW	qnap	001	2021-12-09	191	13	13 ²⁰⁴⁸	-	13 ⁴⁸⁷	59 ⁸	(187) ¹⁴⁴⁹	(187) ¹⁴²⁹	(182) ³⁴⁷²	(183) ⁷³⁷⁵	(186) ¹⁵¹⁵⁹	216 ^{0.11N^{1.2}}
181	Qnap Security	TW	qnap	002	2022-04-15	338	32	16 ²⁰⁴⁸	-	13 ⁴⁸⁹	19 ¹⁷	(158) ⁹⁵⁸	(158) ⁹³⁸	(130) ¹⁸⁶⁶	(137) ⁴³⁵⁹	(130) ⁸⁷⁹²	198 ^{0.12N^{1.1}}
182	Qnap Security	TW	qnap	003	2022-12-09	239	60	18 ²⁰⁴⁸	-	33 ²⁴⁴	147 ¹³	(199) ¹⁶⁷¹	(218) ²⁰³⁹	(193) ⁴⁰¹⁰	(191) ⁸³⁷⁹	(183) ¹⁴⁹¹¹	112 ^{0.87N^{1.0}}
183	Qnap Security	TW	qnap	004	2023-05-05	362	60	14 ²⁰⁴⁸	-	72 ³⁶⁵	108 ¹¹	(209) ¹⁸⁸⁵	(209) ²⁰⁹⁴	(178) ³¹⁹¹	(175) ⁶⁶⁰¹	(178) ¹⁴⁴⁹⁰	28 ^{1.66N^{1.0}}
184	Quantasoft	CZ	quantasoft	1	2018-10-30	276	452	19 ²⁰⁴⁸	k	8 ³⁸⁵	42 ⁶	(277) ¹⁵⁴²²	(284) ¹⁴⁸⁵⁸	(288) ¹⁴⁷¹⁷	(280) ¹⁸²³³	-	-
185	Rank One Computing	US	rankone	4	2018-10-09	0	101	6 ⁸⁵	k	8 ³⁶	46 ⁷	(29) ¹⁰¹	(31) ¹⁰¹	(26) ¹⁹⁰	-	-	33 ^{0.07N^{1.0}}
186	Rank One Computing	US	rankone	5	2018-10-24	0	101	11 ¹³³	k	9 ⁹²	47 ⁷	(37) ¹⁴⁰	(36) ¹⁴⁴	(31) ²⁶⁶	(30) ⁵²⁵	(29) ¹⁰⁴⁹	30 ^{0.11N^{1.0}}
187	Rank One Computing	US	rankone	006	2019-06-03	0	133	13 ¹⁶⁵	k	34 ²⁴⁵	57 ⁸	-	-	-	-	-	-
188	Rank One Computing	US	rankone	007	2019-11-12	0	137	12 ¹⁶⁵	k	21 ²⁷²	51 ⁷	(33) ¹¹⁶	(32) ¹¹⁵	(28) ²¹⁵	(28) ⁴³⁹	(26) ⁸⁷⁷	62 ^{0.07N^{1.0}}
189	Rank One Computing	US	rankone	009	2020-06-26	0	105	23 ²⁶⁰	k	21 ¹⁸⁵	104 ¹¹	(24) ⁹⁵	(27) ⁹⁶	(22) ¹⁸¹	(22) ³⁶²	(23) ⁷²⁷	46 ^{0.06N^{1.0}}
190	Rank One Computing	US	rankone	010	2020-11-05	0	135	27 ²⁶¹	-	24 ¹⁹⁸	98 ¹⁰	(25) ⁹⁵	(23) ⁹⁵	(20) ¹⁷⁸	(20) ³⁵⁷	(21) ⁷¹⁴	41 ^{0.06N^{1.0}}
191	Rank One Computing	US	rankone	011	2021-08-27	0	175	26 ²⁶¹	-	17 ⁵⁶⁶	65 ⁸	(27) ⁹⁶	(24) ⁹⁵	(23) ¹⁸³	(23) ³⁷⁰	(20) ⁷¹⁴	54 ^{0.06N^{1.0}}
192	Rank One Computing	US	rankone	012	2021-12-27	0	257	25 ²⁶¹	-	17 ⁵⁶³	53 ⁸	(26) ⁹⁵	(25) ⁹⁵	(21) ¹⁷⁹	(21) ³⁶¹	(22) ⁷¹⁸	44 ^{0.06N^{1.0}}
193	Rank One Computing	US	rankone	013	2022-07-21	0	223	28 ²⁶¹	-	11 ⁴⁴⁶	186 ¹⁶	(30) ¹⁰¹	(22) ⁸⁹	(19) ¹⁶⁷	(19) ³³⁵	(19) ⁶⁷²	52 ^{0.06N^{1.0}}
194	Rank One Computing	US	rankone	014	2022-12-21	0	237	24 ²⁶¹	-	12 ⁴⁵⁷	58 ⁸	(31) ¹⁰¹	(29) ¹⁰⁰	(25) ¹⁸⁸	(24) ³⁷⁶	(24) ⁷⁷⁵	73 ^{0.06N^{1.0}}
195	Realnetworks Inc	US	realnetworks	2	2018-10-30	105	104	28 ⁴¹⁰⁴	k	32 ²⁴¹	22 ²⁸	(214) ²⁰⁰⁸	(220) ²⁰⁴⁸	(194) ⁴¹⁹⁴	(193) ⁸⁶⁴²	(185) ¹⁵⁰³⁵	80 ^{1.08N^{1.0}}
196	Realnetworks Inc	US	realnetworks	003	2019-06-12	93	102	11 ¹⁸⁴⁸	k	18 ¹⁷³	123 ¹³	(172) ¹¹⁴⁵	(171) ¹¹³²	(140) ²¹⁴²	(153) ⁵²⁴¹	(154) ¹⁰⁴⁹⁵	179 ^{0.21N^{1.1}}
197	Realnetworks Inc	US	realnetworks	004	2019-10-17	94	102	10 ¹⁸⁴⁸	1	16 ¹⁷¹	103 ¹¹	(171) ¹¹⁴³	(173) ¹¹³⁷	(142) ²¹⁴⁹	(146) ⁴⁷⁴⁰	(148) ⁹⁶⁹³	148 ^{0.36N^{1.0}}
198	Realnetworks Inc	US	realnetworks	005	2021-06-23	168	209	24 ²⁰⁵⁶	-	62 ³³²	72 ⁹	(198) ¹⁶⁵⁴	(198) ¹⁶¹⁶	(170) ³⁰³⁰	(165) ⁶⁰⁶⁸	(167) ¹²¹³⁴	50 ^{0.10N^{1.0}}
199	Realnetworks Inc	US	realnetworks	006	2021-12-02	250	56	23 ²⁰⁵⁶	-	17 ¹⁷²	60 ⁸	(141) ⁷⁹¹	(113) ⁵³¹	(87) ⁹⁹⁶	(90) ¹⁹⁹⁸	(84) ³⁹⁹¹	49 ^{0.33N^{1.0}}
200	Realnetworks Inc	US	realnetworks	007	2022-04-11	455	99	23 ²⁰⁵⁶	-	66 ³⁴²	194 ¹⁷	(141) ⁸¹⁵	(130) ⁶⁷⁴	(120) ¹⁵⁹⁷	(126) ³⁶⁸³	(104) ⁵⁷²⁹	180 ^{0.13N^{1.1}}
201	Realnetworks Inc	US	realnetworks	008	2022-08-29	557	99	23 ²⁰⁵⁶	-	158 ⁵²⁴	115 ¹²	(113) ⁵³⁸	(129) ⁶⁷³	(104) ¹²⁶⁴	(117) ³⁰¹¹		

	DEVELOPER	DEVELOPER	SHORT	SEQ.	VALIDATION	CONFIG ¹	LIB ¹	TEMPLATE GENERATION			FINALIZE ²	SEARCH DURATION ⁵ MILLISEC									
								LOCATION	NAME	NUM.	DATE	DATA (MB)	DATA (MB)	SIZE (B)	MULT ³	TIME (MS) ⁴	TIME (S)	L=1	L=50	L=50	L=50
N	=1.6M	N	=1.6M	N	=1.6M	N	=3M	N	=6M	N	=12M										
209	SQIsoft	KR	sqisoft	001	2021-12-20	271	377	239	2056	-	54	312	82	9	(211) 1907	(182) 1319	(151) 2456	(147) 4906	(150) 0755	34	0.90 N ^{1.0}
210	SQIsoft	KR	sqisoft	002	2022-10-26	354	593	238	2056	-	106	425	134	13	(188) 1480	(196) 1596	(171) 3044	(166) 6111	(172) 13138	115	0.68 N ^{1.0}
211	Samsung S1 Corp	KR	s1	000	2021-06-03	257	196	272	4096	-	133	487	207	20	(259) 5149	(277) 6794	(237) 13032	(232) 26372	(230) 55723	118	2.82 N ^{1.0}
212	Samsung S1 Corp	KR	s1	001	2021-11-01	240	198	206	2048	-	141	491	66	8	(221) 2366	(234) 2491	(203) 4718	(201) 9614	(205) 24472	177	0.53 N ^{1.1}
213	Samsung S1 Corp	KR	s1	002	2022-05-04	244	93	157	2048	-	136	488	180	16	(176) 1234	(188) 1450	(161) 2729	(162) 5945	(162) 11923	139	0.51 N ^{1.0}
214	Samsung S1 Corp	KR	s1	003	2022-09-27	471	93	120	2048	-	134	487	144	13	(196) 1620	(189) 1454	(162) 2740	(164) 6025	(159) 11644	122	0.57 N ^{1.0}
215	Samsung S1 Corp	KR	s1	004	2023-02-03	471	58	212	2048	-	137	489	133	13	(191) 1554	(190) 1481	(177) 3184	(176) 6701	(165) 12044	152	0.47 N ^{1.1}
216	Scanovate Ltd	IL	scanovate	000	2020-01-15	250	446	184	2048	-	233	705	162	14	(184) 1419	(186) 1412	(169) 3008	(204) 11616	(163) 12012	222	0.10 N ^{1.2}
217	Scanovate Ltd	IL	scanovate	001	2020-09-10	250	446	176	2048	-	166	545	130	13	(190) 1520	(183) 1320	(154) 2502	(150) 5047	(151) 10163	87	0.65 N ^{1.0}
218	Sensetime Group	CN	sensetime	0	2018-10-30	525	6	279	4104	k	227	693	250	41	(105) 498	(108) 501	(102) 1212	(93) 2281	(93) 5032	188	0.09 N ^{1.1}
219	Sensetime Group	CN	sensetime	1	2018-10-30	525	6	280	4104	k	193	628	256	48	(110) 516	(109) 502	(96) 1146	(95) 2301	(89) 4765	185	0.09 N ^{1.1}
220	Sensetime Group	CN	sensetime	002	2019-06-03	523	6	235	2056	k	182	603	200	18	(76) 359	(96) 370	(133) 1897	(142) 4508	(144) 9543	243	0.00 N ^{1.5}
221	Sensetime Group	CN	sensetime	003	2019-12-02	769	76	238	2056	1	285	910	204	19	(256) 4885	(260) 4989	(232) 12325	(227) 24712	(224) 49445	20	0.67 N ^{1.1}
222	Sensetime Group	CN	sensetime	004	2020-08-10	456	29	80	1032	-	226	690	121	12	(226) 2490	(231) 2477	(201) 4654	(199) 9402	(203) 19651	91	1.22 N ^{1.0}
223	Sensetime Group	CN	sensetime	005	2020-12-17	631	39	78	1032	-	291	980	102	11	-	(249) 3939	(214) 7398	(212) 14768	(201) 19016	21	14.03 N ^{0.9}
224	Sensetime Group	CN	sensetime	006	2021-07-26	526	54	4	-	-	2	-	57	7	-	(230) 2422	(198) 4527	(196) 9128	(197) 18640	69	1.35 N ^{1.0}
225	Sensetime Group	CN	sensetime	007	2022-01-15	526	37	75	1032	-	287	935	67	8	(222) 2432	(229) 2406	(197) 4513	(195) 8994	(199) 18796	78	1.28 N ^{1.0}
226	Sensetime Group	CN	sensetime	008	2022-08-17	567	37	77	1032	-	264	814	78	9	(223) 2444	(215) 2012	(189) 3785	(187) 7551	(189) 15799	78	1.05 N ^{1.0}
227	Sensetime Group	CN	sensetime	009	2023-01-04	883	59	76	1032	-	295	1320	69	9	(217) 2031	(221) 2062	(188) 3747	(186) 7543	(188) 15781	77	1.06 N ^{1.0}
228	Serendipity Ltd	UZ	serendipity	000	2023-06-20	0	366	205	2048	-	281	894	125	13	(87) 400	(87) 371	(76) 827	(57) 1188	(51) 2386	25	0.60 N ^{0.9}
229	Shaman Software	US	shaman	6	2018-10-26	0	200	165	2048	k	234	706	160	14	(121) 603	(125) 612	-	-	-	122	0.25 N ^{1.0}
230	Shaman Software	US	shaman	7	2018-10-26	0	200	150	2048	k	235	707	163	14	(120) 602	(126) 614	(98) 1187	(101) 2448	(96) 5083	122	0.25 N ^{1.0}
231	Shanghai Yitu Technology	CN	yitu	4	2018-10-30	2119	136	245	2070	1	282	897	254	45	(181) 1288	(177) 1203	(150) 2440	(154) 5241	(147) 9671	117	0.52 N ^{1.0}
232	Shanghai Yitu Technology	CN	yitu	5	2018-10-30	2043	136	246	2070	1	273	853	253	44	(177) 1237	(176) 1199	(155) 2513	(149) 5013	(146) 9620	109	0.55 N ^{1.0}
233	Smilart	DE	smilart	4	2018-10-30	65	89	47	512	k	15	167	29	4	(278) 16137	(285) 15633	-	-	-	220	0.00 N ^{1.4}
234	Smilart	DE	smilart	5	2018-10-30	562	89	196	2048	k	145	450	157	14	-	-	-	-	220	0.07 N ^{1.1}	
235	StaQu Technologies	IN	staqu	000	2021-08-30	1018	690	264	4096	-	219	684	220	24	(251) 4527	(259) 4933	-	-	-	209	0.12 N ^{1.1}
236	Synesis	RU	synesis	003	2019-07-04	143	17	152	2048	k	28	211	117	12	(107) 507	(110) 502	(147) 2297	(143) 4564	(142) 9452	238	0.00 N ^{1.4}
237	Synesis	RU	synesis	3	2018-10-30	237	150	274	4096	k	119	99	229	29	(140) 789	(146) 801	(137) 1941	(130) 3888	(131) 8810	210	0.07 N ^{1.1}
238	Synesis	RU	synesis	005	2020-09-08	494	24	281	4104	-	249	756	218	24	(152) 877	(151) 865	(176) 3182	(145) 4658	(147) 9750	222	0.06 N ^{1.2}
239	T4iSB	BR	t4isb	000	2022-08-17	228	15	180	2048	-	241	729	140	13	(59) 250	(74) 311	-	-	-	209	0.12 N ^{1.1}
240	Tech5 SA	CH	tech5	001	2019-08-19	1394	116	101	1536	k	280	887	91	10	(82) 383	(143) 766	(163) 2767	(168) 6149	(113) 6178	209	0.12 N ^{1.1}
241	Tech5 SA	CH	tech5	002	2021-04-07	727	112	51	513	-	228	687	28	4	(243) 3816	(258) 6689	(234) 12541	(229) 25145	(227) 50239	48	4.18 N ^{1.0}
242	Tencent Deepsea Lab	CN	deepsea	001	2019-07-29	250	323	204	2048	1	243	737	120	12	(164) 1021	(160) 1020	(164) 2774	(160) 5767	(168) 12341	228	0.06 N ^{1.2}
243	Tevian	RU	tevian	5	2018-10-30	773	15	202	2048	1	95	405	169	15	(89) 405	(94) 408	(78) 854	(83) 1757	(74) 3380	146	0.14 N ^{1.0}
244	Tevian	RU	tevian	006	2021-04-16	769	19	83	1032	-	167	546	90	10	(76) 343	(72) 295	(56) 578	(56) 1187	(60) 2741	171	0.06 N ^{1.1}
245	Tevian	RU	tevian	007	2021-10-12	703	19	79	1032	-	246	747	33	4	(81) 369	(73) 298	(57) 579	(55) 1179	(50) 2418	138	0.11 N ^{1.0}
246	Thales Group	US	cogent	2	2018-10-30	681	39	80	1043	k	288	945	223	27	(215) 2017	(220) 2144	(195) 4298	(192) 8472	(192) 16429	88	1.08 N ^{1.0}
247	Thales Group	US	cogent	3	2018-10-30	681	39	86	1043	k	289	940	87	9	(175) 1230	(181) 1311	(160) 2687	(155) 5399	(152) 10184	105	0.62 N ^{1.0}
248	Thales Group	US	cogent	004	2021-02-10	1376	59	230	2053	-	290	947	149	14	(231) 2903	(211) 1911	(183) 3566	(184) 7498	(191) 16370	145	0.64 N ^{1.0}
249	Thales Group	US	cogent	005	2021-09-13	1043	56	88	1062	-	102	418	38	5	(121) 648	(162) 996	(131) 1872	(129) 3845	(124) 7555	105	0.44 N ^{1.0}
250	Thales Group	US	cogent	006	2022-05-14	508	70	61	550	-	101	412	54	8	(119) 587	(136) 706	(107) 1328	(100) 2767	(100) 5675	82	0.37 N ^{1.0}
251	Thales Group	US	cogent	007	2023-01-30	597	72	62	550	-	131	485	23	3	(111) 516	(111) 708	(106) 1321	(112) 2839	(106) 5789	98	0.34 N ^{1.0}
252	TigerIT Americas LLC	US	tiger	2	2018-10-29	416	518	228	2052	k	124	461	173	15	(206) 1816	(212) 1921	(190) 3833	(185) 7526	(181) 14820	111	0.83 N ^{1.0}
253	TigerIT Americas LLC	US	tiger	3	2018-10-30	416	518	228	2052	k	123	461	293	474	191	(45)	189	-	-	105	0.62 N ^{1.0}
254	Toshiba	JP	toshiba	0	2018-10-30	961	105	106	1548	k	279	876	110	12	(268) 6153	(270) 6236	(231) 12221	(230) 25355	(225) 49448	217	0.36 N ^{1.2}
255	Toshiba	JP	toshiba	1	2018-10-30	961	105	240	2050	k	278	875	294	247	44701	(267) 6007	(272) 6355	-	-	105	0.44 N ^{1.0}
256	Tripleze	JP	aize	001	2021-08-06	262	150	156	2048	-	30	222	77	9	(230) 2870	(241) 3080	-	-	-</		

	DEVELOPER	DEVELOPER	SHORT	SEQ. NUM.	VALIDATION DATE	CONFIG ¹	LIB ¹	TEMPLATE GENERATION	FINALIZE ²	SEARCH DURATION ⁵ MILLISEC						POWER LAW (μs)								
										DATA (MB)	DATA (MB)	SIZE (B)	MULT ³	TIME (MS) ⁴	TIME (S)	L=1	L=50							
261	Veridas Digital Authentication Solutions S.L.	ES	veridas	003	2021-11-09	346	870	11 ⁹ 2048	-	150	508	70 ⁹	(100)	457	(79)	327	(70)	699	(66)	1401	(83)	3954	22 ⁰ 0.02N ^{1.2}	
262	Veridas Digital Authentication Solutions S.L.	ES	veridas	004	2023-02-03	1074	608	19 ⁵ 2048	-	179	579	142	(98)	440	(100)	426	(62)	618	(33)	620	(79)	3775	36 ⁰ 0.22N ^{1.0}	
263	Verigram	KZ	verigram	000	2023-05-17	1553	20	26 ⁴ 096	-	21 ⁹	681	266	68	(132)	710	(133)	688	-	-	-	-	-	-	
264	Verijelas	ID	verijelas	000	2022-10-11	248	11	11 ⁸ 2048	-	53	310	151	14	(9)	20	(10)	26	-	-	-	-	-	-	
265	Vietnam Posts and Telecommunications Group	VN	vnpt	001	2022-05-05	361	235	17 ⁴ 2048	-	14 ⁷	491	208	(20)	142	813	(152)	867	(122)	1626	(124)	3346	(121)	6808	90 ⁰ 0.43N ^{1.0}
266	Vietnam Posts and Telecommunications Group	VN	vnpt	002	2022-09-08	547	235	14 ⁶ 2048	-	198	636	192	16	(148)	857	(155)	897	(126)	1700	(123)	3320	(117)	6622	60 ⁰ 0.52N ^{1.0}
267	Vietnam Posts and Telecommunications Group	VN	vnpt	003	2023-06-26	547	235	19 ² 2048	-	26 ⁹	816	181	16	-	-	-	-	-	-	-	-	-	-	
268	Viettel Group	VN	vts	000	2021-03-12	250	257	13 ² 2048	-	115	447	276	2295	(3)	3	(2)	4	(2)	6	(4)	11	-	15 ⁰ 0.61N ^{0.6}	
269	Viettel Group	VN	vts	001	2021-07-16	352	600	17 ⁵ 2048	-	117	444	213	21	(218)	2081	(233)	2487	(200)	4644	(197)	9313	(198)	18713	53 ¹ 0.53N ^{1.0}
270	Viettel Group	VN	vts	002	2022-02-08	244	600	13 ⁹ 2048	-	284	903	231	29	(225)	2485	(232)	2485	(203)	4678	(198)	9370	(200)	18833	59 ¹ 0.49N ^{1.0}
271	Viettel Group	VN	vts	003	2022-07-14	493	468	16 ⁴ 2048	-	86	393	241	34	(224)	2482	(222)	2075	(192)	3894	(190)	7883	(190)	15891	66 ¹ 1.18N ^{1.0}
272	Vigilant Solutions	US	vigilant	5	2018-10-30	335	122	10 ¹ 1544	k	29 ⁷	762	203	19	-	(203)	1720	-	-	-	-	-	-	-	
273	Vigilant Solutions	US	vigilant	6	2018-10-30	337	122	10 ⁵ 1544	k	26 ⁸	816	211	21	-	(202)	1713	-	-	-	-	-	-	-	
274	Vigilant Solutions	US	vigilantsolutions	007	2021-01-08	340	51	10 ² 1544	-	16 ⁸	552	191	16	(193)	1570	(185)	1352	(166)	2911	(163)	5966	(158)	11466	17 ⁷ 0.27N ^{1.1}
275	Vigilant Solutions	US	vigilantsolutions	008	2021-07-23	340	51	10 ³ 1544	-	70	360	139	13	(186)	1442	(169)	1061	(148)	2330	(158)	5520	(143)	9499	20 ⁵ 0.11N ^{1.1}
276	Visidon	FI	visidon	1	2018-10-30	166	42	22 ⁰ 2052	k	21 ⁹	667	176	15	(246)	4370	(254)	4472	(210)	8454	(219)	17262	(214)	34288	75 ² 2.40N ^{1.0}
277	Visidon	FI	vd	002	2021-05-18	248	42	2 ² -	-	3	7 ¹	9	-	(228)	2336	-	-	-	-	-	-	-	-	
278	Visidon	FI	vd	003	2021-10-12	497	43	3 ² -	-	4 ²	8 ¹	6 ¹	8	-	(225)	2082	-	-	-	-	-	-	-	
279	Vision-Box	PT	visionbox	000	2021-09-17	252	274	24 ² 2059	-	234	687	190	16	(109)	515	(84)	359	(69)	855	(34)	631	(47)	2096	19 ² 2.46N ^{0.8}
280	VisionLabs	RU	visionlabs	6	2018-10-30	360	17	39 ⁵ 512	1	4 ⁸	289	290	2090	(19)	36	(17)	36	(14)	39	(12)	44	(10)	53	9 ³ 3211.93N ^{0.2}
281	VisionLabs	RU	visionlabs	7	2018-10-30	360	17	50 ⁵ 512	1	45 ⁸	289	292	34666	(21)	63	(19)	63	(15)	72	(15)	80	(13)	115	11 ¹ 2076.32N ^{0.2}
282	VisionLabs	RU	visionlabs	008	2019-06-18	348	17	40 ⁵ 512	1	41 ⁷	272	287	12747	(12)	23	(8)	24	(7)	26	(6)	29	(5)	33	6 ⁶ 2539.61N ^{0.2}
283	VisionLabs	RU	visionlabs	009	2020-08-04	689	20	44 ⁵ 512	-	126 ⁵	467	288	13245	(13)	23	(11)	29	(10)	34	(14)	61	(14)	145	14 ⁸ 8.88N ^{0.6}
284	VisionLabs	RU	visionlabs	010	2021-02-05	1042	20	45 ⁵ 512	-	18 ⁷	617	281	11837	(10)	21	(13)	32	(11)	36	(9)	39	(6)	43	7 ³ 183.79N ^{0.2}
285	VisionLabs	RU	visionlabs	011	2021-10-20	1042	20	38 ⁵ 512	-	190 ⁵	618	286	12255	(14)	23	(7)	23	(6)	26	(7)	34	(9)	51	12 ³ 01.26N ^{0.3}
286	Vixvizion	AU	vixvizion	009	2022-11-28	580	460	16 ³ 2048	-	153	516	148	14	(85)	389	(81)	339	(71)	724	(81)	1750	(55)	2622	15 ³ 0.11N ^{1.1}
287	Vocord	RU	vocord	5	2018-10-30	1035	185	65 ⁷ 768	k	25 ⁹	780	50 ⁷	7	(43)	158	(49)	204	(38)	383	(40)	767	(33)	1466	55 ⁰ 0.12N ^{1.0}
288	Vocord	RU	vocord	6	2018-10-30	1035	185	29 ⁷ 10240	k	25 ⁸	785	27 ²	243	(44)	170	(53)	216	-	-	-	-	-	-	-
289	Xforward AI Technology	CN	xforwardai	000	2020-07-24	236	171	21 ⁹ 2048	-	24 ⁸	753	143	13	(253)	4603	(279)	7647	(239)	15723	(225)	23900	(229)	53729	20 ⁶ 0.56N ^{1.1}
290	Xforward AI Technology	CN	xforwardai	001	2021-01-21	332	50	13 ⁷ 2048	-	69 ⁵	355	187	16	(245)	4338	(252)	4384	(222)	8798	(220)	18553	(233)	48993	21 ⁴ 0.32N ^{1.1}
291	Xforward AI Technology	CN	xforwardai	002	2021-05-24	691	50	26 ⁴ 4096	-	13 ⁹	490	201	18	(271)	6340	(273)	6400	(235)	12659	(239)	31077	(232)	65158	21 ² 0.52N ^{1.1}
292	[**Developer name**]	[**Developer country**]	aadi	000	2023-06-27	95	83	42 ⁵ 12	-	67 ³	346	21 ³	(216)	2024	(206)	1754	-	-	-	-	-	-	-	
293	[**Developer name**]	[**Developer country**]	vtcc	000	2023-06-26	277	312	29 ⁸ 4861	-	50 ⁷	307	29 ²⁹	-	-	-	-	-	-	-	-	-	-	-	
294	[**Developer name**]	[**Developer country**]	psl	001	2023-06-28	795	593	1 ¹ -	-	5 ²	295	-	-	-	-	-	-	-	-	-	-	-	-	
295	useB	KR	useb	000	2023-05-08	979	482	12 ⁹ 2048	-	18 ³	606	248	38	(270)	6280	(269)	6158	-	-	-	-	-	-	-
296	verihubs-inteligensia	ID	verihubs-inteligensia	000	2022-09-29	204	75	14 ⁸ 2048	-	38 ²	260	158	14	(275)	9715	(283)	9677	(243)	18417	(240)	41160	(237)	95915	17 ⁶ 2.05N ^{1.1}
297	verihubs-inteligensia	ID	verihubs-inteligensia	001	2023-06-27	352	16	18 ⁷ 2048	-	12 ⁷	471	116	12	(281)	61464	-	-	-	-	-	-	-	-	

Notes

- Configuration size does not capture static data present in libraries. Libraries are included but the size also includes any ancillary libraries for image processing (e.g. openCV) or numerical computation (e.g. blas).
- Finalization is the processing of converting $N = 1600000$ templates into a searchable data structure an operation which can be a simple copy, or the building of an index or tree, for example. The duration of the operation may be data dependent, and may not be linear in the number of input templates.
- This multiplier expresses the increase in template size when k images are passed to the template generation function.
- All durations are measured on Intel®Xeon®CPU E5-2630 v4 @ 2.20GHz processors. Estimates are made by wrapping the API function call in calls to std::chrono::high_resolution_clock which on the machine in (3) counts 1ns clock ticks. Precision is somewhat worse than that however.
- Search durations are measured as in the prior note. The power-law model in the final column mostly fits the empirical results in Figure 311. However in certain cases the model is not correct and should not be used numerically.

Table 7: Summary of algorithms and properties included in this report. The blue superscripts give ranking for the quantity in that column. Missing search durations, denoted by “-”, are absent because those runs were not executed, usually because we did not run on the larger galleries. Caution: The power-law model is sometimes an incorrect model. It is included here only to show broad sublinear behavior, which is flagged in green. The models should not be used for prediction.

#	ALGORITHM	INVESTIGATION, FNIR(N, R = 1, T = 0)								IDENTIFICATION, FNIR(N, R = L, T ≥ 0) FOR FPIR = 0.001							
		(0, 2]	(2, 4]	(4, 6]	(6, 8]	(8, 10]	(10, 12]	(12, 14]	(14, 18]	(0, 2]	(2, 4]	(4, 6]	(6, 8]	(8, 10]	(10, 12]	(12, 14]	(14, 18]
1	3DIVI-005	⁹⁸ 0.0207	⁹⁷ 0.0304	⁹⁷ 0.0415	⁹⁷ 0.0533	⁹⁷ 0.0646	¹⁶⁸ 0.0735	¹⁶⁸ 0.0884	¹⁶⁹ 0.1148	¹⁰⁷ 0.1580	⁹⁸ 0.2316	⁹⁸ 0.3033	⁹⁸ 0.3740	⁹⁸ 0.4285	¹⁶⁷ 0.4742	¹⁶⁸ 0.5329	¹⁶⁸ 0.5975
2	ADVANCE-000									⁸⁸ 0.0087	⁸⁹ 0.0099	⁹¹ 0.0111					
3	AFISBIOMETRICS-000							¹⁰²	¹⁰²	¹⁰² 0.0118	¹⁰² 0.0146	¹¹³ 0.0185					
4	ANKE-000	⁹⁵ 0.0162	⁹⁵ 0.0245	⁹⁵ 0.0333	⁹⁵ 0.0428	⁹⁵ 0.0515	¹⁶⁶ 0.0615	¹⁶⁶ 0.0780	¹⁶⁵ 0.1028	⁹⁶ 0.1132	⁹⁶ 0.1761	⁹⁶ 0.2402	⁹⁶ 0.3057	⁹⁵ 0.3640	¹⁶⁴ 0.4200	¹⁶⁴ 0.4928	¹⁶⁴ 0.5680
5	ANKE-002	⁴⁹ 0.0055	⁵⁰ 0.0074	⁵⁰ 0.0090	⁴⁹ 0.0103	⁴⁸ 0.0116	¹¹⁷ 0.0135	¹¹⁶ 0.0162	¹¹⁵ 0.0202	⁵⁴ 0.0329	⁵⁴ 0.0560	⁵⁶ 0.0843	⁵⁷ 0.1169	⁵⁷ 0.1481	¹²² 0.1820	¹²² 0.2280	¹²² 0.2831
6	ARMATURA-000									²⁴ 0.0041	²⁶ 0.0047	³⁸ 0.0037					
7	AWARE-005	¹⁰⁶ 0.0328	¹⁰⁶ 0.0519	¹⁰⁶ 0.0712	¹⁰⁴ 0.0910	¹⁰⁴ 0.1078	¹⁷⁵ 0.1235	¹⁷⁵ 0.1457	¹⁷⁶ 0.1831	¹⁰⁶ 0.3605	¹⁰⁷ 0.4949	¹⁰⁷ 0.5948	¹⁰⁷ 0.6783	¹⁰⁸ 0.7393	¹⁷⁷ 0.7905	¹⁷⁷ 0.8408	¹⁷⁷ 0.8831
8	AWARE-006	¹¹⁰ 0.0702	¹¹⁰ 0.1110	¹¹⁰ 0.1502	¹¹⁰ 0.1899	¹¹⁰ 0.2253	¹⁸⁴ 0.2614	¹⁸³ 0.3045	¹⁸³ 0.3659								
9	AYONIX-002	¹¹⁵ 0.3360	¹¹⁴ 0.4389	¹¹⁴ 0.5144	¹¹⁴ 0.5814	¹¹⁴ 0.6340	¹⁸⁷ 0.6818	¹⁸⁷ 0.7297	¹⁸⁸ 0.7774	¹¹⁶ 0.8288	¹¹¹ 0.9013	¹¹¹ 0.9375	¹¹¹ 0.9603	¹¹¹ 0.9744	¹⁸² 0.9837	¹⁸² 0.9893	¹⁸² 0.9927
10	CAMVI-004	¹⁰⁹ 0.0623	¹⁰⁹ 0.0944	¹⁰⁹ 0.1243	¹⁰⁹ 0.1548	¹⁰⁸ 0.1812	¹⁸¹ 0.2056	¹⁸¹ 0.2344	¹⁷⁹ 0.2672	⁹¹ 0.0810	⁹¹ 0.1267	⁸⁸ 0.1721	⁸⁸ 0.2203	⁸⁸ 0.2619	¹⁵⁵ 0.3040	¹⁵⁴ 0.3543	¹⁵⁰ 0.4124
11	CAMVI-005	¹¹¹ 0.0849	¹¹¹ 0.1255	¹¹¹ 0.1631	¹¹¹ 0.1989	¹¹¹ 0.2298	¹⁸³ 0.2585	¹⁸² 0.2915	¹⁸² 0.3246								
12	CANON-001									⁵⁴ 0.0052	⁵¹ 0.0057	⁴⁵ 0.0042					
13	CANON-002									⁷¹ 0.0062	⁷⁰ 0.0070	⁷⁰ 0.0070					
14	CIB-000	¹¹⁴ 0.0022	¹¹⁴ 0.0030	¹⁵ 0.0037	¹⁵ 0.0044	¹⁷ 0.0049	⁶⁵ 0.0057	⁶⁸ 0.0069	⁶⁷ 0.0062	²⁵ 0.0139	²⁶ 0.0240	²⁷ 0.0373	²⁸ 0.0525	²⁸ 0.0689	⁸² 0.0859	⁸³ 0.1109	⁸³ 0.1454
15	CLEARVIEWAI-000	¹ 0.0017	⁴ 0.0023	⁴ 0.0028	⁹ 0.0034	¹¹ 0.0039	⁴⁰ 0.0046	³⁰ 0.0056	⁵ 0.0047	¹⁶ 0.0066	¹⁸ 0.0121	¹⁸ 0.0194	¹⁸ 0.0287	¹⁸ 0.0385	⁶⁶ 0.0493	⁶⁵ 0.0662	⁶⁶ 0.0873
16	CLOUDWALK-HR-000	⁸ 0.0019	⁷ 0.0024	⁸ 0.0029	⁶ 0.0032	⁵ 0.0032	⁸ 0.0036	¹³ 0.0041	⁹ 0.0020	¹ 0.0029	¹ 0.0041	¹ 0.0054	¹ 0.0064	² 0.0073	⁹ 0.0085	⁹ 0.0102	⁹ 0.0112
17	CLOUDWALK-MT-000							¹⁴ 0.0037	¹⁴ 0.0038	¹⁴ 0.0013							
18	CLOUDWALK-MT-001							¹¹ 0.0037	³ 0.0037	³ 0.0012							
19	CLOUDWALK-MT-002							¹⁰ 0.0036	⁴ 0.0038	² 0.0012							
20	COGENT-000	⁹⁰ 0.0128	⁹⁰ 0.0184	⁹² 0.0250	⁹² 0.0327	⁹² 0.0407	¹⁶¹ 0.0488	¹⁵⁹ 0.0611	¹⁵⁹ 0.0794	⁷⁷ 0.0559	⁷⁸ 0.0923	⁷⁶ 0.1342	⁷⁷ 0.1812	⁷⁷ 0.2243	¹⁴⁴ 0.2675	¹⁴⁴ 0.3240	¹⁴⁴ 0.3992
21	COGENT-001	⁹¹ 0.0128	⁹¹ 0.0184	⁹³ 0.0250	⁹³ 0.0327	⁹³ 0.0407	¹⁶⁰ 0.0488	¹⁶⁰ 0.0611	¹⁵⁸ 0.0794	⁷⁸ 0.0559	⁷⁹ 0.0923	⁷⁷ 0.1342	⁷⁶ 0.1812	⁷⁶ 0.2243	¹⁴³ 0.2675	¹⁴³ 0.3240	¹⁴⁷ 0.3992
22	COGENT-002	⁶⁷ 0.0081	⁶⁶ 0.0105	⁶³ 0.0123	⁶⁴ 0.0137	⁶² 0.0157	¹³¹ 0.0175	¹²⁹ 0.0215	¹²⁹ 0.0280	⁶⁹ 0.0499	⁶⁸ 0.0827	⁶⁷ 0.1207	⁶⁷ 0.1639	⁶⁷ 0.2037	¹³⁵ 0.2432	¹³⁵ 0.2972	¹³⁷ 0.3638
23	COGENT-003	⁷¹ 0.0082	⁶⁷ 0.0108	⁶⁷ 0.0128	⁶⁷ 0.0145	⁶⁶ 0.0168	¹³⁷ 0.0191	¹³⁸ 0.0239	¹³⁵ 0.0312	⁸⁰ 0.0582	⁸⁰ 0.0971	⁸⁰ 0.1417	⁸⁰ 0.1918	⁸⁰ 0.2380	¹⁵⁰ 0.2836	¹⁵² 0.3440	¹⁵³ 0.4207
24	COGENT-004	⁵⁹ 0.0066	⁵³ 0.0080	⁴⁵ 0.0085	³⁹ 0.0080	³¹ 0.0083	⁹³ 0.0092	⁹³ 0.0106	⁹¹ 0.0130	⁶³ 0.0410	⁶⁵ 0.0720	⁶⁵ 0.1099	⁶⁵ 0.1539	⁶⁴ 0.1974	¹³² 0.2443	¹³² 0.3043	¹³⁷ 0.3757
25	COGENT-006							³⁶ 0.0045	³⁷ 0.0049	⁴¹ 0.0038							
26	COGENT-007							³⁵ 0.0044	³¹ 0.0049	³⁸ 0.0036							
27	COGNITEC-000	¹⁰⁵ 0.0265	¹⁰³ 0.0423	¹⁰³ 0.0588	¹⁰³ 0.0757	¹⁰² 0.0894	¹⁷³ 0.1014	¹⁷³ 0.1169	¹⁷² 0.1381	¹⁰⁸ 0.1522	⁹⁹ 0.2330	⁹⁹ 0.3051	⁹⁸ 0.3751	⁹⁸ 0.4300	¹⁶⁸ 0.4779	¹⁶⁷ 0.5307	¹⁶⁸ 0.5913
28	COGNITEC-001	⁹³ 0.0149	⁹⁴ 0.0228	⁹⁴ 0.0312	⁹⁴ 0.0399	⁹⁴ 0.0479	¹⁶³ 0.0546	¹⁶² 0.0656	¹⁶⁰ 0.0806	⁹³ 0.0963	⁹³ 0.1562	⁹² 0.2157	⁹² 0.2771	¹⁶¹ 0.3771	¹⁶¹ 0.4433	¹⁶¹ 0.4959	
29	COGNITEC-002	⁷⁰ 0.0101	⁸⁰ 0.0138	⁸¹ 0.0170	⁸¹ 0.0201	⁸¹ 0.0237	¹⁴⁹ 0.0264	¹⁴⁷ 0.0309	¹⁴⁶ 0.0389	⁷² 0.0517	⁷¹ 0.0879	⁷² 0.1269	⁷¹ 0.1707	⁷¹ 0.2098	¹³⁷ 0.2463	¹³⁷ 0.2919	¹³⁷ 0.3535
30	COGNITEC-003	⁷⁸ 0.0104	⁸¹ 0.0140	⁸² 0.0174	⁸² 0.0205	⁸² 0.0238	¹⁵⁰ 0.0266	¹⁴⁸ 0.0311	¹⁴⁸ 0.0401	⁷¹ 0.0504	⁷⁰ 0.0855	⁶⁹ 0.1235	⁶⁹ 0.1662	⁶⁸ 0.2045	¹³⁴ 0.2403	¹³⁴ 0.2854	¹³³ 0.3451
31	COGNITEC-004	⁶⁴ 0.0073	⁶³ 0.0099	⁶² 0.0118	⁵⁹ 0.0130	⁵⁹ 0.0147	¹³⁶ 0.0163	¹²⁵ 0.0189	¹²⁵ 0.0239	⁵³ 0.0325	⁵³ 0.0548	⁵² 0.0798	⁵¹ 0.1074	⁵⁰ 0.1325	¹¹⁵ 0.1591	¹¹⁵ 0.1952	¹¹⁵ 0.2414
32	COGNITEC-006							⁸⁴ 0.0081	⁸² 0.0086	⁸³ 0.0090							
33	CUBOX-000	⁷ 0.0019	⁵ 0.0024	⁵ 0.0028	⁴ 0.0031	⁴ 0.0032	¹² 0.0037	²⁰ 0.0044	²⁰ 0.0044	²⁰ 0.0027	⁶ 0.0039	⁶ 0.0059	⁷ 0.0083	⁸ 0.0111	²⁴ 0.0185	²⁵ 0.0252	²⁶ 0.0339
34	CYBERLINK-002	⁵⁰ 0.0055	⁴⁵ 0.0068	⁴¹ 0.0075	³⁵ 0.0078	³² 0.0084	⁹⁴ 0.0094	⁹⁴ 0.0107	⁹² 0.0114	³² 0.0180	³³ 0.0302	³³ 0.0460	³² 0.0643	³³ 0.0837	⁹² 0.1058	⁹¹ 0.1370	⁹¹ 0.1787
35	CYBERLINK-003	³ 0.0041	³⁴ 0.0052	²⁷ 0.0057	²⁵ 0.0058	²⁵ 0.0061	⁸⁰ 0.0068	⁷⁷ 0.0078	⁷⁷ 0.0078	¹⁹ 0.0109	¹⁹ 0.0175	²⁰ 0.0259	²¹ 0.0356	²¹ 0.0468	⁶⁹ 0.0594	⁷² 0.0787	⁷⁴ 0.1072
36	DAHUA-002	³⁰ 0.0035	²⁸ 0.0047	²⁸ 0.0058	²⁷ 0.0067	²⁸ 0.0074	⁸⁵ 0.0082	⁸⁰ 0.0100	⁸⁸ 0.0108	³⁰ 0.0169	³² 0.0294	³¹ 0.0449	³⁰ 0.0635	³⁰ 0.0817	⁸⁹ 0.1013	⁸⁸ 0.1291	⁸⁷ 0.1638
37	DAHUA-003	¹ 0.0026	¹⁹ 0.0036	¹⁹ 0.0043	²⁰ 0.0050	²⁰ 0.0055	⁷⁰ 0.0062	⁷⁰ 0.0080	⁷⁰ 0.0073	²⁹ 0.0160	³⁰ 0.0280	²⁹ 0.0432	²⁹ 0.0794	⁸⁷ 0.0987	⁸⁷ 0.1270	⁸⁵ 0.1587	
38	DEEGLINT-001	¹⁷ 0.0024	¹⁶ 0.0032	¹⁴ 0.0037	¹³ 0.0040	¹³ 0.0043	⁴⁸ 0.0049	⁵⁹ 0.0060	⁵⁸ 0.0052	¹² 0.0058	¹⁰ 0.0087	¹¹ 0.0119	¹¹ 0.0155	¹¹ 0.0199	³⁰ 0.0249	³⁰ 0.0338	³² 0.0463
39	DEEPSSEA-001	⁷ 0.0081	⁷⁰ 0.0116	⁷³ 0.0149	⁷⁶ 0.0182	⁷⁶ 0.0216	¹⁴⁸ 0.0260	¹⁵⁰ 0.0332	¹⁴⁵ 0.0432	⁶⁶ 0.0458	⁶⁶ 0.0752	⁶⁴ 0.1086	⁶³ 0.1464	⁶³ 0.1812	¹³² 0.2186	¹³² 0.2663	¹³¹ 0.3213
40	DERMALOG-006	⁸² 0.0113	⁸² 0.0142	⁷⁸ 0.0163	⁷⁷ 0.0183	⁷⁴ 0.0200	¹⁴² 0.0218	¹⁴⁰ 0.0251	¹³⁸ 0.0329	⁷⁵ 0.0545	⁷³ 0.0889	⁷³ 0.1271	⁷² 0.1697	⁷⁰ 0.2090	¹³⁹ 0.2498	¹³⁸ 0.3028	¹³⁸ 0.3670
41	DERMALOG-007	⁸ 0.0125	⁸⁸ 0.0170	^{88</}													

MISS RATES		INVESTIGATION, FNIR(N, R = 1, T = 0)								IDENTIFICATION, FNIR(N, R = L, T ≥ 0) FOR FPIR = 0.001							
#	ALGORITHM	(0, 2]	(2, 4]	(4, 6]	(6, 8]	(8, 10]	(10, 12]	(12, 14]	(14, 18]	(0, 2]	(2, 4]	(4, 6]	(6, 8]	(8, 10]	(10, 12]	(12, 14]	(14, 18]
45	DILUSENSE-000																
46	DILUSENSE-001																
47	FIRSTCREDITKZ-001																
48	FUJITSULAB-001																
49	GORILLA-002	100 ^{0.0213}	100 ^{0.0359}	101 ^{0.0528}	102 ^{0.0716}	103 ^{0.0895}	174 ^{0.1088}	174 ^{0.1367}	174 ^{0.1765}	103 ^{0.1828}	104 ^{0.2787}	104 ^{0.3654}	104 ^{0.4485}	104 ^{0.5168}	171 ^{0.5823}	171 ^{0.6508}	171 ^{0.7180}
50	GORILLA-005	38 ^{0.0044}	47 ^{0.0070}	58 ^{0.0102}	62 ^{0.0136}	67 ^{0.0170}	140 ^{0.0204}	143 ^{0.0272}	145 ^{0.0373}	79 ^{0.0566}	81 ^{0.0973}	82 ^{0.1432}	81 ^{0.1937}	81 ^{0.2398}	153 ^{0.2862}	151 ^{0.3437}	151 ^{0.4150}
51	GORILLA-007																
52	GORILLA-008																
53	GRIAULE-001																
54	HYPERVERGE-003																
55	HZAILU-001																
56	HZAILU-002																
57	HZAILU-003																
58	IDEMIA-003	81 ^{0.0110}	86 ^{0.0151}	86 ^{0.0196}	85 ^{0.0238}	84 ^{0.0281}	153 ^{0.0313}	153 ^{0.0368}	152 ^{0.0504}	87 ^{0.0717}	86 ^{0.1147}	86 ^{0.1614}	86 ^{0.2113}	85 ^{0.2553}	154 ^{0.2976}	153 ^{0.3537}	154 ^{0.4334}
59	IDEMIA-004	80 ^{0.0107}	84 ^{0.0148}	85 ^{0.0192}	84 ^{0.0233}	83 ^{0.0277}	152 ^{0.0312}	152 ^{0.0367}	153 ^{0.0512}	58 ^{0.0373}	55 ^{0.0587}	54 ^{0.0833}	53 ^{0.1100}	52 ^{0.1340}	114 ^{0.1580}	111 ^{0.1911}	112 ^{0.2482}
60	IDEMIA-005	84 ^{0.0118}	87 ^{0.0167}	90 ^{0.0218}	89 ^{0.0270}	88 ^{0.0317}	156 ^{0.0357}	155 ^{0.0425}	155 ^{0.0579}	63 ^{0.0440}	60 ^{0.0689}	60 ^{0.0964}	59 ^{0.1254}	58 ^{0.1513}	121 ^{0.1762}	116 ^{0.2113}	119 ^{0.2698}
61	IDEMIA-006	87 ^{0.0124}	89 ^{0.0171}	89 ^{0.0218}	87 ^{0.0263}	86 ^{0.0302}	154 ^{0.0321}	151 ^{0.0356}	151 ^{0.0471}	62 ^{0.0409}	59 ^{0.0620}	57 ^{0.0850}	52 ^{0.1097}	49 ^{0.1309}	107 ^{0.1486}	104 ^{0.1738}	103 ^{0.2200}
62	IDEMIA-007	47 ^{0.0050}	48 ^{0.0071}	48 ^{0.0089}	50 ^{0.0106}	51 ^{0.0124}	119 ^{0.0142}	119 ^{0.0171}	12 ^{0.0220}	36 ^{0.0202}	36 ^{0.0335}	34 ^{0.0491}	33 ^{0.0663}	31 ^{0.0825}	88 ^{0.0999}	85 ^{0.1240}	86 ^{0.1645}
63	IDEMIA-008	5 ^{0.0018}	6 ^{0.0024}	6 ^{0.0029}	5 ^{0.0032}	7 ^{0.0035}	16 ^{0.0039}	24 ^{0.0046}	31 ^{0.0033}	3 ^{0.0034}	3 ^{0.0051}	5 ^{0.0069}	5 ^{0.0087}	5 ^{0.0102}	15 ^{0.0123}	13 ^{0.0146}	13 ^{0.0186}
64	IDEMIA-009																
65	IDEMIA-010																
66	IMAGUS-005	33 ^{0.0039}	33 ^{0.0052}	31 ^{0.0061}	29 ^{0.0067}	30 ^{0.0077}	98 ^{0.0088}	91 ^{0.0103}	89 ^{0.0109}	39 ^{0.0212}	39 ^{0.0357}	40 ^{0.0539}	40 ^{0.0755}	38 ^{0.0967}	97 ^{0.1183}	96 ^{0.1485}	94 ^{0.1893}
67	IMAGUS-008																
68	IMPERIAL-000	34 ^{0.0040}	35 ^{0.0054}	36 ^{0.0067}	38 ^{0.0079}	40 ^{0.0093}	105 ^{0.0112}	104 ^{0.0139}	108 ^{0.0178}	49 ^{0.0286}	51 ^{0.0503}	51 ^{0.0779}	51 ^{0.1116}	56 ^{0.1455}	128 ^{0.1844}	128 ^{0.2341}	127 ^{0.2951}
69	INCODE-003	94 ^{0.0155}	96 ^{0.0247}	96 ^{0.0348}	96 ^{0.0463}	96 ^{0.0571}	167 ^{0.0674}	167 ^{0.0856}	168 ^{0.1114}	102 ^{0.1627}	102 ^{0.2507}	102 ^{0.3322}	100 ^{0.4122}	100 ^{0.4772}	170 ^{0.5368}	170 ^{0.6059}	170 ^{0.6766}
70	INCODE-004	56 ^{0.0061}	59 ^{0.0087}	59 ^{0.0110}	61 ^{0.0136}	64 ^{0.0161}	133 ^{0.0185}	136 ^{0.0236}	134 ^{0.0309}	73 ^{0.0532}	74 ^{0.0908}	75 ^{0.1334}	73 ^{0.1809}	77 ^{0.2245}	143 ^{0.2675}	144 ^{0.3249}	143 ^{0.3932}
71	INNOVATRICS-004	114 ^{0.3594}	115 ^{0.3629}	115 ^{0.3688}	112 ^{0.3754}	112 ^{0.3813}	185 ^{0.3870}	185 ^{0.3960}	185 ^{0.4135}	107 ^{0.4234}	106 ^{0.4642}	106 ^{0.5073}	105 ^{0.5522}	105 ^{0.5902}	174 ^{0.6274}	172 ^{0.6736}	172 ^{0.7253}
72	INNOVATRICS-005	41 ^{0.0046}	41 ^{0.0063}	42 ^{0.0078}	45 ^{0.0092}	45 ^{0.0106}	109 ^{0.0124}	110 ^{0.0149}	109 ^{0.0178}	55 ^{0.0343}	56 ^{0.0590}	58 ^{0.0886}	58 ^{0.1222}	59 ^{0.1544}	128 ^{0.1881}	127 ^{0.2321}	125 ^{0.2874}
73	INNOVATRICS-008																
74	INSPUR-000																
75	INTELLIVISION-002																
76	INTEMA-000																
77	INTEMA-001																
78	IREX-000	24 ^{0.0031}	24 ^{0.0042}	25 ^{0.0051}	26 ^{0.0060}	26 ^{0.0068}	83 ^{0.0080}	86 ^{0.0095}	82 ^{0.0107}	82 ^{0.0313}	82 ^{0.0539}	83 ^{0.0815}	86 ^{0.1137}	85 ^{0.1442}	129 ^{0.1755}	123 ^{0.2181}	121 ^{0.2718}
79	ISYSTEMS-002	76 ^{0.0101}	79 ^{0.0135}	80 ^{0.0169}	79 ^{0.0197}	80 ^{0.0228}	146 ^{0.0256}	146 ^{0.0304}	144 ^{0.0398}	99 ^{0.0779}	96 ^{0.1258}	91 ^{0.1759}	90 ^{0.2299}	90 ^{0.2758}	158 ^{0.3204}	156 ^{0.3763}	156 ^{0.4401}
80	ISYSTEMS-003	75 ^{0.0089}	69 ^{0.0115}	69 ^{0.0139}	69 ^{0.0158}	70 ^{0.0177}	139 ^{0.0198}	135 ^{0.0234}	132 ^{0.0303}	84 ^{0.0647}	84 ^{0.1056}	84 ^{0.1502}	84 ^{0.1986}	83 ^{0.2402}	148 ^{0.2819}	147 ^{0.3351}	145 ^{0.3976}
81	KAKAO-001																
82	KEDACOM-001	83 ^{0.0116}	75 ^{0.0130}	67 ^{0.0135}	60 ^{0.0133}	57 ^{0.0135}	118 ^{0.0141}	111 ^{0.0151}	107 ^{0.0176}	41 ^{0.0241}	41 ^{0.0360}	39 ^{0.0513}	34 ^{0.0689}	34 ^{0.0866}	93 ^{0.1060}	89 ^{0.1327}	89 ^{0.1694}
83	KNOWUTECH-000																
84	LINECLOVA-002																
85	LINECLOVA-003																
86	LOOKMAN-003	86 ^{0.0123}	83 ^{0.0144}	77 ^{0.0158}	70 ^{0.0168}	71 ^{0.0178}	135 ^{0.0188}	128 ^{0.0212}	128 ^{0.0260}	64 ^{0.0438}	62 ^{0.0687}	61 ^{0.0978}	61 ^{0.1296}	60 ^{0.1581}	122 ^{0.1879}	122 ^{0.2294}	123 ^{0.2756}
87	LOOKMAN-005	85 ^{0.0118}	77 ^{0.0134}	70 ^{0.0142}	66 ^{0.0144}	61 ^{0.0150}	128 ^{0.0160}	120 ^{0.0176}	119 ^{0.0213}	51 ^{0.0310}	49 ^{0.0480}	46 ^{0.0698}	46 ^{0.0954}	46 ^{0.1216}	108 ^{0.1491}	110 ^{0.1890}	110 ^{0.2381}
88	MAXVISION-000																

Table 9: Accuracy for the FRVT 2018 mugshot sets under ageing. The second row shows the time lapse between gallery and subsequent probe images, in years. The first two columns identify the algorithm. The next 8 values give rank-based FNIR with $R = 1$, $T = 0$ and $FPIR = 1$. All these are relevant to investigational uses where candidates from all searches would need human review. The second 8 values give threshold-based FNIR with $T \geq 0$, $FPIR = 0.001$ and no rank criterion. The shaded cells indicate the three most accurate algorithms for that elapsed time. The gallery size is 3068801. The total number of searches is 10951064.

2023/07/05

FNIR(N, R, T) =

False neg. identification rate

N = Num. enrolled subjects

R = Num. candidates examined

T = Threshold

 $T = 0 \rightarrow$ Investigation $T > 0 \rightarrow$ Identification

MISS RATES		INVESTIGATION, FNIR(N, R = 1, T = 0)								IDENTIFICATION, FNIR(N, R = L, T ≥ 0) FOR FPIR = 0.001								
#	ALGORITHM	(0, 2]	(2, 4]	(4, 6]	(6, 8]	(8, 10]	(10, 12]	(12, 14]	(14, 18]	(0, 2]	(2, 4]	(4, 6]	(6, 8]	(8, 10]	(10, 12]	(12, 14]	(14, 18]	
89	MAXVISION-001																	
90	MAXVISION-002																	
91	MEGVII-003																	
92	MICROFOCUS-005	115.04269	115.05527	115.06355	116.07024	116.07503	118.0786	118.08234	119.08601	111.08338	111.09113	112.09468	112.09667	112.09771	111.09836	111.09880	111.09924	
93	MICROSOFT-003	28.00034	32.00050	33.00064	36.00078	38.00092	101.0107	103.0135	104.0166	50.0288	50.0503	50.0763	50.1067	54.1359	117.1680	118.2116	117.2644	
94	MICROSOFT-004	25.00032	27.00047	29.00060	32.00075	35.00087	97.0103	101.0131	102.0159	47.0268	48.0470	49.0716	48.1007	48.1291	116.1610	115.2052	115.2590	
95	MICROSOFT-005	22.00031	29.00047	35.00066	43.00084	43.00103	114.0131	117.0164	112.0185	43.0243	44.0432	44.0658	44.0913	45.1172	105.1476	109.1874	105.2272	
96	MICROSOFT-006	26.00032	31.00049	36.00065	42.00081	42.00096	106.0117	106.0144	105.0160	24.0134	24.0233	25.0346	23.0462	22.0578	77.0713	77.0903	77.1156	
97	MUKH-002															180.09761	180.09840	180.09899
98	NEC-000	97.0195	99.0316	99.0445	99.0581	98.0699	170.0817	170.0998	170.1237	89.0759	89.1245	89.1729	89.2240	89.2671	157.3117	155.3639	155.4348	
99	NEC-001	104.0246	102.0382	100.0524	100.0672	101.0793	172.0904	171.1076	171.1317	94.0109	94.1623	94.2214	94.2834	94.3341	163.3844	163.4440	162.5183	
100	NEC-002	27.00033	22.00041	18.0043	16.0044	15.0045	47.0049	49.0056	44.0041	15.0066	11.0090	10.0111	10.0131	9.0149	20.0171	21.0207	21.0267	
101	NEC-003	31.00036	29.00046	29.0051	29.0055	29.0059	67.0067	75.0077	77.0073	9.0091	9.0056	9.0076	9.0091	7.0105	9.0119	10.0137	10.0162	10.0209
102	NEC-004	32.00039	25.00045	22.00047	18.0046	14.0044	43.0046	45.0052	37.0036	7.0046	5.0057	2.0063	2.0066	1.0069	7.0076	7.0090	7.0105	
103	NEC-005															8.0080	8.0091	8.0107
104	NEC-006															2.0030	2.0033	2.0012
105	NEC-007															1.0027	1.0031	1.0010
106	NEUROTECHNOLOGY-003	101.0234	101.0379	102.0549	101.0682	100.0720	169.0747	169.0886	167.1066	168.06802	169.08187	110.08920	110.09355	110.09594	119.09738	119.09828	119.09885	
107	NEUROTECHNOLOGY-004	79.0104	78.0134	79.0156	73.0173	72.0195	14.0212	13.0245	13.0320	83.0642	82.1015	81.1426	79.1881	78.2299	146.2722	145.3269	144.3943	
108	NEUROTECHNOLOGY-005	74.00889	71.0116	69.0136	68.0152	69.0173	13.0196	13.0233	13.0306	76.0556	76.0913	74.1315	74.1766	74.2192	142.2617	141.3174	141.3843	
109	NEUROTECHNOLOGY-007	66.0078	63.0103	63.0124	63.0140	63.0161	13.0185	13.0225	13.0290	82.0641	85.1069	85.1546	85.2075	86.2572	156.3081	157.3713	157.4421	
110	NEUROTECHNOLOGY-010															89.0863	89.1050	89.1333
111	NEUROTECHNOLOGY-012															72.0638	71.0783	72.1027
112	NEUROTECHNOLOGY-013															59.0406	48.0498	47.0654
113	NOBLIS-002	112.01520	112.02419	112.03296	113.04114	113.04856	186.05528	186.06011	186.06532	113.09984	113.09996	113.09998	113.09999	113.09999	183.10000	183.10000	183.10000	
114	NTECHLAB-003	65.00078	76.0131	87.0202	90.0295	91.0405	167.0543	167.0761	166.1035	68.0491	72.0881	79.1384	83.1985	87.02594	159.3270	159.4065	159.4891	
115	NTECHLAB-004	62.00668	68.0110	79.0167	86.0239	89.0330	159.0447	161.0641	163.0891	60.0379	63.0688	66.1108	66.1629	73.2192	151.2846	156.3657	158.4524	
116	NTECHLAB-006	31.00056	62.0095	77.0148	83.0218	85.0301	15.0413	15.0591	16.0814	56.0349	60.0636	63.1023	64.1506	66.2024	141.2617	148.3374	155.4185	
117	NTECHLAB-007	37.00444	43.00666	49.00899	57.0118	60.0150	13.0189	14.0255	14.0342	45.0256	46.0450	48.0705	49.1012	51.1334	118.1692	120.2170	122.2752	
118	NTECHLAB-008	18.0025	21.0038	26.0052	31.0074	44.0104	120.0146	120.0236	142.0348	26.0143	28.0267	32.0459	37.0733	40.1062	104.1469	114.2044	118.2698	
119	NTECHLAB-009	15.00022	15.0031	16.0038	17.0045	19.0055	77.0067	83.0088	86.0100	18.0073	17.0117	17.0170	17.0238	18.0319	38.0419	59.0577	62.0833	
120	NTECHLAB-011														42.0351	48.0475	51.0724	
121	OMNIGARDE-000														59.0413	59.0531	59.0741	
122	PANGIAM-000														62.0503	61.0617	60.0810	
123	PANGIAM-001														69.0545	69.0685	69.0894	
124	PARAVISION-002	53.00058	58.0083	60.0111	63.0137	63.0162	134.0187	133.0229	131.0295	57.0354	58.0618	59.0931	60.1290	61.1625	129.1964	130.2408	129.2924	
125	PARAVISION-003	44.00048	48.0067	51.0090	52.0109	54.0128	121.0148	119.0218	119.0219	57.0354	58.0618	59.0931	60.1290	61.1625	129.1964	130.2408	129.2924	
126	PARAVISION-004	16.00024	17.00032	17.00404	19.0047	18.0053	69.0061	73.0073	73.0072	20.0118	23.0209	24.0327	24.0465	24.0613	79.0779	80.1008	79.1285	
127	PARAVISION-005	12.00021	13.0028	13.0035	14.0041	16.0046	60.0054	66.0067	72.0070	11.0057	12.0093	12.0144	14.0207	15.0278	48.0368	56.0508	50.0715	
128	PARAVISION-007	6.00019	8.0025	7.0029	8.0033	8.0036	27.0042	36.0049	27.0030	10.0057	13.0094	14.0144	13.0206	14.0275	44.0357	46.0485	46.0652	
129	PARAVISION-009														39.0283	36.0371	37.0525	
130	PARAVISION-012														19.0137	17.0167	17.0219	
131	PARAVISION-014														19.0119	19.0148	19.0195	
132	PIXELALL-002	72.00885	73.01119	71.0147	72.0172	73.0198	143.0225	143.0270	143.0349	97.01193	97.01900	97.02601	97.03332	97.03955	166.04565	166.05268	167.06030	

Table 10: **Accuracy for the FRVT 2018 mugshot sets under ageing.** The second row shows the time lapse between gallery and subsequent probe images, in years. The first two columns identify the algorithm. The next 8 values give rank-based FNIR with $R = 1$, $T = 0$ and FPIR = 1. All these are relevant to investigational uses where candidates from all searches would need human review. The second 8 values give threshold-based FNIR with $T \geq 0$, FPIR = 0.001 and no rank criterion. The shaded cells indicate the three most accurate algorithms for that elapsed time. The gallery size is 3068801. The total number of searches is 10951064.

MISS RATES		INVESTIGATION, FNIR(N, R = 1, T = 0)								IDENTIFICATION, FNIR(N, R = L, T ≥ 0) FOR FPIR = 0.001							
#	ALGORITHM	(0, 2]	(2, 4]	(4, 6]	(6, 8]	(8, 10]	(10, 12]	(12, 14]	(14, 18]	(0, 2]	(2, 4]	(4, 6]	(6, 8]	(8, 10]	(10, 12]	(12, 14]	(14, 18]
133	PIXELLALL-003	⁴⁶ 0.0050	⁴² 0.0063	³⁹ 0.0072	³⁴ 0.0077	³³ 0.0085	³⁶ 0.0095	³³ 0.0113	³³ 0.0119	⁴⁴ 0.0248	⁴³ 0.0418	⁴³ 0.0622	⁴³ 0.0861	⁴³ 0.1104	¹⁰¹ 0.1364	¹⁰¹ 0.1723	¹⁰¹ 0.2167
134	PIXELLALL-004	⁴⁵ 0.0049	⁴⁰ 0.0063	⁴⁰ 0.0072	³⁷ 0.0079	³⁶ 0.0089	³³ 0.0103	³³ 0.0127	³³ 0.0146	³⁸ 0.0211	⁴⁰ 0.0360	⁴² 0.0553	⁴² 0.0792	³⁹ 0.1045	¹⁰⁰ 0.1317	¹⁰⁰ 0.1700	¹⁰⁰ 0.2246
135	PTAKURATSATU-000	⁵⁴ 0.0061	⁵⁵ 0.0082	⁵⁵ 0.0097	⁵³ 0.0109	⁴⁹ 0.0120	¹¹³ 0.0131	¹⁰⁸ 0.0146	¹¹⁰ 0.0180	⁵⁹ 0.0375	⁵⁷ 0.0596	⁵⁵ 0.0842	⁵⁵ 0.1116	⁵³ 0.1357	¹¹² 0.1553	¹⁰⁵ 0.1820	¹⁰⁸ 0.2326
136	QNAP-004						¹⁰⁸ 0.0105	¹⁰² 0.0133	¹⁰⁵ 0.0167						⁹⁸ 0.1243	⁹⁹ 0.1556	⁹⁹ 0.2050
137	RANKONE-002	⁹⁹ 0.0212	⁹⁸ 0.0313	⁹⁸ 0.0431	⁹⁸ 0.0562	⁹⁹ 0.0712	¹⁷¹ 0.0881	¹⁷² 0.1130	¹⁷³ 0.1543	⁹⁵ 0.1111	⁹⁵ 0.1707	⁹⁵ 0.2305	⁹⁵ 0.2968	⁹⁶ 0.3646	¹⁶⁵ 0.4345	¹⁶⁵ 0.5172	¹⁶⁸ 0.6110
138	RANKONE-004	¹⁰⁸ 0.0424	¹⁰⁷ 0.0643	¹⁰⁷ 0.0875	¹⁰⁷ 0.1127	¹⁰⁷ 0.1364	¹⁷⁷ 0.1579	¹⁷⁸ 0.1914	¹⁷⁸ 0.2378	¹⁰⁸ 0.1855	¹⁰⁸ 0.2681	¹⁰³ 0.3431	¹⁰¹ 0.4155	¹⁰¹ 0.4785	¹⁶⁹ 0.5350	¹⁶⁹ 0.5980	¹⁶⁸ 0.6722
139	RANKONE-005	⁹² 0.0136	⁹³ 0.0192	⁹¹ 0.0246	⁹¹ 0.0303	⁹⁰ 0.0362	¹⁵⁸ 0.0422	¹⁵⁷ 0.0521	¹⁵⁷ 0.0694	⁸¹ 0.0582	⁷⁵ 0.0910	⁷¹ 0.1260	⁶⁸ 0.1645	⁶⁵ 0.2005	¹³³ 0.2353	¹³³ 0.2816	¹³⁴ 0.3522
140	RANKONE-007	⁶ 0.0078	⁶ 0.0099	⁶ 0.0113	⁵⁸ 0.0123	⁴⁷ 0.0139	¹²¹ 0.0156	¹²⁶ 0.0242	⁴² 0.0242	⁴² 0.0376	⁴¹ 0.0542	³⁸ 0.0737	³⁹ 0.0935	⁹⁶ 0.1130	⁹³ 0.1416	⁹³ 0.1811	
141	RANKONE-009	⁴⁸ 0.0054	⁴⁹ 0.0072	⁴⁶ 0.0085	⁴⁷ 0.0098	⁴⁷ 0.0113	¹¹² 0.0130	¹¹⁸ 0.0169	¹²² 0.0220	³⁷ 0.0208	³⁸ 0.0345	³⁷ 0.0504	³⁶ 0.0706	³⁶ 0.0930	⁹⁶ 0.1174	⁹⁷ 0.1504	⁹⁷ 0.2002
142	RANKONE-010	⁴² 0.0047	³⁹ 0.0061	³⁶ 0.0070	³³ 0.0076	³⁴ 0.0087	⁹⁶ 0.0098	⁹⁷ 0.0113	⁹⁴ 0.0120	³¹ 0.0177	²⁹ 0.0269	²⁶ 0.0368	²⁶ 0.0479	²³ 0.0590	²⁷ 0.0688	⁷³ 0.0803	⁷⁰ 0.0991
143	RANKONE-011	²⁵ 0.0031	²³ 0.0041	²³ 0.0047	²³ 0.0053	²² 0.0058	⁷⁸ 0.0067	⁷⁴ 0.0077	⁷⁶ 0.0073	²³ 0.0127	²⁰ 0.0194	²¹ 0.0265	²⁰ 0.0345	²⁰ 0.0422	⁶¹ 0.0499	⁶⁰ 0.0611	⁵⁶ 0.0756
144	RANKONE-012						⁷⁴ 0.0065	⁶⁹ 0.0069	⁶⁹ 0.0053						³⁴ 0.0460	⁵² 0.0540	⁴⁸ 0.0672
145	RANKONE-013						⁵³ 0.0051	⁴² 0.0051	³⁴ 0.0035						³⁰ 0.0306	³⁵ 0.0355	²⁹ 0.0405
146	RANKONE-014						³² 0.0044	²⁵ 0.0047	²² 0.0029						²⁷ 0.0222	²⁶ 0.0255	²² 0.0287
147	REALNETWORKS-002	¹⁰ 0.0381	¹⁰⁸ 0.0687	¹⁰⁸ 0.1062	¹⁰⁸ 0.1495	¹⁰ 0.1963	¹⁸ 0.2513	¹⁸⁴ 0.3206	¹⁸⁴ 0.3927	¹⁰ 0.2153	¹⁰⁸ 0.3323	¹⁰⁵ 0.4444	¹⁰⁵ 0.5485	¹⁰⁶ 0.6355	¹⁷⁵ 0.7132	¹⁷⁶ 0.7855	¹⁷⁰ 0.8437
148	REALNETWORKS-003	¹⁰³ 0.0245	¹⁰⁵ 0.0437	¹⁰⁵ 0.0686	¹⁰⁶ 0.0975	¹⁰⁶ 0.1312	¹⁸⁰ 0.1719	¹⁸⁰ 0.2294	¹⁸¹ 0.2907	⁹⁸ 0.1468	¹⁰⁰ 0.2370	¹⁰¹ 0.3313	¹⁰³ 0.4269	¹⁰³ 0.5142	¹⁷³ 0.5979	¹⁷⁴ 0.6815	¹⁷⁴ 0.7567
149	REALNETWORKS-004	¹⁰² 0.0244	¹⁰⁴ 0.0428	¹⁰⁴ 0.0663	¹⁰⁵ 0.0939	¹⁰³ 0.1251	¹⁷⁷ 0.1634	¹⁷⁹ 0.2170	¹⁸⁰ 0.2785	⁹⁹ 0.1484	¹⁰¹ 0.2377	¹⁰⁰ 0.3303	¹⁰² 0.4249	¹⁰² 0.5106	¹⁷² 0.5924	¹⁷³ 0.6758	¹⁷² 0.7534
150	REALNETWORKS-006							⁸¹ 0.0069	⁷⁶ 0.0077	⁸⁰ 0.0080					⁹⁰ 0.1022	⁸⁶ 0.1253	⁸⁶ 0.1622
151	REALNETWORKS-008							⁴⁹ 0.0049	⁴⁷ 0.0054	³³ 0.0047					⁵⁵ 0.0462	⁵³ 0.0577	⁵⁵ 0.0745
152	RECOGNITO-000						²⁸ 0.0042	²⁹ 0.0047	²⁴ 0.0030						²¹ 0.0176	²³ 0.0221	²³ 0.0306
153	S1-002							⁴² 0.0046	⁴¹ 0.0051	⁴² 0.0038					⁵⁷ 0.0482	⁵⁸ 0.0597	⁵⁷ 0.0788
154	S1-003							⁶⁴ 0.0057	⁶² 0.0063	⁶⁴ 0.0056					⁷⁸ 0.0681	⁷⁵ 0.0839	⁷⁵ 0.1061
155	S1-004						²⁵ 0.0042	²¹ 0.0045	³⁰ 0.0032					⁴⁵ 0.0360	⁴³ 0.0448	⁴³ 0.0598	
156	SCANOVATE-001	⁶⁸ 0.0079	⁷² 0.0117	⁷⁵ 0.0151	⁷⁸ 0.0185	⁷⁸ 0.0221	¹⁴⁷ 0.0259	¹⁴⁹ 0.0321	¹⁴⁹ 0.0427	⁸⁸ 0.0727	⁸⁸ 0.1169	⁸⁷ 0.1650	⁸⁷ 0.2115	⁸⁴ 0.2528	¹⁵³ 0.2925	¹⁵⁰ 0.3437	¹⁴⁸ 0.4084
157	SENSETIME-002	⁹⁶ 0.0186	⁹² 0.0191	⁸⁴ 0.0183	⁷³ 0.0179	⁶⁸ 0.0173	¹¹⁶ 0.0133	⁸⁴ 0.0089	⁶⁵ 0.0059	⁴⁰ 0.0220	²⁵ 0.0236	¹⁹ 0.0237	¹⁸ 0.0240	¹² 0.0245	²⁶ 0.0219	²⁰ 0.0195	¹⁸ 0.0222
158	SENSETIME-003	¹¹ 0.0021	¹⁰ 0.0028	¹¹ 0.0031	⁷ 0.0033	⁶ 0.0035	²⁰ 0.0040	²⁸ 0.0047	³² 0.0033	⁸ 0.0046	⁸ 0.0064	⁶ 0.0076	⁸ 0.0086	⁴ 0.0101	¹⁴ 0.0122	¹⁵ 0.0155	¹⁵ 0.0196
159	SENSETIME-004	³ 0.0016	³ 0.0022	³ 0.0025	³ 0.0028	³ 0.0030	⁷ 0.0035	¹⁹ 0.0043	¹⁸ 0.0025	⁴ 0.0036	⁴ 0.0052	³ 0.0066	³ 0.0081	³ 0.0099	¹⁶ 0.0126	¹⁸ 0.0169	¹⁹ 0.0230
160	SENSETIME-005	⁴⁰ 0.0015	²⁰ 0.0020	²⁰ 0.0024	²⁰ 0.0026	²⁰ 0.0029	⁶ 0.0035	¹⁶ 0.0043	²¹ 0.0028	⁵ 0.0036	⁷ 0.0059	⁸ 0.0089	⁹ 0.0128	¹⁰ 0.0177	²⁹ 0.0240	³¹ 0.0345	³³ 0.0493
161	SENSETIME-006	¹ 0.0015	¹ 0.0019	¹ 0.0022	¹ 0.0025	¹ 0.0027	¹ 0.0033	¹⁰ 0.0040	¹³ 0.0021	² 0.0031	² 0.0049	⁴ 0.0068	⁶ 0.0097	⁷ 0.0132	²³ 0.0184	²⁷ 0.0262	²⁷ 0.0359
162	SENSETIME-007							⁵ 0.0035	⁵ 0.0038	⁵ 0.0015					¹² 0.0112	¹² 0.0140	¹² 0.0176
163	SENSETIME-008							⁴ 0.0034	⁴ 0.0039	⁷ 0.0017					¹¹ 0.0103	¹¹ 0.0127	¹¹ 0.0163
164	SERENDIPITY-000							⁸⁶ 0.0084	⁸⁵ 0.0092	⁸⁴ 0.0094					⁸⁶ 0.0981	⁸⁴ 0.1180	⁸⁴ 0.1519
165	SIAT-002	¹¹⁷ 0.8309	¹¹⁷ 0.8310	¹¹⁷ 0.8311	¹¹⁷ 0.8306	¹¹⁷ 0.8296	¹⁹⁹ 0.8302	¹⁹⁸ 0.8300	¹⁸⁹ 0.8301	¹¹² 0.8340	¹¹⁰ 0.8368	¹⁰⁵ 0.8404	¹⁰⁹ 0.8445	¹⁰⁹ 0.8480	¹⁷⁸ 0.8532	¹⁷⁸ 0.8595	¹⁷⁷ 0.8691
166	SYNESIS-003	⁸⁹ 0.0125	⁸⁵ 0.0151	⁸³ 0.0174	⁸⁰ 0.0199	⁷⁹ 0.0223	¹⁴⁴ 0.0240	¹⁴⁴ 0.0279	¹³⁹ 0.0311	⁸⁵ 0.0658	⁸³ 0.1052	⁸² 0.1483	⁸² 0.1968	⁸² 0.2399	¹⁴⁹ 0.2834	¹⁴⁸ 0.3405	¹⁴⁸ 0.4046
167	SYNESIS-005	⁴⁰ 0.0044	³⁹ 0.0058	³⁷ 0.0070	⁴⁰ 0.0080	³⁷ 0.0091	⁹⁸ 0.0103	⁹⁸ 0.0125	¹⁰⁰ 0.0152	⁴⁶ 0.0262	⁴⁵ 0.0444	⁴⁵ 0.0666	⁴⁵ 0.0923	⁴⁴ 0.1156	¹⁰² 0.1399	¹⁰³ 0.1736	¹⁰² 0.2185
168	T4ISB-000						¹⁶⁵ 0.0606	¹⁶⁴ 0.0748	¹⁶⁴ 0.0970								
169	TECH5-001	⁵⁷ 0.0061	⁶¹ 0.0093	⁶⁹ 0.0128	⁷¹ 0.0171	⁷⁷ 0.0221	¹⁵¹ 0.0289	¹⁵⁴ 0.0412	¹⁵⁴ 0.0560	⁸⁶ 0.0660	⁸⁷ 0.1156	⁹⁰ 0.1733	⁹¹ 0.2385	⁹¹ 0.2998	¹⁶⁰ 0.3629	¹⁶² 0.4424	¹⁶² 0.5284
170	TOSHIBA-001	⁷³ 0.0086	⁷⁴ 0.0119	⁷⁴ 0.0150	⁷⁴ 0.0178	⁷⁵ 0.0209	¹⁴⁵ 0.0241	¹⁴⁵ 0.0292	¹⁴⁴ 0.0365								
171	TRUEFACE-000	³⁶ 0.0043	³⁶ 0.0057	³⁶ 0.0061	²⁸ 0.0067	²⁷ 0.0073	⁸⁷ 0.0084	⁸⁷ 0.0097	⁸⁵ 0.0099	³⁵ 0.0200	³⁷ 0.0338	³⁸ 0.0504	³⁵ 0.0705	³⁵ 0.0904	⁹¹ 0.1112	⁹² 0.1401	⁹² 0.1792
172	VERIDAS-001	⁵⁸ 0.0063	⁵⁶ 0.0083	⁵⁶ 0.0099	⁵⁶ 0.0113	⁵⁶ 0.0132	¹²³ 0.0148	¹²³ 0.0184	¹²⁰ 0.0219	⁶¹ 0.0403	⁶¹ 0.0684	⁶² 0.1012	⁶² 0.1386	<sup			

MISS RATES		INVESTIGATION, FNIR(N, R = 1, T = 0)								IDENTIFICATION, FNIR(N, R = L, T ≥ 0) FOR FPIR = 0.001							
#	ALGORITHM	(0, 2]	(2, 4]	(4, 6]	(6, 8]	(8, 10]	(10, 12]	(12, 14]	(14, 18]	(0, 2]	(2, 4]	(4, 6]	(6, 8]	(8, 10]	(10, 12]	(12, 14]	(14, 18]
177	VISIONLABS-008	²¹ 0.0028	²⁰ 0.0037	²¹ 0.0047	²² 0.0053	²³ 0.0058	²⁶ 0.0067	⁸¹ 0.0081	⁸¹ 0.0085	²⁷ 0.0143	²¹ 0.0241	²⁸ 0.0373	²⁷ 0.0519	²² 0.0677	⁸¹ 0.0850	⁸² 0.1104	⁸² 0.1444
178	VISIONLABS-009	¹⁰ 0.0020	¹⁰ 0.0026	¹⁰ 0.0030	¹⁰ 0.0034	¹⁰ 0.0038	³⁴ 0.0044	⁴⁴ 0.0052	⁵⁰ 0.0046	¹⁴ 0.0065	¹⁵ 0.0105	¹⁵ 0.0156	¹⁵ 0.0217	¹⁶ 0.0289	⁴⁷ 0.0368	⁴⁹ 0.0499	⁴⁹ 0.0681
179	VISIONLABS-010	⁹ 0.0020	⁹ 0.0025	⁹ 0.0030	¹¹ 0.0034	⁹ 0.0036	³⁰ 0.0043	³⁹ 0.0051	⁵² 0.0047	¹⁷ 0.0069	¹⁶ 0.0113	¹⁶ 0.0170	¹⁶ 0.0238	¹⁷ 0.0316	⁵¹ 0.0411	⁵³ 0.0557	⁵³ 0.0740
180	VISIONLABS-011						²⁶ 0.0042	²³ 0.0046	³⁶ 0.0036						³¹ 0.0270	²⁹ 0.0337	³¹ 0.0432
181	VIXVIZION-009						¹²⁹ 0.0161	¹²⁶ 0.0190	¹²⁴ 0.0238						¹²² 0.1787	¹¹⁷ 0.2116	¹¹⁵ 0.2595
182	VNPT-002						⁵⁶ 0.0053	⁵⁷ 0.0059	⁴⁹ 0.0044						⁶⁶ 0.0534	⁶⁷ 0.0670	⁶⁸ 0.0882
183	VTS-000	¹¹⁶ 0.5878	¹¹⁶ 0.6312	¹¹⁶ 0.6602	¹¹⁵ 0.6863	¹¹⁵ 0.7073	¹⁸⁸ 0.7246	¹⁸⁸ 0.7458	¹⁸⁷ 0.7747	¹⁰⁸ 0.5929	¹⁰⁸ 0.6397	¹⁰⁸ 0.6729	¹⁰⁸ 0.7034	¹⁰⁷ 0.7279	¹⁷⁶ 0.7493	¹⁷⁵ 0.7739	¹⁷⁵ 0.8076
184	VTS-003						⁵⁹ 0.0054	⁵⁴ 0.0059	⁶² 0.0054						⁷⁰ 0.0597	⁶⁹ 0.0731	⁶⁹ 0.0950
185	XFORWARDAI-000	²⁰ 0.0027	¹⁸ 0.0034	²⁰ 0.0044	²¹ 0.0052	²¹ 0.0058	²⁹ 0.0067	⁷⁸ 0.0079	⁷⁸ 0.0076	²⁸ 0.0157	³¹ 0.0281	³⁰ 0.0443	³¹ 0.0635	³² 0.0834	⁹¹ 0.1050	⁹⁰ 0.1330	⁹⁰ 0.1714
186	XFORWARDAI-001	¹⁵ 0.0023	¹¹ 0.0028	¹² 0.0034	¹² 0.0037	¹² 0.0039	³⁷ 0.0045	⁴⁵ 0.0052	⁴⁷ 0.0043	¹⁵ 0.0060	¹⁴ 0.0096	¹³ 0.0144	¹² 0.0200	¹³ 0.0260	³⁹ 0.0334	⁴⁰ 0.0435	⁴⁰ 0.0586
187	YITU-002	⁶⁰ 0.0066	⁵⁷ 0.0083	⁵³ 0.0094	⁴⁸ 0.0101	⁵⁰ 0.0121	¹²⁴ 0.0150	¹³⁰ 0.0223	¹³⁷ 0.0328	³⁹ 0.0189	³⁴ 0.0317	³⁵ 0.0494	³⁹ 0.0750	⁴¹ 0.1066	¹⁰⁹ 0.1494	¹²¹ 0.2171	¹²⁸ 0.2958
188	YITU-003	⁶³ 0.0072	⁶⁰ 0.0089	⁵⁷ 0.0100	⁵¹ 0.0107	⁵⁸ 0.0125	¹²⁵ 0.0153	¹³² 0.0226	¹⁴⁶ 0.0334	³⁴ 0.0194	³⁶ 0.0321	³⁶ 0.0500	⁴¹ 0.0756	⁴² 0.1071	¹¹⁰ 0.1500	¹²² 0.2177	¹²⁹ 0.2964
189	YITU-004	⁵⁵ 0.0061	⁵¹ 0.0075	⁴¹ 0.0081	⁴¹ 0.0081	³⁹ 0.0092	¹⁰² 0.0107	¹¹¹ 0.0154	¹¹⁷ 0.0207	²² 0.0125	²² 0.0204	²³ 0.0314	²⁵ 0.0469	²⁶ 0.0671	⁸⁵ 0.0955	⁸⁰ 0.1421	⁸⁶ 0.2006
190	YITU-005	⁶¹ 0.0067	⁵⁴ 0.0080	⁴⁷ 0.0087	⁴⁴ 0.0085	⁴¹ 0.0094	¹⁰³ 0.0108	¹¹³ 0.0151	¹¹⁶ 0.0204	²¹ 0.0124	²¹ 0.0198	²² 0.0308	²² 0.0462	²⁵ 0.0667	⁸⁴ 0.0953	⁹⁴ 0.1418	⁹⁶ 0.1930

Table 12: **Accuracy for the FRVT 2018 mugshot sets under ageing.** The second row shows the time lapse between gallery and subsequent probe images, in years. The first two columns identify the algorithm. The next 8 values give rank-based FNIR with $R = 1$, $T = 0$ and FPIR = 1. All these are relevant to investigational uses where candidates from all searches would need human review. The second 8 values give threshold-based FNIR with $T \geq 0$, FPIR = 0.001 and no rank criterion. The shaded cells indicate the three most accurate algorithms for that elapsed time. The gallery size is 3068801. The total number of searches is 10951064.

2023/07/05
16:19:47FNIR(N, R, T) = False neg. identification rate
FPIR(N, T) = False pos. identification rateN = Num. enrolled subjects
R = Num. candidates examined
T = ThresholdT = 0 → Investigation
T > 0 → Identification

#	ALGORITHM	INVESTIGATION MODE						IDENTIFICATION MODE						FAILURE TO EXTRACT FEATURES						
		RANK ONE MISS RATE, FNIR(N, 0, 1)						HIGH T → FPIR = 0.001, FNIR(N, T, L)												
		N=1.6M						N=1.6M												
GALLERY	MUGSHOT	MUGSHOT	MUGSHOT	VISA	BORDER	BOR ₁ 10YR	KIOSK	MUGSHOT	MUGSHOT	MUGSHOT	VISA	BORDER	BOR ₁ 10YR	KIOSK	MUGSHOT	MUGSHOT	MUGSHOT	VISA	BORDER	KIOSK
PROBE	MUGSHOT	WEBCAM	PROFILE	BORDER	BOR ₁ 10YR	KIOSK		MUGSHOT	WEBCAM	PROFILE	BORDER	BOR ₁ 10YR	KIOSK		MUGSHOT	WEBCAM	PROFILE	BORDER	BOR ₁ 10YR	KIOSK
1	20FACE-000	³¹⁰ 0.055	³⁰⁰ 0.085	²¹⁴ 0.736	²⁴⁹ 0.056	¹⁶⁶ 0.239	²³⁵ 0.243	³¹⁰ 0.348	²⁹⁷ 0.450	²⁷⁶ 1.000	²⁵⁷ 0.424	¹⁴ 0.772	²³ 0.938	0.000	0.000	0.000	0.000	0.000	0.000	
2	3DIVI-003	³²⁵ 0.083	³¹⁷ 0.206	²⁵⁴ 0.141	²⁶⁰ 0.474	³¹⁹ 0.400	³¹⁴ 0.626	²⁵³ 0.605	²¹³ 0.821	^{0.002}	^{0.005}									
3	3DIVI-004	²⁸² 0.018	²⁸⁸ 0.062	²³⁷ 0.035	²³⁹ 0.279	²⁸⁷ 0.169	²⁸⁷ 0.343	²²⁶ 0.277	¹⁸ 0.607	^{0.002}	^{0.005}									
4	3DIVI-005	²⁸³ 0.018	²⁸⁷ 0.062	²⁶¹ 0.930	²⁷³ 0.821	²⁴⁰ 0.279	²⁸⁶ 0.166	²⁸⁸ 0.339	¹⁹⁵ 0.996	²⁵⁹ 0.864	¹⁸³ 0.597	^{0.002}	^{0.005}	^{0.442}	^{0.000}					
5	3DIVI-006	²⁹ 0.024	²⁹⁵ 0.074	²³⁹ 0.047	²⁴⁷ 0.312	²⁸ 0.168	²⁸⁶ 0.342	²²⁷ 0.283	¹⁸ 0.615	^{0.002}	^{0.005}									
6	AADI-000			³⁵² 1.000	¹⁷² 1.000	³²⁴ 1.000			²⁸⁷ 1.000	²³⁸ 1.000	³⁵⁴ 1.000	^{0.028}	^{0.154}	^{0.990}	^{0.274}					
7	ACER-000	²⁵⁹ 0.011	²⁴⁹ 0.036	²⁴¹ 0.827	²¹⁸ 0.025	²²² 0.209	²⁷⁸ 0.146	²⁶³ 0.246	¹⁴⁴ 0.981	²²⁰ 0.201	¹⁶ 0.490	^{0.000}	^{0.000}	^{0.042}						
8	ACER-001	²¹¹ 0.005	¹⁹⁵ 0.020	¹⁵⁷ 0.422	¹⁷⁹ 0.008	¹⁴⁰ 0.050	¹¹⁹ 0.098	²¹⁸ 0.056	¹⁸⁹ 0.109	²³⁵ 0.999	¹⁷⁶ 0.068	¹²⁵ 0.406	¹⁶⁶ 0.479	^{0.001}	^{0.001}	^{0.041}	^{0.000}			
9	ADVANCE-000	¹²⁵ 0.002	¹²⁸ 0.013	¹⁰³ 0.186	¹⁰⁸ 0.003	¹⁴⁷ 0.060	⁸⁴ 0.081	¹³² 0.020	²⁷⁴ 0.270	¹²⁸ 0.973	²⁰⁵ 0.163	¹⁴⁶ 0.884	¹³⁴ 0.326	^{0.000}	^{0.000}	^{0.043}	^{0.000}			
10	AFISBIOMETRICS-000	⁸⁸ 0.002	⁸³ 0.009	⁸⁵ 0.125	¹⁰³ 0.003	⁸⁸ 0.015	⁹² 0.083	¹⁷⁴ 0.030	¹⁵⁴ 0.081	⁵⁴ 0.517	¹³⁴ 0.034	⁸¹ 0.154	⁸³ 0.172	^{0.000}	^{0.000}	^{0.041}	^{0.000}			
11	AIZE-001	²¹ 0.006	²⁰⁹ 0.022	²⁰⁴ 0.683	²⁰⁸ 0.016	¹⁴² 0.050	²¹⁴ 0.165	²⁴ 0.077	²¹⁷ 0.143	¹⁷³ 0.994	¹⁹⁰ 0.101	¹¹⁸ 0.364	¹⁴ 0.387	^{0.001}	^{0.001}	^{0.047}	^{0.000}			
12	ALCHERA-000	²⁷⁸ 0.016	²⁷⁴ 0.047	²⁴⁸ 0.870	²³⁰ 0.046	²⁴⁵ 0.292	²⁷⁷ 0.138	²⁴⁷ 0.216	²¹⁴ 0.999	²¹⁰ 0.176	²⁰⁹ 0.803	^{0.006}	^{0.014}	^{0.328}						
13	ALCHERA-001	³⁵⁴ 0.987	³⁴⁸ 1.000	²⁷ 1.000	³¹⁹ 1.000	³⁵¹ 0.999	³⁴² 1.000	³⁶⁰ 1.000	²⁵⁹ 1.000	^{0.006}	^{0.013}	^{0.324}								
14	ALCHERA-002	³² 0.095	³¹⁴ 0.166	²⁷⁵ 0.954	²⁷¹ 0.668	²⁵⁸ 0.446	³²⁰ 0.486	³⁰⁹ 0.591	²⁴² 1.000	²⁵⁹ 0.827	²¹⁰ 0.811	^{0.001}	^{0.002}	^{0.106}						
15	ALCHERA-003	²⁵⁶ 0.010	²⁴⁷ 0.035	²¹⁵ 0.741	²⁰⁵ 0.016	²²⁰ 0.206	²⁸⁰ 0.155	²⁵⁹ 0.239	²²⁷ 0.999	²¹³ 0.172	¹⁶¹ 0.464	^{0.001}	^{0.002}	^{0.106}						
16	ALCHERA-004	²⁶ 0.011	²⁵³ 0.038	¹⁴⁸ 0.345	²⁰⁸ 0.017	¹⁵⁴ 0.088	¹⁹³ 0.144	³¹ 0.394	³⁰⁴ 0.529	¹⁶⁵ 0.991	²³⁹ 0.424	¹³³ 0.708	¹⁷ 0.546	^{0.001}	^{0.001}	^{0.046}	^{0.000}			
17	ALLGOVISION-000	²⁶⁵ 0.011	²⁴³ 0.033	²⁵¹ 0.894	²¹³ 0.021	²⁴² 0.282	²⁵² 0.088	²³³ 0.166	¹⁶² 0.990	¹⁹² 0.117	¹⁷³ 0.526	^{0.002}	^{0.003}	^{0.122}						
18	ALLGOVISION-001	²⁴⁸ 0.009	²⁵⁹ 0.038	²⁰⁰ 0.661	²¹⁷ 0.021	²³³ 0.241	²⁵⁹ 0.102	²⁵¹ 0.221	¹⁵¹ 0.986	²⁰⁶ 0.150	¹⁶ 0.491	^{0.001}	^{0.001}	^{0.042}						
19	ALLGOVISION-002	¹⁹⁴ 0.004	²¹⁸ 0.023	¹⁹² 0.585	¹⁸¹ 0.008	¹⁶⁰ 0.161	¹⁸² 0.132	²³¹ 0.065	³⁰³ 0.520	¹¹¹ 0.950	²²² 0.232	¹⁷³ 1.000	¹⁹⁸ 0.716	^{0.000}	^{0.000}	^{0.041}	^{0.000}			
20	ANKE-000	²⁷³ 0.013	²⁸⁵ 0.038	²⁶⁴ 0.931	³⁴⁴ 1.000	³³⁹ 1.000	²⁶ 0.117	²⁵⁰ 0.220	¹⁷² 0.994	²⁸⁰ 1.000	³⁹ 1.000	^{0.000}	^{0.001}	^{0.080}						
21	ANKE-001	²⁷⁴ 0.013	²⁵⁴ 0.038	²⁷⁰ 0.946	²⁷⁶ 1.000	³⁰⁹ 1.000	²⁶⁶ 0.119	²⁴⁹ 0.220	¹⁷⁹ 0.994	³³⁹ 1.000	²⁷¹ 1.000	^{0.000}	^{0.001}	^{0.080}						
22	ANKE-002	¹⁶ 0.003	¹⁶⁸ 0.016	¹⁷⁶ 0.522	¹³⁹ 0.005	¹⁶⁴ 0.119	¹⁷ 0.032	¹⁵¹ 0.079	¹¹⁰ 0.948	¹³⁷ 0.034	¹⁰ 0.245	^{0.001}	^{0.001}	^{0.049}						
23	ARMATURA-000	¹¹⁷ 0.002	¹²⁷ 0.013	⁴⁶ 0.070	⁵¹ 0.002	²³ 0.005	³⁶ 0.062	⁴⁸ 0.004	⁴⁷ 0.025	²² 0.223	²⁹ 0.006	²⁸ 0.048	¹⁹ 0.090	^{0.001}	^{0.001}	^{0.056}	^{0.001}			
24	AWARE-003	³⁰ 0.031	³⁰¹ 0.090	²⁸⁷ 0.966	²⁶¹ 0.316	²⁴⁴ 0.290	²⁷⁷ 0.128	¹⁴⁸ 0.984	²³⁹ 0.428	¹⁷ 0.530	^{0.004}	^{0.003}	^{0.874}							
25	AWARE-004	³²⁰ 0.068	³¹⁶ 0.176	²⁹⁶ 0.976	²⁵⁹ 0.122	²⁵⁶ 0.414	³⁰⁵ 0.269	³⁰² 0.509	²⁴⁶ 1.000	²³⁴ 0.397	²¹¹ 0.816	^{0.003}	^{0.003}	^{0.776}						
26	AWARE-005	³⁰² 0.031	²⁸⁹ 0.067	²⁹⁷ 0.978	²³⁸ 0.048	²⁴⁸ 0.308	³¹³ 0.364	²⁶⁵ 0.253	²⁴⁹ 1.000	²²³ 0.255	²²⁶ 0.916	^{0.001}	^{0.002}	^{0.189}						
27	AWARE-006	³² 0.070	³¹⁰ 0.128	²⁹⁹ 0.983	²⁵¹ 0.111	²⁵⁷ 0.421	³⁰⁷ 0.276	²⁹⁰ 0.398	²³⁸ 0.999	²³⁷ 0.368	²⁰² 0.749	^{0.001}	^{0.002}	^{0.189}						
28	AYONIX-000	³⁴⁷ 0.450	³⁴³ 0.685	³⁴⁸ 0.996	²⁶⁸ 0.607	²⁷⁷ 0.867	³³⁸ 0.811	³³⁶ 0.939	²⁰³ 0.998	²⁶⁴ 0.954	²⁴⁷ 0.982	^{0.010}	^{0.031}	^{0.939}						
29	AYONIX-001	³⁴ 0.341	³³² 0.527	³⁰³ 0.993	²⁷⁷ 0.994	²⁶⁸ 0.778	³⁴¹ 0.824	³³¹ 0.920	²³⁶ 0.999	²⁶⁹ 0.999	²³⁹ 0.969	^{0.010}	^{0.031}	^{0.939}						
30	AYONIX-002	³⁴¹ 0.341	³³³ 0.527	³⁰⁴ 0.993	²⁶⁴ 0.464	²⁶⁹ 0.778	³⁴⁰ 0.824	³³² 0.920	²³⁴ 0.999	²⁶⁰ 0.915	²³⁸ 0.969	^{0.010}	^{0.031}	^{0.939}						
31	CAMVI-003	³¹⁵ 0.052	³⁰² 0.090	²⁵⁴ 0.911	²⁴⁹ 0.093	²⁵³ 0.360	²³⁷ 0.071	²⁰⁹ 0.132	¹²³ 0.970	¹⁹² 0.114	¹⁴ 0.402	^{0.006}	^{0.013}	^{0.675}						
32	CAMVI-004	³¹³ 0.047	²⁹⁶ 0.077	²¹⁷ 0.744	²⁴⁵ 0.072	²⁴⁷ 0.296	²³⁶ 0.072	²¹¹ 0.136	²³² 0.999	¹⁸⁹ 0.100	²⁰⁷ 0.078	^{0.000}	^{0.000}	^{0.000}						
33	CAMVI-005	³¹ 0.065	³⁰⁸ 0.103	²¹⁹ 0.746	²⁴ 0.098	²⁵² 0.341	²⁵⁹ 0.099	²⁴⁰ 0.179	²⁴³ 1.000	²⁰⁷ 0.156	²⁵ 0.999	^{0.000}	^{0.000}	^{0.000}						
34	CANON-001	²⁷ 0.001	⁸ 0.006	⁶³ 0.088	⁴⁸ 0.001	³⁵ 0.007	³⁹ 0.062	⁶² 0.005	⁴² 0.023	³⁶ 0.365	⁴⁷ 0.008	⁴⁶ 0.068	³⁹ 0.139	^{0.001}	^{0.000}	^{0.042}	^{0.000}			
35	CANON-002	³ 0.001	¹¹ 0.006	⁷⁶ 0.106	²⁵ 0.001	³⁸ 0.007	³³ 0.059	⁵⁸ 0.005	³⁵ 0.020	⁴⁰ 0.047	⁷¹ 0.013	³⁷ 0.075	³⁹ 0.188	^{0.001}	^{0.000}	^{0.042}	^{0.000}			
36	CIB-000	⁸¹ 0.002	⁴⁴ 0.008	⁷³ 0.100	⁷⁰ 0.002	⁷⁵ 0.011	⁵⁴ 0.069	¹⁰⁸ 0.012	⁹⁴ 0.045	²⁵⁹ 1.000	⁹⁶ 0.017	⁷¹ 0.141	²²⁵ 0.894	^{0.000}	^{0.000}	^{0.000}				
37	CLEARVIEWAI-000	²⁸ 0.001	²⁴ 0.007	²¹ 0.062	⁴³ 0.001	²⁷ 0.006	²⁵ 0.056	⁶⁹ 0.006	⁵¹ 0.025	¹²⁹ 0.974	⁴⁸ 0.00									

#	ALGORITHM	INVESTIGATION MODE						IDENTIFICATION MODE						FAILURE TO EXTRACT						
		RANK ONE MISS RATE, FNIR(N, 0, 1)						HIGH T → FPIR = 0.001, FNIR(N, T, L)						FEATURES						
		N=1.6M						N=1.6M												
	GALLERY	MUGSHOT	MUGSHOT	MUGSHOT	VISA	BORDER	VISA	MUGSHOT	MUGSHOT	MUGSHOT	VISA	BORDER	VISA	MUGSHOT	MUGSHOT	MUGSHOT	VISA	BORDER	KIOSK	
	PROBE	MUGSHOT	WEBCAM	PROFILE	BORDER	BOR _E 10YR	KIOSK	MUGSHOT	WEBCAM	PROFILE	BORDER	BOR _E 10YR	KIOSK	MUGSHOT	WEBCAM	PROFILE	BORDER	BOR _E 10YR	KIOSK	
47	COGENT-005	90.002	82.010	86.126	70.002	70.010	165.120	86.009	79.037	158.098	69.011	59.082	233.0905	0.000	0.000	0.000	0.000	0.000	0.000	
48	COGENT-006	48.001	29.007	40.067	34.001	44.007	128.101	49.004	43.023	23.028	31.006	126.0422	53.0130	0.000	0.000	0.041	0.000	0.000	0.000	
49	COGENT-007	29.001	43.008	36.004	29.001	30.006	132.103	38.004	36.021	14.194	33.006	27.047	63.0144	0.000	0.000	0.043	0.000	0.000	0.000	
50	COGNITEC-000	295.025	284.059	283.096				284.161	280.303	166.0992				0.003	0.002	0.924				
51	COGNITEC-001	266.012	245.034	278.058				258.102	259.230	35.1000				0.003	0.002	0.924				
52	COGNITEC-002	218.006	227.025	272.049				211.053	239.178	258.1000				0.003	0.002	0.924				
53	COGNITEC-003	22.006	226.025	263.090				207.053	231.162	26.1000				0.004	0.002	0.878				
54	COGNITEC-004	178.003	167.016	238.813	196.013	146.057	192.0143	178.031	177.097	159.0990	175.068	115.316	123.288	0.002	0.001	0.635	0.006			
55	COGNITEC-005	92.002	79.010	211.713	214.021	136.037	159.115	89.010	89.041	341.1000	147.041	82.0157	89.0179	0.002	0.001	0.614	0.017			
56	COGNITEC-006	88.002	68.010	208.703	169.007	113.024	151.111	78.008	89.040	334.1000	122.030	88.0171	199.0681	0.002	0.001	0.568	0.003			
57	CUBOX-000	66.001	76.010	12.058	48.002	14.004	7.049	31.003	30.019	11.168	19.004	15.028	8.073	0.001	0.000	0.042	0.000			
58	CYBERLINK-000	189.004	194.020	212.717	172.007	184.034	219.056	193.116	188.0995	173.0063	139.0339	0.001	0.001	0.063						
59	CYBERLINK-001	183.004	182.018	213.731	165.007	183.033	212.054	190.109	183.0995	170.062	191.0652	0.000	0.000	0.040						
60	CYBERLINK-002	166.003	112.012	196.577	178.004	143.107	115.015	116.053	159.0988	109.024	124.288	0.001	0.000	0.042						
61	CYBERLINK-003	88.002	86.009	167.474	96.003	74.012	89.082	79.008	74.035	126.0972	73.012	62.100	142.368	0.000	0.000	0.039	0.000			
62	CYBERLINK-004	94.002	107.011	130.423	92.003	71.011	134.104	74.007	75.036	27.1000	76.013	63.109	29.0954	0.000	0.000	0.011	0.000			
63	CYBERLINK-005	107.002	87.011	108.209	75.002	64.010	120.098	93.010	86.041	248.1000	80.014	59.089	232.0926	0.000	0.000	0.034	0.000			
64	DAHUA-000	249.009	230.026					248.086	210.135					0.004	0.003					
65	DAHUA-001	220.007	221.024	209.703				238.073	201.122	140.0980				0.002	0.002	0.346				
66	DAHUA-002	111.002	111.012	136.304	91.003	93.084	116.015	96.046	67.0638	87.017	76.0159	0.001	0.000	0.099						
67	DAHUA-003	4.001	26.007	102.206	67.002	59.009	63.073	109.014	88.041	62.0579	75.013	53.0081	56.0134	0.000	0.000	0.000	0.000			
68	DAHUA-004	26.001	31.008	91.144	49.002	37.007	51.069	73.007	53.026	32.0485	35.0008	30.051	45.0113	0.000	0.000	0.000	0.000			
69	DAON-000	192.004	175.017	179.530	140.005	103.020	170.125	148.023	124.061	24.1000	110.025	96.0173	218.0846	0.002	0.002	0.108	0.001			
70	DFCATUR-000	135.002	109.011	117.229	128.004	100.019	147.109	151.023	130.066	72.0675	114.027	89.0173	107.0239	0.001	0.000	0.044	0.001			
71	DEEPLINT-001	7.001	22.007	108.200	88.002	64.073	37.003	21.014	248.1000	35.006	78.0159	0.000	0.000	0.038						
72	DEEPMSEA-001	198.004	165.016	239.814	183.010	191.140	199.046	181.101	149.0985	180.077	135.0326	0.000	0.001	0.047						
73	DERMALOG-003	33.0126	319.0217	259.296	263.0560	325.0482	316.0655	257.0677	22.0870	0.002	0.002	0.103								
74	DERMALOG-004	330.0125	318.0215	262.0930	253.0135	259.0467	324.0480	317.0657	189.0995	251.0603	219.0856	0.001	0.002	0.107						
75	DERMALOG-005	277.015	252.037	207.701	238.242	235.0384	231.088	223.0154	161.0990	238.0300	186.0614	0.001	0.002	0.102						
76	DERMALOG-006	249.008	225.024	197.619	184.010	200.155	206.052	184.0105	14.0981	168.0059	138.0318	0.003	0.006	0.181						
77	DERMALOG-007	248.009	232.027	202.675	200.014	206.170	249.086	222.0152	160.0990	188.0099	181.0557	0.001	0.002	0.102						
78	DERMALOG-008	17.003	157.015	174.516	162.007	128.029	190.139	197.045	170.094	281.0000	165.057	122.382	239.0940	0.000	0.000	0.002	0.000			
79	DERMALOG-009	170.003	149.014	99.167	170.007	171.999	137.106	140.021	131.066	264.1000	124.031	158.0999	216.840	0.001	0.001	0.018	0.003			
80	DERMALOG-010	13.002	104.011	36.066	223.038	159.124	157.113	72.007	115.055	22.0999	186.089	159.0100	175.0522	0.001	0.001	0.018	0.003			
81	DERMALOG-011	86.002	81.010	71.096	107.003	130.031	108.092	143.022	161.087	210.0998	196.0129	159.0991	204.0764	0.000	0.000	0.013	0.000			
82	DIGIDATA-000	330.590	334.0548	259.895	269.642	169.707	271.813	331.610	306.0577	174.0994	255.0646	142.789	214.824	0.002	0.001	0.070	0.001			
83	DILUSENSE-000	141.002	117.012	133.297	175.008	125.028	124.099	126.030	150.078	68.0655	142.039	134.0664	96.0203	0.001	0.001	0.219	0.006			
84	DILUSENSE-001	72.001	66.010	123.250	135.006	91.016	101.088	82.009	73.034	45.0456	83.0105	129.0511	58.0137	0.001	0.001	0.219	0.007			
85	EYEDEA-003	32.080	312.0148	281.960	250.101	254.0379	315.0388	308.0543	198.0994	249.0570	208.0792	0.001	0.003	0.161						
86	F8-001	270.012	201.669	328.1000	348.1000	285.0166	213.0988	285.0166				0.004	1.000	0.158						
87	HINCORE-000	261.011	246.034	225.767	226.032	158.0117	215.191	274.0134	248.0217	254.1000	215.0187	131.0598	159.0458	0.000	0.001	0.043	0.000			
88	FIRSTCREDITZ-001	45.001	47.008	70.094	68.002	65.010	43.065	33.003	31.019	30.291	43.0007	39.061	27.097	0.000	0.001	0.047	0.001			
89	FUJITSULAB-000	142.002	142.014	161.440	12.004	107.023	121.098	141.021	117.056	107.024	91.0177	108.0240	0.000	0.001	0.016	0.000				
90	FUJITSULAB-001	114.002	135.0013	163.455	125.004	116.026	130.106	129.018	119.058	168.0992	108.024	136.0739	111.0247	0.000	0.003	0.150	0.002			
91	GLORY-000	33.0178	325.0320	307.0994	295.0228	265.0678	314.0367	305.0547	182.0995	241.0453	217.0839	0.011	0.013	0.985						
92	GLORY-001	332.0127	322.0267	302.0992	296.0178	264.0594	305.0305	305.0537	170.0993	236.0408	212.0819	0.011	0.013	0.988						

Table 14: **Miss rates by dataset**: At left, rank 1 miss rates relevant to investigations; at right, with threshold set to target FPIR = 0.01 for higher volume, low prior, uses. Yellow indicates most accurate algorithm. Throughout blue superscripts indicate the rank of the algorithm for that column.

2023/07/05
16:19:47

$FNIR(N, K, T) =$ False neg. identification rate
 $FPIR(N, T) =$ False pos. identification rate

N = Num. enrolled subjects
 R = Num. candidates examined

Threshold

$T \geq 0 \rightarrow$ Investigation
 $T > 0 \rightarrow$ Identification

#	ALGORITHM	INVESTIGATION MODE						IDENTIFICATION MODE						FAILURE TO EXTRACT FEATURES					
		RANK ONE MISS RATE, FNIR(N, 0, 1)						HIGH T → FPIR = 0.001, FNIR(N, T, L)											
		N=1.6M						N=1.6M											
	GALLERY PROBE	MUGSHOT MUGSHOT	MUGSHOT WEBCAM	MUGSHOT PROFILE	VISA BORDER	BORDER BOR _L 10YR	KIOSK	MUGSHOT MUGSHOT	MUGSHOT WEBCAM	MUGSHOT PROFILE	VISA BORDER	BORDER BOR _L 10YR	KIOSK	MUGSHOT MUGSHOT	MUGSHOT WEBCAM	MUGSHOT PROFILE	VISA BORDER	BOR _L 10YR	KIOSK
93	GORILLA-001	317.060	304.095	266.0936	244.069	250.329	320.406	298.453	271.1000	242.468	316.1000	0.001	0.001	0.069					
94	GORILLA-002	289.020	268.044	221.0753	219.027	227.214	292.188	272.268	280.1000	224.250	256.1000	0.001	0.001	0.069					
95	GORILLA-003	304.036	291.070	240.821	239.048	237.265	307.318	295.434	298.1000	235.407	329.1000	0.001	0.001	0.069					
96	GORILLA-004	222.006	222.024	206.697	189.012	203.0162	250.089	230.160	115.095	200.135	155.0438	0.000	0.001	0.042					
97	GORILLA-005	177.003	183.018	108.209	154.006	168.0124	225.058	216.0142	74.0700	185.088	131.0315	0.000	0.000	0.040					
98	GORILLA-006	104.002	111.012	82.0122	106.003	95.0018	136.0105	161.0027	165.0089	56.0531	117.0028	86.0166	101.0218	0.000	0.000	0.041	0.000	0.000	
99	GORILLA-007	97.002	86.011	79.0114	80.002	93.016	100.0088	164.0027	149.077	69.0534	111.0026	105.0264	87.0178	0.000	0.000	0.041	0.000	0.000	
100	GORILLA-008	76.001	70.010	61.0085	56.002	78.0012	90.0082	152.0024	157.0083	46.0463	121.0030	117.0319	85.0178	0.000	0.000	0.041	0.000	0.000	
101	GRIAULE-000	159.002	136.014	142.327	187.0111	135.031	172.0126	138.0020	127.0063	184.0995	131.0033	95.0185	96.0198	0.000	0.002	0.090	0.001		
102	GRIAULE-001	43.001	39.008	88.0132	18.0001	109.023	44.0065	54.0005	58.0028	96.0865	40.0007	156.0995	30.0099	0.000	0.000	0.000	0.000		
103	HIK-003	261.012	235.027	205.689	192.012	197.0151	259.0103	226.0158	121.0969	201.0142	157.0445	0.000	0.000	0.048					
104	HIK-004	261.011	233.027	216.0743	190.012	199.0152	255.0099	223.0153	130.0976	201.0137	154.0434	0.000	0.000	0.048					
105	HIK-005	204.005	170.017	181.0535	167.0007	180.0111	194.0044	148.0077	23.0999	174.0068	177.0541	0.000	0.000	0.000					
106	HIK-006	204.005	169.017	182.0535				201.0047	160.0086	274.1000				0.000	0.000				
107	HYPERVERGE-001	62.001	99.011	39.067	47.002	35.0007	35.061	59.0004	66.031	20.0220	41.0007	32.0053	35.101	0.001	0.000	0.041	0.000		
108	HYPERVERGE-002	59.001	93.011	22.063	36.0001	29.0006	32.0058	39.0004	56.027	18.0210	27.0006	29.0048	24.0093	0.001	0.000	0.041	0.000		
109	HYPERVERGE-003	69.001	110.011	53.076	61.0002	50.0008	38.0062	70.0007	90.0042	29.0282	70.012	43.0065	39.0106	0.001	0.000	0.041	0.000		
110	HZAILU-000	146.002	134.013	121.0244	97.0003	89.015	104.0090	130.0020	101.051	118.0967	98.0020	114.0316	70.0153	0.001	0.001	0.054	0.001		
111	HZAILU-001	123.002	98.011	77.0106	76.0002	156.1113	107.0092	83.0009	241.0183	154.0986	219.0196	163.0000	194.0679	0.000	0.000	0.039	0.000		
112	HZAILU-002	129.002	97.011	83.0122	60.0002	66.0010	71.0076	84.0008	75.0074	71.0012	45.0066	137.0330	0.001	0.000	0.041	0.000			
113	HZAILU-003	91.002	89.011	74.0104	33.0001	41.0007	61.0072	81.0008	82.0038	61.0551	66.0009	40.0062	47.0119	0.001	0.000	0.041	0.000		
114	IDEMIA-003	229.007	244.034	276.0958	208.018	224.0210	206.0047	232.0165	191.0123	206.0766	0.000	0.000	0.041						
115	IDEMIA-004	222.007	242.032	271.0947	208.018	223.0210	188.0037	197.0118	127.0973	195.0123	205.0766	0.000	0.000	0.041					
116	IDEMIA-005	239.008	268.039	274.0954	216.0021	228.0217	197.0044	221.0150	130.0978	197.0130	222.0879	0.000	0.000	0.041					
117	IDEMIA-006	250.010	293.072	290.0969	220.030	236.0253	191.0043	253.0226	148.0982	204.0144	200.0733	0.000	0.000	0.041					
118	IDEMIA-007	161.003	161.015	311.000	156.0006	135.036	179.0131	128.0108	114.0055	310.0000	159.052	93.0182	338.0000	0.000	0.000	0.040	0.000		
119	IDEMIA-008	249.001	135.0007	56.079	46.0001	39.0007	70.0075	16.0002	18.0013	17.0204	22.0005	22.036	40.106	0.000	0.000	0.040	0.000		
120	IDEMIA-009	111.001	12.006	33.065	19.0001	20.0005	15.051	9.0002	6.0111	7.141	11.0003	12.027	11.074	0.000	0.000	0.040	0.000		
121	IDEMIA-010	7.001	9.006	13.058	7.0001	9.0004	8.049	1.001	2.008	5.131	6.0002	14.028	6.070	0.000	0.000	0.037	0.000		
122	IMAGUS-002	338.0220	323.0301	301.0988				336.0749	324.0816	259.1000			0.004	0.008	0.550				
123	IMAGUS-003	344.0356	338.0513	305.0993				338.0807	329.0909	261.0000			0.004	0.008	0.550				
124	IMAGUS-005	122.002	115.012	139.0319	153.0006	105.0022	181.0132	132.0018	129.0066	94.0838	117.0029	85.0161	104.0231	0.000	0.000	0.000	0.000		
125	IMAGUS-006	129.002	139.014	132.0293	126.0004	102.0019	153.0112	135.0019	135.0069	104.0897	116.0028	84.0161	115.0260	0.000	0.000	0.000	0.000		
126	IMAGUS-007	133.002	132.013	140.0321	119.0004	106.0022	161.0117	150.0023	141.0073	102.0893	120.0031	87.0169	120.0265	0.000	0.000	0.000	0.000		
127	IMAGUS-008	326.0086	303.0093	137.0305	213.021	153.0081	163.0119	346.0974	321.0774	191.0996	247.0520	160.1000	172.0518	0.000	0.000	0.000	0.000		
128	IMPERIAL-000	158.002	158.015	129.0280	135.0004	116.0097	150.0026	133.0068	218.0999	148.0042	110.0245	0.000	0.000	0.000	0.000	0.000	0.000		
129	INCODE-000	314.049	306.100	273.0951				306.0310	293.0420	209.0998			0.001	0.004	0.173				
130	INCODE-001	289.017	273.046	222.0762				292.0212	276.0296	268.1000			0.001	0.004	0.173				
131	INCODE-002	284.018	275.048	243.0843				291.0184	273.0269	171.0993			0.000	0.001	0.066				
132	INCODE-003	274.013	26.040	226.0764				286.0167	269.0264	239.0999			0.000	0.001	0.066				
133	INCODE-004	184.004	180.017	168.0475	180.0008	186.0135	215.0054	200.0120	181.0995	172.0063	129.0313	0.000	0.001	0.066					
134	INCODE-005	92.002	105.011	94.0147	82.0002	81.0013	82.0079	97.0011	92.0043	56.0528	89.0017	75.0145	73.0155	0.000	0.000	0.042	0.000		
135	INNOVATRICS-002	312.045	294.074	246.0853				308.0234	281.0310	281.0000			0.000	0.001	0.046				
136	INNOVATRICS-003	297.026	279.055	245.0845				296.0221	277.0297	243.0000			0.000	0.001	0.046				
137	INNOVATRICS-004	277.012	264.040	277.0958				277.0132	252.0222	139.0980			0.000	0.001	0.046				
138	INNOVATRICS-005	157.002	148.014	136.0407	138.0005	146.0109	181.0034	164.0089	93.0846	155.0047	112.0251	0.000	0.001	0.041					

Table 15: **Miss rates by dataset**: At left, rank 1 miss rates relevant to investigations; at right, with threshold set to target $FPIR = 0.01$ for higher volume, low prior, uses. Yellow indicates most accurate algorithm. Throughout blue superscripts indicate the rank of the algorithm for that column.

2023/07/05
16:19:47

FNIR(N, R, T) = False neg. identification rate
 FPIRN(T) = False pos. identification rate

R = Num. candidates examined

T = Threshold

$T = 0 \rightarrow$ Investigation
 $T > 0 \rightarrow$ Identification

#	ALGORITHM	INVESTIGATION MODE						IDENTIFICATION MODE						FAILURE TO EXTRACT FEATURES									
		RANK ONE MISS RATE, FNIR(N, 0, 1)						HIGH T → FPIR = 0.001, FNIR(N, T, L)															
		N=1.6M						N=1.6M															
	GALLERY	MUGSHOT	MUGSHOT	MUGSHOT	VISA	BORDER	BOR ₁ 10YR	KIOSK	MUGSHOT	MUGSHOT	MUGSHOT	VISA	BORDER	BOR ₁ 10YR	KIOSK	MUGSHOT	MUGSHOT	MUGSHOT	VISA	BORDER	KIOSK		
	PROBE	MUGSHOT	WEBCAM	PROFILE	BORDER	BOR ₁ 10YR	KIOSK	MUGSHOT	WEBCAM	PROFILE	BORDER	BOR ₁ 10YR	KIOSK	MUGSHOT	WEBCAM	PROFILE	BORDER	BOR ₁ 10YR	KIOSK				
139	INNOVATRICS-007	96.002	103.011	122.048	86.002	83.013	74.077	105.013	105.051	78.0743	88.017	69.093	71.0154	0.000	0.001	0.041	0.000	0.000	0.000	0.000	0.000		
140	INNOVATRICS-008	83.001	51.008	69.082	25.002	104.021	62.072	99.005	76.036	27.1000	77.013	147.0886	69.139	0.000	0.000	0.004	0.000	0.000	0.000	0.000	0.000		
141	INSPUR-000	13.001	340.0606	20.062	221.030	168.0395	217.0195	69.006	330.0915	251.1000	263.0936	249.1000	250.0998	0.000	0.000	0.000	0.000	0.000	0.000	0.000	0.000		
142	INTELIGENSA-000	130.002	121.012	118.210	133.004	134.0033	167.0124	153.024	147.077	88.0786	163.053	103.0235	111.0255	0.001	0.000	0.046	0.001	0.000	0.001	0.000	0.000		
143	INTELLIVISION-001	305.036	307.0102	292.0972	241.0057	165.0222	251.0333	304.0279	291.0404	252.0000	230.0328	138.0749	196.0685	0.001	0.000	0.044	0.000	0.000	0.000	0.000	0.000		
144	INTELLIVISION-002	260.011	241.0031	269.0942	207.018	152.0080	218.0200	279.0154	247.0196	22.0999	199.0134	127.0437	164.0460	0.001	0.000	0.043	0.000	0.000	0.000	0.000	0.000		
145	INTEMA-000	33.001	49.0008	10.058	22.0001	26.0005	13.051	24.0002	26.017	267.1000	24.0005	111.0288	15.081	0.000	0.000	0.040	0.000	0.000	0.000	0.000	0.000		
146	INTEMA-001	1.001	337.601	4.052	7.0001	75.012	4.046	6.0001	311.0603	1.013	16.004	134.0715	15.076	0.001	0.000	0.041	0.000	0.000	0.000	0.000	0.000		
147	INTSYSMSU-000	333.0146	219.0023	189.0562	246.072	180.0132	349.0998	341.0000	244.0000	268.0999	252.0999	0.000	0.000	0.050	0.000	0.000	0.000	0.000	0.000	0.000	0.000	0.000	
148	IREX-000	199.004	63.0010	20.0681	81.0002	76.0012	87.0082	170.0208	122.060	112.0957	151.044	113.0302	8.0170	0.000	0.000	0.042	0.000	0.000	0.000	0.000	0.000		
149	ISYSTEMS-002	224.006	229.0026	244.0844				242.0078	204.0126	201.0998				0.002	0.002	0.142							
150	ISYSTEMS-003	212.005	215.023	229.0791				225.0059	188.0107	250.1000				0.002	0.002	0.142							
151	KAKAO-000	74.001	85.0011	80.119	84.0002	80.013	77.078	118.0015	116.0056	48.0468	95.0019	70.0141	74.0158	0.000	0.000	0.041	0.000	0.000	0.000	0.000	0.000		
152	KAKAO-001	63.001	57.0009	70.058	12.0001	17.0004	6.0047	28.0003	26.017	10.0159	18.0004	25.0042	16.074	0.000	0.000	0.040	0.000	0.000	0.000	0.000	0.000		
153	KEDACOM-001	235.0008	248.0036	293.0972	228.0034			230.0237	149.023	139.0072	153.0986	164.0055	127.0305	0.000	0.000	0.000	0.000	0.000	0.000	0.000	0.000		
154	KNERON-000	219.006	234.027	187.0552	220.028			216.0195						0.000	0.000	0.000	0.000	0.000	0.000	0.000	0.000		
155	KNERON-001	300.030	342.0621	120.0237	235.0144	164.0207	241.0280							0.000	0.000	0.000	0.000	0.000	0.000	0.000	0.000		
156	KNOWUTECH-000	31.001	18.0007	57.080	30.0002	52.0008	56.0070	87.0009	80.0038	33.0318	74.0012	58.0091	52.0129	0.000	0.000	0.041	0.000	0.000	0.000	0.000	0.000		
157	LINE-000	143.002	146.0014	116.0223	146.0005	126.0029	140.0107	177.0031	174.0095		153.0046	108.0278	310.1000	0.000	0.000	0.000	0.000	0.000	0.000	0.000	0.000		
158	LINE-001	32.001	28.0007	29.063	62.0002	53.0008	98.0085	55.0005	54.0027	283.1000	62.0009	48.0072	300.1000	0.000	0.000	0.000	0.000	0.000	0.000	0.000	0.000		
159	LINECLOVA-002	55.001	30.0008	44.070	52.0002	72.0111	31.058	41.0004	206.0130	142.0981	145.0040	161.0000	197.0700	0.000	0.001	0.040	0.000	0.000	0.000	0.000	0.000		
160	LINECLOVA-003	14.001	33.00601	77.0999	20.0001	55.0009	97.0085	30.0003	312.0606		26.0006	157.0974	47.0110	0.000	0.000	0.024	0.000	0.000	0.000	0.000	0.000		
161	LOOKMAN-003	244.009	258.0038	231.0035				232.0239	193.0044	192.0112		184.0084	140.0355	0.000	0.000	0.000	0.000	0.000	0.000	0.000	0.000		
162	LOOKMAN-004	246.009	261.039	295.0973				196.0045	186.0105	131.0977			0.000	0.000	0.000	0.000	0.000	0.000	0.000	0.000	0.000		
163	LOOKMAN-005	238.008	251.0036	294.0972	230.0035			231.0237	175.0030	139.0086	134.0978	171.0062	128.0308	0.000	0.000	0.000	0.000	0.000	0.000	0.000	0.000		
164	MANTRA-000	99.002	77.0010	219.0709	164.0007	114.0024	152.0112	94.0010	87.0041	35.0000	118.0299	79.0152	251.0000	0.002	0.001	0.591	0.003						
165	MAXVISION-000	154.002	153.0015	143.0327	129.0004	143.0051	126.0101	171.0028	256.0237	83.0767	205.0149	157.0997	180.0557	0.000	0.000	0.042	0.000	0.000	0.000	0.000	0.000		
166	MAXVISION-001	44.001	32.0008	38.0064	24.0001	98.0018	29.0057	47.0004	49.0025	219.0000	39.0007	156.0951	36.0100	0.000	0.000	0.042	0.000	0.000	0.000	0.000	0.000		
167	MAXVISION-002	46.001	21.0007	25.063	32.0001	61.0009	53.0069	40.0004	38.0022	16.0197	36.0007	148.0895	37.0104	0.001	0.000	0.044	0.000	0.000	0.000	0.000	0.000		
168	MEGVII-001	268.012	178.017	348.1000				237.0072	178.0097				0.002	0.000	0.000	0.000	0.000	0.000	0.000	0.000	0.000		
169	MEGVII-002	269.012	181.017	162.0450	331.0000			241.0077	176.0096	212.0998			0.002	0.000	0.000	0.000	0.000	0.000	0.000	0.033	0.000		
170	MEGVII-003	49.001	41.0008	19.061	16.0001	15.0004	27.0057	26.0003	7.0011	9.0055	13.0003	13.0027	13.078	0.001	0.000	0.044	0.000	0.000	0.000	0.000	0.000		
171	MICROFOCUS-003	352.0594	346.0781		272.0708			274.0907	344.0931	348.0979		267.0982	246.0991	0.001	0.005								
172	MICROFOCUS-004	349.0576	345.0758		271.0701			273.0904	350.0999	338.0975		265.0974	244.0989	0.001	0.005								
173	MICROFOCUS-005	345.0424	338.0601		266.0494			267.0777	342.0835	338.0928		262.0935	244.0985	0.001	0.005								
174	MICROFOCUS-006	346.0427	336.0583		265.0490			270.0782	347.0978	333.0923		261.0923	240.0971	0.001	0.005								
175	MICROSOFT-003	87.0002	118.0012		116.0004			148.0109	168.0028	168.0091		138.0036	109.0233	0.000	0.001								
176	MICROSOFT-004	77.0001	116.0012		110.0004			149.0109	159.0026	162.0087		132.0033	102.0222	0.000	0.001								
177	MICROSOFT-005	115.0002	92.0111	97.0144	102.0003			122.0099	156.0026	137.0070	63.0587	112.0027	99.0180	0.000	0.000	0.049							
178	MICROSOFT-006	125.0002	108.0111	96.0150	114.0004			123.100	99.0112	77.0037	38.0386	128.0032	86.0178	0.000	0.001	0.049							
179	MUKH-002	296.026	250.0036	198.0638	188.0012	151.0079	175.0129	329.0594	264.0242	260.0000	211.0170	137.0741	148.0389	0.000	0.000	0.042	0.000	0.000	0.000	0.000	0.000		
180	NEC-000	281.017	266.0041	280.0959	217.0025			234.0243	244.0079	215.0140	137.0979	165.0474	0.001	0.002	0.890								
181	NEC-001	290.021	280.056	289.0667	227.0033			238.0277	261.0106	244.0197	152.0986	198.0133	167.0468	0.005	0.003	0.934							
182	NEC-002	22.0001	55.0009	151.0363	109.0003			160.0117	227.0003	34.0020	231.0999	51.0008	193.0676	0.000	0.001	0.041							
183	NEC-003	61.0001	75.0010	150.0352	113.0004	79.0013	166.0020	23.0002	27.0017	91.0824	54.0008	23.0036	197.0668	0.000	0.001	0.041	0.000	0.000	0.000	0.001	0.000		
184	NEC-004	68.0001	52.0009	183.0538	99.0003	46.0007	69.0075	12.0002	17.0013	66.022	20.0004	7.019	33.0100	0.000	0.001	0.041	0.000	0.000	0.000	0.001	0.000		

Table 16: **Miss rates by dataset**: At left, rank 1 miss rates relevant to investigations; at right, with threshold set to target FPIR = 0.01 for higher volume, low prior, uses. Yellow indicates most accurate algorithm. Throughout blue superscripts indicate the rank of the algorithm for that column.

16:19:47
2023/07/03

$FNIR(N, K, T) =$ False neg. identification rate
 $FPIR(N, T) =$ False pos. identification rate

N = Null. enrolled subjects
R = Num. candidates examined

1 INTRODUCTION

$I = 0 \rightarrow$ Investigation
 $T > 0 \rightarrow$ Identification

#	ALGORITHM	INVESTIGATION MODE						IDENTIFICATION MODE						FAILURE TO EXTRACT FEATURES							
		RANK ONE MISS RATE, FNIR(N, 0, 1)						HIGH T → FPIR = 0.01, FNIR(N, T, L)						N=1.6M							
		GALLERY		MUGSHOT	MUGSHOT	MUGSHOT	VISA	BORDER	VISA	MUGSHOT	MUGSHOT	MUGSHOT	VISA	BORDER	VISA	MUGSHOT	MUGSHOT	MUGSHOT	VISA	BORDER	KIOSK
185	NEC-005	41.001	33.008	30.081	38.002	19.005	66.073	10.002	12.012	71.673	14.003	6.019	29.099	0.000	0.001	0.040	0.000	0.001	0.001	0.001	
186	NEC-006	50.001	45.008	34.066	64.002	22.005	46.065	18.002	29.018	47.463	10.004	11.026	25.094	0.000	0.001	0.040	0.000	0.001	0.001	0.001	
187	NEC-007	20.001	5.006	15.059	17.001	3.003	10.049	4.001	3.009	8.147	4.002	1.010	4.065	0.000	0.000	0.040	0.000	0.000	0.000	0.000	
188	NEUROTECHNOLOGY-003	291.022	267.042	287.961						333.636	271.266	336.1.000				0.000	0.001	0.131			
189	NEUROTECHNOLOGY-004	214.006	193.020	291.970						230.063	194.117	176.094				0.000	0.001	0.131			
190	NEUROTECHNOLOGY-005	197.004	224.024	250.893						216.054	207.130	204.098				0.000	0.000	0.030			
191	NEUROTECHNOLOGY-006	285.018	270.045	197.606						301.249	292.418					0.000	0.000				
192	NEUROTECHNOLOGY-007	188.004	201.021	231.796	182.009		212.180	229.062	236.0173	257.1.000	231.339	236.0173	282.1.000	0.001	0.001	0.041					
193	NEUROTECHNOLOGY-008	138.002	147.014	165.457	12.004	110.023	129.101	210.053	153.080	269.1.000	13.035	112.293	97.203	0.000	0.001	0.052	0.001				
194	NEUROTECHNOLOGY-009	70.001	88.011	102.179	74.002	82.013	81.079	119.015	106.052	64.588	97.020	80.153	79.165	0.001	0.000	0.046	0.000				
195	NEUROTECHNOLOGY-010	47.001	62.009	47.070	40.001	45.007	50.068	92.010	80.037	28.277	67.010	82.075	50.126	0.000	0.000	0.041	0.000				
196	NEUROTECHNOLOGY-012	18.001	37.008	23.063	11.001	24.005	28.057	71.007	70.032	114.059	58.008	38.061	227.016	0.000	0.000	0.039	0.000				
197	NEUROTECHNOLOGY-013	19.001	36.008	17.058	10.001	18.004	24.056	46.004	40.023	35.324	30.006	26.046	189.641	0.000	0.000	0.039	0.000				
198	NEWLAND-002	323.079	309.117	267.936						322.0438	299.466	228.0999				0.007	0.012	0.200			
199	NOBLIS-001	340.249	331.522	300.993						352.1.000	353.1.000	270.1.000				0.000	0.000	0.000			
200	NOBLIS-002	336.179	328.392	298.982						348.097	351.1.000	273.1.000				0.000	0.000	0.000			
201	NOTIONTAG-000	156.002	119.012	103.204	123.004	90.016	113.095	123.017	122.059	65.611	102.021	78.150	84.176	0.000	0.000	0.000	0.000				
202	NTECHLAB-003	220.006	212.023	170.504						214.054	195.118	93.837				0.000	0.000	0.040			
203	NTECHLAB-004	207.005	188.019	171.506	174.008		176.129	189.041	185.105	92.833	162.053		117.263	0.000	0.000	0.040					
204	NTECHLAB-005	205.005	184.018	155.367	170.008		162.118	190.042	183.102	84.771	178.073		125.294	0.000	0.000	0.040					
205	NTECHLAB-006	193.004	174.017	149.347	171.007		158.113	184.037	171.094	82.754	166.057		116.260	0.000	0.000	0.040					
206	NTECHLAB-007	163.003	122.012	147.326	13.004		141.107	159.026	132.067	81.750	122.032		103.223	0.000	0.000	0.042					
207	NTECHLAB-008	98.002	64.010	98.157	108.003		94.084	112.014	95.045	57.529	133.033		91.183	0.000	0.000	0.044					
208	NTECHLAB-009	51.001	38.008	81.138	72.002	84.013	68.074	58.005	39.022	42.430	81.015	64.109	63.142	0.000	0.000	0.041	0.001				
209	NTECHLAB-010	30.001	46.008	62.085	37.002	51.008	30.057	25.003	24.015	22.252	37.007	37.059	28.098	0.001	0.001	0.043	0.000				
210	NTECHLAB-011	21.001	17.007	4.072	42.001	49.007	16.051	32.003	23.015	23.228	67.009	50.074	21.091	0.000	0.000	0.040	0.000				
211	OMNIGARDE-000	23.001	14.007	47.074	38.001	34.007	49.068	45.004	41.023	26.252	44.007	33.055	37.136	0.000	0.000	0.041	0.000				
212	PANGIAM-000	40.001	34.008	51.074	66.002	48.007	45.065	66.006	64.030	34.318	69.009	69.136	38.105	0.000	0.001	0.044	0.001				
213	PANGIAM-001	230.007	129.013	51.078	25.001	62.009	42.064	98.011	63.030	37.383	69.009	145.860	62.141	0.003	0.000	0.040	0.000				
214	PARAVISION-000	286.019	257.038	180.534	263.023	423	262.059	253.089	234.170	243.470	231.026	0.000	0.000								
215	PARAVISION-001	186.004	198.020	144.329	262.0414		261.0484	203.049	205.128	219.099	240.444		201.739	0.000	0.000	0.000					
216	PARAVISION-002	191.004	205.022	146.335	202.015		208.175	204.050	198.119	146.983	181.080		169.497	0.000	0.000	0.032					
217	PARAVISION-003	176.003	190.019	121.252	203.015		205.167	182.035	175.096	178.094	16.058		126.296	0.000	0.000	0.032					
218	PARAVISION-004	90.002	80.010	75.104	151.006		154.112	96.010	81.038	282.1.000	92.018		225.098	0.000	0.000	0.032					
219	PARAVISION-005	80.002	69.010	51.079	168.007		138.106	44.004	44.024	138.098	69.011		54.132	0.000	0.000	0.038					
220	PARAVISION-007	37.001	42.008	35.066	144.005	67.010	127.101	42.004	48.025	272.1.000	59.009	65.113	319.1.000	0.000	0.000	0.000					
221	PARAVISION-009	17.001	27.007	31.067	30.001	13.004	21.054	21.003	77.735	12.003	17.033	9.073	0.000	0.001	0.025	0.000					
222	PARAVISION-012	10.001	23.007	15.061	37.001	11.004	17.052	8.002	15.012	49.475	10.002	10.025	5.068	0.000	0.001	0.025	0.000				
223	PARAVISION-014	9.001	20.007	16.059	8.001	7.003	5.047	7.001	8.011	59.533	5.002	18.033	3.061	0.000	0.001	0.025	0.000				
224	PIXELALL-002	202.005	208.022	230.810	186.011		213.187	260.105	289.388	286.1.000	259.602		297.1.000	0.000	0.000	0.000					
225	PIXELALL-003	136.002	146.014	173.515	161.006		196.151	145.022	140.073	241.1.000	141.037		179.554	0.000	0.000	0.000					
226	PIXELALL-004	133.002	154.015	175.523	148.005		198.152	131.018	152.079	261.1.000	157.051		247.094	0.000	0.000	0.000					
227	PIXELALL-005	118.002	91.011	126.264	191.012		122.028	194.146	101.012	99.050	272.1.000	113.027	97.203	254.1.000	0.000	0.000	0.000				
228	PTAKURATSATU-000	174.003	173.017	191.605	14.005	119.027	135.105	183.037	203.124	107.924	15.046	99.206	105.232	0.000	0.001	0.039	0.000				
229	QNAP-000	236.008	237.027	170.522	198.013	144.054	201.158	271.129	258.238	289.1.000	216.191	130.539	249.098	0.001	0.000	0.054	0.000				
230	QNAP-001	195.004	206.022	169.498	158.006	138.041	155.112	213.054	212.137	108.928	18.081	120.368	138.331	0.000	0.000	0.004	0.000				

Table 17: **Miss rates by dataset:** At left, rank 1 miss rates relevant to investigations; at right, with threshold set to target FPIR = 0.01 for higher volume, low prior, uses. Yellow indicates most accurate algorithm. Throughout blue superscripts indicate the rank of the algorithm for that column.

2023/07/05
16:19:47FNIR(N, R, T) = False neg. identification rate
FPIR(N, T) =N = Num. enrolled subjects
T = ThresholdT = 0 → Investigation
T > 0 → Identification

#	ALGORITHM	INVESTIGATION MODE										IDENTIFICATION MODE										FAILURE TO EXTRACT FEATURES									
		RANK ONE MISS RATE, FNIR(N, 0, 1)					HIGH T → FPIR = 0.001, FNIR(N, T, L)					N=1.6M					N=1.6M														
		GALLERY	MUGSHOT	MUGSHOT	MUGSHOT	VISA	BORDER	BOR _{10YR}	KIOSK	MUGSHOT	MUGSHOT	MUGSHOT	VISA	BORDER	VISA	MUGSHOT	MUGSHOT	MUGSHOT	VISA	BORDER	BOR _{10YR}	KIOSK									
231	QNAP-002	²⁰⁸ 0.005	²⁰⁰ 0.021	¹⁰¹ 0.172	¹²⁷ 0.004	¹³² 0.031	¹⁷¹ 0.125	¹⁶⁰ 0.026	⁸³ 0.772	¹⁶¹ 0.052	¹⁰⁹ 0.281	¹²² 0.272	0.001	0.004	0.057	0.001	0.001	0.001	0.001	0.001	0.001	0.001	0.001	0.001	0.001	0.001	0.001	0.001	0.001	0.001	
232	QNAP-003	¹⁶⁸ 0.003	¹⁷⁷ 0.017	⁹⁷ 0.152	¹⁷⁶ 0.008	¹⁴⁸ 0.061	¹¹¹ 0.093	¹³⁴ 0.019	³²⁶ 0.835	¹⁶⁷ 0.992	²⁴⁹ 0.502	¹⁹⁶ 1.000	²²⁰ 0.865	0.000	0.001	0.002	0.001	0.001	0.001	0.001	0.001	0.001	0.001	0.001	0.001	0.001	0.001	0.001	0.001	0.001	0.001
233	QNAP-004	¹¹⁹ 0.002	¹⁵¹ 0.014	⁸¹ 0.119	¹⁴² 0.005	¹³⁹ 0.041	⁹⁹ 0.086	¹¹⁰ 0.014	³²⁸ 0.890	¹⁹⁶ 0.996	²⁴⁵ 0.501	¹⁹⁷ 1.000	²²⁹ 0.922	0.000	0.001	0.002	0.001	0.001	0.001	0.001	0.001	0.001	0.001	0.001	0.001	0.001	0.001	0.001	0.001	0.001	0.001
234	QUANTASOFT-001	³³⁷ 0.218	³⁴⁴ 0.727						³³⁴ 0.639													0.000	0.000								
235	RANKONE-002	²⁸⁸ 0.019	²⁹² 0.071						²⁶⁵ 0.118	²⁶⁷ 0.261												0.000	0.000								
236	RANKONE-003	²⁸⁷ 0.019	²⁹⁰ 0.068						²⁶⁴ 0.118	²⁶⁶ 0.255												0.000	0.000								
237	RANKONE-004	³¹¹ 0.041	³¹¹ 0.141						²⁹³ 0.193	²⁹⁴ 0.426												0.000	0.000								
238	RANKONE-005	²⁵⁰ 0.009	²⁶⁵ 0.041	³⁰⁰ 0.986					²²⁵ 0.059	²³⁷ 0.173	²⁰⁶ 0.998											0.000	0.000	0.489							
239	RANKONE-006	²¹⁰ 0.005	²³³ 0.797						¹⁸⁵ 0.037		¹³² 0.977											0.002	0.167								
240	RANKONE-007	¹⁸⁰ 0.003	¹⁸⁷ 0.019	²³⁰ 0.796					¹⁴⁷ 0.022	¹⁷² 0.095	¹¹⁷ 0.967										0.001	0.001	0.102								
241	RANKONE-009	¹⁵¹ 0.002	¹²⁴ 0.013	¹⁸⁴ 0.549	¹⁵⁰ 0.006	¹⁸⁵ 0.134	¹²⁷ 0.018	¹⁴⁴ 0.076	¹²² 0.969	¹⁶⁰ 0.062	¹³⁶ 0.328										0.000	0.000	0.000								
242	RANKONE-010	¹⁴⁴ 0.002	⁷¹ 0.010	¹⁵³ 0.374	¹⁴¹ 0.005	¹¹⁷ 0.027	¹⁷³ 0.126	¹⁰⁸ 0.014	¹²⁰ 0.058	⁸⁹ 0.802	¹⁶⁰ 0.052	¹⁰⁰ 0.208	¹¹⁴ 0.259	0.000	0.000	0.000	0.000	0.000	0.000	0.000	0.000	0.000	0.000	0.000	0.000	0.000	0.000	0.000	0.000	0.000	
243	RANKONE-011	⁷⁸ 0.002	¹⁰⁶ 0.011	¹¹⁵ 0.223	¹¹² 0.004	⁹⁹ 0.019	⁹¹ 0.082	⁸⁴ 0.009	⁹⁷ 0.048					¹⁴ 0.037	⁹² 0.182	²⁴¹ 0.977				0.000	0.000	0.000									
244	RANKONE-012	⁶⁰ 0.001	⁸⁴ 0.010	⁸⁷ 0.127	¹⁰¹ 0.003	⁸⁶ 0.014	⁵² 0.069	⁷⁷ 0.008	¹¹¹ 0.053					¹¹⁰ 0.029	⁷⁴ 0.144	¹⁶² 0.465				0.000	0.000	0.000									
245	RANKONE-013	²⁵ 0.001	¹⁶ 0.007	⁵² 0.076	²⁷ 0.001	⁵⁴ 0.008	²⁰ 0.054	⁵¹ 0.005	⁷² 0.034	¹⁹⁴ 0.996	⁹³ 0.018	⁷² 0.141	⁶⁴ 0.142	0.000	0.000	0.033	0.000	0.000	0.000	0.000	0.000	0.000	0.000	0.000	0.000	0.000	0.000	0.000	0.000	0.000	
246	RANKONE-014	¹² 0.001	⁷ 0.006	⁴¹ 0.067	¹⁵ 0.001	²⁵ 0.005	¹¹ 0.050	³⁵ 0.003	⁴⁵ 0.024												0.000	0.000	0.000								
247	REALNETWORKS-000	³¹⁰ 0.040	²⁹⁸ 0.078						²⁹⁹ 0.234	²⁸³ 0.319											0.001	0.000									
248	REALNETWORKS-001	³⁰⁹ 0.040	²⁹⁹ 0.078						²⁹¹ 0.234	²⁸⁴ 0.319											0.001	0.000									
249	REALNETWORKS-002	³⁰⁶ 0.039	²⁹⁷ 0.078						²⁹⁷ 0.231	²⁸² 0.315											0.001	0.000									
250	REALNETWORKS-003	²⁹⁴ 0.024	²⁸⁶ 0.062	²²⁶ 0.771	²²⁵ 0.031	²²¹ 0.209	²⁸³ 0.159	²⁷⁰ 0.266	²¹¹ 0.998	²¹⁰ 0.164	¹⁷⁰ 0.500										0.001	0.000	0.009								
251	REALNETWORKS-004	²⁹² 0.024	²⁸³ 0.059	²³² 0.797	²²⁴ 0.031	²²⁶ 0.213	²⁸² 0.158	²⁶⁸ 0.263	²²⁸ 0.999	²¹² 0.170	¹⁸⁸ 0.613										0.001	0.000	0.009								
252	REALNETWORKS-005	¹⁴⁷ 0.002	¹³³ 0.013	¹⁶⁶ 0.433	¹³⁴ 0.004	¹⁰⁸ 0.023	¹³⁰ 0.102	¹⁶⁷ 0.028	¹⁴² 0.074	¹²⁴ 0.971	¹³ 0.037	¹⁰¹ 0.223	¹⁰⁰ 0.215	0.000	0.000	0.006	0.000	0.000	0.000	0.000	0.000	0.000	0.000	0.000	0.000	0.000	0.000	0.000	0.000	0.000	
253	REALNETWORKS-006	⁶⁵ 0.001	⁷³ 0.010	¹³¹ 0.137	⁸⁸ 0.002	⁶⁸ 0.010	⁷⁸ 0.078	¹¹⁵ 0.015	¹⁰⁹ 0.053	¹⁴¹ 0.980	⁸⁴ 0.016	⁶⁶ 0.120	⁷² 0.154								0.000	0.009									
254	REALNETWORKS-007	³⁶ 0.001	⁶¹ 0.009	¹²² 0.267	³⁶ 0.002	⁵⁶ 0.009	⁶⁰ 0.072	⁹³ 0.010	⁹³ 0.043	¹³⁶ 0.979	⁷¹ 0.012	¹²⁸ 0.463	⁶¹ 0.140								0.000	0.000	0.009								
255	REALNETWORKS-008	³⁵ 0.001	³⁵ 0.008	⁶⁴ 0.089	³⁶ 0.002	⁴³ 0.007	¹⁰⁵ 0.091	⁶⁷ 0.006	⁶² 0.029	¹¹⁹ 0.968	⁵⁰ 0.008	⁴⁷ 0.068	³¹ 0.129								0.000	0.000	0.042								
256	RECOGNITO-000	⁸ 0.001	¹⁰ 0.006	²⁷ 0.064	⁶ 0.001	¹²⁰ 0.028	³ 0.045	¹⁹ 0.002	¹⁰ 0.012	¹³ 0.184	⁴⁶ 0.007	¹³⁵ 0.730	²² 0.092	0.000	0.000	0.040	0.000	0.000	0.000	0.000	0.000	0.000	0.000	0.000	0.000	0.000	0.000	0.000	0.000	0.000	0.000
257	RECOGNITO-001			³¹ 0.001		¹² 0.004	¹² 0.050													¹⁹ 0.033											
258	REMARKAI-000	²⁴³ 0.009	²⁴⁰ 0.030						²⁶⁹ 0.128	²⁴⁵ 0.203											0.000	0.001									
259	REMARKAI-000	¹⁸² 0.003	¹⁸⁵ 0.018	¹⁹⁶ 0.660	¹⁷³ 0.008	¹⁹⁵ 0.148	²¹ 0.055	¹⁹⁹ 0.120	²²⁵ 0.999	¹⁷⁷ 0.069	¹⁹⁹ 0.717										0.000	0.000	0.000								
260	REMARKAI-002	²⁴¹ 0.008	²³⁹ 0.029	²³⁴ 0.802					²⁶⁸ 0.124	²⁴³ 0.196	¹⁶⁴ 0.991										0.000	0.001	0.017								
261	RENDIP-000	⁸³ 0.002	¹⁵⁶ 0.015	¹⁵⁹ 0.424	¹⁵⁷ 0.006	¹²¹ 0.028	⁹⁵ 0.084	¹⁶⁰ 0.012	¹²¹ 0.059	¹⁰³ 0.894	¹⁰³ 0.022	⁹⁴ 0.185	⁸⁰ 0.167								0.000	0.000	0.041								
262	REVEALMEDIA-000	¹¹³ 0.002	⁶⁷ 0.010	¹²⁸ 0.275	⁷³ 0.002	⁷⁷ 0.012	⁶⁷ 0.074	¹⁰² 0.012	⁹¹ 0.042	⁷³ 0.680	¹⁰¹ 0.021	⁶¹ 0.093	⁶⁶ 0.143								0.000	0.000	0.041								
263	S1-000	¹⁵³ 0.002	¹⁷² 0.017	¹²⁵ 0.258	¹⁴⁴ 0.005	¹¹⁵ 0.025	¹⁰³ 0.090	¹⁶⁹ 0.028	¹⁵⁸ 0.085	²⁸⁷ 1.000	¹⁵⁰ 0.047	²⁸⁵ 1.000	²⁷⁷ 1.000								0.000	0.000	0.040								
264	S1-001	¹⁷⁸ 0.003	¹⁴³ 0.014	¹¹¹ 0.215	⁹⁴ 0.003	⁹⁶ 0.018	⁷² 0.077	¹²⁰ 0.016	¹⁰⁵ 0.052	¹⁵⁰ 0.985</td																					

#	ALGORITHM	INVESTIGATION MODE						IDENTIFICATION MODE						FAILURE TO EXTRACT						
		RANK ONE MISS RATE, FNIR(N, 0, 1)						HIGH T → FPIR = 0.001, FNIR(N, T, L)						FEATURES						
		N=1.6M						N=1.6M												
	GALLERY	MUGSHOT	MUGSHOT	MUGSHOT	VISA	BORDER	BOR ₁ 10YR	KIOSK	MUGSHOT	MUGSHOT	MUGSHOT	VISA	BORDER	MUGSHOT	MUGSHOT	MUGSHOT	VISA	BORDER	KIOSK	
277	SENSETIME-007	³ 0.001	³ 0.006	³ 0.052	⁵ 0.001	⁰ 0.003	³ 0.062	³ 0.001	³ 0.009	²³⁰ 0.999	¹⁰ 0.003	³ 0.024	¹⁷ 0.085	0.000	0.000	0.025	0.000	0.000	0.000	
278	SENSETIME-008	¹ 0.001	⁴ 0.006	⁶ 0.054	³ 0.001	³ 0.003	⁴⁷ 0.067	³ 0.001	¹ 0.009	³⁹ 0.405	⁷ 0.002	³ 0.021	¹⁴ 0.080	0.000	0.000	0.039	0.000	0.000	0.000	
279	SENSETIME-009	² 0.001	¹ 0.005	¹ 0.052	⁴ 0.001	³ 0.003	⁷ 0.078	² 0.001	¹ 0.007	⁹⁷ 0.868	³⁰ 0.001	³ 0.015	¹⁸ 0.085	0.000	0.000	0.039	0.000	0.000	0.000	
280	SERENDIPITY-000	⁷⁹ 0.002	¹⁵⁵ 0.015	¹³⁵ 0.299	¹³⁰ 0.004	¹⁵⁵ 0.108	⁶⁵ 0.073	¹⁰⁴ 0.012	²⁴⁶ 0.213	⁸⁰ 0.748	⁹¹ 0.018	¹⁶² 1.000	⁶⁵ 0.142	0.000	0.000	0.041	0.000	0.000	0.000	
281	SHAMAN-003	³² 0.124	³¹⁵ 0.172					³² 0.451	³¹¹ 0.597					0.020	0.011					
282	SHAMAN-004	³³⁹ 0.222	³²⁴ 0.319					³³² 0.615	³²⁰ 0.754					0.020	0.011					
283	SHAMAN-006	³⁰⁶ 0.040	²⁸ 0.058	²⁶⁷ 0.938				²⁷ 0.141	²⁵ 0.237	¹²⁵ 0.972				0.020	0.011	0.869				
284	SHAMAN-007	³⁰⁷ 0.040	²⁸¹ 0.057					²⁷ 0.141	²⁶⁰ 0.240					0.020	0.010					
285	SIAT-001	¹⁰⁸ 0.002	³² 0.333	¹³² 0.004		¹²³	^{0.099}	¹²⁴ 0.018	²⁸ 0.365		¹²⁵ 0.031			0.000	0.000					
286	SIAT-002	¹⁰⁹ 0.002	³²⁹ 0.446	²⁶¹ 0.348		¹³¹	^{0.102}	¹⁴⁴ 0.022	³⁰⁰ 0.478	²³³ 0.372		²³⁰ 0.923		0.000	0.000					
287	SIMILART-004	³⁵³ 0.965	³⁴⁷ 0.974					³⁴⁵ 0.968	³³⁹ 0.976					0.011	0.013					
288	SIMILART-005															0.011	0.013			
289	SQISOFT-001	¹⁹⁶ 0.004	¹⁸⁹ 0.019	¹³⁰ 0.282	¹⁴⁵ 0.005	¹¹⁸ 0.027	¹¹⁷ 0.097	²⁷³ 0.132	²⁶⁴ 0.252	⁸⁷ 0.797	¹⁴⁴ 0.040	¹¹⁶ 0.317	¹⁵³ 0.420	0.000	0.000	0.039	0.000	0.000	0.000	
290	SQISOFT-002	⁵⁴ 0.001	²²⁸ 0.026	⁶⁶ 0.090	¹⁴³ 0.005	¹⁶⁷ 0.282	⁸⁸ 0.078	¹⁷³ 0.029		¹⁰⁵ 0.904	²⁵⁴ 0.621		²³⁹ 0.953	0.000	0.000	0.039	0.000	0.000	0.000	
291	STAQU-000	²³² 0.007	¹⁹⁶ 0.020	¹⁹⁶ 0.613	²¹⁰ 0.020	¹⁴⁵ 0.055	²⁰² 0.159		²²⁷ 0.643	²⁵³ 1.000	²⁴⁸ 0.535	¹⁵² 0.961	³⁰⁷ 1.000	0.000	0.000	0.000	0.000	0.000	0.000	
292	SYNESIS-003	²⁷ 0.016	²¹⁶ 0.023	²⁴² 0.827	¹⁹⁴ 0.013		¹⁸⁸ 0.136	²³⁵ 0.065	²⁰⁵ 0.123	¹¹⁵ 0.960	¹⁷⁹ 0.075		¹³ 0.314	0.000	0.001	0.063				
293	SYNESIS-003	³³ 0.170	³²⁰ 0.235					³²⁸ 0.582	³¹⁵ 0.646					0.006	0.015					
294	SYNESIS-005	²⁴ 0.009	¹² 0.013	²¹⁸ 0.744	¹⁰⁵ 0.003		¹⁰⁹ 0.092	¹⁵⁴ 0.025	¹³⁷ 0.072	¹⁴⁷ 0.984	¹³⁰ 0.032		⁹⁹ 0.214	0.001	0.000	0.135				
295	T4ISB-000	²⁵⁸ 0.010	²²⁰ 0.023	¹⁶⁵ 0.462	⁸⁹ 0.003	¹⁵⁹	^{0.115}	⁸⁵ 0.081	¹²¹ 0.016	¹⁰⁸ 0.053	⁵³ 0.510	⁹⁹ 0.021	¹³⁹ 0.759	⁷⁷ 0.161	0.000	0.000	0.000	0.000	0.000	0.000
296	TECH5-001	¹⁹⁰ 0.004	¹⁷¹ 0.017	¹⁹¹ 0.584	¹⁶³ 0.007		¹⁴² 0.107	²²⁸ 0.057	³³⁵ 0.935	²⁸⁸ 0.510	²²³ 0.244		²⁴⁸ 0.994	0.000	0.000	0.006				
297	TECH5-002	¹⁶⁴ 0.003	⁹⁰ 0.011	¹³⁸ 0.312	¹⁰⁴ 0.003	¹²⁹	^{0.029}	¹⁰² 0.089	¹⁶¹ 0.027	¹³⁶ 0.070	⁹⁰ 0.805	¹⁴³ 0.039	⁹⁸ 0.205	¹⁵⁶ 0.440	0.001	0.000	0.041	0.000	0.000	0.000
298	TEVIAN-003	²⁷⁶ 0.015	²⁵⁶ 0.052					²⁹⁰ 0.177	²⁷⁸ 0.298					0.001	0.002					
299	TEVIAN-004	²⁶ 0.011	²⁵⁶ 0.038					²⁶¹ 0.117	²⁵⁴ 0.176					0.001	0.002					
300	TEVIAN-005	²³³ 0.007	²³⁸ 0.028	¹⁶⁶ 0.467				²⁵⁰ 0.087	²¹⁸ 0.144	¹¹⁶ 0.962				0.001	0.002	0.116				
301	TEVIAN-006	¹⁵⁷ 0.002	¹⁰⁷ 0.011	⁸⁴ 0.123	⁹⁵ 0.003	⁸⁸	^{0.013}	⁵⁸ 0.071	⁹¹ 0.010	⁶⁹ 0.032	⁴¹ 0.425	⁸⁵ 0.016	⁵⁹ 0.093	²³⁵ 0.951	0.001	0.000	0.062	^{0.000}		
302	TEVIAN-007	¹⁰⁸ 0.002	⁶⁰ 0.009	⁶⁸ 0.093	⁶⁹ 0.002	⁶³	^{0.009}	⁴⁸ 0.067	⁶¹ 0.005	³⁷ 0.022	³² 0.301	⁶⁴ 0.009	⁴¹ 0.065	⁴⁸ 0.122	0.000	0.000	0.062	^{0.000}		
303	TIGER-000	³¹ 0.062	³⁶ 0.095					³¹⁷ 0.390	³⁰ 0.500					0.000	0.000					
304	TIGER-002	²¹⁹ 0.006	²¹⁴ 0.023	¹⁷² 0.514				²⁴⁶ 0.086	²²⁸ 0.158	²²⁰ 0.999				0.000	0.000	0.056				
305	TIGER-003	²¹⁵ 0.006	²¹³ 0.023					²⁴⁷ 0.086	²²⁷ 0.158					0.000	0.000					
306	TONGYITRANS-000	²² 0.007	²¹¹ 0.022					²³⁹ 0.074	¹⁹ 0.112					0.003	0.001					
307	TONGYITRANS-001	²²⁸ 0.007	²¹⁰ 0.022					²³³ 0.066	¹⁸² 0.101					0.003	0.001					
308	TOSHIBA-000	²⁰⁷ 0.004	²⁰⁵ 0.022	²²⁴ 0.766				²²⁹ 0.062	¹⁹⁸ 0.118	¹⁸⁷ 0.995				0.000	0.000	0.070				
309	TOSHIBA-001	²⁰⁶ 0.005	²⁰⁷ 0.022					²²³ 0.058	¹⁶⁹ 0.092					0.000	0.000					
310	TRUEFACE-000	¹⁷ 0.003	¹⁵⁷ 0.014	¹¹⁸ 0.230	¹⁶⁸ 0.007	¹¹² 0.024	¹¹⁰ 0.092	¹³⁶ 0.018	¹²⁴ 0.062	⁹⁸ 0.882	¹²⁰ 0.030	⁹⁶ 0.194	⁹³ 0.188	0.001	0.001	0.047	^{0.003}			
311	TURINGTECHVIP-001	²⁵¹ 0.009	²³¹ 0.026	³⁸ 0.081	²³⁴ 0.045	¹⁶³ 0.199	²²⁹ 0.220	³⁰⁸ 0.345	³²⁷ 0.850	¹⁶⁹ 0.993	²⁶⁶ 0.978	³²² 1.000	²³³ 0.999	0.001	0.003	0.044	0.000			
312	USEB-000	³⁰⁵ 0.035	²⁷⁸ 0.054	¹⁵⁴ 0.380	²¹² 0.021	¹⁶¹ 0.172	¹⁸ 0.135	³³⁵ 0.715	³¹⁷ 0.722	¹²⁰ 0.968	²⁴⁴ 0.490	¹⁴¹ 0.804	¹⁹ 0.648	0.000	0.001	0.042	0.000			
313	VD-000	³⁴⁸ 0.474	³³⁵ 0.551					³⁴³ 0.917	³³⁷ 0.946					0.011	0.013					
314	VD-001	²⁹ 0.028	²⁷ 0.053					²⁹⁴ 0.201	²⁷⁰ 0.281					0.005	0.001					
315	VD-002	²⁵⁹ 0.010	²³⁶ 0.027	²⁴⁹ 0.893	¹⁹⁷ 0.013	¹⁴¹ 0.050	²⁰⁹ 0.176	²⁴³ 0.079	²²⁰ 0.148	¹⁹⁰ 0.996	¹⁸⁷ 0.095	¹¹⁹ 0.367	¹⁴³ 0.372	0.004	0.003	0.156	^{0.002}			
316	VD-003	²³⁴ 0.008	²³¹ 0.022	²²⁷ 0.773	¹⁷⁷ 0.008	¹²⁰ 0.030	¹⁸ 0.137	¹⁹⁴ 0.046	¹⁸ 0.100	²²² 0.999	¹³⁸ 0.051	¹⁰⁴ 0.244	¹³ 0.315	0.003	0.003	0.144	^{0.002}			
317	VERIDAS-001	¹⁶⁷ 0.003	¹⁴⁴ 0.014	¹⁸⁵ 0.550	¹⁵⁹ 0.006	¹²⁴ 0.028	¹⁷ 0.131	¹⁸⁶ 0.037	¹⁵⁶ 0.082	¹⁵⁵ 0.987	¹⁴⁹ 0.044	¹⁰⁶ 0.266	¹¹⁹ 0.264	0.000	0.002	0.093	0.001			
318	VERIDAS-002	¹⁶⁶ 0.003	¹⁴⁵ 0.014	¹⁸⁶ 0.550	¹⁶⁰ 0.006	¹²³ 0.028	¹⁷⁸ 0.131	¹⁸⁷ 0.037	¹⁵³ 0.082	¹⁵⁶ 0.987	¹⁵⁰ 0.044	¹⁰⁷ 0.266	¹¹⁸ 0.264	0.000	0.002	0.093	0.001			
319	VERIDAS-003	¹⁰⁸ 0.002	¹⁰⁰ 0.011	¹³⁴ 0.297	¹²⁰ 0.004	⁹² 0.016	¹⁴³ 0.108	¹²² 0.017	¹¹⁷ 0.055	¹⁹⁷ 0.997	⁹⁶ 0.020	¹⁵¹ 0.180	⁸⁷ 0.178	0.000	0.002	0.093	0.001			
320	VERIDAS-004	⁵⁸ 0.001	⁴⁰ 0.008	¹⁰⁴ 0.186	⁹⁰ 0.003	⁶⁰ 0.009	¹¹⁸ 0.097	⁶⁴ 0.006	⁵⁰ 0.025	¹³⁵ 0.979	⁵⁰ 0.008	³⁶ 0.058	⁴⁶ 0.118	0.000	0.002	0.094	0.001			
321	VERIGRAM-000	¹⁶⁷ 0.003	¹⁶² 0.016	²⁹ 0.064	⁶³ 0.002	⁴⁷ 0.007	¹⁸ 0.052	⁵⁷ 0.005	⁶⁹ 0.028	²¹ 0.221	³² 0.006	⁵⁶ 0.088	¹⁶ 0.083	0.001	0.004	0.046	0.001			
322	VERIJELAS-000	³⁴³ 0.355	³²⁷ 0.369	²⁸⁹ 0.968	²⁴⁷ 0.086	¹⁶² 0.191	²⁴⁶ 0.292	³³⁷ 0.799	³²³ 0.813	²¹⁷ 0.999	²²⁹ 0.324	¹⁴⁹ 0.933	¹⁸² 0.589	0.002	0.001	0.070	^{0.001}			

Table 19: **Miss rates by dataset**: At left, rank 1 miss rates relevant to investigations; at right, with threshold set to target FPIR = 0.01 for higher volume, low prior, uses. Yellow indicates most accurate algorithm. Throughout blue superscripts indicate the rank of the algorithm for that column.

16:19:47
2023/07/05

$FNIR(N, R, D) =$ False neg. identification rate
 $FPIR(N, T) =$ False pos. identification rate

N = Num. enrolled subjects
R = Num. candidates examined

1 ≡ 1_{threshold}

$I \equiv 0 \rightarrow$ Investigation
 $T > 0 \rightarrow$ Identification

#	ALGORITHM	INVESTIGATION MODE										IDENTIFICATION MODE										FAILURE TO EXTRACT FEATURES												
		RANK ONE MISS RATE, FNIR(N, 0, 1)										HIGH T → FPIR = 0.001, FNIR(N, T, L)																						
		N=1.6M					N=1.6M					N=1.6M					N=1.6M					N=1.6M					N=1.6M							
		GALLERY	MUGSHOT	MUGSHOT	WEBCAM	PROFILE	VISA	BORDER	BOR _L 10YR	KIOSK	MUGSHOT	MUGSHOT	WEBCAM	PROFILE	BORDER	BOR _L 10YR	KIOSK	MUGSHOT	MUGSHOT	WEBCAM	PROFILE	BORDER	BOR _L 10YR	KIOSK	MUGSHOT	MUGSHOT	WEBCAM	PROFILE	BORDER	BOR _L 10YR	KIOSK			
323	VIGILANTSOLUTIONS-003	³²¹ 0.069	³¹³ 0.151	²⁷⁷ 0.958							³²¹ 0.408	³¹⁸ 0.660	²¹⁶ 0.999																					
324	VIGILANTSOLUTIONS-004	³²⁹ 0.125	³²¹ 0.244	²⁸⁴ 0.965							³²⁷ 0.549	³²⁵ 0.817	¹⁹³ 0.996																					
325	VIGILANTSOLUTIONS-005	²⁴⁷ 0.009		²⁵⁷ 0.920							³¹⁶ 0.388		²⁶⁸ 1.000																					
326	VIGILANTSOLUTIONS-006	²⁵⁴ 0.010		²⁵⁷ 0.921							³¹¹ 0.353		²⁸⁸ 1.000																					
327	VIGILANTSOLUTIONS-007	¹⁸¹ 0.003	¹⁷⁶ 0.017	²⁶³ 0.925	¹⁹⁵ 0.013	¹⁴⁹ 0.068	²⁰⁷ 0.175	¹⁷² 0.028	¹⁶³ 0.088	¹⁹² 0.996	¹⁸³ 0.081	¹²¹ 0.371	¹⁴⁷ 0.391																					^{0.001}
328	VIGILANTSOLUTIONS-008	¹⁷³ 0.003	¹⁷⁸ 0.017	²⁵⁷ 0.913	¹⁹⁹ 0.014	¹⁵⁰ 0.072	²¹⁰ 0.178	¹⁵⁹ 0.021	¹⁴⁶ 0.077	²¹⁹ 0.999	¹⁹¹ 0.104	¹²⁴ 0.398	¹⁷¹ 0.511																				^{0.001}	
329	VISIONBOX-000	¹²⁰ 0.002	¹⁰² 0.011	²²⁵ 0.752	¹³⁷ 0.005	⁹⁴ 0.017	⁷⁹ 0.078	¹²⁷ 0.018	¹¹⁸ 0.057	¹⁶³ 0.990	¹⁰³ 0.023	⁷⁶ 0.146	⁷⁸ 0.162																			^{0.001}		
330	VISIONLABS-004	¹⁶⁵ 0.003	¹⁹² 0.020	¹⁴⁷ 0.343							²²¹ 0.058	²²⁹ 0.159	¹⁰⁸ 0.890																			^{0.046}		
331	VISIONLABS-005	¹⁵² 0.002	¹⁸⁶ 0.019	¹⁴⁵ 0.334							²⁰⁵ 0.050	²¹⁹ 0.147	⁹⁹ 0.888																			^{0.046}		
332	VISIONLABS-006	¹¹⁰ 0.002	¹⁶⁰ 0.015	¹¹⁷ 0.211	¹¹⁵ 0.004						¹¹⁵ 0.096	¹⁶² 0.027	¹⁶⁷ 0.090	⁶⁹ 0.672																	^{0.051}			
333	VISIONLABS-007	¹⁰⁴ 0.002	¹⁵⁹ 0.015	¹¹¹ 0.211	¹¹¹ 0.004						¹¹⁴ 0.095	¹⁶¹ 0.027	¹⁶⁶ 0.090	⁷⁰ 0.672	¹²⁶ 0.031		⁹² 0.185														^{0.051}			
334	VISIONLABS-008	¹³¹ 0.002	¹³⁸ 0.014	⁹¹ 0.141	⁷⁷ 0.002						⁸³ 0.081	¹⁰⁶ 0.013	¹⁰⁴ 0.051	⁵¹ 0.481	⁸⁸ 0.017		⁶⁹ 0.151													^{0.075}				
335	VISIONLABS-009	³⁴ 0.001	⁵⁰ 0.008	⁶⁷ 0.091	⁴¹ 0.001						⁵⁷ 0.071	⁵² 0.005	⁵² 0.025	⁸⁸ 0.799	⁵⁷ 0.008		⁴³ 0.113														^{0.060}			
336	VISIONLABS-010	⁶⁴ 0.001	⁸³ 0.010	⁴⁷ 0.069	²⁵ 0.001	²⁸ 0.006	⁵⁵ 0.069	⁶⁰ 0.005	⁵⁷ 0.027		⁴⁹ 0.008	³⁴ 0.055	⁴¹ 0.109																^{0.040}					
337	VISIONLABS-011	³⁹ 0.001	⁵⁴ 0.009	³¹ 0.064	³⁰ 0.001	¹⁶ 0.004	⁴⁰ 0.063	³⁶ 0.003	³³ 0.020		²¹ 0.004	²¹ 0.034	²⁰ 0.090																^{0.032}					
338	VIXVIZION-009	¹⁴⁵ 0.002	¹²⁵ 0.013	¹¹⁴ 0.220	¹³⁶ 0.005	¹³¹ 0.031	¹⁴⁴ 0.107	¹⁶⁵ 0.027	¹⁴⁵ 0.077	⁷⁹ 0.745	¹⁴⁶ 0.041	¹¹⁰ 0.286	¹⁶⁴ 0.472																^{0.000}					
339	VNPPT-001	¹³⁷ 0.002	¹⁵⁰ 0.014	⁹¹ 0.145	⁸⁷ 0.002	¹¹¹ 0.023	⁵⁹ 0.071	¹¹¹ 0.014	¹³⁴ 0.068	⁷⁶ 0.718	¹³⁶ 0.035	¹⁵⁴ 0.990	¹⁴¹ 0.362															^{0.042}						
340	VNPPT-002	¹¹⁶ 0.002	¹²⁰ 0.012	⁴⁷ 0.068	²⁶ 0.001	³² 0.006	²² 0.054	⁷⁰ 0.007	⁶⁷ 0.032	³¹ 0.292	⁴⁹ 0.007	²⁶ 0.096																^{0.042}						
341	VNPPT-003	⁸⁹ 0.002									⁶⁸ 0.006																		^{0.041}					
342	VOCORD-003	²²¹ 0.006	²²³ 0.024	²³⁵ 0.804	²⁴³ 0.061			²¹⁴ 0.188	²⁶⁷ 0.122	²²⁵ 0.155	²⁰⁷ 0.998	²⁰⁸ 0.157	¹⁵⁰ 0.404																^{0.425}					
343	VOCORD-004	²³⁷ 0.008	¹⁹⁹ 0.021	²²⁷ 0.792	¹⁹⁵ 0.012			¹⁷⁴ 0.127	³¹² 0.355	²³⁵ 0.173	²⁵⁶ 1.000	²¹⁸ 0.193	²⁴⁵ 0.991																^{0.000}					
344	VOCORD-005	²³¹ 0.007	²¹⁷ 0.023	²³⁷ 0.812	²³⁹ 0.055			²¹⁹ 0.206	²⁸¹ 0.158	²⁰⁸ 0.130	¹⁹⁹ 0.997	²⁰² 0.138	¹⁴⁴ 0.381															^{0.554}						
345	VOCORD-006	³⁵⁵ 1.000	³⁵⁶ 1.000	³¹⁷ 1.000	³²⁵ 1.000			³⁴⁶ 1.000	³⁵⁴ 1.000	³⁵⁶ 1.000	²⁹⁴ 1.000	²⁹³ 1.000	³³³ 1.000															^{0.554}						
346	VTCC-000	²⁰⁰ 0.004									²²⁴ 0.059																	^{0.000}						
347	VTS-000	³⁵¹ 0.594	³⁴¹ 0.608	²⁵³ 0.909	²⁶⁷ 0.607	¹⁷⁰ 0.724	²⁶⁶ 0.739	³³⁰ 0.598	³¹³ 0.619	²⁵⁹ 0.999	²⁵³ 0.613	¹⁴⁰ 0.760	²⁰³ 0.761														^{0.047}							
348	VTS-001	⁸² 0.002	⁷⁴ 0.010	¹⁰⁷ 0.167	¹⁵² 0.006	⁹⁷ 0.018	⁷⁵ 0.077	¹⁰⁷ 0.013	¹⁰³ 0.051	¹⁷⁴ 0.994	¹⁰⁴ 0.022	⁷³ 0.141	⁹⁵ 0.192														^{0.040}							
349	VTS-002	¹²¹ 0.002	¹³⁰ 0.013	¹¹⁷ 0.233	²⁰⁷ 0.014	¹³⁷ 0.038	¹⁶⁹ 0.125	¹⁵⁷ 0.026	¹⁴³ 0.075	²³⁹ 1.000	¹⁵⁹ 0.045	¹⁰² 0.231	¹⁵² 0.417													^{0.029}								
350	VTS-003	³⁶ 0.001	²⁵ 0.007	⁵¹ 0.074	⁵¹ 0.002	⁵⁷ 0.009	¹⁹ 0.053	⁷⁵ 0.007	⁷¹ 0.033	²⁶² 1.000	⁷⁹ 0.014	¹⁵¹ 0.954	¹⁸⁸ 0.635												^{0.029}									
351	XFORWARDAI-000	¹⁴⁶ 0.002	¹⁴¹ 0.014	⁶¹ 0.089	¹¹⁷ 0.004	⁸⁷ 0.015	¹¹² 0.094	¹¹⁷ 0.015	¹¹² 0.053	⁴³ 0.440	¹⁰³ 0.021	⁸³ 0.159	⁸¹ 0.169													^{0.000}								
352	XFORWARDAI-001	¹³⁴ 0.002	¹²³ 0.013	³¹ 0.067	⁹⁸ 0.003	⁵⁸ 0.009	⁸⁸ 0.082	⁵⁶ 0.005	⁶¹ 0.028	⁴⁴ 0.448	³⁵ 0.008	⁴¹ 0.062	⁴⁹ 0.123												^{0.000}									
353	XFORWARDAI-002	¹²⁴ 0.002	¹¹⁵ 0.012	¹⁴ 0.059	⁸⁵ 0.002	³⁶ 0.007	⁷³ 0.077	³⁴ 0.003	²⁵ 0.016	⁵³ 0.525	²⁵ 0.005	²⁴ 0.041	³² 0.099												^{0.000}									
354	YISHENG-001	²⁹⁸ 0.027	²⁸⁵ 0.060	²⁴² 0.058			²⁴³ 0.287	³⁰⁹ 0.346	³²² 0.808		²⁵⁶ 0.666		²²⁸ 0.919												^{0.005}									
355	YITU-002	¹¹² 0.002	⁷⁸ 0.010							¹²⁵ 0.018	⁹⁸ 0.049													^{0.000}										
356	YITU-003	¹⁷² 0.003	¹⁶⁶ 0.016							¹³³ 0.019	¹⁰⁷ 0.052												^{0.003}											
357	YITU-004	⁵² 0.001	⁴⁸ 0.008	²⁴⁷ 0.866						⁸⁸ 0.010	³⁵ 0.027	¹⁰⁹ 0.936											^{0.000}											
358	YITU-005	¹⁴⁸ 0.002	¹⁵² 0.014							⁹⁵ 0.010	⁶⁹ 0.032												^{0.003}											

Table 20: **Miss rates by dataset:** At left, rank 1 miss rates relevant

#	ALGORITHM	MISSES BELOW THRESHOLD, T	ENROL, MOST RECENT			
		DATASET: FRVT 2018 MUGSHOTS				
		N=0.64M	N=1.6M	N=3.0M	N=6.0M	N=12.0M
1	3DIVI-005	²⁸⁶ 0.1358	²⁸⁶ 0.1664	²⁵³ 0.1915	²⁴³ 0.2370	²³³ 0.3054
2	ACER-000	²⁷⁹ 0.1185	²⁷⁸ 0.1455	²⁴⁷ 0.1714	²³⁶ 0.2074	²²⁸ 0.2537
3	ADVANCE-000	¹⁵ 0.0142	¹³⁷ 0.0199	¹³ 0.0246	¹³¹ 0.0404	¹³ 0.1282
4	AFISBIOMETRICS-000	¹⁷³ 0.0204	¹⁷⁴ 0.0298	¹⁷⁰ 0.0381	¹⁶⁸ 0.0562	¹¹⁵ 0.1176
5	ALCHERA-003	²⁷ 0.1176	²⁸⁰ 0.1553	²⁴⁹ 0.1853	²⁴⁴ 0.2409	²⁴ 0.3553
6	ALLGOVISION-000	²⁵¹ 0.0688	²⁵² 0.0881	²³⁰ 0.1084	²²¹ 0.1389	²⁰⁸ 0.2129
7	ALLGOVISION-001	²⁵ 0.0785	²⁵⁷ 0.1017	²³⁷ 0.1218	²²⁸ 0.1584	²¹ 0.2273
8	ANKE-000	²⁸⁴ 0.0942	²⁶² 0.1169	²⁴² 0.1404	²³³ 0.1776	²²⁹ 0.2559
9	ANKE-002	¹⁷ 0.0229	¹⁷⁹ 0.0318	¹⁷ 0.0406	¹⁶⁹ 0.0605	¹⁵ 0.1466
10	ARMATURA-000	⁵³ 0.0034	⁴⁸ 0.0043	⁴³ 0.0055	³⁴ 0.0099	²³ 0.0616
11	AWARE-003	²⁷ 0.1098	²⁷⁰ 0.1283	²⁴⁷ 0.1447	²³¹ 0.1768	²² 0.2364
12	AWARE-005	³¹⁵ 0.3389	³¹³ 0.3643	²⁶⁰ 0.3993	²⁵² 0.4526	²²⁷ 0.2531
13	AYONIX-002	³⁴ 0.7862	³⁴⁰ 0.8242	²⁶ 0.8508	²⁸ 0.8704	²⁵ 0.8939
14	CAMVI-004	²⁰⁶ 0.0367	²³⁶ 0.0716	²²³ 0.0983	²⁴⁶ 0.2508	²³² 0.2701
15	CANON-001	⁶² 0.0039	⁶² 0.0054	⁶¹ 0.0074	⁵⁶ 0.0158	⁶⁰ 0.0924
16	CANON-002	⁵⁵ 0.0036	⁵³ 0.0047	⁵⁴ 0.0061	⁴⁶ 0.0124	⁴⁵ 0.0808
17	CIB-000	⁹⁹ 0.0086	¹⁰³ 0.0125	¹⁰⁸ 0.0160	¹⁰⁶ 0.0303	¹² 0.1251
18	CLEARVIEWAI-000	⁶⁴ 0.0040	⁶⁵ 0.0058	⁶⁵ 0.0078	⁵⁸ 0.0159	⁷⁰ 0.0971
19	CLOUDWALK-HR-000	² 0.0019	²¹ 0.0020	¹⁷ 0.0023	²³ 0.0072	³⁰ 0.0701
20	CLOUDWALK-MT-000	²² 0.0019	²⁰ 0.0020	¹⁸ 0.0022	⁹ 0.0049	¹³ 0.0466
21	CLOUDWALK-MT-001	¹⁷ 0.0018	¹⁷ 0.0019	¹⁵ 0.0020	¹¹ 0.0052	²⁰ 0.0555
22	CLOUDWALK-MT-002	²⁰ 0.0018	¹⁵ 0.0019	¹⁰ 0.0019	¹⁰ 0.0051	²² 0.0587
23	COGENT-000	²²⁴ 0.0430	²⁰⁸ 0.0527	²⁰⁸ 0.0695	²⁰⁷ 0.1133	¹⁹⁷ 0.1960
24	COGENT-001	²² 0.0430	²⁰⁹ 0.0527	²⁰⁹ 0.0695	²⁰⁶ 0.1133	¹⁹ 0.1960
25	COGENT-002	¹⁹² 0.0322	¹⁹⁵ 0.0444	¹⁹² 0.0610	²⁰⁴ 0.1116	²¹⁰ 0.2180
26	COGENT-003	¹⁹³ 0.0328	²⁰⁰ 0.0463	²⁰⁴ 0.0683	²¹⁴ 0.1294	²² 0.2445
27	COGENT-004	¹⁷⁶ 0.0210	¹⁸⁰ 0.0331	¹⁸⁷ 0.0527	²⁰⁹ 0.1138	²⁰⁷ 0.2119
28	COGENT-005	⁸⁸ 0.0064	⁸⁶ 0.0091	⁸⁸ 0.0123	¹⁰⁵ 0.0303	¹² 0.1233
29	COGENT-006	⁴⁸ 0.0032	⁴⁹ 0.0044	⁴⁸ 0.0057	⁴¹ 0.0120	⁴⁷ 0.0830
30	COGENT-007	³⁶ 0.0028	³⁸ 0.0036	⁴⁶ 0.0049	³⁷ 0.0111	³⁷ 0.0756
31	COGNITEC-000	²⁸⁸ 0.1377	²⁸⁴ 0.1606	²⁵⁹ 0.1870	²³⁸ 0.2176	²³⁴ 0.2831
32	COGNITEC-001	²⁵⁹ 0.0807	²⁵⁸ 0.1017	²⁵⁶ 0.1214	²²⁴ 0.1513	²¹³ 0.2238
33	COGNITEC-002	²¹⁷ 0.0406	²¹¹ 0.0531	²⁰⁰ 0.0666	¹⁹² 0.0935	¹⁹² 0.1874
34	COGNITEC-003	²¹⁴ 0.0400	²⁰⁷ 0.0526	¹⁹⁵ 0.0650	¹⁸⁷ 0.0895	¹⁸⁵ 0.1772
35	COGNITEC-004	¹⁷⁸ 0.0222	¹⁷⁸ 0.0313	¹⁷⁷ 0.0388	¹⁵⁹ 0.0540	⁹⁸ 0.1103
36	COGNITEC-005	⁸⁵ 0.0063	⁸⁹ 0.0096	⁹⁴ 0.0144	⁹⁹ 0.0287	⁶⁸ 0.0967
37	COGNITEC-006	⁷ 0.0053	⁷⁸ 0.0077	⁸⁰ 0.0117	⁸⁵ 0.0254	⁶¹ 0.0919
38	CYBERLINK-000	²¹⁹ 0.0414	²¹⁹ 0.0565	²¹¹ 0.0707	²⁰⁸ 0.1031	²⁰³ 0.2050
39	CYBERLINK-001	²¹⁰ 0.0392	²¹² 0.0536	²⁰⁸ 0.0695	¹⁹⁷ 0.0973	¹⁸⁷ 0.1794
40	CYBERLINK-002	¹¹² 0.0105	¹¹⁵ 0.0148	¹¹⁸ 0.0202	¹²⁹ 0.0399	¹²⁶ 0.1255
41	CYBERLINK-003	²⁸ 0.0056	²⁹ 0.0077	⁷¹ 0.0100	⁸¹ 0.0235	¹²⁷ 0.1237
42	CYBERLINK-004	²⁷ 0.0051	⁷⁴ 0.0071	⁷⁷ 0.0102	⁶⁹ 0.0199	¹² 0.1269
43	CYBERLINK-005	⁹⁰ 0.0067	⁹³ 0.0099	⁹² 0.0138	¹²⁶ 0.0394	¹⁷⁰ 0.1566
44	DAHUA-001	²⁴ 0.0569	²³⁸ 0.0727	²¹⁹ 0.0878	²¹⁰ 0.1148	¹⁹ 0.1867
45	DAHUA-002	¹¹⁷ 0.0108	¹¹⁶ 0.0151	¹¹³ 0.0191	¹⁰¹ 0.0291	¹¹⁰ 0.1153
46	DAHUA-003	¹⁰ 0.0100	¹⁰⁹ 0.0139	¹⁰⁸ 0.0180	¹⁰² 0.0296	¹⁰ 0.1130
47	DAHUA-004	⁷⁰ 0.0048	⁷³ 0.0069	⁷⁰ 0.0090	⁶¹ 0.0164	⁴⁸ 0.0853
48	DAON-000	¹⁴ 0.0161	¹⁴⁸ 0.0226	¹⁴⁷ 0.0293	¹⁶⁷ 0.0562	¹⁷ 0.1702
49	DECATUR-000	¹⁵¹ 0.0173	¹⁵¹ 0.0229	¹⁴⁸ 0.0305	¹⁴¹ 0.0464	¹⁵³ 0.1433
50	DEEGLINT-001	³⁰ 0.0027	³⁷ 0.0033	³⁶ 0.0043	⁴³ 0.0121	⁶ 0.0922
51	DEEPSSEA-001	²⁰² 0.0347	¹⁹⁹ 0.0462	¹⁹¹ 0.0586	¹⁸⁸ 0.0802	¹⁸¹ 0.1708
52	DERMALOG-005	²⁵ 0.0700	²⁵¹ 0.0880	²⁵⁸ 0.1144	²²⁷ 0.1578	²² 0.2451
53	DERMALOG-006	²¹¹ 0.0395	²⁰⁶ 0.0517	¹⁹⁶ 0.0659	¹⁹⁶ 0.0973	¹⁸⁴ 0.1745
54	DERMALOG-007	²⁵² 0.0691	²⁴⁹ 0.0863	²³¹ 0.1107	²²³ 0.1504	²¹⁸ 0.2299
55	DERMALOG-008	¹⁹⁸ 0.0338	¹⁹⁷ 0.0455	¹⁹¹ 0.0626	²⁰¹ 0.1060	²¹⁰ 0.2276
56	DERMALOG-009	¹⁴⁰ 0.0148	¹⁴⁰ 0.0206	¹³⁸ 0.0268	¹³⁴ 0.0416	¹⁴⁵ 0.1374
57	DERMALOG-010	⁷¹ 0.0052	⁷² 0.0069	⁶⁹ 0.0088	⁷¹ 0.0207	⁷¹ 0.0971
58	DERMALOG-011	¹⁴² 0.0149	¹⁴³ 0.0215	¹⁴⁴ 0.0279	¹⁴⁰ 0.0461	¹¹⁸ 0.1192
59	DILUSENSE-000	¹⁷⁵ 0.0208	¹⁷⁶ 0.0305	¹⁶⁹ 0.0377	¹⁶³ 0.0543	¹⁵ 0.1429
60	DILUSENSE-001	⁸¹ 0.0061	⁸² 0.0085	⁷⁹ 0.0109		¹¹² 0.1161
61	FIRSTCREDITKZ-001	³¹ 0.0023	³³ 0.0030	³⁶ 0.0039	³¹ 0.0093	³⁸ 0.0760
62	FUJITSULAB-000	¹⁴¹ 0.0148	¹⁴¹ 0.0206	¹⁴² 0.0277	¹⁶¹ 0.0541	¹⁸³ 0.1739
63	FUJITSULAB-001	¹² 0.0126	¹²⁹ 0.0182	¹³⁰ 0.0251	¹⁷² 0.0646	²⁰ 0.2079
64	GORILLA-002	²⁹² 0.1539	²⁹² 0.1880	²⁵⁸ 0.2184	²⁴⁷ 0.2596	²⁴² 0.3398
65	GORILLA-004	²⁵⁴ 0.0699	²⁵⁴ 0.0892	²²⁹ 0.1048	²¹⁹ 0.1370	²⁰ 0.1969
66	GORILLA-005	²²⁰ 0.0453	²²³ 0.0583	²¹⁰ 0.0704	¹⁹⁸ 0.0974	¹⁵ 0.1474
67	GORILLA-006	¹⁶⁶ 0.0196	¹⁶⁶ 0.0275	¹⁵⁸ 0.0331	¹⁵¹ 0.0516	¹⁰¹ 0.1113
68	GORILLA-007	¹⁶³ 0.0190	¹⁶⁴ 0.0271	¹⁶¹ 0.0348	¹⁵⁵ 0.0520	¹⁰ 0.1129
69	GORILLA-008	¹⁵⁰ 0.0170	¹⁵² 0.0238	¹⁴⁹ 0.0308	¹⁴² 0.0469	¹⁰² 0.1120
70	GRIAULE-000	¹⁵ 0.0145	¹³⁸ 0.0201	¹³⁴ 0.0253	¹³² 0.0407	¹⁵ 0.1440
71	GRIAULE-001	⁵⁰ 0.0033	⁵⁴ 0.0047	⁵⁶ 0.0064	⁵⁴ 0.0153	⁵⁷ 0.0910
72	HIK-003	²⁶⁰ 0.0828	²⁵⁹ 0.1028	²³⁹ 0.1202	²²⁶ 0.1525	²² 0.2480

Table 21: **Identification-mode: Effect of N on FNIR at high threshold.** Values are threshold-based miss rates i.e. FNIR at FPIR = 0.001 for five enrollment population sizes, N. The right six columns apply for enrollment of one image. Missing entries usually apply because another algorithm from the same developer was run instead. Some developers are missing because less accurate algorithms were not run on galleries with $N \geq 3\,000\,000$. Throughout blue superscripts indicate the rank of the algorithm for that column.

#	ALGORITHM	MISSES BELOW THRESHOLD, T		ENROL MOST RECENT					
		FNIR(N, T > 0, R > L)		DATASET: FRVT 2018 MUGSHOTS					
73	HIK-004	²⁵⁸ 0.0796	²⁵⁵ 0.0988	²³³ 0.1147	²²² 0.1474	²²⁶ 0.2483			
74	HIK-005	¹⁹⁰ 0.0312	¹⁹² 0.0436	¹⁹⁴ 0.0560	¹⁸⁹ 0.0911	²⁰⁹ 0.2129			
75	HYPERVERGE-001	⁴⁹ 0.0033	⁵⁰ 0.0045	⁵⁰ 0.0059	³⁸ 0.0117	⁵¹ 0.0872			
76	HYPERVERGE-002	⁴⁰ 0.0028	³⁹ 0.0037	³⁷ 0.0046	¹⁸ 0.0064	¹⁷ 0.0538			
77	HYPERVERGE-003	⁷⁷ 0.0055	⁷⁶ 0.0074	⁷³ 0.0100	⁶⁸ 0.0189	⁷⁴ 0.0986			
78	HZAILU-000	¹³⁴ 0.0143	¹³⁶ 0.0197	¹³⁴ 0.0255	¹³³ 0.0411	¹¹¹ 0.1174			
79	HZAILU-001	⁸⁹ 0.0066	⁸³ 0.0086	⁷⁸ 0.0109	⁷² 0.0207	⁹⁰ 0.1052			
80	HZAILU-002	⁸² 0.0061	⁸⁰ 0.0080	⁷⁹ 0.0101	⁶⁶ 0.0187	³⁹ 0.0914			
81	HZAILU-003	⁸⁰ 0.0060	⁸¹ 0.0082	⁸⁰ 0.0111	⁶⁴ 0.0183	⁶⁹ 0.0969			
82	IDEMIA-003	²⁰⁰ 0.0346	²⁰² 0.0471	²²⁰ 0.0892	²⁴⁹ 0.2789	²⁴⁶ 0.4311			
83	IDEMIA-004	¹⁸⁹ 0.0300	¹⁸⁸ 0.0373	¹⁷⁹ 0.0447	¹⁷⁰ 0.0617	¹⁷⁸ 0.1635			
84	IDEMIA-005	²⁰⁵ 0.0360	¹⁹⁴ 0.0440	¹⁸⁸ 0.0537	¹⁸⁴ 0.0764	¹⁹³ 0.1915			
85	IDEMIA-006	²⁰³ 0.0351	¹⁹¹ 0.0433	¹⁸⁶ 0.0525	¹⁸⁰ 0.0734	²¹¹ 0.2201			
86	IDEMIA-007	¹³⁰ 0.0136	¹²⁸ 0.0181	¹²⁰ 0.0228	¹¹⁸ 0.0357	¹⁴⁹ 0.1402			
87	IDEMIA-008	¹² 0.0016	¹⁶ 0.0019	¹⁷ 0.0024	¹² 0.0053	¹⁴ 0.0470			
88	IDEMIA-009	⁸ 0.0013	⁹ 0.0016	⁷ 0.0018	¹⁷ 0.0061	¹⁹ 0.0550			
89	IDEMIA-010	² 0.0010	¹ 0.0011	¹ 0.0012	² 0.0027	¹ 0.0193			
90	IMAGUS-005	¹³¹ 0.0137	¹³² 0.0185	¹²⁹ 0.0237	¹²⁰ 0.0368	⁹³ 0.1067			
91	IMAGUS-006	¹³² 0.0137	¹³⁵ 0.0190	¹³⁰ 0.0244	¹²⁷ 0.0396	¹¹¹ 0.1159			
92	IMAGUS-007	¹⁴⁶ 0.0160	¹⁵⁰ 0.0228	¹⁴⁵ 0.0284	¹³⁷ 0.0444	¹¹⁰ 0.1179			
93	IMPERIAL-000	¹⁵⁹ 0.0187	¹⁵⁸ 0.0259	¹⁶⁷ 0.0358	¹⁷⁹ 0.0733	¹⁸⁷ 0.1794			
94	INCODE-003	²⁸ 0.1324	²⁸ 0.1672	²⁵ 0.1961	²¹ 0.2345	²³ 0.3123			
95	INCODE-004	²¹⁵ 0.0403	²¹⁵ 0.0538	¹⁹⁹ 0.0662	¹⁹¹ 0.0917	¹⁷⁵ 0.1619			
96	INCODE-005	⁹⁷ 0.0083	⁹⁷ 0.0113	⁹⁶ 0.0145	⁸² 0.0247	⁹⁸ 0.0912			
97	INNOVATRICS-007	¹⁰⁴ 0.0093	¹⁰⁵ 0.0125	¹⁰¹ 0.0159	⁸⁷ 0.0259	⁹⁴ 0.1092			
98	INNOVATRICS-008	⁵⁸ 0.0037	⁵⁹ 0.0050	⁵⁶ 0.0066	⁷⁰ 0.0206	⁹⁹ 0.1093			
99	INSPUR-000	⁶⁸ 0.0045	⁶⁹ 0.0064	⁶⁸ 0.0086	⁶⁵ 0.0185	⁷² 0.0981			
100	INTEMA-000	²⁸ 0.0019	²⁴ 0.0024	²⁶ 0.0032	³² 0.0098	³⁸ 0.0745			
101	INTEMA-001	⁹ 0.0014	⁶ 0.0014	¹⁶ 0.0023	²² 0.0071	²⁸ 0.0678			
102	INTSYSMSU-000	³³¹ 0.9982	³⁴⁹ 0.9984	²⁷¹ 0.9985	²⁵¹ 0.9987	²⁵⁴ 0.9988			
103	IREX-000	¹⁶⁴ 0.0190	¹⁷⁰ 0.0280	¹⁷³ 0.0391	¹⁷⁵ 0.0677	¹⁶⁰ 0.1479			
104	ISYSTEMS-002	²⁴² 0.0584	²⁴² 0.0783	²²⁸ 0.0973	²²⁰ 0.1373	²¹⁷ 0.2295			
105	ISYSTEMS-003	²² 0.0438	²²⁵ 0.0590	²¹⁷ 0.0807	²¹² 0.1259	²¹⁹ 0.2357			
106	KAKAO-000	¹¹⁸ 0.0109	¹¹⁶ 0.0151	¹¹⁵ 0.0196	¹¹² 0.0324	⁸⁰ 0.1010			
107	KAKAO-001	²⁸ 0.0021	²⁸ 0.0026	²⁷ 0.0032	²⁸ 0.0085	²⁹ 0.0693			
108	KEDACOM-001	¹⁵⁴ 0.0181	¹⁴⁹ 0.0227	¹³⁶ 0.0265	¹⁴⁰ 0.0422	¹⁴⁰ 0.1340			
109	KNOWUTECH-000	⁸⁷ 0.0065	⁸⁷ 0.0093	⁸⁴ 0.0121	⁷⁵ 0.0217	⁷³ 0.0985			
110	LINECLOVA-002	³⁹ 0.0028	⁴¹ 0.0040	³⁹ 0.0049	⁴² 0.0120	⁴⁵ 0.0824			
111	LINECLOVA-003	³⁵ 0.0026	³⁰ 0.0026	³⁸ 0.0049	³⁷ 0.0158	²⁹ 0.0989			
112	LOOKMAN-003	²⁰¹ 0.0346	¹⁹³ 0.0437	¹⁸⁴ 0.0514	¹⁷⁸ 0.0724	¹⁷⁶ 0.1620			
113	LOOKMAN-005	¹⁸ 0.0240	¹⁷⁵ 0.0301	¹⁶⁸ 0.0356	¹⁵⁰ 0.0512	¹⁵⁹ 0.1334			
114	MANTRA-000	⁸⁸ 0.0065	⁹⁴ 0.0101	⁹⁶ 0.0151	¹⁰⁷ 0.0308	⁸⁶ 0.1035			
115	MAXVISION-000	¹⁷⁴ 0.0206	¹⁷¹ 0.0282	¹⁶³ 0.0355	¹⁵² 0.0517	¹⁴¹ 0.1340			
116	MAXVISION-001	⁴⁵ 0.0031	⁴⁷ 0.0043	⁴² 0.0055	⁴⁴ 0.0122	⁵⁶ 0.0895			
117	MAXVISION-002	⁴ 0.0030	⁴⁰ 0.0039	⁴¹ 0.0051	⁴⁵ 0.0123	⁶⁹ 0.0949			
118	MEGVII-001	²⁵⁸ 0.0562	²⁵⁷ 0.0722	²¹⁸ 0.0872	²¹⁶ 0.1309	²³³ 0.2713			
119	MEGVII-003	²⁸ 0.0021	²⁶ 0.0025	²⁵ 0.0032	²⁹ 0.0085	⁴⁹ 0.0784			
120	MICROFOCUS-005	³⁴⁸ 0.9732	³⁴² 0.8354	²⁶⁸ 0.8555	²⁵⁹ 0.8755	²⁵³ 0.8954			
121	MICROSOFT-003	¹⁶ 0.0198	¹⁶⁸ 0.0278	¹⁶⁵ 0.0356	¹⁵⁸ 0.0538	¹⁶⁰ 0.1539			
122	MICROSOFT-004	¹⁵⁷ 0.0185	¹⁵⁹ 0.0259	¹⁵⁸ 0.0333	¹⁵³ 0.0517	¹⁶⁴ 0.1510			
123	MICROSOFT-005	¹⁵⁵ 0.0181	¹⁵⁶ 0.0256	¹⁵⁷ 0.0320	¹⁴⁹ 0.0512	¹⁶² 0.1491			
124	MICROSOFT-006	¹⁰² 0.0091	⁹⁹ 0.0120	¹⁰³ 0.0162	¹⁰⁴ 0.0301	¹⁰ 0.1482			
125	MUKH-002	³²⁹ 0.5041	³²⁹ 0.5942	²⁶⁵ 0.6674	²⁵⁶ 0.7314	²⁵¹ 0.8276			
126	NEC-000	²⁴⁶ 0.0637	²⁴⁴ 0.0789	²²⁸ 0.0933	²¹¹ 0.1163	¹⁹⁹ 0.1941			
127	NEC-001	²⁶¹ 0.0863	²⁶¹ 0.1055	²³⁸ 0.1249	²²⁵ 0.1519	²¹⁴ 0.2253			
128	NEC-002	²⁷ 0.0020	²⁷ 0.0026	²⁵ 0.0033	³⁰ 0.0135	²⁹ 0.0653			
129	NEC-003	²⁷ 0.0021	²³ 0.0024	²⁵ 0.0028	¹⁵ 0.0059	¹⁸ 0.0540			
130	NEC-004	⁷ 0.0017	¹² 0.0018	¹¹ 0.0020	⁶ 0.0037	⁸ 0.0329			
131	NEC-005	¹¹ 0.0015	¹⁰ 0.0017	⁹ 0.0019	¹⁹ 0.0065	⁶ 0.0307			
132	NEC-006	¹⁸ 0.0018	¹⁸ 0.0020	²⁹ 0.0026	³⁵ 0.0103	²¹ 0.0573			
133	NEC-007	⁶ 0.0013	⁴ 0.0013	³ 0.0015	³ 0.0029	⁴ 0.0268			
134	NEUROTECHNOLOGY-003	³³² 0.5698	³³³ 0.6362	²⁶⁶ 0.7035	²⁵⁷ 0.7602	²⁵⁰ 0.8224			
135	NEUROTECHNOLOGY-004	²³¹ 0.0466	²³⁰ 0.0629	²¹⁸ 0.0779	²⁰⁸ 0.1135	²⁰⁶ 0.2102			
136	NEUROTECHNOLOGY-005	²¹² 0.0396	²¹⁶ 0.0538	²⁰² 0.0675	¹⁹⁵ 0.0950	¹⁹⁹ 0.1966			
137	NEUROTECHNOLOGY-007	²²⁰ 0.0436	²²⁹ 0.0623	²¹⁷ 0.0802	²¹⁷ 0.1320	²²¹ 0.2393			
138	NEUROTECHNOLOGY-008	¹⁹⁹ 0.0339	²¹⁰ 0.0530	²²¹ 0.0893	²³² 0.1769	²⁴⁰ 0.3288			
139	NEUROTECHNOLOGY-009	¹¹⁸ 0.0108	¹¹⁹ 0.0152	¹¹⁸ 0.0196	¹¹⁰ 0.0324	⁹⁷ 0.1102			
140	NEUROTECHNOLOGY-010	⁹³ 0.0069	⁹² 0.0099	⁹² 0.0138	¹³⁹ 0.0449	¹⁸² 0.1727			
141	NEUROTECHNOLOGY-012	⁶⁹ 0.0047	⁷¹ 0.0068	⁷² 0.0097	⁹¹ 0.0265	¹⁴³ 0.1343			
142	NEUROTECHNOLOGY-013	⁴¹ 0.0029	⁴⁶ 0.0043	⁴⁹ 0.0057	⁷³ 0.0208	¹¹⁹ 0.1202			
143	NOTIONTAG-000	¹²³ 0.0128	¹²³ 0.0175	¹²¹ 0.0228	¹¹⁹ 0.0357	¹³⁰ 0.1270			
144	NTECHLAB-003	²²¹ 0.0421	²¹⁴ 0.0537	²⁰¹ 0.0674	¹⁸⁸ 0.0907	¹⁷² 0.1582			

Table 22: Identification-mode: Effect of N on FNIR at high threshold. Values are threshold-based miss rates i.e. FNIR at FPIR = 0.001 for five enrollment population sizes, N. The right six columns apply for enrollment of one image. Missing entries usually apply because another algorithm from the same developer was run instead. Some developers are missing because less accurate algorithms were not run on galleries with $N \geq 3\,000\,000$. Throughout blue superscripts indicate the rank of the algorithm for that column.

MISSES BELOW THRESHOLD, T FNIR(N, T > 0, R > L)		ENROL MOST RECENT DATASET: FRVT 2018 MUGSHOTS				
#	ALGORITHM	N=0.64M	N=1.6M	N=3.0M	N=6.0M	N=12.0M
145	NTechLab-004	¹⁹¹ 0.0312	¹⁸⁹ 0.0405	¹⁸⁸ 0.0519	¹⁷⁷ 0.0722	¹⁶³ 0.1503
146	NTechLab-005	¹⁹⁵ 0.0334	¹⁹⁰ 0.0424	¹⁸⁹ 0.0537	¹⁸³ 0.0760	¹⁶⁹ 0.1543
147	NTechLab-006	¹⁸⁷ 0.0288	¹⁸⁴ 0.0367	¹⁸² 0.0471	¹⁷⁴ 0.0670	¹⁶⁵ 0.1523
148	NTechLab-007	¹⁶¹ 0.0188	¹⁵⁵ 0.0256	¹⁵¹ 0.0317	¹⁴⁷ 0.0495	¹³⁴ 0.1306
149	NTechLab-008	¹¹⁴ 0.0107	¹¹² 0.0145	¹¹¹ 0.0187	⁹⁸ 0.0286	⁷⁸ 0.0995
150	NTechLab-009	⁵⁷ 0.0037	⁵⁸ 0.0049	⁵⁶ 0.0062	⁴⁷ 0.0125	³⁴ 0.0735
151	NTechLab-010	²⁴ 0.0020	²⁵ 0.0025	²³ 0.0030	²⁶ 0.0077	³² 0.0710
152	NTechLab-011	³⁰ 0.0022	³² 0.0030	³² 0.0038	²⁴ 0.0075	²⁴ 0.0625
153	OMNIGARDE-000	⁴⁶ 0.0032	⁴⁵ 0.0042	⁴⁸ 0.0055	⁴⁹ 0.0131	⁵⁴ 0.0879
154	PANGIAM-000	⁶⁶ 0.0042	⁶⁶ 0.0060	⁶⁵ 0.0080	⁵⁹ 0.0160	⁵³ 0.0876
155	PANGIAM-001	¹⁰⁸ 0.0098	⁹⁸ 0.0113	⁸⁹ 0.0134	⁷⁷ 0.0232	⁵⁹ 0.0865
156	PARAVISION-003	¹⁸³ 0.0260	¹⁸² 0.0351	¹⁸⁰ 0.0447	¹⁷³ 0.0657	¹⁷⁷ 0.1630
157	PARAVISION-004	⁹³ 0.0074	⁹⁶ 0.0101	⁹¹ 0.0136	⁹² 0.0267	¹² 0.1256
158	PARAVISION-005	⁴⁷ 0.0032	⁴⁴ 0.0041	⁴⁷ 0.0057	⁶³ 0.0174	⁸⁷ 0.1037
159	PARAVISION-007	⁴² 0.0030	⁴² 0.0040	⁴⁴ 0.0055	⁷⁴ 0.0211	⁹⁶ 0.1097
160	PARAVISION-009	²⁵ 0.0020	²⁹ 0.0026	³¹ 0.0038	³³ 0.0098	⁴⁹ 0.0857
161	PARAVISION-012	⁷ 0.0013	⁸ 0.0015	⁹ 0.0018	²⁰ 0.0065	³⁹ 0.0770
162	PARAVISION-014	⁴ 0.0012	⁷ 0.0014	⁶ 0.0017	¹⁶ 0.0060	³⁵ 0.0720
163	PIXELALL-002	²⁴⁶ 0.0716	²⁶⁰ 0.1052	²⁴⁸ 0.1475	²⁴⁵ 0.2489	²⁴⁵ 0.3904
164	PIXELALL-003	¹⁴⁵ 0.0158	¹⁴⁵ 0.0218	¹⁴⁶ 0.0288	¹⁴³ 0.0474	¹⁰⁵ 0.1138
165	PIXELALL-004	¹²⁶ 0.0129	¹³¹ 0.0183	¹³¹ 0.0245	¹²¹ 0.0378	¹⁴⁶ 0.1375
166	PIXELALL-005	¹⁰⁰ 0.0087	¹⁰¹ 0.0121	¹⁰⁸ 0.0171	⁸⁴ 0.0250	⁸⁹ 0.1052
167	PTAKURATSATU-000	¹⁸⁴ 0.0275	¹⁸³ 0.0366	¹⁸¹ 0.0458	¹⁵⁶ 0.0523	¹⁶ 0.0523
168	QNAP-001	²¹⁶ 0.0404	²¹³ 0.0536	¹⁹⁸ 0.0661	¹⁹⁰ 0.0916	¹⁷ 0.1595
169	QNAP-002	¹⁶⁸ 0.0200	¹⁶⁰ 0.0265	¹⁵⁴ 0.0327	¹⁴⁵ 0.0490	¹⁴² 0.1341
170	QNAP-003	¹³ 0.0139	¹³⁴ 0.0189	¹²⁸ 0.0239	¹²² 0.0379	¹⁵⁹ 0.1414
171	QNAP-004	¹⁰⁶ 0.0096	¹¹⁰ 0.0139	¹¹⁰ 0.0184	¹¹⁶ 0.0346	¹³⁸ 0.1321
172	QUANTASOFT-001	³³⁴ 0.6387	³³⁴ 0.6387	²⁶⁴ 0.6387	²⁴⁸ 0.6387	
173	RANKONE-002	²⁷⁰ 0.0973	²⁶⁸ 0.1175	²³⁸ 0.1359	²³⁰ 0.1718	²³¹ 0.2613
174	RANKONE-003	²⁴⁹ 0.0973	²⁶⁴ 0.1175	²⁴⁹ 0.1359	²²⁹ 0.1718	²³⁰ 0.2613
175	RANKONE-005	²³² 0.0473	²²⁶ 0.0592	²⁰⁸ 0.0700	¹⁹³ 0.0944	²⁰¹ 0.1998
176	RANKONE-007	¹⁴⁹ 0.0168	¹⁴⁷ 0.0222	¹³⁷ 0.0266	¹²⁴ 0.0381	¹⁰⁵ 0.1132
177	RANKONE-009	¹² 0.0132	¹²⁶ 0.0177	¹²² 0.0230	¹¹⁴ 0.0344	⁶³ 0.0921
178	RANKONE-010	¹¹³ 0.0106	¹⁰⁸ 0.0136	¹⁰⁶ 0.0174	⁹⁸ 0.0265	⁴¹ 0.0785
179	RANKONE-011	⁸⁴ 0.0063	⁸⁴ 0.0087	⁸¹ 0.0115	⁹³ 0.0269	¹⁰ 0.1135
180	RANKONE-012	²⁹ 0.0058	⁷⁷ 0.0077	⁷⁵ 0.0100	⁷⁶ 0.0220	¹⁰⁰ 0.1111
181	RANKONE-013	⁵² 0.0034	⁵¹ 0.0046	⁵¹ 0.0059	⁴⁸ 0.0127	⁵² 0.0875
182	RANKONE-014	³³ 0.0025	³⁵ 0.0035	³⁴ 0.0043	³⁶ 0.0106	²⁶ 0.0656
183	REALNETWORKS-002	²⁹⁸ 0.1943	²⁹⁷ 0.2314	²⁵⁹ 0.2656	²⁵¹ 0.3134	²³⁹ 0.3208
184	REALNETWORKS-003	²⁸⁴ 0.1300	²⁸³ 0.1594	²⁵¹ 0.1858	²³⁹ 0.2246	²³⁹ 0.3076
185	REALNETWORKS-004	²⁸³ 0.1279	²⁸² 0.1581	²⁵⁰ 0.1857	²⁴⁰ 0.2329	²³⁸ 0.3179
186	REALNETWORKS-005	¹⁶ 0.0202	¹⁶⁷ 0.0277	¹⁶¹ 0.0355	¹⁶⁶ 0.0560	¹⁵ 0.1431
187	REALNETWORKS-006	¹⁰⁷ 0.0097	¹¹³ 0.0145	¹⁰⁹ 0.0182	¹⁰⁸ 0.0308	²⁷ 0.0991
188	REALNETWORKS-007	⁹² 0.0068	⁹⁰ 0.0097	⁸⁶ 0.0125	⁷⁹ 0.0233	⁶⁹ 0.0917
189	REALNETWORKS-008	⁶⁷ 0.0044	⁶⁷ 0.0062	⁶⁶ 0.0082	⁵¹ 0.0139	⁴⁴ 0.0824
190	RECOGNITO-000	¹⁰ 0.0016	¹⁹ 0.0020	²¹ 0.0026	¹⁴ 0.0057	¹² 0.0519
191	REMARKAI-000	²¹⁸ 0.0406	²¹⁷ 0.0552	²⁰³ 0.0676	¹⁹⁹ 0.1028	²⁰² 0.2003
192	RENDIP-000	⁹⁶ 0.0085	¹⁰⁰ 0.0121	⁹⁶ 0.0156	⁹⁷ 0.0277	¹¹ 0.1182
193	REVEALMEDIA-000	¹⁰¹ 0.0090	¹⁰² 0.0122	⁹⁹ 0.0158	⁹⁶ 0.0277	⁸³ 0.1019
194	S1-000	¹²⁷ 0.0204	¹⁶⁹ 0.0279	¹⁷⁷ 0.0382	¹⁷¹ 0.0630	¹⁸⁰ 0.1707
195	S1-001	¹¹⁷ 0.0115	¹²⁰ 0.0156	¹¹⁷ 0.0199	¹²⁵ 0.0392	¹²⁸ 0.1256
196	S1-002	⁶³ 0.0040	⁶³ 0.0056	⁶² 0.0077	⁸⁹ 0.0264	¹³³ 0.1285
197	S1-003	⁸³ 0.0061	⁸⁵ 0.0088	⁸² 0.0116	⁹⁴ 0.0277	¹³ 0.1298
198	S1-004	⁴³ 0.0030	⁴³ 0.0040	⁴⁶ 0.0056	⁶⁰ 0.0162	²⁶ 0.0989
199	SCANOVATE-000	²³ 0.0498	²³⁴ 0.0667	²¹⁷ 0.0804	²⁰³ 0.1097	⁹⁹ 0.1109
200	SCANOVATE-001	²⁴⁵ 0.0630	²⁴⁵ 0.0815	²²⁶ 0.0993	²¹³ 0.1292	⁹⁸ 0.1960
201	SENSETIME-000	¹⁴ 0.0158	¹⁴² 0.0208	¹⁴⁶ 0.0270	¹²⁸ 0.0398	¹² 0.1232
202	SENSETIME-001	¹⁴⁷ 0.0161	¹⁴⁶ 0.0219	¹⁴³ 0.0277	¹³⁵ 0.0420	¹³⁵ 0.1304
203	SENSETIME-002	¹³⁸ 0.0146	¹¹⁴ 0.0148	⁹⁷ 0.0153	⁸⁰ 0.0234	²⁷ 0.0657
204	SENSETIME-003	¹³ 0.0016	¹¹ 0.0018	¹⁴ 0.0021	¹³ 0.0054	¹¹ 0.0451
205	SENSETIME-004	¹² 0.0015	¹¹ 0.0018	¹³ 0.0021	⁷ 0.0040	³ 0.0354
206	SENSETIME-005	¹³ 0.0016	²² 0.0022	²³ 0.0031	³⁰ 0.0089	¹² 0.0454
207	SENSETIME-006	¹⁰ 0.0014	¹³ 0.0018	¹⁸ 0.0023	⁸ 0.0047	¹⁰ 0.0372
208	SENSETIME-007	³ 0.0012	⁵ 0.0014	³ 0.0016	⁵ 0.0036	⁷ 0.0316
209	SENSETIME-008	³ 0.0011	³ 0.0013	⁴ 0.0015	⁴ 0.0031	⁵ 0.0288
210	SENSETIME-009	¹ 0.0010	² 0.0011	² 0.0012	¹ 0.0024	³ 0.0238
211	SERENDIPITY-000	¹⁰³ 0.0092	¹⁰⁴ 0.0125	¹⁰³ 0.0159	⁹⁵ 0.0277	⁸¹ 0.1016
212	SHAMAN-007	²⁸ 0.1212	²⁷ 0.1413	²⁴ 0.1587	²³⁴ 0.1879	²² 0.2460
213	SIAT-001	¹²⁹ 0.0136	¹²⁴ 0.0176	¹²⁴ 0.0230	¹¹³ 0.0344	⁸⁵ 0.1035
214	SIAT-002	¹⁴⁷ 0.0154	¹⁴⁴ 0.0216	¹⁴¹ 0.0273	¹³⁰ 0.0404	¹³² 0.1283
215	SQISOFT-001	²⁶² 0.0921	²⁷³ 0.1322	²⁴⁸ 0.1781	²⁴² 0.2348	²⁵⁴ 0.9271
216	SQISOFT-002	¹⁵² 0.0177	¹⁷³ 0.0290	¹⁷⁷ 0.0415	¹⁸¹ 0.0739	¹⁴⁴ 0.1351

Table 23: Identification-mode: Effect of N on FNIR at high threshold. Values are threshold-based miss rates i.e. FNIR at FPIR = 0.001 for five enrollment population sizes, N. The right six columns apply for enrollment of one image. Missing entries usually apply because another algorithm from the same developer was run instead. Some developers are missing because less accurate algorithms were not run on galleries with $N \geq 3\ 000\ 000$. Throughout blue superscripts indicate the rank of the algorithm for that column.

#	ALGORITHM	MISSES BELOW THRESHOLD, T					
		ENROL MOST RECENT					
		FNIR(N, T > 0, R > L)		DATASET: FRVT 2018 MUGSHOTS			
		N=0.64M	N=1.6M	N=3.0M	N=6.0M	N=12.0M	
217	SYNESIS-003	²³⁵ 0.0499	²³² 0.0652	²¹⁶ 0.0804	²⁰² 0.1095	¹⁹⁴ 0.1916	
218	SYNESIS-003	³³⁰ 0.5341	³²⁸ 0.5821	²⁶⁹ 0.6113	²⁵⁵ 0.6479	²⁴⁹ 0.6822	
219	SYNESIS-005	¹⁵³ 0.0181	¹⁵⁴ 0.0248	¹⁵⁹ 0.0319	¹⁵⁴ 0.0518	¹⁷¹ 0.1580	
220	TECH5-001	²²⁰ 0.0420	²²⁰ 0.0574	²²² 0.0911	²³⁷ 0.2106	²⁴⁴ 0.3725	
221	TECH5-002	¹⁶⁵ 0.0194	¹⁶³ 0.0269	¹⁶⁷ 0.0346	¹⁵⁷ 0.0537	¹⁷⁴ 0.1607	
222	TEVIAN-005	²⁵³ 0.0692	²⁵⁰ 0.0873	²²⁹ 0.1066	²¹⁵ 0.1301	¹⁸⁹ 0.1840	
223	TEVIAN-006	⁹⁸ 0.0078	⁹¹ 0.0098	⁸⁸ 0.0130	⁸⁸ 0.0261	¹³⁰ 0.1305	
224	TEVIAN-007	⁶¹ 0.0038	⁶¹ 0.0052	⁵⁷ 0.0065	⁵⁵ 0.0154	⁶⁷ 0.0957	
225	TIGER-002	²⁴⁸ 0.0647	²⁴⁶ 0.0861	²²⁷ 0.1036	²¹⁸ 0.1332	²¹² 0.2231	
226	TOSHIBA-000	²³⁰ 0.0460	²²⁸ 0.0620	²¹³ 0.0780	²⁰⁵ 0.1117	²⁰⁵ 0.2082	
227	TRUEFACE-000	¹²⁴ 0.0134	¹³⁰ 0.0182	¹²² 0.0238	¹²⁵ 0.0380	¹⁴⁸ 0.1385	
228	VD-001	²⁹⁴ 0.1642	²⁹⁴ 0.2015	²⁵⁹ 0.2351	²⁴⁸ 0.2736	²⁴¹ 0.3293	
229	VERIDAS-001	¹⁸⁵ 0.0278	¹⁸⁶ 0.0373	¹⁸⁸ 0.0491	¹⁸² 0.0753	¹⁶ 0.1541	
230	VERIDAS-002	¹⁸⁵ 0.0278	¹⁸⁷ 0.0373	¹⁶⁸ 0.0373	¹⁴⁶ 0.0491	³⁶ 0.0753	
231	VERIDAS-003	¹²⁰ 0.0117	¹²² 0.0166	¹¹⁹ 0.0219	¹³⁸ 0.0446	¹⁶⁸ 0.1543	
232	VERIDAS-004	⁶⁵ 0.0042	⁶⁴ 0.0058	⁶⁹ 0.0077	²⁵ 0.0077	² 0.0232	
233	VIGILANTSOLUTIONS-008	¹³⁹ 0.0146	¹³⁹ 0.0205	¹³⁹ 0.0269	¹⁴⁴ 0.0489	¹¹³ 0.1164	
234	VISIONBOX-000	¹²¹ 0.0122	¹²⁷ 0.0177	¹²⁹ 0.0239		²⁵⁵ 0.9538	
235	VISIONLABS-004	²²³ 0.0427	²²¹ 0.0578	²⁰⁹ 0.0703	¹⁹⁴ 0.0949	¹⁹⁰ 0.1853	
236	VISIONLABS-005	²⁰⁸ 0.0369	²⁰⁵ 0.0502	¹⁹⁷ 0.0626	¹⁸⁶ 0.0847	¹⁸⁸ 0.1815	
237	VISIONLABS-006	¹⁶¹ 0.0188	¹⁶² 0.0267	¹⁵⁸ 0.0336	¹⁶² 0.0542	¹⁵⁸ 0.1478	
238	VISIONLABS-007	¹⁶² 0.0188	¹⁶¹ 0.0266	¹⁵⁷ 0.0335	¹⁶⁰ 0.0540	¹⁵⁹ 0.1479	
239	VISIONLABS-008	¹⁰⁵ 0.0096	¹⁰⁶ 0.0131	¹⁰⁸ 0.0166	¹⁰⁰ 0.0291	¹²⁴ 0.1247	
240	VISIONLABS-009	³² 0.0034	⁵² 0.0046	⁵⁶ 0.0060	⁵² 0.0140	³² 0.0881	
241	VISIONLABS-010	⁶⁰ 0.0038	⁶⁹ 0.0051	⁶⁹ 0.0070	⁵³ 0.0149	⁶² 0.0920	
242	VISIONLABS-011	³⁴ 0.0025	³⁶ 0.0033	³⁶ 0.0044	⁴⁰ 0.0120	⁴⁶ 0.0825	
243	VIXVIZION-009	¹⁷¹ 0.0203	¹⁶⁵ 0.0273	¹⁶⁹ 0.0348	¹⁶⁴ 0.0545	¹⁴⁷ 0.1377	
244	VNPPT-001	¹¹¹ 0.0104	¹¹¹ 0.0143	¹¹² 0.0190	¹⁰³ 0.0296	⁸⁴ 0.1028	
245	VNPPT-002	⁷² 0.0051	⁷⁰ 0.0065	⁶⁷ 0.0083	⁶² 0.0172	⁷⁹ 0.1005	
246	VCORD-005	²⁷⁸ 0.1179	²⁸¹ 0.1577	²⁸⁵ 0.2183	²⁵⁰ 0.3122	²⁴⁷ 0.4490	
247	VTS-001	¹¹⁰ 0.0102	¹⁰⁷ 0.0133	¹⁰⁹ 0.0175	¹⁰⁹ 0.0322	¹² 0.1243	
248	VTS-002	¹⁵⁶ 0.0185	¹⁵⁷ 0.0259	¹⁵⁹ 0.0344	¹⁶⁵ 0.0549	¹⁵⁵ 0.1447	
249	VTS-003	⁷⁶ 0.0053	⁷⁵ 0.0073	⁷¹ 0.0096	⁶⁷ 0.0188	⁸² 0.1017	
250	XFORWARDAI-000	¹¹⁵ 0.0107	¹¹⁷ 0.0151	¹¹⁴ 0.0195	¹¹¹ 0.0324	⁹¹ 0.1057	
251	XFORWARDAI-001	³⁸ 0.0037	⁵⁶ 0.0049	⁵⁷ 0.0060	³⁹ 0.0120	⁴² 0.0800	
252	XFORWARDAI-002	³⁶ 0.0026	³⁴ 0.0030	³⁹ 0.0035	²⁷ 0.0078	³¹ 0.0706	
253	YITU-002	¹² 0.0129	¹²⁵ 0.0177	¹²² 0.0228	¹¹⁵ 0.0345	¹⁶ 0.1133	
254	YITU-003	¹³³ 0.0138	¹³³ 0.0185	¹²⁹ 0.0236	¹¹⁷ 0.0353	¹⁰⁹ 0.1148	
255	YITU-004	⁹¹ 0.0067	⁸⁸ 0.0096	⁸⁷ 0.0129	⁷⁸ 0.0232	⁸⁸ 0.1046	
256	YITU-005	⁹⁵ 0.0074	⁹⁵ 0.0101	⁹⁰ 0.0135	⁸⁶ 0.0255	⁹² 0.1057	

Table 24: Identification-mode: Effect of N on FNIR at high threshold. Values are threshold-based miss rates i.e. FNIR at FPIR = 0.001 for five enrollment population sizes, N. The right six columns apply for enrollment of one image. Missing entries usually apply because another algorithm from the same developer was run instead. Some developers are missing because less accurate algorithms were not run on galleries with $N \geq 3\,000\,000$. Throughout blue superscripts indicate the rank of the algorithm for that column.

MISSES AT GIVEN RANK		ENROL MOST RECENT													
#	ALGORITHM	RANK 1					aN ^b	RANK 50							
		N=0.64M	N=1.6M	N=3.0M	N=6.0M	N=12.0M	aN ^b	N=0.64M	N=1.6M	N=3.0M	N=6.0M	N=12.0M	aN ^b		
1	3DIVI-005	²⁸⁵ 0.0137	²⁸³ 0.0176	²⁴⁶ 0.0210	²³⁹ 0.0253	²³⁴ 0.0302	¹⁸⁰ 0.0004 N ^{0.271} ²¹⁶	²⁶² 0.0040	²⁶³ 0.0049	²³⁵ 0.0057	²³¹ 0.0068	²²⁶ 0.0081	⁴⁹ 0.0002 N ^{0.240} ²²¹		
2	ACER-000	²⁵¹ 0.0081	²⁵⁹ 0.0106	²³¹ 0.0128	²³¹ 0.0157	²²⁷ 0.0195	⁷² 0.0001 N ^{0.299} ²⁴¹	²⁰⁸ 0.0020	²²⁵ 0.0026	²¹² 0.0031	²¹¹ 0.0037	²⁰⁷ 0.0045	¹⁹ 0.0000 N ^{0.284} ²³⁵		
3	ADVANCE-000	¹¹⁸ 0.0017	¹²⁰ 0.0020	¹²² 0.0022	¹²⁴ 0.0025	¹²⁶ 0.0029	⁸⁹ 0.0002 N ^{0.173} ¹⁴⁶	¹⁵⁵ 0.0014	¹⁴⁴ 0.0014	¹⁴⁰ 0.0015	¹³⁸ 0.0015	¹² 0.0016	¹⁴⁴ 0.0007 N ^{0.049} ¹²⁸		
4	AFISBIOMETRICS-000	⁶⁴ 0.0013	⁸⁸ 0.0016	¹⁰⁸ 0.0019	¹¹⁶ 0.0024	¹¹⁹ 0.0029	¹⁵ 0.0000 N ^{0.272} ²²²	³⁰ 0.0009	³³ 0.0009	⁴⁵ 0.0010	⁴¹ 0.0010	³⁹ 0.0010	⁸² 0.0004 N ^{0.061} ¹⁴⁴		
5	ALCHERA-003	²⁴⁷ 0.0079	²⁵⁹ 0.0104	²³³ 0.0123	²⁴⁰ 0.0147	²²³ 0.0180	¹⁰⁷ 0.0002 N ^{0.278} ²²⁸	²⁴³ 0.0027	²⁴² 0.0032	²¹⁸ 0.0035	²¹¹ 0.0042	²⁰⁸ 0.0048	⁵⁷ 0.0002 N ^{0.199} ²¹¹		
6	ALLGOVISION-000	²⁶⁷ 0.0101	²⁶⁵ 0.0114	²³³ 0.0127	²²⁹ 0.0145	²²⁴ 0.0166	²²⁸ 0.0010 N ^{0.171} ¹⁴⁸	²⁸³ 0.0063	²⁸⁰ 0.0067	²⁴¹ 0.0071	²³⁴ 0.0075	²²⁵ 0.0081	^{0.020} 0.0020 N ^{0.086} ¹⁶⁵		
7	ALLGOVISION-001	²³⁷ 0.0069	²⁴ 0.0090	²² 0.0107	²²⁴ 0.0128	²²¹ 0.0157	⁹¹ 0.0002 N ^{0.277} ²³⁸	²²⁸ 0.0023	²³⁰ 0.0027	²¹ 0.0031	²⁰⁸ 0.0036	²⁰ 0.0043	⁴ 0.0001 N ^{0.211} ²¹⁶		
8	ANKE-000	²⁷⁰ 0.0102	²⁷³ 0.0132	²⁴¹ 0.0155	²³⁶ 0.0188	²³⁸ 0.0225	¹⁵¹ 0.0003 N ^{0.270} ²¹⁸	²⁵⁸ 0.0032	²⁵⁴ 0.0040	²³¹ 0.0046	²²⁵ 0.0056	²¹⁶ 0.0066	⁴⁰ 0.0001 N ^{0.247} ²²³		
9	ANKE-002	¹⁶⁷ 0.0024	¹⁶ 0.0028	¹⁶⁸ 0.0032	¹⁶³ 0.0037	¹⁵⁰ 0.0043	⁸² 0.0002 N ^{0.203} ¹⁶⁵	¹⁷³ 0.0016	¹⁷³ 0.0017	¹⁶⁵ 0.0017	¹⁵⁷ 0.0018	¹⁵² 0.0019	¹¹⁷ 0.0006 N ^{0.067} ¹⁵²		
10	ARMATURA-000	¹³³ 0.0019	¹¹⁷ 0.0019	¹⁰⁵ 0.0019	⁹² 0.0020	⁸² 0.0022	²²⁷ 0.0009 N ^{0.050} ¹⁴	¹⁹⁸ 0.0018	¹⁹⁰ 0.0018	¹⁸¹ 0.0018	¹⁶¹ 0.0018	¹⁴³ 0.0018	²³³ 0.0017 N ^{0.003} ¹³		
11	AWARE-003	³⁰³ 0.0238	³⁰¹ 0.0306	²⁵⁸ 0.0361	²⁵¹ 0.0431	²⁴⁸ 0.0506	²²⁴ 0.0008 N ^{0.258} ²¹⁰	²⁷⁹ 0.0055	²⁸⁸ 0.0075	²⁵² 0.0092	²⁴⁶ 0.0113	²⁴⁵ 0.0143	³⁶ 0.0001 N ^{0.325} ²⁴⁵		
12	AWARE-005	³⁰⁴ 0.0245	³⁰² 0.0311	²⁵⁹ 0.0366	²⁵⁴ 0.0434	²³⁸ 0.0312	²⁴⁹ 0.0056 N ^{0.118} ⁸⁷	²⁸³ 0.0062	²⁹⁴ 0.0082	²⁵⁴ 0.0101	²⁴⁸ 0.0128	²²⁸ 0.0089	¹⁵⁷ 0.0007 N ^{0.169} ²⁰⁶		
13	AYONIX-002	³⁴¹ 0.2935	³⁴ 0.3414	²⁶⁷ 0.3736	²⁶¹ 0.4101	²⁵¹ 0.4465	²⁵⁴ 0.0440 N ^{0.143} ¹¹²	³⁴⁰ 0.0950	³⁴² 0.1274	²⁶⁹ 0.1524	²⁵⁹ 0.1828	²⁵³ 0.2150	²³⁹ 0.023 N ^{0.229} ²³²		
14	CAMVI-004	²⁷⁸ 0.0124	³¹ 0.0468	²⁶ 0.0719	²⁵⁹ 0.2363	²⁵¹ 0.2367	³ 0.0000 N ^{0.185} ²⁵⁵	³¹² 0.0117	³²⁷ 0.0464	²⁶⁵ 0.0715	²⁶¹ 0.2361	²⁵⁴ 0.2364	³ 0.0000 N ^{0.171} ²⁵⁵		
15	CANON-001	³¹ 0.0011	²⁷ 0.0011	²⁸ 0.0012	³⁰ 0.0013	²⁶ 0.0014	¹²⁸ 0.0002 N ^{0.113} ¹⁸⁹	³² 0.0009	³³ 0.0009	³³ 0.0009	³² 0.0010	¹¹⁸ 0.0006 N ^{0.026} ⁸⁴			
16	CANON-002	³⁴ 0.0011	³⁸ 0.0012	⁴⁶ 0.0013	⁴⁸ 0.0014	⁴⁷ 0.0016	⁸¹ 0.0002 N ^{0.142} ¹¹¹	³³ 0.0009	³¹ 0.0009	²⁹ 0.0009	²⁷ 0.0009	¹⁸⁴ 0.0007 N ^{0.015} ⁸¹			
17	CIB-000	⁸⁵ 0.0014	⁸¹ 0.0015	⁸⁰ 0.0017	⁸⁴ 0.0019	²¹⁵ 0.0131	⁴ 0.0000 N ^{0.635} ²⁸⁴	⁸⁹ 0.0012	⁸² 0.0012	⁸¹ 0.0012	⁸⁰ 0.0012	⁸⁰ 0.0012	⁴ 0.0000 N ^{0.647} ²⁵⁴		
18	CLEARVIEWAI-000	²⁷ 0.0010	²⁹ 0.0011	²⁹ 0.0012	³³ 0.0013	³⁴ 0.0015	⁹⁶ 0.0002 N ^{0.129} ¹⁰⁰	³⁶ 0.0009	³² 0.0009	³⁰ 0.0009	²⁹ 0.0009	²⁸ 0.0009	⁹ 0.0000 N ^{0.466} ²⁸⁰		
19	CLOUDWALK-HR-000	⁹¹ 0.0015	⁷³ 0.0015	⁷⁰ 0.0015	⁶¹ 0.0016	⁵⁶ 0.0017	²¹⁸ 0.0007 N ^{0.054} ¹⁶	¹⁵³ 0.0014	¹³⁹ 0.0014	¹²⁹ 0.0014	¹²⁰ 0.0014	¹⁰¹ 0.0014	²¹⁶ 0.0012 N ^{0.112} ³⁸		
20	CLOUDWALK-MT-000	¹²³ 0.0018	¹⁰³ 0.0018	⁹³ 0.0018	⁸⁰ 0.0019	⁷⁰ 0.0020	²³⁰ 0.0011 N ^{0.058} ⁸	¹⁸⁹ 0.0018	¹⁸⁵ 0.0018	¹⁶⁸ 0.0018	¹⁵⁸ 0.0018	¹³⁸ 0.0018	²³¹ 0.0017 N ^{0.002} ⁴		
21	CLOUDWALK-MT-001	¹²² 0.0018	¹⁰¹ 0.0018	⁸⁷ 0.0018	⁷⁵ 0.0018	⁶⁸ 0.0019	²³² 0.0012 N ^{0.029} ⁶	¹⁸⁸ 0.0017	¹⁸⁴ 0.0018	¹⁷¹ 0.0018	¹⁵⁰ 0.0018	¹³⁹ 0.0018	²³⁰ 0.0017 N ^{0.003} ¹¹		
22	CLOUDWALK-MT-002	¹²⁵ 0.0018	¹⁰⁸ 0.0018	⁸⁹ 0.0018	⁷⁴ 0.0018	⁶⁶ 0.0019	²³³ 0.0012 N ^{0.027} ⁵	¹⁹⁰ 0.0018	¹⁸³ 0.0018	¹⁷² 0.0018	¹⁵⁴ 0.0018	¹³² 0.0018	²³² 0.0017 N ^{0.002} ⁵		
23	COCENT-000	²⁶⁸ 0.0101	²⁵⁸ 0.0105	²²⁸ 0.0110	²²⁰ 0.0115	²¹⁵ 0.0125	²⁴⁶ 0.0038 N ^{0.071} ³³	²¹⁶ 0.0021	²¹⁸ 0.0024	²⁰⁷ 0.0028	²⁰⁸ 0.0036	²³¹ 0.0095	⁹ 0.0000 N ^{0.466} ²⁸⁰		
24	COCENT-001	²⁶⁹ 0.0101	²⁵ 0.0105	²²⁹ 0.0109	²¹⁹ 0.0115	²¹⁵ 0.0125	²⁴⁸ 0.0038 N ^{0.071} ³²	²¹⁷ 0.0021	²¹⁷ 0.0024	²⁰⁸ 0.0028	²⁰⁹ 0.0036	²²² 0.0095	⁹ 0.0000 N ^{0.466} ²⁵¹		
25	COCENT-002	¹⁸² 0.0029	¹⁸⁵ 0.0036	¹⁸¹ 0.0041	¹⁷⁸ 0.0049	¹⁷⁴ 0.0059	⁴⁷ 0.0001 N ^{0.244} ²⁰⁴	¹⁵⁰ 0.0014	¹⁶² 0.0015	¹⁵⁹ 0.0017	¹⁶⁵ 0.0019	¹⁶⁶ 0.0021	⁵⁴ 0.0002 N ^{0.144} ²⁰⁰		
26	COCENT-003	¹⁸⁸ 0.0031	¹⁸⁰ 0.0031	¹⁸⁶ 0.0043	¹⁸¹ 0.0051	¹⁷⁸ 0.0060	⁶⁷ 0.0001 N ^{0.230} ¹⁸⁹	¹⁶⁵ 0.0015	¹⁷⁴ 0.0017	¹⁸² 0.0018	¹⁷⁷ 0.0020	¹⁷² 0.0022	⁵⁶ 0.0002 N ^{0.143} ¹⁹⁹		
27	COCENT-004	¹²⁶ 0.0018	¹²⁷ 0.0020	¹²² 0.0022	¹²³ 0.0025	¹¹⁴ 0.0028	¹¹² 0.0002 N ^{0.159} ¹³²	¹⁴¹ 0.0013	¹³⁸ 0.0014	¹³⁵ 0.0014	¹²⁸ 0.0015	¹¹⁶ 0.0015	¹³⁰ 0.0007 N ^{0.050} ¹³⁰		
28	COCENT-005	⁹⁹ 0.0016	⁹⁵ 0.0017	⁹⁴ 0.0018	⁸⁹ 0.0020	⁸¹ 0.0021	¹⁷⁹ 0.0004 N ^{0.108} ⁷²	¹⁴³ 0.0013	¹²⁹ 0.0013	¹²¹ 0.0014	¹⁰⁸ 0.0014	¹⁰⁰ 0.0014	²⁰⁴ 0.0011 N ^{0.17} ⁵⁷		
29	COCENT-006	³¹ 0.0012	⁴⁸ 0.0012	⁴⁷ 0.0013	⁴⁴ 0.0014	⁴⁰ 0.0015	¹⁷⁸ 0.0004 N ^{0.088} ⁵¹	⁶⁷ 0.0011	⁶⁸ 0.0011	⁶¹ 0.0011	⁵⁹ 0.0011	⁵⁷ 0.0011	¹⁷⁵ 0.0008 N ^{0.119} ⁶⁵		
30	COCENT-007	³⁰ 0.0010	²⁹ 0.0011	³³ 0.0012	³² 0.0013	³³ 0.0015	¹¹¹ 0.0002 N ^{0.122} ⁹²	⁴⁶ 0.0009	⁴⁴ 0.0010	⁴¹ 0.0010	³⁹ 0.0010	³⁶ 0.0010	¹³⁷ 0.0007 N ^{0.022} ⁷⁴		
31	COGNITEC-000	²⁹⁶ 0.0195	²⁵⁹ 0.0252	²⁵⁹ 0.0297	²⁴⁸ 0.0352	²⁴⁷ 0.0417	²¹³ 0.0006 N ^{0.259} ²¹¹	²⁷⁴ 0.0050	²⁷⁸ 0.0065	²⁴⁸ 0.0077	²⁴⁷ 0.0097	²³⁹ 0.0122	³⁷ 0.0001 N ^{0.305} ²³⁹		
32	COGNITEC-001	²⁶² 0.0090	²⁶⁶ 0.0117	²³⁹ 0.0139	²³⁴ 0.0166	²²⁸ 0.0199	¹⁴⁰ 0.0002 N ^{0.271} ²¹⁸	²⁴⁸ 0.0030	²⁴⁷ 0.0034	²²⁷ 0.0040	²²² 0.0046	²¹² 0.0054	⁵² 0.0002 N ^{0.207} ²¹⁵		
33	COGNITEC-002	²²⁰ 0.0048	²¹⁸ 0.0057	²⁰⁶ 0.0067	²⁰⁰ 0.0079	¹⁹⁷ 0.0094	¹²⁰ 0.0002 N ^{0.232} ¹⁹²	²³⁰ 0.0024	²²⁷ 0.0026	²¹⁰ 0.0028	²⁰³ 0.0030	¹⁹¹ 0.0034	⁹⁵ 0.0005 N ^{0.117} ¹⁸⁶		
34	COGNITEC-003	²²³ 0.0053	²⁰² 0.0072	¹⁹⁶ 0.0085	¹⁹⁰ 0.0105	¹⁸⁵ 0.0130	²⁰⁴ 0.0003 N ^{0.110} ⁷⁵	²⁹ 0.0028	²³⁹ 0.0030	²¹⁵ 0.0032	²⁰⁴ 0.0035	¹⁹⁶ 0.0037	¹⁶⁸ 0.0008 N ^{0.097} ¹⁷⁴		
35	COGNITEC-004	¹⁷⁷ 0.0027	¹⁷⁶ 0.0032	¹⁷³ 0.0045	¹⁷⁷ 0.0056	¹⁷⁵ 0.0060	³⁵ 0.0001 N ^{0.253} ²⁰⁷	¹³⁸ 0.0013	¹⁴¹ 0.0014	¹⁴¹ 0.0015	¹⁴⁰ 0.0017	¹⁴⁰ 0.0019	⁶⁶ 0.0002 N ^{0.123} ¹⁹¹		
36	COGNITEC-005	⁸⁸ 0.0014	⁹⁶ 0.0016	⁹⁶ 0.0018	⁹³ 0.0021	⁹⁷ 0.0024	⁷³ 0.0001 N ^{0.169} ¹⁴¹	⁷							

MISSES AT GIVEN RANK		ENROL MOST RECENT											
#	FNIR(N, T= 0, R)	RANK 1					RANK 50						
		N=0.64M	N=1.6M	N=3.0M	N=6.0M	N=12.0M	aN^b	N=0.64M	N=1.6M	N=3.0M	N=6.0M	N=12.0M	aN^b
73	HIK-004	²⁶¹ 0.0088	²⁶⁴ 0.0113	²⁷⁷ 0.0134	²³² 0.0163	²²⁶ 0.0195	¹³⁴ 0.0002 N ^{-0.271} ²²¹	²³³ 0.0024	²³⁴ 0.0030	²¹⁹ 0.0035	²¹⁵ 0.0042	²¹⁰ 0.0052	³¹ 0.0001 N ^{-0.259} ²²⁸
74	HIK-005	²⁰¹ 0.0036	²⁰³ 0.0046	¹⁹⁸ 0.0053	¹⁹¹ 0.0065	¹⁹⁶ 0.0081	³⁷ 0.0001 N ^{-0.274} ²²³	¹⁰³ 0.0012	¹⁵³ 0.0015	¹³⁵ 0.0016	¹⁶⁴ 0.0019	¹⁶⁸ 0.0022	³⁵ 0.0001 N ^{-0.262} ²¹³
75	HYPERVERGE-001	⁶⁸ 0.0013	⁶² 0.0014	⁵⁸ 0.0014	⁵⁸ 0.0015	⁵⁵ 0.0017	¹⁸⁹ 0.0004 N ^{-0.084} ⁴⁶	¹²⁹ 0.0013	¹¹⁹ 0.0013	¹⁰⁶ 0.0013	⁹¹ 0.0013	⁸⁰ 0.0013	²¹⁸ 0.0012 N ^{-0.084} ¹⁷
76	HYPERVERGE-002	⁶⁹ 0.0013	⁵⁹ 0.0014	⁵⁷ 0.0014	⁴⁹ 0.0015	⁴¹ 0.0016	²¹⁹ 0.0007 N ^{-0.047} ¹³	¹²³ 0.0013	¹⁰⁹ 0.0013	¹⁰⁴ 0.0013	⁸⁸ 0.0013	⁸¹ 0.0013	²¹⁵ 0.0011 N ^{-0.088} ²⁶
77	HYPERVERGE-003	⁷⁴ 0.0014	⁶⁹ 0.0014	⁶⁴ 0.0015	⁶⁵ 0.0017	⁶⁵ 0.0019	¹⁶³ 0.0003 N ^{-0.105} ⁷⁰	¹²⁴ 0.0013	¹¹⁸ 0.0013	¹⁰⁵ 0.0013	⁹² 0.0013	⁸² 0.0013	²¹⁴ 0.0011 N ^{-0.09} ³³
78	HZAILU-000	¹⁴¹ 0.0019	¹⁴⁰ 0.0022	¹³⁵ 0.0025	¹³⁶ 0.0028	¹³⁴ 0.0033	⁸³ 0.0002 N ^{-0.185} ¹⁵⁵	¹⁵⁹ 0.0014	¹⁴⁸ 0.0014	¹⁴¹ 0.0015	¹³⁴ 0.0015	¹²⁰ 0.0016	¹⁹⁴ 0.0009 N ^{-0.032} ⁹⁶
79	HZAILU-001	¹²⁹ 0.0018	¹²⁵ 0.0020	¹¹⁵ 0.0021	¹⁰³ 0.0022	⁹⁹ 0.0025	²⁰⁵ 0.0005 N ^{-0.095} ⁵⁹	¹⁶ 0.0014	¹⁵⁹ 0.0015	¹⁵¹ 0.0016	¹⁴¹ 0.0016	¹²⁹ 0.0016	¹⁶³ 0.0008 N ^{-0.048} ¹²⁵
80	HZAILU-002	¹³¹ 0.0018	¹²⁸ 0.0020	¹¹⁸ 0.0021	¹¹¹ 0.0023	¹⁰⁴ 0.0026	¹⁸⁴ 0.0004 N ^{-0.114} ⁸²	¹⁶⁷ 0.0014	¹⁵⁸ 0.0015	¹⁴⁹ 0.0015	¹⁴³ 0.0016	¹³¹ 0.0017	¹⁶⁴ 0.0008 N ^{-0.048} ¹²⁷
81	HZAILU-003	⁹⁵ 0.0015	⁹¹ 0.0016	⁸⁶ 0.0018	⁸⁸ 0.0020	⁸⁴ 0.0022	¹⁵⁶ 0.0003 N ^{-0.123} ⁹³	¹¹¹ 0.0012	¹⁰⁶ 0.0013	¹¹⁸ 0.0013	¹⁰⁹ 0.0014	⁹⁹ 0.0014	¹²⁵ 0.0007 N ^{-0.046} ¹²²
82	IDEMIA-003	²²⁶ 0.0054	²²⁹ 0.0069	²¹⁸ 0.0084	²¹⁷ 0.0101	²¹¹ 0.0122	⁵⁷ 0.0001 N ^{-0.281} ²³⁰	²²⁴ 0.0023	²³¹ 0.0027	²¹¹ 0.0031	²⁰⁷ 0.0036	²⁰¹ 0.0041	⁴⁶ 0.0002 N ^{-0.201} ²¹²
83	IDEMIA-004	²²⁹ 0.0054	²²⁵ 0.0066	²¹⁵ 0.0079	²¹⁹ 0.0097	²¹⁰ 0.0117	⁷⁰ 0.0001 N ^{-0.270} ²¹⁴	¹⁹⁷ 0.0018	²⁰⁴ 0.0021	²⁰⁴ 0.0026	²⁰⁰ 0.0030	¹⁹⁵ 0.0036	²⁵ 0.0001 N ^{-0.241} ²²²
84	IDEMIA-005	²³⁴ 0.0064	²³⁹ 0.0081	²²⁴ 0.0097	²²¹ 0.0118	²¹⁸ 0.0143	⁷⁹ 0.0002 N ^{-0.277} ²²⁷	²²³ 0.0022	²³⁶ 0.0030	²²¹ 0.0036	²²⁰ 0.0044	²¹³ 0.0055	¹⁷ 0.0000 N ^{-0.300} ²³⁸
85	IDEMIA-006	²⁴⁴ 0.0076	²³³ 0.0096	²³¹ 0.0113	²²⁹ 0.0135	²²² 0.0161	¹³⁸ 0.0002 N ^{-0.259} ²¹²	²⁴⁴ 0.0028	²⁵¹ 0.0037	²³⁰ 0.0046	²²⁵ 0.0059	²²² 0.0076	¹⁵ 0.0000 N ^{-0.341} ²⁴⁷
86	IDEMIA-007	¹⁵¹ 0.0021	¹⁶¹ 0.0026	¹⁶¹ 0.0030	¹⁵⁸ 0.0036	¹⁵⁹ 0.0044	²⁷ 0.0001 N ^{-0.250} ²⁰⁵	⁷⁴ 0.0011	⁸⁸ 0.0012	⁹² 0.0012	¹¹² 0.0014	¹¹⁴ 0.0015	⁶⁵ 0.0002 N ^{-0.110} ¹⁸³
87	IDEMIA-008	¹⁸ 0.0010	²⁴ 0.0011	²⁴ 0.0013	²³ 0.0014	²⁴ 0.0014	¹⁰³ 0.0002 N ^{-0.121} ⁹¹	³¹ 0.0009	²⁸ 0.0009	²⁵ 0.0009	²⁵ 0.0009	¹⁴⁶ 0.0007 N ^{-0.016} ⁵³	
88	IDEMIA-009	¹³ 0.0009	¹¹ 0.0010	¹² 0.0010	¹¹ 0.0011	¹² 0.0012	¹⁴² 0.0002 N ^{-0.097} ⁶¹	²¹ 0.0008	¹⁸ 0.0009	¹⁶ 0.0009	¹⁵ 0.0009	¹¹ 0.0009	¹⁶⁶ 0.0008 N ^{-0.007} ²¹
89	IDEMIA-010	⁷ 0.0009	⁷ 0.0009	⁶ 0.0009	⁶ 0.0010	⁵ 0.0010	¹⁸³ 0.0003 N ^{-0.059} ²⁰	²² 0.0008	¹⁷ 0.0009	¹⁵ 0.0009	¹¹ 0.0009	⁹ 0.0009	¹⁷⁶ 0.0008 N ^{-0.002} ¹⁰
90	IMAGUS-005	¹²⁴ 0.0018	¹²² 0.0019	¹²² 0.0022	¹²¹ 0.0025	¹¹² 0.0028	¹¹⁸ 0.0002 N ^{-0.158} ¹³¹	¹²³ 0.0013	¹²⁸ 0.0013	¹²³ 0.0014	¹¹⁸ 0.0014	¹¹⁹ 0.0016	⁹⁹ 0.0005 N ^{-0.056} ¹⁸¹
91	IMAGUS-006	¹²⁷ 0.0018	¹²⁷ 0.0020	¹²⁸ 0.0022	¹²⁸ 0.0025	¹¹⁷ 0.0029	¹²² 0.0002 N ^{-0.156} ¹²⁵	¹⁴⁷ 0.0014	¹⁴⁶ 0.0014	¹⁴² 0.0015	¹²⁴ 0.0016	¹⁴⁴ 0.0016	¹⁴⁰ 0.0007 N ^{-0.049} ¹²⁹
92	IMAGUS-007	¹¹⁷ 0.0017	¹³² 0.0020	¹³⁰ 0.0022	¹²⁹ 0.0026	¹²³ 0.0030	⁶⁹ 0.0001 N ^{-0.189} ¹⁵⁷	¹⁰⁸ 0.0012	¹⁰⁵ 0.0013	⁹⁸ 0.0013	⁹⁶ 0.0013	¹⁰⁶ 0.0015	⁹⁸ 0.0005 N ^{-0.064} ¹⁴⁹
93	IMPERIAL-000	¹⁵⁹ 0.0022	¹⁵⁸ 0.0024	¹⁵³ 0.0027	¹⁴⁸ 0.0030	¹⁴¹ 0.0035	¹⁴⁶ 0.0003 N ^{-0.157} ¹²⁷	¹⁸¹ 0.0016	¹⁷⁵ 0.0017	¹⁶⁷ 0.0017	¹⁵⁶ 0.0018	¹⁴⁴ 0.0018	¹⁹⁵ 0.0009 N ^{-0.041} ¹¹²
94	INCODE-003	²⁶⁶ 0.0098	²⁹² 0.0129	²⁴¹ 0.0154	²³⁹ 0.0191	²³¹ 0.0233	¹⁰⁸ 0.0002 N ^{-0.296} ²³⁸	²³³ 0.0024	²⁴⁰ 0.0031	²²⁵ 0.0036	²²¹ 0.0046	²¹⁴ 0.0056	²⁵ 0.0001 N ^{-0.285} ²³⁶
95	INCODE-004	¹⁸³ 0.0029	¹⁸⁴ 0.0035	¹⁸² 0.0041	¹⁷⁹ 0.0049	¹⁷⁶ 0.0060	⁴⁶ 0.0001 N ^{-0.244} ²⁰²	¹⁹³ 0.0018	¹⁹¹ 0.0019	¹⁸⁸ 0.0020	¹⁸³ 0.0021	¹⁷⁰ 0.0022	¹¹⁷ 0.0006 N ^{-0.077} ¹⁵⁹
96	INCODE-005	⁹⁴ 0.0015	⁹³ 0.0017	⁹¹ 0.0018	⁹⁰ 0.0020	⁸⁹ 0.0023	¹³⁶ 0.0002 N ^{-0.140} ¹⁰⁵	¹⁰⁸ 0.0012	¹⁰³ 0.0013	¹⁰² 0.0013	¹⁰¹ 0.0013	⁹⁶ 0.0014	¹⁴² 0.0007 N ^{-0.041} ¹⁰⁹
97	INNOVATRICS-007	¹⁰¹ 0.0016	⁹⁶ 0.0017	⁹⁸ 0.0019	⁹⁵ 0.0021	⁹⁸ 0.0024	¹²⁷ 0.0002 N ^{-0.143} ¹¹⁴	¹⁰⁷ 0.0012	⁹⁹ 0.0012	⁹⁵ 0.0013	⁹³ 0.0013	⁹⁰ 0.0013	¹⁵¹ 0.0007 N ^{-0.037} ¹⁰⁶
98	INNOVATRICS-008	³⁵ 0.0012	³³ 0.0013	³¹ 0.0014	³¹ 0.0015	³⁰ 0.0016	¹⁵⁹ 0.0003 N ^{-0.120} ⁶⁶	⁶⁸ 0.0011	⁶⁶ 0.0011	⁵⁸ 0.0011	⁵⁴ 0.0011	⁵¹ 0.0011	¹⁸⁰ 0.0008 N ^{-0.018} ⁶¹
99	INSPUR-000	⁹ 0.0009	¹³ 0.0010	¹⁵ 0.0010	¹⁸ 0.0012	²³ 0.0014	⁶⁵ 0.0001 N ^{-0.139} ¹⁰⁶	¹⁵ 0.0008	¹⁴ 0.0008	¹³ 0.0009	⁸ 0.0009	¹³¹ 0.0007 N ^{-0.014} ⁴⁷	
100	INTEMA-000	³⁵ 0.0011	³⁵ 0.0011	³¹ 0.0012	³¹ 0.0013	³¹ 0.0016	¹⁰⁹ 0.0002 N ^{-0.124} ⁹⁵	⁵⁰ 0.0010	⁵⁹ 0.0010	⁶⁴ 0.0011	⁵⁹ 0.0011	⁷⁶ 0.0013	⁷⁶ 0.0003 N ^{-0.079} ¹⁶⁰
101	INTEMA-001	¹ 0.0008	¹ 0.0008	⁶ 0.0009	⁷ 0.0010	¹⁶ 0.0013	⁴³ 0.0001 N ^{-0.151} ¹²¹	⁷ 0.0008	⁶ 0.0008	¹¹ 0.0008	¹² 0.0009	⁴⁵ 0.0011	⁶² 0.0002 N ^{-0.091} ¹⁷⁰
102	LINECLOVA-000	³³³ 0.1395	³³³ 0.1457	²⁶³ 0.1498	²⁵⁹ 0.1544	²⁵⁹ 0.1591	²⁵⁶ 0.0768 N ^{-0.045} ¹¹	³⁴⁵ 0.1098	³⁴⁶ 0.1163	²⁶⁸ 0.1206	²⁵⁸ 0.1252	²⁵² 0.1296	²⁵⁶ 0.0519 N ^{-0.056} ¹³⁷
103	IREX-000	²¹⁰ 0.0043	¹⁹⁹ 0.0044	¹⁸⁷ 0.0044	¹⁷⁴ 0.0046	¹⁶⁸ 0.0048	²⁴² 0.0028 N ^{-0.032} ⁷	²⁶⁸ 0.0043	²⁵⁹ 0.0043	²²⁹ 0.0043	²¹⁷ 0.0043	²⁰² 0.0043	²⁴⁵ 0.0042 N ^{-0.002} ⁸
104	ISYSTEMS-002	²²⁵ 0.0053	²²⁴ 0.0064	²¹¹ 0.0072	²⁰⁸ 0.0083	²⁰⁰ 0.0096	¹⁷³ 0.0003 N ^{-0.204} ¹⁶⁷	²⁵⁷ 0.0033	²⁴⁸ 0.0034	²²⁰ 0.0036	²¹² 0.0038	²⁰⁰ 0.0041	²²⁰ 0.0013 N ^{-0.071} ¹⁵⁴
105	ISYSTEMS-003	²¹⁴ 0.0046	²¹² 0.0052	¹⁹³ 0.0057	¹⁹³ 0.0066	¹⁸⁸ 0.0076	¹⁹³ 0.0004 N ^{-0.174} ¹⁴⁸	²⁵⁰ 0.0031	²⁴⁴ 0.0033	²¹⁶ 0.0034	²⁰⁵ 0.0035	¹⁹⁸ 0.0037	²²¹ 0.0013 N ^{-0.063} ¹⁴⁸
106	KAKAO-000	⁶⁰ 0.0013	⁷⁴ 0.0015	⁸² 0.0019	⁸⁰ 0.0022	⁷⁶ 0.0024	⁴⁶ 0.0001 N ^{-0.192} ¹⁶¹	⁴² 0.0009	⁴⁴ 0.0010	⁴⁶ 0.0010	⁴⁶ 0.0011	⁴¹ 0.0011	⁹¹ 0.0005 N ^{-0.050} ¹³⁰
107	KAKAO-001	⁷⁵ 0.0014	⁶⁰ 0.0015	⁵¹ 0.0015	⁵⁰ 0.0016	⁴⁶ 0.0016	²⁴³ 0.0030 N ^{-0.076} ³⁸	²⁹⁷ 0.0072	²⁸⁷ 0.0074	²⁴⁷ 0.0075	²³⁵ 0.0076	²²³ 0.0077	²⁴⁸ 0.0054 N ^{-0.022} ⁷²
108	KEDACOM-001	²⁴⁵ 0.0076	²³⁵ 0.0077	²¹⁶ 0.0079	²⁰⁸ 0.0083	¹⁹⁸ 0.0087	²⁴ 0.0040 N ^{-0.024} ¹²¹	²⁹¹ 0.0071	²⁸⁴ 0.0072	²⁴⁵ 0.0072	²²⁴ 0.0073	²¹⁷ 0.0073	²⁴⁹ 0.0060 N ^{-0.013} ⁴⁴
109	KNERON-000	²¹⁹ 0.0048	²¹⁹ 0.0059	²⁰⁷ 0.0067	²⁰¹ 0.0079	¹⁹⁸ 0.0093	¹³² 0.0002 N ^{-0.226} ¹⁸⁵	²⁷¹ 0.0048	²⁷² 0.0059	²³⁹ 0.0067	^{237</}		

MISSES AT GIVEN RANK		ENROL MOST RECENT											
FNIR(N, T = 0, R)		RANK 1					RANK 50						
#	ALGORITHM	N=0.64M	N=1.6M	N=3.0M	N=6.0M	N=12.0M	aN ^b	N=0.64M	N=1.6M	N=3.0M	N=6.0M	N=12.0M	aN ^b
145	NTechLab-003	²¹⁷ 0.0046	²²⁰ 0.0062	²¹⁵ 0.0076	²¹³ 0.0094	²⁰⁹ 0.0114	²⁸ 0.0001 N ^{0.310} ²⁴³	¹³⁸ 0.0013	¹⁶⁷ 0.0016	¹⁸⁰ 0.0018	¹⁸⁵ 0.0022	¹⁸¹ 0.0026	²⁴ 0.0001 N ^{0.237} ²²⁰
146	NTechLab-004	²⁰² 0.0037	²⁰⁷ 0.0048	²⁰⁰ 0.0058	¹⁹⁸ 0.0071	¹⁹² 0.0085	³⁰ 0.0001 N ^{0.291} ²³⁴	⁸³ 0.0011	¹²⁸ 0.0013	¹⁴⁵ 0.0015	¹⁴⁶ 0.0017	¹⁶² 0.0021	³⁴ 0.0001 N ^{0.198} ²¹⁰
147	NTechLab-005	¹⁹⁶ 0.0035	¹⁹⁵ 0.0047	²⁰¹ 0.0058	¹⁹⁷ 0.0073	¹⁹⁹ 0.0092	¹⁷ 0.0000 N ^{0.334} ²⁴⁹	¹⁶ 0.0008	⁶¹ 0.0011	⁸⁶ 0.0012	¹³⁷ 0.0015	¹⁵⁰ 0.0019	¹¹ 0.0000 N ^{0.283} ²³⁴
148	NTechLab-006	¹⁸⁴ 0.0030	¹⁹³ 0.0041	¹⁹³ 0.0050	¹⁸⁹ 0.0062	¹⁸⁹ 0.0078	¹⁶ 0.0000 N ^{0.326} ²⁴⁸	⁶ 0.0008	³⁶ 0.0009	⁶² 0.0011	⁹⁰ 0.0013	¹²⁵ 0.0016	¹³ 0.0000 N ^{0.253} ²²⁴
149	NTechLab-007	¹⁵⁶ 0.0022	¹⁶³ 0.0027	¹⁶³ 0.0031	¹⁶² 0.0037	¹⁶¹ 0.0044	³² 0.0001 N ^{0.245} ²⁰³	⁸⁰ 0.0011	⁹³ 0.0012	⁹⁹ 0.0013	¹¹⁵ 0.0014	¹¹⁷ 0.0015	⁶⁸ 0.0003 N ^{0.109} ¹⁸²
150	NTechLab-008	⁸⁶ 0.0014	⁹⁸ 0.0017	¹⁰⁷ 0.0020	¹¹⁵ 0.0024	¹⁰⁸ 0.0027	²⁹ 0.0001 N ^{0.224} ¹⁸³	⁵⁹ 0.0010	⁵⁷ 0.0010	⁵⁵ 0.0011	⁶² 0.0011	⁶⁴ 0.0012	⁸⁴ 0.0004 N ^{0.065} ¹⁵⁰
151	NTechLab-009	⁴⁸ 0.0012	⁵¹ 0.0013	³⁷ 0.0014	⁵⁶ 0.0015	³⁹ 0.0018	⁹⁷ 0.0002 N ^{0.140} ¹⁰⁷	⁴³ 0.0009	⁴² 0.0009	⁴² 0.0010	⁴⁰ 0.0010	⁴¹ 0.0010	¹⁰ 0.0005 N ^{0.041} ¹¹⁰
152	NTechLab-010	³³ 0.0011	³⁰ 0.0011	²⁹ 0.0012	²⁹ 0.0013	²⁴ 0.0014	¹⁵⁸ 0.0003 N ^{0.091} ⁵⁶	⁶⁰ 0.0010	⁵⁴ 0.0010	⁴⁷ 0.0010	⁴³ 0.0010	³⁸ 0.0010	¹⁹⁶ 0.0009 N ^{0.005} ¹⁹
153	NTechLab-011	²³ 0.0010	²¹ 0.0010	¹⁹ 0.0011	¹⁹ 0.0012	¹⁹ 0.0013	¹³⁶ 0.0002 N ^{0.103} ⁶⁸	²⁸ 0.0009	²⁶ 0.0009	²⁴ 0.0009	²³ 0.0009	²¹ 0.0009	¹³⁸ 0.0007 N ^{0.017} ⁵⁸
154	OMNIGARDE-000	¹⁵ 0.0010	²³ 0.0011	²⁰ 0.0011	²⁶ 0.0013	²⁰ 0.0014	⁶⁹ 0.0001 N ^{0.140} ¹⁰⁹	¹⁴ 0.0008	¹⁵ 0.0008	¹⁸ 0.0009	¹⁹ 0.0009	¹⁵ 0.0009	¹⁰⁶ 0.0006 N ^{0.028} ⁹⁰
155	PANGIAM-000	⁴⁴ 0.0011	⁴⁰ 0.0012	⁴⁴ 0.0013	⁴¹ 0.0014	⁴⁶ 0.0016	¹²⁶ 0.0002 N ^{0.118} ⁸⁸	⁵⁴ 0.0010	⁵¹ 0.0010	⁴⁷ 0.0011	⁴⁷ 0.0011	¹³⁴ 0.0007 N ^{0.027} ⁸⁷	
156	PANGIAM-001	²³⁷ 0.0068	²³⁰ 0.0069	²⁰⁷ 0.0070	¹⁹⁶ 0.0071	¹⁸⁸ 0.0073	²⁴⁸ 0.0052 N ^{0.020} ⁴	²⁸⁹ 0.0068	²⁸¹ 0.0068	²⁴⁰ 0.0068	²¹⁸ 0.0068	²⁵¹ 0.0066 N ^{0.002} ⁶	
157	PARAVISION-003	¹⁷⁶ 0.0026	¹⁷⁶ 0.0031	¹⁷³ 0.0035	¹⁶⁹ 0.0042	¹⁶⁷ 0.0048	⁷⁹ 0.0002 N ^{0.210} ¹⁷³	¹⁸⁰ 0.0016	¹⁸¹ 0.0017	¹⁷⁸ 0.0018	¹⁷³ 0.0020	¹⁶³ 0.0021	⁹³ 0.0005 N ^{0.089} ¹⁶⁷
158	PARAVISION-004	⁹⁷ 0.0015	⁹⁰ 0.0016	⁸⁸ 0.0017	⁸¹ 0.0019	⁷⁹ 0.0021	¹⁸⁶ 0.0003 N ^{0.111} ⁷⁶	¹³¹ 0.0013	¹²⁰ 0.0013	¹¹¹ 0.0013	¹⁰² 0.0013	⁹⁵ 0.0014	²⁰⁰ 0.0010 N ^{0.020} ⁷⁰
159	PARAVISION-005	⁹⁰ 0.0015	⁸⁸ 0.0015	⁷⁵ 0.0016	⁷⁰ 0.0018	⁶⁷ 0.0019	¹⁸⁶ 0.0004 N ^{0.094} ⁵⁸	¹³⁶ 0.0013	¹²⁵ 0.0013	¹¹⁵ 0.0013	¹⁰⁵ 0.0013	⁹⁴ 0.0014	²⁰⁶ 0.0011 N ^{0.015} ⁵⁰
160	PARAVISION-007	⁴⁰ 0.0011	³⁷ 0.0012	³⁷ 0.0012	²⁸ 0.0013	³⁰ 0.0015	¹⁶² 0.0003 N ^{0.091} ⁵⁴	⁵⁸ 0.0010	⁵¹ 0.0010	⁴⁵ 0.0010	⁴⁵ 0.0010	¹⁷¹ 0.0008 N ^{0.018} ⁶³	
161	PARAVISION-009	²¹ 0.0010	¹⁷ 0.0010	²⁰ 0.0011	²⁰ 0.0012	²¹ 0.0014	¹⁰⁵ 0.0002 N ^{0.118} ⁸⁶	⁴⁰ 0.0009	³⁸ 0.0009	³⁷ 0.0009	³⁵ 0.0010	¹¹¹ 0.0006 N ^{0.032} ⁹⁴	
162	PARAVISION-012	¹² 0.0009	¹⁰ 0.0009	⁸ 0.0010	⁸ 0.0010	⁷ 0.0012	¹⁷ 0.0003 N ^{0.072} ²⁹	³⁸ 0.0009	³³ 0.0009	³⁰ 0.0009	²² 0.0009	¹⁸⁵ 0.0009 N ^{0.003} ¹²	
163	PARAVISION-014	¹¹ 0.0009	⁹ 0.0009	⁸ 0.0010	⁹ 0.0011	⁷ 0.0011	¹⁷⁶ 0.0003 N ^{0.070} ³¹	³⁴ 0.0009	³⁰ 0.0009	²⁸ 0.0009	²⁶ 0.0009	¹⁹ 0.0009	¹⁸⁴ 0.0008 N ^{0.005} ¹⁸
164	PIXELALL-002	²⁰⁴ 0.0037	²⁰² 0.0045	¹⁹⁵ 0.0052	¹⁹⁶ 0.0062	¹⁸⁷ 0.0075	⁷³ 0.0002 N ^{0.238} ¹⁹⁶	¹⁸³ 0.0017	¹⁹⁷ 0.0019	¹⁹³ 0.0021	¹⁹⁰ 0.0024	¹⁸² 0.0027	⁵⁸ 0.0002 N ^{0.154} ²⁰³
165	PIXELALL-003	¹³⁶ 0.0019	¹³⁶ 0.0021	¹³⁹ 0.0024	¹³² 0.0028	¹³¹ 0.0032	⁸⁰ 0.0002 N ^{0.182} ¹⁵⁴	¹⁴⁸ 0.0014	¹⁴³ 0.0014	¹³⁴ 0.0014	¹²² 0.0015	¹²¹ 0.0016	¹⁶¹ 0.0007 N ^{0.045} ¹²⁰
166	PIXELALL-004	¹¹³ 0.0017	¹³³ 0.0020	¹³¹ 0.0023	¹²⁶ 0.0026	¹²⁴ 0.0030	⁶¹ 0.0001 N ^{0.192} ¹⁶⁰	¹³³ 0.0013	¹²⁶ 0.0013	¹¹⁷ 0.0014	¹¹⁰ 0.0015	¹³⁵ 0.0007 N ^{0.046} ¹²¹	
167	PIXELALL-005	¹²⁰ 0.0018	¹¹⁸ 0.0019	¹⁰⁸ 0.0020	⁹⁹ 0.0021	⁹⁷ 0.0024	¹⁹⁹ 0.0005 N ^{0.098} ⁶²	¹⁷⁶ 0.0015	¹⁶⁶ 0.0016	¹⁵⁴ 0.0016	¹³⁹ 0.0016	¹²⁸ 0.0016	²¹⁷ 0.0012 N ^{0.070} ⁶⁰
168	PTAKURATSATU-000	¹⁷² 0.0025	¹⁷⁴ 0.0030	¹⁷⁵ 0.0036	¹⁶⁶ 0.0040	¹⁵³ 0.0040	¹⁵³ 0.0003 N ^{0.167} ¹³⁹	¹⁶⁹ 0.0015	¹⁶⁹ 0.0016	¹⁸³ 0.0018	¹⁷¹ 0.0020	¹⁵⁴ 0.0020	⁸⁵ 0.0004 N ^{0.086} ¹⁷³
169	QNAP-001	¹⁹⁷ 0.0035	¹⁹⁵ 0.0041	¹⁹¹ 0.0047	¹⁸⁷ 0.0054	¹⁸¹ 0.0063	¹³⁷ 0.0002 N ^{0.200} ¹⁶³	²²⁷ 0.0022	²¹⁶ 0.0023	²⁰³ 0.0024	¹⁹⁵ 0.0025	¹⁸⁶ 0.0028	¹⁸ 0.0008 N ^{0.102} ¹⁵⁶
170	QNAP-002	²¹⁸ 0.0047	²⁰⁸ 0.0049	¹⁹⁴ 0.0052	¹⁸⁹ 0.0054	¹⁷⁵ 0.0059	²³⁸ 0.0016 N ^{0.079} ⁴¹	²⁶³ 0.0041	²⁵⁸ 0.0042	²²⁸ 0.0042	²¹⁸ 0.0043	²⁰⁵ 0.0044	²⁴² 0.0032 N ^{0.019} ⁶⁹
171	QNAP-003	¹⁷¹ 0.0025	¹⁶⁸ 0.0028	¹⁶¹ 0.0031	¹⁵⁷ 0.0035	¹⁵⁸ 0.0040	¹⁵³ 0.0003 N ^{0.161} ¹³⁴	¹⁶⁴ 0.0014	¹⁵⁸ 0.0016	¹⁵¹ 0.0018	¹⁵⁸ 0.0020	¹⁷⁷ 0.0004 N ^{0.104} ¹⁷⁷	
172	QNAP-004	¹¹⁶ 0.0017	¹¹⁹ 0.0019	¹²¹ 0.0021	¹¹⁸ 0.0024	¹¹⁵ 0.0028	⁹⁰ 0.0002 N ^{0.171} ¹⁴⁴	¹⁴⁷ 0.0013	¹³⁴ 0.0014	¹²⁵ 0.0014	¹²¹ 0.0014	¹¹² 0.0015	¹⁷⁷ 0.0008 N ^{0.035} ⁹⁹
173	QUANTASOFT-001	³⁴⁰ 0.2177	³⁰⁷ 0.2177	²⁶¹ 0.2177	²⁵⁹ 0.2177	²⁵¹ 0.2177	²⁵¹ 0.2177 N ^{0.000} ¹	³⁴³ 0.1116	³³⁹ 0.1116	³⁶⁷ 0.1116	²⁶⁷ 0.1116	²⁵¹ 0.1116	²⁵ 0.1116 N ^{0.000} ¹
174	RANKONE-002	²⁸⁹ 0.0155	²⁸⁸ 0.0194	²⁴⁸ 0.0224	²⁴⁰ 0.0262	²³⁷ 0.0304	²²¹ 0.0007 N ^{0.230} ¹⁸⁷	²⁷⁰ 0.0048	²⁷⁴ 0.0060	²⁴³ 0.0071	²⁴¹ 0.0085	²³⁵ 0.0102	⁴⁷ 0.0002 N ^{0.254} ²²⁷
175	RANKONE-003	²⁸⁸ 0.0155	²⁸⁹ 0.0194	²⁴⁹ 0.0224	²⁴¹ 0.0262	²³⁹ 0.0304	²²⁰ 0.0007 N ^{0.230} ¹⁸⁸	²⁷² 0.0048	²⁷⁵ 0.0060	²⁴² 0.0071	²⁴⁰ 0.0085	²³⁶ 0.0102	⁴⁸ 0.0002 N ^{0.254} ²²⁶
176	RANKONE-005	²⁴³ 0.0075	²⁸⁰ 0.0094	²³⁹ 0.0110	²²⁹ 0.0132	²²⁰ 0.0156	¹⁴⁴ 0.0003 N ^{0.251} ²⁰⁶	²⁴¹ 0.0026	²⁴¹ 0.0032	²²⁴ 0.0036	²¹⁶ 0.0043	²⁰⁹ 0.0050	⁴⁵ 0.0001 N ^{0.221} ²¹⁷
177	RANKONE-007	¹⁸¹ 0.0028	¹⁸⁰ 0.0034	¹⁷⁷ 0.0038	¹⁷¹ 0.0045	¹⁷⁰ 0.0053	⁸⁴ 0.0002 N ^{0.207} ¹⁷⁴	¹⁶⁰ 0.0015	¹⁷⁴ 0.0017	¹⁶⁸ 0.0019	¹⁶⁷ 0.0021	¹⁶⁰ 0.0021	²⁰ 0.0003 N ^{0.123} ¹⁹⁰
178	RANKONE-009	¹⁴³ 0.0020	¹⁵¹ 0.0025	¹⁵⁹ 0.0029	¹³² 0.0032	¹²⁴ 0.0040	¹²⁴ 0.0002 N ^{0.164} ¹³⁸	¹⁵⁸ 0.0014	¹⁵⁰ 0.0015	¹⁴⁶ 0.0015	¹³⁷ 0.0017	¹²⁰ 0.0006 N ^{0.108} ¹³⁹	
179	RANKONE-010	¹⁴⁷ 0.0020	¹⁴⁴ 0.0022	¹⁴¹ 0.0025	¹³⁹ 0.0029	¹³² 0.0032	¹²⁴ 0.0002 N ^{0.164} ¹³⁸	¹⁵⁸ 0.0014	¹⁵⁰ 0.0015	¹⁴⁶ 0.0015	¹³⁷ 0.0017	¹²⁰ 0.0006 N ^{0.108} ¹³⁹	
180	RANKONE-011	⁷³ 0.0014	⁷⁸ 0.0015	⁷¹ 0.0017	⁷⁶ 0.0018	⁸⁰ 0.0021	⁹⁸ 0.0002 N ^{0.150} ¹²⁰	⁸⁶ 0.0011	⁷⁹ 0.0012	⁷⁸ 0.0012	⁷³ 0.0012	⁶⁹ 0.0012	¹⁸³ 0.0008 N ^{0.023} ⁷⁶
181	RANKONE-012	⁸⁸ 0.0013	⁶⁰ 0.0014	⁶⁹ 0.0015	⁶⁹ 0.0017	⁶⁹ 0.0020	¹⁰⁸ 0.0002 N ^{0.144} ¹¹⁵	⁷³ 0.0011	⁷⁴ 0.0011	⁶⁹ 0.0011	⁶¹ 0.0011	⁵⁶ 0.0012	¹⁸⁹ 0.0009 N ^{0.017} ⁵²
182	RANKONE-013	²⁰ 0.0010											

MISSES AT GIVEN RANK		ENROL MOST RECENT															
FNIR(N, T = 0, R)		RANK 1							RANK 50								
#	ALGORITHM	N=0.64M	N=1.6M	N=3.0M	N=6.0M	N=12.0M	aN ^b	N=0.64M	N=1.6M	N=3.0M	N=6.0M	N=12.0M	aN ^b				
217	SQISOFT-002	46.0012	54.00013	65.00015	77.00019	89.00023	10.0000 N ^{0.232} 191	37.00009	35.00009	38.00009	38.00010	37.00010	104.00005 N ^{0.039} 105				
218	SYNESSIS-003	290.0161	279.0162	245.0163	238.0165	232.0254	241.00027 N ^{0.127} 98	317.00160	314.00160	259.00160	252.00160	247.00245	197.00009 N ^{0.192} 209				
219	SYNESSIS-003	334.01456	334.01700	266.01876	259.02088	252.02317	259.0177 N ^{0.158} 130	336.00828	336.00869	266.00920	257.00998	250.01104	235.00218 N ^{0.098} 175				
220	SYNESSIS-005	257.00085	242.00085	221.00085	208.00086	195.00088	250.00072 N ^{0.012} 3	301.0085	295.00085	251.00085	239.00085	227.00085	252.00085 N ^{0.000} 2				
221	TECH5-001	190.00032	190.00040	191.00047	188.00057	188.00071	30.00001 N ^{0.271} 217	171.00016	176.00017	177.00018	172.00020	173.00023	71.00003 N ^{0.119} 187				
222	TECH5-002	146.00020	164.00027	166.00031	161.00037	163.00047	18.00000 N ^{0.285} 232	35.00009	50.00010	39.00011	57.00012	86.00013	50.00002 N ^{0.127} 194				
223	TEVIAN-005	230.00056	233.00073	222.00084	219.01015	217.00130	56.00001 N ^{0.283} 231	209.00020	212.00023	205.00025	198.00028	192.00034	81.00002 N ^{0.178} 207				
224	TEVIAN-006	163.00023	155.00024	151.00026	133.00028	127.00031	209.00005 N ^{0.106} 71	175.00017	172.00017	160.00017	149.00017	142.00018	193.00009 N ^{0.041} 111				
225	TEVIAN-007	115.00017	105.00018	95.00018	91.00020	79.00021	214.00006 N ^{0.073} 37	118.00013	107.00013	107.00013	103.00013	91.00013	187.00009 N ^{0.026} 82				
226	TIGER-002	212.00044	216.00056	208.00068	209.00086	205.00105	31.00001 N ^{0.299} 240	127.00013	135.00015	170.00018	182.00021	183.00027	18.00000 N ^{0.253} 225				
227	TOSHIBA-000	198.00035	201.00045	197.00052	188.00061	219.00154	8.00000 N ^{0.449} 252	174.00016	189.00018	186.00019	184.00021	237.00105	5.00000 N ^{0.539} 253				
228	TRUEFACE-000	187.00031	179.00035	165.00039	157.00043	215.00066 N ^{0.115} 83	239.00027	223.00026	206.00026	197.00027	188.00028	226.00015 N ^{0.038} 108					
229	VD-001	302.00230	299.00276	256.00315	259.00363	243.00418	239.00015 N ^{0.204} 168	311.00120	308.00130	258.00140	251.00154	246.00170	240.00024 N ^{0.120} 188				
230	VERIDAS-001	164.00023	167.00028	167.00032	164.00037	161.00045	44.00001 N ^{0.231} 190	156.00014	151.00015	147.00015	144.00016	141.00018	89.00005 N ^{0.083} 163				
231	VERIDAS-002	162.00023	166.00028	158.00028	159.00032	149.00037	159.00003 N ^{0.158} 128	150.00014	149.00015	137.00015	132.00015	126.00016	158.00007 N ^{0.047} 124				
232	VERIDAS-003	108.00017	108.00018	105.00020	104.00022	103.00026	121.00002 N ^{0.150} 119	120.00013	117.00013	114.00013	107.00014	102.00014	139.00007 N ^{0.043} 116				
233	VERIDAS-004	66.00013	58.00014	54.00014	42.00014	38.00015	222.00007 N ^{0.043} 10	108.0012	98.00012	89.00012	79.00012	73.00012	208.00111 N ^{0.048} 25				
234	VIGILANTSOLUTIONS-008	169.00025	173.00029	172.00034	168.00040	162.00047	56.00001 N ^{0.224} 182	92.00012	110.00013	133.00014	136.00015	134.00017	55.00002 N ^{0.130} 195				
235	VISIONBOX-000	119.00017	120.00019	125.00022	291.00000	257.00027	7.00000 N ^{0.270} 257	113.00012	108.00013	116.00013	263.00000	237.00025	1.00000 N ^{0.270} 195				
236	VISIONLABS-004	158.00022	165.00027	169.00032	170.00044	183.00070	7.00000 N ^{0.387} 250	111.00012	137.00014	161.00017	193.00025	206.00045	6.00000 N ^{0.435} 249				
237	VISIONLABS-005	142.00020	152.00024	160.00029	166.00037	169.00051	11.00000 N ^{0.322} 247	108.00012	115.00013	153.00016	169.00019	189.00029	12.00000 N ^{0.298} 237				
238	VISIONLABS-006	105.00016	110.00018	110.00022	137.00028	150.00041	10.00000 N ^{0.314} 245	105.00012	111.00013	139.00015	163.00019	184.00027	14.00000 N ^{0.275} 230				
239	VISIONLABS-007	103.00016	104.00018	109.00020	113.00023	138.00034	21.00001 N ^{0.248} 204	95.00012	94.00012	94.00013	156.00020	44.00001 N ^{0.152} 201					
240	VISIONLABS-008	132.00019	131.00020	120.00021	122.00025	122.00030	10.00002 N ^{0.169} 140	180.00116	178.00017	166.00017	174.00020	174.00023	75.00003 N ^{0.114} 184				
241	VISIONLABS-009	38.00011	34.00011	34.00012	43.00014	57.00017	52.00001 N ^{0.160} 133	51.00010	47.00010	50.00010	60.00011	98.00014	60.00002 N ^{0.109} 180				
242	VISIONLABS-010	72.00014	64.00014	6.00015	66.00017	72.00021	111.00002 N ^{0.137} 105	111.0013	104.00013	117.00013	117.00014	130.00017	79.00004 N ^{0.090} 169				
243	VISIONLABS-011	39.00011	39.00012	40.00012	40.00014	61.00018	51.00001 N ^{0.162} 136	62.00010	63.00011	66.00011	74.00012	111.00015	57.00003 N ^{0.114} 185				
244	VIXVIZION-009	139.0019	145.00019	151.00023	152.00026	156.00032	142.00037	39.00001 N ^{0.226} 184	69.00011	92.00012	101.00013	105.00013	104.00015	67.00003 N ^{0.106} 178			
245	VNPPT-001	148.00020	137.00022	132.00023	122.00025	110.00028	206.00005 N ^{0.104} 64	192.00018	186.00018	179.00018	159.00018	145.00019	223.00014 N ^{0.018} 59				
246	VNPPT-002	128.00018	116.00019	103.00020	98.00021	90.00023	217.00007 N ^{0.072} 34	186.00017	182.00017	169.00018	153.00018	140.00018	227.00015 N ^{0.009} 32				
247	VOCORD-005	231.00060	230.00107	217.00082	219.00097	209.00117	148.00003 N ^{0.232} 193	259.00033	249.00035	226.00037	213.00040	204.00043	198.00010 N ^{0.090} 168				
248	VTS-001	71.00014	82.00015	83.00017	87.00019	93.00023	53.00001 N ^{0.179} 152	52.00010	49.00010	52.00010	59.00011	54.00011	94.00005 N ^{0.051} 132				
249	VTS-002	110.00017	121.00019	125.00022	128.00026	128.00032	36.00001 N ^{0.215} 176	79.00011	72.00011	83.00012	84.00013	81.00044 N ^{0.079} 161					
250	VTS-003	37.00011	36.00011	32.00012	36.00013	41.00015	110.00002 N ^{0.124} 96	27.00009	24.00009	26.00009	24.00009	26.00009	115.00006 N ^{0.126} 83				
251	XFORWARDAI-000	153.00021	146.00023	135.00024	130.00027	121.00029	198.00005 N ^{0.111} 77	209.00019	196.00019	187.00019	175.00020	159.00020	225.00015 N ^{0.018} 62				
252	XFORWARDAI-001	145.00020	134.00020	117.00021	102.00022	95.00024	226.00009 N ^{0.055} 18	201.00019	195.00019	185.00019	167.00019	151.00019	235.00018 N ^{0.004} 15				
253	XFORWARDAI-002	140.00019	124.00020	110.00020	99.00021	83.00022	231.00011 N ^{0.038} 9	209.00019	194.00019	184.00019	166.00019	148.00019	234.00018 N ^{0.003} 14				
254	YITU-002	100.0016	112.00018	118.00021	119.00024	125.00029	36.00001 N ^{0.213} 175	47.00009	52.00010	53.00010	51.00011	61.00012	78.00004 N ^{0.073} 157				
255	YITU-003	175.00026	172.00027	169.00031	158.00035	159.00039	188.00004 N ^{0.141} 110	211.00020	205.00021	196.00022	187.00023	177.00024	199.00010 N ^{0.054} 133				
256	YITU-004	41.00011	52.00013	68.00015	69.00017	164.00047	7.00000 N ^{0.438} 251	20.00008	19.00009	21.00009	20.00009	194.00036	7.00000 N ^{0.395} 248				
257	YITU-005	160.00022	148.00023	142.00025	131.00027	125.00031	201.00005 N ^{0.113} 79	203.00020	199.00020	191.00020	177.00020	161.00020	228.00017 N ^{0.012} 39				

Table 28: Investigation-mode: Effect of N on FNIR on recent images For five enrollment population sizes, N, with T = 0 and FPIR = 1. The left five columns are rank 1 miss rates The right five columns are rank 50 miss rates Missing entries usually apply because another algorithm from the same developer was run instead. Some developers are missing because less accurate algorithms were not run on galleries with $N > 1\,600\,000$. Throughout blue superscripts indicate the rank of the algorithm for that column, and yellow highlighting indicates the most accurate value. Caution: The Power-low models are mostly intended to draw attention to the kind of behavior, not as a model to be used for prediction.

MISSES OUTSIDE RANK R		RESOURCE USAGE		ENROL MOST RECENT, N = 1.6M						
#	ALGORITHM	BYTES	MSEC	R=1	R=5	R=10	R=20	R=50	WORK-10	
1	20FACE-000	358	358	310.0552	310.0269	307.0198	306.0146	299.0099	311.1.275	
2	3DIVI-003	358	358	325.0.0833	320.0.0444	320.0.0349	316.0.0270	316.0.0191	321.1.447	
3	3DIVI-004	358	358	281.0.0175	273.0.0091	271.0.0075	267.0.0061	262.0.0049	278.1.092	
4	3DIVI-005	358	358	281.0.0176	274.0.0091	269.0.0074	266.0.0061	263.0.0049	279.1.092	
5	3DIVI-006	358	358	293.0.0240	301.0.0171	303.0.0160	307.0.0154	312.0.0148	299.1.162	
6	AADI-000	358	358						356.10.0000	
7	ACER-000	358	358	259.0.0106	240.0.0051	235.0.0041	233.0.0034	225.0.0026	241.1.053	
8	ACER-001	358	358	217.0.0051	212.0.0032	211.0.0028	210.0.0025	208.0.0022	211.1.031	
9	ADVANCE-000	358	358	126.0.0200	136.0.0116	139.0.0016	139.0.0015	144.0.0014	129.1.015	
10	AFISBIOMETRICS-000	358	358	89.0.0016	49.0.0011	42.0.0010	43.0.0010	32.0.0009	57.1.011	
11	AIZE-001	358	358	217.0.0056	216.0.0037	221.0.0033	222.0.0030	229.0.0027	217.1.035	
12	ALCHERA-000	358	358	271.0.0161	287.0.0124	291.0.0117	299.0.0111	302.0.0105	286.1.116	
13	ALCHERA-001	358	358	354.0.9869	354.0.9782	354.0.9735	354.0.9679	353.0.9590	354.9.811	
14	ALCHERA-002	358	358	321.0.0049	325.0.0555	322.0.0443	321.0.0354	318.0.0254	325.1.544	
15	ALCHERA-003	358	358	256.0.0104	243.0.0054	244.0.0045	242.0.0038	242.0.0032	248.1.055	
16	ALCHERA-004	358	358	261.0.0110	239.0.0049	231.0.0038	227.0.0032	222.0.0025	238.1.051	
17	ALLGOVISION-000	358	358	261.0.0114	268.0.0084	274.0.0078	275.0.0073	280.0.0067	268.1.079	
18	ALLGOVISION-001	358	358	249.0.0090	237.0.0048	234.0.0040	232.0.0033	230.0.0027	237.1.048	
19	ALLGOVISION-002	358	358	194.0.0041	196.0.0026	196.0.0022	189.0.0019	177.0.0017	196.1.025	
20	ANKE-000	358	358	273.0.0132	259.0.0073	257.0.0060	256.0.0050	254.0.0040	264.1.072	
21	ANKE-001	358	358	271.0.0132	260.0.0073	259.0.0061	257.0.0050	255.0.0040	268.1.073	
22	ANKE-002	358	358	169.0.0028	167.0.0020	166.0.0018	172.0.0018	173.0.0017	169.1.019	
23	ARMATURA-000	358	358	117.0.0019	133.0.0018	161.0.0018	178.0.0018	190.0.0018	149.1.017	
24	AWARE-003	358	358	301.0.0306	299.0.0162	296.0.0127	292.0.0100	288.0.0075	300.1.163	
25	AWARE-004	358	358	321.0.0679	317.0.0348	314.0.0274	311.0.0145	317.1.354		
26	AWARE-005	358	358	302.0.0311	300.0.0167	298.0.0134	295.0.0107	294.0.0082	302.1.167	
27	AWARE-006	358	358	321.0.0697	319.0.0369	315.0.0288	315.0.0223	313.0.0158	319.1.371	
28	AYONIX-000	358	358	341.0.4505	348.0.3540	348.0.3176	348.0.2834	347.0.2381	348.4.288	
29	AYONIX-001	358	358	341.0.3414	341.0.2338	341.0.1977	341.0.1652	341.0.1274	341.3.226	
30	AYONIX-002	358	358	341.0.3414	342.0.2338	342.0.1977	341.0.1652	342.0.1274	342.3.226	
31	CAMVI-003	358	358	316.0.0520	324.0.0517	323.0.0517	328.0.0517	328.0.0517	323.1.466	
32	CAMVI-004	358	358	311.0.0468	322.0.0465	322.0.0465	325.0.0464	327.0.0464	328.1.419	
33	CAMVI-005	358	358	319.0.0652	326.0.0648	330.0.0648	331.0.0648	333.0.0647	328.1.584	
34	CANON-001	358	358	29.0.0011	38.0.0010	36.0.0010	35.0.0009	34.0.0009	34.1.009	
35	CANON-002	358	358	38.0.0012	35.0.0010	30.0.0009	28.0.0009	31.0.0009	31.1.009	
36	CIB-000	358	358	81.0.0015	86.0.0013	79.0.0012	81.0.0012	82.0.0012	86.1.012	
37	CLEARVIEWAI-000	358	358	28.0.0011	37.0.0010	37.0.0010	32.0.0009	29.0.0009	32.1.009	
38	CLOUDWALK-HR-000	358	358	79.0.0015	108.0.0014	118.0.0014	130.0.0014	139.0.0014	103.1.013	
39	CLOUDWALK-MT-000	358	358	103.0.0018	145.0.0018	158.0.0018	165.0.0018	188.0.0018	140.1.016	
40	CLOUDWALK-MT-001	358	358	101.0.0018	147.0.0018	157.0.0018	164.0.0018	184.0.0018	139.1.016	
41	CLOUDWALK-MT-002	358	358	102.0.0018	144.0.0018	154.0.0018	169.0.0018	183.0.0018	141.1.016	
42	COGENT-000	358	358	259.0.0105	279.0.0096	284.0.0095	226.0.0032	218.0.0024	276.1.088	
43	COGENT-001	358	358	257.0.0105	280.0.0096	288.0.0095	227.0.0032	217.0.0024	278.1.088	
44	COGENT-002	358	358	181.0.0036	179.0.0022	176.0.0020	170.0.0018	162.0.0015	180.1.021	
45	COGENT-003	358	358	187.0.0038	190.0.0024	188.0.0021	187.0.0019	174.0.0017	189.1.023	
46	COGENT-004	358	358	129.0.0020	127.0.0016	126.0.0015	134.0.0015	138.0.0014	123.1.015	
47	COGENT-005	358	358	98.0.0017	107.0.0014	108.0.0014	110.0.0014	129.0.0013	106.1.013	
48	COGENT-006	358	358	48.0.0012	54.0.0011	53.0.0011	60.0.0011	68.0.0011	52.1.010	
49	COGENT-007	358	358	29.0.0011	39.0.0010	46.0.0010	41.0.0010	44.0.0010	37.1.009	
50	COGNITEC-000	358	358	295.0.0252	293.0.0136	29.0.0107	288.0.0085	278.0.0065	294.1.136	
51	COGNITEC-001	358	358	261.0.0117	251.0.0062	250.0.0051	251.0.0042	247.0.0034	252.1.062	
52	COGNITEC-002	358	358	218.0.0057	215.0.0037	216.0.0032	217.0.0029	227.0.0026	216.1.035	
53	COGNITEC-003	358	358	22.0.0062	224.0.0040	223.0.0036	231.0.0033	239.0.0030	224.1.039	
54	COGNITEC-004	358	358	178.0.0032	170.0.0020	157.0.0018	146.0.0015	141.0.0014	174.1.020	
55	COGNITEC-005	358	358	92.0.0016	78.0.0013	77.0.0012	73.0.0012	75.0.0011	79.1.012	
56	COGNITEC-006	358	358	81.0.0016	77.0.0013	71.0.0012	71.0.0012	73.0.0011	79.1.012	
57	CUBOX-000	358	358	66.0.0014	98.0.0014	109.0.0014	121.0.0014	132.0.0014	93.1.012	
58	CYBERLINK-000	358	358	189.0.0040	202.0.0028	206.0.0026	209.0.0024	209.0.0022	201.1.027	
59	CYBERLINK-001	358	358	183.0.0035	185.0.0023	184.0.0021	177.0.0018	180.0.0017	184.1.022	
60	CYBERLINK-002	358	358	161.0.0026	181.0.0023	191.0.0022	190.0.0021	203.0.0021	178.1.021	
61	CYBERLINK-003	358	358	85.0.0016	84.0.0013	84.0.0013	82.0.0012	80.0.0012	90.1.012	
62	CYBERLINK-004	358	358	91.0.0017	114.0.0015	124.0.0015	131.0.0014	142.0.0014	116.1.014	
63	CYBERLINK-005	358	358	107.0.0018	126.0.0016	133.0.0015	142.0.0015	145.0.0014	120.1.015	
64	DAHUA-000	358	358	249.0.0093	254.0.0066	259.0.0061	264.0.0057	267.0.0054	253.1.062	
65	DAHUA-001	358	358	229.0.0067	225.0.0040	222.0.0036	229.0.0033	233.0.0029	226.1.040	
66	DAHUA-002	358	358	111.0.0018	112.0.0015	120.0.0014	126.0.0014	127.0.0013	113.1.014	
67	DAHUA-003	358	358	47.0.0012	28.0.0010	24.0.0009	23.0.0009	20.0.0009	29.1.009	
68	DAHUA-004	358	358	26.0.0011	24.0.0010	27.0.0009	26.0.0009	27.0.0009	26.1.009	
69	DAON-000	358	358	192.0.0041	217.0.0038	228.0.0037	238.0.0037	250.0.0036	215.1.034	
70	DECATUR-000	358	358	135.0.0021	128.0.0016	130.0.0015	127.0.0014	121.0.0013	128.1.015	
71	DEEPLINKI-001	358	358	71.0.0014	95.0.0014	97.0.0013	105.0.0013	112.0.0013	92.1.012	
72	DEEPSA-001	358	358	198.0.0043	180.0.0022	161.0.0018	154.0.0016	135.0.0014	180.1.022	

Table 29: Rank-based accuracy for the FRVT 2018 mugshot sets. In columns 3 and 4 are template size and template generation duration. Thereafter values are rank-based FNIR with $T = 0$ and FPIR = 1. This is appropriate to investigational uses but not those with higher volumes where candidates from all searches would need review. The next column is a workload statistic, a small value shows an algorithm front-loads mates into the first 10 candidates. Throughout, blue superscripts indicate the rank of the algorithm for that column, and the best value is highlighted in yellow.

MISSES OUTSIDE RANK R		RESOURCE USAGE		ENROL MOST RECENT, N = 1.6M					
#	ALGORITHM	BYTES	MSEC	R=1	R=5	R=10	R=20	R=50	WORK-10
73	DERMALOG-003	358	358	³³ 0.1259	³³⁰ 0.0744	³²⁸ 0.0603	³²⁷ 0.0480	³²⁶ 0.0347	³³⁰ 1.731
74	DERMALOG-004	358	358	³³⁰ 0.1251	³²⁹ 0.0739	³²⁷ 0.0598	³²⁶ 0.0475	³²⁵ 0.0343	³²⁹ 1.727
75	DERMALOG-005	358	358	²⁷ 0.0149	²⁹⁰ 0.0129	²⁹⁵ 0.0125	³⁰¹ 0.0123	³⁰⁷ 0.0122	²⁸⁷ 1.118
76	DERMALOG-006	358	358	²⁴⁰ 0.0081	²⁵⁸ 0.0069	²⁶⁰ 0.0066	²⁶⁸ 0.0065	²⁷⁶ 0.0063	²⁵⁶ 1.063
77	DERMALOG-007	358	358	²⁴ 0.0092	²⁵⁵ 0.0066	²⁵⁶ 0.0060	²⁶ 0.0057	²⁷⁰ 0.0054	²⁵⁴ 1.062
78	DERMALOG-008	358	358	¹⁷ 0.0029	¹⁶⁶ 0.0020	¹⁶¹ 0.0018	¹⁵⁷ 0.0017	¹⁶⁰ 0.0015	¹⁶⁸ 1.019
79	DERMALOG-009	358	358	¹⁷ 0.0028	¹⁸⁸ 0.0024	¹⁹⁸ 0.0023	²⁰⁶ 0.0023	²¹⁰ 0.0022	¹⁸² 1.022
80	DERMALOG-010	358	358	¹³ 0.0022	¹⁷⁵ 0.0021	¹⁸³ 0.0021	¹⁹ 0.0020	²⁰⁰ 0.0020	¹⁶⁷ 1.019
81	DERMALOG-011	358	358	⁸⁶ 0.0016	⁷⁰ 0.0012	⁶⁷ 0.0012	⁶⁵ 0.0011	⁶⁹ 0.0011	⁶⁹ 1.011
82	DIGIDATA-000	358	358	³⁵⁹ 0.5897	³⁵¹ 0.5892	³⁵¹ 0.5891	³⁵¹ 0.5891	³⁵¹ 0.5891	³⁵¹ 6.303
83	DILUSENSE-000	358	358	¹⁴¹ 0.0022	¹²³ 0.0015	¹¹⁶ 0.0014	¹¹⁵ 0.0013	¹⁰⁰ 0.0013	¹²⁴ 1.015
84	DILUSENSE-001	358	358	⁷⁷ 0.0015	⁷⁴ 0.0013	⁷² 0.0012	⁷⁰ 0.0012	⁷⁸ 0.0011	⁷¹ 1.011
85	EYEDEA-003	358	358	³²⁴ 0.0800	³²¹ 0.0451	³²¹ 0.0362	³¹⁷ 0.0289	³¹⁷ 0.0211	³²² 1.448
86	F8-001	358	358	²⁷ 0.0120	²⁸² 0.0105	²⁸⁸ 0.0102	²⁹⁰ 0.0100	²⁹⁸ 0.0099	²⁸² 1.096
87	FINCORE-000	358	358	²⁶¹ 0.0108	²⁴² 0.0052	²³⁷ 0.0042	²³⁵ 0.0034	²²⁸ 0.0026	²⁴⁸ 1.054
88	FIRSTCREDITKZ-001	358	358	⁴⁷ 0.0012	⁶¹ 0.0012	⁶⁶ 0.0012	⁷⁰ 0.0012	⁸³ 0.0012	⁵⁸ 1.011
89	FUJITSULAB-000	358	358	¹⁴² 0.0022	¹³³ 0.0016	¹³⁵ 0.0015	¹³⁵ 0.0015	¹³¹ 0.0014	¹³⁴ 1.015
90	FUJITSULAB-001	358	358	¹¹⁸ 0.0019	¹¹⁹ 0.0015	¹²² 0.0015	¹²⁶ 0.0014	¹³⁶ 0.0014	¹¹⁶ 1.014
91	GLORY-000	358	358	³³⁵ 0.1781	³³⁷ 0.1391	³³⁷ 0.1266	³³⁷ 0.1154	³³⁷ 0.1007	³³⁶ 2.298
92	GLORY-001	358	358	³³⁸ 0.1268	³³² 0.0967	³³² 0.0869	³³⁸ 0.0778	³³⁴ 0.0673	³³² 1.903
93	GORILLA-001	358	358	³¹⁷ 0.0603	³¹² 0.0304	³¹¹ 0.0230	³¹¹ 0.0174	³⁰⁴ 0.0117	³¹² 1.309
94	GORILLA-002	358	358	²⁸ 0.0197	²⁷⁵ 0.0092	²⁶⁵ 0.0070	²⁵⁹ 0.0054	²⁵⁶ 0.0041	²⁸¹ 1.096
95	GORILLA-003	358	358	³⁰⁷ 0.0361	²⁹⁶ 0.0146	²⁹⁶ 0.0106	²⁸² 0.0078	²⁶⁹ 0.0054	²⁹⁸ 1.158
96	GORILLA-004	358	358	²²³ 0.0063	²¹¹ 0.0032	²⁰⁷ 0.0026	²⁰³ 0.0023	¹⁸⁷ 0.0018	²¹² 1.033
97	GORILLA-005	358	358	¹⁷ 0.0032	¹⁸⁵ 0.0019	¹⁴⁹ 0.0017	¹³⁷ 0.0015	¹¹³ 0.0013	¹⁶⁵ 1.018
98	GORILLA-006	358	358	¹⁰⁷ 0.0017	⁷⁵ 0.0013	⁷⁴ 0.0012	⁶⁹ 0.0012	⁶⁹ 0.0011	⁸⁹ 1.012
99	GORILLA-007	358	358	⁹ 0.0017	⁶⁹ 0.0012	⁶⁵ 0.0012	⁵⁸ 0.0011	⁶² 0.0011	⁷⁴ 1.012
100	GORILLA-008	358	358	⁷⁶ 0.0015	⁶⁰ 0.0012	⁵⁹ 0.0011	⁵⁵ 0.0011	⁶⁰ 0.0011	⁶² 1.011
101	GRIAULE-000	358	358	¹⁵⁹ 0.0025	¹⁶⁴ 0.0020	¹⁶⁸ 0.0019	¹⁷⁰ 0.0018	¹⁷¹ 0.0017	¹⁶² 1.018
102	GRIAULE-001	358	358	⁴² 0.0012	⁴⁶ 0.0011	⁴⁸ 0.0011	⁴⁹ 0.0010	⁵⁶ 0.0010	⁴⁹ 1.010
103	HIK-003	358	358	²⁶ 0.0117	²⁴⁹ 0.0060	²⁴⁸ 0.0048	²⁴⁷ 0.0039	²³⁷ 0.0030	²⁵⁰ 1.061
104	HIK-004	358	358	²⁶¹ 0.0113	²⁴⁷ 0.0059	²⁴⁷ 0.0047	²⁴⁰ 0.0037	²³⁴ 0.0030	²⁴⁸ 1.060
105	HIK-005	358	358	²⁰³ 0.0046	¹⁹³ 0.0025	¹⁸⁰ 0.0020	¹⁶² 0.0017	¹⁵³ 0.0015	¹⁹⁴ 1.025
106	HIK-006	358	358	²⁰ 0.0046	¹⁹⁴ 0.0025	¹⁷⁹ 0.0020	¹⁶⁷ 0.0017	¹⁵² 0.0015	¹⁹⁵ 1.025
107	HYPERVERGE-001	358	358	⁶² 0.0014	⁸⁰ 0.0013	⁹² 0.0013	¹⁰⁰ 0.0013	¹¹⁹ 0.0013	⁷⁸ 1.012
108	HYPERVERGE-002	358	358	⁵⁹ 0.0014	⁸¹ 0.0013	⁹³ 0.0013	⁹⁸ 0.0013	¹⁰⁹ 0.0013	⁷⁷ 1.012
109	HYPERVERGE-003	358	358	⁶⁹ 0.0014	⁸⁷ 0.0013	⁹¹ 0.0013	⁹⁹ 0.0013	¹¹⁸ 0.0013	⁸³ 1.012
110	HZAILU-000	358	358	¹⁴⁸ 0.0022	¹³¹ 0.0016	¹³⁶ 0.0015	¹⁴⁸ 0.0014	¹³² 0.0015	¹³¹ 1.015
111	HZAILU-001	358	358	¹²⁰ 0.0020	¹⁴¹ 0.0017	¹⁴⁶ 0.0016	¹⁵³ 0.0016	¹⁵⁹ 0.0015	¹³⁸ 1.016
112	HZAILU-002	358	358	¹²⁰ 0.0020	¹⁴⁰ 0.0017	¹⁴⁴ 0.0016	¹⁵⁰ 0.0016	¹⁵⁸ 0.0015	¹³² 1.016
113	HZAILU-003	358	358	⁹¹ 0.0016	¹⁰⁵ 0.0014	¹¹⁶ 0.0014	¹²⁰ 0.0014	¹⁰⁶ 0.0013	¹⁰² 1.013
114	IDEMIA-003	358	358	²²⁹ 0.0069	²³³ 0.0045	²³² 0.0039	²³⁴ 0.0034	²³¹ 0.0027	²³⁰ 1.043
115	IDEMIA-004	358	358	²²⁹ 0.0066	²²¹ 0.0038	²¹⁷ 0.0032	²¹⁶ 0.0027	²⁰⁴ 0.0021	²¹⁹ 1.038
116	IDEMIA-005	358	358	²³⁹ 0.0081	²³¹ 0.0044	²²⁶ 0.0036	²²⁸ 0.0032	²³⁶ 0.0030	²³³ 1.044
117	IDEMIA-006	358	358	²⁵ 0.0096	²⁴¹ 0.0052	²³⁸ 0.0042	²⁴⁵ 0.0039	²⁵¹ 0.0037	²⁴⁰ 1.052
118	IDEMIA-007	358	358	¹⁶¹ 0.0026	¹²⁹ 0.0016	¹¹⁷ 0.0014	⁹⁵ 0.0013	⁸⁸ 0.0012	¹³⁸ 1.015
119	IDEMIA-008	358	358	²⁸ 0.0011	²⁵ 0.0009	²⁶ 0.0009	³⁰ 0.0009	²⁸ 0.0009	²¹ 1.009
120	IDEMIA-009	358	358	¹¹ 0.0010	¹¹ 0.0009	¹⁴ 0.0009	¹⁶ 0.0009	¹⁸ 0.0009	¹¹ 1.008
121	IDEMIA-010	358	358	⁷ 0.0009	⁹ 0.0009	¹³ 0.0009	¹⁵ 0.0009	¹⁷ 0.0009	⁷ 1.008
122	IMAGUS-002	358	358	³³⁶ 0.2203	³³⁶ 0.1342	³³⁵ 0.1090	³³⁴ 0.0871	³³² 0.0632	³³² 2.308
123	IMAGUS-003	358	358	³⁴ 0.3559	³⁴³ 0.2491	³⁴³ 0.2132	³⁴ 0.1791	³⁴³ 0.1397	³⁴³ 3.363
124	IMAGUS-005	358	358	¹²⁸ 0.0019	¹³⁰ 0.0016	¹²⁵ 0.0015	¹² 0.0014	¹²⁶ 0.0013	¹²⁵ 1.015
125	IMAGUS-006	358	358	¹²⁹ 0.0020	¹³⁵ 0.0016	¹³⁷ 0.0015	¹³⁸ 0.0015	¹⁴⁶ 0.0014	¹³⁰ 1.015
126	IMAGUS-007	358	358	¹³⁷ 0.0020	¹¹⁵ 0.0015	¹¹² 0.0014	¹⁰ 0.0013	¹⁰⁵ 0.0013	¹¹⁴ 1.014
127	IMAGUS-008	358	358	³²⁶ 0.0860	³²⁷ 0.0701	³²⁹ 0.0646	³²⁹ 0.0590	³²⁹ 0.0518	³²² 1.648
128	IMPERIAL-000	358	358	¹⁵⁹ 0.0024	¹⁵⁷ 0.0019	¹⁶³ 0.0018	¹⁷ 0.0018	¹⁷⁵ 0.0017	¹⁵⁷ 1.018
129	INCODE-000	358	358	³¹⁴ 0.0489	³⁰⁹ 0.0261	³¹⁰ 0.0204	³⁰⁸ 0.0160	³⁰⁵ 0.0117	³⁰⁹ 1.262
130	INCODE-001	358	358	²⁸ 0.0166	²⁶⁹ 0.0084	²⁶² 0.0067	²⁶ 0.0055	²⁶⁰ 0.0043	²⁷¹ 1.086
131	INCODE-002	358	358	²⁸⁴ 0.0178	²⁷² 0.0090	²⁶⁸ 0.0070	²⁶² 0.0056	²⁶¹ 0.0043	²⁷⁷ 1.092
132	INCODE-003	358	358	²⁷ 0.0129	²⁵³ 0.0064	²⁵¹ 0.0051	²⁴⁸ 0.0040	²⁴⁰ 0.0031	²⁵⁰ 1.066
133	INCODE-004	358	358	¹⁸³ 0.0035	¹⁸⁶ 0.0024	¹⁸⁸ 0.0021	¹⁹¹ 0.0020	¹⁹¹ 0.0019	¹⁸⁶ 1.023
134	INCODE-005	358	358	⁹⁸ 0.0017	⁹⁶ 0.0014	¹⁰⁶ 0.0014	¹⁰³ 0.0013	¹⁰³ 0.0013	⁹⁷ 1.013
135	INNOVATRICS-002	358	358	³¹⁷ 0.0451	³¹⁴ 0.0342	³¹⁷ 0.0322	³¹⁰ 0.0308	³²¹ 0.0297	³¹⁶ 1.321
136	INNOVATRICS-003	358	358	²⁹⁷ 0.0263	²⁸⁸ 0.0126	²⁸³ 0.0095	²⁷⁷ 0.0074	²⁶⁶ 0.0053	²⁹¹ 1.129
137	INNOVATRICS-004	358	358	²⁷ 0.0123	²⁵² 0.0063	²⁴⁹ 0.0050	²⁴³ 0.0040	²⁴³ 0.0032	²⁵⁷ 1.064
138	INNOVATRICS-005	358	358	¹⁵⁷ 0.0024	¹⁵⁰ 0.0018	¹⁵⁰ 0.0017	¹⁵⁰ 0.0016	¹⁴⁷ 0.0014	¹⁵¹ 1.017
139	INNOVATRICS-007	358	358	⁹⁸ 0.0017	¹⁰³ 0.0014	⁹⁹ 0.0013	⁹⁹ 0.0012	¹⁰⁰ 0.0012	¹⁰⁰ 1.013
140	INNOVATRICS-008	358	358	⁵⁹ 0.0013	⁵⁶ 0.0011	⁵⁷ 0.0011	⁵⁹ 0.0011	⁶⁶ 0.0011	⁵⁴ 1.010
141	INSPUR-000	358	358	¹³ 0.0010	⁸ 0.0009	¹² 0.0009	¹⁴ 0.0008	¹⁴ 0.0008	⁹ 1.008
142	INTELLIGENSIA-000	358	358	¹³⁰ 0.0020	¹¹⁰ 0.0015	¹⁰¹ 0.0013	⁹⁰ 0.0013	⁸⁶ 0.0012	¹¹¹ 1.014
143	INTELLIVISION-001	358	358	³⁰ 0.0365	³⁰⁷ 0.0199	³⁰³ 0.0160	³⁰² 0.0126	²⁹⁷ 0.0095	³⁰⁵ 1.199
144	INTELLIVISION-002	358	358	²⁶⁰ 0.0107	²				

MISSES OUTSIDE RANK R		RESOURCE USAGE		ENROL MOST RECENT, N = 1.6M					
#	ALGORITHM	BYTES	MSEC	R=1	R=5	R=10	R=20	R=50	WORK-10
145	INTEMA-000	358	358	33 ^{0.0011}	45 ^{0.0011}	49 ^{0.0011}	51 ^{0.0010}	59 ^{0.0010}	42 ^{1.010}
146	INTEMA-001	358	358	1 ^{0.0008}	1 ^{0.0008}	2 ^{0.0008}	4 ^{0.0008}	6 ^{0.0008}	1 ^{1.007}
147	INTSYSMSU-000	358	358	333 ^{0.1457}	335 ^{0.1320}	338 ^{0.1272}	338 ^{0.1225}	340 ^{0.1163}	332 ^{2.203}
148	IREX-000	358	358	199 ^{0.0044}	227 ^{0.0043}	241 ^{0.0043}	252 ^{0.0043}	259 ^{0.0043}	225 ^{1.039}
149	ISYSTEMS-002	358	358	224 ^{0.0064}	228 ^{0.0043}	233 ^{0.0039}	237 ^{0.0037}	246 ^{0.0034}	222 ^{1.041}
150	ISYSTEMS-003	358	358	212 ^{0.0052}	222 ^{0.0039}	227 ^{0.0036}	236 ^{0.0034}	244 ^{0.0033}	218 ^{1.037}
151	KAKAO-000	358	358	74 ^{0.0015}	52 ^{0.0011}	58 ^{0.0011}	44 ^{0.0010}	45 ^{0.0010}	51 ^{1.010}
152	KAKAO-001	358	358	63 ^{0.0014}	89 ^{0.0013}	96 ^{0.0013}	109 ^{0.0013}	116 ^{0.0013}	84 ^{1.012}
153	KEDACOM-001	358	358	235 ^{0.0077}	261 ^{0.0074}	266 ^{0.0073}	274 ^{0.0072}	284 ^{0.0072}	259 ^{1.067}
154	KNERON-000	358	358	219 ^{0.0059}	248 ^{0.0059}	258 ^{0.0059}	265 ^{0.0059}	272 ^{0.0059}	242 ^{1.053}
155	KNERON-001	358	358	300 ^{0.0295}	311 ^{0.0295}	318 ^{0.0295}	320 ^{0.0295}	310 ^{1.266}	
156	KNOWUTECH-000	358	358	31 ^{0.0011}	16 ^{0.0009}	18 ^{0.0009}	19 ^{0.0009}	22 ^{0.0009}	19 ^{1.008}
157	LINE-000	358	358	143 ^{0.0022}	121 ^{0.0015}	111 ^{0.0014}	89 ^{0.0013}	81 ^{0.0012}	122 ^{1.015}
158	LINE-001	358	358	32 ^{0.0011}	36 ^{0.0010}	39 ^{0.0010}	35 ^{0.0009}	37 ^{0.0009}	35 ^{1.009}
159	LINECLOVA-002	358	358	55 ^{0.0013}	66 ^{0.0012}	70 ^{0.0012}	79 ^{0.0012}	87 ^{0.0012}	65 ^{1.011}
160	LINECLOVA-003	358	358	14 ^{0.0010}	10 ^{0.0009}	10 ^{0.0008}	13 ^{0.0008}	7 ^{0.0008}	10 ^{1.008}
161	LOOKMAN-003	358	358	244 ^{0.0088}	266 ^{0.0078}	273 ^{0.0076}	279 ^{0.0075}	287 ^{0.0074}	262 ^{1.071}
162	LOOKMAN-004	358	358	246 ^{0.0091}	266 ^{0.0079}	277 ^{0.0076}	278 ^{0.0075}	286 ^{0.0073}	263 ^{1.072}
163	LOOKMAN-005	358	358	238 ^{0.0080}	263 ^{0.0075}	270 ^{0.0074}	276 ^{0.0073}	285 ^{0.0072}	260 ^{1.068}
164	MANTRA-000	358	358	99 ^{0.0017}	92 ^{0.0013}	88 ^{0.0013}	88 ^{0.0012}	91 ^{0.0012}	95 ^{1.013}
165	MAXVISION-000	358	358	154 ^{0.0024}	142 ^{0.0017}	140 ^{0.0016}	141 ^{0.0015}	133 ^{0.0014}	147 ^{1.016}
166	MAXVISION-001	358	358	44 ^{0.0012}	53 ^{0.0011}	58 ^{0.0011}	63 ^{0.0011}	67 ^{0.0011}	51 ^{1.010}
167	MAXVISION-002	358	358	46 ^{0.0012}	57 ^{0.0011}	62 ^{0.0011}	68 ^{0.0011}	76 ^{0.0011}	53 ^{1.010}
168	MEGVII-001	358	358	268 ^{0.0118}	276 ^{0.0093}	278 ^{0.0087}	286 ^{0.0084}	297 ^{0.0080}	271 ^{1.086}
169	MEGVII-002	358	358	269 ^{0.0118}	277 ^{0.0093}	278 ^{0.0088}	285 ^{0.0084}	297 ^{0.0080}	273 ^{1.087}
170	MEGVII-003	358	358	49 ^{0.0012}	64 ^{0.0012}	69 ^{0.0012}	77 ^{0.0012}	84 ^{0.0012}	59 ^{1.011}
171	MICROFOCUS-003	358	358	352 ^{0.5942}	350 ^{0.4692}	359 ^{0.4204}	350 ^{0.3724}	350 ^{0.3095}	359 ^{5.361}
172	MICROFOCUS-004	358	358	349 ^{0.5763}	349 ^{0.4519}	349 ^{0.4026}	349 ^{0.3560}	349 ^{0.2957}	349 ^{5.199}
173	MICROFOCUS-005	358	358	345 ^{0.4242}	345 ^{0.3028}	344 ^{0.2606}	344 ^{0.2209}	345 ^{0.1724}	346 ^{3.861}
174	MICROFOCUS-006	358	358	346 ^{0.4268}	346 ^{0.3049}	345 ^{0.2623}	346 ^{0.2233}	346 ^{0.1746}	346 ^{3.880}
175	MICROSOFT-003	358	358	87 ^{0.0016}	33 ^{0.0010}	15 ^{0.0009}	3 ^{0.0008}	2 ^{0.0006}	39 ^{1.009}
176	MICROSOFT-004	358	358	27 ^{0.0015}	22 ^{0.0009}	1 ^{0.0008}	1 ^{0.0007}	1 ^{0.0006}	36 ^{1.009}
177	MICROSOFT-005	358	358	115 ^{0.0019}	26 ^{0.0010}	30 ^{0.0008}	2 ^{0.0008}	3 ^{0.0006}	46 ^{1.010}
178	MICROSOFT-006	358	358	125 ^{0.0020}	55 ^{0.0011}	35 ^{0.0010}	5 ^{0.0008}	4 ^{0.0007}	66 ^{1.011}
179	MUKH-002	358	358	296 ^{0.0258}	294 ^{0.0139}	299 ^{0.0112}	289 ^{0.0090}	281 ^{0.0070}	291 ^{1.140}
180	NEC-000	358	358	281 ^{0.0170}	271 ^{0.0086}	261 ^{0.0066}	258 ^{0.0052}	253 ^{0.0038}	274 ^{1.087}
181	NEC-001	358	358	299 ^{0.0209}	295 ^{0.0141}	297 ^{0.0128}	300 ^{0.0119}	303 ^{0.0113}	293 ^{1.135}
182	NEC-002	358	358	22 ^{0.0010}	13 ^{0.0009}	8 ^{0.0008}	7 ^{0.0008}	3 ^{0.0008}	12 ^{1.008}
183	NEC-003	358	358	61 ^{0.0014}	73 ^{0.0012}	76 ^{0.0012}	84 ^{0.0012}	87 ^{0.0012}	68 ^{1.011}
184	NEC-004	358	358	68 ^{0.0014}	93 ^{0.0013}	108 ^{0.0013}	104 ^{0.0013}	114 ^{0.0013}	91 ^{1.012}
185	NEC-005	358	358	41 ^{0.0012}	51 ^{0.0011}	55 ^{0.0011}	61 ^{0.0011}	64 ^{0.0011}	50 ^{1.010}
186	NEC-006	358	358	50 ^{0.0013}	68 ^{0.0012}	78 ^{0.0012}	72 ^{0.0012}	77 ^{0.0011}	61 ^{1.011}
187	NEC-007	358	358	20 ^{0.0010}	31 ^{0.0010}	38 ^{0.0010}	40 ^{0.0010}	41 ^{0.0009}	27 ^{1.009}
188	NEUROTECHNOLOGY-003	358	358	291 ^{0.0225}	289 ^{0.0126}	288 ^{0.0100}	283 ^{0.0078}	277 ^{0.0057}	290 ^{1.125}
189	NEUROTECHNOLOGY-004	358	358	214 ^{0.0056}	214 ^{0.0036}	219 ^{0.0032}	221 ^{0.0029}	229 ^{0.0025}	215 ^{1.035}
190	NEUROTECHNOLOGY-005	358	358	197 ^{0.0043}	204 ^{0.0029}	208 ^{0.0027}	208 ^{0.0024}	213 ^{0.0023}	205 ^{1.028}
191	NEUROTECHNOLOGY-006	358	358	285 ^{0.0180}	267 ^{0.0079}	259 ^{0.0059}	254 ^{0.0046}	247 ^{0.0033}	269 ^{1.083}
192	NEUROTECHNOLOGY-007	358	358	188 ^{0.0039}	199 ^{0.0027}	204 ^{0.0025}	204 ^{0.0023}	206 ^{0.0022}	197 ^{1.026}
193	NEUROTECHNOLOGY-008	358	358	188 ^{0.0022}	116 ^{0.0015}	12 ^{0.0014}	122 ^{0.0014}	121 ^{0.0013}	121 ^{1.015}
194	NEUROTECHNOLOGY-009	358	358	70 ^{0.0014}	67 ^{0.0012}	68 ^{0.0012}	67 ^{0.0011}	70 ^{0.0011}	67 ^{1.011}
195	NEUROTECHNOLOGY-010	358	358	47 ^{0.0012}	42 ^{0.0011}	49 ^{0.0010}	45 ^{0.0010}	55 ^{0.0010}	46 ^{1.010}
196	NEUROTECHNOLOGY-012	358	358	18 ^{0.0010}	32 ^{0.0010}	31 ^{0.0010}	34 ^{0.0009}	40 ^{0.0009}	25 ^{1.009}
197	NEUROTECHNOLOGY-013	358	358	19 ^{0.0010}	30 ^{0.0010}	32 ^{0.0010}	38 ^{0.0010}	43 ^{0.0010}	24 ^{1.009}
198	NEWLAND-002	358	358	323 ^{0.0786}	323 ^{0.0480}	322 ^{0.0397}	322 ^{0.0332}	319 ^{0.0263}	324 ^{4.468}
199	NOBLIS-001	358	358	340 ^{0.2492}	340 ^{0.1772}	340 ^{0.1542}	340 ^{0.1339}	338 ^{0.1112}	340 ^{2.679}
200	NOBLIS-002	358	358	336 ^{0.1794}	333 ^{0.1108}	333 ^{0.0903}	332 ^{0.0722}	331 ^{0.0535}	332 ^{2.077}
201	NOTIONTAG-000	358	358	156 ^{0.0024}	176 ^{0.0021}	182 ^{0.0021}	194 ^{0.0020}	198 ^{0.0019}	171 ^{1.019}
202	NTECHLAB-003	358	358	220 ^{0.0062}	207 ^{0.0029}	199 ^{0.0023}	188 ^{0.0019}	167 ^{0.0016}	210 ^{1.030}
203	NTECHLAB-004	358	358	207 ^{0.0048}	183 ^{0.0023}	171 ^{0.0019}	156 ^{0.0016}	128 ^{0.0013}	192 ^{1.024}
204	NTECHLAB-005	358	358	205 ^{0.0047}	178 ^{0.0022}	153 ^{0.0017}	108 ^{0.0013}	61 ^{0.0011}	181 ^{1.023}
205	NTECHLAB-006	358	358	193 ^{0.0041}	156 ^{0.0019}	128 ^{0.0015}	80 ^{0.0012}	36 ^{0.0009}	173 ^{1.019}
206	NTECHLAB-007	358	358	163 ^{0.0027}	137 ^{0.0017}	118 ^{0.0014}	114 ^{0.0013}	93 ^{0.0012}	146 ^{1.016}
207	NTECHLAB-008	358	358	98 ^{0.0017}	65 ^{0.0012}	61 ^{0.0012}	62 ^{0.0011}	57 ^{0.0010}	73 ^{1.012}
208	NTECHLAB-009	358	358	51 ^{0.0013}	44 ^{0.0011}	46 ^{0.0010}	42 ^{0.0010}	42 ^{0.0009}	48 ^{1.010}
209	NTECHLAB-010	358	358	30 ^{0.0011}	40 ^{0.0010}	43 ^{0.0010}	46 ^{0.0010}	54 ^{0.0010}	38 ^{1.009}
210	NTECHLAB-011	358	358	21 ^{0.0010}	20 ^{0.0009}	23 ^{0.0009}	24 ^{0.0009}	26 ^{0.0009}	20 ^{1.008}
211	OMNIGARDE-000	358	358	23 ^{0.0011}	14 ^{0.0009}	19 ^{0.0009}	18 ^{0.0009}	15 ^{0.0008}	18 ^{1.008}
212	PANGIAM-000	358	358	40 ^{0.0012}	47 ^{0.0011}	50 ^{0.0011}	50 ^{0.0010}	53 ^{0.0010}	47 ^{1.010}
213	PANGIAM-001	358	358	230 ^{0.0069}	256 ^{0.0068}	260 ^{0.0068}	270 ^{0.0068}	287 ^{0.0068}	251 ^{1.061}
214	PARAVISION-000	358	358	286 ^{0.0188}	302 ^{0.0171}	307 ^{0.0167}	310 ^{0.0165}	315 ^{0.0164}	297 ^{1.156}
215	PARAVISION-001	358	358	186 ^{0.0038}	189 ^{0.0024}	188 ^{0.0022}	195 ^{0.0020}	192 ^{0.0019}	190 ^{1.023}
216	PARAVISION-002	358	358	191 ^{0.0040}	195 ^{0.0025}	195 ^{0.0022}	1		

MISSES OUTSIDE RANK R		RESOURCE USAGE		ENROL MOST RECENT, N = 1.6M						
FNIR(N, T=0, R)		TEMPLATE		FRVT 2018 MUGSHOTS						
#	ALGORITHM	BYTES	MSEC	R=1	R=5	R=10	R=20	R=50	WORK-10	
217	PARAVISION-003	358	-	17 ⁶ 0.0031	17 ⁶ 0.0022	18 ¹ 0.0020	18 ¹ 0.0019	18 ¹ 0.0017	17 ¹ 1.021	
218	PARAVISION-004	358	-	90 ¹ 0.0016	99 ¹ 0.0014	103 ¹ 0.0013	112 ¹ 0.0013	120 ¹ 0.0013	99 ¹ 1.013	
219	PARAVISION-005	358	-	80 ¹ 0.0015	97 ¹ 0.0014	108 ¹ 0.0013	115 ¹ 0.0013	125 ¹ 0.0013	91 ¹ 1.013	
220	PARAVISION-007	358	-	37 ¹ 0.0012	48 ¹ 0.0011	47 ¹ 0.0010	48 ¹ 0.0010	51 ¹ 0.0010	43 ¹ 1.010	
221	PARAVISION-009	358	-	17 ¹ 0.0010	25 ¹ 0.0010	31 ¹ 0.0010	37 ¹ 0.0009	38 ¹ 0.0009	25 ¹ 1.009	
222	PARAVISION-012	358	-	10 ¹ 0.0009	18 ¹ 0.0009	25 ¹ 0.0009	29 ¹ 0.0009	32 ¹ 0.0009	17 ¹ 1.008	
223	PARAVISION-014	358	-	5 ¹ 0.0009	17 ¹ 0.0009	25 ¹ 0.0009	27 ¹ 0.0009	30 ¹ 0.0009	15 ¹ 1.008	
224	PIXELALL-002	358	-	202 ¹ 0.0045	205 ¹ 0.0029	209 ¹ 0.0025	201 ¹ 0.0022	197 ¹ 0.0019	209 ¹ 1.028	
225	PIXELALL-003	358	-	136 ¹ 0.0021	132 ¹ 0.0016	134 ¹ 0.0015	132 ¹ 0.0014	141 ¹ 0.0014	133 ¹ 1.015	
226	PIXELALL-004	358	-	133 ¹ 0.0020	120 ¹ 0.0015	124 ¹ 0.0015	129 ¹ 0.0014	130 ¹ 0.0013	117 ¹ 1.014	
227	PIXELALL-005	358	-	118 ¹ 0.0019	139 ¹ 0.0017	142 ¹ 0.0016	135 ¹ 0.0016	166 ¹ 0.0016	131 ¹ 1.015	
228	PTAKURATSU-000	358	-	17 ⁴ 0.0030	17 ⁴ 0.0021	17 ⁴ 0.0019	168 ¹ 0.0018	169 ¹ 0.0016	17 ¹ 1.020	
229	QNAP-000	358	-	236 ¹ 0.0078	230 ¹ 0.0044	229 ¹ 0.0037	230 ¹ 0.0033	232 ¹ 0.0028	231 ¹ 1.043	
230	QNAP-001	358	-	195 ¹ 0.0041	206 ¹ 0.0029	207 ¹ 0.0027	211 ¹ 0.0025	216 ¹ 0.0023	207 ¹ 1.028	
231	QNAP-002	358	-	208 ¹ 0.0049	229 ¹ 0.0044	242 ¹ 0.0043	253 ¹ 0.0043	258 ¹ 0.0042	227 ¹ 1.040	
232	QNAP-003	358	-	165 ¹ 0.0028	172 ¹ 0.0021	167 ¹ 0.0019	159 ¹ 0.0017	167 ¹ 0.0015	17 ¹ 1.019	
233	QNAP-004	358	-	119 ¹ 0.0019	122 ¹ 0.0015	120 ¹ 0.0015	123 ¹ 0.0014	134 ¹ 0.0014	117 ¹ 1.014	
234	QUANTASOFT-001	358	-	337 ¹ 0.2177	339 ¹ 0.1643	339 ¹ 0.1468	339 ¹ 0.1312	339 ¹ 0.1116	339 ¹ 2.539	
235	RANKONE-002	358	-	288 ¹ 0.0194	283 ¹ 0.0112	280 ¹ 0.0093	281 ¹ 0.0077	275 ¹ 0.0060	284 ¹ 1.111	
236	RANKONE-003	358	-	287 ¹ 0.0194	284 ¹ 0.0112	281 ¹ 0.0093	280 ¹ 0.0077	275 ¹ 0.0060	283 ¹ 1.111	
237	RANKONE-004	358	-	311 ¹ 0.0145	308 ¹ 0.0226	308 ¹ 0.0177	304 ¹ 0.0141	300 ¹ 0.0102	308 ¹ 1.225	
238	RANKONE-005	358	-	250 ¹ 0.0094	244 ¹ 0.0054	245 ¹ 0.0046	245 ¹ 0.0039	241 ¹ 0.0032	244 ¹ 1.054	
239	RANKONE-006	358	-	210 ¹ 0.0050	210 ¹ 0.0030	210 ¹ 0.0027	205 ¹ 0.0024	202 ¹ 0.0021	209 ¹ 1.030	
240	RANKONE-007	358	-	180 ¹ 0.0034	184 ¹ 0.0023	186 ¹ 0.0021	180 ¹ 0.0018	170 ¹ 0.0017	181 ¹ 1.022	
241	RANKONE-009	358	-	151 ¹ 0.0024	134 ¹ 0.0016	138 ¹ 0.0015	140 ¹ 0.0015	140 ¹ 0.0014	136 ¹ 1.015	
242	RANKONE-010	358	-	144 ¹ 0.0022	146 ¹ 0.0018	145 ¹ 0.0016	148 ¹ 0.0015	150 ¹ 0.0015	146 ¹ 1.016	
243	RANKONE-011	358	-	78 ¹ 0.0015	72 ¹ 0.0012	75 ¹ 0.0012	75 ¹ 0.0012	75 ¹ 0.0012	72 ¹ 1.011	
244	RANKONE-012	358	-	60 ¹ 0.0014	63 ¹ 0.0012	60 ¹ 0.0011	66 ¹ 0.0011	74 ¹ 0.0011	69 ¹ 1.011	
245	RANKONE-013	358	-	25 ¹ 0.0011	19 ¹ 0.0009	21 ¹ 0.0009	22 ¹ 0.0009	23 ¹ 0.0009	18 ¹ 1.008	
246	RANKONE-014	358	-	12 ¹ 0.0010	15 ¹ 0.0009	18 ¹ 0.0009	21 ¹ 0.0009	21 ¹ 0.0009	14 ¹ 1.008	
247	REALNETWORKS-000	358	-	310 ¹ 0.0402	305 ¹ 0.0195	301 ¹ 0.0149	298 ¹ 0.0111	290 ¹ 0.0077	307 ¹ 1.201	
248	REALNETWORKS-001	358	-	369 ¹ 0.0402	306 ¹ 0.0195	307 ¹ 0.0149	297 ¹ 0.0111	291 ¹ 0.0077	308 ¹ 1.201	
249	REALNETWORKS-002	358	-	306 ¹ 0.0393	304 ¹ 0.0189	300 ¹ 0.0142	296 ¹ 0.0108	288 ¹ 0.0076	304 ¹ 1.195	
250	REALNETWORKS-003	358	-	294 ¹ 0.0242	286 ¹ 0.0117	273 ¹ 0.0090	273 ¹ 0.0070	280 ¹ 0.0054	281 ¹ 1.120	
251	REALNETWORKS-004	358	-	292 ¹ 0.0236	285 ¹ 0.0112	277 ¹ 0.0087	271 ¹ 0.0068	264 ¹ 0.0050	289 ¹ 1.116	
252	REALNETWORKS-005	358	-	147 ¹ 0.0023	125 ¹ 0.0016	113 ¹ 0.0014	116 ¹ 0.0013	94 ¹ 0.0012	127 ¹ 1.015	
253	REALNETWORKS-006	358	-	65 ¹ 0.0014	62 ¹ 0.0012	60 ¹ 0.0011	54 ¹ 0.0011	48 ¹ 0.0010	61 ¹ 1.011	
254	REALNETWORKS-007	358	-	56 ¹ 0.0013	58 ¹ 0.0012	54 ¹ 0.0011	52 ¹ 0.0011	46 ¹ 0.0010	56 ¹ 1.011	
255	REALNETWORKS-008	358	-	35 ¹ 0.0011	27 ¹ 0.0010	29 ¹ 0.0009	31 ¹ 0.0009	21 ¹ 0.0009	28 ¹ 1.009	
256	RECOGNITO-000	358	-	8 ¹ 0.0009	7 ¹ 0.0009	11 ¹ 0.0008	12 ¹ 0.0008	13 ¹ 0.0008	8 ¹ 1.008	
257	RECOGNITO-001	358	-						357 ¹ 10.000	
258	REMARKAI-000	358	-	243 ¹ 0.0086	232 ¹ 0.0044	223 ¹ 0.0036	224 ¹ 0.0031	221 ¹ 0.0025	234 ¹ 1.045	
259	REMARKAI-0001	358	-	182 ¹ 0.0034	173 ¹ 0.0021	167 ¹ 0.0019	158 ¹ 0.0017	163 ¹ 0.0015	174 ¹ 1.020	
260	REMARKAI-002	358	-	241 ¹ 0.0081	223 ¹ 0.0040	214 ¹ 0.0031	212 ¹ 0.0026	201 ¹ 0.0021	228 ¹ 1.041	
261	RENIDIP-000	358	-	83 ¹ 0.0015	83 ¹ 0.0013	78 ¹ 0.0012	83 ¹ 0.0012	90 ¹ 0.0012	87 ¹ 1.012	
262	REVEALMEDIA-000	358	-	113 ¹ 0.0019	90 ¹ 0.0013	93 ¹ 0.0013	93 ¹ 0.0013	92 ¹ 0.0012	96 ¹ 1.013	
263	S1-000	358	-	153 ¹ 0.0024	143 ¹ 0.0018	147 ¹ 0.0017	151 ¹ 0.0016	155 ¹ 0.0015	150 ¹ 1.017	
264	S1-001	358	-	175 ¹ 0.0031	192 ¹ 0.0025	200 ¹ 0.0024	206 ¹ 0.0024	215 ¹ 0.0023	188 ¹ 1.023	
265	S1-002	358	-	57 ¹ 0.0014	91 ¹ 0.0013	98 ¹ 0.0013	110 ¹ 0.0013	123 ¹ 0.0013	89 ¹ 1.012	
266	S1-003	358	-	73 ¹ 0.0015	88 ¹ 0.0013	87 ¹ 0.0013	97 ¹ 0.0013	102 ¹ 0.0013	88 ¹ 1.012	
267	S1-004	358	-	57 ¹ 0.0013	79 ¹ 0.0013	85 ¹ 0.0013	96 ¹ 0.0013	101 ¹ 0.0013	76 ¹ 1.012	
268	SCANOVATE-000	358	-	209 ¹ 0.0050	198 ¹ 0.0026	199 ¹ 0.0022	176 ¹ 0.0018	164 ¹ 0.0015	209 ¹ 1.026	
269	SCANOVATE-001	358	-	213 ¹ 0.0053	200 ¹ 0.0027	196 ¹ 0.0022	179 ¹ 0.0018	161 ¹ 0.0015	204 ¹ 1.028	
270	SENSETIME-000	358	-	147 ¹ 0.0023	168 ¹ 0.0020	171 ¹ 0.0019	174 ¹ 0.0018	175 ¹ 0.0017	161 ¹ 1.018	
271	SENSETIME-001	358	-	150 ¹ 0.0023	165 ¹ 0.0020	170 ¹ 0.0019	163 ¹ 0.0017	168 ¹ 0.0016	160 ¹ 1.018	
272	SENSETIME-002	358	-	275 ¹ 0.0137	292 ¹ 0.0136	299 ¹ 0.0136	303 ¹ 0.0136	303 ¹ 0.0136	289 ¹ 1.122	
273	SENSETIME-003	358	-	16 ¹ 0.0010	29 ¹ 0.0010	30 ¹ 0.0010	36 ¹ 0.0009	39 ¹ 0.0009	24 ¹ 1.009	
274	SENSETIME-004	358	-	15 ¹ 0.0010	12 ¹ 0.0009	16 ¹ 0.0009	17 ¹ 0.0009	16 ¹ 0.0009	13 ¹ 1.008	
275	SENSETIME-005	358	-	6 ¹ 0.0009	6 ¹ 0.0008	4 ¹ 0.0008	6 ¹ 0.0008	5 ¹ 0.0008	5 ¹ 1.008	
276	SENSETIME-006	358	-	5 ¹ 0.0009	5 ¹ 0.0008	7 ¹ 0.0008	11 ¹ 0.0008	11 ¹ 0.0008	6 ¹ 1.008	
277	SENSETIME-007	358	-	3 ¹ 0.0008	4 ¹ 0.0008	3 ¹ 0.0008	9 ¹ 0.0008	12 ¹ 0.0008	4 ¹ 1.007	
278	SENSETIME-008	358	-	4 ¹ 0.0008	2 ¹ 0.0008	3 ¹ 0.0008	8 ¹ 0.0008	8 ¹ 0.0008	2 ¹ 1.007	
279	SENSETIME-009	358	-	2 ¹ 0.0008	3 ¹ 0.0008	4 ¹ 0.0008	10 ¹ 0.0008	10 ¹ 0.0008	3 ¹ 1.007	
280	SERENDIPITY-000									

#	ALGORITHM	MISSES OUTSIDE RANK R		RESOURCE USAGE		ENROL MOST RECENT, N = 1.6M									
		FNIR(N, T=0, R)		TEMPLATE		FRVT 2018 MUGSHOTS					WORK-10				
		BYTES	MSEC	R=1	R=5	R=10	R=20	R=50							
289	SQISOFT-001	358	-	196	0.0042	108	0.0014	83	0.0013	70	0.0012	58	0.0010	144	1.016
290	SQISOFT-002	358	-	54	0.0013	41	0.0010	41	0.0010	39	0.0010	36	0.0009	41	1.010
291	STAQU-000	358	-	232	0.0071	250	0.0060	252	0.0057	260	0.0055	268	0.0053	247	1.056
292	SYNEISIS-003	358	-	279	0.0162	296	0.0160	304	0.0160	309	0.0160	315	0.0160	291	1.144
293	SYNEISIS-003	358	-	334	0.1700	334	0.1172	334	0.1047	335	0.0953	336	0.0869	334	2.120
294	SYNEISIS-005	358	-	242	0.0085	270	0.0085	278	0.0085	287	0.0085	297	0.0085	267	1.076
295	T4HSB-000	358	-	255	0.0104	281	0.0103	289	0.0103	294	0.0103	301	0.0103	280	1.093
296	TECH5-001	358	-	190	0.0040	187	0.0024	187	0.0021	181	0.0018	176	0.0017	191	1.024
297	TECH5-002	358	-	164	0.0027	106	0.0014	81	0.0012	64	0.0011	56	0.0010	118	1.014
298	TEVIAN-003	358	-	276	0.0147	262	0.0074	253	0.0059	255	0.0047	252	0.0037	266	1.075
299	TEVIAN-004	358	-	263	0.0113	246	0.0057	246	0.0047	241	0.0037	239	0.0030	248	1.058
300	TEVIAN-005	358	-	233	0.0073	220	0.0038	215	0.0031	215	0.0027	212	0.0023	223	1.038
301	TEVIAN-006	358	-	155	0.0024	151	0.0018	159	0.0018	161	0.0017	177	0.0017	151	1.017
302	TEVIAN-007	358	-	105	0.0018	94	0.0014	100	0.0013	111	0.0013	107	0.0013	96	1.013
303	TIGER-000	358	-	318	0.0616	315	0.0310	317	0.0236	312	0.0178	308	0.0120	317	1.315
304	TIGER-002	358	-	216	0.0056	208	0.0029	201	0.0024	182	0.0019	159	0.0015	207	1.030
305	TIGER-003	358	-	215	0.0056	209	0.0029	200	0.0024	184	0.0019	158	0.0015	208	1.030
306	TONGYITRANS-000	358	-	227	0.0069	218	0.0038	220	0.0032	219	0.0029	220	0.0026	220	1.038
307	TONGYITRANS-001	358	-	228	0.0069	219	0.0038	218	0.0032	220	0.0029	224	0.0026	221	1.038
308	TOSHIBA-000	358	-	201	0.0045	197	0.0026	192	0.0022	189	0.0020	198	0.0018	198	1.026
309	TOSHIBA-001	358	-	206	0.0048	201	0.0027	197	0.0023	196	0.0020	188	0.0018	202	1.027
310	TRUEFACE-000	358	-	179	0.0033	205	0.0028	217	0.0028	214	0.0026	222	0.0026	199	1.026
311	TURINGTECHVIP-001	358	-	251	0.0095	278	0.0093	282	0.0093	291	0.0093	296	0.0093	270	1.084
312	USEB-000	358	-	303	0.0345	297	0.0157	294	0.0119	290	0.0092	277	0.0063	301	1.165
313	VD-000	358	-	348	0.4737	347	0.3204	346	0.2695	345	0.2215	344	0.1678	347	4.058
314	VD-001	358	-	299	0.0276	305	0.0181	305	0.0162	305	0.0146	308	0.0130	303	1.174
315	VD-002	358	-	252	0.0095	264	0.0077	268	0.0073	272	0.0070	282	0.0068	261	1.071
316	VD-003	358	-	234	0.0076	257	0.0069	26	0.0067	269	0.0066	27	0.0066	25	1.063
317	VERIDAS-001	358	-	167	0.0028	161	0.0019	151	0.0017	149	0.0015	151	0.0015	161	1.018
318	VERIDAS-002	358	-	166	0.0028	160	0.0019	146	0.0017	147	0.0015	146	0.0015	159	1.018
319	VERIDAS-003	358	-	108	0.0018	115	0.0015	114	0.0014	117	0.0013	117	0.0013	109	1.014
320	VERIDAS-004	358	-	58	0.0014	76	0.0013	80	0.0012	87	0.0012	98	0.0012	70	1.011
321	VERIGRAM-000	358	-	160	0.0025	191	0.0024	202	0.0024	207	0.0024	219	0.0024	183	1.022
322	VERIJELAS-000	358	-	343	0.3547	344	0.2975	347	0.2805	347	0.2655	348	0.2489	344	3.744
323	VIGILANTSOLUTIONS-003	358	-	321	0.0694	318	0.0349	313	0.0262	313	0.0201	310	0.0140	318	1.355
324	VIGILANTSOLUTIONS-004	358	-	329	0.1249	328	0.0706	326	0.0557	324	0.0434	322	0.0305	328	1.699
325	VIGILANTSOLUTIONS-005	358	-	247	0.0092	234	0.0045	222	0.0036	218	0.0029	207	0.0022	235	1.046
326	VIGILANTSOLUTIONS-006	358	-	254	0.0099	236	0.0048	230	0.0038	223	0.0030	211	0.0022	238	1.049
327	VIGILANTSOLUTIONS-007	358	-	181	0.0034	163	0.0020	159	0.0017	145	0.0015	122	0.0013	170	1.019
328	VIGILANTSOLUTIONS-008	358	-	173	0.0029	154	0.0018	141	0.0016	135	0.0015	110	0.0013	158	1.018
329	VISIONBOX-000	358	-	120	0.0019	117	0.0015	122	0.0014	118	0.0013	108	0.0013	111	1.014
330	VISIONLABS-004	358	-	165	0.0027	148	0.0018	143	0.0016	144	0.0015	137	0.0014	154	1.017
331	VISIONLABS-005	358	-	152	0.0024	138	0.0017	131	0.0015	124	0.0014	117	0.0013	142	1.016
332	VISIONLABS-006	358	-	110	0.0018	111	0.0015	107	0.0014	107	0.0013	111	0.0013	108	1.014
333	VISIONLABS-007	358	-	104	0.0018	104	0.0014	94	0.0013	91	0.0013	95	0.0012	104	1.013
334	VISIONLABS-008	358	-	131	0.0020	152	0.0018	168	0.0018	167	0.0018	178	0.0017	148	1.017
335	VISIONLABS-009	358	-	34	0.0011	43	0.0011	45	0.0010	47	0.0010	47	0.0010	40	1.010
336	VISIONLABS-010	358	-	64	0.0014	82	0.0013	96	0.0013	94	0.0013	104	0.0013	81	1.012
337	VISIONLABS-011	358	-	39	0.0012	50	0.0011	56	0.0011	57	0.0011	63	0.0011	49	1.010
338	VIXVIZION-009	358	-	145	0.0023	124	0.0016	118	0.0014	106	0.0013	92	0.0012	126	1.015
339	VNPT-001	358	-	137	0.0022	158	0.0019	165	0.0018	175	0.0018	186	0.0018	155	1.017
340	VNPT-002	358	-	116	0.0019	149	0.0018	159	0.0018	166	0.0018	182	0.0017	141	1.016
341	VNPT-003	358	-	89	0.0016	118	0.0015	132	0.0015	143	0.0015	150	0.0015	112	1.014
342	VOCORD-003	358	-	221	0.0062	215	0.0035	213	0.0030	213	0.0026	214	0.0023	214	1.035
343	VOCORD-004	358	-	237	0.0079	238	0.0049	240	0.0043	244	0.0038	246	0.0034	236	1.048
344	VOCORD-005	358	-	231	0.0070	233	0.0046	236	0.0041	243	0.0038	249	0.0035	232	1.044
345	VOCORD-006	358	-	355	1.0000	357	1.0000	355	1.0000	355	1.0000	355	1.0000	355	10.000
346	VTCC-000	358	-	200	0.0044	226	0.0043	239	0.0042	250	0.0042	257	0.0042	223	1.039
347	VTS-000	358	-	351	0.5937	352	0.5936	353	0.5936	352	0.5936	353	0.5936	36	3.343
348	VTS-001	358	-	82	0.0015	99	0.0012	92	0.0011	93	0.0011	49	0.0010	64	1.011
349	VTS-002	358	-	121	0.0019	101	0.0014	88	0.0013	86	0.0012	77	0.0011	10	1.013
350	VTS-003	358	-	36	0.0011	34	0.0010	28	0.0009	25	0.0009	24	0.0009	30	1.009
351	XFORWARDAI-000	358	-	146	0.0023	166	0.0020	172	0.0020	190	0.0019	196	0.0019	161	1.018
352	XFORWARDAI-001	358	-	134	0.0020	162	0.0019	174	0.0019	186	0.0019	196	0.0019	156	1.018
353	XFORWARDAI-002	358	-	124	0.0020	159	0.0019	172	0.0019	185	0.0019	194	0.0019	153	1.017
354	YISHENG-001	358	-	298	0.0265	291	0.0130	289	0.0102	284	0.0080	277	0.0059	292	1.134
355	YITU-002	358	-	112	0.0018	71	0.0012	61	0.0011	56	0.0011	52	0.0010	60	1.012
356	YITU-003	358	-	172	0.0029	182	0.0023	192	0.0022	200	0.0021	209	0.0021	179	1.021
357	YITU-004	358	-	52	0.0013	21	0.0009	20	0.0009	20	0.0009	19	0.0009	33	1.009
358	YITU-005	358	-	148	0.0023	171	0.0021	178	0.0020	193	0.0020	196	0.0020	166	1.019

Table 33: Rank-based accuracy for the FRVT 2018 mugshot sets. In columns 3 and 4 are template size and template generation duration. Thereafter values are rank-based FNIR with T

MISSES BELOW THRESHOLD, T		ENROL RECENT MUGSHOT, N = 1.6M												ENROL APPLICATION PORTRAIT, N = 1.6M											
#	ALGORITHM	ENROL: MUGSHOT			ENROL: MUGSHOT			ENROL: PROFILE			ENROL: VISA			ENROL: BORDER			PROBE: BORDER 10+YR			PROBE: KIOSK					
		FPIR=0.0003	FPIR=0.001	FPIR=0.01	FPIR=0.0003	FPIR=0.001	FPIR=0.01	FPIR=0.0003	FPIR=0.001	FPIR=0.01	FPIR=0.001	FPIR=0.001	FPIR=0.01	FPIR=0.001	FPIR=0.01	FPIR=0.001	FPIR=0.01	FPIR=0.001	FPIR=0.01	FPIR=0.001	FPIR=0.01	FPIR=0.001	FPIR=0.01		
1	20FACE-000	²⁹⁹ 0.462	³¹⁰ 0.348	³¹⁸ 0.230	³⁰⁷ 0.763	²⁹⁷ 0.450	³⁰¹ 0.301	²⁶⁷ 1.000	²⁷⁶ 1.000	²⁸⁵ 1.000	²³⁷ 0.424	²⁴⁰ 0.255	¹⁴¹ 0.772	¹⁵³ 0.599	²³³ 0.938	²⁴⁹ 0.836									
2	3DIVI-003	³⁰¹ 0.482	³¹⁹ 0.400	³²⁴ 0.282	³⁰¹ 0.685	³¹⁸ 0.626	³¹⁷ 0.497				²⁵² 0.605	²⁵⁹ 0.445											²¹³ 0.821	²³⁸ 0.717	
3	3DIVI-004	²⁷¹ 0.256	²⁸⁹ 0.169	²⁹⁴ 0.093	²⁶⁵ 0.400	²⁸⁷ 0.343	²⁹⁵ 0.237				²²⁶ 0.277	²³³ 0.172											¹⁸⁴ 0.607	²¹⁷ 0.485	
4	3DIVI-005	²⁷⁰ 0.255	²⁸⁶ 0.166	²⁹⁵ 0.093	²⁶⁷ 0.395	²⁸⁵ 0.339	²⁹⁴ 0.234	¹⁸⁴ 0.998	¹⁹⁵ 0.996	²¹⁵ 0.990	²⁵⁹ 0.864	²⁶⁷ 0.846											¹⁸³ 0.597	²¹⁶ 0.484	
5	3DIVI-006	²⁶⁹ 0.253	²⁸⁸ 0.168	²⁹⁶ 0.096	²⁶⁸ 0.403	²⁸⁶ 0.342	²⁹⁶ 0.238				²²⁷ 0.283	²³⁴ 0.174											¹⁸⁷ 0.615	²¹⁸ 0.490	
6	AADI-000										²⁸² 1.000	³⁴⁷ 1.000	²³⁵ 1.000	¹⁶⁹ 1.000	³⁵⁴ 1.000	³³⁶ 1.000									
7	ACER-000	²⁵⁹ 0.208	²⁷⁸ 0.146	²⁸³ 0.074	²⁴⁷ 0.300	²⁶³ 0.246	²⁶⁹ 0.157	¹²² 0.987	¹⁴⁴ 0.981	¹²⁷ 0.955	²²⁰ 0.201	²²⁹ 0.114											¹⁶² 0.490	¹⁹⁸ 0.363	
8	ACER-001	²⁰⁰ 0.109	²¹⁸ 0.056	²²⁴ 0.026	¹⁸⁹ 0.136	¹⁸⁹ 0.109	¹⁹⁸ 0.069	²²⁰ 1.000	²³⁵ 0.999	²⁶ 0.998	¹⁷⁶ 0.068	¹⁷⁸ 0.036	¹²⁵ 0.406	¹³⁶ 0.250									¹⁶⁶ 0.479	¹⁴⁷ 0.206	
9	ADVANCE-000	¹¹⁶ 0.038	¹³⁷ 0.020	¹³¹ 0.008	²⁶² 0.371	²⁷⁴ 0.270	²⁴⁸ 0.112	¹⁷² 0.997	¹²⁸ 0.973	⁸⁶ 0.476	²⁰⁹ 0.163	¹⁹² 0.047	¹⁴⁶ 0.884	¹⁵⁶ 0.667									¹³⁴ 0.326	¹⁴⁷ 0.209	
10	AFISBIOMETRICS-000	¹⁵³ 0.054	¹⁷⁴ 0.030	¹⁶¹ 0.011	¹⁴⁴ 0.104	¹⁵⁴ 0.081	¹⁴⁶ 0.044	⁴⁷ 0.623	⁵⁴ 0.517	⁷ 0.347	¹³⁴ 0.034	¹² 0.015	⁸¹ 0.154	⁸⁶ 0.080	⁸³ 0.172	⁹⁶ 0.127									
11	AIZE-001	²¹¹ 0.127	²⁴⁰ 0.077	²³⁹ 0.034	²¹¹ 0.187	²¹⁷ 0.143	²²¹ 0.087	¹⁵⁶ 0.995	¹⁷³ 0.994	²⁰² 0.983	¹⁹⁰ 0.101	¹⁹⁷ 0.052	¹¹⁸ 0.364	¹³¹ 0.216	¹⁴⁵ 0.387	¹⁸⁰ 0.289									
12	ALCHERA-000	²⁶² 0.231	²⁷⁵ 0.138	²⁷⁷ 0.070	²⁵⁶ 0.259	²⁴ 0.216	²⁶² 0.146	¹⁹⁶ 0.999	²¹⁴ 0.999	²⁴ 0.996	²¹⁴ 0.176	²² 0.111											²⁰⁹ 0.803	²¹⁷ 0.456	
13	ALCHERA-001	³⁵¹ 1.000	³⁵¹ 0.999	³⁵³ 0.999	³⁴² 1.000	³⁴² 1.000	³⁴⁹ 1.000						³⁵⁰ 1.000	²⁷⁶ 1.000									²⁵⁹ 1.000	²⁹⁷ 1.000	
14	ALCHERA-002	³²⁶ 0.807	³²⁶ 0.486	³² 0.302	³⁶⁷ 0.685	³⁶⁷ 0.591	³¹² 0.442	²³⁹ 1.000	²⁴² 1.000	²⁶⁹ 0.999	²⁵⁸ 0.827	²⁶⁷ 0.770											²¹⁰ 0.811	²³⁸ 0.705	
15	ALCHERA-003	²⁹⁵ 0.450	²⁸⁰ 0.155	²⁷⁸ 0.070	²⁴⁸ 0.304	²⁵⁹ 0.239	²⁶⁷ 0.152	²³³ 1.000	²²⁷ 0.999	²⁵⁰ 0.997	²¹³ 0.172	²²⁰ 0.097											¹⁶¹ 0.464	¹⁹⁷ 0.362	
16	ALCHERA-004	³⁰⁶ 0.520	³¹⁸ 0.394	³¹⁷ 0.211	²⁹⁷ 0.642	³⁰⁴ 0.529	³⁰⁶ 0.327	¹⁵⁷ 0.995	¹⁶⁵ 0.991	¹³⁶ 0.813	²³⁸ 0.424	²³⁸ 0.232	¹³³ 0.708	¹⁴⁷ 0.515									¹⁷⁸ 0.546	²⁰⁸ 0.398	
17	ALLGOVISION-000	²²¹ 0.138	²⁵² 0.088	²⁵⁹ 0.045	²²³ 0.202	²³³ 0.166	²⁴⁵ 0.106	¹⁴³ 0.993	¹⁶² 0.990	²⁰¹ 0.982	¹⁹³ 0.117	²⁰⁴ 0.066											¹⁷⁵ 0.526	²⁰⁷ 0.396	
18	ALLGOVISION-001	²³⁰ 0.155	²⁵⁷ 0.102	²⁶⁵ 0.053	²⁴¹ 0.275	²⁵¹ 0.221	²⁶¹ 0.141	¹⁴⁷ 0.993	¹⁵¹ 0.986	¹⁶⁰ 0.933	²⁰⁶ 0.150	²¹⁵ 0.081											¹⁶⁸ 0.491	²⁰⁶ 0.389	
19	ALLGOVISION-002	²¹⁶ 0.133	²³¹ 0.065	²²² 0.028	³⁰⁶ 0.753	³⁰³ 0.520	²⁴⁹ 0.113	¹¹⁷ 0.983	¹¹¹ 0.950	¹⁴ 0.870	²²² 0.232	¹⁹⁷ 0.049	¹⁷³ 1.000	¹⁶⁶ 1.000	¹⁹⁸ 0.716	²⁰⁶ 0.366								²⁵² 1.000	³³⁴ 1.000
20	ANKE-000	²⁴¹ 0.184	²⁶² 0.117	²⁷⁴ 0.063	²⁵⁵ 0.256	²⁵⁰ 0.220	²⁶⁵ 0.151	¹⁵³ 0.995	¹⁷² 0.994	²¹³ 0.990	²⁸⁰ 1.000	³⁵¹ 1.000												²⁷¹ 1.000	³⁰⁹ 1.000
21	ANKE-001	²³⁹ 0.183	²⁶⁶ 0.119	²⁷⁷ 0.063	²⁴⁷ 0.256	²⁴² 0.220	²⁶⁶ 0.151	¹⁵⁹ 0.995	¹⁷⁹ 0.994	²² 0.992	³³⁹ 1.000	²⁹⁷ 1.000												¹⁰⁹ 0.245	¹³⁷ 0.190
22	ANKE-002	¹⁶³ 0.062	¹⁷⁹ 0.032	¹⁸⁰ 0.014	¹⁴³ 0.103	¹⁵¹ 0.079	¹⁶⁰ 0.050	¹⁰¹ 0.975	¹¹⁰ 0.948	¹³² 0.795	¹³⁵ 0.034	¹⁴⁰ 0.018													
23	ARMATURA-000	³⁶ 0.009	⁴⁸ 0.004	⁶ 0.003	⁴⁴ 0.031	⁴ 0.025	⁶² 0.018	²¹⁰ 0.291	²² 0.223	² 0.134	²⁸ 0.006	²⁸ 0.003	²⁸ 0.048	²⁴ 0.019	¹⁹ 0.090	¹⁷ 0.073									
24	AWARE-003	²³⁸ 0.174	²⁷⁰ 0.128	²⁸⁶ 0.082	²⁵⁹ 0.351	²⁷⁹ 0.298	²⁸⁸ 0.204	¹²⁴ 0.987	¹⁴⁸ 0.984	¹⁹⁶ 0.977	²³⁹ 0.428	²⁴⁷ 0.378											¹⁷⁶ 0.530	²¹⁰ 0.443	
25	AWARE-004	²⁸⁷ 0.355	³⁰² 0.269	³¹¹ 0.175	²⁹³ 0.619	³⁰² 0.509	³¹⁰ 0.375	²³⁵ 1.000	²⁴⁶ 1.000	²⁷⁷ 0.999	²³⁴ 0.397	²⁴⁷ 0.279											²¹¹ 0.816	²³⁸ 0.631	
26	AWARE-005	³¹² 0.608	³¹³ 0.364	²⁸⁸ 0.085	²⁵⁴ 0.342	²⁶⁵ 0.253	²⁷¹ 0.163	²³² 1.000	²⁴⁹ 1.000	²⁷⁵ 0.999	²²⁵ 0.255	²³¹ 0.122											²²⁶ 0.916	²³⁷ 0.714	
27	AWARE-006	³⁰⁰ 0.475	³⁰³ 0.276	³¹⁷ 0.175	²⁷² 0.466	²⁹⁰ 0.398	²⁹⁹ 0.283	²¹⁶ 1.000	²³⁸ 0.999	²⁶ 0.999	²³² 0.368	²³⁹ 0.254											²⁰² 0.749	²²⁷ 0.623	
28	AYONIX-000	³³⁰ 0.846	³³⁹ 0.811	³⁴⁵ 0.724	³²² 0.956	³³⁶ 0.939	³³⁸ 0.892	¹⁸⁵ 0.998	²⁰³ 0.998	²⁴² 0.995	²⁶⁴ 0.954	²⁶⁶ 0.891											²⁴² 0.982	²⁵⁹ 0.959	
29	AYONIX-001	³³² 0.875	³⁴¹ 0.824	³⁴³ 0.701	³¹⁷ 0.946	³³¹ 0.920	³³⁴ 0.845	²²⁸ 1.000	²³⁴ 0.999	²⁴⁶ 0.996	²⁶⁰ 0.915	²⁶⁷ 0.821											²³⁹ 0.969	²⁵⁷ 0.926	
30	AYONIX-002	³³³ 0.876	³⁴⁰ 0.824	³⁴⁴ 0.702	³¹⁸ 0.946	³³² 0.920	³³³ 0.845	²³⁰ 1.000	²³⁴ 0.999	²⁴⁶ 0.996	²⁶⁰ 0.915	²⁶⁷ 0.821											²³⁸ 0.969	²⁵⁹ 0.926	
31	CAMVI-003	¹⁸⁹ 0.094	²³⁵ 0.071	²⁷⁰ 0.058	¹⁹¹ 0.152	²⁰⁹ 0.132	²⁴⁶ 0.108	¹⁰⁹ 0.979	¹²⁵ 0.970	¹⁶⁷ 0.940	¹⁹² 0.114	²²¹ 0.100											¹⁴⁹ 0.402	²⁰³ 0.377	
32	CAMVI-004	¹⁹⁸ 0.107	²³⁶ 0.072	²⁰⁸ 0.054	²²¹ 0.136	²³⁵ 0.100	²¹⁸ 1.000	²³² 0.999	²⁵⁹ 0.998	¹⁸⁹ 0.100	²¹⁹ 0.081												²⁰⁷ 0.787	²²⁸ 0.507	
33	CAMVI-005	²²² 0.139	²⁵⁰ 0.099	²⁸⁵ 0.076	²⁴⁰ 0.175	²⁵⁶ 0.132	²²² 1.000	²⁴³ 1.000	²⁶¹ 0.998	²⁰⁷ 0.156	²²⁸ 0.112												²⁵¹ 0.999	²⁶² 0.983	
34	CANON-001	⁵² 0.012	⁶² 0.005	⁶⁰ 0.002	⁴² 0.027	⁴³ 0																			

MISSES BELOW THRESHOLD, T		ENROL RECENT MUGSHOT, N = 1.6M												ENROL APPLICATION PORTRAIT, N = 1.6M															
		ENROL: MUGSHOT				ENROL: MUGSHOT				ENROL: WEBCAM				ENROL: MUGSHOT				PROBE: PROFILE				ENROL: VISA		ENROL: BORDER		ENROL: BORDER 10+YR		ENROL: VISA	
#	ALGORITHM	FPIR=0.0003	FPIR=0.001	FPIR=0.01	FPIR=0.0003	FPIR=0.001	FPIR=0.01	FPIR=0.0003	FPIR=0.001	FPIR=0.01	FPIR=0.0003	FPIR=0.001	FPIR=0.01	FPIR=0.0003	FPIR=0.001	FPIR=0.01	FPIR=0.0003	FPIR=0.001	FPIR=0.01	FPIR=0.0003	FPIR=0.001	FPIR=0.01	FPIR=0.0003	FPIR=0.001	FPIR=0.01	FPIR=0.0003	FPIR=0.001		
47	COGENT-005	¹⁴³ 0.050	⁸⁶ 0.009	⁸⁶ 0.004	⁷⁴ 0.050	⁷⁹ 0.037	⁸⁵ 0.023	¹⁶¹ 0.996	¹⁵⁸ 0.989	⁷⁰ 0.323	⁶⁹ 0.011	⁷¹ 0.006	³⁵ 0.082	⁶ 0.043	²²⁴ 0.905	¹³⁹ 0.202													
48	COGENT-006	⁴⁸ 0.010	⁴⁹ 0.004	⁴⁹ 0.002	⁴⁶ 0.033	⁴³ 0.023	⁴⁵ 0.015	²⁸ 0.383	²⁵ 0.238	²⁹ 0.145	³¹ 0.006	³⁵ 0.003	¹²⁶ 0.422	⁴⁰ 0.028	⁵³ 0.130	⁸⁰ 0.120													
49	COGENT-007	³² 0.008	³⁸ 0.004	³⁸ 0.002	³⁵ 0.027	³⁶ 0.021	⁴¹ 0.014	¹⁰ 0.250	¹⁴ 0.194	²² 0.126	³³ 0.006	³⁵ 0.003	²⁷ 0.047	²⁶ 0.022	⁶⁷ 0.144	⁹² 0.129													
50	COGNITEC-000	²⁶⁰ 0.226	²⁸⁴ 0.161	²⁹⁵ 0.095	²⁷³ 0.439	²⁸⁰ 0.303	²⁸⁶ 0.200	¹⁶⁰ 0.996	¹⁶⁶ 0.992	¹⁸⁵ 0.971																			
51	COGNITEC-001	²⁵¹ 0.192	²⁵⁸ 0.102	²⁶⁶ 0.053	³³⁷ 0.997	²⁵ 0.230	²⁵⁸ 0.135	²⁸⁴ 1.000	³⁵⁵ 1.000	¹⁸ 0.965																			
52	COGNITEC-002	²⁰⁷ 0.122	²¹¹ 0.053	²¹⁹ 0.025	³³³ 0.990	²³⁹ 0.178	²⁴² 0.101	³² 1.000	²⁵⁸ 1.000	¹⁷⁸ 0.956																			
53	COGNITEC-003	¹⁹³ 0.099	²⁰⁷ 0.053	²² 0.025	²² 0.222	²³ 0.162	²³⁶ 0.100	²⁸⁸ 1.000	¹⁶ 0.946																				
54	COGNITEC-004	¹⁵⁵ 0.055	¹⁷⁸ 0.031	¹⁸¹ 0.014	¹⁶⁸ 0.127	¹⁷⁷ 0.097	¹⁷⁸ 0.058	¹⁵⁵ 0.995	¹⁵⁹ 0.990	¹⁵⁵ 0.919	¹⁷⁵ 0.068	¹⁸⁰ 0.038	¹¹⁵ 0.316	¹³⁰ 0.196	¹²³ 0.288	¹⁵⁴ 0.218													
55	COGNITEC-005	¹⁵⁶ 0.055	⁸⁹ 0.010	⁸² 0.004	⁸⁶ 0.058	⁸⁹ 0.041	⁸⁰ 0.022	²⁹⁷ 1.000	³⁴¹ 1.000	¹⁴⁸ 0.878	¹⁴⁷ 0.041	¹⁶ 0.028	⁸² 0.157	⁹⁷ 0.092	⁸⁹ 0.179	¹⁰⁶ 0.145													
56	COGNITEC-006	¹⁰⁰ 0.029	⁷⁸ 0.008	⁷⁴ 0.003	⁹² 0.065	⁸⁵ 0.040	⁷⁶ 0.022	³⁰⁶ 1.000	³³² 1.000	²⁶⁶ 0.999	¹²² 0.030	¹¹⁹ 0.013	⁸⁸ 0.171	⁸⁰ 0.081	¹⁹⁵ 0.681	¹⁵¹ 0.214													
57	CUBOX-000	²² 0.005	³¹ 0.003	³⁷ 0.002	²⁸ 0.022	³⁰ 0.019	³⁵ 0.014	¹⁶ 0.276	¹¹ 0.168	¹⁷ 0.104	¹⁹ 0.004	²¹ 0.003	¹⁵ 0.028	¹⁶ 0.014	⁸ 0.073	⁹ 0.062													
58	CYBERLINK-000	²²⁰ 0.137	²¹⁹ 0.056	²¹¹ 0.023	¹⁹⁷ 0.162	¹⁹³ 0.116	²⁰¹ 0.070	¹⁷⁶ 0.997	¹⁸⁸ 0.995	²⁰ 0.981	¹⁷³ 0.063	¹⁷ 0.032	¹⁹¹ 0.652	¹⁶ 0.232															
59	CYBERLINK-001	¹⁹⁴ 0.096	²¹¹ 0.054	²⁰⁹ 0.022	¹⁸⁴ 0.138	¹⁹⁰ 0.109	¹⁹⁴ 0.067	¹⁷⁵ 0.997	¹⁸³ 0.995	²⁰³ 0.984	¹⁷⁰ 0.062	¹⁶⁹ 0.031																	
60	CYBERLINK-002	¹¹⁷ 0.038	¹¹⁵ 0.015	¹¹⁶ 0.006	¹⁰² 0.068	¹¹⁰ 0.053	¹¹¹ 0.032	¹⁴⁹ 0.994	¹⁵⁷ 0.988	¹⁷⁰ 0.957	¹⁰⁹ 0.024	¹¹ 0.013	¹²⁴ 0.288	¹¹⁶ 0.157															
61	CYBERLINK-003	¹³⁰ 0.045	⁷⁹ 0.008	⁸⁰ 0.004	⁶⁵ 0.045	⁷⁴ 0.035	⁷¹ 0.021	¹⁵⁰ 0.995	¹²⁶ 0.972	¹⁴¹ 0.845	⁷³ 0.012	²⁹ 0.007	⁶² 0.100	⁶⁸ 0.051	¹⁴² 0.368	⁸² 0.120													
62	CYBERLINK-004	²⁴⁹ 0.188	⁷⁴ 0.007	⁷² 0.003	⁹⁰ 0.063	⁷⁵ 0.036	⁷⁸ 0.022	²⁸⁰ 1.000	²⁷⁸ 1.000	²⁷ 0.999	⁷⁶ 0.013	²⁹ 0.007	⁶³ 0.109	⁶⁷ 0.050	²³⁷ 0.954	¹⁸³ 0.291													
63	CYBERLINK-005	²⁵⁰ 0.208	⁹³ 0.010	⁸⁸ 0.004	⁸¹ 0.054	⁸⁶ 0.041	⁸⁴ 0.026	²⁴⁶ 1.000	²⁴⁸ 1.000	¹⁴⁹ 0.888	⁸⁰ 0.014	⁵⁷ 0.089	⁵⁹ 0.043	²³² 0.926	¹⁷³ 0.266														
64	DAHUA-000	²¹³ 0.128	²⁴⁸ 0.086	²⁵⁰ 0.045	²⁰ 0.179	²¹ 0.135	²¹⁹ 0.083																						
65	DAHUA-001	¹⁹⁷ 0.106	²³⁸ 0.073	²⁴⁵ 0.037	¹⁹⁰ 0.151	²⁰¹ 0.122	²¹⁰ 0.075	¹²⁶ 0.987	¹⁴⁰ 0.980	¹⁶¹ 0.933																			
66	DAHUA-002	⁹³ 0.026	¹¹⁶ 0.015	¹¹⁷ 0.006	⁸⁷ 0.060	⁹⁶ 0.046	¹⁰⁰ 0.029	⁵⁵ 0.681	⁶⁷ 0.638	⁹² 0.522	⁸⁷ 0.017	⁸⁷ 0.008																	
67	DAHUA-003	⁹⁰ 0.025	¹⁰⁵ 0.014	¹⁰² 0.005	⁸⁰ 0.054	⁸⁸ 0.041	⁸⁸ 0.024	⁵⁰ 0.647	⁶² 0.579	⁸¹ 0.447	⁷⁵ 0.013	⁷⁷ 0.006	⁵³ 0.081	⁶⁹ 0.043	⁵⁶ 0.134	⁶⁸ 0.109													
68	DAHUA-004	⁶⁰ 0.014	⁷³ 0.007	⁶⁸ 0.003	⁴⁸ 0.033	⁵³ 0.026	⁵⁰ 0.016	³⁷ 0.552	⁵² 0.485	⁷³ 0.345	⁵⁵ 0.008	⁵⁶ 0.004	³⁰ 0.051	³⁵ 0.027	⁴⁵ 0.113	⁵³ 0.094													
69	DAON-000	²¹⁸ 0.135	¹⁴⁸ 0.023	¹⁴⁹ 0.009	¹¹⁶ 0.079	¹²⁴ 0.061	¹³¹ 0.039	²³⁸ 1.000	²⁴⁷ 1.000	²⁶⁰ 0.998	¹¹⁰ 0.025	¹¹¹ 0.013	⁹⁰ 0.173	⁹⁶ 0.091	²¹⁸ 0.846	¹²³ 0.172													
70	DECATAR-000	¹²² 0.043	¹⁵¹ 0.023	¹⁵³ 0.010	¹²¹ 0.085	¹³⁰ 0.066	¹³⁴ 0.040	⁶⁰ 0.757	⁷² 0.675	⁹¹ 0.509	¹¹⁴ 0.027	¹²³ 0.014	⁸⁹ 0.173	¹⁰³ 0.098	¹⁰⁷ 0.239	¹¹¹ 0.156													
71	DEEPLINT-001	⁴³ 0.010	³⁷ 0.003	³⁹ 0.002	²¹ 0.018	²¹ 0.014	²⁰ 0.010	²⁵⁶ 1.000	²⁴⁰ 1.000	³⁰ 0.503	³⁵ 0.006	³⁹ 0.004																	
72	DEEPSA-001	¹⁷⁵ 0.073	¹⁹⁹ 0.046	²⁰⁷ 0.022	¹²⁷ 0.129	¹⁸¹ 0.101	¹⁸¹ 0.059	¹³⁰ 0.988	¹⁴⁹ 0.985	¹⁹⁰ 0.973	¹⁸⁰ 0.077	¹⁸⁵ 0.041																	
73	DERMALOG-003	³⁰⁸ 0.550	³²⁵ 0.482	³³⁰ 0.360	³⁰⁴ 0.715	³¹⁶ 0.655	³²¹ 0.526	¹⁷⁰ 0.997	¹⁸⁹ 0.995	²²³ 0.991	²⁵⁷ 0.677	²⁵⁹ 0.554																	
74	DERMALOG-004	³¹⁰ 0.554	³²⁴ 0.480	³²⁹ 0.358	³⁰³ 0.711	³¹⁷ 0.657	³¹⁹ 0.526	¹⁶⁹ 0.997	¹⁸⁹ 0.995	²²³ 0.991	²⁵¹ 0.603	²⁵⁴ 0.458	²¹⁹ 0.856	²⁴¹ 0.751															
75	DERMALOG-005	²⁵⁰ 0.189	²⁵¹ 0.088	²⁵ 0.043	²¹⁹ 0.201	²² 0.152	²²⁹ 0.093	¹⁶⁵ 0.996	¹⁶⁰ 0.990	¹⁷ 0.950	²²⁸ 0.300	²⁴ 0.267																	
76	DERMALOG-006	¹⁹² 0.098	²⁰⁶ 0.052	²²⁵ 0.026	¹⁸² 0.137	¹⁸⁴ 0.105	¹⁹³ 0.067	¹³² 0.989	¹⁴³ 0.981	¹⁶² 0.933	¹⁶⁸ 0.059	¹⁷¹ 0.031																	
77	DERMALOG-007	²⁴⁷ 0.188	²⁴⁹ 0.086	²⁴⁹ 0.040	²¹ 0.200	²² 0.152	²²⁹ 0.093	¹⁶⁶ 0.996	¹⁶⁰ 0.990	¹⁷ 0.950	¹⁸⁸ 0.099	¹⁹⁶ 0.052																	
78	DERMALOG-008	²⁷⁴ 0.268	¹⁹⁷ 0.045	¹⁹⁰ 0.017	²²⁸ 0.231	¹⁷⁰ 0.094	¹⁷¹ 0.054	²⁵² 1.000	²⁸² 1.000	¹⁶⁵ 0.057	¹⁶⁰ 0.025	<																	

MISSES BELOW THRESHOLD, T		ENROL RECENT MUGSHOT, N = 1.6M												ENROL APPLICATION PORTRAIT, N = 1.6M												
#	ALGORITHM	ENROL: MUGSHOT			ENROL: MUGSHOT			ENROL: MUGSHOT			ENROL: VISA			ENROL: BORDER			ENROL: BORDER 10+YR			ENROL: KIOSK						
		FPIR=0.0003	FPIR=0.001	FPIR=0.01	FPIR=0.0003	FPIR=0.001	FPIR=0.01	FPIR=0.0003	FPIR=0.001	FPIR=0.01	FPIR=0.0001	FPIR=0.001	FPIR=0.01	FPIR=0.0001	FPIR=0.001	FPIR=0.01	FPIR=0.0001	FPIR=0.001	FPIR=0.01	FPIR=0.0001	FPIR=0.001	FPIR=0.01				
93	GORILLA-001	³²² 0.747	³²⁰ 0.406	³²⁰ 0.246	²⁹⁸ 0.590	²⁹⁸ 0.453	³⁰⁴ 0.314	²⁷⁵ 1.000	²⁷¹ 1.000	²⁹⁷ 1.000	²⁴² 0.468	²⁴³ 0.299										³¹⁶ 1.000	²³⁶ 0.710			
94	GORILLA-002	²⁷³ 0.266	²⁹² 0.188	³⁰⁸ 0.106	²⁵⁹ 0.342	²⁷⁷ 0.268	²⁷⁷ 0.170	²⁶² 1.000	²⁸⁰ 1.000	²²⁹ 0.993	²²⁴ 0.250	²³⁹ 0.137											²⁵⁶ 1.000	²¹⁹ 0.466		
95	GORILLA-003	³²⁰ 0.694	³⁰⁷ 0.318	³¹¹ 0.157	²⁹⁹ 0.684	²⁹⁵ 0.434	²⁹⁷ 0.247	³⁵⁶ 1.000	²⁹⁸ 1.000	²³⁵ 0.407	²³⁵ 0.213												²²⁹ 1.000	²²⁴ 0.562		
96	GORILLA-004	²¹⁷ 0.135	²⁵⁴ 0.089	²⁵⁹ 0.043	²²⁸ 0.202	²³⁰ 0.160	²⁴⁰ 0.101	⁹⁷ 0.972	¹¹³ 0.959	¹⁵ 0.903	²⁰⁰ 0.135	²⁰⁹ 0.072											¹⁵⁵ 0.438	¹⁸⁹ 0.309		
97	GORILLA-005	¹⁸⁶ 0.086	²²³ 0.058	²²⁵ 0.026	²⁰⁵ 0.179	²¹⁶ 0.142	²²³ 0.088	⁶³ 0.770	⁷⁴ 0.700	¹⁰⁰ 0.553	¹⁸⁸ 0.088	¹⁸⁴ 0.040											¹³¹ 0.315	¹⁵⁶ 0.223		
98	GORILLA-006	¹³⁵ 0.046	¹⁶⁶ 0.027	¹⁶² 0.011	¹⁵⁸ 0.118	¹⁶⁵ 0.089	¹⁶⁷ 0.053	⁴⁴ 0.602	⁵⁸ 0.531	⁷⁶ 0.369	¹¹⁵ 0.028	¹¹⁸ 0.013	⁸⁶ 0.166	¹⁰⁰ 0.093	¹⁰¹ 0.218	¹¹² 0.154								³⁰ 0.099	³¹ 0.081	
99	GORILLA-007	¹³¹ 0.046	¹⁶⁴ 0.027	¹⁵⁷ 0.010	¹⁴⁰ 0.101	¹⁴⁹ 0.077	¹⁴⁹ 0.045	⁴⁸ 0.626	⁶⁰ 0.534	⁷⁷ 0.369	¹¹¹ 0.026	¹⁰⁸ 0.012	¹⁰⁵ 0.264	¹⁰⁶ 0.108	⁸⁷ 0.178	¹⁰⁷ 0.138								⁸⁵ 0.178	⁹⁵ 0.132	
100	GORILLA-008	¹²⁴ 0.044	¹⁵² 0.024	¹⁴⁰ 0.009	¹⁵⁰ 0.111	¹⁵⁷ 0.083	¹⁵⁷ 0.048	³⁵ 0.541	⁴⁶ 0.463	⁶⁷ 0.295	¹²¹ 0.030	¹²¹ 0.011	¹¹⁷ 0.319	⁹⁵ 0.090	¹⁰⁶ 0.178	¹⁰⁸ 0.138								¹⁷⁷ 0.541	¹⁷⁹ 0.258	
101	GRIAULE-000	¹²⁵ 0.044	¹³⁸ 0.020	¹⁴⁵ 0.009	¹¹⁹ 0.082	¹²⁷ 0.063	¹³⁰ 0.038	¹⁷⁹ 0.997	¹⁸⁴ 0.995	¹⁷³ 0.952	¹³¹ 0.033	¹⁴⁸ 0.020	⁹⁵ 0.185	¹⁰⁸ 0.107	⁹⁶ 0.198	¹²⁰ 0.166								³⁰ 0.099	³¹ 0.081	
102	GRIAULE-001	⁵⁵ 0.013	⁵⁴ 0.005	⁴⁸ 0.002	²⁶ 0.051	⁵⁸ 0.028	⁵² 0.016	⁸⁶ 0.928	⁹⁶ 0.865	⁶² 0.625	⁴⁰ 0.007	³⁰ 0.003	¹⁵⁶ 0.995	¹⁵³ 0.610										¹⁵⁷ 0.445	¹⁹⁹ 0.359	
103	HIK-003	²³⁵ 0.159	²⁵⁹ 0.103	²⁶⁹ 0.057	²¹⁸ 0.190	²²⁶ 0.158	²⁴⁴ 0.105	¹¹¹ 0.980	¹²¹ 0.969	¹⁵⁹ 0.925	²⁰³ 0.142	²¹⁹ 0.080												¹⁵⁰ 0.445	¹⁹⁹ 0.359	
104	HIK-004	²³² 0.156	²⁵⁵ 0.099	²⁶⁷ 0.054	²⁰⁹ 0.182	²²³ 0.153	²⁴¹ 0.101	¹²⁰ 0.983	¹³⁰ 0.976	¹⁷⁰ 0.947	²⁰¹ 0.137	²¹² 0.077												¹⁵⁴ 0.434	¹⁹⁴ 0.353	
105	HIK-005	¹⁹⁵ 0.102	¹⁹² 0.044	¹⁹⁹ 0.019	¹³⁴ 0.098	¹⁴⁸ 0.077	¹⁵⁸ 0.048	²²⁵ 1.000	²³⁷ 0.999	²⁵⁹ 0.998	¹⁷⁴ 0.068	¹⁷⁷ 0.036												¹⁷⁷ 0.541	¹⁷⁹ 0.258	
106	HIK-006	²²⁴ 0.142	²⁰¹ 0.047	¹⁹⁸ 0.020	¹⁴⁹ 0.111	¹⁶⁰ 0.086	¹⁶⁵ 0.052	²⁶⁹ 1.000	²⁷⁴ 1.000	²⁷⁶ 0.999													²⁰⁶ 0.766	²²⁹ 0.630		
107	HYPERVERGE-001	³⁷ 0.009	⁵⁰ 0.004	⁵⁶ 0.002	⁵⁹ 0.039	⁶⁶ 0.031	⁶⁹ 0.020	¹⁵ 0.275	²⁰ 0.220	³⁶ 0.146	⁴¹ 0.007	⁴⁹ 0.004	³² 0.053	³⁶ 0.027	³⁵ 0.101	³⁴ 0.083								²⁰⁵ 0.766	²²⁸ 0.630	
108	HYPERVERGE-002	³⁴ 0.008	³⁹ 0.004	⁴² 0.002	⁵¹ 0.034	⁵⁶ 0.027	⁵⁹ 0.018	¹⁸ 0.278	¹⁸ 0.210	²⁴ 0.131	²⁷ 0.006	²⁹ 0.003	²⁹ 0.048	²⁴ 0.023	²⁴ 0.093	²⁴ 0.077								³⁹ 0.106	³⁷ 0.085	
109	HYPERVERGE-003	⁶⁷ 0.016	⁷⁶ 0.007	⁷⁹ 0.003	⁷⁹ 0.053	⁹⁰ 0.042	⁹⁶ 0.026	²⁵ 0.353	²⁹ 0.282	⁴⁸ 0.183	⁷⁰ 0.012	⁶⁷ 0.005	⁴³ 0.065	⁴⁶ 0.033										²²² 0.879	²³⁹ 0.743	
110	HZAILU-000	¹¹⁰ 0.035	¹³⁶ 0.020	¹⁴⁴ 0.009	⁹¹ 0.064	¹⁰¹ 0.051	¹⁰⁵ 0.031	¹¹⁸ 0.983	¹¹⁸ 0.967	¹³⁷ 0.813	⁹⁸ 0.020	⁹³ 0.010	¹¹⁴ 0.316	⁸¹ 0.077	⁷⁰ 0.153	⁸⁹ 0.120								²⁰⁰ 0.733	²²³ 0.531	
111	HZAILU-001	⁶⁸ 0.016	⁸³ 0.009	⁹⁰ 0.004	²⁶⁹ 0.414	²⁴¹ 0.183	⁹¹ 0.024	¹⁸⁹ 0.998	¹⁵⁴ 0.986	⁶¹ 0.282	²¹⁹ 0.196	¹⁵¹ 0.021	¹⁶³ 1.000	¹⁶² 0.997	¹⁹⁴ 0.679	¹⁹⁶ 0.360								³⁵⁸ 1.000	²⁶⁸ 0.982	
112	HZAILU-002	⁶³ 0.015	⁸⁰ 0.008	⁹⁰ 0.004	⁷⁵ 0.050	⁸⁴ 0.039	⁹⁰ 0.024	¹³⁵ 0.990	⁷⁵ 0.704	⁶⁵ 0.299	⁷¹ 0.012	⁷¹ 0.006	⁴⁵ 0.066	⁵² 0.034	¹³⁷ 0.330	⁶⁹ 0.110								¹¹ 0.074	¹² 0.064	
113	HZAILU-003	⁶⁴ 0.015	⁸¹ 0.008	⁹¹ 0.004	⁷⁷ 0.051	⁸² 0.038	⁷⁹ 0.022	⁵⁷ 0.715	⁶¹ 0.551	⁶² 0.287	⁶⁶ 0.009	⁶⁰ 0.004	⁴⁰ 0.062	⁴⁷ 0.031	⁴⁷ 0.119	⁵¹ 0.096								²⁰⁶ 0.766	²²⁹ 0.630	
114	IDEMIA-003	³⁰⁹ 0.552	²⁰² 0.047	²⁰² 0.021	³³⁴ 1.000	²³² 0.165	²¹⁴ 0.079	¹⁰⁵ 0.976	¹²⁷ 0.973	¹⁸² 0.968	¹⁹⁵ 0.123	²⁰⁰ 0.061											²⁰⁶ 0.766	²²⁹ 0.630		
115	IDEMIA-004	¹⁵⁴ 0.055	¹⁸⁸ 0.037	²⁰¹ 0.021	¹⁸⁶ 0.144	¹⁹⁷ 0.118	²¹³ 0.079	¹¹⁰ 0.979	¹³³ 0.978	¹⁸⁷ 0.973	¹⁹⁷ 0.130	²⁰⁷ 0.070											²⁰⁵ 0.766	²²⁸ 0.630		
116	IDEMIA-005	¹⁷⁰ 0.066	¹⁹⁴ 0.044	²²² 0.026	²⁰⁸ 0.181	²²¹ 0.150	²⁴³ 0.102	¹¹⁰ 0.979	¹³³ 0.978	¹⁸⁷ 0.973	¹⁹⁷ 0.130	²⁰⁷ 0.070											²²² 0.879	²³⁹ 0.743		
117	IDEMIA-006	¹⁶⁸ 0.065	¹⁹¹ 0.043	²²⁰ 0.025	²³⁹ 0.266	²⁵³ 0.226	²⁷⁰ 0.161	¹²³ 0.984	¹⁴⁵ 0.982	¹⁹⁹ 0.980	²⁰⁴ 0.144	²¹⁸ 0.090											²⁰⁰ 0.733	²²³ 0.531		
118	IDEMIA-007	¹¹¹ 0.035	¹²⁸ 0.018	¹³⁰ 0.008	¹¹⁰ 0.073	¹¹⁴ 0.055	¹¹⁴ 0.033	³³¹ 1.000	³¹⁰ 1.000	³⁵⁹ 1.000	¹⁵⁹ 0.052	¹⁵⁷ 0.022	⁹³ 0.182	¹⁰⁸ 0.109	³⁵⁸ 1.000	²⁶⁸ 0.982								³⁵⁸ 1.000	²⁶⁸ 0.982	
119	IDEMIA-008	¹⁴ 0.004	¹⁶ 0.002	¹⁷ 0.001	²⁰ 0.016	¹⁸ 0.013	¹³ 0.009	¹⁷ 0.276	¹⁷ 0.204	²⁷ 0.136	²² 0.005	²³ 0.003	²² 0.036	²⁵ 0.019	⁴⁰ 0.106	⁴⁸ 0.092								¹¹ 0.074	¹² 0.064	
120	IDEMIA-009	¹³ 0.004	⁹ 0.002	⁷ 0.001	⁷ 0.012	⁷ 0.011	⁶ 0.008	⁶ 0.202	⁷ 0.141	¹² 0.099	¹¹ 0.003	¹¹ 0.002	¹² 0.027	¹⁴ 0.013	¹⁴ 0.013	¹¹ 0.074	¹² 0.064								¹²¹ 0.313	¹⁵⁷ 0.226
121	IDEMIA-010	⁴ 0.002	¹ 0.001	¹ 0.001	⁷ 0.009	⁷ 0.008	³ 0.007	⁸ 0.228	⁵ 0.131	⁷ 0.078	⁶ 0.002	⁶ 0.001	¹⁴ 0.028	⁹ 0.009	⁶ 0.070	⁶ 0.058								¹¹² 0.251	¹³³ 0.182	
122	IMAGUS-002	³³⁶ 0.908	³³⁶ 0.749	³³⁸ 0.564	³¹⁶ 0.944	³²⁴ 0.816	³²⁸ 0.645	²⁶⁵ 1.000	²⁷⁹ 1.000	²⁸⁶ 1.000													¹¹⁰ 0.245	¹²¹ 0.168		
123	IMAGUS-003	³³⁵ 0.898	³³⁸ 0.807	³⁴¹ 0.669	³² 0.954	³²⁹ 0.486	²⁹ 0.420	<sup																		

MISSES BELOW THRESHOLD, T		ENROL RECENT MUGSHOT, N = 1.6M												ENROL APPLICATION PORTRAIT, N = 1.6M																																																																																																																																																																																																
#	ALGORITHM	ENROL: MUGSHOT			ENROL: MUGSHOT			ENROL: WEBCAM			ENROL: MUGSHOT			PROBE: PROFILE			ENROL: VISA			ENROL: BORDER			ENROL: BORDER 10+YR			ENROL: VISA																																																																																																																																																																																				
		FPIR=0.0003	FPIR=0.001	FPIR=0.01	FPIR=0.0003	FPIR=0.001	FPIR=0.01	FPIR=0.0003	FPIR=0.001	FPIR=0.01	FPIR=0.0003	FPIR=0.001	FPIR=0.01	FPIR=0.0003	FPIR=0.001	FPIR=0.01	FPIR=0.001	FPIR=0.001	FPIR=0.01	FPIR=0.001	FPIR=0.001	FPIR=0.01	FPIR=0.001	FPIR=0.01	FPIR=0.001	FPIR=0.01																																																																																																																																																																																				
139	INNOVATRICS-007	82.024	105.013	105.005	93.065	102.051	107.032	68.086	78.0743	101.0567	88.017	91.009	60.093	70.053	71.054	80.0120	60.139	67.0108	60.139	67.0108	60.139	67.0108	60.139	67.0108	60.139	67.0108	60.139	67.0108																																																																																																																																																																																		
140	INNOVATRICS-008	82.025	59.005	36.002	183.138	76.036	58.018	261.1000	277.1000	241.095	77.013	81.007	147.086	141.0430	263.099	259.0584	249.1000	211.000	250.0998	257.099	250.0998	257.099	250.0998	257.099	250.0998	257.099	250.0998	257.099	250.0998																																																																																																																																																																																	
141	INSPUR-000	65.015	69.006	63.003	324.0963	330.0915	331.0740	240.1000	251.1000	264.0999	163.053	176.036	103.0235	117.0145	113.0255	146.0208	113.0255	146.0208	113.0255	146.0208	113.0255	146.0208	113.0255	146.0208	113.0255	146.0208	113.0255	146.0208																																																																																																																																																																																		
142	INTELLIGENSIA-000	146.051	153.024	160.011	132.097	147.077	159.049	115.0982	86.0786	90.0507	163.053	176.036	103.0235	117.0145	113.0255	146.0208	113.0255	146.0208	113.0255	146.0208	113.0255	146.0208	113.0255	146.0208	113.0255	146.0208	113.0255	146.0208																																																																																																																																																																																		
143	INTELLIVISION-001	304.508	304.279	312.158	27.0459	291.404	302.302	247.1000	252.1000	277.0999	230.0328	239.0219	138.0749	153.0598	196.0685	225.0562	196.0685	225.0562	196.0685	225.0562	196.0685	225.0562	196.0685	225.0562	196.0685	225.0562	196.0685	225.0562	196.0685	225.0562																																																																																																																																																																																
144	INTELLIVISION-002	278.282	279.154	282.072	242.096	250.127	242.096	206.0999	221.0999	252.0997	199.0134	210.073	127.0437	140.0297	160.0460	192.0348	160.0460	192.0348	160.0460	192.0348	160.0460	192.0348	160.0460	192.0348	160.0460	192.0348	160.0460	192.0348	160.0460	192.0348																																																																																																																																																																																
145	INTEMA-000	35.009	24.002	19.001	29.022	26.017	26.012	267.1000	14.0100	24.005	17.002	111.0288	56.042	15.0081	13.0067	12.0076	8.0062	134.0715	139.0294	12.0076	8.0062	134.0715	139.0294	12.0076	8.0062	134.0715	139.0294	12.0076	8.0062																																																																																																																																																																																	
146	INTEMA-001	2.002	6.001	4.001	291.604	311.603	324.602	3.0137	3.103	4.073	16.004	15.002	134.0715	139.0294	12.0076	8.0062	134.0715	139.0294	12.0076	8.0062	134.0715	139.0294	12.0076	8.0062	134.0715	139.0294	12.0076	8.0062																																																																																																																																																																																		
147	INTSYSMSU-000	346.999	349.998	359.0990	339.1000	341.1000	343.0998	234.1000	244.1000	259.0998	268.0999	269.0989	113.0302	73.0062	82.0170	99.0135	100.0135	101.0135	102.0135	103.0135	104.0135	105.0135	106.0135	107.0135	108.0135	109.0135	110.0135	111.0135	112.0135	113.0135	114.0135																																																																																																																																																																															
148	IREX-000	172.068	170.028	132.008	137.099	123.060	109.032	129.0988	112.0957	121.0680	151.044	152.044	153.044	154.044	155.044	156.044	157.044	158.044	159.044	160.044	161.044	162.044	163.044	164.044	165.044	166.044	167.044	168.044	169.044																																																																																																																																																																																	
149	ISYSTEMS-002	231.055	242.078	239.032	19.0161	208.126	216.080	188.0998	201.0998	222.0993	113.0302	114.0302	115.0302	116.0302	117.0302	118.0302	119.0302	120.0302	121.0302	122.0302	123.0302	124.0302	125.0302	126.0302	127.0302	128.0302	129.0302	130.0302	131.0302																																																																																																																																																																																	
150	ISYSTEMS-003	254.204	225.059	216.024	179.135	188.107	196.068	248.1000	250.1000	253.0997	113.0302	114.0302	115.0302	116.0302	117.0302	118.0302	119.0302	120.0302	121.0302	122.0302	123.0302	124.0302	125.0302	126.0302	127.0302	128.0302	129.0302	130.0302	131.0302																																																																																																																																																																																	
151	KAKAO-000	98.028	118.015	118.006	108.071	116.056	120.034	34.0539	48.0468	71.0327	95.019	96.010	70.0141	81.0075	74.0158	83.0120	74.0158	83.0120	74.0158	83.0120	74.0158	83.0120	74.0158	83.0120	74.0158	83.0120	74.0158	83.0120	74.0158	83.0120	74.0158	83.0120																																																																																																																																																																														
152	KAKAO-001	26.006	28.003	31.002	27.022	28.017	29.013	7.0226	10.0159	15.0101	18.004	19.004	16.0002	25.0042	26.0042	27.0042	28.0042	29.0042	30.0042	31.0042	32.0042	33.0042	34.0042	35.0042	36.0042	37.0042	38.0042	39.0042	40.0042	41.0042	42.0042	43.0042																																																																																																																																																																														
153	KEDACOM-001	120.041	149.023	179.013	131.096	139.072	170.054	133.0989	153.0986	179.073	164.0055	165.0055	166.0055	167.0055	168.0055	169.0055	170.0055	171.0055	172.0055	173.0055	174.0055	175.0055	176.0055	177.0055	178.0055	179.0055	180.0055	181.0055	182.0055	183.0055	184.0055	185.0055																																																																																																																																																																														
154	KNERON-000																																																																																																																																																																																																													
155	KNERON-001																																																																																																																																																																																																													
156	KNOWUTECH-000	69.017	87.009	84.004	73.049	83.038	81.023	29.0399	33.0318	31.0206	74.0112	76.006	88.0091	63.0046	52.0129	63.0103	64.0103	65.0103	66.0103	67.0103	68.0103	69.0103	70.0103	71.0103	72.0103	73.0103	74.0103	75.0103	76.0103	77.0103	78.0103	79.0103	80.0103																																																																																																																																																																													
157	LINE-000	164.062	177.031	176.012	175.0132	174.0095	172.0054				28.0000	153.0046	154.0021	108.0278	122.0151	310.0000	174.0268	175.0268	176.0268	177.0268	178.0268	179.0268	180.0268	181.0268	182.0268	183.0268	184.0268	185.0268	186.0268	187.0268	188.0268	189.0268	190.0268	191.0268	192.0268	193.0268	194.0268																																																																																																																																																																									
158	LINEF-001	101.030	55.005	46.002	44.066	54.027	48.015	288.1000	283.1000	291.0000	141.0992	142.0981	106.0577	145.0040	39.0004	161.0000	159.0000	160.0000	161.0000	162.0000	163.0000	164.0000	165.0000	166.0000	167.0000	168.0000	169.0000	170.0000	171.0000	172.0000	173.0000	174.0000	175.0000	176.0000	177.0000	178.0000	179.0000	180.0000	181.0000	182.0000	183.0000	184.0000	185.0000	186.0000	187.0000	188.0000	189.0000	190.0000	191.0000	192.0000	193.0000	194.0000	195.0000	196.0000	197.0000	198.0000	199.0000	200.0000	201.0000	202.0000	203.0000	204.0000	205.0000	206.0000	207.0000	208.0000	209.0000	210.0000	211.0000	212.0000	213.0000	214.0000	215.0000	216.0000	217.0000	218.0000	219.0000	220.0000	221.0000	222.0000	223.0000	224.0000	225.0000	226.0000	227.0000	228.0000	229.0000	230.0000	231.0000	232.0000	233.0000	234.0000	235.0000	236.0000	237.0000	238.0000	239.0000	240.0000	241.0000	242.0000	243.0000	244.0000	245.0000	246.0000	247.0000	248.0000	249.0000	250.0000	251.0000	252.0000	253.0000	254.0000	255.0000	256.0000	257.0000	258.0000	259.0000	260.0000	261.0000	262.0000	263.0000	264.0000	265.0000	266.0000	267.0000	268.0000	269.0000	270.0000	271.0000	272.0000	273.0000	274.0000	275.0000	276.0000	277.0000	278.0000	279.0000	280.0000	281.0000	282.0000	283.0000	284.0000	285.0000	286.0000	287.0000	288.0000	289.0000	290.0000	291.0000	292.0000	293.0000	294.0000	295.0000	296.0000	297.0000	298.0000	299.0000	300.0000	301.0000	302.0000	303.0000	304.0000	305.0000	306.0000	307.0000	308.0000	309.0000	310.0000	311.0000	312.0000	313.0000	314.0000	315.0000	316.0000	317.0000	318.0000	319.0000	320.0000	321.0000	322.0000	323.0000	324.0000	325.0000	326.0000	327.0000	328.0000	329.0000	330.0000	331.0000	332.0000	333.0000	334.0000	335.0000	336.0000	337.0000	338.0000	339.0000	340.0000	341.0000	342.0000	343.0000	344.0000	345.0000	346.0000	347.0000	

MISSES BELOW THRESHOLD, T		ENROL RECENT MUGSHOT, N = 1.6M												ENROL APPLICATION PORTRAIT, N = 1.6M										
#	ALGORITHM	ENROL: MUGSHOT			ENROL: MUGSHOT			ENROL: WEBCAM			PROBE: PROFILE			ENROL: VISA		ENROL: BORDER		PROBE: BORDER 10+YR		ENROL: KIOSK				
		FPIR=0.0003	FPIR=0.001	FPIR=0.01	FPIR=0.0003	FPIR=0.001	FPIR=0.01	FPIR=0.0003	FPIR=0.001	FPIR=0.01	FPIR=0.0003	FPIR=0.001	FPIR=0.01	FPIR=0.001	FPIR=0.01	FPIR=0.001	FPIR=0.01	FPIR=0.001	FPIR=0.01	FPIR=0.001	FPIR=0.01			
185	NEC-005	²⁹ 0.007	¹⁰ 0.002	¹⁶ 0.001	¹¹ 0.014	¹² 0.012	¹³ 0.009	⁸⁰ 0.901	⁷¹ 0.673	⁴² 0.177	¹⁴ 0.003	¹⁸ 0.002	⁶ 0.019	⁸ 0.011	²⁰ 0.099	⁴¹ 0.087								
186	NEC-006	⁴⁰ 0.010	¹⁸ 0.002	²¹ 0.002	³¹ 0.024	²⁹ 0.018	²⁸ 0.013	⁷⁵ 0.857	⁴⁷ 0.463	²⁰ 0.122	¹⁵ 0.004	²² 0.003	¹¹ 0.026	¹³ 0.013	²⁵ 0.094	³² 0.081								
187	NEC-007	³ 0.002	⁴ 0.001	¹⁰ 0.001	³ 0.001	³ 0.009	⁵ 0.007	⁹ 0.241	⁸ 0.147	⁸ 0.089	⁴ 0.002	⁷ 0.001	¹ 0.010	² 0.006	⁴ 0.065	⁵ 0.057								
188	NEUROTECHNOLOGY-003	³⁴⁷ 0.999	³³³ 0.636	²⁹⁸ 0.099	³⁰⁸ 0.773	²⁷¹ 0.266	²⁷² 0.164	³¹² 1.000	³³⁶ 1.000	³¹³ 1.000														
189	NEUROTECHNOLOGY-004	²⁰⁵ 0.120	²³⁰ 0.063	²²⁷ 0.028	¹⁸⁷ 0.146	¹⁹⁴ 0.117	²⁰⁴ 0.073	¹⁶⁷ 0.996	¹⁷⁶ 0.994	²¹⁴ 0.990														
190	NEUROTECHNOLOGY-005	²⁰⁴ 0.117	²¹⁶ 0.054	²⁰⁸ 0.022	²³³ 0.252	²⁰⁷ 0.130	²⁰⁷ 0.074	¹⁹⁴ 0.999	²⁰⁴ 0.998	²¹⁰ 0.989														
191	NEUROTECHNOLOGY-006	³⁴⁴ 0.987	³⁰¹ 0.249	³⁰⁴ 0.121	³⁵⁶ 1.000	²⁹⁷ 0.418	²⁸⁹ 0.206																	
192	NEUROTECHNOLOGY-007	²⁶⁸ 0.252	²²⁹ 0.062	²⁰⁸ 0.021	³³⁸ 0.996	²³⁶ 0.173	¹⁹⁵ 0.068	²³⁵ 1.000	²⁵⁷ 1.000	²⁵¹ 0.997	²³¹ 0.339	¹⁷⁸ 0.036								²⁸² 1.000	²⁶⁶ 0.989			
193	NEUROTECHNOLOGY-008	³²⁵ 0.797	²¹⁰ 0.053	¹⁷³ 0.012	¹⁴⁶ 0.110	¹⁵⁰ 0.080	¹³⁵ 0.047	²⁷⁰ 1.000	²⁶⁹ 1.000	²⁹⁴ 1.000	¹³⁷ 0.035	¹³⁷ 0.017	¹¹² 0.293	¹²⁰ 0.149	⁹⁷ 0.203	¹¹¹ 0.152								
194	NEUROTECHNOLOGY-009	⁹⁴ 0.027	¹¹⁹ 0.015	¹¹⁸ 0.006	⁹⁶ 0.066	¹⁰⁸ 0.052	¹⁰⁸ 0.032	⁵³ 0.661	⁶⁴ 0.588	⁸² 0.436	⁹⁷ 0.020	⁹⁷ 0.010	⁸⁰ 0.153	⁹² 0.082	⁷⁰ 0.165	⁹³ 0.129								
195	NEUROTECHNOLOGY-010	²⁸⁴ 0.346	⁹² 0.010	⁷⁷ 0.003	⁶⁹ 0.047	⁸⁰ 0.037	⁸⁶ 0.023	²⁶ 0.377	²⁸ 0.277	³⁹ 0.170	⁶⁷ 0.010	⁶³ 0.005	⁵² 0.075	⁵⁷ 0.039	⁵⁰ 0.126	⁵⁷ 0.097								
196	NEUROTECHNOLOGY-012	¹⁸⁸ 0.092	⁷¹ 0.007	⁵⁷ 0.002	⁶⁶ 0.045	⁷⁰ 0.032	⁶⁴ 0.019	²⁴¹ 1.000	¹¹⁴ 0.959	³¹ 0.149	³⁸ 0.008	⁴⁴ 0.004	³⁸ 0.061	⁴² 0.028	²² 0.916	⁴³ 0.088								
197	NEUROTECHNOLOGY-013	¹⁶⁰ 0.059	⁴⁶ 0.004	³² 0.002	⁴¹ 0.030	⁴⁰ 0.023	⁴⁰ 0.014	¹⁰² 0.975	³⁵ 0.324	¹⁸ 0.117	³⁴ 0.006	²⁴ 0.003	²⁶ 0.046	²⁷ 0.022	¹⁸⁹ 0.641	³⁶ 0.083								
198	NEWLAND-002	³⁰⁷ 0.523	³²² 0.438	³²⁵ 0.294	²⁸⁴ 0.535	²⁹⁹ 0.466	³⁰⁷ 0.335	²⁰⁸ 0.999	²²⁴ 0.999	²⁵⁸ 0.999														
199	NOBLIS-001	³⁵² 1.000	³⁵² 1.000	³⁵³ 0.991	³⁵⁷ 1.000	³⁵³ 1.000	³⁵³ 1.000	²⁷¹ 1.000	²⁷⁰ 1.000	²⁹⁸ 1.000														
200	NOBLIS-002	³⁵⁰ 1.000	³⁴⁸ 0.997	³³⁴ 0.488	³⁵⁷ 1.000	³⁵⁴ 1.000	³⁵⁴ 1.000	²⁷³ 1.000	²⁹⁸ 1.000															
201	NOTIONTAG-000	¹⁰⁵ 0.032	¹²³ 0.017	¹²⁸ 0.007	¹¹¹ 0.076	¹²² 0.059	¹²⁶ 0.036	⁵⁴ 0.671	⁶⁵ 0.611	⁸³ 0.467	¹⁰² 0.021	¹⁰⁵ 0.011	⁷⁸ 0.150	⁹³ 0.084	⁸⁴ 0.176	¹⁰² 0.140								
202	NTECHLAB-003	¹⁸⁰ 0.080	²¹⁴ 0.054	²²⁸ 0.028	¹⁸⁸ 0.148	¹⁹⁵ 0.118	²¹⁹ 0.075	⁷⁷ 0.873	⁹³ 0.837	¹³⁰ 0.752														
203	NTECHLAB-004	¹⁶⁶ 0.063	¹⁸⁹ 0.041	²⁰³ 0.021	¹⁷³ 0.131	¹⁸⁵ 0.105	¹⁹² 0.065	⁷⁶ 0.868	⁹² 0.833	¹²⁸ 0.746	¹⁶² 0.053	¹⁶⁸ 0.030								¹¹⁷ 0.263	¹⁵³ 0.214			
204	NTECHLAB-005	¹⁶⁵ 0.062	¹⁹⁰ 0.042	²⁰⁴ 0.021	¹⁷² 0.130	¹⁸⁷ 0.102	¹⁹¹ 0.063	⁶⁹ 0.816	⁸⁴ 0.771	¹¹⁵ 0.661	¹⁷⁸ 0.073	¹⁸² 0.039	¹²² 0.294	¹⁵⁸ 0.227										
205	NTECHLAB-006	¹⁵⁷ 0.056	¹⁸⁴ 0.037	¹⁹³ 0.018	¹⁶² 0.121	¹⁷¹ 0.094	¹⁷⁹ 0.059	⁶⁷ 0.802	⁸² 0.754	¹¹⁴ 0.635	¹⁶⁶ 0.057	¹⁷² 0.032								¹¹⁶ 0.260	¹⁴⁵ 0.207			
206	NTECHLAB-007	¹¹⁹ 0.040	¹⁵³ 0.026	¹⁷⁰ 0.012	¹²⁰ 0.085	¹³² 0.067	¹³⁹ 0.041	⁶⁶ 0.796	⁸¹ 0.750	¹¹⁵ 0.642	¹²⁹ 0.032	¹³⁸ 0.017	¹⁰³ 0.223	¹²⁵ 0.176										
207	NTECHLAB-008	⁸⁶ 0.024	¹¹² 0.014	¹²¹ 0.007	⁸⁰ 0.057	⁹⁹ 0.045	¹⁰¹ 0.029	⁴³ 0.601	⁵⁷ 0.529	⁸¹ 0.391	¹³³ 0.033	¹⁴² 0.018	⁹¹ 0.183	¹⁰³ 0.140										
208	NTECHLAB-009	⁴² 0.010	⁵⁸ 0.005	⁶¹ 0.003	³⁷ 0.028	³⁹ 0.022	³⁸ 0.014	³³ 0.522	⁴² 0.430	⁶² 0.311	⁸² 0.015	⁸⁵ 0.008	⁶⁴ 0.109	⁷² 0.061	⁶³ 0.142	⁷² 0.114								
209	NTECHLAB-010	²³ 0.005	²⁵ 0.003	²⁶ 0.002	²⁵ 0.018	²⁴ 0.015	²⁰ 0.011	²⁴ 0.334	²⁷ 0.252	³⁸ 0.169	³⁷ 0.007	⁴⁸ 0.004	³⁹ 0.059	⁴⁵ 0.031	²⁹ 0.098	²³ 0.077								
210	NTECHLAB-011	²⁴ 0.006	³² 0.003	²⁴ 0.002	²² 0.018	²³ 0.015	¹⁹ 0.010	²⁰ 0.291	²³ 0.228	³⁴ 0.150	⁶¹ 0.009	⁵⁸ 0.004	⁵⁰ 0.074	⁵⁶ 0.038	²¹ 0.091	²⁰ 0.075								
211	OMNIGARDE-000	⁴⁶ 0.010	⁴⁵ 0.004	⁴⁷ 0.002	³⁶ 0.029	⁴¹ 0.023	³⁹ 0.014	²³ 0.332	²⁶ 0.252	³⁶ 0.160	⁴⁴ 0.007	³⁷ 0.003	³³ 0.055	³⁹ 0.027	⁵⁷ 0.136	⁴⁹ 0.092								
212	PANGIAM-000	⁵⁸ 0.014	⁶⁶ 0.006	⁶² 0.003	⁶¹ 0.039	⁶⁴ 0.030	⁶⁰ 0.018	¹⁰⁰ 0.974	³⁴ 0.318	⁴⁰ 0.175	⁶⁵ 0.009	⁶¹ 0.005	⁶⁹ 0.136	⁵⁰ 0.033	³⁸ 0.105	³⁵ 0.083								
213	PANGIAM-001	⁷⁸ 0.023	⁹⁸ 0.011	¹³⁵ 0.008	⁵⁶ 0.039	⁶¹ 0.030	⁶⁸ 0.020	⁵¹ 0.650	³⁷ 0.383	⁴³ 0.180	⁶¹ 0.009	⁴⁷ 0.004	⁴³ 0.004	¹⁴ 0.860	⁸⁸ 0.081	⁶¹ 0.141	³⁸ 0.085							
214	PARAVISION-000	²⁷⁷ 0.278	²⁵³ 0.089	²⁵⁸ 0.045	²⁷⁴ 0.447	²³⁴ 0.170	²³⁹ 0.100	²⁵⁹ 1.000	²²⁶ 0.999	²⁴⁹ 0.997	²⁴³ 0.470	²⁵² 0.443								²³¹ 0.926	²⁴⁴ 0.779			
215	PARAVISION-001	²²³ 0.140	²⁰³ 0.049	²⁰⁸ 0.020	²²⁴ 0.207	²⁰⁸ 0.128	²⁰⁶ 0.074	²⁵⁹ 1.000	²¹⁵ 0.999	²³² 0.994	²⁴⁰ 0.444	²⁵¹ 0.428								²⁰ 0.739	²²⁶ 0.573			
216	PARAVISION-002	¹⁸⁸ 0.085	²⁰⁴ 0.050	²¹⁰ 0.022	¹⁹² 0.152	¹⁹⁸ 0.119	²¹¹ 0.076	¹⁴⁰ 0.992	¹⁴⁶ 0.983	¹²⁹ 0.748	¹⁸¹ 0.080	¹⁸⁹ 0.043								¹⁶⁹ 0.497	¹⁷⁵ 0.268			
217	PARAVISION-003	¹⁶⁷ 0.063	¹⁸² 0.035	¹⁸⁴ 0.016	¹⁶⁷ 0.124	¹⁷⁵ 0.096	¹⁸² 0.060	¹⁷⁴ 0.997	¹⁷⁸ 0.994	¹²⁴ 0.733	¹⁶⁷ 0.058	¹⁷⁵ 0.034								¹²⁶ 0.296	¹⁶¹ 0.232			
218	PARAVISION-004	⁸⁸ 0.025	⁹⁶ 0.010	⁹⁴ 0.004	⁷² 0.049	⁸¹ 0.038	⁸⁷ 0.024	²⁶⁰ 1.000	²⁸² 1.000	¹³⁴ 0.797	⁹² 0.018	¹⁰¹ 0.011								²² 0.908	¹⁴⁹ 0.211			
219	PARAVISION-005	⁶² 0.014	⁴⁴ 0.004	⁵² 0.002	⁴³ 0.031</td																			

MISSES BELOW THRESHOLD, T		ENROL RECENT MUGSHOT, N = 1.6M												ENROL APPLICATION PORTRAIT, N = 1.6M											
		ENROL: MUGSHOT				ENROL: MUGSHOT				ENROL: WEBCAM				PROBE: PROFILE				ENROL: VISA		ENROL: BORDER		ENROL: BORDER 10+YR		ENROL: KIOSK	
#	ALGORITHM	FPIR=0.0003	FPIR=0.001	FPIR=0.01	FPIR=0.0003	FPIR=0.001	FPIR=0.01	FPIR=0.0003	FPIR=0.001	FPIR=0.01	FPIR=0.0003	FPIR=0.001	FPIR=0.01	FPIR=0.0003	FPIR=0.001	FPIR=0.01	FPIR=0.001	FPIR=0.001	FPIR=0.01	FPIR=0.001	FPIR=0.01	FPIR=0.001	FPIR=0.01		
231	QNAP-002	129 0.045	160 0.026	178 0.013	181 0.136	187 0.106	197 0.068	70 0.820	85 0.772	108 0.622	161 0.052	16 0.025	109 0.281	12 0.171	122 0.272	152 0.214									
232	QNAP-003	113 0.036	134 0.019	141 0.009	329 0.980	326 0.835	177 0.057	342 1.000	167 0.992	79 0.372	246 0.502	205 0.066	196 1.000	167 1.000	220 0.865	202 0.373									
233	QNAP-004	106 0.034	110 0.014	106 0.006	338 0.999	328 0.890	129 0.038	272 1.000	196 0.996	66 0.303	245 0.501	197 0.056	164 0.999	197 1.000	164 0.999	229 0.922	223 0.530								
234	QUANTASOFT-001	321 0.713	334 0.639	335 0.493																					
235	RANKONE-002	243 0.184	263 0.118	277 0.071	249 0.308	269 0.261	283 0.190																		
236	RANKONE-003	242 0.184	264 0.118	280 0.071	246 0.300	266 0.255	281 0.187																		
237	RANKONE-004	267 0.250	293 0.193	305 0.124	281 0.482	297 0.426	305 0.324																		
238	RANKONE-005	191 0.096	226 0.059	237 0.033	225 0.212	237 0.173	252 0.119	209 0.999	206 0.998	233 0.994															
239	RANKONE-006	162 0.061	183 0.037	196 0.020				125 0.987	132 0.977	16 0.937															
240	RANKONE-007	107 0.034	147 0.022	166 0.011	159 0.118	172 0.095	185 0.061	116 0.983	122 0.969	142 0.859	169 0.062	167 0.029									136 0.328	144 0.206			
241	RANKONE-009	102 0.031	126 0.018	138 0.008	133 0.098	144 0.076	147 0.045	116 0.983	122 0.969	142 0.859	169 0.062	167 0.029													
242	RANKONE-010	79 0.023	108 0.014	120 0.007	111 0.077	120 0.058	125 0.036	82 0.905	89 0.802	118 0.652	160 0.052	168 0.027	100 0.208	111 0.119	114 0.259	138 0.194									
243	RANKONE-011	101 0.049	84 0.009	89 0.004	117 0.079	97 0.048	102 0.029				140 0.037	139 0.017	92 0.182	97 0.092	241 0.977	218 0.465									
244	RANKONE-012	75 0.020	77 0.008	88 0.004	107 0.072	111 0.053	103 0.030				119 0.029	122 0.014	74 0.144	78 0.072	162 0.465	91 0.128									
245	RANKONE-013	47 0.010	51 0.005	51 0.002	68 0.046	72 0.034	67 0.020	186 0.998	194 0.996	52 0.214	93 0.018	83 0.008	72 0.141	67 0.050	64 0.142	58 0.097									
246	RANKONE-014	31 0.008	35 0.003	29 0.002	47 0.033	45 0.024	44 0.015				63 0.009	51 0.004	54 0.081	34 0.026	328 1.000	330 0.083									
247	REALNETWORKS-000	280 0.374	299 0.234	308 0.138	291 0.433	283 0.319	291 0.209																		
248	REALNETWORKS-001	289 0.374	296 0.234	307 0.138	277 0.433	285 0.319	292 0.209																		
249	REALNETWORKS-002	288 0.370	297 0.231	307 0.137	270 0.416	282 0.315	293 0.209														170 0.500	199 0.364			
250	REALNETWORKS-003	275 0.273	283 0.159	290 0.090	255 0.342	270 0.266	278 0.172	205 0.999	211 0.998	206 0.987	210 0.164	222 0.103									185 0.613	207 0.370			
251	REALNETWORKS-004	265 0.242	282 0.158	289 0.090	261 0.353	286 0.263	278 0.169	223 1.000	228 0.999	222 0.992	212 0.170	222 0.103													
252	REALNETWORKS-005	147 0.052	167 0.028	172 0.012	130 0.094	142 0.074	152 0.047	121 0.984	124 0.971	150 0.896	139 0.037	135 0.017	101 0.223	114 0.123	100 0.215	119 0.165									
253	REALNETWORKS-006	91 0.025	113 0.015	107 0.006	103 0.068	109 0.053	112 0.032	142 0.993	141 0.980	140 0.838	84 0.016	88 0.008	66 0.120	71 0.063	72 0.154	74 0.116									
254	REALNETWORKS-007	74 0.019	90 0.010	87 0.004	84 0.057	93 0.043	92 0.027	138 0.992	136 0.979	132 0.855	72 0.012	68 0.005	128 0.463	73 0.063	61 0.140	69 0.100									
255	REALNETWORKS-008	54 0.012	67 0.006	69 0.003	62 0.037	61 0.029	61 0.018	131 0.988	119 0.968	119 0.971	56 0.008	47 0.004	56 0.035	51 0.129	76 0.110										
256	RECOGNITO-000	15 0.004	19 0.002	14 0.001	14 0.015	10 0.012	10 0.009	13 0.266	13 0.184	21 0.123	46 0.007	36 0.003	135 0.730	145 0.437	22 0.092	16 0.070									
257	RECOGNITO-001										19 0.033	16 0.016													
258	REMARKAI-000	252 0.197	269 0.128	272 0.059	238 0.263	245 0.203	254 0.123																		
259	REMARKAI-000	210 0.125	217 0.055	212 0.023	201 0.173	199 0.120	200 0.070	214 0.999	225 0.999	236 0.995	177 0.069	174 0.033									199 0.717	190 0.315			
260	REMARKAI-002	248 0.188	268 0.124	271 0.059	232 0.248	243 0.196	253 0.122	146 0.993	164 0.991	198 0.980															
261	RENDIP-000	80 0.023	100 0.012	101 0.005	213 0.189	121 0.059	118 0.034	93 0.945	103 0.894	127 0.744	103 0.022	114 0.013	94 0.185	94 0.089	80 0.167	94 0.130									
262	REVEALMEDIA-000	81 0.024	102 0.012	104 0.006	82 0.054	91 0.042	93 0.025	59 0.755	73 0.680	99 0.539	101 0.021	107 0.011	61 0.093	69 0.051	66 0.143	77 0.118									
263	S1-000	219 0.137	169 0.028	164 0.011	170 0.129	158 0.085	156 0.048	229 1.000	287 1.000	105 0.596	156 0.047	143 0.018	285 1.000	113 0.123	277 1.000	231 0.632									
264	S1-001	152 0.054	120 0.016	12 0.007	95 0.066	105 0.052	117 0.033	139 0.992	150 0.985	175 0.952	94 0.019	96 0.010	68 0.136	88 0.075	68 0.148	78 0.119									
265	S1-002	161 0.060	63 0.006	59 0.002	122 0.085	65 0.031	57 0.018	84 0.924	15 0.196	10 0.095	42 0.007	32 0.003	143 0.792	123 0.151	217 0.841	108 0.144									
266	S1-003	144 0.050	85 0.009	78 0.003	78 0.052	78 0.037	75 0.022	251 1.000	255 1.000	21 0.989	81 0.014	78 0.006	123 0.396	56 0.037	292 1.000	148 0.209									
267	S1-004	84 0.024	43 0.004	44 0.002	49 0.034	46 0.025	51 0.016	243 1.000	198 0.997	47 0.191	30 0.006	28 0.003	42 0.064	32 0.024	287 1.000	39 0.086									
268	SCANOVATE-000	196 0.103	234 0.067	23 0.030	24 0.296	26 0.240	264 0.150	88 0.931	101 0.893	13 0.803	221 0.215	23 0.118									148 0.400	186 0.299			
269	SCANOVATE-001	212 0.128	245 0.081	245 0.037	244 0.281	254 0.227	260 0.140	89 0.935	106 0.911	139 0.834	217 0.192	224 0.103									151 0.404	182 0.290			
270	SENSETIME-000	112 0.036	142 0.021	147 0.009	114 0.078	126 0.063	136 0.040	283 1.000	354 1.000	208 0.988															
271	SENSETIME-001	114 0.036	146 0.022	151 0.010	118 0.080	128 0.064	142 0.041				170 0.997	175 0.994	197 0.979	127 0.032	136 0.017						174 0.523	118 0.160			
272	SENSETIME-002	115 0.037	114 0.015	183 0.014	166 0.124	59 0.028	84 0.023				170 0.997	175 0.994	197 0.979	127 0.032	136 0.017						35 0.133	73 0.115			
273	SENSETIME-003	17 0.004	14 0.002	13 0.001	12 0.014	13 0.012	12 0.009	45 0.607	50 0.477	63 0.311	52 0.008	69 0.005									44 0.113	59 0.100			
274	SENSETIME-004	10 0.003	11 0.002	12 0.001	15 0.015	16 0.013	17 0.010</																		

MISSES BELOW THRESHOLD, T		ENROL RECENT MUGSHOT, N = 1.6M												ENROL APPLICATION PORTRAIT, N = 1.6M													
#	ALGORITHM	ENROL: MUGSHOT			ENROL: MUGSHOT			ENROL: WEBCAM			ENROL: MUGSHOT			PROBE: PROFILE			ENROL: VISA		ENROL: BORDER		ENROL: BORDER 10+YR		ENROL: VISA				
		FPIR=0.0003	FPIR=0.001	FPIR=0.01	FPIR=0.0003	FPIR=0.001	FPIR=0.01	FPIR=0.0003	FPIR=0.001	FPIR=0.01	FPIR=0.0003	FPIR=0.001	FPIR=0.01	FPIR=0.0003	FPIR=0.001	FPIR=0.01	FPIR=0.001	FPIR=0.001	FPIR=0.01	FPIR=0.001	FPIR=0.01	FPIR=0.001	FPIR=0.01	FPIR=0.001	FPIR=0.01		
277	SENSETIME-007	⁹ 0.003	⁵ 0.001	¹ 0.001	¹⁰ 0.012	⁷ 0.009	⁴ 0.007	²²⁴ 1.000	²³⁰ 0.999	⁹ 0.538	¹⁰ 0.003	³ 0.001	⁹ 0.024	⁷ 0.011	¹⁷ 0.085	¹⁹ 0.074											
278	SENSETIME-008	⁵ 0.002	³ 0.001	³ 0.001	⁴ 0.011	⁴ 0.009	²⁰ 0.007	¹³⁴ 0.990	³⁹ 0.405	⁷ 0.086	⁷ 0.002	⁵ 0.001	⁸ 0.021	⁵ 0.009	¹⁴ 0.080	¹⁸ 0.074											
279	SENSETIME-009	¹ 0.002	² 0.001	¹ 0.001	¹ 0.008	¹ 0.007	¹⁰ 0.006	²⁰³ 0.999	⁹⁷ 0.868	³ 0.068	³ 0.001	³ 0.001	³ 0.015	⁴ 0.007	¹⁸ 0.085	³⁰ 0.081											
280	SERENDIPITY-000	⁸³ 0.024	¹⁰⁴ 0.012	¹⁰⁰ 0.005	²⁸⁰ 0.474	²⁴⁶ 0.213	¹²⁷ 0.036	⁷³ 0.844	⁸⁰ 0.748	¹⁰⁴ 0.579	⁹¹ 0.018	⁹⁴ 0.010	¹⁶² 1.000	¹⁶⁵ 0.999	⁶⁵ 0.142	⁶⁵ 0.106											
281	SHAMAN-003	³⁰³ 0.506	³²³ 0.451	³² 0.347	²⁹⁸ 0.650	³¹⁰ 0.597	³¹⁶ 0.472																				
282	SHAMAN-004	³¹⁸ 0.679	³³² 0.615	³³³ 0.488	³¹¹ 0.812	³²⁰ 0.754	³² 0.639																				
283	SHAMAN-006	²⁴⁵ 0.185	²⁷⁶ 0.141	²⁹² 0.092	²⁴ 0.278	²⁵ 0.237	²⁷⁴ 0.168	¹⁰⁷ 0.978	¹²⁵ 0.972	¹⁸⁰ 0.960																	
284	SHAMAN-007	²⁴⁰ 0.183	²⁷⁷ 0.141	²⁹¹ 0.092	²⁴³ 0.280	²⁶⁰ 0.240	²⁶ 0.169																				
285	SIAT-001	²¹⁵ 0.132	¹²⁴ 0.018	¹² 0.007	²⁹⁶ 0.641	²⁸⁸ 0.365	³⁰⁸ 0.348																				
286	SIAT-002	²⁹² 0.417	¹⁴⁴ 0.022	¹²⁷ 0.007	³¹⁵ 0.942	³⁰⁰ 0.478	³¹⁴ 0.460																				
287	SMILART-004	³⁴¹ 0.970	³⁴⁵ 0.968	³⁵⁰ 0.965	³² 0.977	³³ 0.976	³⁴² 0.973																				
288	SMILART-005																										
289	SQISOFT-001	²⁶¹ 0.226	²⁷³ 0.132	²⁵⁸ 0.044	²³³ 0.340	²⁶⁴ 0.252	²⁴⁷ 0.111	⁹⁶ 0.956	⁸⁷ 0.797	¹⁰⁶ 0.608	¹⁴⁴ 0.040	¹⁴⁵ 0.019	¹¹⁶ 0.317	¹²¹ 0.150	¹³³ 0.420	¹³⁶ 0.189											
290	SQISOFT-002	¹⁷⁷ 0.074	¹⁷³ 0.029	¹¹² 0.006				³³⁹ 0.908	¹⁰⁵ 0.904	³⁹ 0.266	²⁵⁴ 0.621	²¹¹ 0.074															
291	STAQU-000	²⁸³ 0.334	²²⁷ 0.062	²⁰⁶ 0.022	³¹² 0.848	²⁹⁶ 0.443	¹⁸⁴ 0.061	²⁴⁴ 1.000	²⁵³ 1.000	²⁷⁰ 0.999	²⁴⁸ 0.535	¹⁸³ 0.039	¹⁵² 0.961	¹²⁹ 0.183	²⁰⁷ 1.000	²⁶⁹ 0.999											
292	SYNESIS-003	²⁰² 0.111	²³² 0.065	²³⁴ 0.032	¹⁹³ 0.155	²⁰² 0.123	²¹² 0.078	⁹⁹ 0.973	¹¹⁵ 0.960	¹⁵² 0.911	¹⁷⁹ 0.075	¹⁸¹ 0.039															
293	SYNESIS-003	³¹⁵ 0.648	³²⁸ 0.582	³³² 0.443	³⁰² 0.708	³¹⁵ 0.646	³¹⁸ 0.524																				
294	SYNESIS-005	¹⁴¹ 0.050	¹⁵⁴ 0.025	¹⁶⁸ 0.011	¹² 0.088	¹³⁸ 0.072	¹⁴⁵ 0.043	¹⁵⁴ 0.995	¹⁴⁷ 0.984	¹³¹ 0.795	¹³⁰ 0.032	¹³⁰ 0.016															
295	T4ISB-000	⁹⁵ 0.027	¹²¹ 0.016	¹⁶³ 0.011	¹⁰¹ 0.068	¹⁰⁸ 0.053	¹¹⁹ 0.034	³⁹ 0.566	⁵³ 0.510	⁸⁴ 0.463	⁹⁹ 0.021	⁹⁸ 0.010	¹³⁹ 0.759	¹²⁸ 0.177	⁷⁷ 0.161	⁸⁷ 0.125											
296	TECH5-001	³²⁷ 0.807	²²⁰ 0.057	¹⁹² 0.018	³³ 0.994	³³⁵ 0.935	¹⁷⁵ 0.055	³⁰³ 1.000	²⁸⁸ 1.000	²⁸ 1.000	²²³ 0.244	¹⁶ 0.028															
297	TECH5-002	¹⁵¹ 0.053	¹⁶³ 0.027	¹⁷¹ 0.012	¹²⁹ 0.094	¹³⁶ 0.070	¹³⁸ 0.040	⁷⁸ 0.874	⁹⁰ 0.805	¹¹⁰ 0.627	¹⁴³ 0.039	¹⁴⁴ 0.019	⁹⁸ 0.205	¹⁰⁹ 0.111	¹⁵⁶ 0.440	¹³³ 0.182											
298	TEVIAN-003	²⁶⁴ 0.239	²⁹⁰ 0.177	²⁹ 0.096	²⁵ 0.346	²⁷⁸ 0.298	²⁸⁵ 0.198																				
299	TEVIAN-004	²³⁷ 0.170	²⁶³ 0.117	²⁷⁶ 0.063	²²⁶ 0.216	²³⁸ 0.176	²⁵⁰ 0.115																				
300	TEVIAN-005	²¹⁴ 0.129	²⁵⁰ 0.087	²³⁷ 0.045	²⁰⁷ 0.180	²¹⁸ 0.144	²²⁴ 0.089	¹²⁸ 0.988	¹¹⁶ 0.962	¹³² 0.796																	
301	TEVIAN-006	⁸⁵ 0.024	⁹¹ 0.010	⁹⁰ 0.005	⁶³ 0.041	⁶⁸ 0.032	⁷³ 0.021	³⁸ 0.562	⁴¹ 0.425	⁶⁵ 0.291	⁸⁵ 0.016	⁸⁹ 0.009	⁵⁹ 0.093	⁶⁸ 0.050	²³⁵ 0.951	⁷⁶ 0.117											
302	TEVIAN-007	⁵⁰ 0.011	⁶¹ 0.005	⁶⁶ 0.003	³⁶ 0.028	³⁷ 0.022	⁴² 0.015	³² 0.504	³² 0.301	⁴⁵ 0.183	⁶⁴ 0.009	⁶⁴ 0.005	⁴⁴ 0.065	⁴⁹ 0.033	⁴⁸ 0.122	⁶³ 0.102											
303	TIGER-000	²⁹⁸ 0.462	³¹⁷ 0.390	³² 0.261	²⁸⁹ 0.565	³⁰ 0.500	³⁰⁹ 0.366																				
304	TIGER-002	¹⁵⁰ 0.158	²⁴⁶ 0.086	²⁴⁸ 0.039	²²² 0.202	²²⁸ 0.158	²³¹ 0.095	²¹⁵ 0.999	²²⁰ 0.999	¹⁹⁴ 0.975																	
305	TIGER-003	²³³ 0.158	²⁴⁷ 0.086	²⁴ 0.039	²² 0.202	²² 0.158	²³⁰ 0.095																				
306	TONGYITRANS-000	¹⁹⁹ 0.107	²³⁹ 0.074	²⁴⁶ 0.038	¹⁸⁵ 0.141	¹⁹¹ 0.112	¹⁹⁹ 0.069																				
307	TONGYITRANS-001	²⁰⁹ 0.124	²³³ 0.066	²³⁸ 0.032	¹⁶⁹ 0.128	¹⁸² 0.101	¹⁸⁸ 0.062																				
308	TOSHIBA-000	²⁰⁸ 0.123	²²⁸ 0.062	²²⁶ 0.027	¹⁸⁹ 0.150	¹⁹⁶ 0.118	²⁰⁵ 0.074	¹⁷³ 0.997	¹⁸⁷ 0.995	²⁰⁹ 0.988																	
309	TOSHIBA-001	²⁵⁹ 0.225	²²² 0.058	¹⁹ 0.019	¹⁷ 0.133	¹⁶ 0.092	¹⁷⁴ 0.054																				
310	TRUEFACE-000	¹³² 0.046	¹³⁰ 0.018	¹³⁷ 0.008	¹¹⁵ 0.079	¹²⁵ 0.062	¹³² 0.039	¹⁵⁸ 0.995	⁹⁸ 0.882	⁸⁸ 0.499	¹²⁰ 0.030	¹³³ 0.016	⁹⁶ 0.194	¹¹⁰ 0.111	⁹³ 0.188	¹⁰⁷ 0.145											
311	TURINGTECHVIP-001	³³¹ 0.865	³⁰⁸ 0.345	³⁰ 0.041	³² 0.967	³² 0.850	²⁹ 0.173	²¹³ 0.999	¹⁶⁹ 0.993	⁵⁰ 0.205	²⁶⁶ 0.978	²⁹ 0.754	³²² 1.000	¹⁶ 1.000	²⁵³ 0.999	²⁶ 0.984											
312	USEB-000	³²⁴ 0.789	³³³ 0.715	³³⁶ 0.509	³¹⁰ 0.803	³¹⁹ 0.722	³²² 0.531	¹¹⁴ 0.980	¹²⁰ 0.968	¹⁵⁴ 0.915	²⁴⁴ 0.490	²⁴⁴ 0.301	¹⁴⁴ 0.804	¹⁵⁵ 0.651	¹⁹⁰ 0.648	²¹⁹ 0.506											
313	VD-000	³³⁸ 0.950	³⁴³ 0.917	³⁴ 0.827	³² 0.968	³³ 0.946	³³⁷ 0.871																				
314	VD-001	²⁷⁶ 0.278	²⁹⁴ 0.201	³⁰³ 0.1																							

MISSES BELOW THRESHOLD, T		ENROL RECENT MUGSHOT, N = 1.6M												ENROL APPLICATION PORTRAIT, N = 1.6M								
#	ALGORITHM	ENROL: MUGSHOT			ENROL: MUGSHOT			ENROL: MUGSHOT			PROBE: PROFILE			ENROL: VISA		ENROL: BORDER		ENROL: VISA				
		FPIR=0.0003	FPIR=0.001	FPIR=0.01	FPIR=0.0003	FPIR=0.001	FPIR=0.01	FPIR=0.0003	FPIR=0.001	FPIR=0.01	FPIR=0.0003	FPIR=0.001	FPIR=0.01	FPIR=0.001	FPIR=0.001	FPIR=0.01	FPIR=0.001	FPIR=0.01	FPIR=0.001	FPIR=0.01		
323	VIGILANTSOLUTIONS-003	³⁰² 0.482	³²¹ 0.408	³²³ 0.282	³⁰⁵ 0.730	³¹⁸ 0.660	³²⁰ 0.526	²⁰⁷ 0.999	²¹⁶ 0.999	²³⁸ 0.995												
324	VIGILANTSOLUTIONS-004	³¹⁴ 0.624	³²⁷ 0.549	³³¹ 0.422	³¹³ 0.858	³²⁸ 0.817	³³⁰ 0.709	¹⁸⁷ 0.998	¹⁹³ 0.996	²¹⁹ 0.991												
325	VIGILANTSOLUTIONS-005	³³⁷ 0.936	³¹⁶ 0.388	²⁵⁰ 0.043				²⁷⁷ 1.000	²⁶⁸ 1.000	²⁹⁴ 1.000												
326	VIGILANTSOLUTIONS-006	³⁴⁰ 0.959	³¹¹ 0.353	²⁵⁷ 0.043				²⁵⁰ 1.000	²⁸⁵ 1.000	²⁹⁷ 1.000												
327	VIGILANTSOLUTIONS-007	¹⁷⁸ 0.076	¹⁷² 0.028	¹⁶⁷ 0.011	¹⁵³ 0.113	¹⁶³ 0.088	¹⁶⁸ 0.053	¹⁷⁸ 0.997	¹⁹² 0.996	²²² 0.991	¹⁸³ 0.081	¹⁹¹ 0.047	¹²¹ 0.371	¹³⁵ 0.242	¹⁴⁷ 0.391	¹⁸⁸ 0.295						
328	VIGILANTSOLUTIONS-008	¹⁴⁵ 0.051	¹³⁹ 0.021	¹⁵⁰ 0.010	¹⁴⁷ 0.105	¹⁴⁶ 0.077	¹⁵⁰ 0.046	²¹⁷ 1.000	²¹⁹ 0.999	²¹⁸ 0.991	¹⁹¹ 0.104	¹⁹⁸ 0.054	¹²⁴ 0.398	¹³⁷ 0.259	¹⁷ 0.511	¹⁹¹ 0.316						
329	VISIONBOX-000	¹⁷⁴ 0.073	¹²⁷ 0.018	¹²³ 0.007	¹⁰⁷ 0.071	¹¹⁸ 0.057	¹²³ 0.035	¹⁵¹ 0.995	¹⁶³ 0.990	¹⁹² 0.974	¹⁰⁶ 0.023	¹¹⁰ 0.012	⁷⁶ 0.146	⁸⁷ 0.081	⁷⁸ 0.162	⁸⁸ 0.126						
330	VISIONLABS-004	¹⁸⁷ 0.091	²²¹ 0.058	²¹⁵ 0.024	²¹¹ 0.199	²²⁵ 0.159	²³³ 0.097	⁹¹ 0.944	¹⁰⁰ 0.890	¹²⁶ 0.742												
331	VISIONLABS-005	¹⁸³ 0.080	²⁰⁵ 0.050	¹⁹⁹ 0.020	²¹⁰ 0.183	²¹⁹ 0.147	²²² 0.087	⁹² 0.945	⁹⁹ 0.888	¹²³ 0.736												
332	VISIONLABS-006	¹²⁸ 0.044	¹⁶² 0.027	¹⁵⁹ 0.010	¹⁵⁷ 0.117	¹⁶⁹ 0.090	¹⁶⁴ 0.051	⁶² 0.764	⁶⁹ 0.672	⁹⁴ 0.511												
333	VISIONLABS-007	¹²⁷ 0.044	¹⁶¹ 0.027	¹⁵⁰ 0.010	¹⁵⁰ 0.117	¹⁶⁶ 0.090	¹⁶³ 0.051	⁶¹ 0.764	⁷⁰ 0.672	⁹³ 0.511	¹²⁶ 0.031	¹²⁴ 0.014			⁹² 0.185	¹⁰⁸ 0.145						
334	VISIONLABS-008	⁹⁷ 0.028	¹⁰⁶ 0.013	¹⁰⁴ 0.006	¹⁰⁰ 0.068	¹⁰⁴ 0.051	¹¹⁰ 0.032	⁴¹ 0.574	⁵¹ 0.481	⁶⁹ 0.317	⁸⁶ 0.017	⁸⁴ 0.008			⁶⁹ 0.151	⁷⁹ 0.119						
335	VISIONLABS-009	⁵³ 0.012	⁵² 0.005	⁴¹ 0.002	⁴⁵ 0.032	⁵² 0.025	³⁵ 0.017	⁸⁷ 0.930	⁸⁸ 0.799	⁴⁹ 0.196	⁵⁷ 0.008	⁵⁷ 0.004			⁴¹ 0.113	⁵² 0.093						
336	VISIONLABS-010	⁶¹ 0.014	⁶⁰ 0.005	⁵⁸ 0.002	⁵² 0.034	⁵⁷ 0.027	⁶³ 0.019			³⁷ 0.169	⁴⁹ 0.008	⁴⁸ 0.004	³⁴ 0.055	³⁶ 0.027	⁴¹ 0.109	⁴⁵ 0.089						
337	VISIONLABS-011	⁵¹ 0.011	³⁶ 0.003	²⁸ 0.002	³⁶ 0.024	³⁶ 0.020	³⁴ 0.014			⁴⁸ 0.194	²¹ 0.004	¹⁹ 0.002	²¹ 0.034	²¹ 0.017	²⁰ 0.090	²⁶ 0.079						
338	VIXVIZION-009	¹⁴⁹ 0.053	¹⁶⁵ 0.027	¹⁷⁴ 0.012	¹³⁵ 0.098	¹⁴⁵ 0.077	¹³⁵ 0.048	¹⁰⁶ 0.976	⁷⁹ 0.745	⁹⁹ 0.519	¹⁴⁶ 0.041	¹⁵⁰ 0.021	¹¹⁶ 0.286	¹²⁶ 0.165	¹⁶⁴ 0.472	¹²⁷ 0.178						
339	VNPT-001	⁹⁶ 0.027	¹¹¹ 0.014	¹¹⁷ 0.006	¹⁹⁴ 0.158	¹³⁴ 0.068	¹²⁴ 0.036	⁸³ 0.922	⁷⁶ 0.718	⁸⁶ 0.373	¹³⁶ 0.035	¹⁰⁴ 0.011	¹⁵⁴ 0.990	¹⁴⁸ 0.537	¹⁴ 0.362	⁹⁷ 0.134						
340	VNPT-002	⁵⁷ 0.013	⁷⁰ 0.007	⁷⁶ 0.003	⁶² 0.040	⁶⁷ 0.032	⁷² 0.021	⁴⁰ 0.568	³¹ 0.292	³⁹ 0.154	⁴⁵ 0.007	⁴¹ 0.004	⁴⁹ 0.072	⁴⁶ 0.031	²⁶ 0.096	²² 0.075						
341	VNPT-003	⁵⁹ 0.014	⁶⁸ 0.006	⁷³ 0.003																		
342	VOCORD-003	²⁸⁵ 0.354	²⁶⁷ 0.122	²⁶¹ 0.048	²¹⁸ 0.195	²²⁸ 0.155	²²⁸ 0.093	¹⁹⁵ 0.999	²⁰⁷ 0.998	²¹⁸ 0.991	²⁰⁸ 0.157	²²⁸ 0.105				¹⁵⁰ 0.404	¹⁸¹ 0.289					
343	VOCORD-004	³²⁸ 0.826	³¹² 0.355	²⁶⁴ 0.051	²⁶⁶ 0.401	²³⁵ 0.173	²²⁶ 0.093	²⁴⁹ 1.000	²⁵⁶ 1.000	²⁶⁹ 0.999	²¹⁸ 0.193	²⁰³ 0.065				²⁴⁵ 0.991	²⁴³ 0.776					
344	VOCORD-005	³¹⁹ 0.689	²⁸¹ 0.158	²⁵⁹ 0.044	¹⁹⁶ 0.161	²⁰⁹ 0.130	²¹⁵ 0.080	²⁰¹ 0.999	¹⁹⁹ 0.997	¹⁸¹ 0.968	²⁰² 0.138	²¹⁹ 0.090				¹⁴⁴ 0.381	¹⁷⁹ 0.287					
345	VOCORD-006	³⁵³ 1.000	³⁵⁴ 1.000	³⁵⁸ 1.000	³⁵¹ 1.000	³⁵⁶ 1.000	³⁵⁵ 1.000	³⁵¹ 1.000	²⁹⁰ 1.000	³³⁴ 1.000	²⁹⁴ 1.000	³³⁴ 1.000				³³³ 1.000	³⁵⁵ 1.000					
346	VTC-C-000	³²³ 0.784	²²⁴ 0.059	¹¹⁷ 0.006																		
347	VTS-000	³¹¹ 0.605	³³⁰ 0.598	³³⁹ 0.595	²⁹⁴ 0.624	³¹³ 0.619	³²⁶ 0.613	²¹⁰ 0.999	²²⁹ 0.999	²⁶² 0.998	²⁵³ 0.613	²⁵⁷ 0.609	¹⁴⁰ 0.760	¹⁵⁹ 0.739	²⁰³ 0.761	²⁴⁰ 0.749						
348	VTS-001	¹⁰⁹ 0.035	¹⁰⁷ 0.013	¹⁰⁸ 0.006	⁹⁹ 0.067	¹⁰⁵ 0.051	¹⁰⁴ 0.031	¹⁸¹ 0.998	¹⁷⁴ 0.994	⁹² 0.510	¹⁰⁴ 0.022	¹¹¹ 0.012	⁷³ 0.141	⁸⁵ 0.079	⁹⁵ 0.192	⁸⁹ 0.126						
349	VTS-002	¹⁵⁰ 0.053	¹⁵⁷ 0.026	¹⁵⁸ 0.010	¹³⁶ 0.098	¹⁴³ 0.075	¹⁵¹ 0.046	²²⁹ 1.000	²³⁹ 1.000	¹⁷⁶ 0.953	¹⁵² 0.045	¹⁶² 0.026	¹⁰² 0.231	¹¹⁶ 0.133	¹⁵² 0.417	¹³⁴ 0.187						
350	VTS-003	⁶⁶ 0.015	⁷⁵ 0.007	⁷¹ 0.003	⁷¹ 0.048	⁷¹ 0.033	⁶⁵ 0.019	²⁶¹ 1.000	²⁶² 1.000	¹¹⁷ 0.632	⁷⁹ 0.014	⁶⁵ 0.005	¹⁵¹ 0.954	⁷¹ 0.060	¹⁸ 0.635	⁴⁶ 0.089						
351	XFORWARDAI-000	⁹⁹ 0.029	¹¹⁷ 0.006	¹⁰⁹ 0.070	¹¹² 0.053	¹²¹ 0.034	⁹⁶ 0.698	⁴³ 0.440	⁵⁰ 0.250	¹⁰⁰ 0.021	⁹⁹ 0.011	⁸³ 0.159	⁹¹ 0.082	⁸¹ 0.169	⁹⁶ 0.134							
352	XFORWARDAI-001	⁴⁴ 0.010	⁵⁶ 0.005	⁶⁷ 0.003	⁵⁶ 0.036	⁶¹ 0.028	⁶⁶ 0.020	⁷² 0.838	⁴⁴ 0.448	²⁸ 0.143	³³ 0.008	⁶⁶ 0.005	⁴¹ 0.062	⁴⁴ 0.030	⁴⁸ 0.123	⁶¹ 0.102						
353	XFORWARDAI-002	²⁸ 0.007	³⁴ 0.003	⁵⁰ 0.002	²⁵ 0.018	²⁹ 0.016	³³ 0.014	¹⁰³ 0.975	⁵⁵ 0.525	⁹ 0.095	²⁵ 0.005	³⁴ 0.003	²⁴ 0.041	²³ 0.018	³² 0.099	⁴⁴ 0.089						
354	YISHENG-001	²⁹⁶ 0.452	³⁰⁹ 0.346	³¹⁶ 0.206	³³⁰ 0.983	³²³ 0.808	²⁹⁸ 0.269					²³⁶ 0.666	²⁵⁰ 0.396							²²⁸ 0.919	²³⁴ 0.695	
355	YITU-002	¹⁰³ 0.031	¹²⁵ 0.018	¹³⁰ 0.008	⁸⁹ 0.063	⁹⁹ 0.049	⁹⁹ 0.028															
356	YITU-003	¹⁰⁴ 0.032	¹³³ 0.019	¹⁴² 0.009	⁹⁷ 0.067	¹⁰⁷ 0.052	¹¹⁶ 0.033															
357	YITU-004	⁷³ 0.019	⁸⁸ 0.010	⁹⁹ 0.004	⁵¹ 0.035	⁵⁹ 0.027	³⁶ 0.017	⁹⁵ 0.948	¹⁰⁹ 0.936	¹³¹ 0.913												
358	YITU-005	⁷⁷ 0.022	⁹⁵ 0.010	⁹⁸ 0.005	⁶⁰ 0.039	⁶⁹ 0.032	⁸² 0.023															

Table 41: **Threshold-based accuracy.** Values are $\text{FNIR}(N, T, L)$ with $N = 1.6$ million with thresholds set to produce $\text{FPIR} = 0.0003, 0.001$, and 0.01 in non-mate searches. Throughout blue superscripts indicate the rank of the algorithm for that column. Caution: The Power-low models are mostly intended to draw attention to the kind of behavior, not as a model to be used for prediction.

Appendices

Appendix A Accuracy on large-population FRVT 2018 mugshots

2023/07/05
16:19:47

FNIR(N, R, T) = False neg. identification rate
FPTR(N, T) = False pos. identification rate

N = Num. enrolled subjects
R = Num. candidates examined

T = Threshold
T = 0 → Investigation
T > 0 → Identification

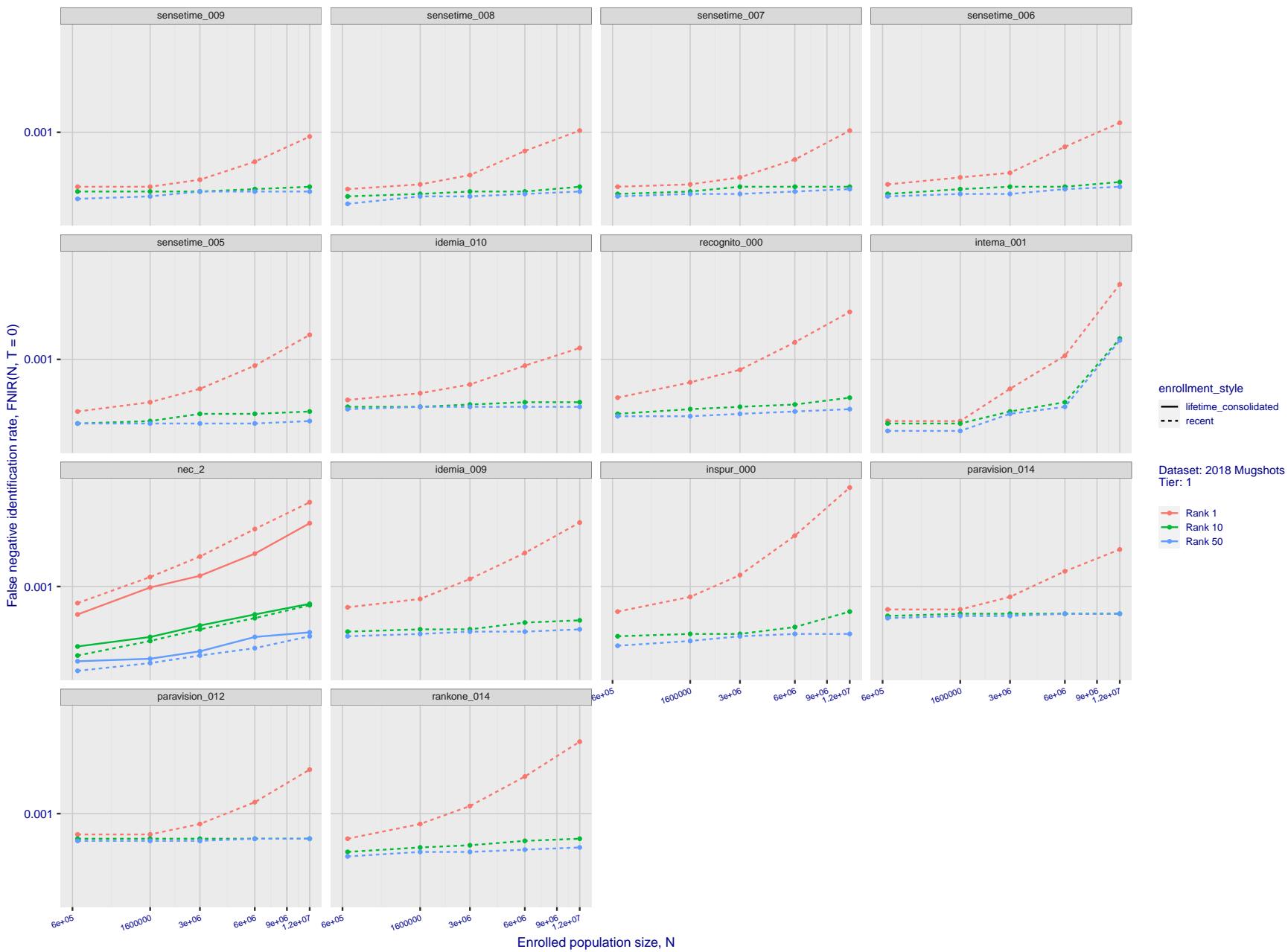


Figure 20: [FRVT-2018 Mugshot Dataset] Rank-based identification miss rates vs. number of enrolled subjects. The figure shows false negative identification rates, $\text{FNIR}(N, R)$, across various gallery sizes and ranks 1, 10 and 50. The threshold is set to zero, so this metric rewards even weak scoring rank 1 mates. This also means $\text{FPIR} = 1$, so any search without an enrolled mate will return non-mated candidates. For clarity, results are sorted and reported into tiers spanning multiple pages, the tiering criteria being rank 1 hit rate on a gallery size of 640 000.

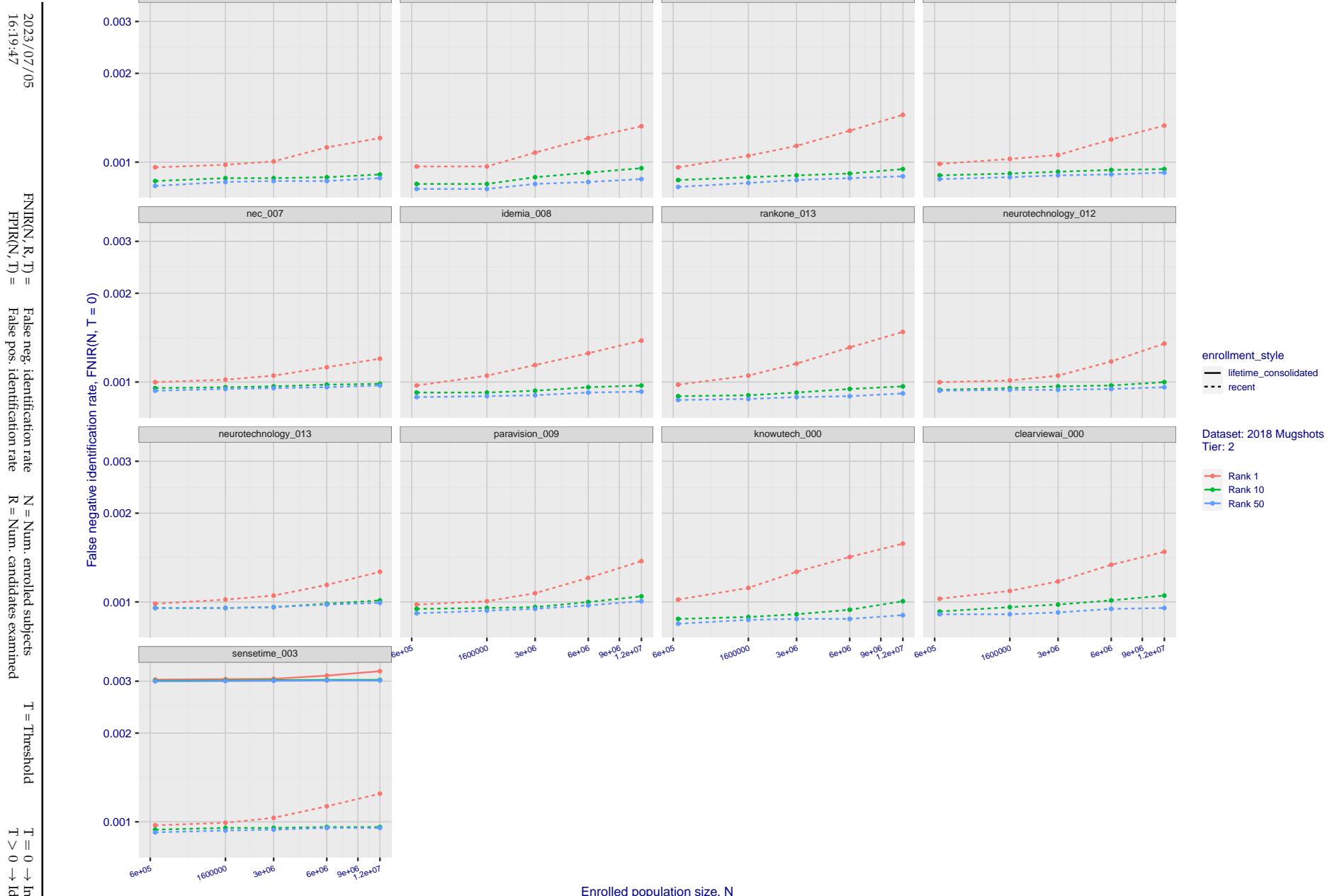


Figure 21: [FRVT-2018 Mugshot Dataset] Rank-based identification miss rates vs. number of enrolled subjects. The figure shows false negative identification rates, $\text{FNIR}(N, R)$, across various gallery sizes and ranks 1, 10 and 50. The threshold is set to zero, so this metric rewards even weak scoring rank 1 mates. This also means $\text{FPIR} = 1$, so any search without an enrolled mate will return non-mated candidates. For clarity, results are sorted and reported into tiers spanning multiple pages, the tiering criteria being rank 1 hit rate on a gallery size of 640 000.

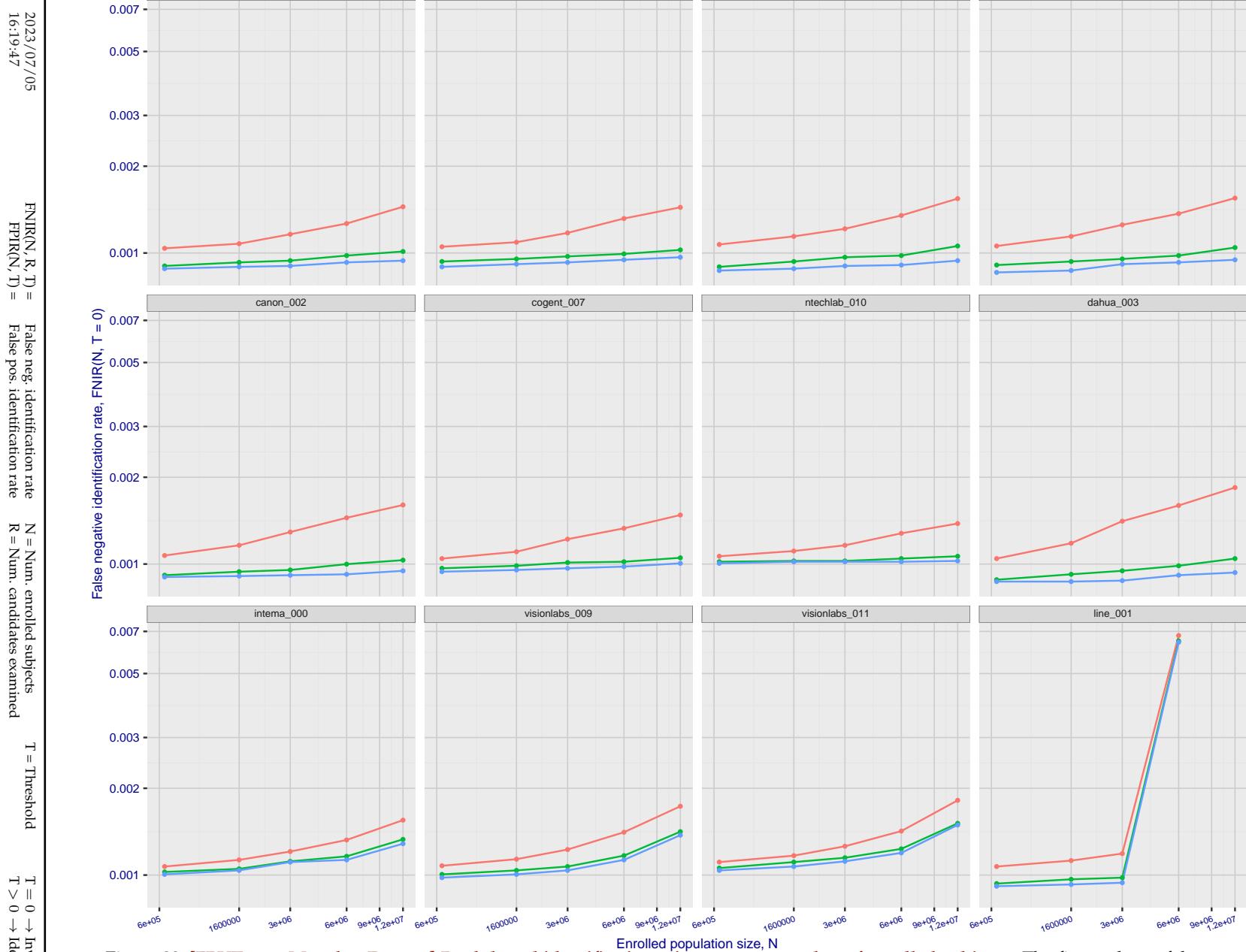


Figure 22: [FRVT-2018 Mugshot Dataset] Rank-based identification miss rates vs. number of enrolled subjects. The figure shows false negative identification rates, $\text{FNIR}(N, R)$, across various gallery sizes and ranks 1, 10 and 50. The threshold is set to zero, so this metric rewards even weak scoring rank 1 mates. This also means $\text{FPIR} = 1$, so any search without an enrolled mate will return non-mated candidates. For clarity, results are sorted and reported into tiers spanning multiple pages, the tiering criteria being rank 1 hit rate on a gallery size of 640 000.

2023/07/05
16:19:47FNIR(N, R, T) = False neg. identification rate
FPIR(N, T) = False pos. identification rateN = Num. enrolled subjects
R = Num. candidates examined

T = Threshold

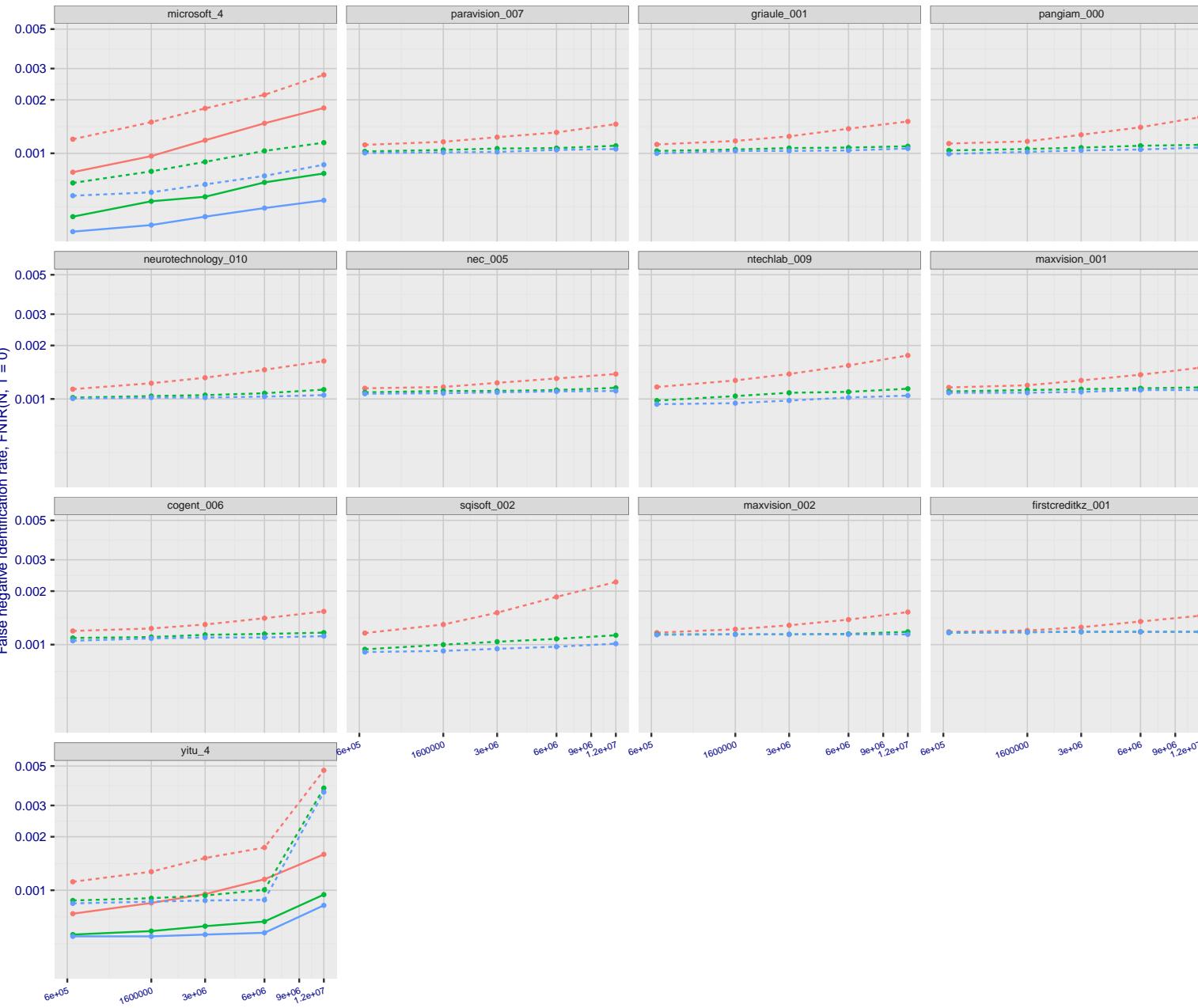
T = 0 → Investigation
 $T > 0 \rightarrow$ Identification

Figure 23: [FRVT-2018 Mugshot Dataset] Rank-based identification miss rates vs. number of enrolled subjects. The figure shows false negative identification rates, $\text{FNIR}(N, R)$, across various gallery sizes and ranks 1, 10 and 50. The threshold is set to zero, so this metric rewards even weak scoring rank 1 mates. This also means $\text{FPIR} = 1$, so any search without an enrolled mate will return non-mated candidates. For clarity, results are sorted and reported into tiers spanning multiple pages, the tiering criteria being rank 1 hit rate on a gallery size of 640 000.

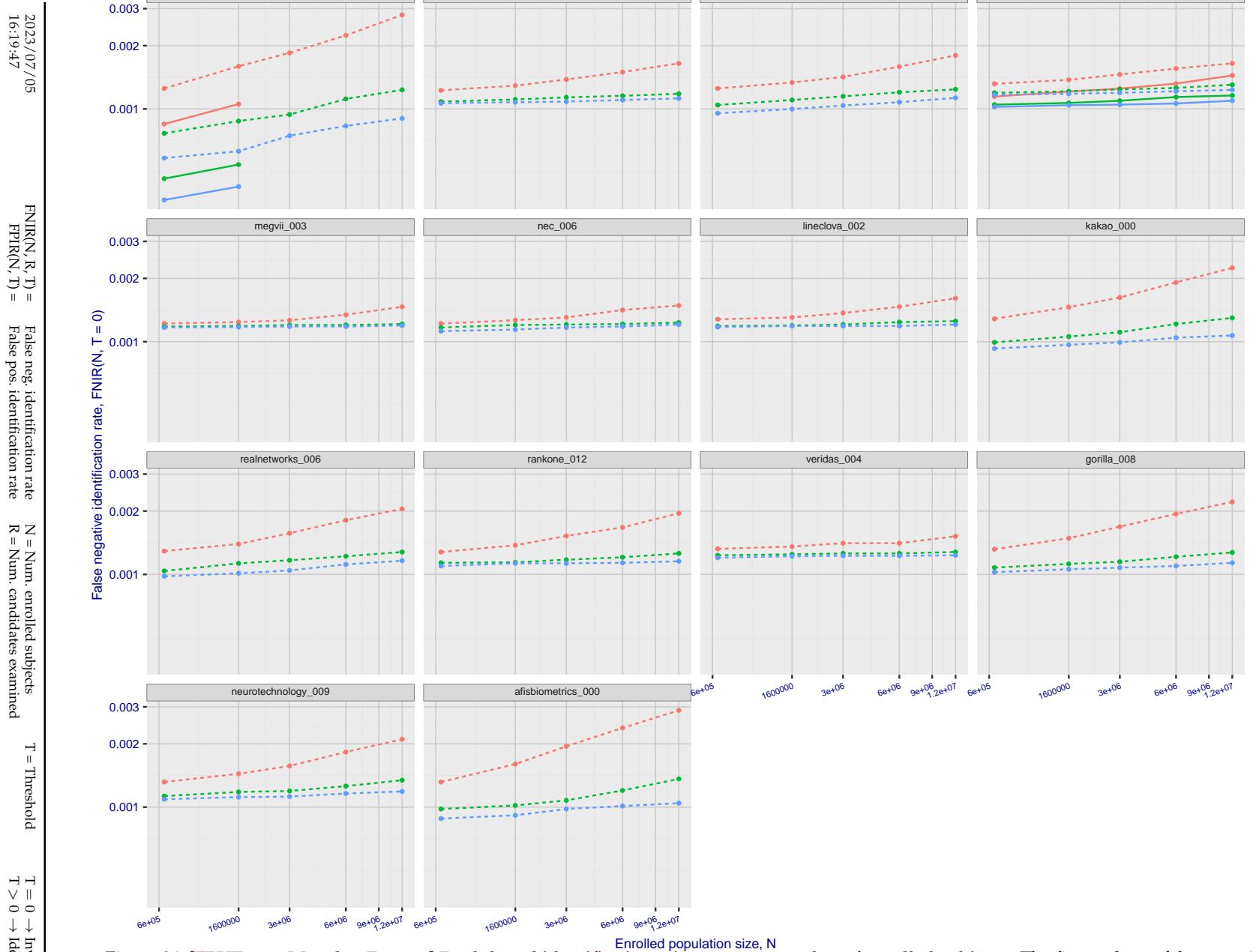


Figure 24: [FRVT-2018 Mugshot Dataset] Rank-based identification miss rates vs. number of enrolled subjects. The figure shows false negative identification rates, $\text{FNIR}(N, R)$, across various gallery sizes and ranks 1, 10 and 50. The threshold is set to zero, so this metric rewards even weak scoring rank 1 mates. This also means $\text{FPIR} = 1$, so any search without an enrolled mate will return non-mated candidates. For clarity, results are sorted and reported into tiers spanning multiple pages, the tiering criteria being rank 1 hit rate on a gallery size of 640 000.

2023/07/05
16:19:47

 $\text{FNIR}(N, R, T) =$
 False neg. identification rate
 $\text{FPIR}(N, T) =$
 False pos. identification rate
 $N = \text{Num. enrolled subjects}$
 $R = \text{Num. candidates examined}$
 $T = \text{Threshold}$
 $T = 0 \rightarrow \text{Investigation}$
 $T > 0 \rightarrow \text{Identification}$

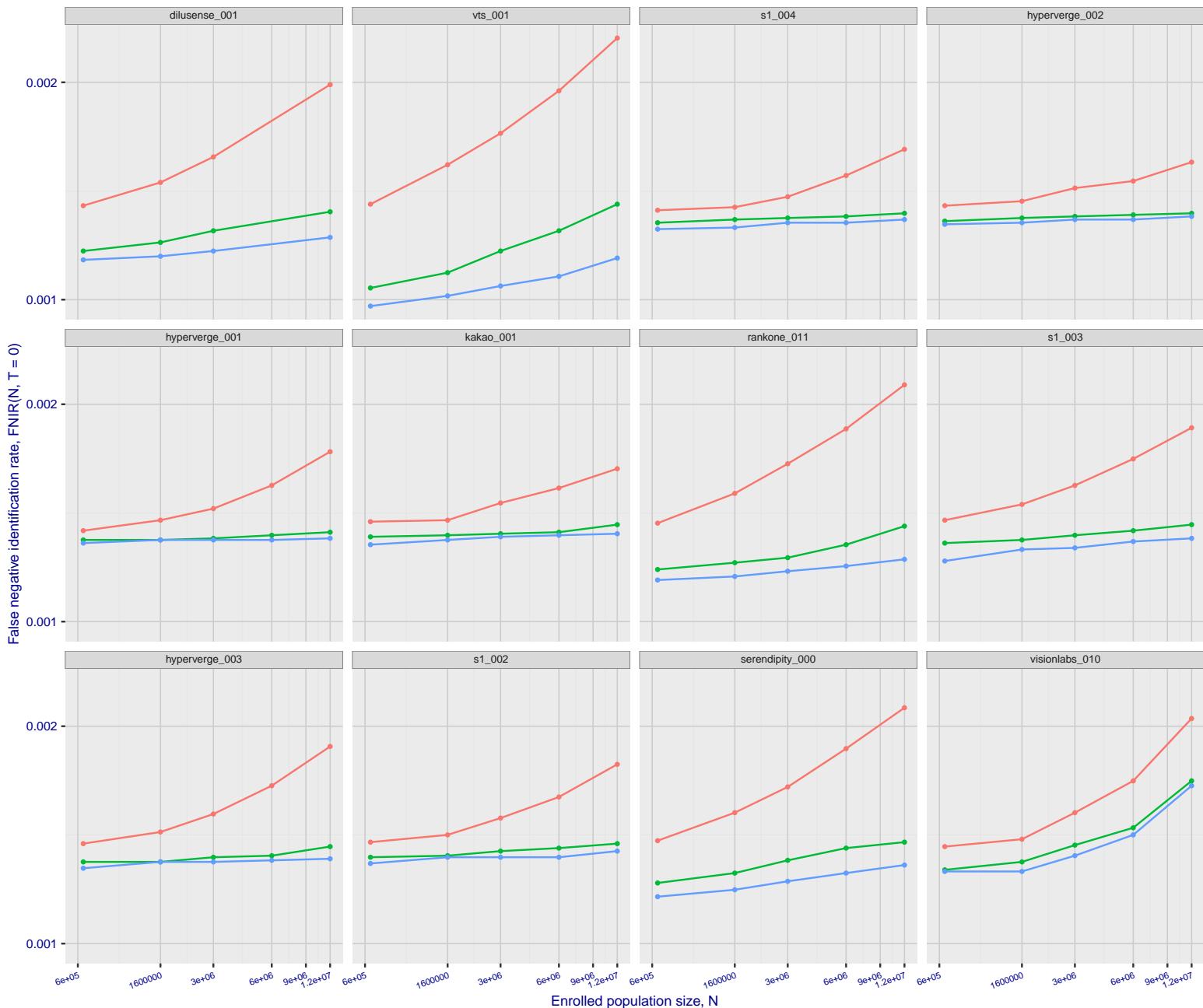


Figure 25: [FRVT-2018 Mugshot Dataset] Rank-based identification miss rates vs. number of enrolled subjects. The figure shows false negative identification rates, $\text{FNIR}(N, R)$, across various gallery sizes and ranks 1, 10 and 50. The threshold is set to zero, so this metric rewards even weak scoring rank 1 mates. This also means $\text{FPIR} = 1$, so any search without an enrolled mate will return non-mated candidates. For clarity, results are sorted and reported into tiers spanning multiple pages, the tiering criteria being rank 1 hit rate on a gallery size of 640 000.

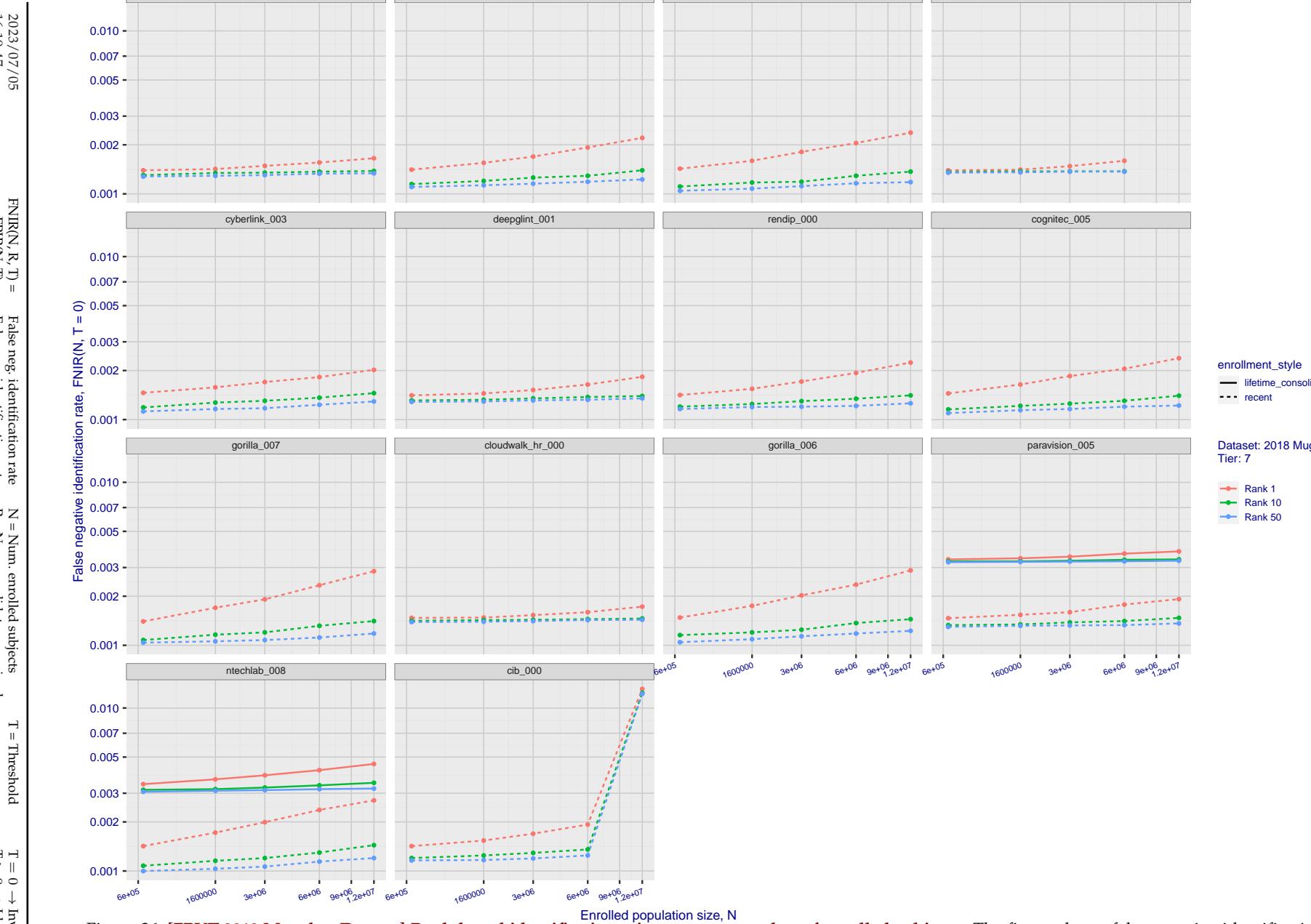


Figure 26: [FRVT-2018 Mugshot Dataset] Rank-based identification miss rates vs. number of enrolled subjects. The figure shows false negative identification rates, $\text{FNIR}(N, R)$, across various gallery sizes and ranks 1, 10 and 50. The threshold is set to zero, so this metric rewards even weak scoring rank 1 mates. This also means $\text{FPIR} = 1$, so any search without an enrolled mate will return non-mated candidates. For clarity, results are sorted and reported into tiers spanning multiple pages, the tiering criteria being rank 1 hit rate on a gallery size of 640 000.

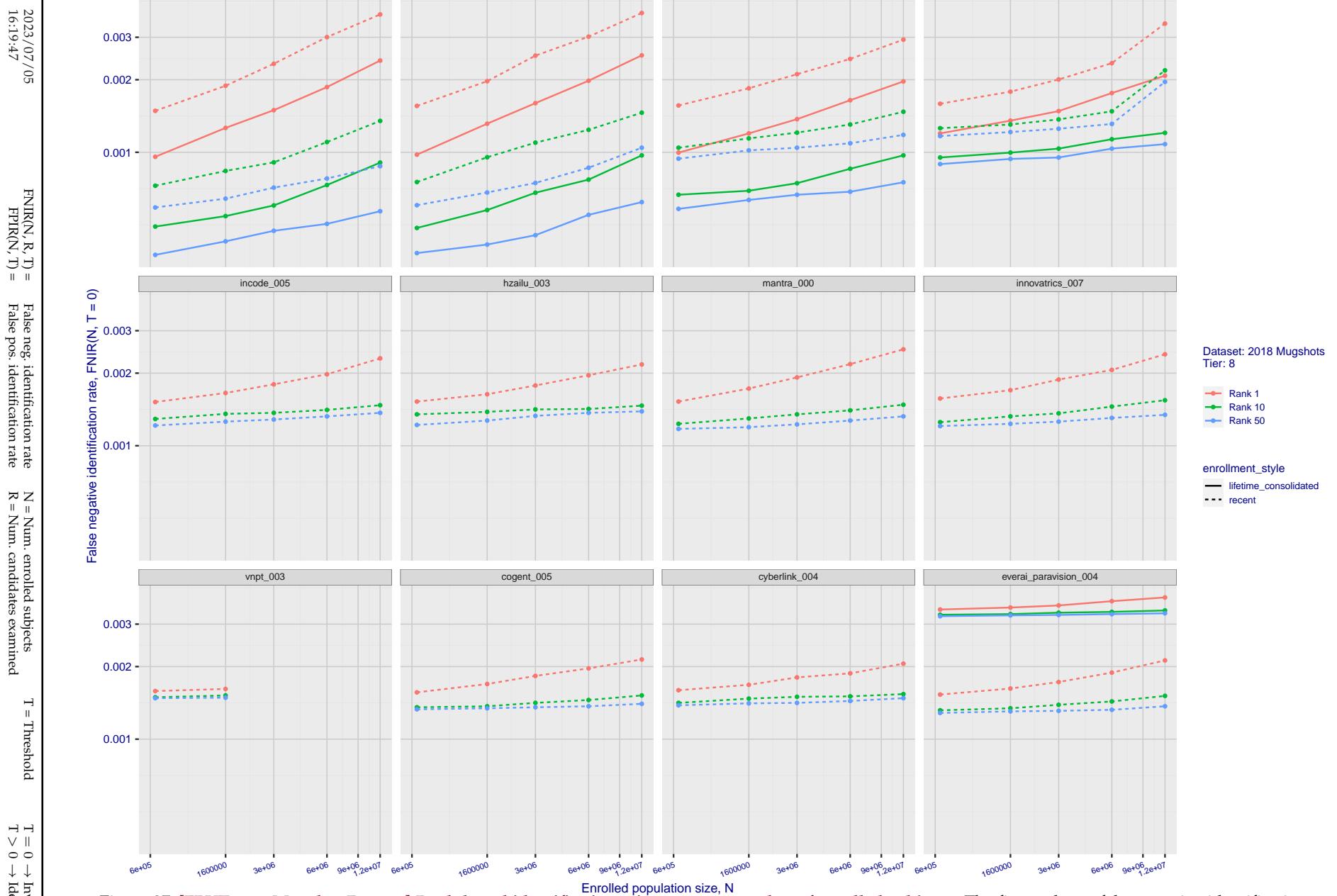


Figure 27: [FRVT-2018 Mugshot Dataset] Rank-based identification miss rates vs. number of enrolled subjects. The figure shows false negative identification rates, $\text{FNIR}(N, R)$, across various gallery sizes and ranks 1, 10 and 50. The threshold is set to zero, so this metric rewards even weak scoring rank 1 mates. This also means $\text{FPIR} = 1$, so any search without an enrolled mate will return non-mated candidates. For clarity, results are sorted and reported into tiers spanning multiple pages, the tiering criteria being rank 1 hit rate on a gallery size of 640 000.

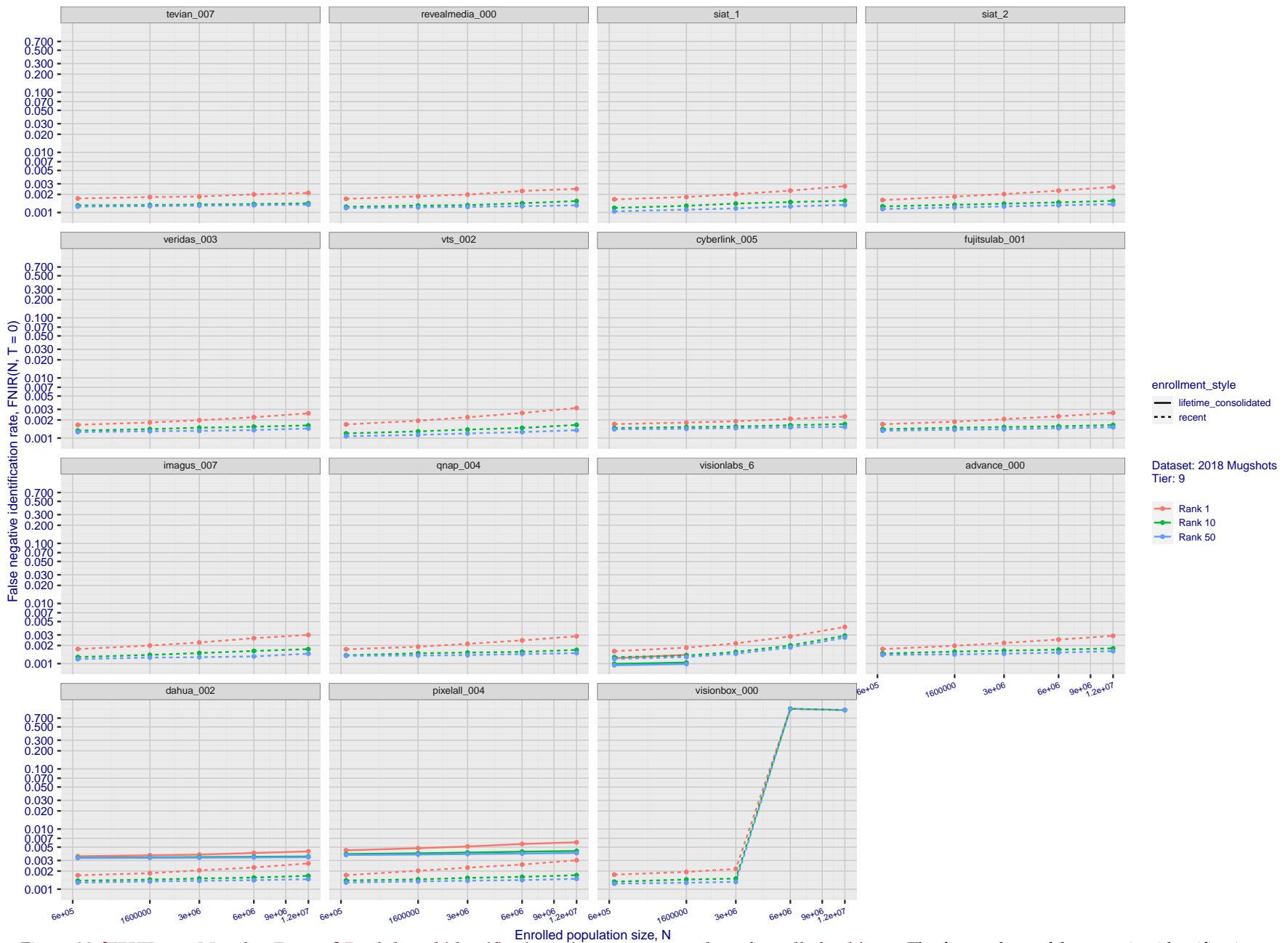


Figure 28: [FRVT-2018 Mugshot Dataset] Rank-based identification miss rates vs. number of enrolled subjects. The figure shows false negative identification rates, $\text{FNIR}(N, R)$, across various gallery sizes and ranks 1, 10 and 50. The threshold is set to zero, so this metric rewards even weak scoring rank 1 mates. This also means $\text{FPIR} = 1$, so any search without an enrolled mate will return non-mated candidates. For clarity, results are sorted and reported into tiers spanning multiple pages, the tiering criteria being rank 1 hit rate on a gallery size of 640 000.

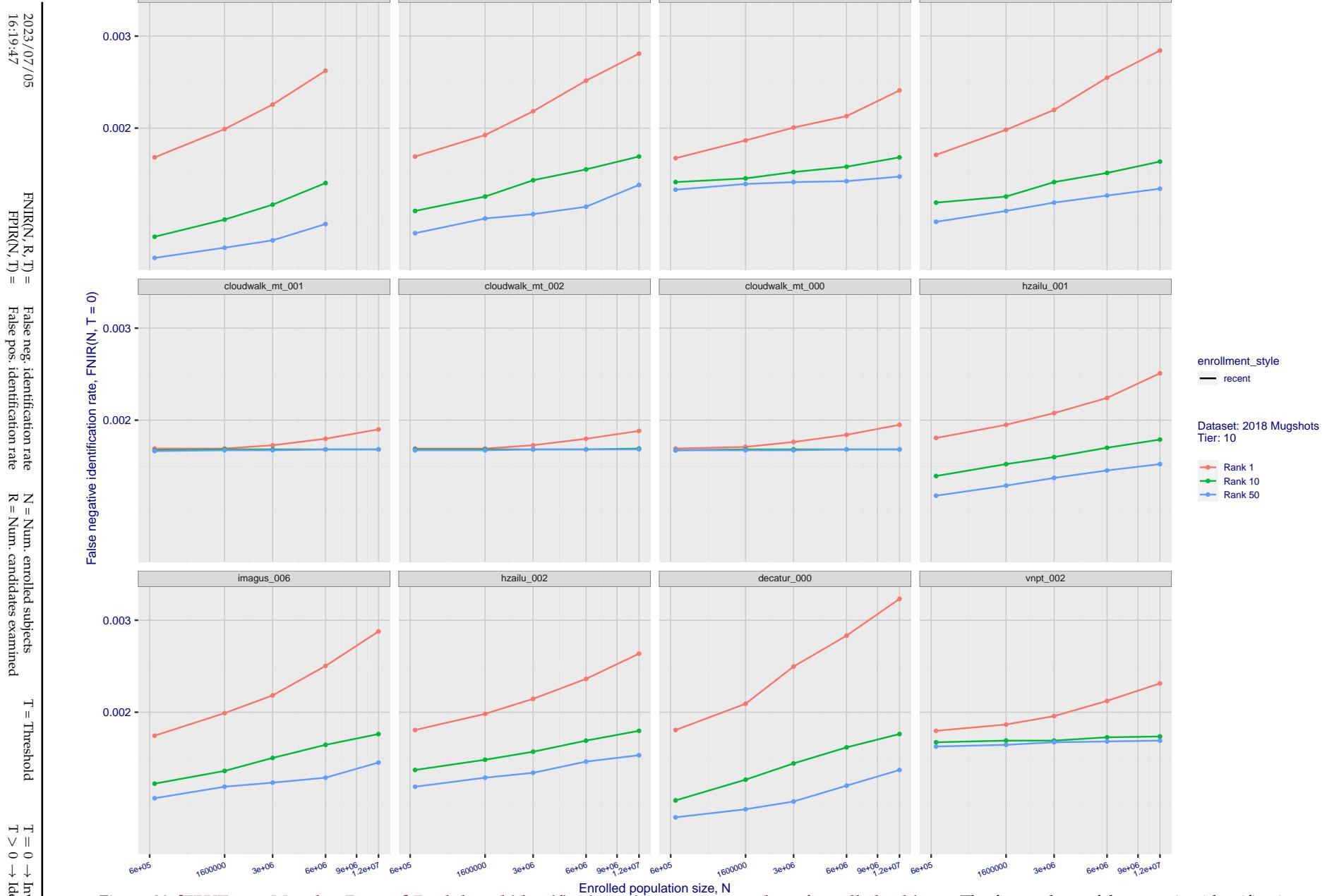


Figure 29: [FRVT-2018 Mugshot Dataset] Rank-based identification miss rates vs. number of enrolled subjects. The figure shows false negative identification rates, $\text{FNIR}(N, R)$, across various gallery sizes and ranks 1, 10 and 50. The threshold is set to zero, so this metric rewards even weak scoring rank 1 mates. This also means $\text{FPIR} = 1$, so any search without an enrolled mate will return non-mated candidates. For clarity, results are sorted and reported into tiers spanning multiple pages, the tiering criteria being rank 1 hit rate on a gallery size of 640 000.

2023/07/05
16:19:47

 $\text{FNIR}(N, R, T) = \text{False neg. identification rate}$
 $\text{FPIR}(N, T) = \text{False pos. identification rate}$
 $N = \text{Num. enrolled subjects}$
 $R = \text{Num. candidates examined}$
 $T = \text{Threshold}$
 $T = 0 \rightarrow \text{Investigation}$
 $T > 0 \rightarrow \text{Identification}$

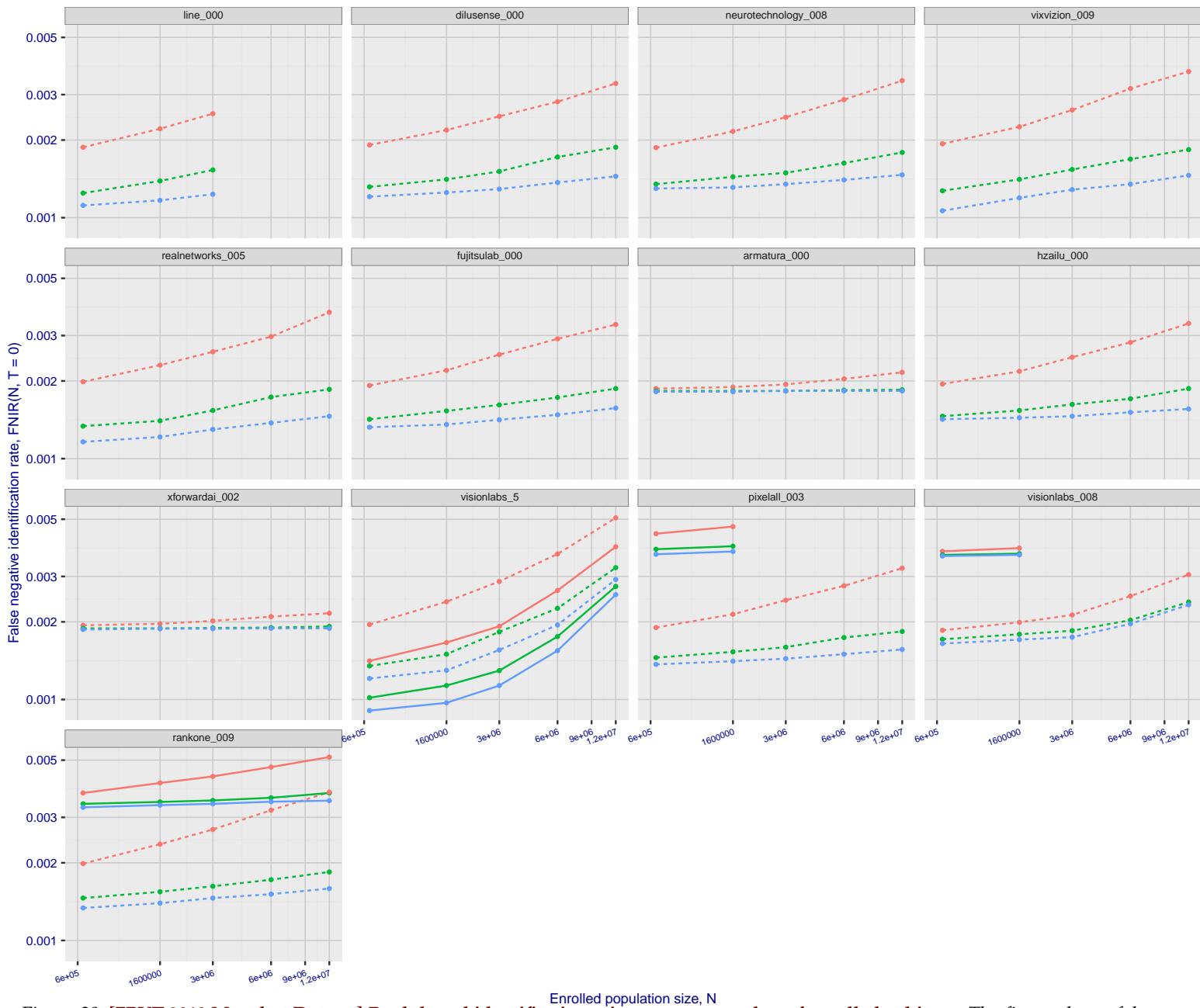


Figure 30: [FRVT-2018 Mugshot Dataset] Rank-based identification miss rates vs. number of enrolled subjects. The figure shows false negative identification rates, $\text{FNIR}(N, R)$, across various gallery sizes and ranks 1, 10 and 50. The threshold is set to zero, so this metric rewards even weak scoring rank 1 mates. This also means $\text{FPIR} = 1$, so any search without an enrolled mate will return non-mated candidates. For clarity, results are sorted and reported into tiers spanning multiple pages, the tiering criteria being rank 1 hit rate on a gallery size of 640 000.

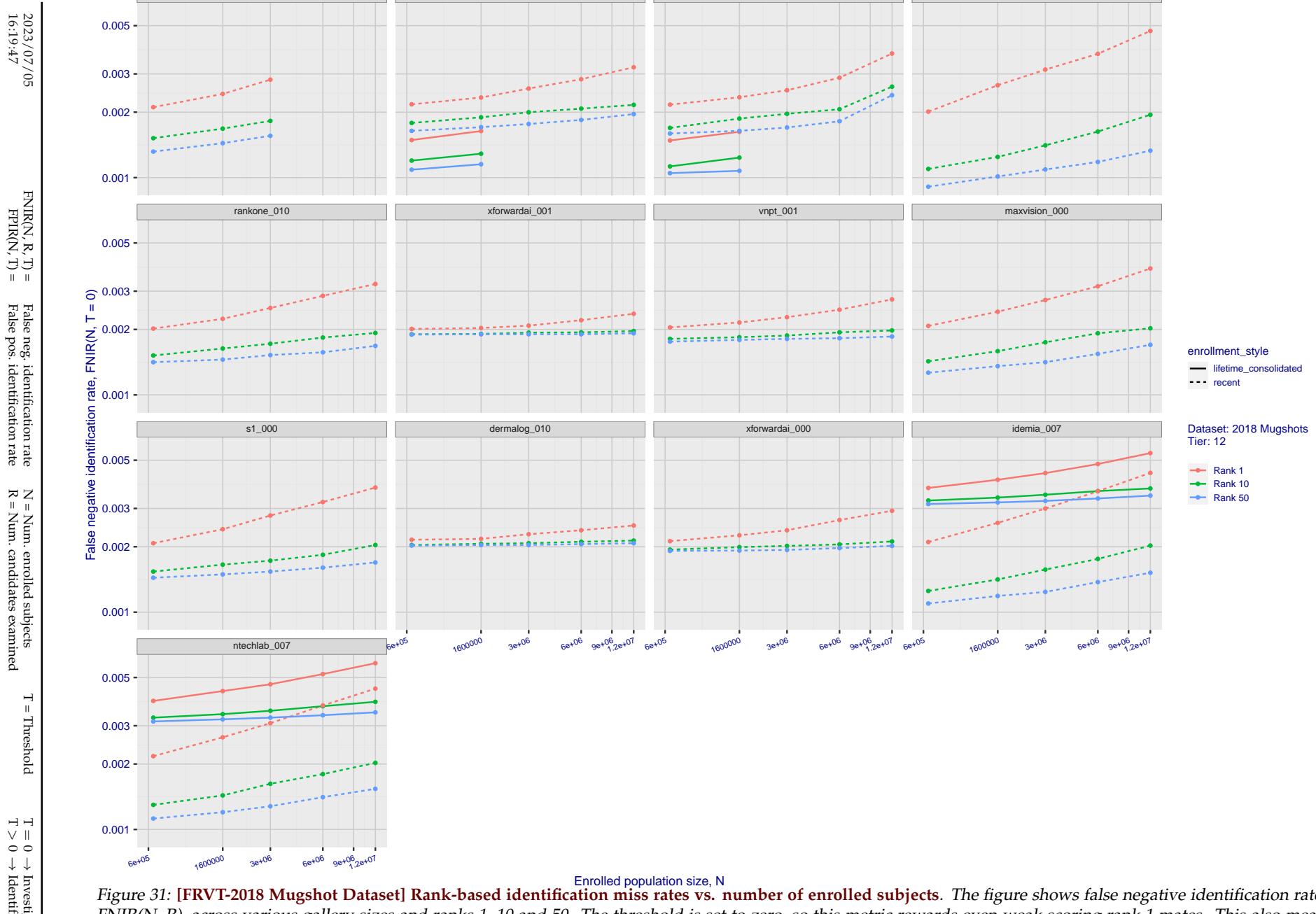


Figure 31: [FRVT-2018 Mugshot Dataset] Rank-based identification miss rates vs. number of enrolled subjects. The figure shows false negative identification rates, $\text{FNIR}(N, R)$, across various gallery sizes and ranks 1, 10 and 50. The threshold is set to zero, so this metric rewards even weak scoring rank 1 mates. This also means $\text{FPIR} = 1$, so any search without an enrolled mate will return non-mated candidates. For clarity, results are sorted and reported into tiers spanning multiple pages, the tiering criteria being rank 1 hit rate on a gallery size of 640 000.

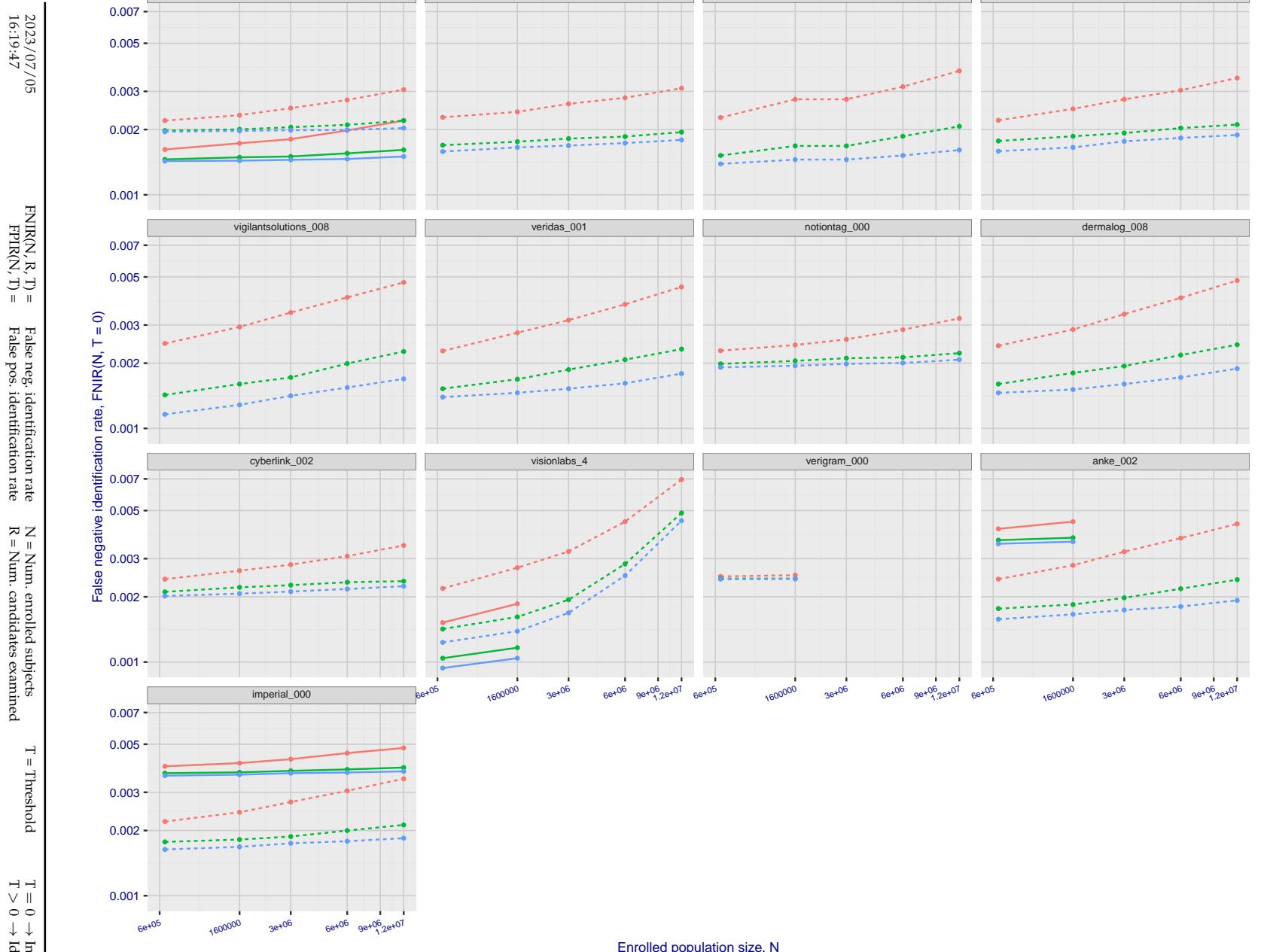


Figure 32: [FRVT-2018 Mugshot Dataset] Rank-based identification miss rates vs. number of enrolled subjects. The figure shows false negative identification rates, $\text{FNIR}(N, R)$, across various gallery sizes and ranks 1, 10 and 50. The threshold is set to zero, so this metric rewards even weak scoring rank 1 mates. This also means $\text{FPIR} = 1$, so any search without an enrolled mate will return non-mated candidates. For clarity, results are sorted and reported into tiers spanning multiple pages, the tiering criteria being rank 1 hit rate on a gallery size of 640 000.

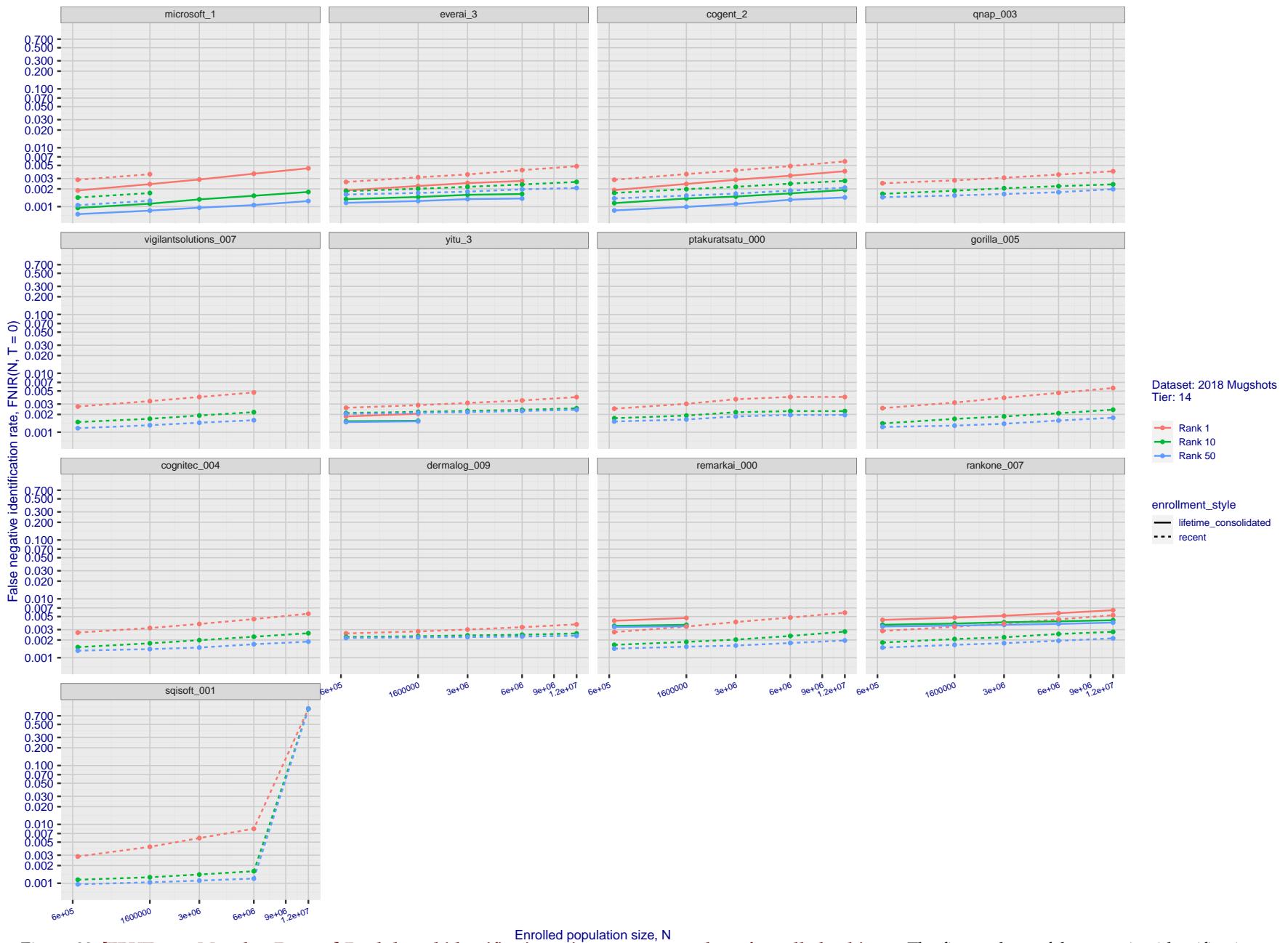


Figure 33: [FRVT-2018 Mugshot Dataset] Rank-based identification miss rates vs. number of enrolled subjects. The figure shows false negative identification rates, $\text{FNIR}(N, R)$, across various gallery sizes and ranks 1, 10 and 50. The threshold is set to zero, so this metric rewards even weak scoring rank 1 mates. This also means $\text{FPIR} = 1$, so any search without an enrolled mate will return non-mated candidates. For clarity, results are sorted and reported into tiers spanning multiple pages, the tiering criteria being rank 1 hit rate on a gallery size of 640 000.

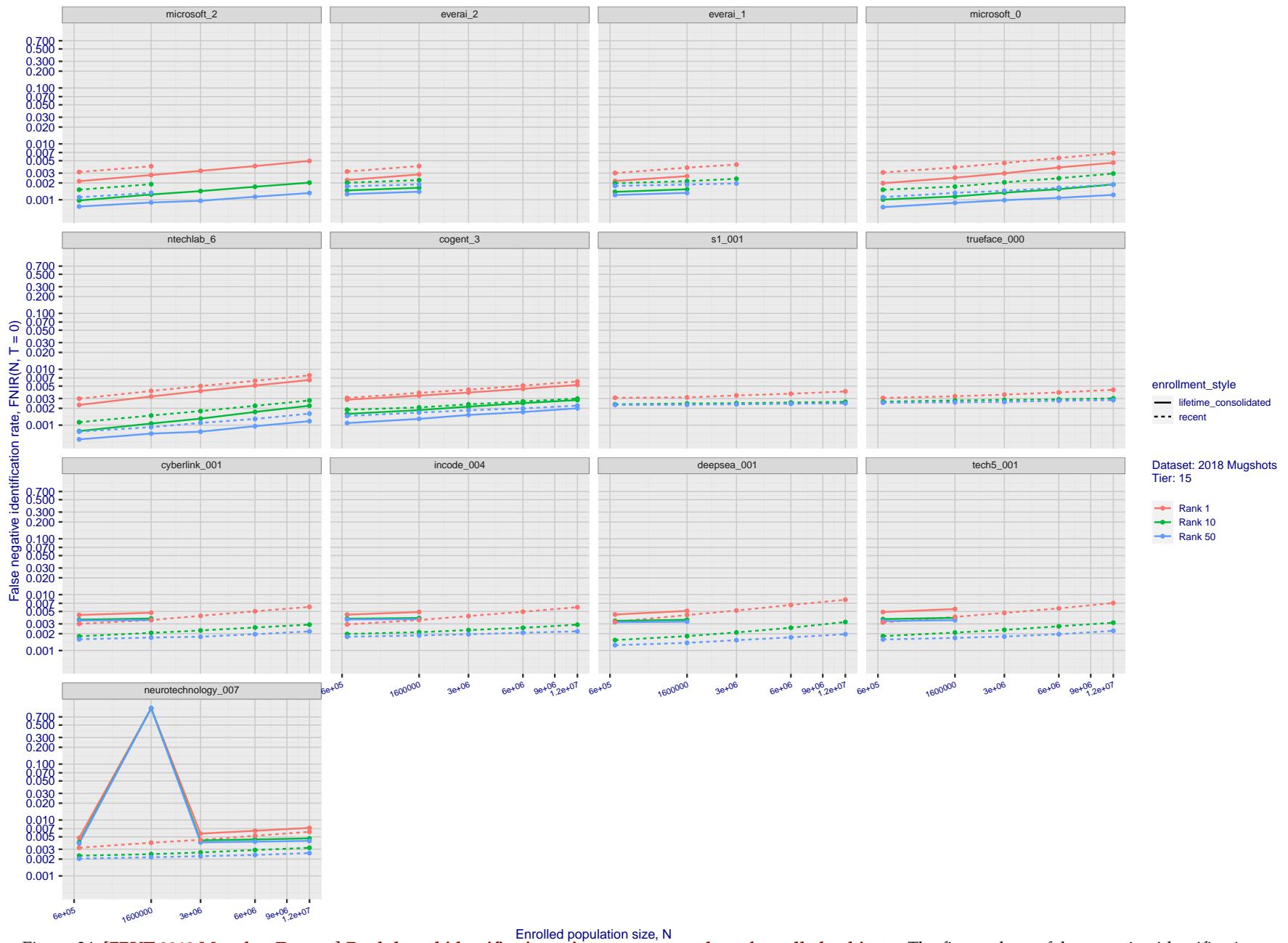


Figure 34: [FRVT-2018 Mugshot Dataset] Rank-based identification miss rates vs. number of enrolled subjects. The figure shows false negative identification rates, $\text{FNIR}(N, R)$, across various gallery sizes and ranks 1, 10 and 50. The threshold is set to zero, so this metric rewards even weak scoring rank 1 mates. This also means $\text{FPIR} = 1$, so any search without an enrolled mate will return non-mated candidates. For clarity, results are sorted and reported into tiers spanning multiple pages, the tiering criteria being rank 1 hit rate on a gallery size of 640 000.

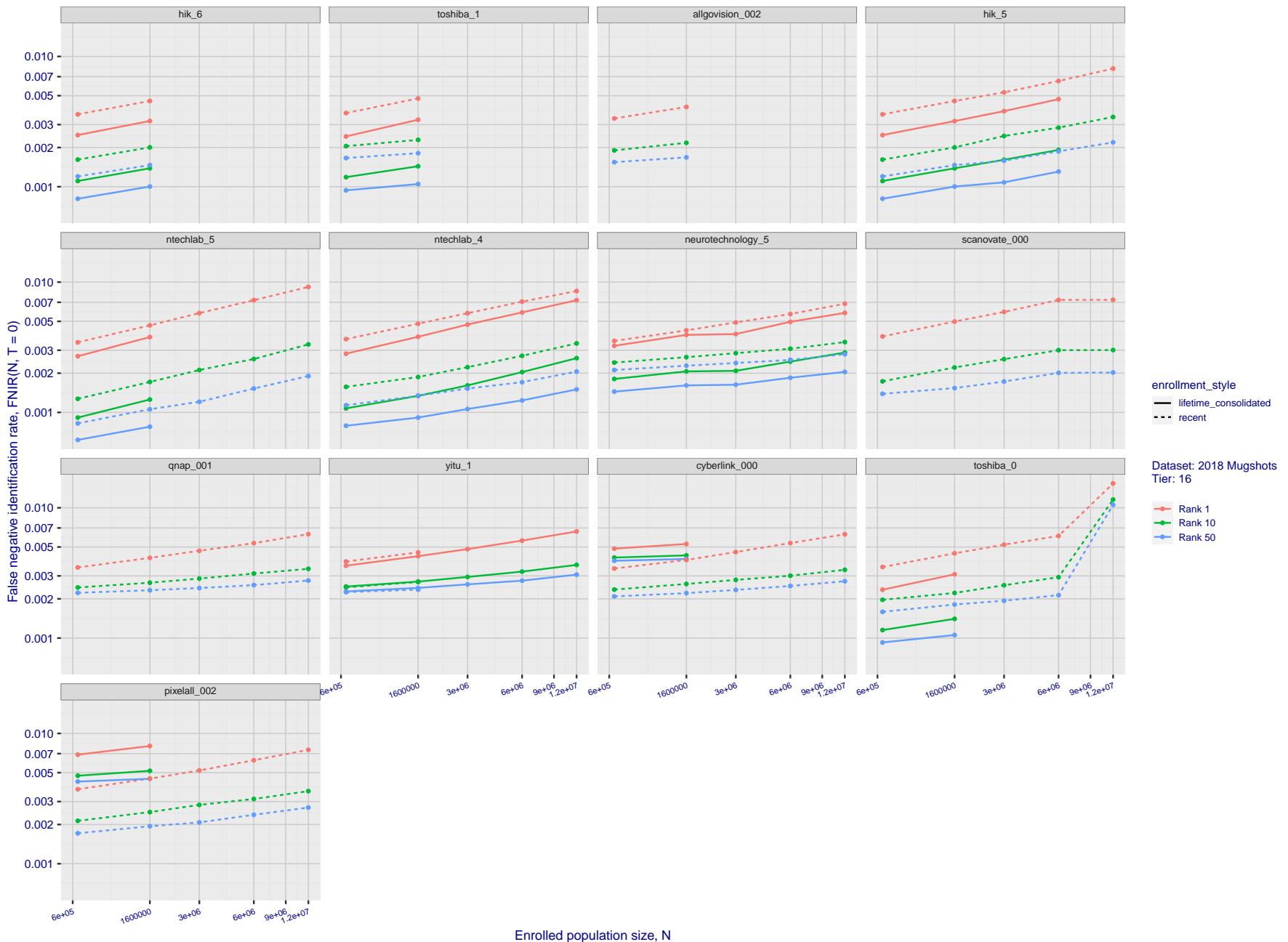


Figure 35: [FRVT-2018 Mugshot Dataset] Rank-based identification miss rates vs. number of enrolled subjects. The figure shows false negative identification rates, $\text{FNIR}(N, R)$, across various gallery sizes and ranks 1, 10 and 50. The threshold is set to zero, so this metric rewards even weak scoring rank 1 mates. This also means $\text{FPIR} = 1$, so any search without an enrolled mate will return non-mated candidates. For clarity, results are sorted and reported into tiers spanning multiple pages, the tiering criteria being rank 1 hit rate on a gallery size of 640 000.

2023/07/05
16:19:47

 $\text{FNIR}(N, R, T) =$
False neg. identification rate
 $\text{FPIR}(N, T) =$
False pos. identification rate
 $N = \text{Num. enrolled subjects}$
 $R = \text{Num. candidates examined}$
 $T = \text{Threshold}$
 $T = 0 \rightarrow \text{Investigation}$
 $T > 0 \rightarrow \text{Identification}$

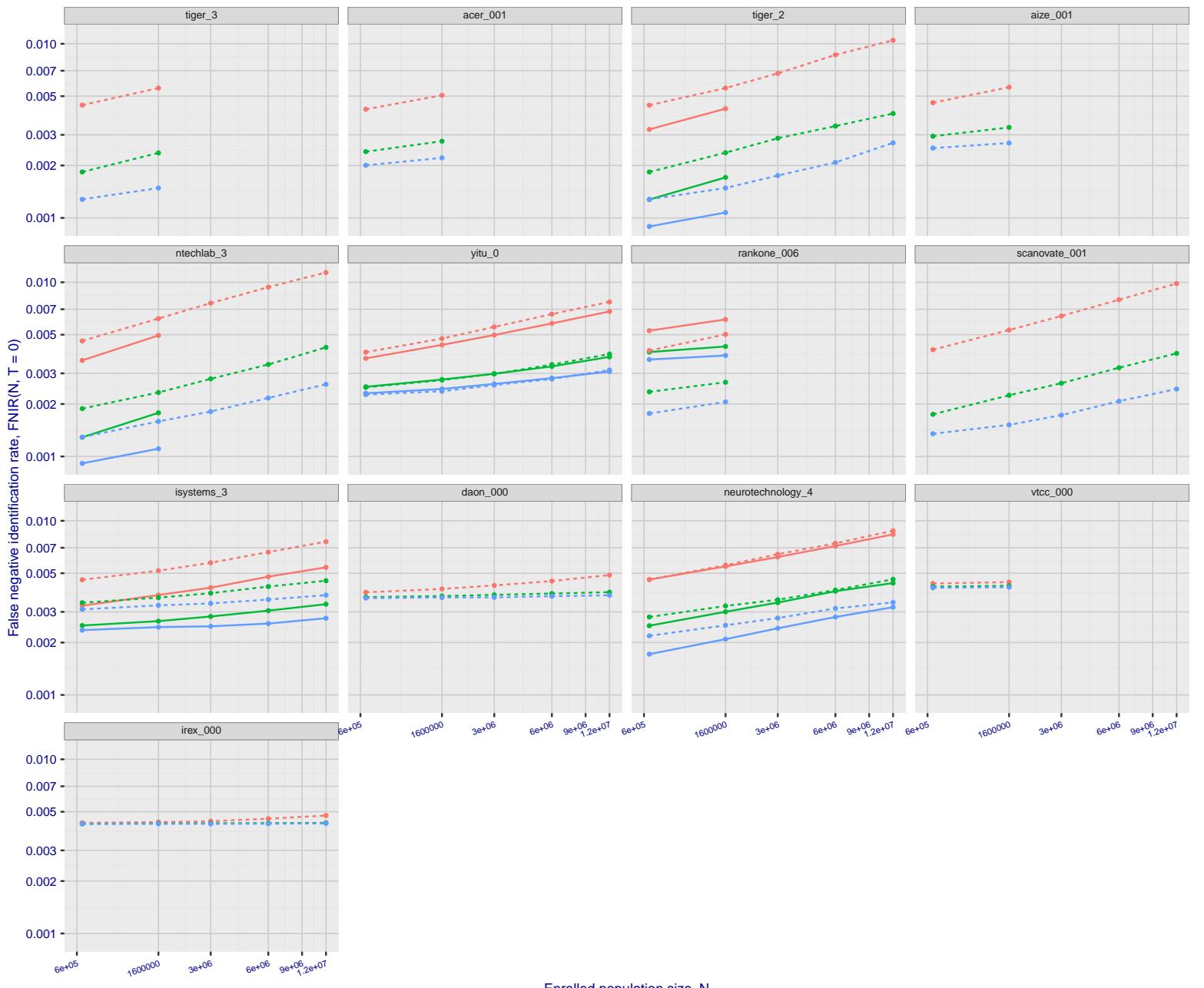


Figure 36: [FRVT-2018 Mugshot Dataset] Rank-based identification miss rates vs. number of enrolled subjects. The figure shows false negative identification rates, $\text{FNIR}(N, R)$, across various gallery sizes and ranks 1, 10 and 50. The threshold is set to zero, so this metric rewards even weak scoring rank 1 mates. This also means $\text{FPIR} = 1$, so any search without an enrolled mate will return non-mated candidates. For clarity, results are sorted and reported into tiers spanning multiple pages, the tiering criteria being rank 1 hit rate on a gallery size of 640 000.

2023/07/05
16:19:47

 $\text{FNIR}(N, R, T) =$
False neg. identification rate
 $\text{FPIR}(N, T) =$
False pos. identification rate
 $N = \text{Num. enrolled subjects}$
 $R = \text{Num. candidates examined}$
 $T = \text{Threshold}$
 $T = 0 \rightarrow \text{Investigation}$
 $T > 0 \rightarrow \text{Identification}$

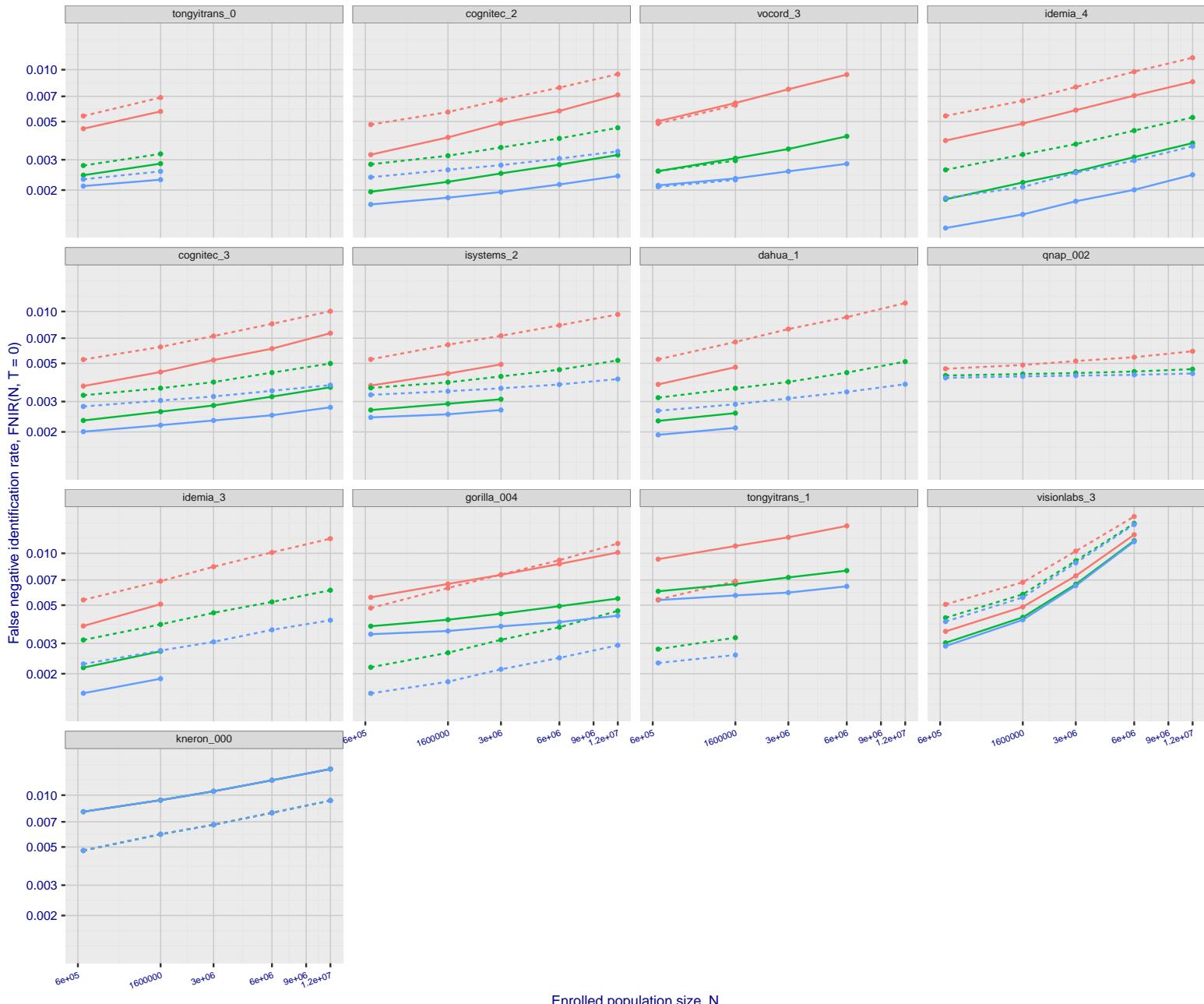


Figure 37: [FRVT-2018 Mugshot Dataset] Rank-based identification miss rates vs. number of enrolled subjects. The figure shows false negative identification rates, $\text{FNIR}(N, R)$, across various gallery sizes and ranks 1, 10 and 50. The threshold is set to zero, so this metric rewards even weak scoring rank 1 mates. This also means $\text{FPIR} = 1$, so any search without an enrolled mate will return non-mated candidates. For clarity, results are sorted and reported into tiers spanning multiple pages, the tiering criteria being rank 1 hit rate on a gallery size of 640 000.

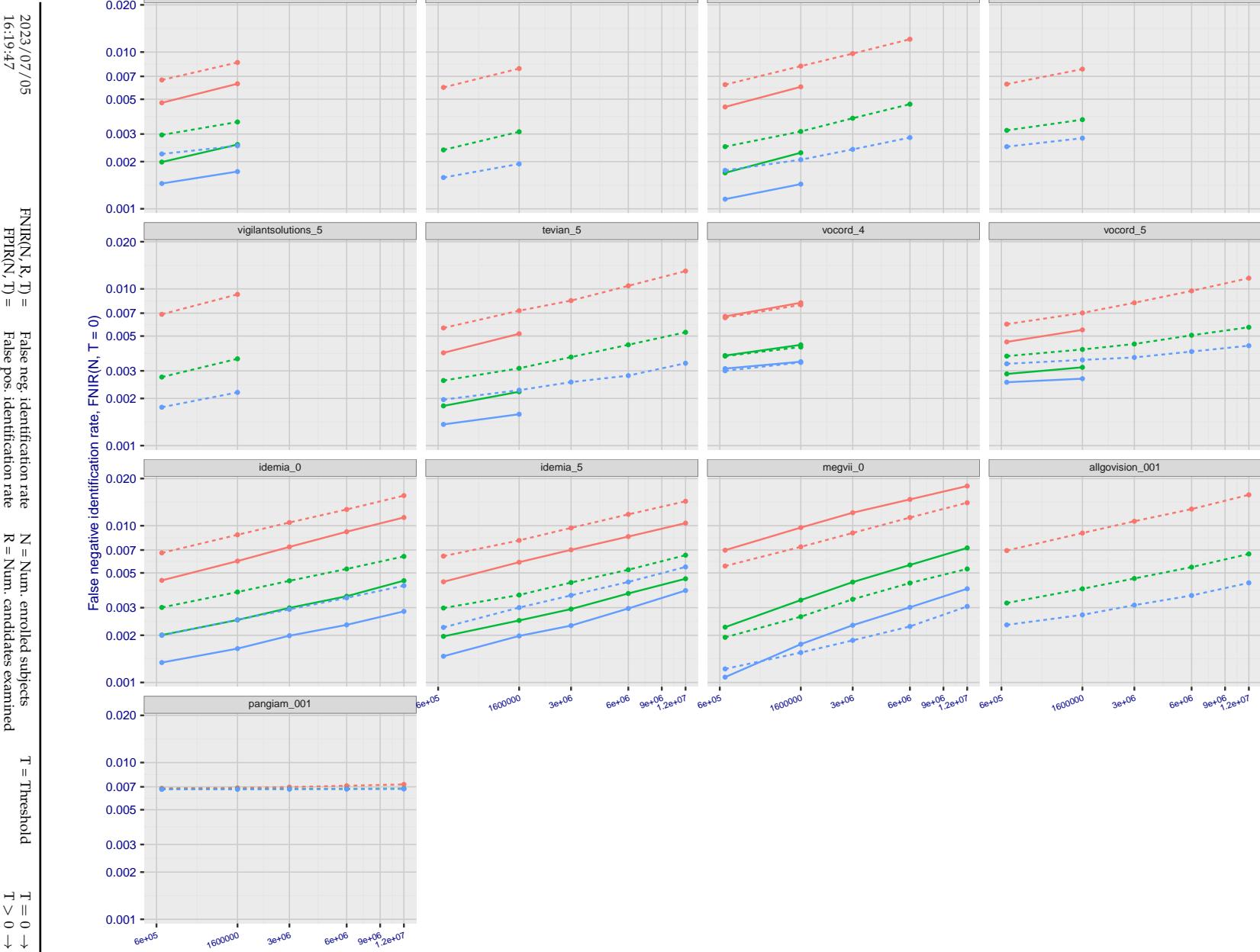


Figure 38: [FRVT-2018 Mugshot Dataset] Rank-based identification miss rates vs. number of enrolled subjects. The figure shows false negative identification rates, $\text{FNIR}(N, R)$, across various gallery sizes and ranks 1, 10 and 50. The threshold is set to zero, so this metric rewards even weak scoring rank 1 mates. This also means $\text{FPIR} = 1$, so any search without an enrolled mate will return non-mated candidates. For clarity, results are sorted and reported into tiers spanning multiple pages, the tiering criteria being rank 1 hit rate on a gallery size of 640 000.

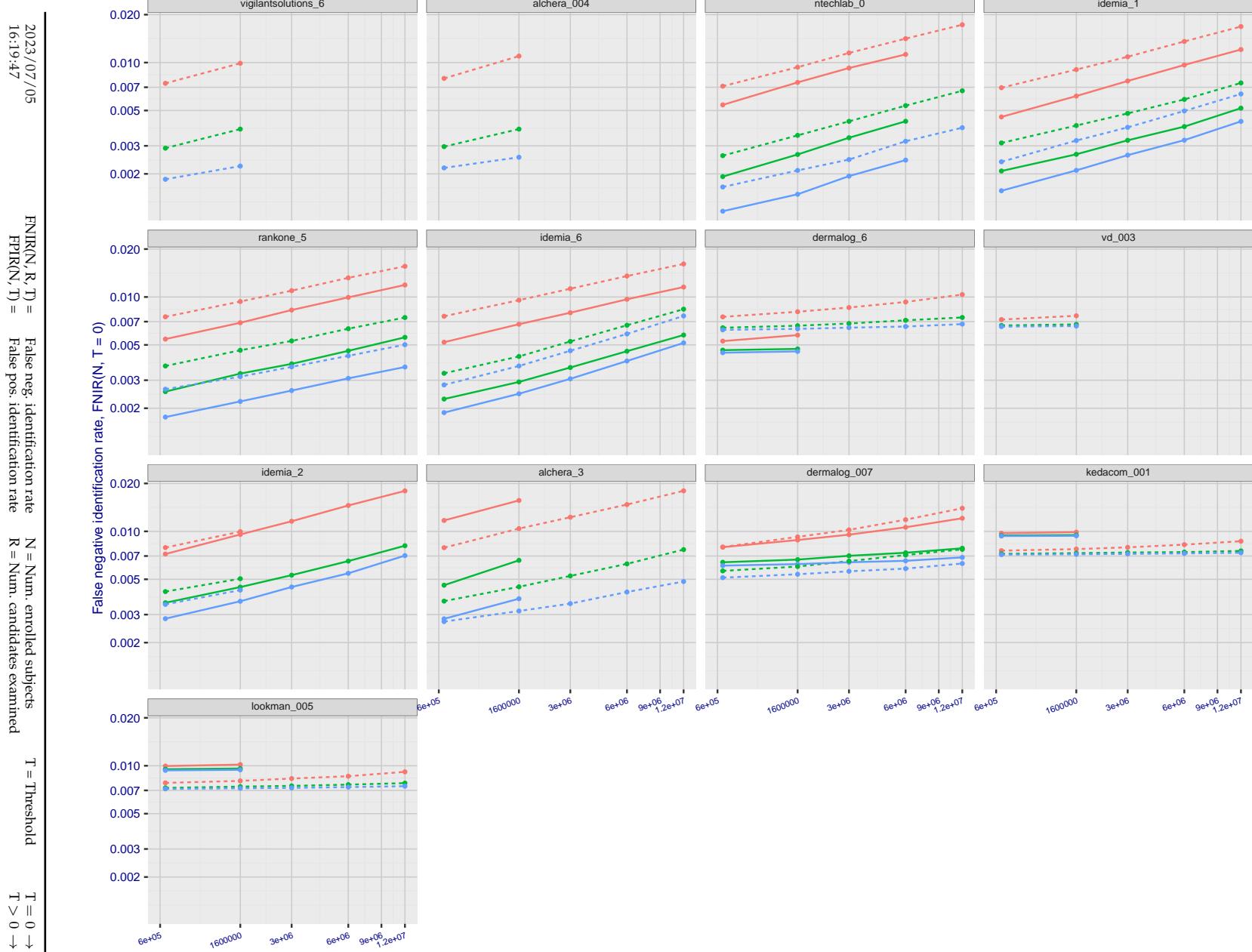
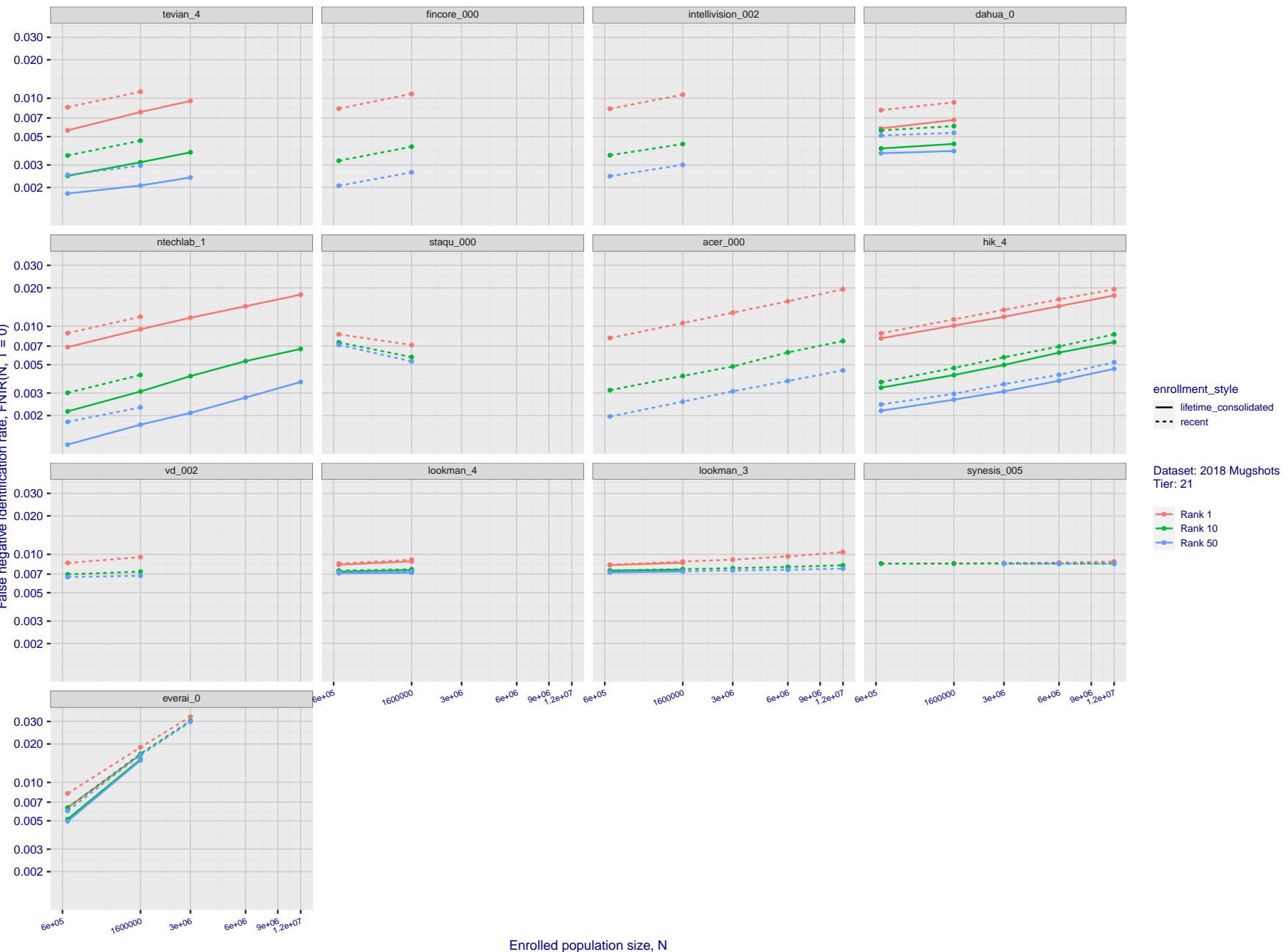


Figure 39: [FRVT-2018 Mugshot Dataset] Rank-based identification miss rates vs. number of enrolled subjects. The figure shows false negative identification rates, $\text{FNIR}(N, R)$, across various gallery sizes and ranks 1, 10 and 50. The threshold is set to zero, so this metric rewards even weak scoring rank 1 mates. This also means $\text{FPIR} = 1$, so any search without an enrolled mate will return non-mated candidates. For clarity, results are sorted and reported into tiers spanning multiple pages, the tiering criteria being rank 1 hit rate on a gallery size of 640 000.

2023/07/05
16:19:47

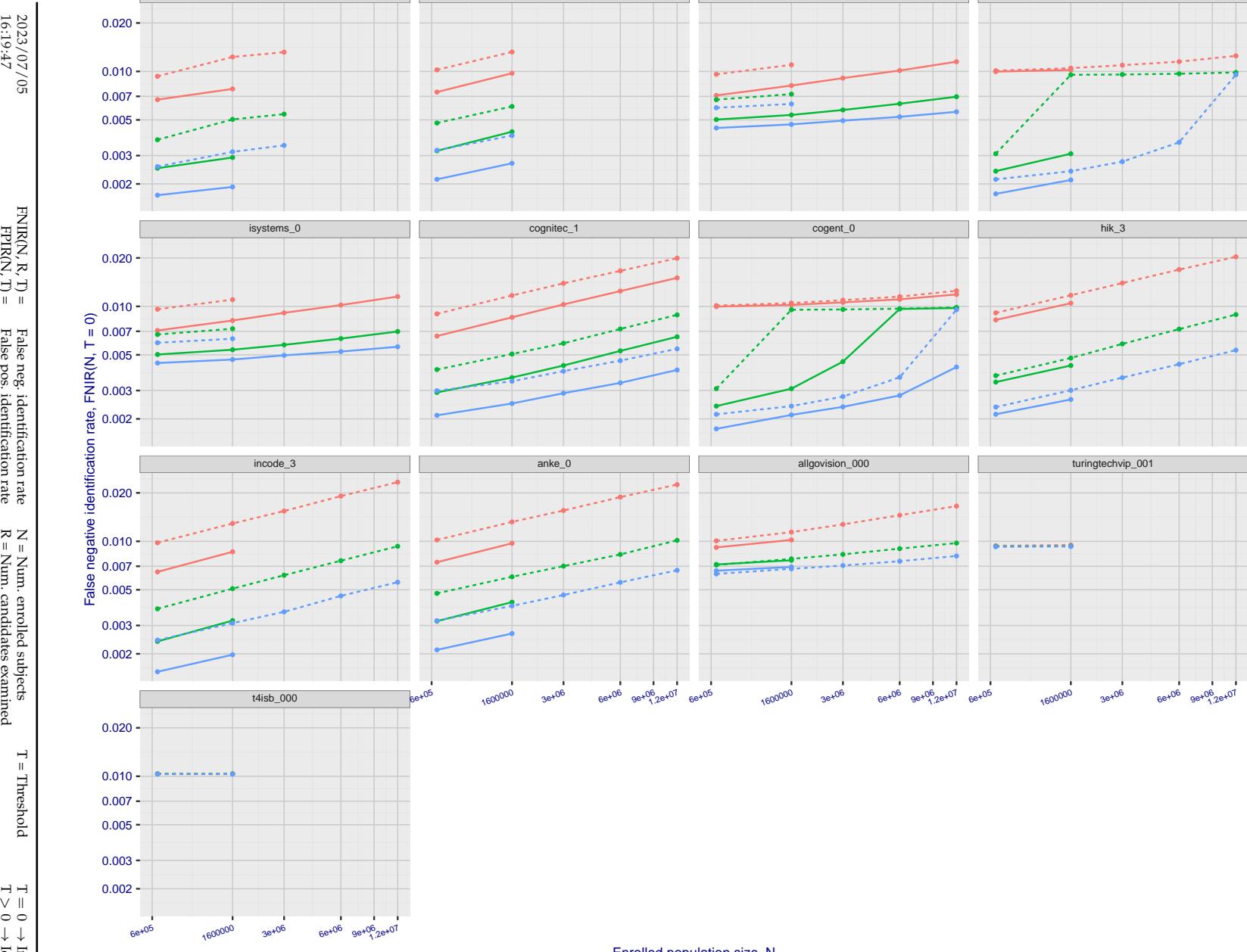


Figure 41: [FRVT-2018 Mugshot Dataset] Rank-based identification miss rates vs. number of enrolled subjects. The figure shows false negative identification rates, $\text{FNIR}(N, R)$, across various gallery sizes and ranks 1, 10 and 50. The threshold is set to zero, so this metric rewards even weak scoring rank 1 mates. This also means $\text{FPIR} = 1$, so any search without an enrolled mate will return non-mated candidates. For clarity, results are sorted and reported into tiers spanning multiple pages, the tiering criteria being rank 1 hit rate on a gallery size of 640 000.

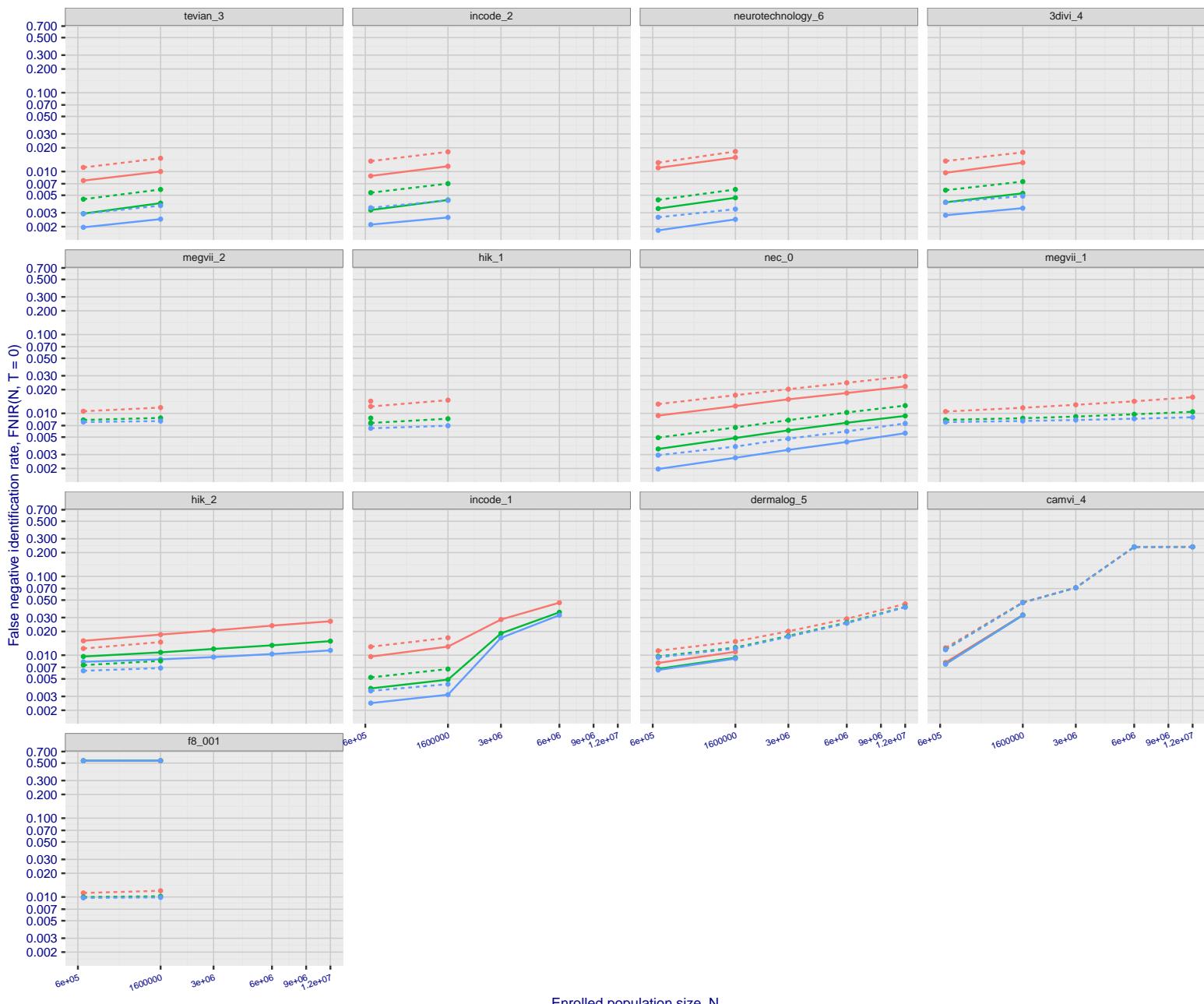


Figure 42: [FRVT-2018 Mugshot Dataset] Rank-based identification miss rates vs. number of enrolled subjects. The figure shows false negative identification rates, $\text{FNIR}(N, R)$, across various gallery sizes and ranks 1, 10 and 50. The threshold is set to zero, so this metric rewards even weak scoring rank 1 mates. This also means $\text{FPIR} = 1$, so any search without an enrolled mate will return non-mated candidates. For clarity, results are sorted and reported into tiers spanning multiple pages, the tiering criteria being rank 1 hit rate on a gallery size of 640 000.

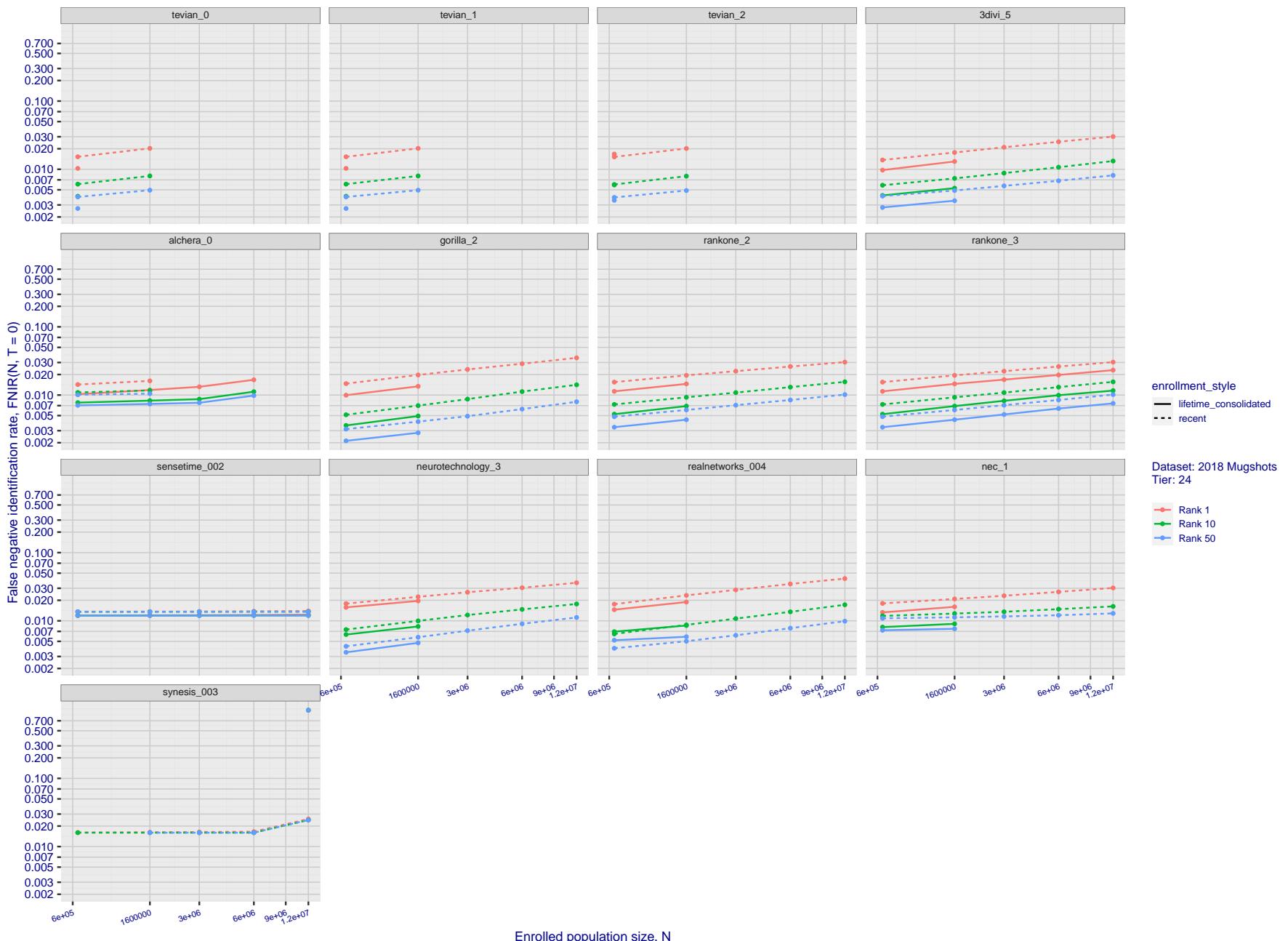


Figure 43: [FRVT-2018 Mugshot Dataset] Rank-based identification miss rates vs. number of enrolled subjects. The figure shows false negative identification rates, $\text{FNIR}(N, R)$, across various gallery sizes and ranks 1, 10 and 50. The threshold is set to zero, so this metric rewards even weak scoring rank 1 mates. This also means $\text{FPIR} = 1$, so any search without an enrolled mate will return non-mated candidates. For clarity, results are sorted and reported into tiers spanning multiple pages, the tiering criteria being rank 1 hit rate on a gallery size of 640 000.

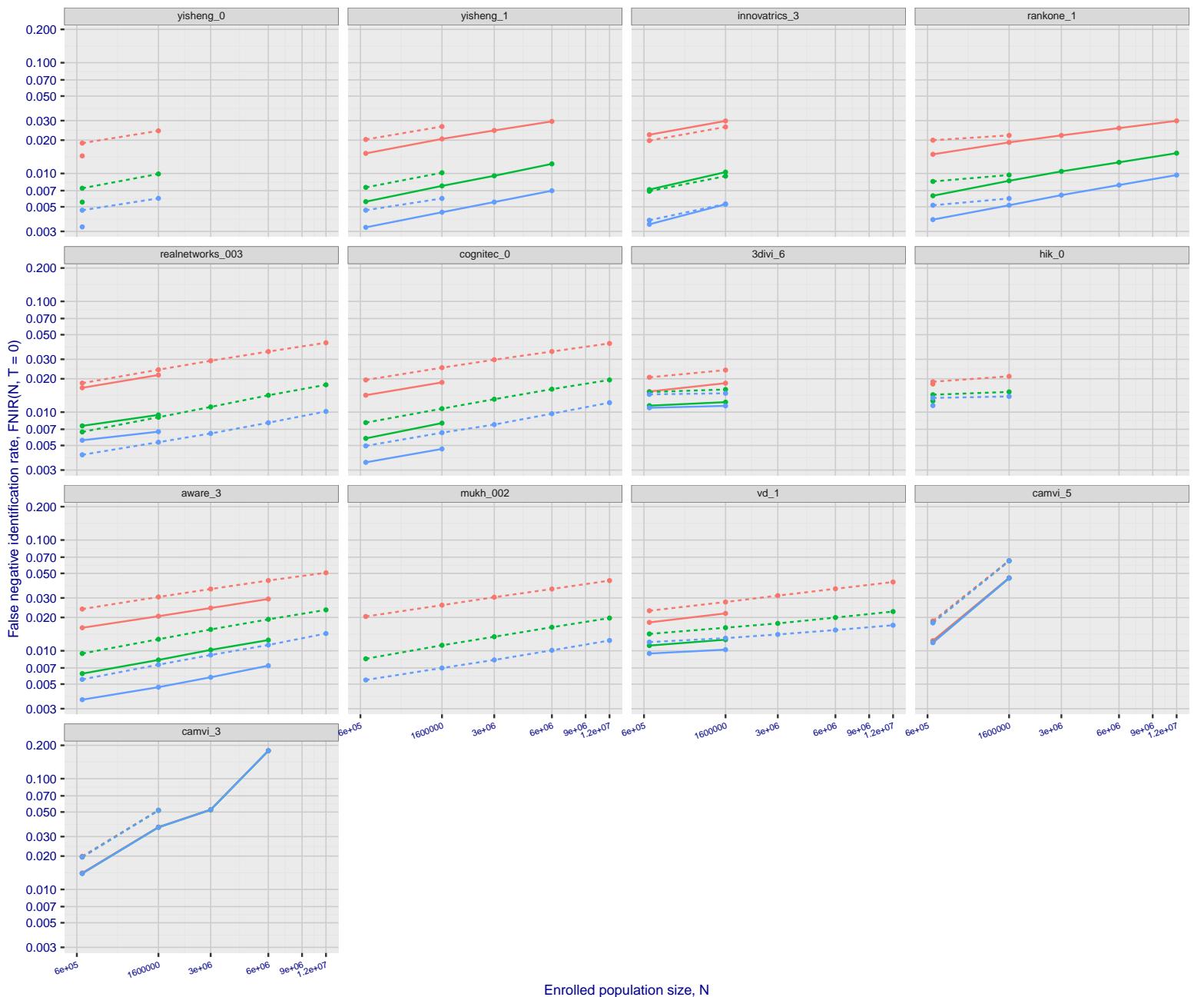


Figure 44: [FRVT-2018 Mugshot Dataset] Rank-based identification miss rates vs. number of enrolled subjects. The figure shows false negative identification rates, $\text{FNIR}(N, R)$, across various gallery sizes and ranks 1, 10 and 50. The threshold is set to zero, so this metric rewards even weak scoring rank 1 mates. This also means $\text{FPIR} = 1$, so any search without an enrolled mate will return non-mated candidates. For clarity, results are sorted and reported into tiers spanning multiple pages, the tiering criteria being rank 1 hit rate on a gallery size of 640 000.

2023/07/05
16:19:47FNIR(N, R, T) = False neg. identification rate
FPIR(N, T) = False pos. identification rate N = Num. enrolled subjects
 R = Num. candidates examined T = Threshold $T = 0 \rightarrow$ Investigation
 $T > 0 \rightarrow$ Identification

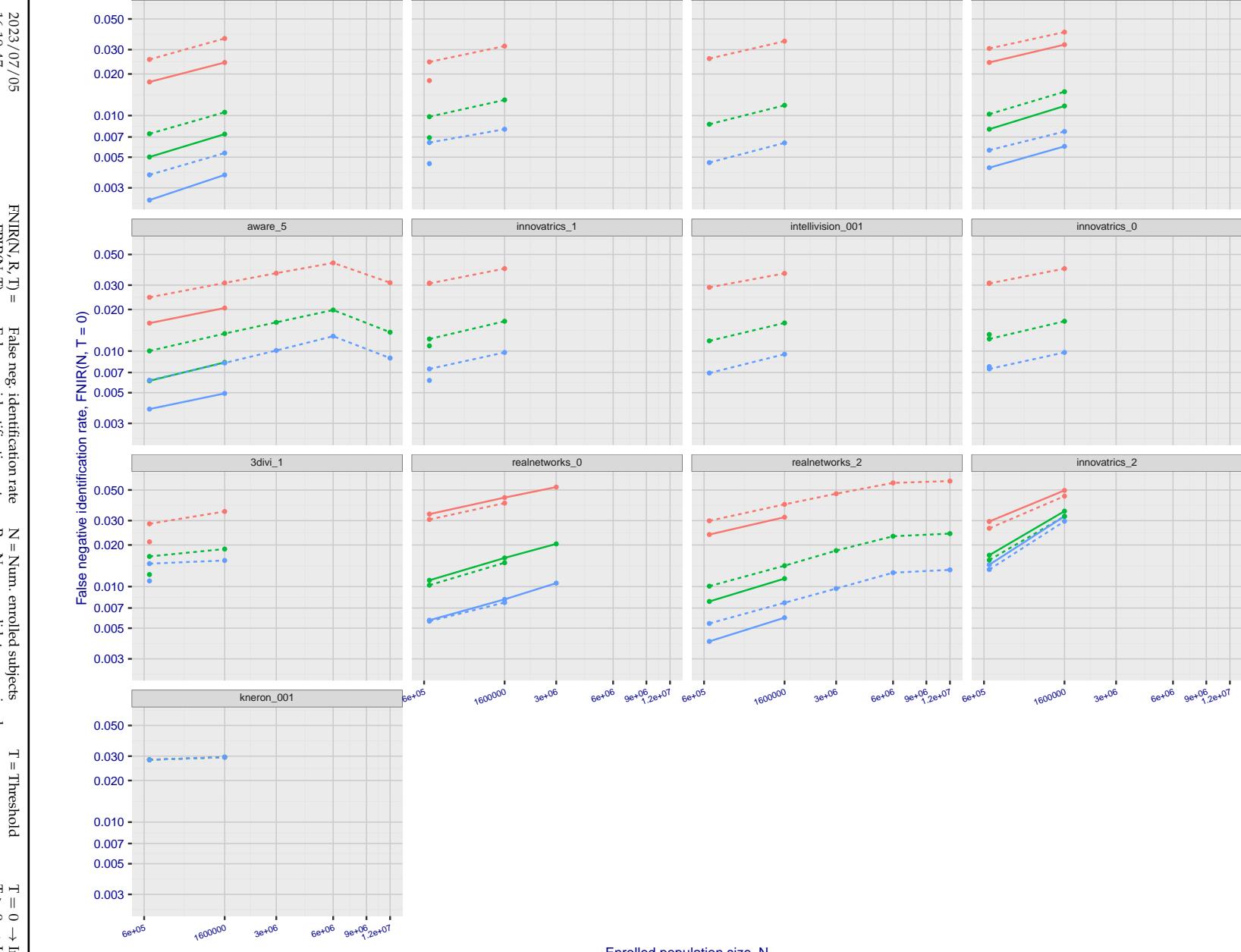


Figure 45: [FRVT-2018 Mugshot Dataset] Rank-based identification miss rates vs. number of enrolled subjects. The figure shows false negative identification rates, $\text{FNIR}(N, R)$, across various gallery sizes and ranks 1, 10 and 50. The threshold is set to zero, so this metric rewards even weak scoring rank 1 mates. This also means $\text{FPIR} = 1$, so any search without an enrolled mate will return non-mated candidates. For clarity, results are sorted and reported into tiers spanning multiple pages, the tiering criteria being rank 1 hit rate on a gallery size of 640 000.

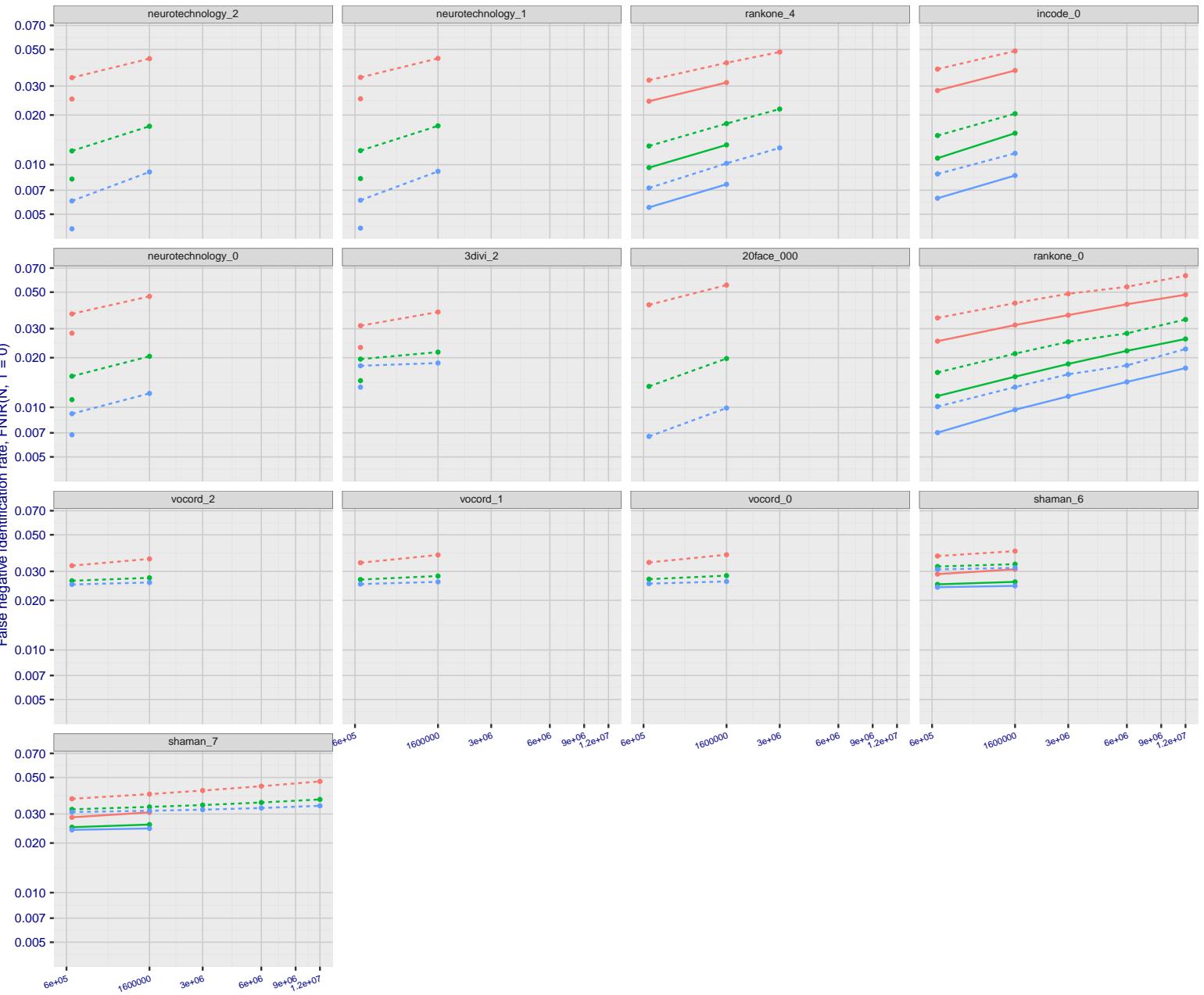
2023/07/05
16:19:47FNIR(N, R, T) = False neg. identification rate
FPIR(N, T) = False pos. identification rate
N = Num. enrolled subjects
R = Num. candidates examinedT = Threshold
T = 0 → Investigation
T > 0 → Identification

Figure 46: [FRVT-2018 Mugshot Dataset] Rank-based identification miss rates vs. number of enrolled subjects. The figure shows false negative identification rates, $\text{FNIR}(N, R)$, across various gallery sizes and ranks 1, 10 and 50. The threshold is set to zero, so this metric rewards even weak scoring rank 1 mates. This also means $\text{FPIR} = 1$, so any search without an enrolled mate will return non-mated candidates. For clarity, results are sorted and reported into tiers spanning multiple pages, the tiering criteria being rank 1 hit rate on a gallery size of 640 000.

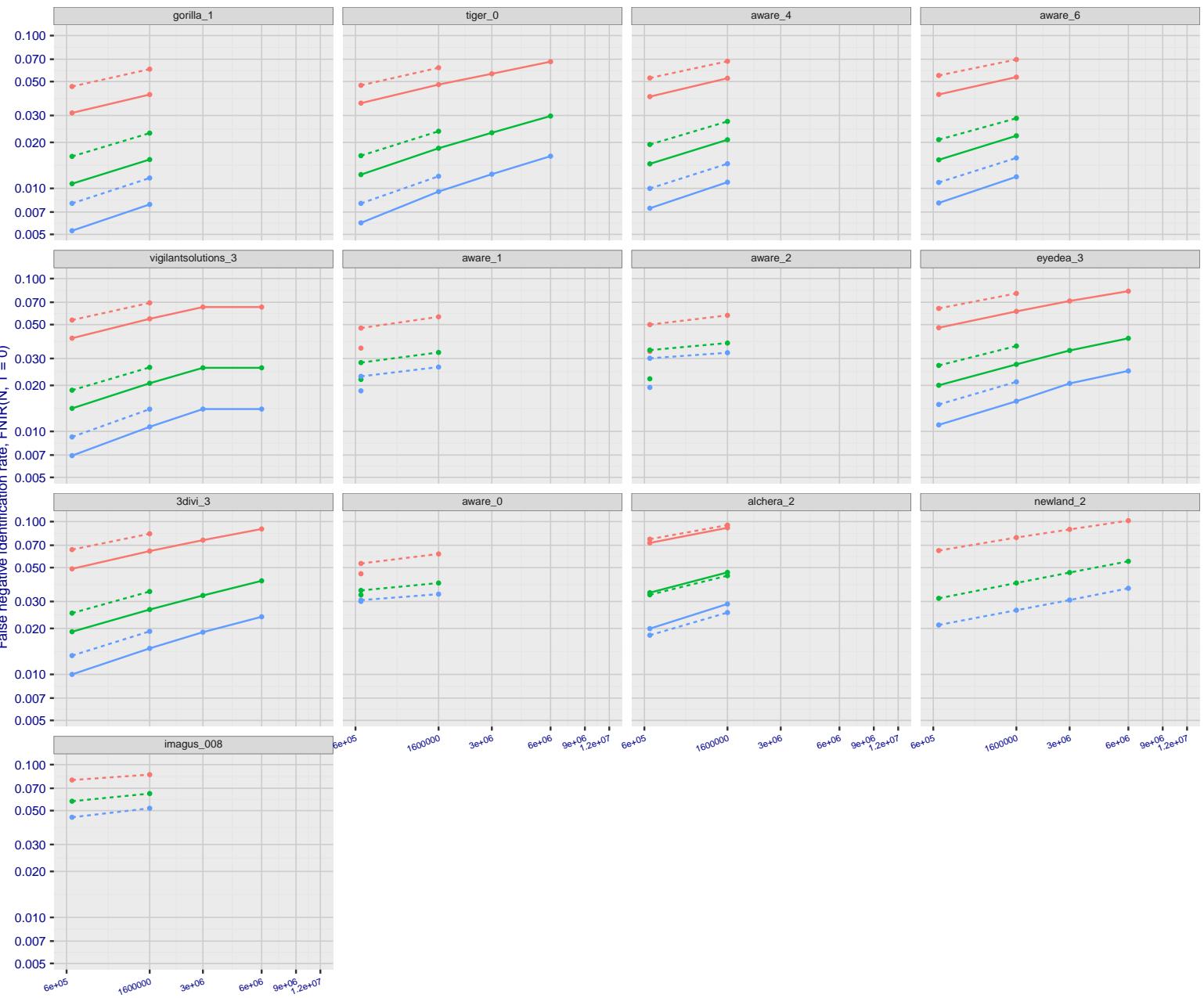
2023/07/05
16:19:47

Figure 47: [FRVT-2018 Mugshot Dataset] Rank-based identification miss rates vs. number of enrolled subjects. The figure shows false negative identification rates, $\text{FNIR}(N, R)$, across various gallery sizes and ranks 1, 10 and 50. The threshold is set to zero, so this metric rewards even weak scoring rank 1 mates. This also means $\text{FPIR} = 1$, so any search without an enrolled mate will return non-mated candidates. For clarity, results are sorted and reported into tiers spanning multiple pages, the tiering criteria being rank 1 hit rate on a gallery size of 640 000.

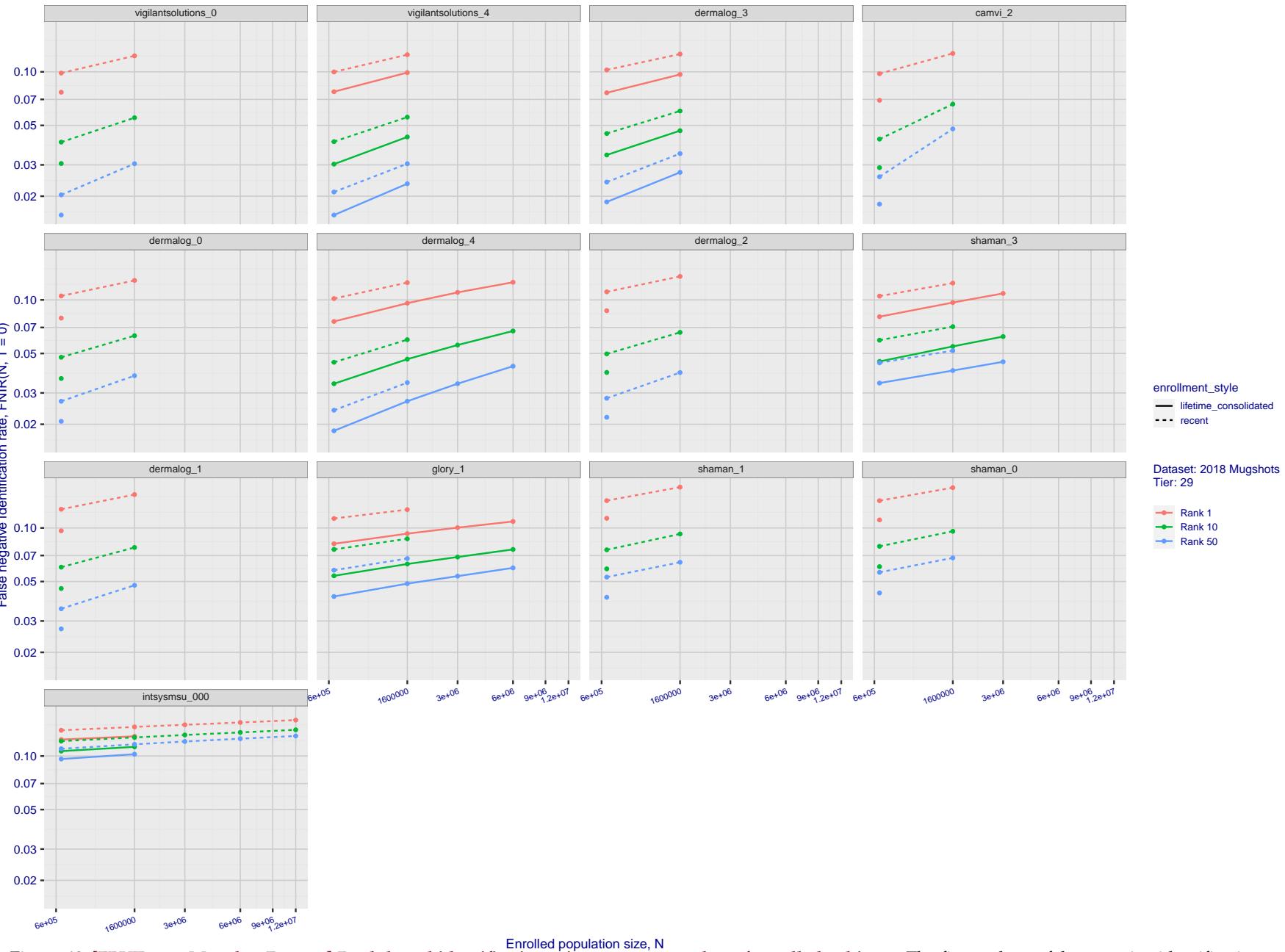
2023/07/05
16:19:47

Figure 48: [FRVT-2018 Mugshot Dataset] Rank-based identification miss rates vs. number of enrolled subjects. The figure shows false negative identification rates, $\text{FNIR}(N, R)$, across various gallery sizes and ranks 1, 10 and 50. The threshold is set to zero, so this metric rewards even weak scoring rank 1 mates. This also means $\text{FPIR} = 1$, so any search without an enrolled mate will return non-mated candidates. For clarity, results are sorted and reported into tiers spanning multiple pages, the tiering criteria being rank 1 hit rate on a gallery size of 640 000.

2023/07/05
16:19:47

 $\text{FNIR}(N, R, T) =$
False neg. identification rate
 $\text{FPIR}(N, T) =$
False pos. identification rate

 $N =$ Num. enrolled subjects
 $R =$ Num. candidates examined

 $T =$ Threshold
 $T = 0 \rightarrow$ Investigation
 $T > 0 \rightarrow$ Identification

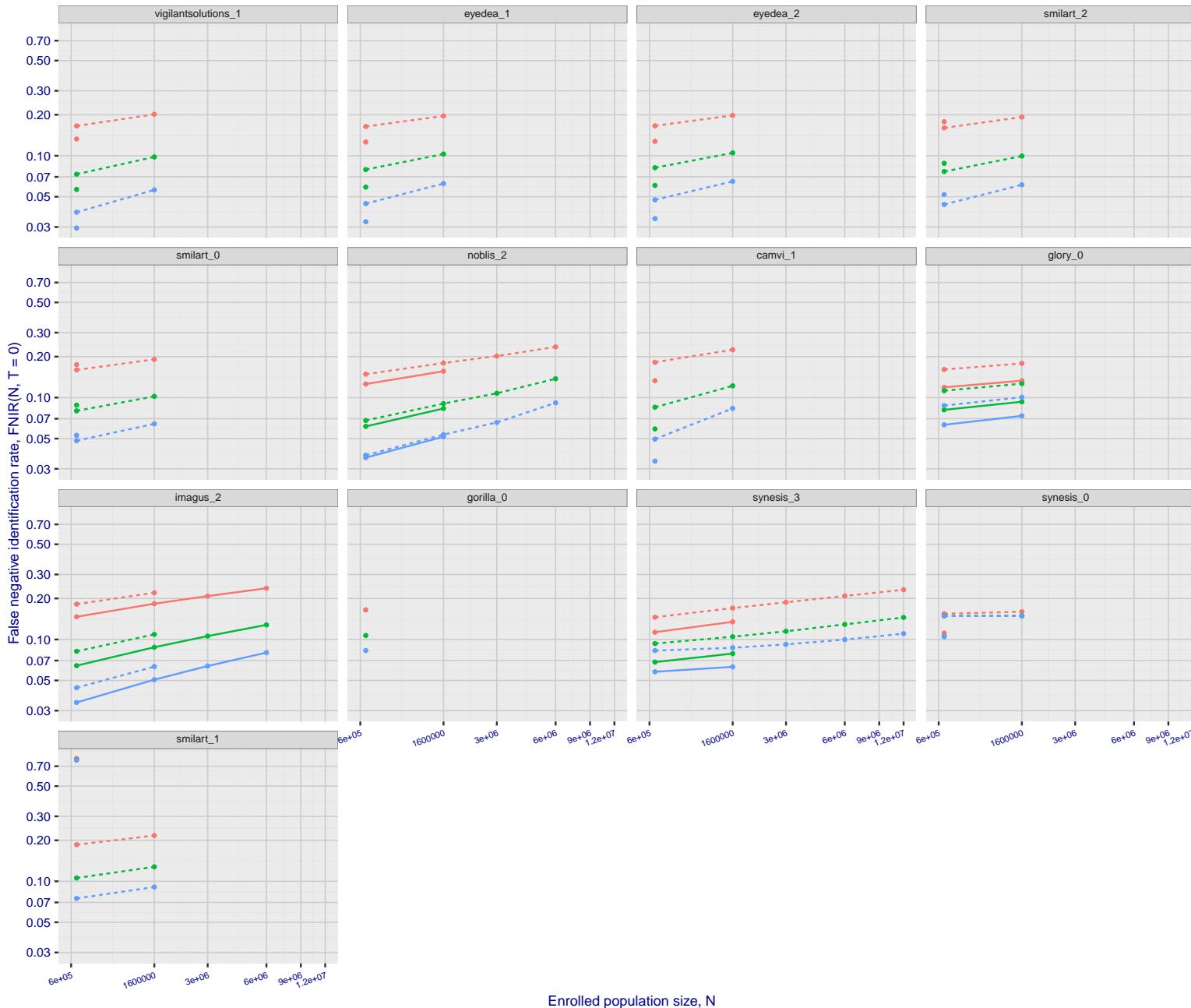


Figure 49: [FRVT-2018 Mugshot Dataset] Rank-based identification miss rates vs. number of enrolled subjects. The figure shows false negative identification rates, $\text{FNIR}(N, R)$, across various gallery sizes and ranks 1, 10 and 50. The threshold is set to zero, so this metric rewards even weak scoring rank 1 mates. This also means $\text{FPIR} = 1$, so any search without an enrolled mate will return non-mated candidates. For clarity, results are sorted and reported into tiers spanning multiple pages, the tiering criteria being rank 1 hit rate on a gallery size of 640 000.

2023/07/05
16:19:47

 $\text{FNIR}(N, R, T) =$
False neg. identification rate
 $\text{FPIR}(N, T) =$
False pos. identification rate

 $N =$ Num. enrolled subjects
 $R =$ Num. candidates examined

 $T =$ Threshold
 $T = 0 \rightarrow$ Investigation
 $T > 0 \rightarrow$ Identification

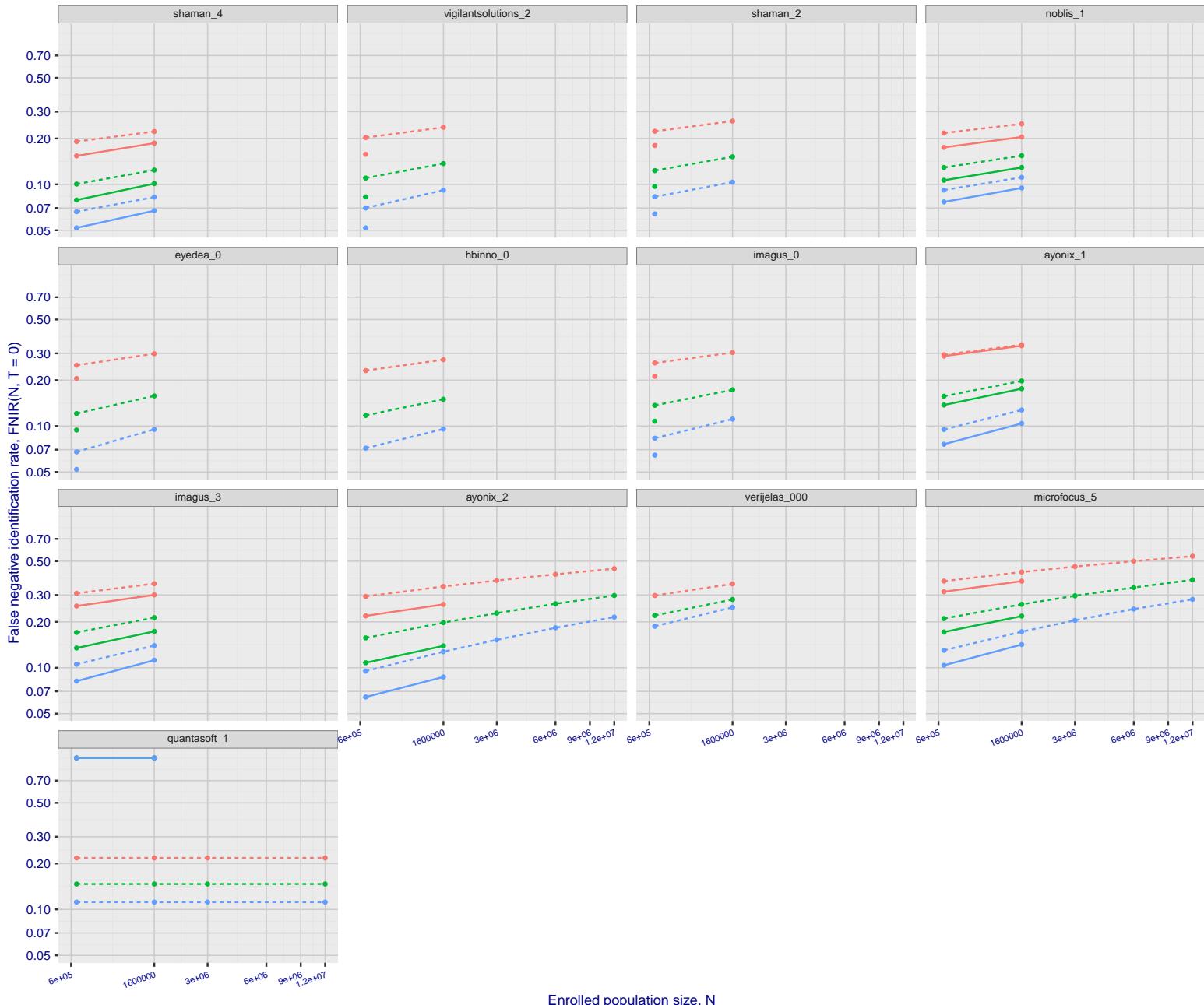
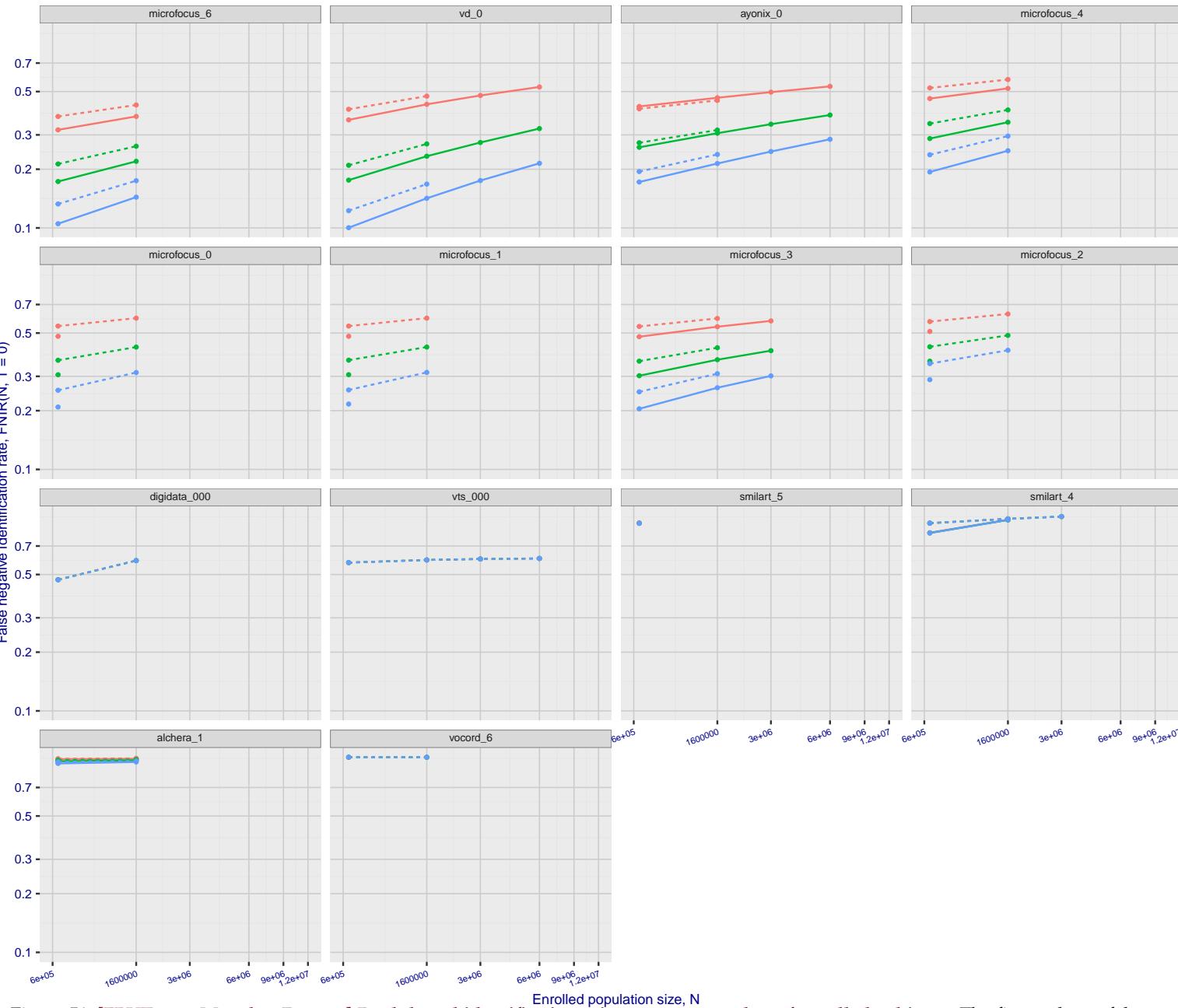


Figure 50: [FRVT-2018 Mugshot Dataset] Rank-based identification miss rates vs. number of enrolled subjects. The figure shows false negative identification rates, $\text{FNIR}(N, R)$, across various gallery sizes and ranks 1, 10 and 50. The threshold is set to zero, so this metric rewards even weak scoring rank 1 mates. This also means $\text{FPIR} = 1$, so any search without an enrolled mate will return non-mated candidates. For clarity, results are sorted and reported into tiers spanning multiple pages, the tiering criteria being rank 1 hit rate on a gallery size of 640 000.

2023/07/05
16:19:47FNIR(N, R, T) = False neg. identification rate
FPIR(N, T) = False pos. identification rateN = Num. enrolled subjects
R = Num. candidates examined

T = Threshold

T = 0 → Investigation
T > 0 → Identification

enrollment_style
 — lifetime_consolidated
 - recent

Dataset: 2018 Mugshots
 Tier: 32

- Rank 1
- Rank 10
- Rank 50

Figure 51: [FRVT-2018 Mugshot Dataset] Rank-based identification miss rates vs. number of enrolled subjects. The figure shows false negative identification rates, $\text{FNIR}(N, R)$, across various gallery sizes and ranks 1, 10 and 50. The threshold is set to zero, so this metric rewards even weak scoring rank 1 mates. This also means $\text{FPIR} = 1$, so any search without an enrolled mate will return non-mated candidates. For clarity, results are sorted and reported into tiers spanning multiple pages, the tiering criteria being rank 1 hit rate on a gallery size of 640 000.

2023/07/05
16:19:47

FNIR(N, R, T) = False neg. identification rate
FPTR(N, T) = False pos. identification rate

N = Num. enrolled subjects
R = Num. candidates examined

T = Threshold
T > 0 → Identification

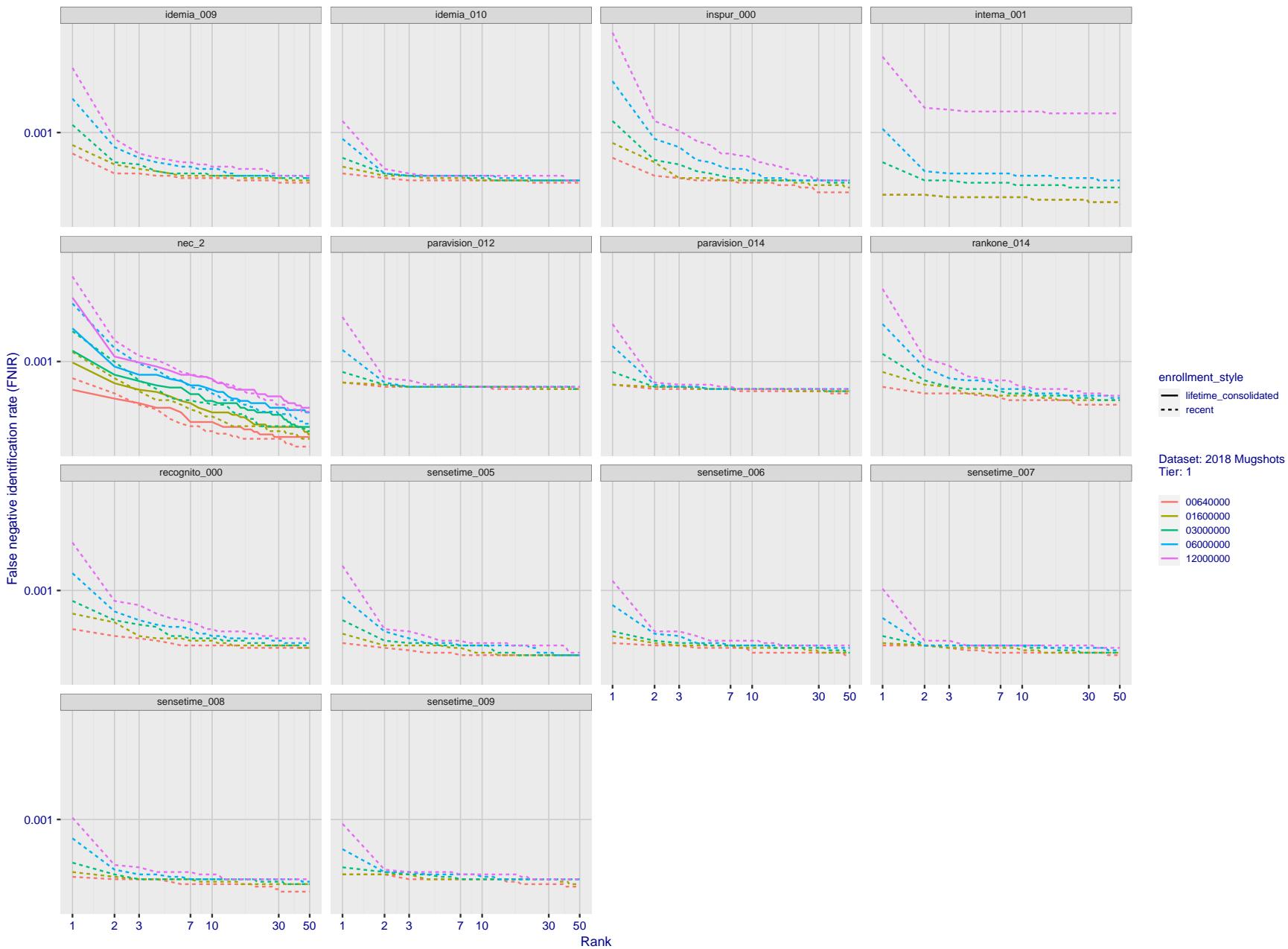


Figure 52: [FRVT-2018 Mugshot Dataset] Rank-based identification miss rates vs. rank. The figure shows false negative identification rates (FNIR) for ranks up to 50. This metric is appropriate to investigational applications where human reviewers will adjudicate sorted candidate lists. Note that with threshold set to zero, FPIR = 1, i.e. any search without an enrolled mate will return non-mated candidates. Results are sorted and reported into tiers for clarity, with the tiering criteria being rank 1 hit rate on a gallery size of $N = 640\,000$ subjects.

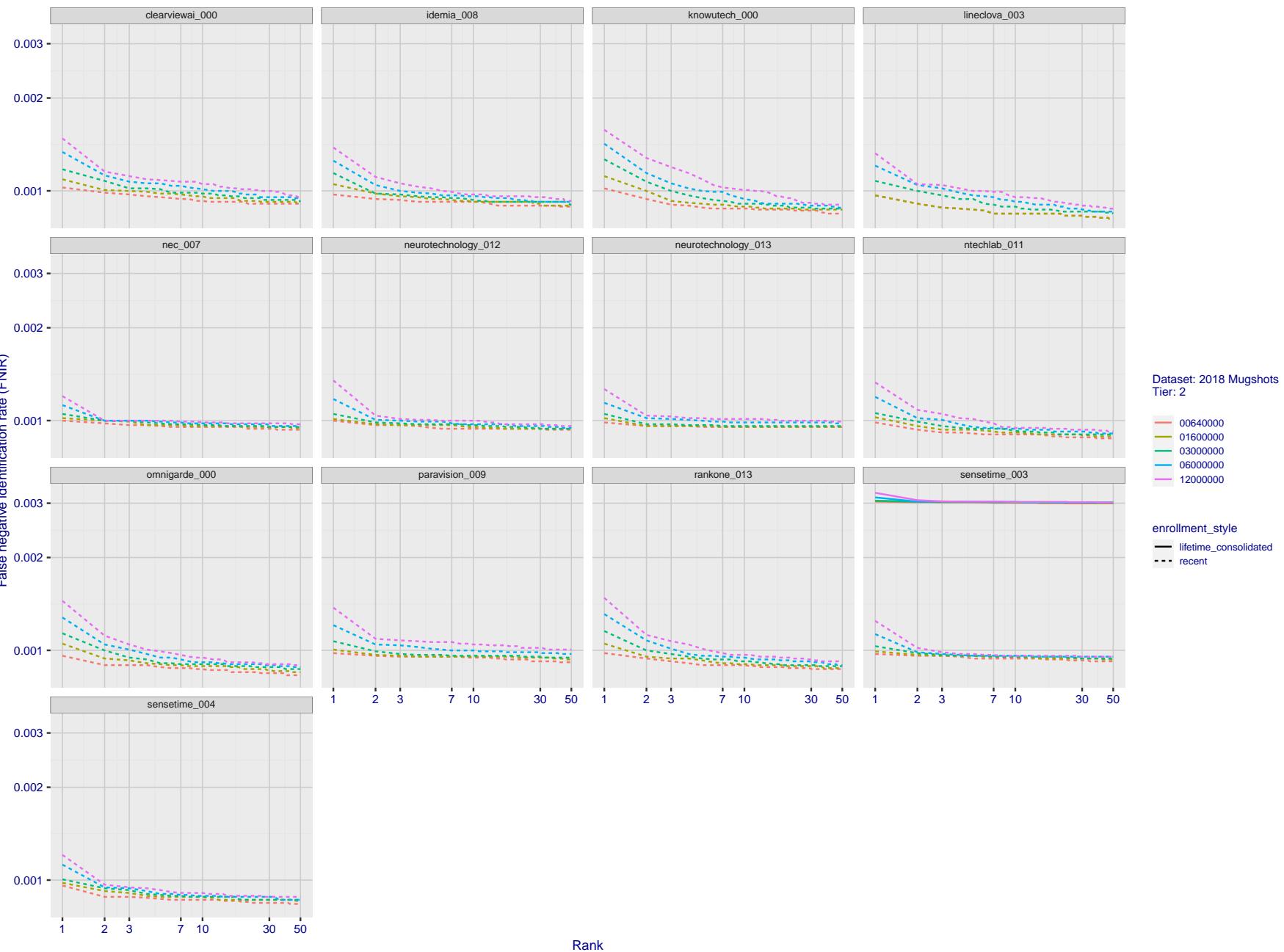
2023/07/05
16:19:47

Figure 53: [FRVT-2018 Mugshot Dataset] Rank-based identification miss rates vs. rank. The figure shows false negative identification rates (FNIR) for ranks up to 50. This metric is appropriate to investigational applications where human reviewers will adjudicate sorted candidate lists. Note that with threshold set to zero, FPIR = 1, i.e. any search without an enrolled mate will return non-mated candidates. Results are sorted and reported into tiers for clarity, with the tiering criteria being rank 1 hit rate on a gallery size of $N = 640\,000$ subjects.

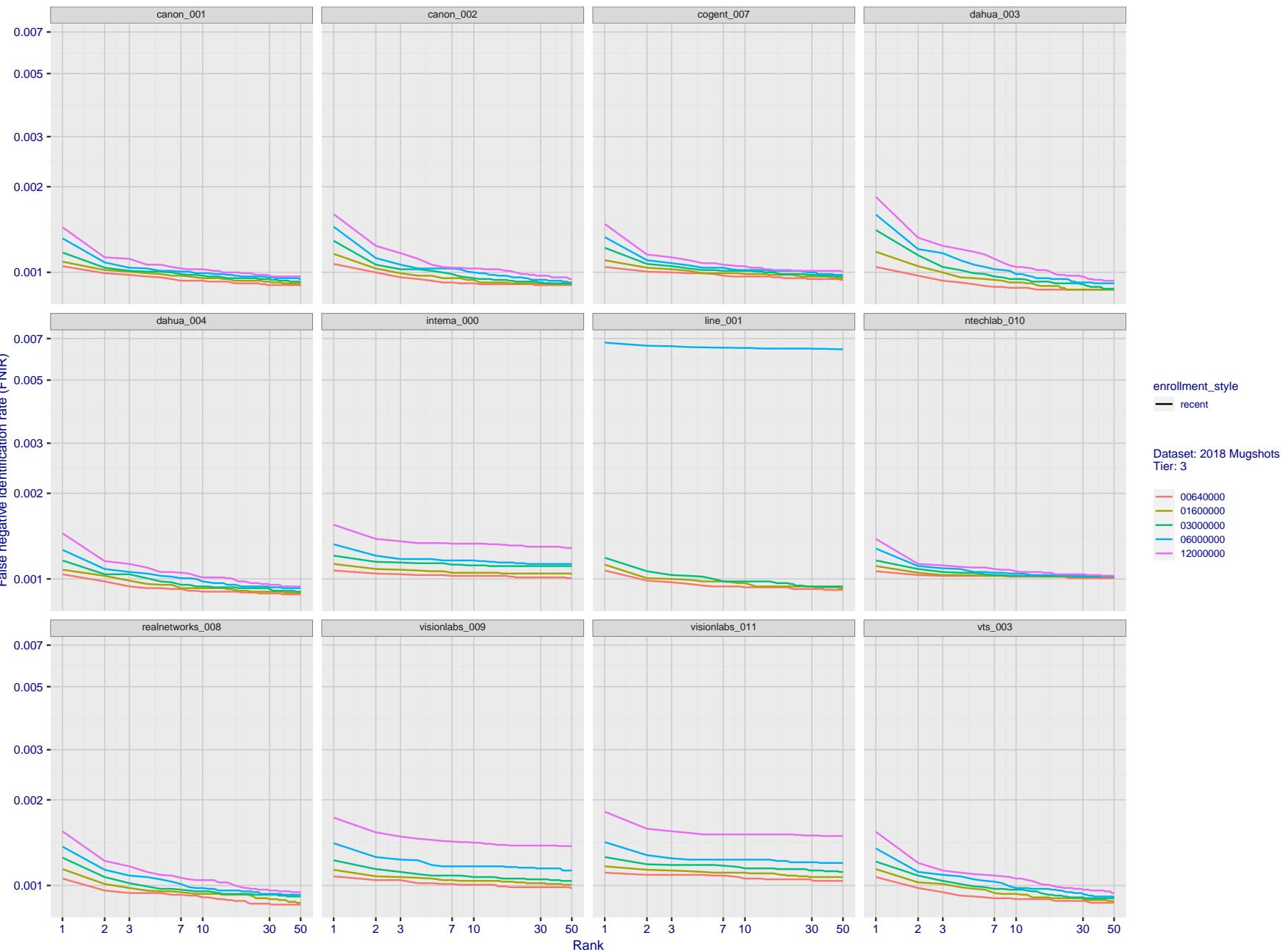
2023/07/05
16:19:47

Figure 54: [FRVT-2018 Mugshot Dataset] Rank-based identification miss rates vs. rank. The figure shows false negative identification rates (FNIR) for ranks up to 50. This metric is appropriate to investigational applications where human reviewers will adjudicate sorted candidate lists. Note that with threshold set to zero, FPIR = 1, i.e. any search without an enrolled mate will return non-mated candidates. Results are sorted and reported into tiers for clarity, with the tiering criteria being rank 1 hit rate on a gallery size of $N = 640\,000$ subjects.

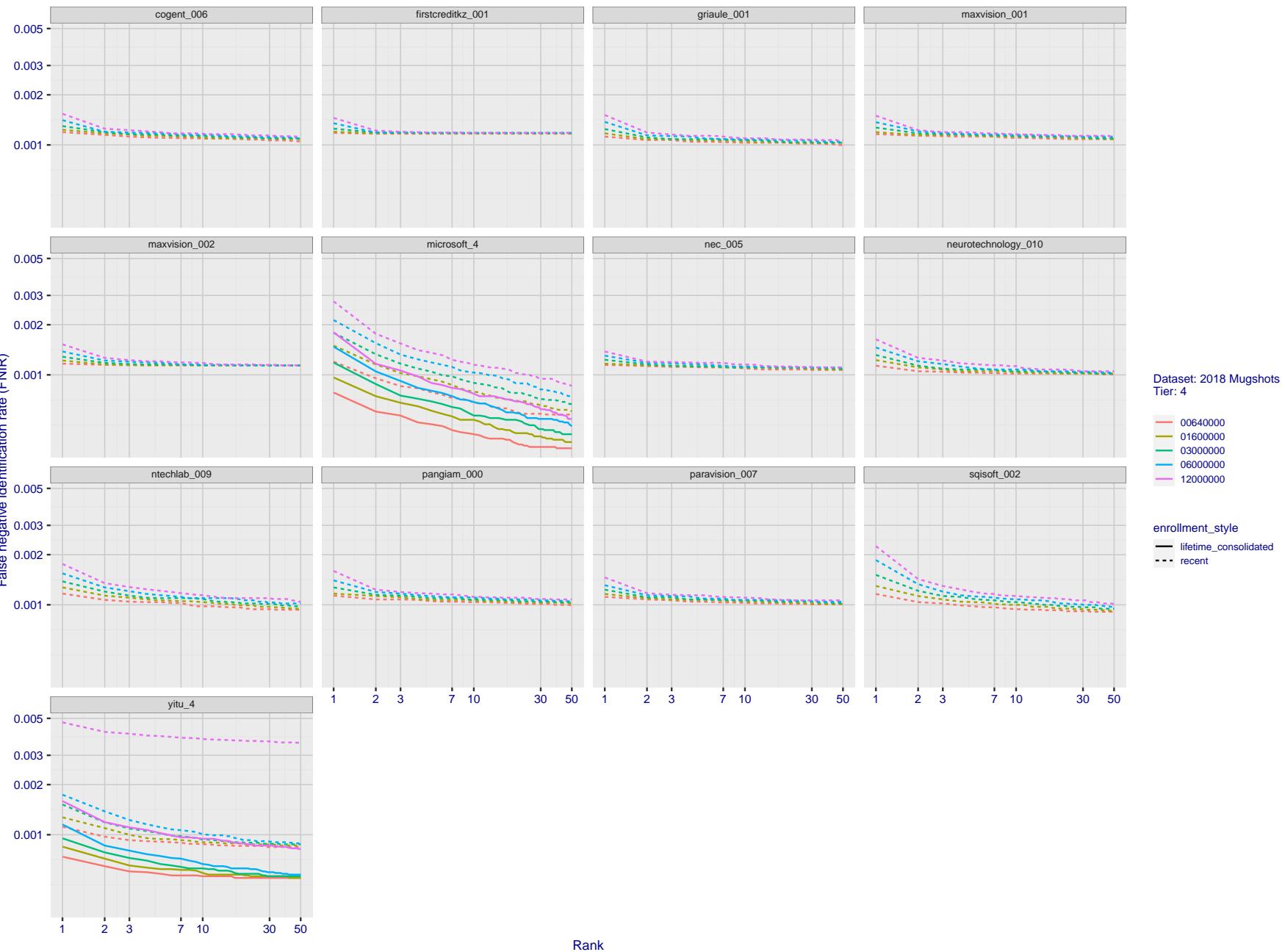
2023/07/05
16:19:47

Figure 55: [FRVT-2018 Mugshot Dataset] Rank-based identification miss rates vs. rank. The figure shows false negative identification rates (FNIR) for ranks up to 50. This metric is appropriate to investigational applications where human reviewers will adjudicate sorted candidate lists. Note that with threshold set to zero, FPIR = 1, i.e. any search without an enrolled mate will return non-mated candidates. Results are sorted and reported into tiers for clarity, with the tiering criteria being rank 1 hit rate on a gallery size of $N = 640\,000$ subjects.

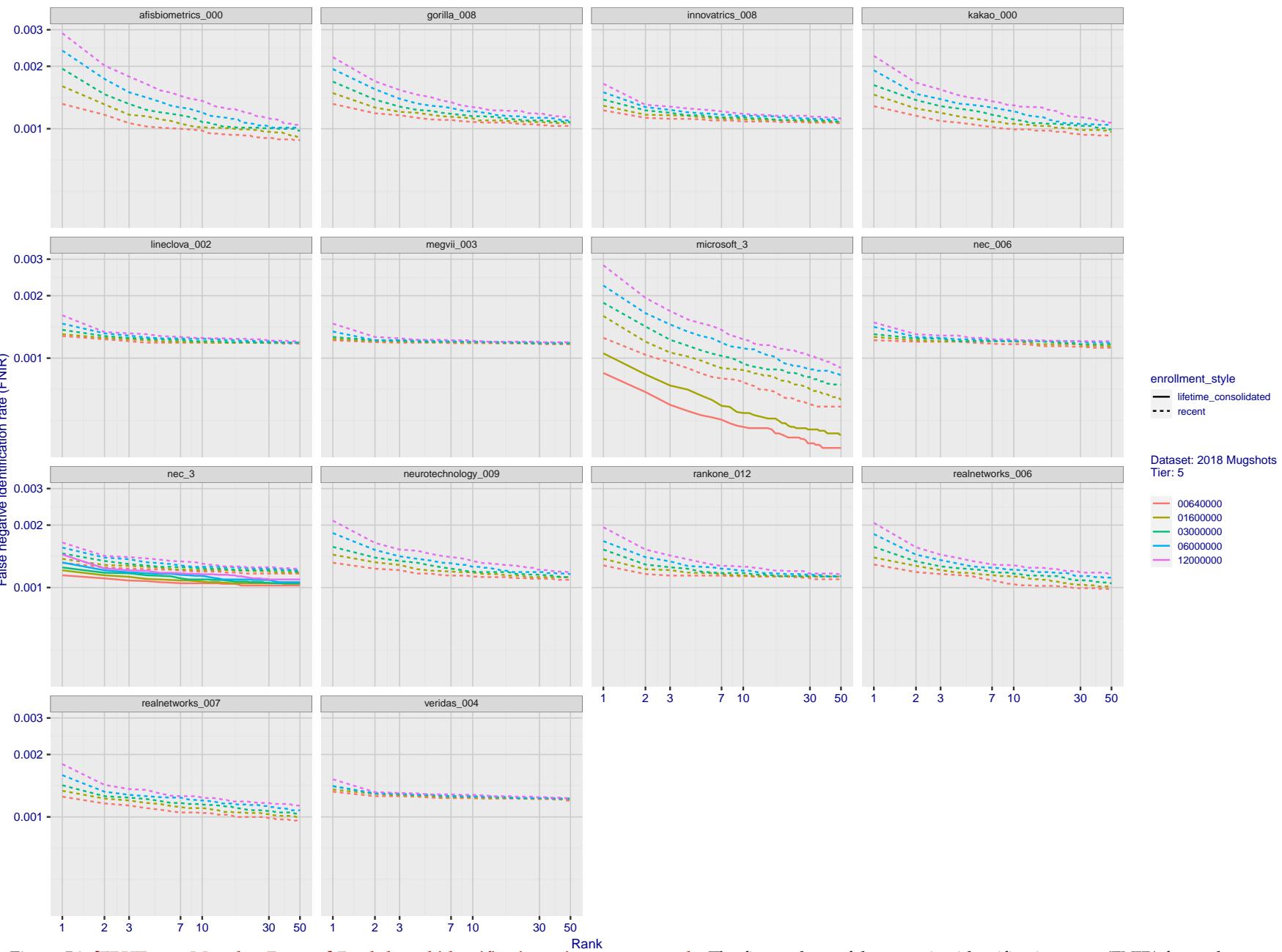
2023/07/05
16:19:47

Figure 56: [FRVT-2018 Mugshot Dataset] Rank-based identification miss rates vs. rank. The figure shows false negative identification rates (FNIR) for ranks up to 50. This metric is appropriate to investigational applications where human reviewers will adjudicate sorted candidate lists. Note that with threshold set to zero, FPIR = 1, i.e. any search without an enrolled mate will return non-mated candidates. Results are sorted and reported into tiers for clarity, with the tiering criteria being rank 1 hit rate on a gallery size of N = 640 000 subjects.

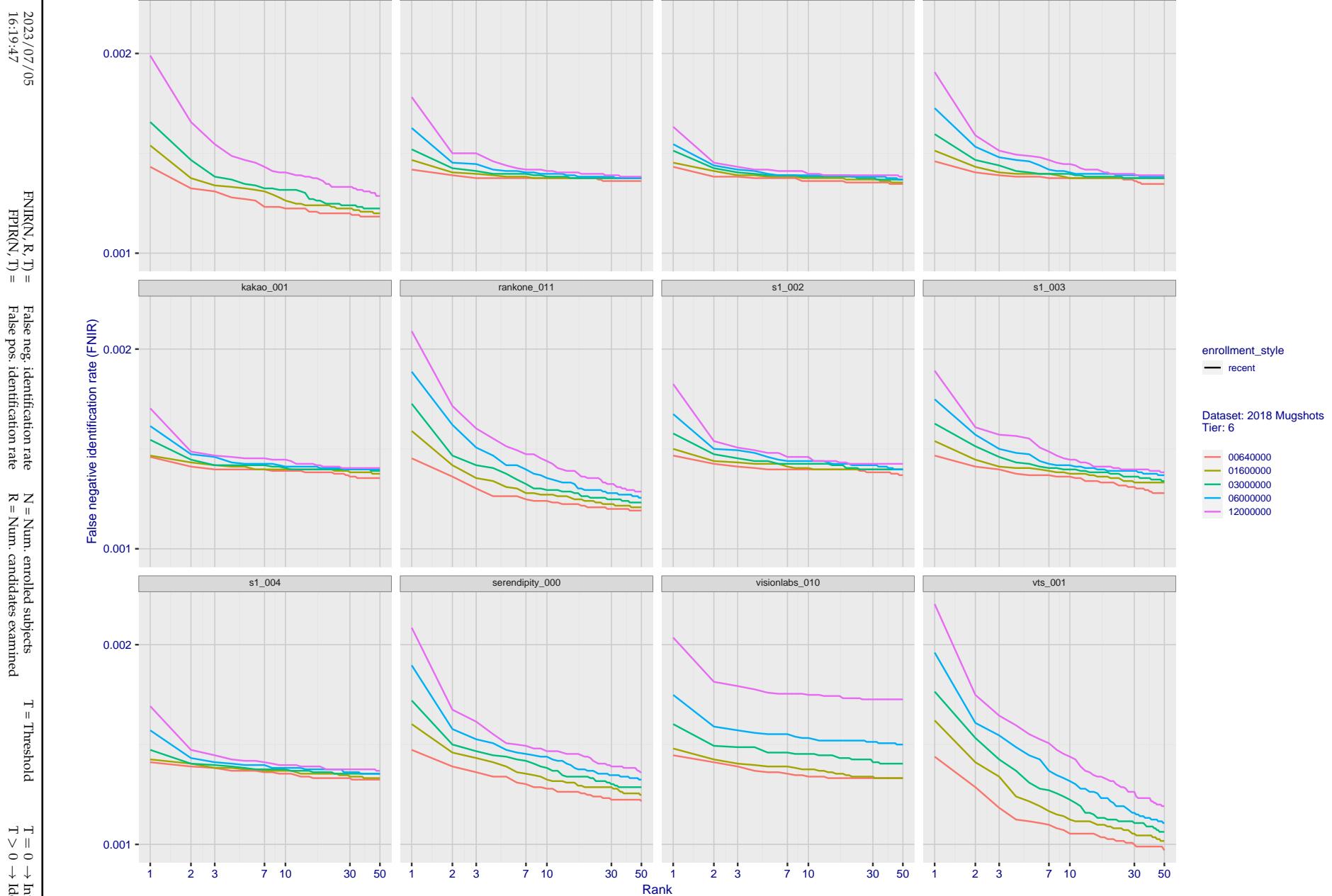


Figure 57: [FRVT-2018 Mugshot Dataset] Rank-based identification miss rates vs. rank. The figure shows false negative identification rates (FNIR) for ranks up to 50. This metric is appropriate to investigational applications where human reviewers will adjudicate sorted candidate lists. Note that with threshold set to zero, FPIR = 1, i.e. any search without an enrolled mate will return non-mated candidates. Results are sorted and reported into tiers for clarity, with the tiering criteria being rank 1 hit rate on a gallery size of N = 640 000 subjects.

2023/07/05
16:19:47FNIR(N, R, T) = False neg. identification rate
FPIR(N, T) = False pos. identification rateN = Num. enrolled subjects
R = Num. candidates examined

T = Threshold

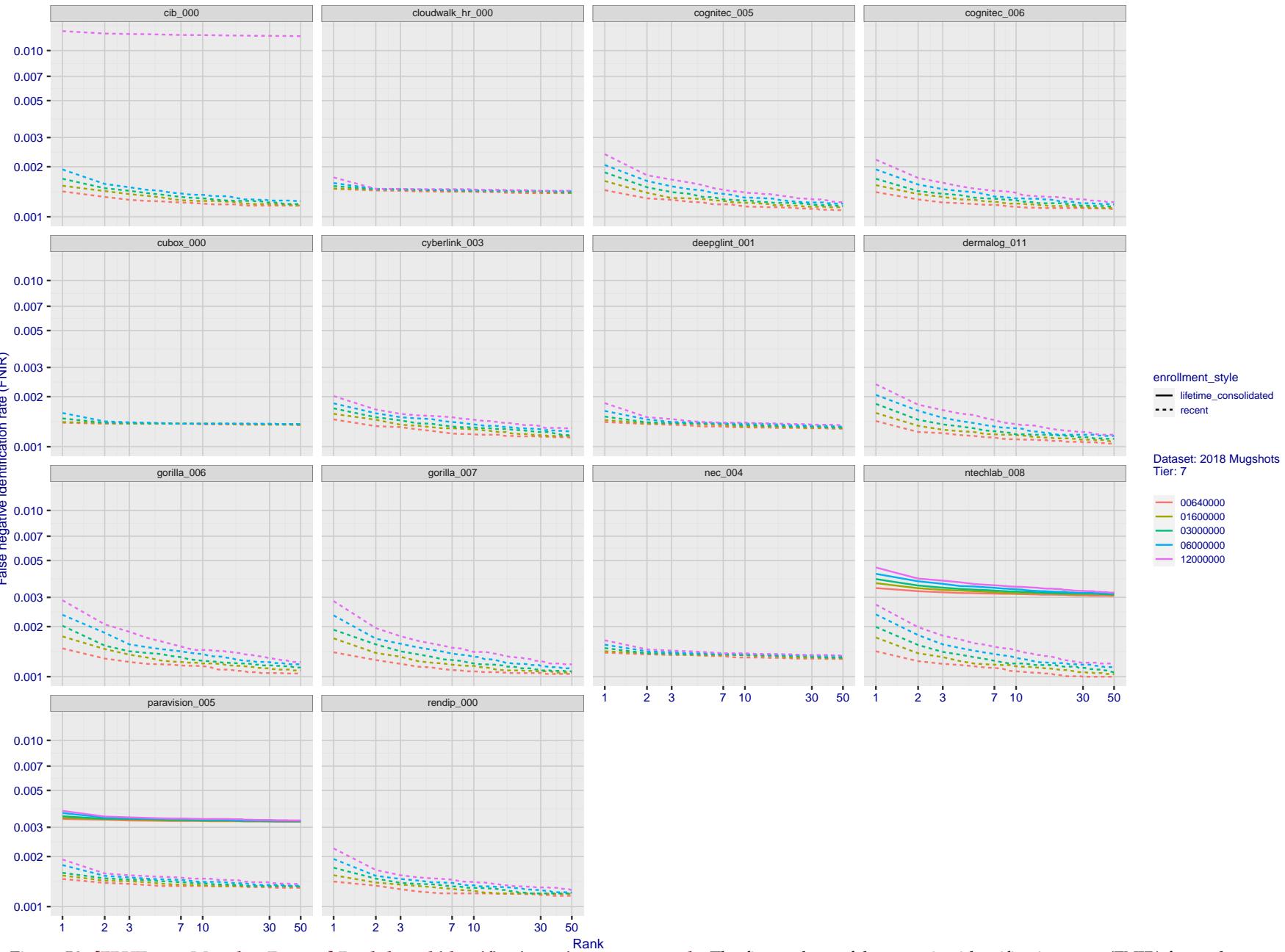
T = 0 → Investigation
T > 0 → Identification

Figure 58: [FRVT-2018 Mugshot Dataset] Rank-based identification miss rates vs. rank. The figure shows false negative identification rates (FNIR) for ranks up to 50. This metric is appropriate to investigational applications where human reviewers will adjudicate sorted candidate lists. Note that with threshold set to zero, FPIR = 1, i.e. any search without an enrolled mate will return non-mated candidates. Results are sorted and reported into tiers for clarity, with the tiering criteria being rank 1 hit rate on a gallery size of N = 640 000 subjects.

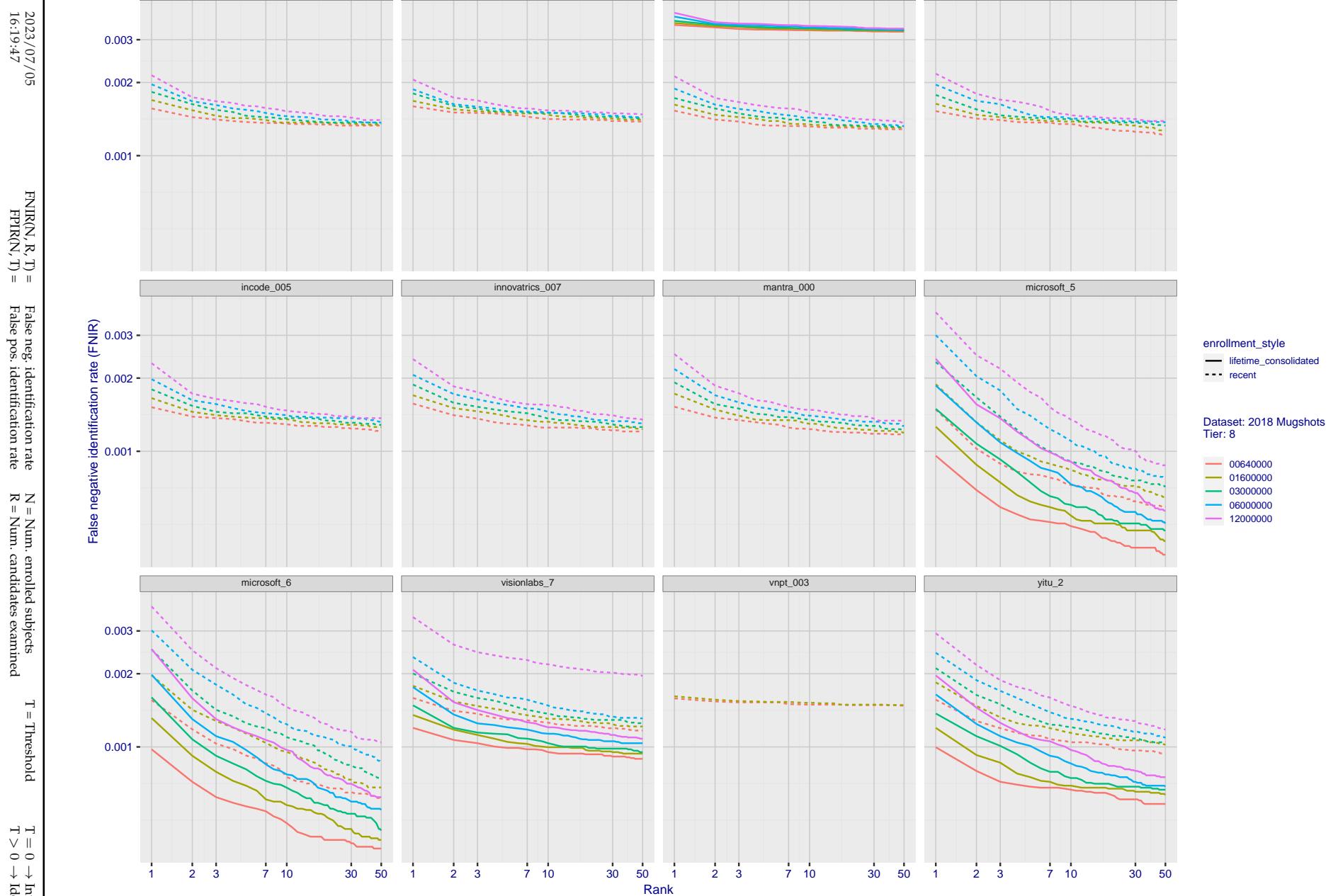


Figure 59: [FRVT-2018 Mugshot Dataset] Rank-based identification miss rates vs. rank. The figure shows false negative identification rates (FNIR) for ranks up to 50. This metric is appropriate to investigational applications where human reviewers will adjudicate sorted candidate lists. Note that with threshold set to zero, FPIR = 1, i.e. any search without an enrolled mate will return non-mated candidates. Results are sorted and reported into tiers for clarity, with the tiering criteria being rank 1 hit rate on a gallery size of N = 640 000 subjects.

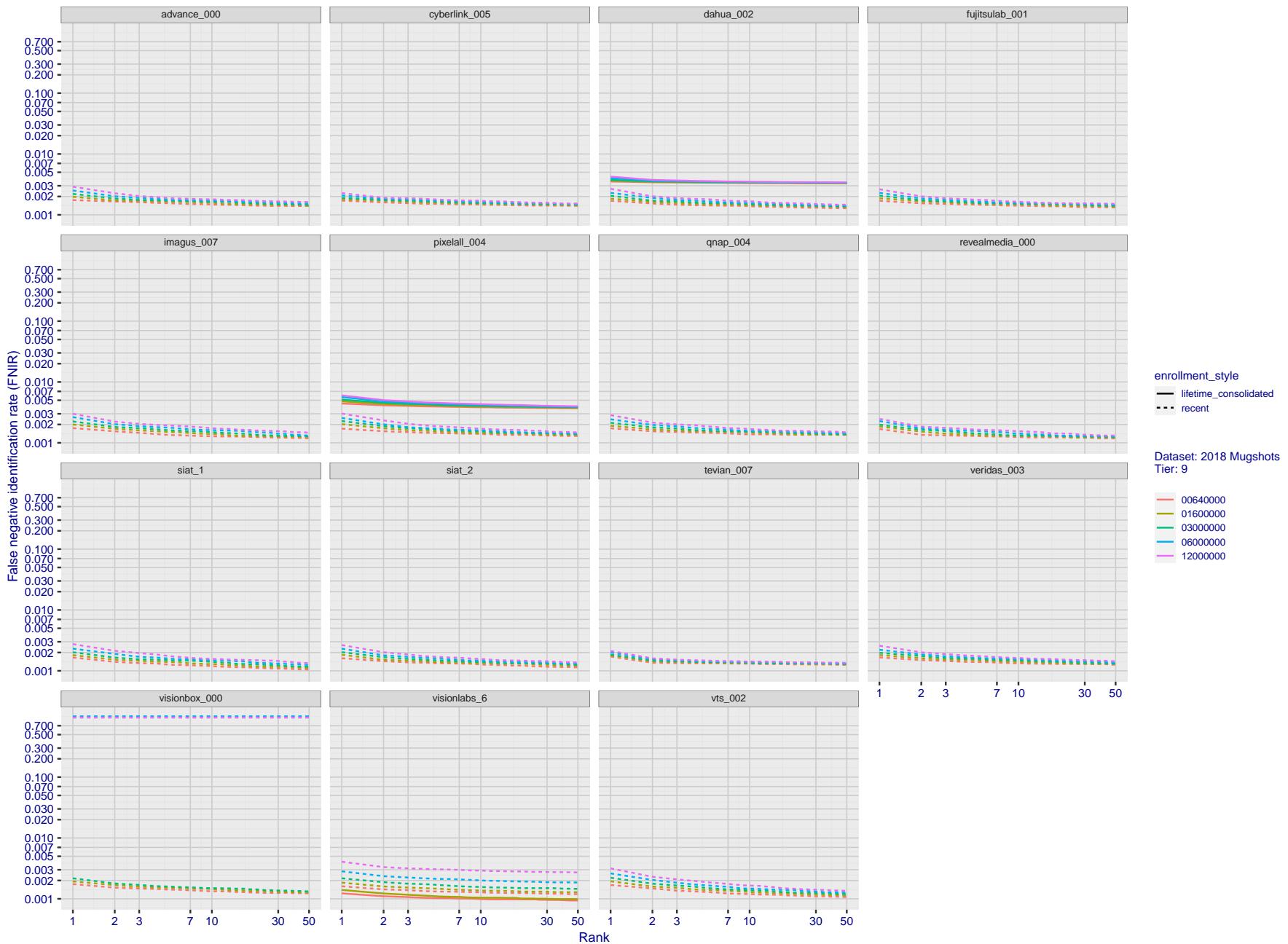


Figure 60: [FRVT-2018 Mugshot Dataset] Rank-based identification miss rates vs. rank. The figure shows false negative identification rates (FNIR) for ranks up to 50. This metric is appropriate to investigational applications where human reviewers will adjudicate sorted candidate lists. Note that with threshold set to zero, FPIR = 1, i.e. any search without an enrolled mate will return non-mated candidates. Results are sorted and reported into tiers for clarity, with the tiering criteria being rank 1 hit rate on a gallery size of $N = 640\,000$ subjects.

2023/07/05
16:19:47FNIR(N, R, T) = False neg. identification rate
FPIR(N, T) = False pos. identification rateN = Num. enrolled subjects
R = Num. candidates examinedT = Threshold
T = 0 → Investigation

T > 0 → Identification

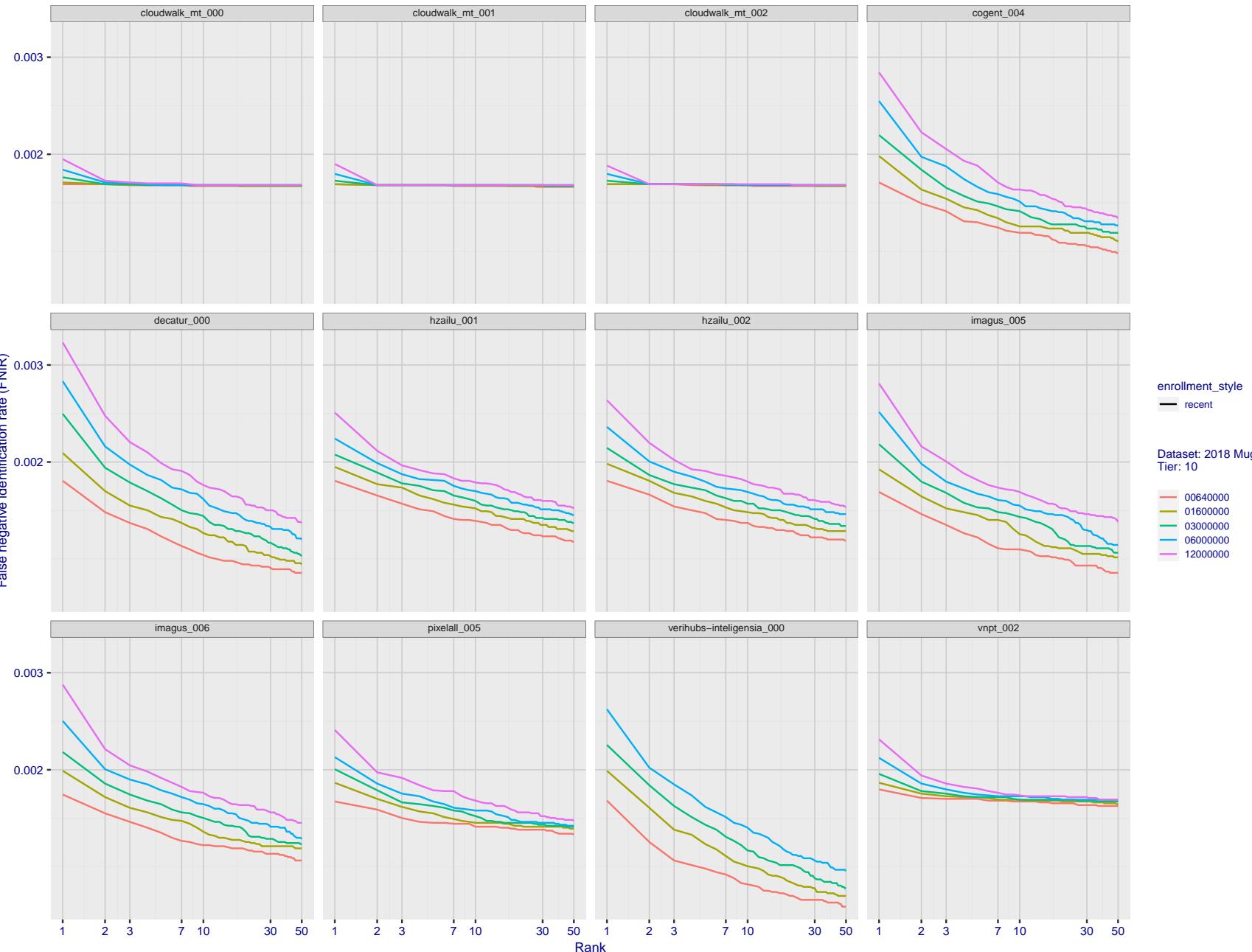


Figure 61: [FRVT-2018 Mugshot Dataset] Rank-based identification miss rates vs. rank. The figure shows false negative identification rates (FNIR) for ranks up to 50. This metric is appropriate to investigational applications where human reviewers will adjudicate sorted candidate lists. Note that with threshold set to zero, FPIR = 1, i.e. any search without an enrolled mate will return non-mated candidates. Results are sorted and reported into tiers for clarity, with the tiering criteria being rank 1 hit rate on a gallery size of N = 640 000 subjects.

2023/07/05
16:19:47FNIR(N, R, T) = False neg. identification rate
FPIR(N, T) = False pos. identification rateN = Num. enrolled subjects
R = Num. candidates examined

T = Threshold

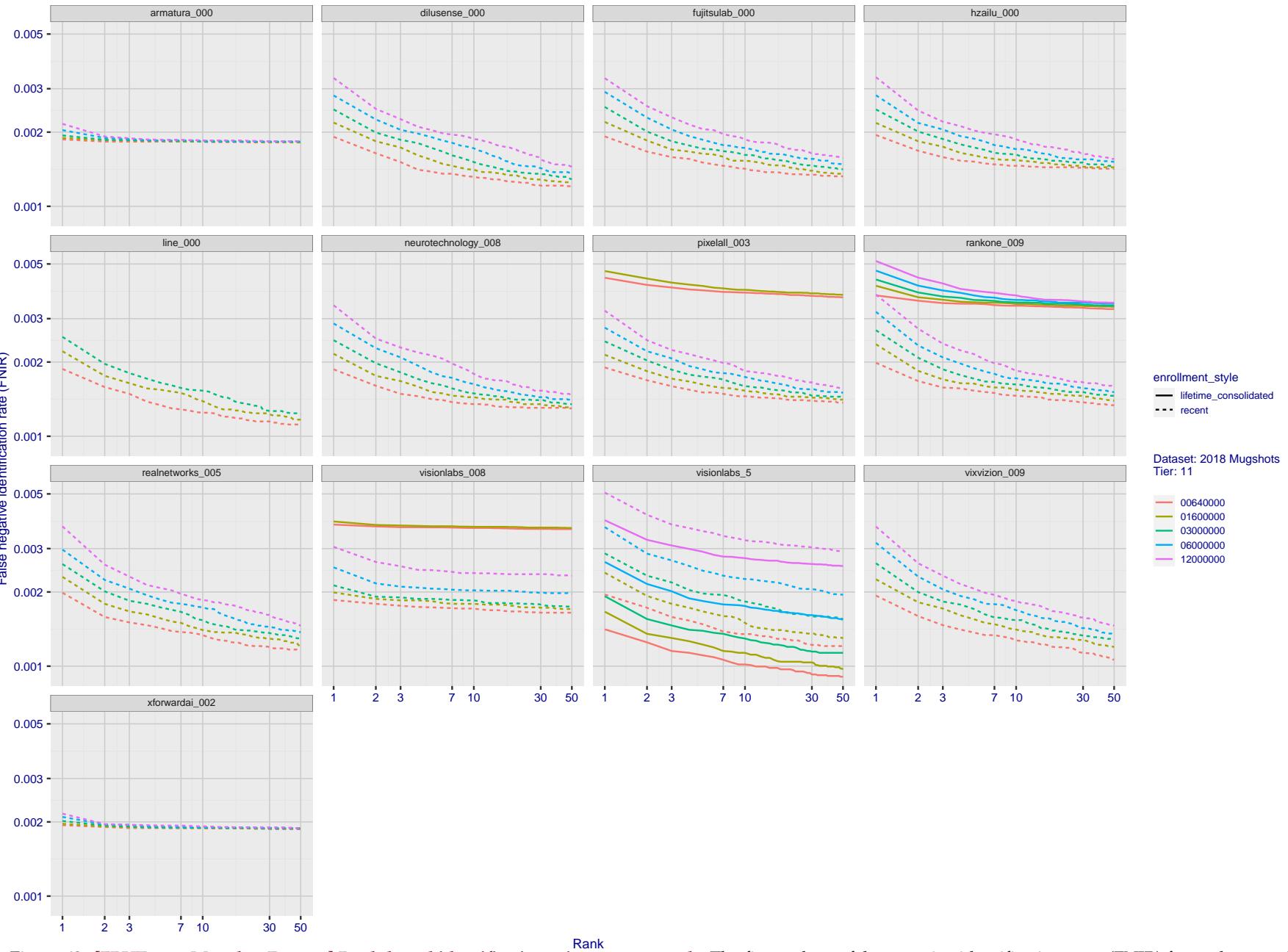
T = 0 → Investigation
T > 0 → Identification

Figure 62: [FRVT-2018 Mugshot Dataset] Rank-based identification miss rates vs. rank. The figure shows false negative identification rates (FNIR) for ranks up to 50. This metric is appropriate to investigational applications where human reviewers will adjudicate sorted candidate lists. Note that with threshold set to zero, FPIR = 1, i.e. any search without an enrolled mate will return non-mated candidates. Results are sorted and reported into tiers for clarity, with the tiering criteria being rank 1 hit rate on a gallery size of N = 640 000 subjects.

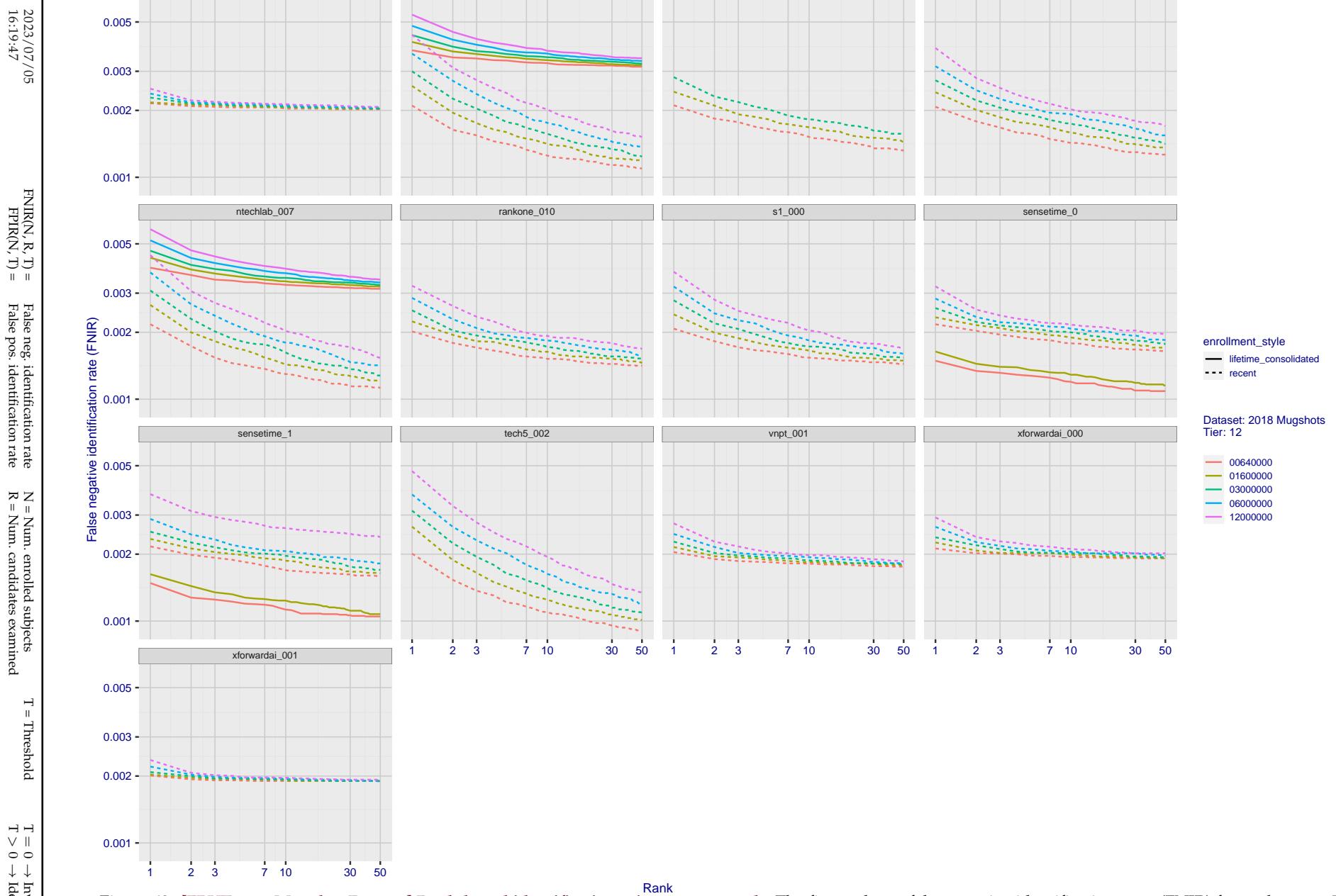


Figure 63: [FRVT-2018 Mugshot Dataset] Rank-based identification miss rates vs. rank. The figure shows false negative identification rates (FNIR) for ranks up to 50. This metric is appropriate to investigational applications where human reviewers will adjudicate sorted candidate lists. Note that with threshold set to zero, FPIR = 1, i.e. any search without an enrolled mate will return non-mated candidates. Results are sorted and reported into tiers for clarity, with the tiering criteria being rank 1 hit rate on a gallery size of $N = 640\,000$ subjects.

2023/07/05
16:19:47FNIR(N, R, T) = False neg. identification rate
FPIR(N, T) = False pos. identification rateN = Num. enrolled subjects
R = Num. candidates examined

T = Threshold

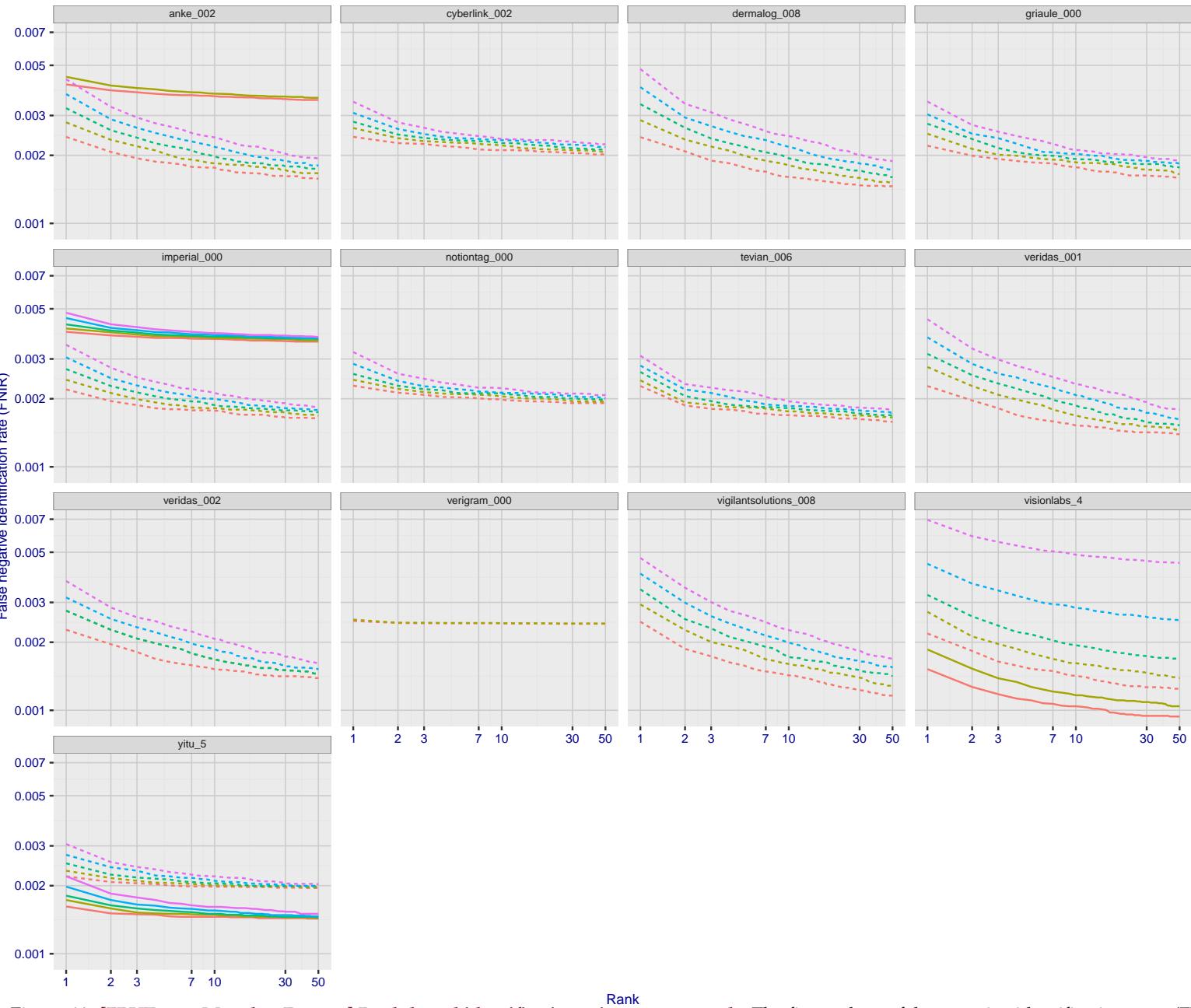
T = 0 → Investigation
T > 0 → Identification

Figure 64: [FRVT-2018 Mugshot Dataset] Rank-based identification miss rates vs. rank. The figure shows false negative identification rates (FNIR) for ranks up to 50. This metric is appropriate to investigational applications where human reviewers will adjudicate sorted candidate lists. Note that with threshold set to zero, FPIR = 1, i.e. any search without an enrolled mate will return non-mated candidates. Results are sorted and reported into tiers for clarity, with the tiering criteria being rank 1 hit rate on a gallery size of N = 640 000 subjects.

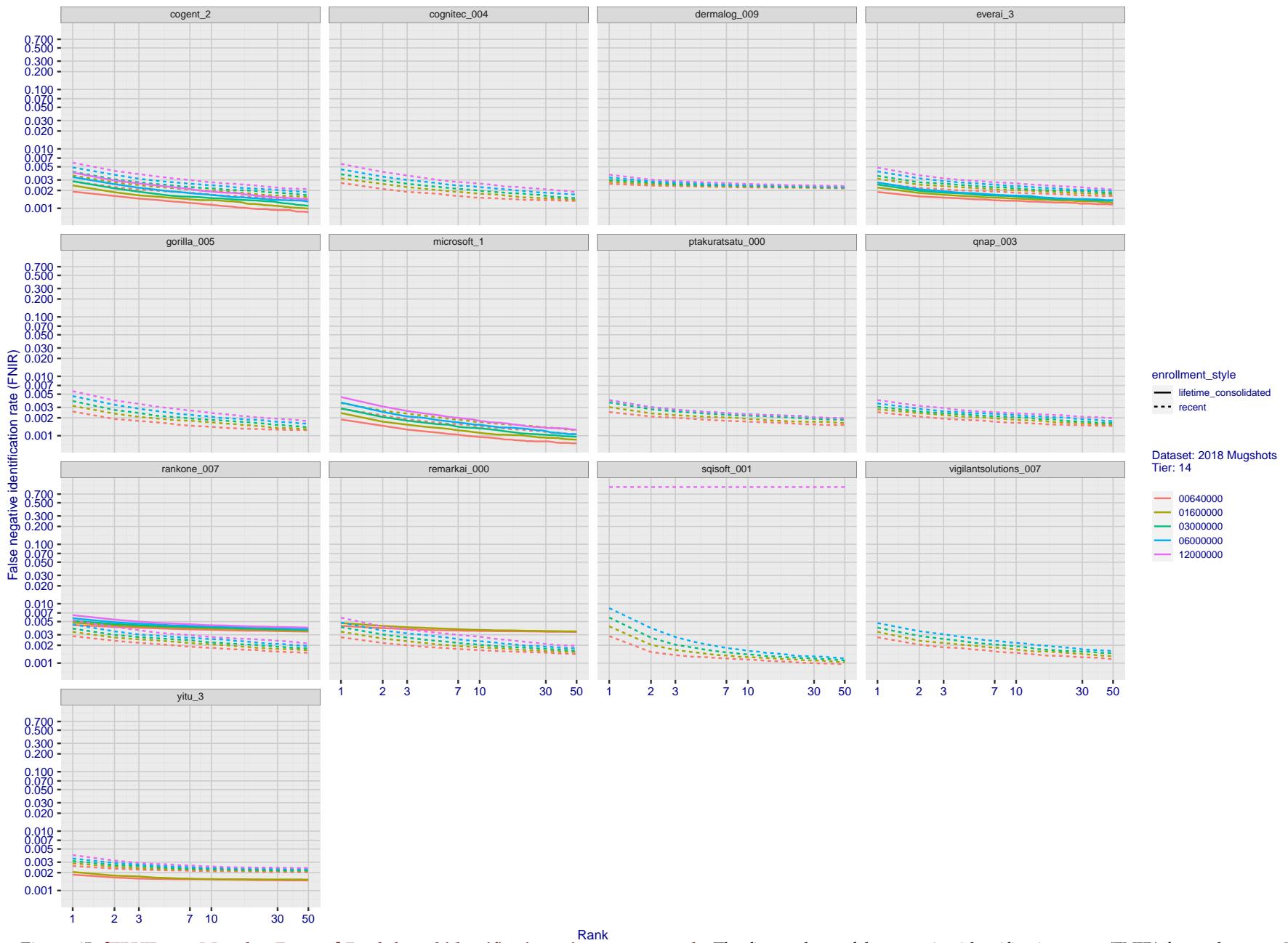


Figure 65: [FRVT-2018 Mugshot Dataset] Rank-based identification miss rates vs. rank. The figure shows false negative identification rates (FNIR) for ranks up to 50. This metric is appropriate to investigational applications where human reviewers will adjudicate sorted candidate lists. Note that with threshold set to zero, FPIR = 1, i.e. any search without an enrolled mate will return non-mated candidates. Results are sorted and reported into tiers for clarity, with the tiering criteria being rank 1 hit rate on a gallery size of $N = 640\,000$ subjects.

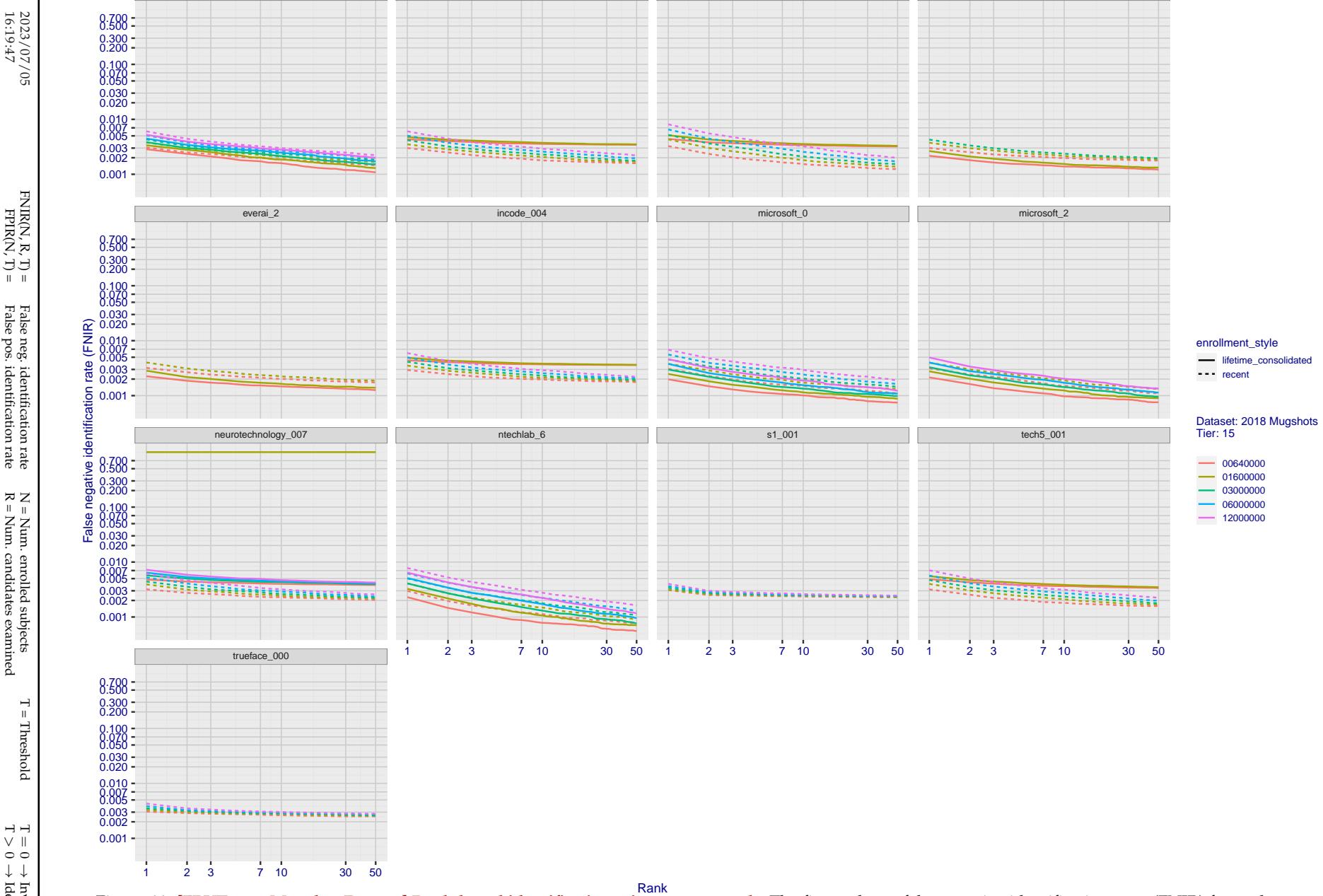


Figure 66: [FRVT-2018 Mugshot Dataset] Rank-based identification miss rates vs. rank. The figure shows false negative identification rates (FNIR) for ranks up to 50. This metric is appropriate to investigational applications where human reviewers will adjudicate sorted candidate lists. Note that with threshold set to zero, FPIR = 1, i.e. any search without an enrolled mate will return non-mated candidates. Results are sorted and reported into tiers for clarity, with the tiering criteria being rank 1 hit rate on a gallery size of N = 640 000 subjects.

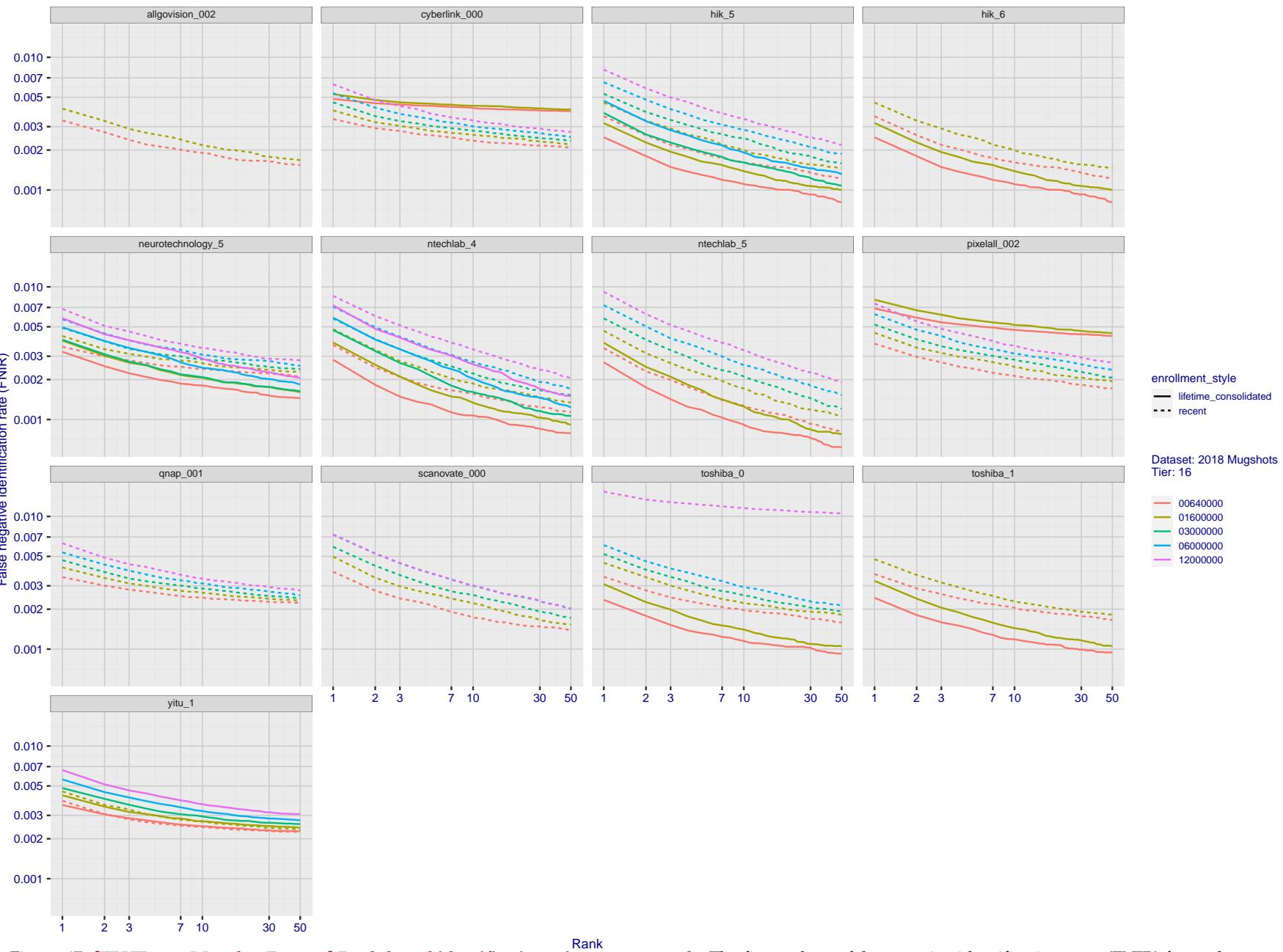
2023/07/05
16:19:47

Figure 67: [FRVT-2018 Mugshot Dataset] Rank-based identification miss rates vs. rank. The figure shows false negative identification rates (FNIR) for ranks up to 50. This metric is appropriate to investigational applications where human reviewers will adjudicate sorted candidate lists. Note that with threshold set to zero, FPIR = 1, i.e. any search without an enrolled mate will return non-mated candidates. Results are sorted and reported into tiers for clarity, with the tiering criteria being rank 1 hit rate on a gallery size of N = 640 000 subjects.

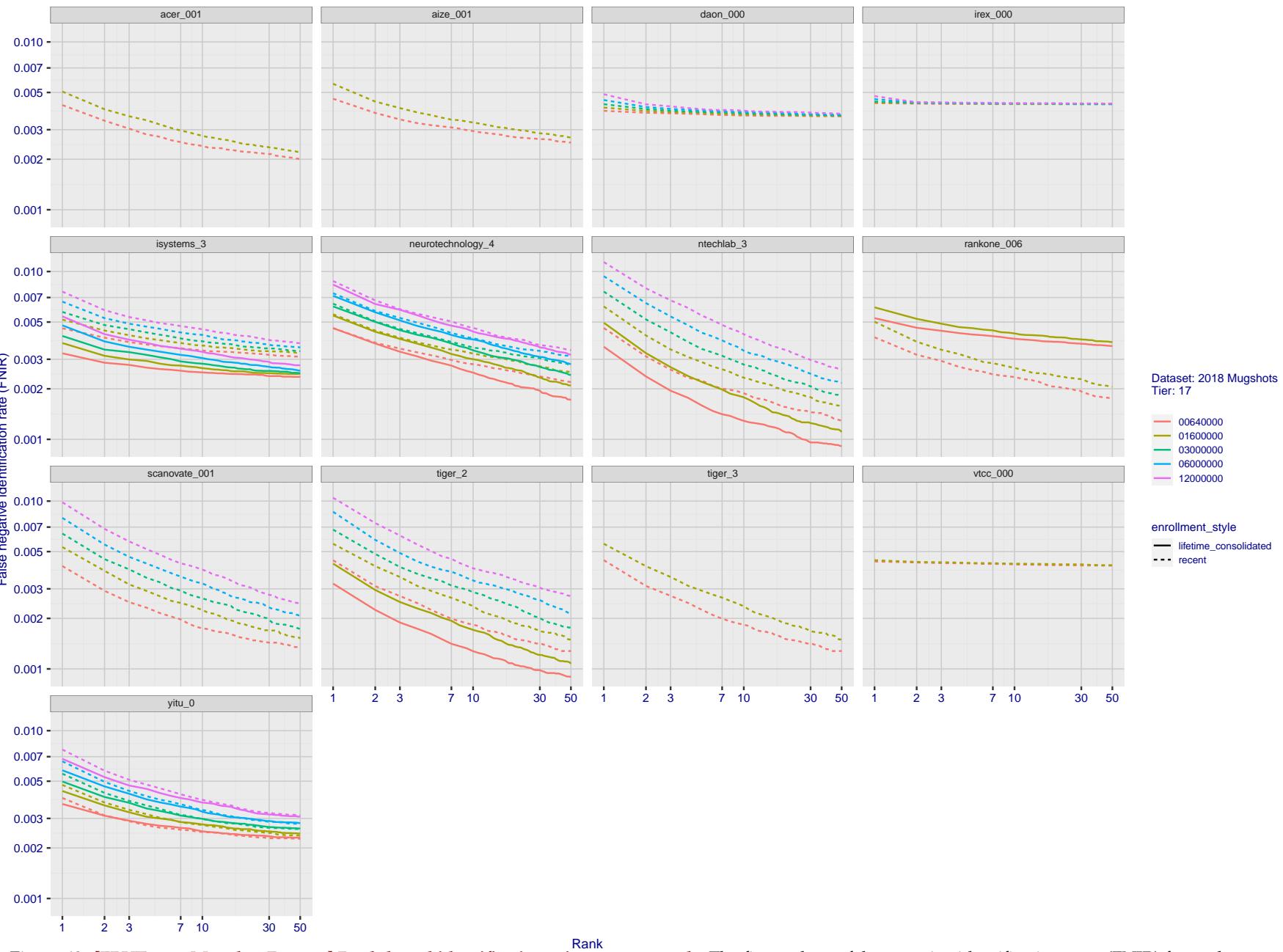
2023/07/05
16:19:47

Figure 68: [FRVT-2018 Mugshot Dataset] Rank-based identification miss rates vs. rank. The figure shows false negative identification rates (FNIR) for ranks up to 50. This metric is appropriate to investigational applications where human reviewers will adjudicate sorted candidate lists. Note that with threshold set to zero, FPIR = 1, i.e. any search without an enrolled mate will return non-mated candidates. Results are sorted and reported into tiers for clarity, with the tiering criteria being rank 1 hit rate on a gallery size of $N = 640\,000$ subjects.

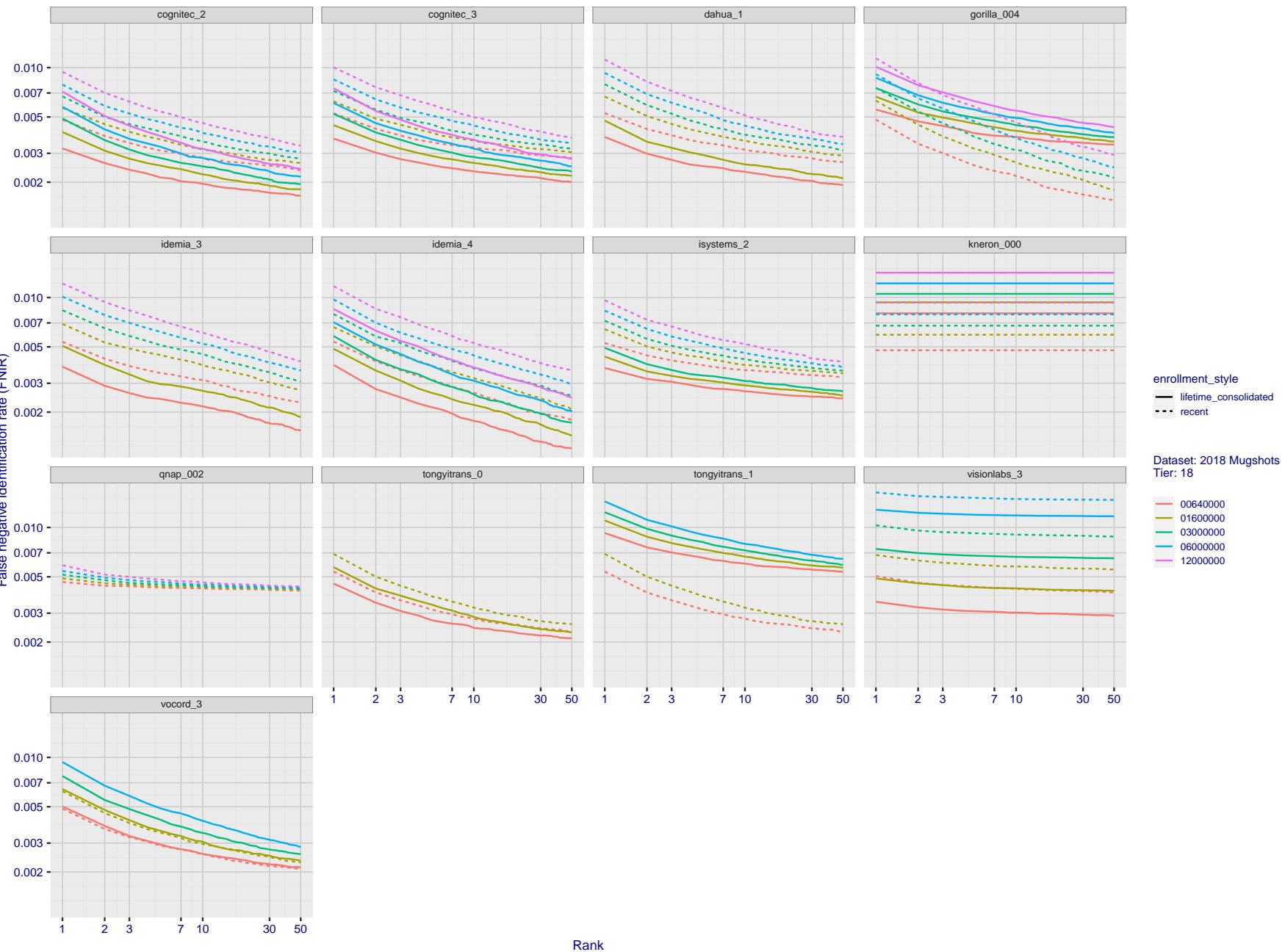
2023/07/05
16:19:47

Figure 69: [FRVT-2018 Mugshot Dataset] Rank-based identification miss rates vs. rank. The figure shows false negative identification rates (FNIR) for ranks up to 50. This metric is appropriate to investigational applications where human reviewers will adjudicate sorted candidate lists. Note that with threshold set to zero, $FPIR = 1$, i.e. any search without an enrolled mate will return non-mated candidates. Results are sorted and reported into tiers for clarity, with the tiering criteria being rank 1 hit rate on a gallery size of $N = 640\,000$ subjects.

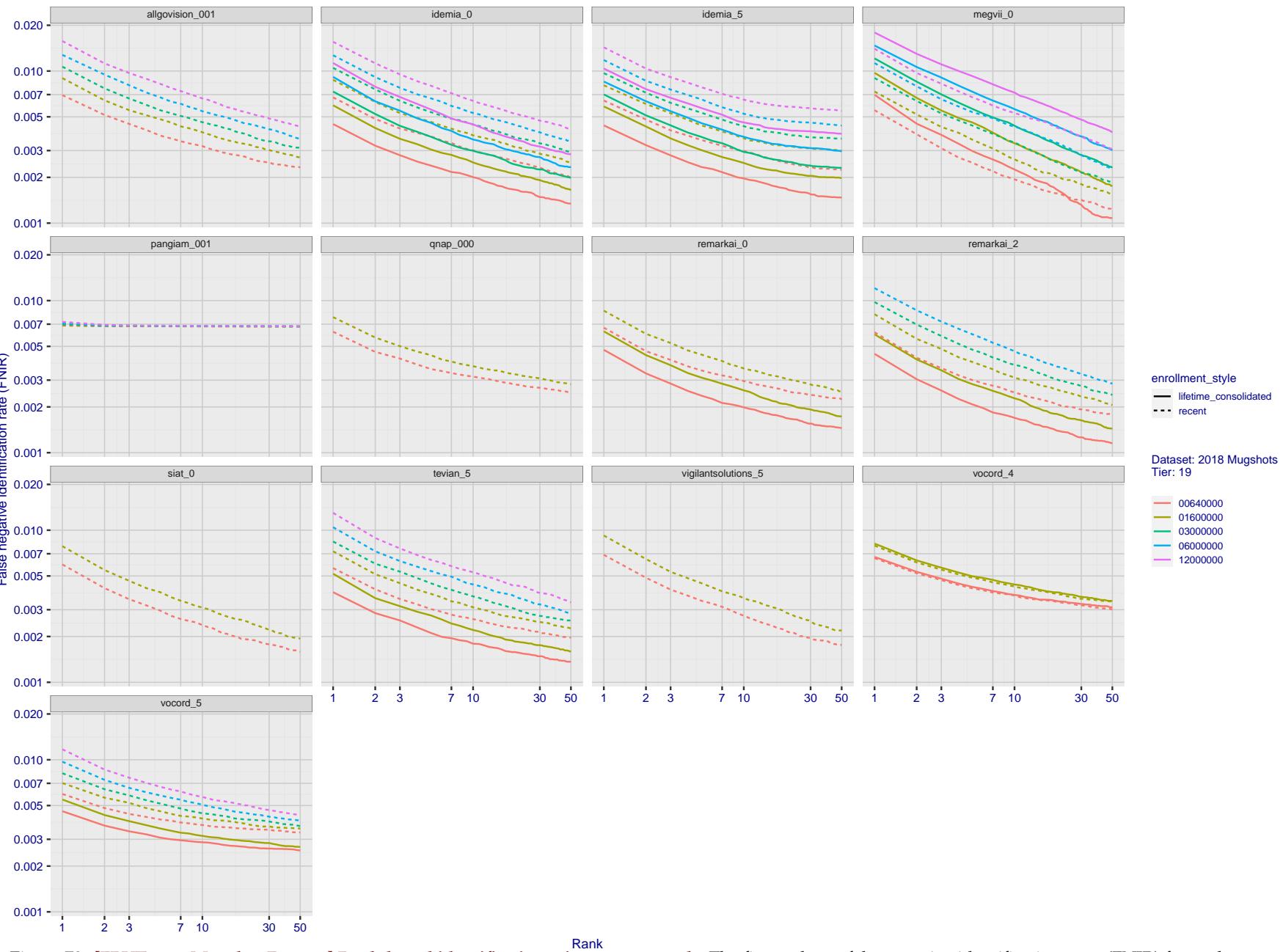
2023/07/05
16:19:47

Figure 70: [FRVT-2018 Mugshot Dataset] Rank-based identification miss rates vs. rank. The figure shows false negative identification rates (FNIR) for ranks up to 50. This metric is appropriate to investigational applications where human reviewers will adjudicate sorted candidate lists. Note that with threshold set to zero, FPIR = 1, i.e. any search without an enrolled mate will return non-mated candidates. Results are sorted and reported into tiers for clarity, with the tiering criteria being rank 1 hit rate on a gallery size of $N = 640\,000$ subjects.

2023/07/05
16:19:47

 $\text{FNIR}(N, R, T)$ = False neg. identification rate
 $\text{FPIR}(N, T)$ = False pos. identification rate

 N = Num. enrolled subjects
 R = Num. candidates examined

 T = Threshold
 $T = 0 \rightarrow$ Investigation
 $T > 0 \rightarrow$ Identification

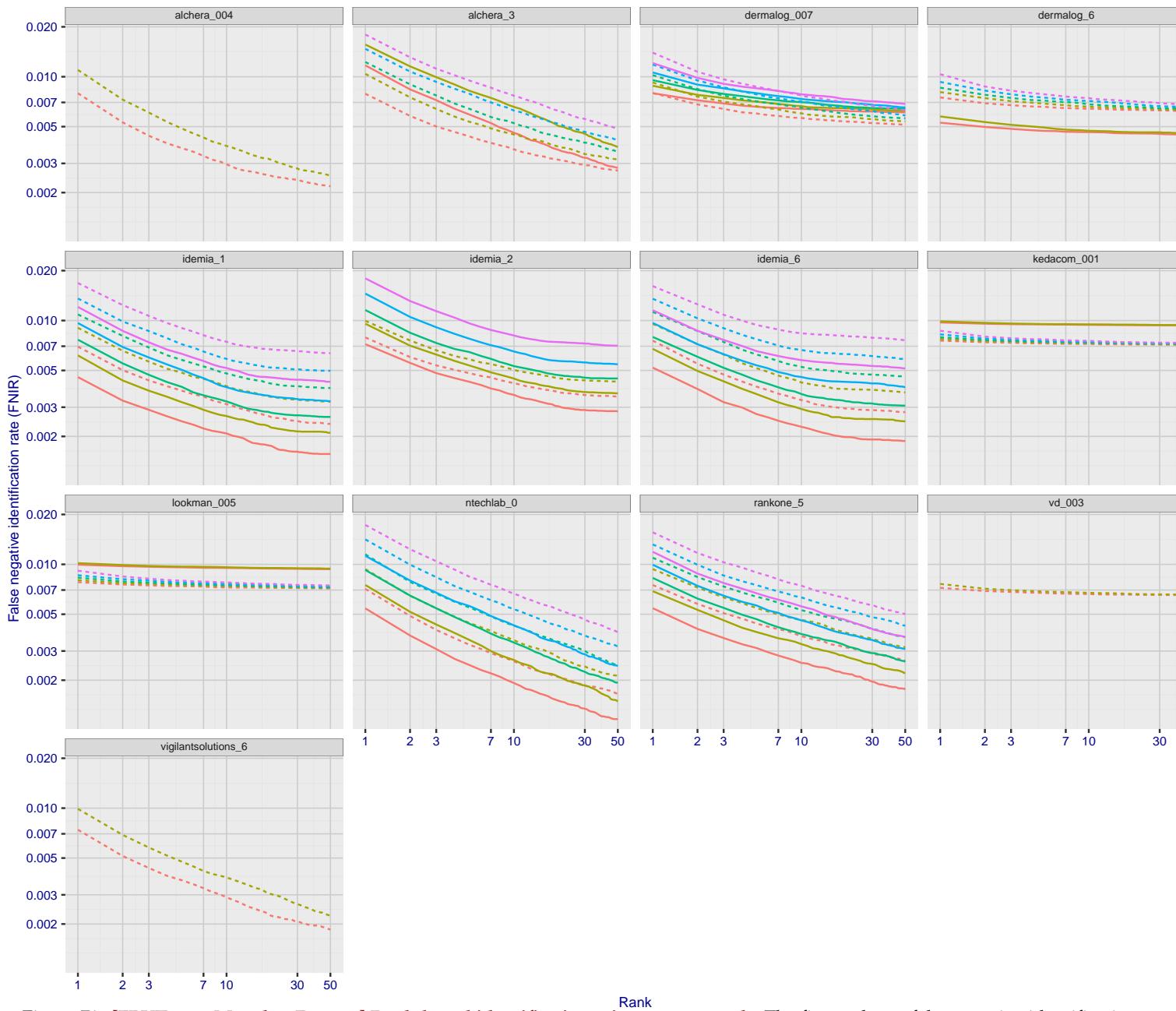


Figure 71: [FRVT-2018 Mugshot Dataset] Rank-based identification miss rates vs. rank. The figure shows false negative identification rates (FNIR) for ranks up to 50. This metric is appropriate to investigational applications where human reviewers will adjudicate sorted candidate lists. Note that with threshold set to zero, FPIR = 1, i.e. any search without an enrolled mate will return non-mated candidates. Results are sorted and reported into tiers for clarity, with the tiering criteria being rank 1 hit rate on a gallery size of $N = 640\,000$ subjects.

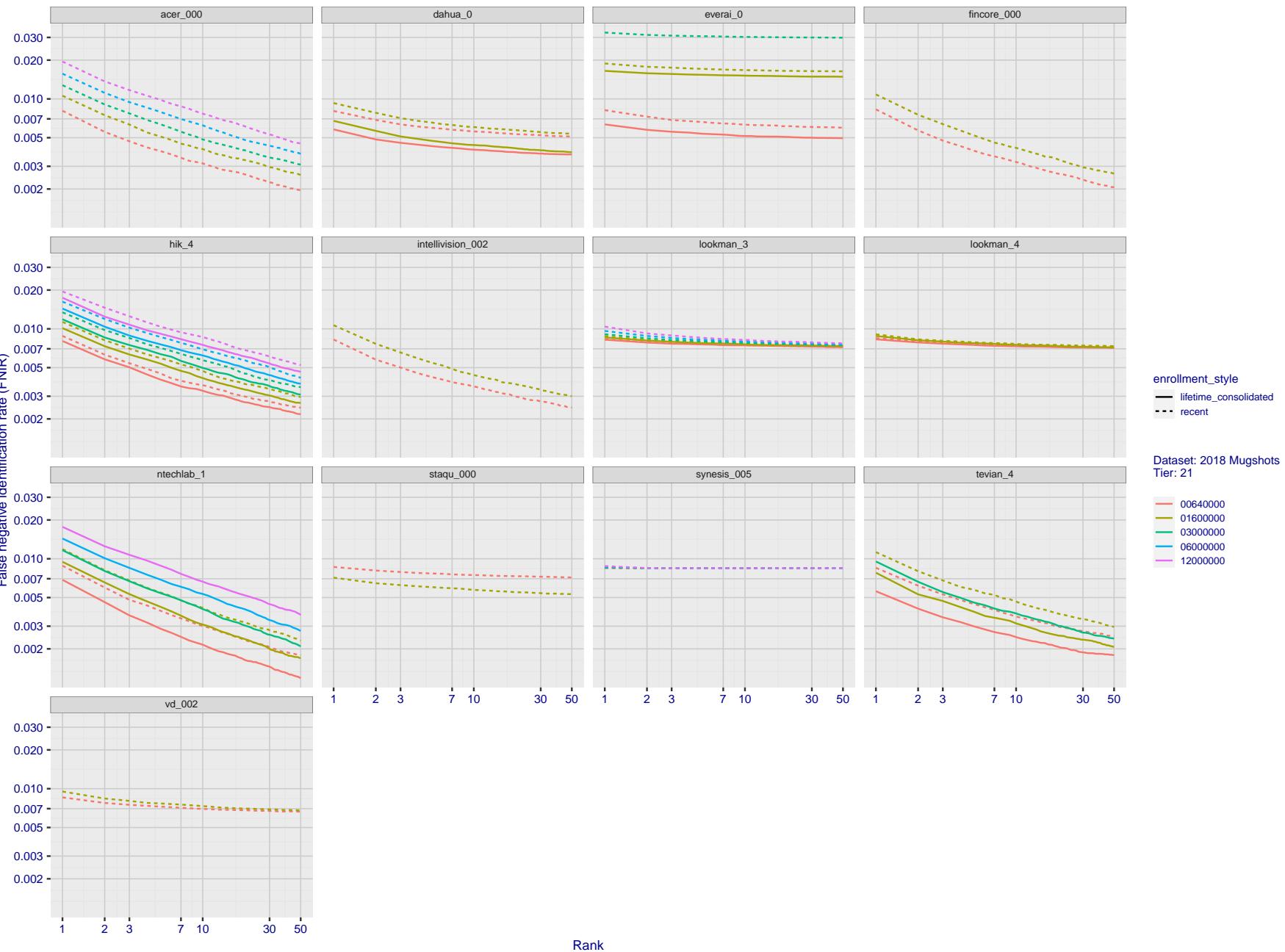
2023/07/05
16:19:47

Figure 72: [FRVT-2018 Mugshot Dataset] Rank-based identification miss rates vs. rank. The figure shows false negative identification rates (FNIR) for ranks up to 50. This metric is appropriate to investigational applications where human reviewers will adjudicate sorted candidate lists. Note that with threshold set to zero, $FPIR = 1$, i.e. any search without an enrolled mate will return non-mated candidates. Results are sorted and reported into tiers for clarity, with the tiering criteria being rank 1 hit rate on a gallery size of $N = 640\,000$ subjects.

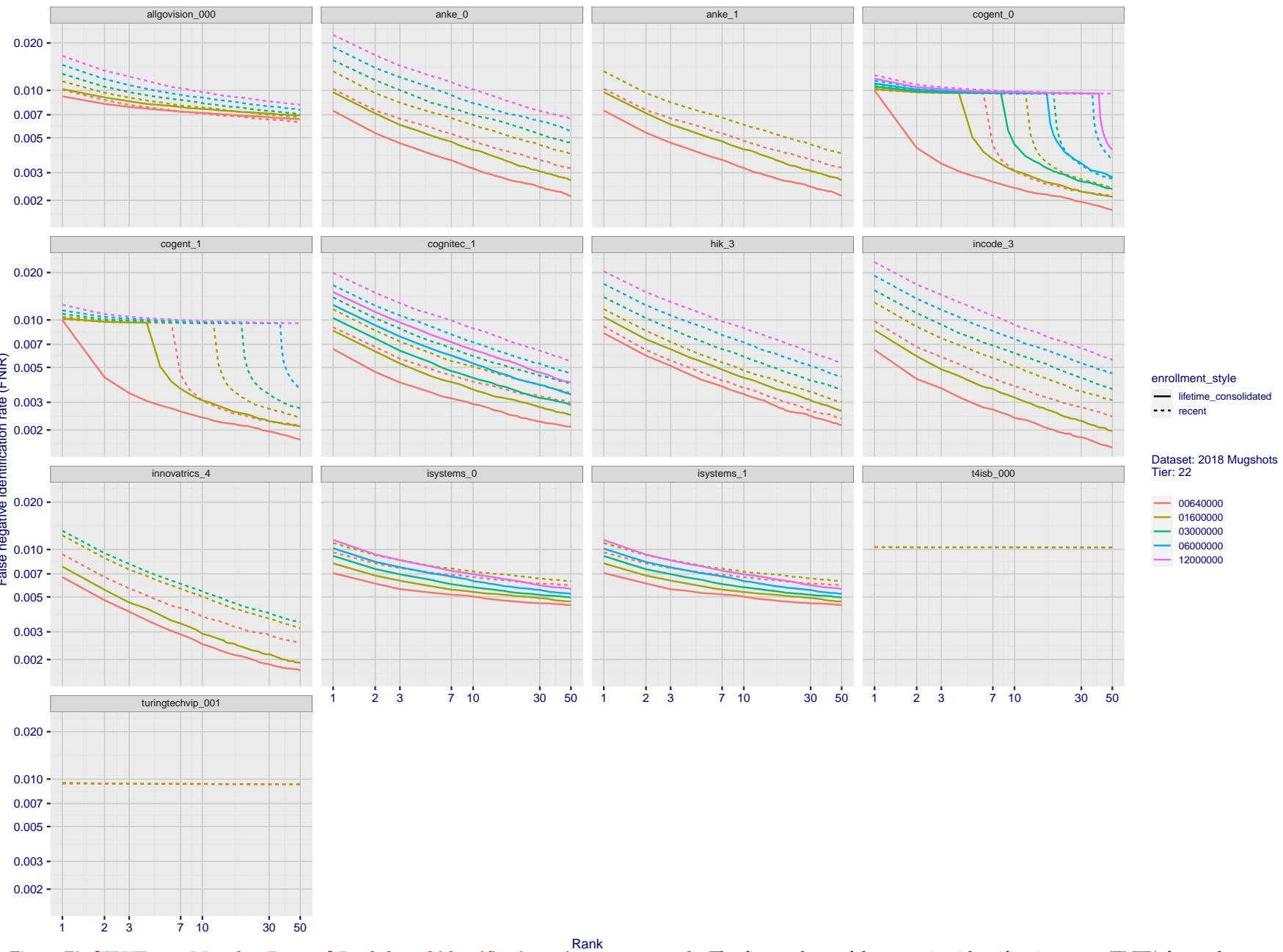
2023/07/05
16:19:47

Figure 73: [FRVT-2018 Mugshot Dataset] Rank-based identification miss rates vs. rank. The figure shows false negative identification rates (FNIR) for ranks up to 50. This metric is appropriate to investigational applications where human reviewers will adjudicate sorted candidate lists. Note that with threshold set to zero, FPIR = 1, i.e. any search without an enrolled mate will return non-mated candidates. Results are sorted and reported into tiers for clarity, with the tiering criteria being rank 1 hit rate on a gallery size of N = 640 000 subjects.

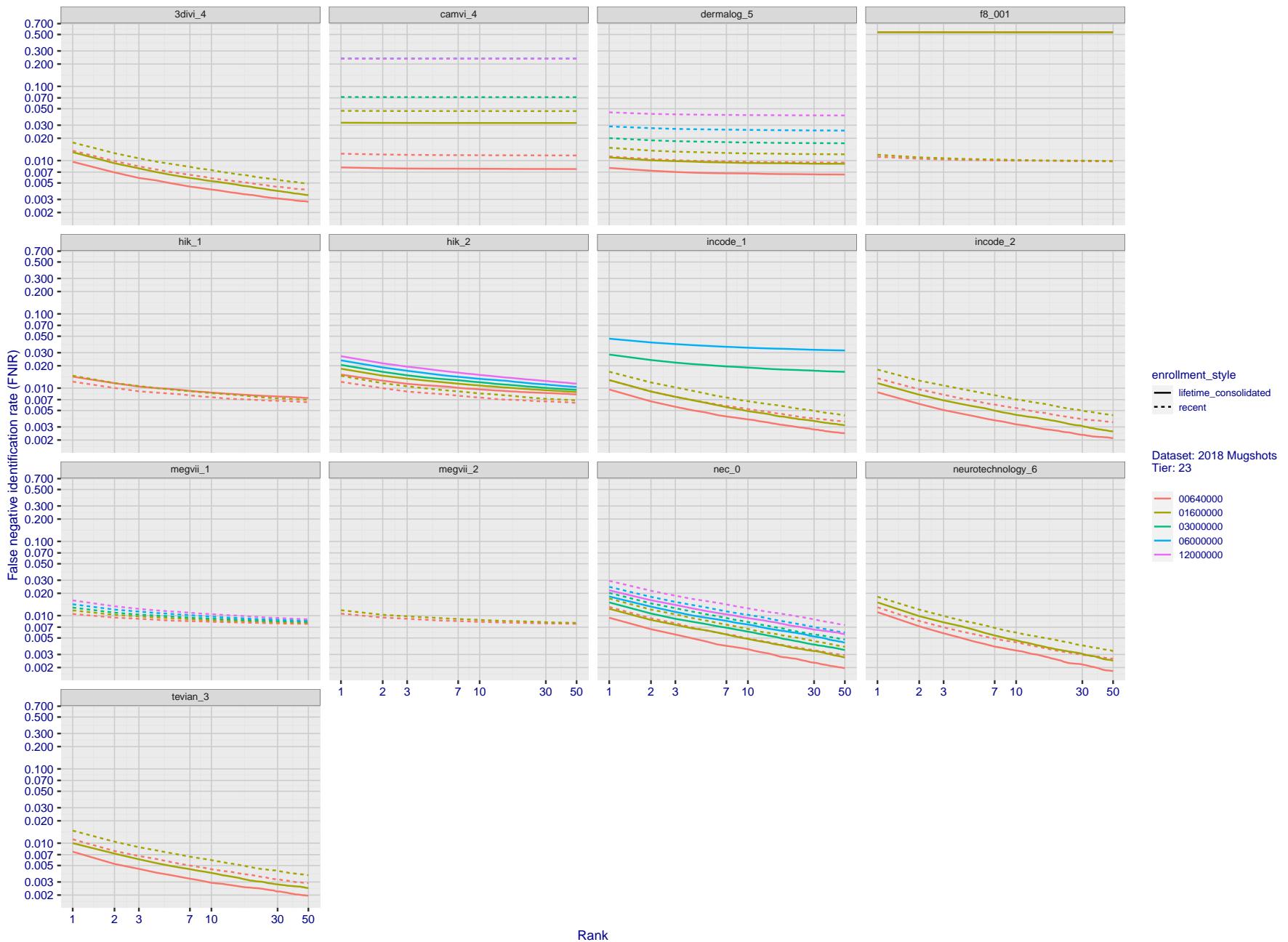


Figure 74: [FRVT-2018 Mugshot Dataset] Rank-based identification miss rates vs. rank. The figure shows false negative identification rates (FNIR) for ranks up to 50. This metric is appropriate to investigational applications where human reviewers will adjudicate sorted candidate lists. Note that with threshold set to zero, FPIR = 1, i.e. any search without an enrolled mate will return non-mated candidates. Results are sorted and reported into tiers for clarity, with the tiering criteria being rank 1 hit rate on a gallery size of $N = 640\,000$ subjects.

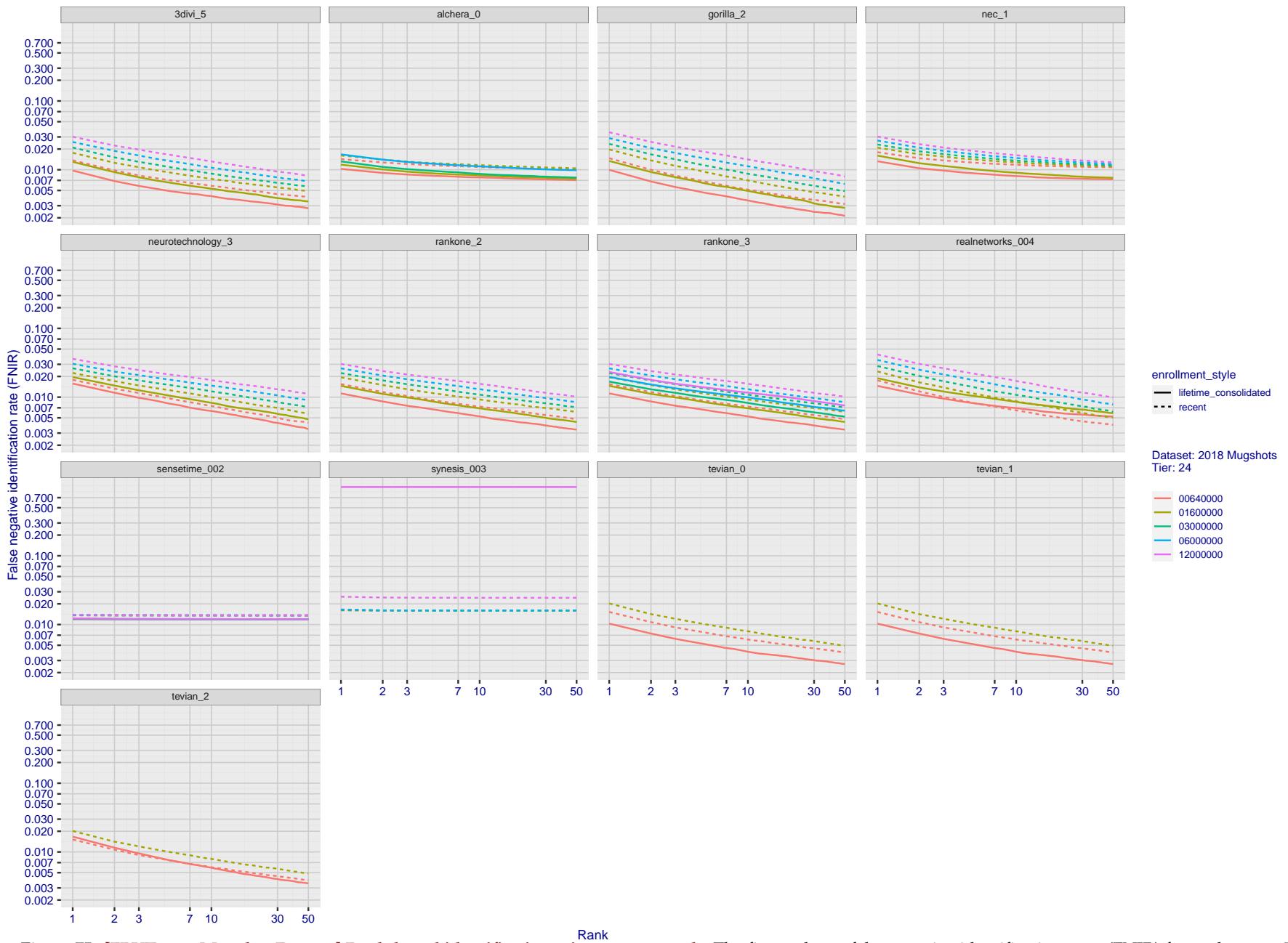


Figure 75: [FRVT-2018 Mugshot Dataset] Rank-based identification miss rates vs. rank. The figure shows false negative identification rates (FNIR) for ranks up to 50. This metric is appropriate to investigational applications where human reviewers will adjudicate sorted candidate lists. Note that with threshold set to zero, FPIR = 1, i.e. any search without an enrolled mate will return non-mated candidates. Results are sorted and reported into tiers for clarity, with the tiering criteria being rank 1 hit rate on a gallery size of $N = 640\,000$ subjects.

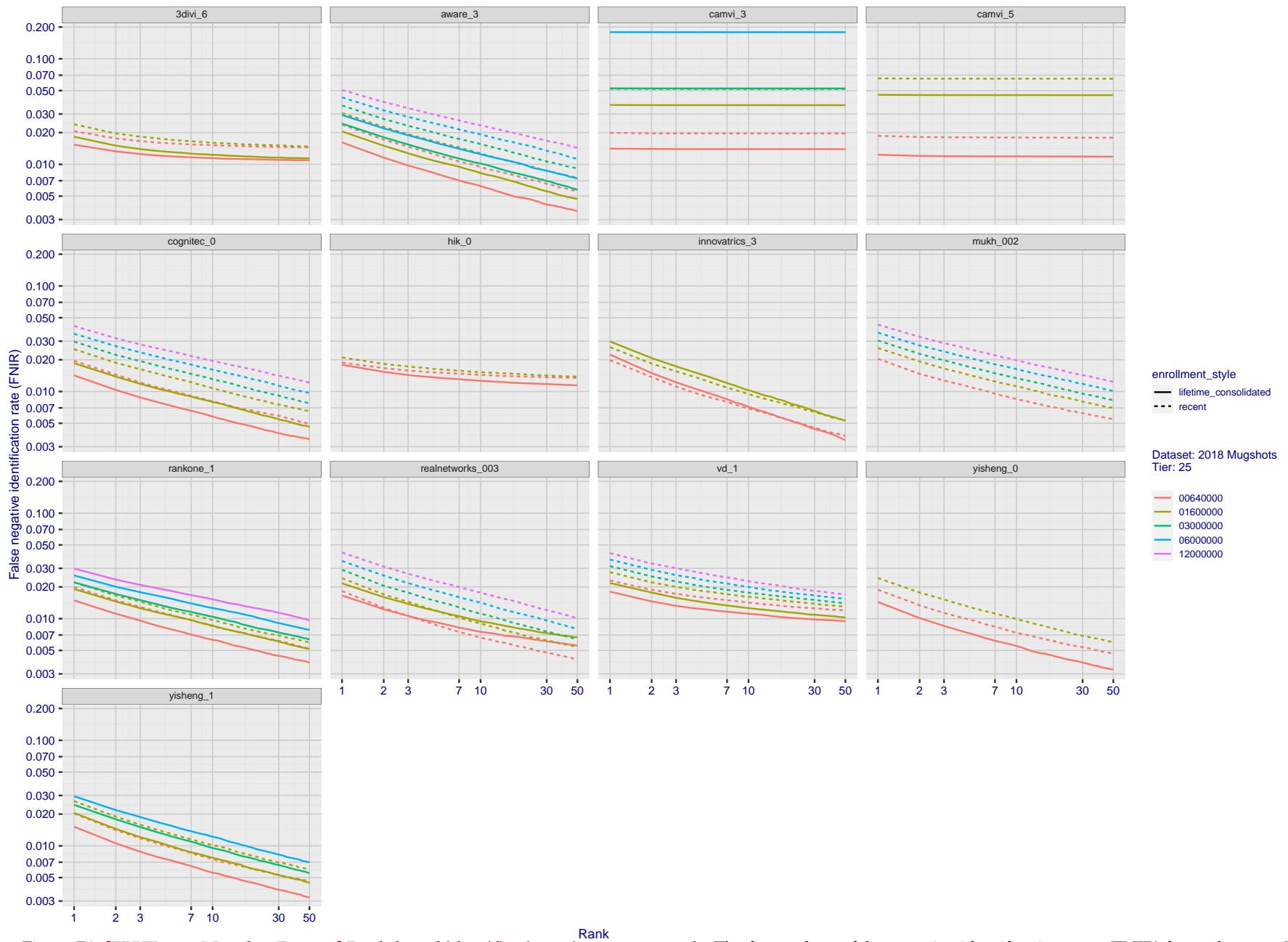


Figure 76: [FRVT-2018 Mugshot Dataset] Rank-based identification miss rates vs. rank. The figure shows false negative identification rates (FNIR) for ranks up to 50. This metric is appropriate to investigational applications where human reviewers will adjudicate sorted candidate lists. Note that with threshold set to zero, FPIR = 1, i.e. any search without an enrolled mate will return non-mated candidates. Results are sorted and reported into tiers for clarity, with the tiering criteria being rank 1 hit rate on a gallery size of $N = 640\,000$ subjects.

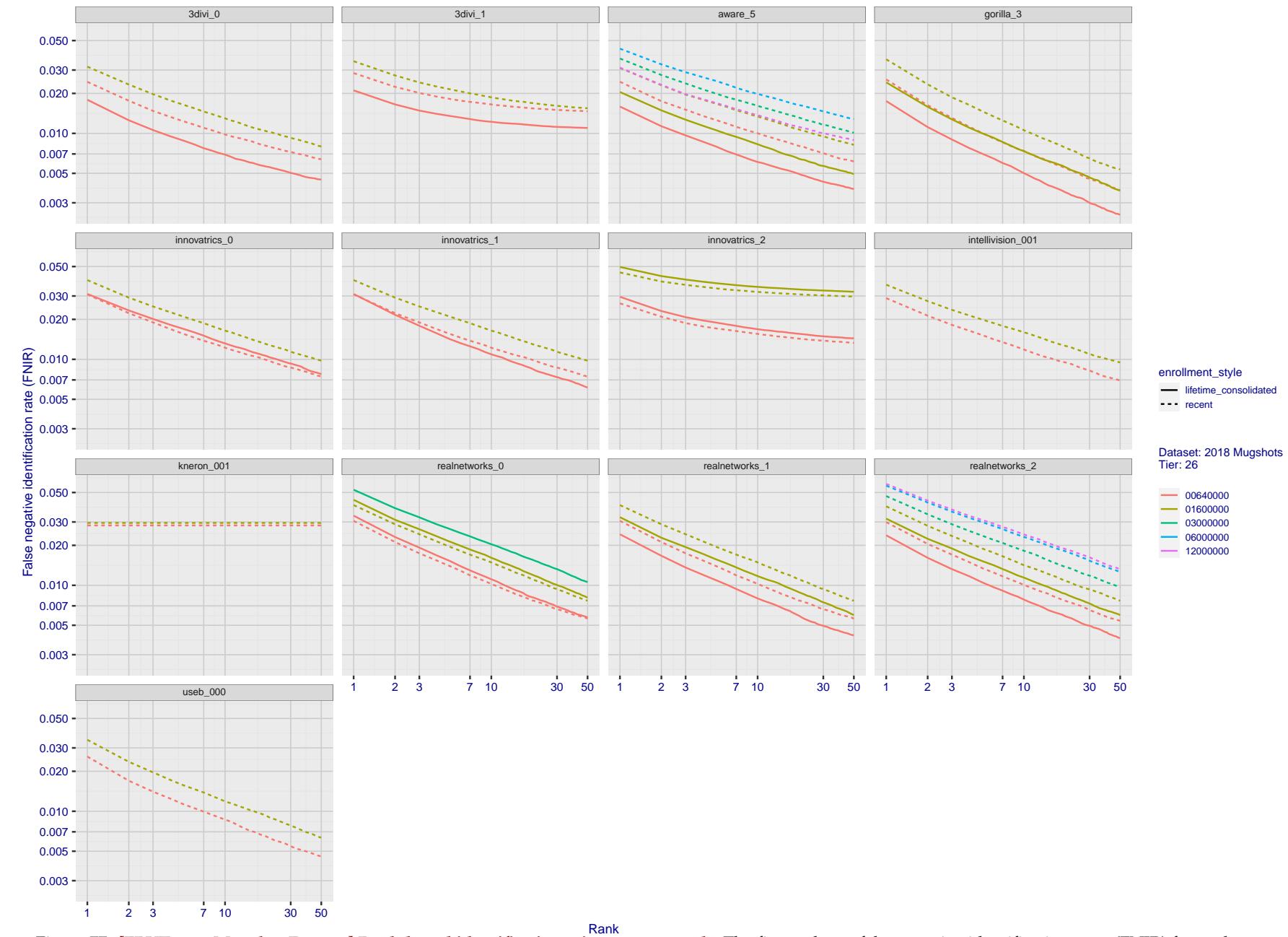
2023/07/05
16:19:47

Figure 77: [FRVT-2018 Mugshot Dataset] Rank-based identification miss rates vs. rank. The figure shows false negative identification rates (FNIR) for ranks up to 50. This metric is appropriate to investigational applications where human reviewers will adjudicate sorted candidate lists. Note that with threshold set to zero, $FPIR = 1$, i.e. any search without an enrolled mate will return non-mated candidates. Results are sorted and reported into tiers for clarity, with the tiering criteria being rank 1 hit rate on a gallery size of $N = 640\,000$ subjects.

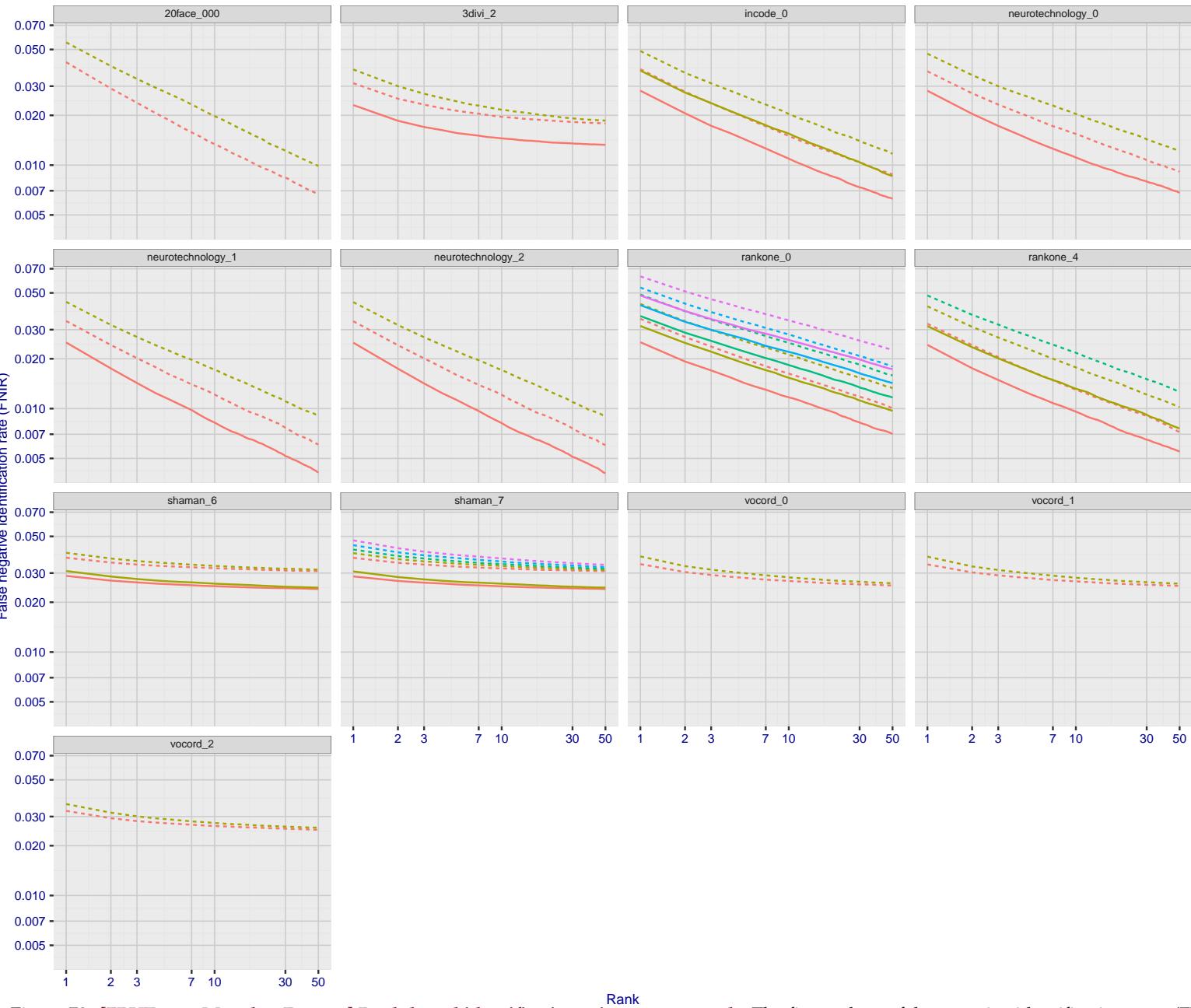
2023/07/05
16:19:47FNIR(N, R, T) = False neg. identification rate
FPIR(N, T) = False pos. identification rateN = Num. enrolled subjects
R = Num. candidates examinedT = Threshold
 $T = 0 \rightarrow$ Investigation
 $T > 0 \rightarrow$ Identification

Figure 78: [FRVT-2018 Mugshot Dataset] Rank-based identification miss rates vs. rank. The figure shows false negative identification rates (FNIR) for ranks up to 50. This metric is appropriate to investigational applications where human reviewers will adjudicate sorted candidate lists. Note that with threshold set to zero, FPIR = 1, i.e. any search without an enrolled mate will return non-mated candidates. Results are sorted and reported into tiers for clarity, with the tiering criteria being rank 1 hit rate on a gallery size of N = 640 000 subjects.

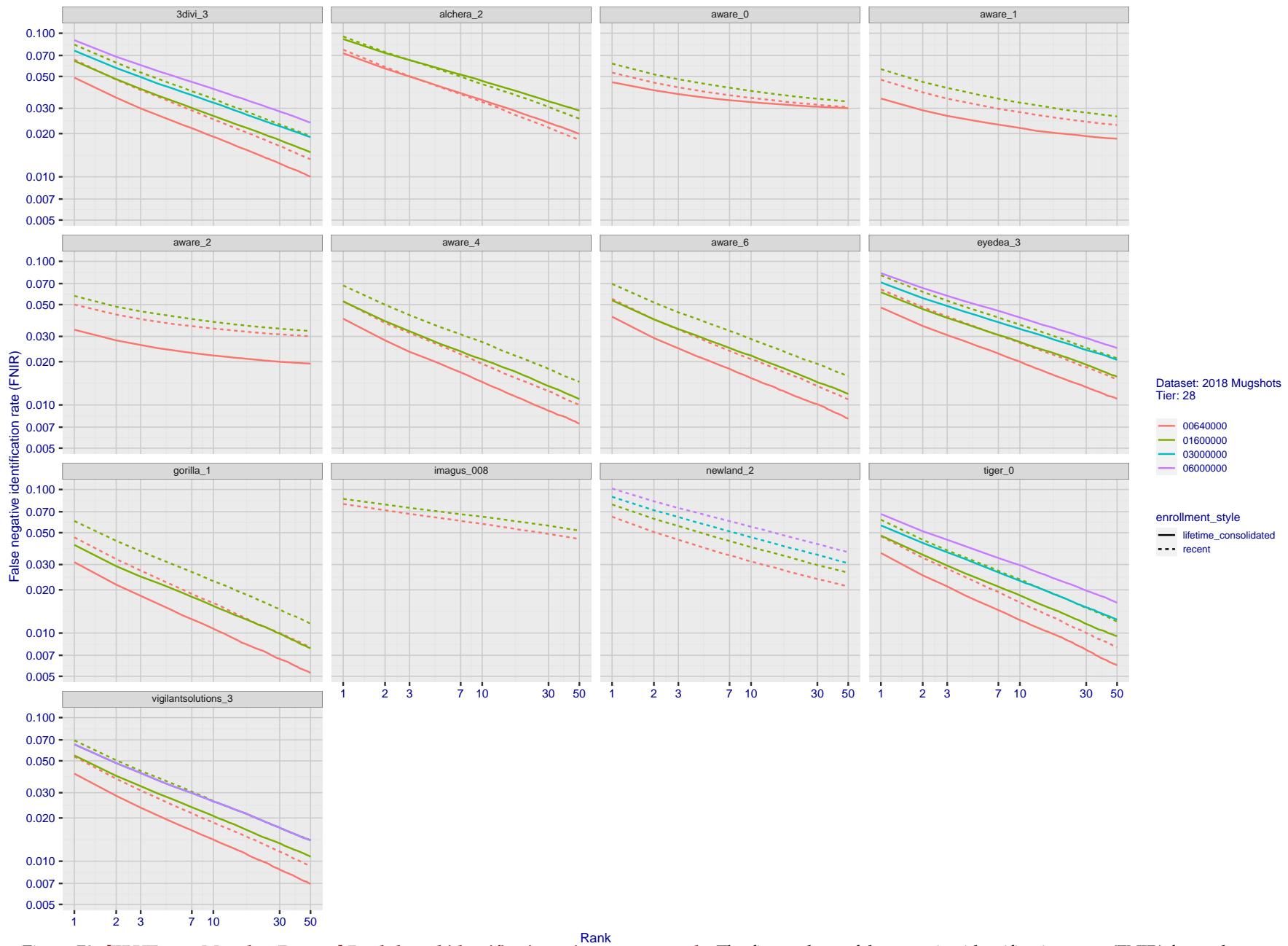


Figure 79: [FRVT-2018 Mugshot Dataset] Rank-based identification miss rates vs. rank. The figure shows false negative identification rates (FNIR) for ranks up to 50. This metric is appropriate to investigational applications where human reviewers will adjudicate sorted candidate lists. Note that with threshold set to zero, FPIR = 1, i.e. any search without an enrolled mate will return non-mated candidates. Results are sorted and reported into tiers for clarity, with the tiering criteria being rank 1 hit rate on a gallery size of N = 640 000 subjects.

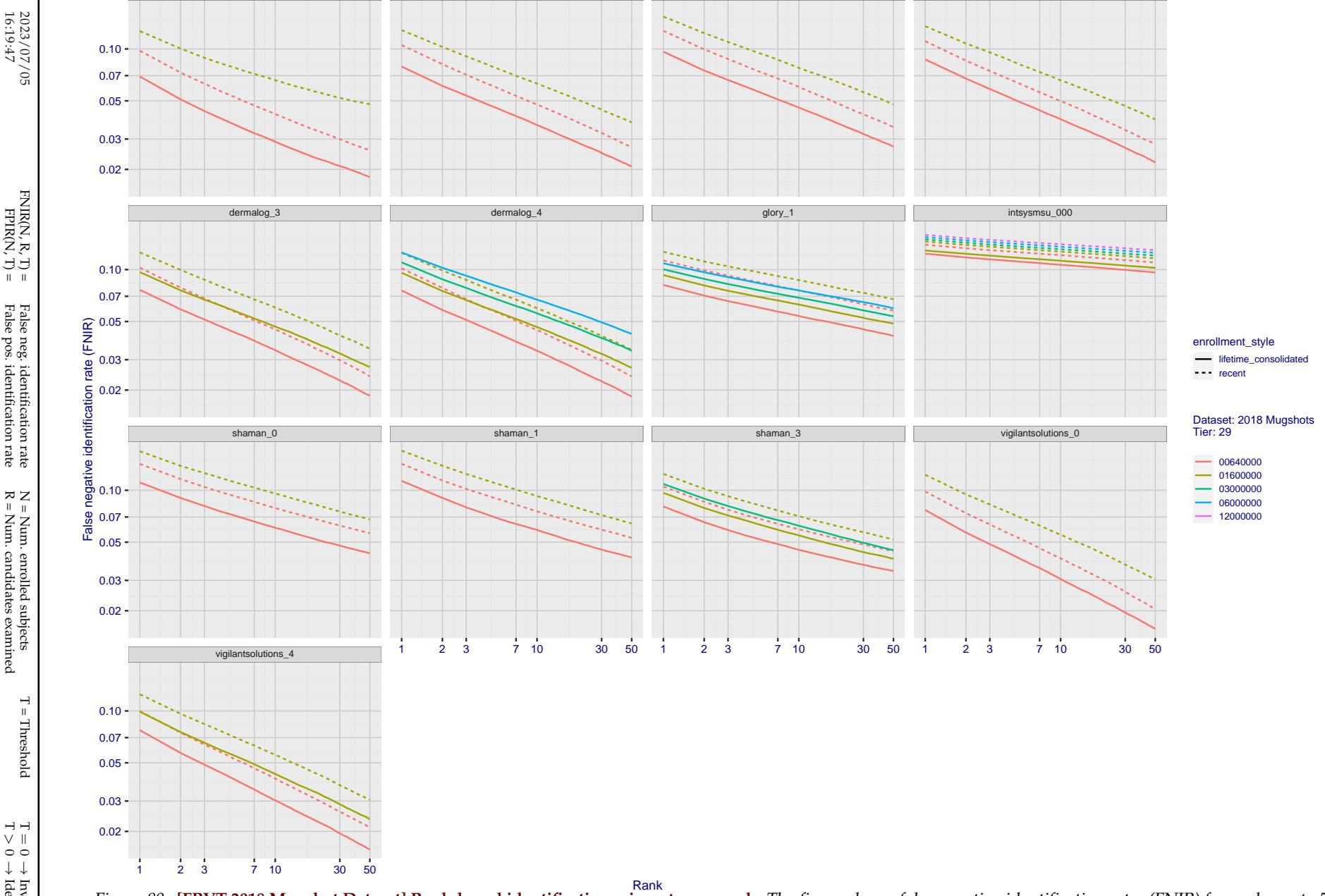


Figure 80: [FRVT-2018 Mugshot Dataset] Rank-based identification miss rates vs. rank. The figure shows false negative identification rates (FNIR) for ranks up to 50. This metric is appropriate to investigational applications where human reviewers will adjudicate sorted candidate lists. Note that with threshold set to zero, FPIR = 1, i.e. any search without an enrolled mate will return non-mated candidates. Results are sorted and reported into tiers for clarity, with the tiering criteria being rank 1 hit rate on a gallery size of N = 640 000 subjects.

2023/07/05
16:19:47FNIR(N, R, T) = False neg. identification rate
FPIR(N, T) = False pos. identification rateN = Num. enrolled subjects
R = Num. candidates examined

T = Threshold

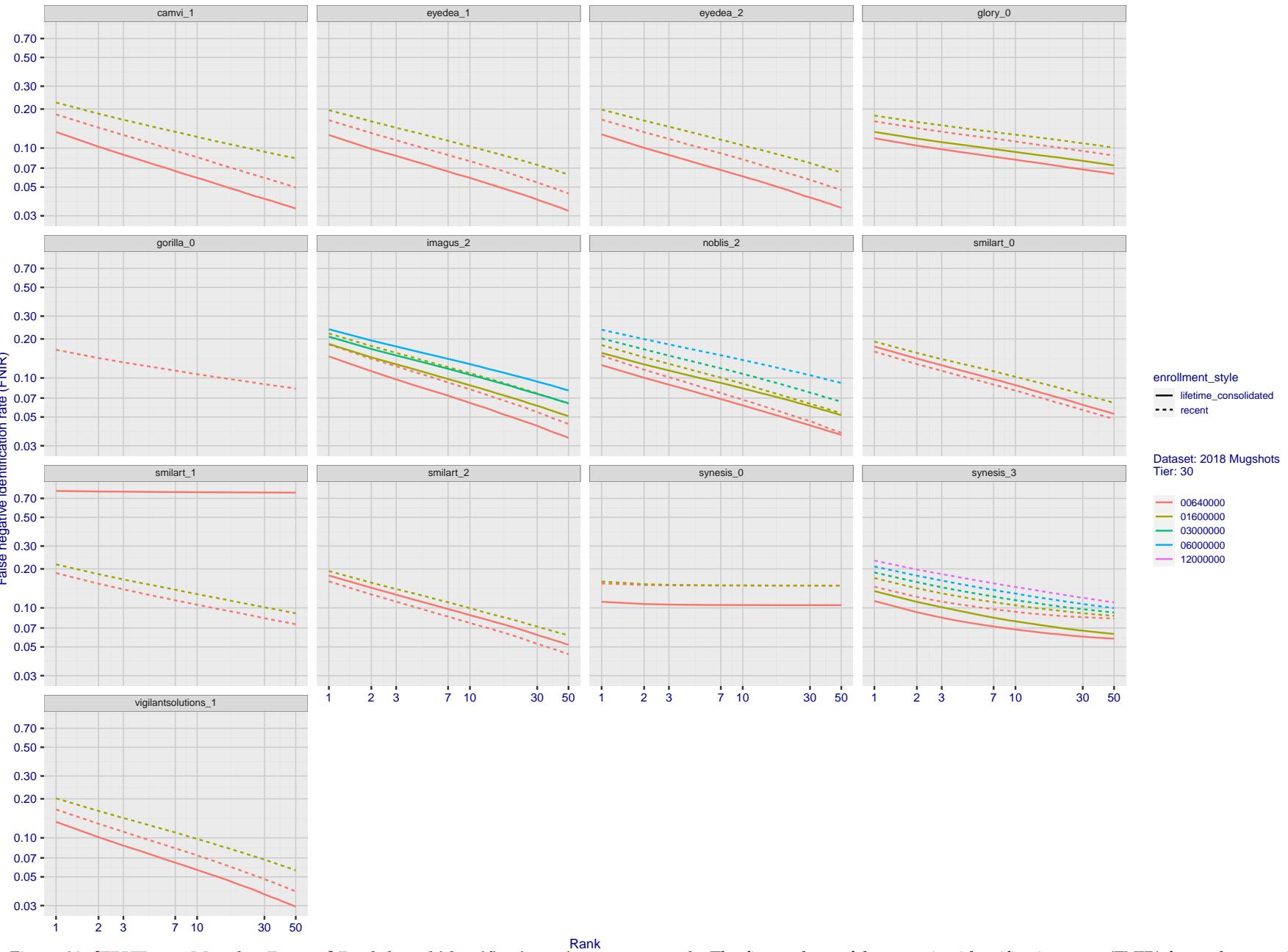
T = 0 → Investigation
T > 0 → Identification

Figure 81: [FRVT-2018 Mugshot Dataset] Rank-based identification miss rates vs. rank. The figure shows false negative identification rates (FNIR) for ranks up to 50. This metric is appropriate to investigational applications where human reviewers will adjudicate sorted candidate lists. Note that with threshold set to zero, FPIR = 1, i.e. any search without an enrolled mate will return non-mated candidates. Results are sorted and reported into tiers for clarity, with the tiering criteria being rank 1 hit rate on a gallery size of N = 640 000 subjects.

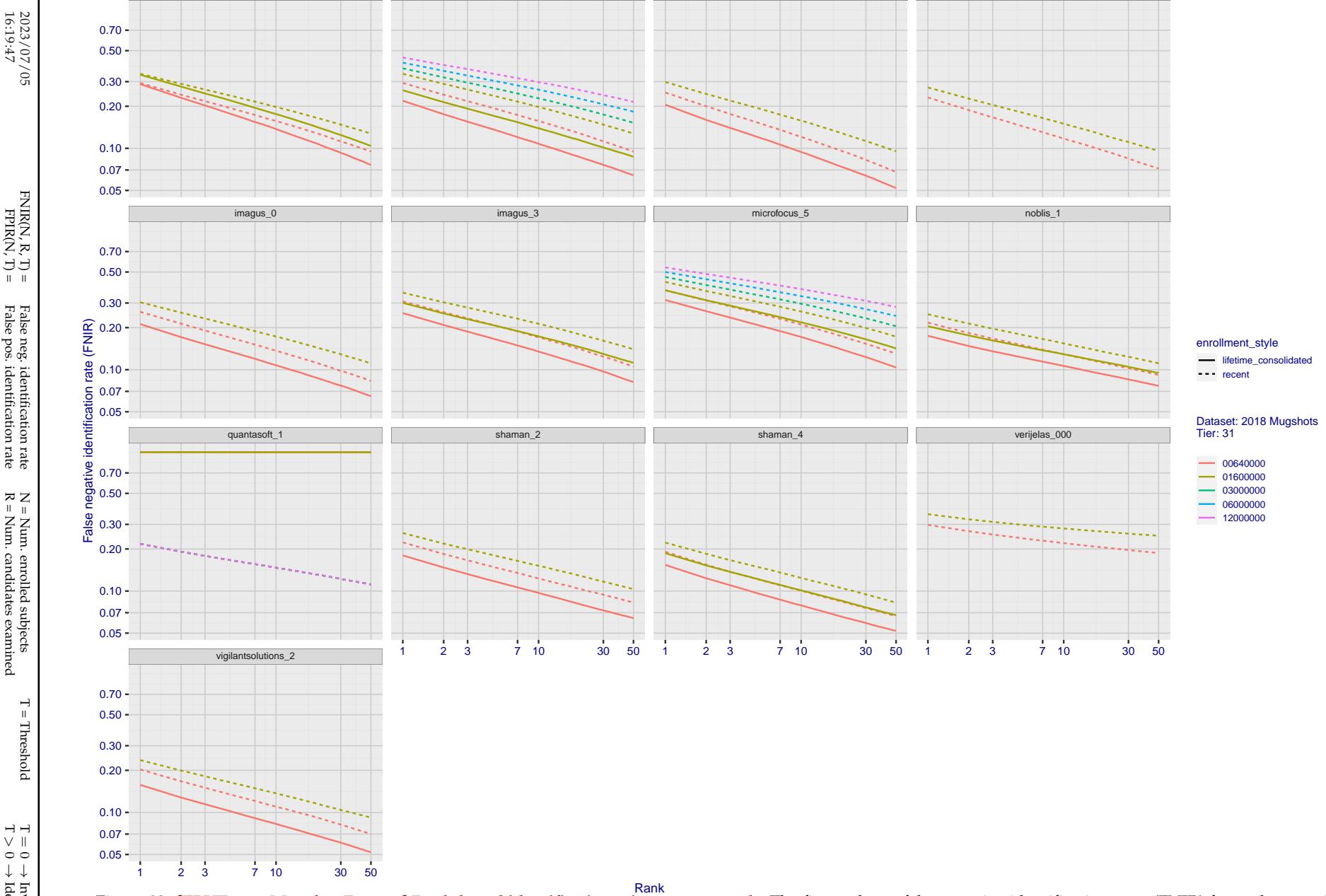


Figure 82: [FRVT-2018 Mugshot Dataset] Rank-based identification miss rates vs. rank. The figure shows false negative identification rates (FNIR) for ranks up to 50. This metric is appropriate to investigational applications where human reviewers will adjudicate sorted candidate lists. Note that with threshold set to zero, FPIR = 1, i.e. any search without an enrolled mate will return non-mated candidates. Results are sorted and reported into tiers for clarity, with the tiering criteria being rank 1 hit rate on a gallery size of N = 640 000 subjects.

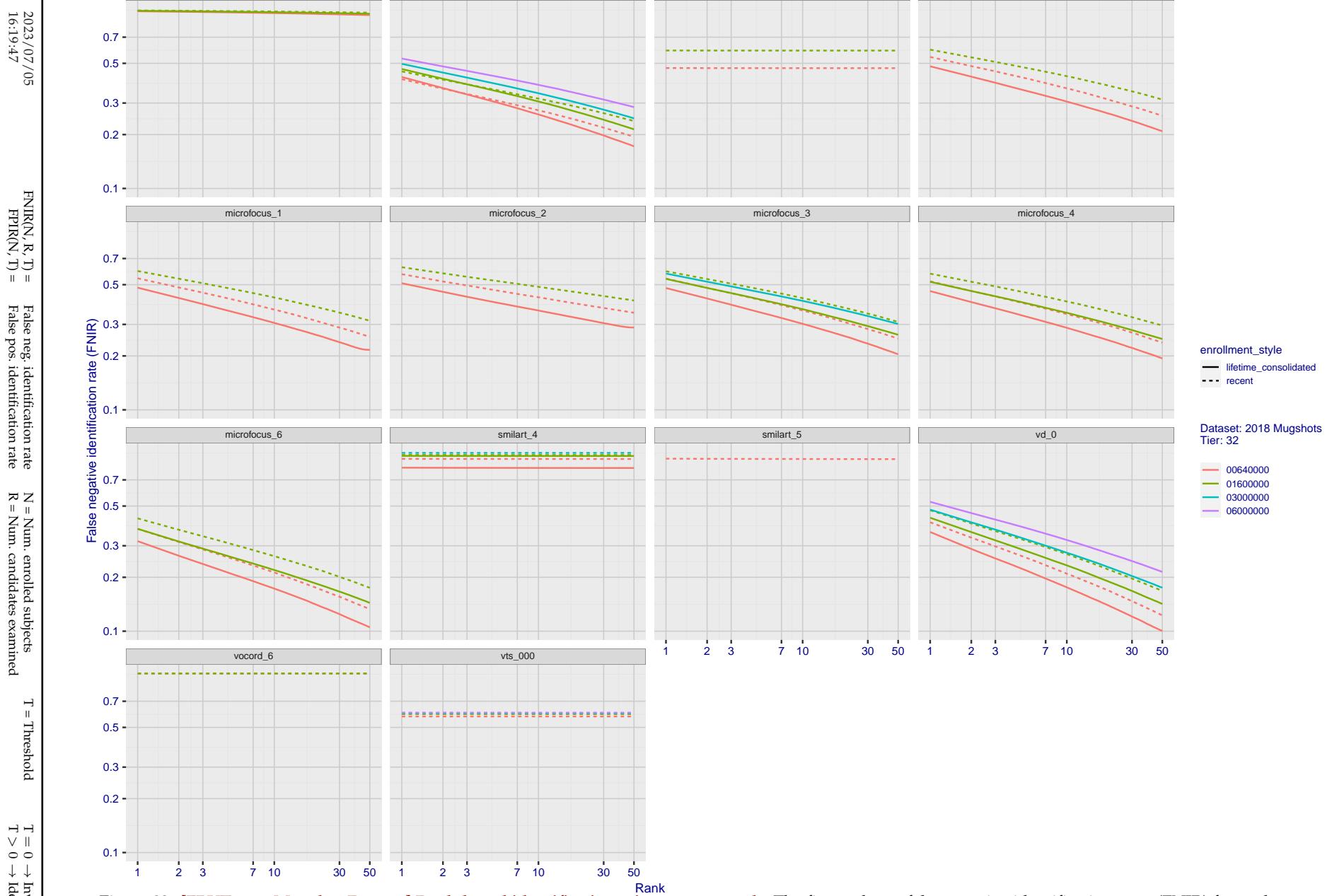


Figure 83: [FRVT-2018 Mugshot Dataset] Rank-based identification miss rates vs. rank. The figure shows false negative identification rates (FNIR) for ranks up to 50. This metric is appropriate to investigational applications where human reviewers will adjudicate sorted candidate lists. Note that with threshold set to zero, FPIR = 1, i.e. any search without an enrolled mate will return non-mated candidates. Results are sorted and reported into tiers for clarity, with the tiering criteria being rank 1 hit rate on a gallery size of N = 640 000 subjects.

2023/07/05
16:19:47

FNIR(N, R, T) = False neg. identification rate
FPTR(N, T) = False pos. identification rate

N = Num. enrolled subjects
R = Num. candidates examined

T = Threshold
T = 0 → Investigation
T > 0 → Identification

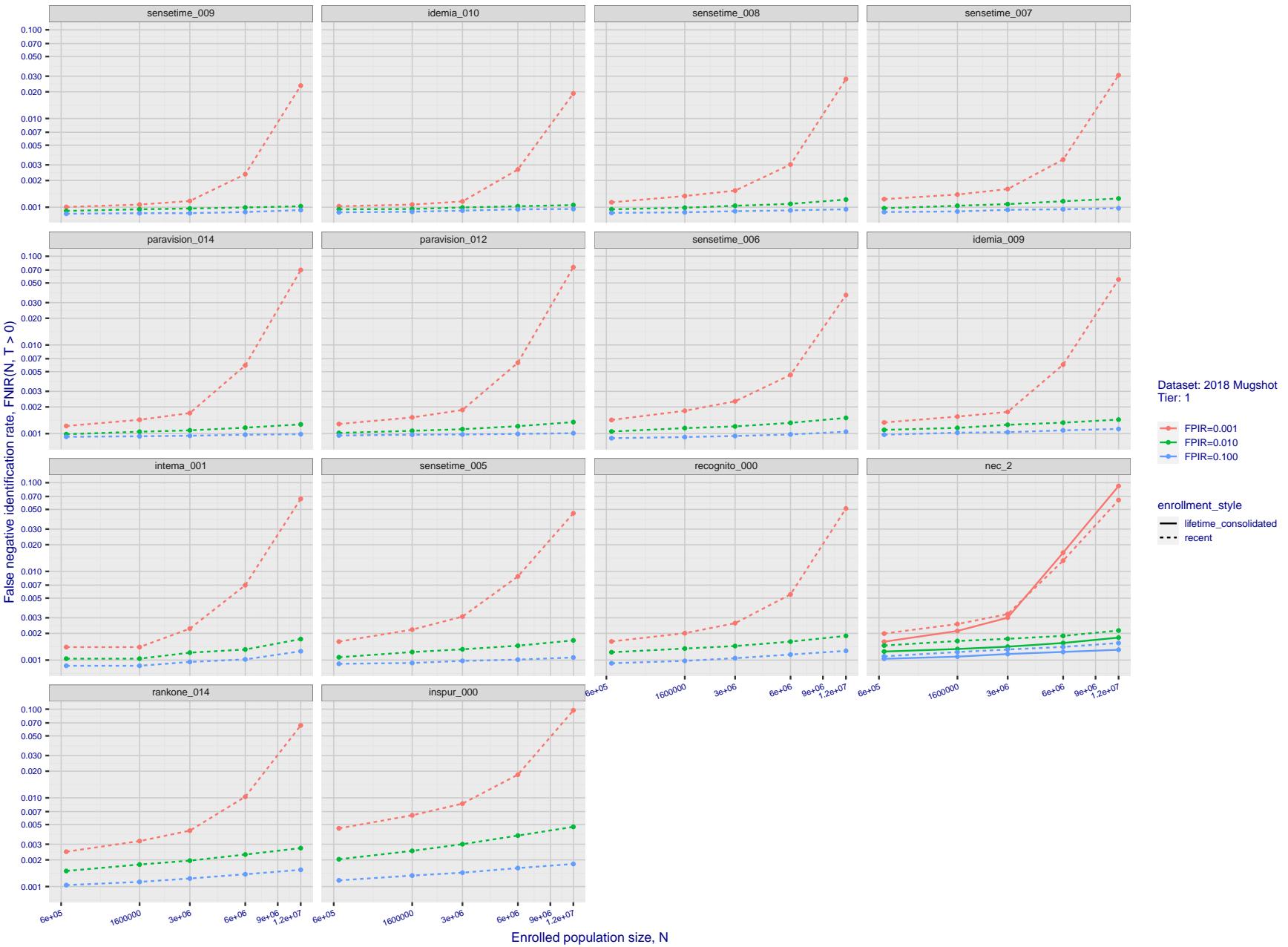


Figure 84: [FRVT-2018 Mugshot Dataset] Threshold-based identification miss rates vs. number of enrolled subjects. The figure shows $\text{FNIR}(N, T)$ across various gallery sizes when the threshold is set to achieve the given FPIRs. The rank criterion is irrelevant at high thresholds as mates are always at rank 1. The results are computed from the trials listed in rows 1-10 of Table 1. Less accurate algorithms were not run on large N , so results are missing. For clarity, results are sorted and reported into tiers spanning multiple pages. The tiering criteria is complicated: First paging by $\text{FNIR}(N_b, 1, 0)$, then sorting by median $\text{FNIR}(N_b, T)$, $N_b = 640\,000$.

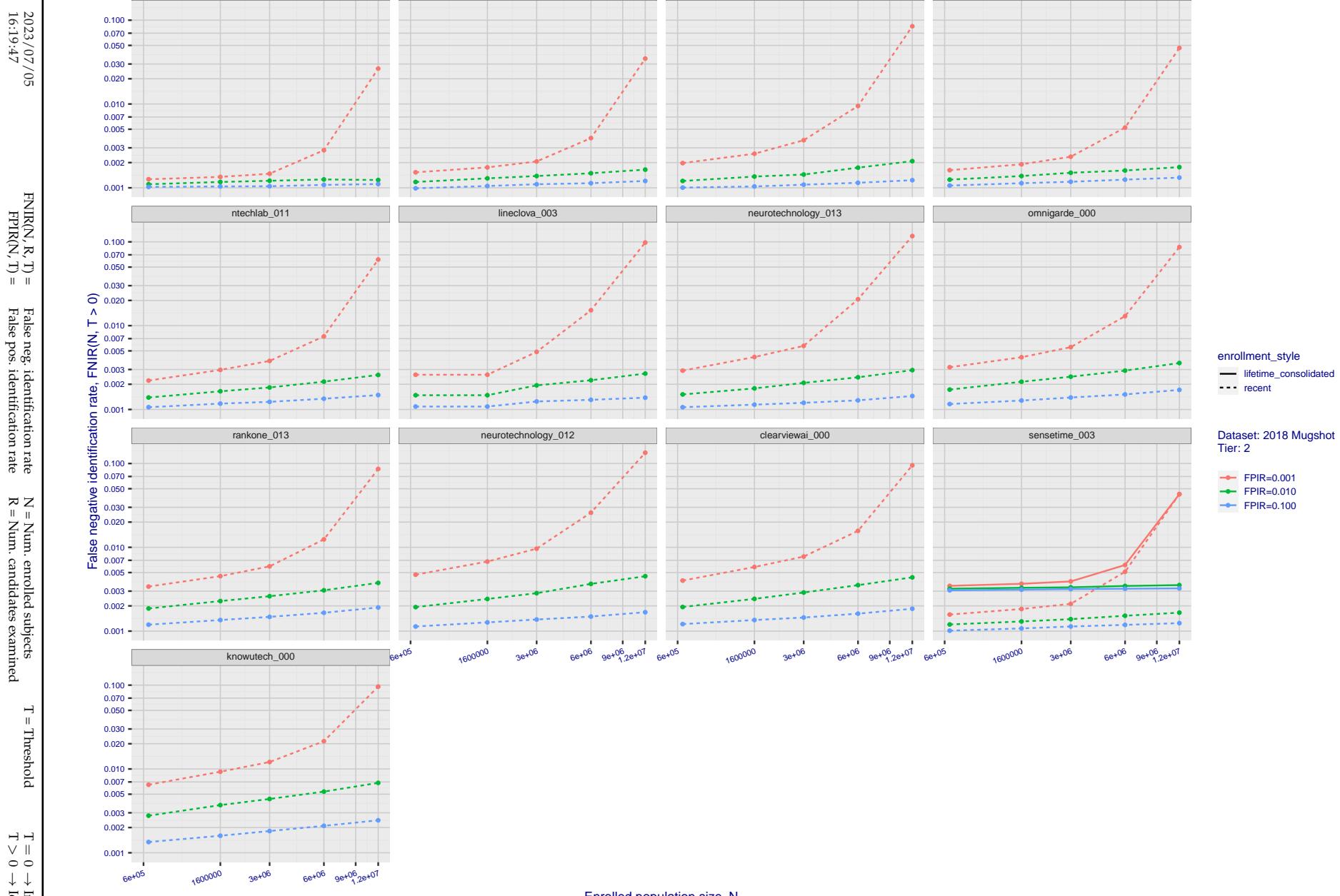


Figure 85: [FRVT-2018 Mugshot Dataset] Threshold-based identification miss rates vs. number of enrolled subjects. The figure shows $\text{FNIR}(N, T)$ across various gallery sizes when the threshold is set to achieve the given FPIRs. The rank criterion is irrelevant at high thresholds as mates are always at rank 1. The results are computed from the trials listed in rows 1-10 of Table 1. Less accurate algorithms were not run on large N , so results are missing. For clarity, results are sorted and reported into tiers spanning multiple pages. The tiering criteria is complicated: First paging by $\text{FNIR}(N_b, 1, 0)$, then sorting by median $\text{FNIR}(N_b, T)$, $N_b = 640\,000$.

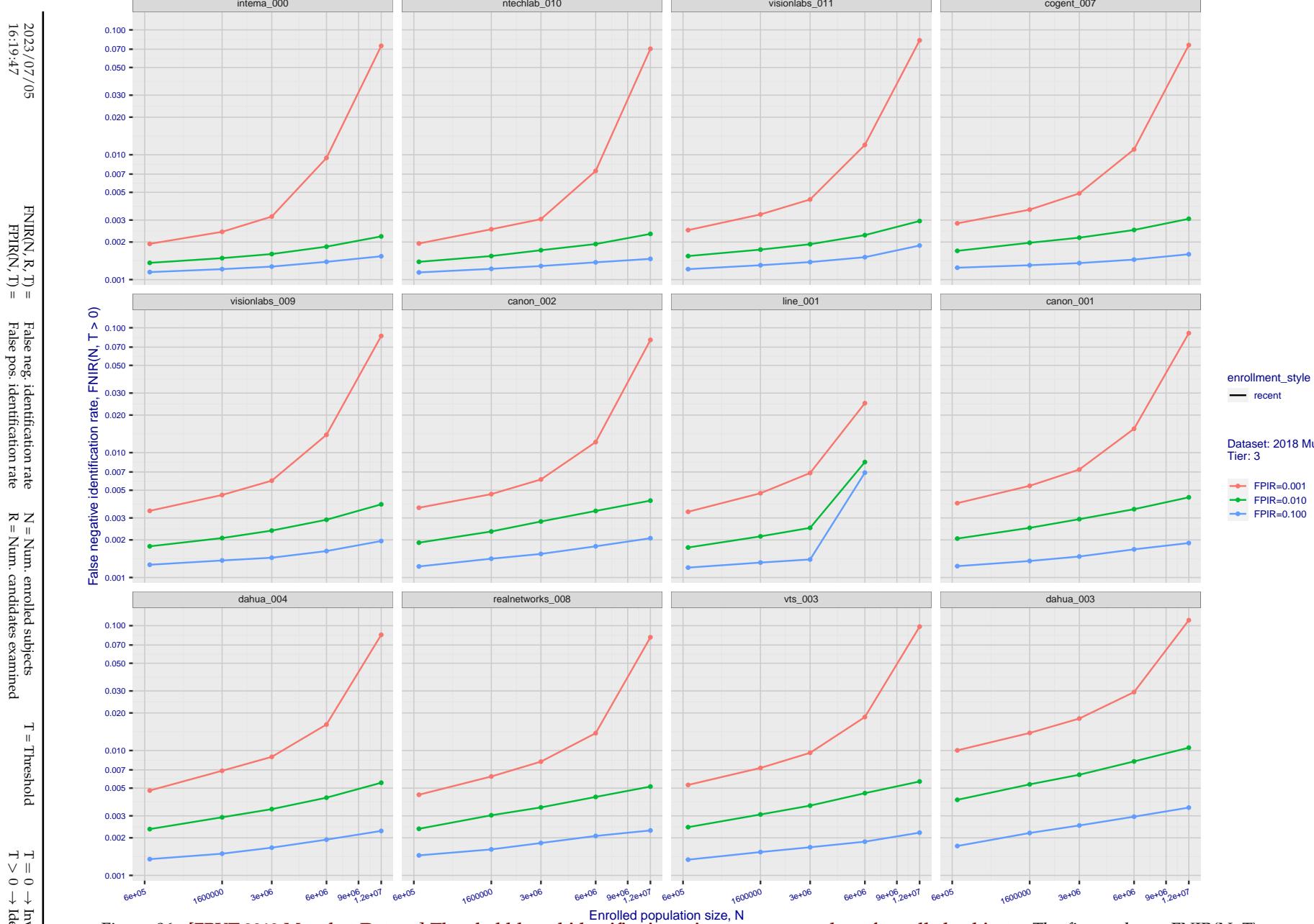


Figure 86: [FRVT-2018 Mugshot Dataset] Threshold-based identification miss rates vs. number of enrolled subjects. The figure shows $\text{FNIR}(N, T)$ across various gallery sizes when the threshold is set to achieve the given FPIRs. The rank criterion is irrelevant at high thresholds as mates are always at rank 1. The results are computed from the trials listed in rows 1-10 of Table 1. Less accurate algorithms were not run on large N , so results are missing. For clarity, results are sorted and reported into tiers spanning multiple pages. The tiering criteria is complicated: First paging by $\text{FNIR}(N_b, 1, 0)$, then sorting by median $\text{FNIR}(N_b, T)$, $N_b = 640\,000$.

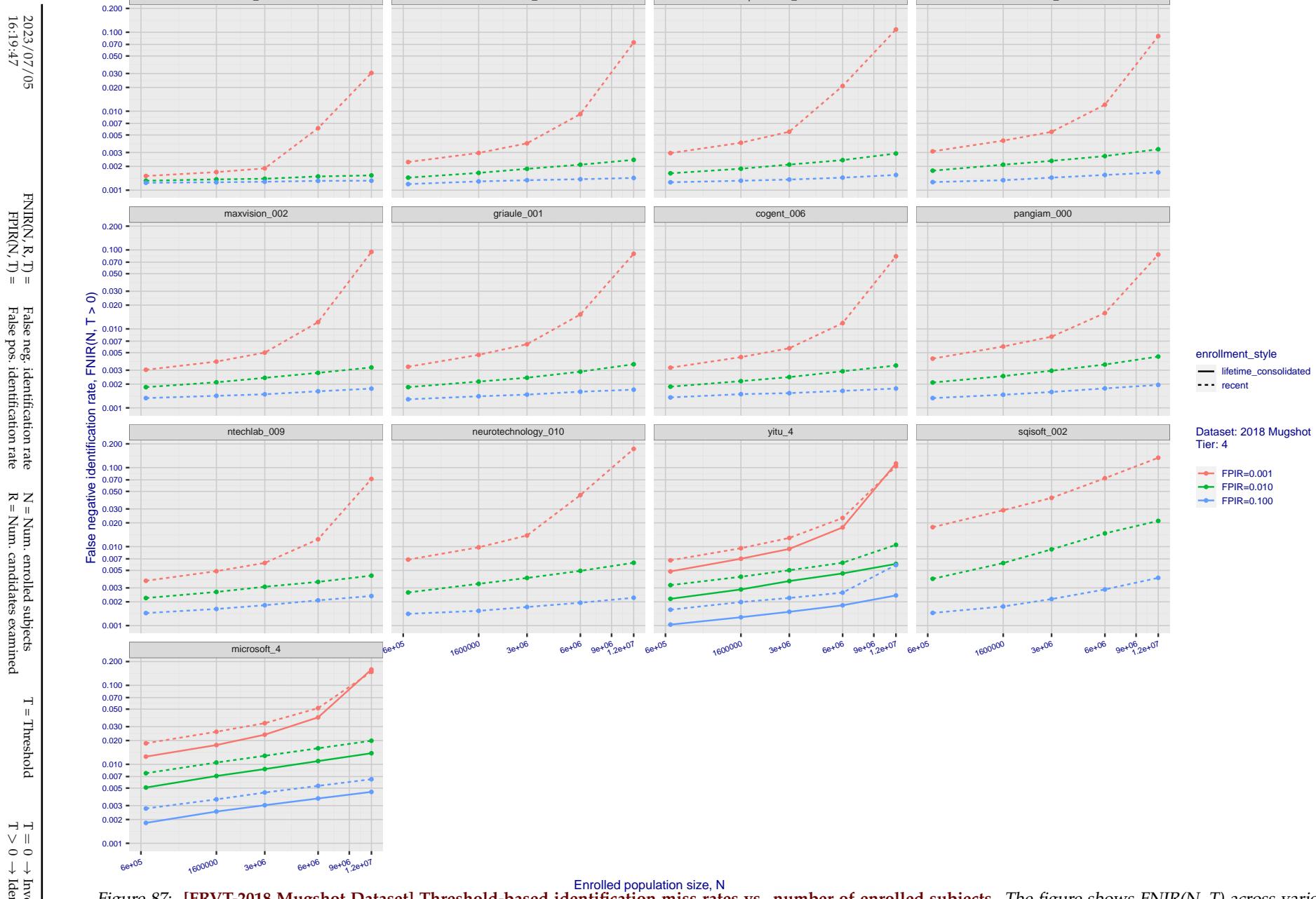


Figure 87: [FRVT-2018 Mugshot Dataset] Threshold-based identification miss rates vs. number of enrolled subjects. The figure shows $\text{FNIR}(N, T)$ across various gallery sizes when the threshold is set to achieve the given FPIRs. The rank criterion is irrelevant at high thresholds as mates are always at rank 1. The results are computed from the trials listed in rows 1-10 of Table 1. Less accurate algorithms were not run on large N , so results are missing. For clarity, results are sorted and reported into tiers spanning multiple pages. The tiering criteria is complicated: First paging by $\text{FNIR}(N_b, 1, 0)$, then sorting by median $\text{FNIR}(N_b, T)$, $N_b = 640\,000$.

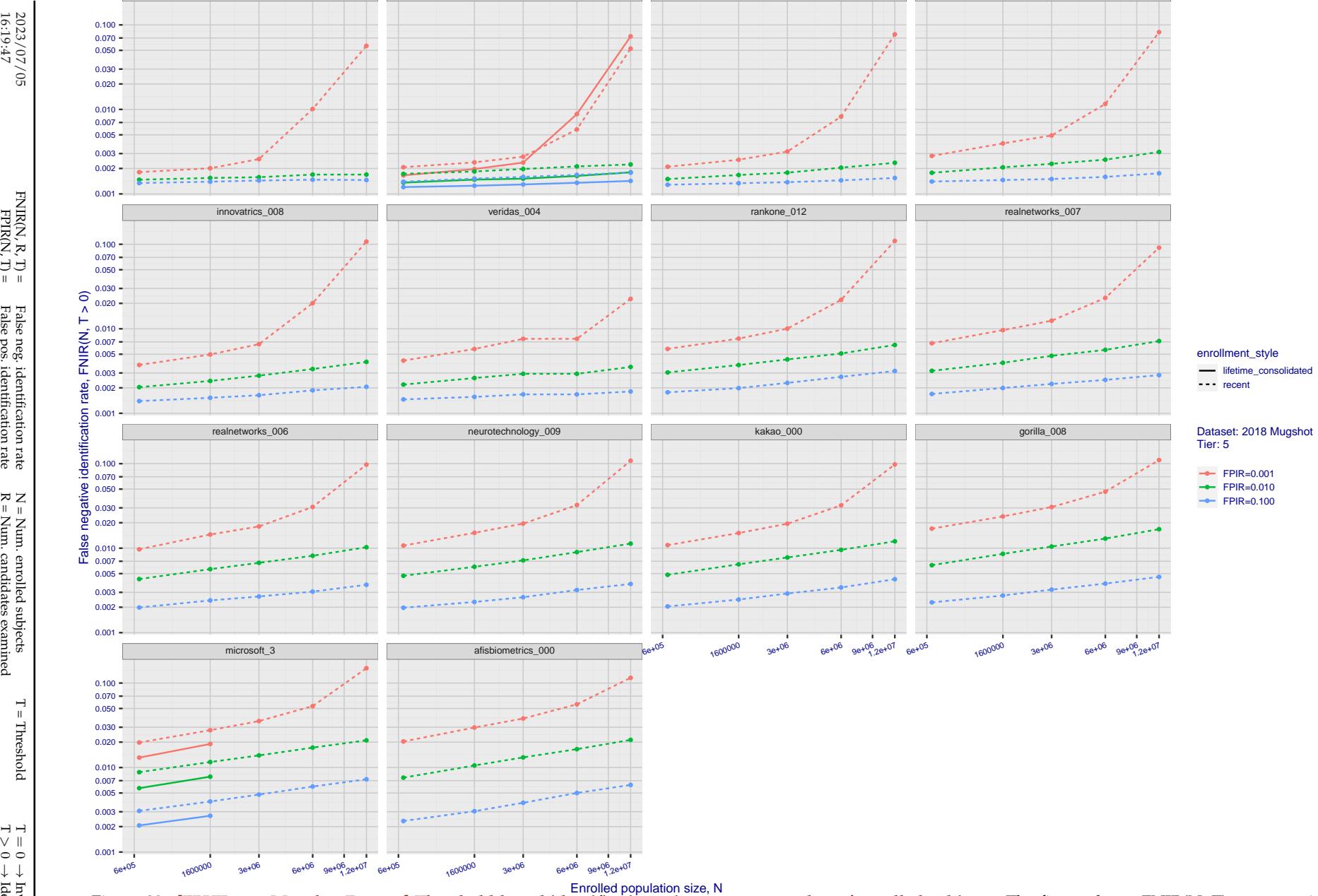


Figure 88: [FRVT-2018 Mugshot Dataset] Threshold-based identification miss rates vs. number of enrolled subjects. The figure shows $\text{FNIR}(N, T)$ across various gallery sizes when the threshold is set to achieve the given FPIRs. The rank criterion is irrelevant at high thresholds as mates are always at rank 1. The results are computed from the trials listed in rows 1-10 of Table 1. Less accurate algorithms were not run on large N , so results are missing. For clarity, results are sorted and reported into tiers spanning multiple pages. The tiering criteria is complicated: First paging by $\text{FNIR}(N_b, 1, 0)$, then sorting by median $\text{FNIR}(N_b, T)$, $N_b = 640\,000$.

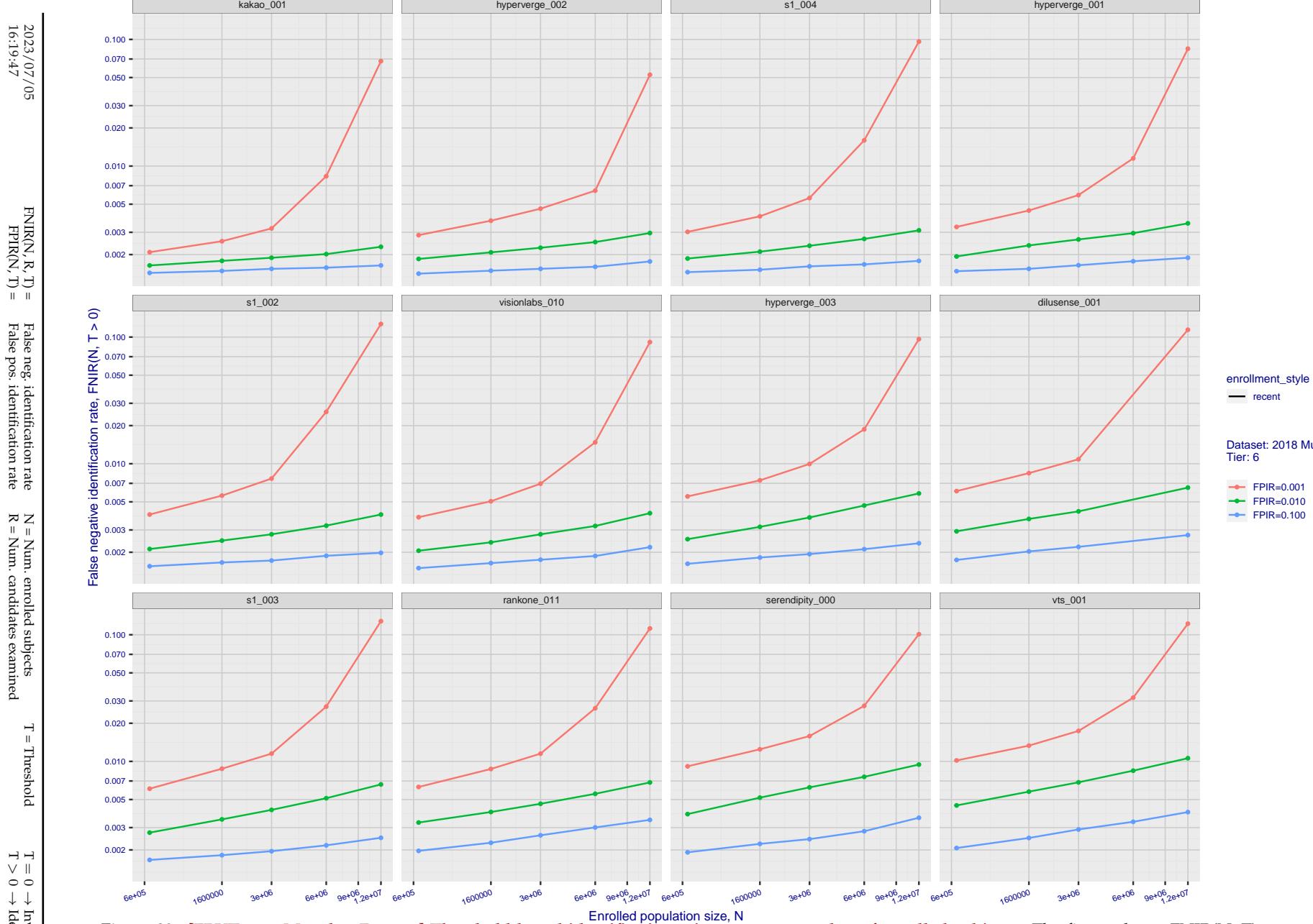


Figure 89: [FRVT-2018 Mugshot Dataset] Threshold-based identification miss rates vs. number of enrolled subjects. The figure shows FNIR(N, T) across various gallery sizes when the threshold is set to achieve the given FPIRs. The rank criterion is irrelevant at high thresholds as mates are always at rank 1. The results are computed from the trials listed in rows 1-10 of Table 1. Less accurate algorithms were not run on large N , so results are missing. For clarity, results are sorted and reported into tiers spanning multiple pages. The tiering criteria is complicated: First paging by FNIR($N_b, 1, 0$), then sorting by median FNIR(N_b, T), $N_b = 640\,000$.

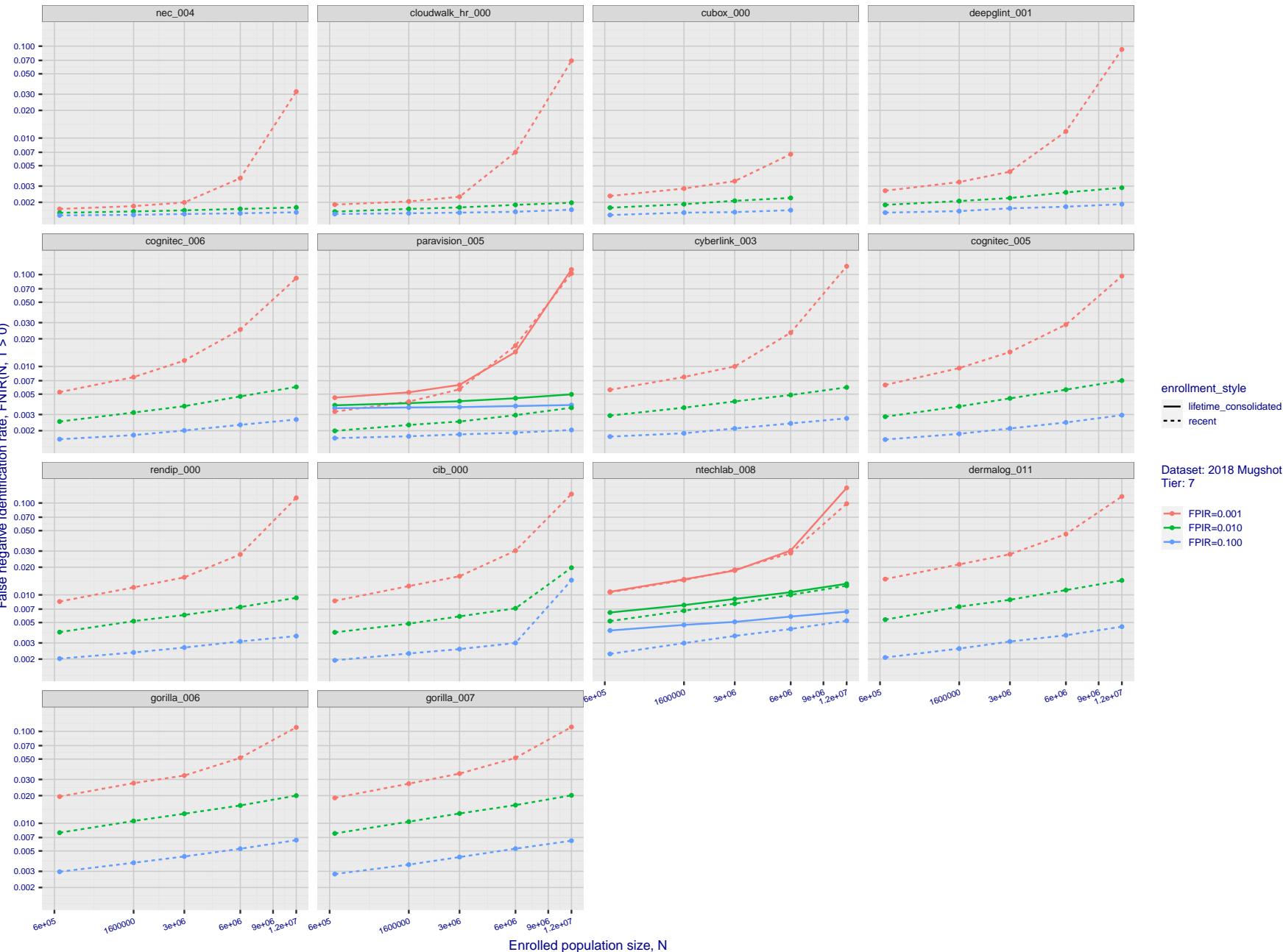
2023/07/05
16:19:47

Figure 90: [FRVT-2018 Mugshot Dataset] Threshold-based identification miss rates vs. number of enrolled subjects. The figure shows $\text{FNIR}(N, T)$ across various gallery sizes when the threshold is set to achieve the given FPIRs. The rank criterion is irrelevant at high thresholds as mates are always at rank 1. The results are computed from the trials listed in rows 1-10 of Table 1. Less accurate algorithms were not run on large N , so results are missing. For clarity, results are sorted and reported into tiers spanning multiple pages. The tiering criteria is complicated: First paging by $\text{FNIR}(N_b, 1, 0)$, then sorting by median $\text{FNIR}(N_b, T)$, $N_b = 640\,000$.

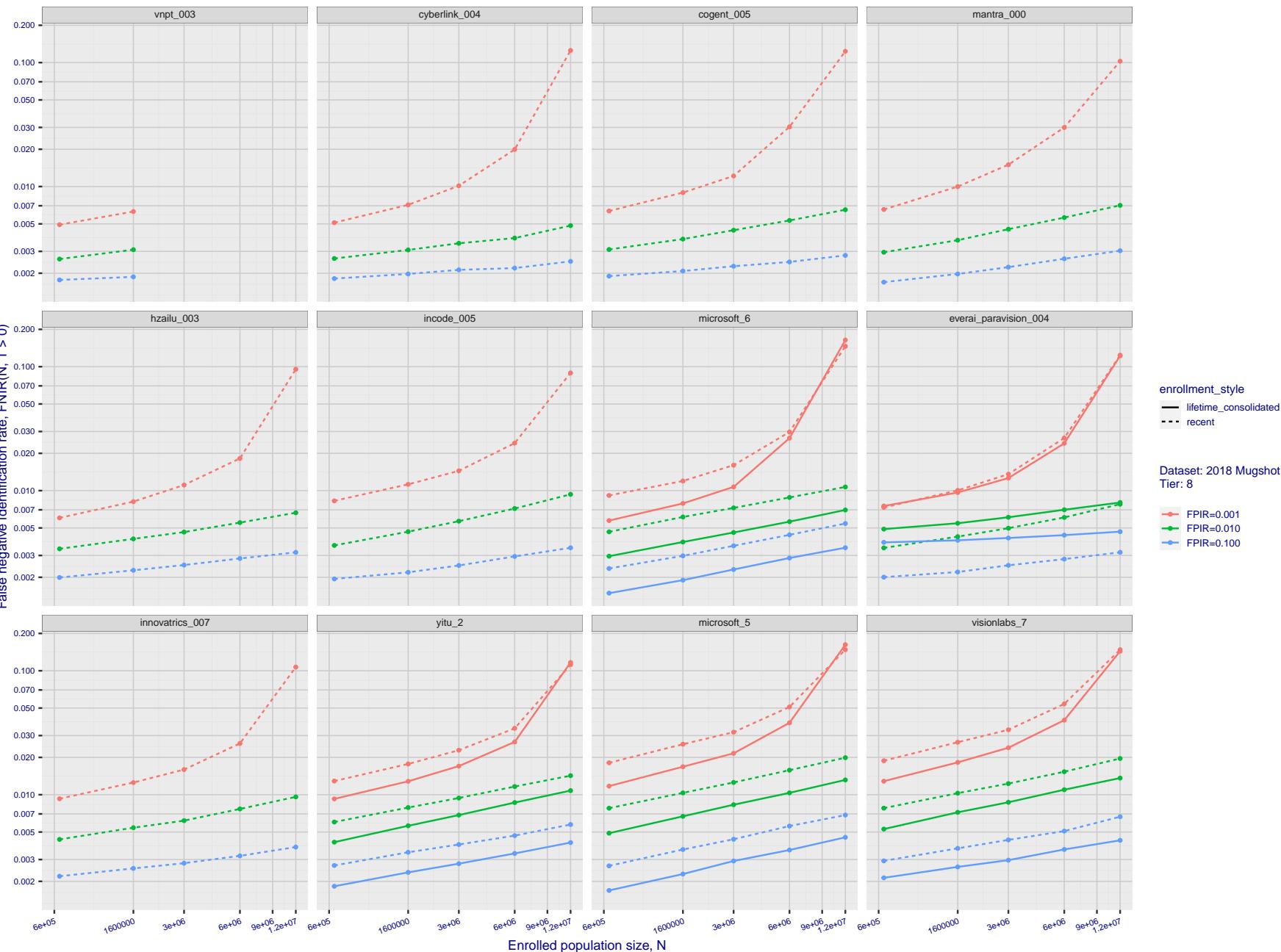
2023/07/05
16:19:47

Figure 91: [FRVT-2018 Mugshot Dataset] Threshold-based identification miss rates vs. number of enrolled subjects. The figure shows $\text{FNIR}(N, T)$ across various gallery sizes when the threshold is set to achieve the given FPIRs. The rank criterion is irrelevant at high thresholds as mates are always at rank 1. The results are computed from the trials listed in rows 1-10 of Table 1. Less accurate algorithms were not run on large N , so results are missing. For clarity, results are sorted and reported into tiers spanning multiple pages. The tiering criteria is complicated: First paging by $\text{FNIR}(N_b, 1, 0)$, then sorting by median $\text{FNIR}(N_b, T)$, $N_b = 640\,000$.

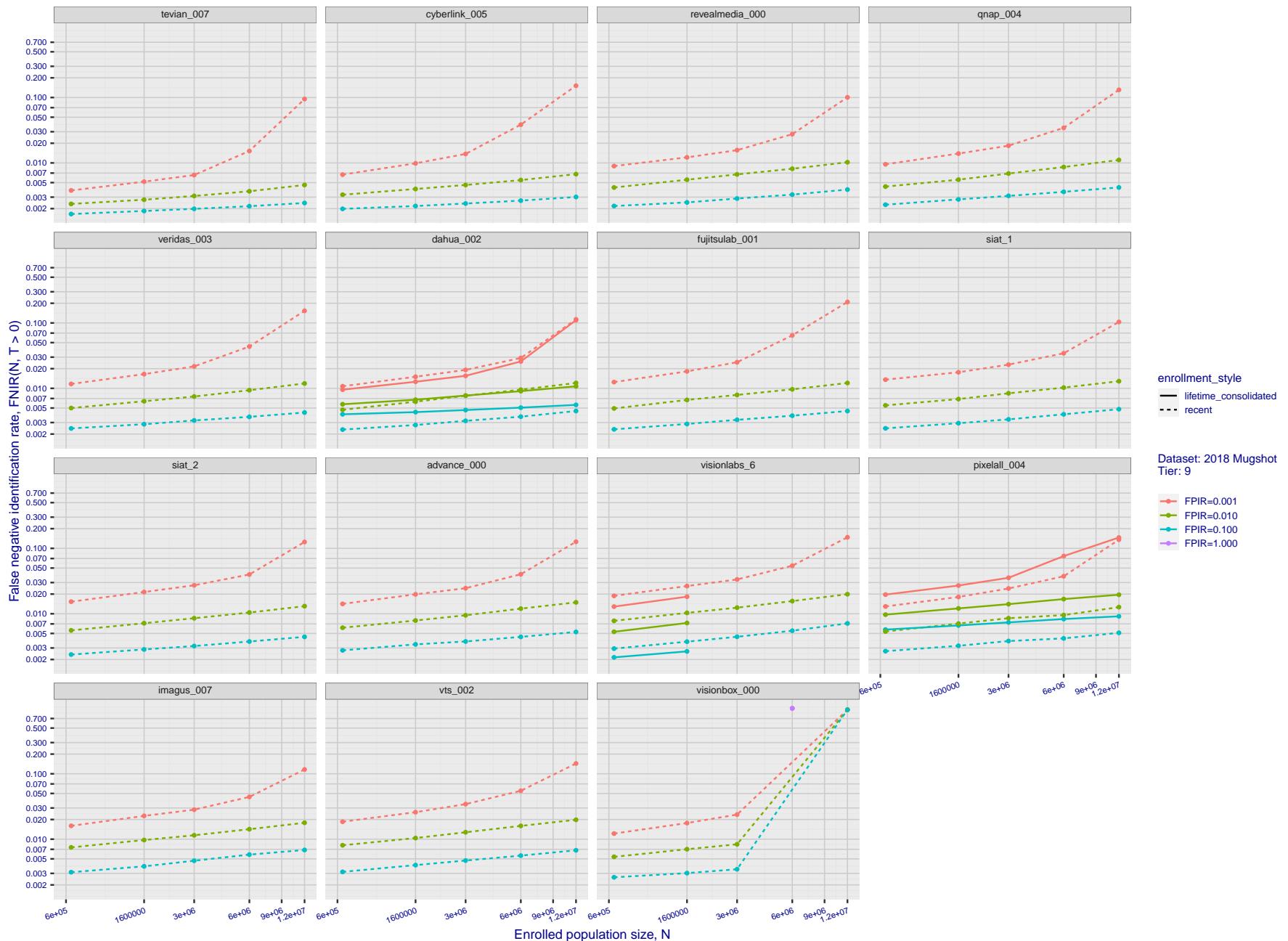


Figure 92: [FRVT-2018 Mugshot Dataset] Threshold-based identification miss rates vs. number of enrolled subjects. The figure shows $\text{FNIR}(N, T)$ across various gallery sizes when the threshold is set to achieve the given FPIRs. The rank criterion is irrelevant at high thresholds as mates are always at rank 1. The results are computed from the trials listed in rows 1-10 of Table 1. Less accurate algorithms were not run on large N , so results are missing. For clarity, results are sorted and reported into tiers spanning multiple pages. The tiering criteria is complicated: First paging by $\text{FNIR}(N_b, 1, 0)$, then sorting by median $\text{FNIR}(N_b, T)$, $N_b = 640\,000$.

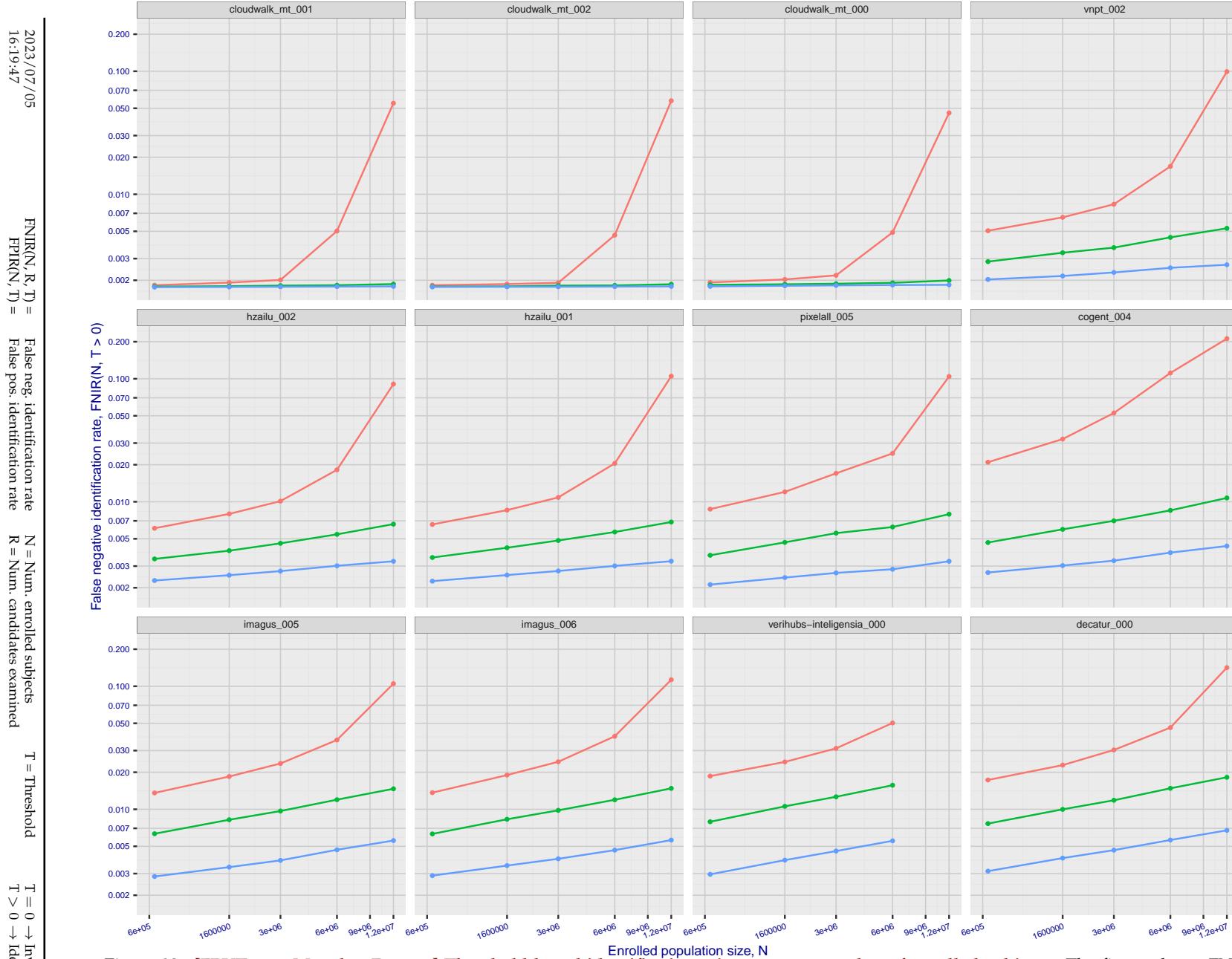


Figure 93: [FRVT-2018 Mugshot Dataset] Threshold-based identification miss rates vs. number of enrolled subjects. The figure shows FNIR(N, T) across various gallery sizes when the threshold is set to achieve the given FPIRs. The rank criterion is irrelevant at high thresholds as mates are always at rank 1. The results are computed from the trials listed in rows 1-10 of Table 1. Less accurate algorithms were not run on large N , so results are missing. For clarity, results are sorted and reported into tiers spanning multiple pages. The tiering criteria is complicated: First paging by FNIR($N_b, 1, 0$), then sorting by median FNIR(N_b, T), $N_b = 640\,000$.

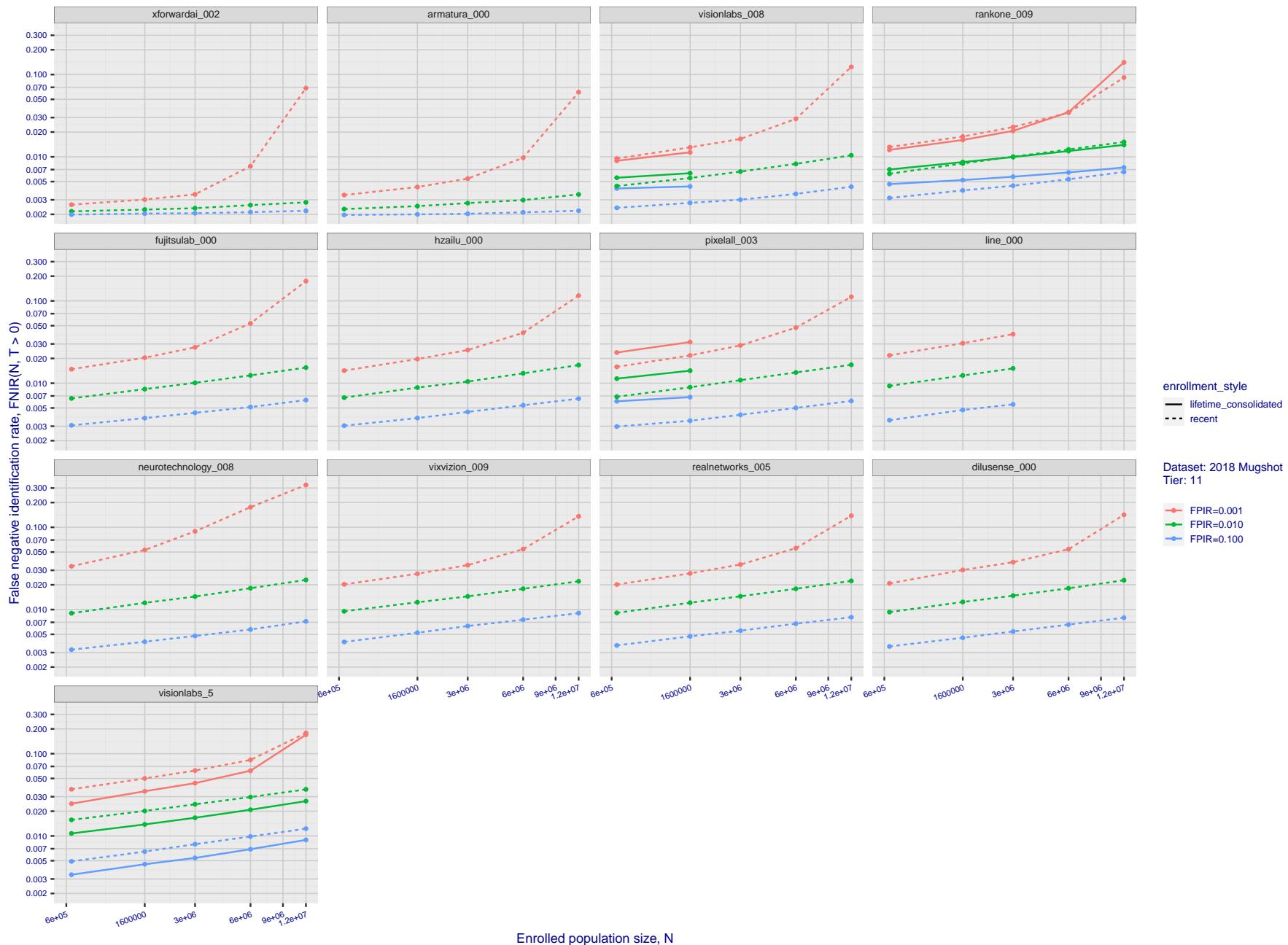


Figure 94: [FRVT-2018 Mugshot Dataset] Threshold-based identification miss rates vs. number of enrolled subjects. The figure shows FNIR(N, T) across various gallery sizes when the threshold is set to achieve the given FPIRs. The rank criterion is irrelevant at high thresholds as mates are always at rank 1. The results are computed from the trials listed in rows 1-10 of Table 1. Less accurate algorithms were not run on large N , so results are missing. For clarity, results are sorted and reported into tiers spanning multiple pages. The tiering criteria is complicated: First paging by $FNIR(N_b, 1, 0)$, then sorting by median $FNIR(N_b, T)$, $N_b = 640\,000$.

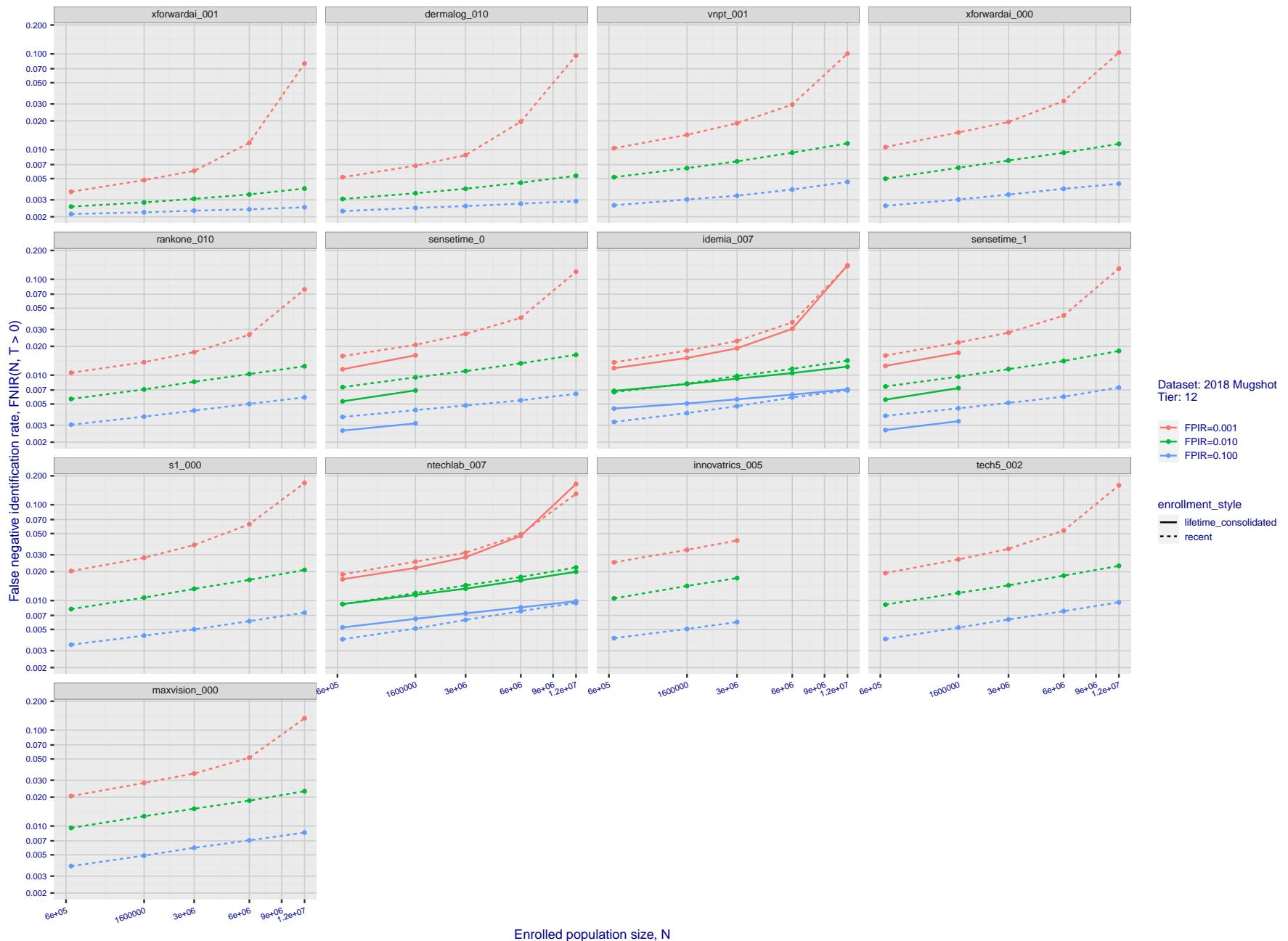


Figure 95: [FRVT-2018 Mugshot Dataset] Threshold-based identification miss rates vs. number of enrolled subjects. The figure shows $\text{FNIR}(N, T)$ across various gallery sizes when the threshold is set to achieve the given FPIRs. The rank criterion is irrelevant at high thresholds as mates are always at rank 1. The results are computed from the trials listed in rows 1-10 of Table 1. Less accurate algorithms were not run on large N , so results are missing. For clarity, results are sorted and reported into tiers spanning multiple pages. The tiering criteria is complicated: First paging by $\text{FNIR}(N_b, 1, 0)$, then sorting by median $\text{FNIR}(N_b, T)$, $N_b = 640\,000$.

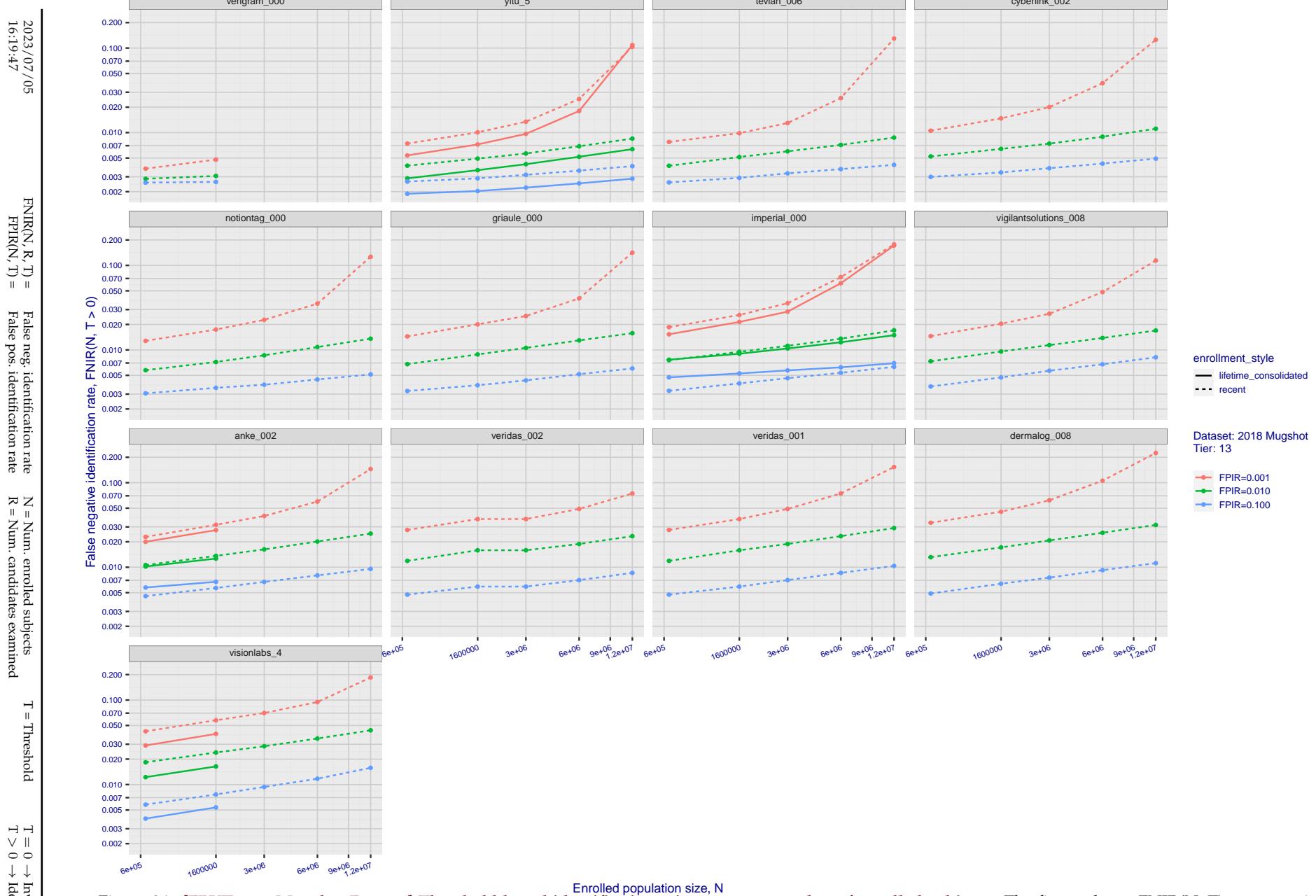


Figure 96: [FRVT-2018 Mugshot Dataset] Threshold-based identification miss rates vs. number of enrolled subjects. The figure shows $\text{FNIR}(N, T)$ across various gallery sizes when the threshold is set to achieve the given FPIRs. The rank criterion is irrelevant at high thresholds as mates are always at rank 1. The results are computed from the trials listed in rows 1-10 of Table 1. Less accurate algorithms were not run on large N , so results are missing. For clarity, results are sorted and reported into tiers spanning multiple pages. The tiering criteria is complicated: First paging by $\text{FNIR}(N_b, 1, 0)$, then sorting by median $\text{FNIR}(N_b, T)$, $N_b = 640\,000$.

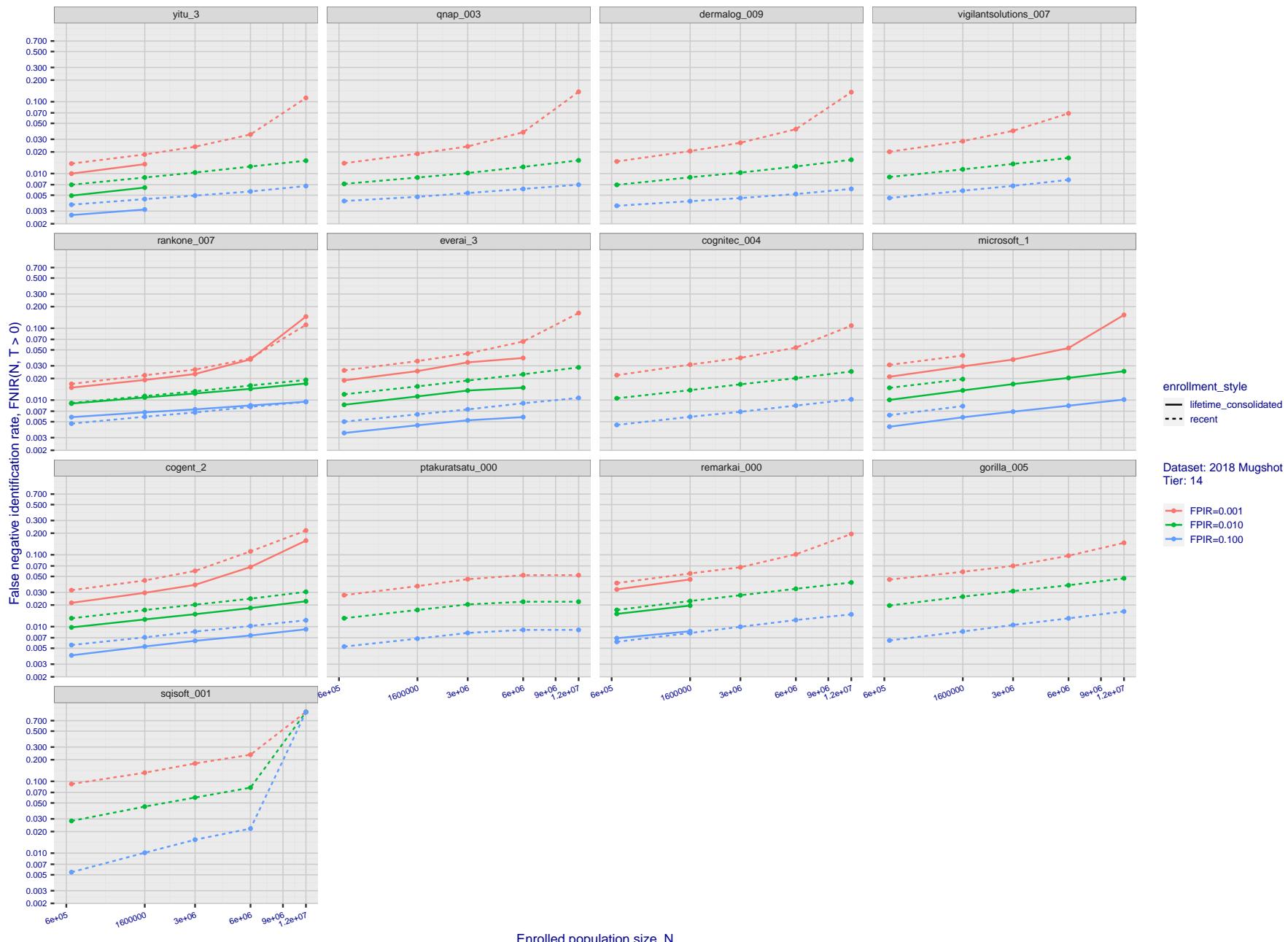


Figure 97: [FRVT-2018 Mugshot Dataset] Threshold-based identification miss rates vs. number of enrolled subjects. The figure shows $\text{FNIR}(N, T)$ across various gallery sizes when the threshold is set to achieve the given FPIRs. The rank criterion is irrelevant at high thresholds as mates are always at rank 1. The results are computed from the trials listed in rows 1-10 of Table 1. Less accurate algorithms were not run on large N , so results are missing. For clarity, results are sorted and reported into tiers spanning multiple pages. The tiering criteria is complicated: First paging by $\text{FNIR}(N_b, 1, 0)$, then sorting by median $\text{FNIR}(N_b, T)$, $N_b = 640\,000$.

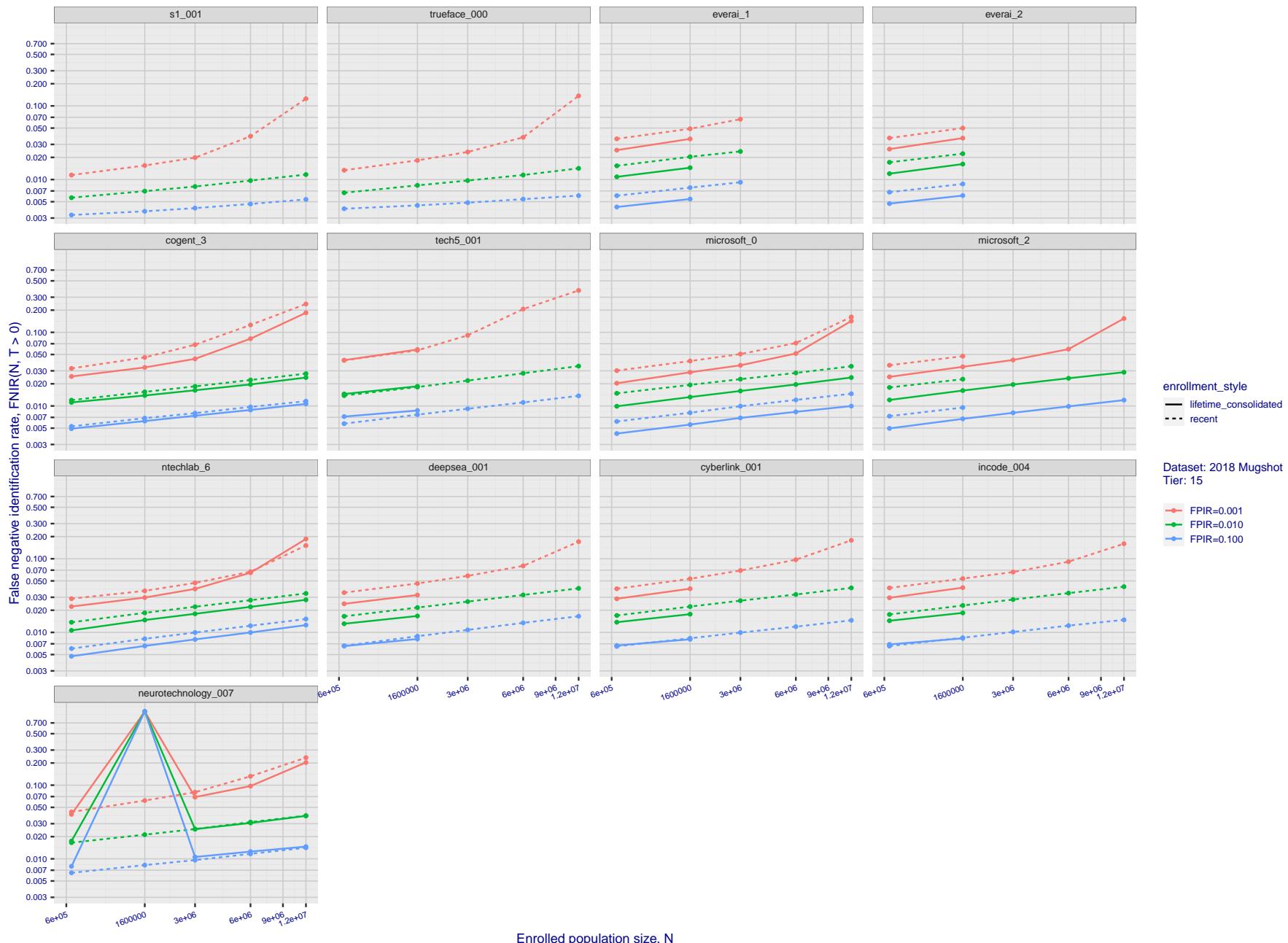


Figure 98: [FRVT-2018 Mugshot Dataset] Threshold-based identification miss rates vs. number of enrolled subjects. The figure shows $\text{FNIR}(N, T)$ across various gallery sizes when the threshold is set to achieve the given FPIRs. The rank criterion is irrelevant at high thresholds as mates are always at rank 1. The results are computed from the trials listed in rows 1-10 of Table 1. Less accurate algorithms were not run on large N , so results are missing. For clarity, results are sorted and reported into tiers spanning multiple pages. The tiering criteria is complicated: First paging by $\text{FNIR}(N_b, 1, 0)$, then sorting by median $\text{FNIR}(N_b, T)$, $N_b = 640\,000$.

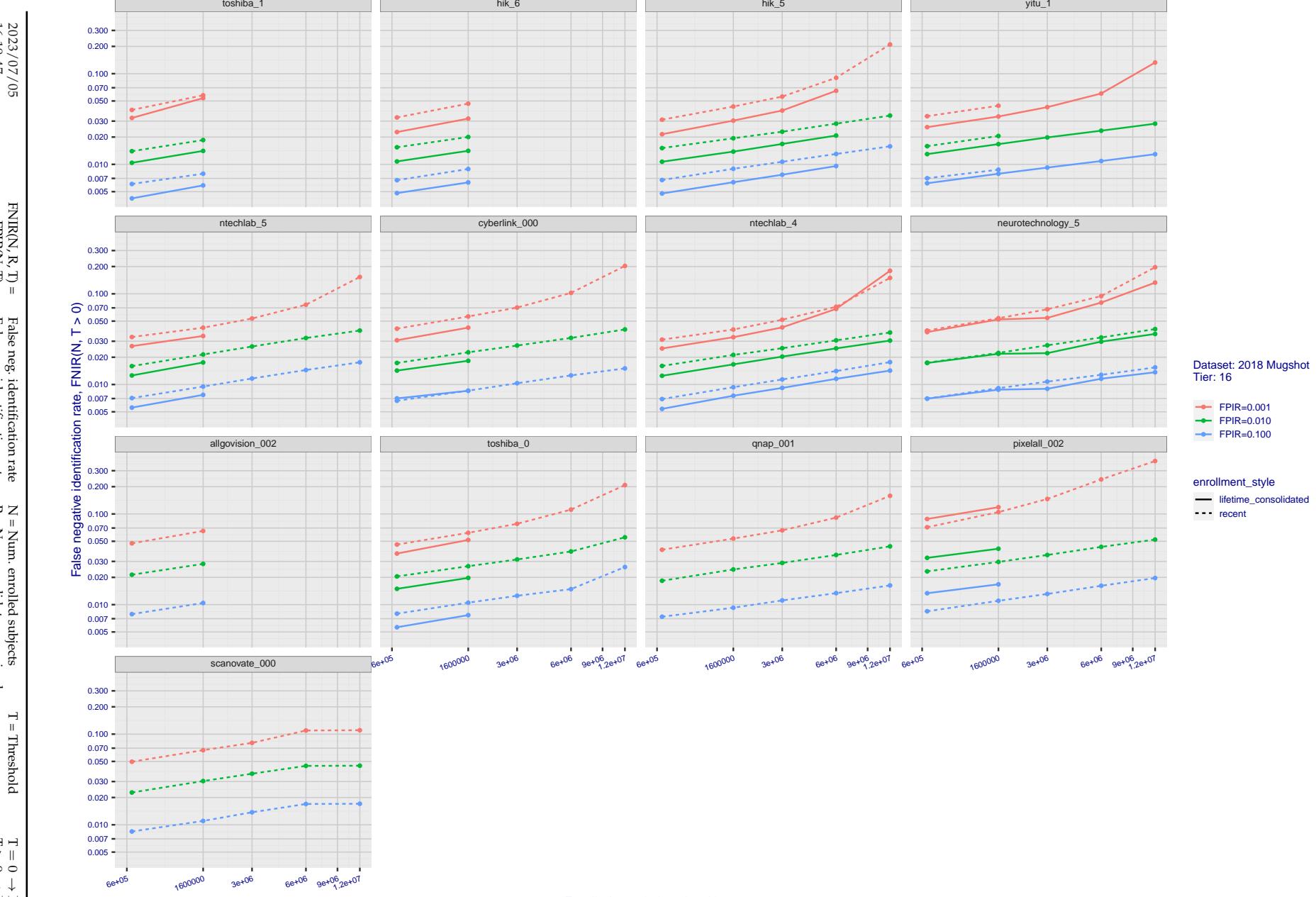


Figure 99: [FRVT-2018 Mugshot Dataset] Threshold-based identification miss rates vs. number of enrolled subjects. The figure shows $\text{FNIR}(N, T)$ across various gallery sizes when the threshold is set to achieve the given FPIRs. The rank criterion is irrelevant at high thresholds as mates are always at rank 1. The results are computed from the trials listed in rows 1-10 of Table 1. Less accurate algorithms were not run on large N , so results are missing. For clarity, results are sorted and reported into tiers spanning multiple pages. The tiering criteria is complicated: First paging by $\text{FNIR}(N_b, 1, 0)$, then sorting by median $\text{FNIR}(N_b, T)$, $N_b = 640\,000$.

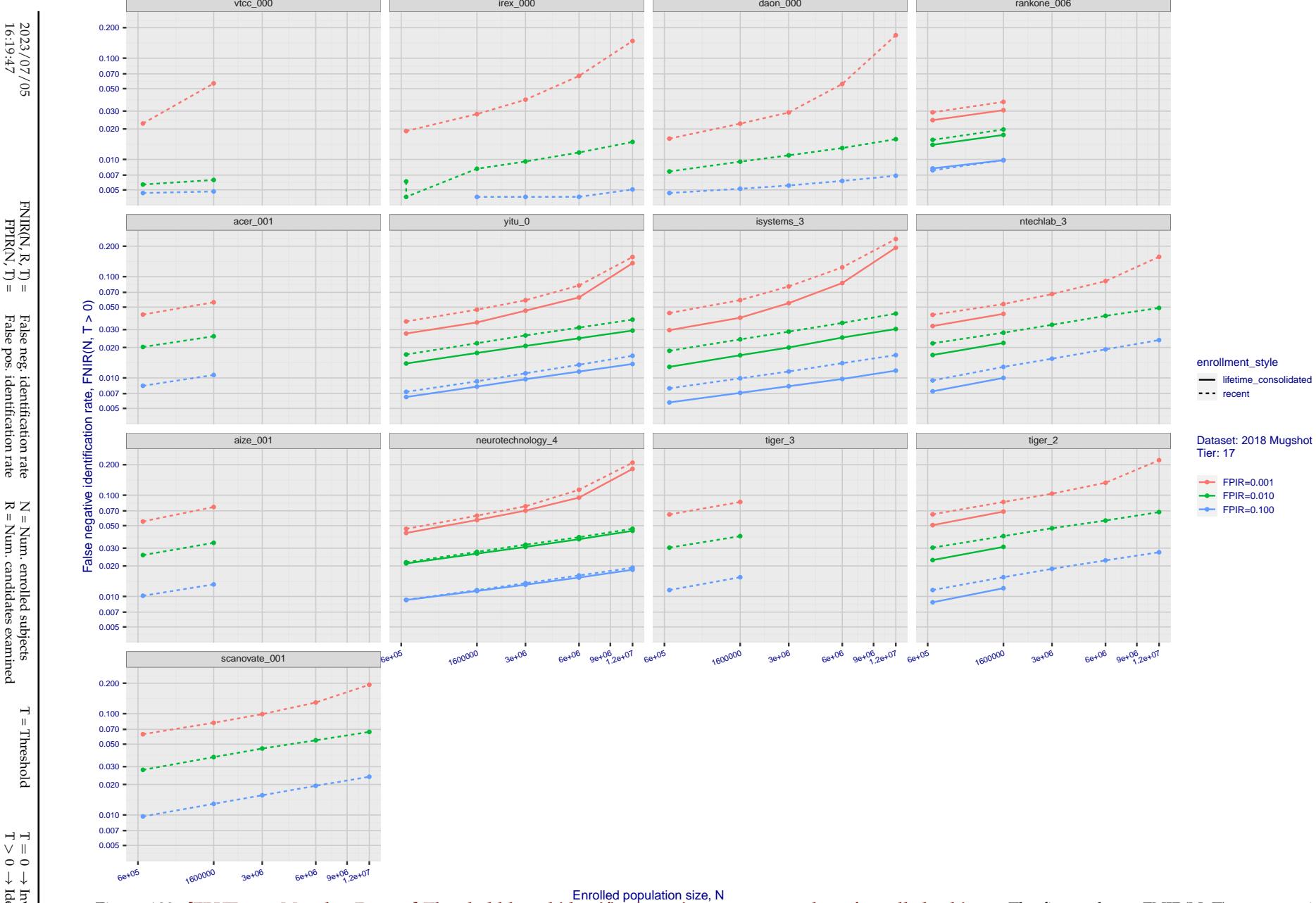


Figure 100: [FRVT-2018 Mugshot Dataset] Threshold-based identification miss rates vs. number of enrolled subjects. The figure shows $\text{FNIR}(N, T)$ across various gallery sizes when the threshold is set to achieve the given FPIRs. The rank criterion is irrelevant at high thresholds as mates are always at rank 1. The results are computed from the trials listed in rows 1-10 of Table 1. Less accurate algorithms were not run on large N , so results are missing. For clarity, results are sorted and reported into tiers spanning multiple pages. The tiering criteria is complicated: First paging by $\text{FNIR}(N_b, 1, 0)$, then sorting by median $\text{FNIR}(N_b, T)$, $N_b = 640\,000$.

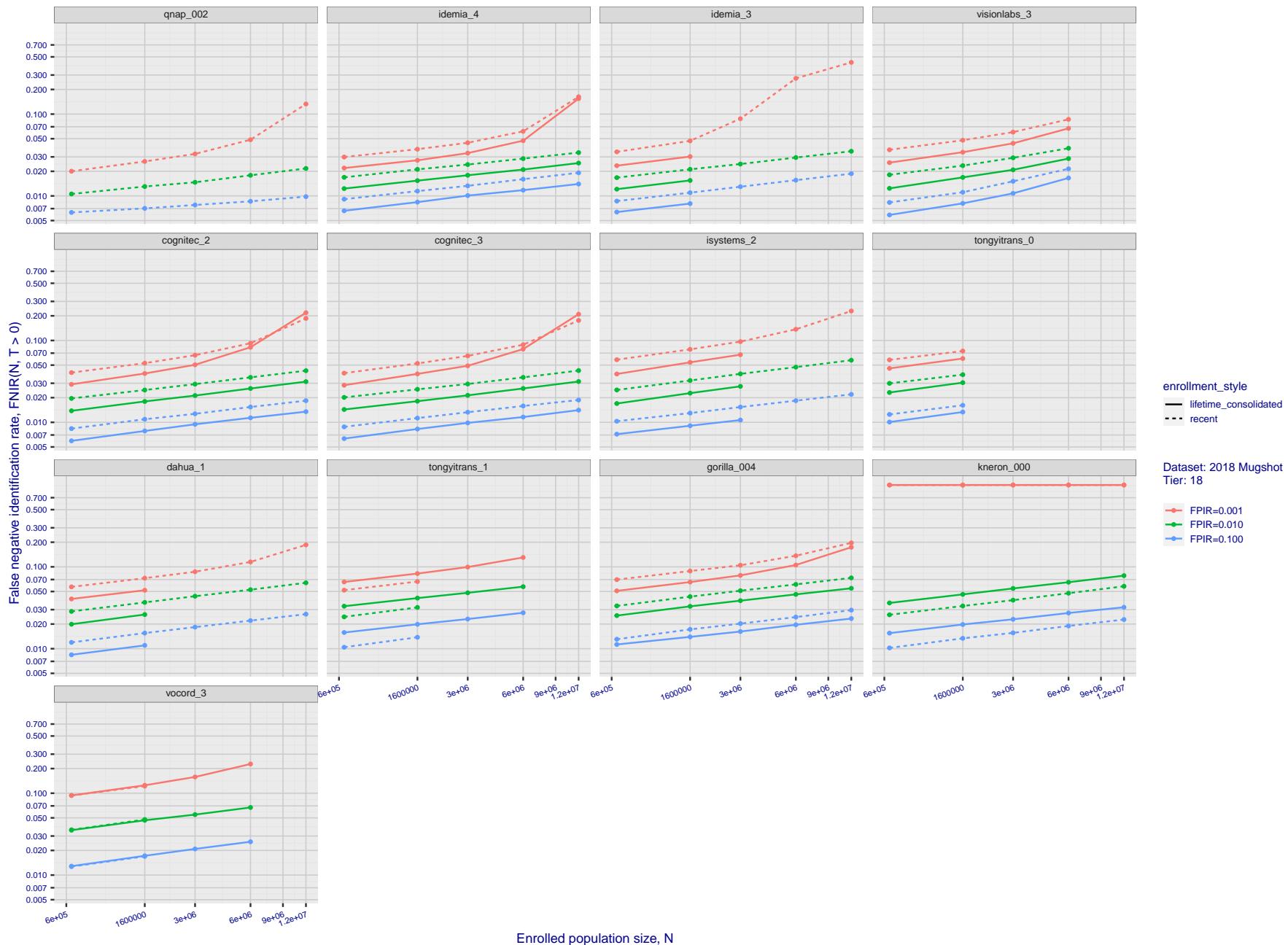


Figure 101: [FRVT-2018 Mugshot Dataset] Threshold-based identification miss rates vs. number of enrolled subjects. The figure shows $\text{FNIR}(N, T)$ across various gallery sizes when the threshold is set to achieve the given FPIRs. The rank criterion is irrelevant at high thresholds as mates are always at rank 1. The results are computed from the trials listed in rows 1-10 of Table 1. Less accurate algorithms were not run on large N , so results are missing. For clarity, results are sorted and reported into tiers spanning multiple pages. The tiering criteria is complicated: First paging by $\text{FNIR}(N_b, 1, 0)$, then sorting by median $\text{FNIR}(N_b, T)$, $N_b = 640\,000$.

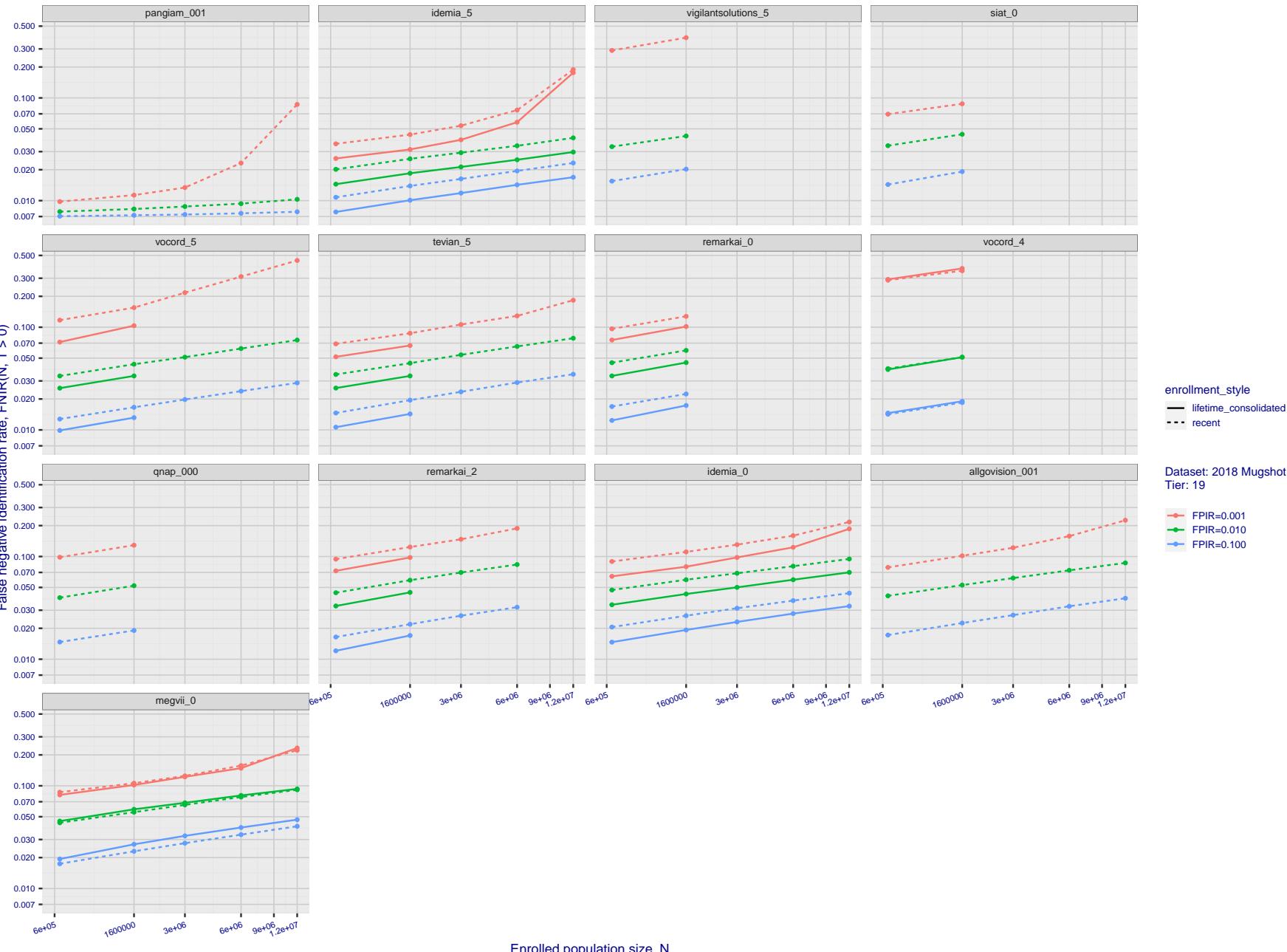


Figure 102: [FRVT-2018 Mugshot Dataset] Threshold-based identification miss rates vs. number of enrolled subjects. The figure shows FNIR(N, T) across various gallery sizes when the threshold is set to achieve the given FPIRs. The rank criterion is irrelevant at high thresholds as mates are always at rank 1. The results are computed from the trials listed in rows 1-10 of Table 1. Less accurate algorithms were not run on large N , so results are missing. For clarity, results are sorted and reported into tiers spanning multiple pages. The tiering criteria is complicated: First paging by $\text{FNIR}(N_b, 1, 0)$, then sorting by median $\text{FNIR}(N_b, T)$, $N_b = 640\,000$.

2023/07/05
16:19:47FNIR(N, R, T) = False neg. identification rate
FPIR(N, T) = False pos. identification rateN = Num. enrolled subjects
R = Num. candidates examinedT = Threshold
T = 0 → Investigation

T > 0 → Identification

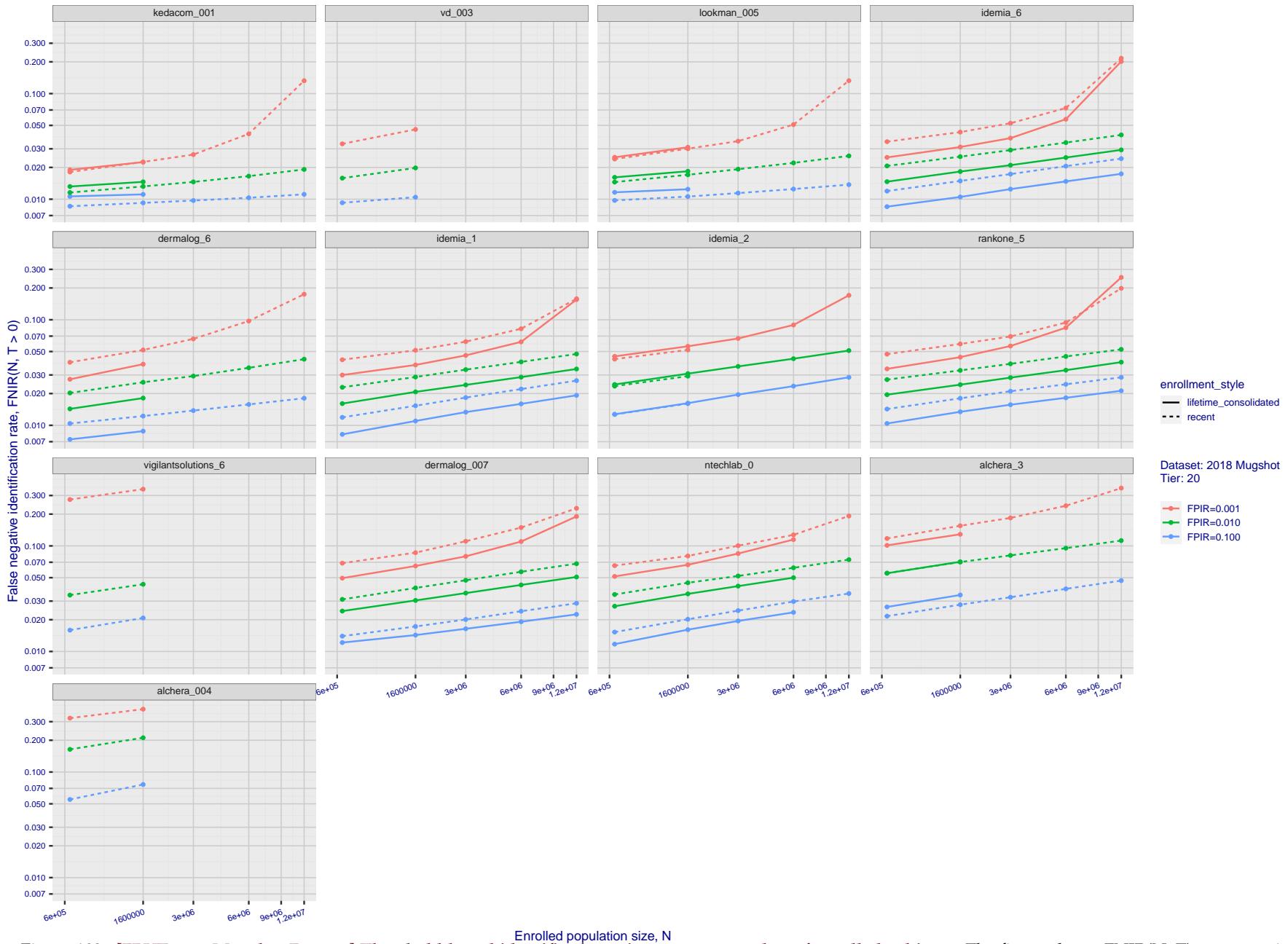


Figure 103: [FRVT-2018 Mugshot Dataset] Threshold-based identification miss rates vs. number of enrolled subjects. The figure shows FNIR(N, T) across various gallery sizes when the threshold is set to achieve the given FPIRs. The rank criterion is irrelevant at high thresholds as mates are always at rank 1. The results are computed from the trials listed in rows 1-10 of Table 1. Less accurate algorithms were not run on large N , so results are missing. For clarity, results are sorted and reported into tiers spanning multiple pages. The tiering criteria is complicated: First paging by $\text{FNIR}(N_b, 1, 0)$, then sorting by median $\text{FNIR}(N_b, T)$, $N_b = 640\,000$.

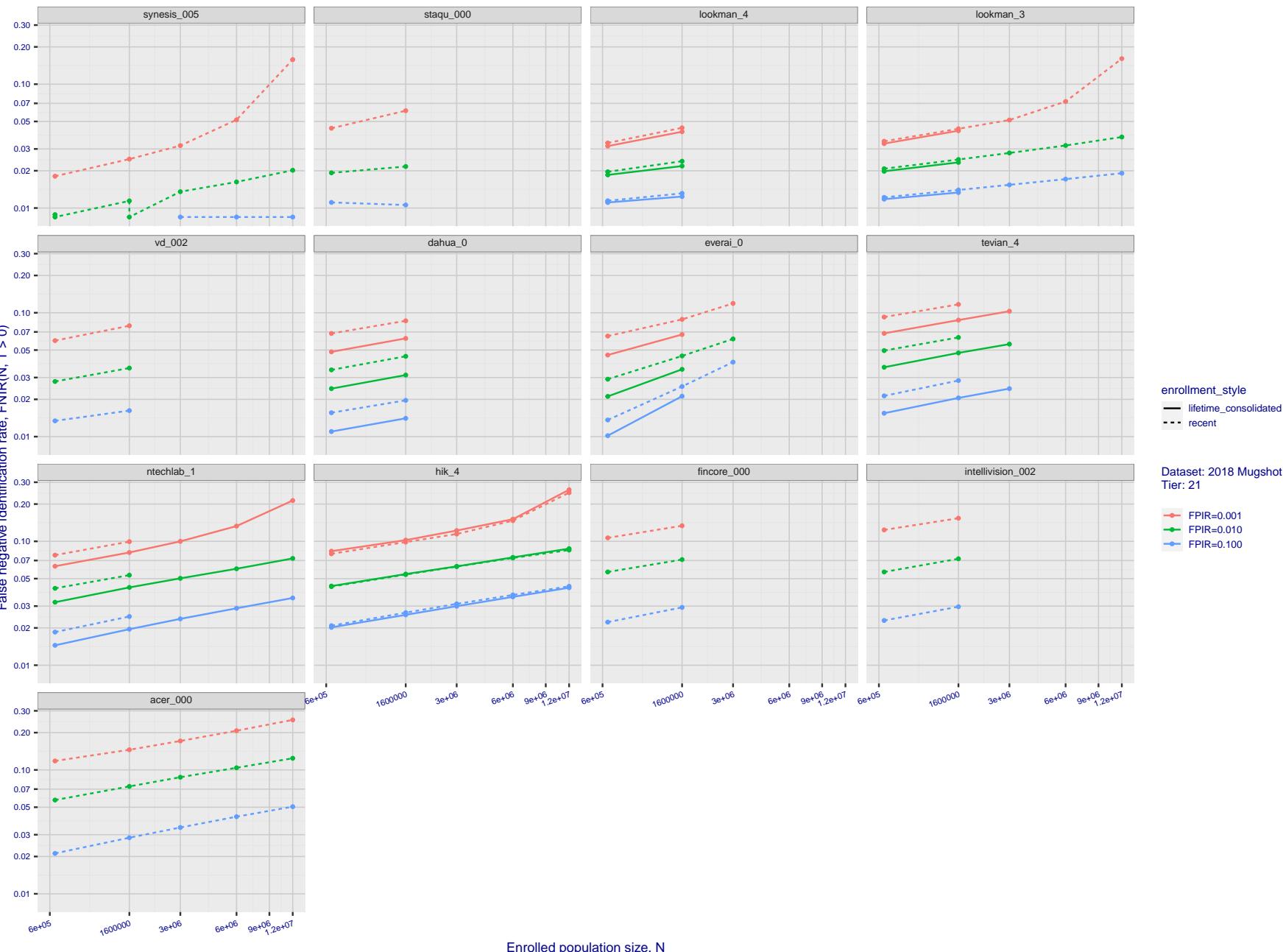
2023/07/05
16:19:47

Figure 104: [FRVT-2018 Mugshot Dataset] Threshold-based identification miss rates vs. number of enrolled subjects. The figure shows FNIR(N, T) across various gallery sizes when the threshold is set to achieve the given FPIRs. The rank criterion is irrelevant at high thresholds as mates are always at rank 1. The results are computed from the trials listed in rows 1-10 of Table 1. Less accurate algorithms were not run on large N , so results are missing. For clarity, results are sorted and reported into tiers spanning multiple pages. The tiering criteria is complicated: First paging by FNIR($N_b, 1, 0$), then sorting by median FNIR(N_b, T), $N_b = 640\,000$.

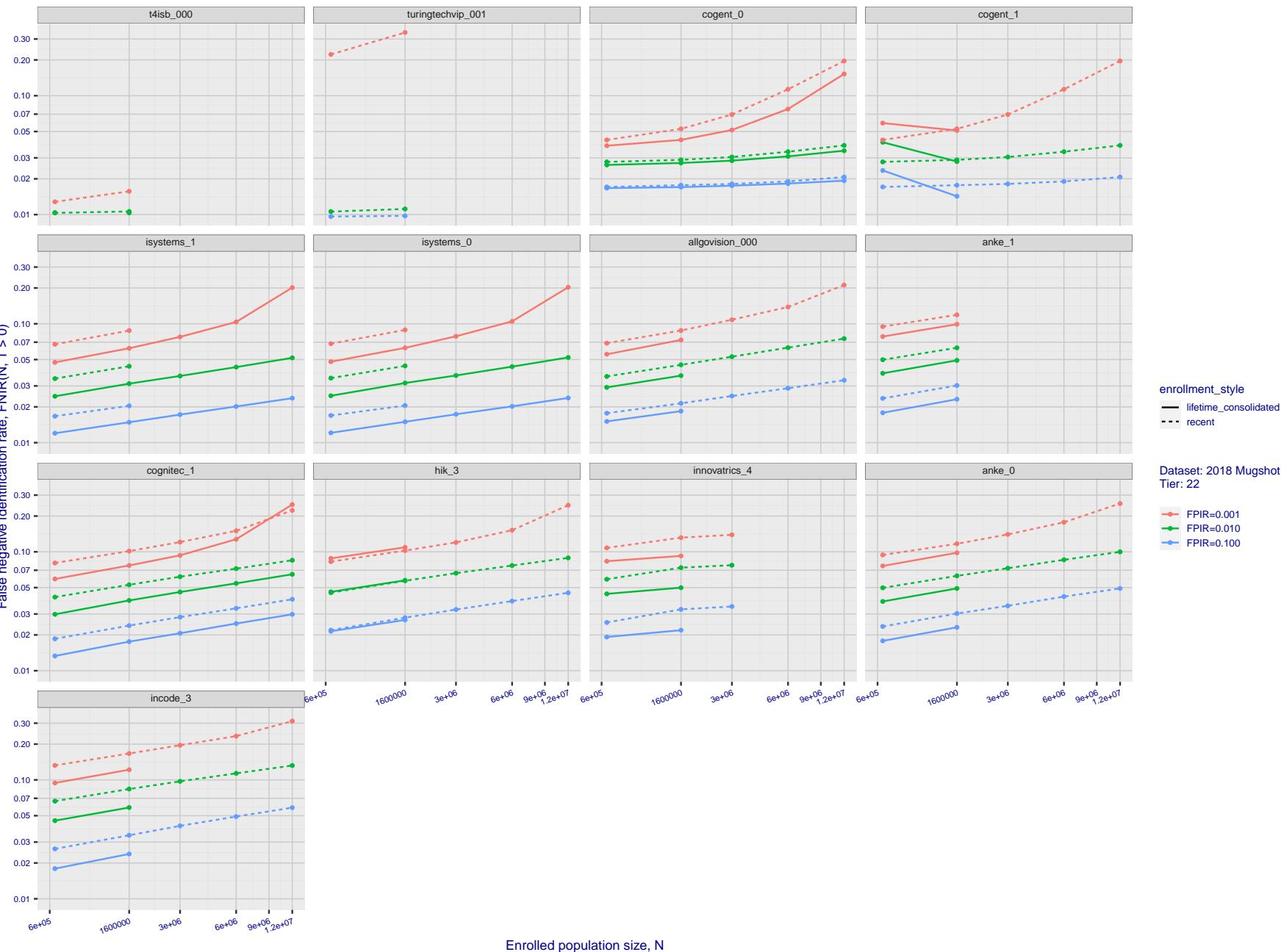
2023/07/05
16:19:47

Figure 105: [FRVT-2018 Mugshot Dataset] Threshold-based identification miss rates vs. number of enrolled subjects. The figure shows FNIR(N, T) across various gallery sizes when the threshold is set to achieve the given FPIRs. The rank criterion is irrelevant at high thresholds as mates are always at rank 1. The results are computed from the trials listed in rows 1-10 of Table 1. Less accurate algorithms were not run on large N , so results are missing. For clarity, results are sorted and reported into tiers spanning multiple pages. The tiering criteria is complicated: First paging by $FNIR(N_b, 1, 0)$, then sorting by median $FNIR(N_b, T)$, $N_b = 640\,000$.

2023/07/05
16:19:47FNIR(N, R, T) = False neg. identification rate
FPIR(N, T) = False pos. identification rateN = Num. enrolled subjects
R = Num. candidates examined

T = Threshold

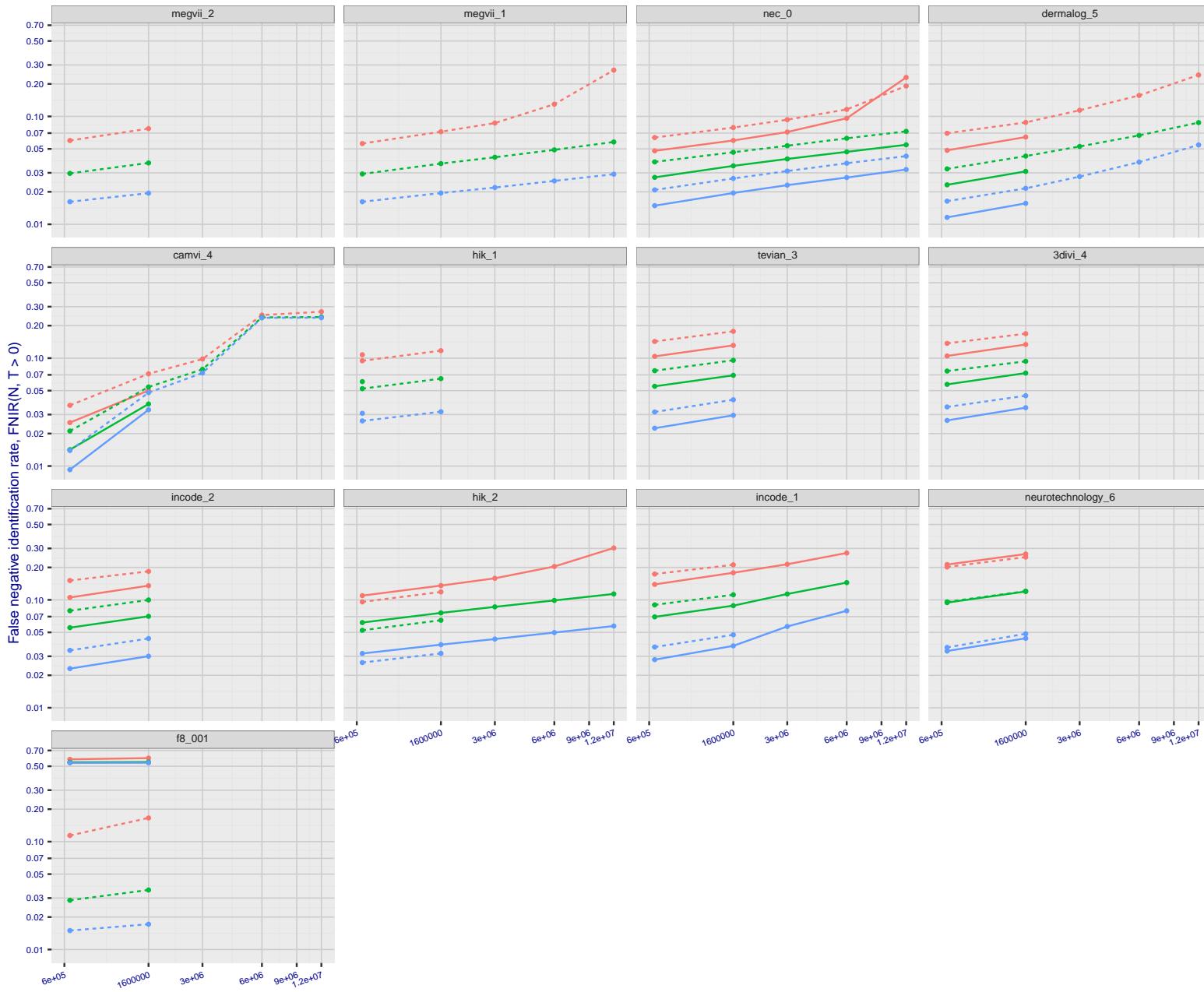
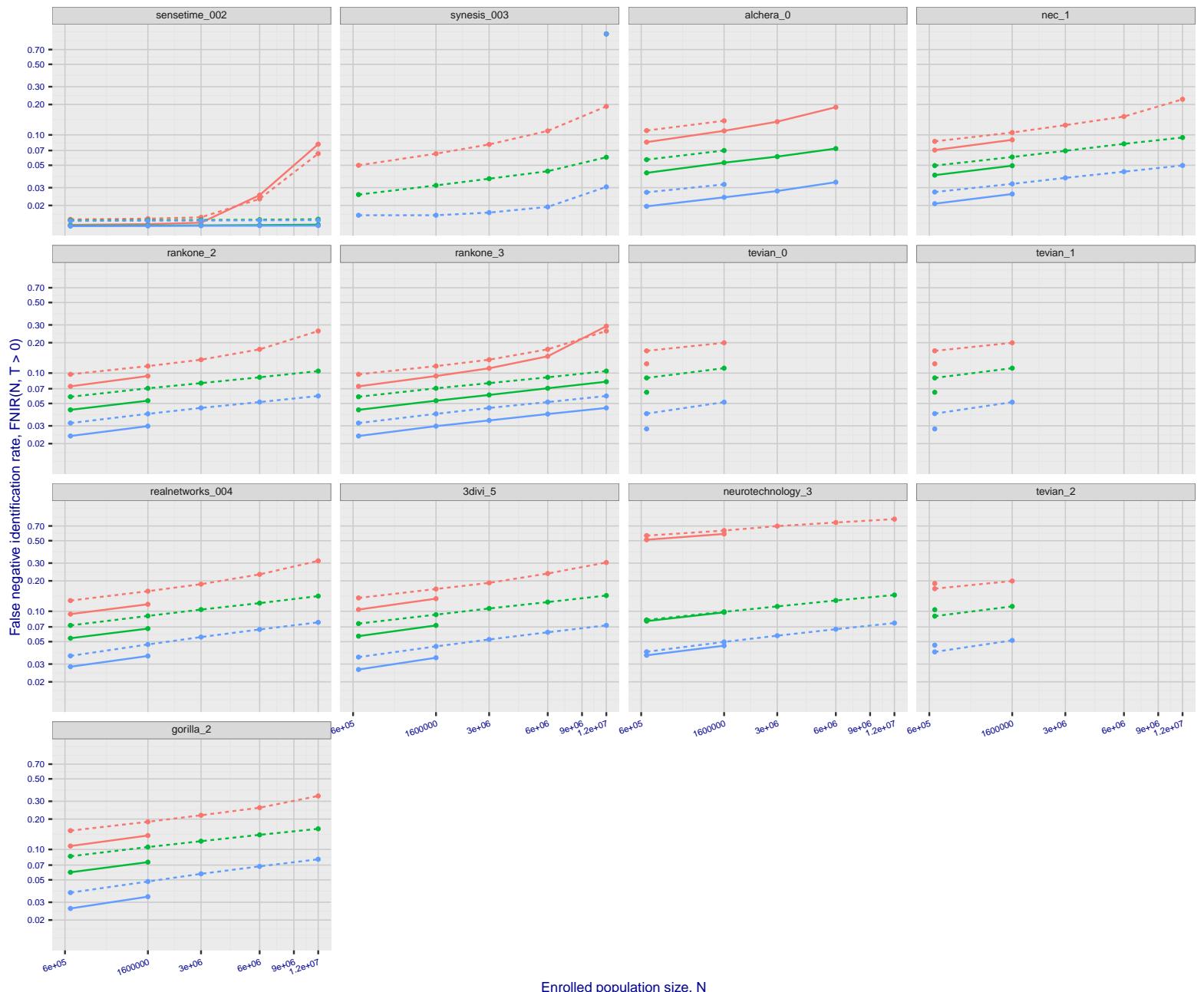
T = 0 → Investigation
 $T > 0 \rightarrow$ Identification

Figure 106: [FRVT-2018 Mugshot Dataset] Threshold-based identification miss rates vs. number of enrolled subjects. The figure shows FNIR(N, T) across various gallery sizes when the threshold is set to achieve the given FPIRs. The rank criterion is irrelevant at high thresholds as mates are always at rank 1. The results are computed from the trials listed in rows 1-10 of Table 1. Less accurate algorithms were not run on large N, so results are missing. For clarity, results are sorted and reported into tiers spanning multiple pages. The tiering criteria is complicated: First paging by $\text{FNIR}(N_b, 1, 0)$, then sorting by median $\text{FNIR}(N_b, T)$, $N_b = 640\,000$.



Dataset: 2018 Mugshot
Tier: 24

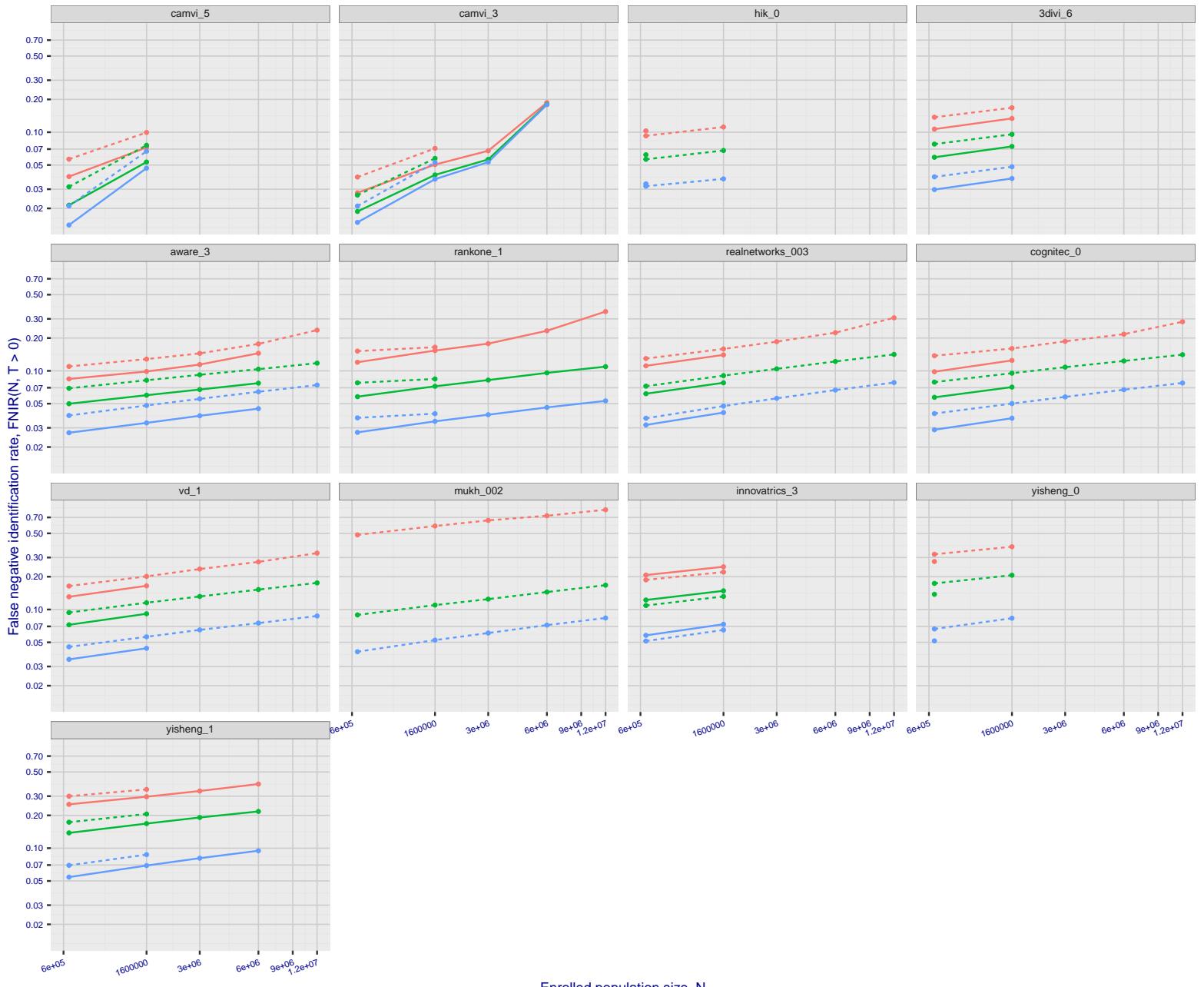
FPIR=0.001
FPIR=0.010
FPIR=0.100

enrollment_style
— lifetime Consolidated
- - recent

Figure 107: [FRVT-2018 Mugshot Dataset] Threshold-based identification miss rates vs. number of enrolled subjects. The figure shows FNIR(N, T) across various gallery sizes when the threshold is set to achieve the given FPIRs. The rank criterion is irrelevant at high thresholds as mates are always at rank 1. The results are computed from the trials listed in rows 1-10 of Table 1. Less accurate algorithms were not run on large N , so results are missing. For clarity, results are sorted and reported into tiers spanning multiple pages. The tiering criteria is complicated: First paging by $\text{FNIR}(N_b, 1, 0)$, then sorting by median $\text{FNIR}(N_b, T)$, $N_b = 640\,000$.

2023/07/05
16:19:47FNIR(N, R, T) = False neg. identification rate
FPIR(N, T) = False pos. identification rateN = Num. enrolled subjects
R = Num. candidates examined

T = Threshold

T = 0 → Investigation
T > 0 → Identification

enrollment_style
— lifetime-consolidated
- - - recent

Dataset: 2018 Mugshot
Tier: 25

FPIR=0.001
FPIR=0.010
FPIR=0.100

Figure 108: [FRVT-2018 Mugshot Dataset] Threshold-based identification miss rates vs. number of enrolled subjects. The figure shows FNIR(N, T) across various gallery sizes when the threshold is set to achieve the given FPIRs. The rank criterion is irrelevant at high thresholds as mates are always at rank 1. The results are computed from the trials listed in rows 1-10 of Table 1. Less accurate algorithms were not run on large N, so results are missing. For clarity, results are sorted and reported into tiers spanning multiple pages. The tiering criteria is complicated: First paging by FNIR(N_b , 1, 0), then sorting by median FNIR(N_b , T), $N_b = 640\,000$.

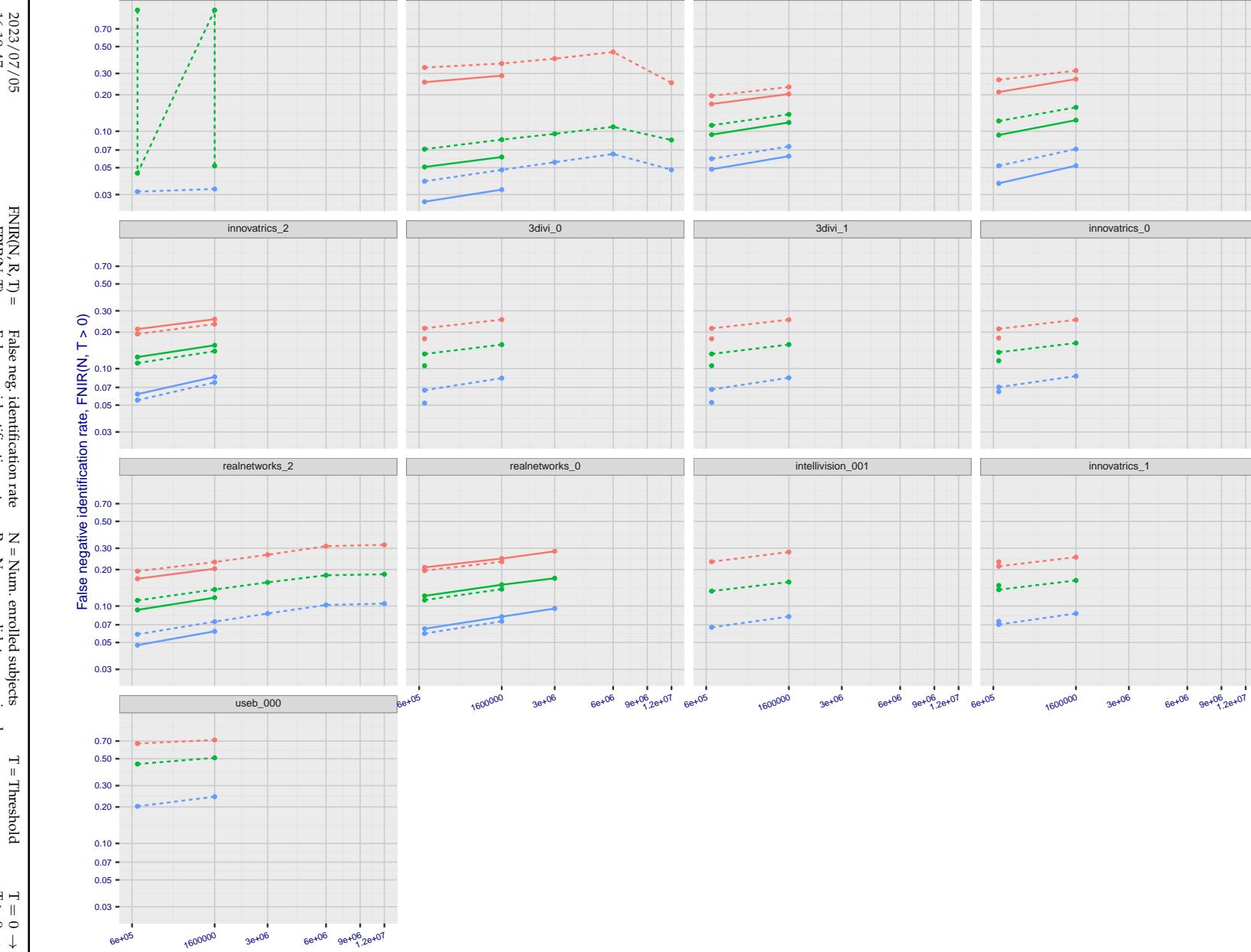


Figure 109: [FRVT-2018 Mugshot Dataset] Threshold-based identification miss rates vs. number of enrolled subjects. The figure shows $\text{FNIR}(N, T)$ across various gallery sizes when the threshold is set to achieve the given FPIRs. The rank criterion is irrelevant at high thresholds as mates are always at rank 1. The results are computed from the trials listed in rows 1-10 of Table 1. Less accurate algorithms were not run on large N , so results are missing. For clarity, results are sorted and reported into tiers spanning multiple pages. The tiering criteria is complicated: First paging by $\text{FNIR}(N_b, 1, 0)$, then sorting by median $\text{FNIR}(N_b, T)$, $N_b = 640\,000$.

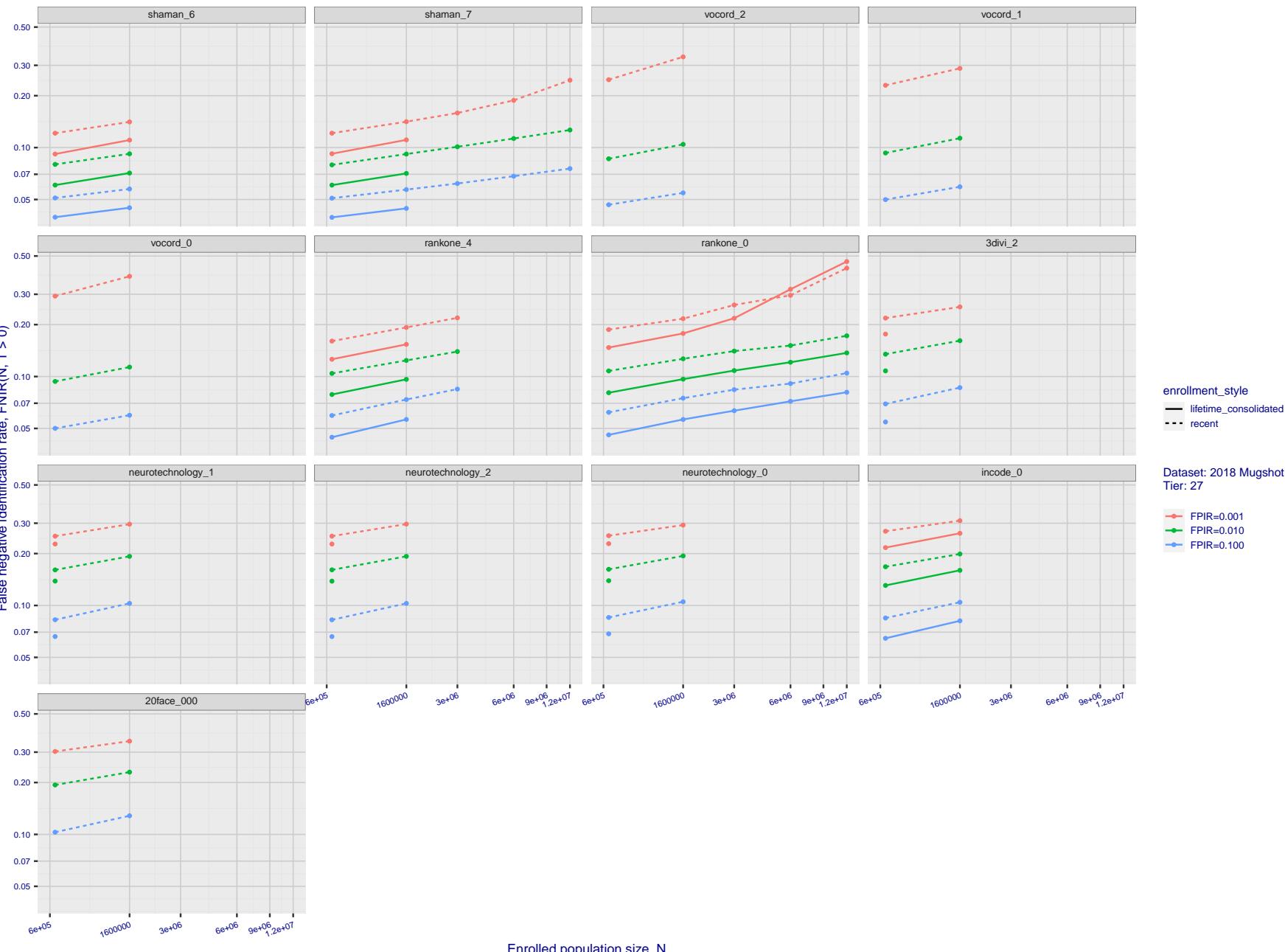
2023/07/05
16:19:47

Figure 110: [FRVT-2018 Mugshot Dataset] Threshold-based identification miss rates vs. number of enrolled subjects. The figure shows FNIR(N, T) across various gallery sizes when the threshold is set to achieve the given FPIRs. The rank criterion is irrelevant at high thresholds as mates are always at rank 1. The results are computed from the trials listed in rows 1-10 of Table 1. Less accurate algorithms were not run on large N , so results are missing. For clarity, results are sorted and reported into tiers spanning multiple pages. The tiering criteria is complicated: First paging by $\text{FNIR}(N_b, 1, 0)$, then sorting by median $\text{FNIR}(N_b, T)$, $N_b = 640\,000$.

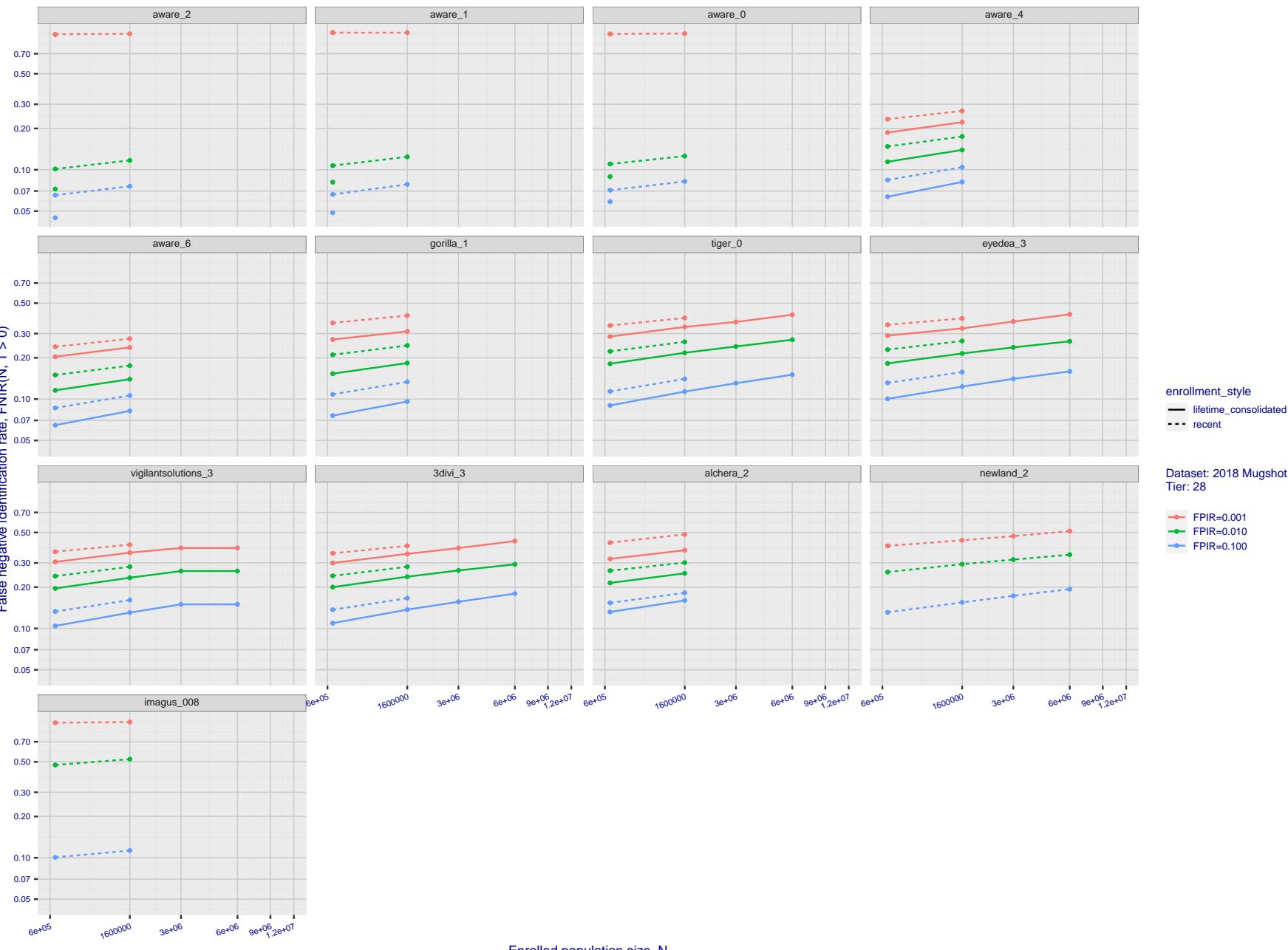
2023/07/05
16:19:47

Figure 111: [FRVT-2018 Mugshot Dataset] Threshold-based identification miss rates vs. number of enrolled subjects. The figure shows FNIR(N, T) across various gallery sizes when the threshold is set to achieve the given FPIRs. The rank criterion is irrelevant at high thresholds as mates are always at rank 1. The results are computed from the trials listed in rows 1-10 of Table 1. Less accurate algorithms were not run on large N , so results are missing. For clarity, results are sorted and reported into tiers spanning multiple pages. The tiering criteria is complicated: First paging by $FNIR(N_b, 1, 0)$, then sorting by median $FNIR(N_b, T)$, $N_b = 640\,000$.

2023/07/05
16:19:47FNIR(N, R, T) = False neg. identification rate
FPIR(N, T) = False pos. identification rateN = Num. enrolled subjects
R = Num. candidates examined

T = Threshold

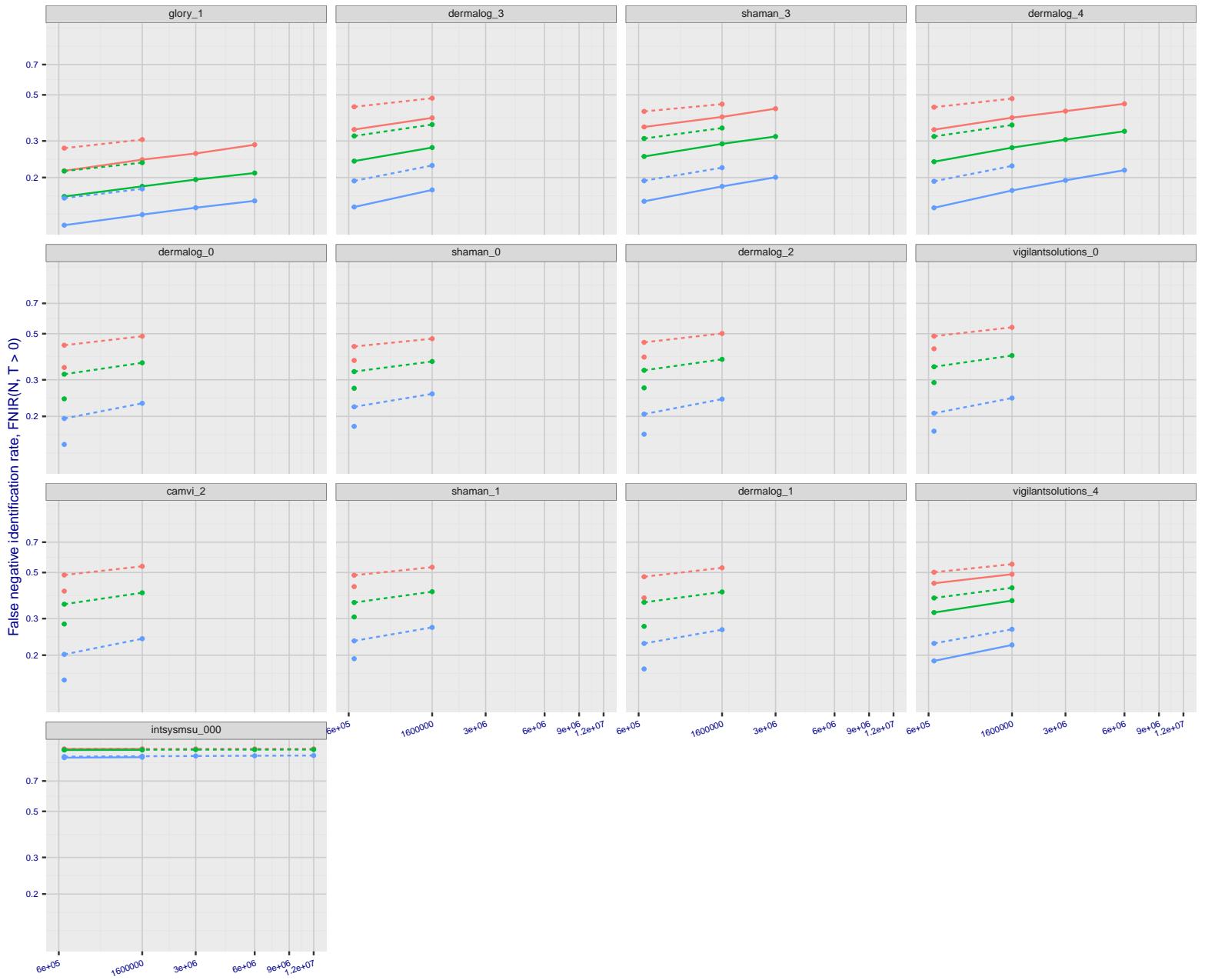
T = 0 → Investigation
T > 0 → Identification

Figure 112: [FRVT-2018 Mugshot Dataset] Threshold-based identification miss rates vs. number of enrolled subjects. The figure shows FNIR(N, T) across various gallery sizes when the threshold is set to achieve the given FPIRs. The rank criterion is irrelevant at high thresholds as mates are always at rank 1. The results are computed from the trials listed in rows 1-10 of Table 1. Less accurate algorithms were not run on large N, so results are missing. For clarity, results are sorted and reported into tiers spanning multiple pages. The tiering criteria is complicated: First paging by FNIR(N_b , 1, 0), then sorting by median FNIR(N_b , T), $N_b = 640\,000$.

2023/07/05
16:19:47FNIR(N, R, T) = False neg. identification rate
FPIR(N, T) = False pos. identification rateN = Num. enrolled subjects
R = Num. candidates examined

T = Threshold

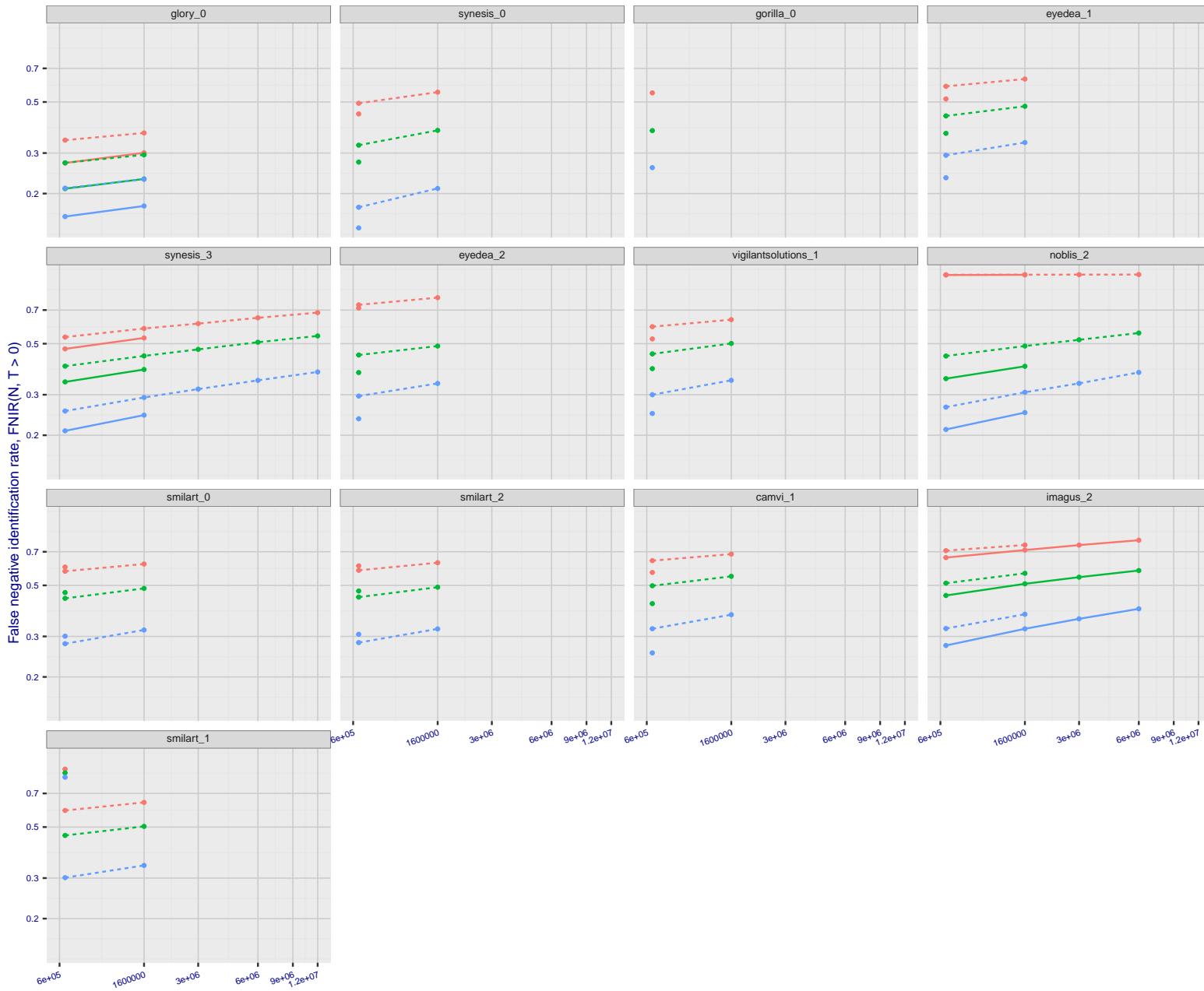
T = 0 → Investigation
T > 0 → Identification

Figure 113: [FRVT-2018 Mugshot Dataset] Threshold-based identification miss rates vs. number of enrolled subjects. The figure shows FNIR(N, T) across various gallery sizes when the threshold is set to achieve the given FPIRs. The rank criterion is irrelevant at high thresholds as mates are always at rank 1. The results are computed from the trials listed in rows 1-10 of Table 1. Less accurate algorithms were not run on large N , so results are missing. For clarity, results are sorted and reported into tiers spanning multiple pages. The tiering criteria is complicated: First paging by $\text{FNIR}(N_b, 1, 0)$, then sorting by median $\text{FNIR}(N_b, T)$, $N_b = 640\,000$.

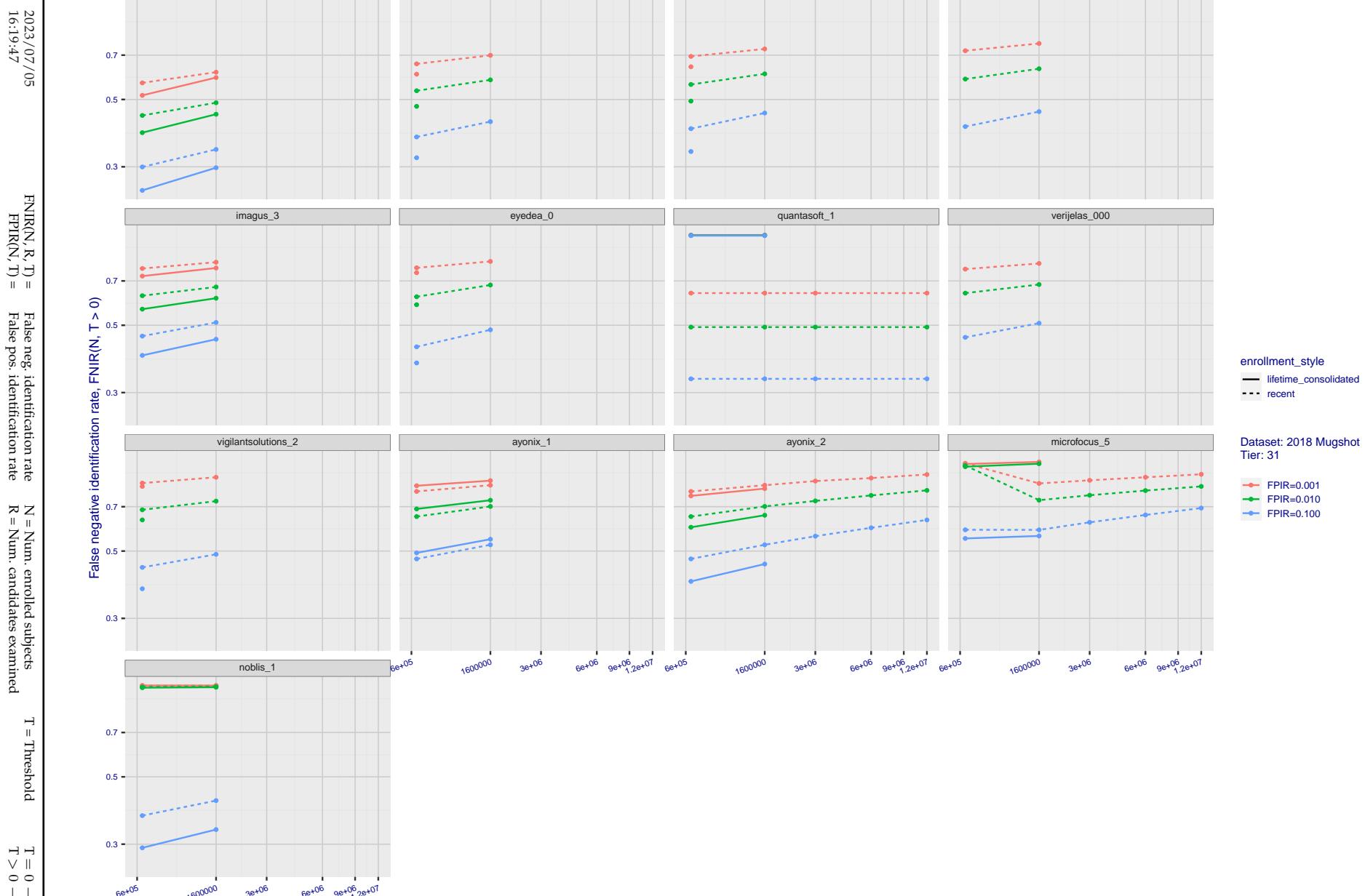


Figure 114: [FRVT-2018 Mugshot Dataset] Threshold-based identification miss rates vs. number of enrolled subjects. The figure shows FNIR(N, T) across various gallery sizes when the threshold is set to achieve the given FPIRs. The rank criterion is irrelevant at high thresholds as mates are always at rank 1. The results are computed from the trials listed in rows 1-10 of Table 1. Less accurate algorithms were not run on large N , so results are missing. For clarity, results are sorted and reported into tiers spanning multiple pages. The tiering criteria is complicated: First paging by $\text{FNIR}(N_b, 1, 0)$, then sorting by median $\text{FNIR}(N_b, T)$, $N_b = 640\,000$.

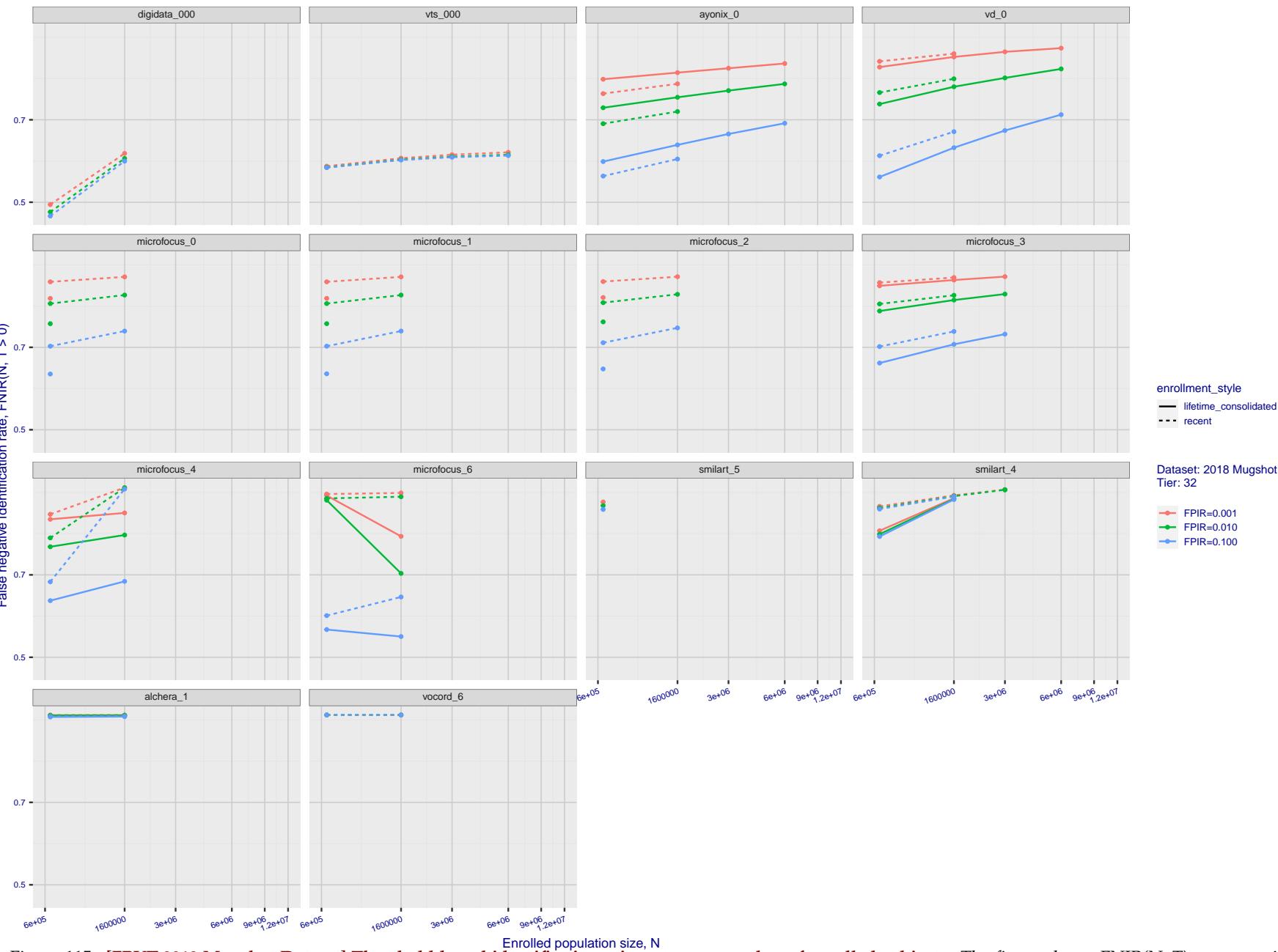
2023/07/05
16:19:47

Figure 115: [FRVT-2018 Mugshot Dataset] Threshold-based identification miss rates vs. number of enrolled subjects. The figure shows FNIR(N, T) across various gallery sizes when the threshold is set to achieve the given FPIRs. The rank criterion is irrelevant at high thresholds as mates are always at rank 1. The results are computed from the trials listed in rows 1-10 of Table 1. Less accurate algorithms were not run on large N , so results are missing. For clarity, results are sorted and reported into tiers spanning multiple pages. The tiering criteria is complicated: First paging by $\text{FNIR}(N_b, 1, 0)$, then sorting by median $\text{FNIR}(N_b, T)$, $N_b = 640\,000$.

2023/07/05
16:19:47

FNIR(N, R, T) = False neg. identification rate
FPTR(N, T) = False pos. identification rate

N = Num. enrolled subjects
R = Num. candidates examined
T = Threshold
T = 0 → Investigation
T > 0 → Identification

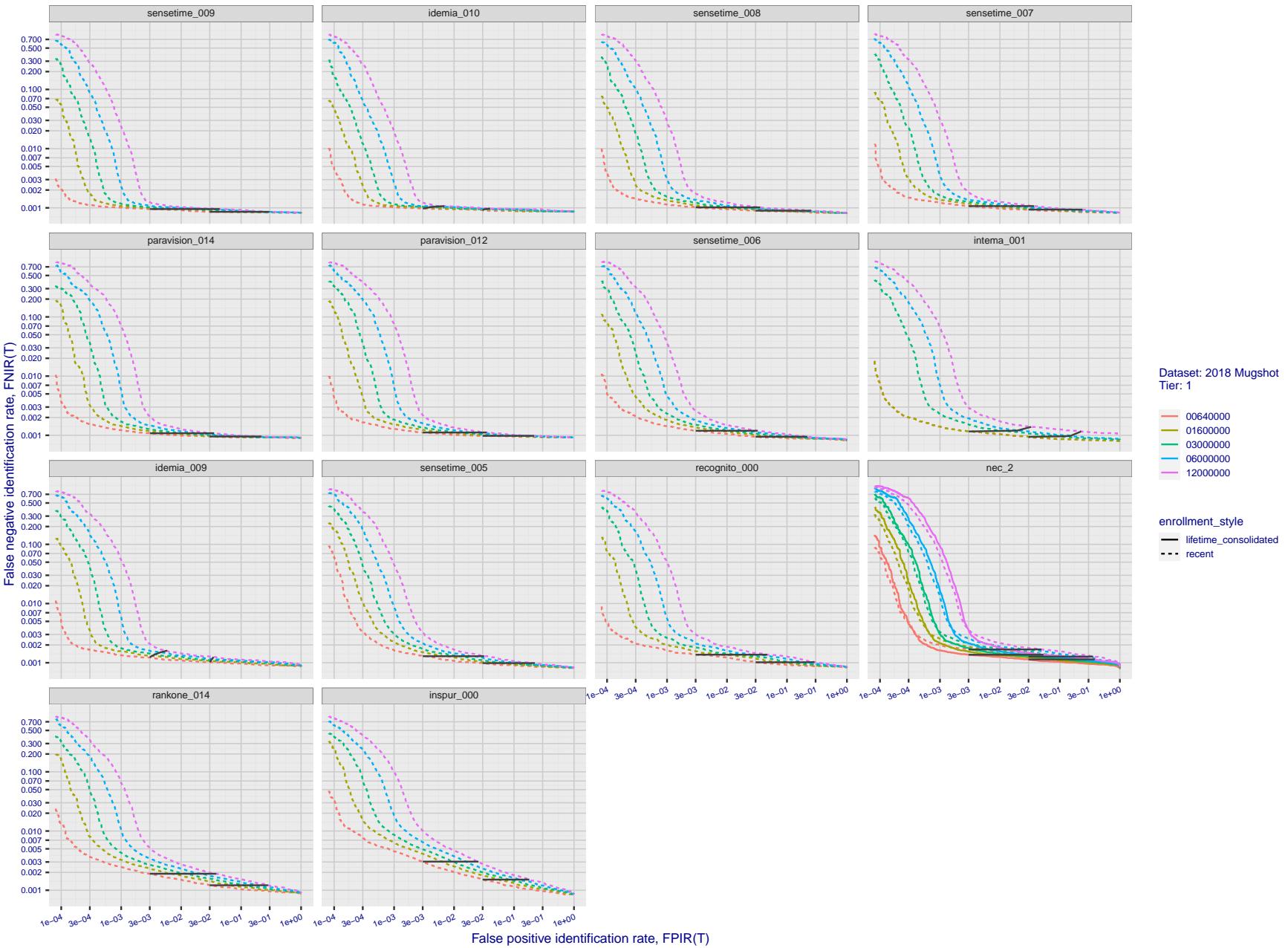
2023/07/05
16:19:47FNIR(N, R, T) = False neg. identification rate
FPIR(N, T) = False pos. identification rateN = Num. enrolled subjects
R = Num. candidates examinedT = Threshold
T = 0 → Investigation
T > 0 → Identification

Figure 116: [FRVT-2018 Mugshot Dataset] Identification miss rates vs. false positive rates. The figure shows miss rates $\text{FNIR}(N, L, T)$ as a function of $\text{FPIR}(N, T)$, with N ranging from 640 000 to 12 000 000 as noted in rows 1-10 of Table 1. These error tradeoff characteristics are useful for applications where a threshold must be elevated to limit false positives, such as when human reviewer labor is not matched to the volume of searches. Dark lines join points of equal threshold: If horizontal, $\text{FPIR}(T)$ rises with N , and mate scores are independent of N . Other algorithms adjust scores in an attempt to make FPIR independent of N .

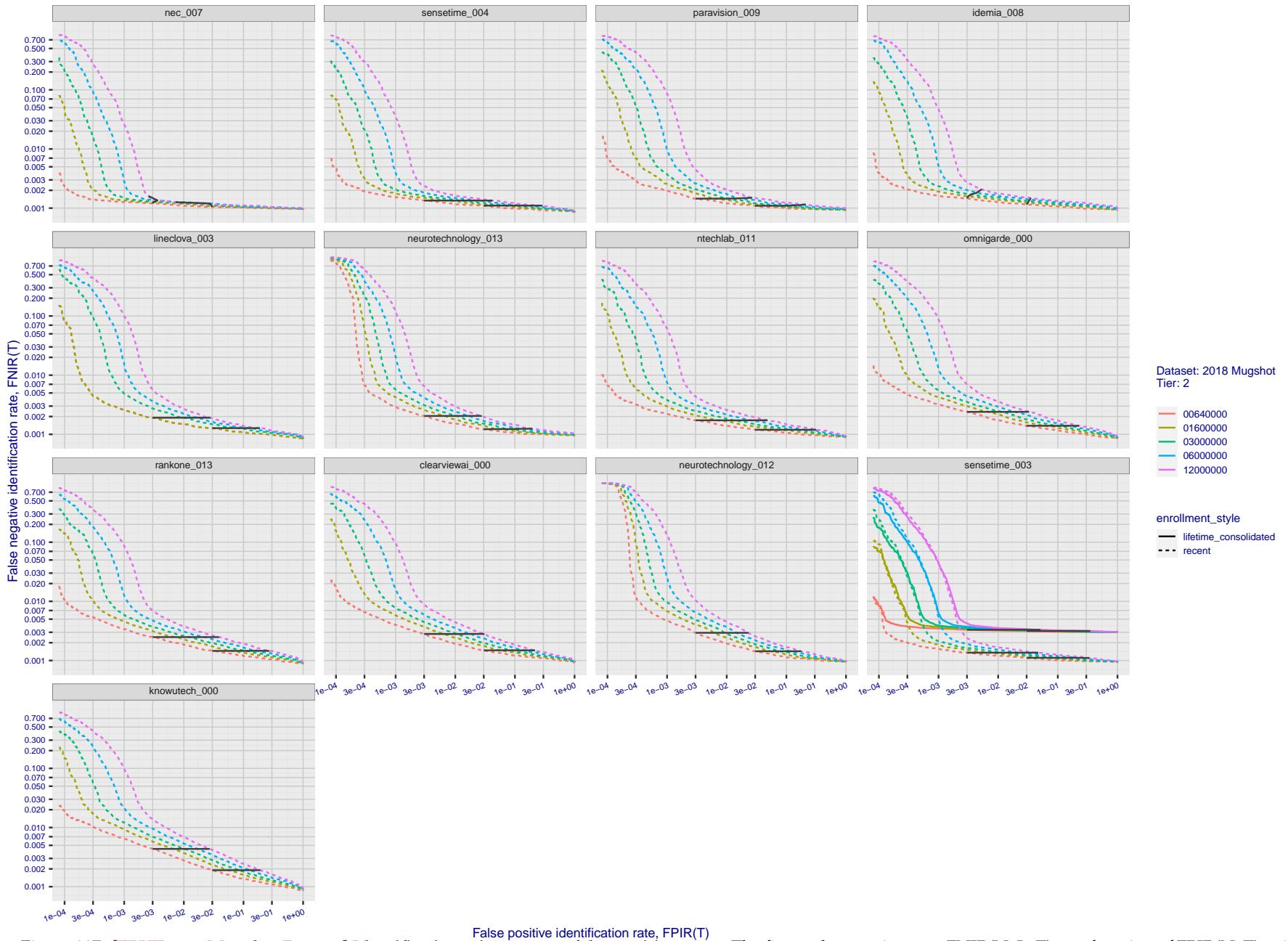


Figure 117: [FRVT-2018 Mugshot Dataset] Identification miss rates vs. false positive rates. The figure shows miss rates $\text{FNIR}(N, L, T)$ as a function of $\text{FPIR}(N, T)$, with N ranging from 640 000 to 12 000 000 as noted in rows 1-10 of Table 1. These error tradeoff characteristics are useful for applications where a threshold must be elevated to limit false positives, such as when human reviewer labor is not matched to the volume of searches. Dark lines join points of equal threshold: If horizontal, $\text{FPIR}(T)$ rises with N , and mate scores are independent of N . Other algorithms adjust scores in an attempt to make FPIR independent of N .

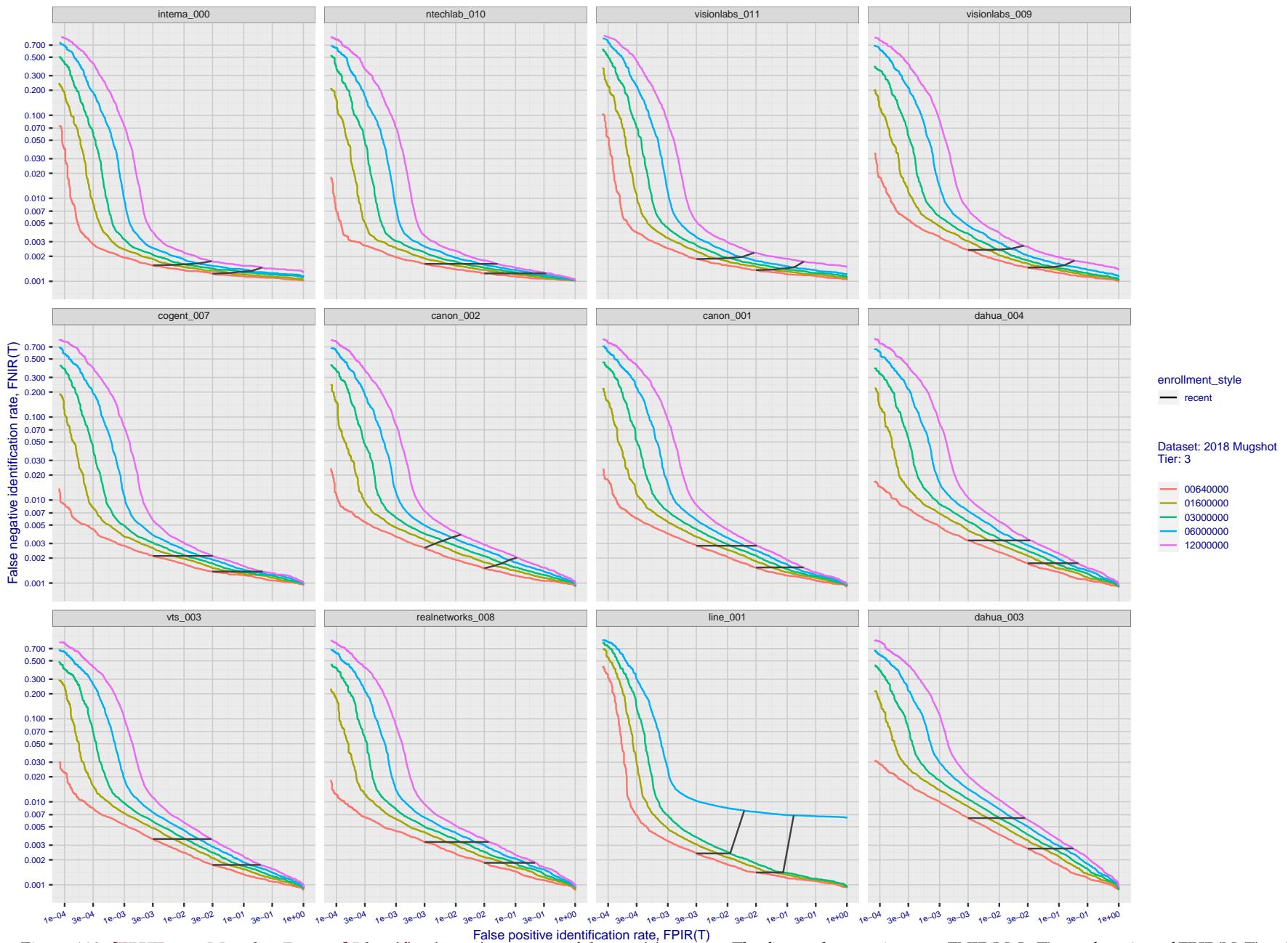


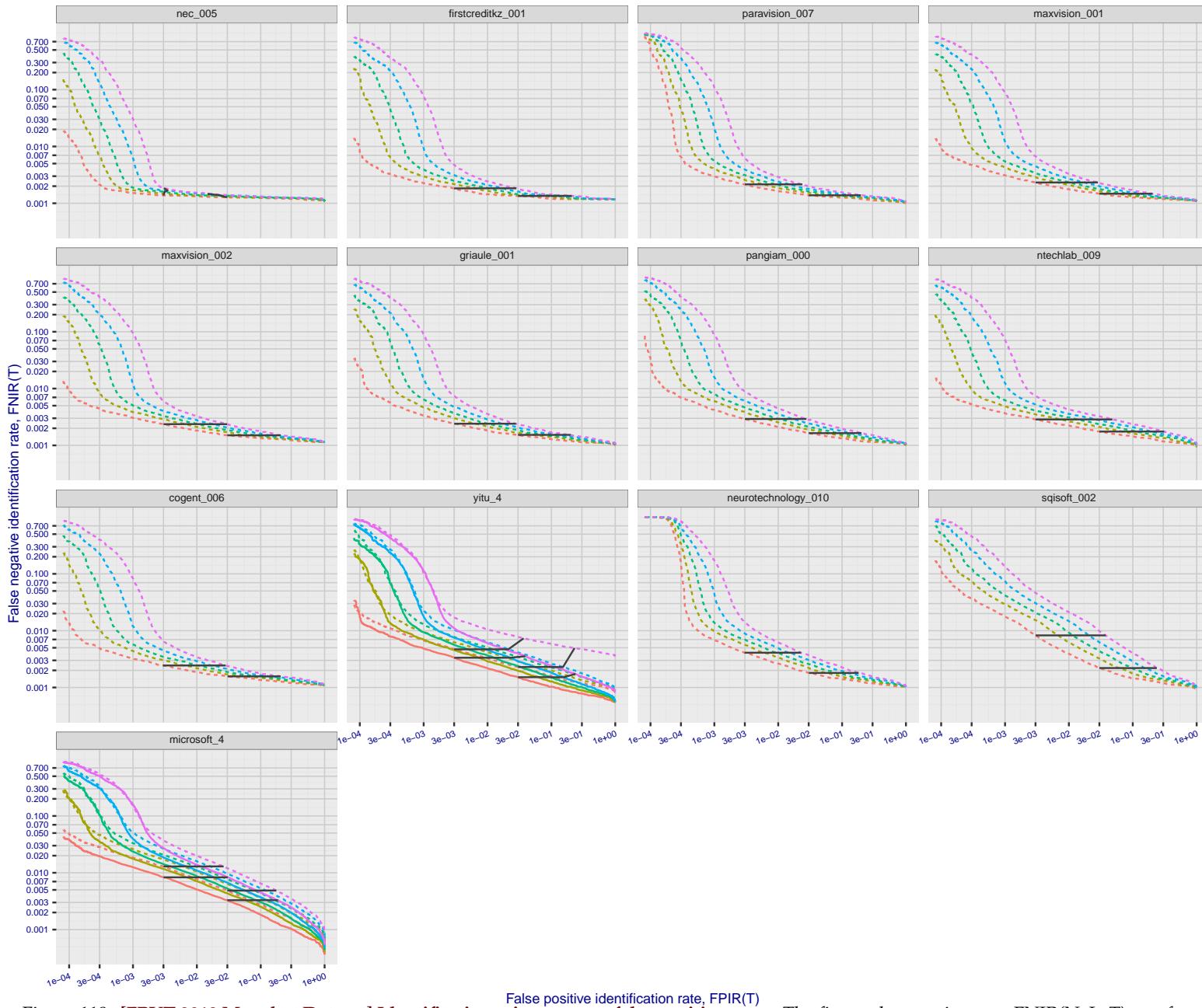
Figure 118: [FRVT-2018 Mugshot Dataset] Identification miss rates vs. false positive rates. The figure shows miss rates $\text{FNIR}(N, L, T)$ as a function of $\text{FPIR}(N, T)$, with N ranging from 640 000 to 12 000 000 as noted in rows 1-10 of Table 1. These error tradeoff characteristics are useful for applications where a threshold must be elevated to limit false positives, such as when human reviewer labor is not matched to the volume of searches. Dark lines join points of equal threshold: If horizontal, $\text{FPIR}(T)$ rises with N , and mate scores are independent of N . Other algorithms adjust scores in an attempt to make FPIR independent of N .

2023/07/05
16:19:47

$\text{FNIR}(N, R, T) =$ False neg. identification rate
 $\text{FPIR}(N, T) =$ False pos. identification rate

$N =$ Num. enrolled subjects
 $R =$ Num. candidates examined

$T =$ Threshold
 $T = 0 \rightarrow$ Investigation
 $T > 0 \rightarrow$ Identification



Dataset: 2018 Mugshot
Tier: 4

- 00640000
- 01600000
- 03000000
- 06000000
- 12000000

enrollment_style

- lifetime Consolidated
- recent

Figure 119: [FRVT-2018 Mugshot Dataset] Identification miss rates vs. false positive rates. The figure shows miss rates $\text{FNIR}(N, L, T)$ as a function of $\text{FPIR}(N, T)$, with N ranging from 640 000 to 12 000 000 as noted in rows 1-10 of Table 1. These error tradeoff characteristics are useful for applications where a threshold must be elevated to limit false positives, such as when human reviewer labor is not matched to the volume of searches. Dark lines join points of equal threshold: If horizontal, $\text{FPIR}(T)$ rises with N , and mate scores are independent of N . Other algorithms adjust scores in an attempt to make FPIR independent of N .

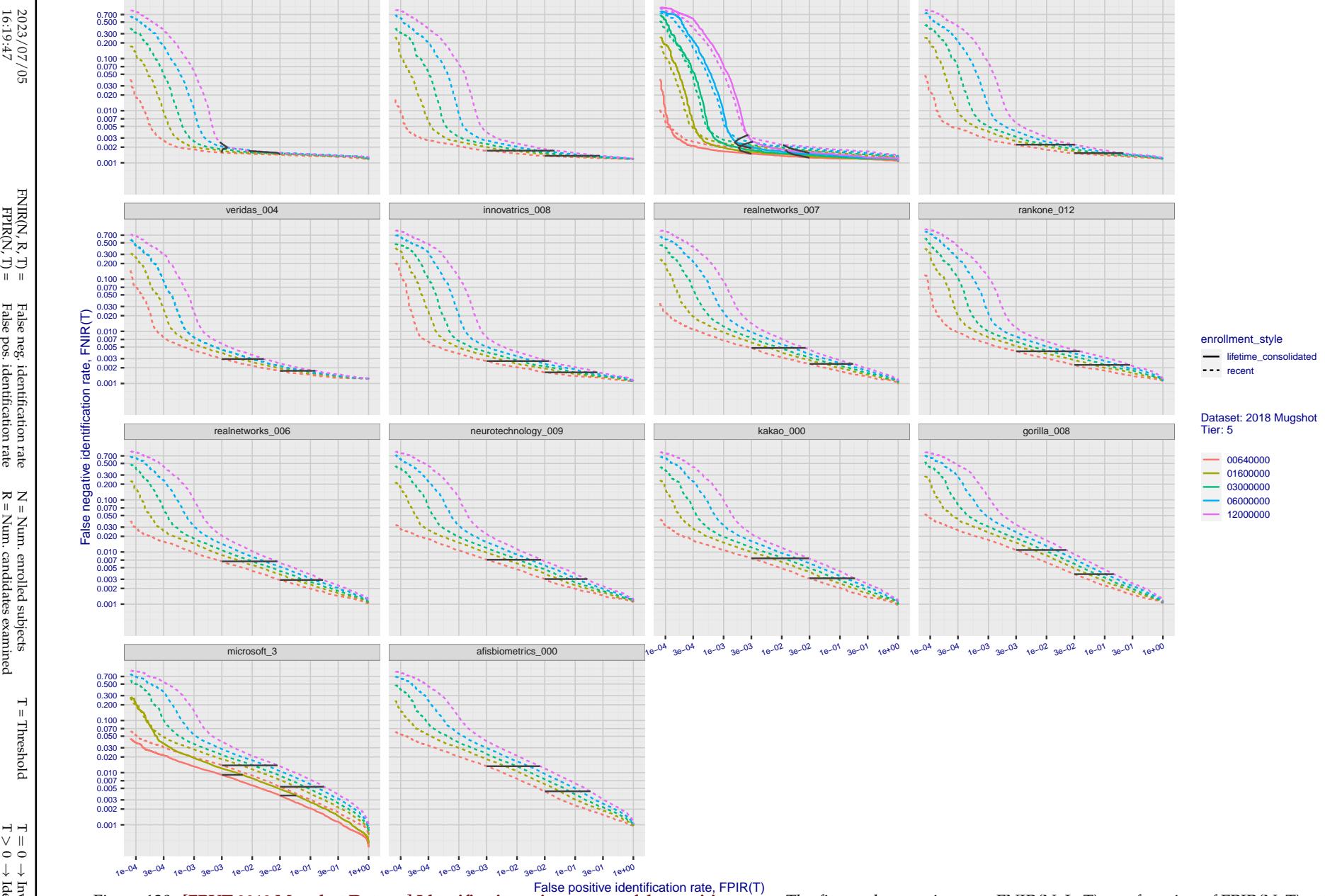


Figure 120: [FRVT-2018 Mugshot Dataset] Identification miss rates vs. false positive rates. The figure shows miss rates $\text{FNIR}(N, L, T)$ as a function of $\text{FPIR}(N, T)$, with N ranging from 640 000 to 12 000 000 as noted in rows 1-10 of Table 1. These error tradeoff characteristics are useful for applications where a threshold must be elevated to limit false positives, such as when human reviewer labor is not matched to the volume of searches. Dark lines join points of equal threshold: If horizontal, $\text{FPIR}(T)$ rises with N , and mate scores are independent of N . Other algorithms adjust scores in an attempt to make FPIR independent of N .

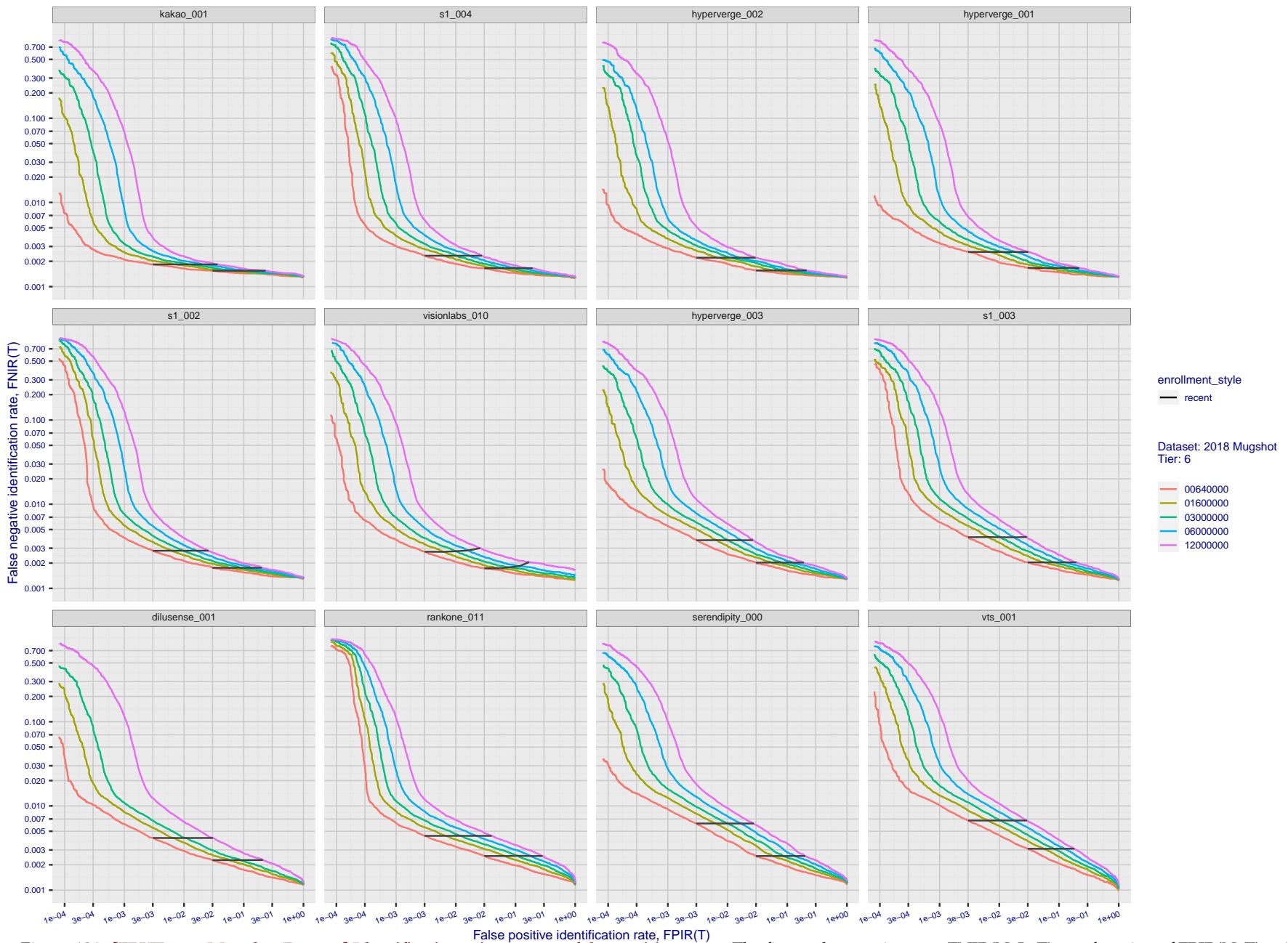


Figure 121: [FRVT-2018 Mugshot Dataset] Identification miss rates vs. false positive rates. The figure shows miss rates $\text{FNIR}(N, L, T)$ as a function of $\text{FPIR}(N, T)$, with N ranging from 640 000 to 12 000 000 as noted in rows 1-10 of Table 1. These error tradeoff characteristics are useful for applications where a threshold must be elevated to limit false positives, such as when human reviewer labor is not matched to the volume of searches. Dark lines join points of equal threshold: If horizontal, $\text{FPIR}(T)$ rises with N , and mate scores are independent of N . Other algorithms adjust scores in an attempt to make FPIR independent of N .

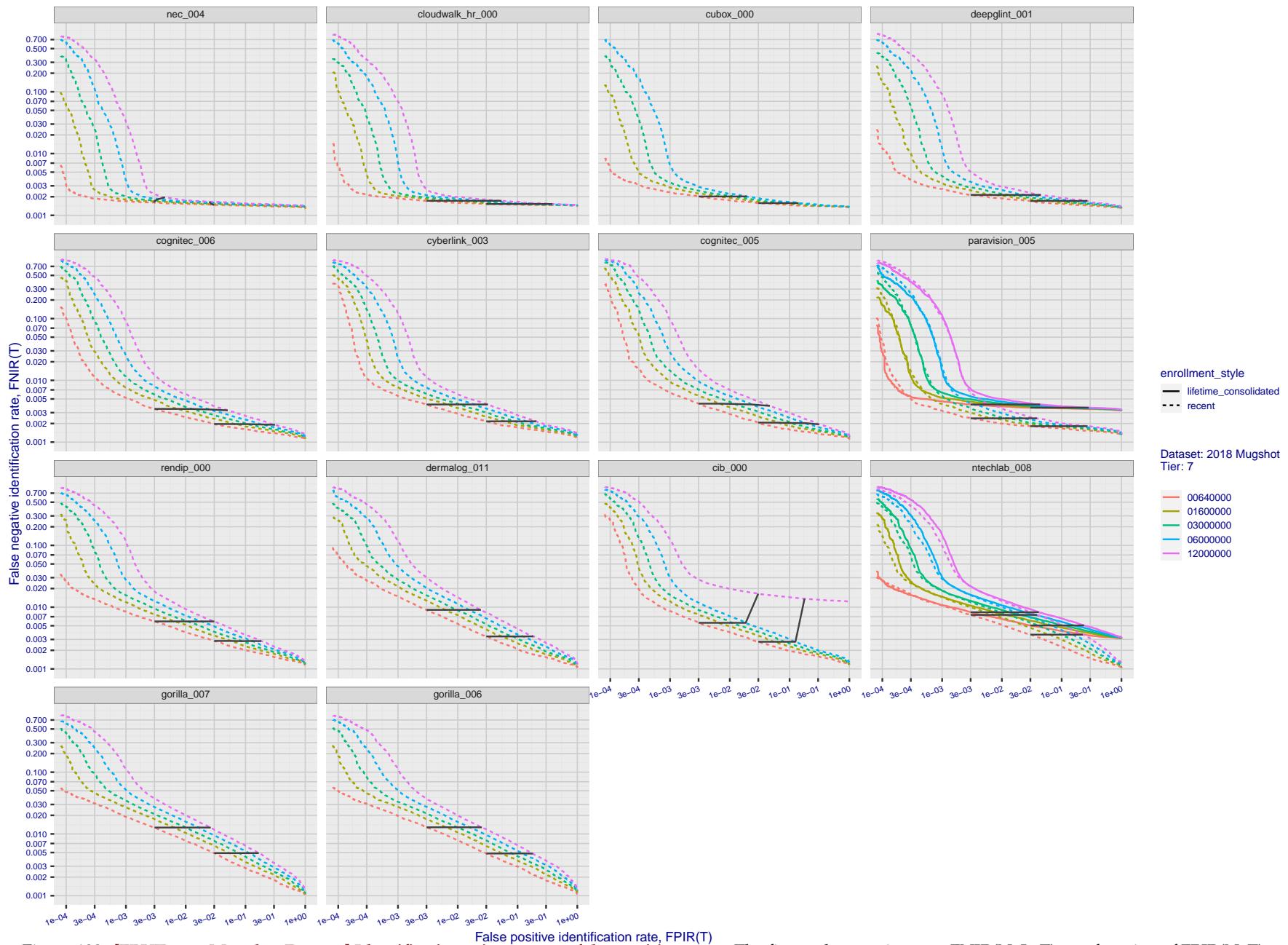


Figure 122: [FRVT-2018 Mugshot Dataset] Identification miss rates vs. false positive rates. The figure shows miss rates $\text{FNIR}(N, L, T)$ as a function of $\text{FPIR}(N, T)$, with N ranging from 640 000 to 12 000 000 as noted in rows 1-10 of Table 1. These error tradeoff characteristics are useful for applications where a threshold must be elevated to limit false positives, such as when human reviewer labor is not matched to the volume of searches. Dark lines join points of equal threshold: If horizontal, $\text{FPIR}(T)$ rises with N , and mate scores are independent of N . Other algorithms adjust scores in an attempt to make FPIR independent of N .

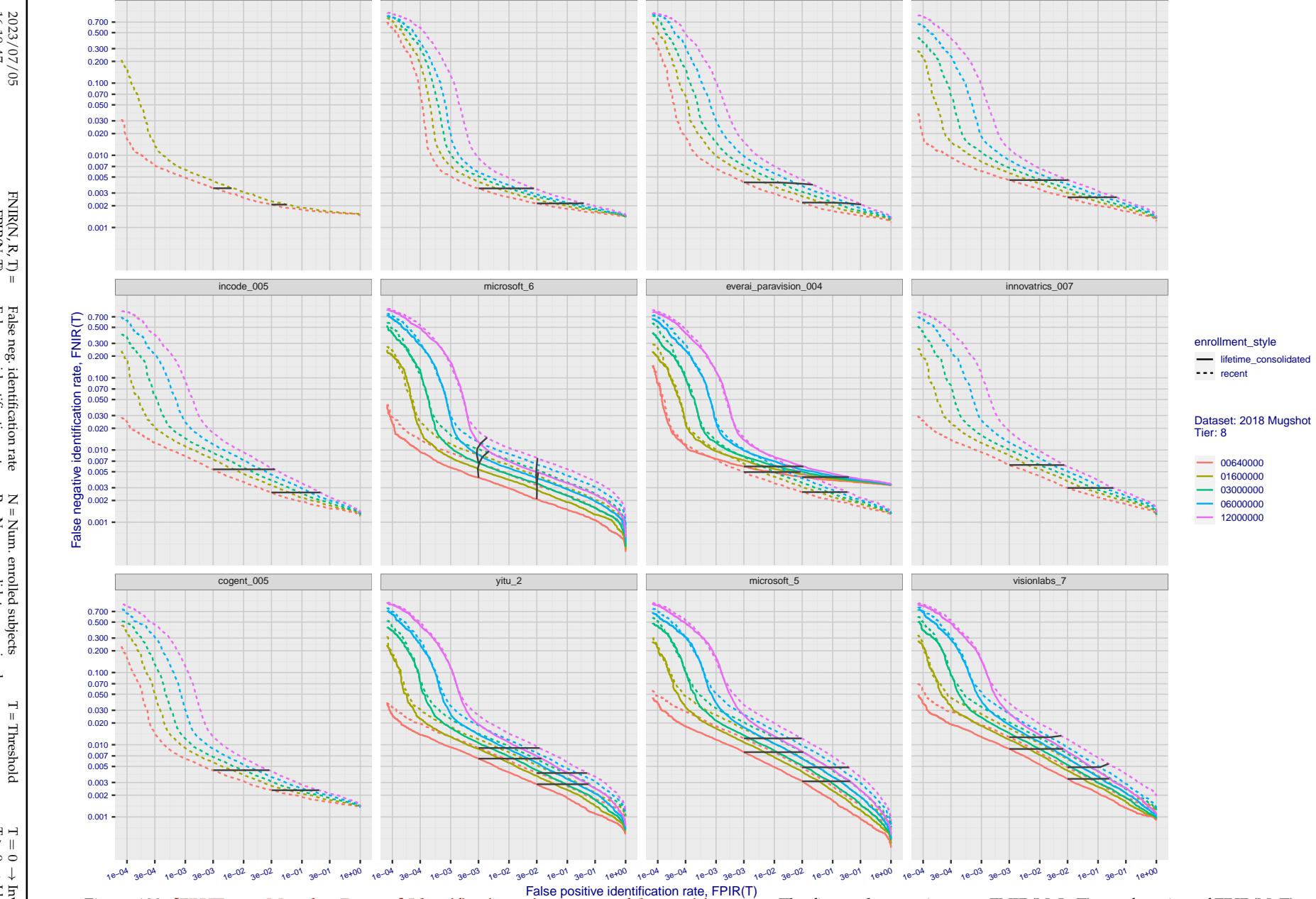


Figure 123: [FRVT-2018 Mugshot Dataset] Identification miss rates vs. false positive rates. The figure shows miss rates $\text{FNIR}(N, L, T)$ as a function of $\text{FPIR}(N, T)$, with N ranging from 640 000 to 12 000 000 as noted in rows 1-10 of Table 1. These error tradeoff characteristics are useful for applications where a threshold must be elevated to limit false positives, such as when human reviewer labor is not matched to the volume of searches. Dark lines join points of equal threshold: If horizontal, $\text{FPIR}(T)$ rises with N , and mate scores are independent of N . Other algorithms adjust scores in an attempt to make FPIR independent of N .

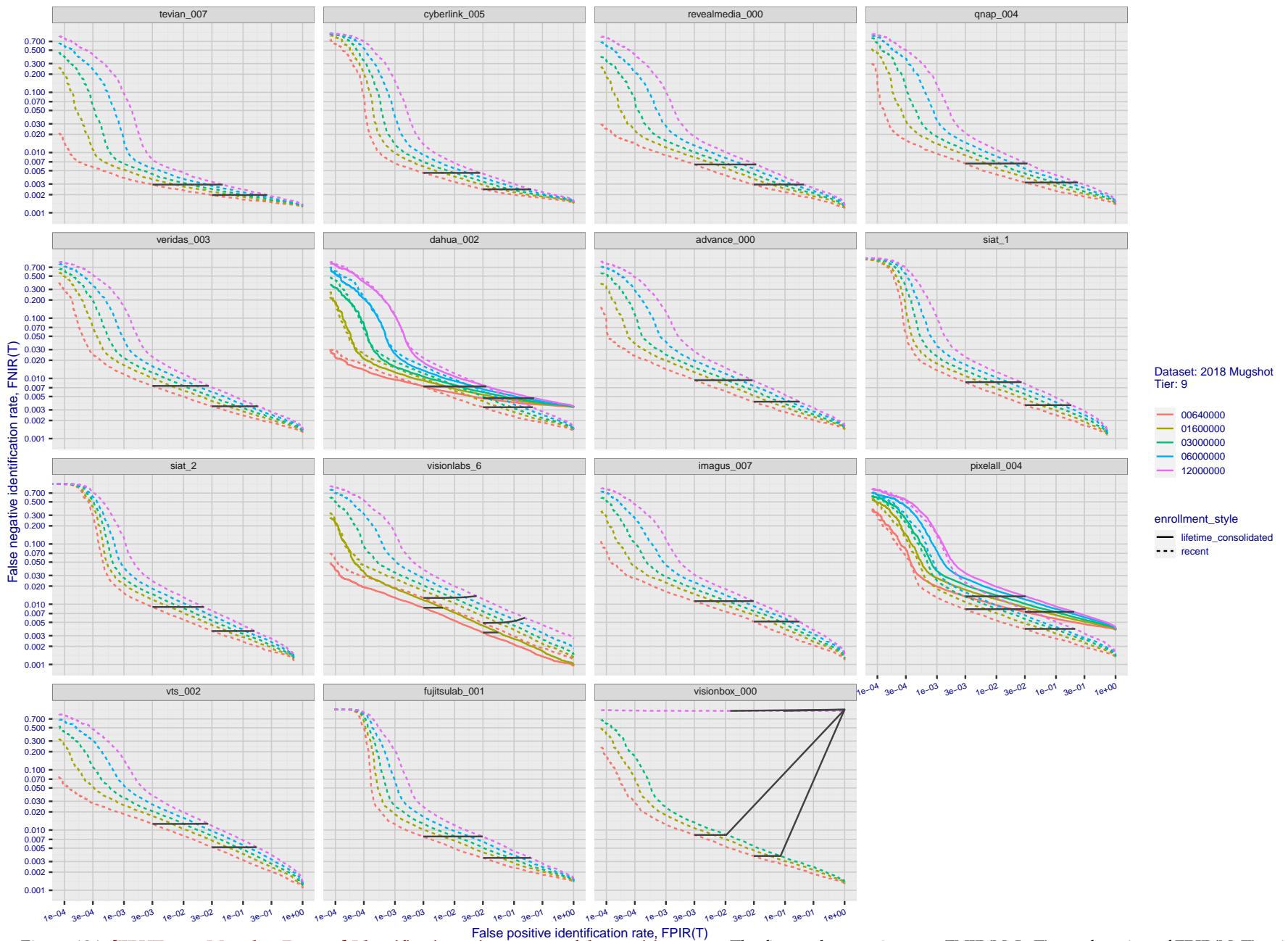


Figure 124: [FRVT-2018 Mugshot Dataset] Identification miss rates vs. false positive rates. The figure shows miss rates $\text{FNIR}(N, L, T)$ as a function of $\text{FPIR}(N, T)$, with N ranging from 640 000 to 12 000 000 as noted in rows 1-10 of Table 1. These error tradeoff characteristics are useful for applications where a threshold must be elevated to limit false positives, such as when human reviewer labor is not matched to the volume of searches. Dark lines join points of equal N . If horizontal, $\text{FPIR}(T)$ rises with N , and mate scores are independent of N . Other algorithms adjust scores in an attempt to make FPIR independent of N .

2023/07/05
16:19:47

 $\text{FNIR}(N, R, T) = \text{False neg. identification rate}$
 $\text{FPIR}(N, T) = \text{False pos. identification rate}$
 $N = \text{Num. enrolled subjects}$
 $R = \text{Num. candidates examined}$
 $T = \text{Threshold}$
 $T = 0 \rightarrow \text{Investigation}$
 $T > 0 \rightarrow \text{Identification}$

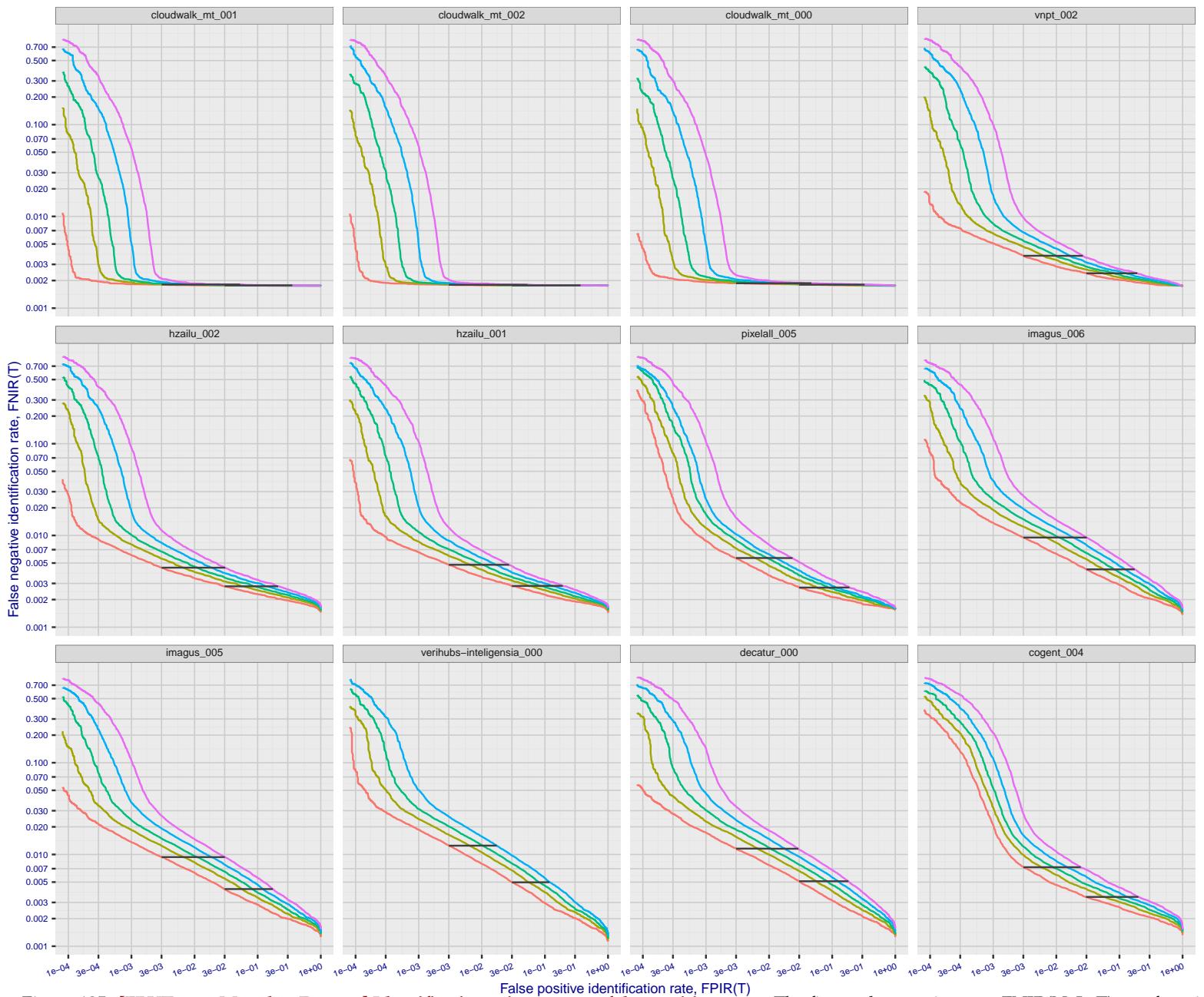


Figure 125: [FRVT-2018 Mugshot Dataset] Identification miss rates vs. false positive rates. The figure shows miss rates $\text{FNIR}(N, L, T)$ as a function of $\text{FPIR}(N, T)$, with N ranging from 640 000 to 12 000 000 as noted in rows 1-10 of Table 1. These error tradeoff characteristics are useful for applications where a threshold must be elevated to limit false positives, such as when human reviewer labor is not matched to the volume of searches. Dark lines join points of equal threshold: If horizontal, $\text{FPIR}(T)$ rises with N , and mate scores are independent of N . Other algorithms adjust scores in an attempt to make FPIR independent of N .

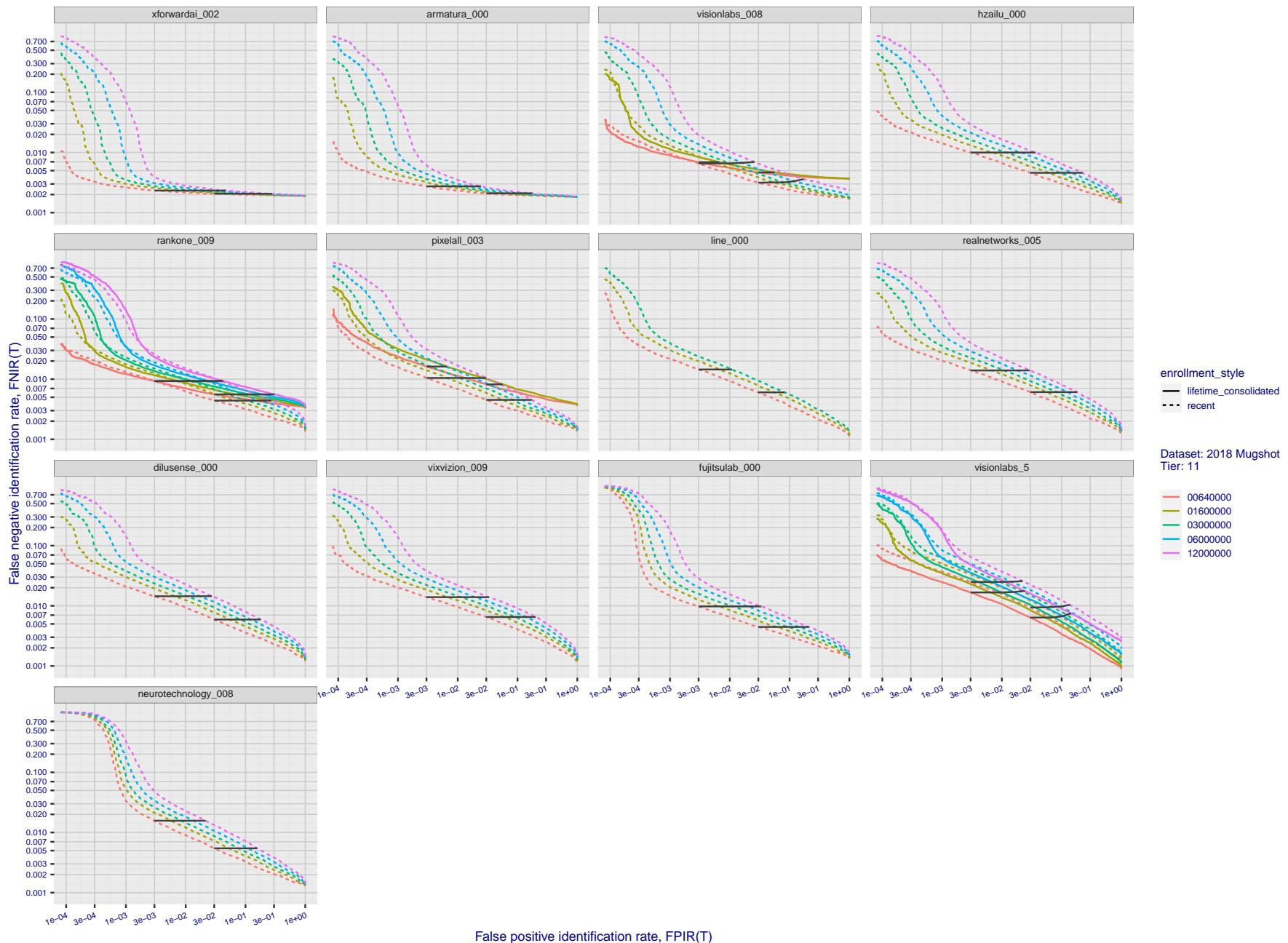


Figure 126: [FRVT-2018 Mugshot Dataset] Identification miss rates vs. false positive rates. The figure shows miss rates $\text{FNIR}(N, L, T)$ as a function of $\text{FPIR}(N, T)$, with N ranging from 640 000 to 12 000 000 as noted in rows 1-10 of Table 1. These error tradeoff characteristics are useful for applications where a threshold must be elevated to limit false positives, such as when human reviewer labor is not matched to the volume of searches. Dark lines join points of equal threshold: If horizontal, $\text{FPIR}(T)$ rises with N , and mate scores are independent of N . Other algorithms adjust scores in an attempt to make FPIR independent of N .

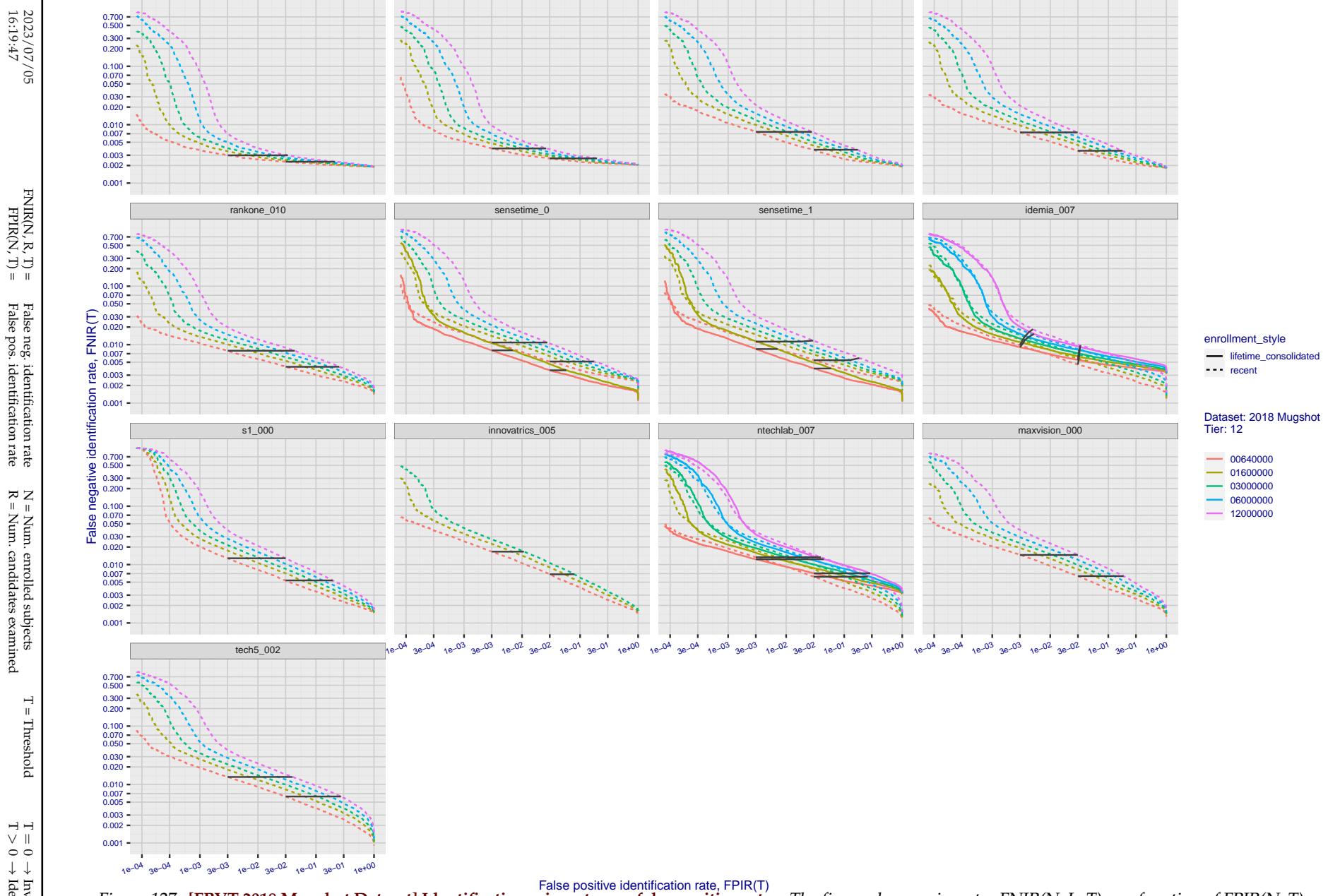


Figure 127: [FRVT-2018 Mugshot Dataset] Identification miss rates vs. false positive rates. The figure shows miss rates $\text{FNIR}(N, L, T)$ as a function of $\text{FPIR}(N, T)$, with N ranging from 640 000 to 12 000 000 as noted in rows 1-10 of Table 1. These error tradeoff characteristics are useful for applications where a threshold must be elevated to limit false positives, such as when human reviewer labor is not matched to the volume of searches. Dark lines join points of equal threshold: If horizontal, $\text{FPIR}(T)$ rises with N , and mate scores are independent of N . Other algorithms adjust scores in an attempt to make FPIR independent of N .

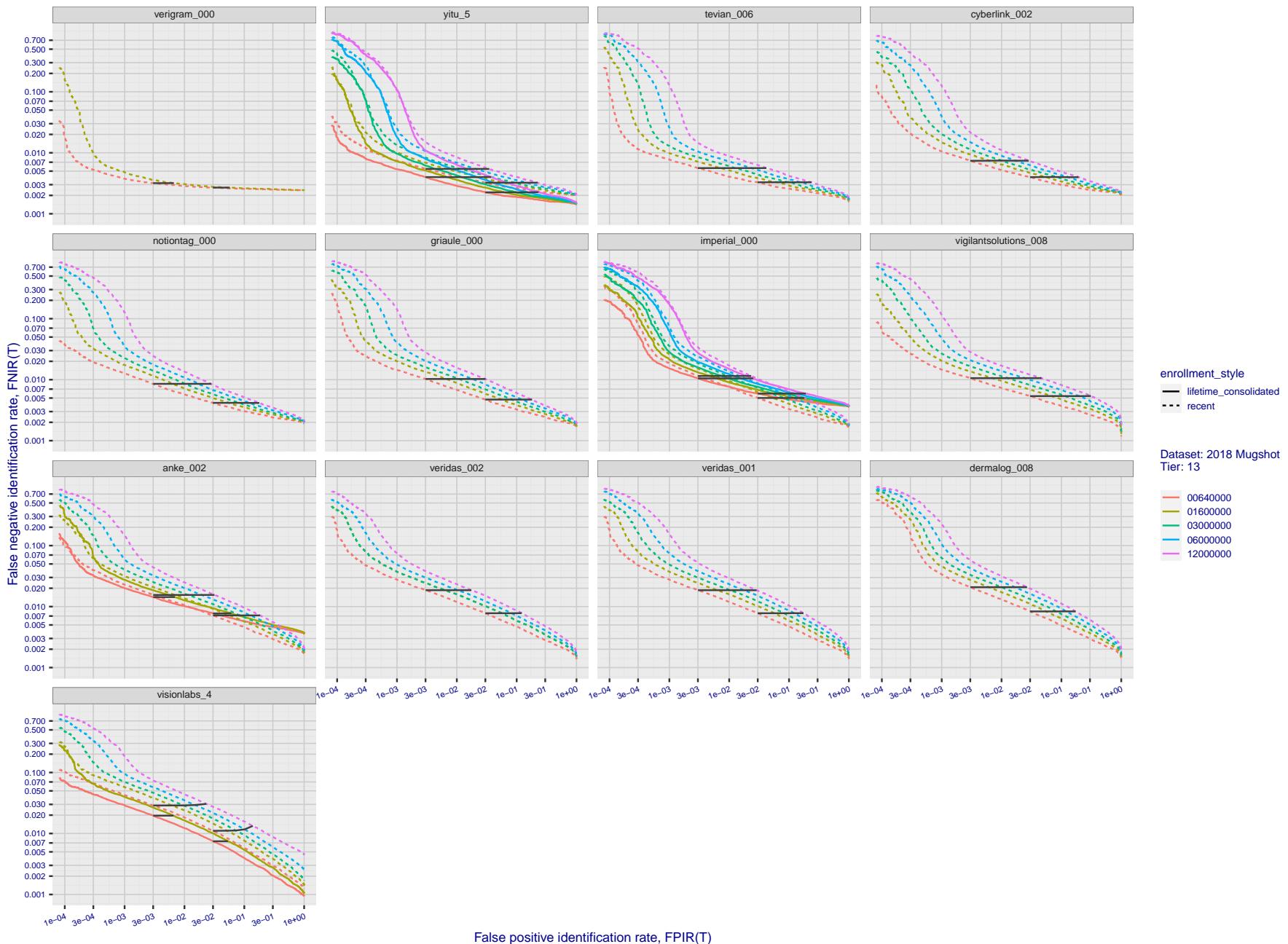


Figure 128: [FRVT-2018 Mugshot Dataset] Identification miss rates vs. false positive rates. The figure shows miss rates $\text{FNIR}(N, L, T)$ as a function of $\text{FPIR}(N, T)$, with N ranging from 640 000 to 12 000 000 as noted in rows 1-10 of Table 1. These error tradeoff characteristics are useful for applications where a threshold must be elevated to limit false positives, such as when human reviewer labor is not matched to the volume of searches. Dark lines join points of equal threshold: If horizontal, $\text{FPIR}(T)$ rises with N , and mate scores are independent of N . Other algorithms adjust scores in an attempt to make FPIR independent of N .

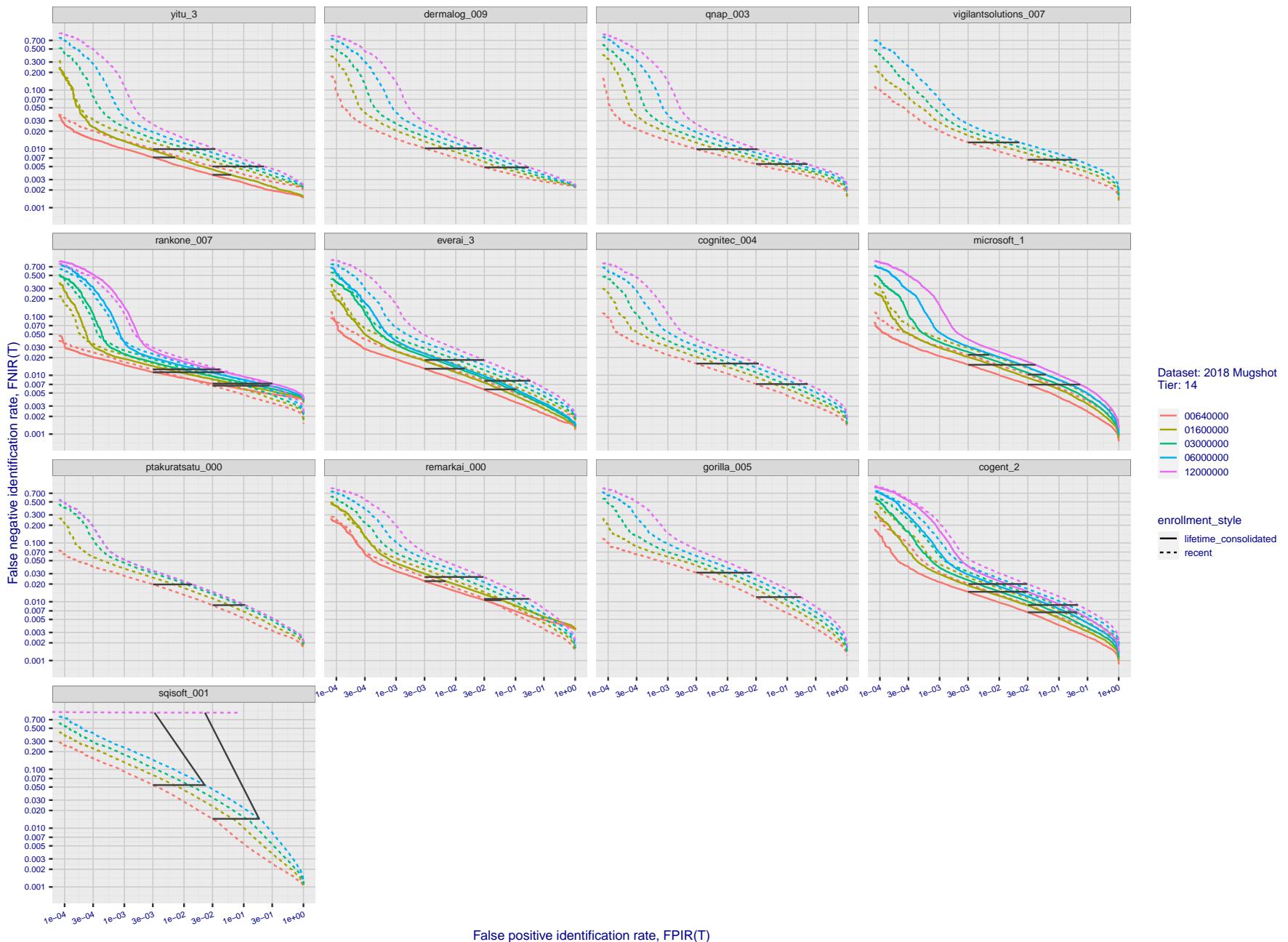


Figure 129: [FRVT-2018 Mugshot Dataset] Identification miss rates vs. false positive rates. The figure shows miss rates $\text{FNIR}(N, L, T)$ as a function of $\text{FPIR}(N, T)$, with N ranging from 640 000 to 12 000 000 as noted in rows 1-10 of Table 1. These error tradeoff characteristics are useful for applications where a threshold must be elevated to limit false positives, such as when human reviewer labor is not matched to the volume of searches. Dark lines join points of equal threshold: If horizontal, $\text{FPIR}(T)$ rises with N , and mate scores are independent of N . Other algorithms adjust scores in an attempt to make FPIR independent of N .

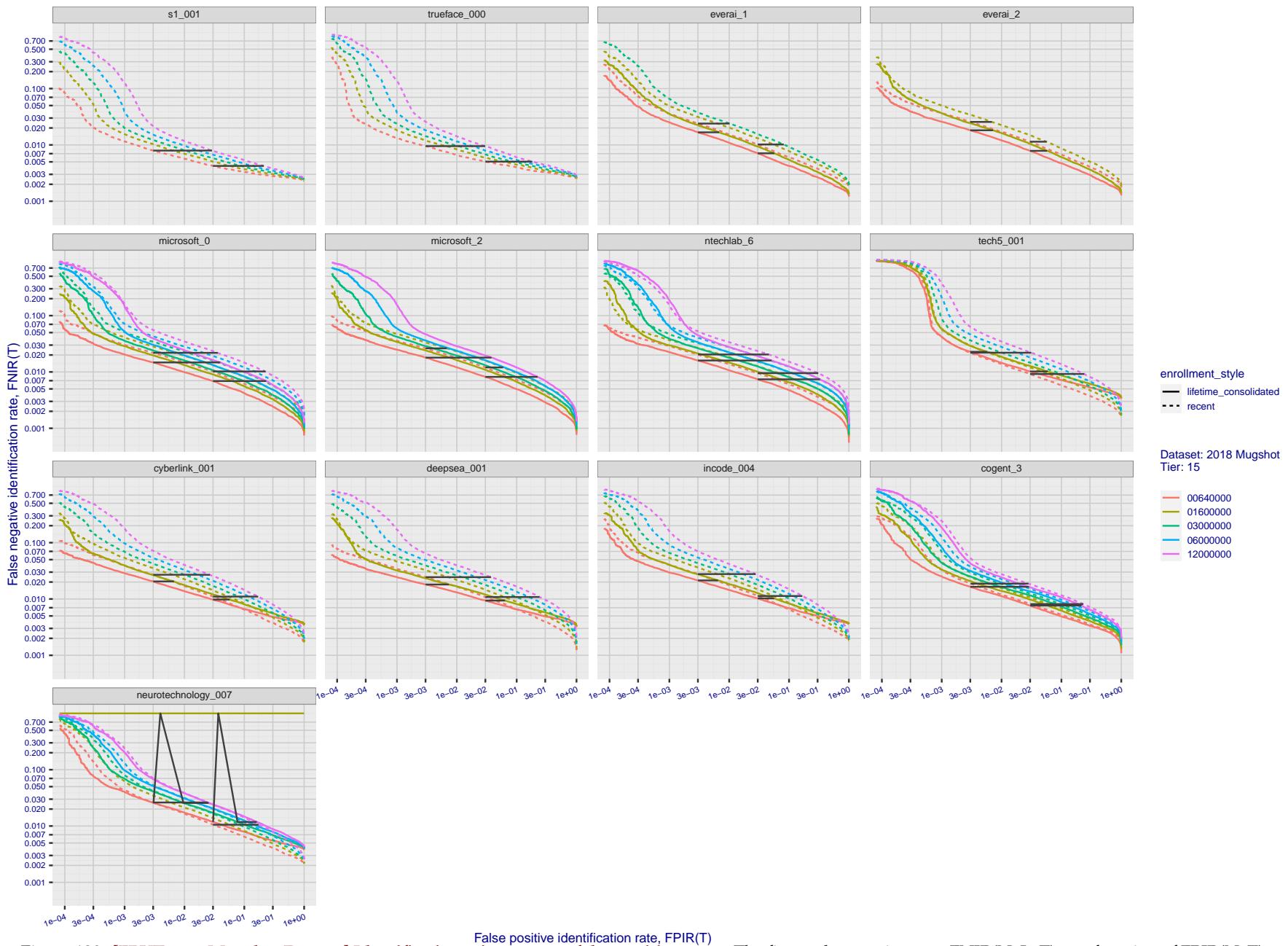


Figure 130: [FRVT-2018 Mugshot Dataset] Identification miss rates vs. false positive rates. The figure shows miss rates $\text{FNIR}(N, L, T)$ as a function of $\text{FPIR}(N, T)$, with N ranging from 640 000 to 12 000 000 as noted in rows 1-10 of Table 1. These error tradeoff characteristics are useful for applications where a threshold must be elevated to limit false positives, such as when human reviewer labor is not matched to the volume of searches. Dark lines join points of equal threshold: If horizontal, $\text{FPIR}(T)$ rises with N , and mate scores are independent of N . Other algorithms adjust scores in an attempt to make FPIR independent of N .

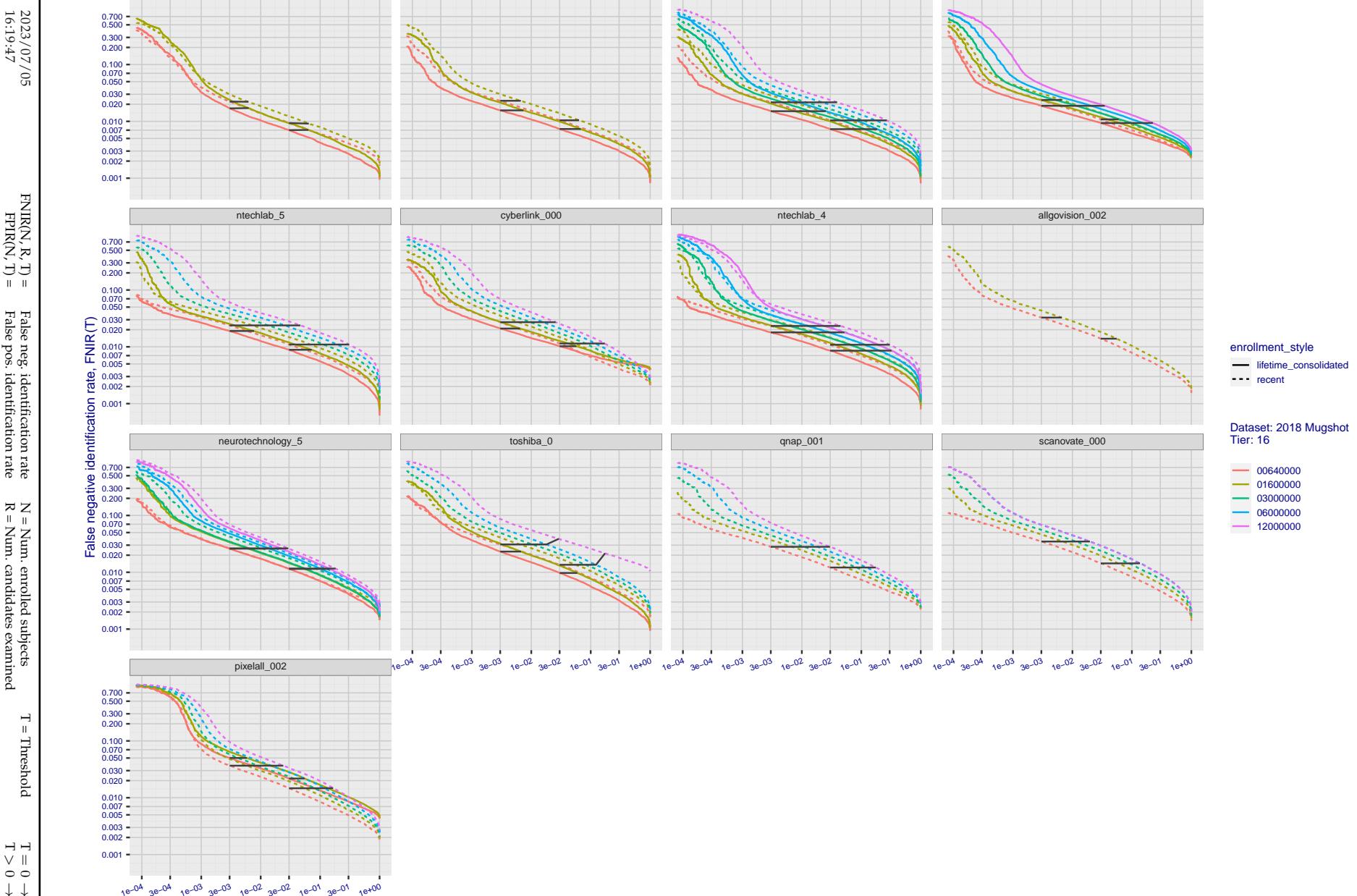


Figure 131: [FRVT-2018 Mugshot Dataset] Identification miss rates vs. false positive rates. The figure shows miss rates $\text{FNIR}(N, L, T)$ as a function of $\text{FPIR}(N, T)$, with N ranging from 64 000 to 12 000 000 as noted in rows 1-10 of Table 1. These error tradeoff characteristics are useful for applications where a threshold must be elevated to limit false positives, such as when human reviewer labor is not matched to the volume of searches. Dark lines join points of equal threshold: If horizontal, $\text{FPIR}(T)$ rises with N , and mate scores are independent of N . Other algorithms adjust scores in an attempt to make FPIR independent of N .

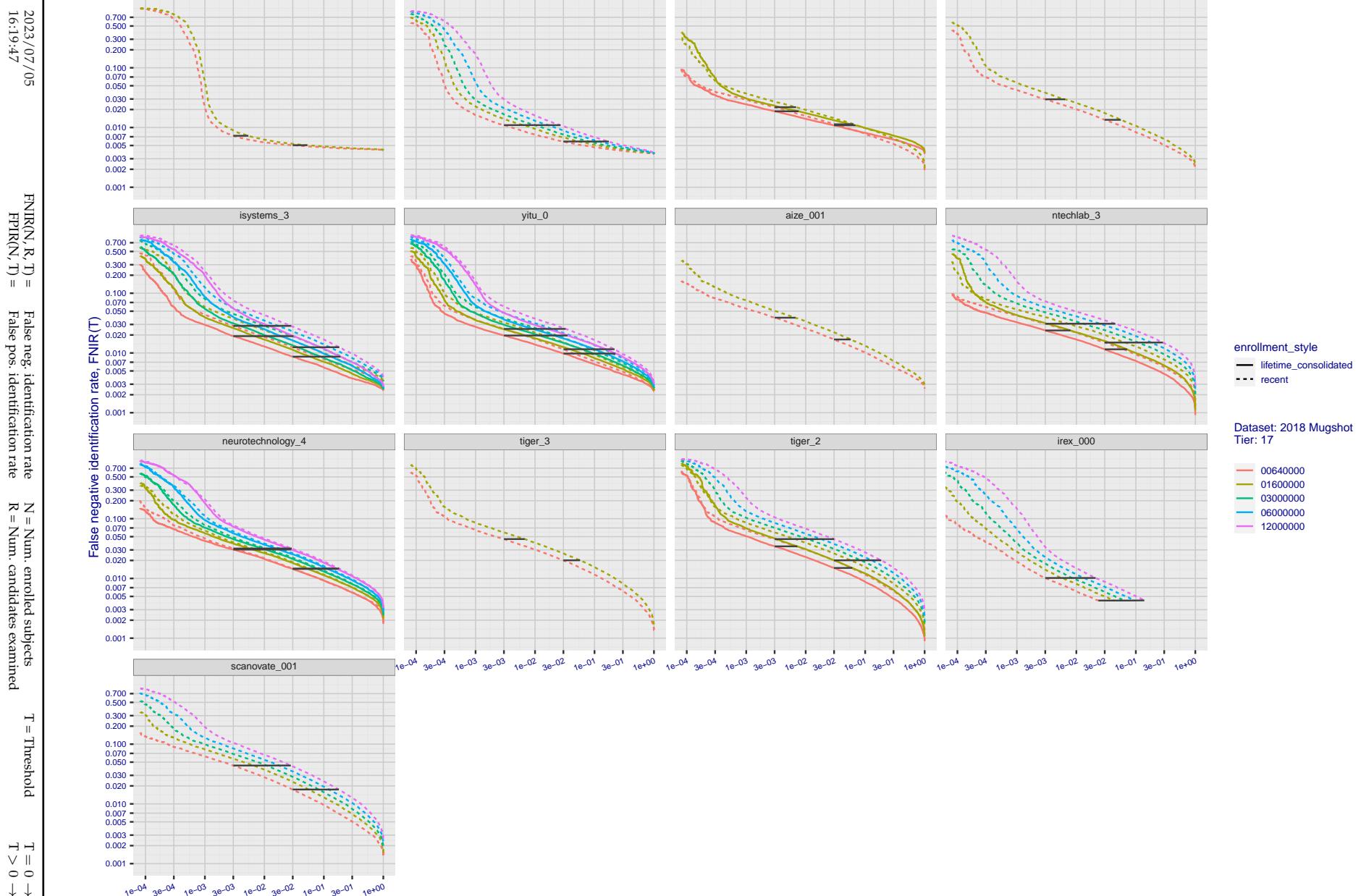


Figure 132: [FRVT-2018 Mugshot Dataset] Identification miss rates vs. false positive rates. The figure shows miss rates $\text{FNIR}(N, L, T)$ as a function of $\text{FPIR}(N, T)$, with N ranging from 640 000 to 12 000 000 as noted in rows 1-10 of Table 1. These error tradeoff characteristics are useful for applications where a threshold must be elevated to limit false positives, such as when human reviewer labor is not matched to the volume of searches. Dark lines join points of equal threshold: If horizontal, $\text{FPIR}(T)$ rises with N , and mate scores are independent of N . Other algorithms adjust scores in an attempt to make FPIR independent of N .

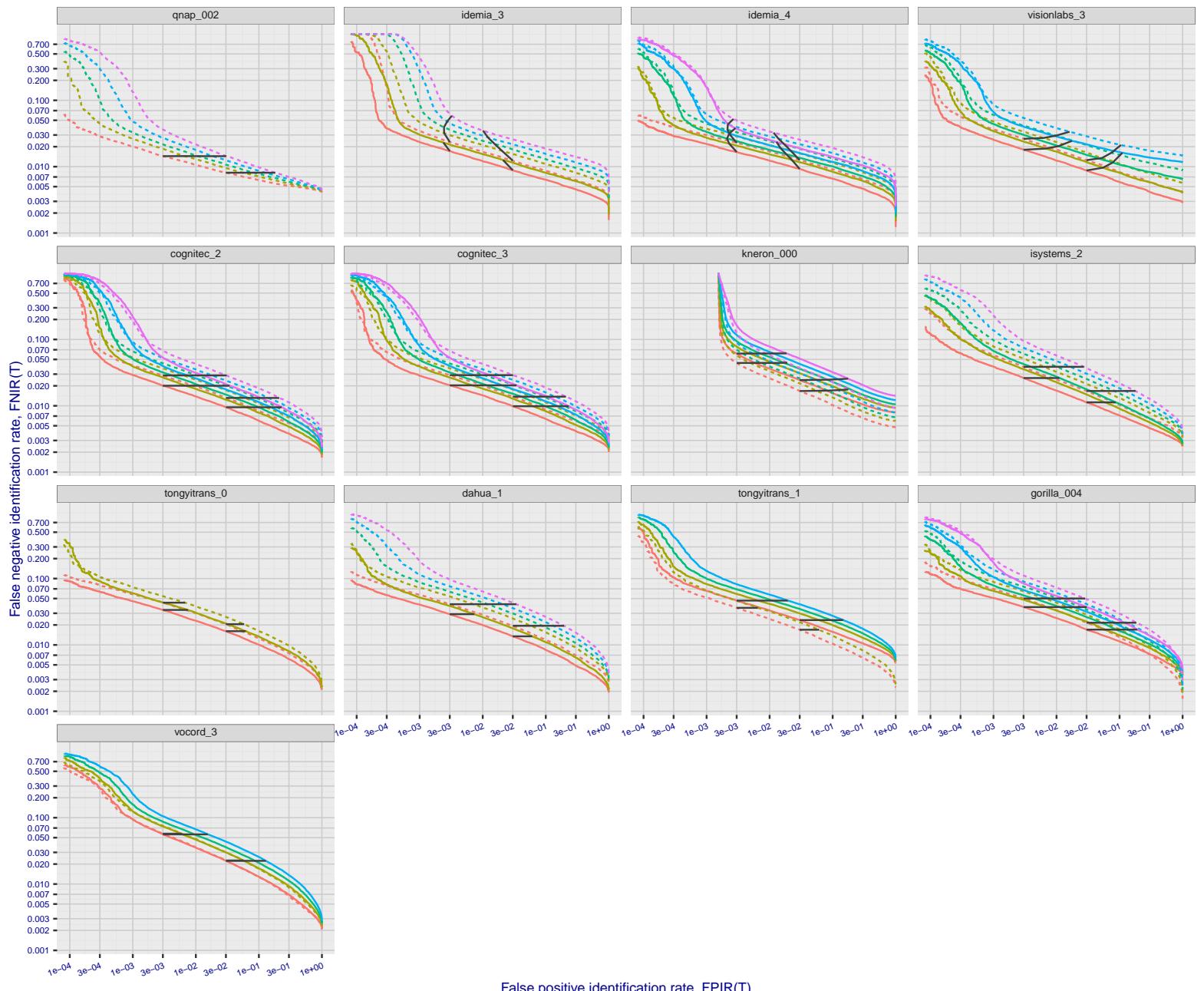


Figure 133: [FRVT-2018 Mugshot Dataset] Identification miss rates vs. false positive rates. The figure shows miss rates $\text{FNIR}(N, L, T)$ as a function of $\text{FPIR}(N, T)$, with N ranging from 64 000 to 12 000 000 as noted in rows 1-10 of Table 1. These error tradeoff characteristics are useful for applications where a threshold must be elevated to limit false positives, such as when human reviewer labor is not matched to the volume of searches. Dark lines join points of equal threshold: If horizontal, $\text{FPIR}(T)$ rises with N , and mate scores are independent of N . Other algorithms adjust scores in an attempt to make FPIR independent of N .

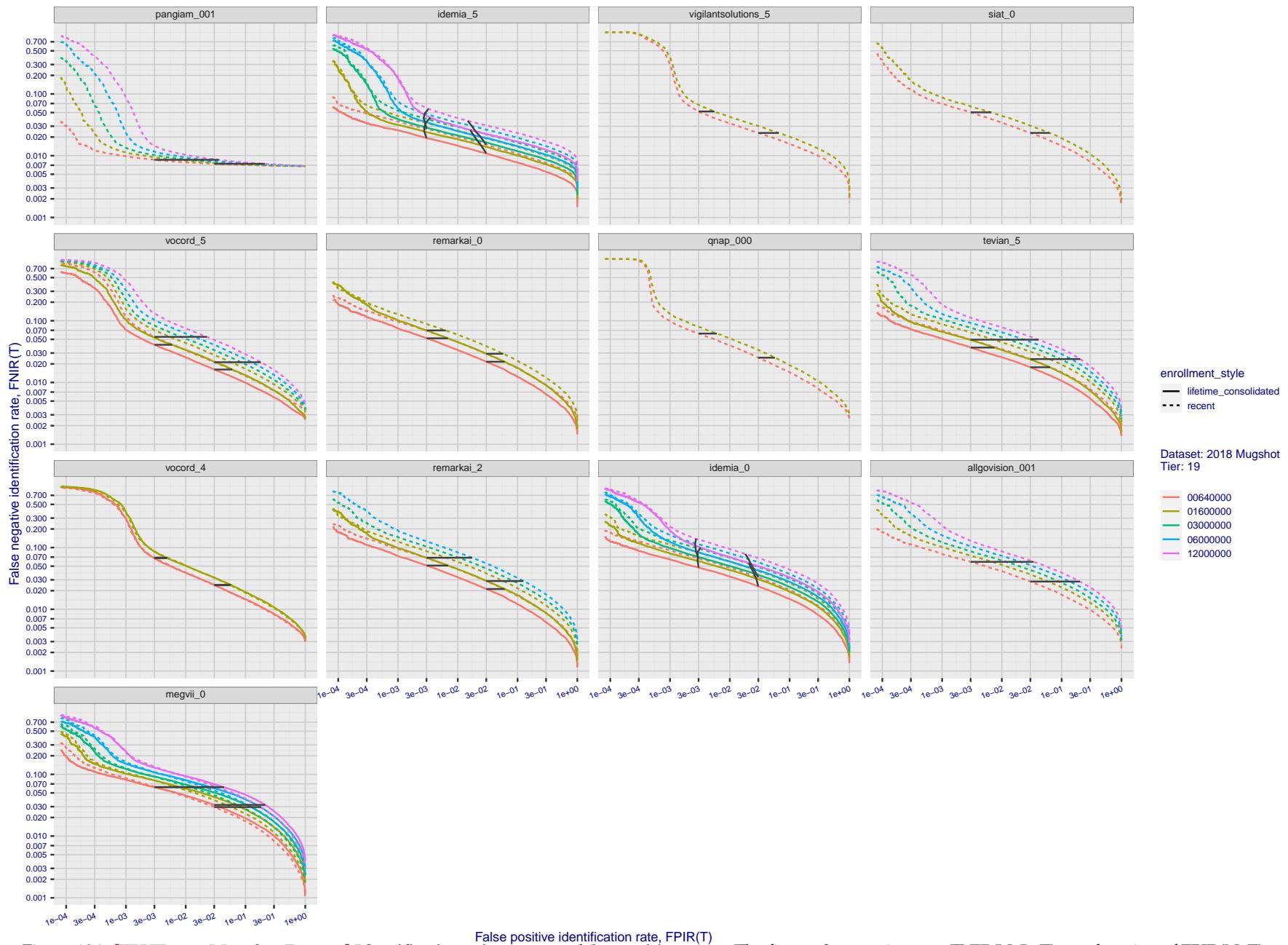


Figure 134: [FRVT-2018 Mugshot Dataset] Identification miss rates vs. false positive rates. The figure shows miss rates $\text{FNIR}(N, L, T)$ as a function of $\text{FPIR}(N, T)$, with N ranging from 640 000 to 12 000 000 as noted in rows 1-10 of Table 1. These error tradeoff characteristics are useful for applications where a threshold must be elevated to limit false positives, such as when human reviewer labor is not matched to the volume of searches. Dark lines join points of equal threshold: If horizontal, $\text{FPIR}(T)$ rises with N , and mate scores are independent of N . Other algorithms adjust scores in an attempt to make FPIR independent of N .

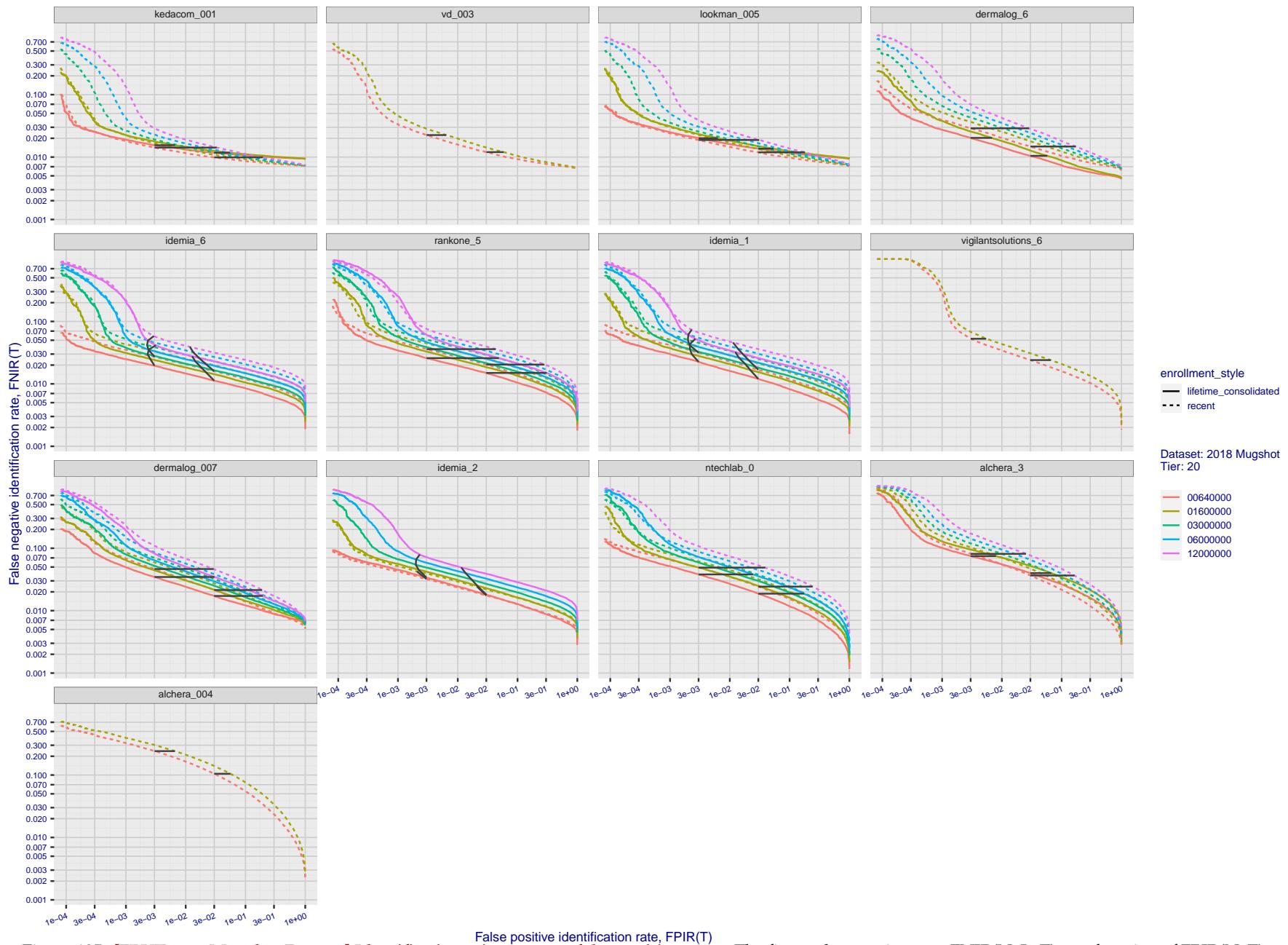


Figure 135: [FRVT-2018 Mugshot Dataset] Identification miss rates vs. false positive rates. The figure shows miss rates $\text{FNIR}(N, L, T)$ as a function of $\text{FPIR}(N, T)$, with N ranging from 640 000 to 12 000 000 as noted in rows 1-10 of Table 1. These error tradeoff characteristics are useful for applications where a threshold must be elevated to limit false positives, such as when human reviewer labor is not matched to the volume of searches. Dark lines join points of equal N . Other algorithms adjust scores in an attempt to make FPIR independent of N .

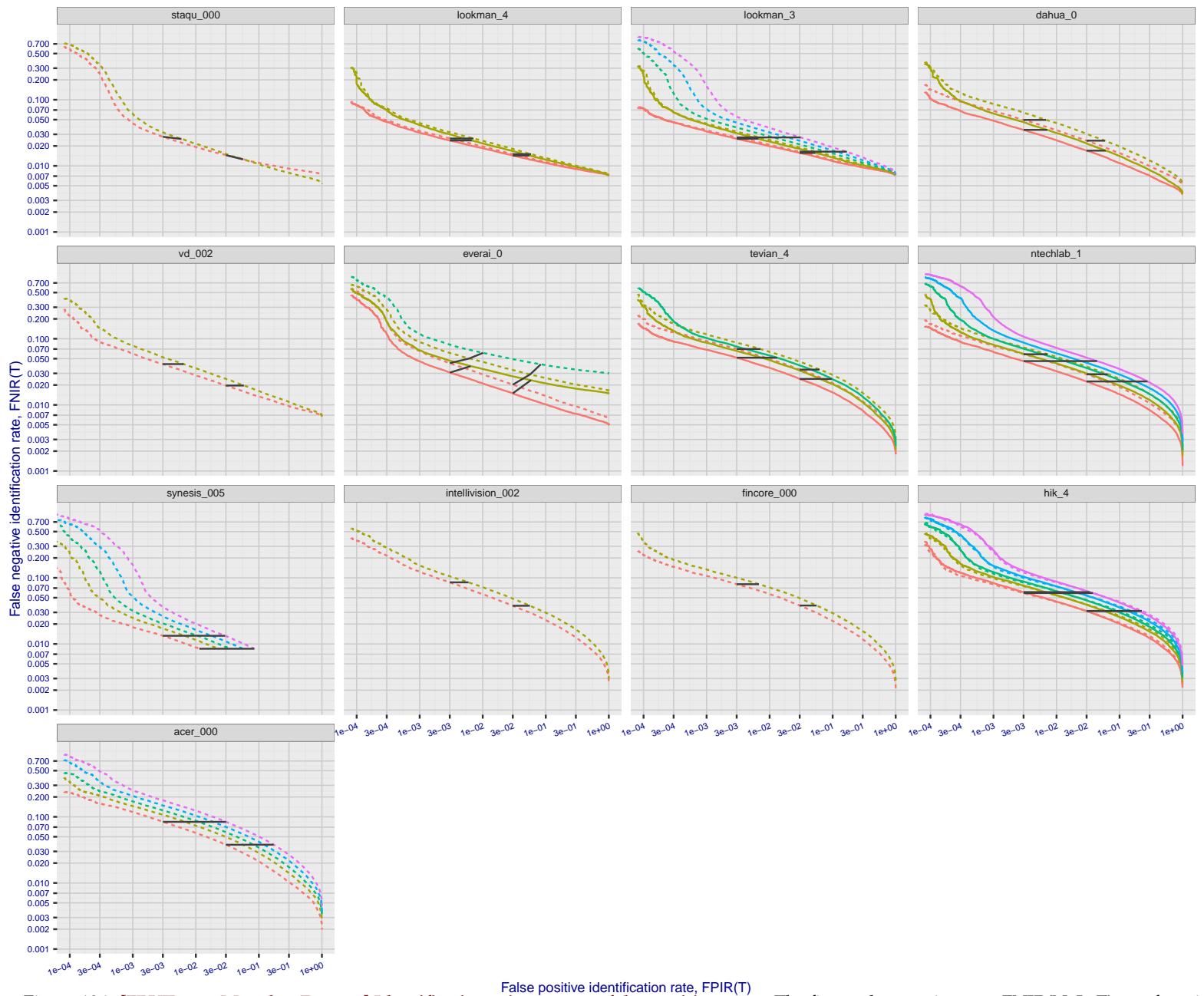


Figure 136: [FRVT-2018 Mugshot Dataset] Identification miss rates vs. false positive rates. The figure shows miss rates $\text{FNIR}(N, L, T)$ as a function of $\text{FPIR}(N, T)$, with N ranging from 64 000 to 12 000 000 as noted in rows 1-10 of Table 1. These error tradeoff characteristics are useful for applications where a threshold must be elevated to limit false positives, such as when human reviewer labor is not matched to the volume of searches. Dark lines join points of equal threshold: If horizontal, $\text{FPIR}(T)$ rises with N , and mate scores are independent of N . Other algorithms adjust scores in an attempt to make FPIR independent of N .

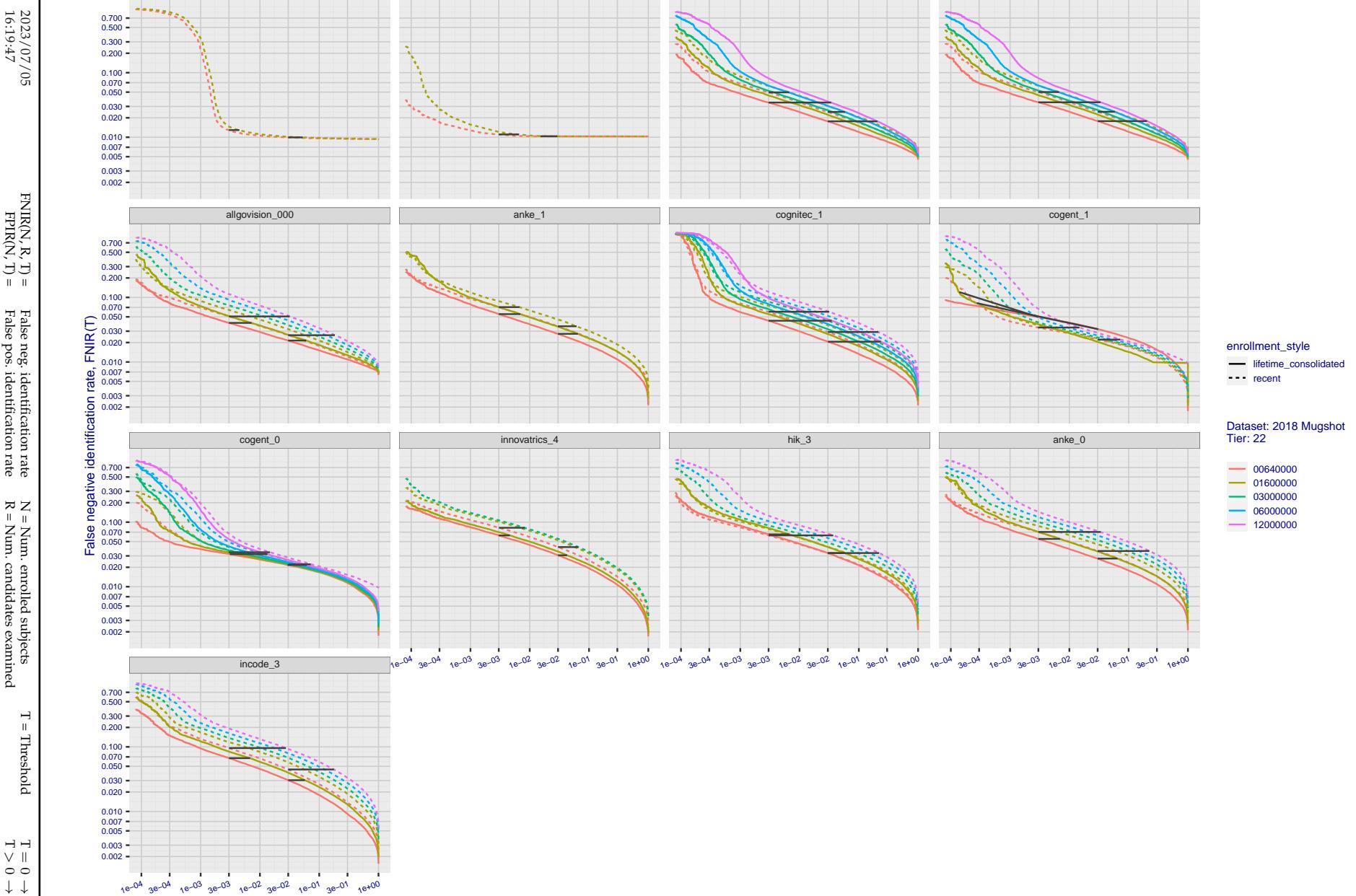


Figure 137: [FRVT-2018 Mugshot Dataset] Identification miss rates vs. false positive rates. The figure shows miss rates $\text{FNIR}(N, L, T)$ as a function of $\text{FPIR}(N, T)$, with N ranging from 640 000 to 12 000 000 as noted in rows 1-10 of Table 1. These error tradeoff characteristics are useful for applications where a threshold must be elevated to limit false positives, such as when human reviewer labor is not matched to the volume of searches. Dark lines join points of equal threshold: If horizontal, $\text{FPIR}(T)$ rises with N , and mate scores are independent of N . Other algorithms adjust scores in an attempt to make FPIR independent of N .

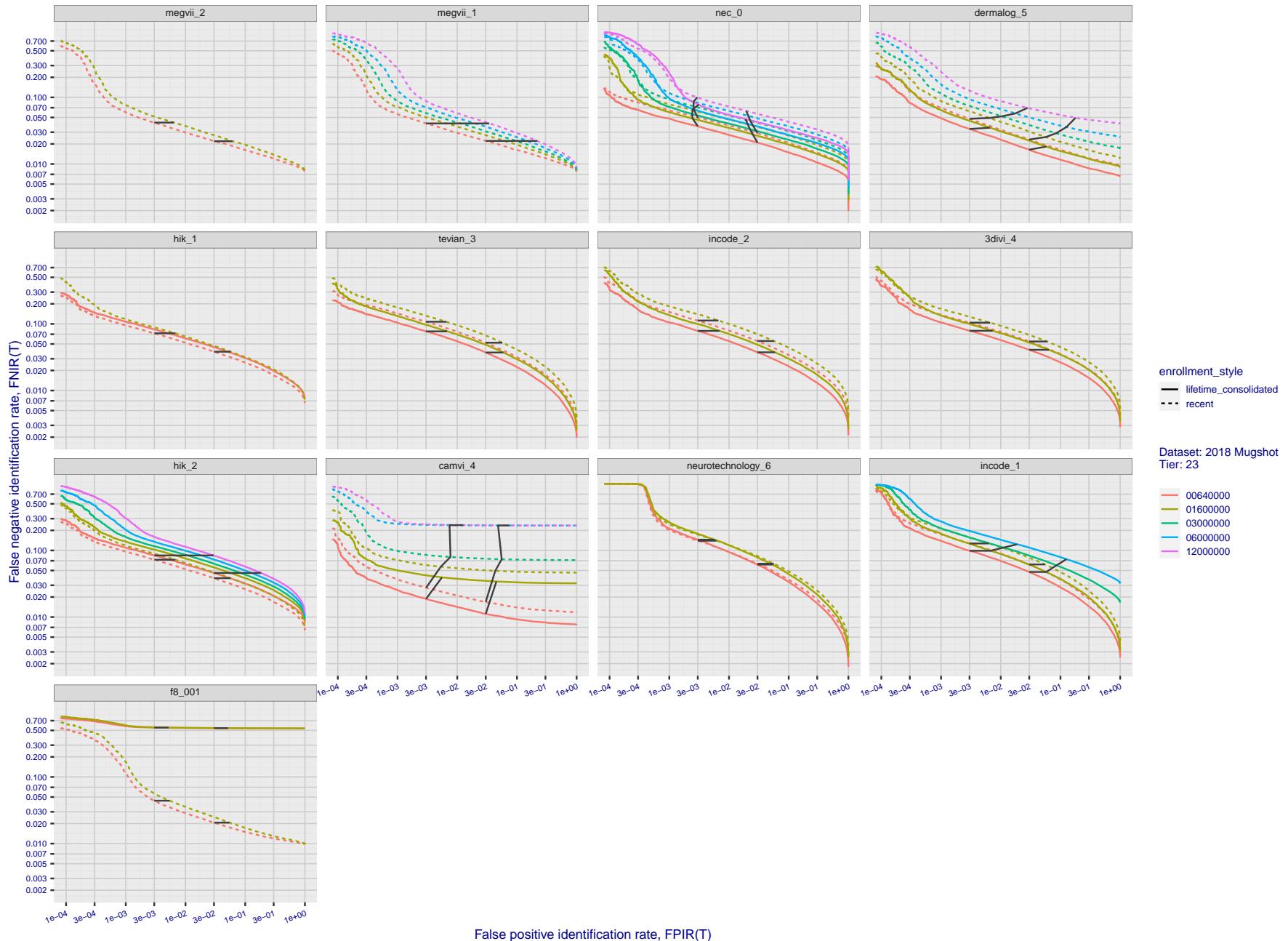


Figure 138: [FRVT-2018 Mugshot Dataset] Identification miss rates vs. false positive rates. The figure shows miss rates $\text{FNIR}(N, L, T)$ as a function of $\text{FPIR}(N, T)$, with N ranging from 640 000 to 12 000 000 as noted in rows 1-10 of Table 1. These error tradeoff characteristics are useful for applications where a threshold must be elevated to limit false positives, such as when human reviewer labor is not matched to the volume of searches. Dark lines join points of equal threshold: If horizontal, $\text{FPIR}(T)$ rises with N , and mate scores are independent of N . Other algorithms adjust scores in an attempt to make FPIR independent of N .

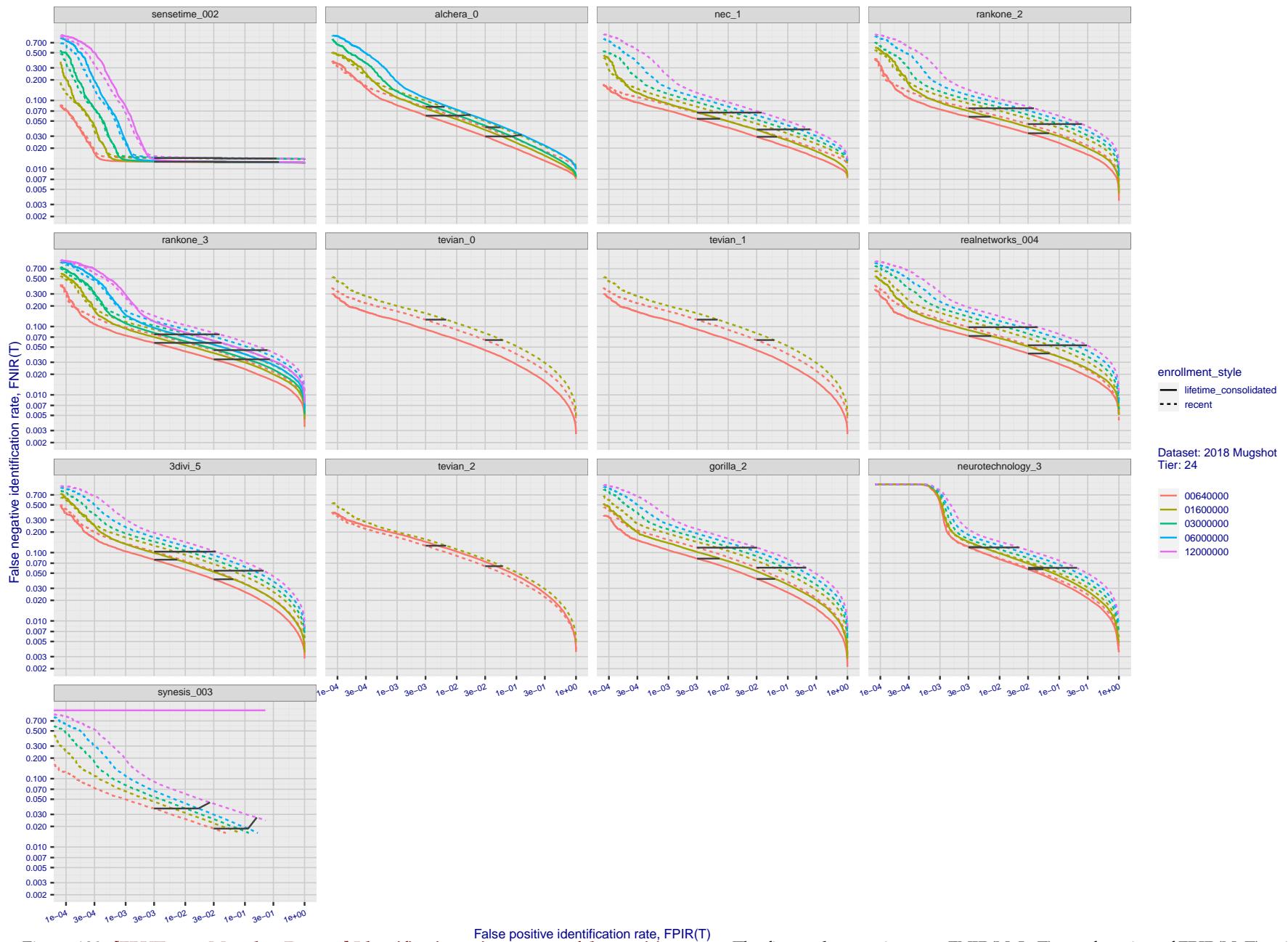


Figure 139: [FRVT-2018 Mugshot Dataset] Identification miss rates vs. false positive rates. The figure shows miss rates $\text{FNIR}(N, L, T)$ as a function of $\text{FPIR}(N, T)$, with N ranging from 640 000 to 12 000 000 as noted in rows 1-10 of Table 1. These error tradeoff characteristics are useful for applications where a threshold must be elevated to limit false positives, such as when human reviewer labor is not matched to the volume of searches. Dark lines join points of equal threshold: If horizontal, $\text{FPIR}(T)$ rises with N , and mate scores are independent of N . Other algorithms adjust scores in an attempt to make FPIR independent of N .

2023/07/05
16:19:47FNIR(N, R, T) = False neg. identification rate
FPIR(N, T) = False pos. identification rateN = Num. enrolled subjects
R = Num. candidates examined

T = Threshold

T = 0 → Investigation
 $T > 0 \rightarrow$ Identification

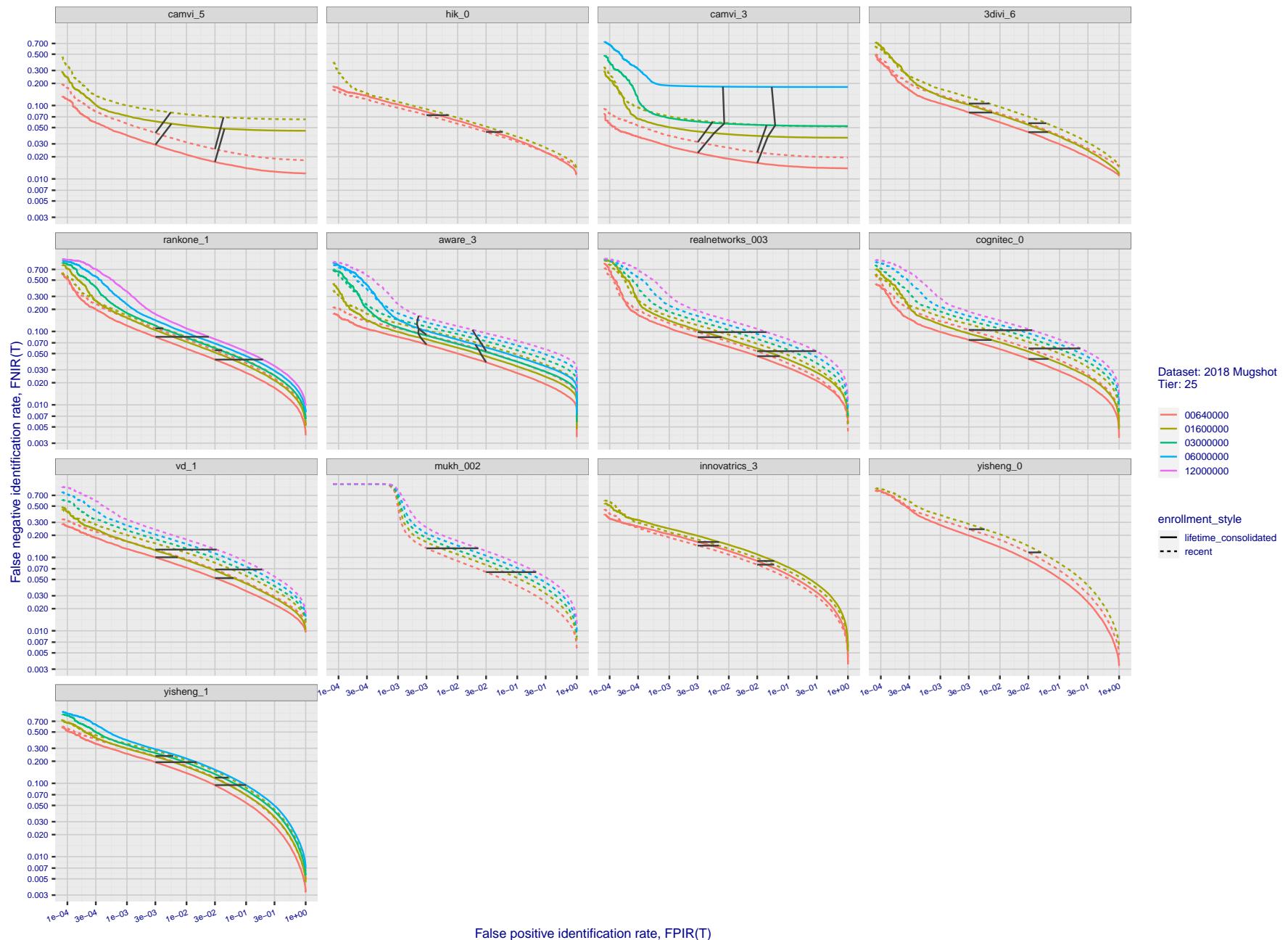


Figure 140: [FRVT-2018 Mugshot Dataset] Identification miss rates vs. false positive rates. The figure shows miss rates $\text{FNIR}(N, L, T)$ as a function of $\text{FPIR}(N, T)$, with N ranging from 640 000 to 12 000 000 as noted in rows 1-10 of Table 1. These error tradeoff characteristics are useful for applications where a threshold must be elevated to limit false positives, such as when human reviewer labor is not matched to the volume of searches. Dark lines join points of equal threshold: If horizontal, $\text{FPIR}(T)$ rises with N , and mate scores are independent of N . Other algorithms adjust scores in an attempt to make FPIR independent of N .

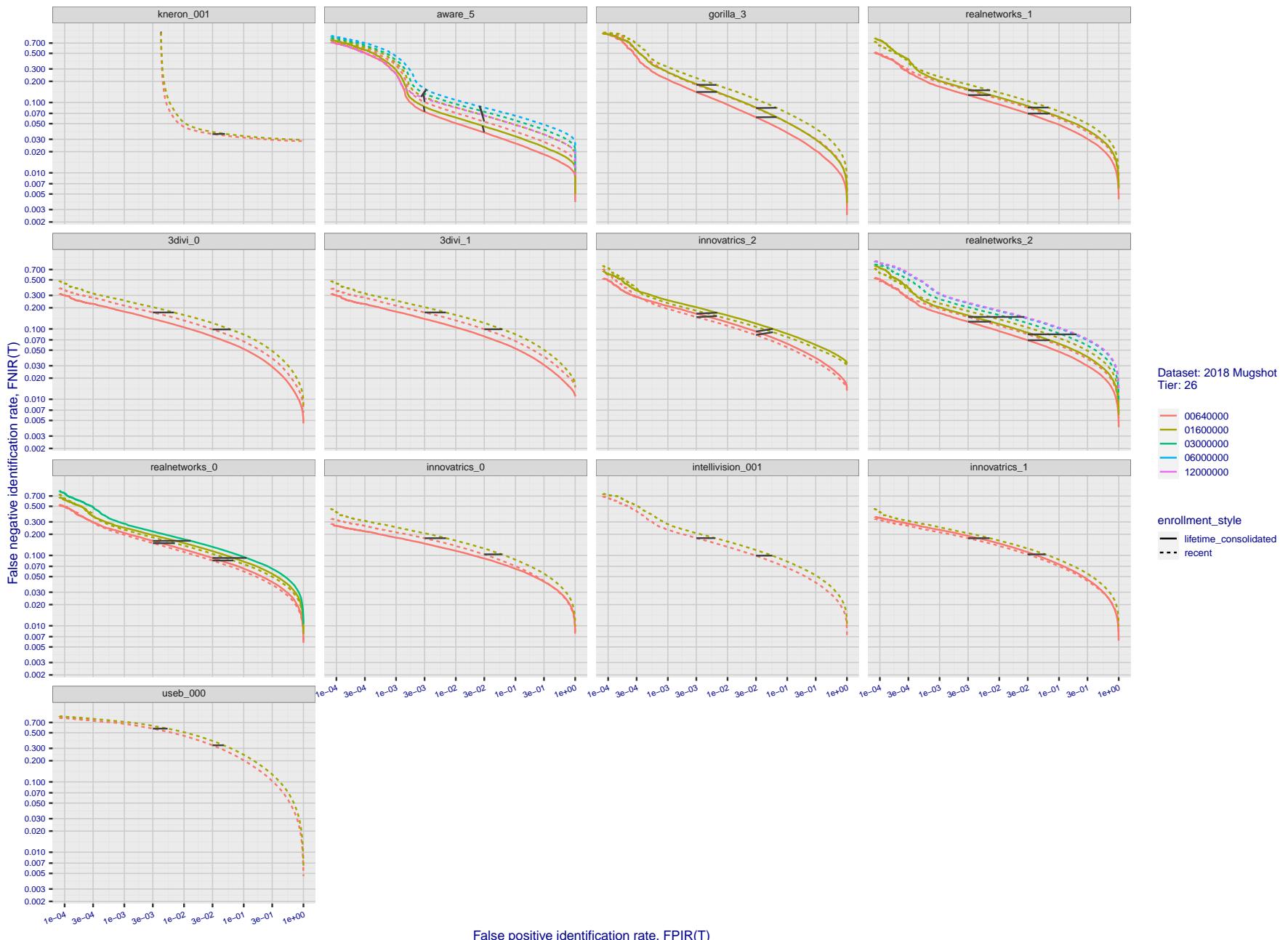


Figure 141: [FRVT-2018 Mugshot Dataset] Identification miss rates vs. false positive rates. The figure shows miss rates $\text{FNIR}(N, L, T)$ as a function of $\text{FPIR}(N, T)$, with N ranging from 640 000 to 12 000 000 as noted in rows 1-10 of Table 1. These error tradeoff characteristics are useful for applications where a threshold must be elevated to limit false positives, such as when human reviewer labor is not matched to the volume of searches. Dark lines join points of equal threshold: If horizontal, $\text{FPIR}(T)$ rises with N , and mate scores are independent of N . Other algorithms adjust scores in an attempt to make FPIR independent of N .

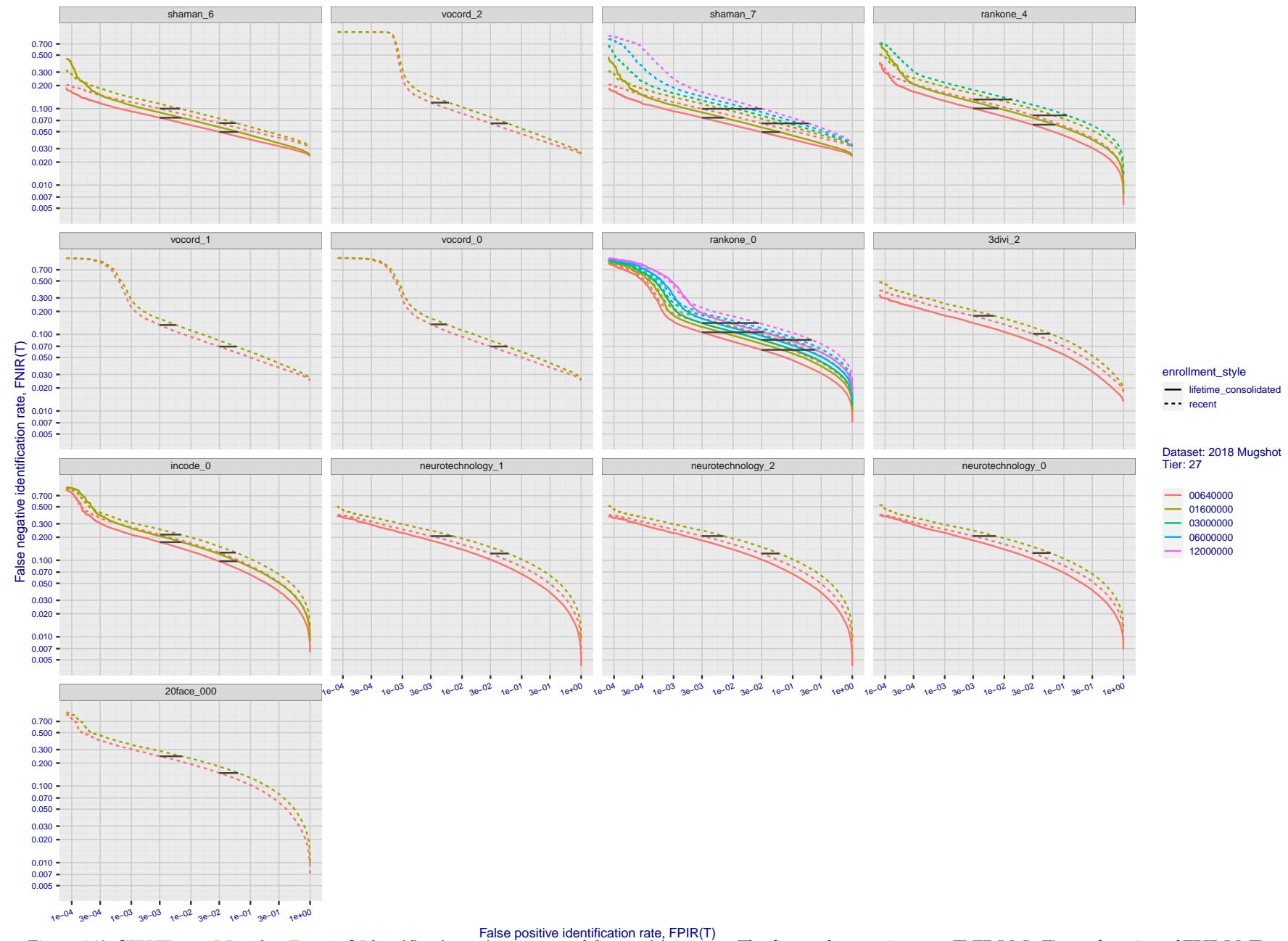


Figure 142: [FRVT-2018 Mugshot Dataset] Identification miss rates vs. false positive rates. The figure shows miss rates $\text{FNIR}(N, L, T)$ as a function of $\text{FPIR}(N, T)$, with N ranging from 640 000 to 12 000 000 as noted in rows 1-10 of Table 1. These error tradeoff characteristics are useful for applications where a threshold must be elevated to limit false positives, such as when human reviewer labor is not matched to the volume of searches. Dark lines join points of equal threshold: If horizontal, $\text{FPIR}(T)$ rises with N , and mate scores are independent of N . Other algorithms adjust scores in an attempt to make FPIR independent of N .

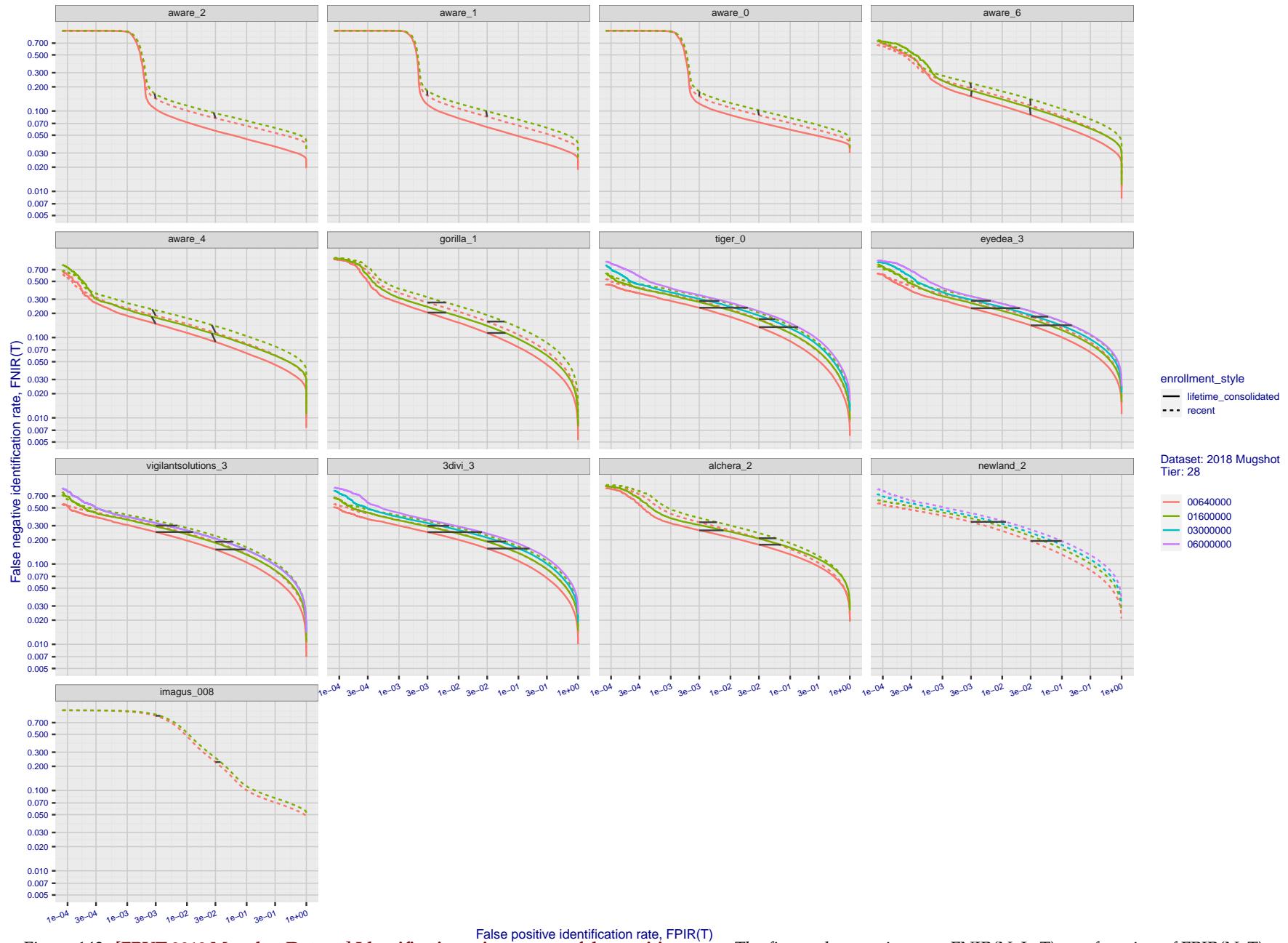


Figure 143: [FRVT-2018 Mugshot Dataset] Identification miss rates vs. false positive rates. The figure shows miss rates $\text{FNIR}(N, L, T)$ as a function of $\text{FPIR}(N, T)$, with N ranging from 640 000 to 12 000 000 as noted in rows 1-10 of Table 1. These error tradeoff characteristics are useful for applications where a threshold must be elevated to limit false positives, such as when human reviewer labor is not matched to the volume of searches. Dark lines join points of equal threshold: If horizontal, $\text{FPIR}(T)$ rises with N , and mate scores are independent of N . Other algorithms adjust scores in an attempt to make FPIR independent of N .

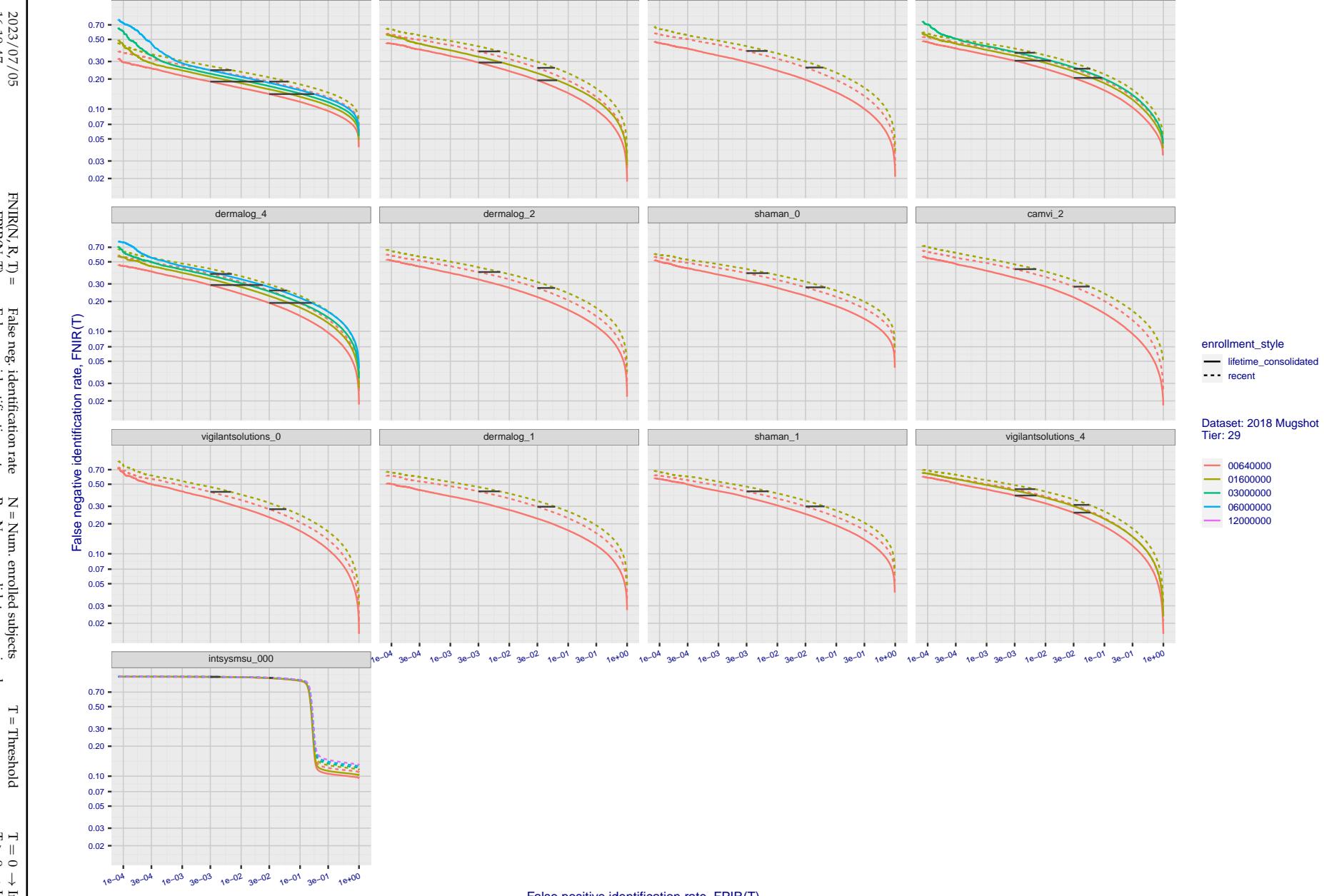


Figure 144: [FRVT-2018 Mugshot Dataset] Identification miss rates vs. false positive rates. The figure shows miss rates $\text{FNIR}(N, L, T)$ as a function of $\text{FPIR}(N, T)$, with N ranging from 640 000 to 12 000 000 as noted in rows 1-10 of Table 1. These error tradeoff characteristics are useful for applications where a threshold must be elevated to limit false positives, such as when human reviewer labor is not matched to the volume of searches. Dark lines join points of equal threshold: If horizontal, $\text{FPIR}(T)$ rises with N , and mate scores are independent of N . Other algorithms adjust scores in an attempt to make FPIR independent of N .

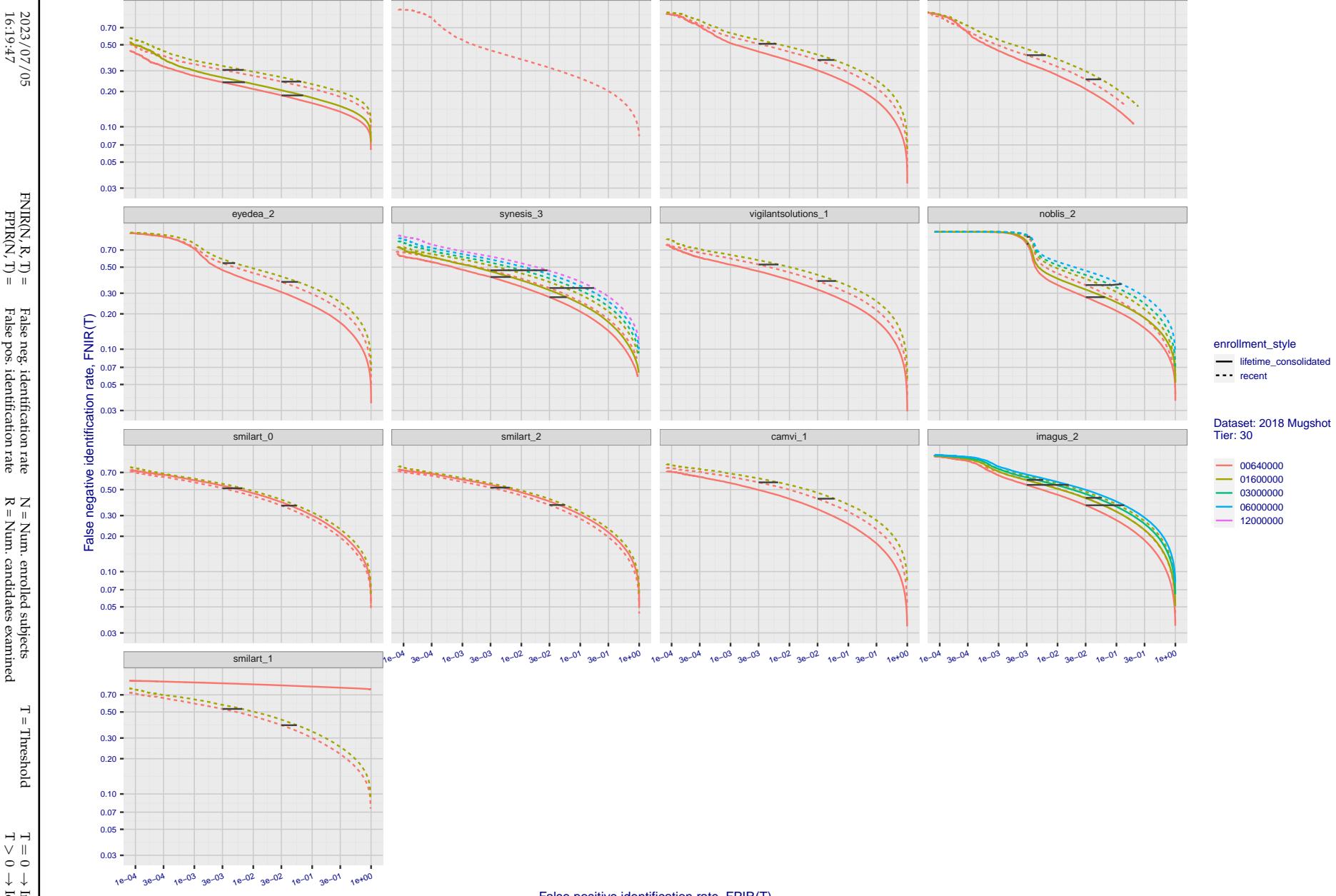


Figure 145: [FRVT-2018 Mugshot Dataset] Identification miss rates vs. false positive rates. The figure shows miss rates $\text{FNIR}(N, L, T)$ as a function of $\text{FPIR}(N, T)$, with N ranging from 640 000 to 12 000 000 as noted in rows 1-10 of Table 1. These error tradeoff characteristics are useful for applications where a threshold must be elevated to limit false positives, such as when human reviewer labor is not matched to the volume of searches. Dark lines join points of equal threshold: If horizontal, $\text{FPIR}(T)$ rises with N , and mate scores are independent of N . Other algorithms adjust scores in an attempt to make FPIR independent of N .

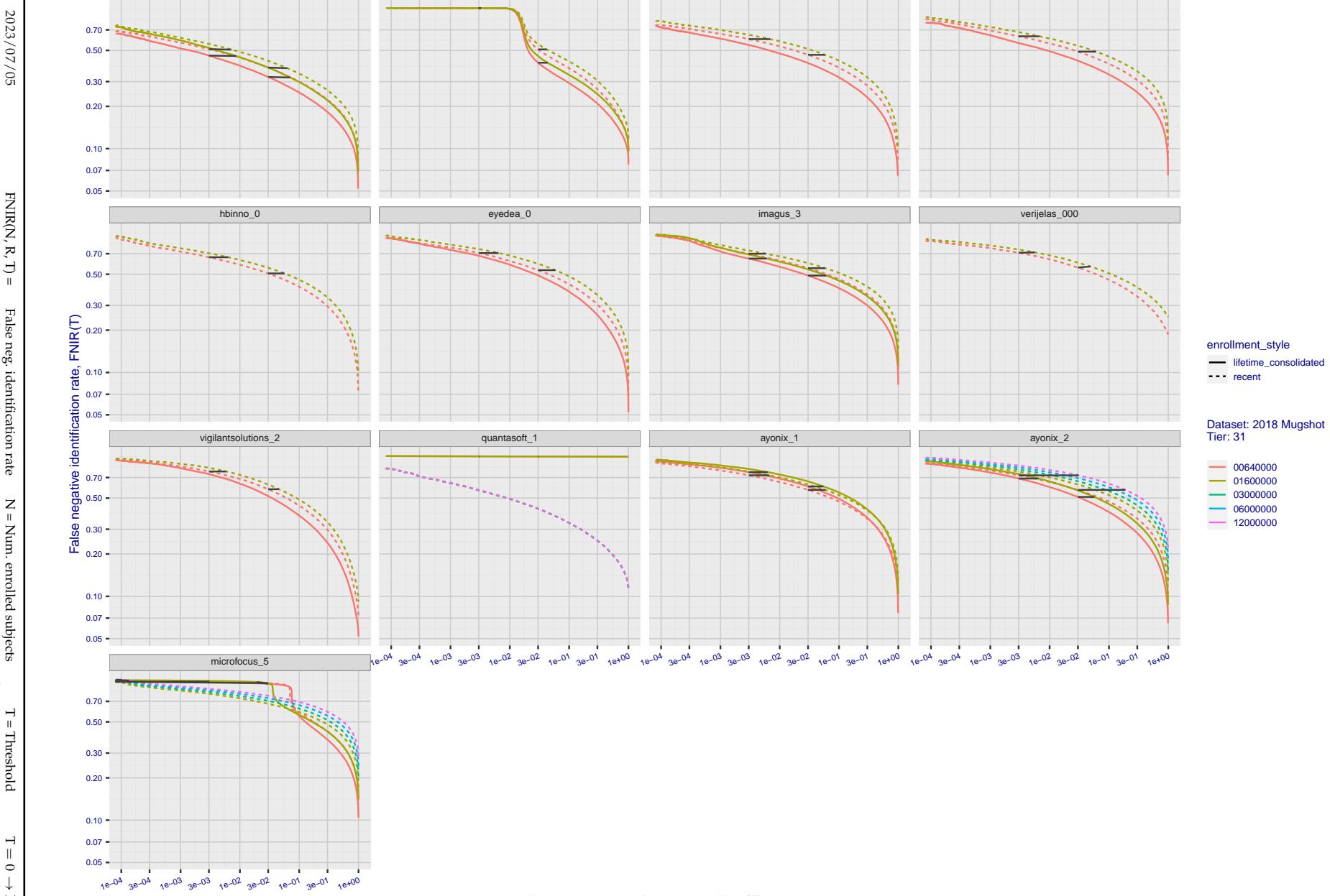


Figure 146: [FRVT-2018 Mugshot Dataset] Identification miss rates vs. false positive rates. The figure shows miss rates $\text{FNIR}(N, L, T)$ as a function of $\text{FPIR}(N, T)$, with N ranging from 640 000 to 12 000 000 as noted in rows 1-10 of Table 1. These error tradeoff characteristics are useful for applications where a threshold must be elevated to limit false positives, such as when human reviewer labor is not matched to the volume of searches. Dark lines join points of equal threshold: If horizontal, $\text{FPIR}(T)$ rises with N , and mate scores are independent of N . Other algorithms adjust scores in an attempt to make FPIR independent of N .

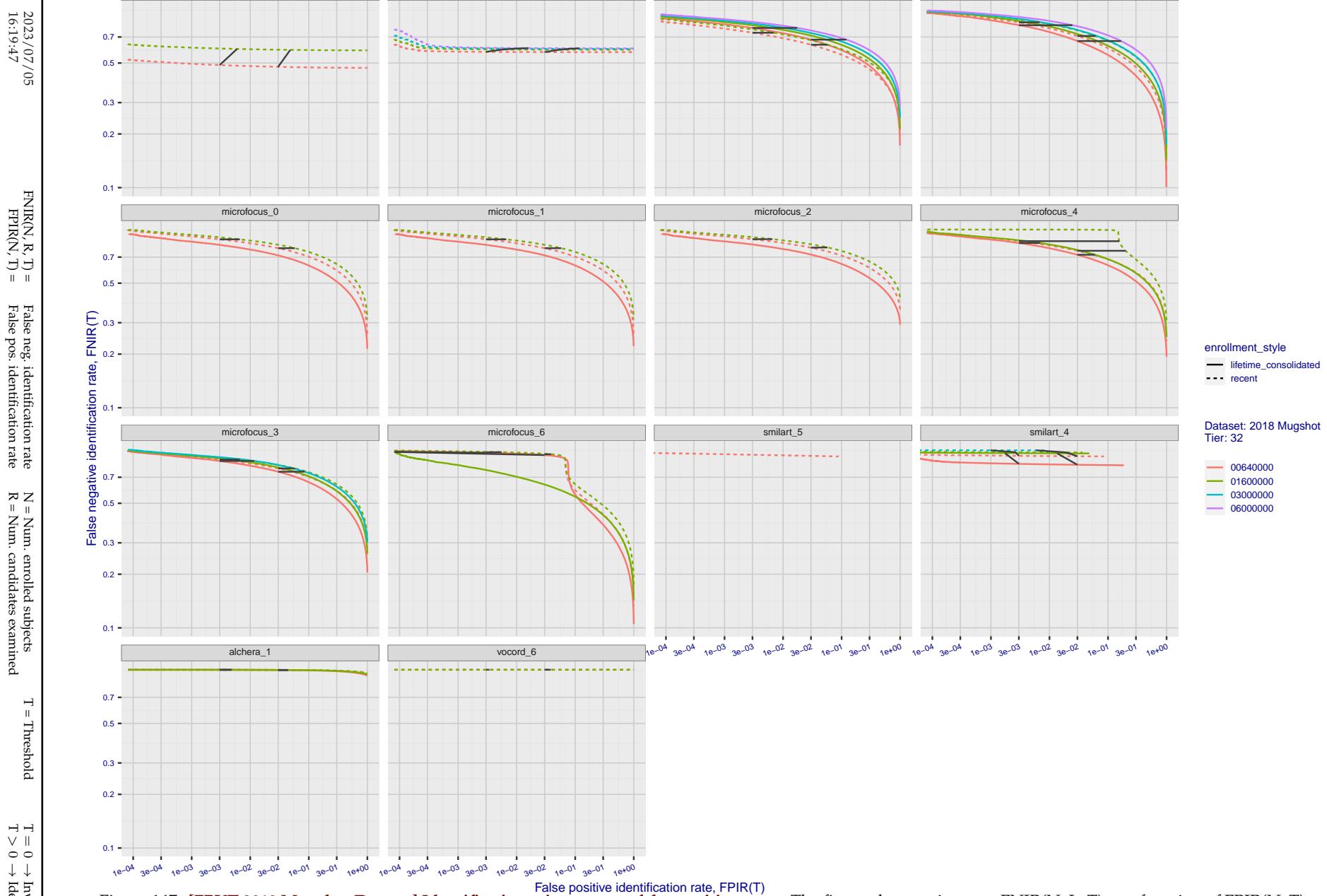


Figure 147: [FRVT-2018 Mugshot Dataset] Identification miss rates vs. false positive rates. The figure shows miss rates $\text{FNIR}(N, L, T)$ as a function of $\text{FPIR}(N, T)$, with N ranging from 640 000 to 12 000 000 as noted in rows 1-10 of Table 1. These error tradeoff characteristics are useful for applications where a threshold must be elevated to limit false positives, such as when human reviewer labor is not matched to the volume of searches. Dark lines join points of equal threshold: If horizontal, $\text{FPIR}(T)$ rises with N , and mate scores are independent of N . Other algorithms adjust scores in an attempt to make FPIR independent of N .

Appendix B Effect of time-lapse: Accuracy after face ageing

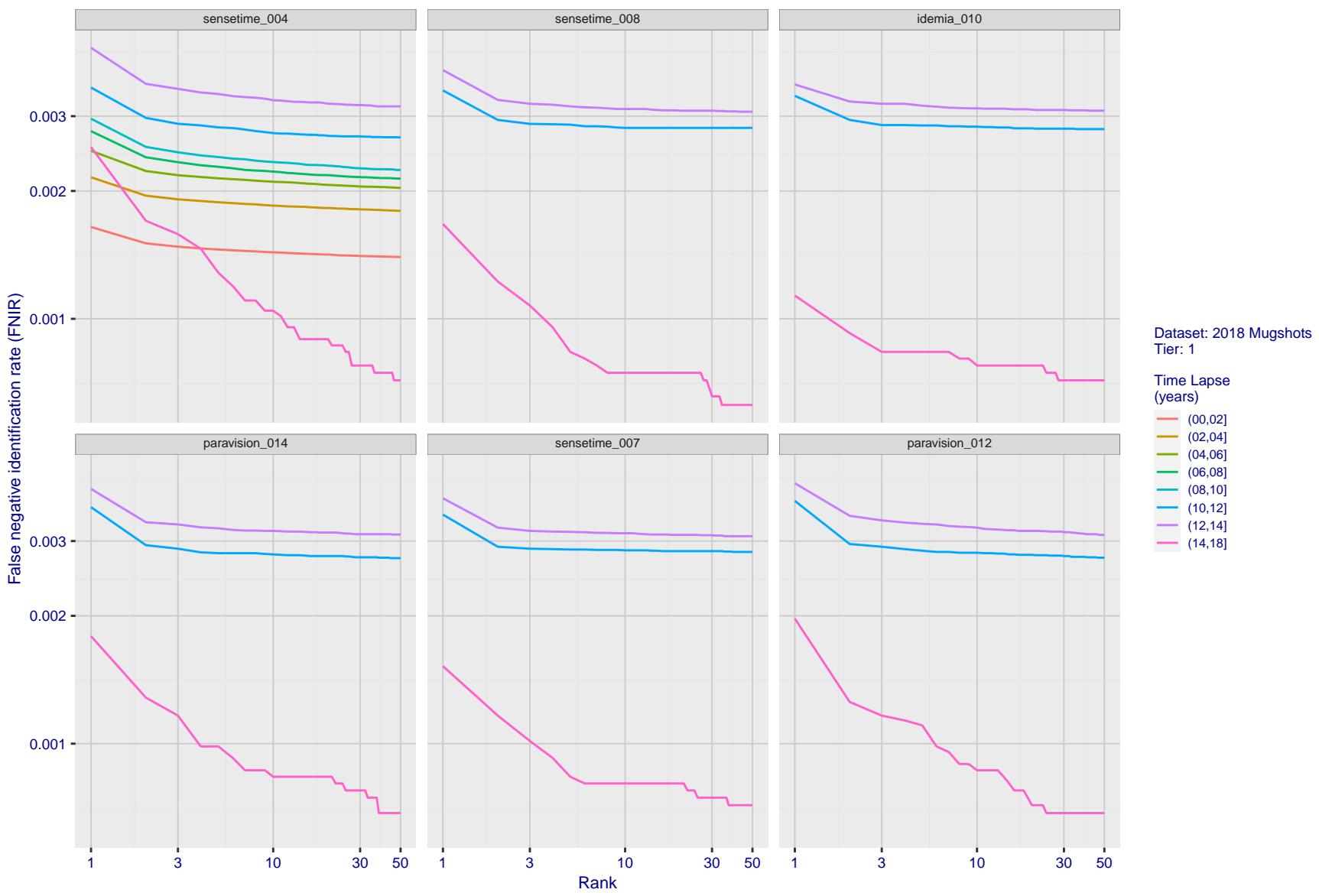


Figure 148: [FRVT-2018 Mugshot Ageing Dataset] Identification miss rates vs. rank by time-elapsed. The oldest image of each individual is enrolled. Thereafter, all more recent images are searched. Miss rates are computed over all searches noted in row 17 of Table 1 and binned by number of years between search and initial enrollment.

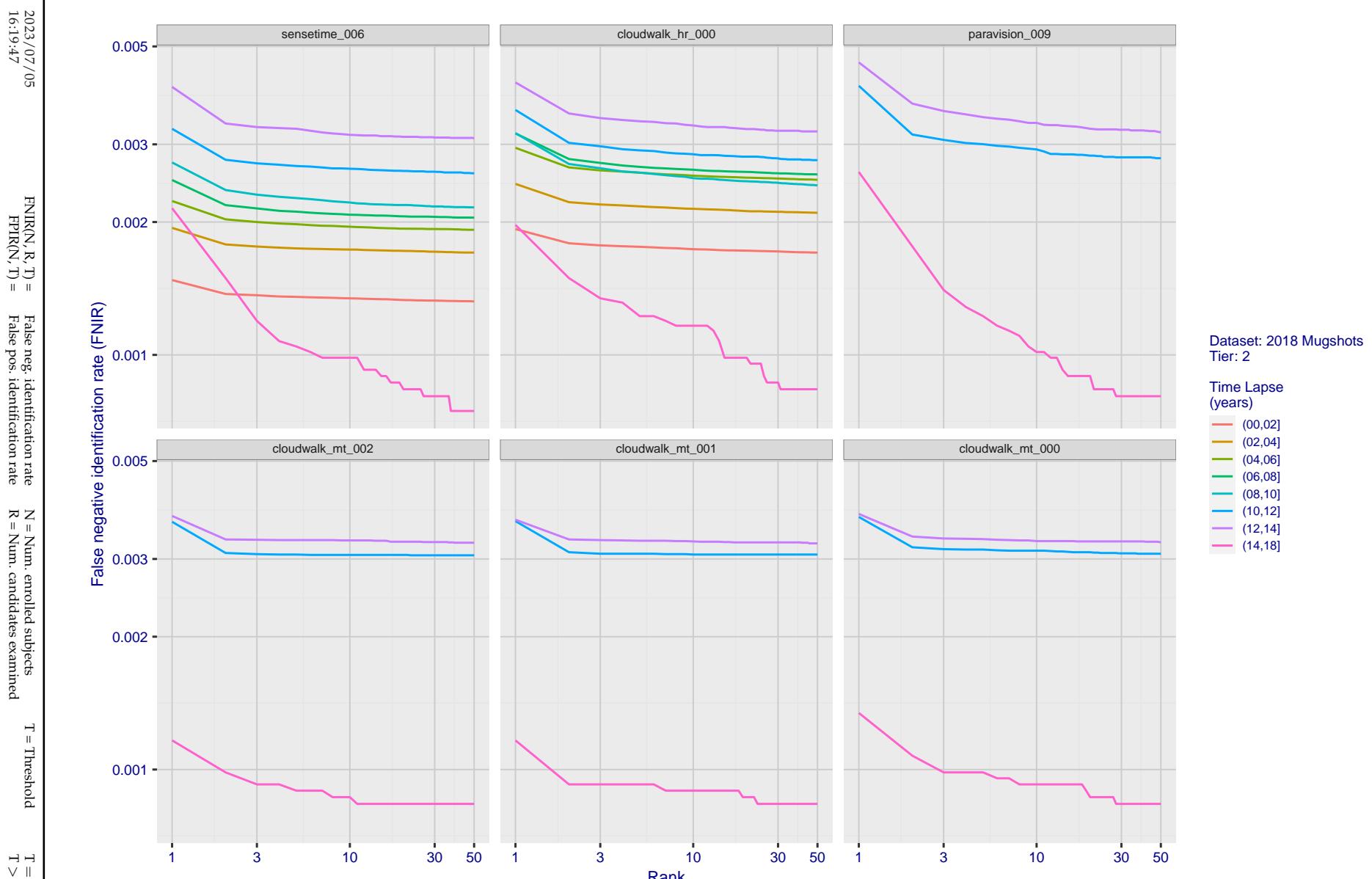


Figure 149: [FRVT-2018 Mugshot Ageing Dataset] Identification miss rates vs. rank by time elapsed. The oldest image of each individual is enrolled. Thereafter, all more recent images are searched. Miss rates are computed over all searches noted in row 17 of Table 1 and binned by number of years between search and initial enrollment.

2023/07/05
16:19:47FNIR(N, R, T) = False neg. identification rate
FPIR(N, T) = False pos. identification rateN = Num. enrolled subjects
R = Num. candidates examinedT = Threshold
T = 0 → Investigation

T > 0 → Identification

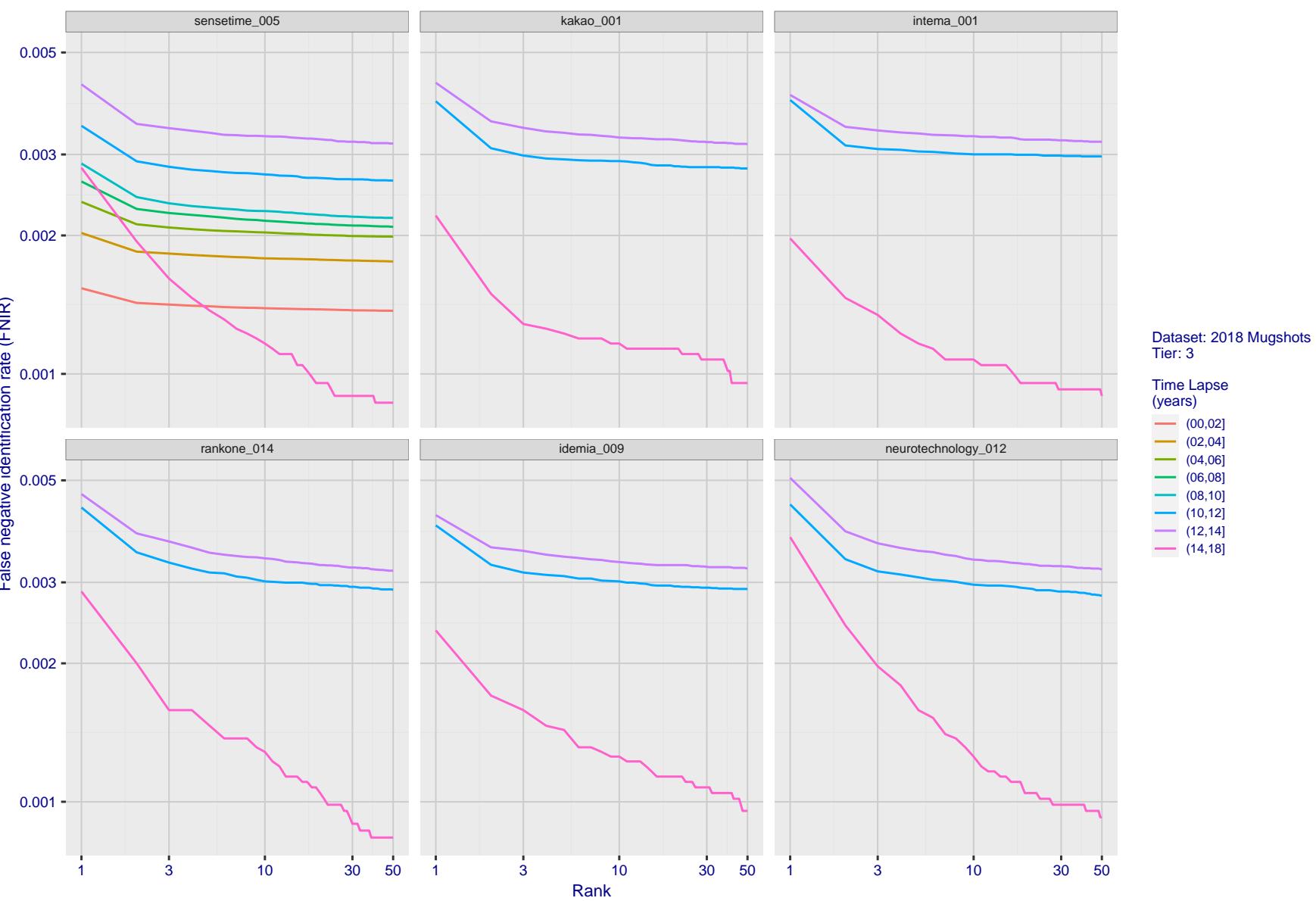


Figure 150: [FRVT-2018 Mugshot Ageing Dataset] Identification miss rates vs. rank by time elapsed. The oldest image of each individual is enrolled. Thereafter, all more recent images are searched. Miss rates are computed over all searches noted in row 17 of Table 1 and binned by number of years between search and initial enrollment.

2023/07/05
16:19:47FNIR(N, R, T) = False neg. identification rate
FPIR(N, T) = False pos. identification rateN = Num. enrolled subjects
R = Num. candidates examinedT = Threshold
T = 0 → Investigation

T > 0 → Identification

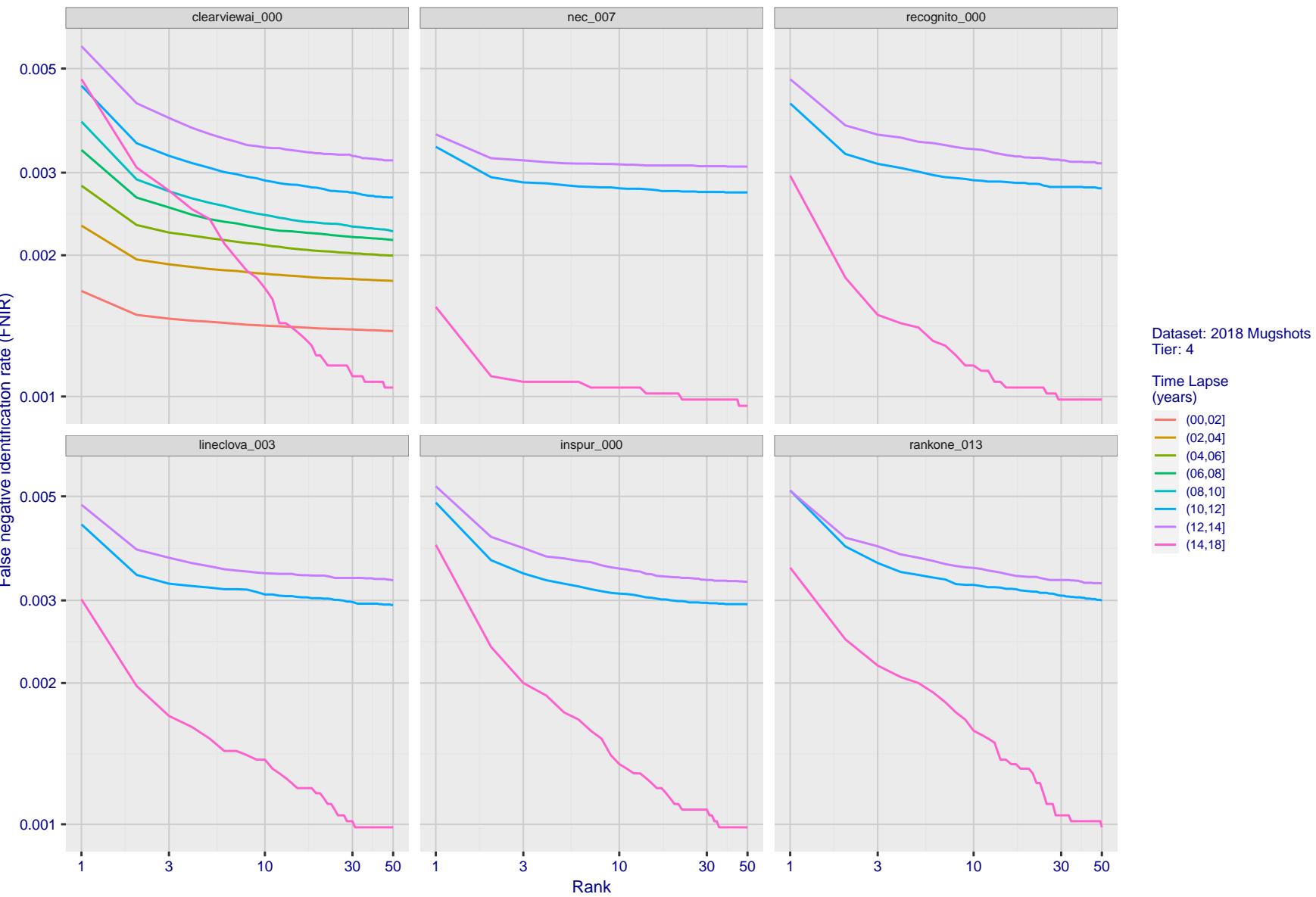


Figure 151: [FRVT-2018 Mugshot Ageing Dataset] Identification miss rates vs. rank by time elapsed. The oldest image of each individual is enrolled. Thereafter, all more recent images are searched. Miss rates are computed over all searches noted in row 17 of Table 1 and binned by number of years between search and initial enrollment.

2023/07/05
16:19:47FNIR(N, R, T) = False neg. identification rate
FPIR(N, T) = False pos. identification rateN = Num. enrolled subjects
R = Num. candidates examinedT = Threshold
T = 0 → Investigation

T > 0 → Identification

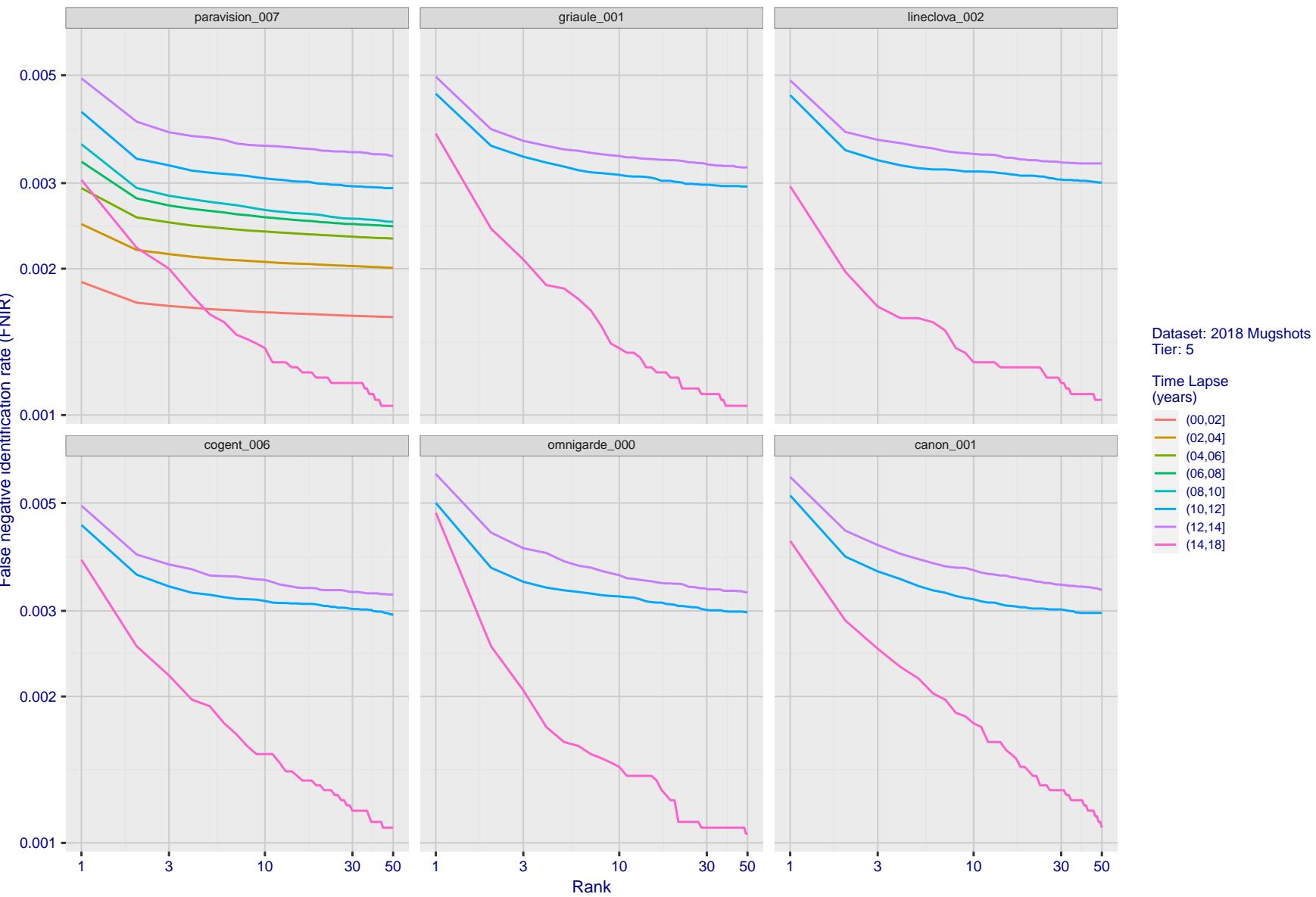


Figure 152: [FRVT-2018 Mugshot Ageing Dataset] Identification miss rates vs. rank by time elapsed. The oldest image of each individual is enrolled. Thereafter, all more recent images are searched. Miss rates are computed over all searches noted in row 17 of Table 1 and binned by number of years between search and initial enrollment.

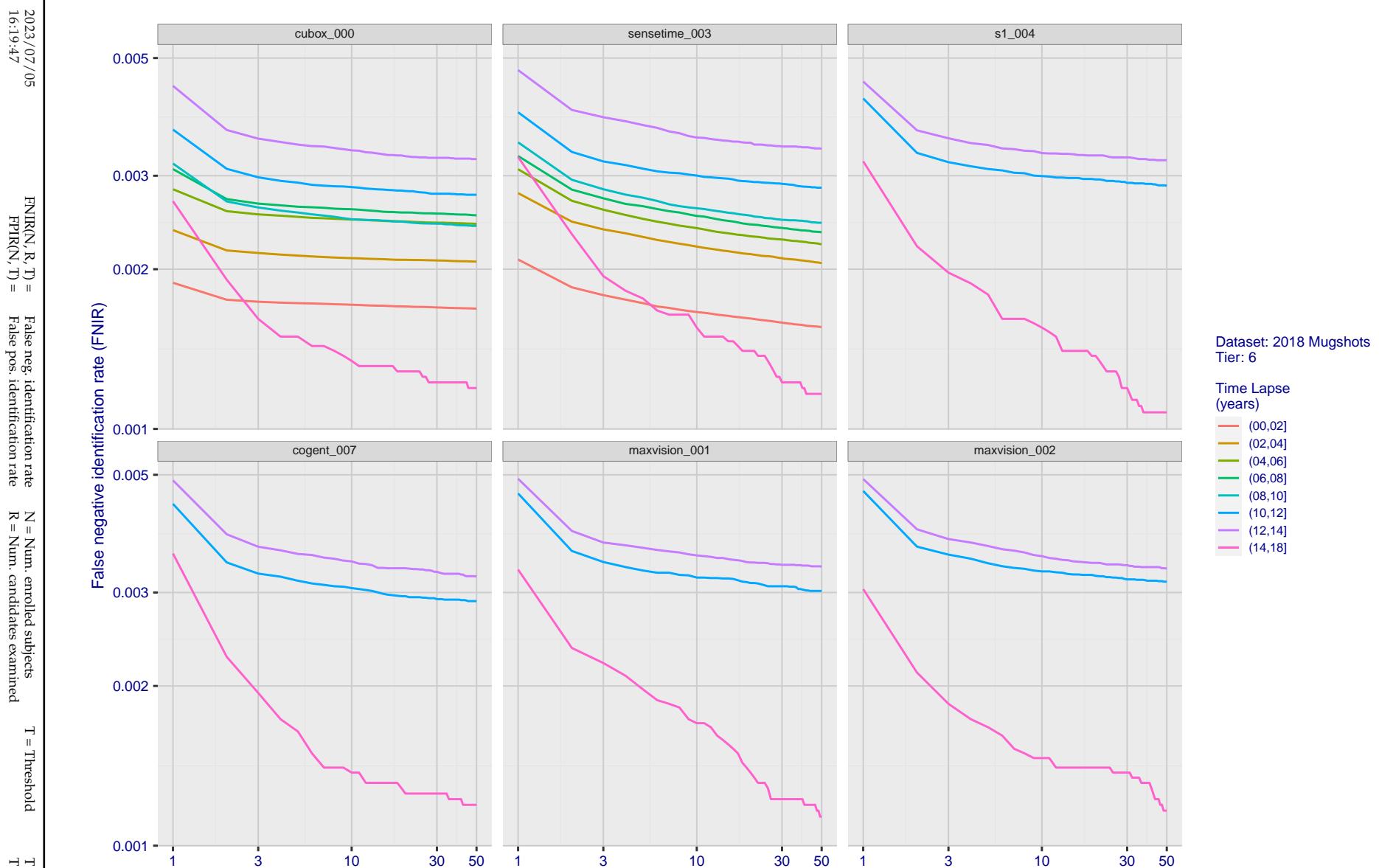


Figure 153: [FRVT-2018 Mugshot Ageing Dataset] Identification miss rates vs. rank by time elapsed. The oldest image of each individual is enrolled. Thereafter, all more recent images are searched. Miss rates are computed over all searches noted in row 17 of Table 1 and binned by number of years between search and initial enrollment.

2023/07/05
16:19:47FNIR(N, R, T) = False neg. identification rate
FPIR(N, T) = False pos. identification rateN = Num. enrolled subjects
R = Num. candidates examinedT = Threshold
T = 0 → Investigation

T > 0 → Identification

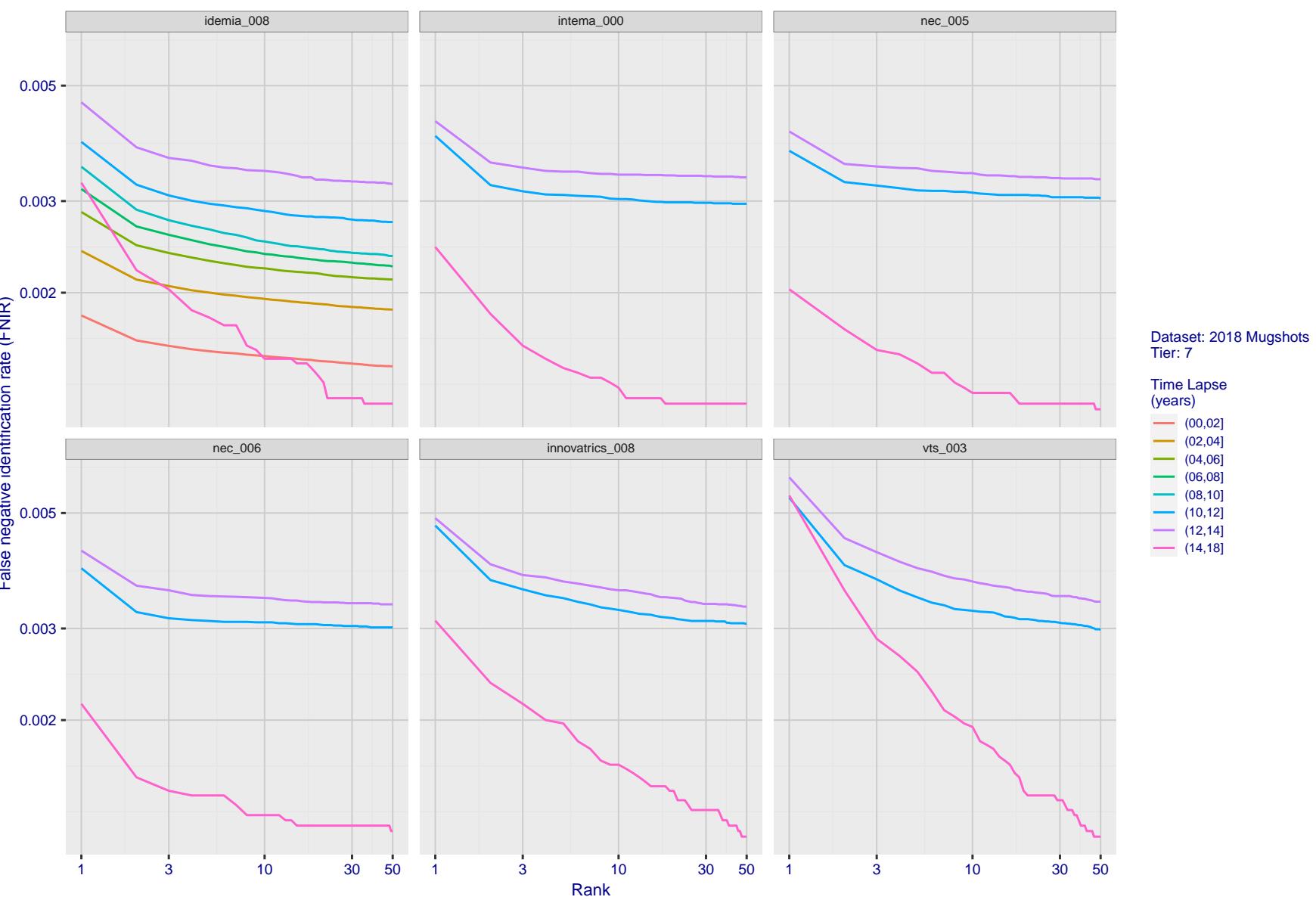


Figure 154: [FRVT-2018 Mugshot Ageing Dataset] Identification miss rates vs. rank by time elapsed. The oldest image of each individual is enrolled. Thereafter, all more recent images are searched. Miss rates are computed over all searches noted in row 17 of Table 1 and binned by number of years between search and initial enrollment.

2023/07/05
16:19:47FNIR(N, R, T) = False neg. identification rate
FPIR(N, T) = False pos. identification rateN = Num. enrolled subjects
R = Num. candidates examinedT = Threshold
T = 0 → Investigation

T > 0 → Identification

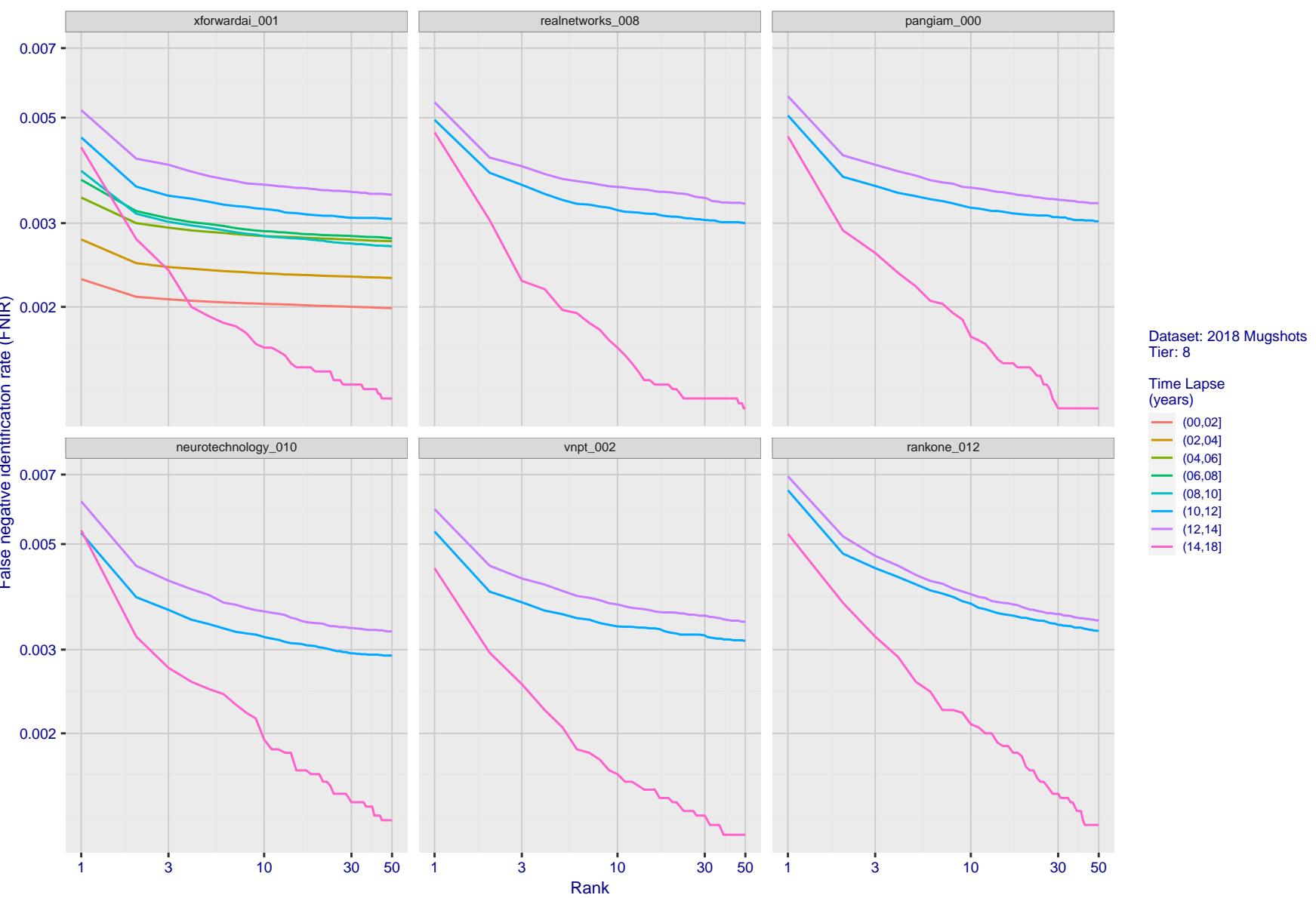


Figure 155: [FRVT-2018 Mugshot Ageing Dataset] Identification miss rates vs. rank by time elapsed. The oldest image of each individual is enrolled. Thereafter, all more recent images are searched. Miss rates are computed over all searches noted in row 17 of Table 1 and binned by number of years between search and initial enrollment.

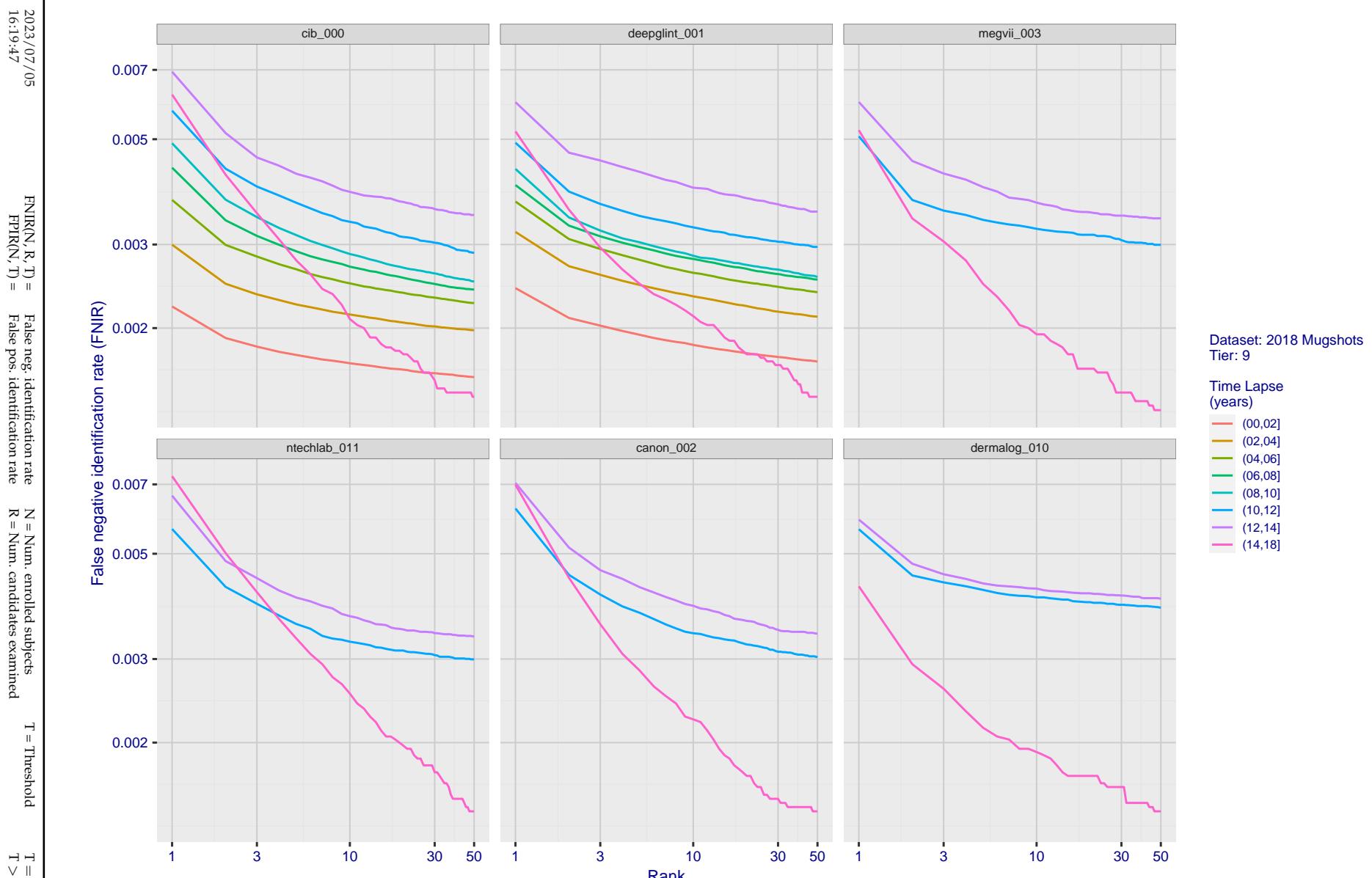


Figure 156: [FRVT-2018 Mugshot Ageing Dataset] Identification miss rates vs. rank by time elapsed. The oldest image of each individual is enrolled. Thereafter, all more recent images are searched. Miss rates are computed over all searches noted in row 17 of Table 1 and binned by number of years between search and initial enrollment.

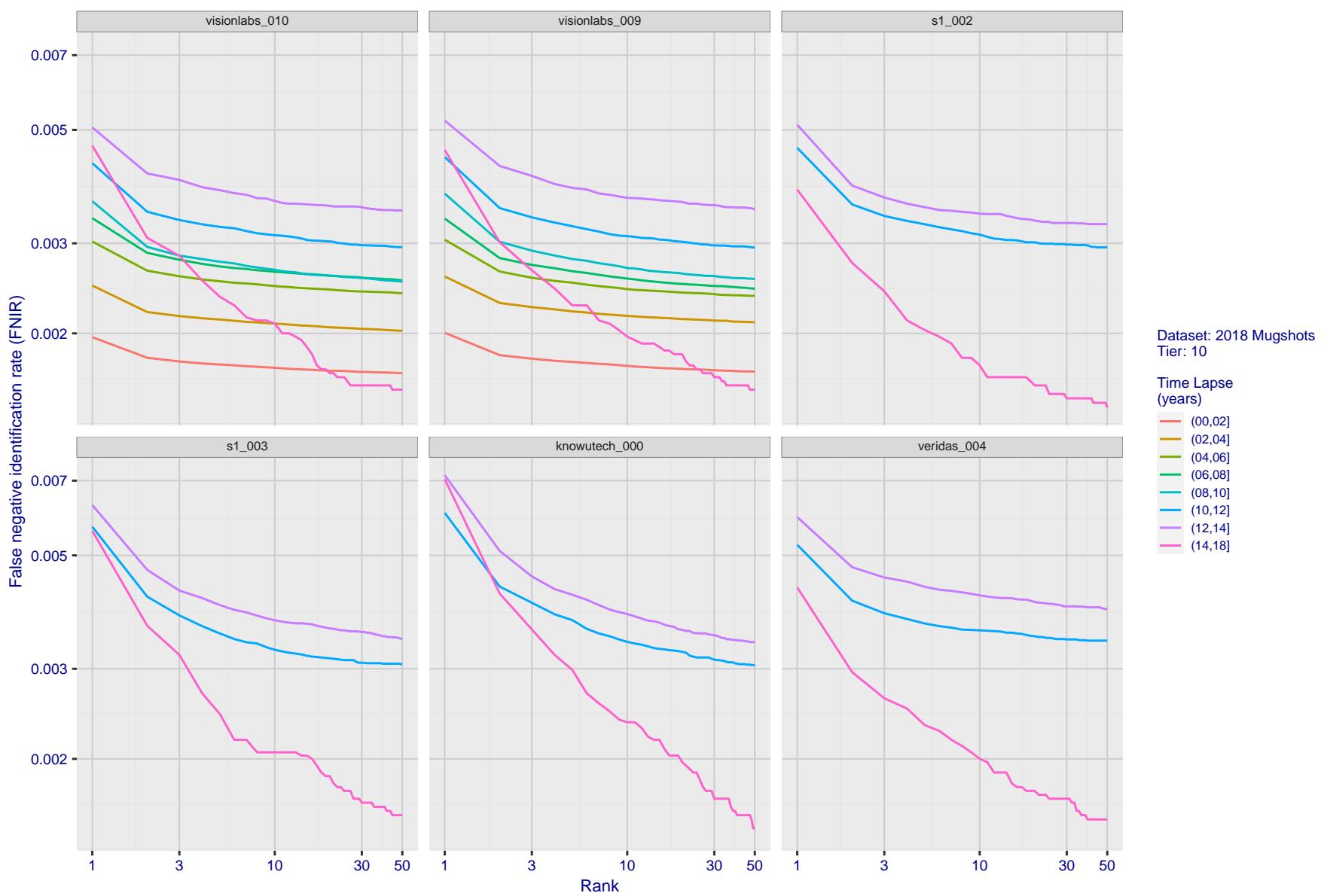
2023/07/05
16:19:47

Figure 157: [FRVT-2018 Mugshot Ageing Dataset] Identification miss rates vs. rank by time-elapsed. The oldest image of each individual is enrolled. Thereafter, all more recent images are searched. Miss rates are computed over all searches noted in row 17 of Table 1 and binned by number of years between search and initial enrollment.

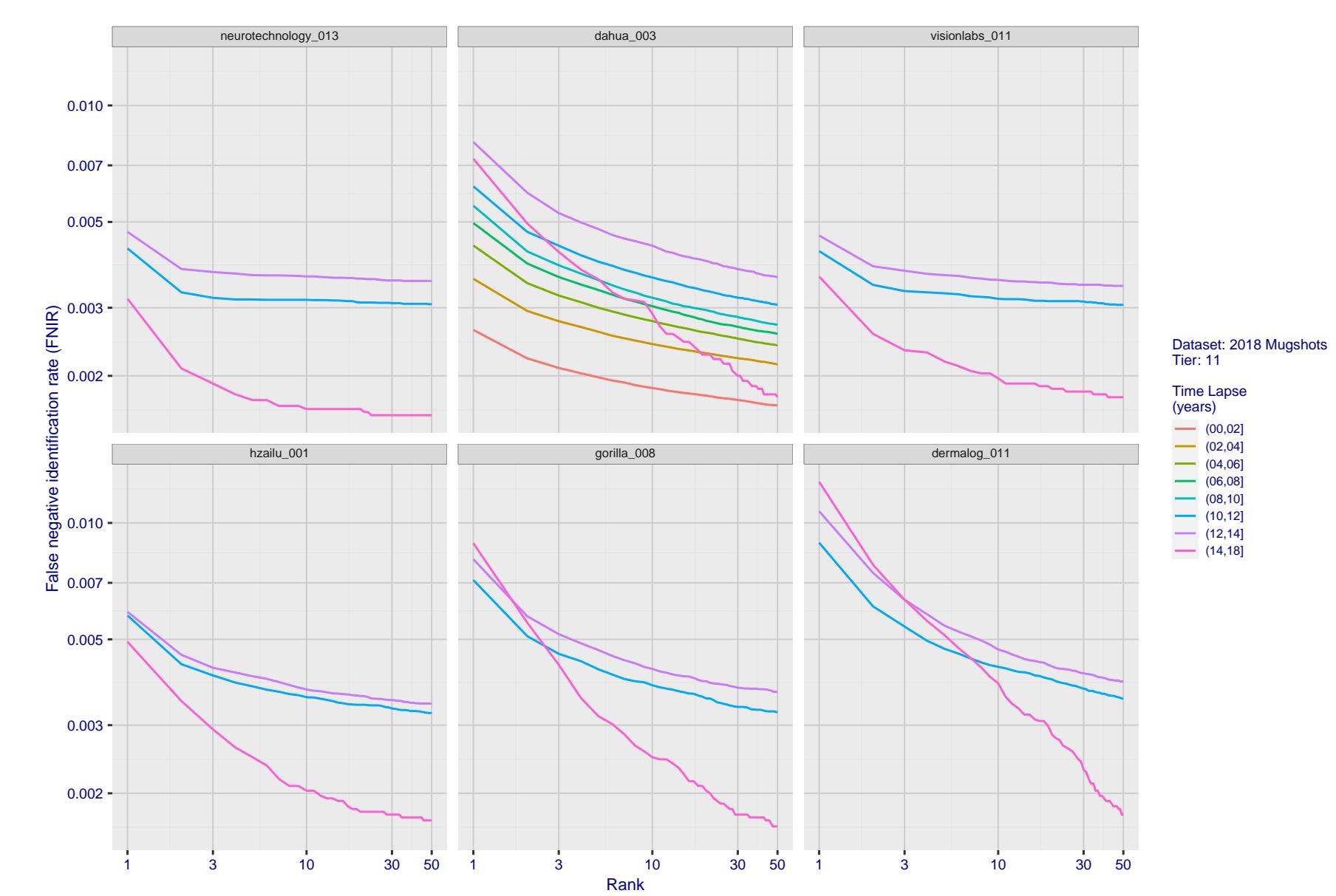
2023/07/05
16:19:47

Figure 158: [FRVT-2018 Mugshot Ageing Dataset] Identification miss rates vs. rank by time-elapsed. The oldest image of each individual is enrolled. Thereafter, all more recent images are searched. Miss rates are computed over all searches noted in row 17 of Table 1 and binned by number of years between search and initial enrollment.

2023/07/05
16:19:47FNIR(N, R, T) = False neg. identification rate
FPIR(N, T) = False pos. identification rateN = Num. enrolled subjects
R = Num. candidates examinedT = Threshold
T = 0 → Investigation

T > 0 → Identification

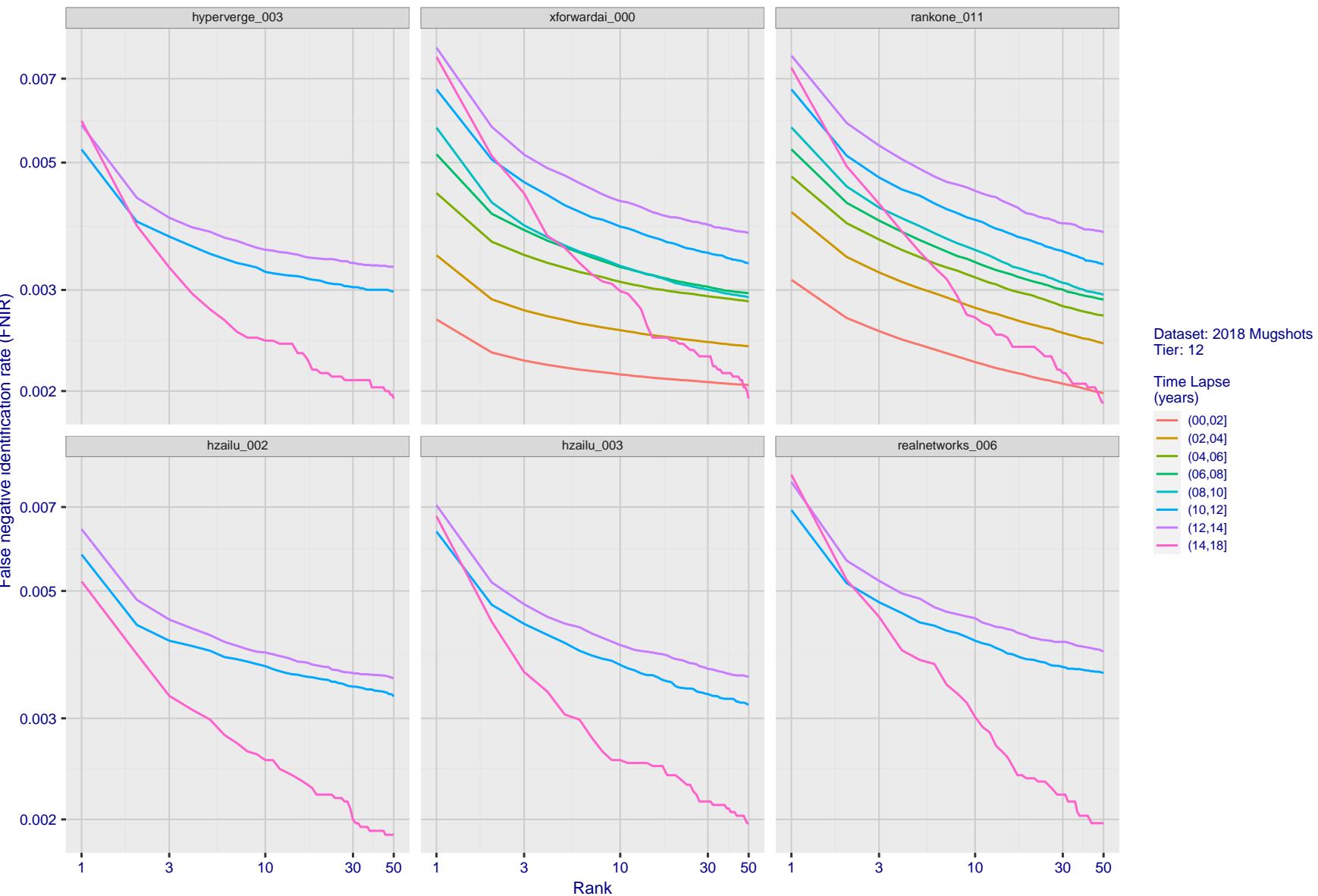


Figure 159: [FRVT-2018 Mugshot Ageing Dataset] Identification miss rates vs. rank by time elapsed. The oldest image of each individual is enrolled. Thereafter, all more recent images are searched. Miss rates are computed over all searches noted in row 17 of Table 1 and binned by number of years between search and initial enrollment.

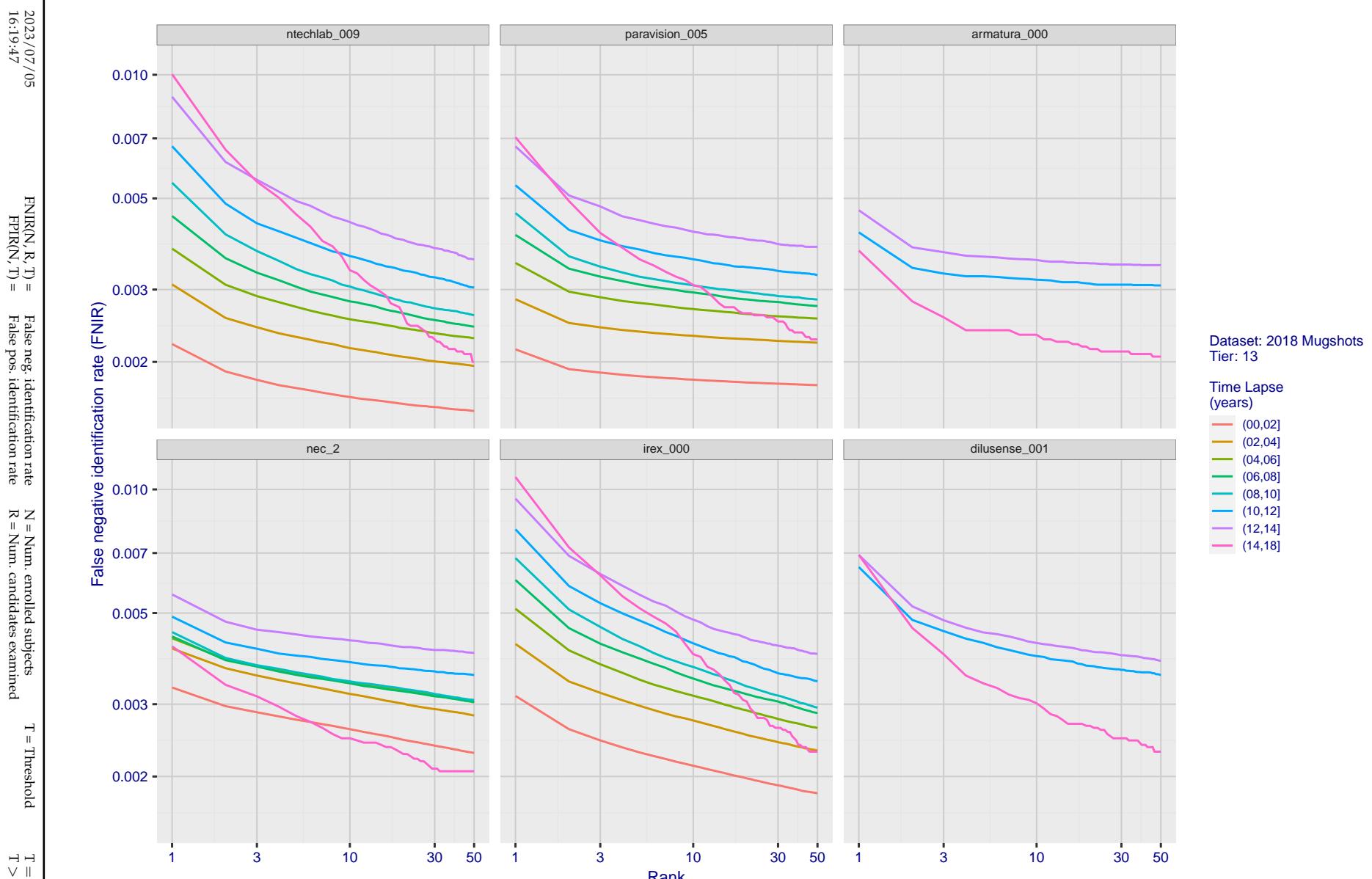


Figure 160: [FRVT-2018 Mugshot Ageing Dataset] Identification miss rates vs. rank by time-elapsed. The oldest image of each individual is enrolled. Thereafter, all more recent images are searched. Miss rates are computed over all searches noted in row 17 of Table 1 and binned by number of years between search and initial enrollment.

2023/07/05
16:19:47FNIR(N, R, T) = False neg. identification rate
FPIR(N, T) = False pos. identification rateN = Num. enrolled subjects
R = Num. candidates examinedT = Threshold
T = 0 → Investigation

T > 0 → Identification

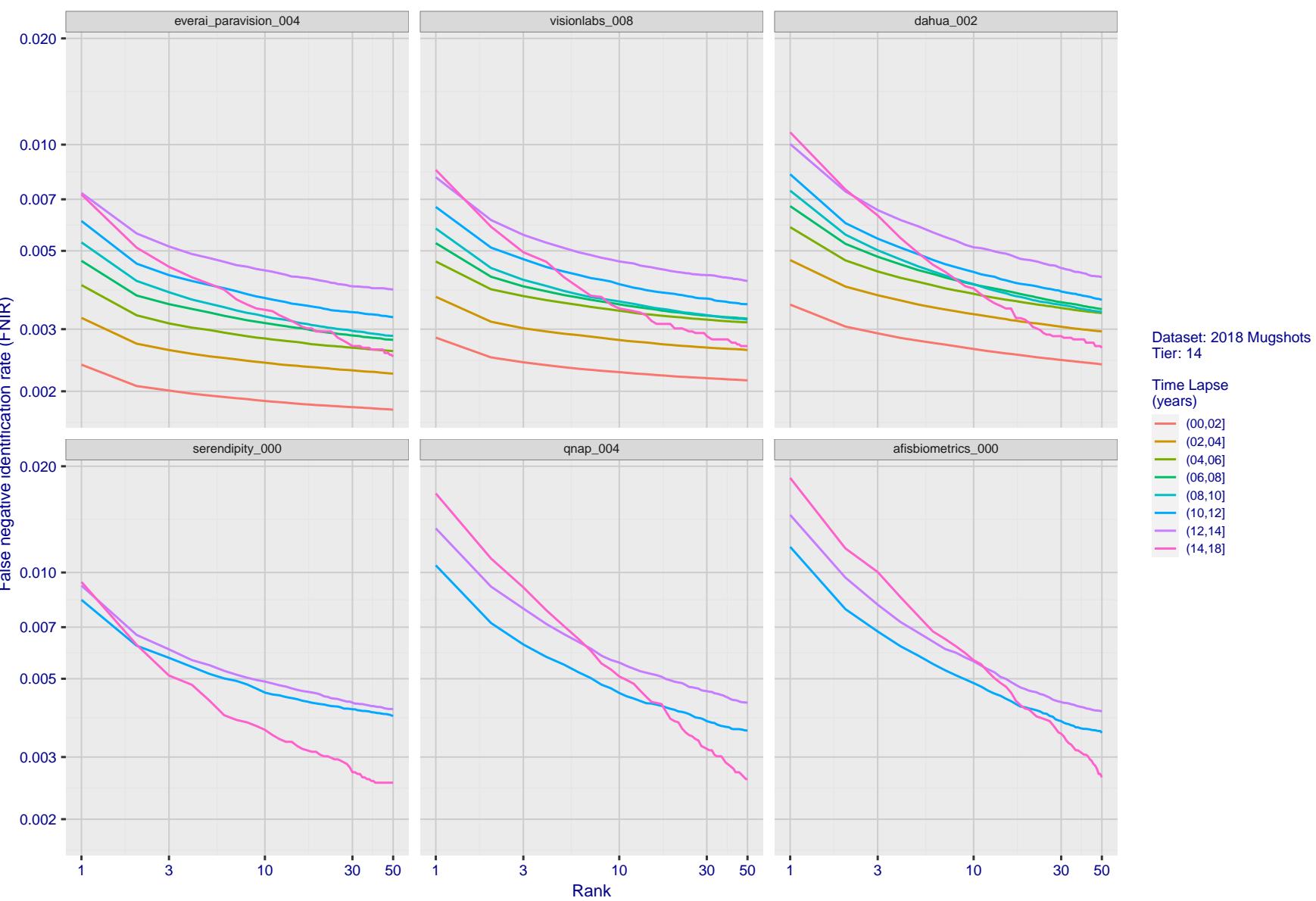


Figure 161: [FRVT-2018 Mugshot Ageing Dataset] Identification miss rates vs. rank by time-elapsed. The oldest image of each individual is enrolled. Thereafter, all more recent images are searched. Miss rates are computed over all searches noted in row 17 of Table 1 and binned by number of years between search and initial enrollment.

2023/07/05
16:19:47FNIR(N, R, T) = False neg. identification rate
FPIR(N, T) = False pos. identification rateN = Num. enrolled subjects
R = Num. candidates examinedT = Threshold
T = 0 → Investigation

T > 0 → Identification

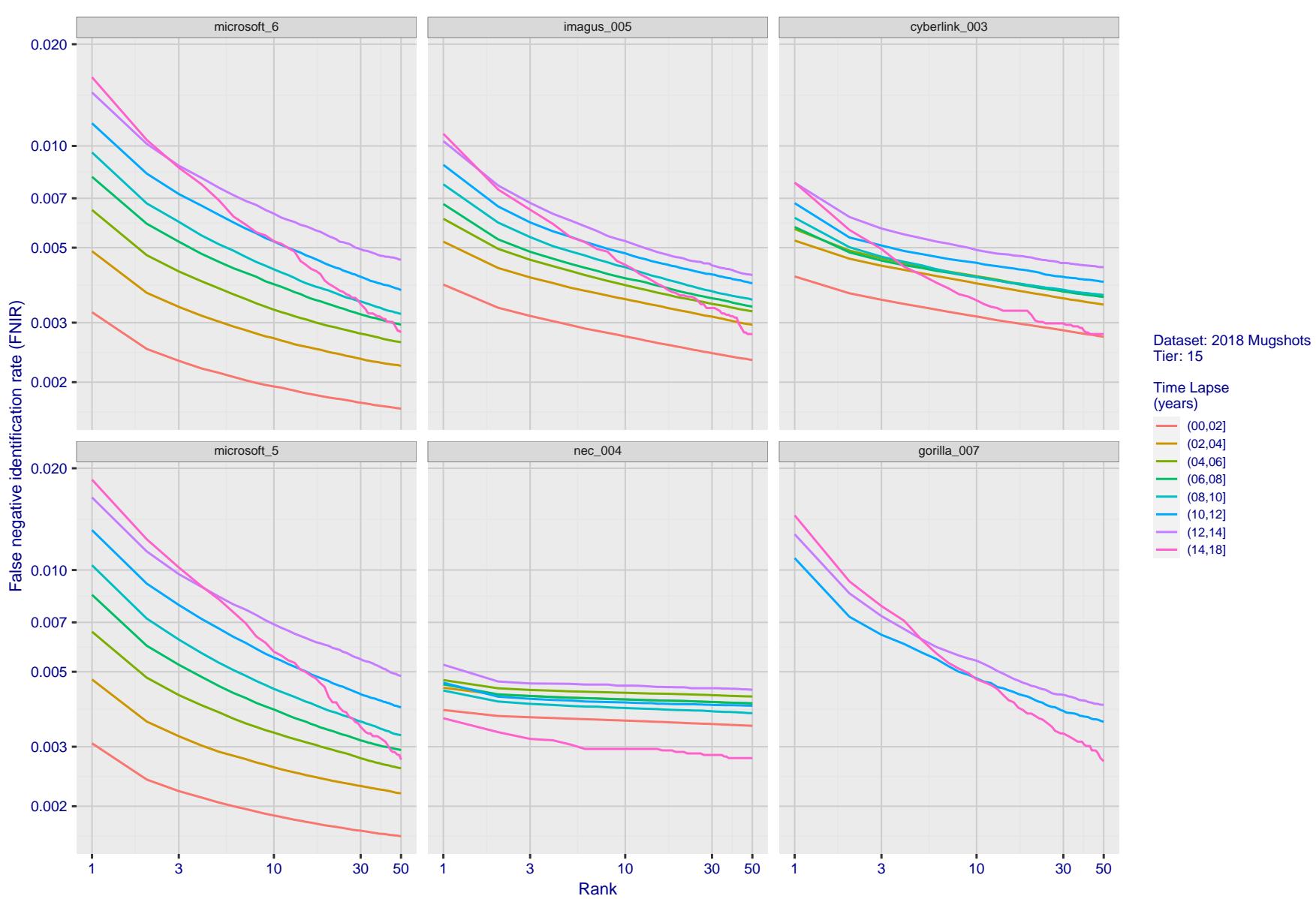


Figure 162: [FRVT-2018 Mugshot Ageing Dataset] Identification miss rates vs. rank by time elapsed. The oldest image of each individual is enrolled. Thereafter, all more recent images are searched. Miss rates are computed over all searches noted in row 17 of Table 1 and binned by number of years between search and initial enrollment.

2023/07/05
16:19:47FNIR(N, R, T) = False neg. identification rate
FPIR(N, T) = False pos. identification rateN = Num. enrolled subjects
R = Num. candidates examined

T = Threshold

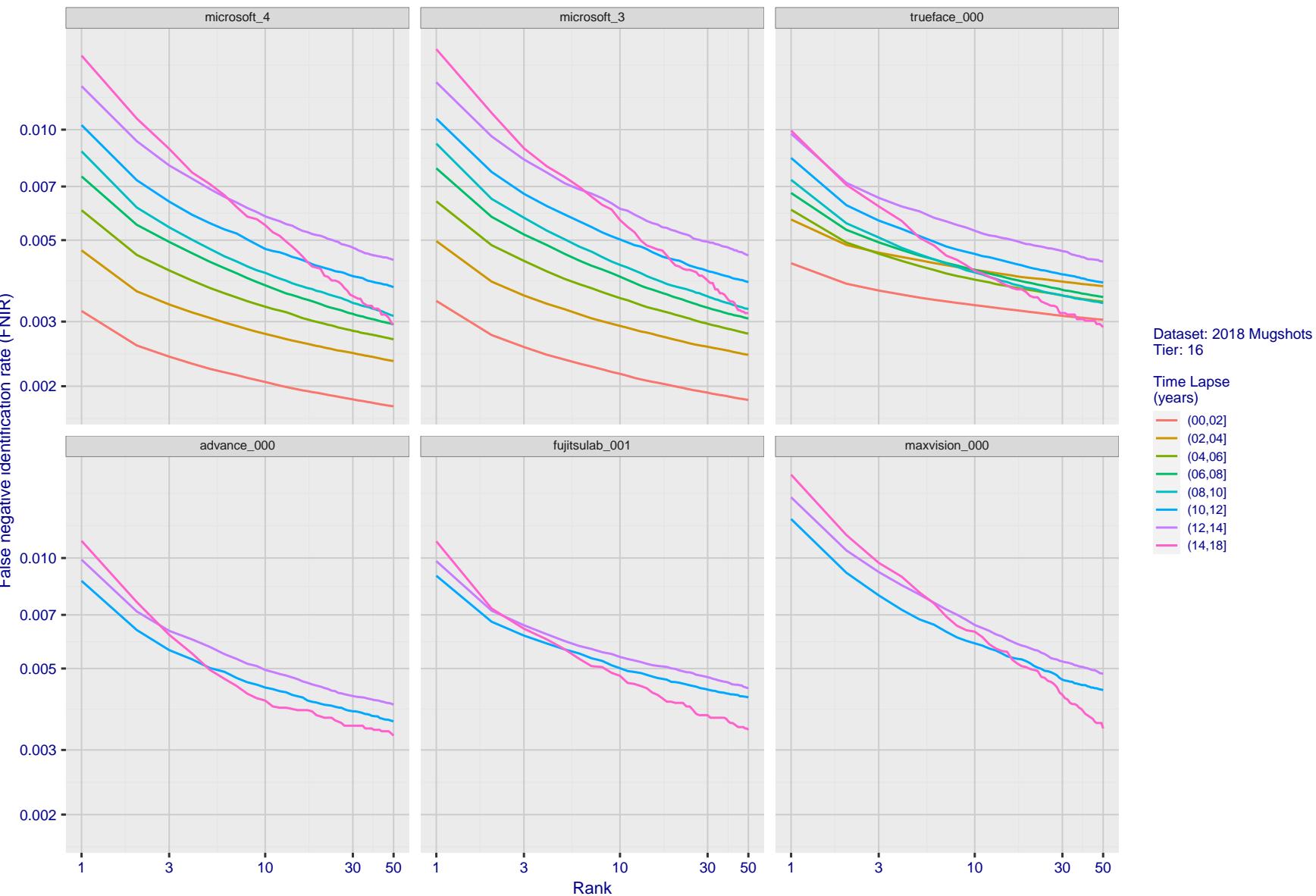
T = 0 → Investigation
T > 0 → Identification

Figure 163: [FRVT-2018 Mugshot Ageing Dataset] Identification miss rates vs. rank by time elapsed. The oldest image of each individual is enrolled. Thereafter, all more recent images are searched. Miss rates are computed over all searches noted in row 17 of Table 1 and binned by number of years between search and initial enrollment.

2023/07/05
16:19:47FNIR(N, R, T) = False neg. identification rate
FPIR(N, T) = False pos. identification rateN = Num. enrolled subjects
R = Num. candidates examinedT = Threshold
T = 0 → Investigation

T > 0 → Identification

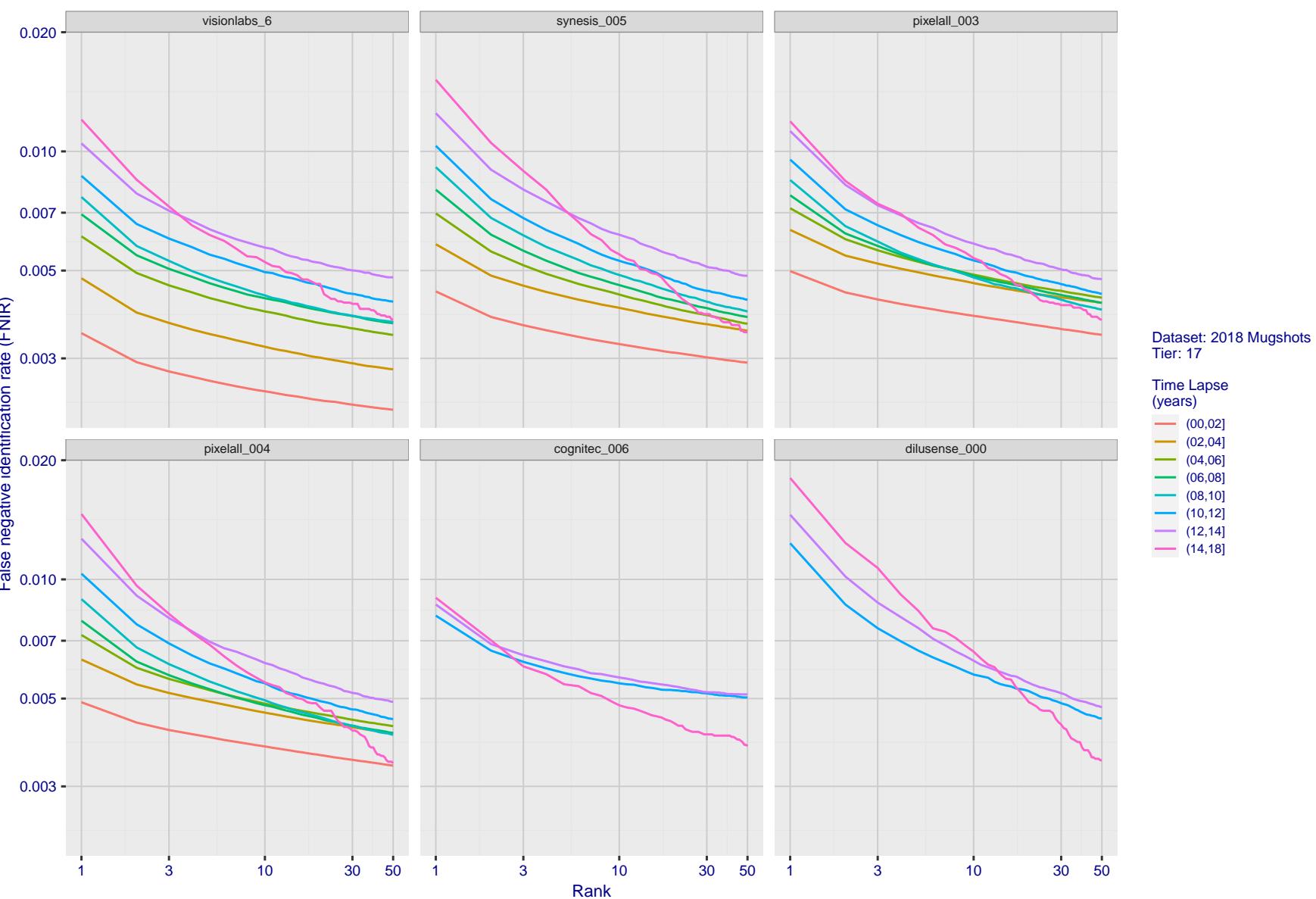


Figure 164: [FRVT-2018 Mugshot Ageing Dataset] Identification miss rates vs. rank by time elapsed. The oldest image of each individual is enrolled. Thereafter, all more recent images are searched. Miss rates are computed over all searches noted in row 17 of Table 1 and binned by number of years between search and initial enrollment.

2023/07/05
16:19:47FNIR(N, R, T) = False neg. identification rate
FPIR(N, T) = False pos. identification rateN = Num. enrolled subjects
R = Num. candidates examinedT = Threshold
T = 0 → Investigation

T > 0 → Identification

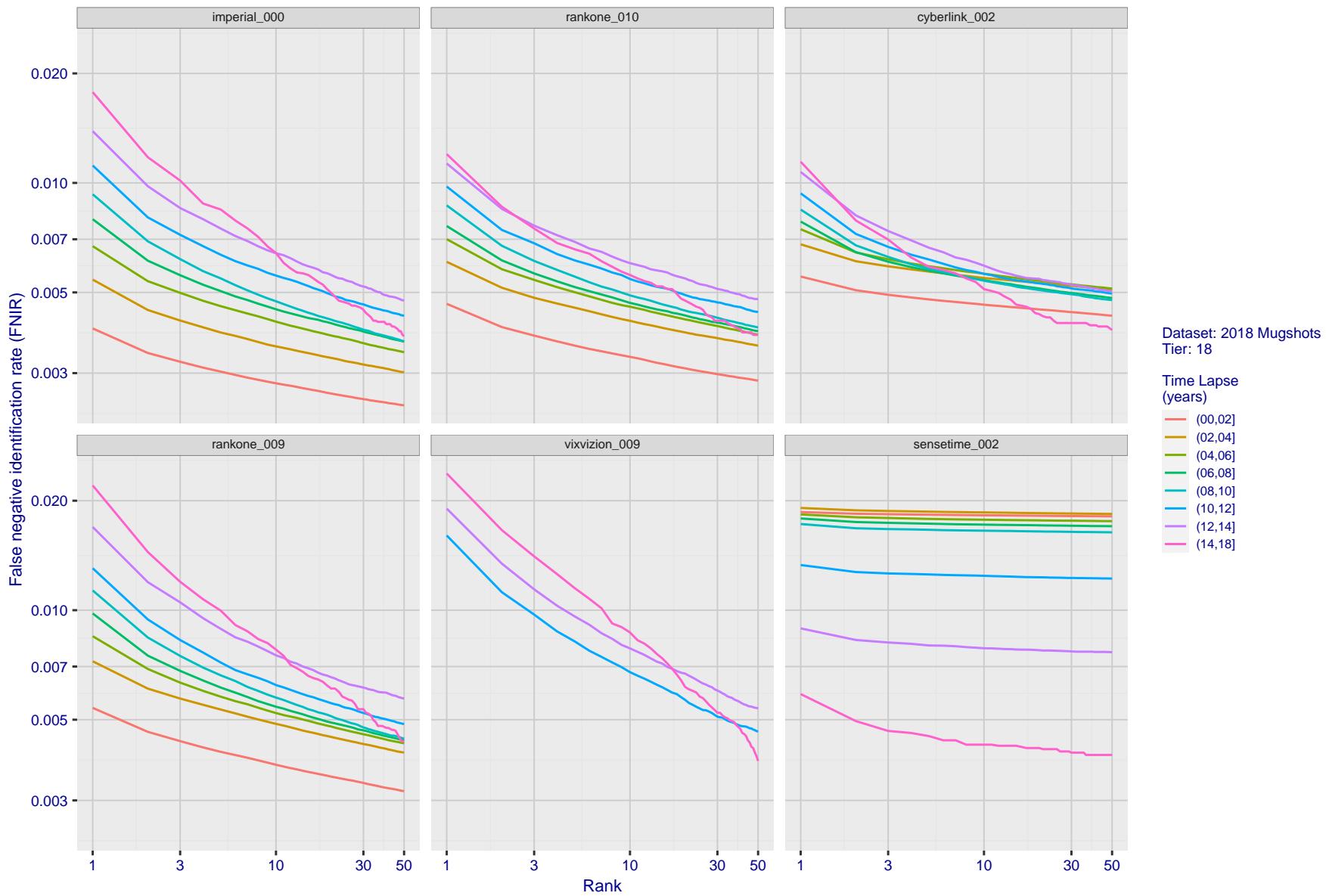


Figure 165: [FRVT-2018 Mugshot Ageing Dataset] Identification miss rates vs. rank by time elapsed. The oldest image of each individual is enrolled. Thereafter, all more recent images are searched. Miss rates are computed over all searches noted in row 17 of Table 1 and binned by number of years between search and initial enrollment.

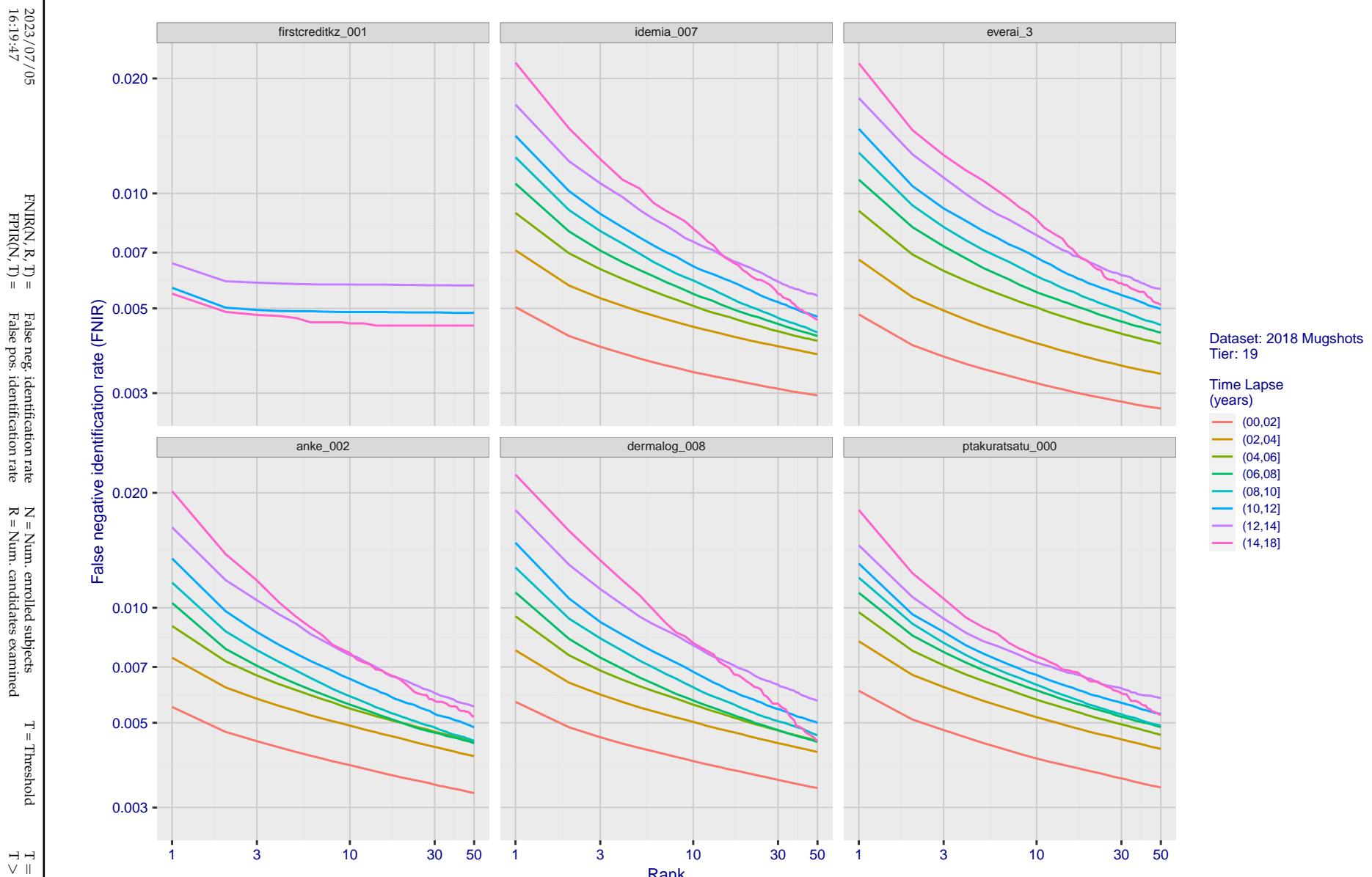


Figure 166: [FRVT-2018 Mugshot Ageing Dataset] Identification miss rates vs. rank by time elapsed. The oldest image of each individual is enrolled. Thereafter, all more recent images are searched. Miss rates are computed over all searches noted in row 17 of Table 1 and binned by number of years between search and initial enrollment.

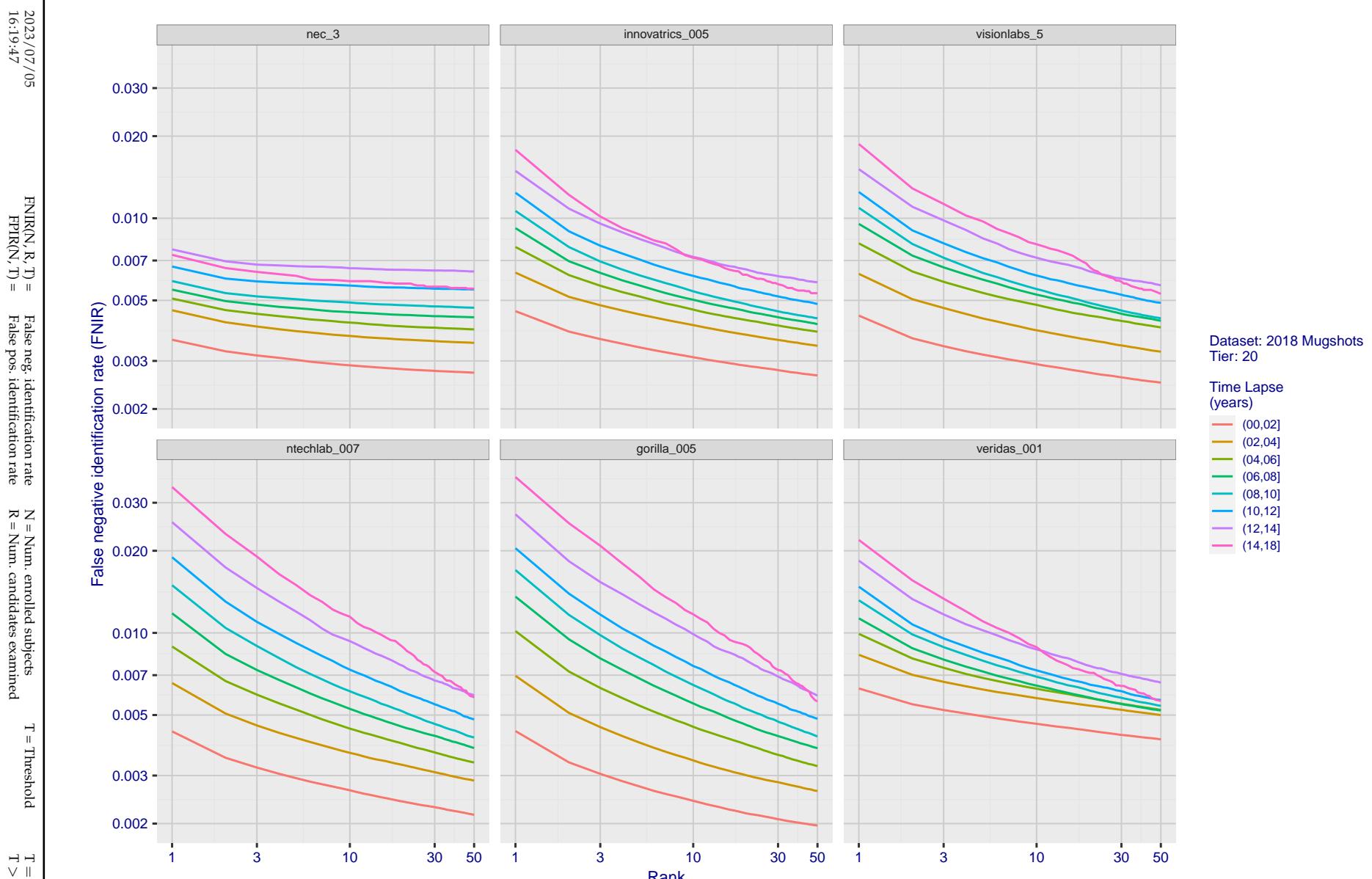


Figure 167: [FRVT-2018 Mugshot Ageing Dataset] Identification miss rates vs. rank by time-elapsed. The oldest image of each individual is enrolled. Thereafter, all more recent images are searched. Miss rates are computed over all searches noted in row 17 of Table 1 and binned by number of years between search and initial enrollment.

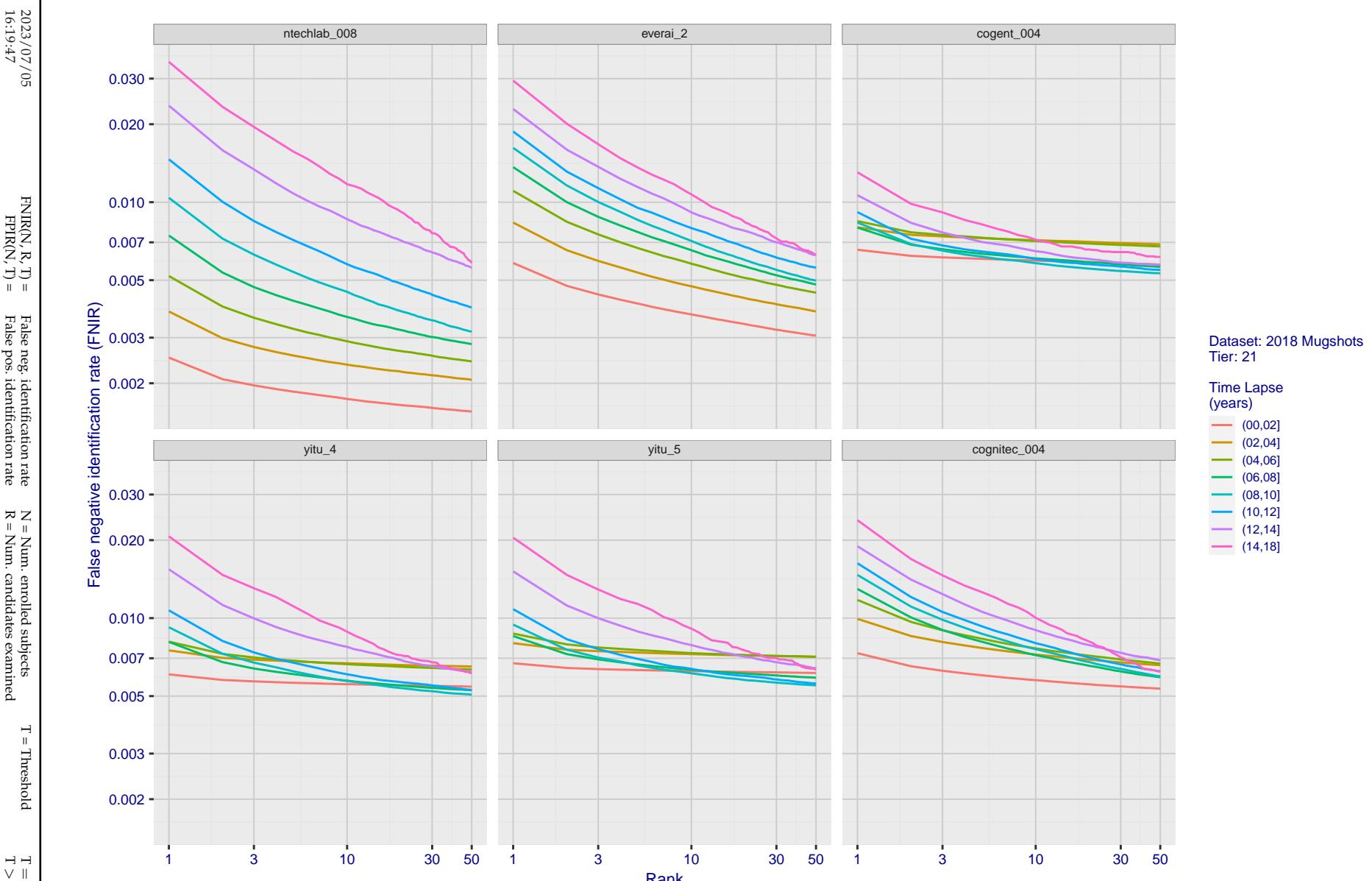


Figure 168: [FRVT-2018 Mugshot Ageing Dataset] Identification miss rates vs. rank by time elapsed. The oldest image of each individual is enrolled. Thereafter, all more recent images are searched. Miss rates are computed over all searches noted in row 17 of Table 1 and binned by number of years between search and initial enrollment.

2023/07/05
16:19:47FNIR(N, R, T) = False neg. identification rate
FPIR(N, T) = False pos. identification rateN = Num. enrolled subjects
R = Num. candidates examined

T = Threshold

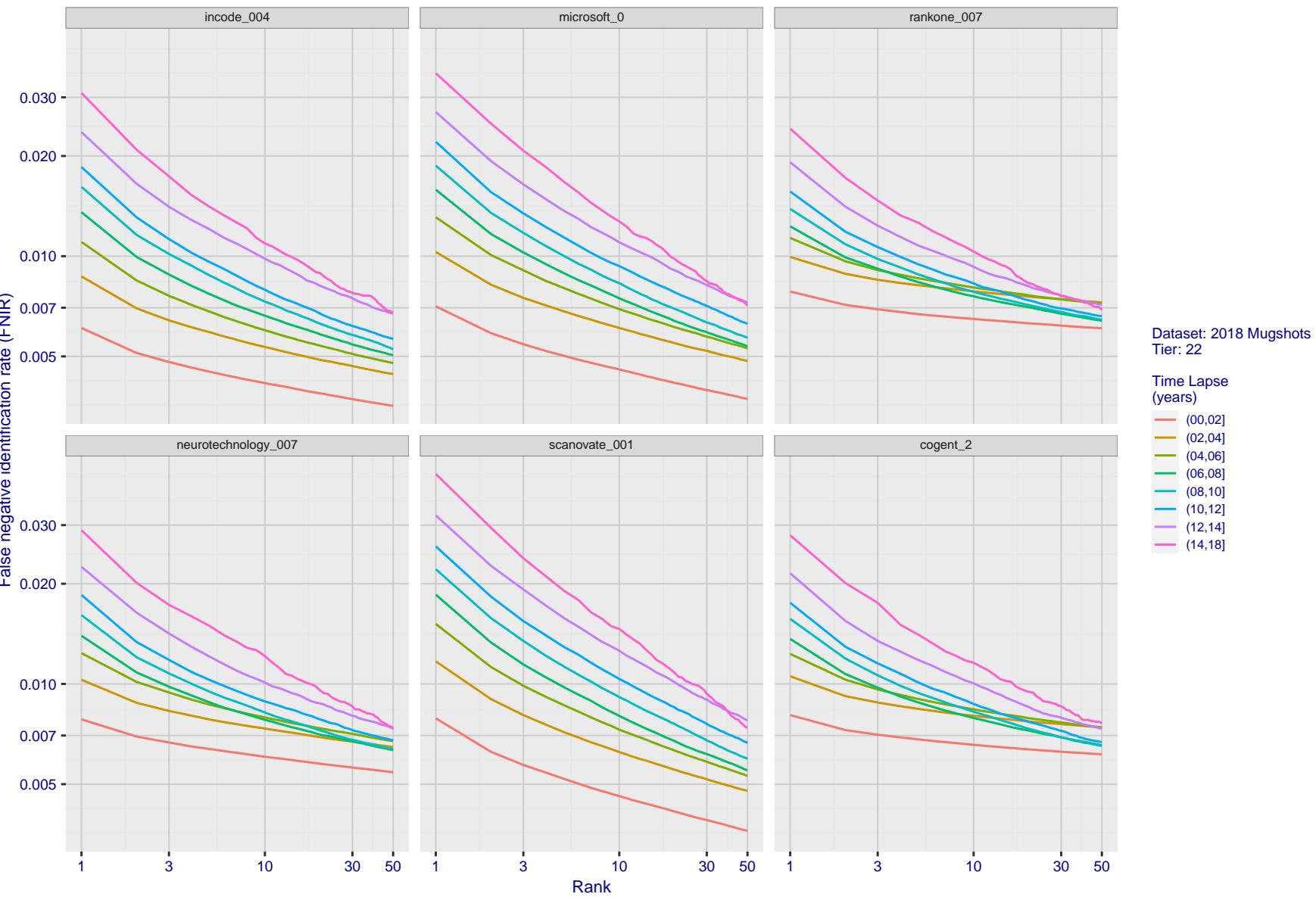
T = 0 → Investigation
T > 0 → Identification

Figure 169: [FRVT-2018 Mugshot Ageing Dataset] Identification miss rates vs. rank by time elapsed. The oldest image of each individual is enrolled. Thereafter, all more recent images are searched. Miss rates are computed over all searches noted in row 17 of Table 1 and binned by number of years between search and initial enrollment.

2023/07/05
16:19:47FNIR(N, R, T) = False neg. identification rate
FPIR(N, T) = False pos. identification rateN = Num. enrolled subjects
R = Num. candidates examinedT = Threshold
T = 0 → Investigation

T > 0 → Identification

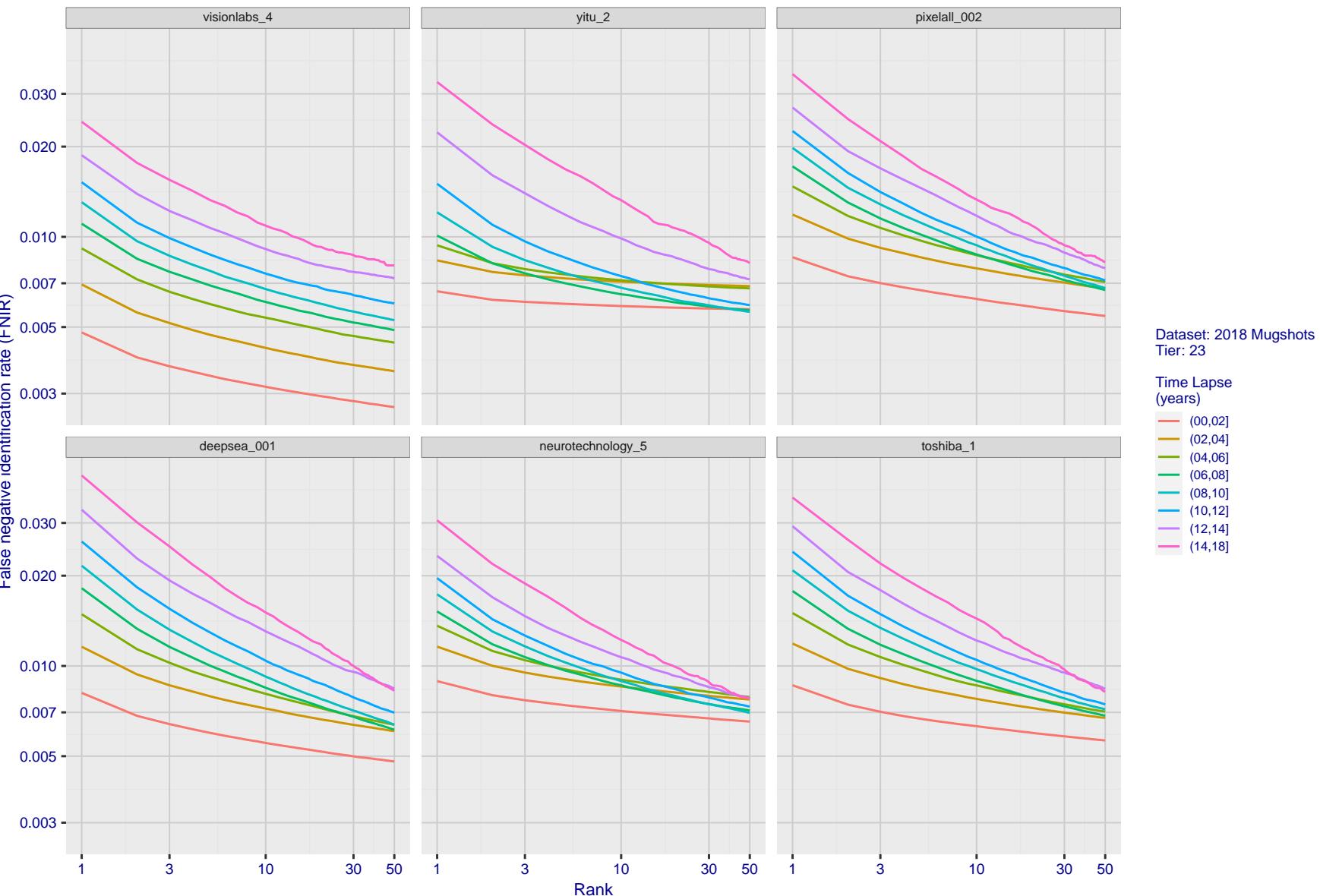


Figure 170: [FRVT-2018 Mugshot Ageing Dataset] Identification miss rates vs. rank by time elapsed. The oldest image of each individual is enrolled. Thereafter, all more recent images are searched. Miss rates are computed over all searches noted in row 17 of Table 1 and binned by number of years between search and initial enrollment.

2023/07/05
16:19:47FNIR(N, R, T) = False neg. identification rate
FPIR(N, T) = False pos. identification rateN = Num. enrolled subjects
R = Num. candidates examinedT = Threshold
T = 0 → Investigation

T > 0 → Identification

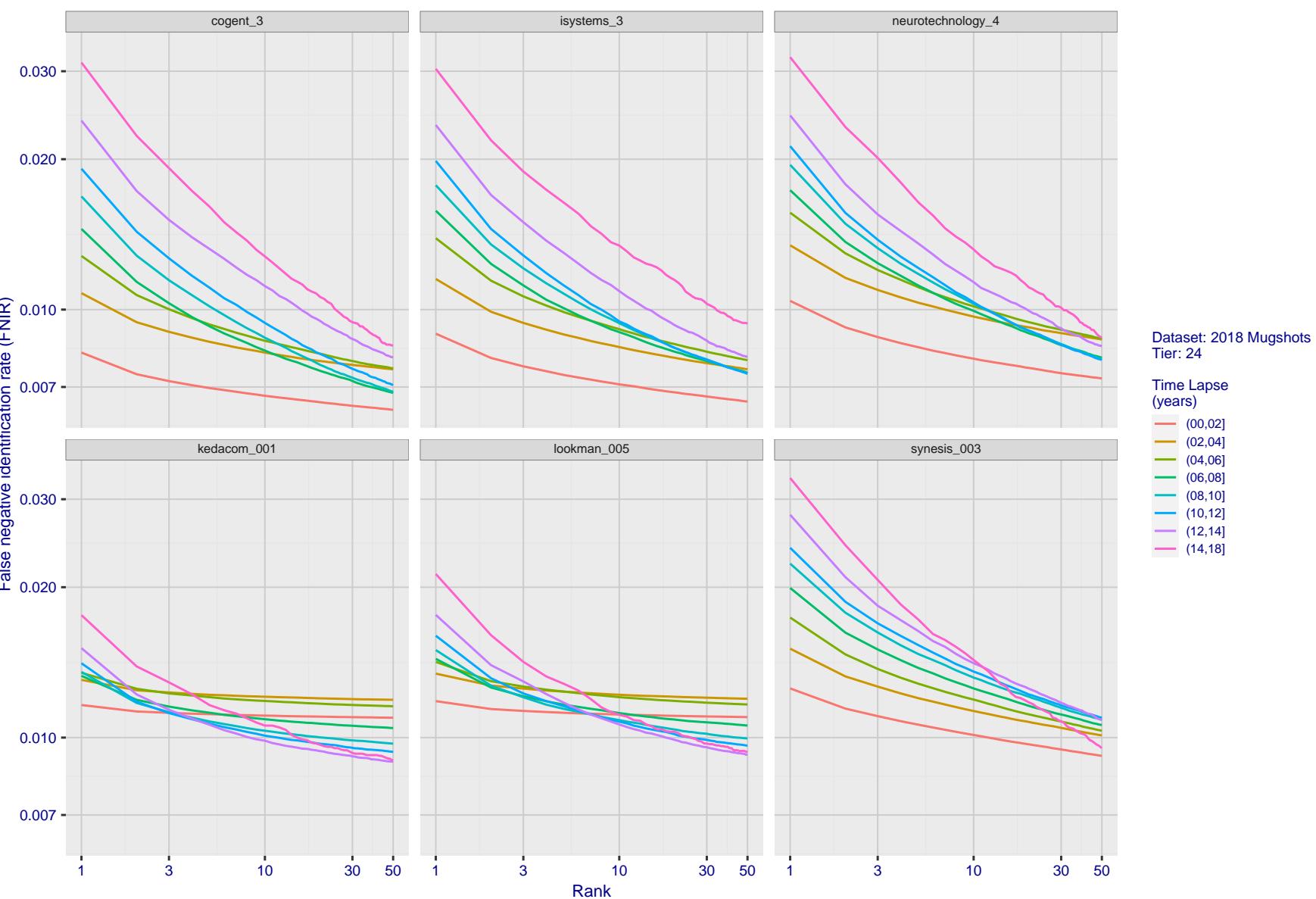


Figure 171: [FRVT-2018 Mugshot Ageing Dataset] Identification miss rates vs. rank by time elapsed. The oldest image of each individual is enrolled. Thereafter, all more recent images are searched. Miss rates are computed over all searches noted in row 17 of Table 1 and binned by number of years between search and initial enrollment.

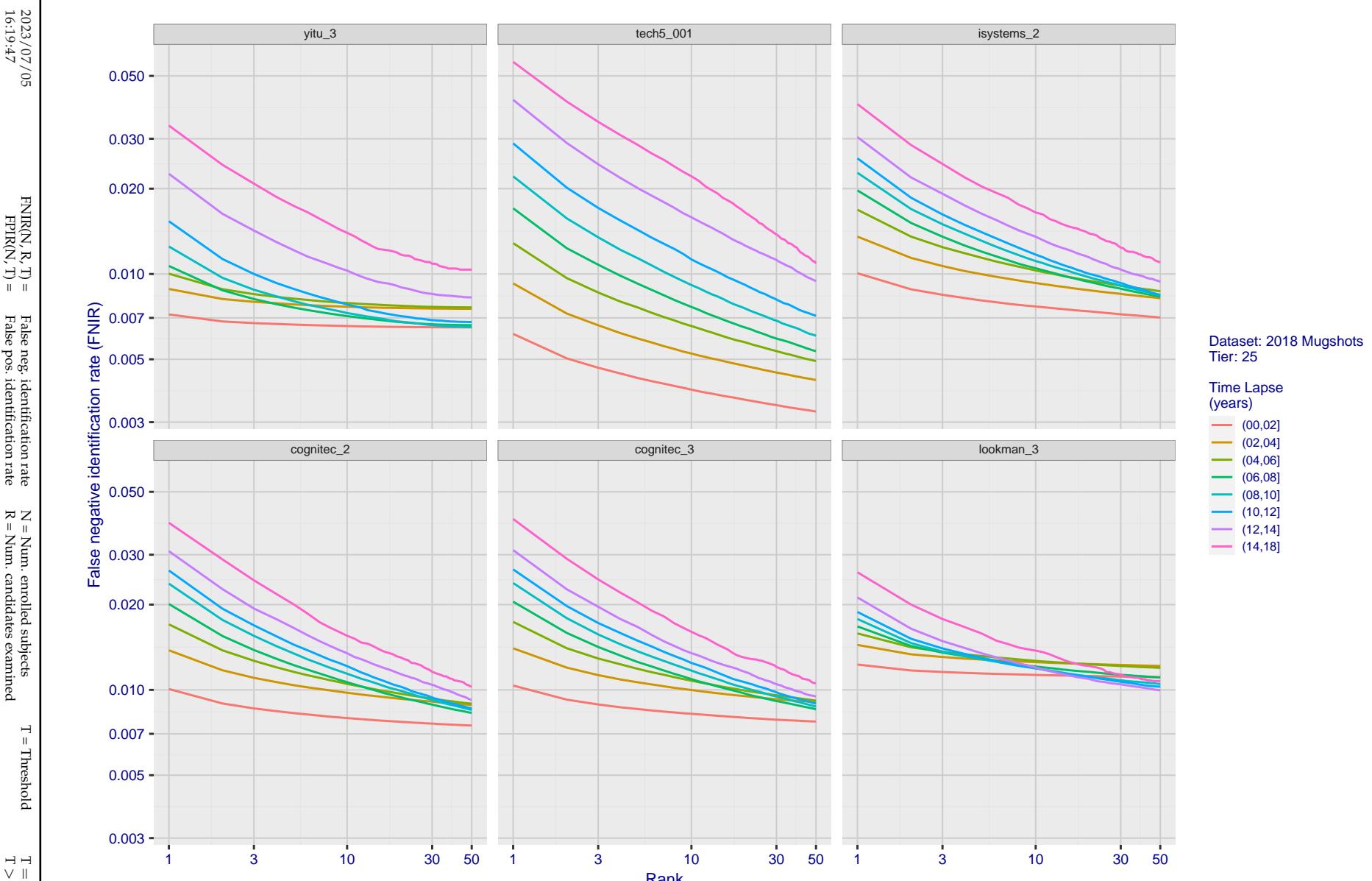


Figure 172: [FRVT-2018 Mugshot Ageing Dataset] Identification miss rates vs. rank by time-elapsed. The oldest image of each individual is enrolled. Thereafter, all more recent images are searched. Miss rates are computed over all searches noted in row 17 of Table 1 and binned by number of years between search and initial enrollment.

2023/07/05
16:19:47FNIR(N, R, T) = False neg. identification rate
FPIR(N, T) = False pos. identification rateN = Num. enrolled subjects
R = Num. candidates examined

T = Threshold

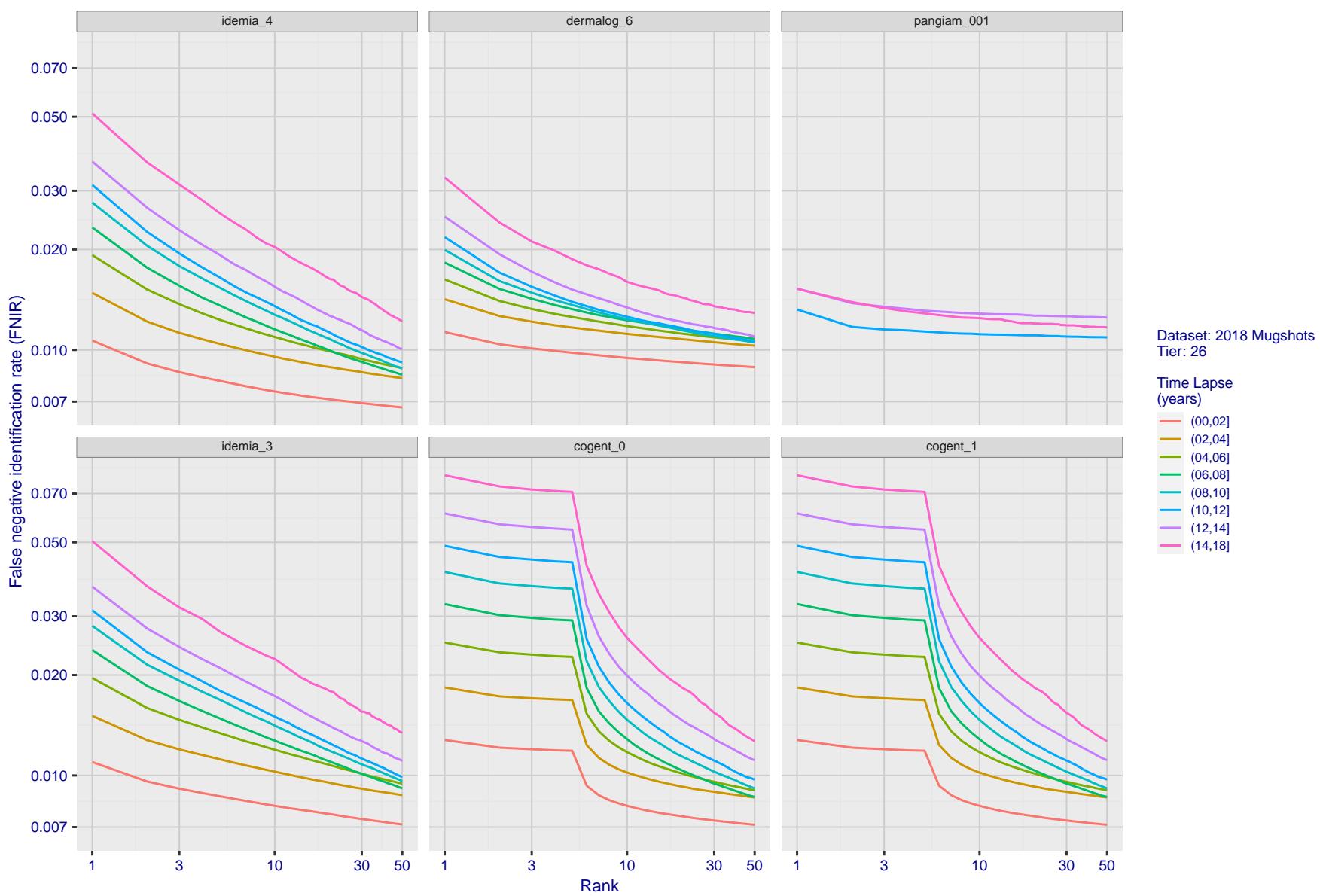
T = 0 → Investigation
T > 0 → Identification

Figure 173: [FRVT-2018 Mugshot Ageing Dataset] Identification miss rates vs. rank by time elapsed. The oldest image of each individual is enrolled. Thereafter, all more recent images are searched. Miss rates are computed over all searches noted in row 17 of Table 1 and binned by number of years between search and initial enrollment.

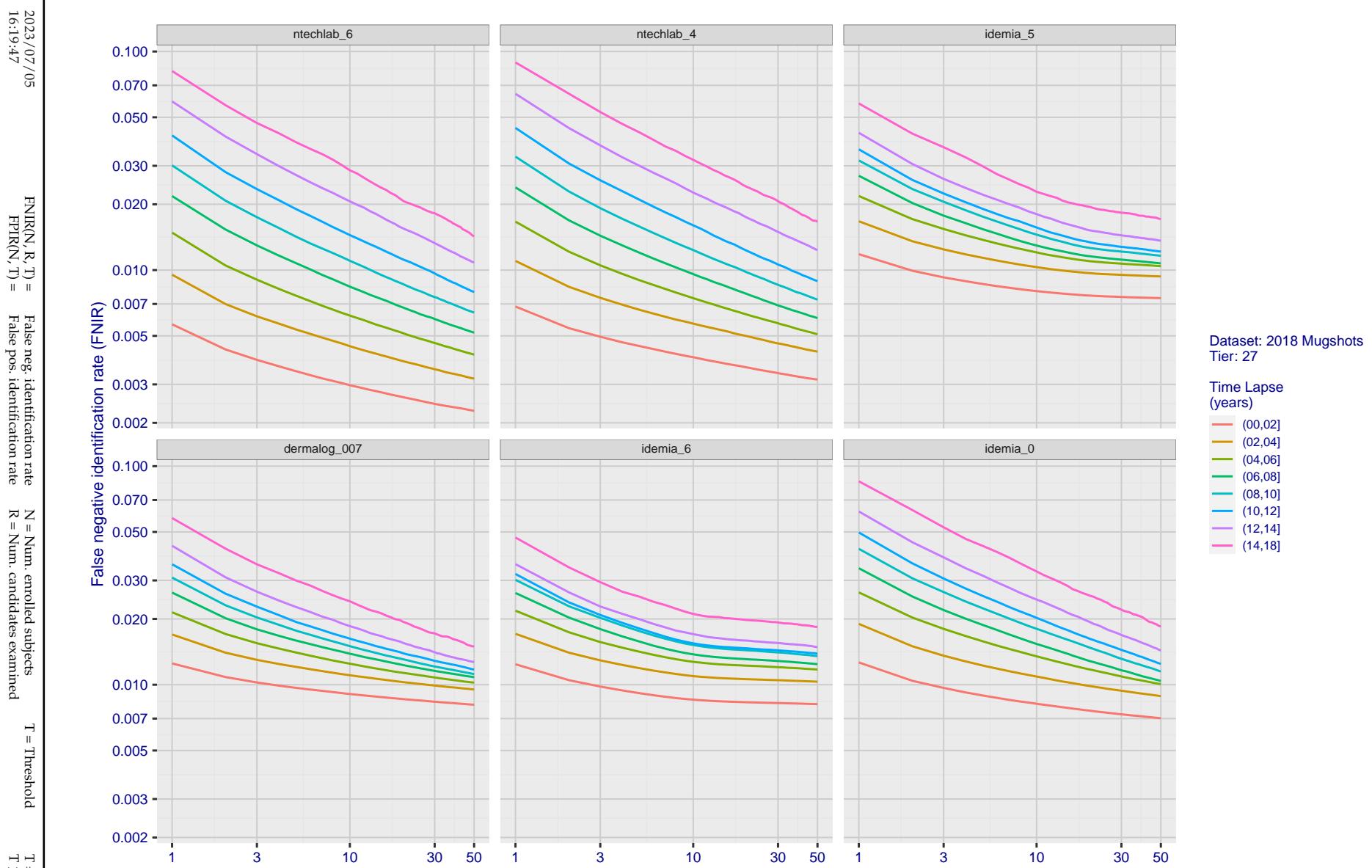


Figure 174: [FRVT-2018 Mugshot Ageing Dataset] Identification miss rates vs. rank by time elapsed. The oldest image of each individual is enrolled. Thereafter, all more recent images are searched. Miss rates are computed over all searches noted in row 17 of Table 1 and binned by number of years between search and initial enrollment.

2023/07/05
16:19:47FNIR(N, R, T) = False neg. identification rate
FPIR(N, T) = False pos. identification rateN = Num. enrolled subjects
R = Num. candidates examinedT = Threshold
T = 0 → Investigation

T > 0 → Identification

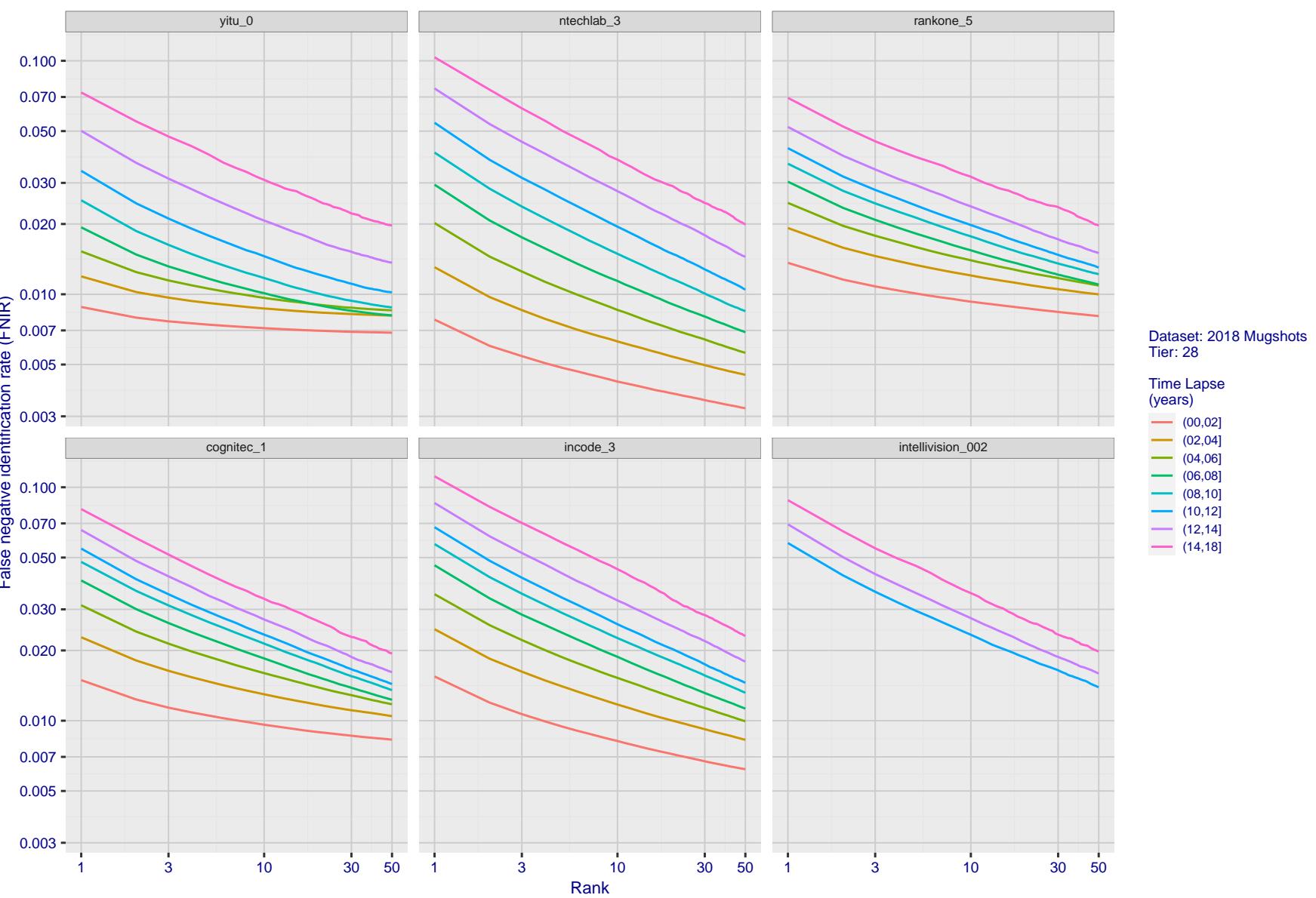


Figure 175: [FRVT-2018 Mugshot Ageing Dataset] Identification miss rates vs. rank by time elapsed. The oldest image of each individual is enrolled. Thereafter, all more recent images are searched. Miss rates are computed over all searches noted in row 17 of Table 1 and binned by number of years between search and initial enrollment.

2023/07/05
16:19:47FNIR(N, R, T) = False neg. identification rate
FPIR(N, T) = False pos. identification rateN = Num. enrolled subjects
R = Num. candidates examined

T = Threshold

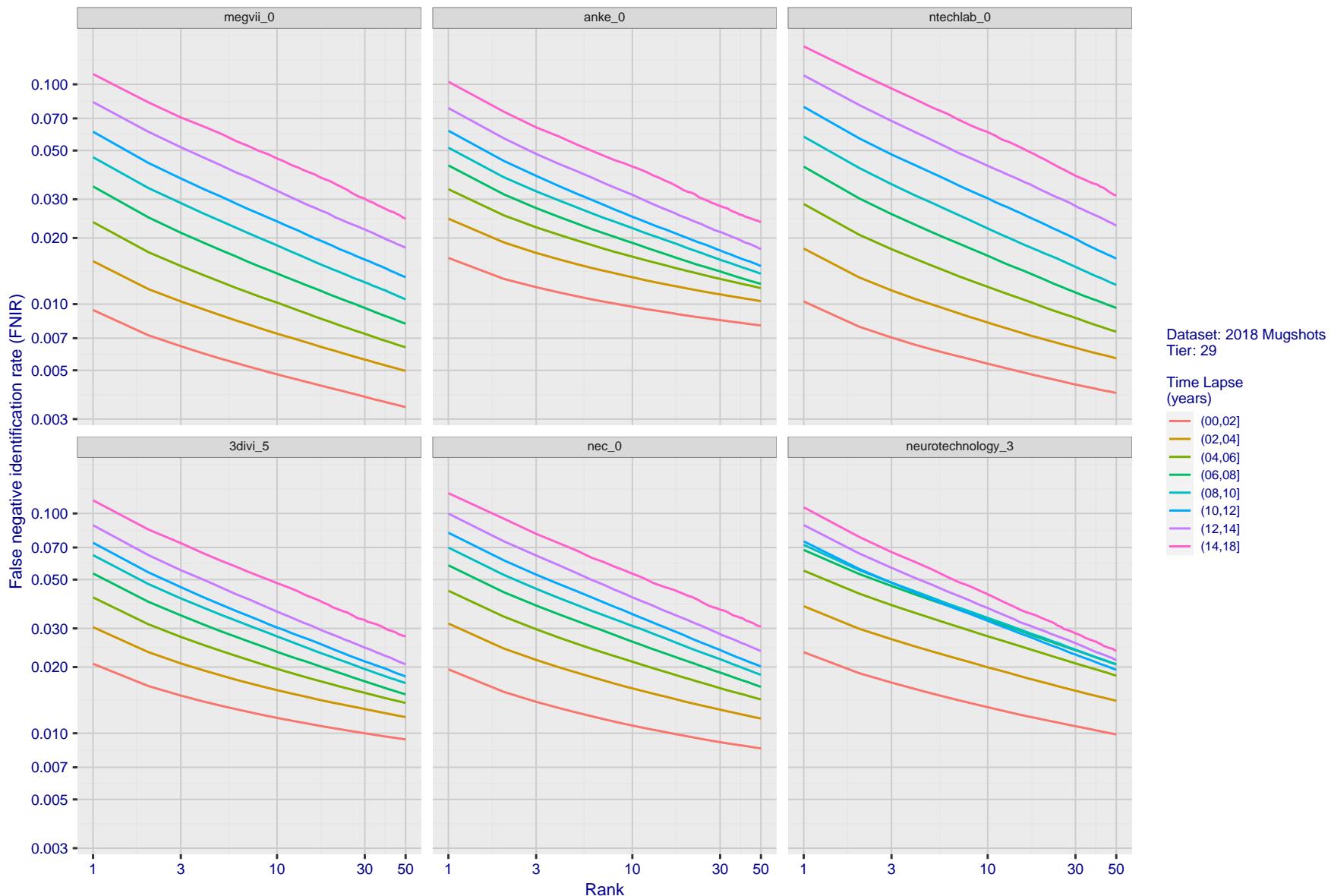
T = 0 → Investigation
T > 0 → Identification

Figure 176: [FRVT-2018 Mugshot Ageing Dataset] Identification miss rates vs. rank by time-elapsed. The oldest image of each individual is enrolled. Thereafter, all more recent images are searched. Miss rates are computed over all searches noted in row 17 of Table 1 and binned by number of years between search and initial enrollment.

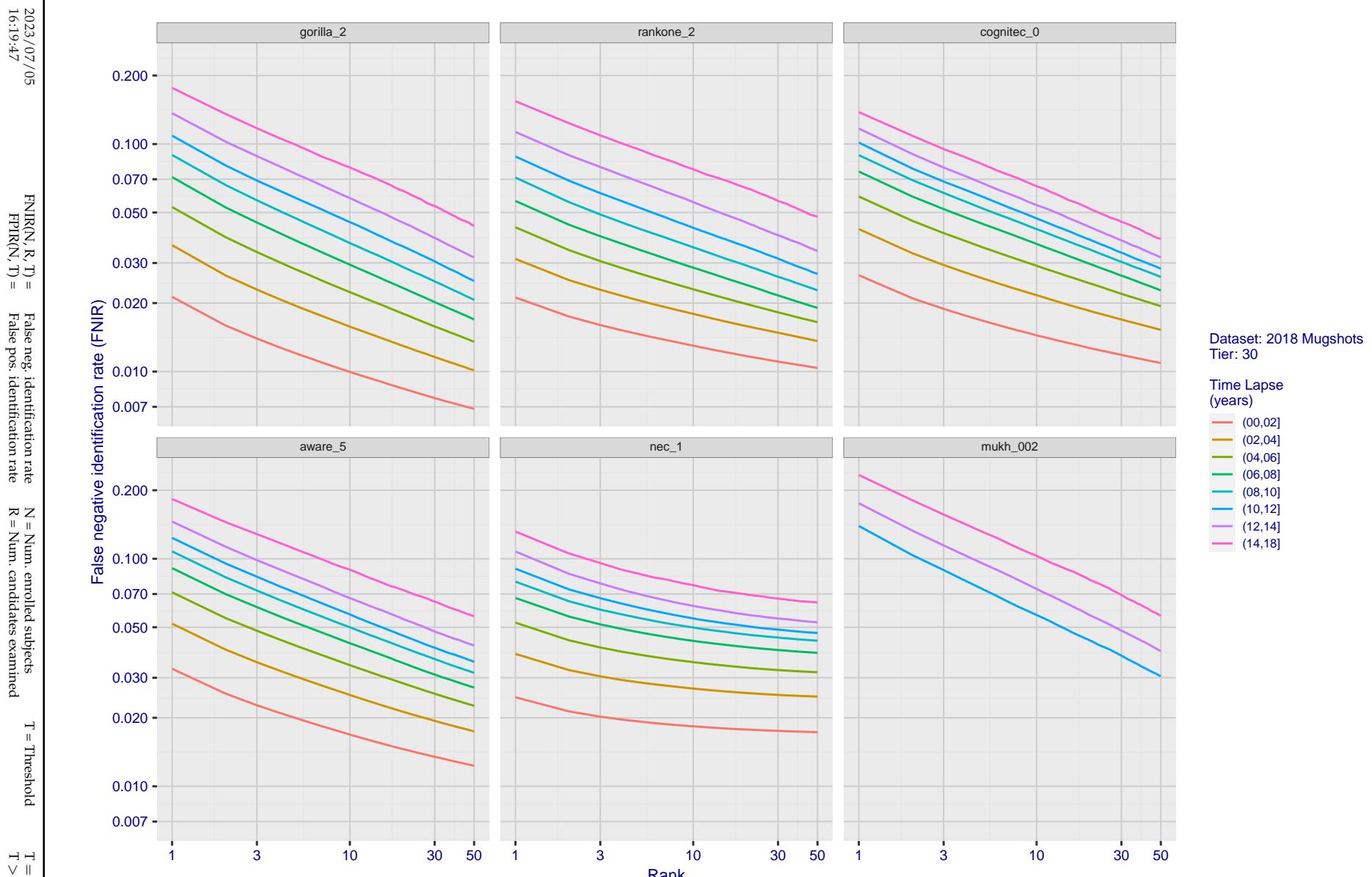


Figure 177: [FRVT-2018 Mugshot Ageing Dataset] Identification miss rates vs. rank by time elapsed. The oldest image of each individual is enrolled. Thereafter, all more recent images are searched. Miss rates are computed over all searches noted in row 17 of Table 1 and binned by number of years between search and initial enrollment.

2023/07/05
16:19:47FNIR(N, R, T) = False neg. identification rate
FPIR(N, T) = False pos. identification rateN = Num. enrolled subjects
R = Num. candidates examinedT = Threshold
T = 0 → Investigation

T > 0 → Identification

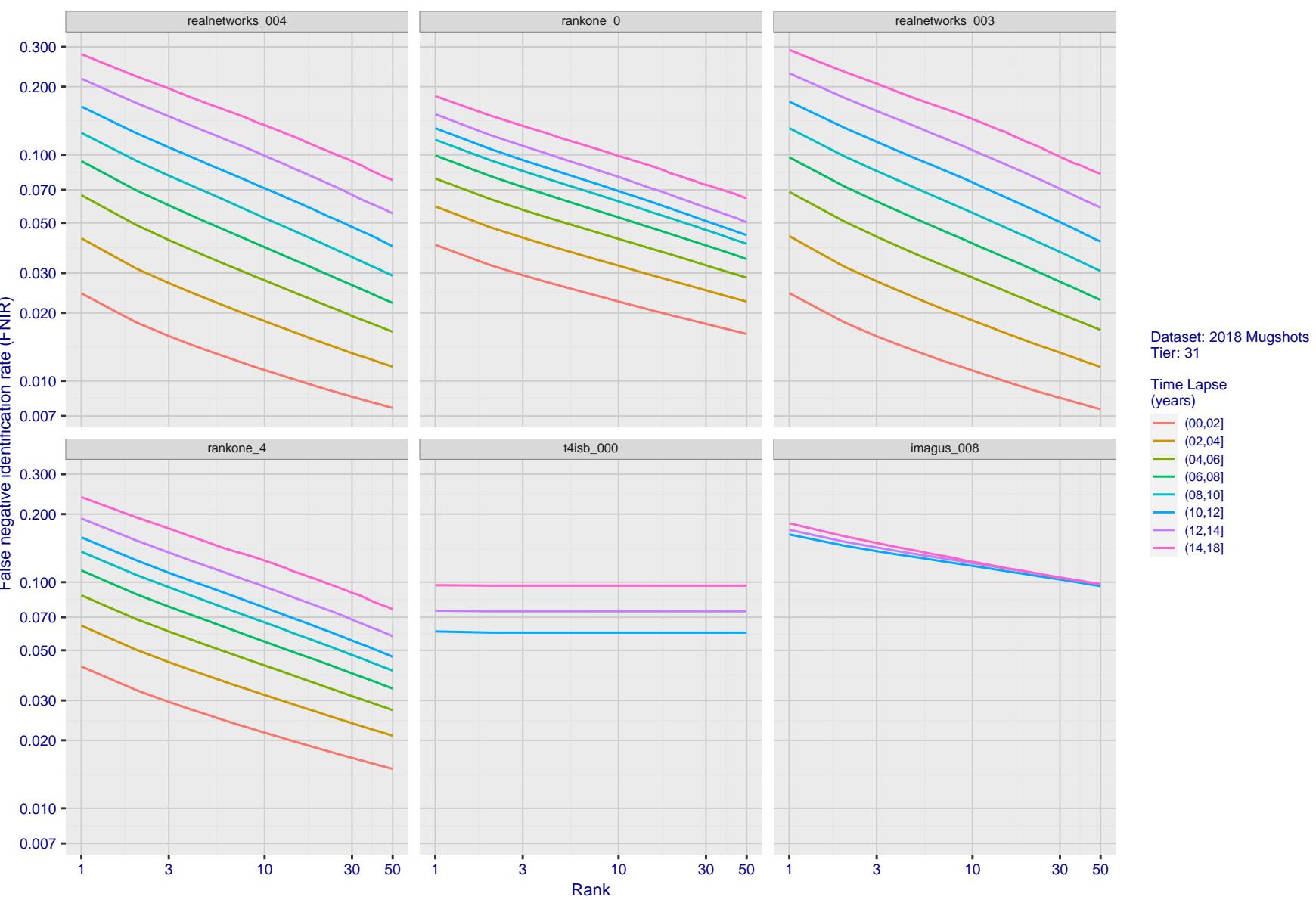


Figure 178: [FRVT-2018 Mugshot Ageing Dataset] Identification miss rates vs. rank by time elapsed. The oldest image of each individual is enrolled. Thereafter, all more recent images are searched. Miss rates are computed over all searches noted in row 17 of Table 1 and binned by number of years between search and initial enrollment.

2023/07/05
16:19:47FNIR(N, R, T) = False neg. identification rate
FPIR(N, T) = False pos. identification rateN = Num. enrolled subjects
R = Num. candidates examined

T = Threshold

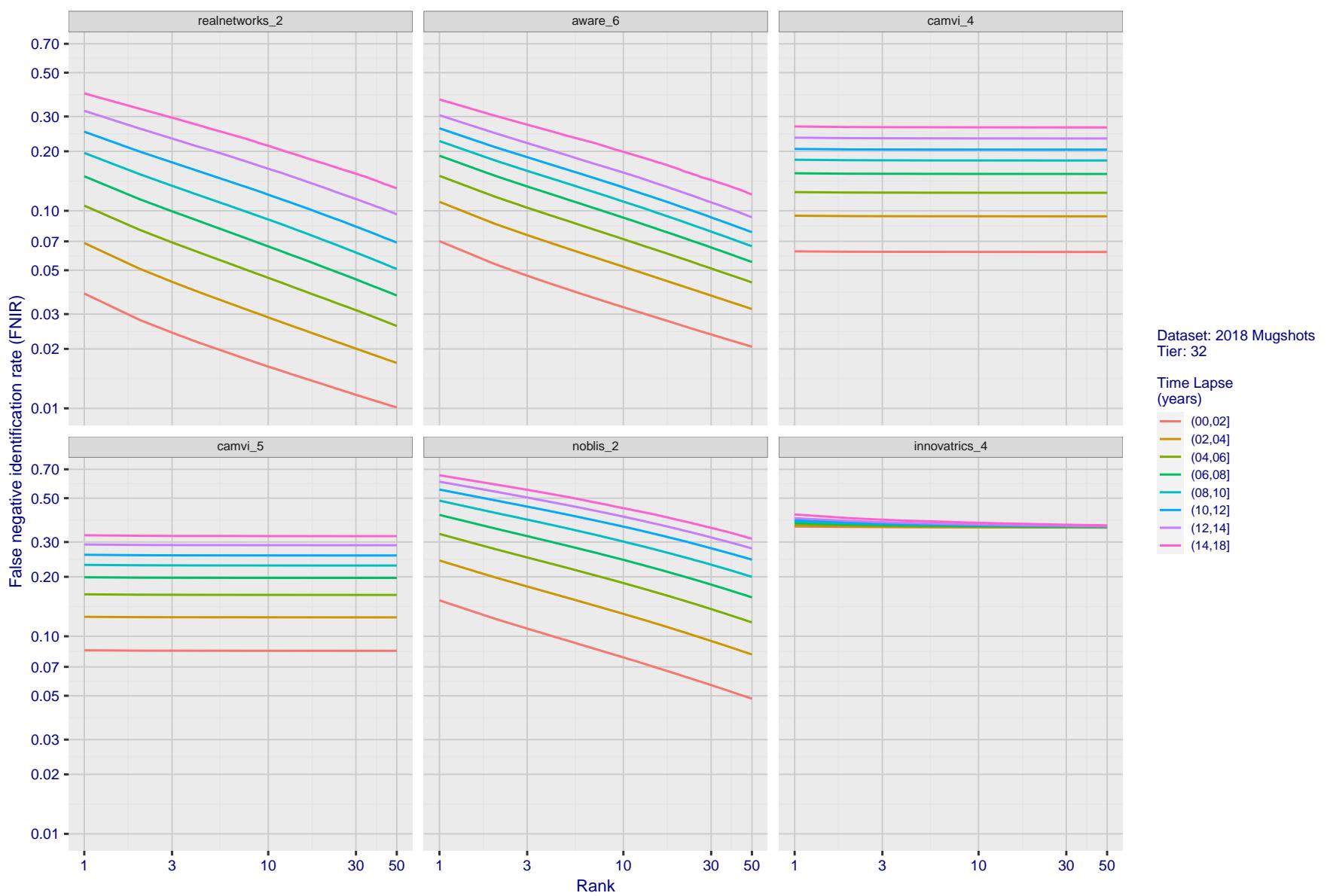
T = 0 → Investigation
T > 0 → Identification

Figure 179: [FRVT-2018 Mugshot Ageing Dataset] Identification miss rates vs. rank by time elapsed. The oldest image of each individual is enrolled. Thereafter, all more recent images are searched. Miss rates are computed over all searches noted in row 17 of Table 1 and binned by number of years between search and initial enrollment.

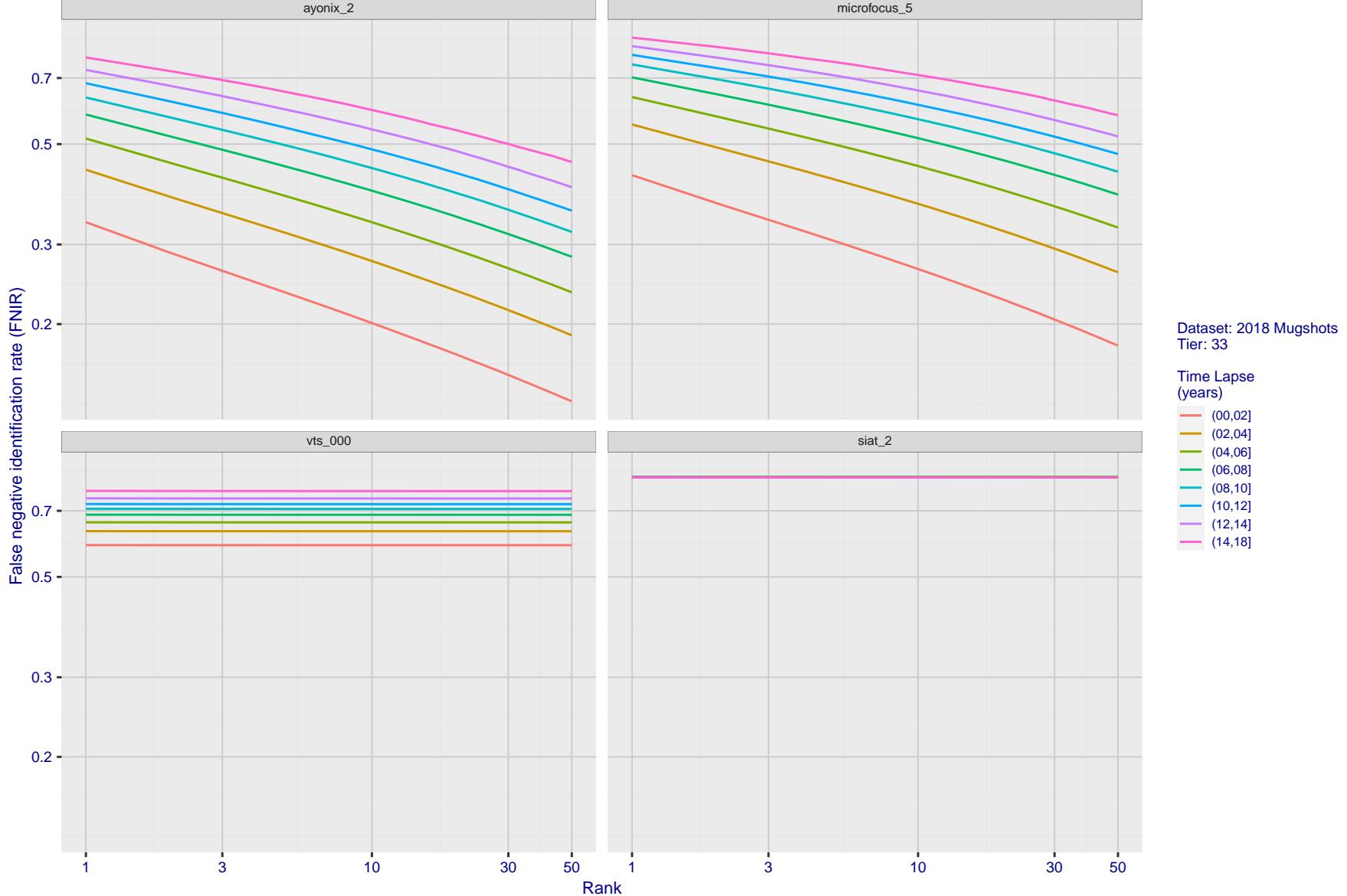


Figure 180: [FRVT-2018 Mugshot Ageing Dataset] Identification miss rates vs. rank by time-elapsed. The oldest image of each individual is enrolled. Thereafter, all more recent images are searched. Miss rates are computed over all searches noted in row 17 of Table 1 and binned by number of years between search and initial enrollment.

2023/07/05
16:19:47

FNIR(N, R, T) = False neg. identification rate
FPTR(N, T) = False pos. identification rate

N = Num. enrolled subjects
R = Num. candidates examined

T = Threshold
T > 0 → Identification

2023/07/05
16:19:47

 $FNIR(N, R, T)$ = False neg. identification rate
 $FPIR(N, T)$ = False pos. identification rate
 N = Num. enrolled subjects
 R = Num. candidates examined
 T = Threshold
 $T = 0 \rightarrow$ Investigation
 $T > 0 \rightarrow$ Identification

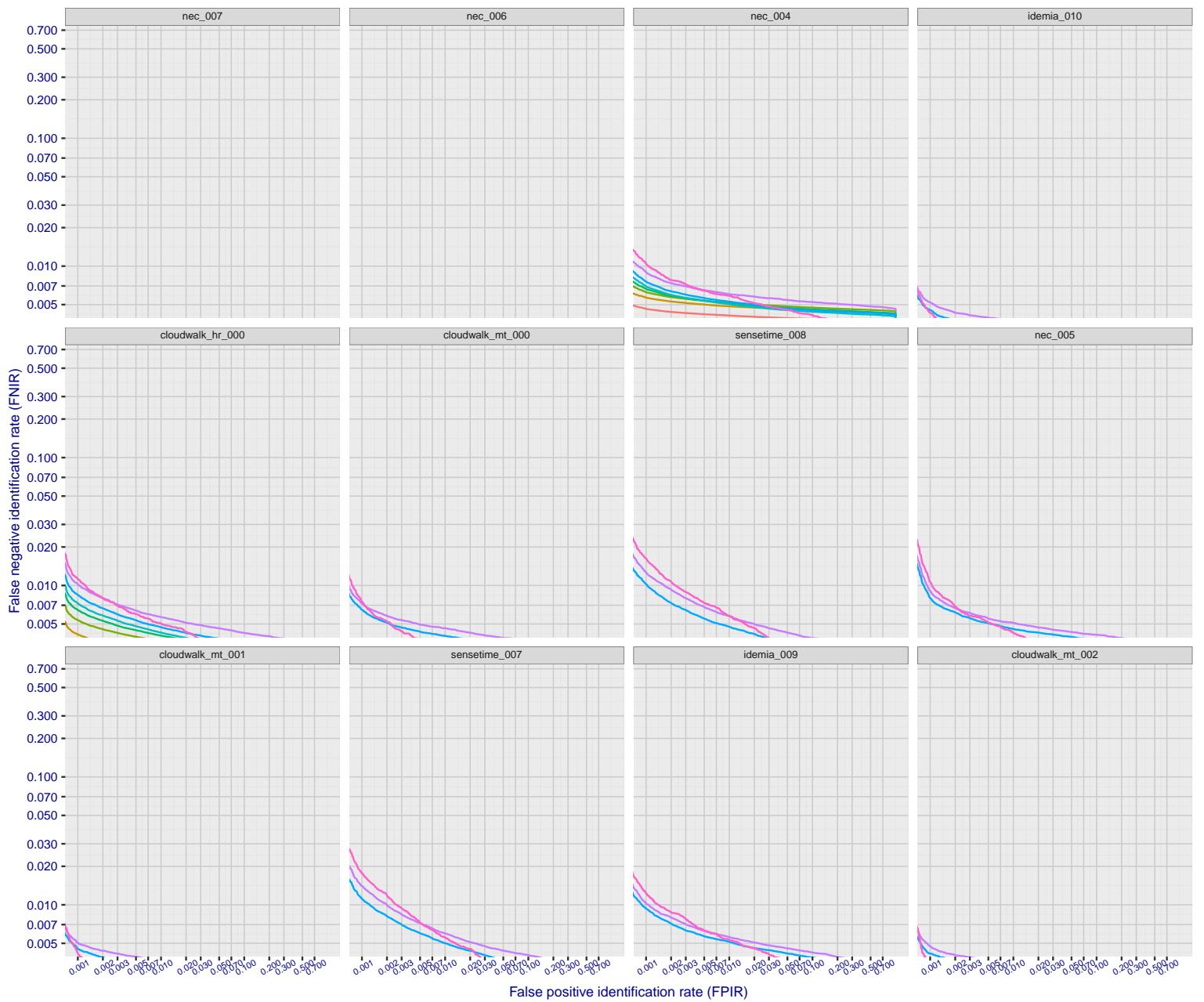


Figure 181: [FRVT-2018 Mugshot Ageing Dataset] Identification miss rates vs. FPIR by time-elapsed. The oldest image of each individual is enrolled. Thereafter, all more recent images are searched. Miss rates are computed over all searches noted in row 17 of Table 1 and binned by number of years between search and initial enrollment. FPIR is computed from the same FRVT 2018 non-mates noted in row 3 of Table 1 with $N = 3000\,000$.

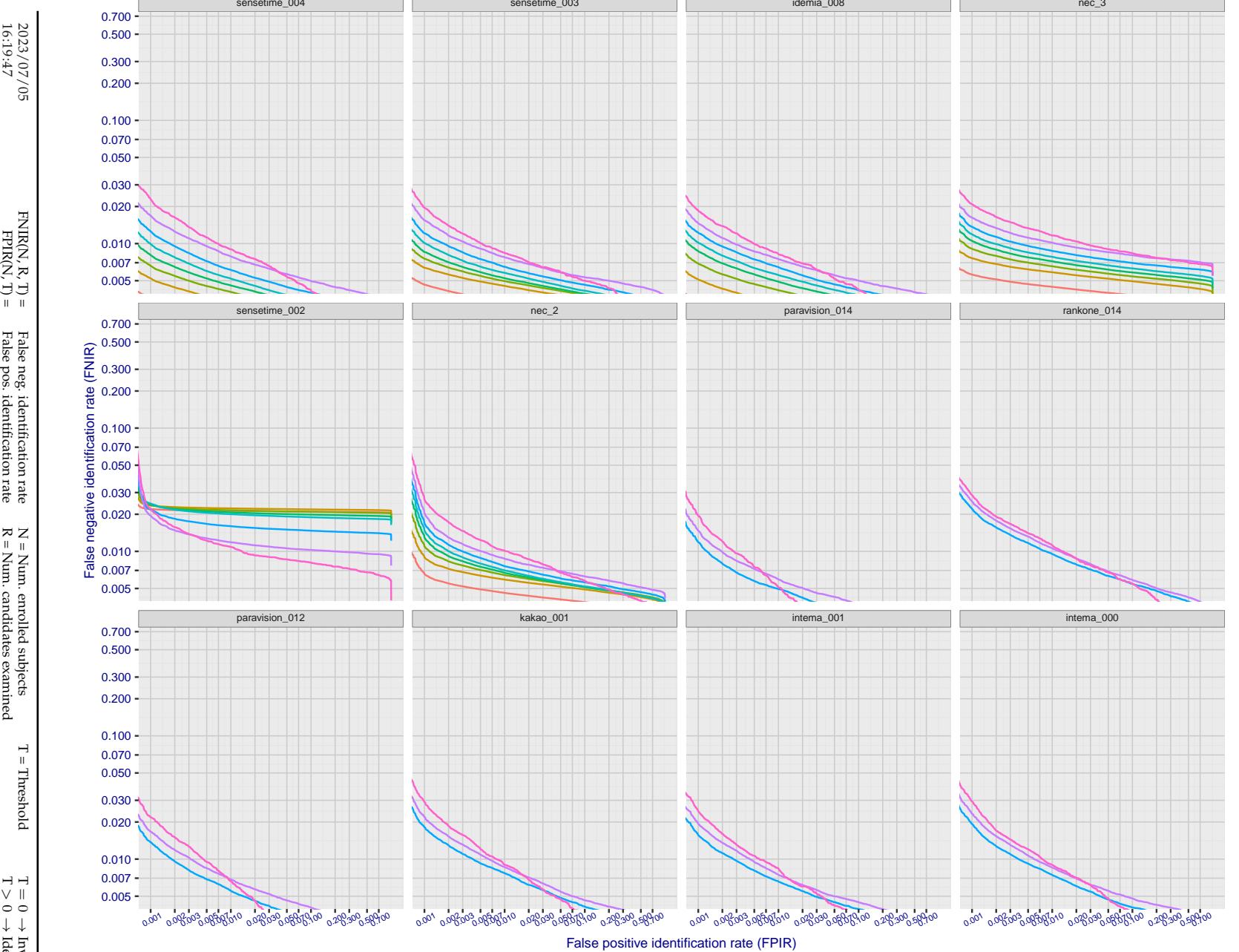


Figure 182: [FRVT-2018 Mugshot Ageing Dataset] Identification miss rates vs. FPIR by time-elapsed. The oldest image of each individual is enrolled. Thereafter, all more recent images are searched. Miss rates are computed over all searches noted in row 17 of Table 1 and binned by number of years between search and initial enrollment. FPIR is computed from the same FRVT 2018 non-mates noted in row 3 of Table 1 with $N = 3\,000\,000$.

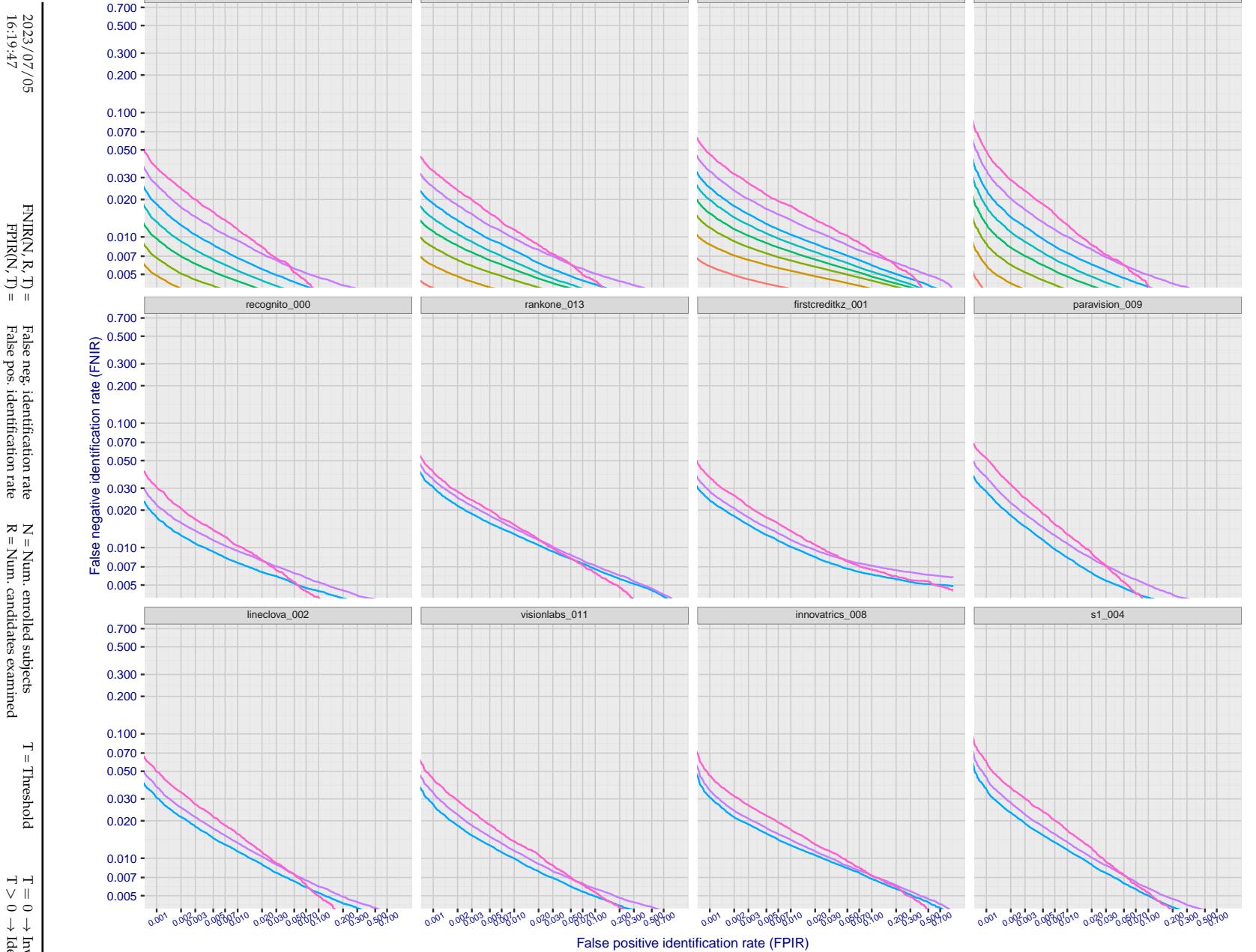


Figure 183: [FRVT-2018 Mugshot Ageing Dataset] Identification miss rates vs. FPIR by time-elapsed. The oldest image of each individual is enrolled. Thereafter, all more recent images are searched. Miss rates are computed over all searches noted in row 17 of Table 1 and binned by number of years between search and initial enrollment. FPIR is computed from the same FRVT 2018 non-mates noted in row 3 of Table 1 with $N = 3\,000\,000$.

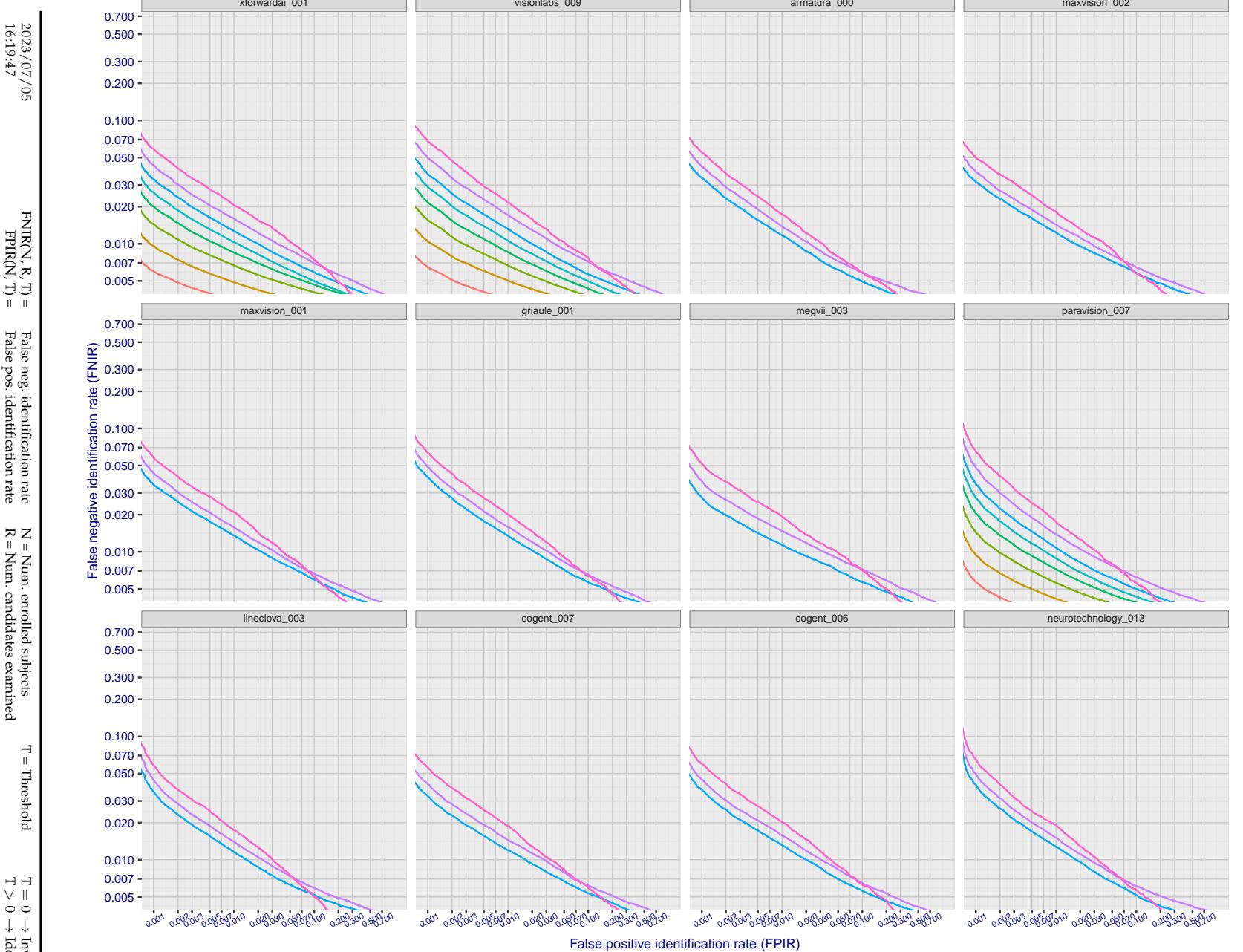


Figure 184: [FRVT-2018 Mugshot Ageing Dataset] Identification miss rates vs. FPIR by time-elapsed. The oldest image of each individual is enrolled. Thereafter, all more recent images are searched. Miss rates are computed over all searches noted in row 17 of Table 1 and binned by number of years between search and initial enrollment. FPIR is computed from the same FRVT 2018 non-mates noted in row 3 of Table 1 with $N = 3\,000\,000$.

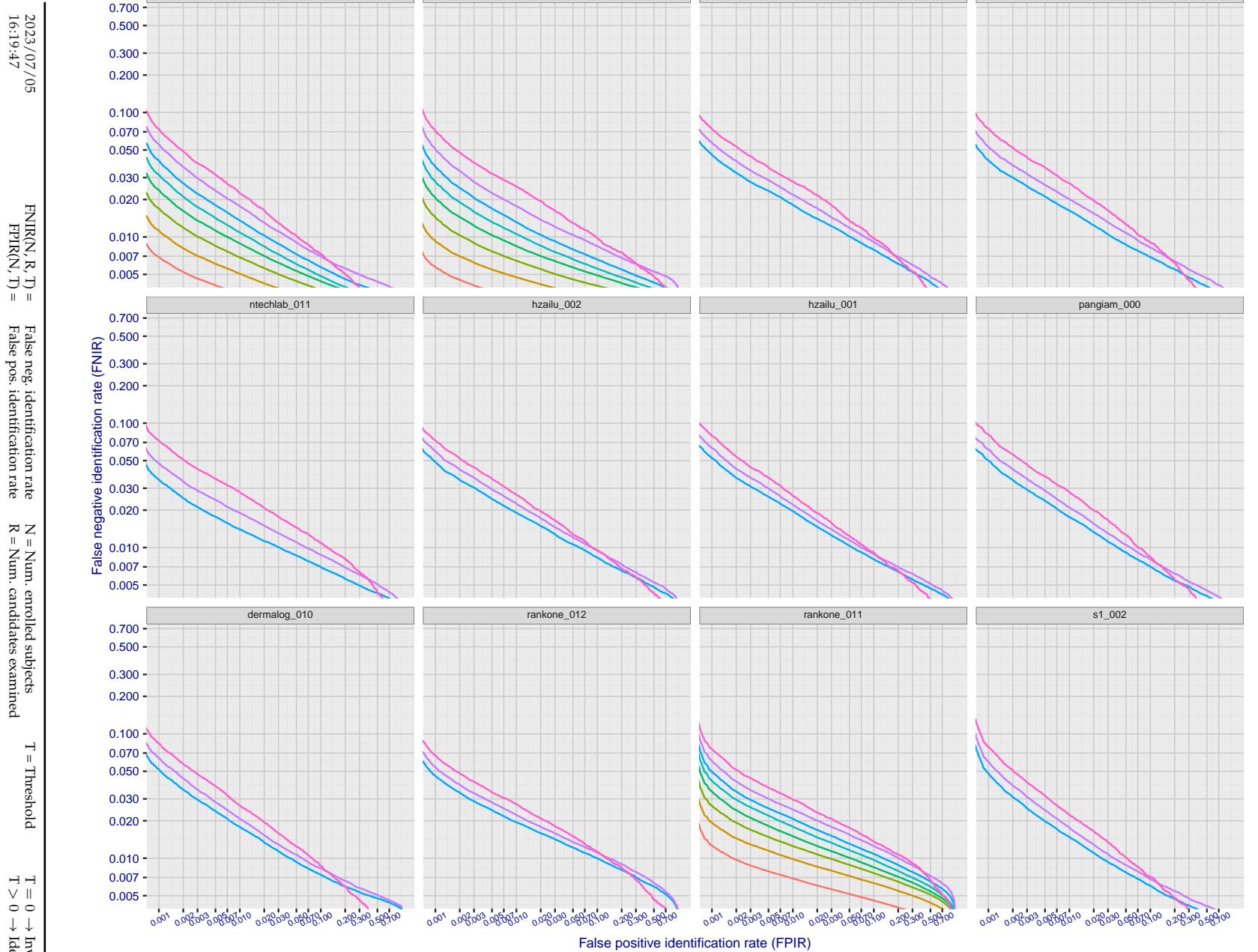


Figure 185: [FRVT-2018 Mugshot Ageing Dataset] Identification miss rates vs. FPIR by time-elapsed. The oldest image of each individual is enrolled. Thereafter, all more recent images are searched. Miss rates are computed over all searches noted in row 17 of Table 1 and binned by number of years between search and initial enrollment. FPIR is computed from the same FRVT 2018 non-mates noted in row 3 of Table 1 with $N = 3\,000\,000$.

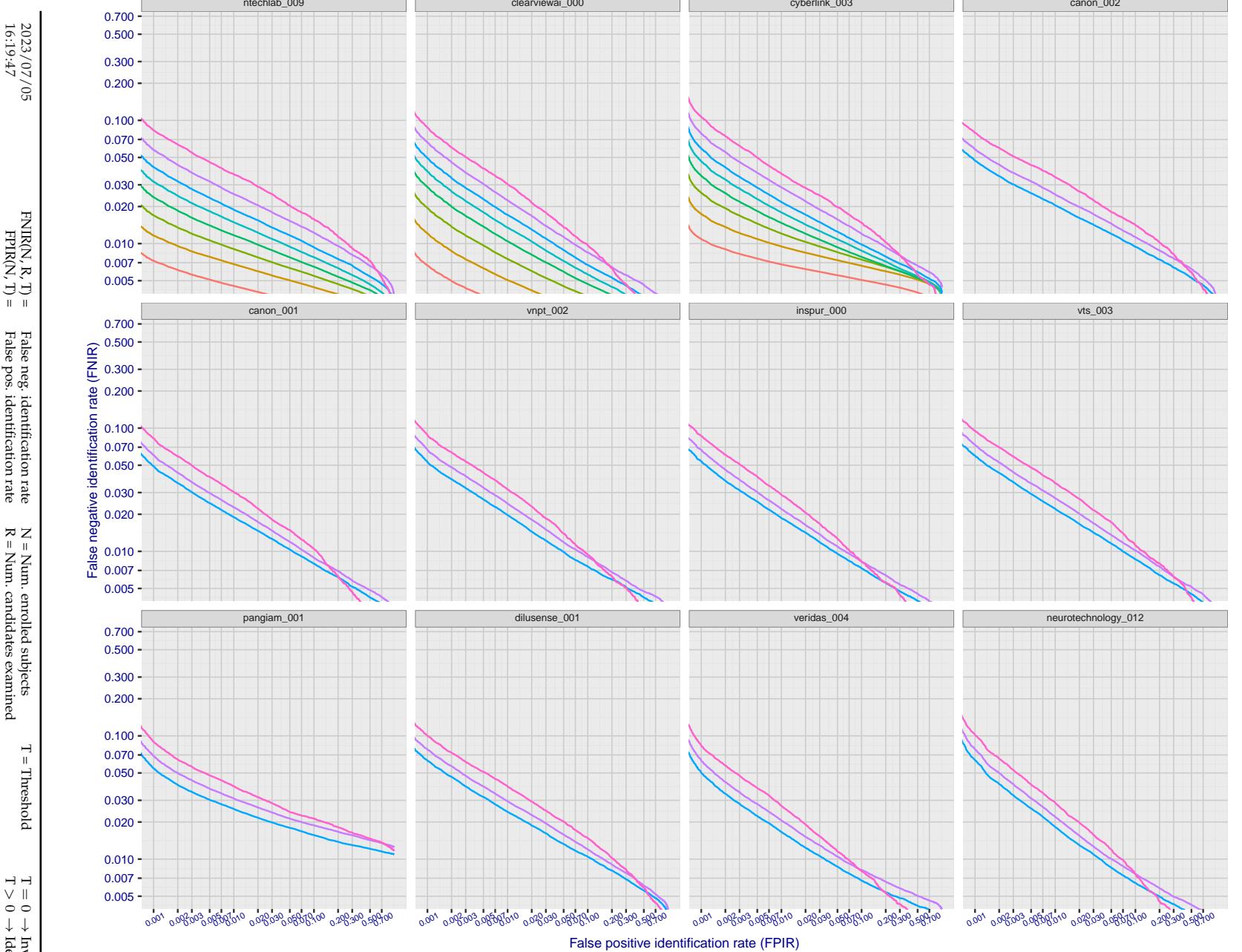


Figure 186: [FRVT-2018 Mugshot Ageing Dataset] Identification miss rates vs. FPIR by time-elapsed. The oldest image of each individual is enrolled. Thereafter, all more recent images are searched. Miss rates are computed over all searches noted in row 17 of Table 1 and binned by number of years between search and initial enrollment. FPIR is computed from the same FRVT 2018 non-mates noted in row 3 of Table 1 with $N = 3\,000\,000$.

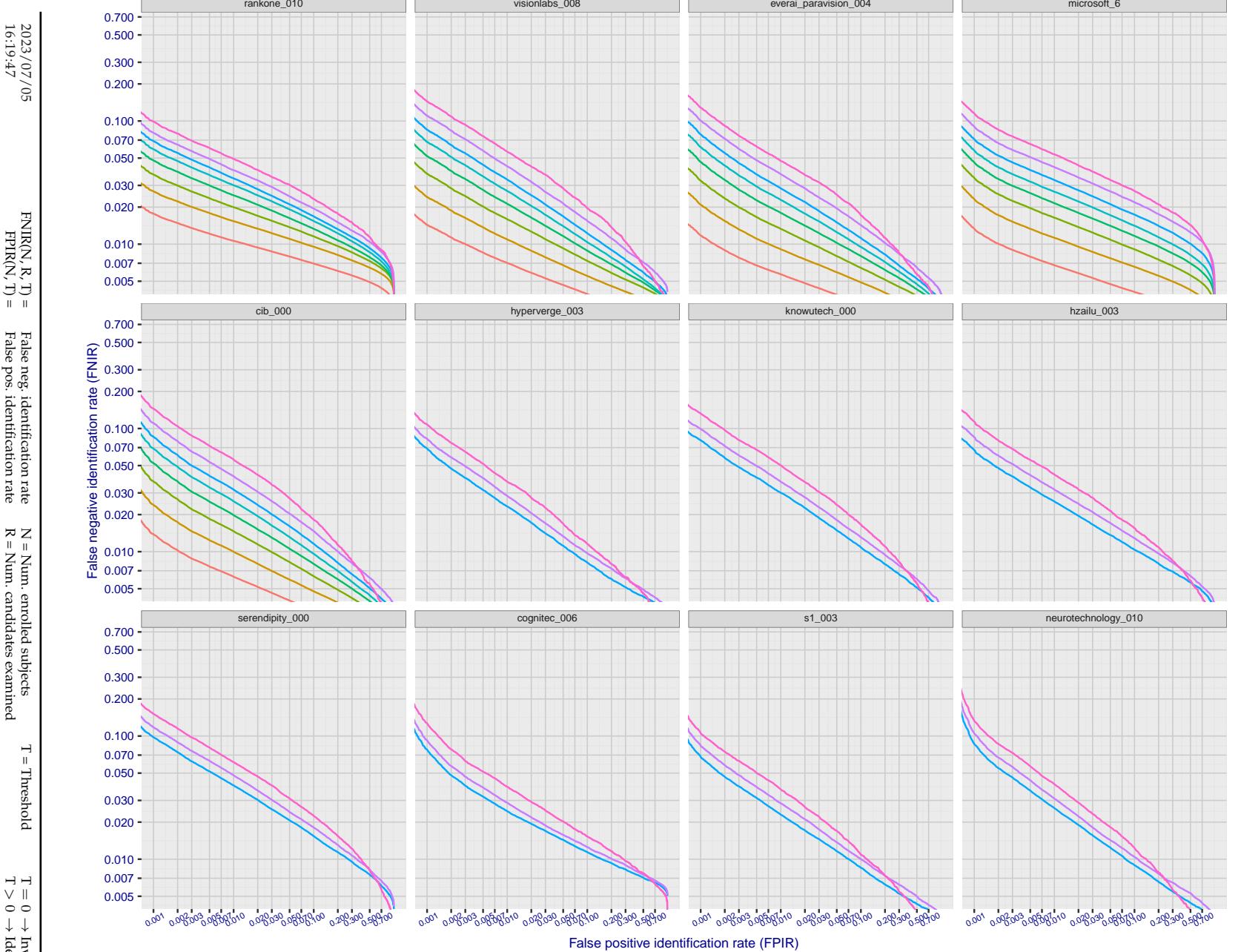


Figure 187: [FRVT-2018 Mugshot Ageing Dataset] Identification miss rates vs. FPIR by time-elapsed. The oldest image of each individual is enrolled. Thereafter, all more recent images are searched. Miss rates are computed over all searches noted in row 17 of Table 1 and binned by number of years between search and initial enrollment. FPIR is computed from the same FRVT 2018 non-mates noted in row 3 of Table 1 with $N = 3\,000\,000$.

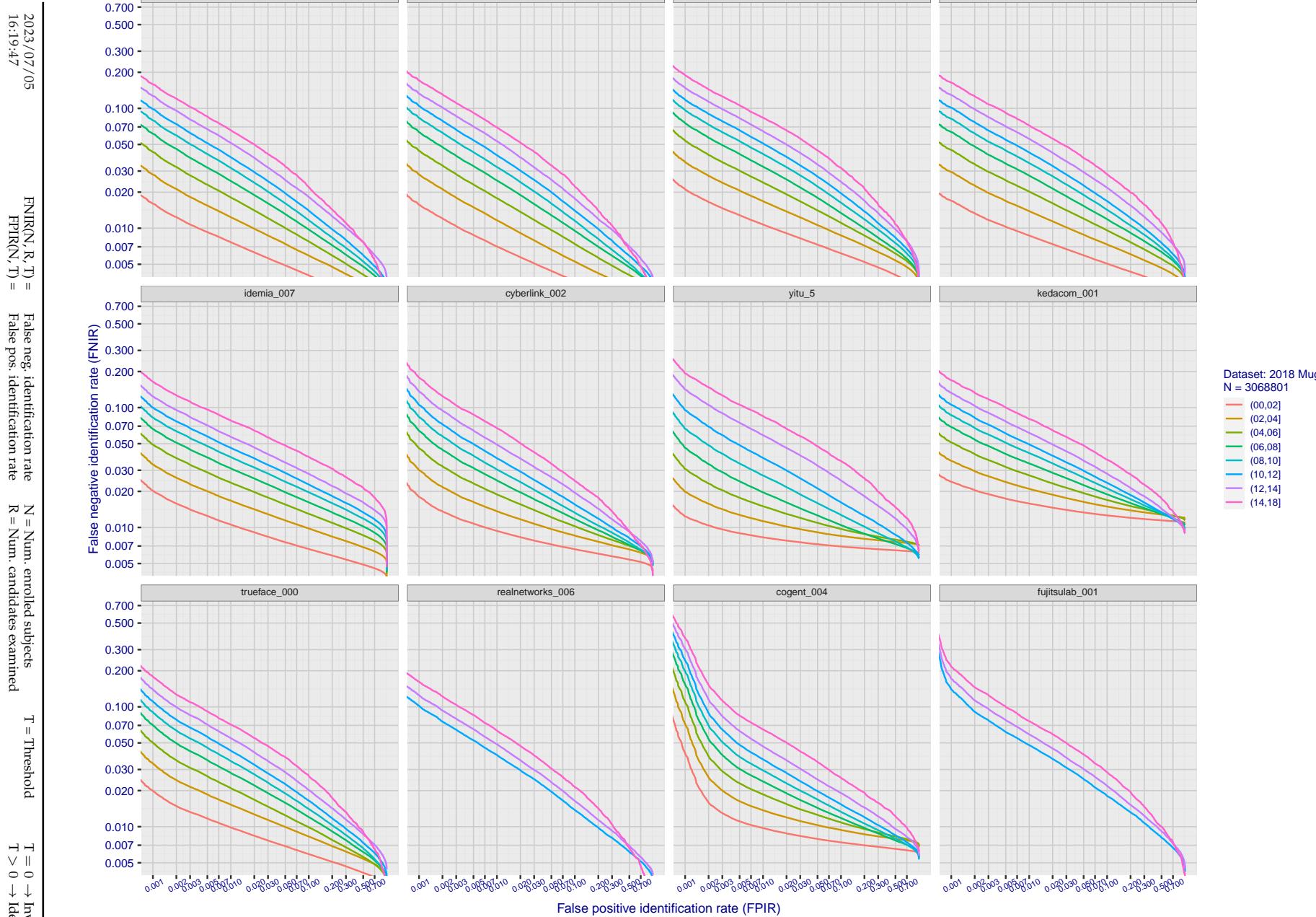


Figure 188: [FRVT-2018 Mugshot Ageing Dataset] Identification miss rates vs. FPIR by time-elapsed. The oldest image of each individual is enrolled. Thereafter, all more recent images are searched. Miss rates are computed over all searches noted in row 17 of Table 1 and binned by number of years between search and initial enrollment. FPIR is computed from the same FRVT 2018 non-mates noted in row 3 of Table 1 with $N = 3\,000\,000$.

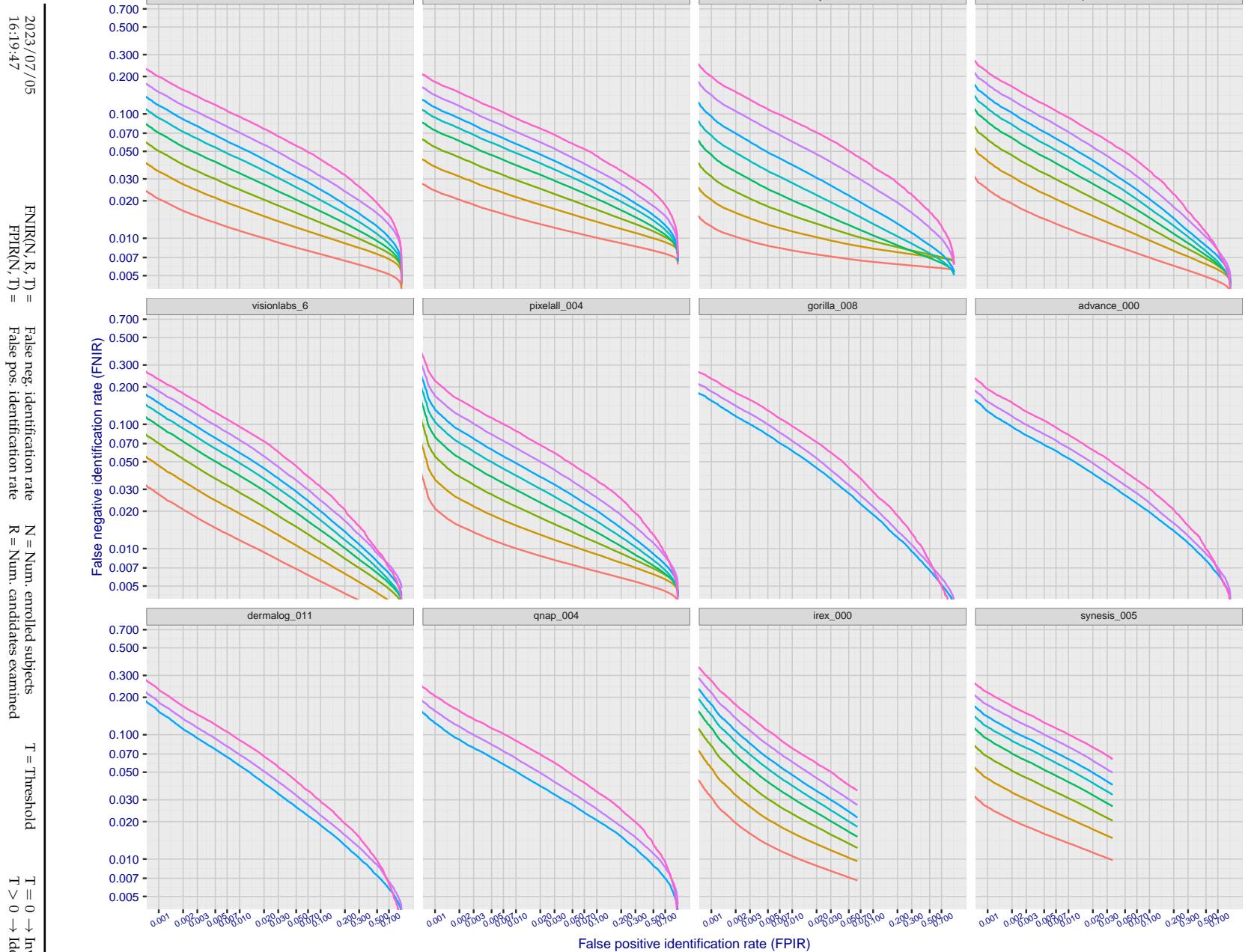


Figure 189: [FRVT-2018 Mugshot Ageing Dataset] Identification miss rates vs. FPIR by time-elapsed. The oldest image of each individual is enrolled. Thereafter, all more recent images are searched. Miss rates are computed over all searches noted in row 17 of Table 1 and binned by number of years between search and initial enrollment. FPIR is computed from the same FRVT 2018 non-mates noted in row 3 of Table 1 with $N = 3\,000\,000$.

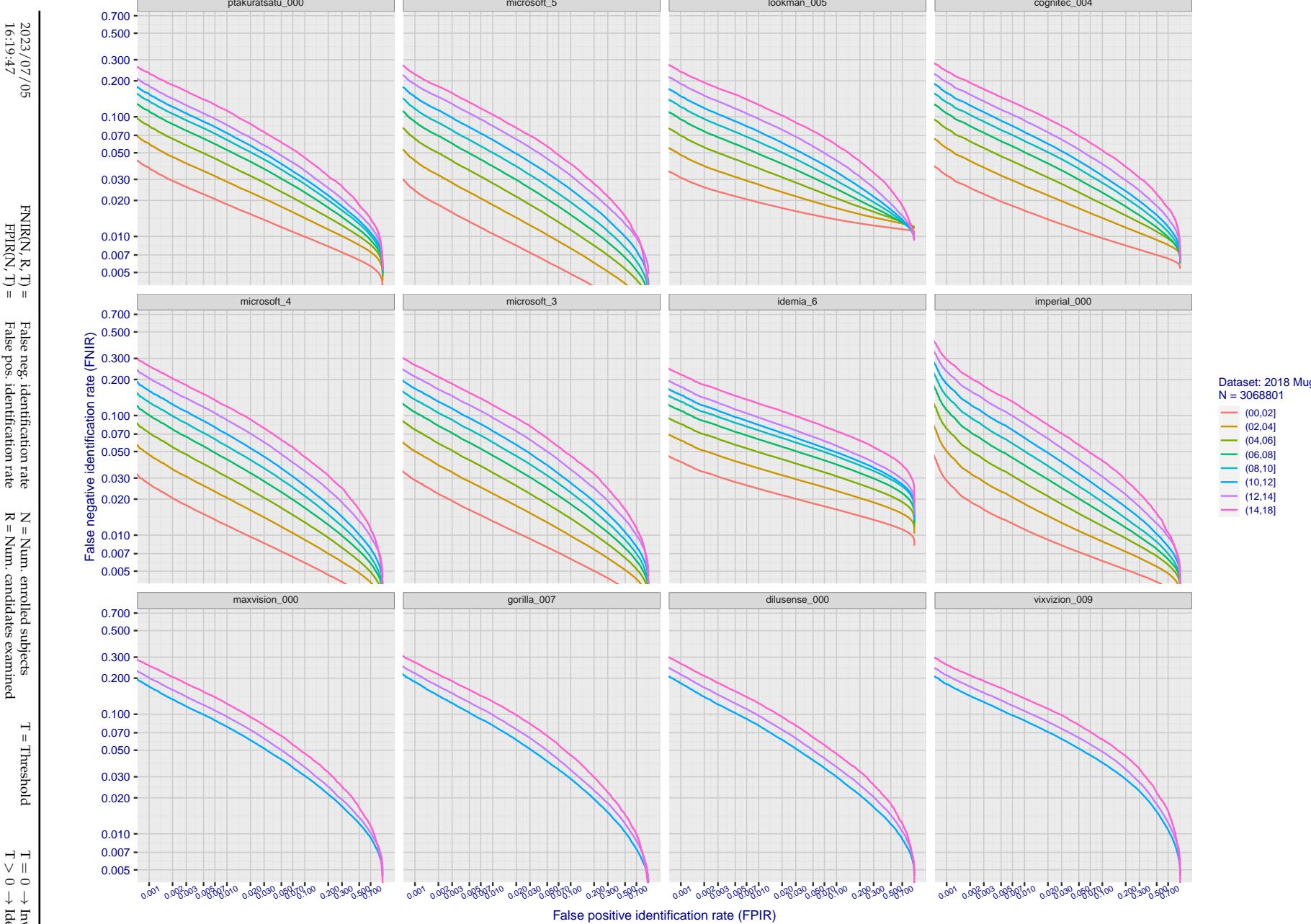


Figure 190: [FRVT-2018 Mugshot Ageing Dataset] Identification miss rates vs. FPIR by time-elapsed. The oldest image of each individual is enrolled. Thereafter, all more recent images are searched. Miss rates are computed over all searches noted in row 17 of Table 1 and binned by number of years between search and initial enrollment. FPIR is computed from the same FRVT 2018 non-mates noted in row 3 of Table 1 with $N = 3\,000\,000$.

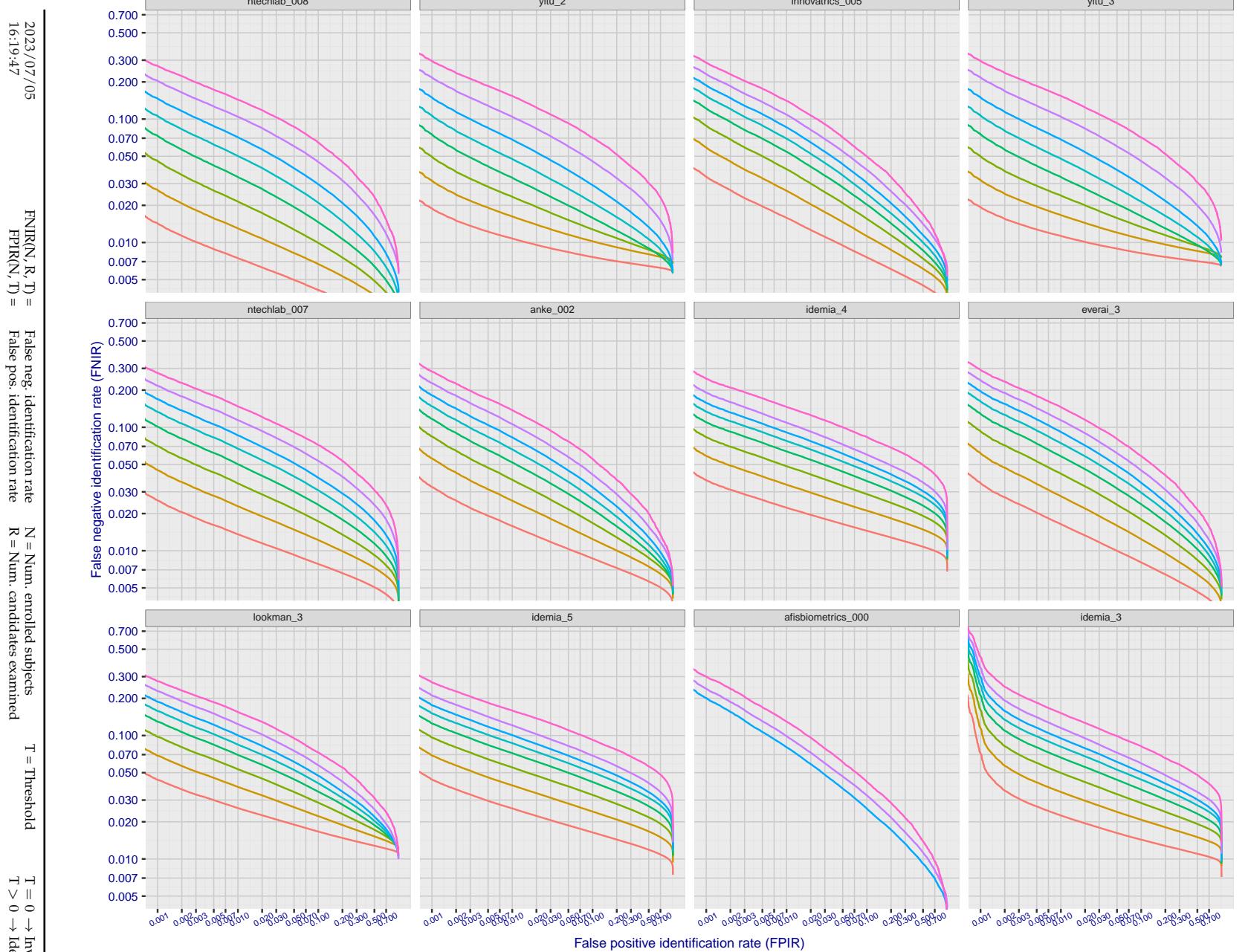


Figure 191: [FRVT-2018 Mugshot Ageing Dataset] Identification miss rates vs. FPIR by time-elapsed. The oldest image of each individual is enrolled. Thereafter, all more recent images are searched. Miss rates are computed over all searches noted in row 17 of Table 1 and binned by number of years between search and initial enrollment. FPIR is computed from the same FRVT 2018 non-mates noted in row 3 of Table 1 with $N = 3\,000\,000$.

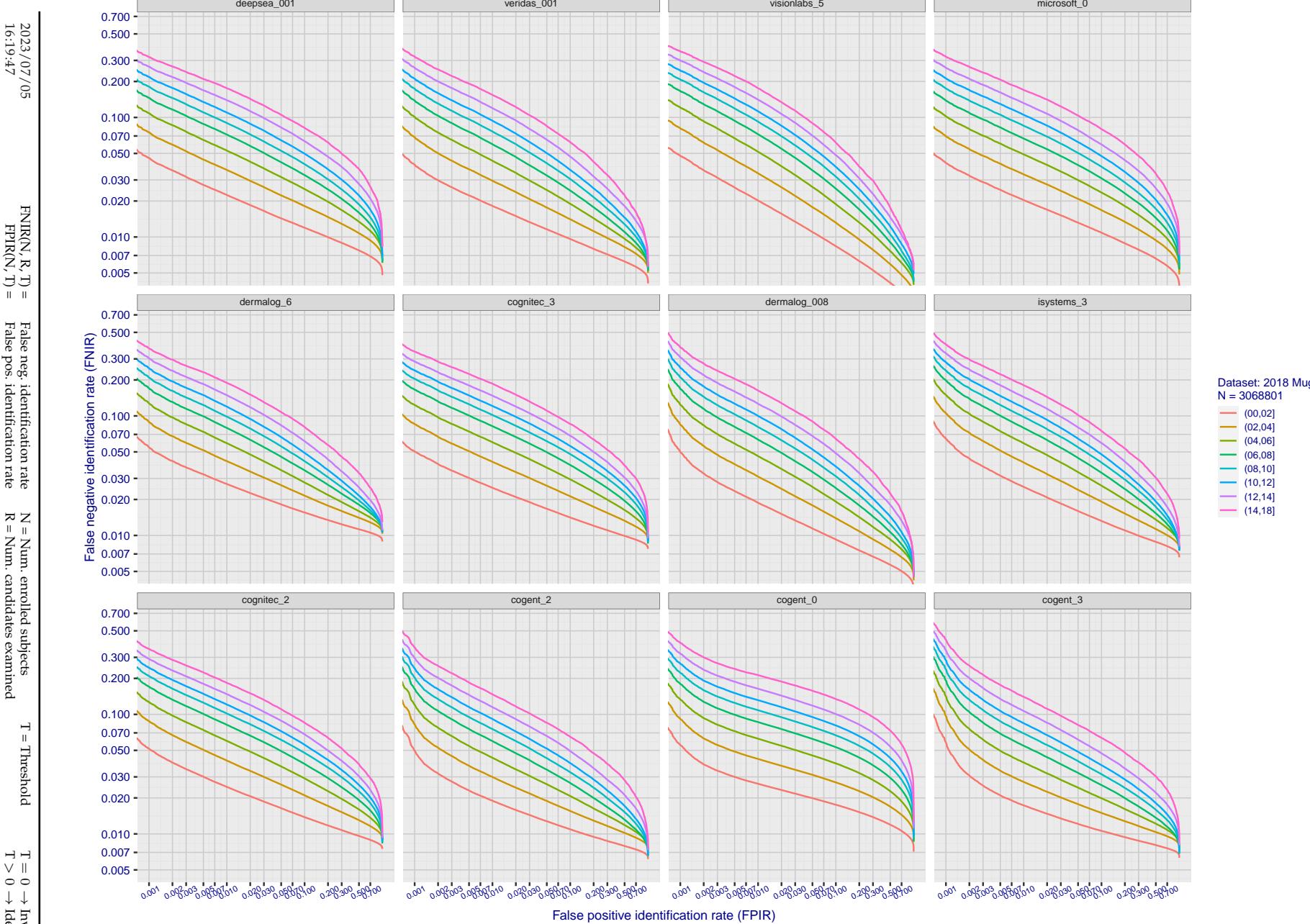


Figure 192: [FRVT-2018 Mugshot Ageing Dataset] Identification miss rates vs. FPIR by time-elapsed. The oldest image of each individual is enrolled. Thereafter, all more recent images are searched. Miss rates are computed over all searches noted in row 17 of Table 1 and binned by number of years between search and initial enrollment. FPIR is computed from the same FRVT 2018 non-mates noted in row 3 of Table 1 with $N = 3\,000\,000$.

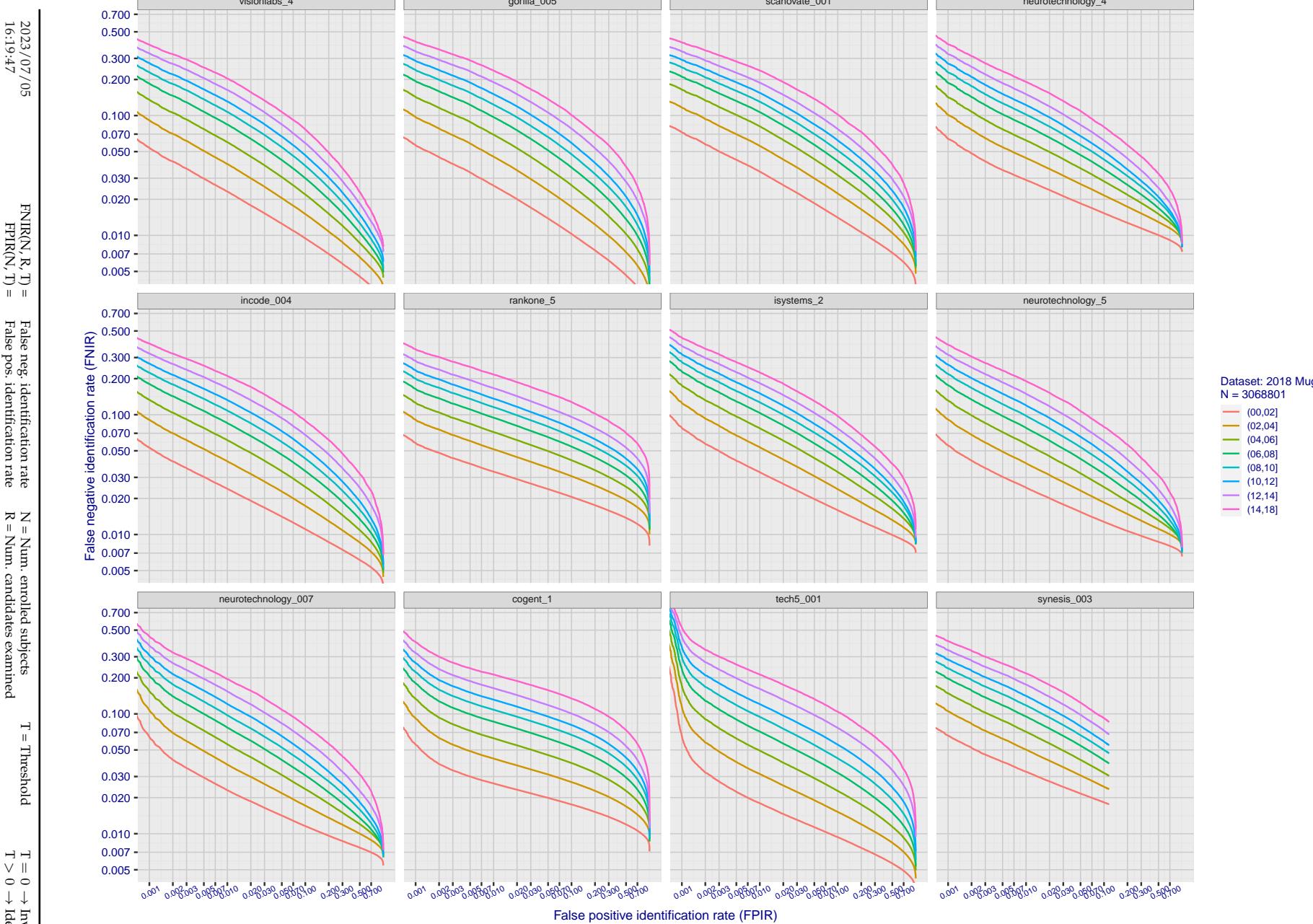


Figure 193: [FRVT-2018 Mugshot Ageing Dataset] Identification miss rates vs. FPIR by time-elapsed. The oldest image of each individual is enrolled. Thereafter, all more recent images are searched. Miss rates are computed over all searches noted in row 17 of Table 1 and binned by number of years between search and initial enrollment. FPIR is computed from the same FRVT 2018 non-mates noted in row 3 of Table 1 with $N = 3\,000\,000$.

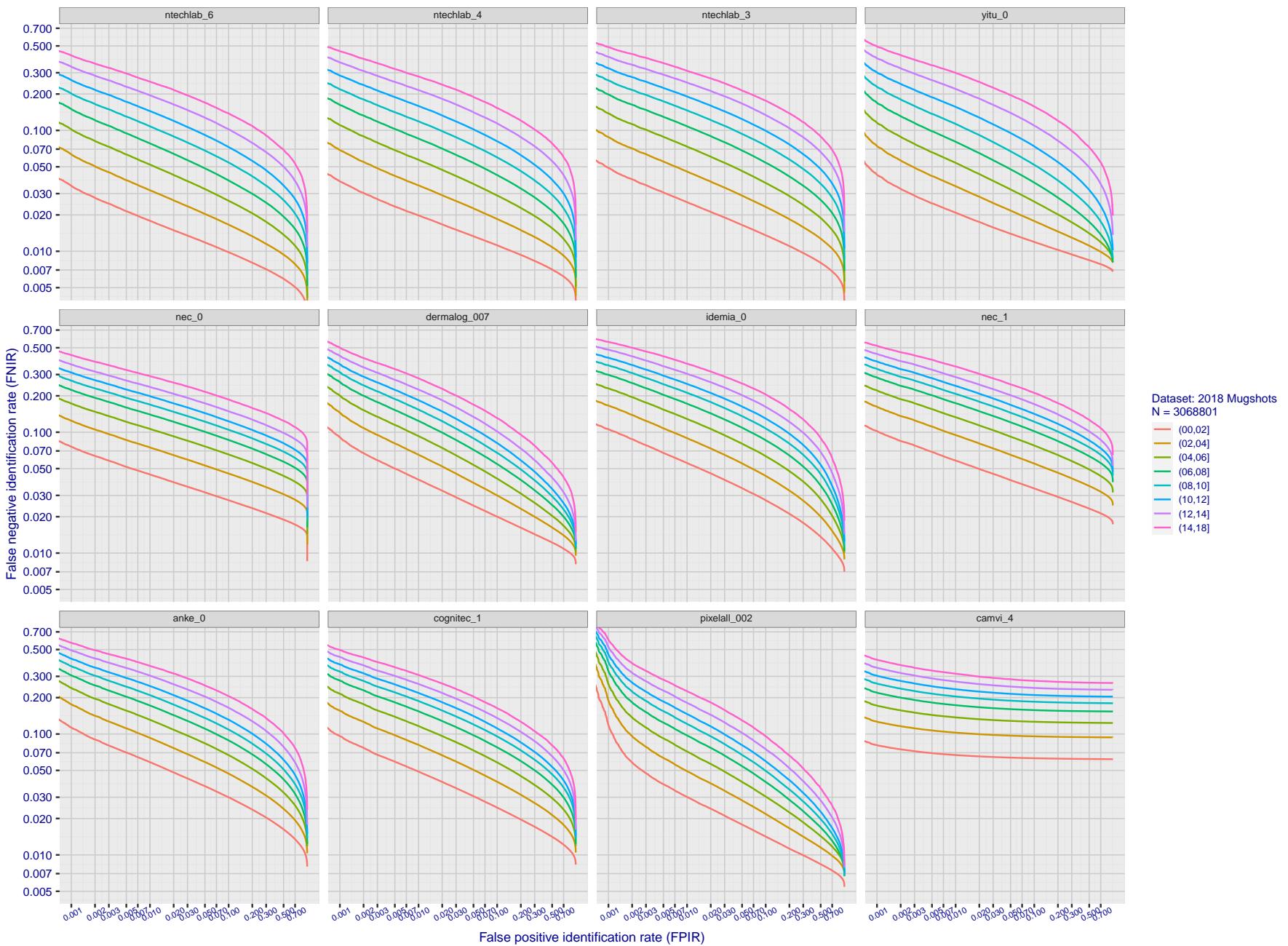


Figure 194: [FRVT-2018 Mugshot Ageing Dataset] Identification miss rates vs. FPIR by time-elapsed. The oldest image of each individual is enrolled. Thereafter, all more recent images are searched. Miss rates are computed over all searches noted in row 17 of Table 1 and binned by number of years between search and initial enrollment. FPIR is computed from the same FRVT 2018 non-mates noted in row 3 of Table 1 with $N = 3\,000\,000$.

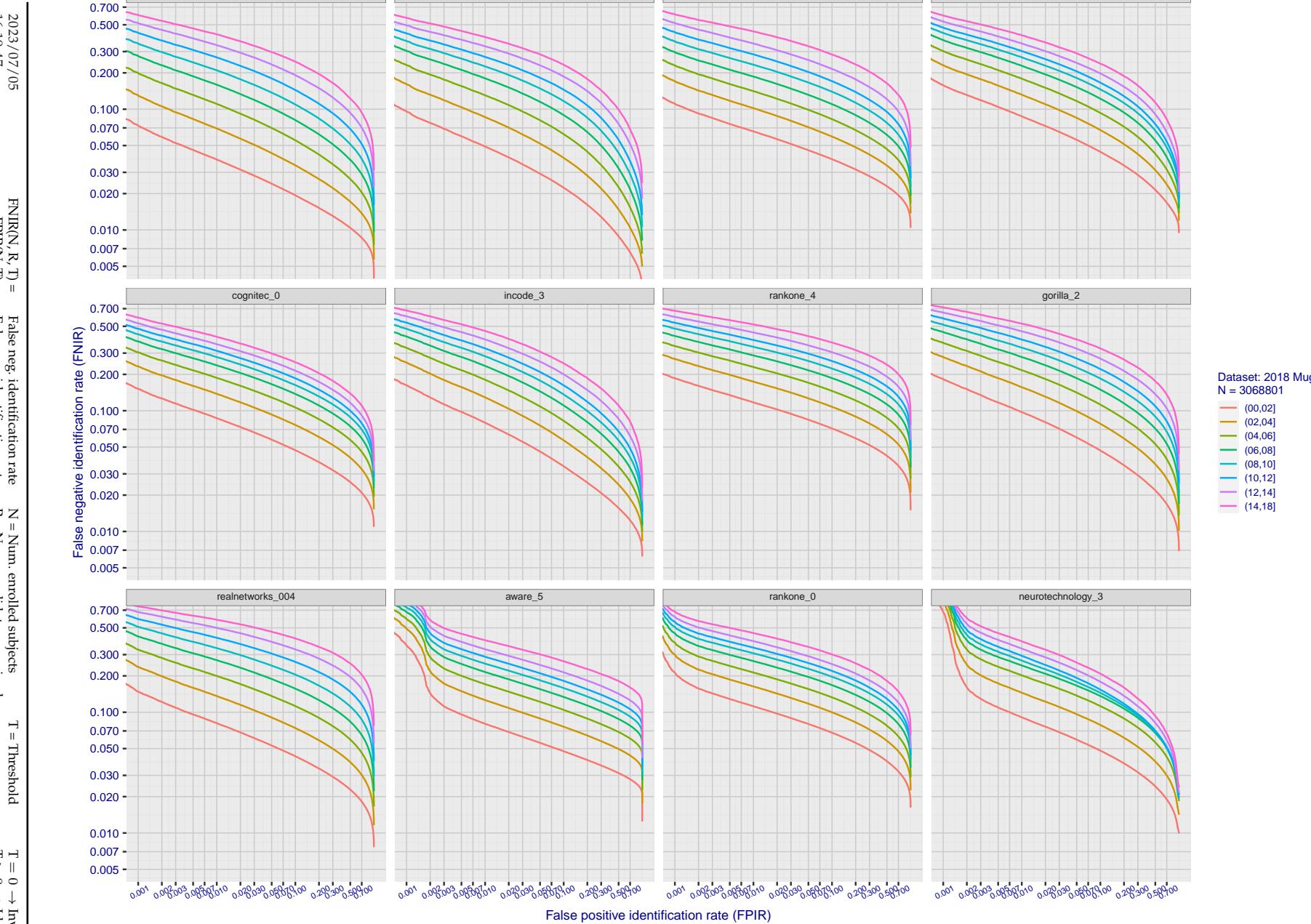


Figure 195: [FRVT-2018 Mugshot Ageing Dataset] Identification miss rates vs. FPIR by time-elapsed. The oldest image of each individual is enrolled. Thereafter, all more recent images are searched. Miss rates are computed over all searches noted in row 17 of Table 1 and binned by number of years between search and initial enrollment. FPIR is computed from the same FRVT 2018 non-mates noted in row 3 of Table 1 with $N = 3\,000\,000$.

2023/07/05
16:19:47FNIR(N, R, T) = False neg. identification rate
FPIR(N, T) = False pos. identification rateN = Num. enrolled subjects
R = Num. candidates examined

T = Threshold

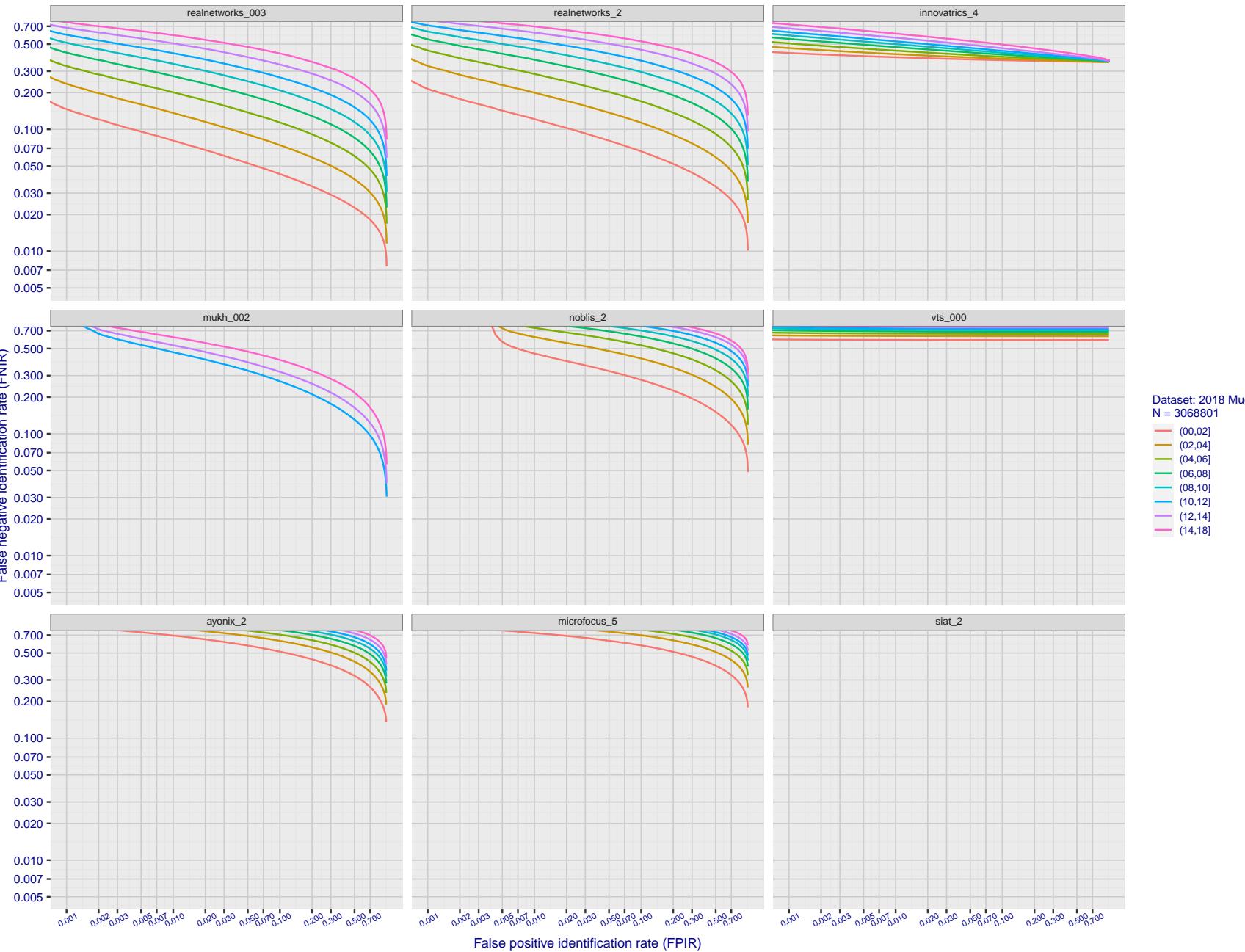
T = 0 → Investigation
T > 0 → Identification

Figure 196: [FRVT-2018 Mugshot Ageing Dataset] Identification miss rates vs. FPIR by time-elapsed. The oldest image of each individual is enrolled. Thereafter, all more recent images are searched. Miss rates are computed over all searches noted in row 17 of Table 1 and binned by number of years between search and initial enrollment. FPIR is computed from the same FRVT 2018 non-mates noted in row 3 of Table 1 with $N = 3\,000\,000$.

2023/07/05
16:19:47

FNIR(N, R, T) = False neg. identification rate
FPTR(N, T) = False pos. identification rate

N = Num. enrolled subjects
R = Num. candidates examined

T = Threshold
T > 0 → Identification

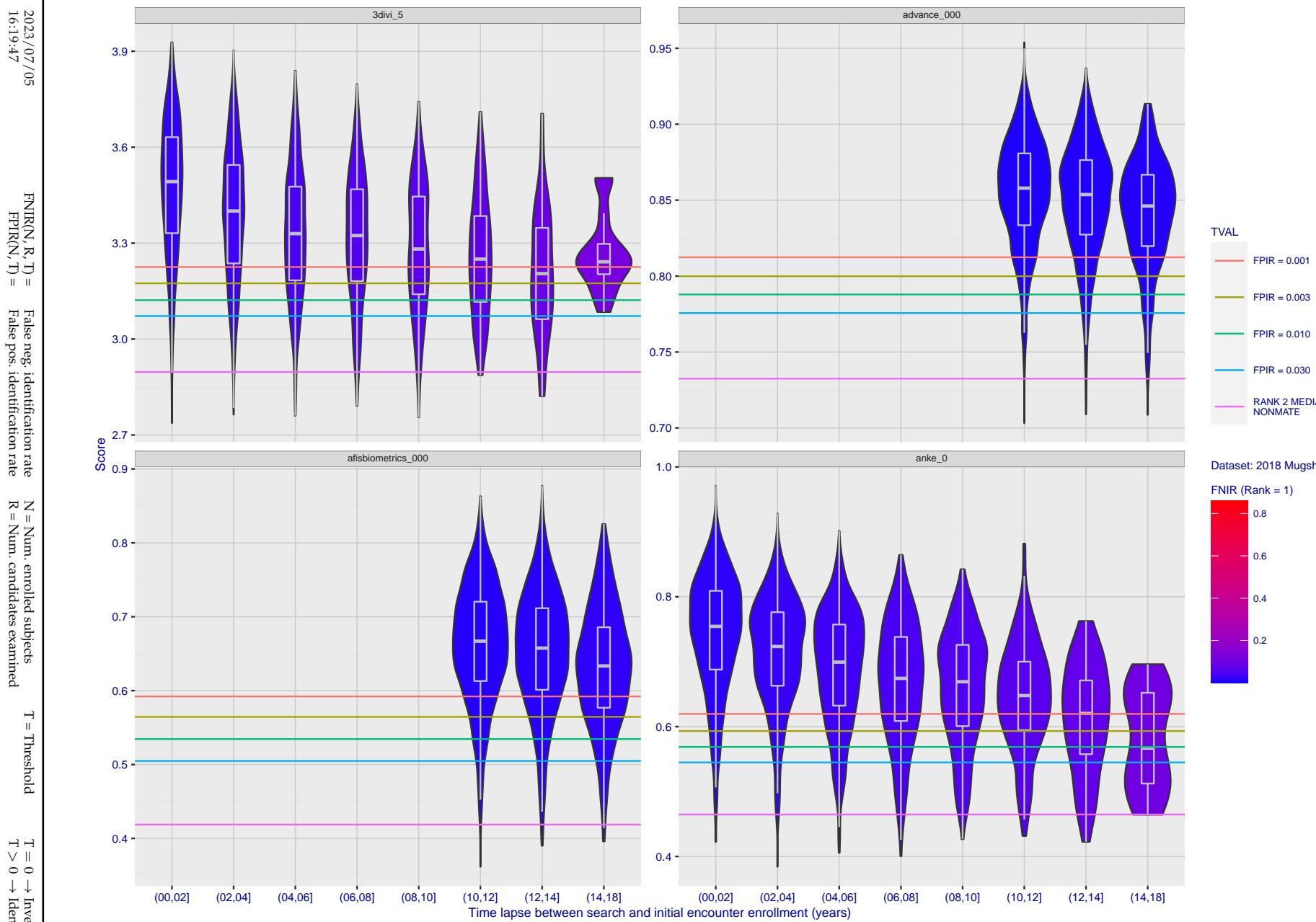


Figure 197: [FRVT-2018 Mugshot Ageing Dataset] Native mate scores vs. time-elapsed. The oldest image of each individual is enrolled. Thereafter, all more recent images are searched. Mated score distributions are computed over all searches noted in row 17 of Table 1 binned by number of years between search and initial enrollment.

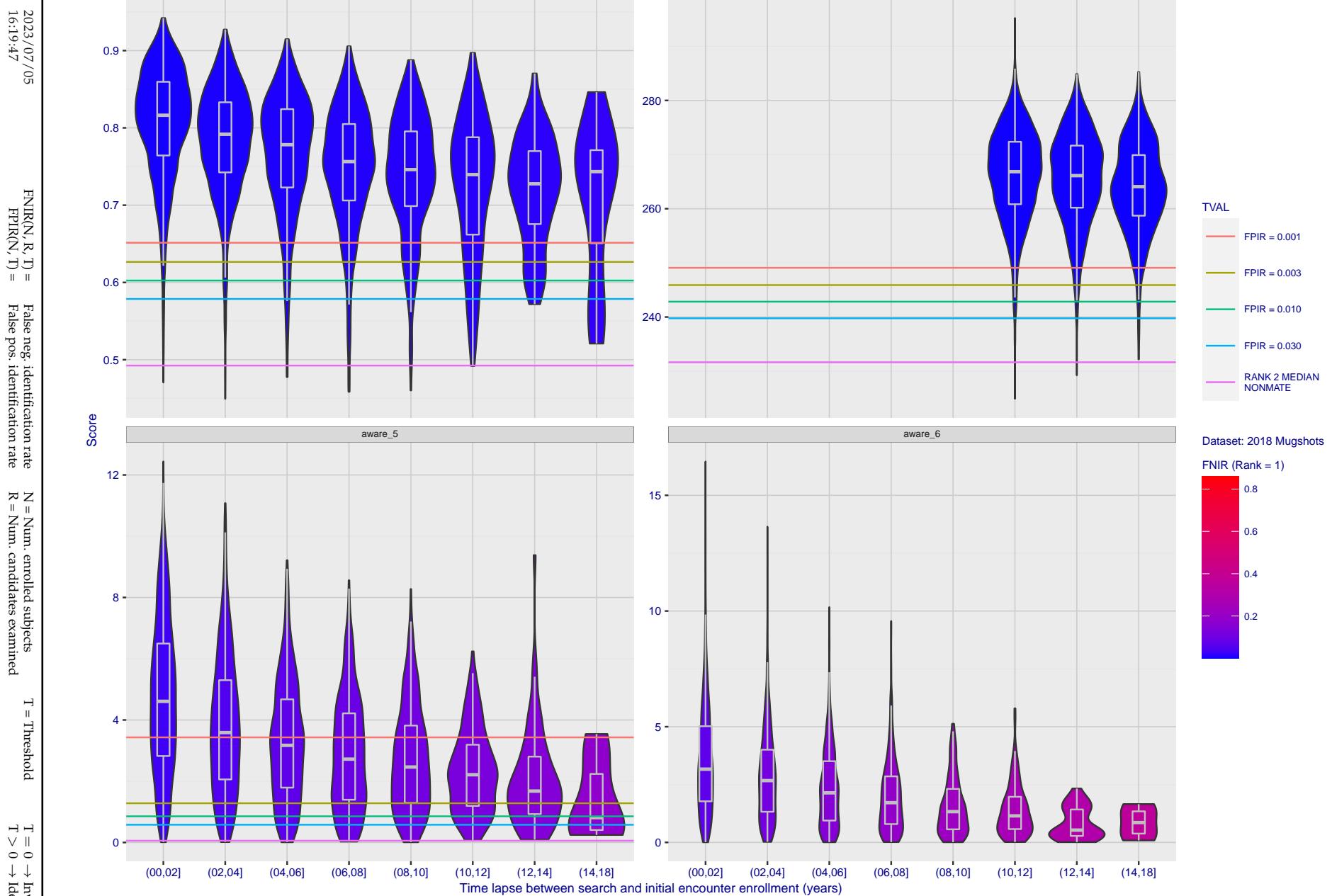


Figure 198: [FRVT-2018 Mugshot Ageing Dataset] Native mate scores vs. time-elapsed. The oldest image of each individual is enrolled. Thereafter, all more recent images are searched. Mated score distributions are computed over all searches noted in row 17 of Table 1 binned by number of years between search and initial enrollment.

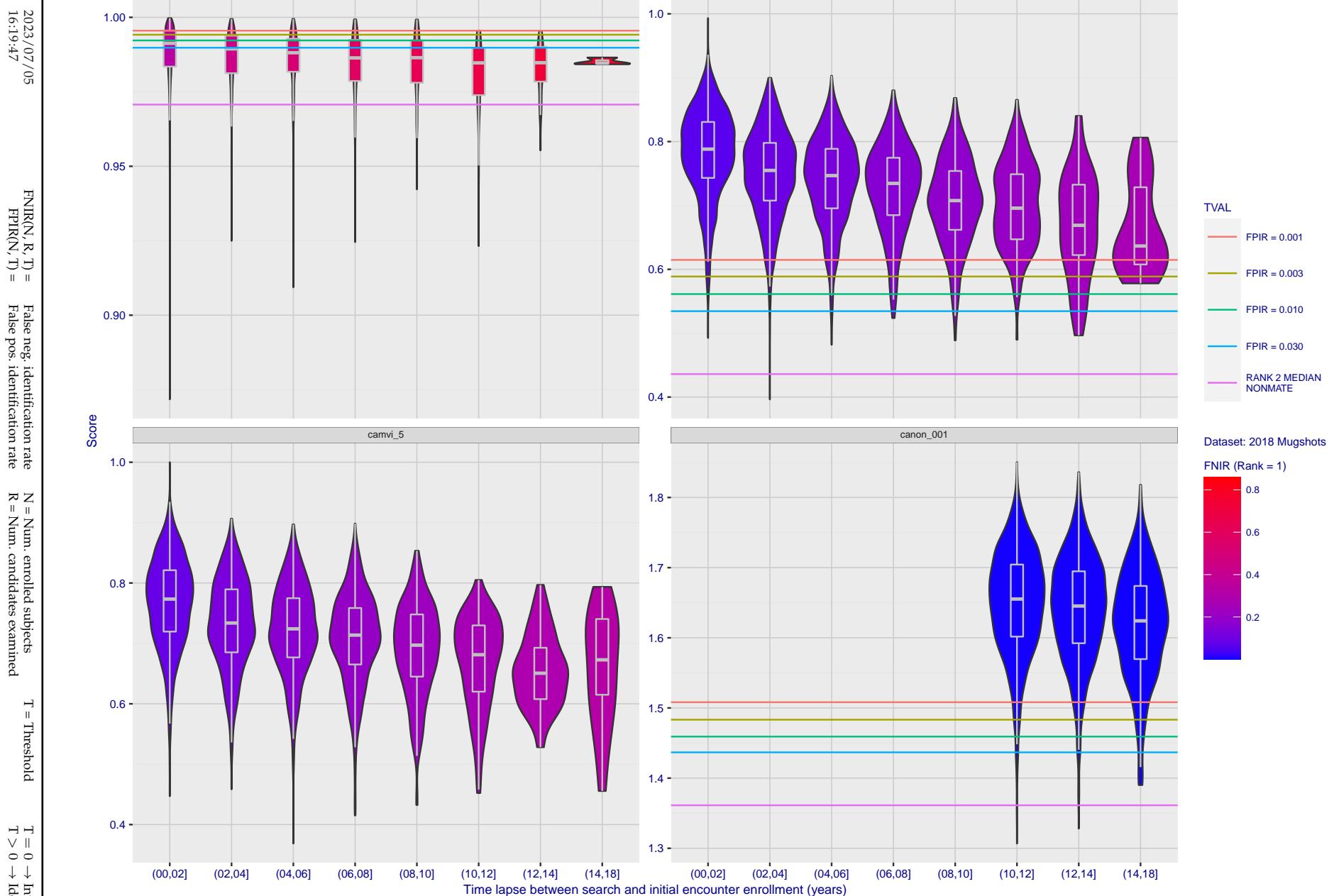


Figure 199: [FRVT-2018 Mugshot Ageing Dataset] Native mate scores vs. time-elapsed. The oldest image of each individual is enrolled. Thereafter, all more recent images are searched. Mated score distributions are computed over all searches noted in row 17 of Table 1 binned by number of years between search and initial enrollment.

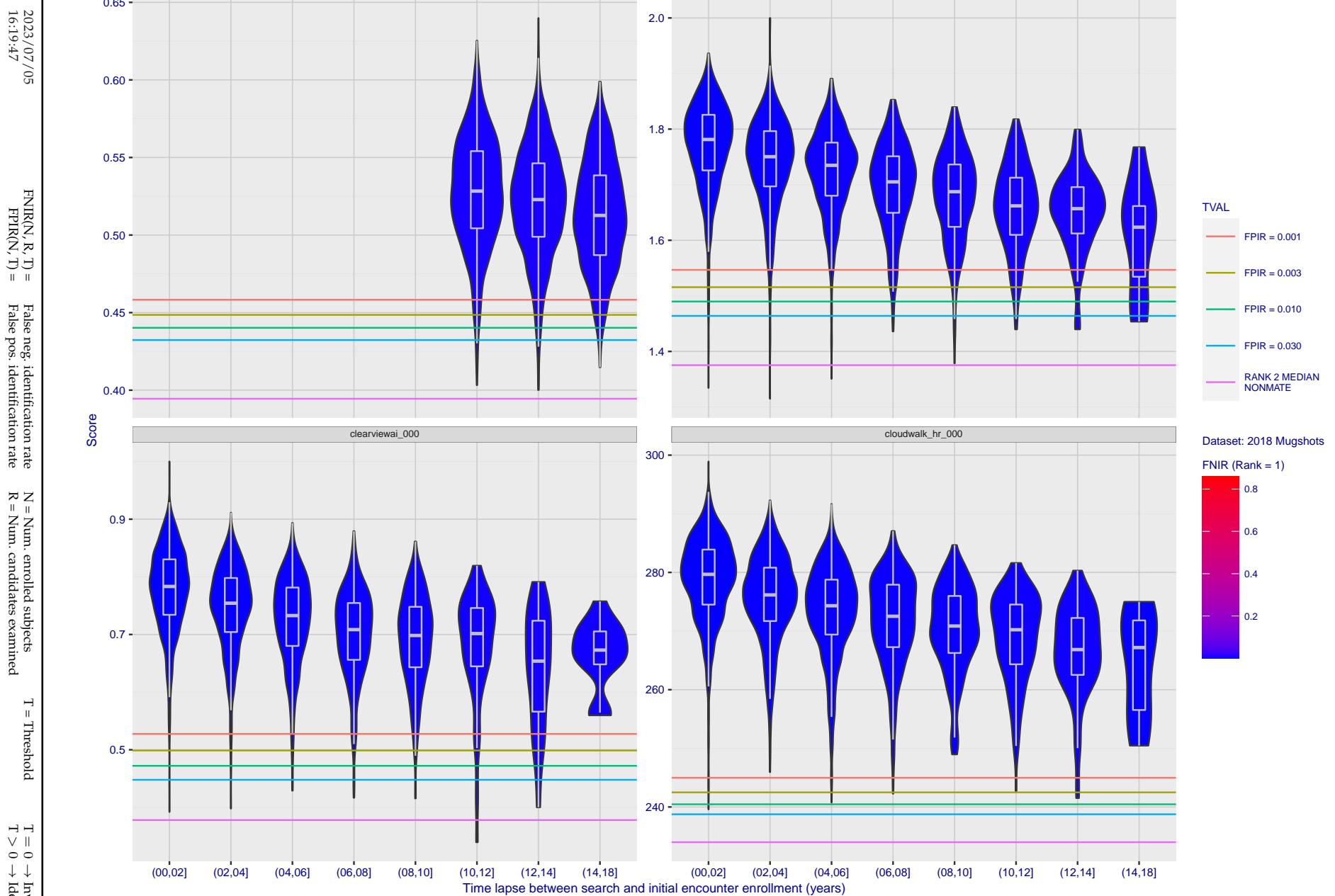


Figure 200: [FRVT-2018 Mugshot Ageing Dataset] Native mate scores vs. time-elapsed. The oldest image of each individual is enrolled. Thereafter, all more recent images are searched. Mated score distributions are computed over all searches noted in row 17 of Table 1 binned by number of years between search and initial enrollment.

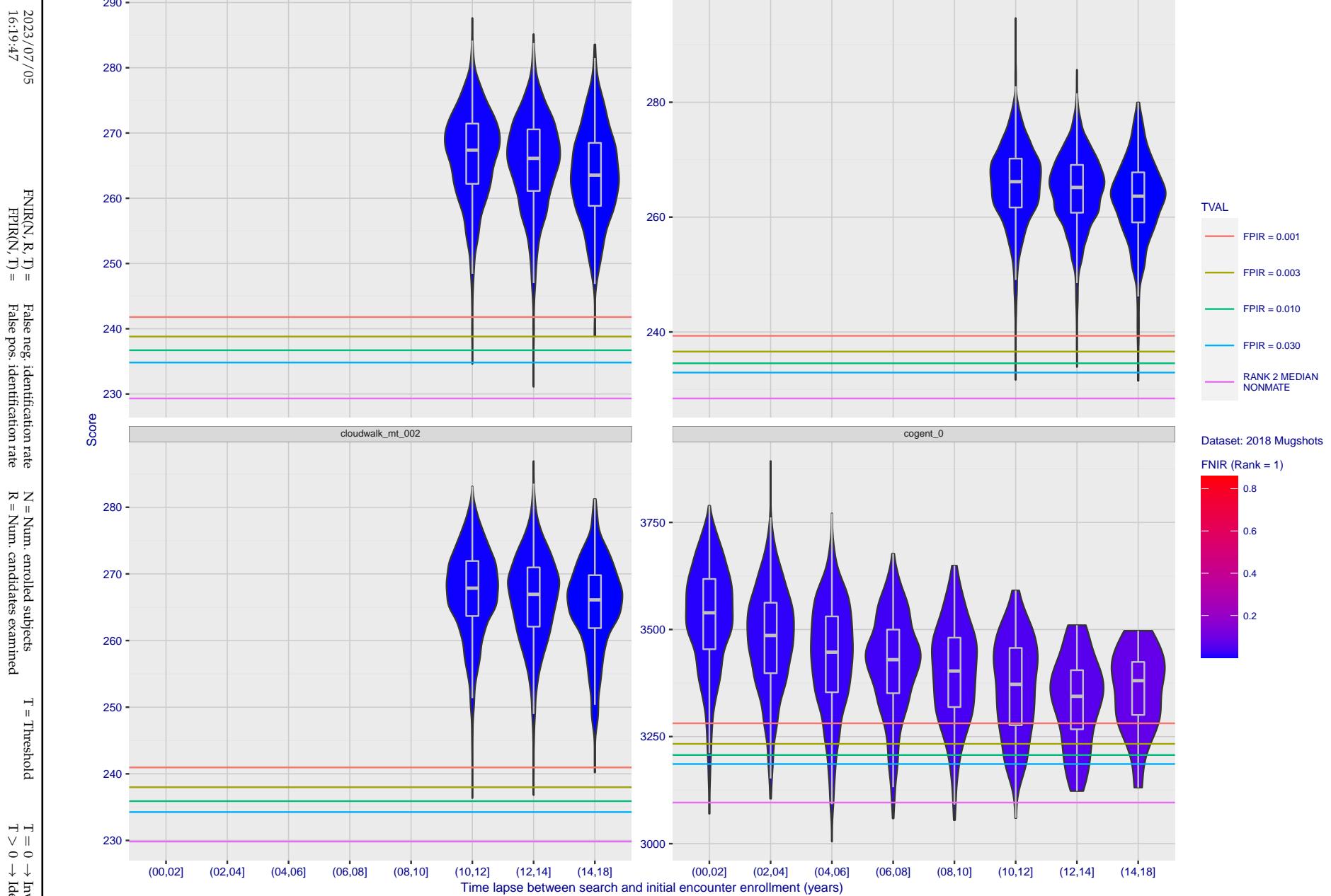


Figure 201: [FRVT-2018 Mugshot Ageing Dataset] Native mate scores vs. time-elapsed. The oldest image of each individual is enrolled. Thereafter, all more recent images are searched. Mated score distributions are computed over all searches noted in row 17 of Table 1 binned by number of years between search and initial enrollment.

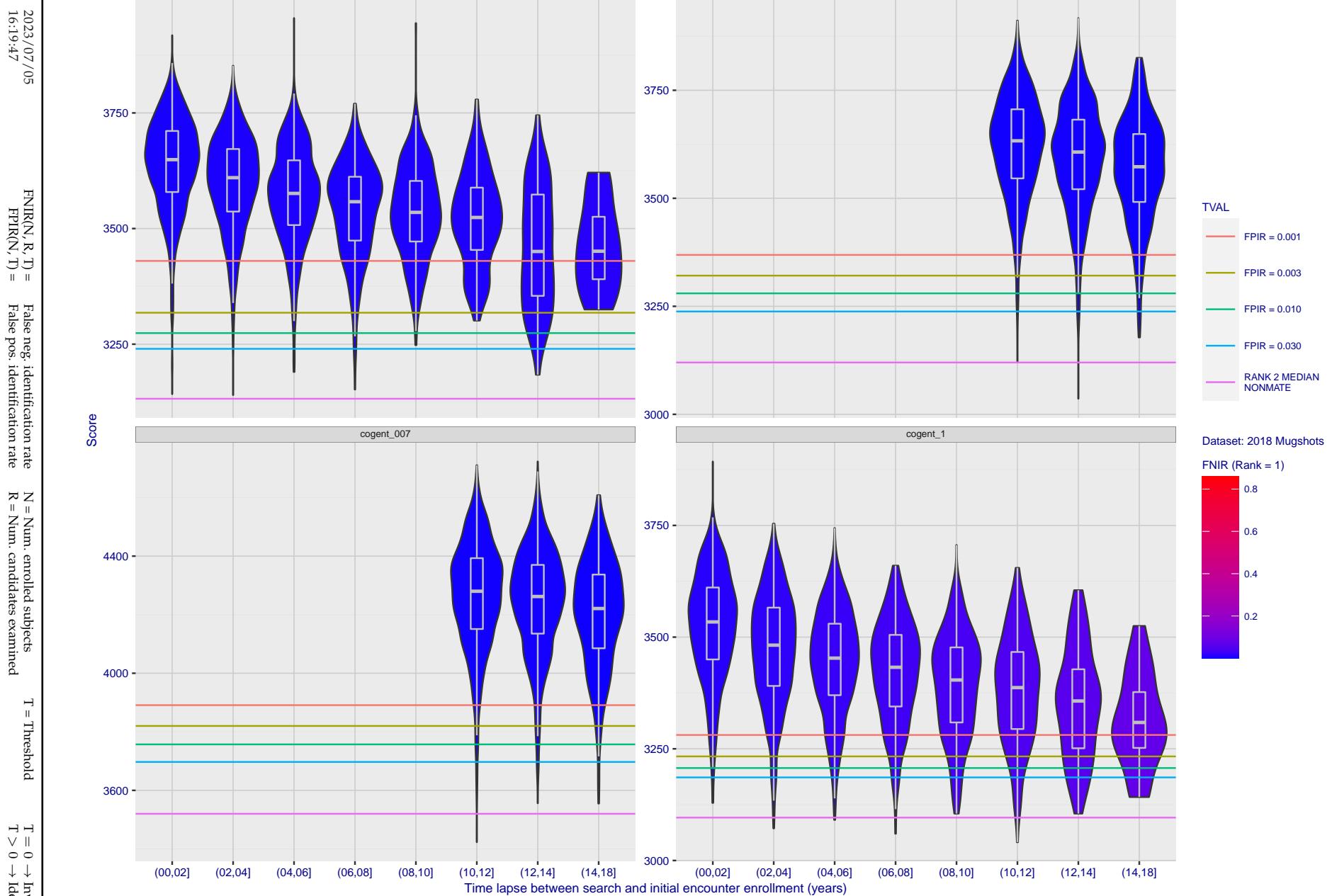


Figure 202: [FRVT-2018 Mugshot Ageing Dataset] Native mate scores vs. time-elapsed. The oldest image of each individual is enrolled. Thereafter, all more recent images are searched. Mated score distributions are computed over all searches noted in row 17 of Table 1 binned by number of years between search and initial enrollment.

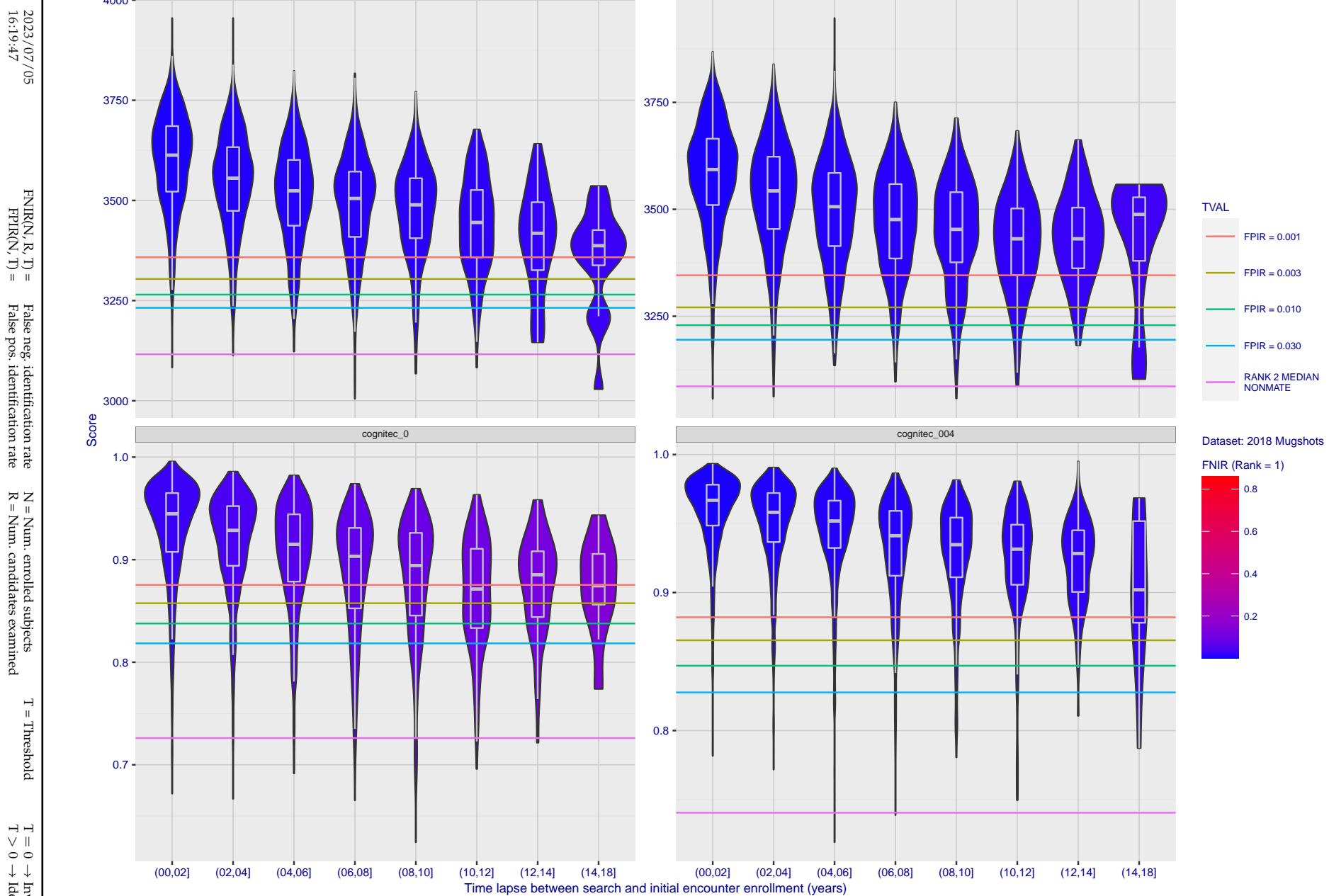


Figure 203: [FRVT-2018 Mugshot Ageing Dataset] Native mate scores vs. time-elapsed. The oldest image of each individual is enrolled. Thereafter, all more recent images are searched. Mated score distributions are computed over all searches noted in row 17 of Table 1 binned by number of years between search and initial enrollment.

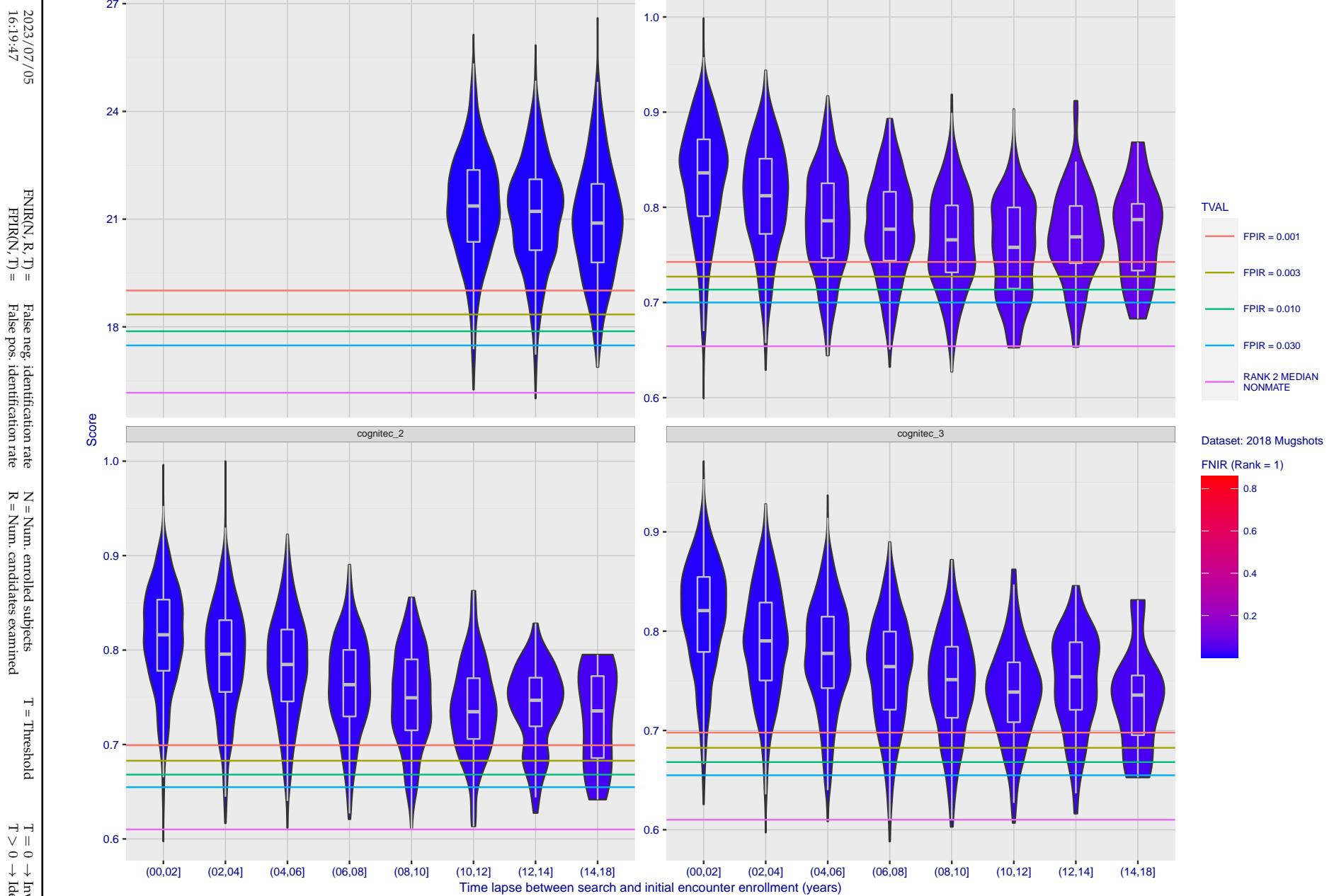


Figure 204: [FRVT-2018 Mugshot Ageing Dataset] Native mate scores vs. time-elapsed. The oldest image of each individual is enrolled. Thereafter, all more recent images are searched. Mated score distributions are computed over all searches noted in row 17 of Table 1 binned by number of years between search and initial enrollment.

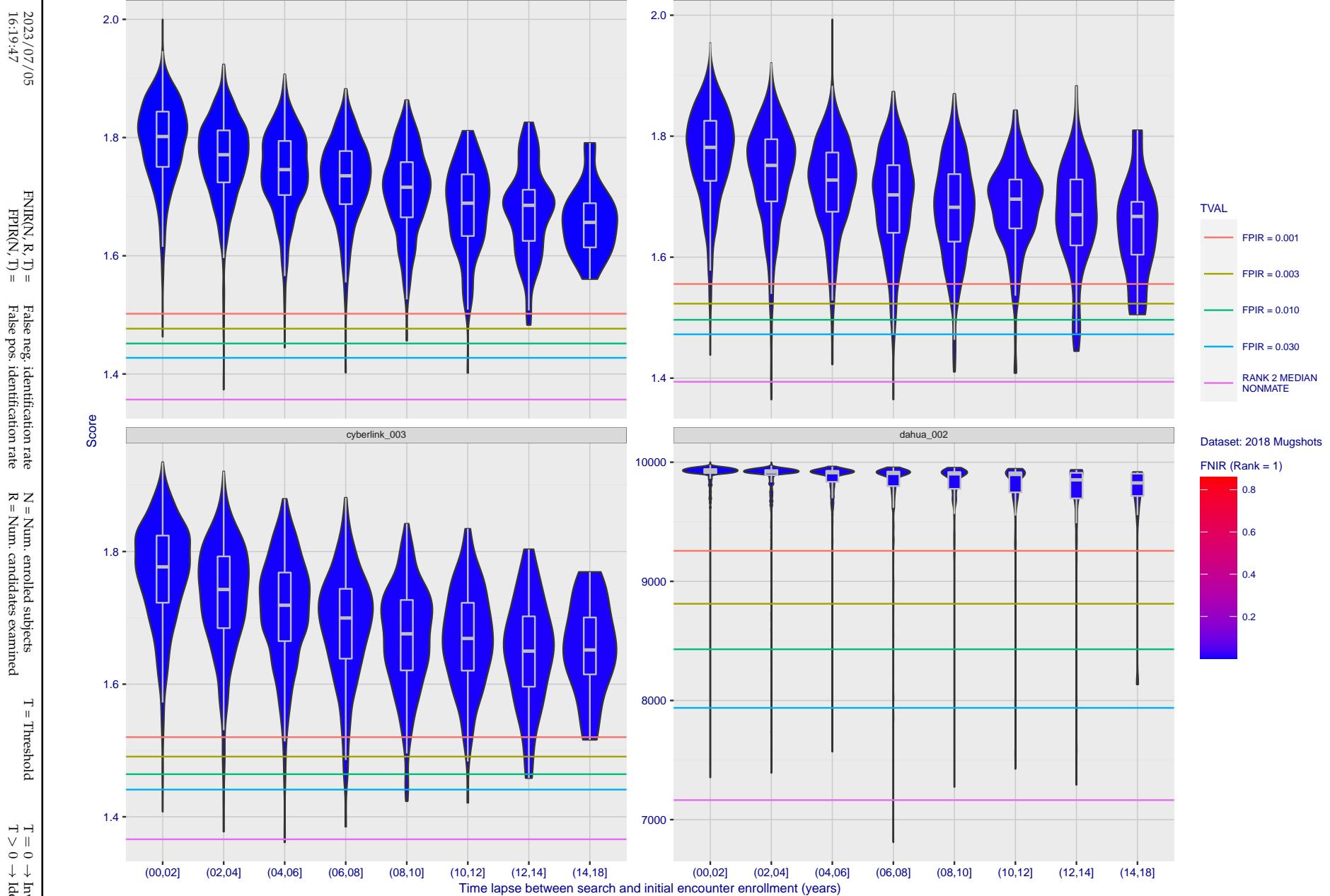


Figure 205: [FRVT-2018 Mugshot Ageing Dataset] Native mate scores vs. time-elapsed. The oldest image of each individual is enrolled. Thereafter, all more recent images are searched. Mated score distributions are computed over all searches noted in row 17 of Table 1 binned by number of years between search and initial enrollment.

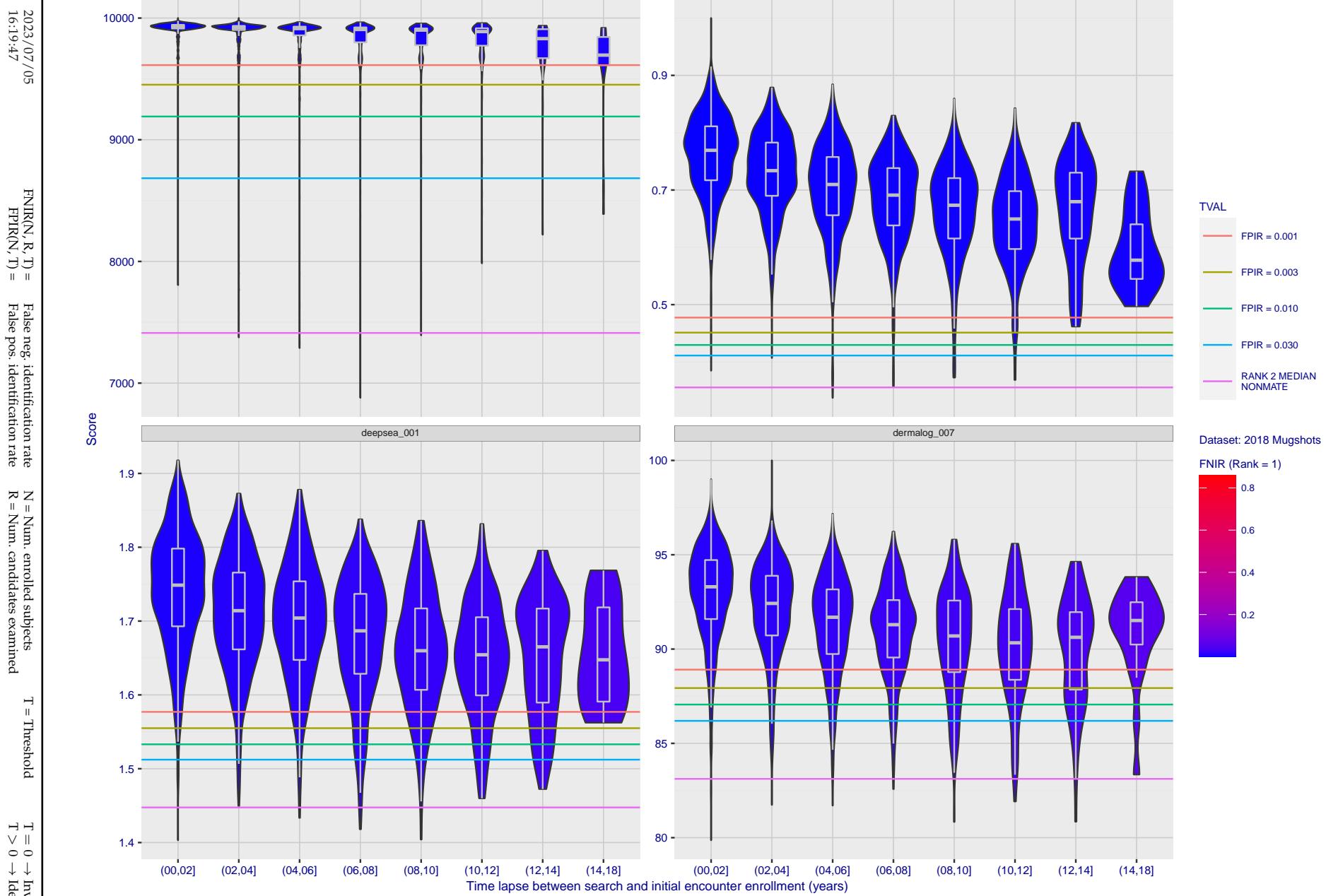


Figure 206: [FRVT-2018 Mugshot Ageing Dataset] Native mate scores vs. time-elapsed. The oldest image of each individual is enrolled. Thereafter, all more recent images are searched. Mated score distributions are computed over all searches noted in row 17 of Table 1 binned by number of years between search and initial enrollment.

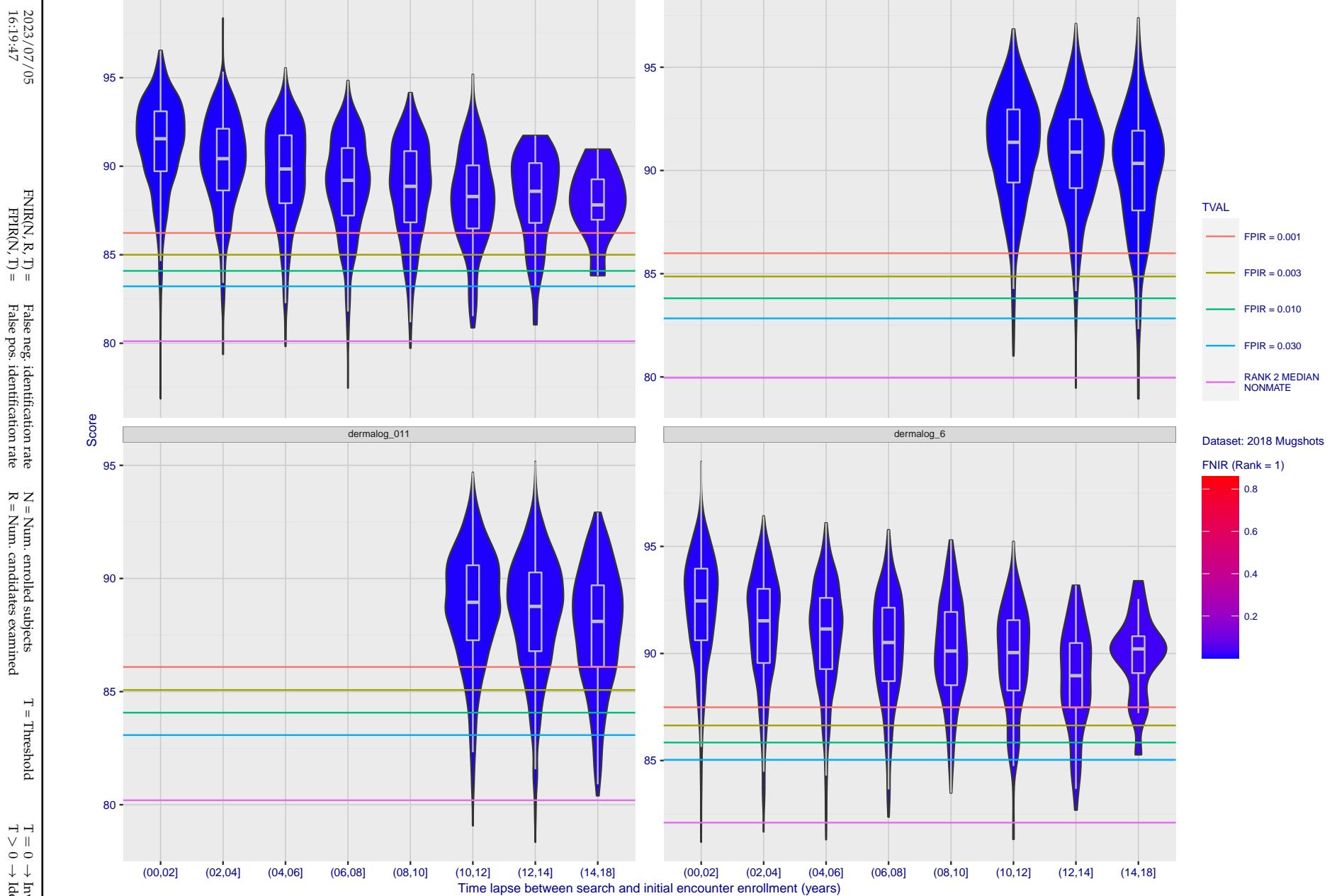


Figure 207: [FRVT-2018 Mugshot Ageing Dataset] Native mate scores vs. time-elapsed. The oldest image of each individual is enrolled. Thereafter, all more recent images are searched. Mated score distributions are computed over all searches noted in row 17 of Table 1 binned by number of years between search and initial enrollment.

2023/07/05
16:19:47FNIR(N, R, T) = False neg. identification rate
FPTR(N, T) = False pos. identification rateN = Num. enrolled subjects
R = Num. candidates examinedT = Threshold
T = 0 → Investigation

T > 0 → Identification

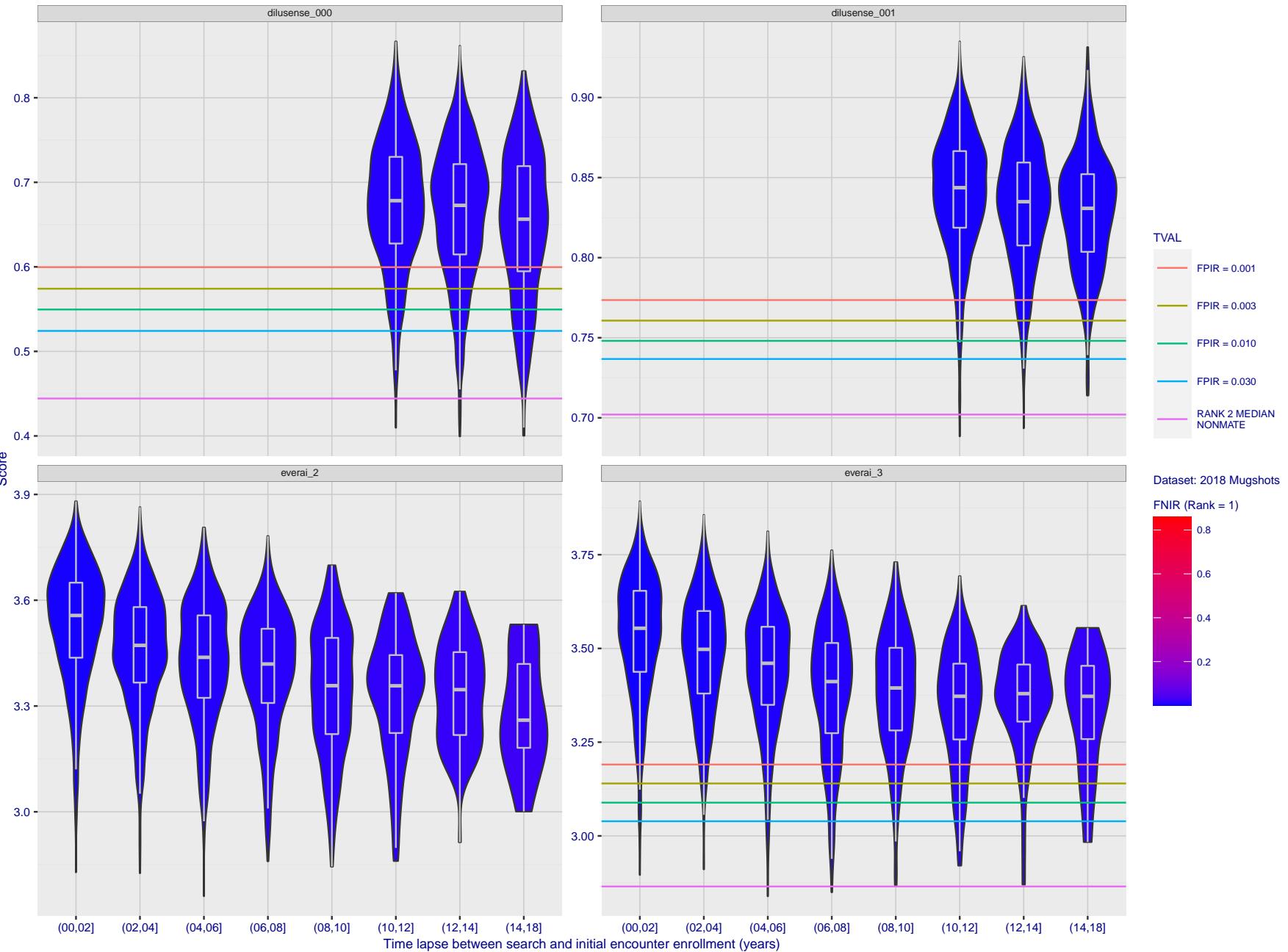


Figure 208: [FRVT-2018 Mugshot Ageing Dataset] Native mate scores vs. time-elapsed. The oldest image of each individual is enrolled. Thereafter, all more recent images are searched. Mated score distributions are computed over all searches noted in row 17 of Table 1 binned by number of years between search and initial enrollment.

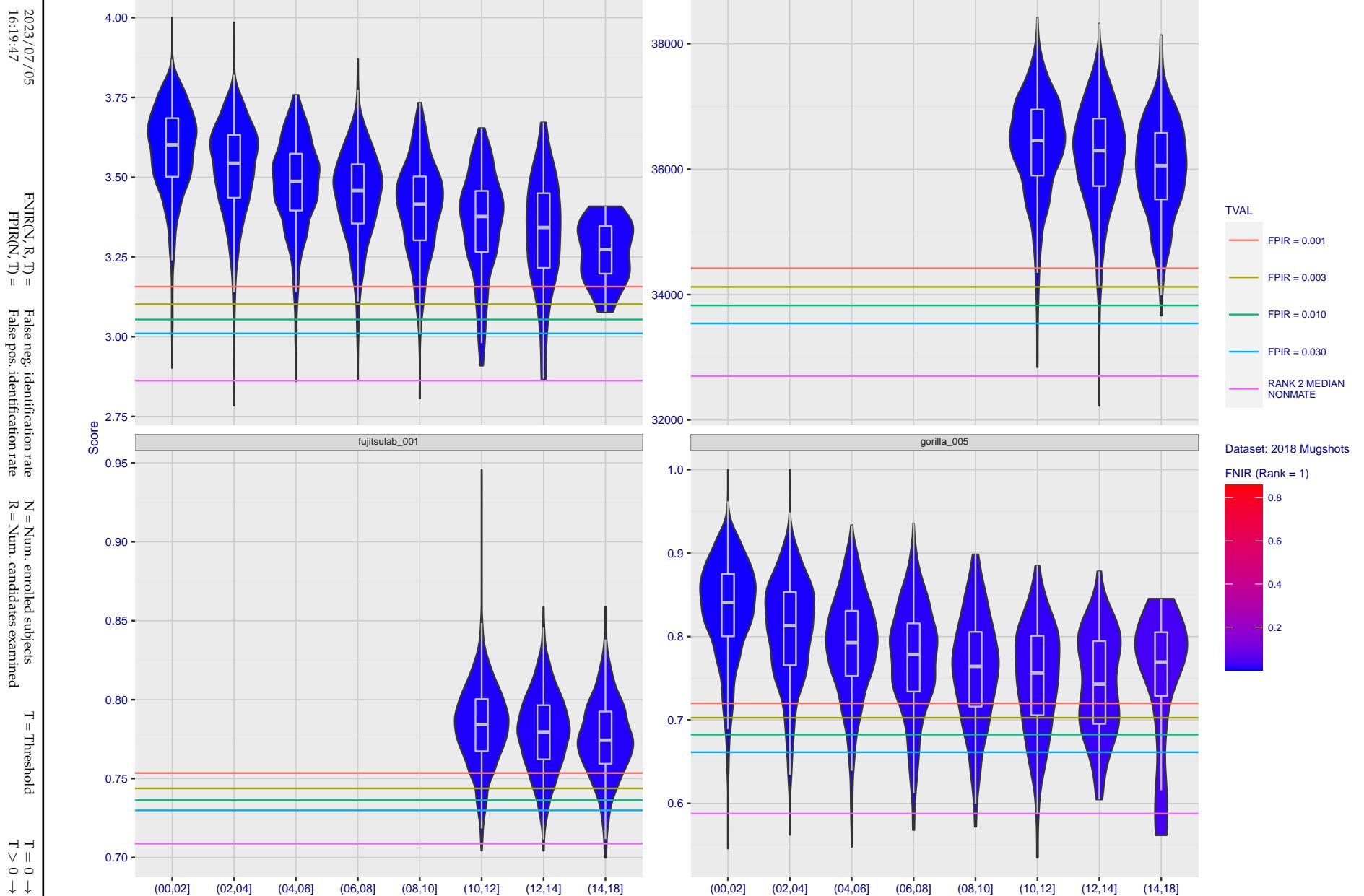


Figure 209: [FRVT-2018 Mugshot Ageing Dataset] Native mate scores vs. time-elapsed. The oldest image of each individual is enrolled. Thereafter, all more recent images are searched. Mated score distributions are computed over all searches noted in row 17 of Table 1 binned by number of years between search and initial enrollment.

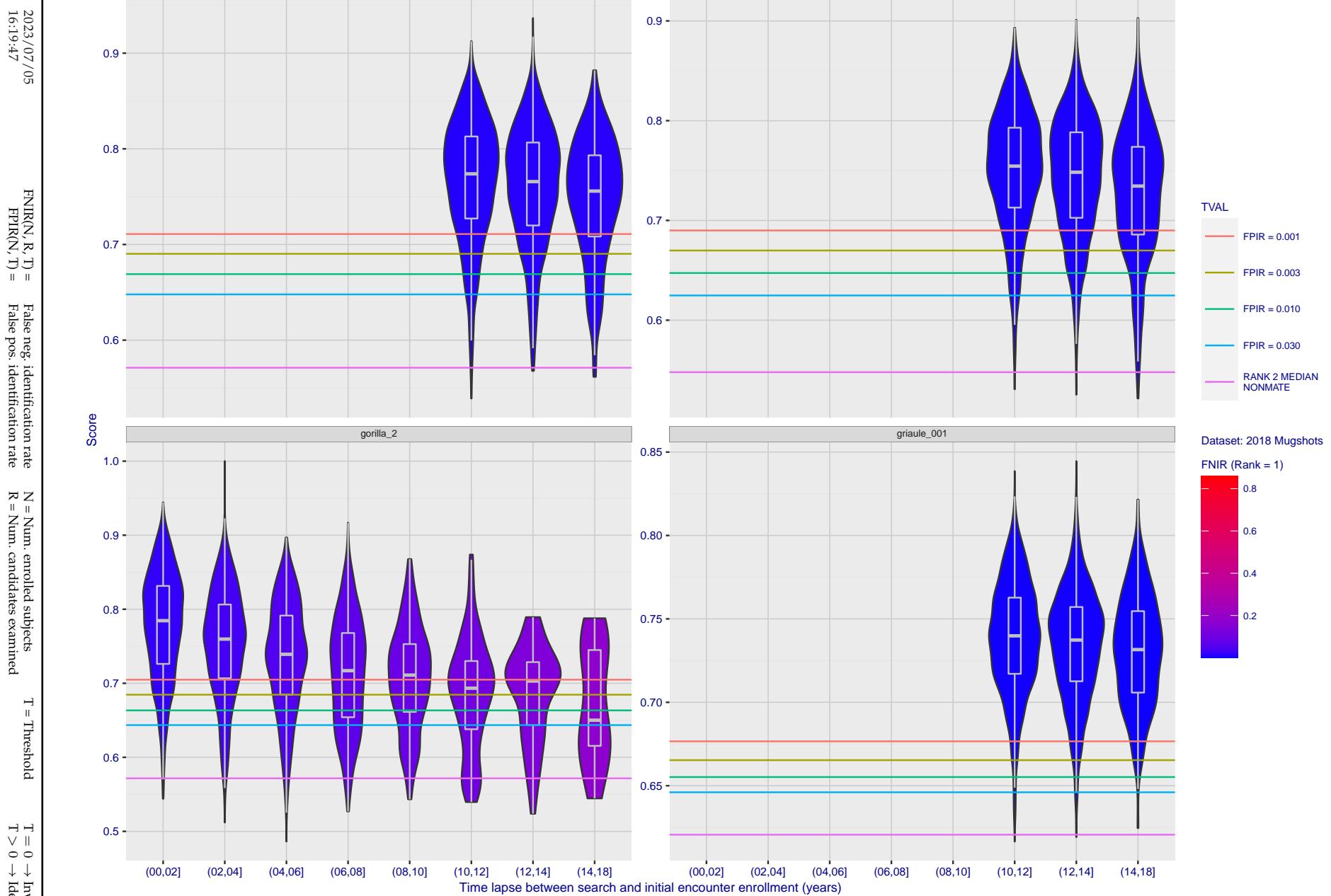


Figure 210: [FRVT-2018 Mugshot Ageing Dataset] Native mate scores vs. time-elapsed. The oldest image of each individual is enrolled. Thereafter, all more recent images are searched. Mated score distributions are computed over all searches noted in row 17 of Table 1 binned by number of years between search and initial enrollment.

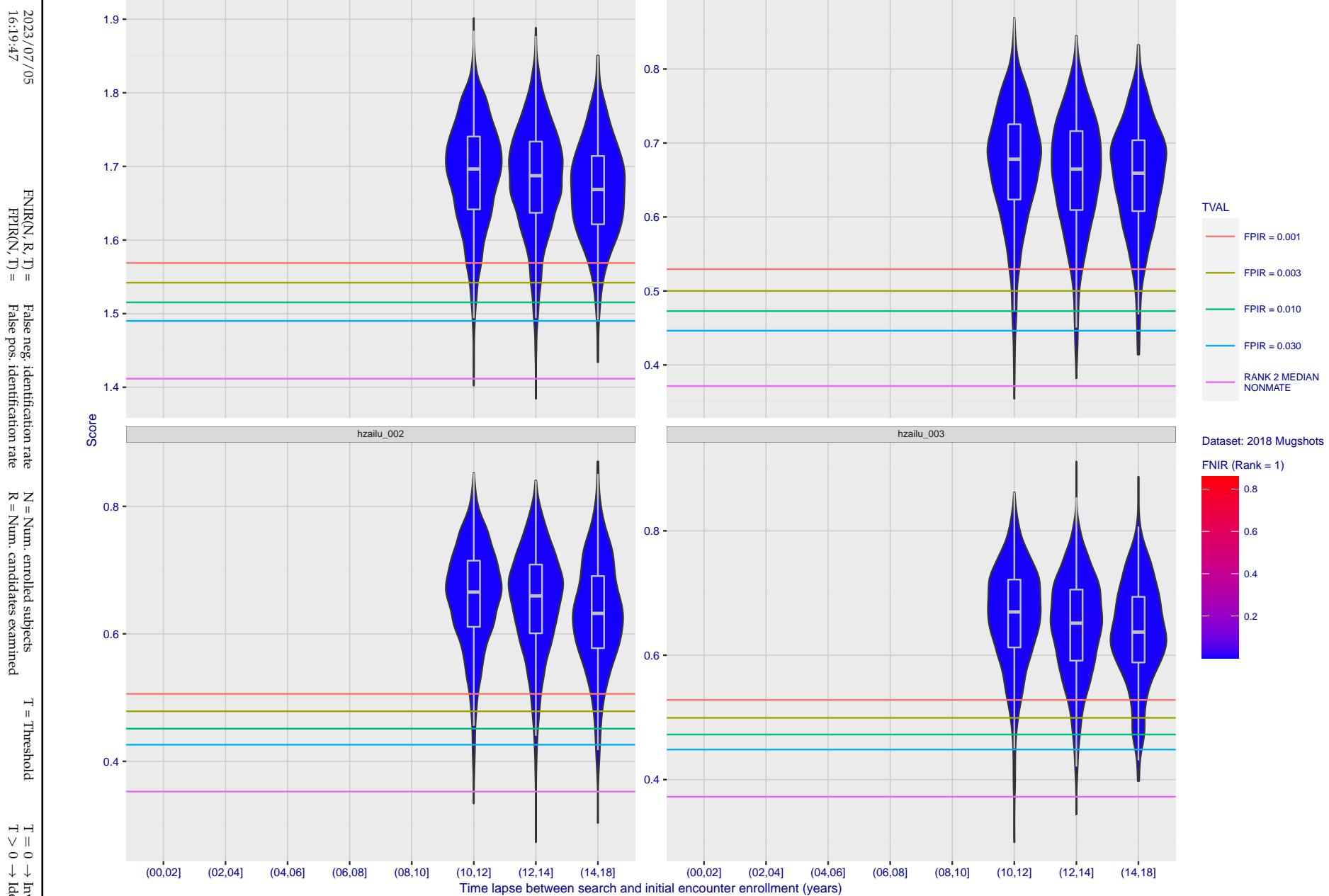


Figure 211: [FRVT-2018 Mugshot Ageing Dataset] Native mate scores vs. time-elapsed. The oldest image of each individual is enrolled. Thereafter, all more recent images are searched. Mated score distributions are computed over all searches noted in row 17 of Table 1 binned by number of years between search and initial enrollment.

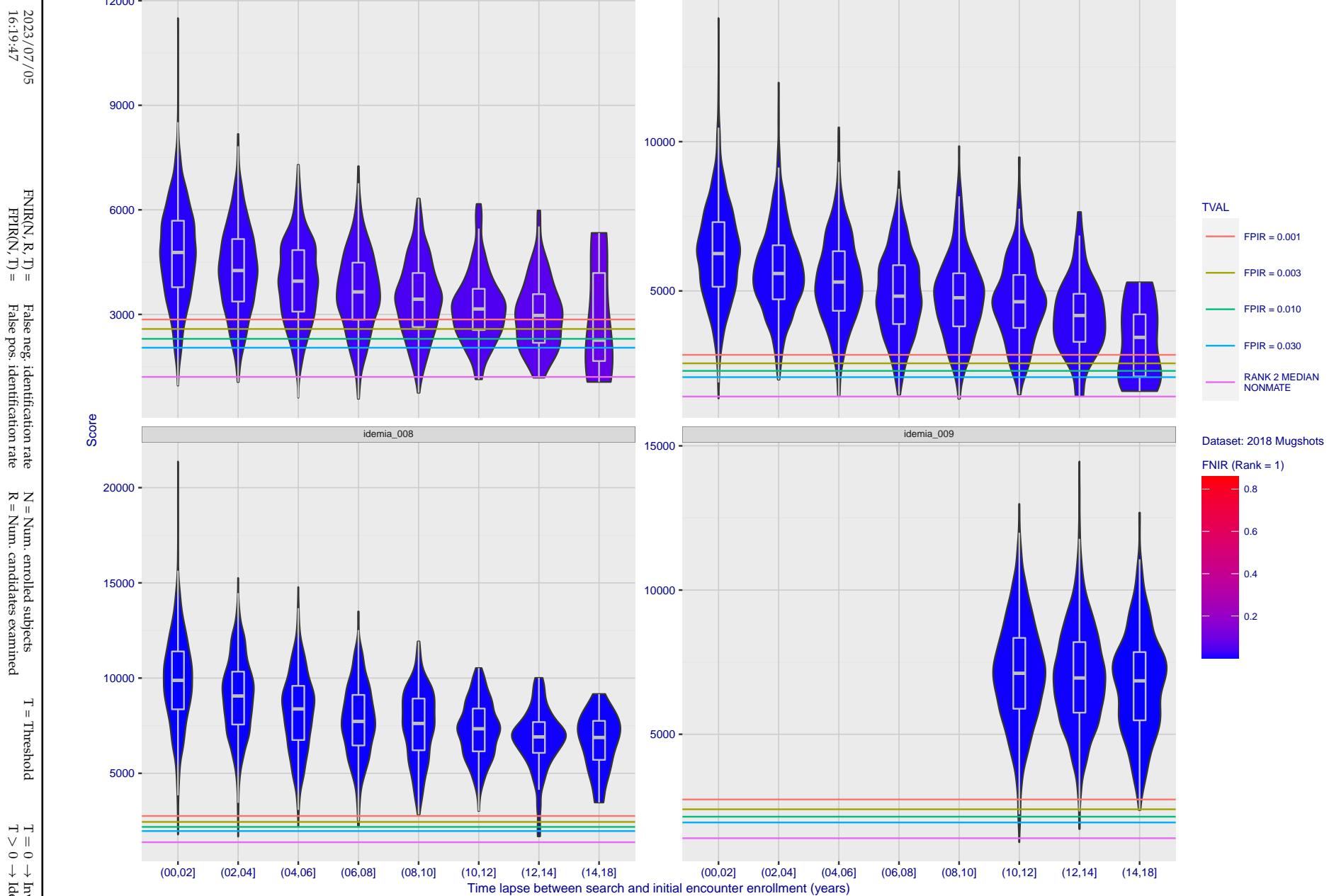


Figure 212: [FRVT-2018 Mugshot Ageing Dataset] Native mate scores vs. time-elapsed. The oldest image of each individual is enrolled. Thereafter, all more recent images are searched. Mated score distributions are computed over all searches noted in row 17 of Table 1 binned by number of years between search and initial enrollment.

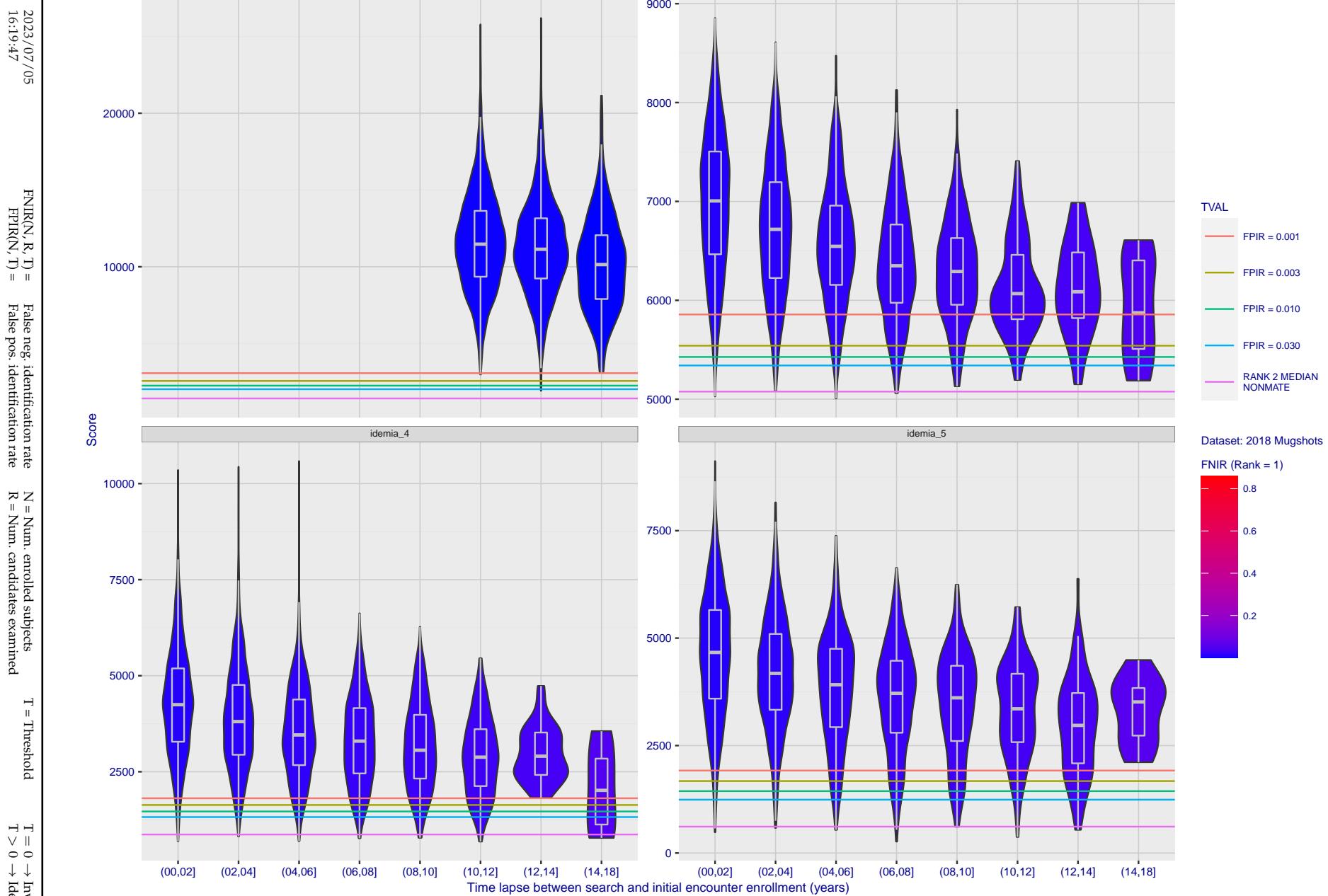


Figure 213: [FRVT-2018 Mugshot Ageing Dataset] Native mate scores vs. time-elapsed. The oldest image of each individual is enrolled. Thereafter, all more recent images are searched. Mated score distributions are computed over all searches noted in row 17 of Table 1 binned by number of years between search and initial enrollment.

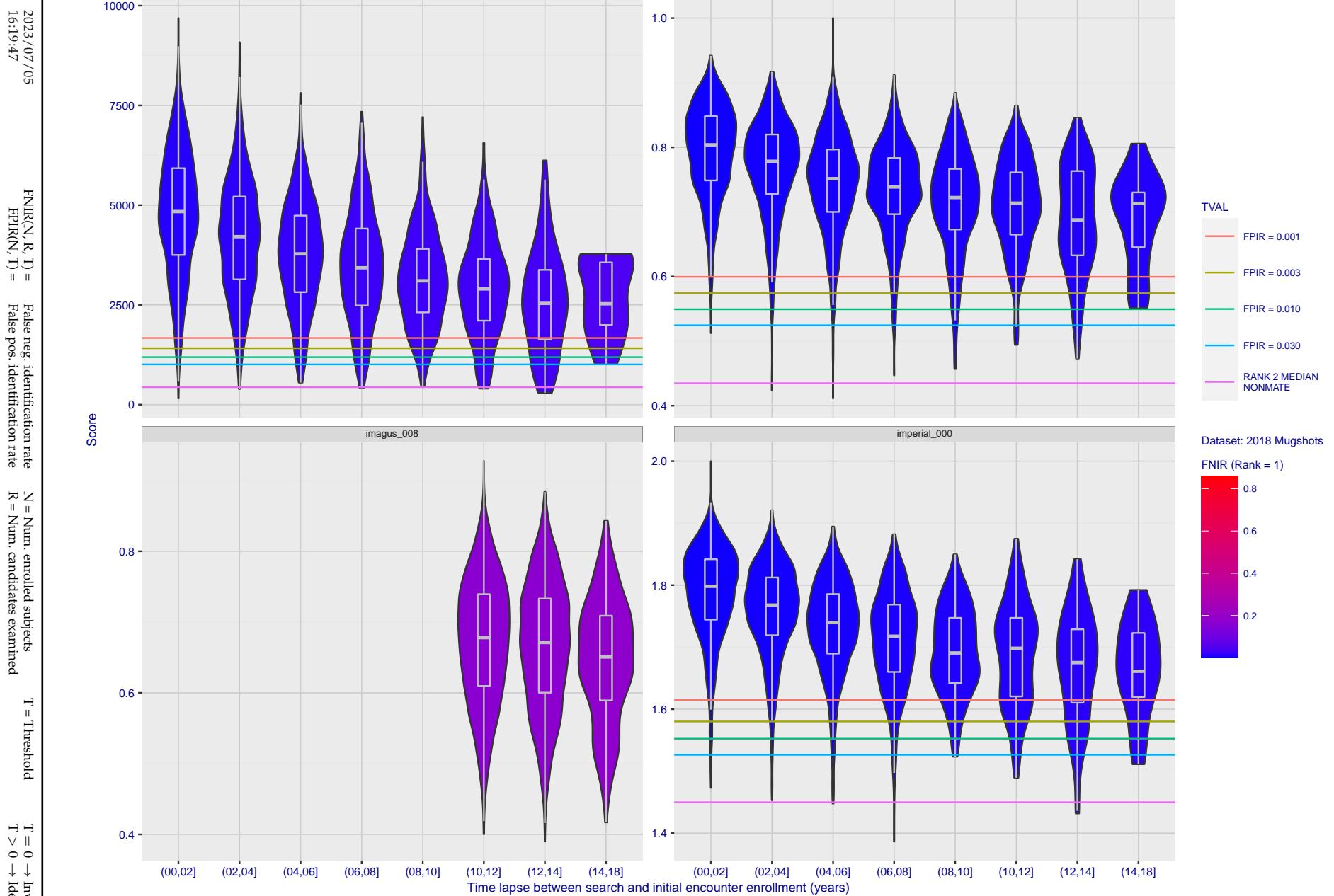


Figure 214: [FRVT-2018 Mugshot Ageing Dataset] Native mate scores vs. time-elapsed. The oldest image of each individual is enrolled. Thereafter, all more recent images are searched. Mated score distributions are computed over all searches noted in row 17 of Table 1 binned by number of years between search and initial enrollment.

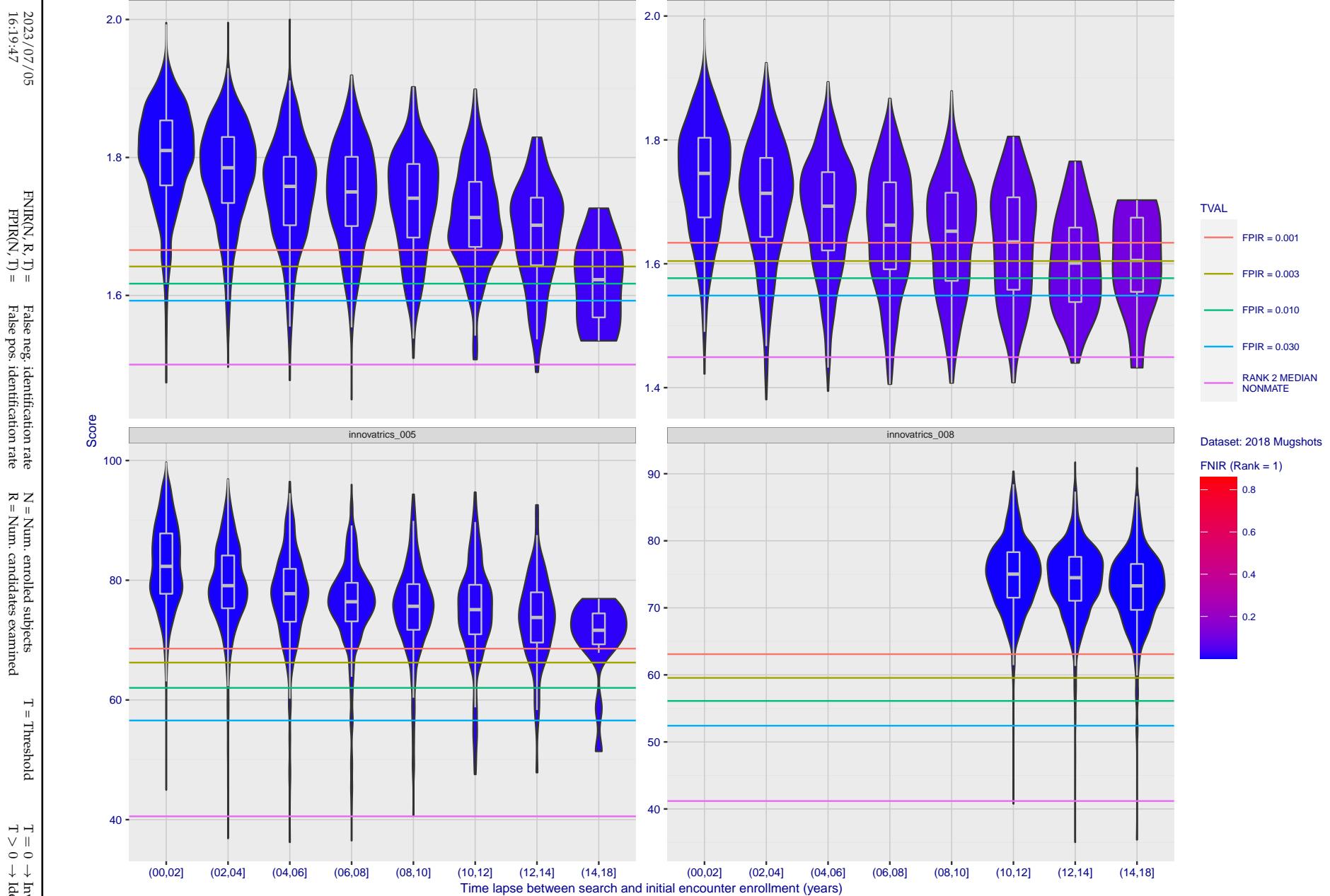


Figure 215: [FRVT-2018 Mugshot Ageing Dataset] Native mate scores vs. time-elapsed. The oldest image of each individual is enrolled. Thereafter, all more recent images are searched. Mated score distributions are computed over all searches noted in row 17 of Table 1 binned by number of years between search and initial enrollment.

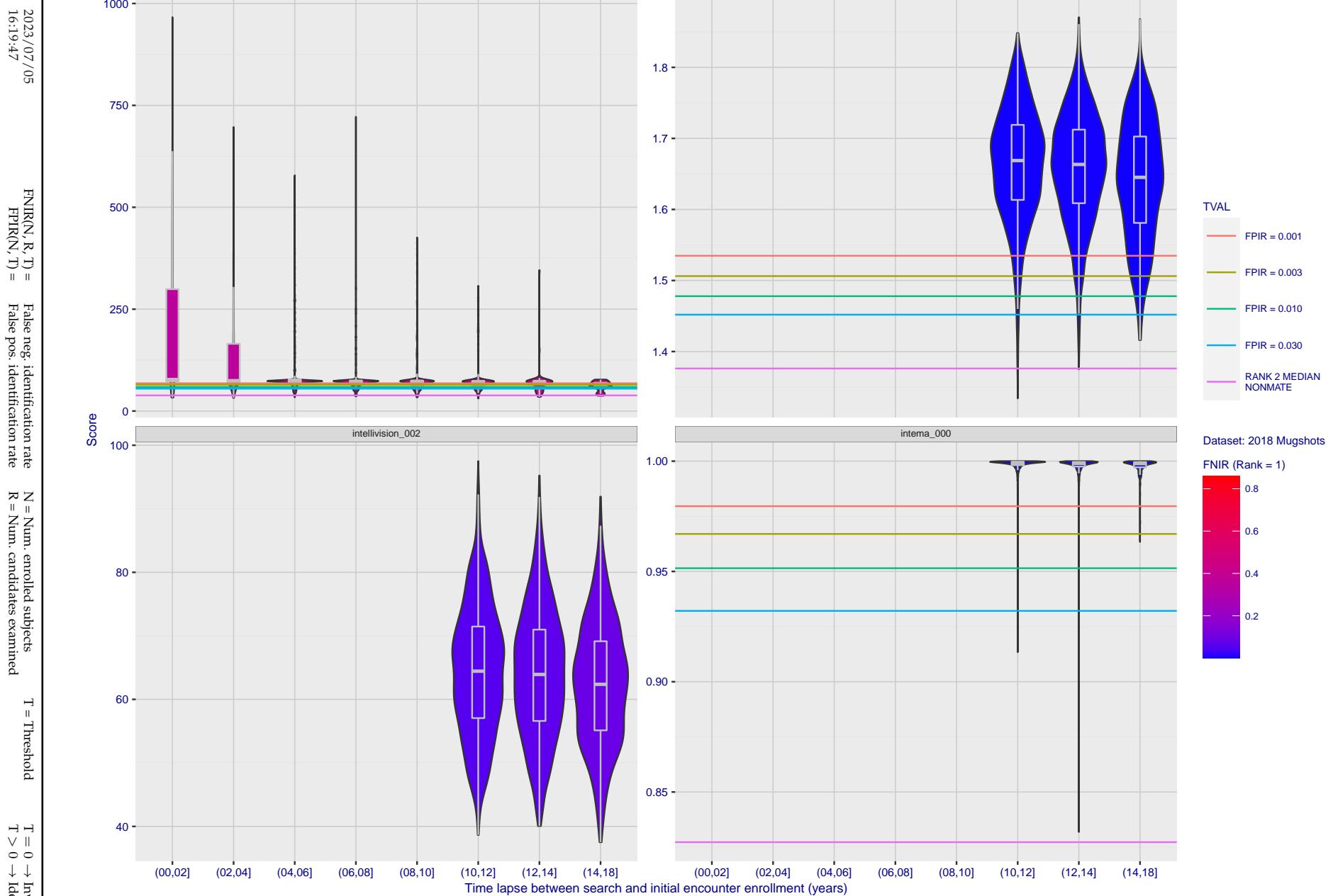


Figure 216: [FRVT-2018 Mugshot Ageing Dataset] Native mate scores vs. time-elapsed. The oldest image of each individual is enrolled. Thereafter, all more recent images are searched. Mated score distributions are computed over all searches noted in row 17 of Table 1 binned by number of years between search and initial enrollment.

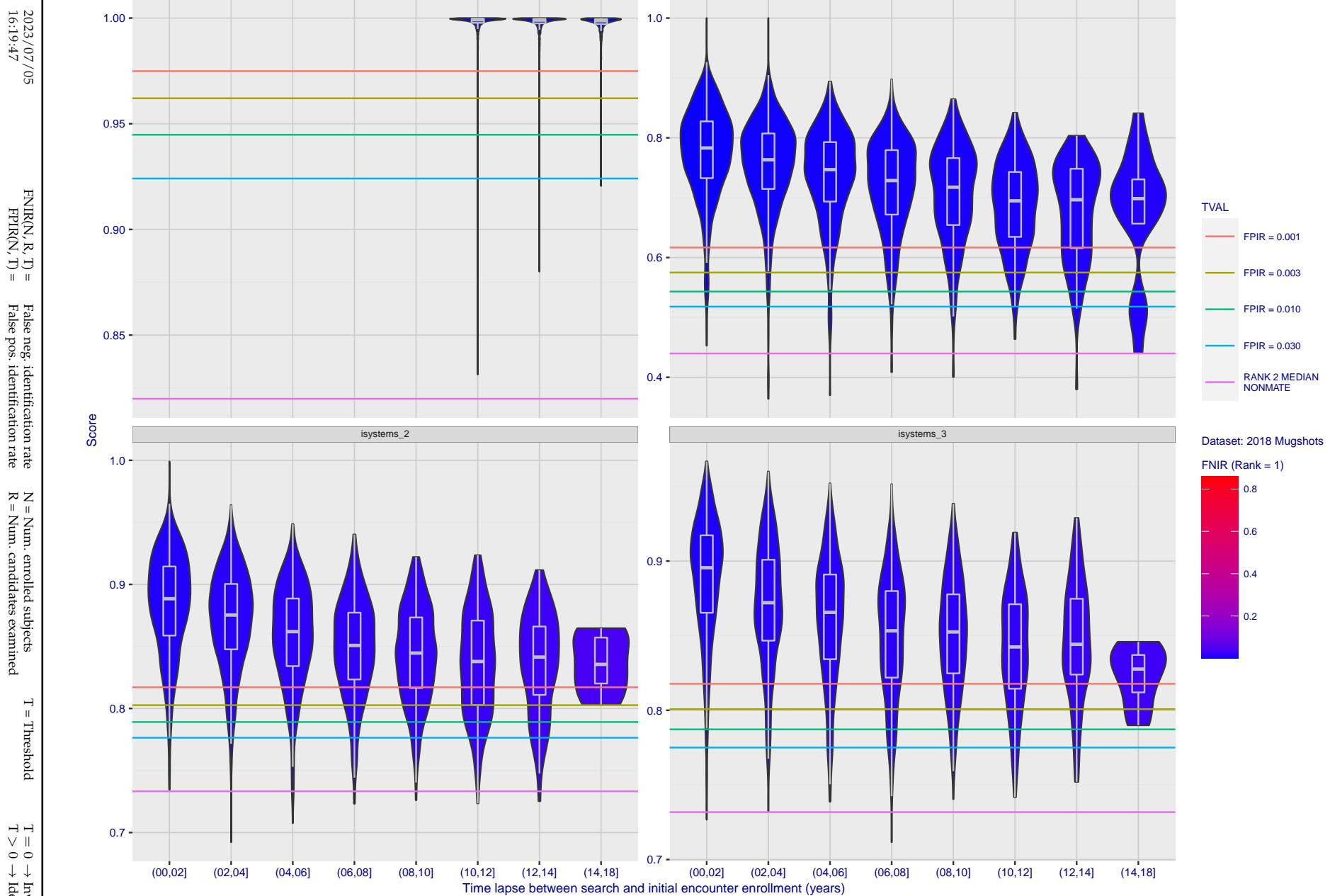


Figure 217: [FRVT-2018 Mugshot Ageing Dataset] Native mate scores vs. time-elapsed. The oldest image of each individual is enrolled. Thereafter, all more recent images are searched. Mated score distributions are computed over all searches noted in row 17 of Table 1 binned by number of years between search and initial enrollment.

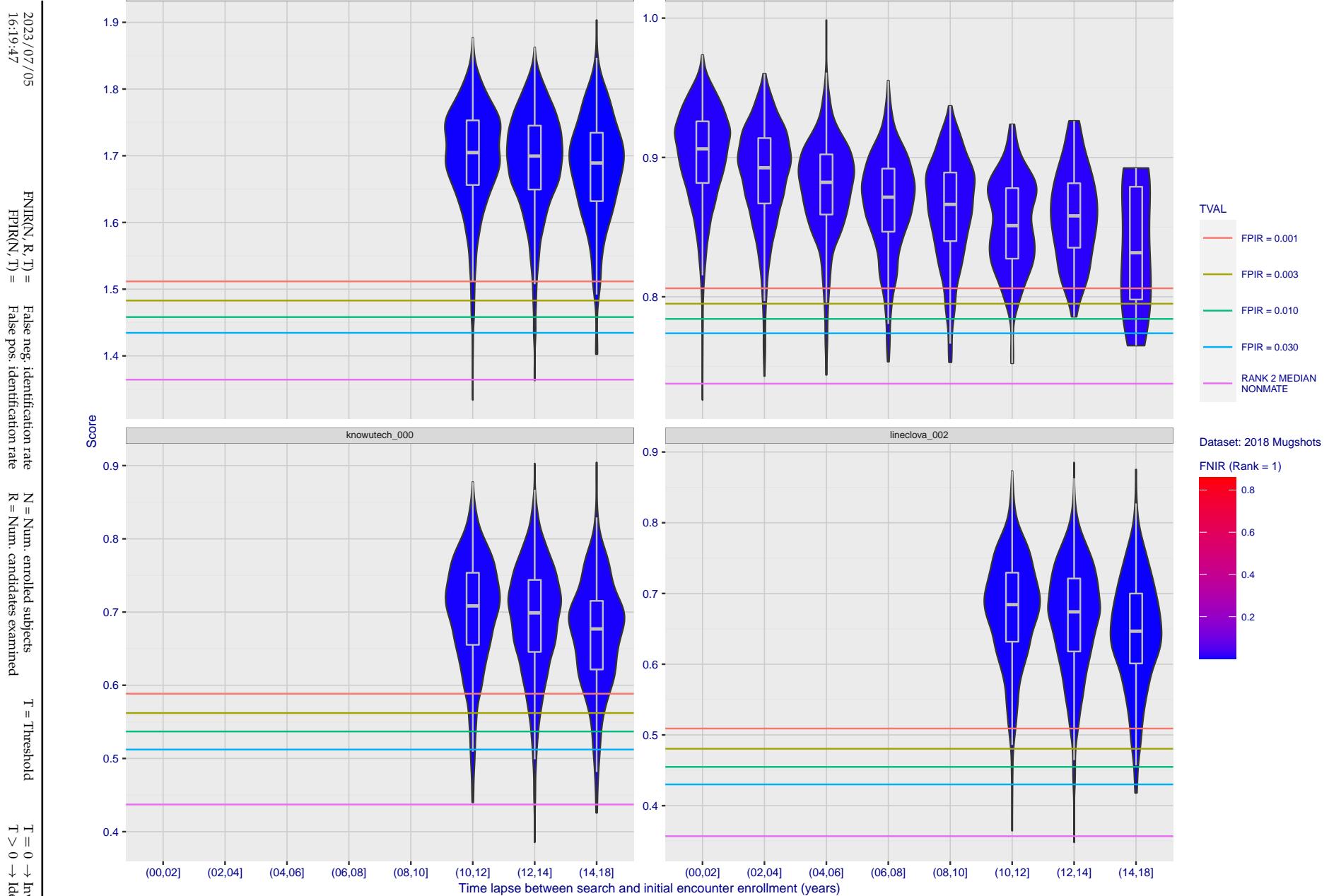


Figure 218: [FRVT-2018 Mugshot Ageing Dataset] Native mate scores vs. time-elapsed. The oldest image of each individual is enrolled. Thereafter, all more recent images are searched. Mated score distributions are computed over all searches noted in row 17 of Table 1 binned by number of years between search and initial enrollment.

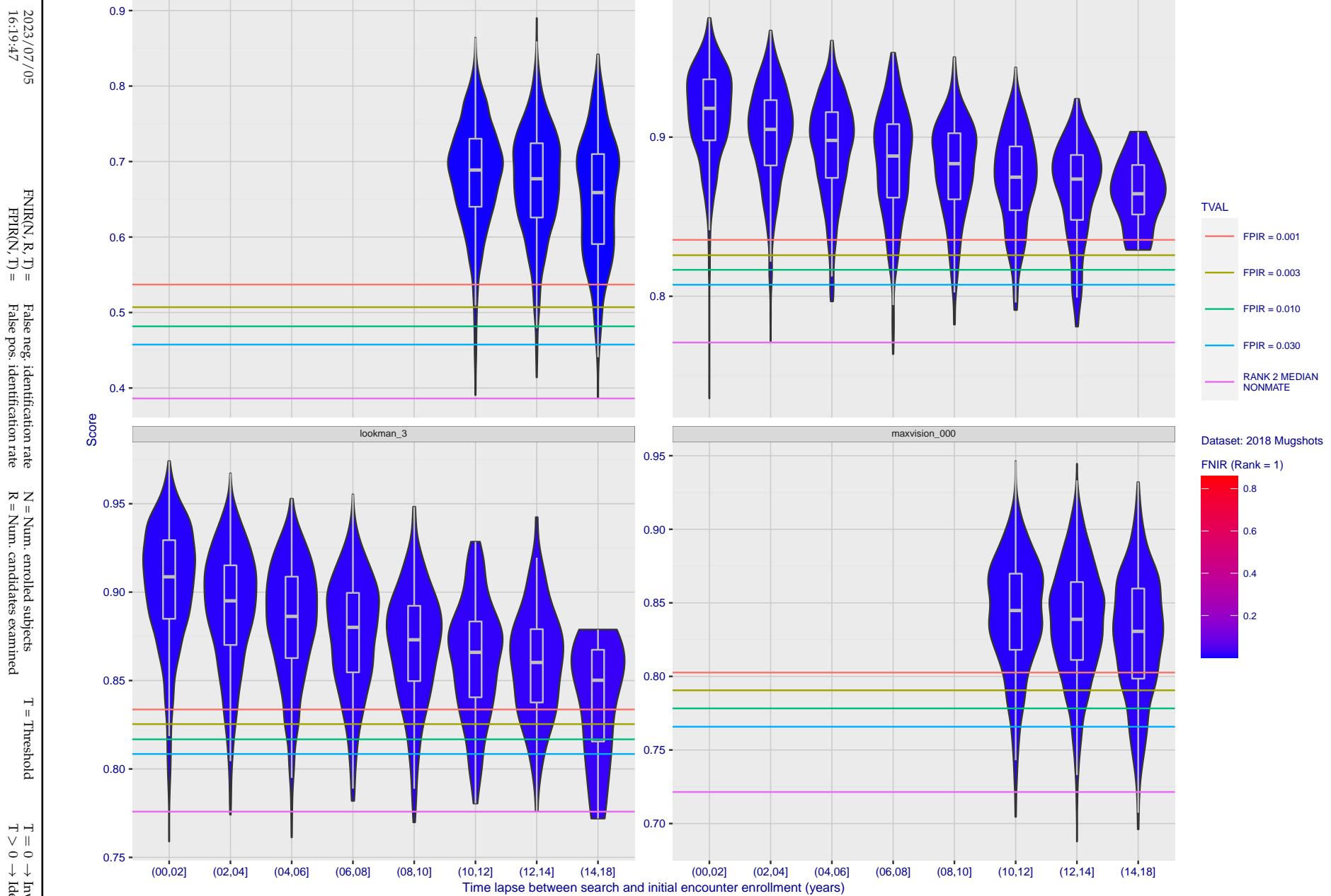


Figure 219: [FRVT-2018 Mugshot Ageing Dataset] Native mate scores vs. time-elapsed. The oldest image of each individual is enrolled. Thereafter, all more recent images are searched. Mated score distributions are computed over all searches noted in row 17 of Table 1 binned by number of years between search and initial enrollment.

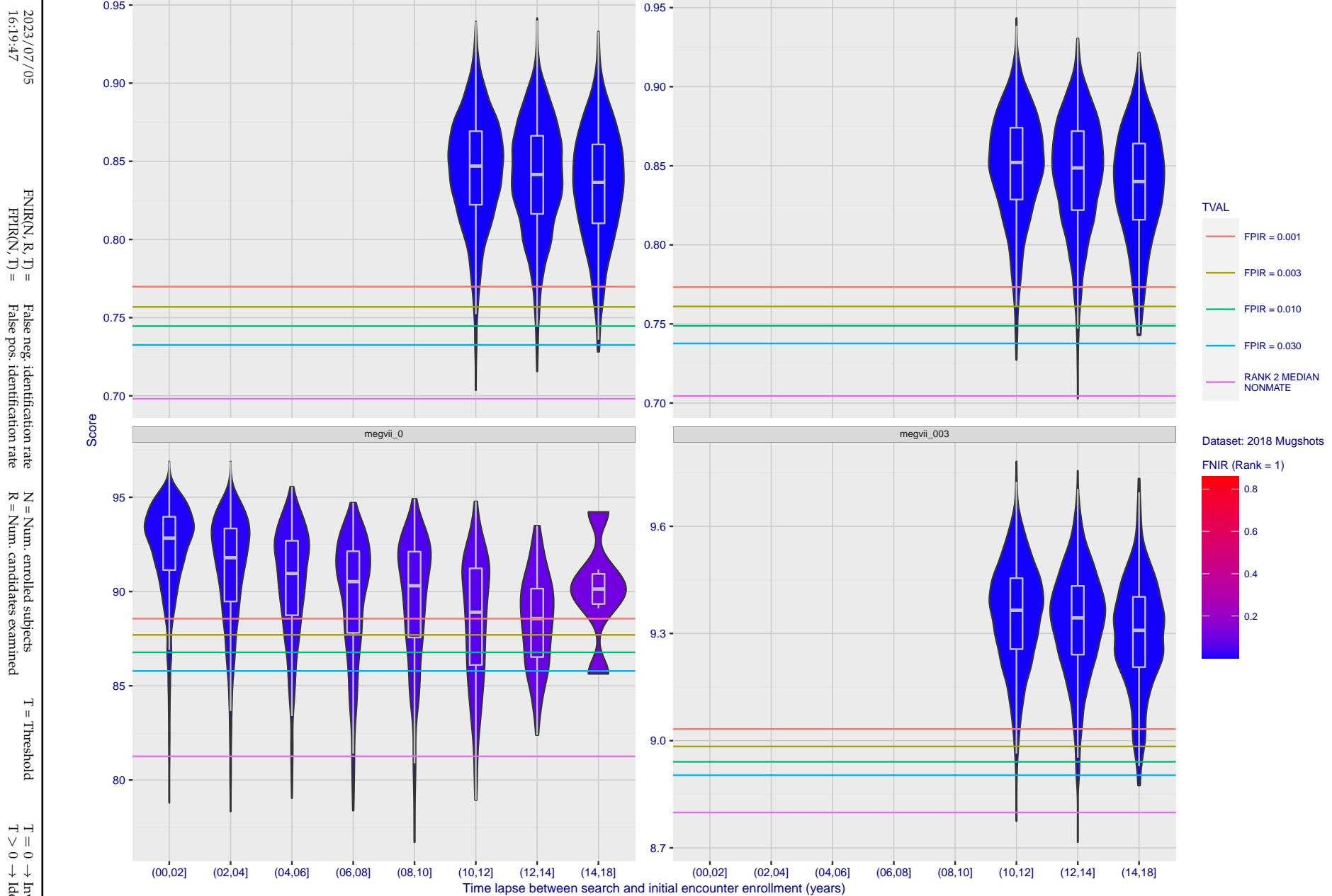


Figure 220: [FRVT-2018 Mugshot Ageing Dataset] Native mate scores vs. time-elapsed. The oldest image of each individual is enrolled. Thereafter, all more recent images are searched. Mated score distributions are computed over all searches noted in row 17 of Table 1 binned by number of years between search and initial enrollment.

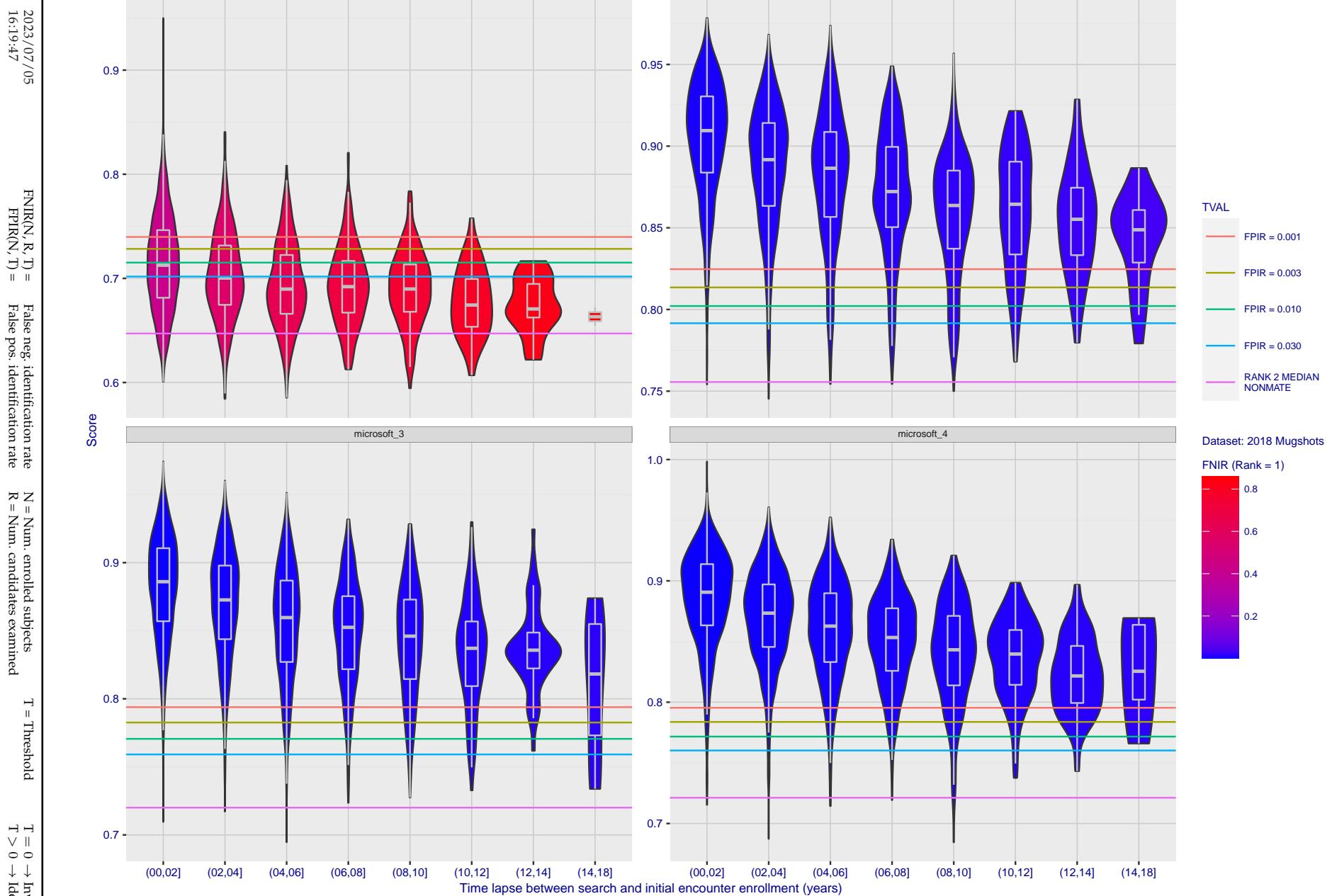


Figure 221: [FRVT-2018 Mugshot Ageing Dataset] Native mate scores vs. time-elapsed. The oldest image of each individual is enrolled. Thereafter, all more recent images are searched. Mated score distributions are computed over all searches noted in row 17 of Table 1 binned by number of years between search and initial enrollment.

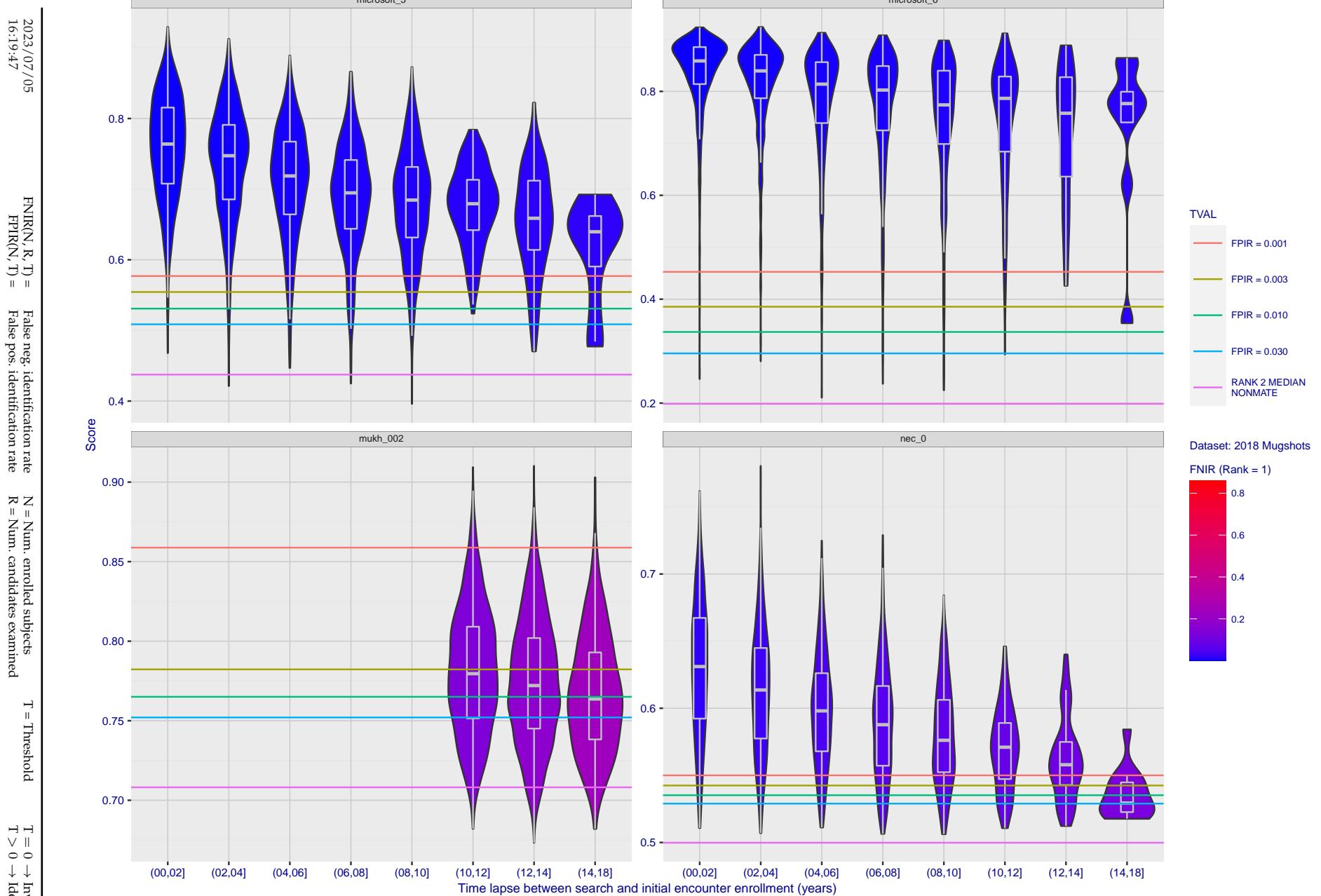


Figure 222: [FRVT-2018 Mugshot Ageing Dataset] Native mate scores vs. time-elapsed. The oldest image of each individual is enrolled. Thereafter, all more recent images are searched. Mated score distributions are computed over all searches noted in row 17 of Table 1 binned by number of years between search and initial enrollment.

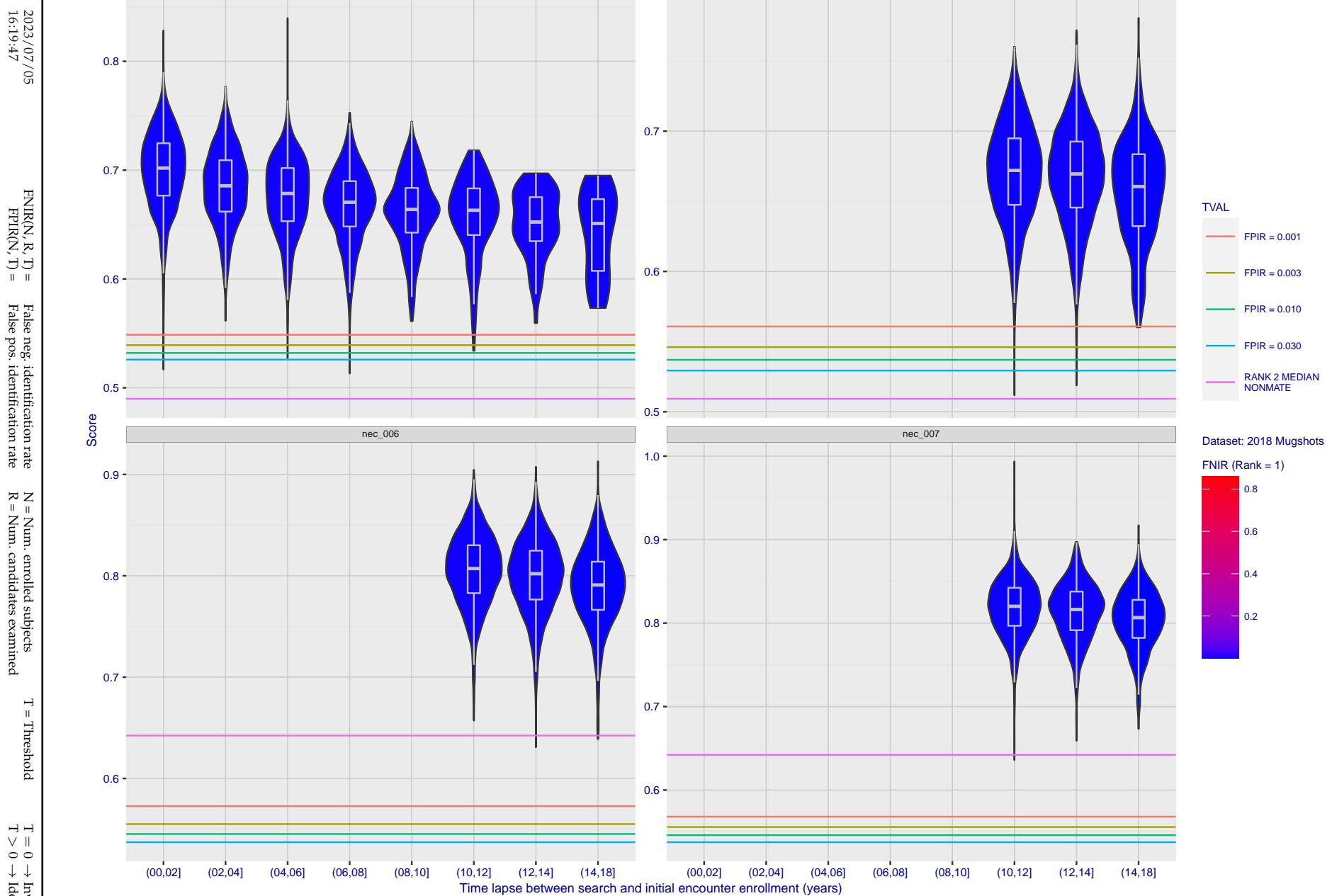


Figure 223: [FRVT-2018 Mugshot Ageing Dataset] Native mate scores vs. time-elapsed. The oldest image of each individual is enrolled. Thereafter, all more recent images are searched. Mated score distributions are computed over all searches noted in row 17 of Table 1 binned by number of years between search and initial enrollment.

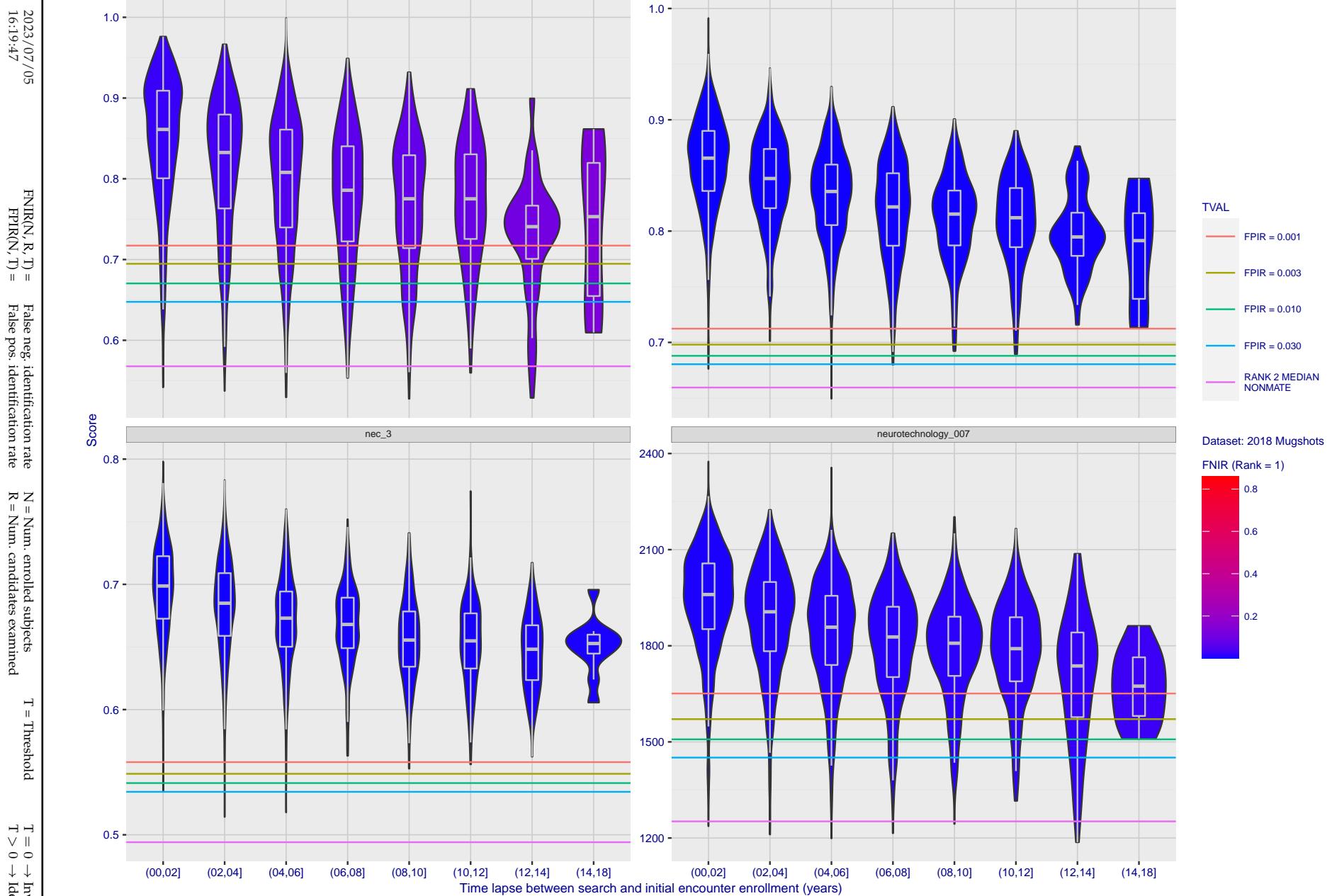


Figure 224: [FRVT-2018 Mugshot Ageing Dataset] Native mate scores vs. time-elapsed. The oldest image of each individual is enrolled. Thereafter, all more recent images are searched. Mated score distributions are computed over all searches noted in row 17 of Table 1 binned by number of years between search and initial enrollment.

2023/07/05
16:19:47FNIR(N, R, T) = False neg. identification rate
FPIR(N, T) = False pos. identification rateN = Num. enrolled subjects
R = Num. candidates examined

T = Threshold

T = 0 → Investigation
T > 0 → Identification

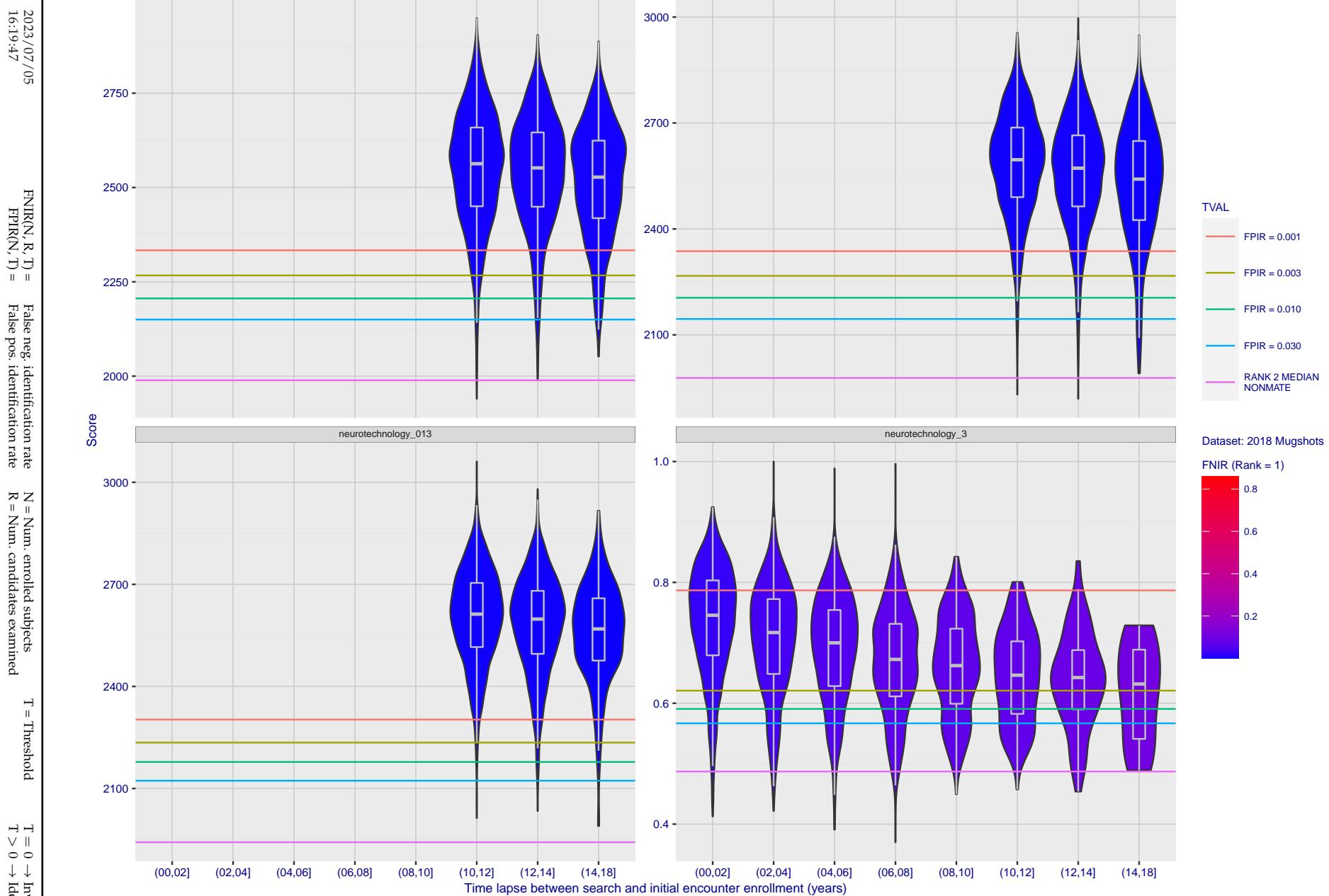


Figure 225: [FRVT-2018 Mugshot Ageing Dataset] Native mate scores vs. time-elapsed. The oldest image of each individual is enrolled. Thereafter, all more recent images are searched. Mated score distributions are computed over all searches noted in row 17 of Table 1 binned by number of years between search and initial enrollment.

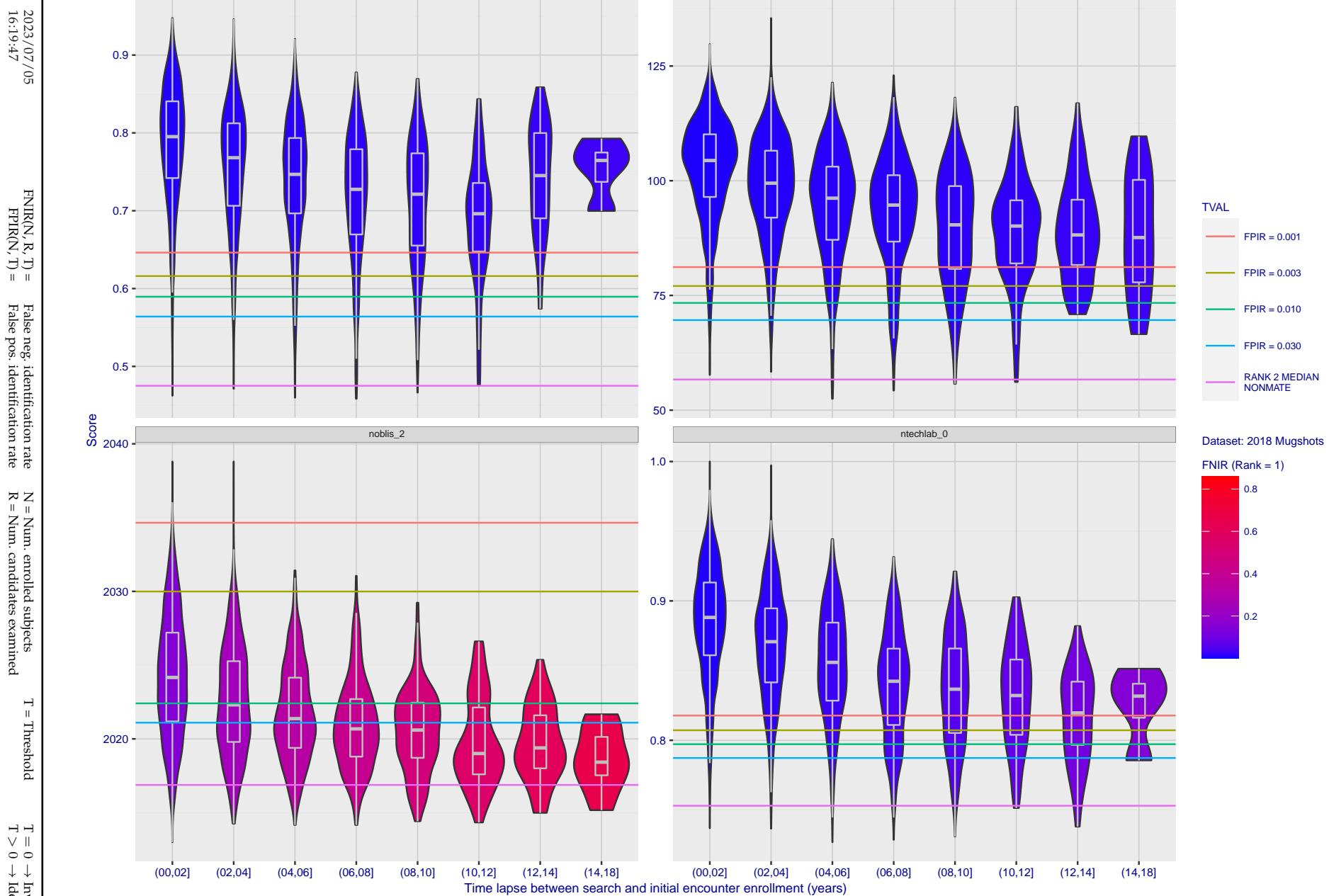


Figure 226: [FRVT-2018 Mugshot Ageing Dataset] Native mate scores vs. time-elapsed. The oldest image of each individual is enrolled. Thereafter, all more recent images are searched. Mated score distributions are computed over all searches noted in row 17 of Table 1 binned by number of years between search and initial enrollment.

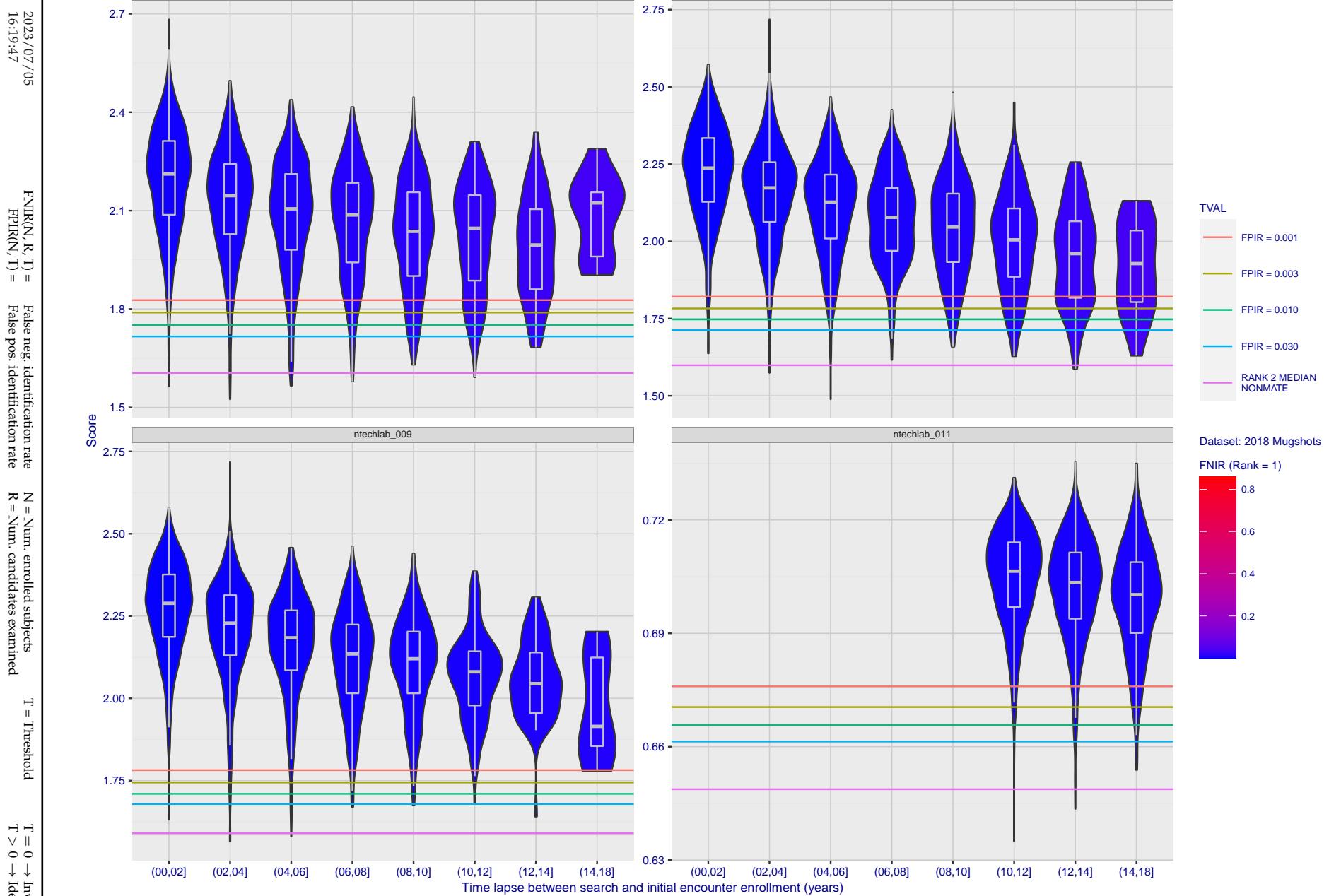


Figure 227: [FRVT-2018 Mugshot Ageing Dataset] Native mate scores vs. time-elapsed. The oldest image of each individual is enrolled. Thereafter, all more recent images are searched. Mated score distributions are computed over all searches noted in row 17 of Table 1 binned by number of years between search and initial enrollment.

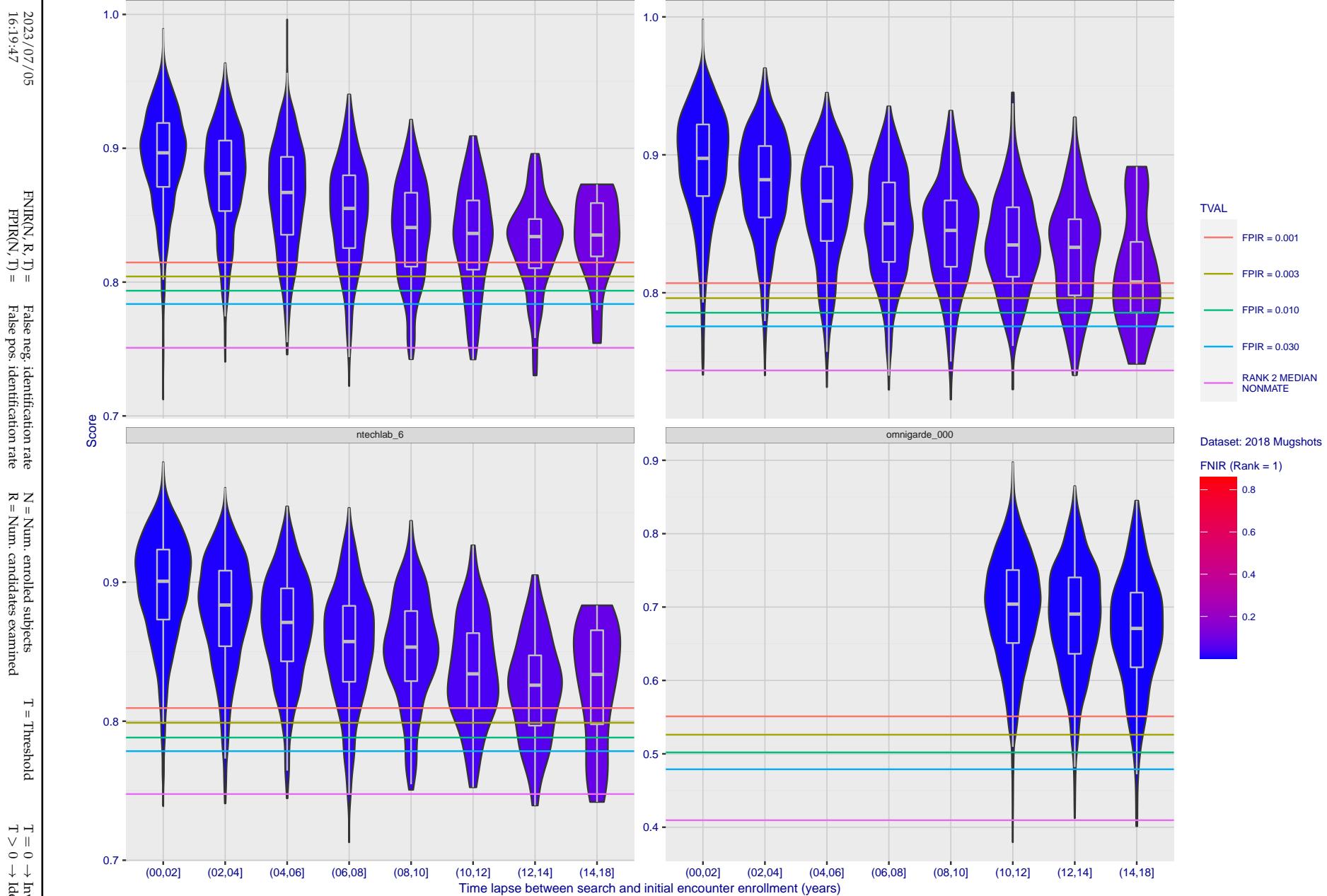


Figure 228: [FRVT-2018 Mugshot Ageing Dataset] Native mate scores vs. time-elapsed. The oldest image of each individual is enrolled. Thereafter, all more recent images are searched. Mated score distributions are computed over all searches noted in row 17 of Table 1 binned by number of years between search and initial enrollment.

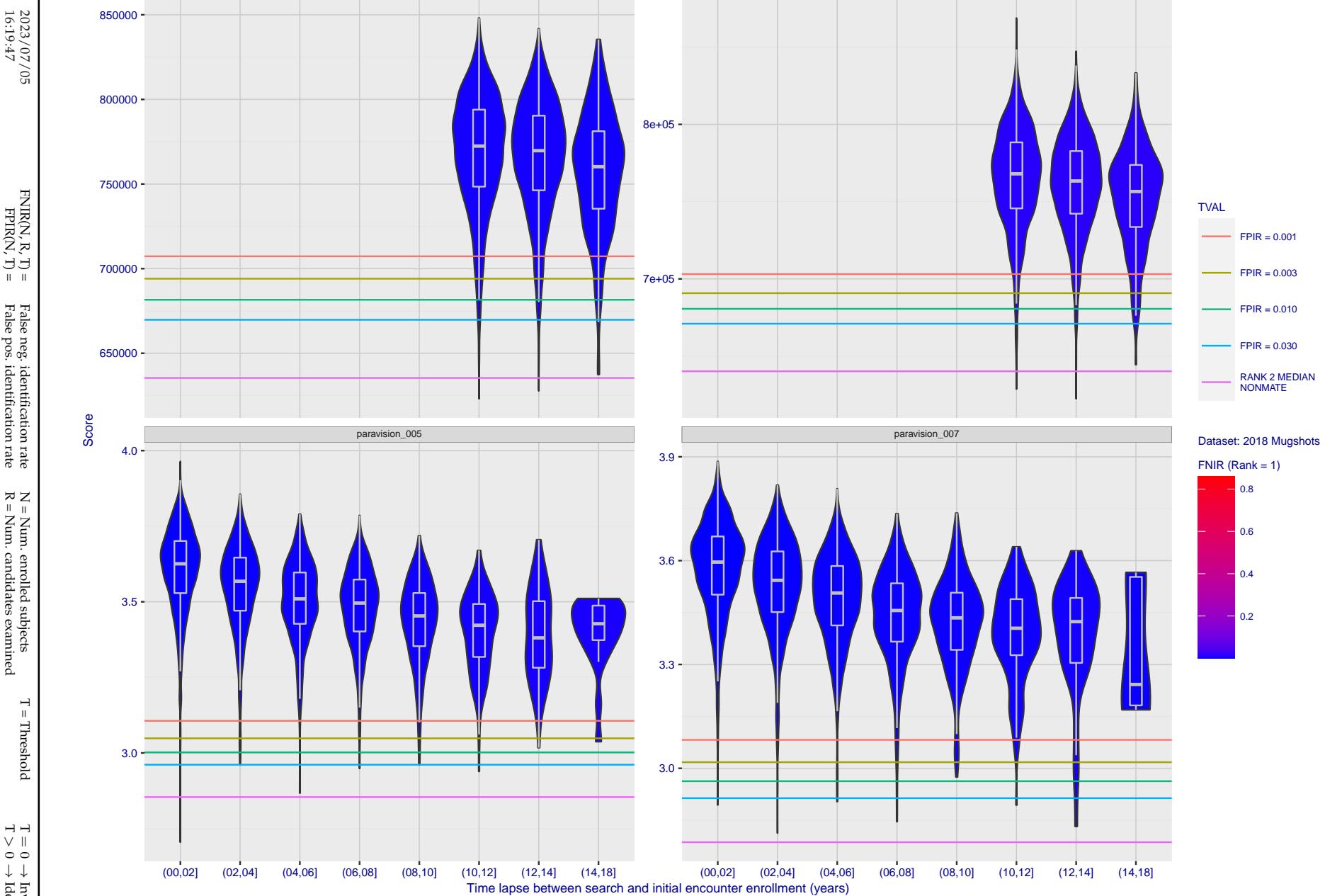


Figure 229: [FRVT-2018 Mugshot Ageing Dataset] Native mate scores vs. time-elapsed. The oldest image of each individual is enrolled. Thereafter, all more recent images are searched. Mated score distributions are computed over all searches noted in row 17 of Table 1 binned by number of years between search and initial enrollment.

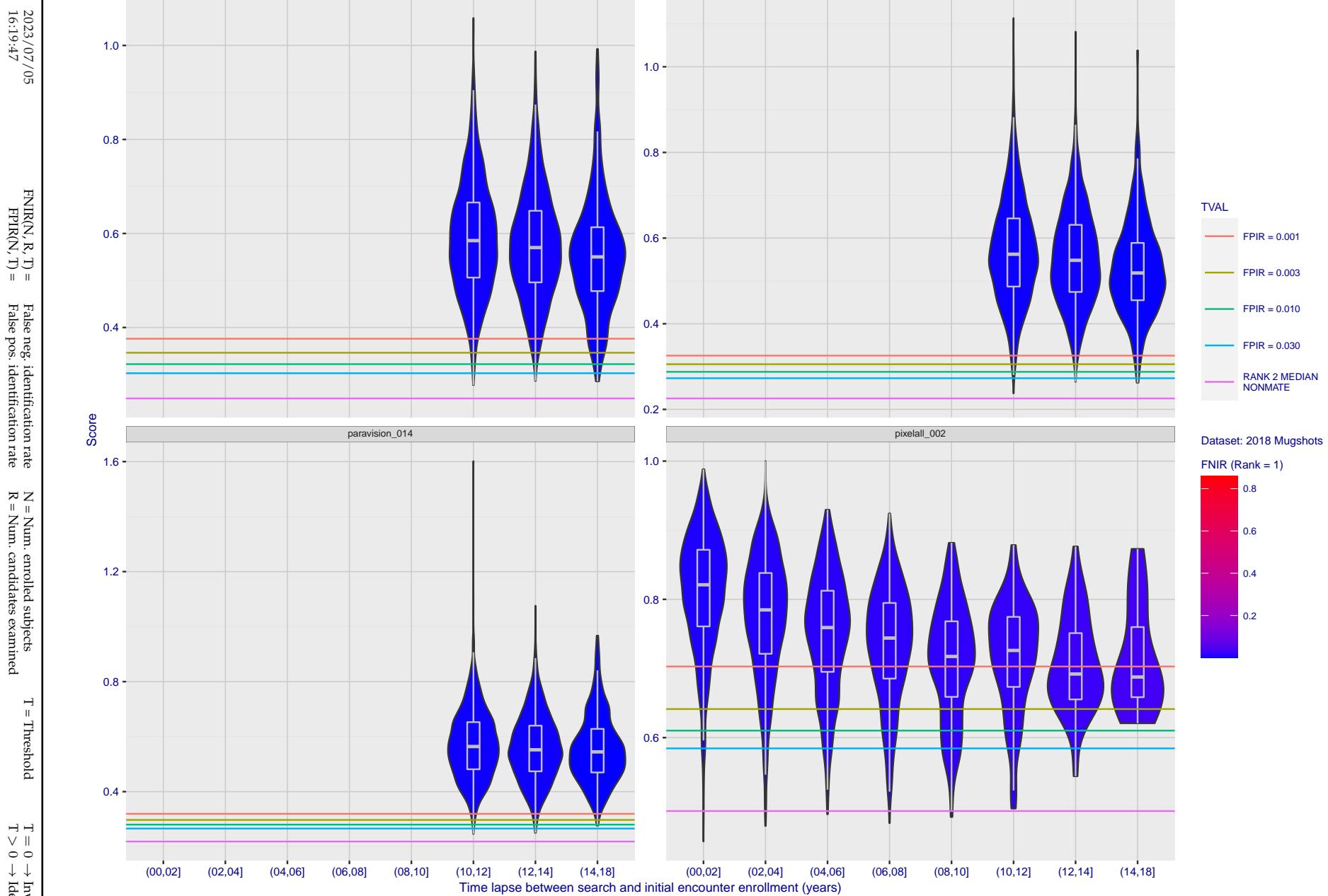


Figure 230: [FRVT-2018 Mugshot Ageing Dataset] Native mate scores vs. time-elapsed. The oldest image of each individual is enrolled. Thereafter, all more recent images are searched. Mated score distributions are computed over all searches noted in row 17 of Table 1 binned by number of years between search and initial enrollment.

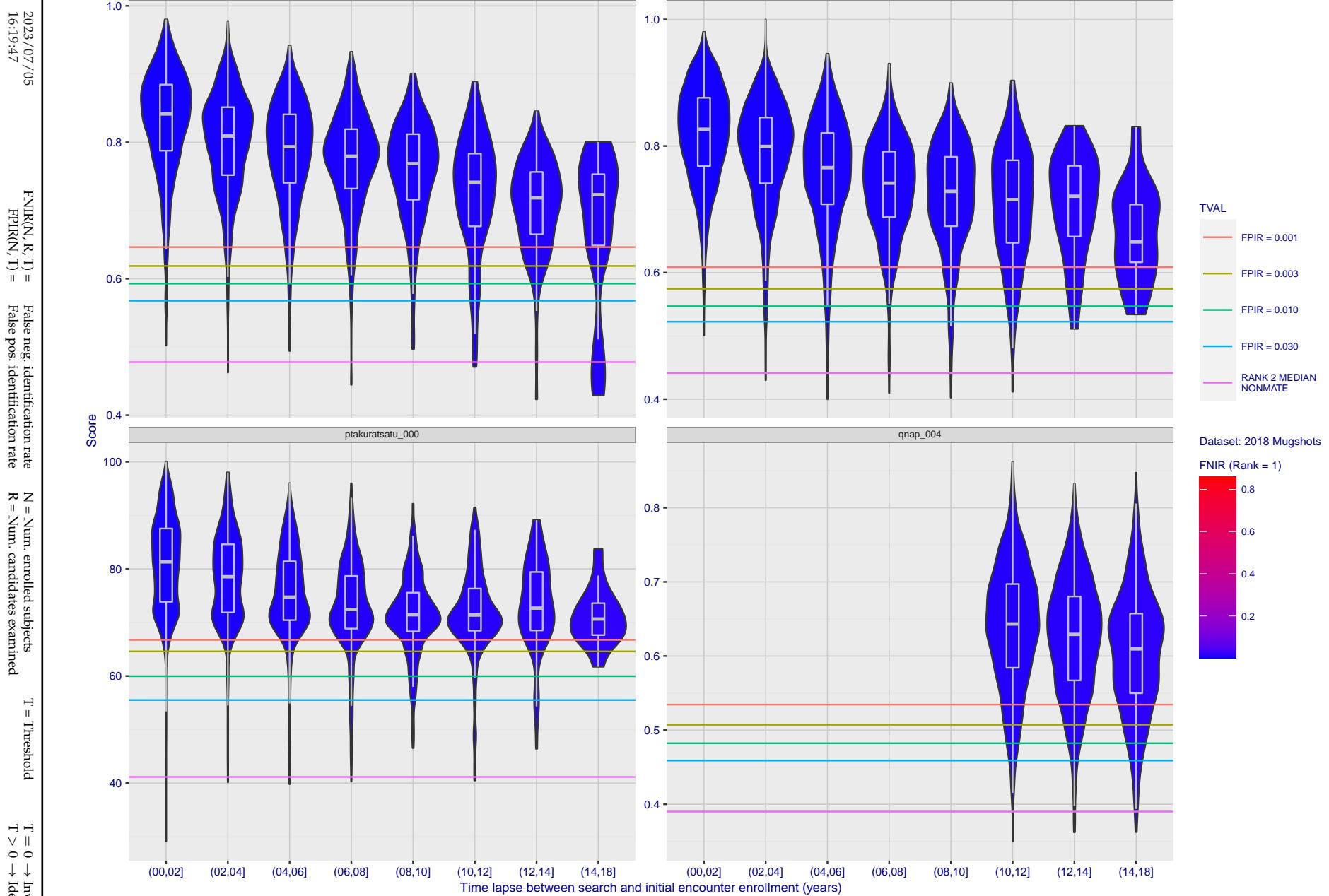


Figure 231: [FRVT-2018 Mugshot Ageing Dataset] Native mate scores vs. time-elapsed. The oldest image of each individual is enrolled. Thereafter, all more recent images are searched. Mated score distributions are computed over all searches noted in row 17 of Table 1 binned by number of years between search and initial enrollment.

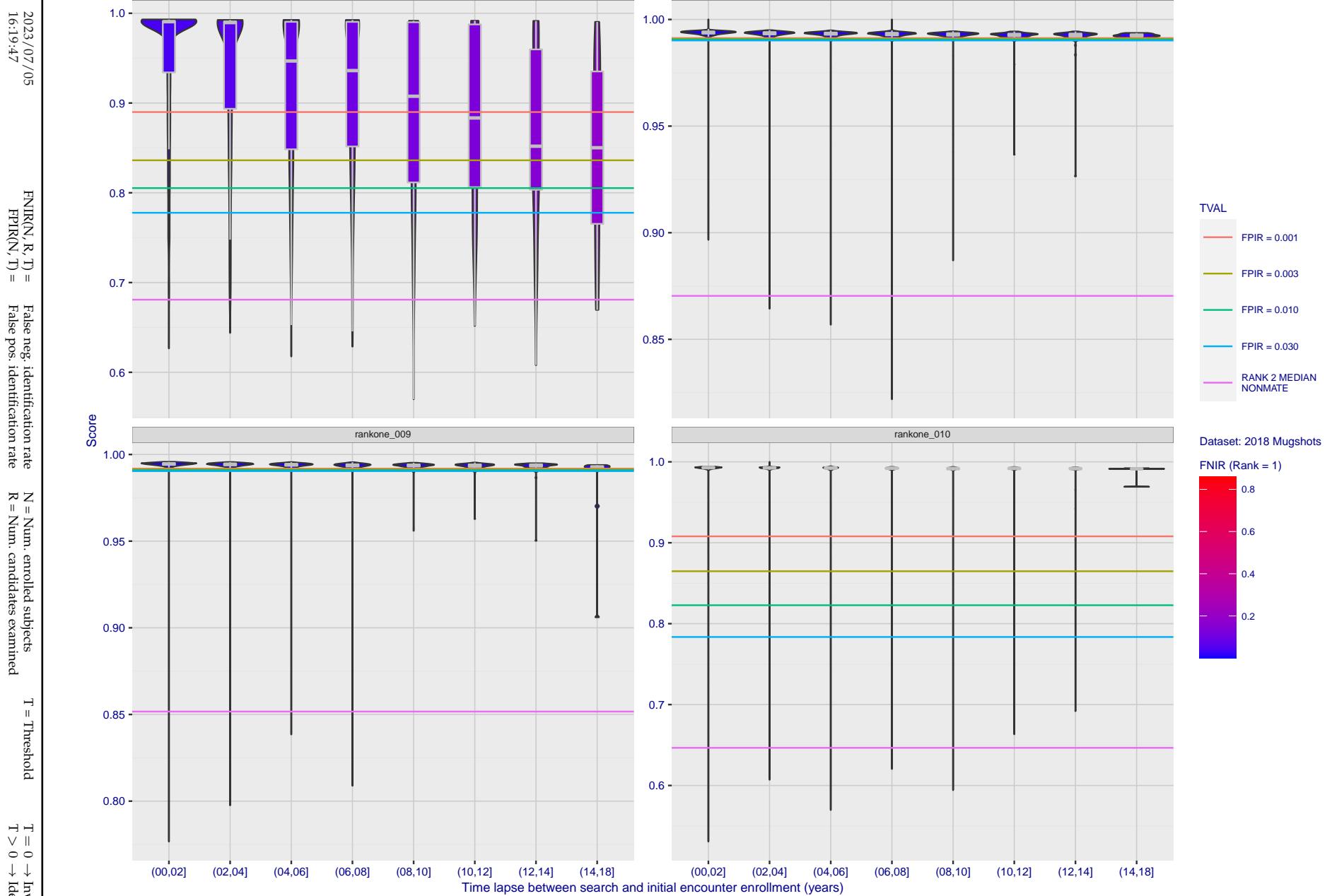


Figure 232: [FRVT-2018 Mugshot Ageing Dataset] Native mate scores vs. time-elapsed. The oldest image of each individual is enrolled. Thereafter, all more recent images are searched. Mated score distributions are computed over all searches noted in row 17 of Table 1 binned by number of years between search and initial enrollment.

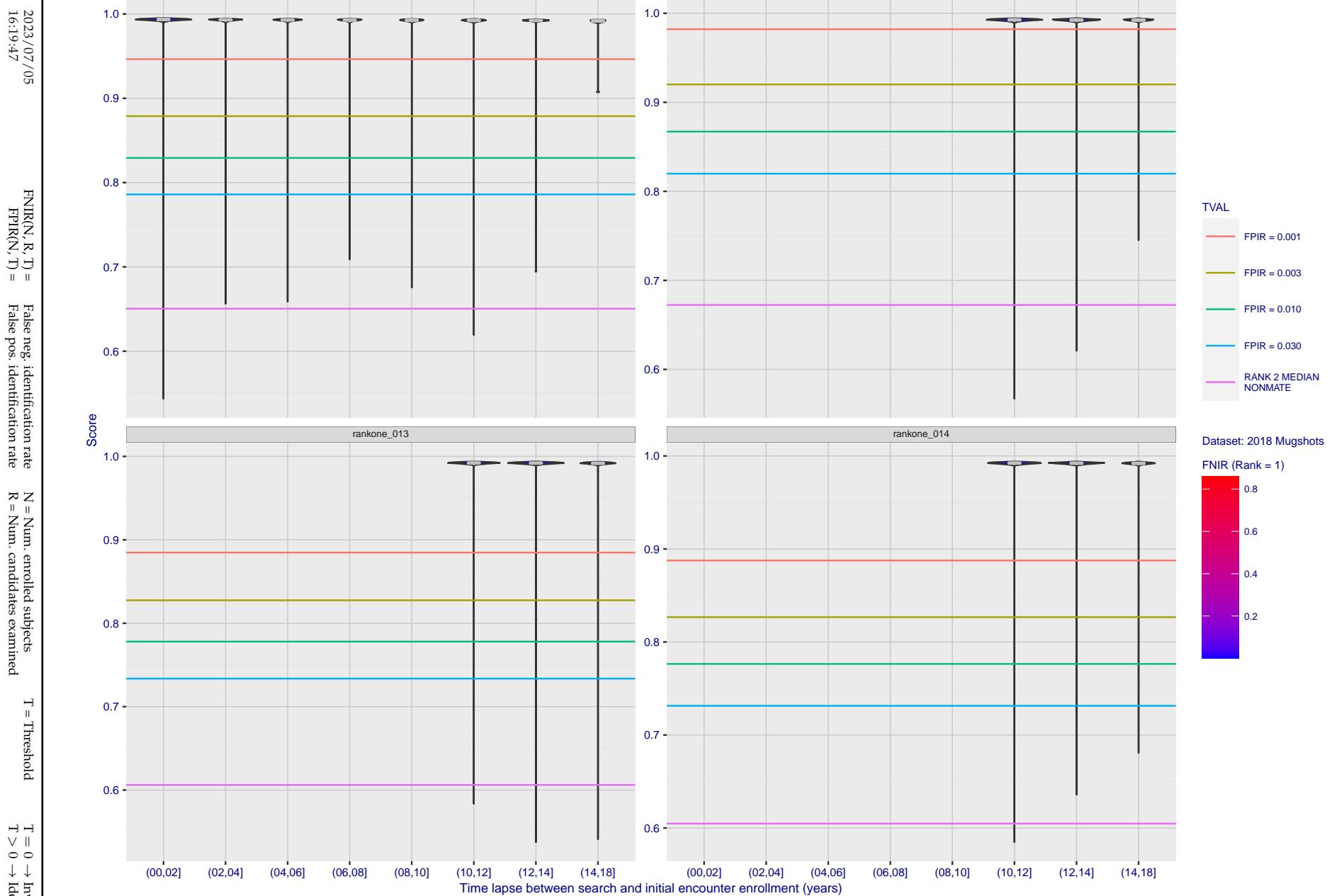


Figure 233: [FRVT-2018 Mugshot Ageing Dataset] Native mate scores vs. time-elapsed. The oldest image of each individual is enrolled. Thereafter, all more recent images are searched. Mated score distributions are computed over all searches noted in row 17 of Table 1 binned by number of years between search and initial enrollment.

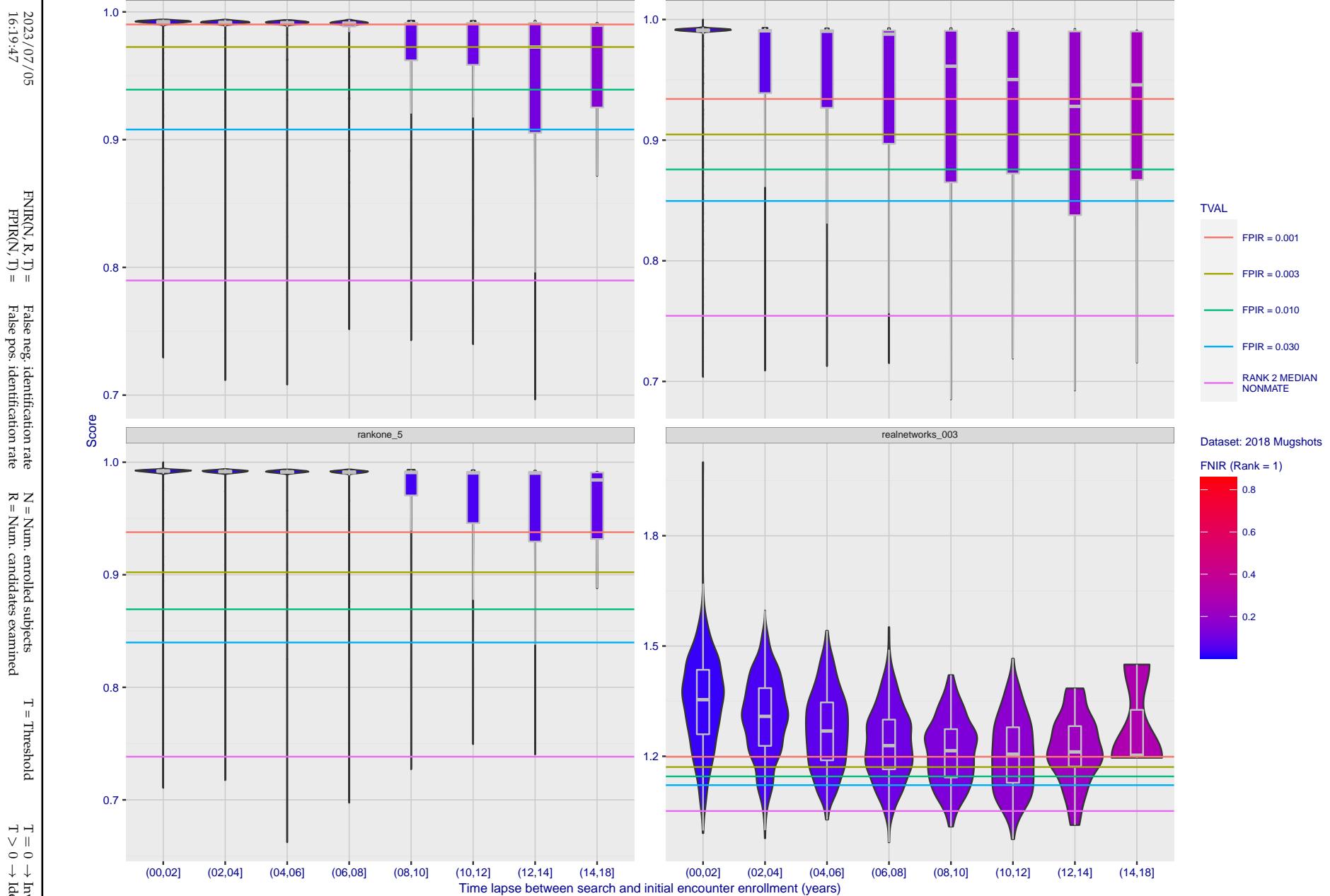


Figure 234: [FRVT-2018 Mugshot Ageing Dataset] Native mate scores vs. time-elapsed. The oldest image of each individual is enrolled. Thereafter, all more recent images are searched. Mated score distributions are computed over all searches noted in row 17 of Table 1 binned by number of years between search and initial enrollment.

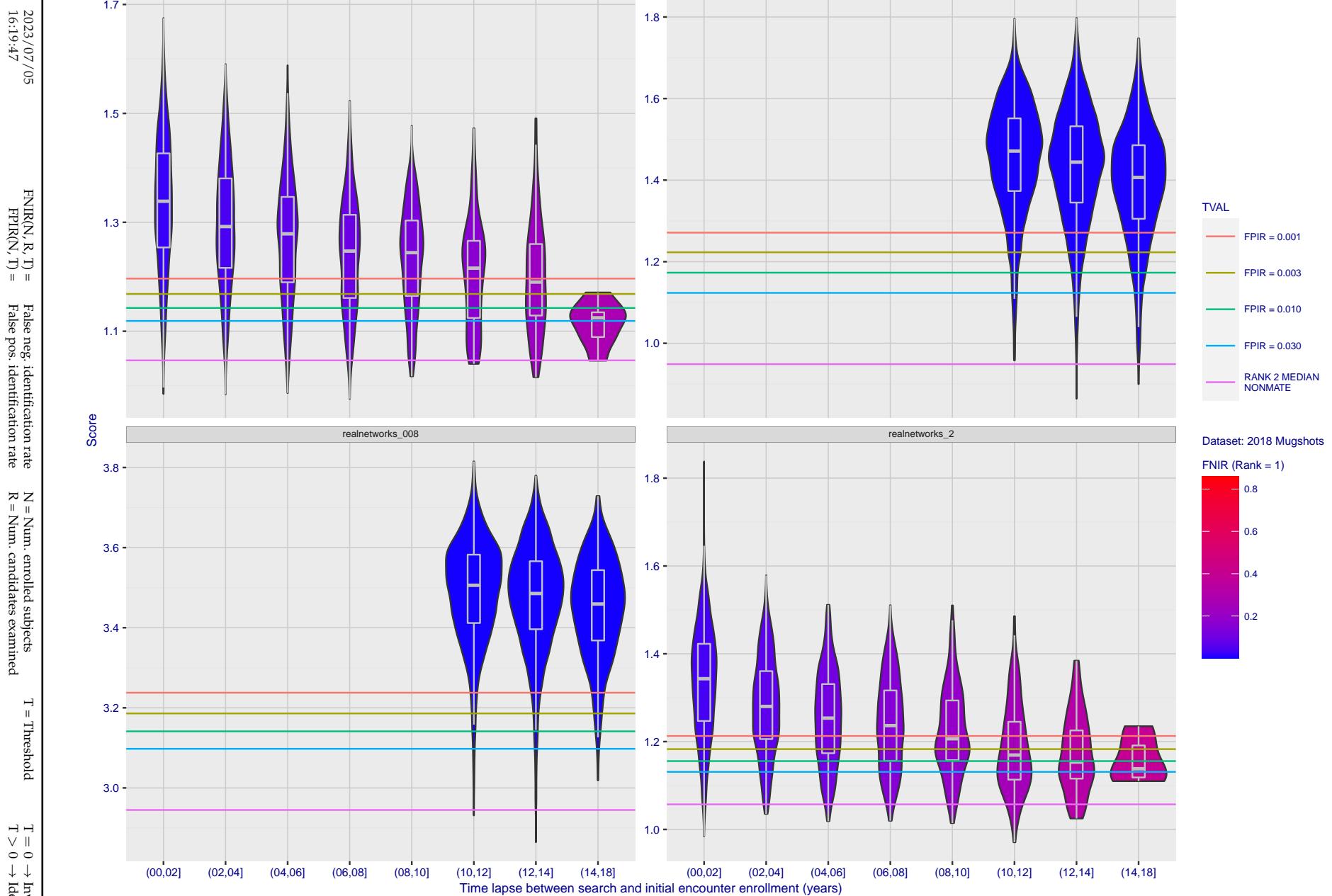


Figure 235: [FRVT-2018 Mugshot Ageing Dataset] Native mate scores vs. time-elapsed. The oldest image of each individual is enrolled. Thereafter, all more recent images are searched. Mated score distributions are computed over all searches noted in row 17 of Table 1 binned by number of years between search and initial enrollment.

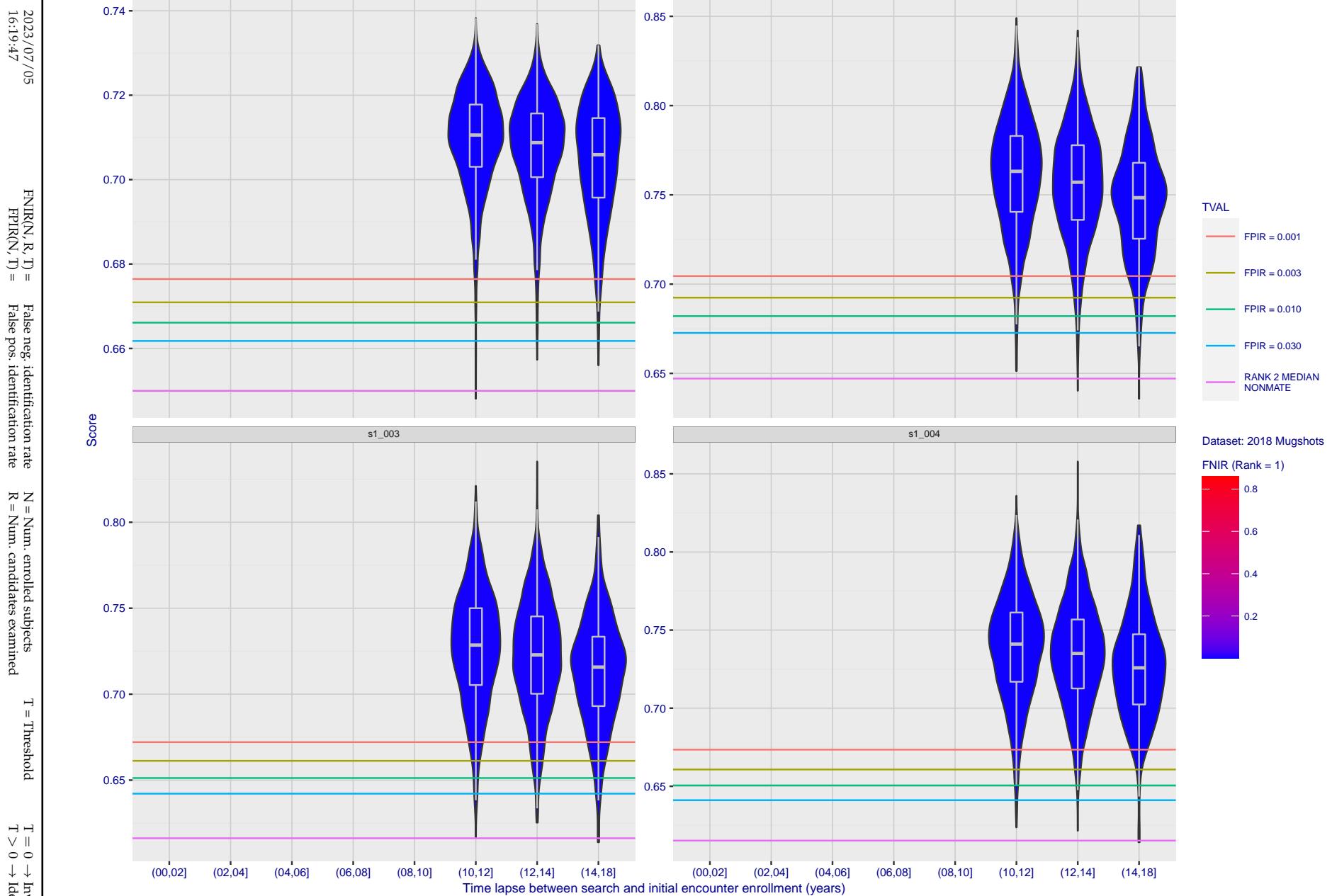


Figure 236: [FRVT-2018 Mugshot Ageing Dataset] Native mate scores vs. time-elapsed. The oldest image of each individual is enrolled. Thereafter, all more recent images are searched. Mated score distributions are computed over all searches noted in row 17 of Table 1 binned by number of years between search and initial enrollment.

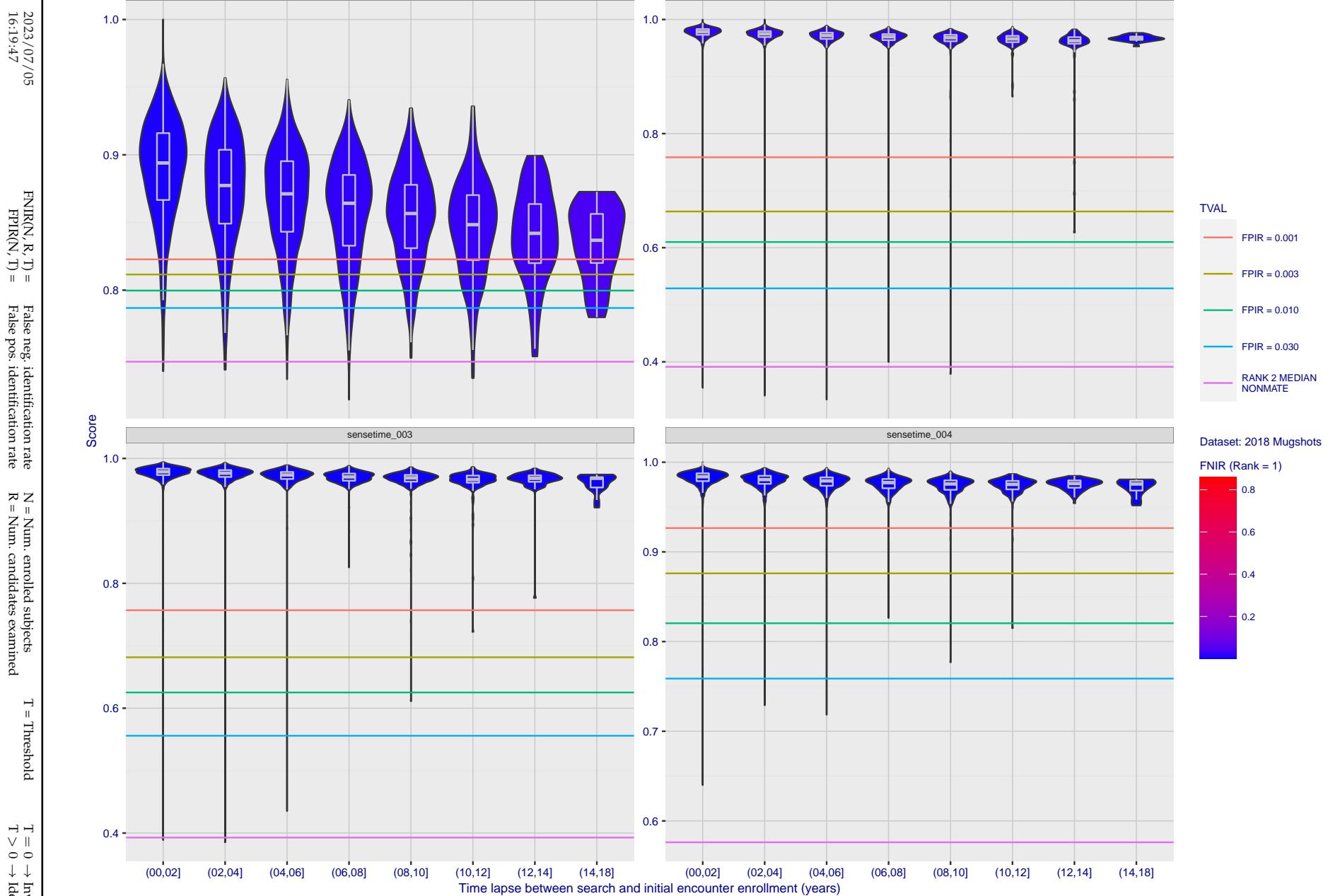


Figure 237: [FRVT-2018 Mugshot Ageing Dataset] Native mate scores vs. time-elapsed. The oldest image of each individual is enrolled. Thereafter, all more recent images are searched. Mated score distributions are computed over all searches noted in row 17 of Table 1 binned by number of years between search and initial enrollment.

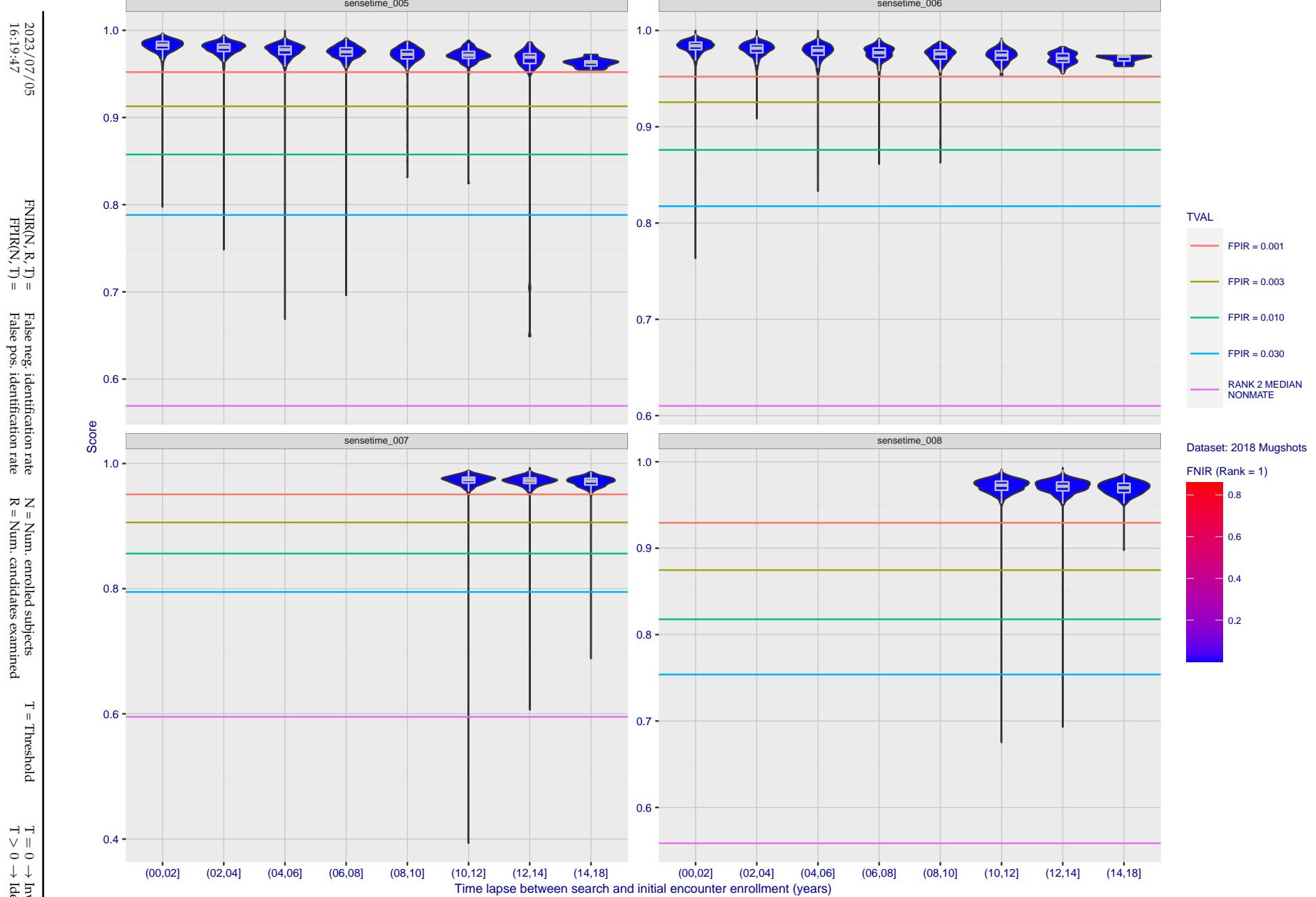


Figure 238: [FRVT-2018 Mugshot Ageing Dataset] Native mate scores vs. time-elapsed. The oldest image of each individual is enrolled. Thereafter, all more recent images are searched. Mated score distributions are computed over all searches noted in row 17 of Table 1 binned by number of years between search and initial enrollment.

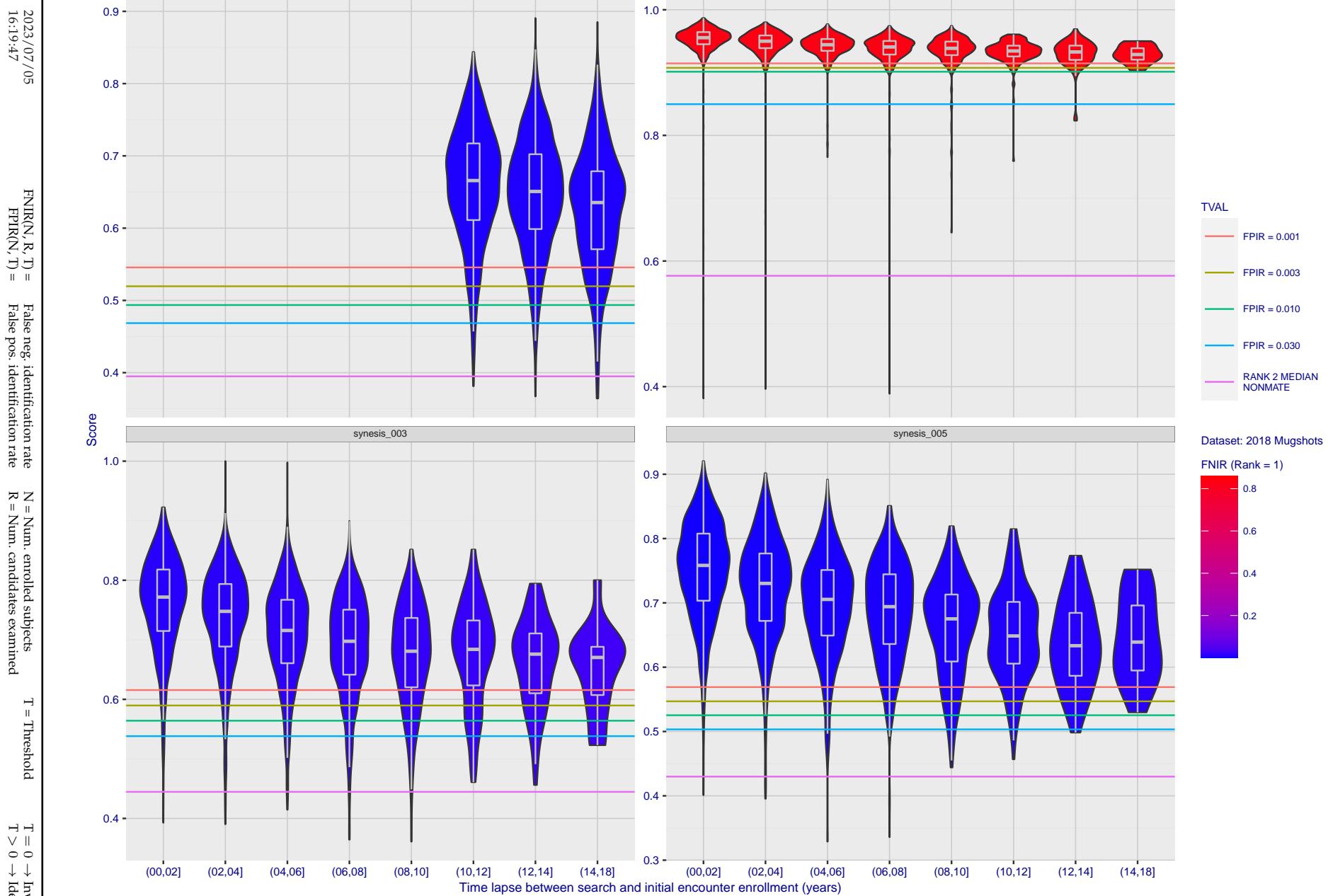


Figure 239: [FRVT-2018 Mugshot Ageing Dataset] Native mate scores vs. time-elapsed. The oldest image of each individual is enrolled. Thereafter, all more recent images are searched. Mated score distributions are computed over all searches noted in row 17 of Table 1 binned by number of years between search and initial enrollment.

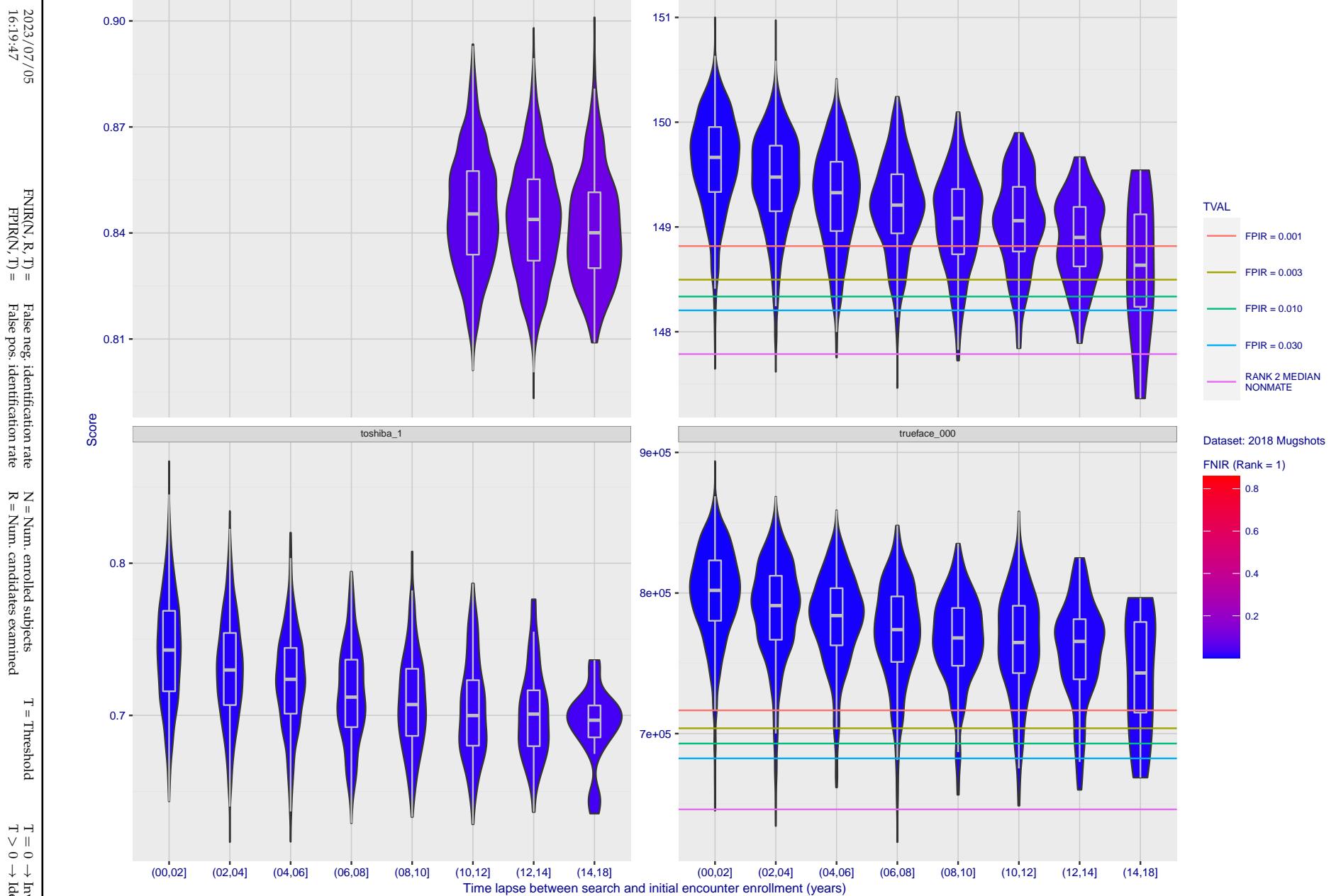


Figure 240: [FRVT-2018 Mugshot Ageing Dataset] Native mate scores vs. time-elapsed. The oldest image of each individual is enrolled. Thereafter, all more recent images are searched. Mated score distributions are computed over all searches noted in row 17 of Table 1 binned by number of years between search and initial enrollment.

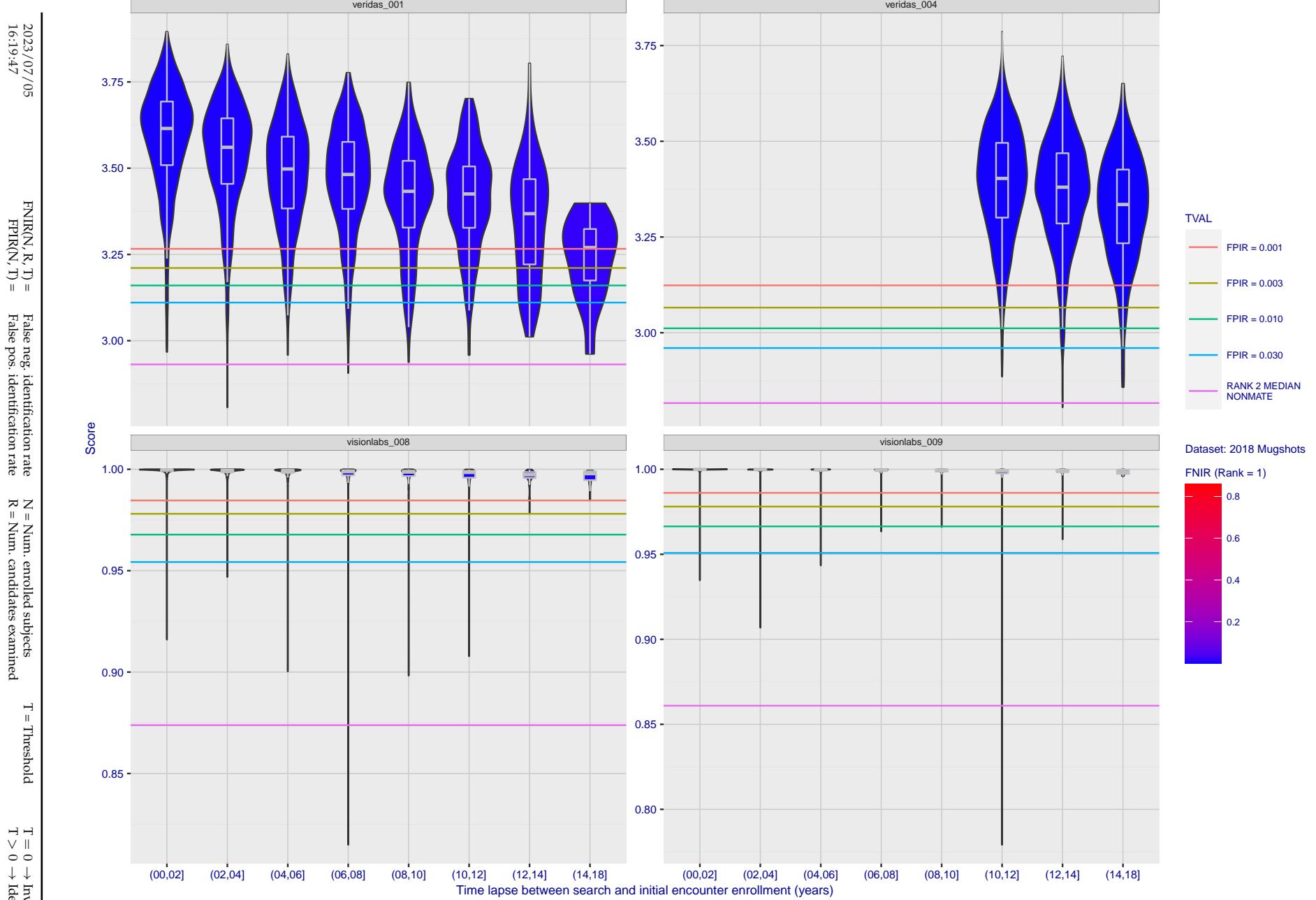


Figure 241: [FRVT-2018 Mugshot Ageing Dataset] Native mate scores vs. time-elapsed. The oldest image of each individual is enrolled. Thereafter, all more recent images are searched. Mated score distributions are computed over all searches noted in row 17 of Table 1 binned by number of years between search and initial enrollment.

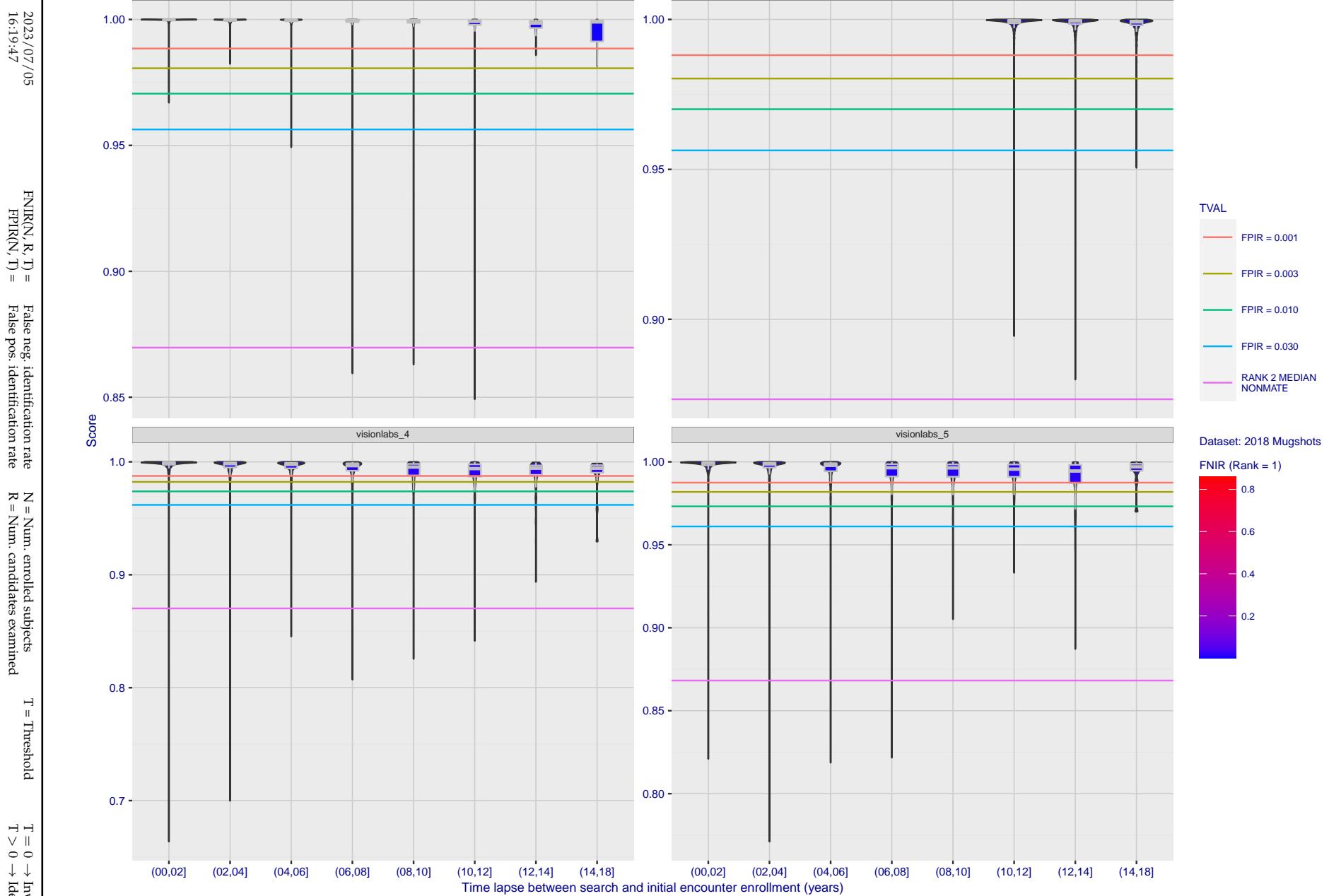


Figure 242: [FRVT-2018 Mugshot Ageing Dataset] Native mate scores vs. time-elapsed. The oldest image of each individual is enrolled. Thereafter, all more recent images are searched. Mated score distributions are computed over all searches noted in row 17 of Table 1 binned by number of years between search and initial enrollment.

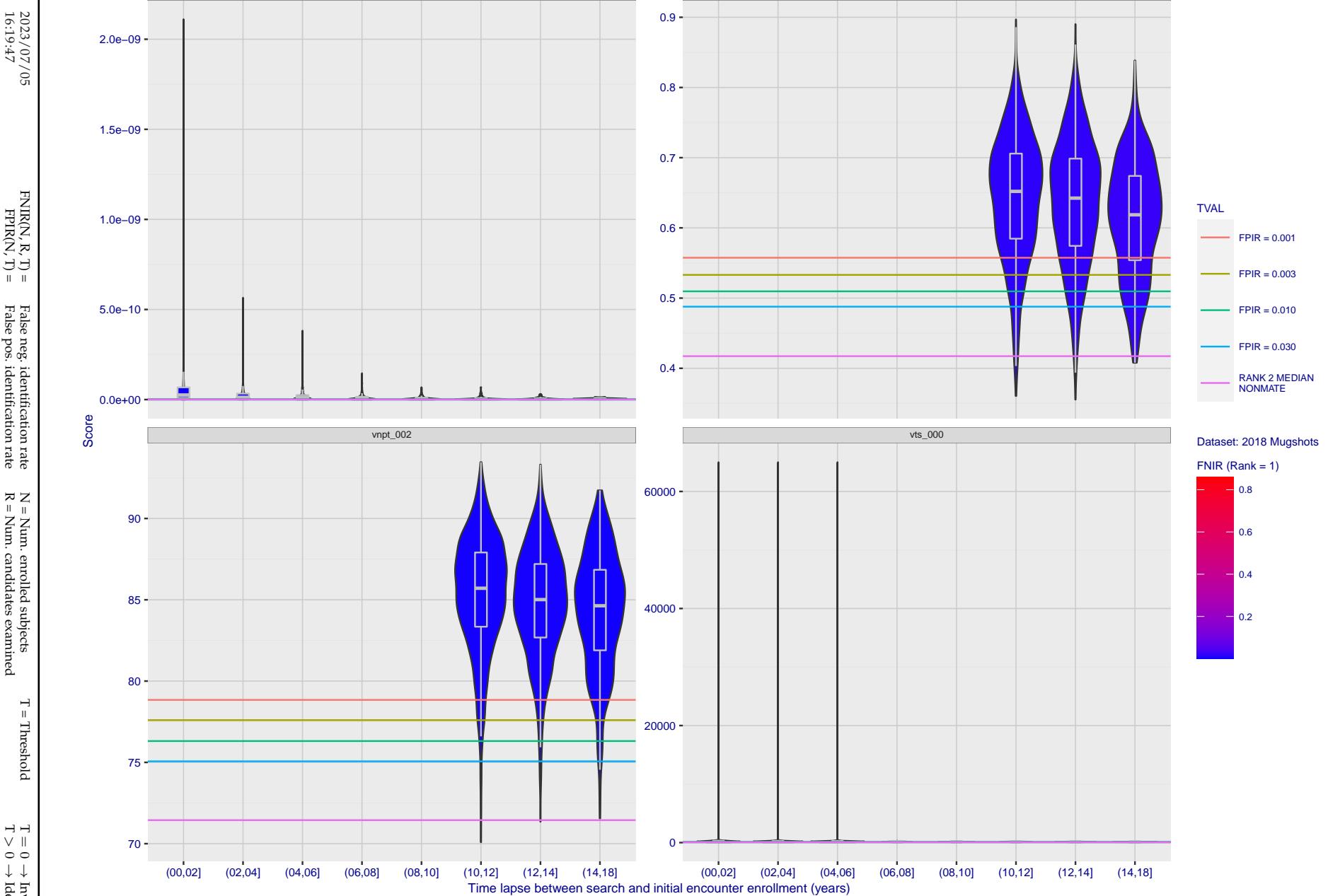


Figure 243: [FRVT-2018 Mugshot Ageing Dataset] Native mate scores vs. time-elapsed. The oldest image of each individual is enrolled. Thereafter, all more recent images are searched. Mated score distributions are computed over all searches noted in row 17 of Table 1 binned by number of years between search and initial enrollment.

2023/07/05
16:19:47FNIR(N, R, T) = False neg. identification rate
FPFR(N, T) = False pos. identification rateN = Num. enrolled subjects
R = Num. candidates examinedT = Threshold
T = 0 → Investigation

T > 0 → Identification

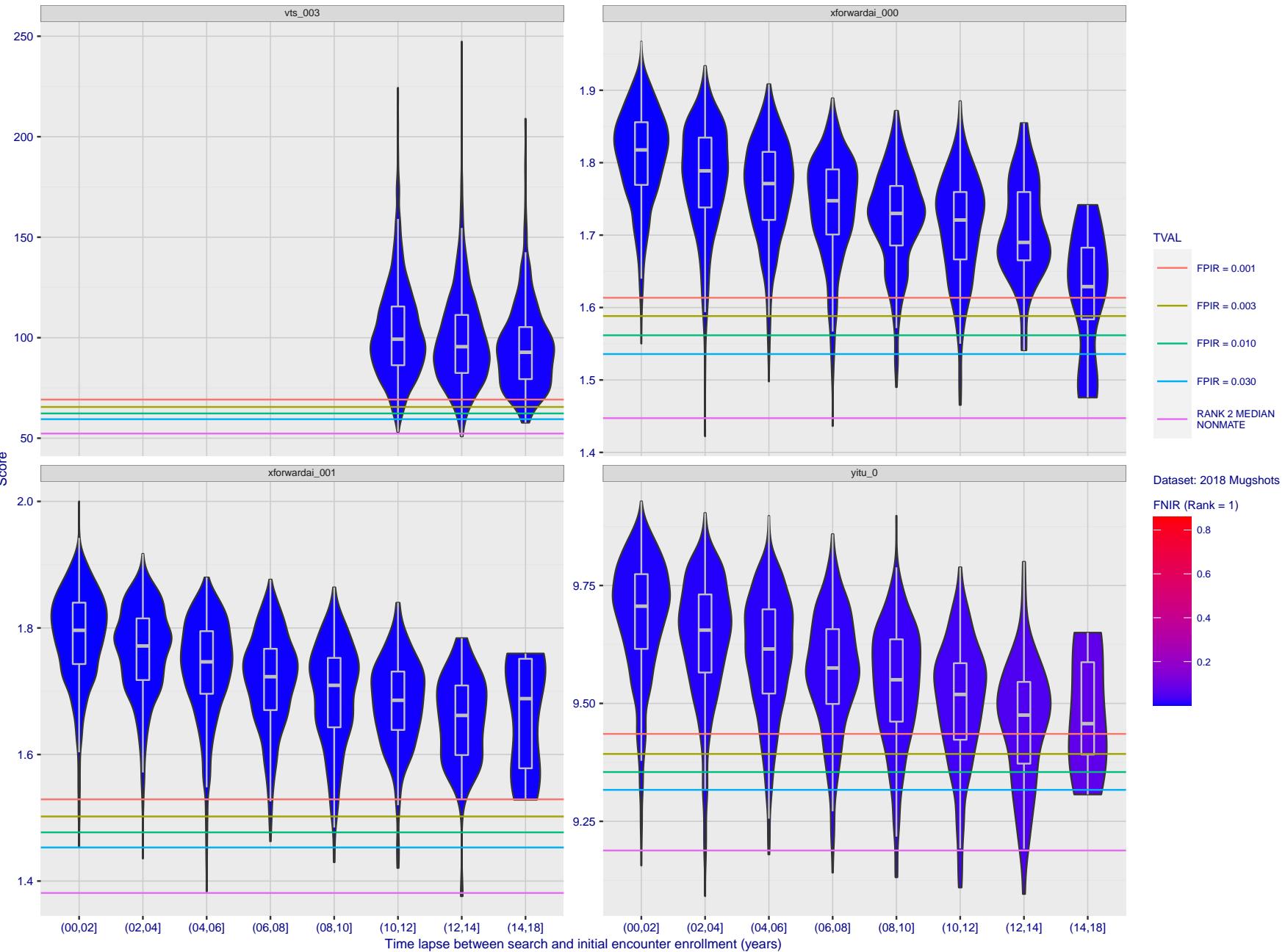


Figure 244: [FRVT-2018 Mugshot Ageing Dataset] Native mate scores vs. time-elapsed. The oldest image of each individual is enrolled. Thereafter, all more recent images are searched. Mated score distributions are computed over all searches noted in row 17 of Table 1 binned by number of years between search and initial enrollment.

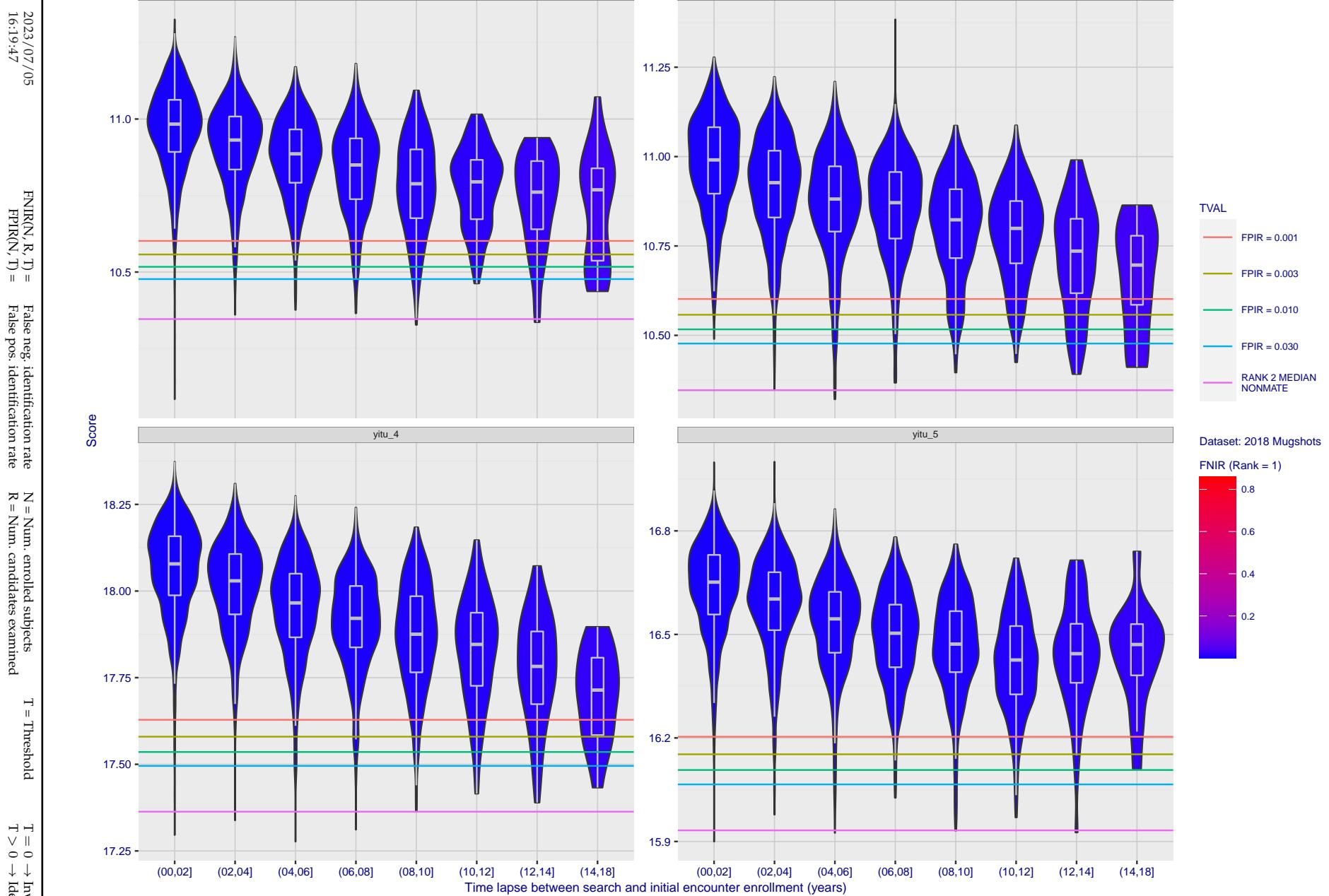


Figure 245: [FRVT-2018 Mugshot Ageing Dataset] Native mate scores vs. time-elapsed. The oldest image of each individual is enrolled. Thereafter, all more recent images are searched. Mated score distributions are computed over all searches noted in row 17 of Table 1 binned by number of years between search and initial enrollment.

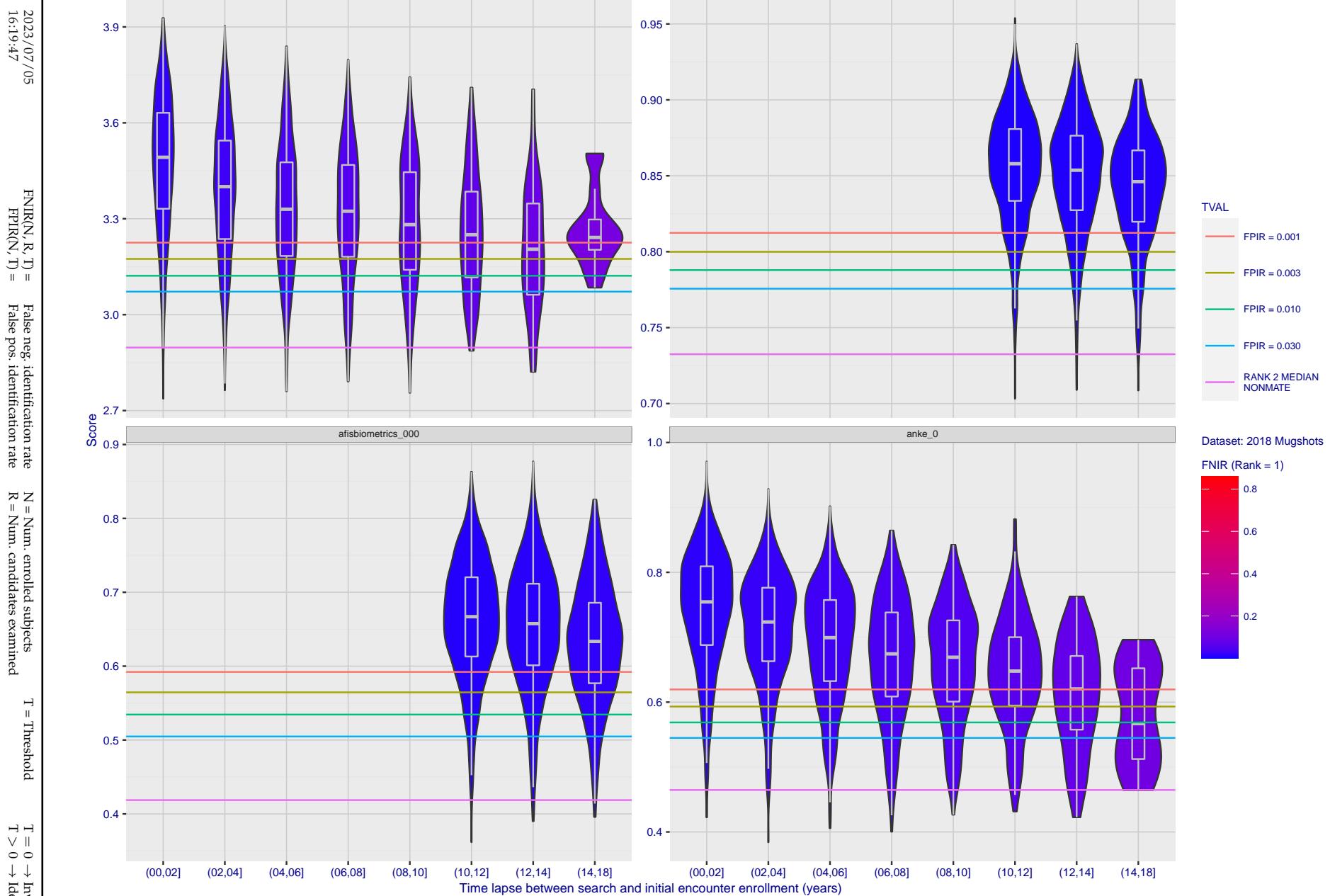


Figure 246: [FRVT-2018 Mugshot Ageing Dataset] Native mate scores vs. time-elapsed. The oldest image of each individual is enrolled. Thereafter, all more recent images are searched. Mated score distributions are computed over all searches noted in row 17 of Table 1 binned by number of years between search and initial enrollment.

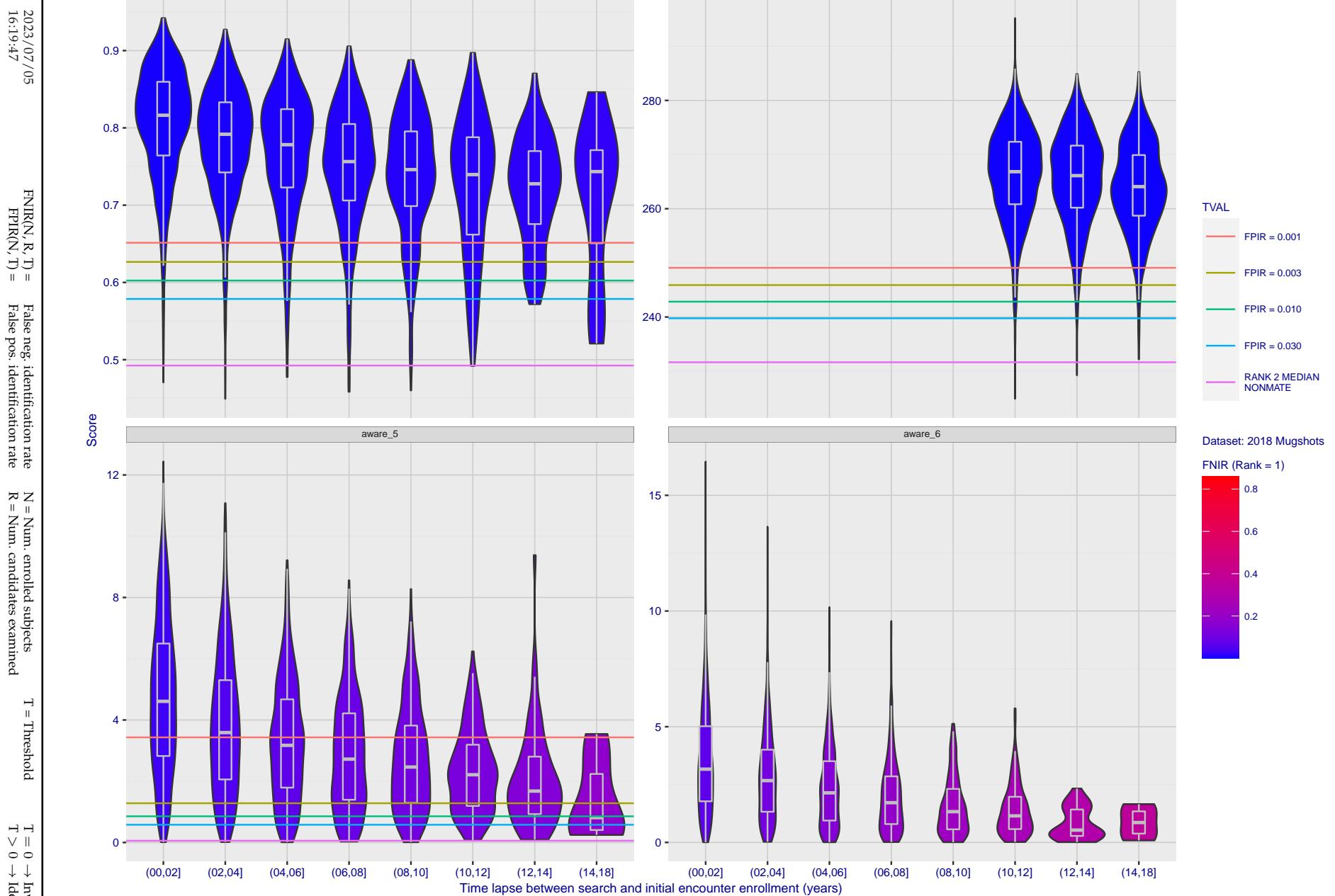


Figure 247: [FRVT-2018 Mugshot Ageing Dataset] Native mate scores vs. time-elapsed. The oldest image of each individual is enrolled. Thereafter, all more recent images are searched. Mated score distributions are computed over all searches noted in row 17 of Table 1 binned by number of years between search and initial enrollment.

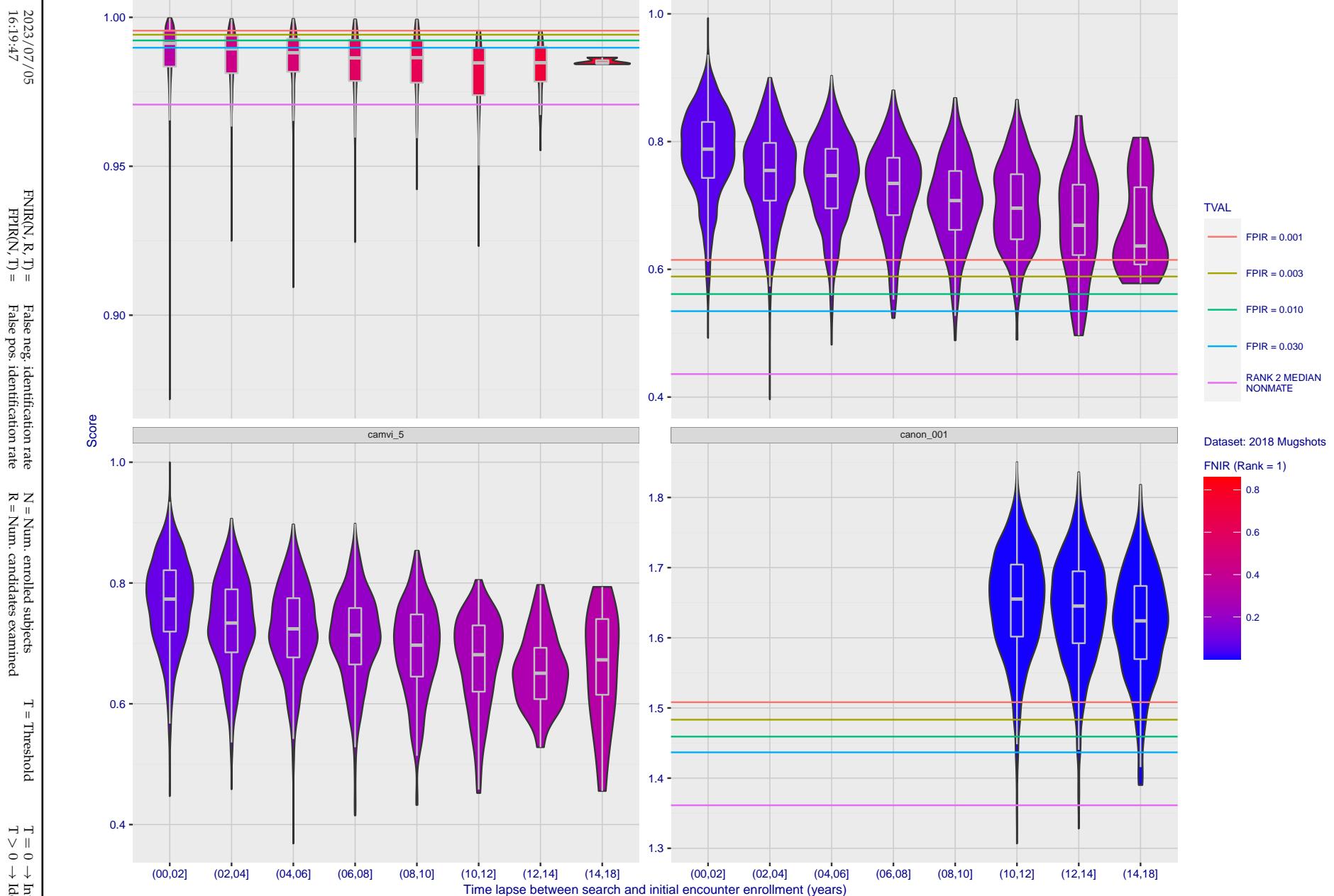


Figure 248: [FRVT-2018 Mugshot Ageing Dataset] Native mate scores vs. time-elapsed. The oldest image of each individual is enrolled. Thereafter, all more recent images are searched. Mated score distributions are computed over all searches noted in row 17 of Table 1 binned by number of years between search and initial enrollment.

2023/07/05
16:19:47FNIR(N, R, T) = False neg. identification rate
FPIR(N, T) = False pos. identification rateN = Num. enrolled subjects
R = Num. candidates examined

T = Threshold

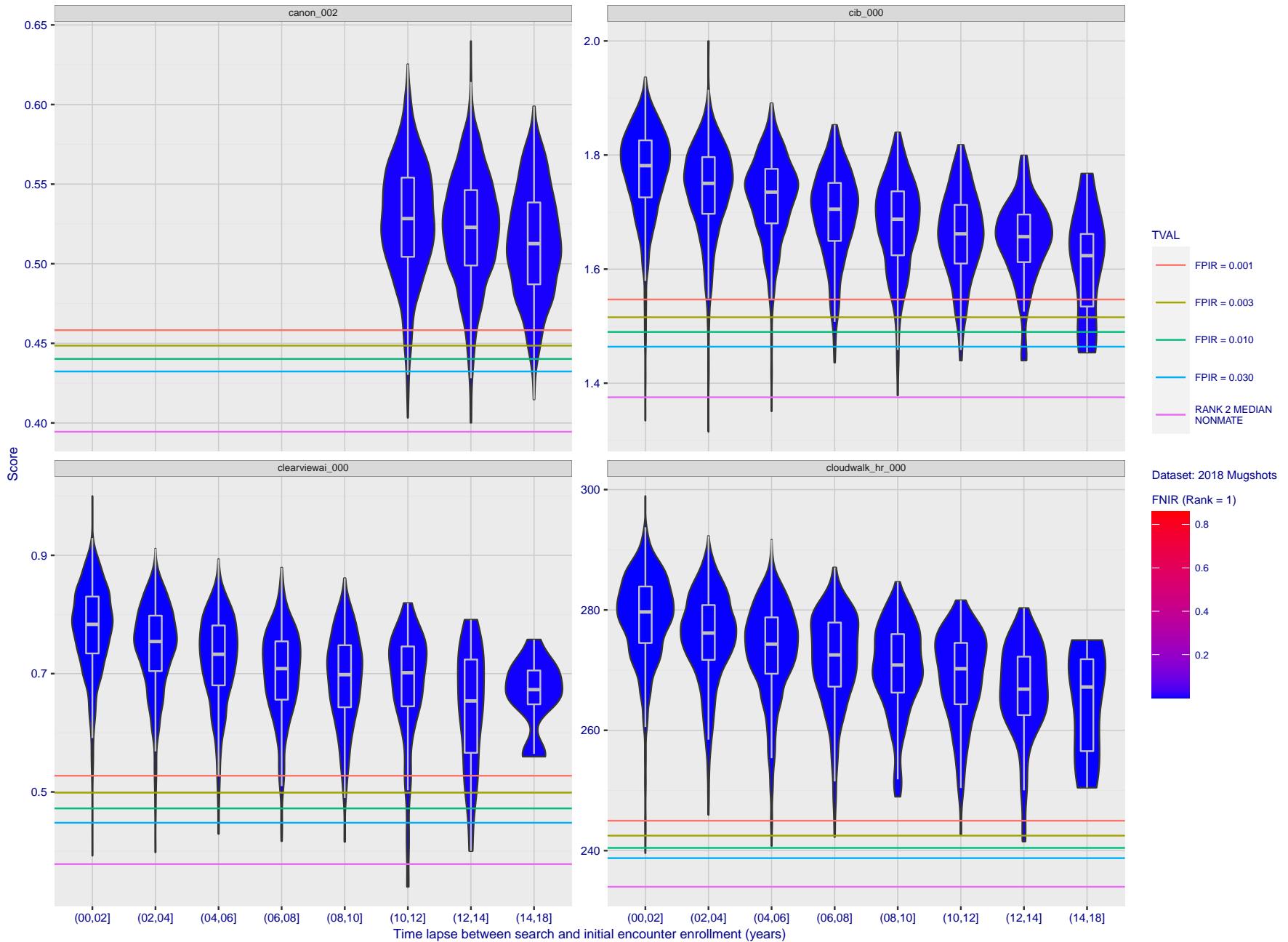
T = 0 → Investigation
T > 0 → Identification

Figure 249: [FRVT-2018 Mugshot Ageing Dataset] Native mate scores vs. time-elapsed. The oldest image of each individual is enrolled. Thereafter, all more recent images are searched. Mated score distributions are computed over all searches noted in row 17 of Table 1 binned by number of years between search and initial enrollment.

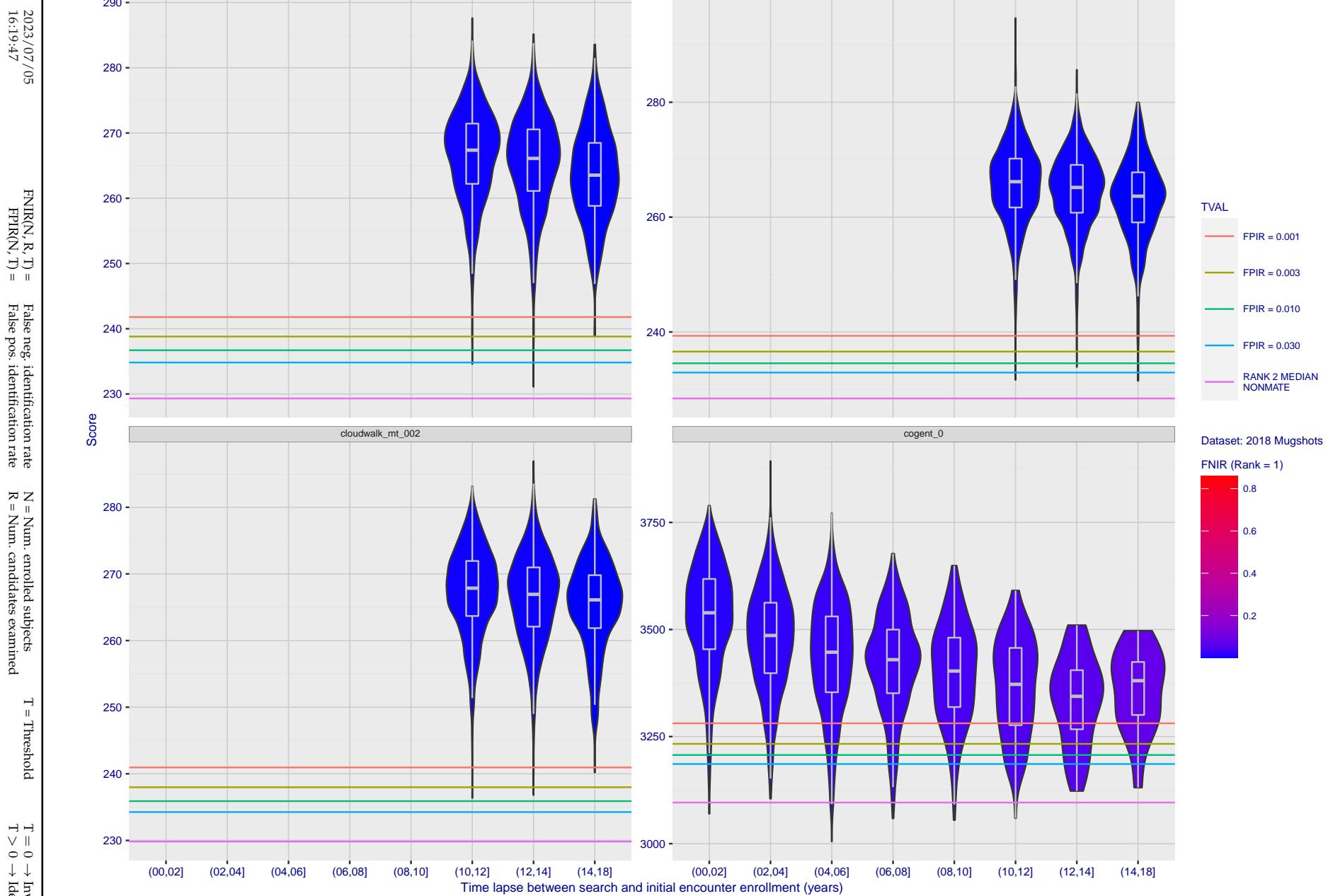


Figure 250: [FRVT-2018 Mugshot Ageing Dataset] Native mate scores vs. time-elapsed. The oldest image of each individual is enrolled. Thereafter, all more recent images are searched. Mated score distributions are computed over all searches noted in row 17 of Table 1 binned by number of years between search and initial enrollment.

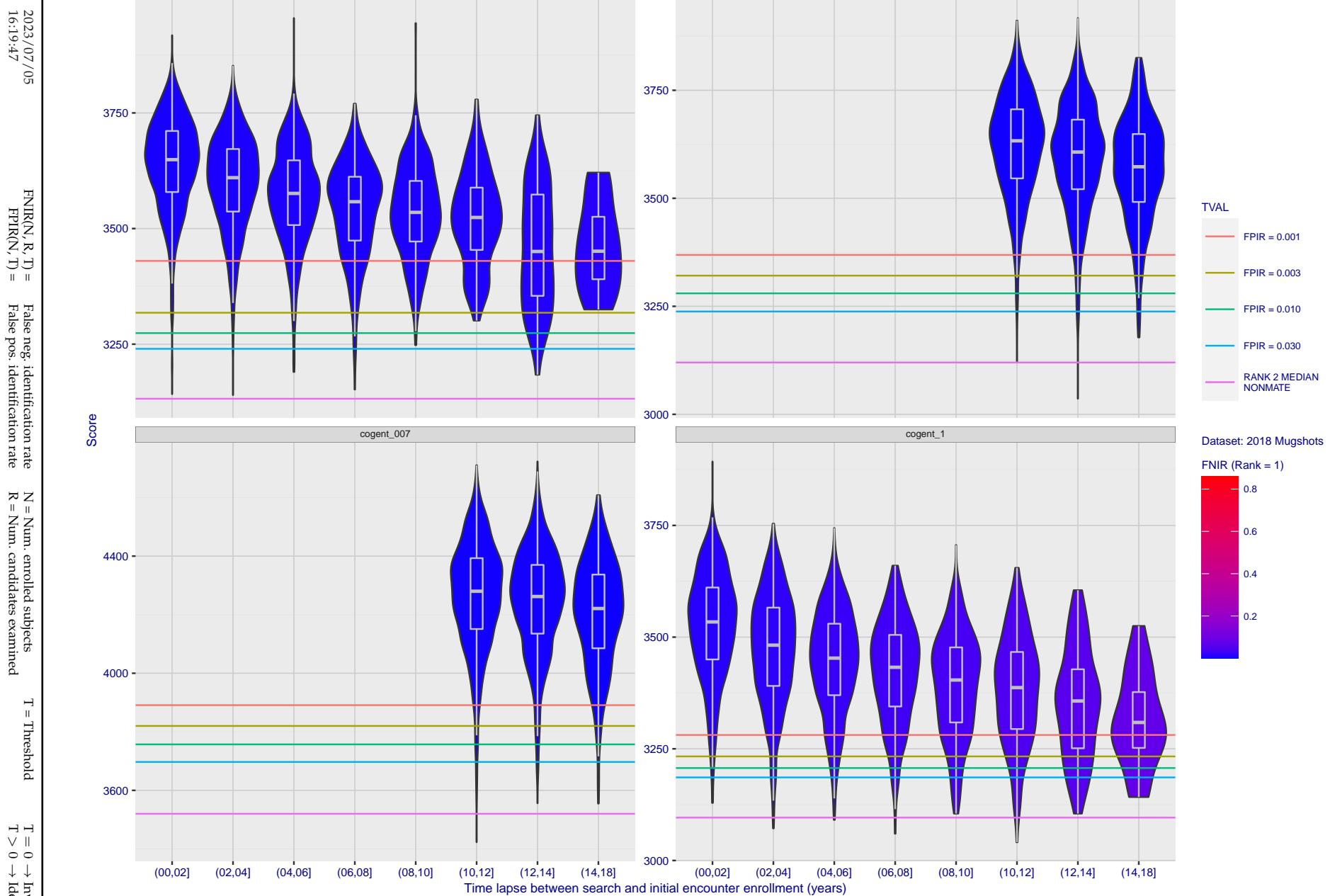


Figure 251: [FRVT-2018 Mugshot Ageing Dataset] Native mate scores vs. time-elapsed. The oldest image of each individual is enrolled. Thereafter, all more recent images are searched. Mated score distributions are computed over all searches noted in row 17 of Table 1 binned by number of years between search and initial enrollment.

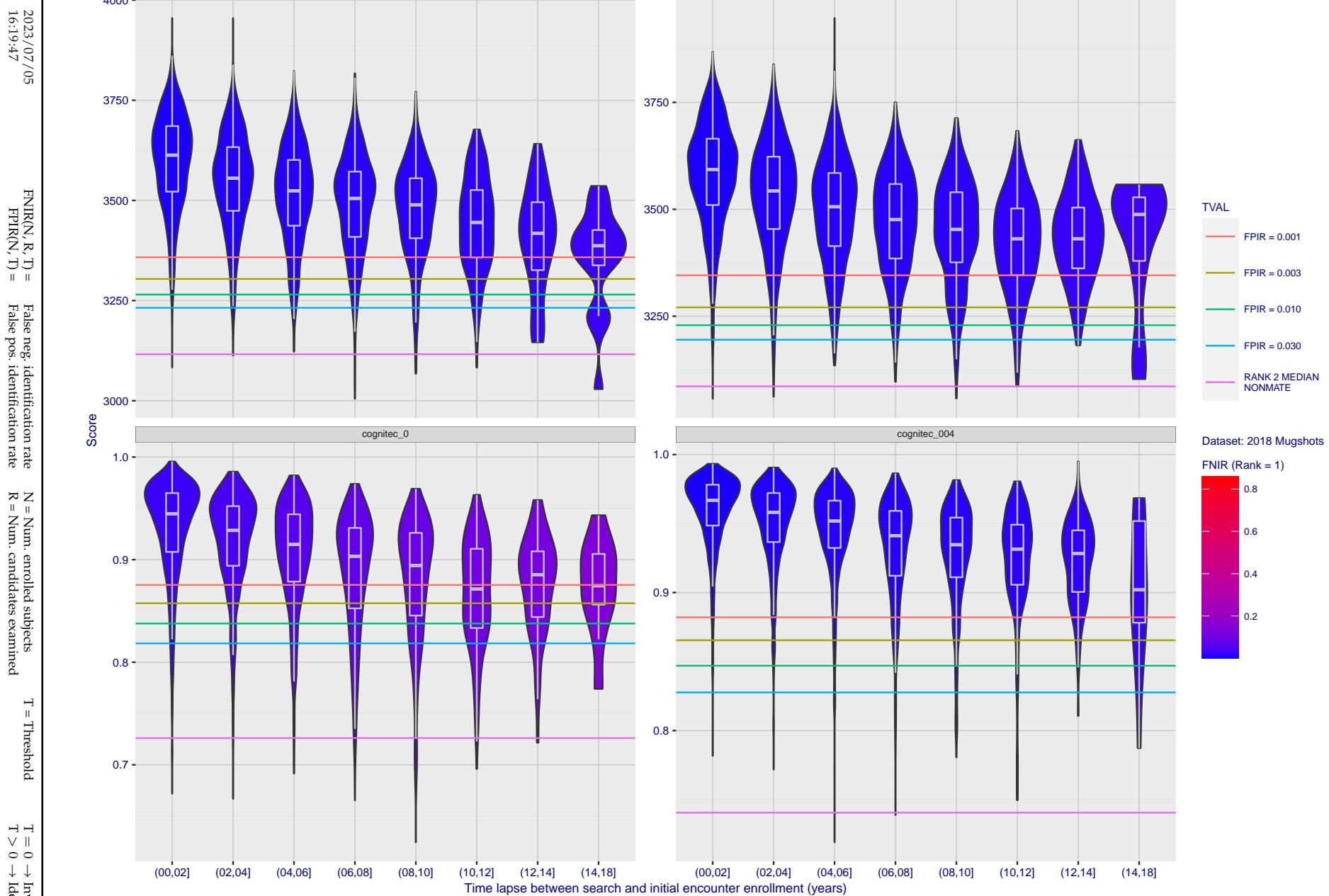


Figure 252: [FRVT-2018 Mugshot Ageing Dataset] Native mate scores vs. time-elapsed. The oldest image of each individual is enrolled. Thereafter, all more recent images are searched. Mated score distributions are computed over all searches noted in row 17 of Table 1 binned by number of years between search and initial enrollment.

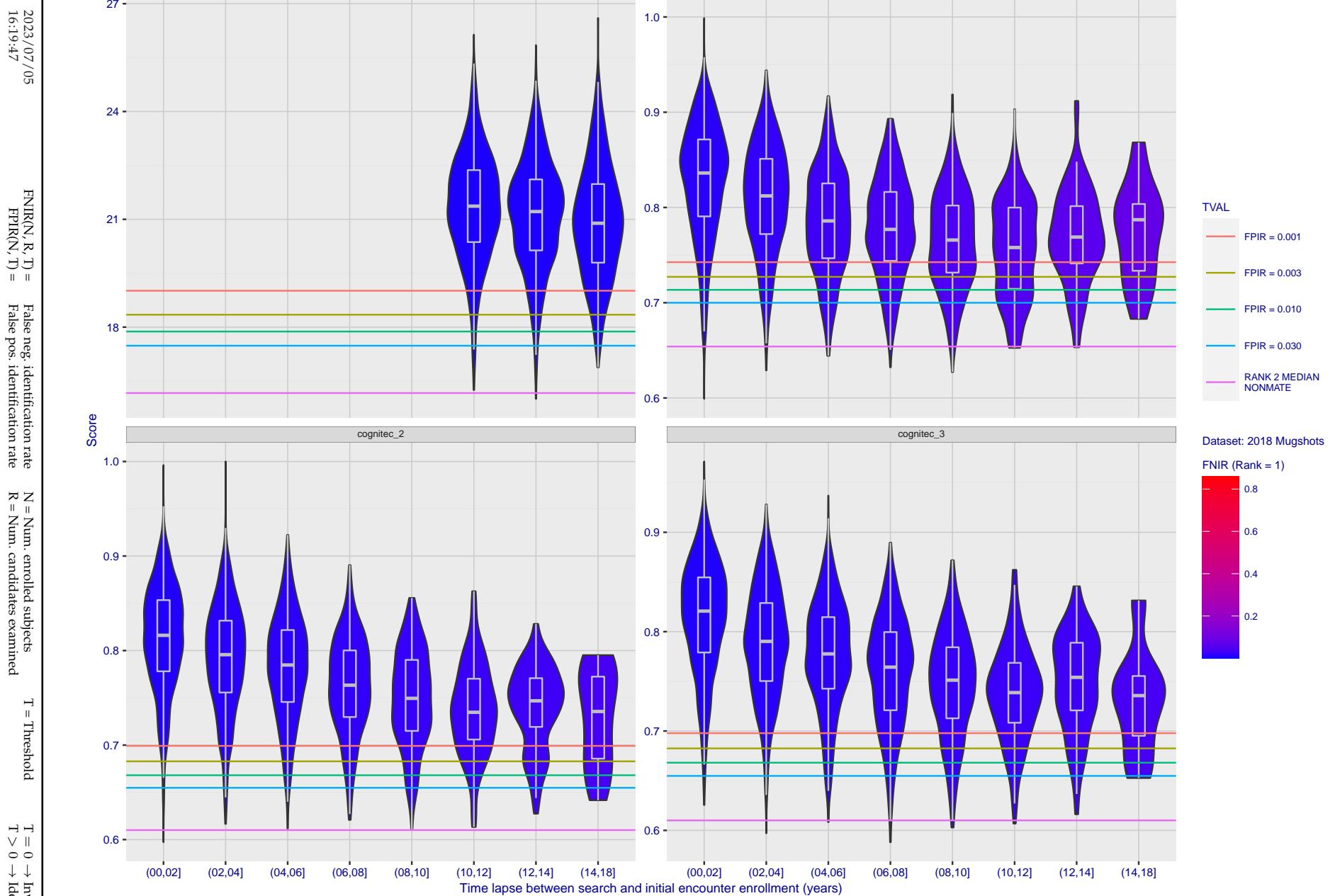


Figure 253: [FRVT-2018 Mugshot Ageing Dataset] Native mate scores vs. time-elapsed. The oldest image of each individual is enrolled. Thereafter, all more recent images are searched. Mated score distributions are computed over all searches noted in row 17 of Table 1 binned by number of years between search and initial enrollment.

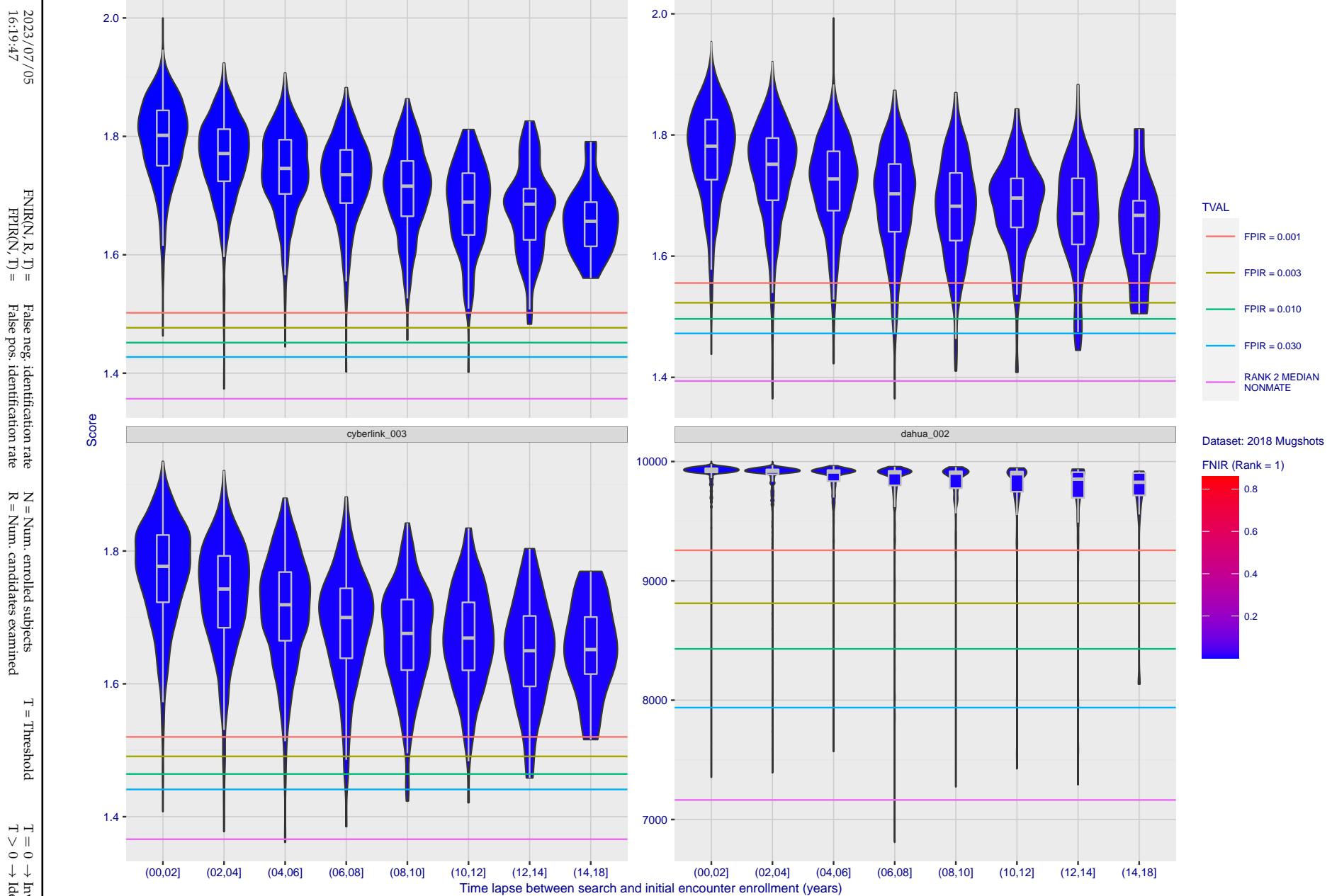


Figure 254: [FRVT-2018 Mugshot Ageing Dataset] Native mate scores vs. time-elapsed. The oldest image of each individual is enrolled. Thereafter, all more recent images are searched. Mated score distributions are computed over all searches noted in row 17 of Table 1 binned by number of years between search and initial enrollment.

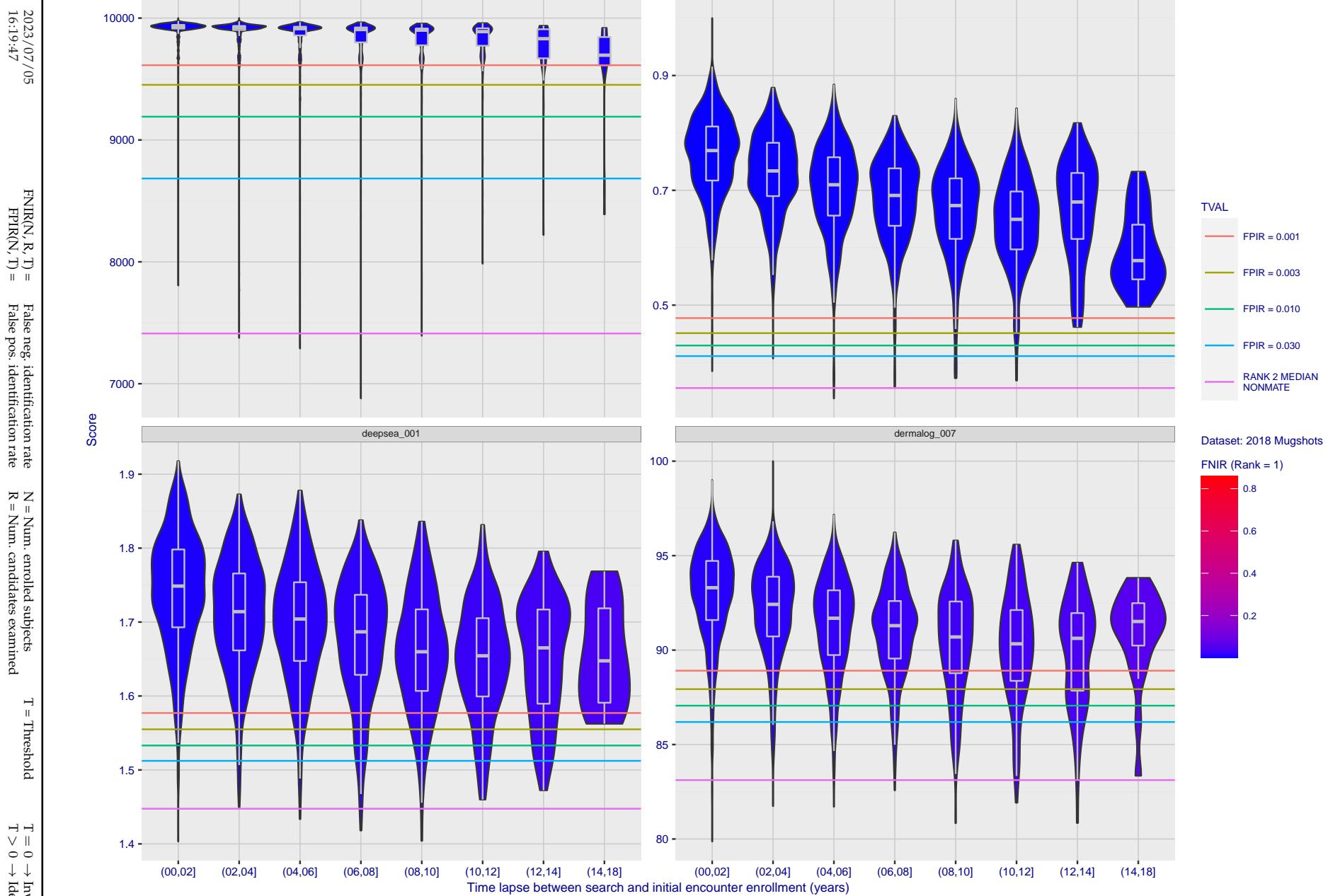


Figure 255: [FRVT-2018 Mugshot Ageing Dataset] Native mate scores vs. time-elapsed. The oldest image of each individual is enrolled. Thereafter, all more recent images are searched. Mated score distributions are computed over all searches noted in row 17 of Table 1 binned by number of years between search and initial enrollment.

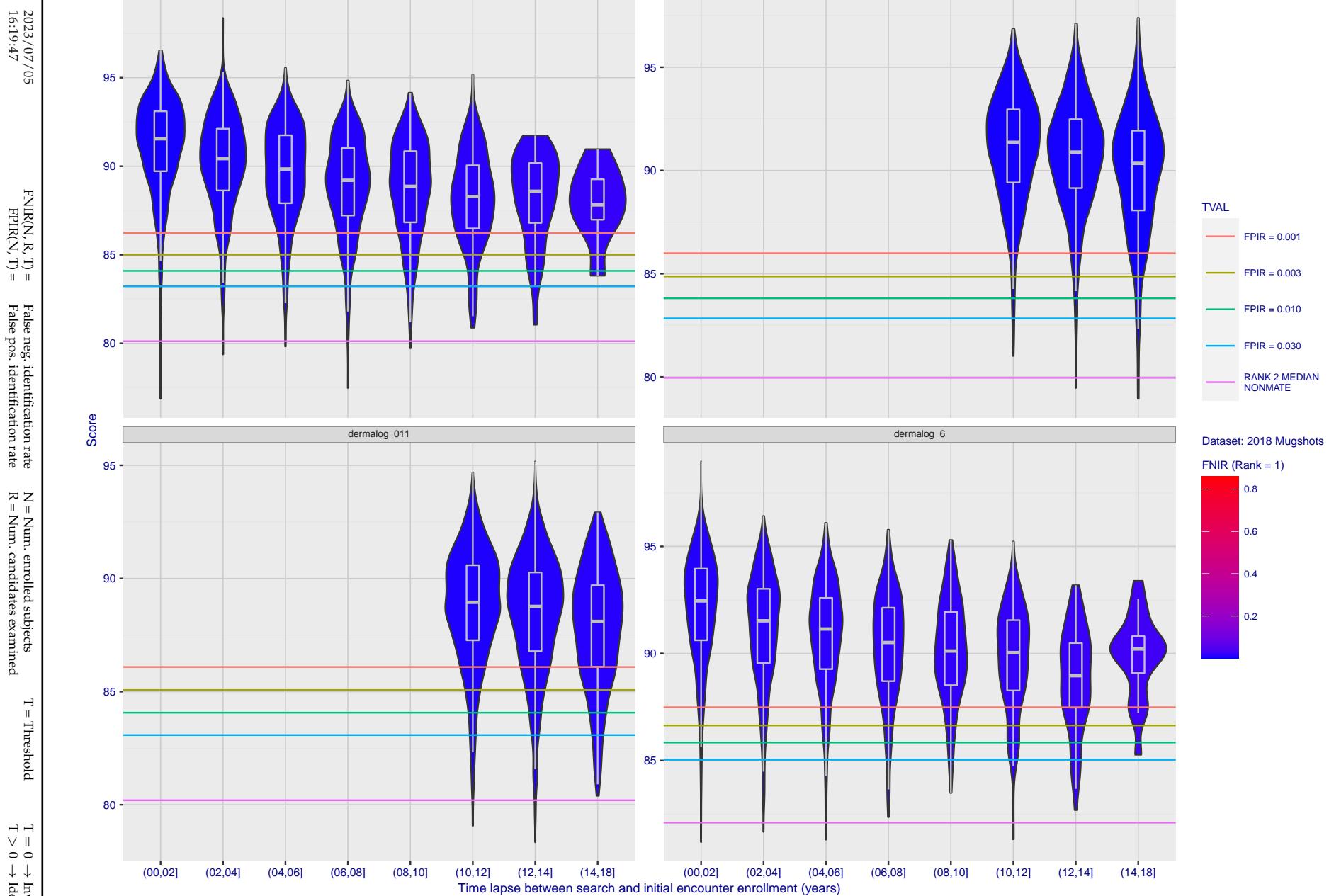


Figure 256: [FRVT-2018 Mugshot Ageing Dataset] Native mate scores vs. time-elapsed. The oldest image of each individual is enrolled. Thereafter, all more recent images are searched. Mated score distributions are computed over all searches noted in row 17 of Table 1 binned by number of years between search and initial enrollment.

2023/07/05
16:19:47FNIR(N, R, T) = False neg. identification rate
FPTR(N, T) = False pos. identification rateN = Num. enrolled subjects
R = Num. candidates examinedT = Threshold
T = 0 → Investigation

T > 0 → Identification

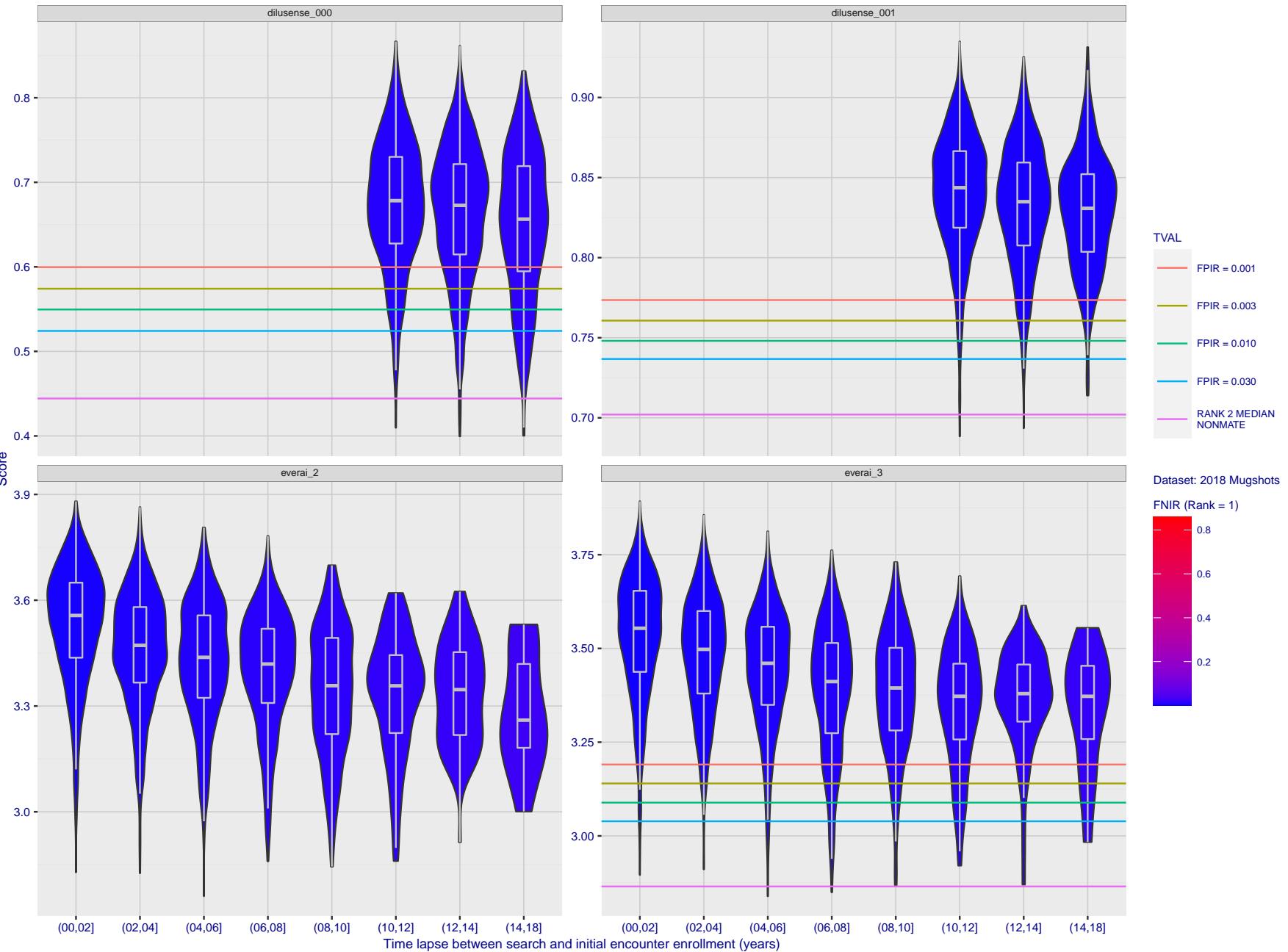


Figure 257: [FRVT-2018 Mugshot Ageing Dataset] Native mate scores vs. time-elapsed. The oldest image of each individual is enrolled. Thereafter, all more recent images are searched. Mated score distributions are computed over all searches noted in row 17 of Table 1 binned by number of years between search and initial enrollment.

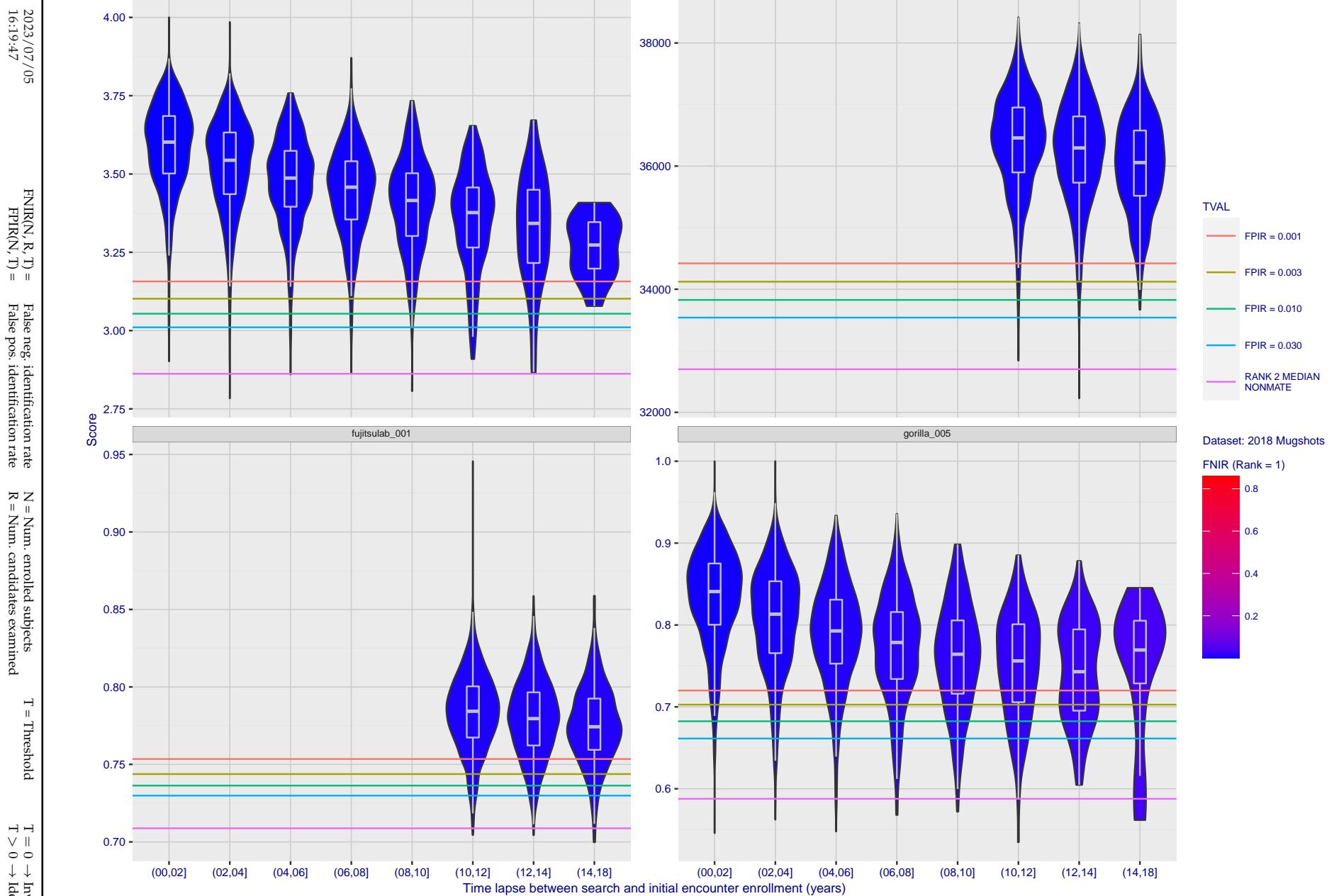


Figure 258: [FRVT-2018 Mugshot Ageing Dataset] Native mate scores vs. time-elapsed. The oldest image of each individual is enrolled. Thereafter, all more recent images are searched. Mated score distributions are computed over all searches noted in row 17 of Table 1 binned by number of years between search and initial enrollment.

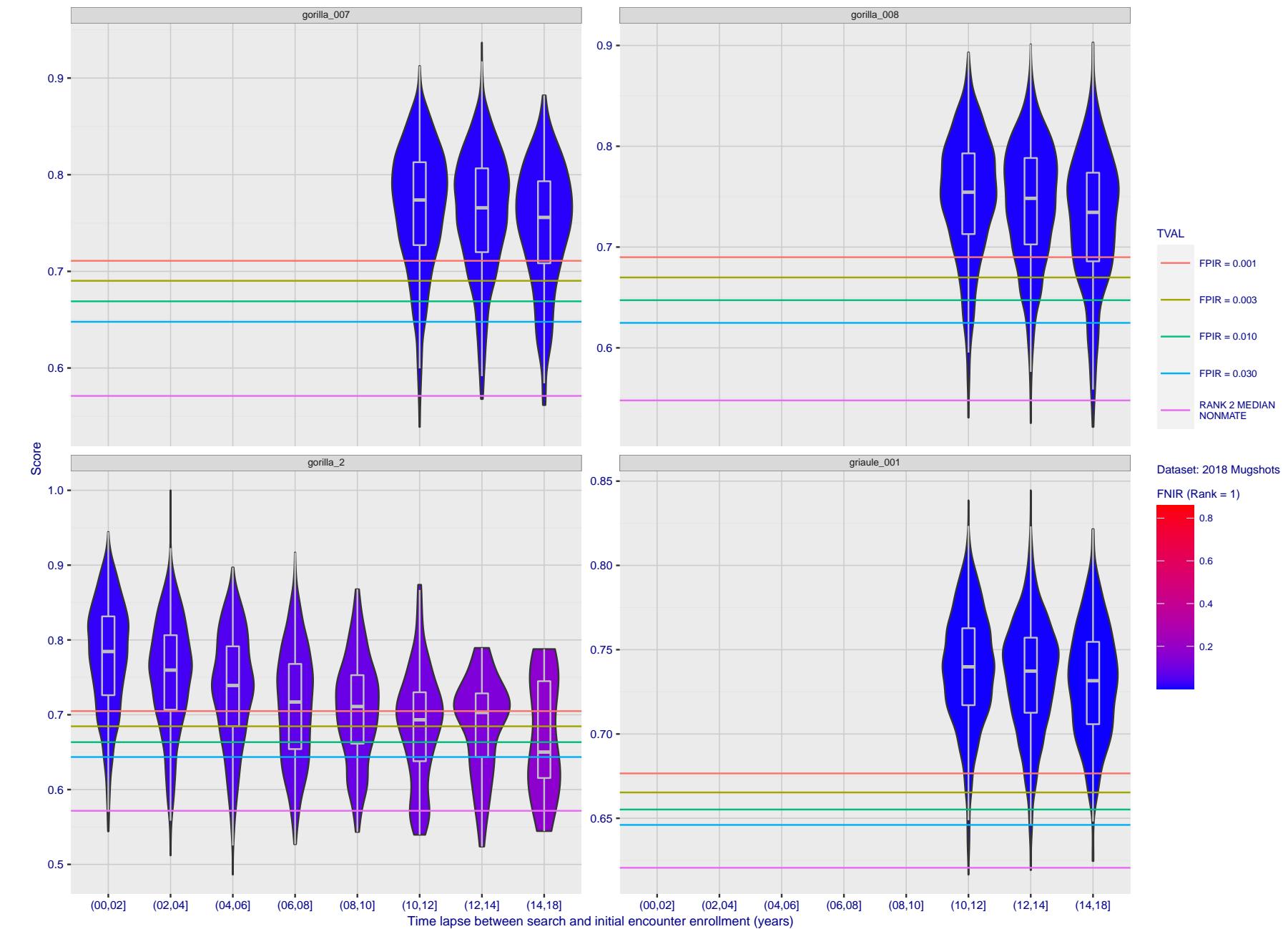
2023/07/05
16:19:47

Figure 259: [FRVT-2018 Mugshot Ageing Dataset] Native mate scores vs. time-elapsed. The oldest image of each individual is enrolled. Thereafter, all more recent images are searched. Mated score distributions are computed over all searches noted in row 17 of Table 1 binned by number of years between search and initial enrollment.

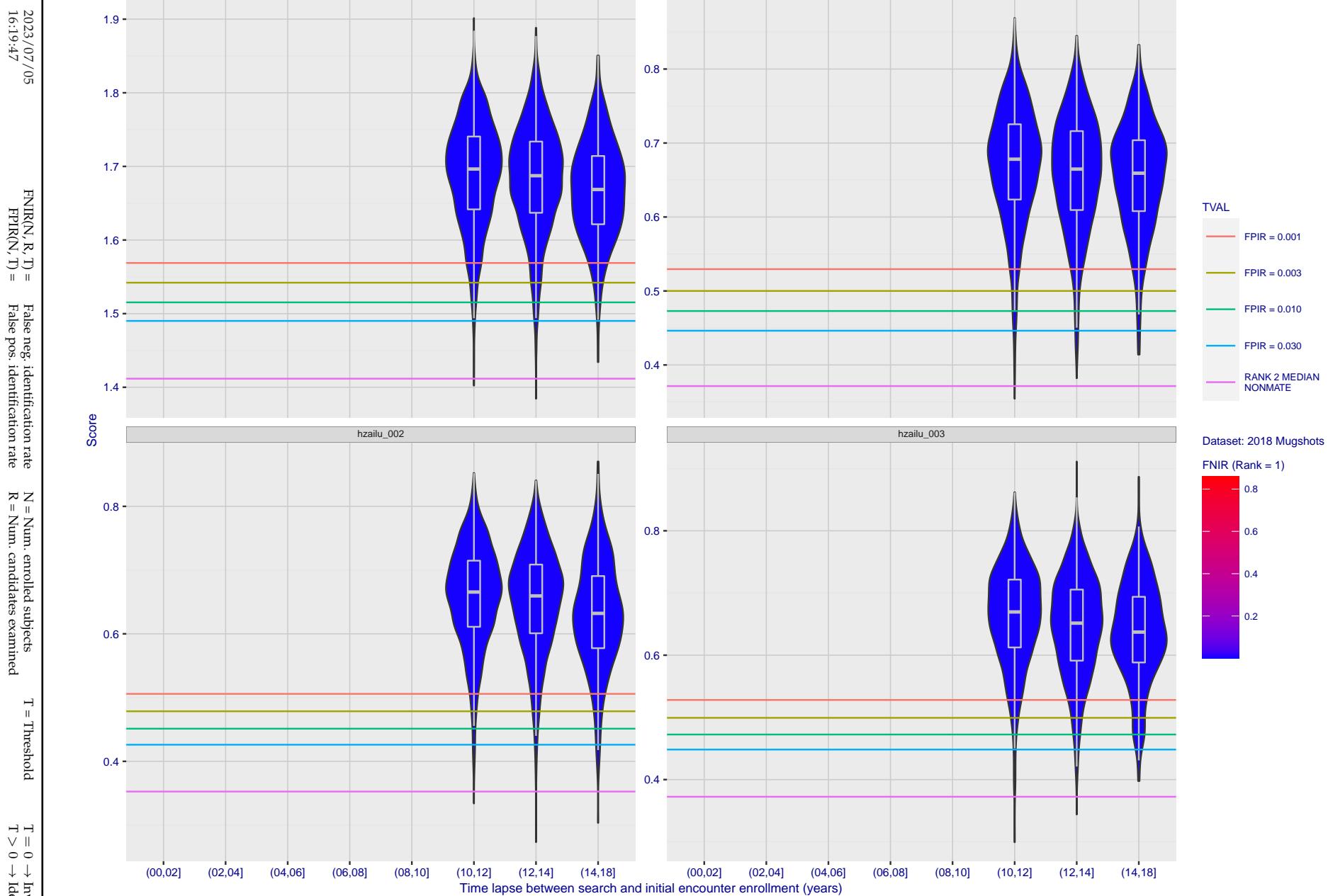


Figure 260: [FRVT-2018 Mugshot Ageing Dataset] Native mate scores vs. time-elapsed. The oldest image of each individual is enrolled. Thereafter, all more recent images are searched. Mated score distributions are computed over all searches noted in row 17 of Table 1 binned by number of years between search and initial enrollment.

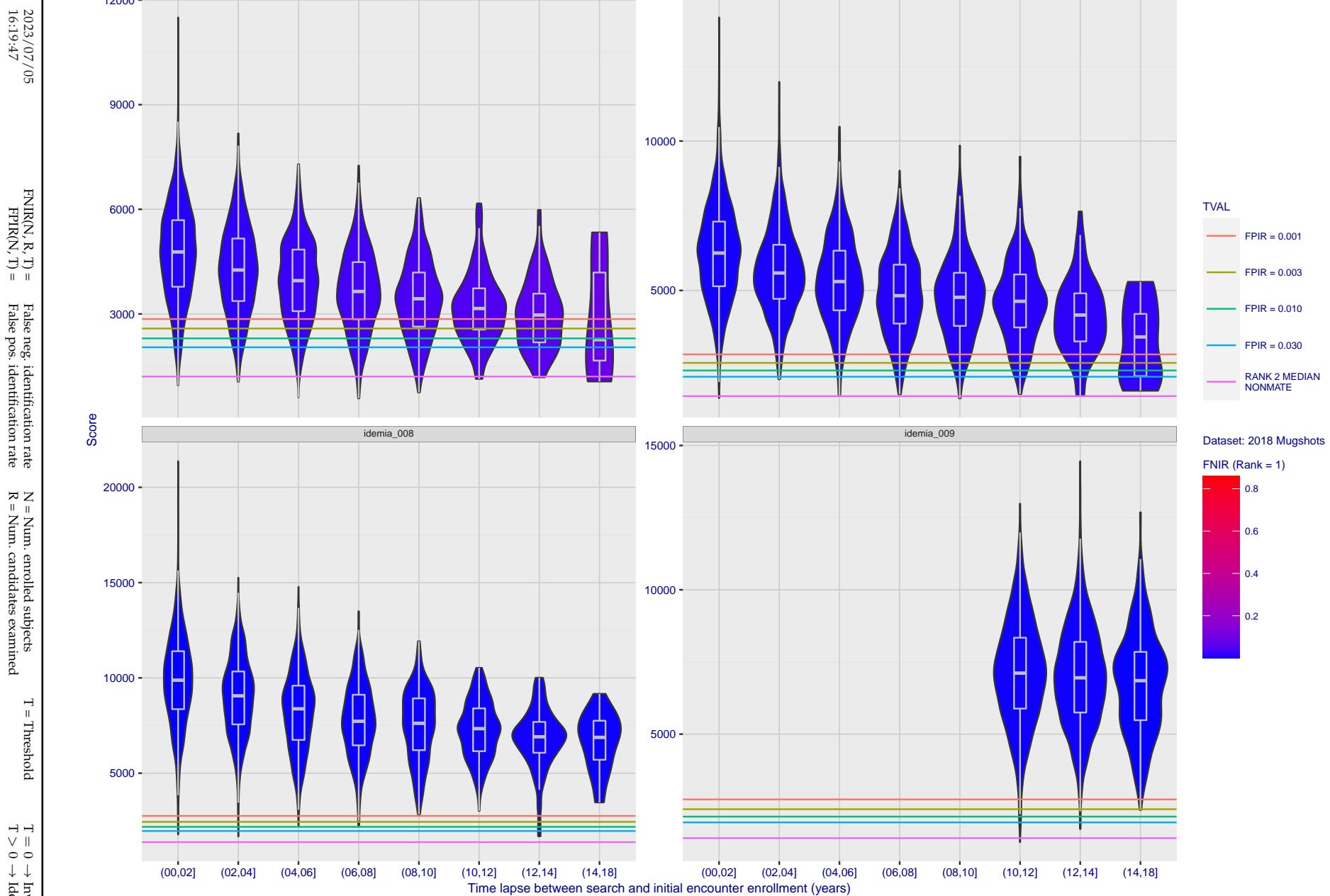


Figure 261: [FRVT-2018 Mugshot Ageing Dataset] Native mate scores vs. time-elapsed. The oldest image of each individual is enrolled. Thereafter, all more recent images are searched. Mated score distributions are computed over all searches noted in row 17 of Table 1 binned by number of years between search and initial enrollment.

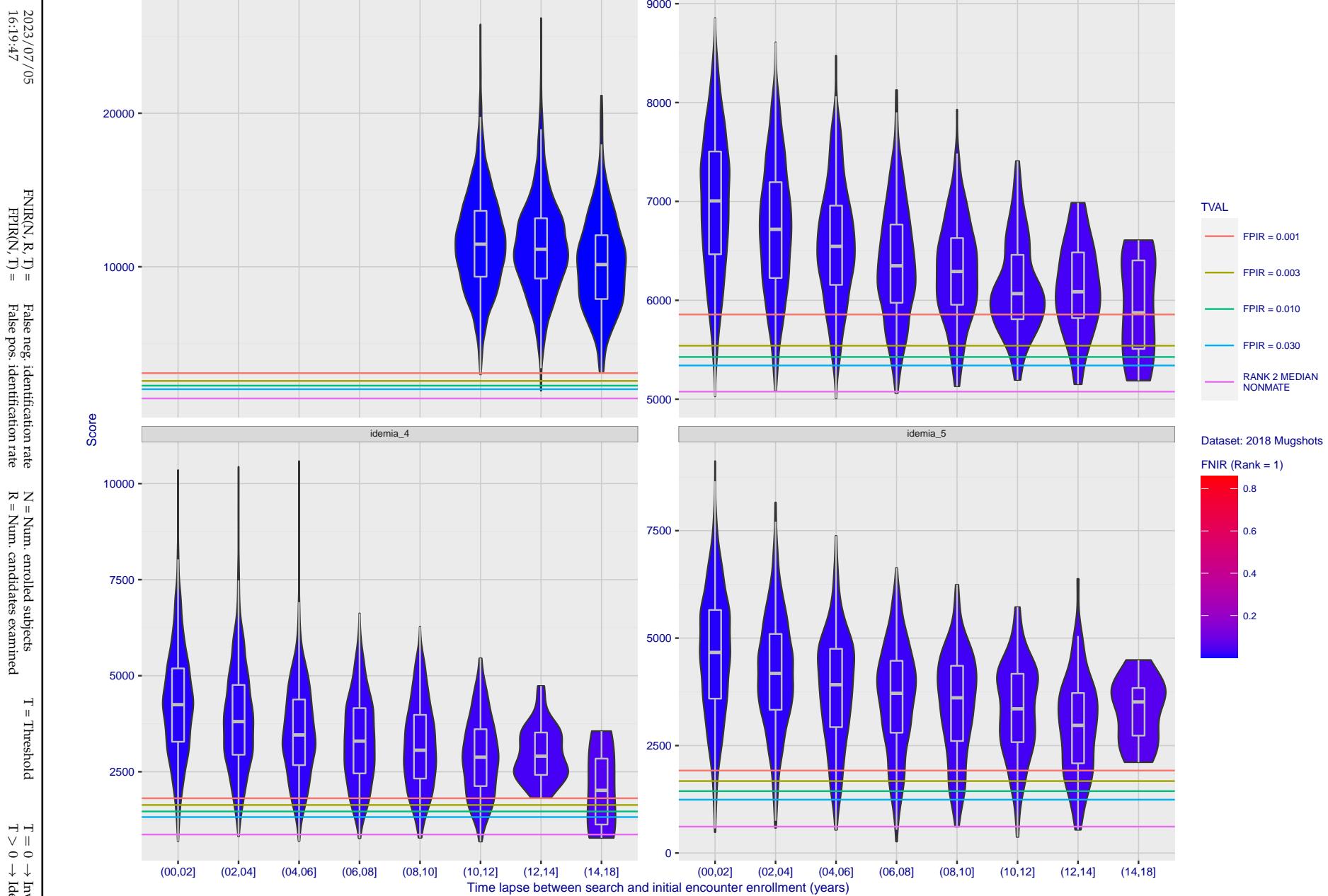


Figure 262: [FRVT-2018 Mugshot Ageing Dataset] Native mate scores vs. time-elapsed. The oldest image of each individual is enrolled. Thereafter, all more recent images are searched. Mated score distributions are computed over all searches noted in row 17 of Table 1 binned by number of years between search and initial enrollment.

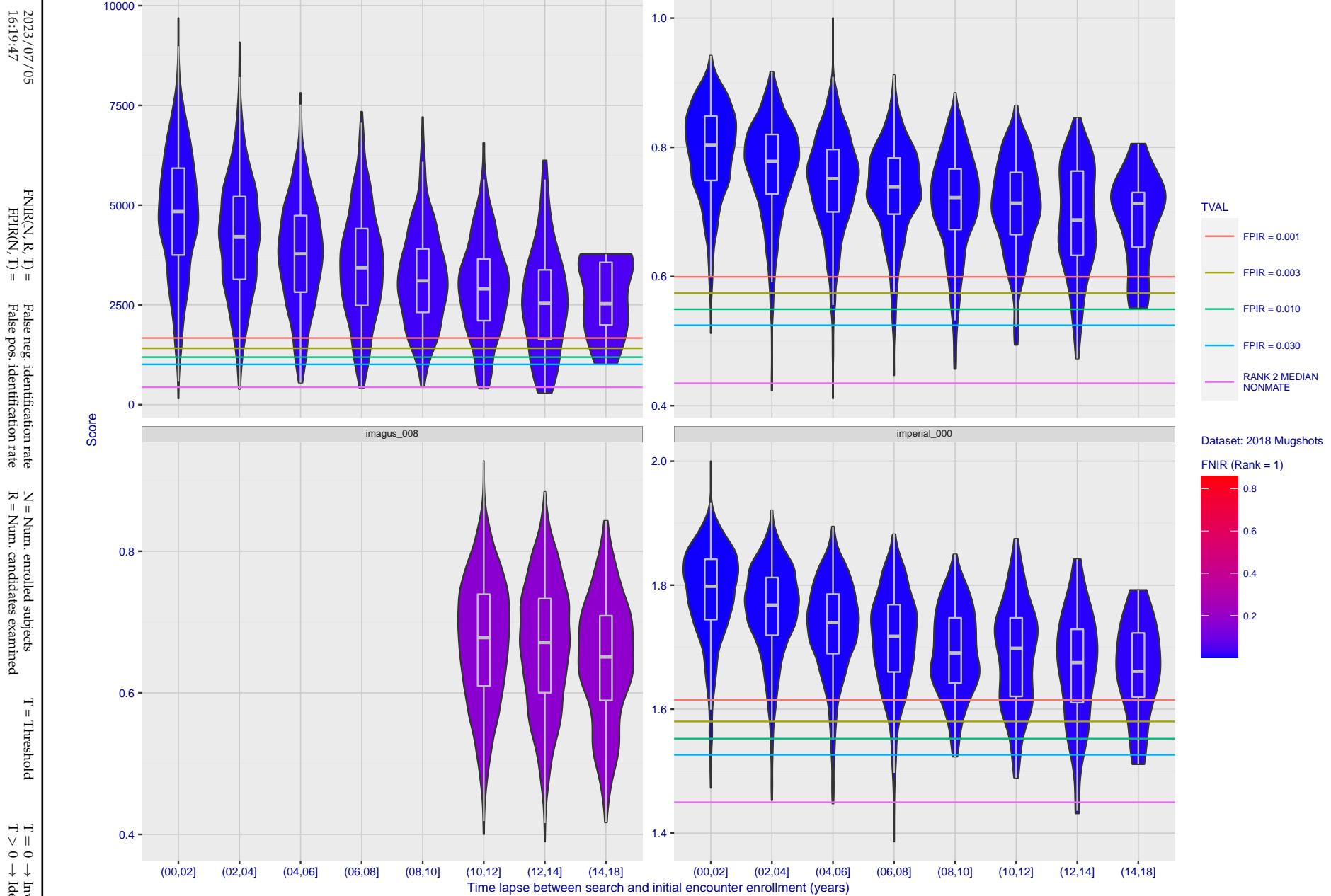


Figure 263: [FRVT-2018 Mugshot Ageing Dataset] Native mate scores vs. time-elapsed. The oldest image of each individual is enrolled. Thereafter, all more recent images are searched. Mated score distributions are computed over all searches noted in row 17 of Table 1 binned by number of years between search and initial enrollment.

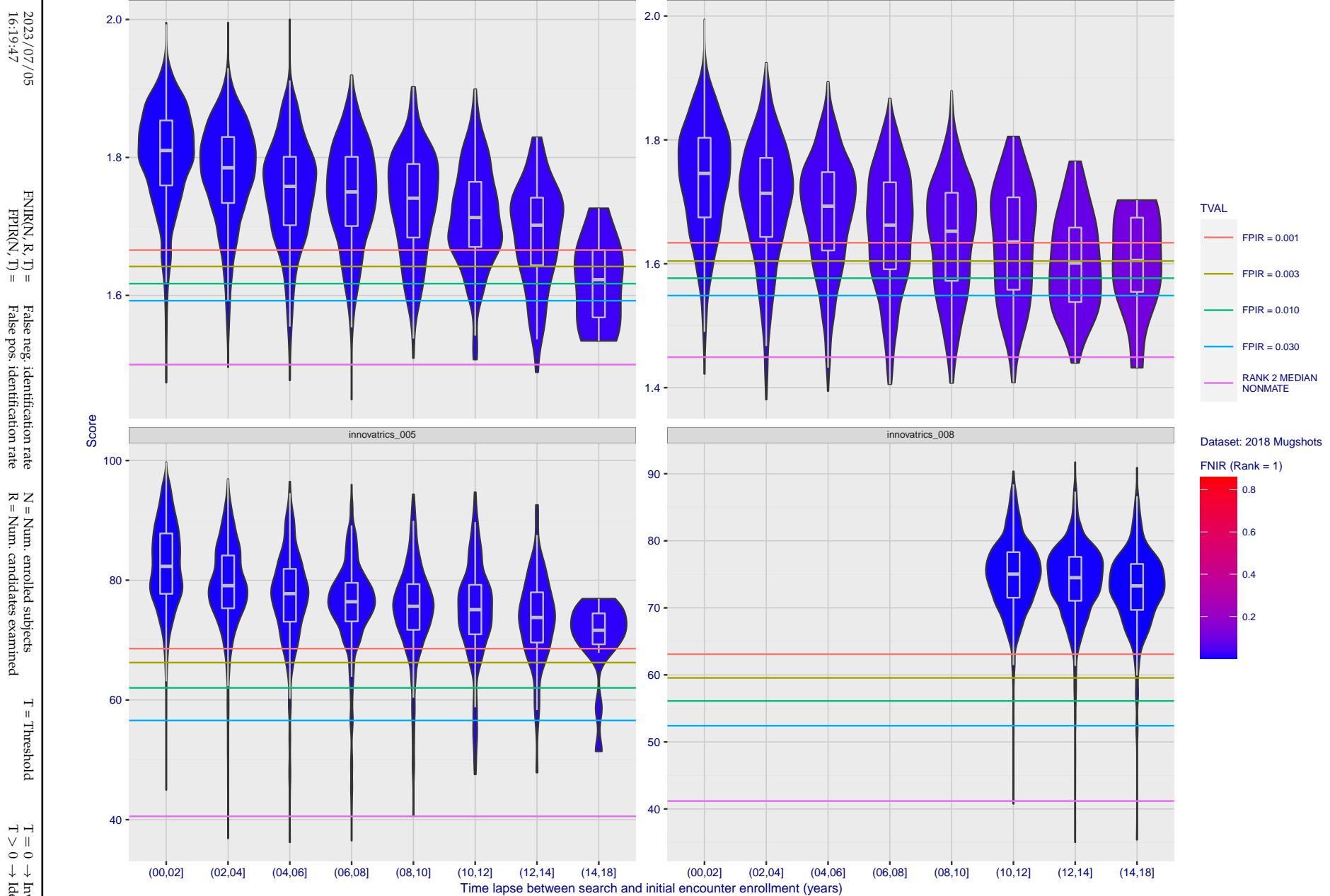


Figure 264: [FRVT-2018 Mugshot Ageing Dataset] Native mate scores vs. time-elapsed. The oldest image of each individual is enrolled. Thereafter, all more recent images are searched. Mated score distributions are computed over all searches noted in row 17 of Table 1 binned by number of years between search and initial enrollment.

2023/07/05
16:19:47FNIR(N, R, T) = False neg. identification rate
FPTR(N, T) = False pos. identification rateN = Num. enrolled subjects
R = Num. candidates examinedT = Threshold
T = 0 → Investigation

T > 0 → Identification

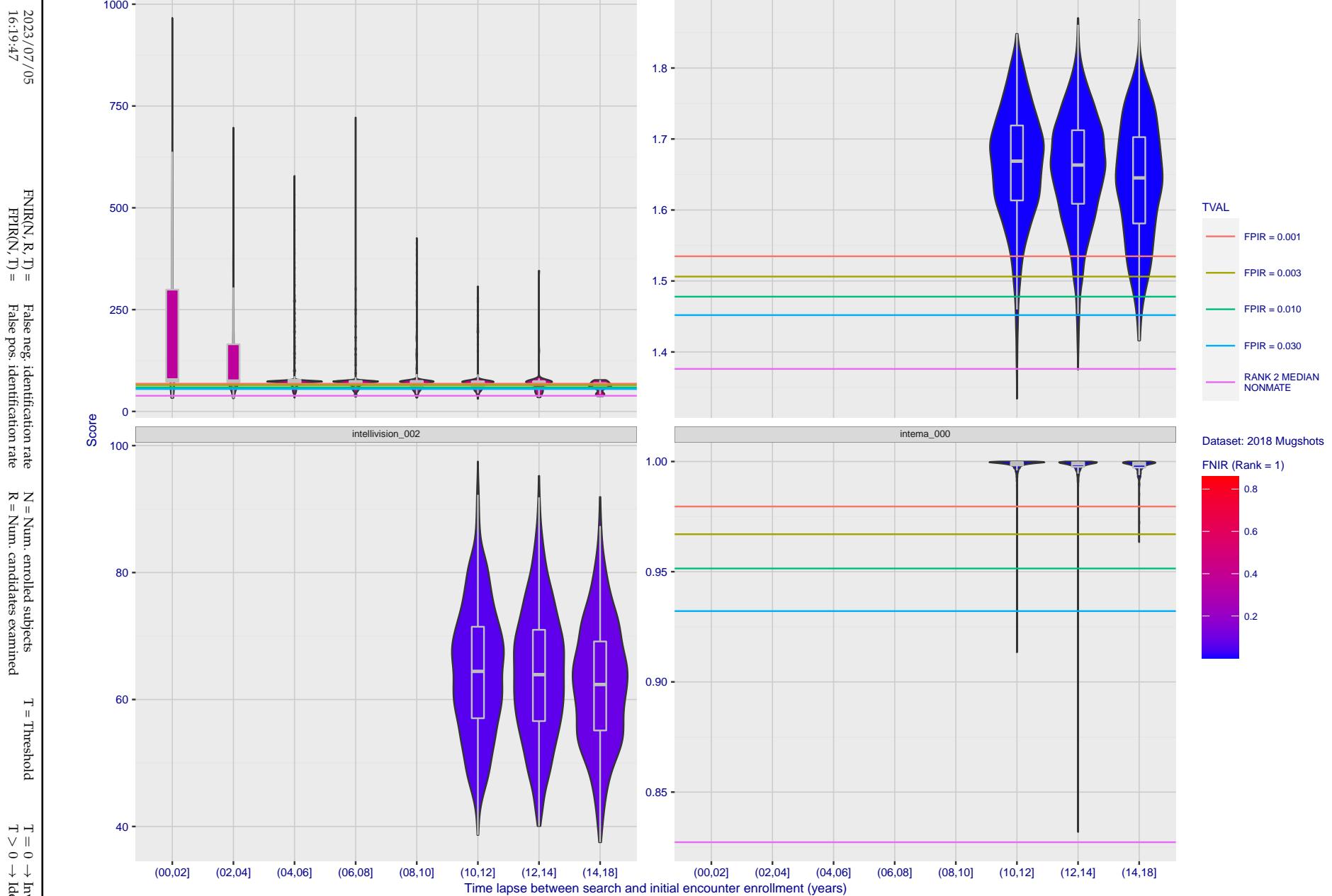


Figure 265: [FRVT-2018 Mugshot Ageing Dataset] Native mate scores vs. time-elapsed. The oldest image of each individual is enrolled. Thereafter, all more recent images are searched. Mated score distributions are computed over all searches noted in row 17 of Table 1 binned by number of years between search and initial enrollment.

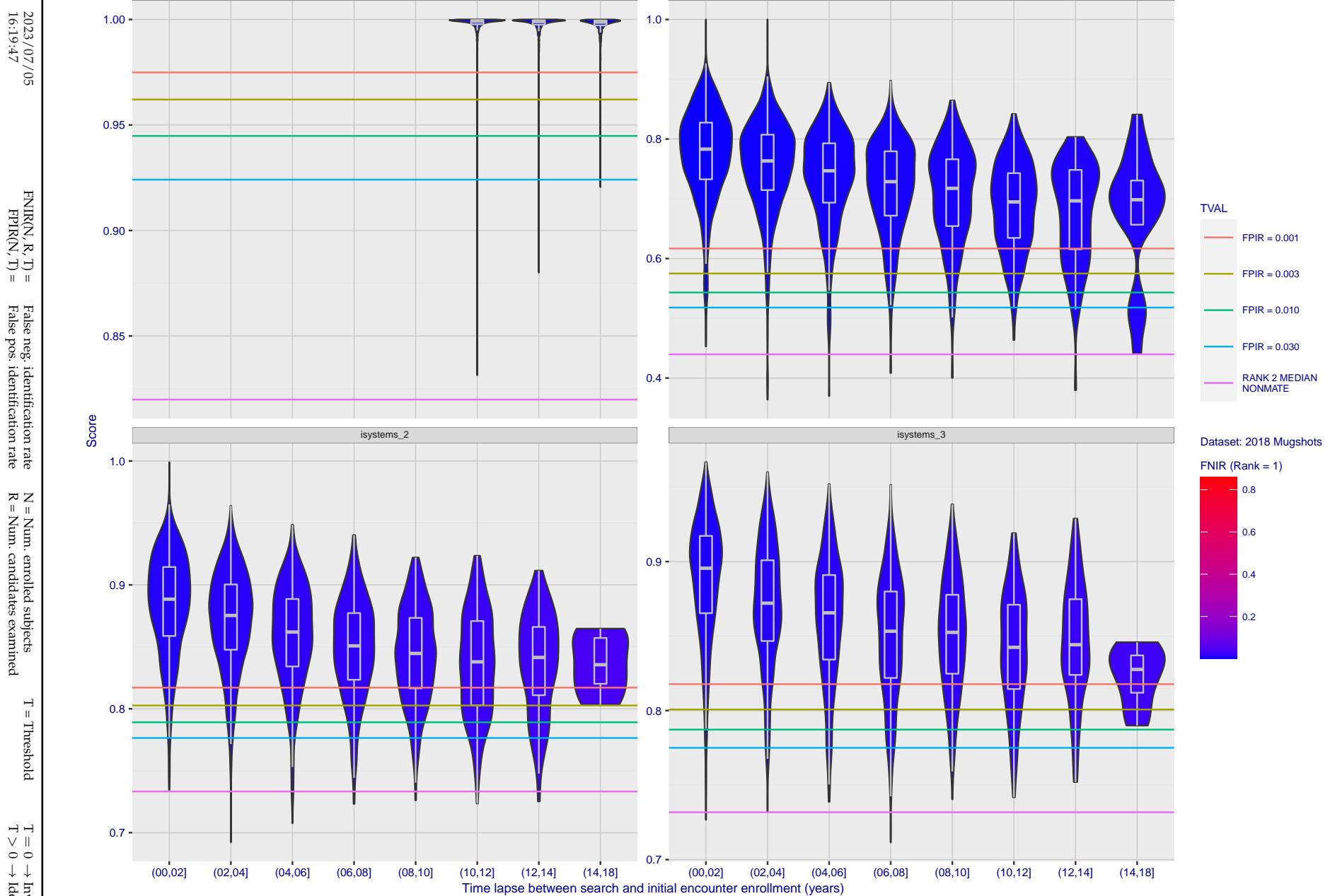


Figure 266: [FRVT-2018 Mugshot Ageing Dataset] Native mate scores vs. time-elapsed. The oldest image of each individual is enrolled. Thereafter, all more recent images are searched. Mated score distributions are computed over all searches noted in row 17 of Table 1 binned by number of years between search and initial enrollment.

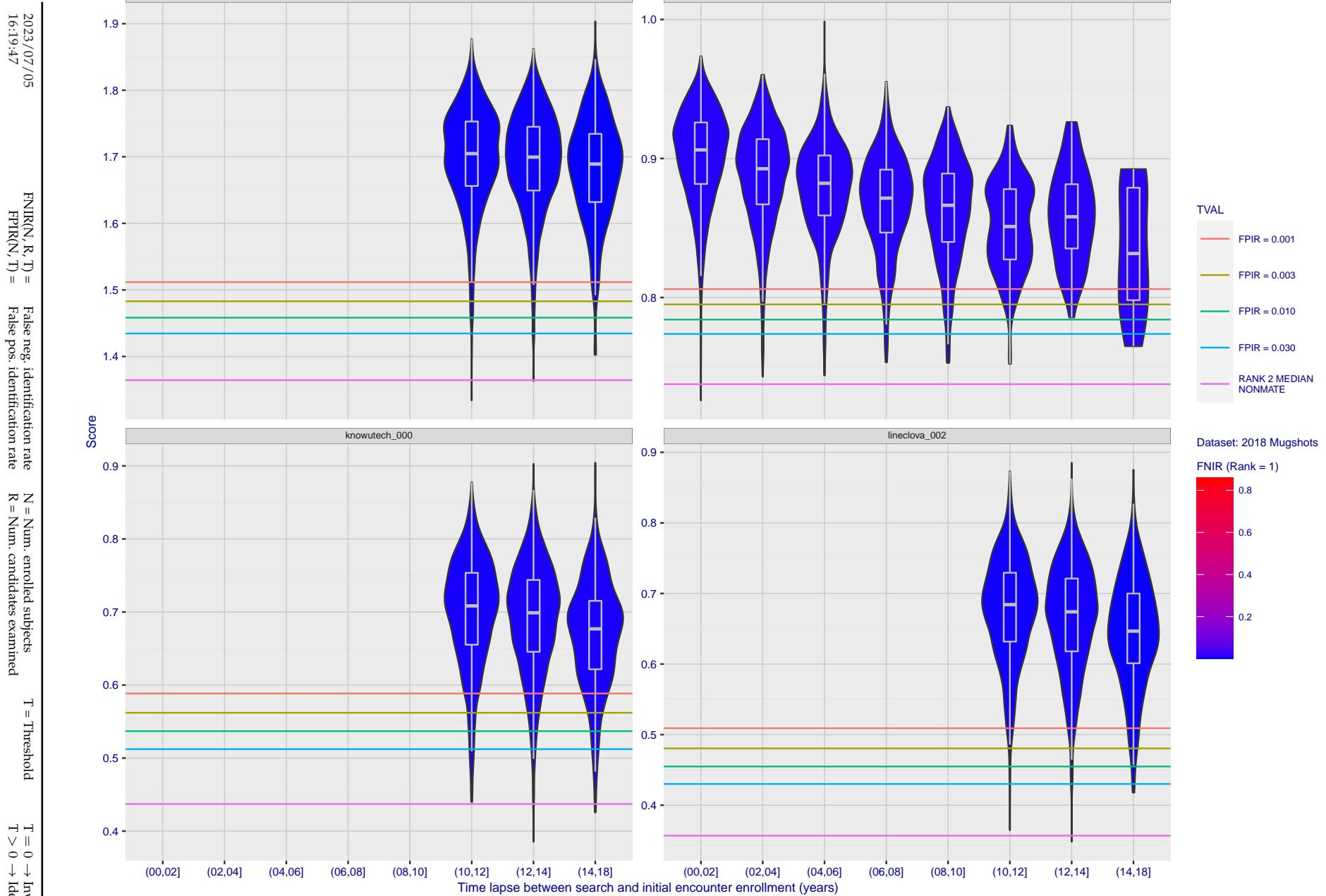


Figure 267: [FRVT-2018 Mugshot Ageing Dataset] Native mate scores vs. time-elapsed. The oldest image of each individual is enrolled. Thereafter, all more recent images are searched. Mated score distributions are computed over all searches noted in row 17 of Table 1 binned by number of years between search and initial enrollment.

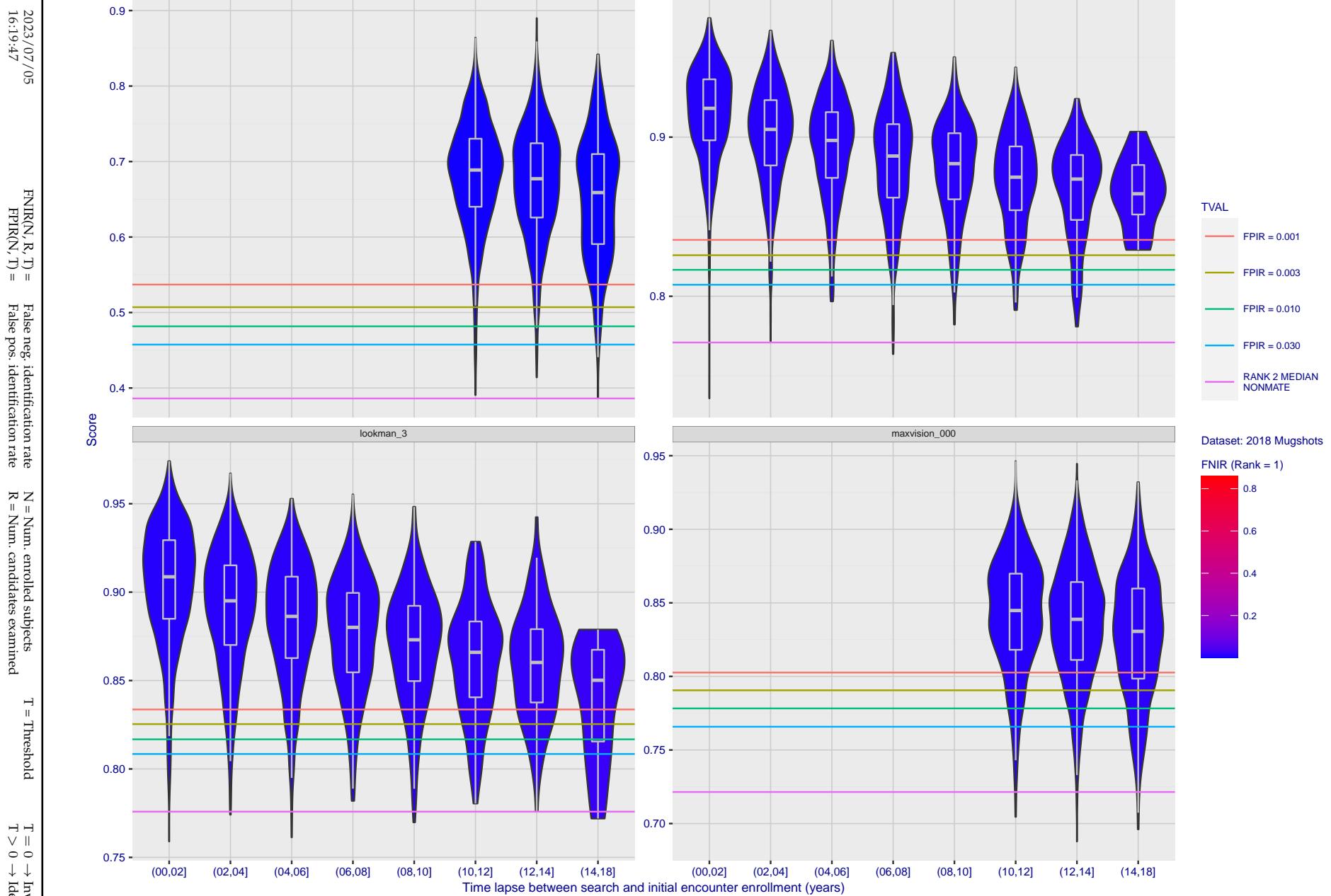


Figure 268: [FRVT-2018 Mugshot Ageing Dataset] Native mate scores vs. time-elapsed. The oldest image of each individual is enrolled. Thereafter, all more recent images are searched. Mated score distributions are computed over all searches noted in row 17 of Table 1 binned by number of years between search and initial enrollment.

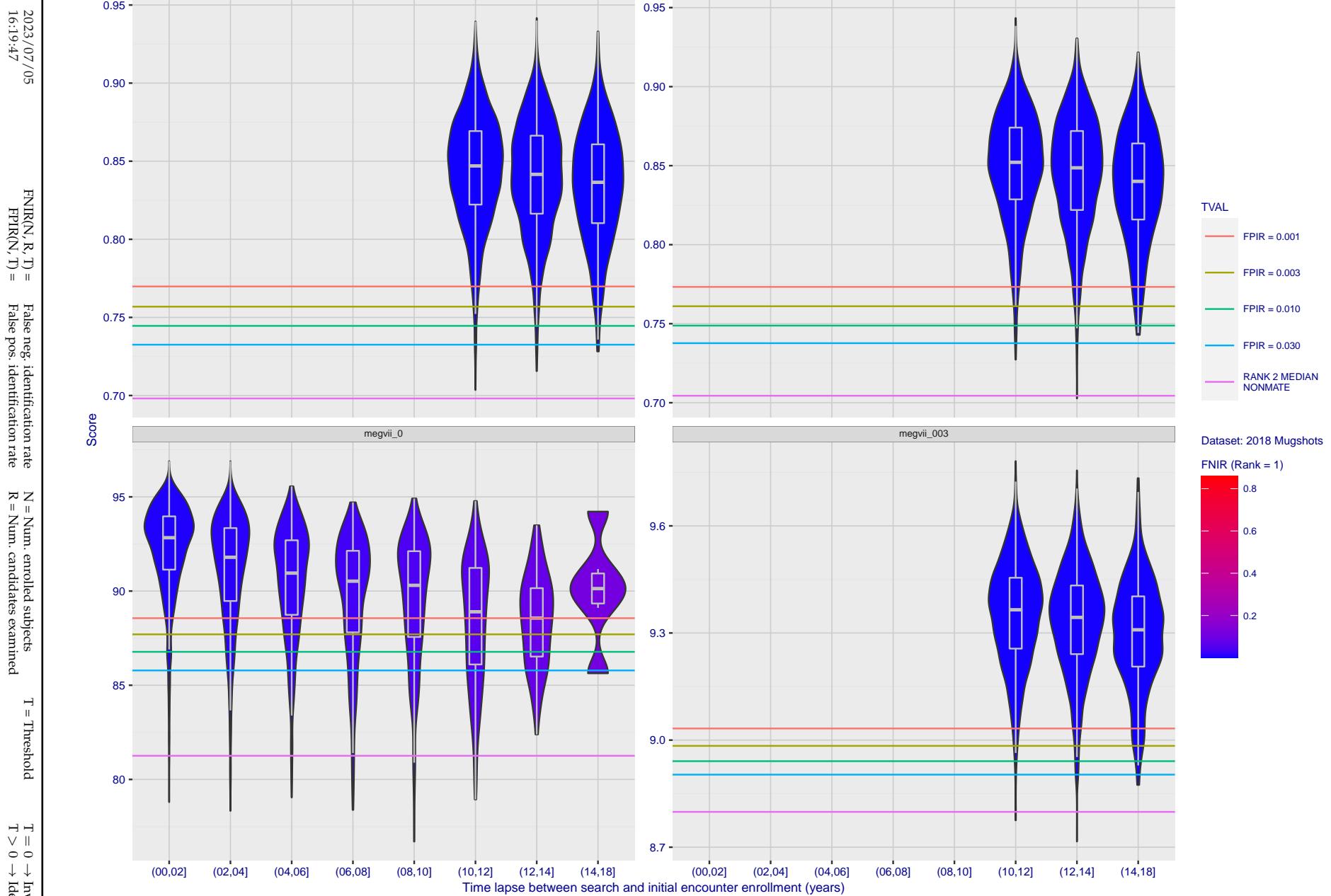


Figure 269: [FRVT-2018 Mugshot Ageing Dataset] Native mate scores vs. time-elapsed. The oldest image of each individual is enrolled. Thereafter, all more recent images are searched. Mated score distributions are computed over all searches noted in row 17 of Table 1 binned by number of years between search and initial enrollment.

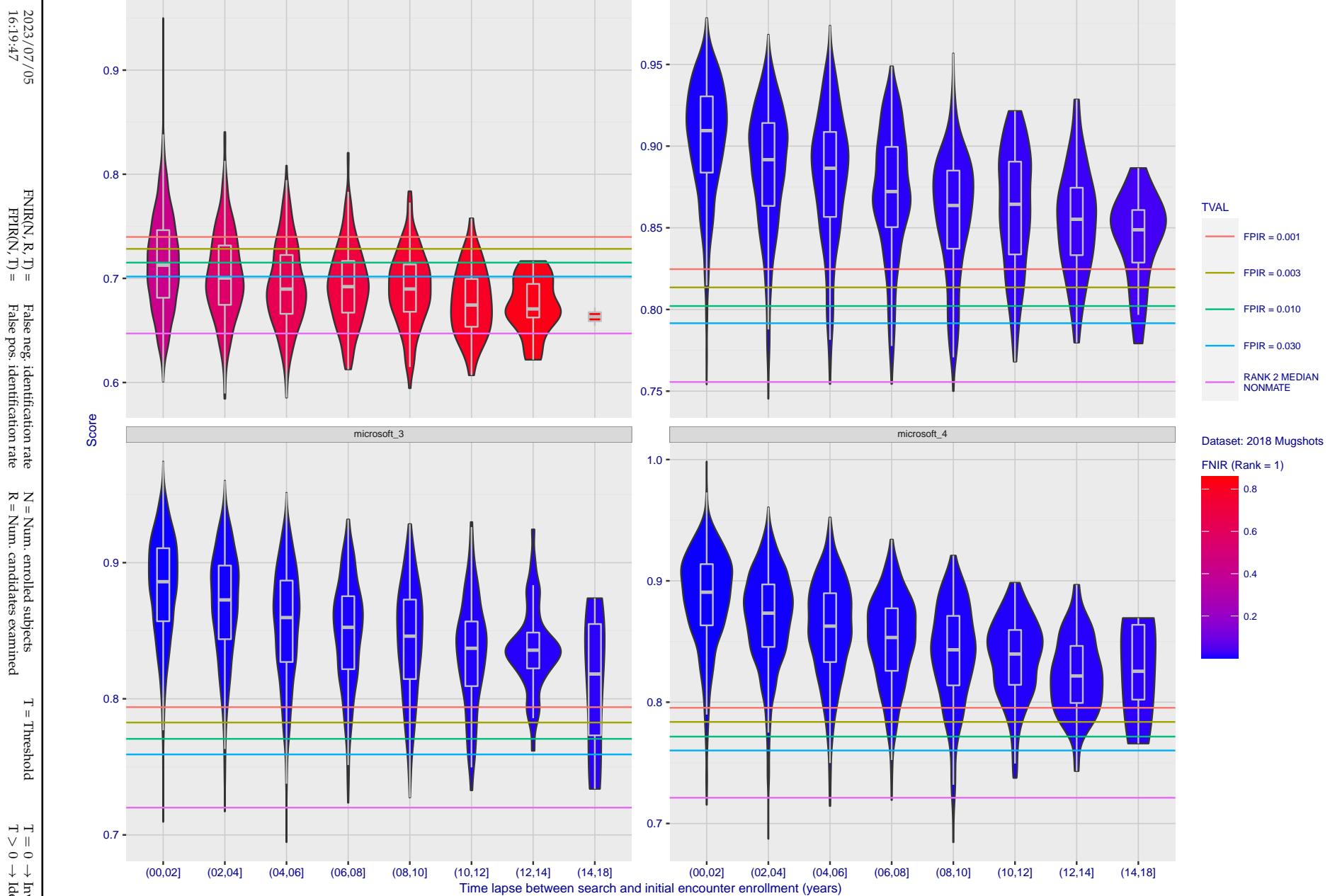


Figure 270: [FRVT-2018 Mugshot Ageing Dataset] Native mate scores vs. time-elapsed. The oldest image of each individual is enrolled. Thereafter, all more recent images are searched. Mated score distributions are computed over all searches noted in row 17 of Table 1 binned by number of years between search and initial enrollment.

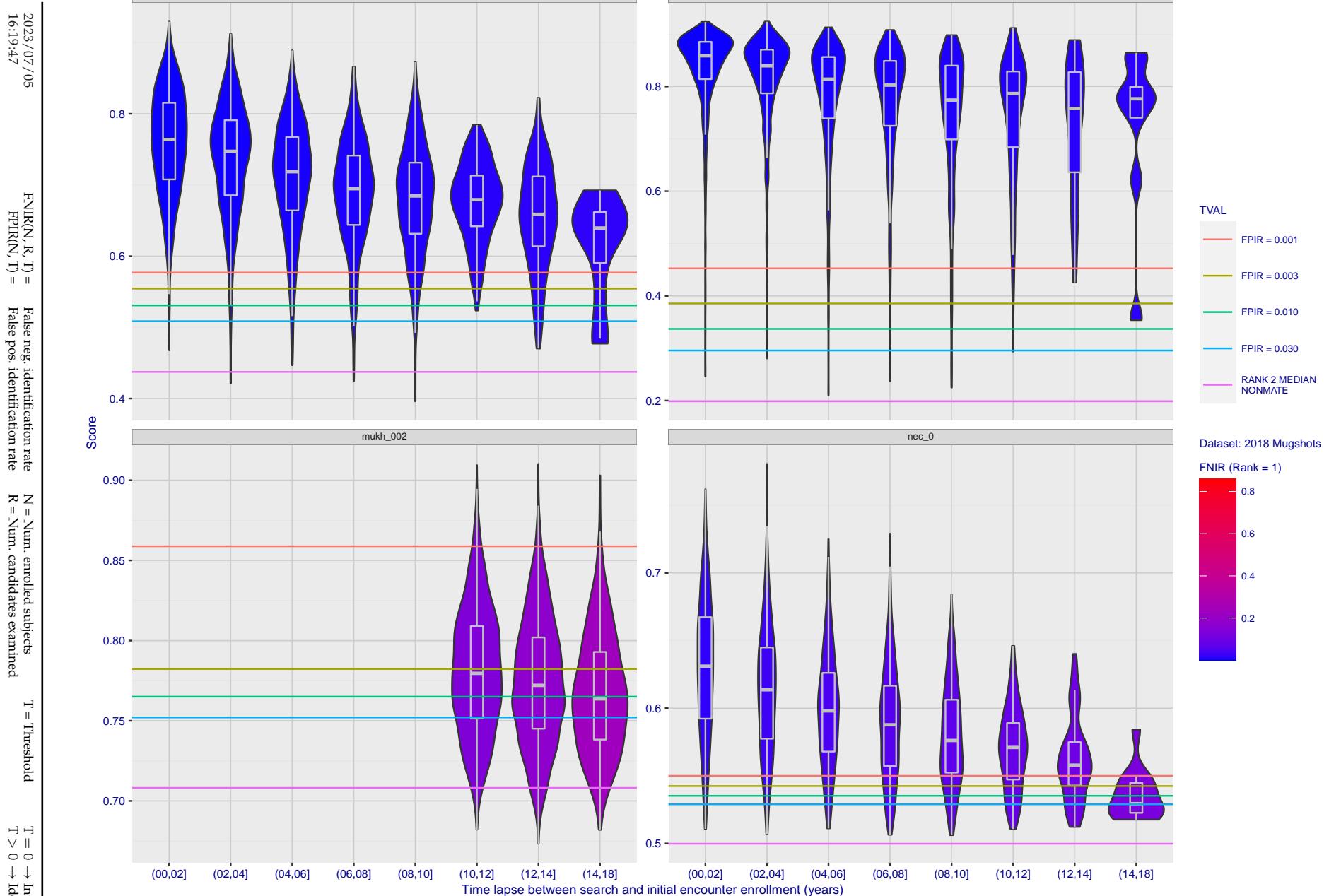


Figure 271: [FRVT-2018 Mugshot Ageing Dataset] Native mate scores vs. time-elapsed. The oldest image of each individual is enrolled. Thereafter, all more recent images are searched. Mated score distributions are computed over all searches noted in row 17 of Table 1 binned by number of years between search and initial enrollment.

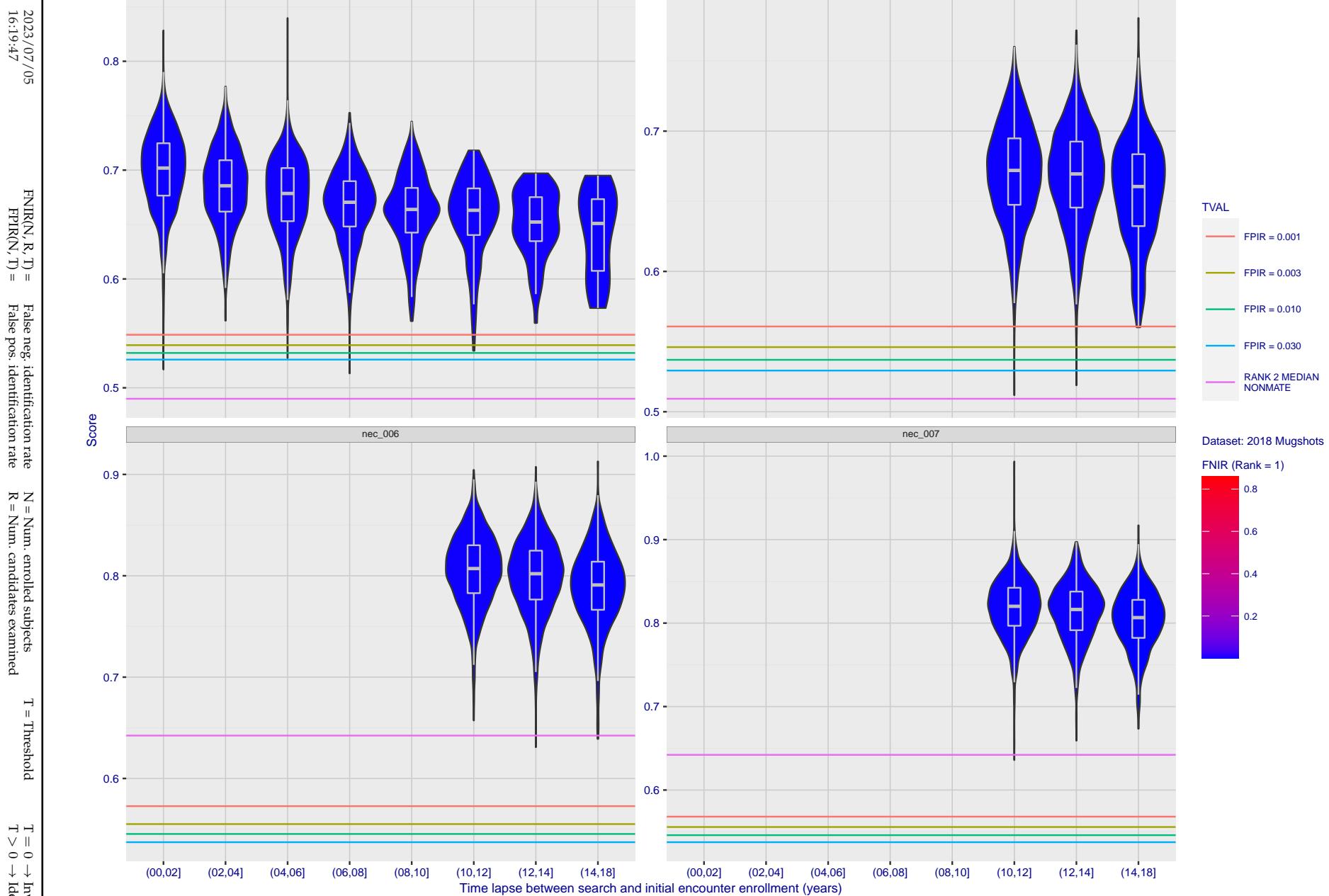


Figure 272: [FRVT-2018 Mugshot Ageing Dataset] Native mate scores vs. time-elapsed. The oldest image of each individual is enrolled. Thereafter, all more recent images are searched. Mated score distributions are computed over all searches noted in row 17 of Table 1 binned by number of years between search and initial enrollment.

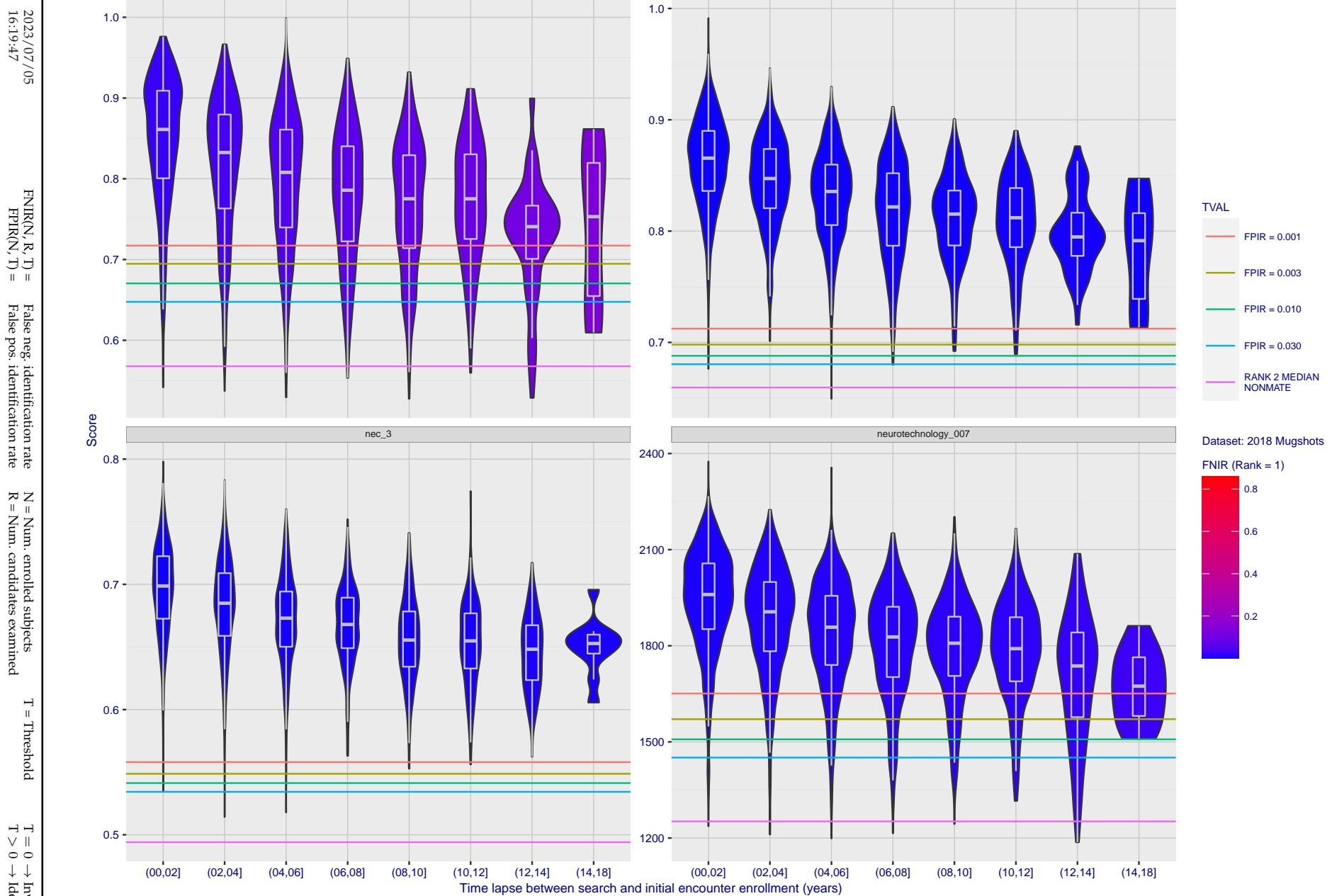


Figure 273: [FRVT-2018 Mugshot Ageing Dataset] Native mate scores vs. time-elapsed. The oldest image of each individual is enrolled. Thereafter, all more recent images are searched. Mated score distributions are computed over all searches noted in row 17 of Table 1 binned by number of years between search and initial enrollment.

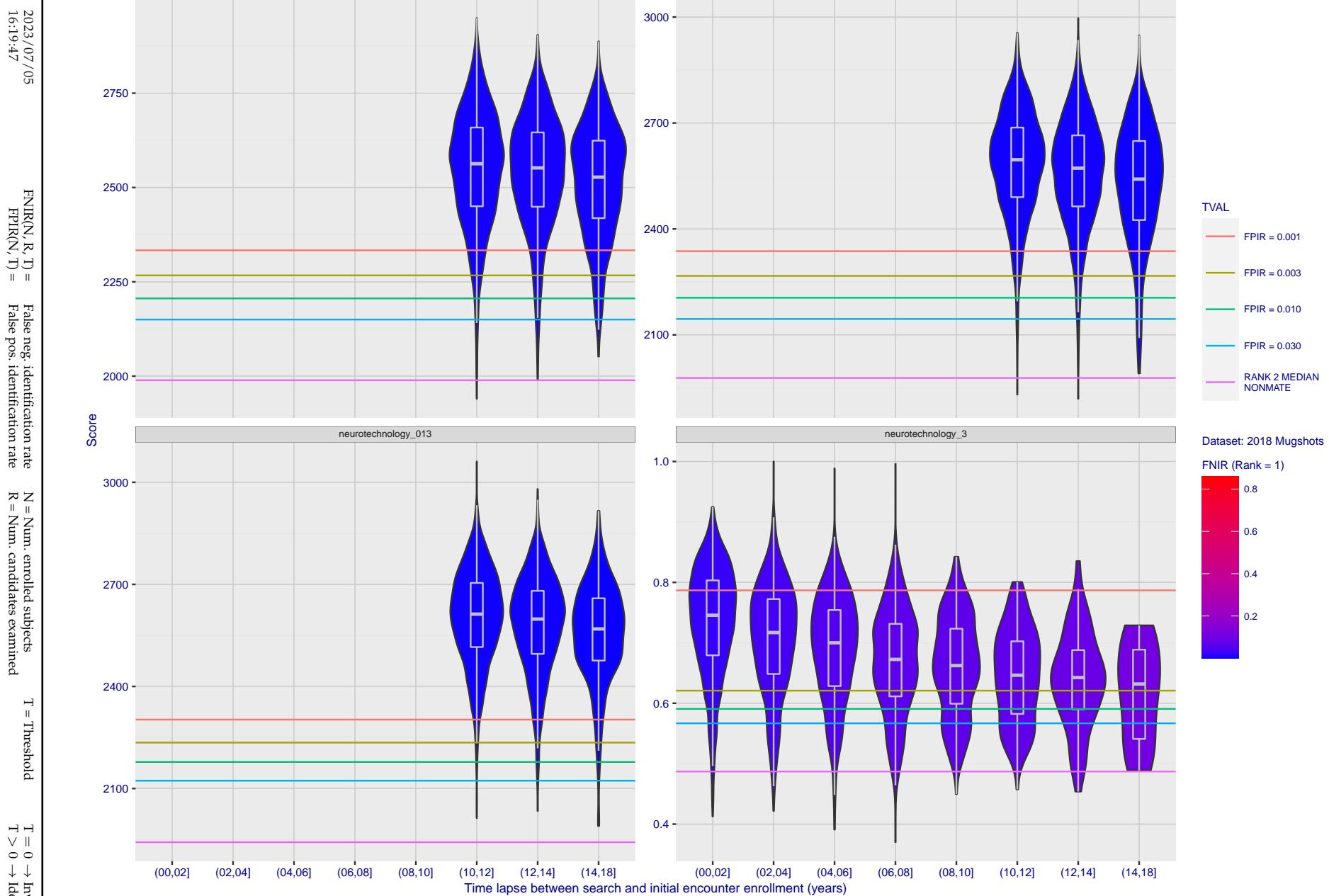


Figure 274: [FRVT-2018 Mugshot Ageing Dataset] Native mate scores vs. time-elapsed. The oldest image of each individual is enrolled. Thereafter, all more recent images are searched. Mated score distributions are computed over all searches noted in row 17 of Table 1 binned by number of years between search and initial enrollment.

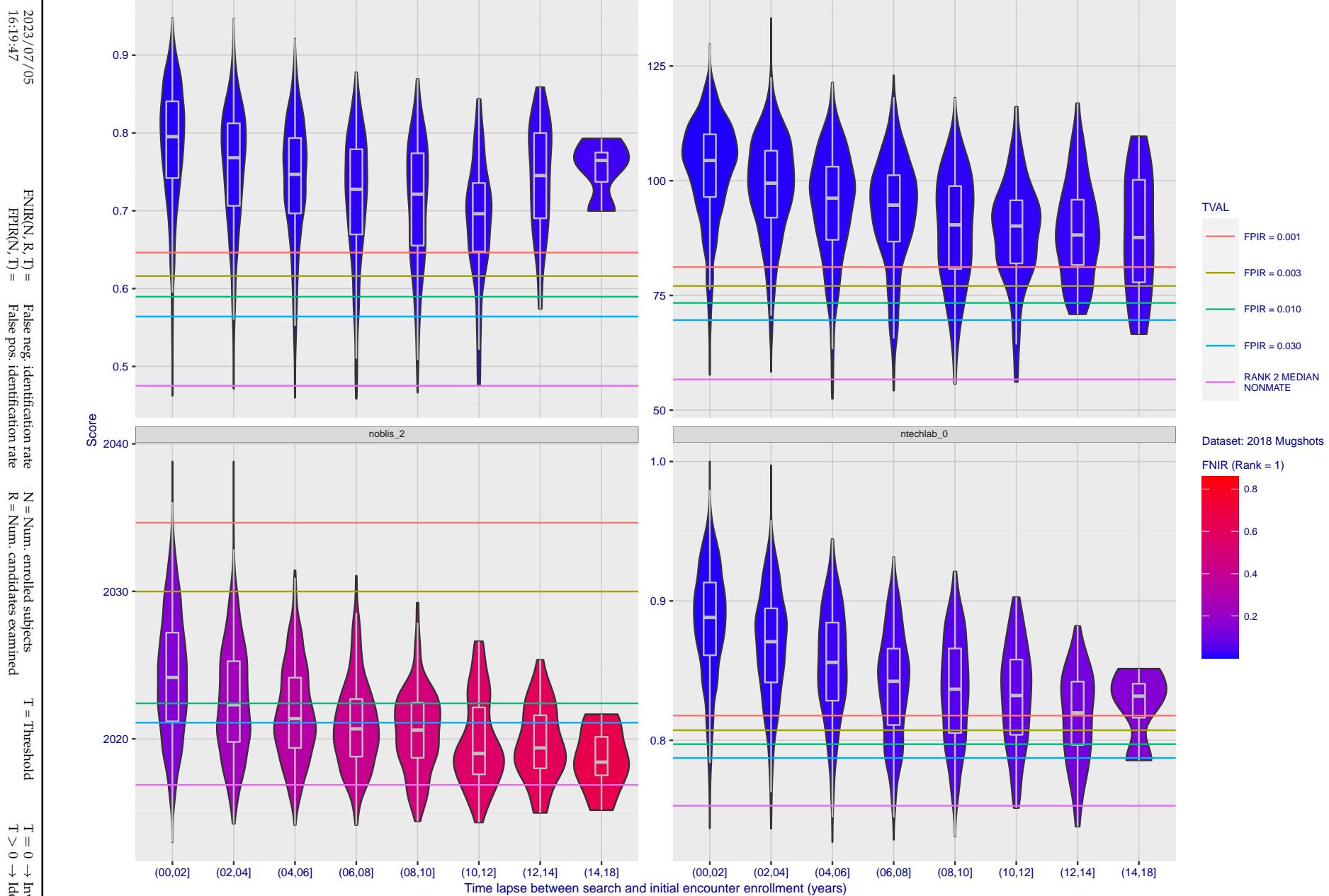


Figure 275: [FRVT-2018 Mugshot Ageing Dataset] Native mate scores vs. time-elapsed. The oldest image of each individual is enrolled. Thereafter, all more recent images are searched. Mated score distributions are computed over all searches noted in row 17 of Table 1 binned by number of years between search and initial enrollment.

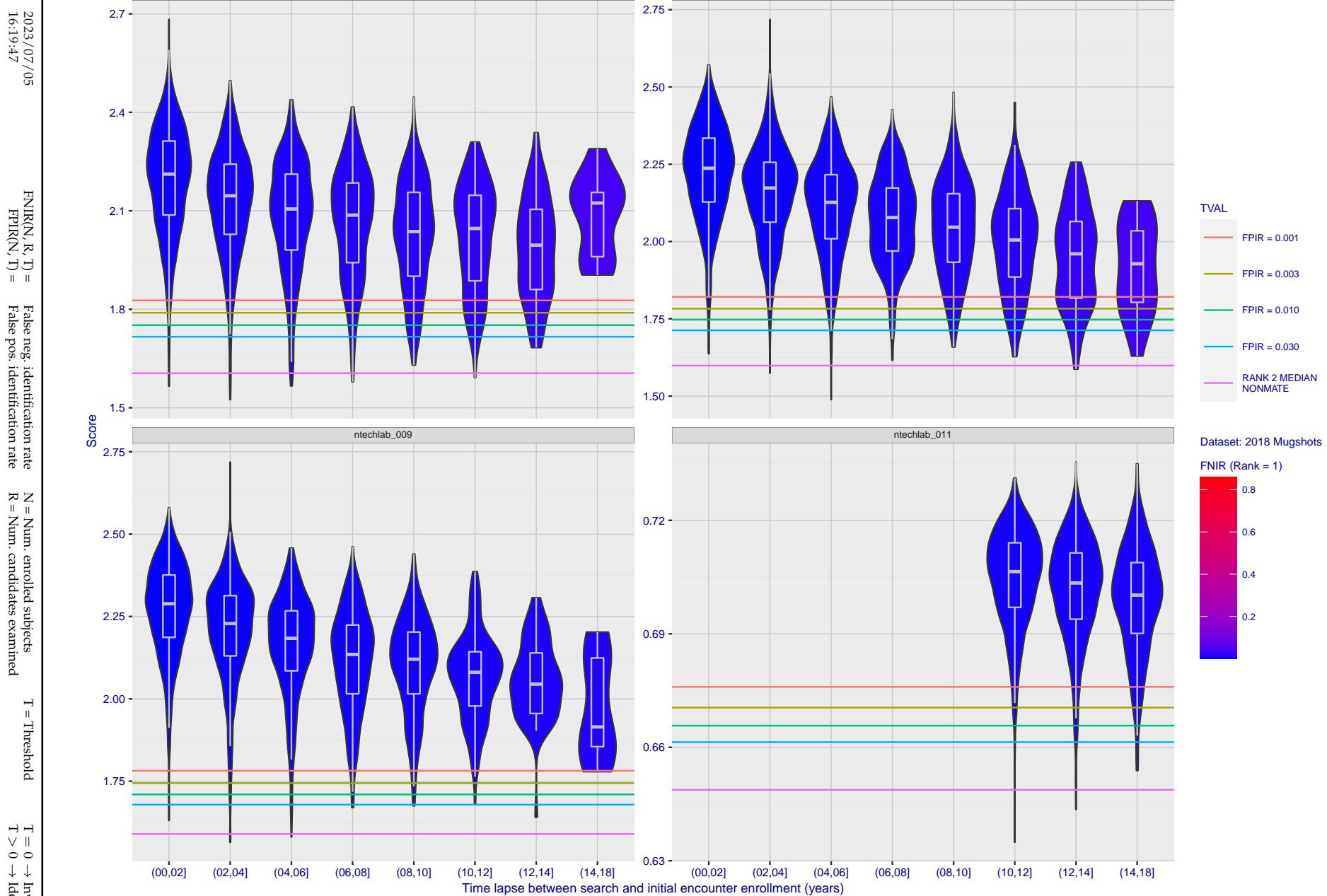


Figure 276: [FRVT-2018 Mugshot Ageing Dataset] Native mate scores vs. time-elapsed. The oldest image of each individual is enrolled. Thereafter, all more recent images are searched. Mated score distributions are computed over all searches noted in row 17 of Table 1 binned by number of years between search and initial enrollment.

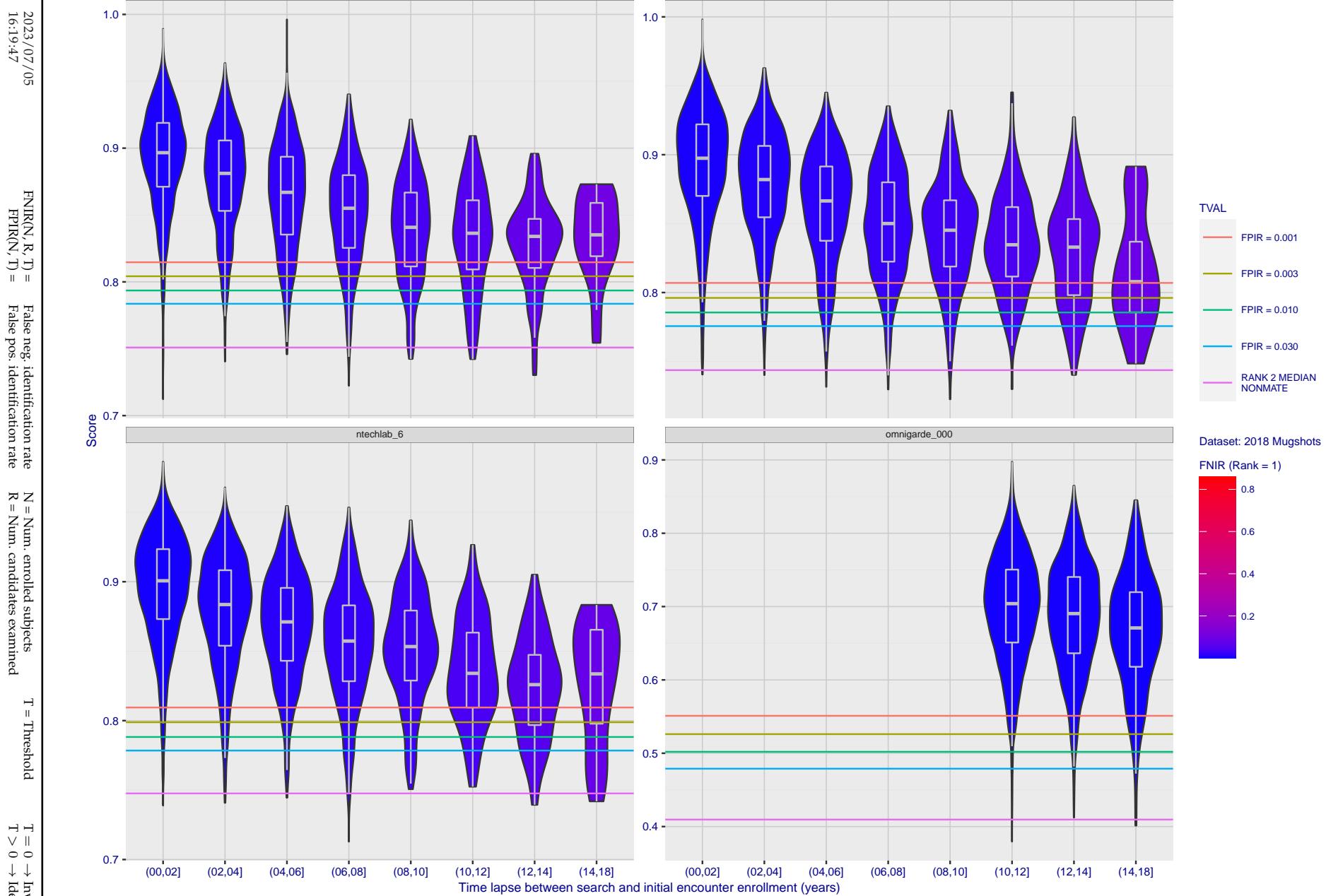


Figure 277: [FRVT-2018 Mugshot Ageing Dataset] Native mate scores vs. time-elapsed. The oldest image of each individual is enrolled. Thereafter, all more recent images are searched. Mated score distributions are computed over all searches noted in row 17 of Table 1 binned by number of years between search and initial enrollment.

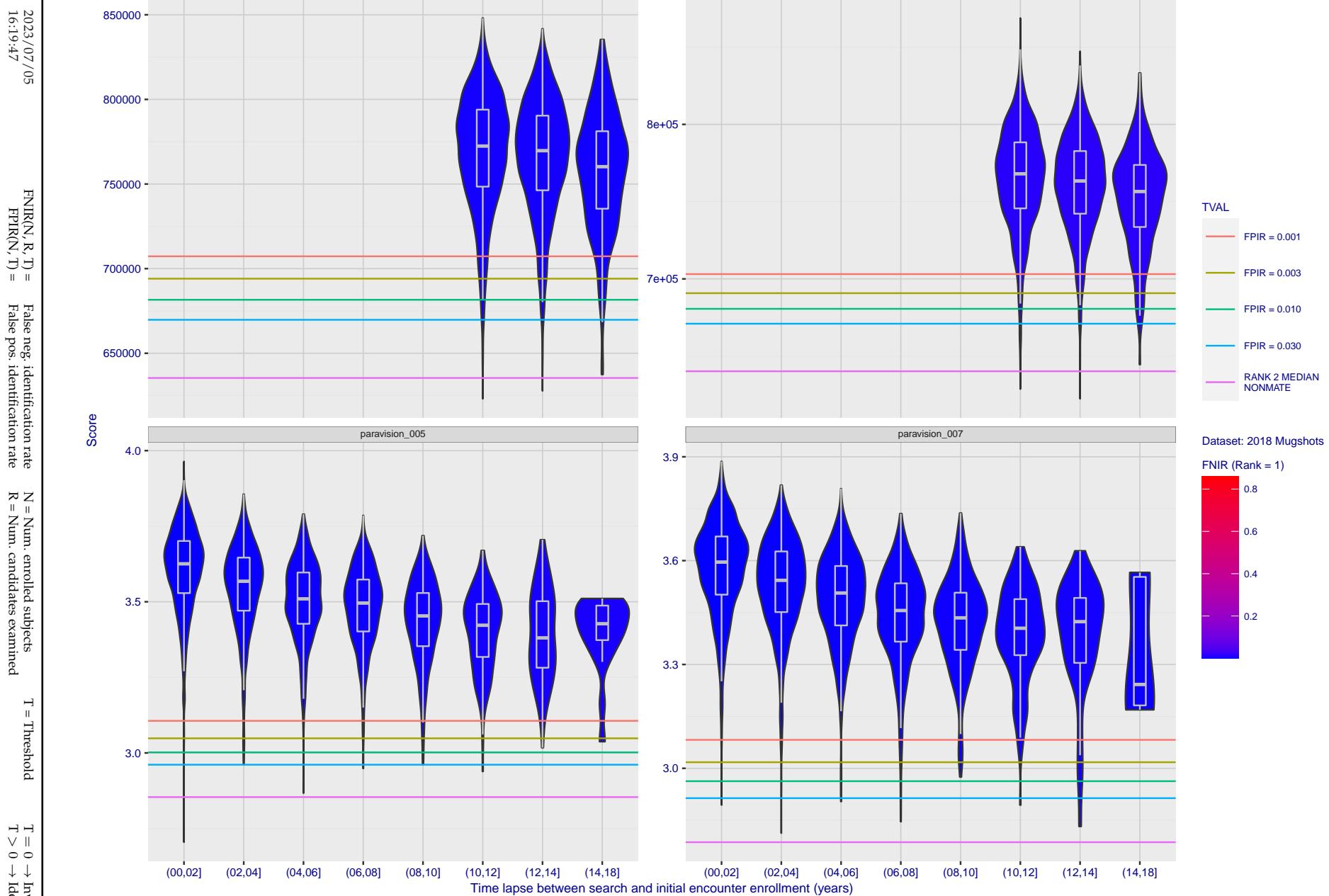


Figure 278: [FRVT-2018 Mugshot Ageing Dataset] Native mate scores vs. time-elapsed. The oldest image of each individual is enrolled. Thereafter, all more recent images are searched. Mated score distributions are computed over all searches noted in row 17 of Table 1 binned by number of years between search and initial enrollment.

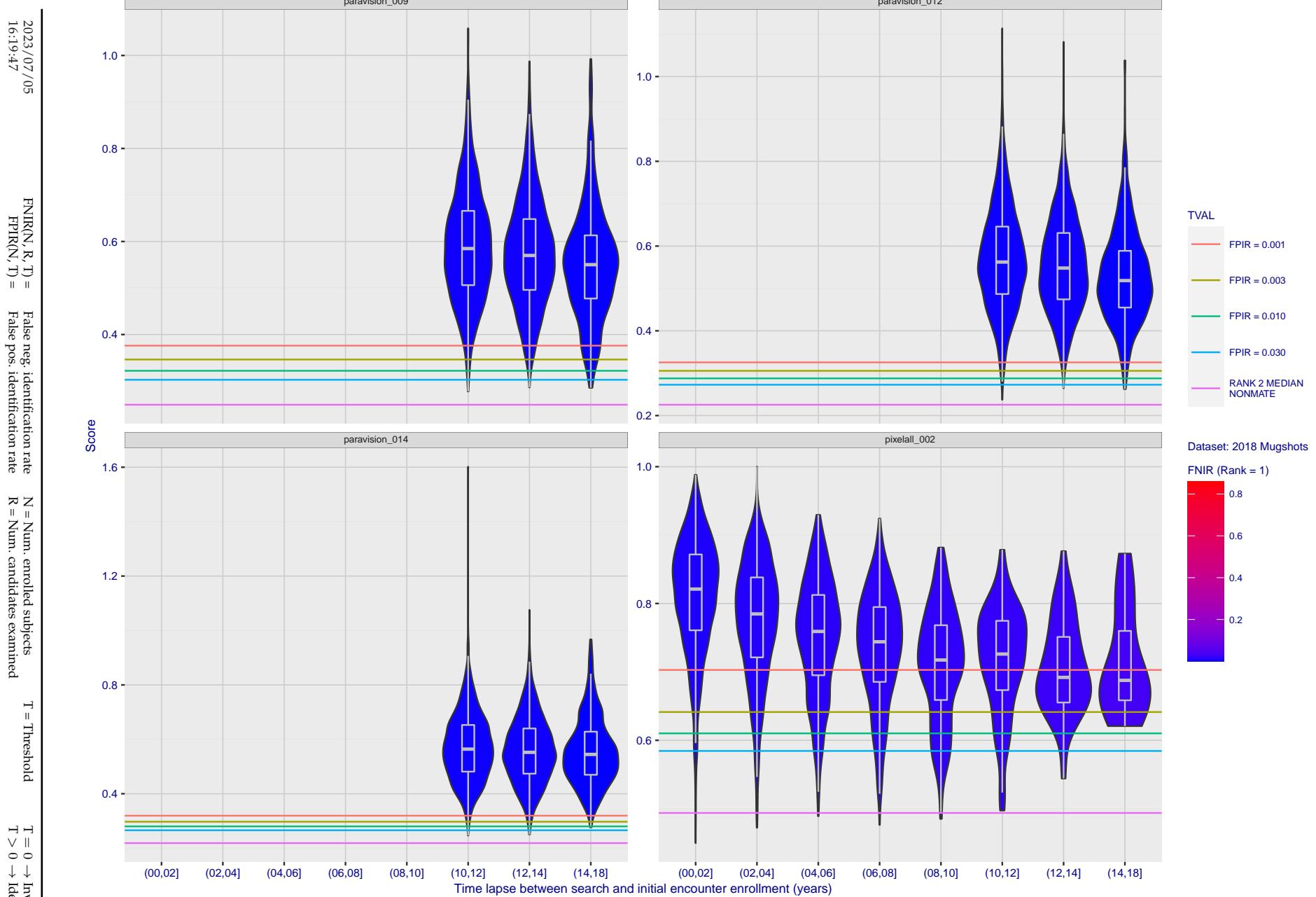


Figure 279: [FRVT-2018 Mugshot Ageing Dataset] Native mate scores vs. time-elapsed. The oldest image of each individual is enrolled. Thereafter, all more recent images are searched. Mated score distributions are computed over all searches noted in row 17 of Table 1 binned by number of years between search and initial enrollment.

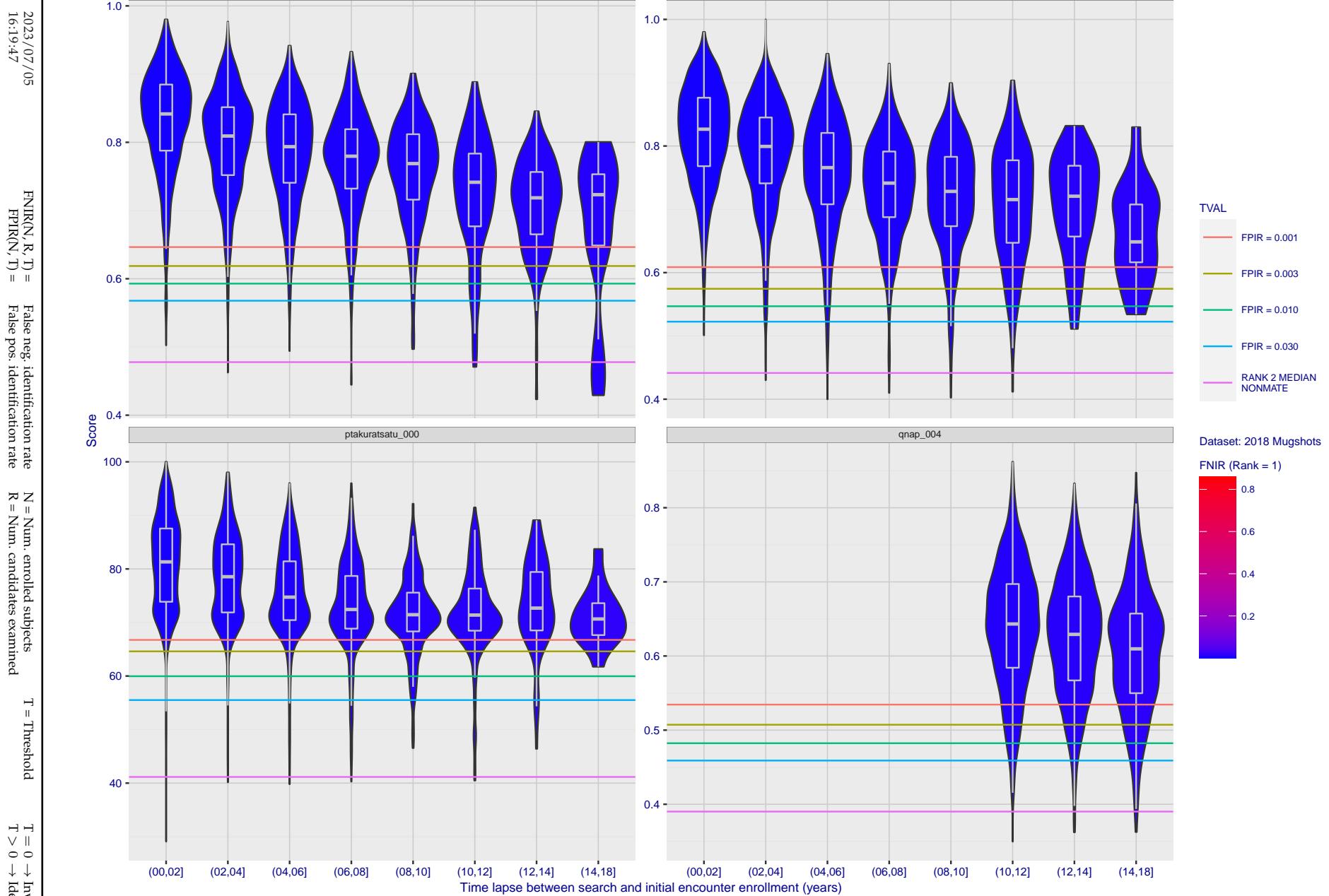


Figure 280: [FRVT-2018 Mugshot Ageing Dataset] Native mate scores vs. time-elapsed. The oldest image of each individual is enrolled. Thereafter, all more recent images are searched. Mated score distributions are computed over all searches noted in row 17 of Table 1 binned by number of years between search and initial enrollment.

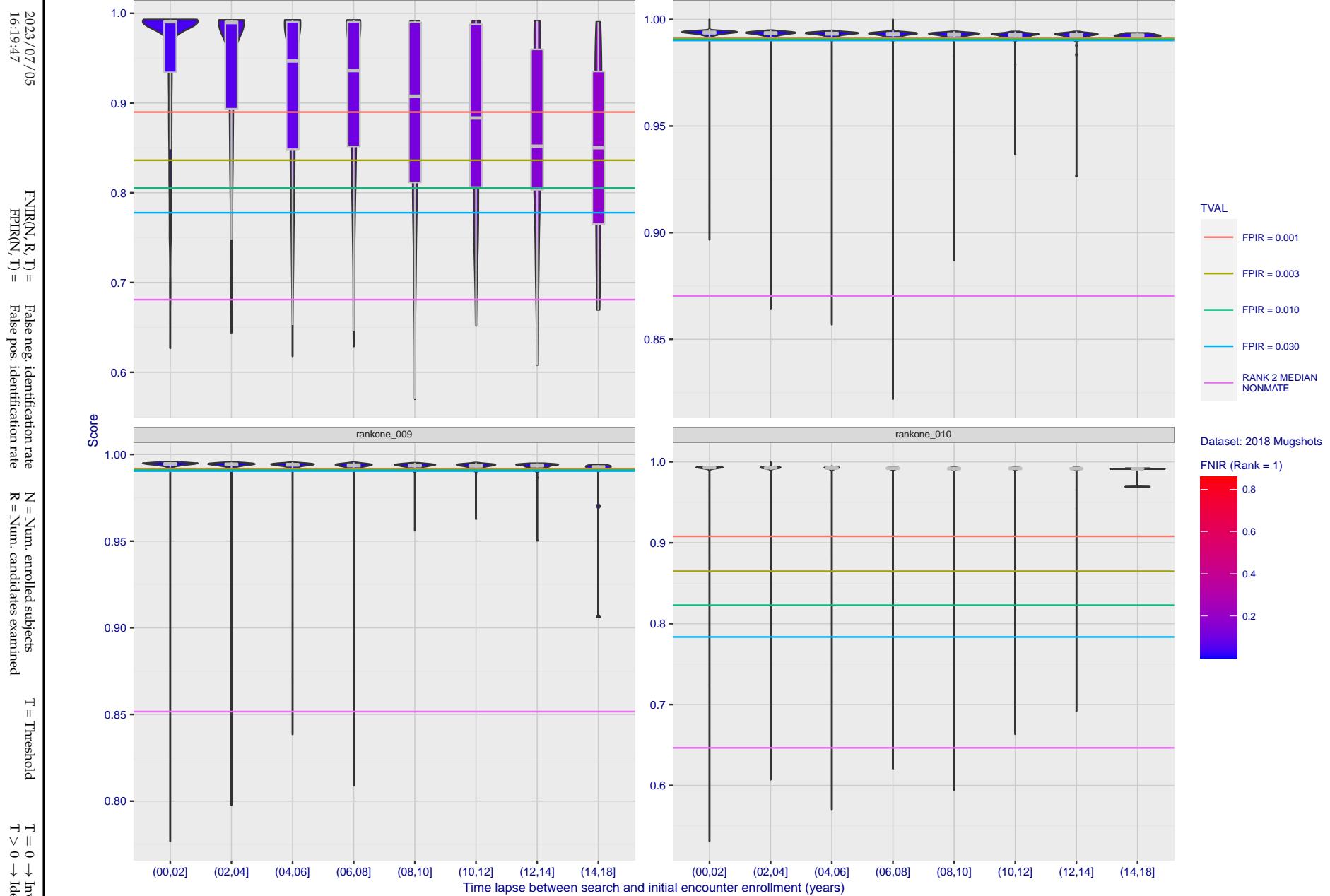


Figure 281: [FRVT-2018 Mugshot Ageing Dataset] Native mate scores vs. time-elapsed. The oldest image of each individual is enrolled. Thereafter, all more recent images are searched. Mated score distributions are computed over all searches noted in row 17 of Table 1 binned by number of years between search and initial enrollment.

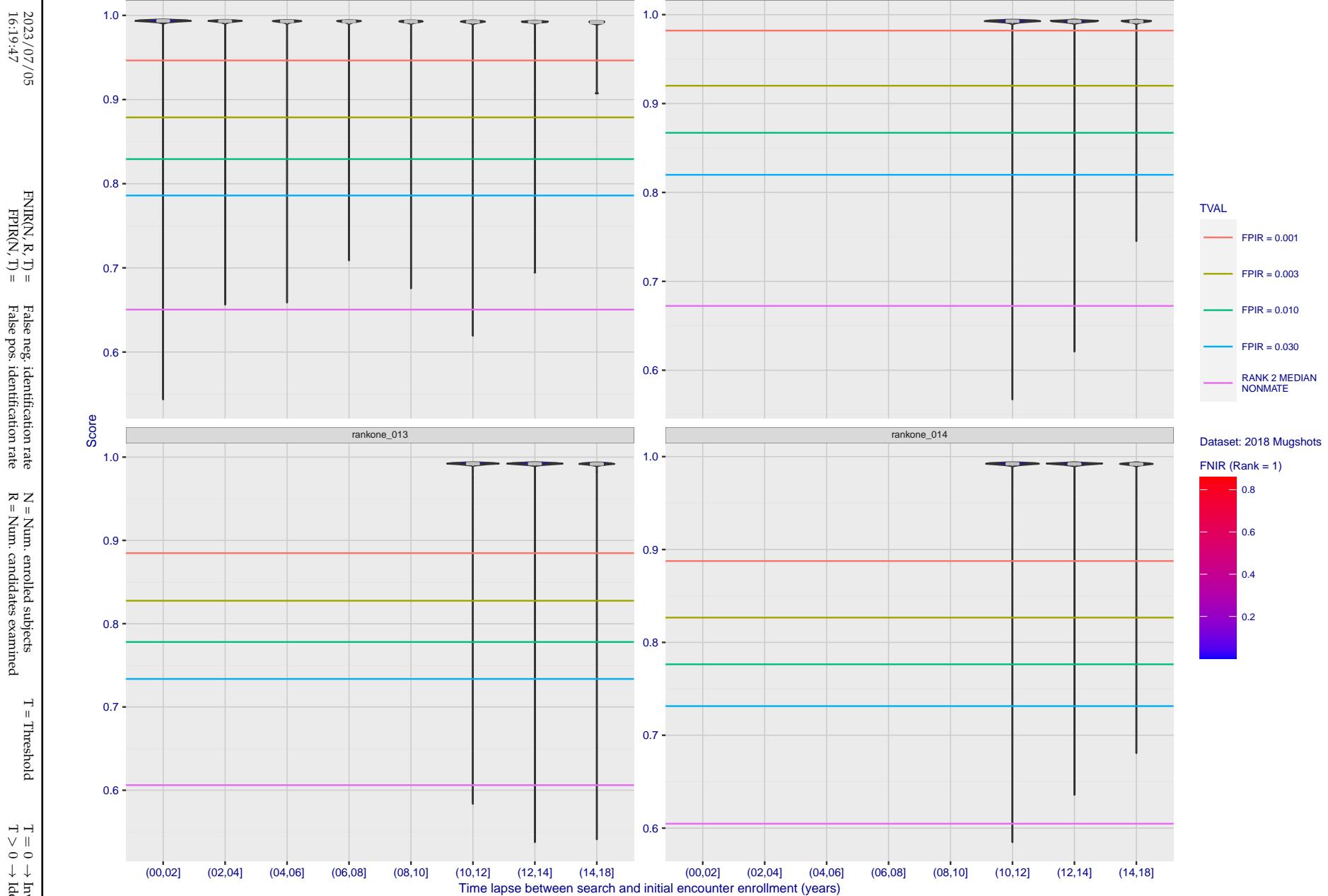


Figure 282: [FRVT-2018 Mugshot Ageing Dataset] Native mate scores vs. time-elapsed. The oldest image of each individual is enrolled. Thereafter, all more recent images are searched. Mated score distributions are computed over all searches noted in row 17 of Table 1 binned by number of years between search and initial enrollment.

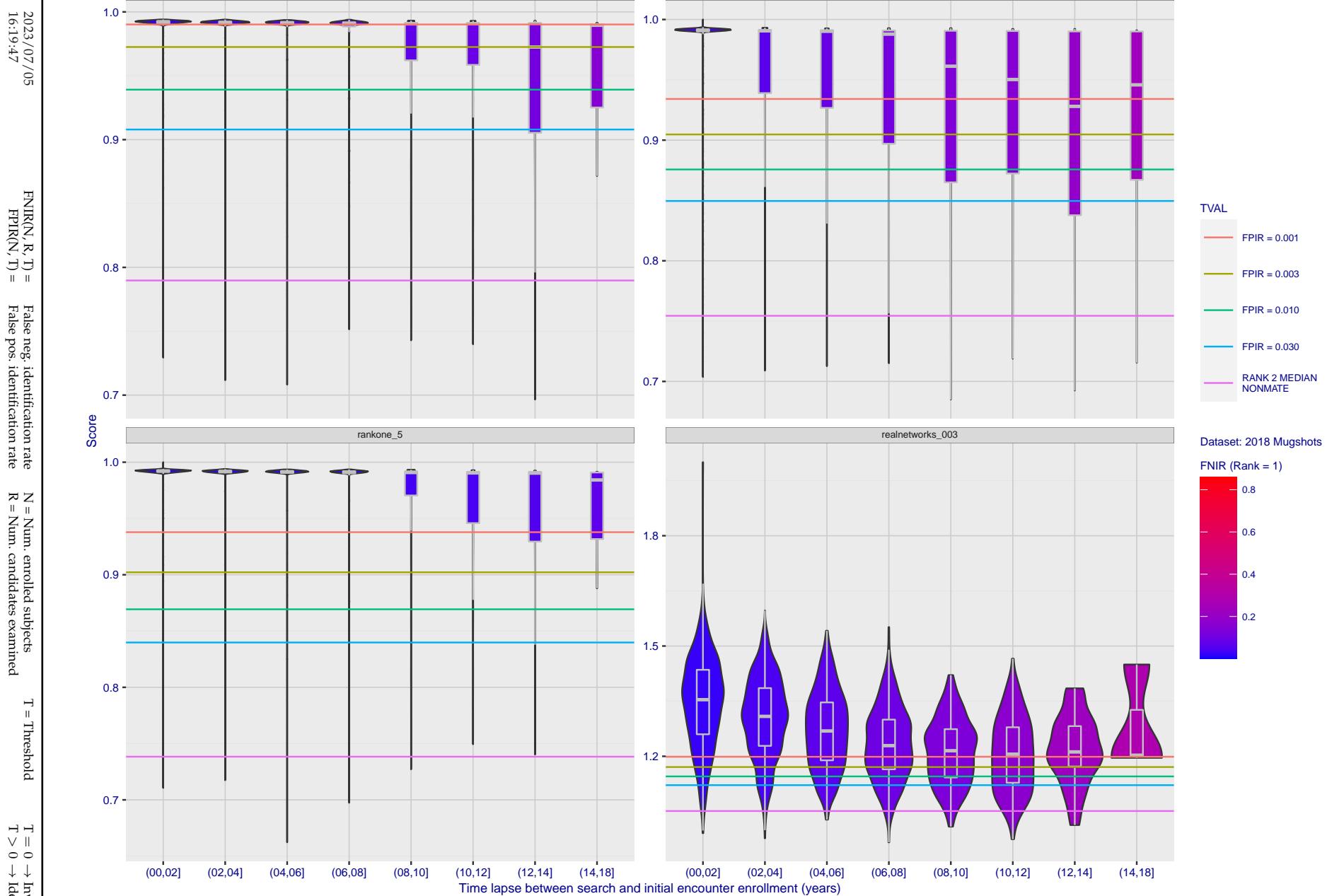


Figure 283: [FRVT-2018 Mugshot Ageing Dataset] Native mate scores vs. time-elapsed. The oldest image of each individual is enrolled. Thereafter, all more recent images are searched. Mated score distributions are computed over all searches noted in row 17 of Table 1 binned by number of years between search and initial enrollment.

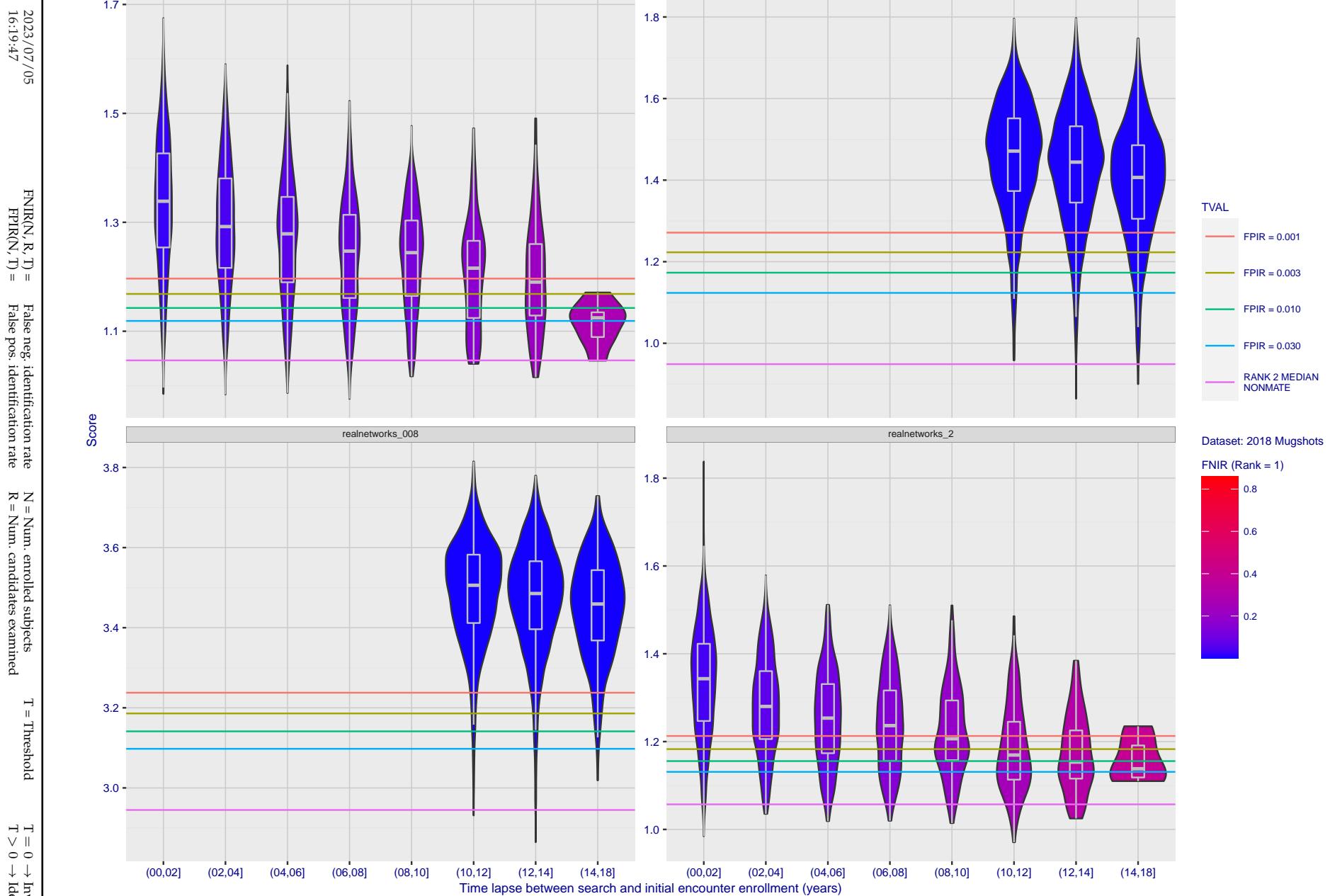


Figure 284: [FRVT-2018 Mugshot Ageing Dataset] Native mate scores vs. time-elapsed. The oldest image of each individual is enrolled. Thereafter, all more recent images are searched. Mated score distributions are computed over all searches noted in row 17 of Table 1 binned by number of years between search and initial enrollment.

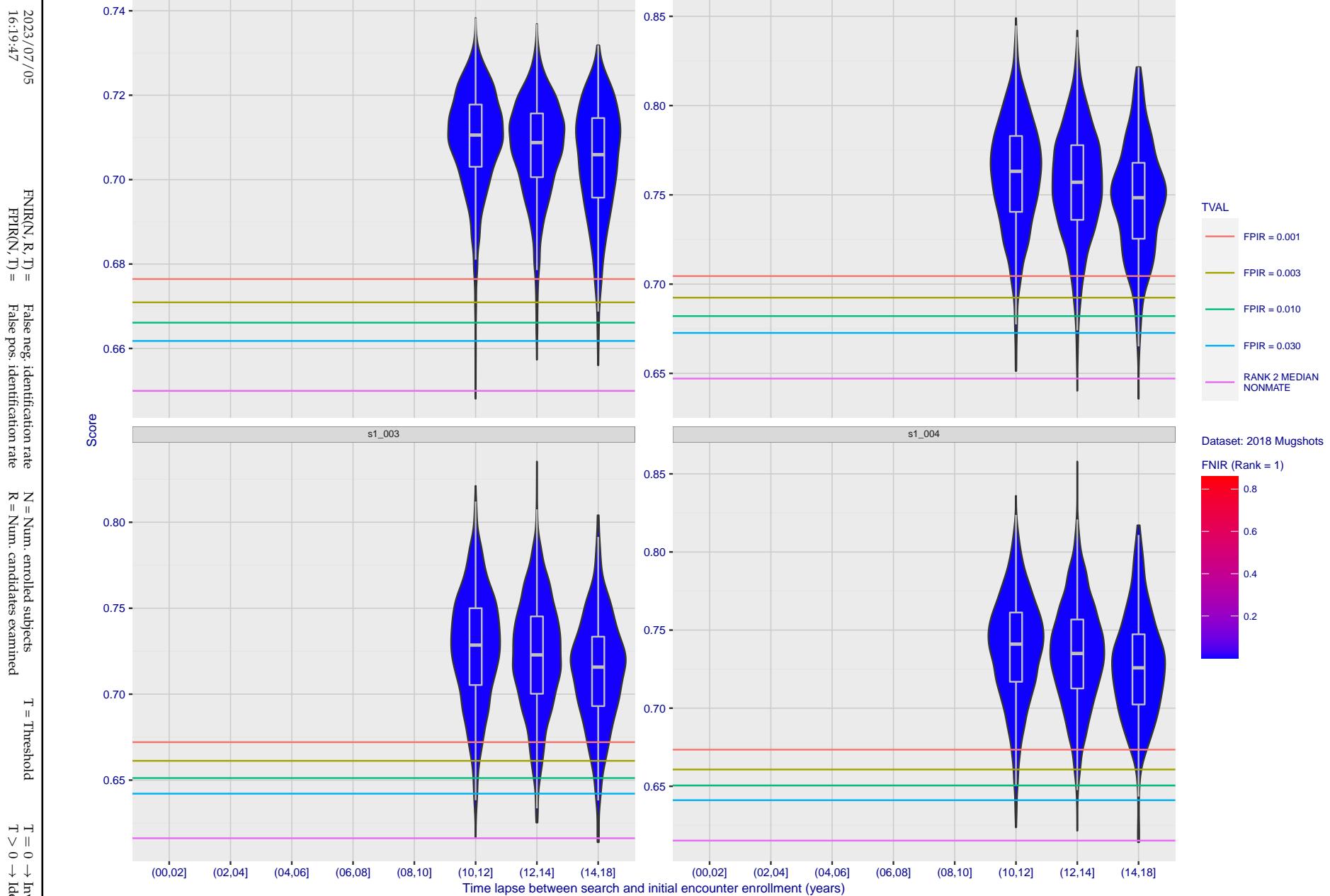


Figure 285: [FRVT-2018 Mugshot Ageing Dataset] Native mate scores vs. time-elapsed. The oldest image of each individual is enrolled. Thereafter, all more recent images are searched. Mated score distributions are computed over all searches noted in row 17 of Table 1 binned by number of years between search and initial enrollment.

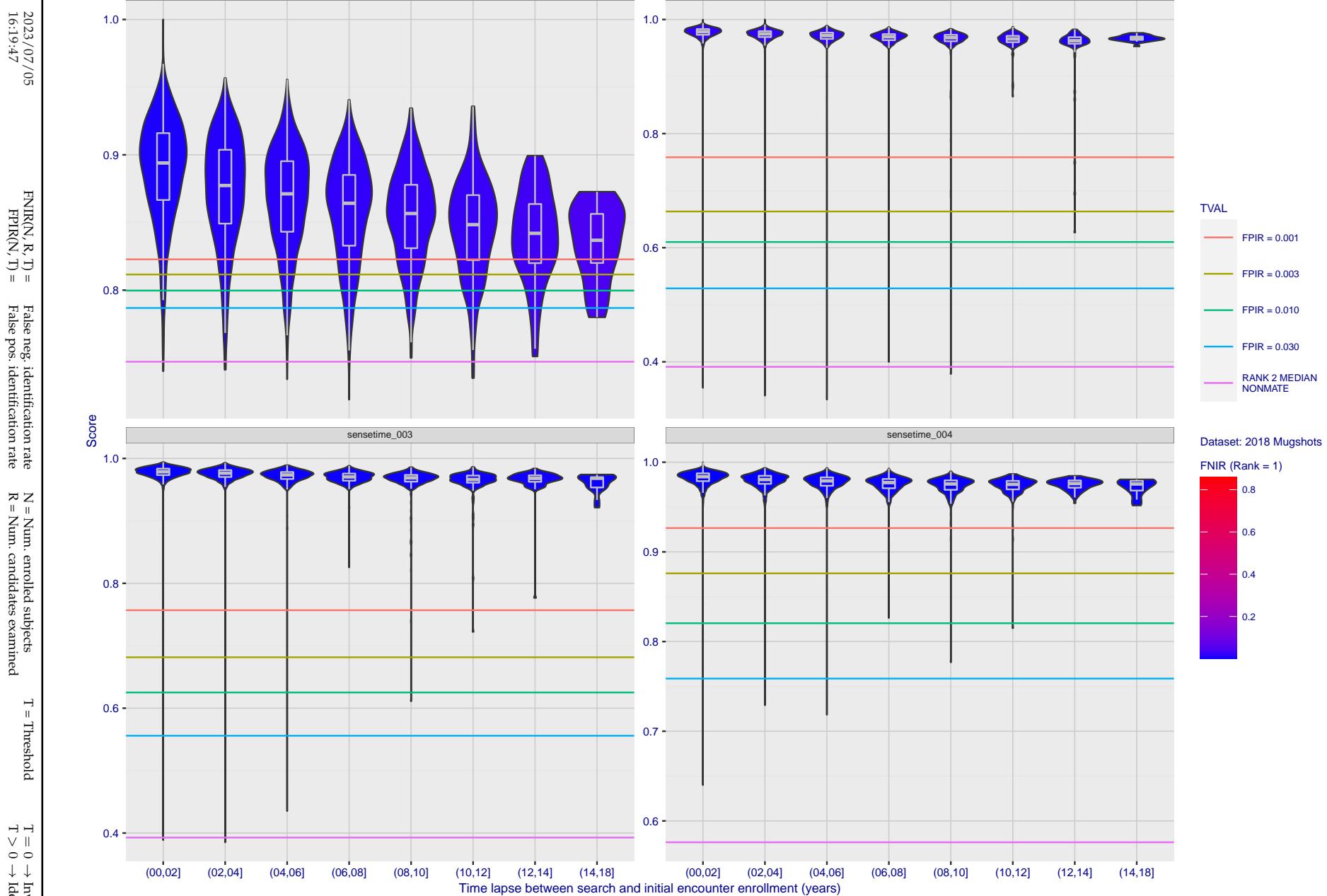


Figure 286: [FRVT-2018 Mugshot Ageing Dataset] Native mate scores vs. time-elapsed. The oldest image of each individual is enrolled. Thereafter, all more recent images are searched. Mated score distributions are computed over all searches noted in row 17 of Table 1 binned by number of years between search and initial enrollment.

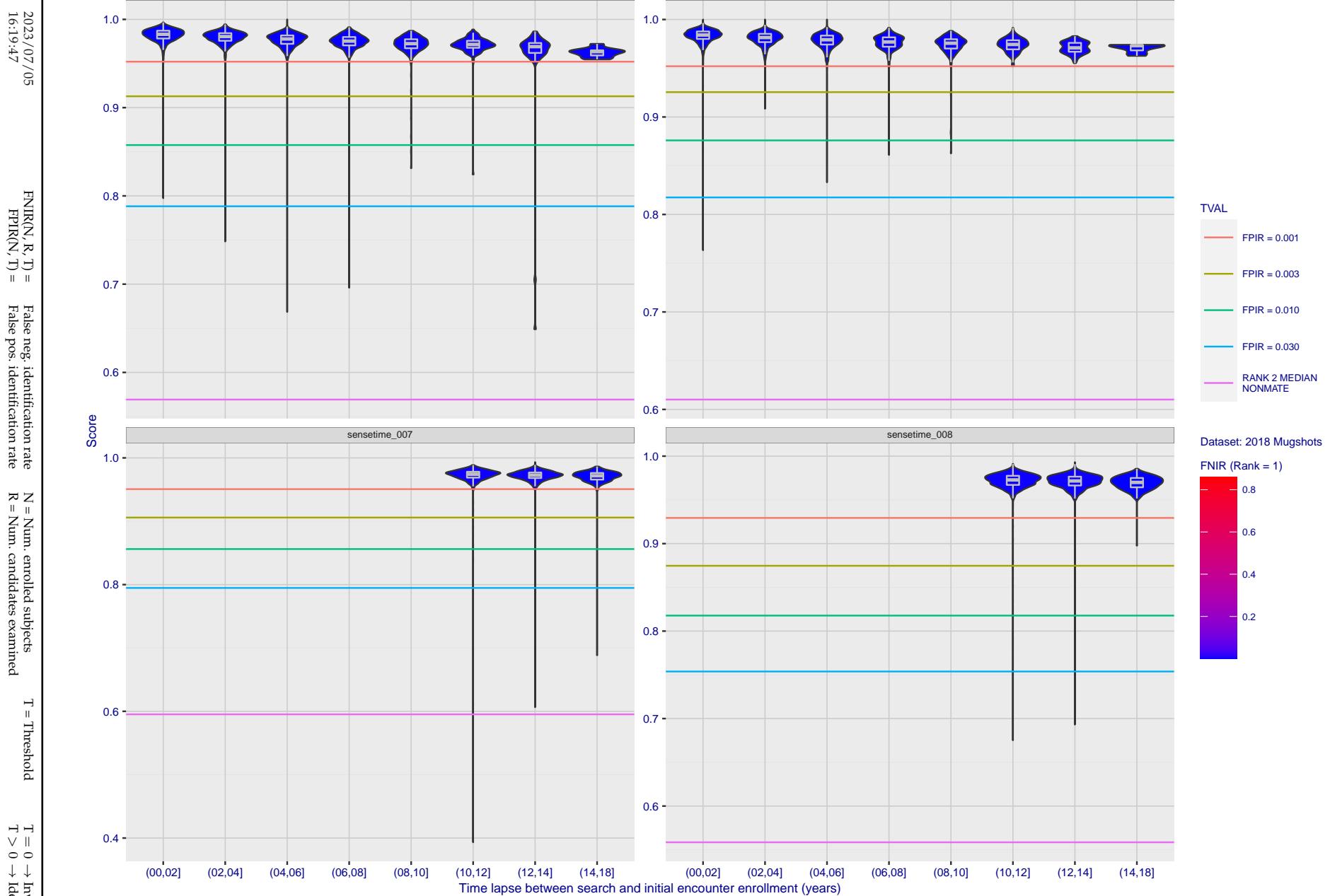


Figure 287: [FRVT-2018 Mugshot Ageing Dataset] Native mate scores vs. time-elapsed. The oldest image of each individual is enrolled. Thereafter, all more recent images are searched. Mated score distributions are computed over all searches noted in row 17 of Table 1 binned by number of years between search and initial enrollment.

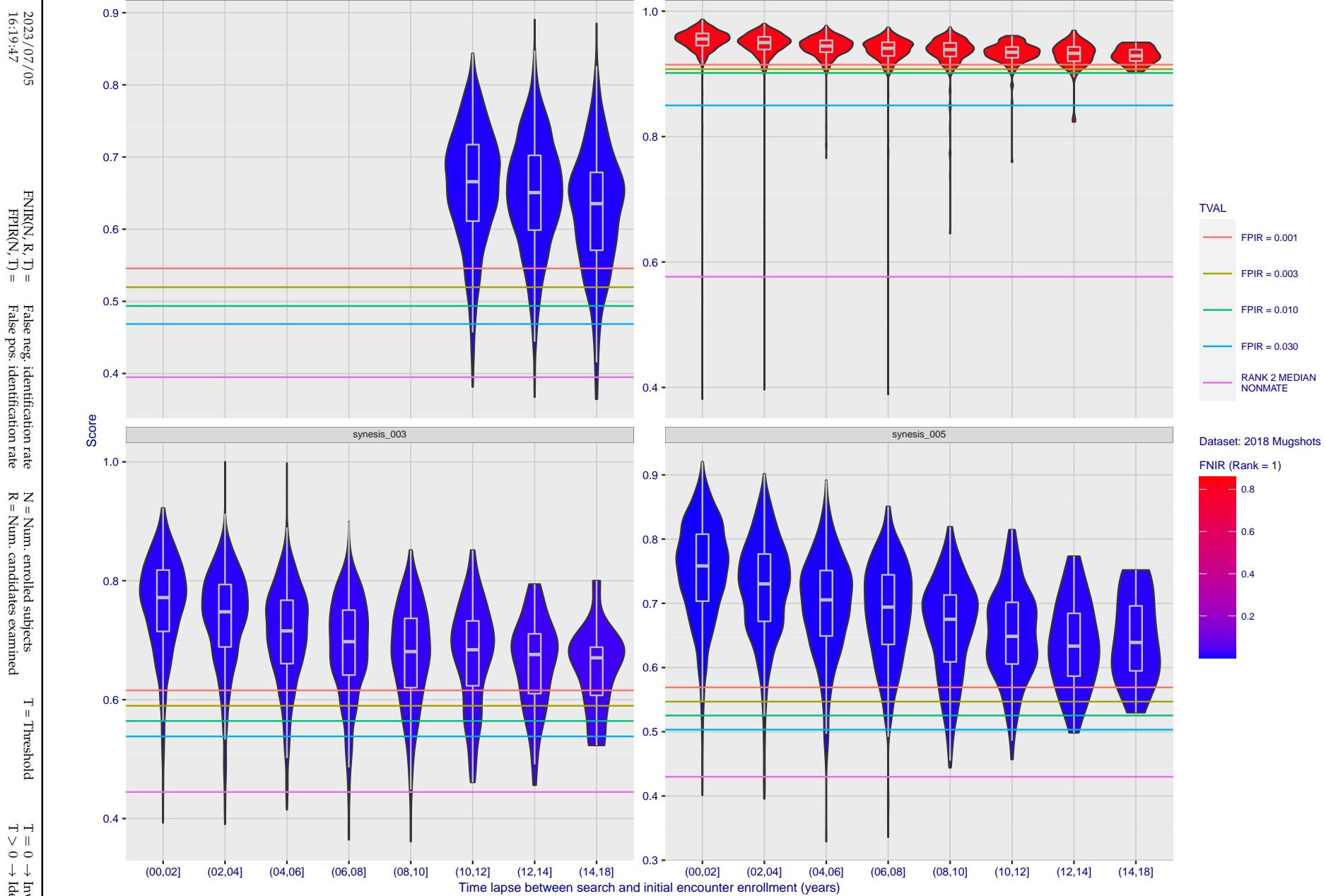


Figure 288: [FRVT-2018 Mugshot Ageing Dataset] Native mate scores vs. time-elapsed. The oldest image of each individual is enrolled. Thereafter, all more recent images are searched. Mated score distributions are computed over all searches noted in row 17 of Table 1 binned by number of years between search and initial enrollment.

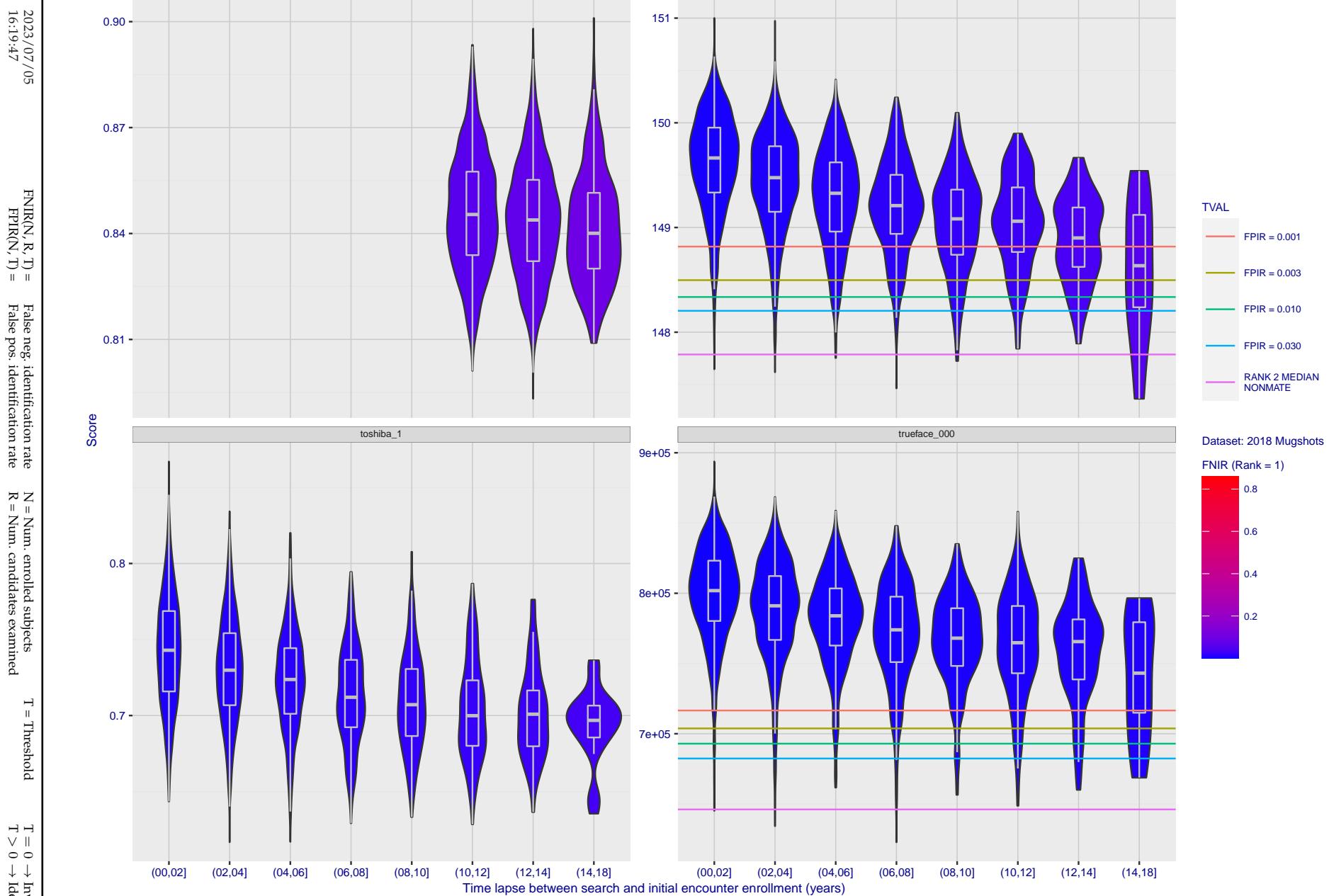


Figure 289: [FRVT-2018 Mugshot Ageing Dataset] Native mate scores vs. time-elapsed. The oldest image of each individual is enrolled. Thereafter, all more recent images are searched. Mated score distributions are computed over all searches noted in row 17 of Table 1 binned by number of years between search and initial enrollment.

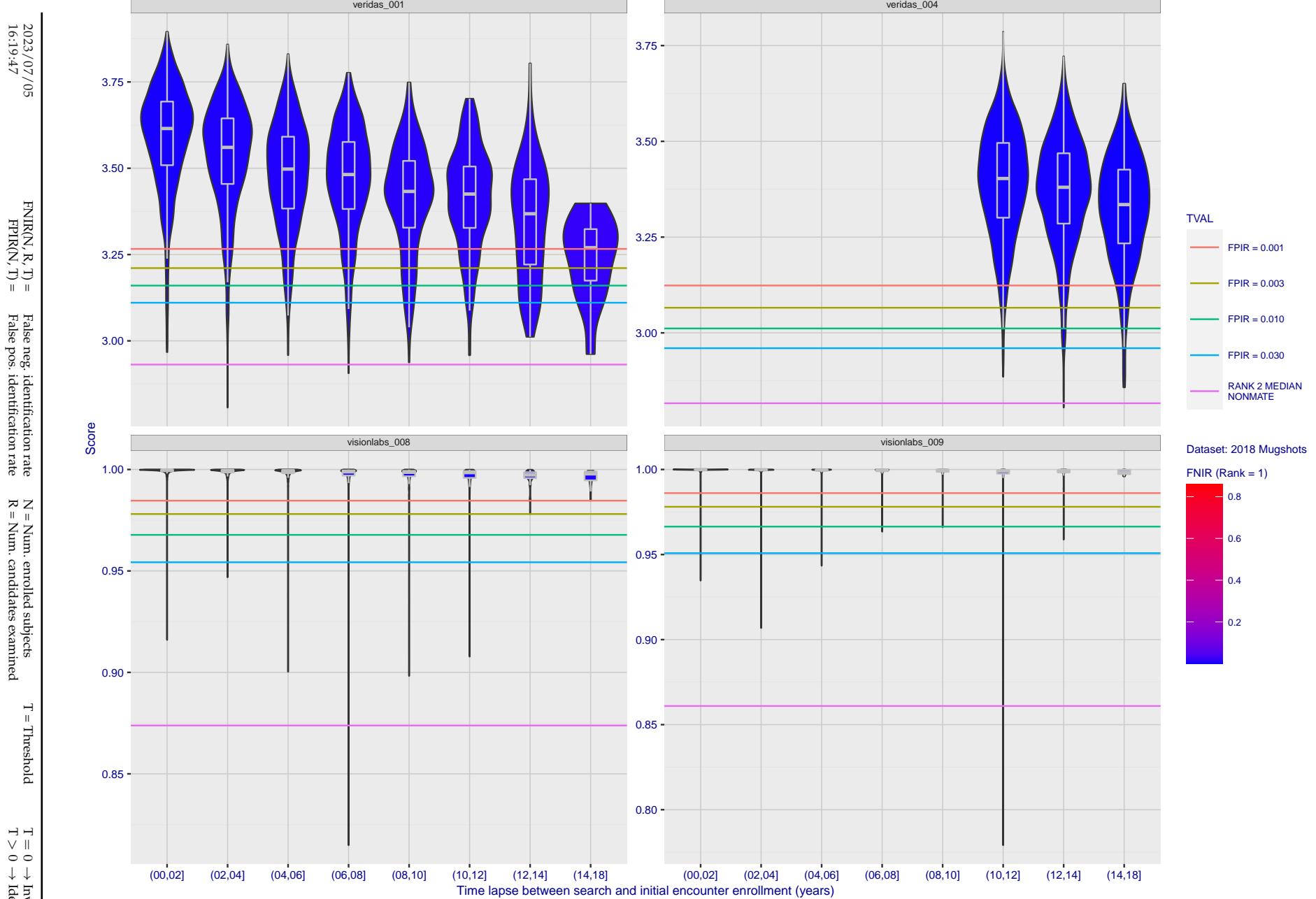


Figure 290: [FRVT-2018 Mugshot Ageing Dataset] Native mate scores vs. time-elapsed. The oldest image of each individual is enrolled. Thereafter, all more recent images are searched. Mated score distributions are computed over all searches noted in row 17 of Table 1 binned by number of years between search and initial enrollment.

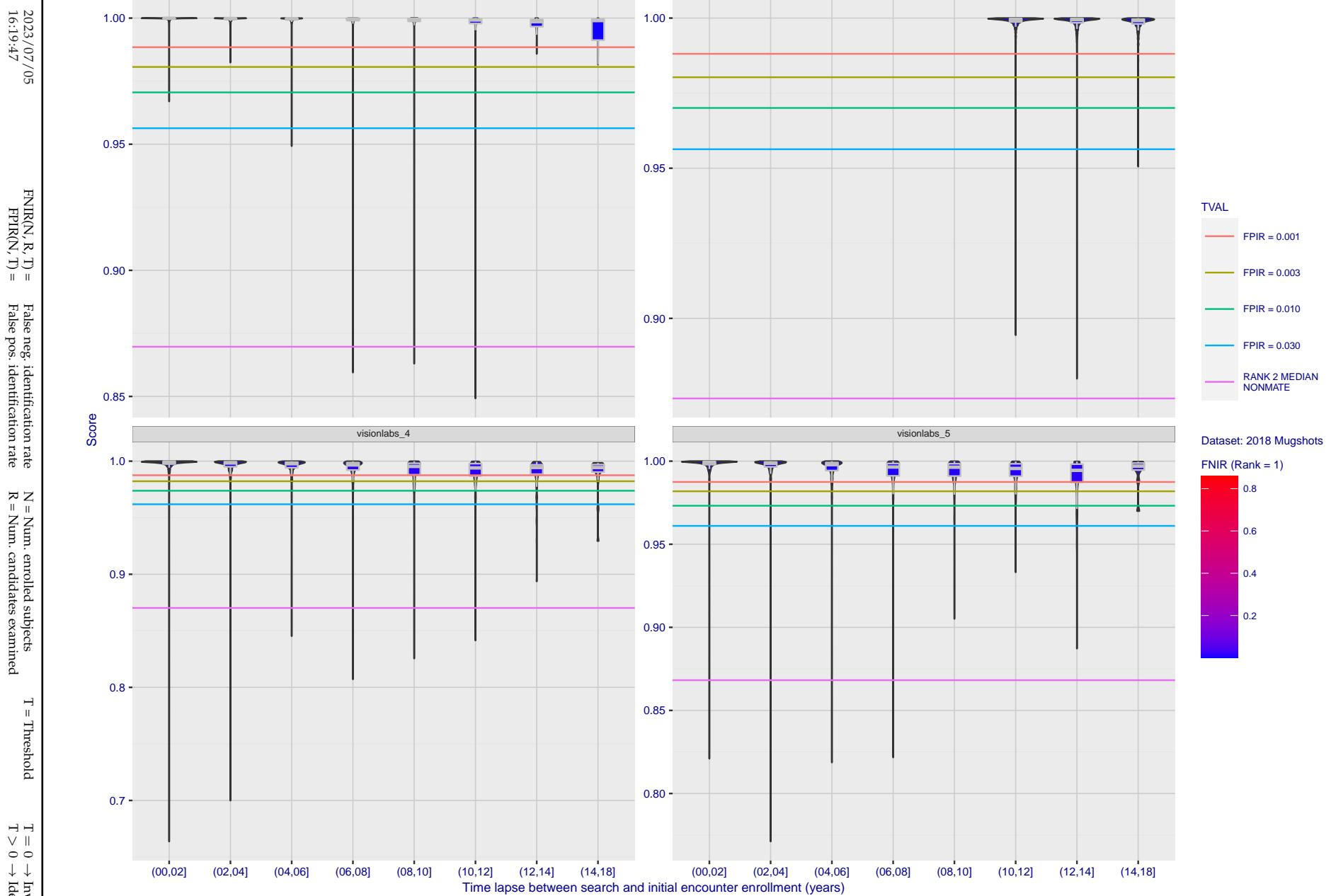


Figure 291: [FRVT-2018 Mugshot Ageing Dataset] Native mate scores vs. time-elapsed. The oldest image of each individual is enrolled. Thereafter, all more recent images are searched. Mated score distributions are computed over all searches noted in row 17 of Table 1 binned by number of years between search and initial enrollment.

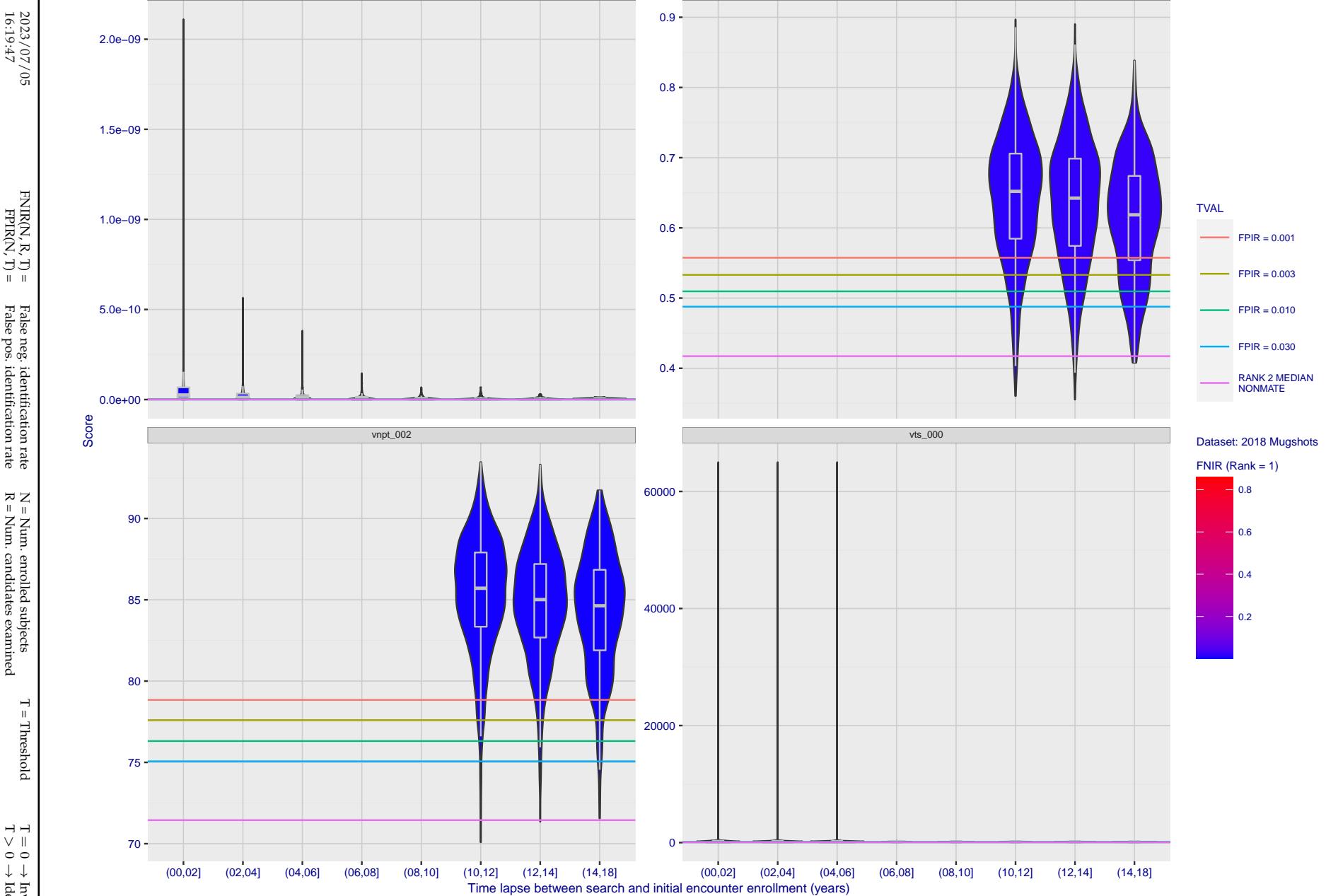


Figure 292: [FRVT-2018 Mugshot Ageing Dataset] Native mate scores vs. time-elapsed. The oldest image of each individual is enrolled. Thereafter, all more recent images are searched. Mated score distributions are computed over all searches noted in row 17 of Table 1 binned by number of years between search and initial enrollment.

2023/07/05
16:19:47FNIR(N, R, T) = False neg. identification rate
FPFR(N, T) = False pos. identification rateN = Num. enrolled subjects
R = Num. candidates examinedT = Threshold
T = 0 → Investigation

T > 0 → Identification

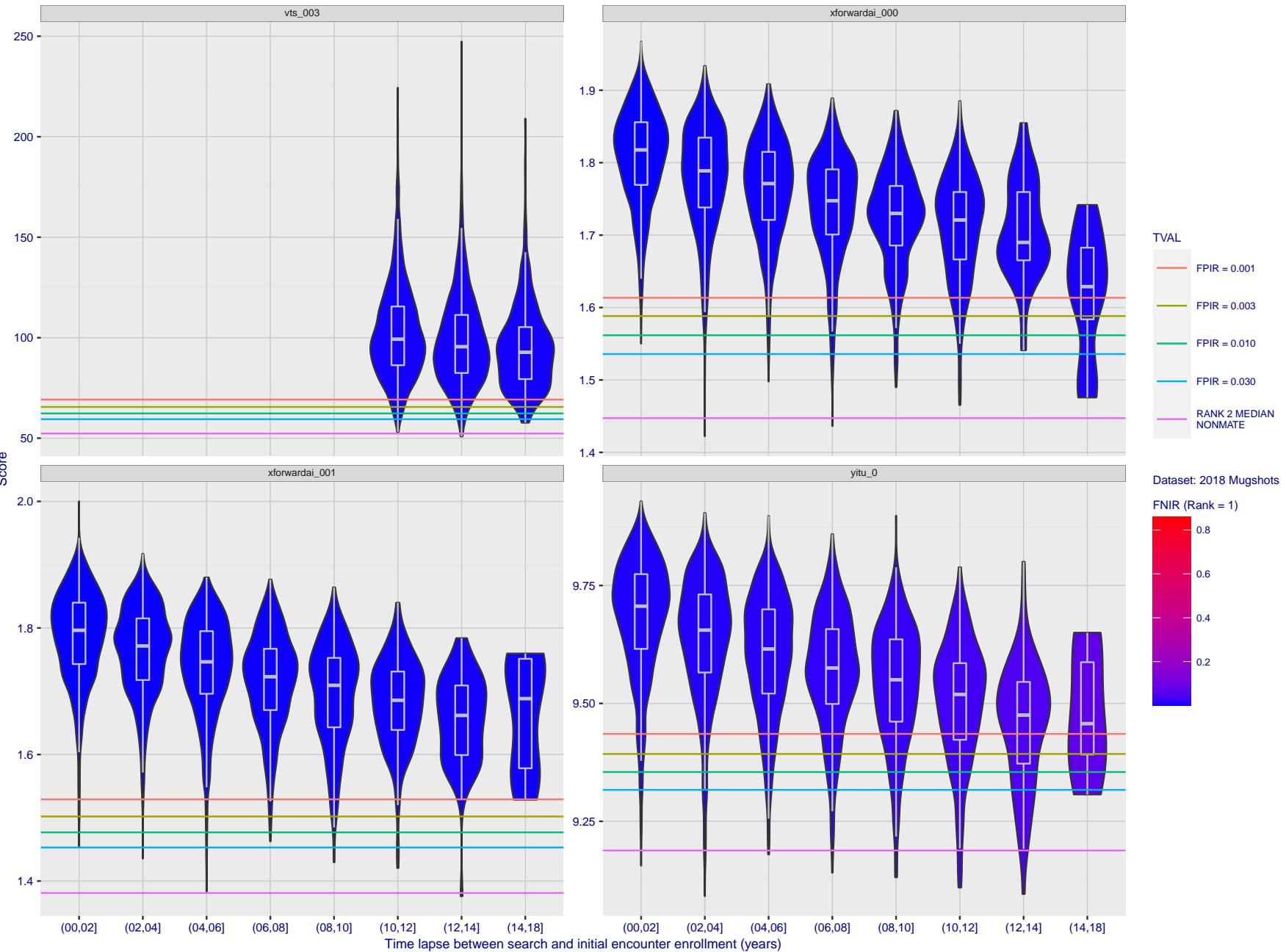


Figure 293: [FRVT-2018 Mugshot Ageing Dataset] Native mate scores vs. time-elapsed. The oldest image of each individual is enrolled. Thereafter, all more recent images are searched. Mated score distributions are computed over all searches noted in row 17 of Table 1 binned by number of years between search and initial enrollment.

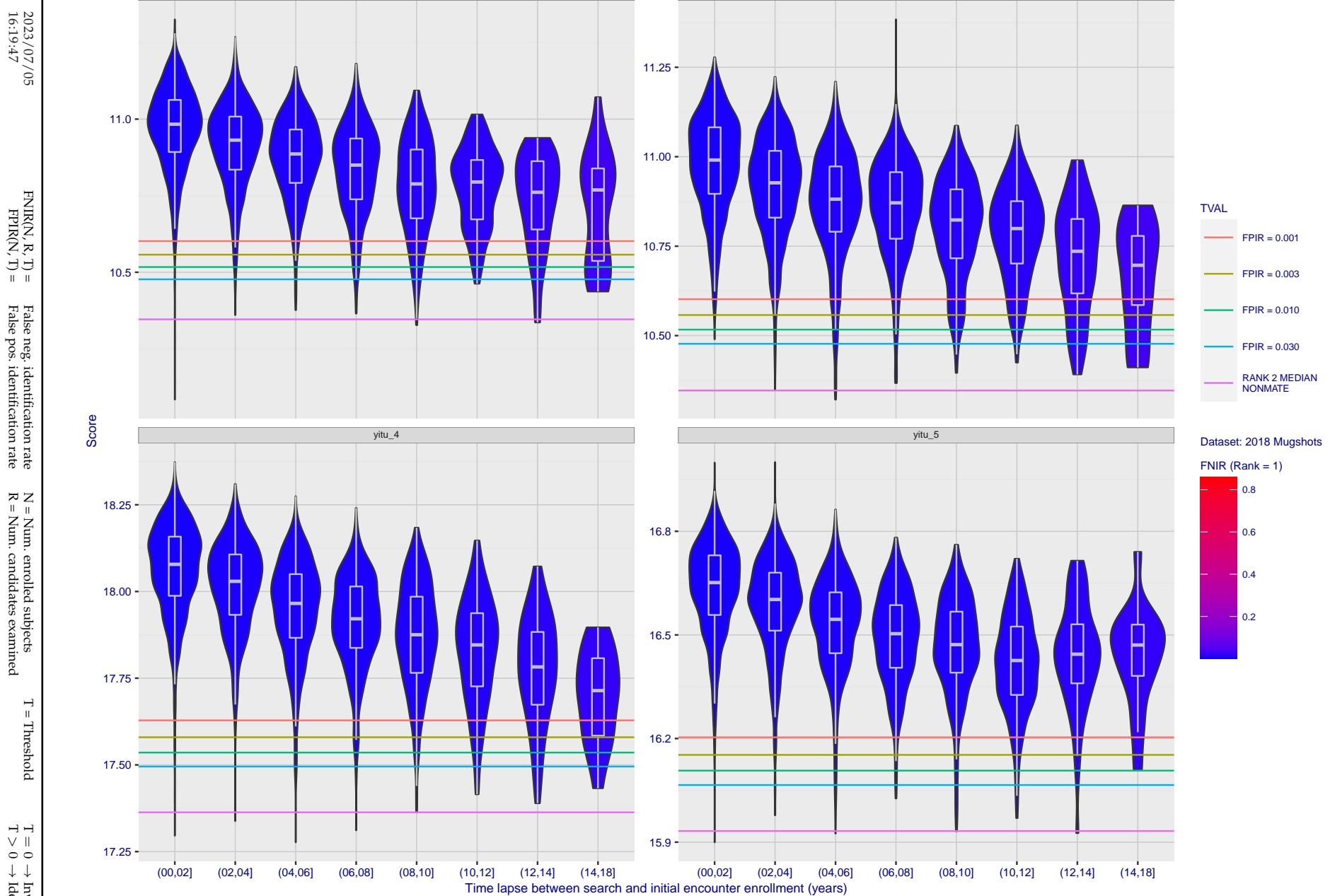


Figure 294: [FRVT-2018 Mugshot Ageing Dataset] Native mate scores vs. time-elapsed. The oldest image of each individual is enrolled. Thereafter, all more recent images are searched. Mated score distributions are computed over all searches noted in row 17 of Table 1 binned by number of years between search and initial enrollment.

Appendix C Effect of enrolling multiple images

2023/07/05
16:19:47FNIR(N, R, T) = False neg. identification rate
FPIR(N, T) = False pos. identification rateN = Num. enrolled subjects
R = Num. candidates examinedT = Threshold
T = 0 → Investigation

T > 0 → Identification

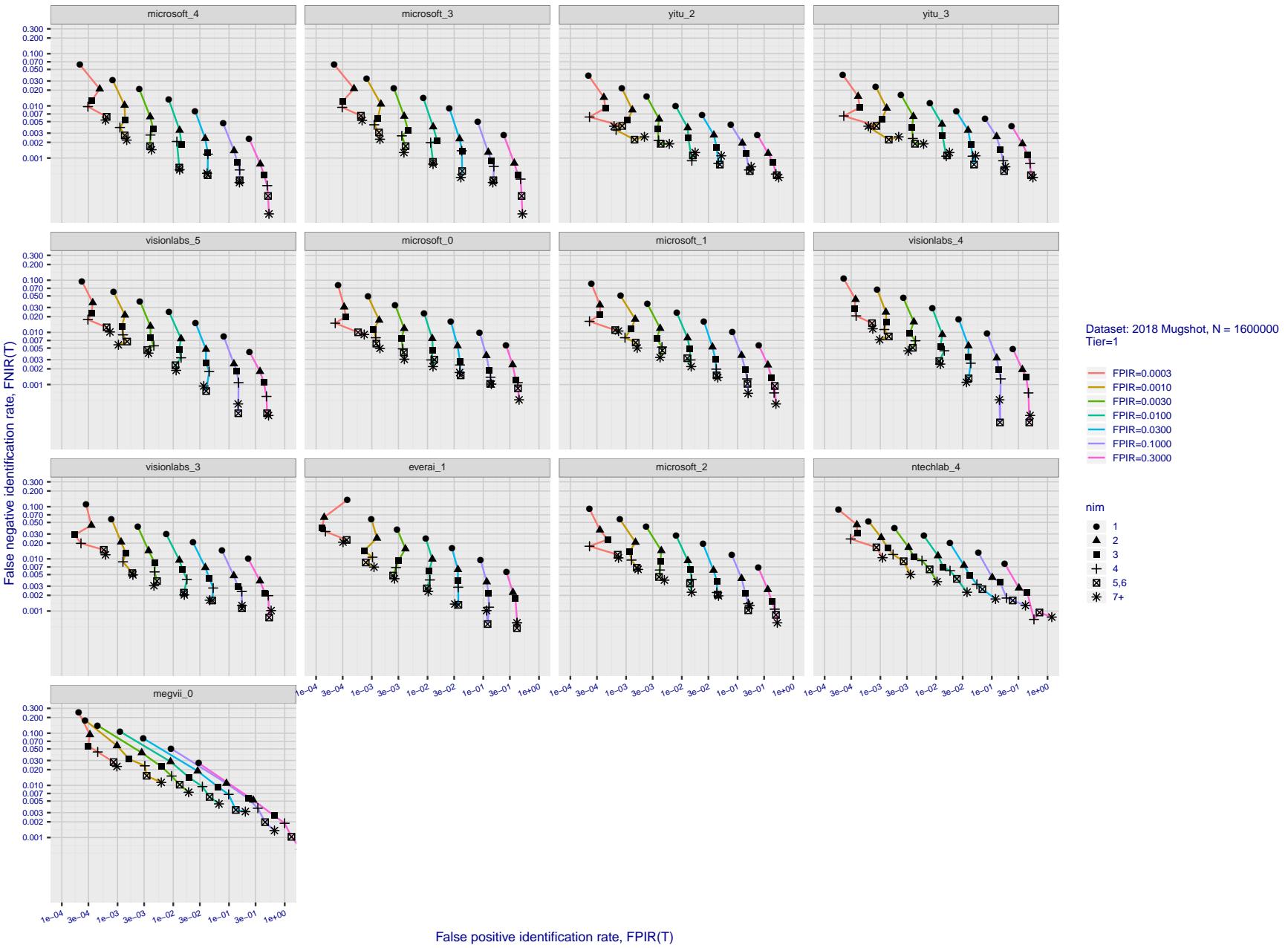


Figure 295: [FRVT-2018 Mugshot Dataset] Effect of enrolling multiple images for each identity. The plot shows an identification miss rates vs. false positive rates, at seven operating thresholds. The enrolled population size is fixed. The images are enrolled with lifetime-consolidation - see section 2.3.

2023/07/05
16:19:47

 $FNIR(N, R, T) =$
False neg. identification rate
 $FPIR(N, T) =$
False pos. identification rate

 $N =$ Num. enrolled subjects
 $R =$ Num. candidates examined

 $T =$ Threshold
 $T = 0 \rightarrow$ Investigation
 $T > 0 \rightarrow$ Identification

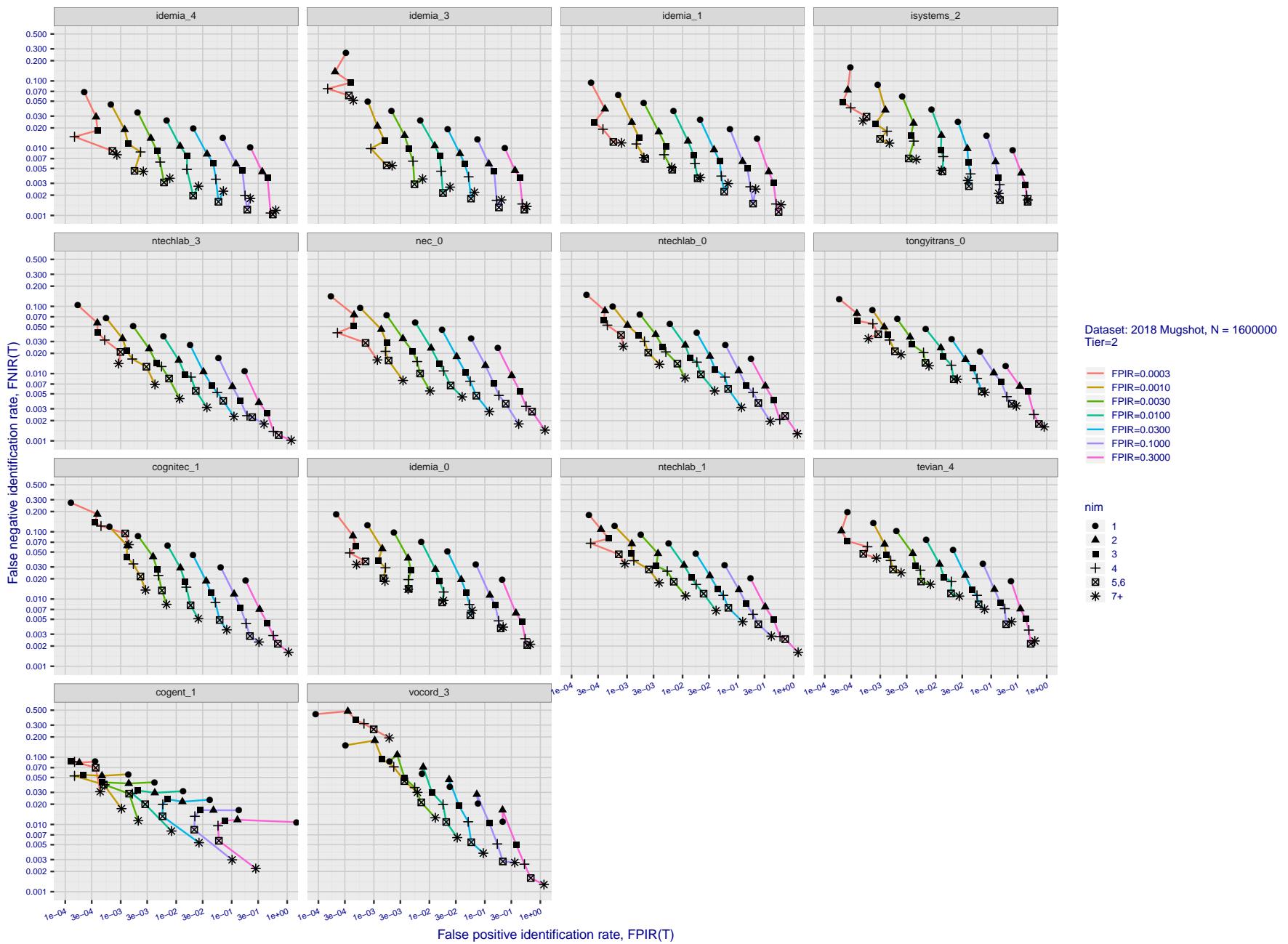


Figure 296: [FRVT-2018 Mugshot Dataset] Effect of enrolling multiple images for each identity. The plot shows an identification miss rates vs. false positive rates, at seven operating thresholds. The enrolled population size is fixed. The images are enrolled with lifetime-consolidation - see section 2.3.

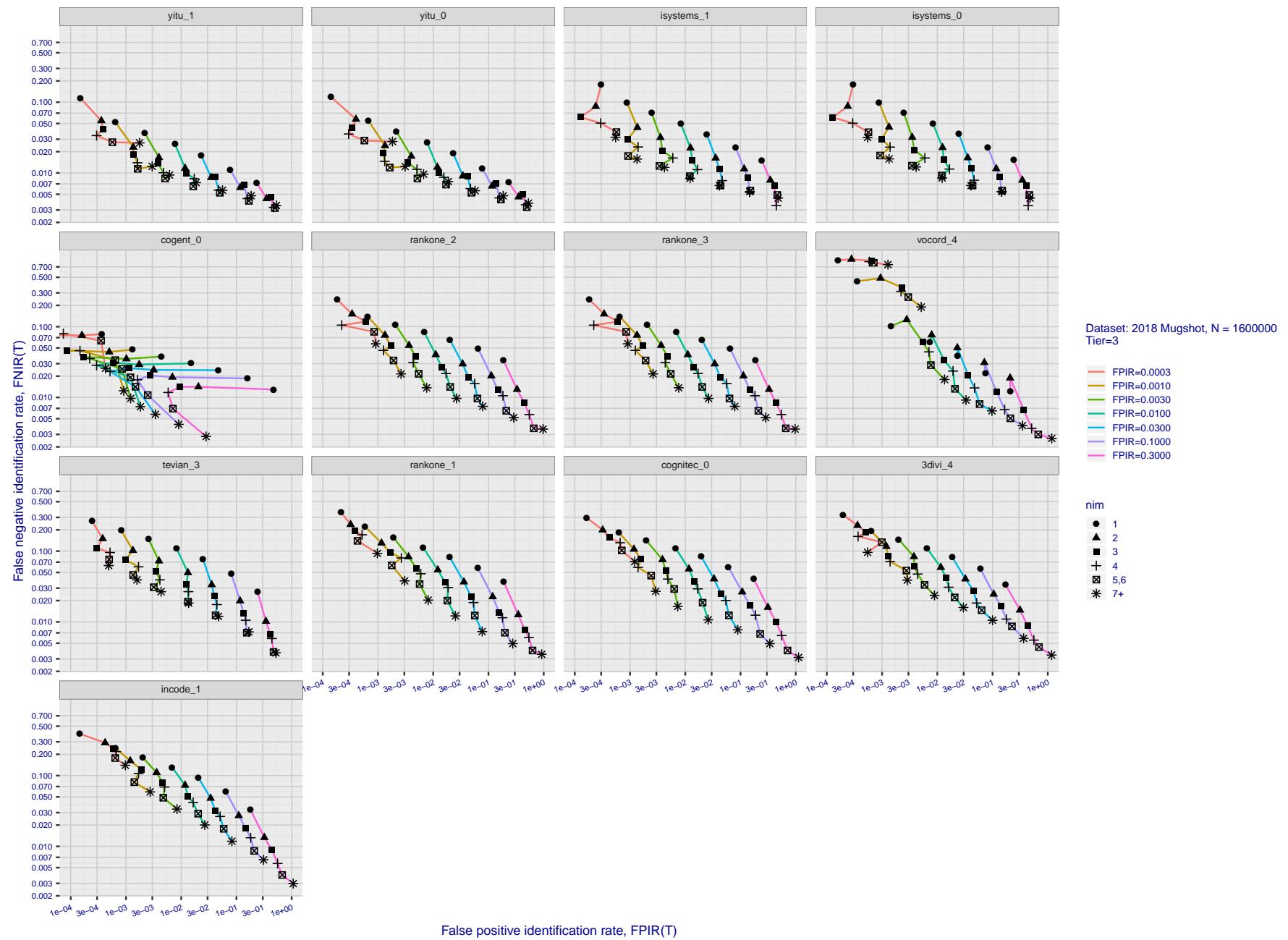


Figure 297: [FRVT-2018 Mugshot Dataset] Effect of enrolling multiple images for each identity. The plot shows an identification miss rates vs. false positive rates, at seven operating thresholds. The enrolled population size is fixed. The images are enrolled with lifetime-consolidation - see section 2.3.

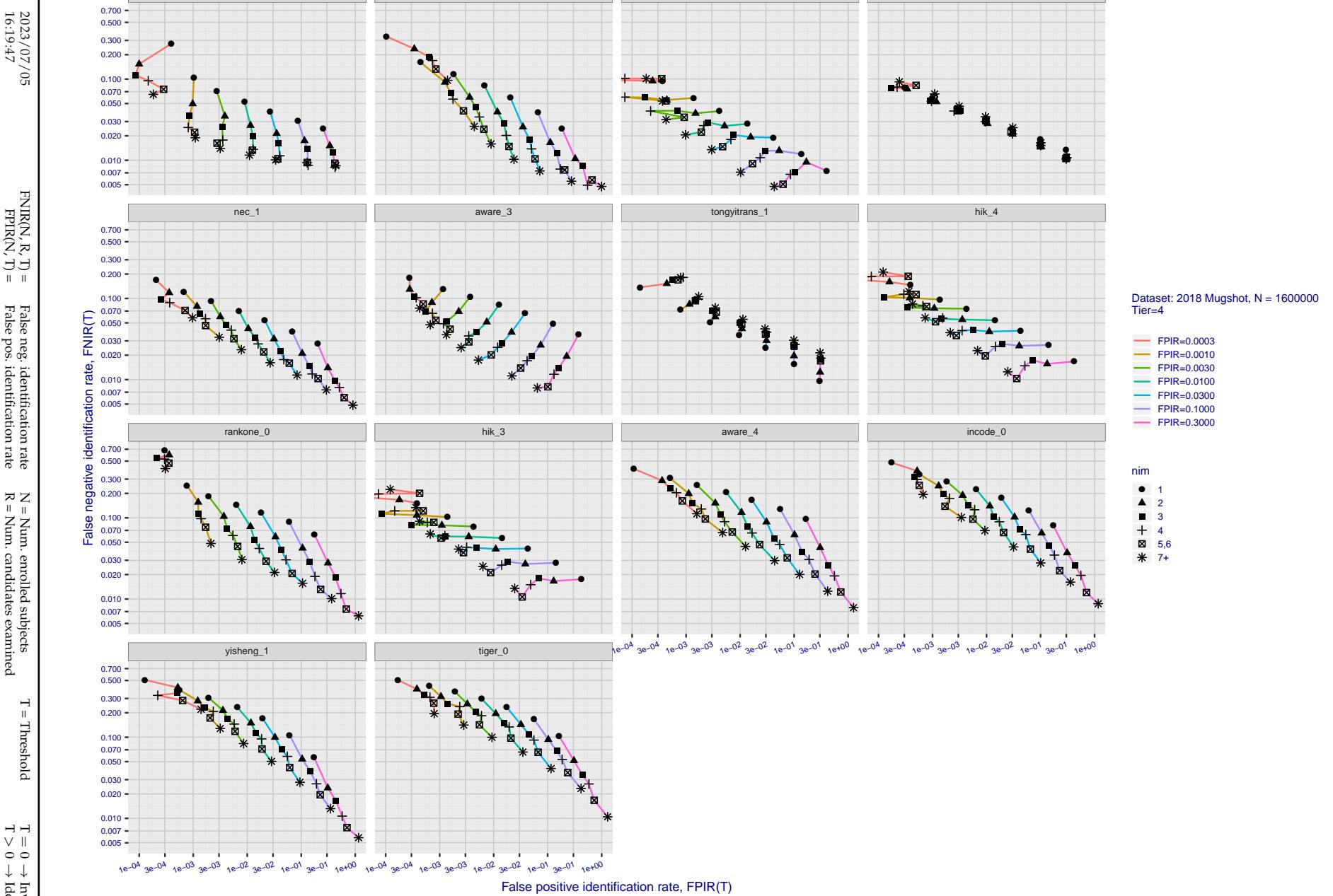


Figure 298: [FRVT-2018 Mugshot Dataset] Effect of enrolling multiple images for each identity. The plot shows an identification miss rates vs. false positive rates, at seven operating thresholds. The enrolled population size is fixed. The images are enrolled with lifetime-consolidation - see section 2.3.

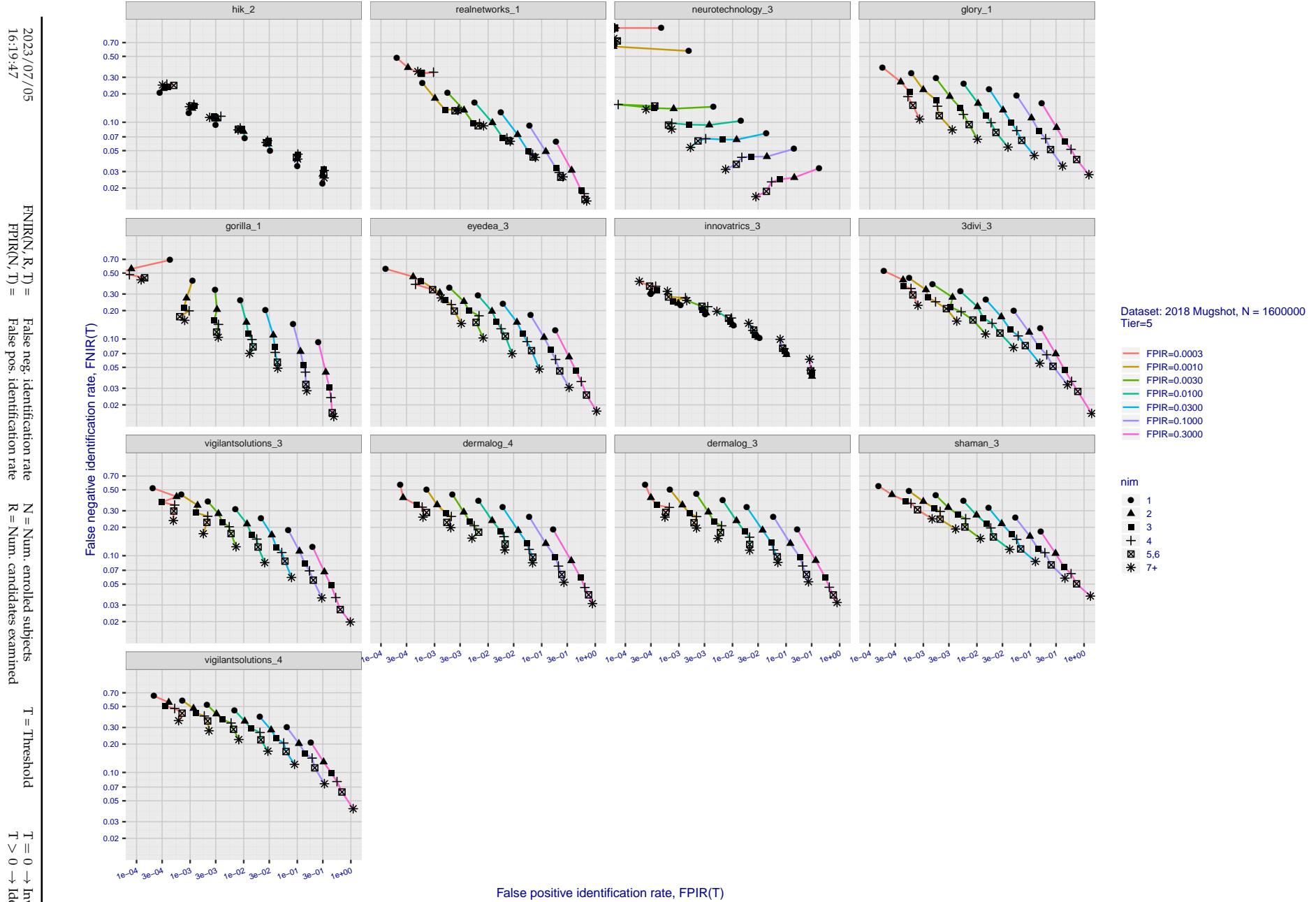


Figure 299: [FRVT-2018 Mugshot Dataset] Effect of enrolling multiple images for each identity. The plot shows an identification miss rates vs. false positive rates, at seven operating thresholds. The enrolled population size is fixed. The images are enrolled with lifetime-consolidation - see section 2.3.

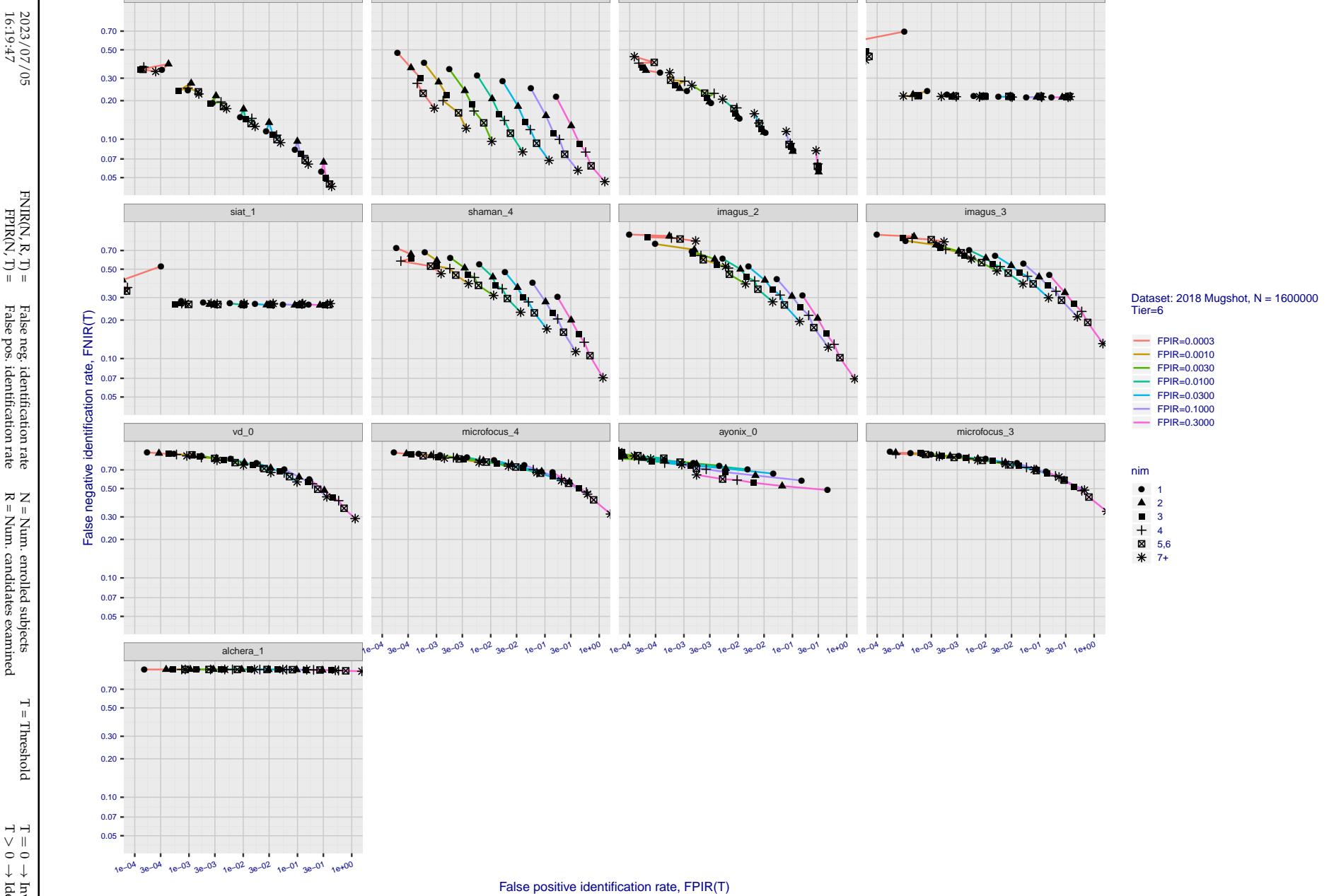


Figure 300: [FRVT-2018 Mugshot Dataset] Effect of enrolling multiple images for each identity. The plot shows an identification miss rates vs. false positive rates, at seven operating thresholds. The enrolled population size is fixed. The images are enrolled with lifetime-consolidation - see section 2.3.

Appendix D Accuracy with poor quality webcam images

2023/07/05
16:19:47

FNIR(N, R, T) = False neg. identification rate
FPTR(N, T) = False pos. identification rate

N = Num. enrolled subjects
R = Num. candidates examined

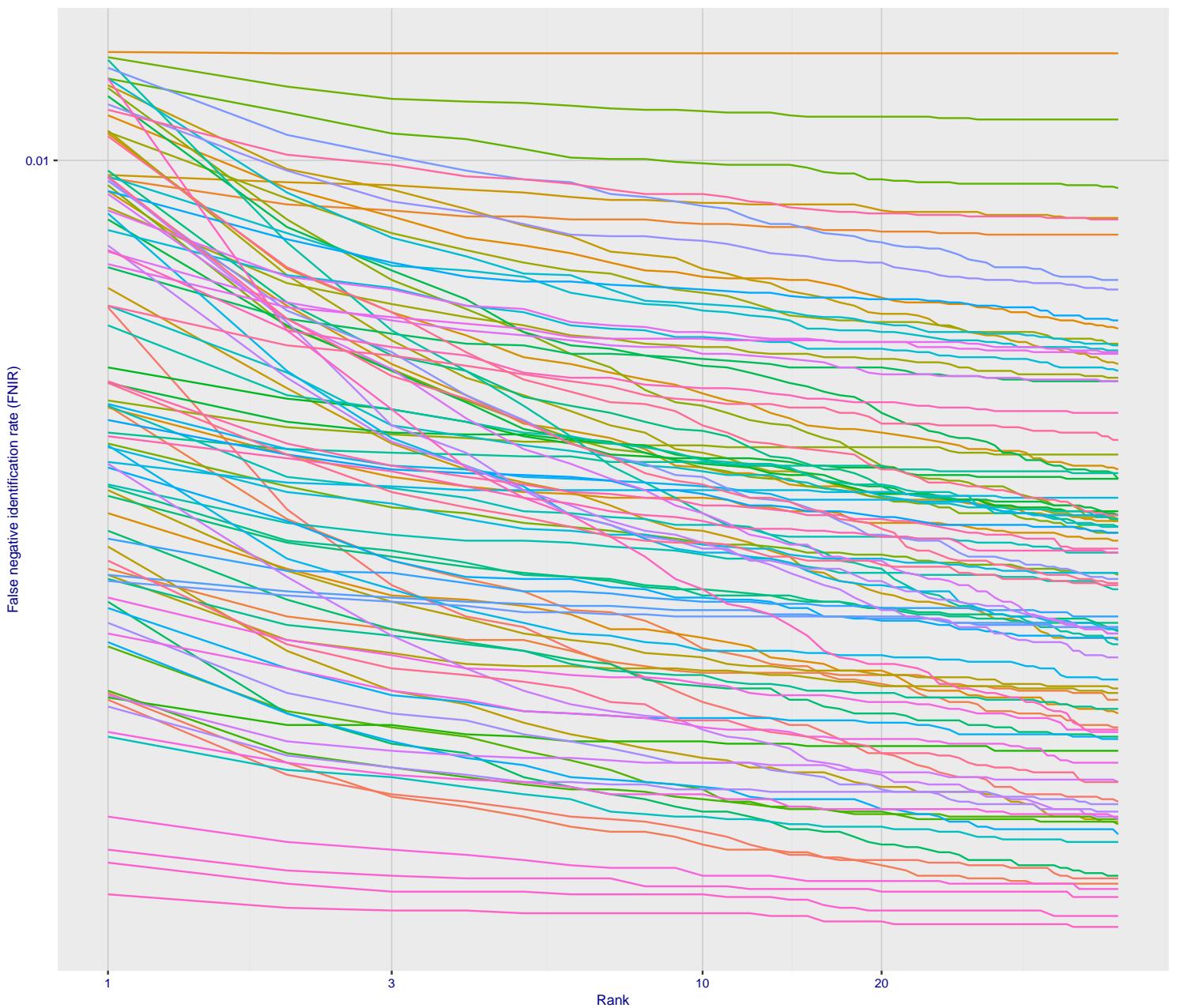
T = Threshold
T > 0 → Identification

2023/07/05

16:19:47

FNIR(N, R, T) = False neg. identification rate
FPTR(N, T) = False pos. identification rateN = Num. enrolled subjects
R = Num. candidates examined

T = Threshold

T = 0 → Investigation
T > 0 → Identification

- 0.010 cogent_005
- 0.010 dermalog_011
- 0.010 everai_paravision_004
- 0.010 cognitec_005
- 0.010 yitu_2
- 0.010 mantra_000
- 0.010 cubox_000
- 0.010 nec_3
- 0.010 vts_001
- 0.010 cloudwalk_hr_000
- 0.010 realnetworks_006
- 0.010 rankone_010
- 0.010 gorilla_008
- 0.010 cognitec_006
- 0.010 paravision_005
- 0.010 revealmedia_000
- 0.010 dilusense_001
- 0.010 s1_003
- 0.010 ntechlab_008
- 0.010 irex_000
- 0.009 neurotechnology_010
- 0.009 realnetworks_007
- 0.009 tevian_007
- 0.009 s1_002
- 0.009 s1_004
- 0.009 kakao_001
- 0.009 cyberlink_003
- 0.009 visionlabs_011
- 0.009 afisbiometrics_000
- 0.009 nec_004
- 0.008 innovates_008
- 0.008 visionlabs_009
- 0.008 intemu_000
- 0.008 yitu_4
- 0.008 firstcreditkz_001
- 0.008 ntechlab_010
- 0.008 cib_000
- 0.008 nec_006
- 0.008 cogent_007
- 0.008 paravision_007
- 0.008 megvii_003
- 0.008 veridas_004
- 0.008 graule_001
- 0.008 ntechlab_009
- 0.008 neurotechnology_012
- 0.008 neurotechnology_013
- 0.008 realnetworks_008
- 0.008 pangiam_000
- 0.008 nec_005
- 0.008 maxvision_001
- 0.008 dahua_004
- 0.008 lineclova_002
- 0.007 cogent_006
- 0.007 line_001
- 0.007 paravision_009
- 0.007 dahua_003
- 0.007 vts_003
- 0.007 clearviewai_000
- 0.007 deepgint_001
- 0.007 paravision_012
- 0.007 maxvision_002
- 0.007 paravision_014
- 0.007 sensetime_004
- 0.007 knowtotech_000
- 0.007 ntechlab_011
- 0.007 rankone_013
- 0.007 sensetime_003

Figure 301: [Webcam Dataset] Identification miss rates vs. rank. The results apply to cross-domain recognition in which webcams are searched against enrolled mugshots. The FNIR values are higher than those for mugshot-mugshot identification due to low image resolution, lighting and less constrained subject pose in webcam images - see Figure 6.

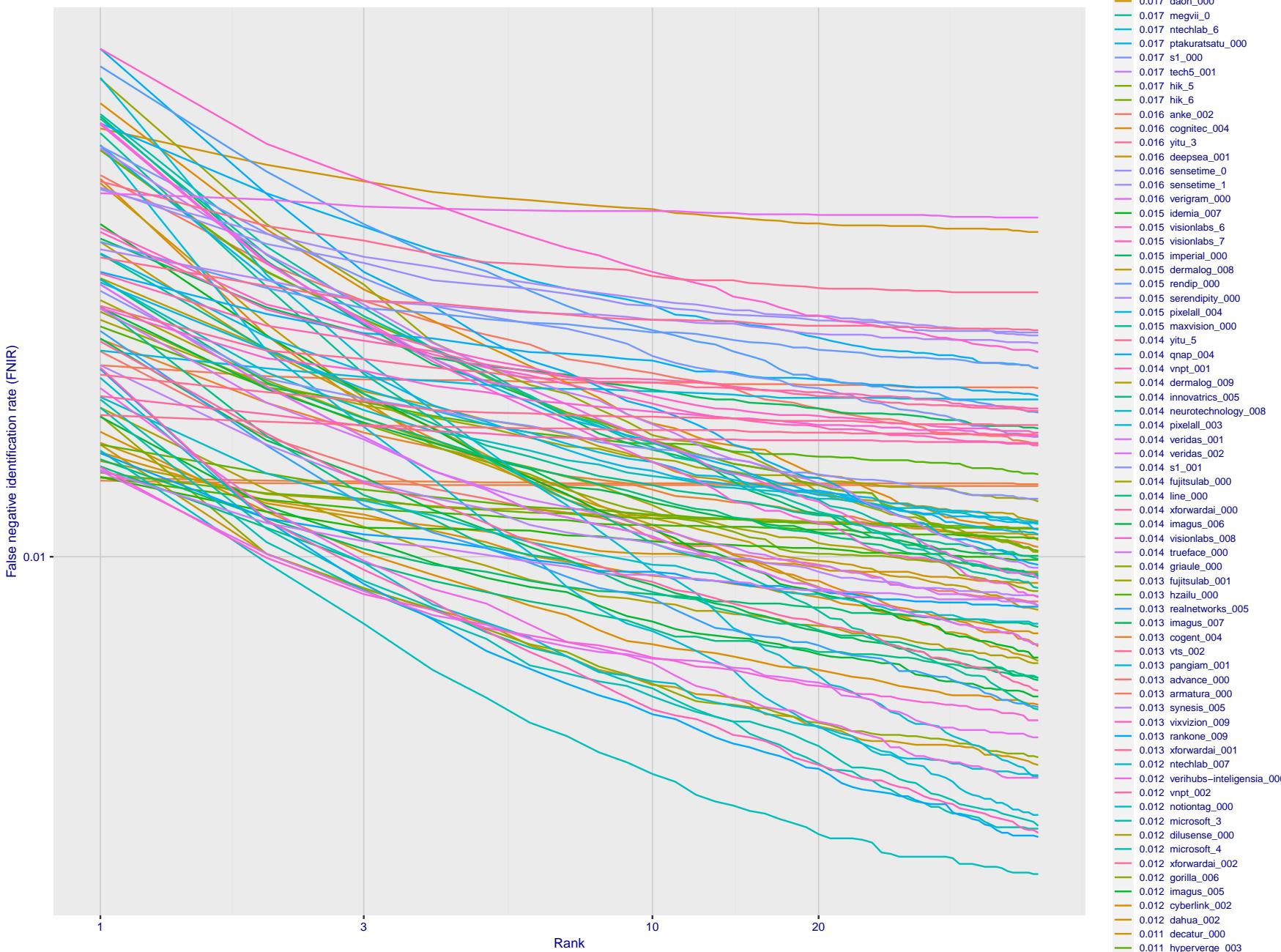


Figure 302: [Webcam Dataset] Identification miss rates vs. rank. The results apply to cross-domain recognition in which webcams are searched against enrolled mugshots. The FNIR values are higher than those for mugshot-mugshot identification due to low image resolution, lighting and less constrained subject pose in webcam images - see Figure 6.

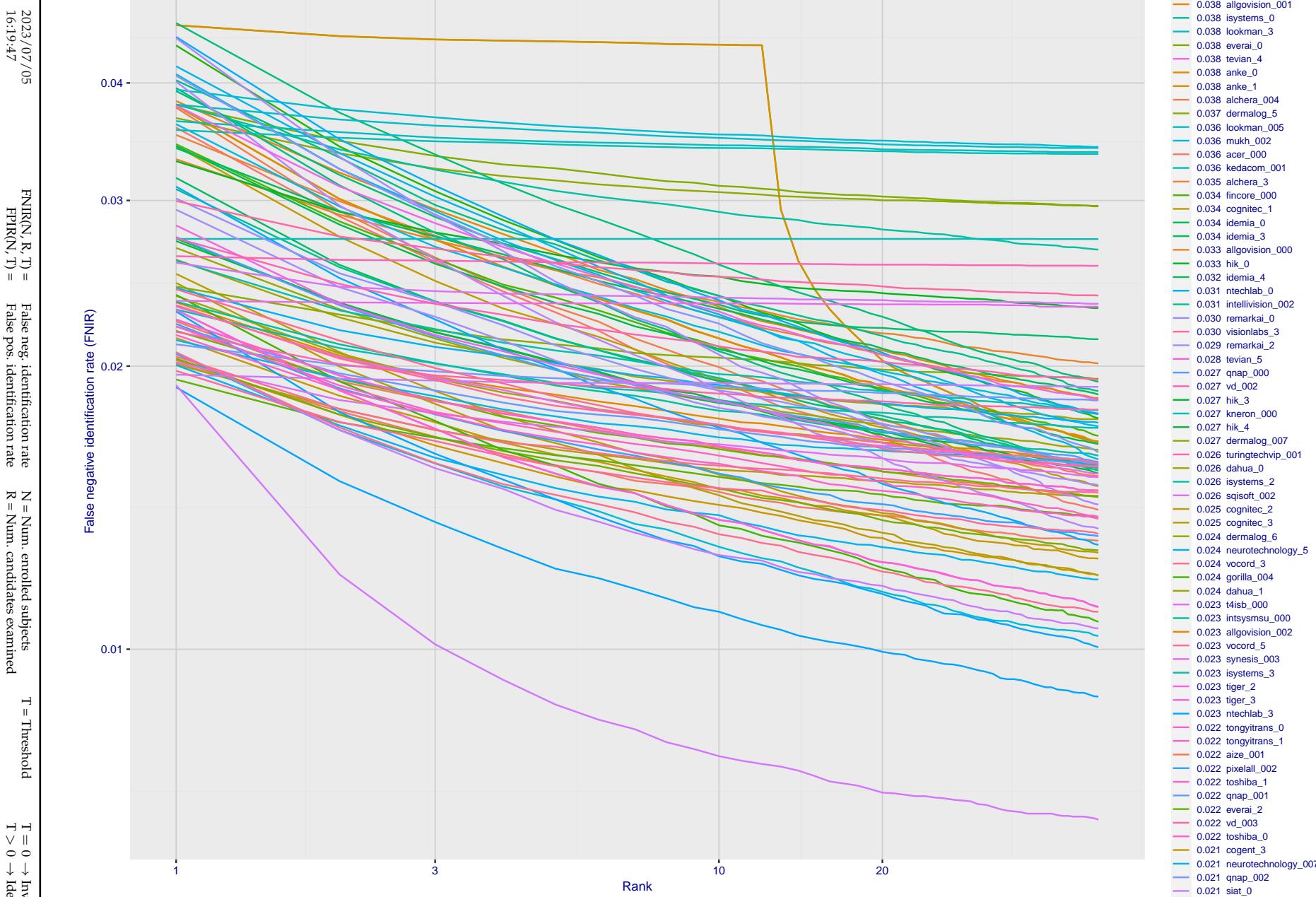


Figure 303: [Webcam Dataset] Identification miss rates vs. rank. The results apply to cross-domain recognition in which webcams are searched against enrolled mugshots. The FNIR values are higher than those for mugshot-mugshot identification due to low image resolution, lighting and less constrained subject pose in webcam images - see Figure 6.

2023/07/05
16:19:47
 $\text{FNIR}(N, R, T) =$ False neg. identification rate
 $\text{FPIR}(N, T) =$ False pos. identification rate
 $N =$ Num. enrolled subjects
 $R =$ Num. candidates examined
 $T =$ Threshold
 $T = 0 \rightarrow$ Investigation
 $T > 0 \rightarrow$ Identification

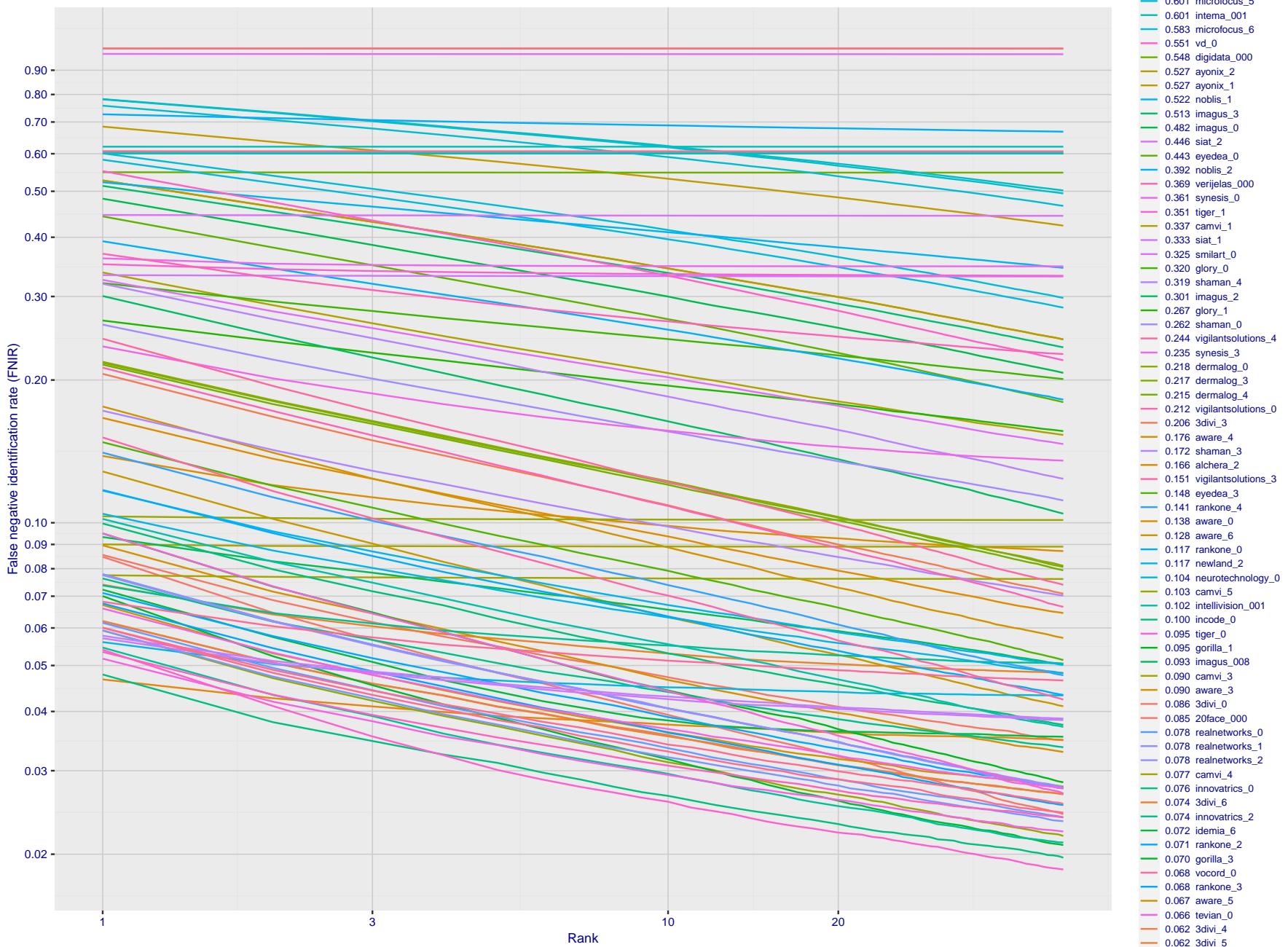


Figure 304: [Webcam Dataset] Identification miss rates vs. rank. The results apply to cross-domain recognition in which webcams are searched against enrolled mugshots. The FNIR values are higher than those for mugshot-mugshot identification due to low image resolution, lighting and less constrained subject pose in webcam images - see Figure 6.

2023/07/05
16:19:47

FNIR(N, R, T) = False neg. identification rate
FPTR(N, T) = False pos. identification rate

N = Num. enrolled subjects
R = Num. candidates examined

T = Threshold
T > 0 → Identification

2023/07/05
16:19:47FNIR(N, R, T) = False neg. identification rate
FPIR(N, T) = False pos. identification rateN = Num. enrolled subjects
R = Num. candidates examined

T = Threshold

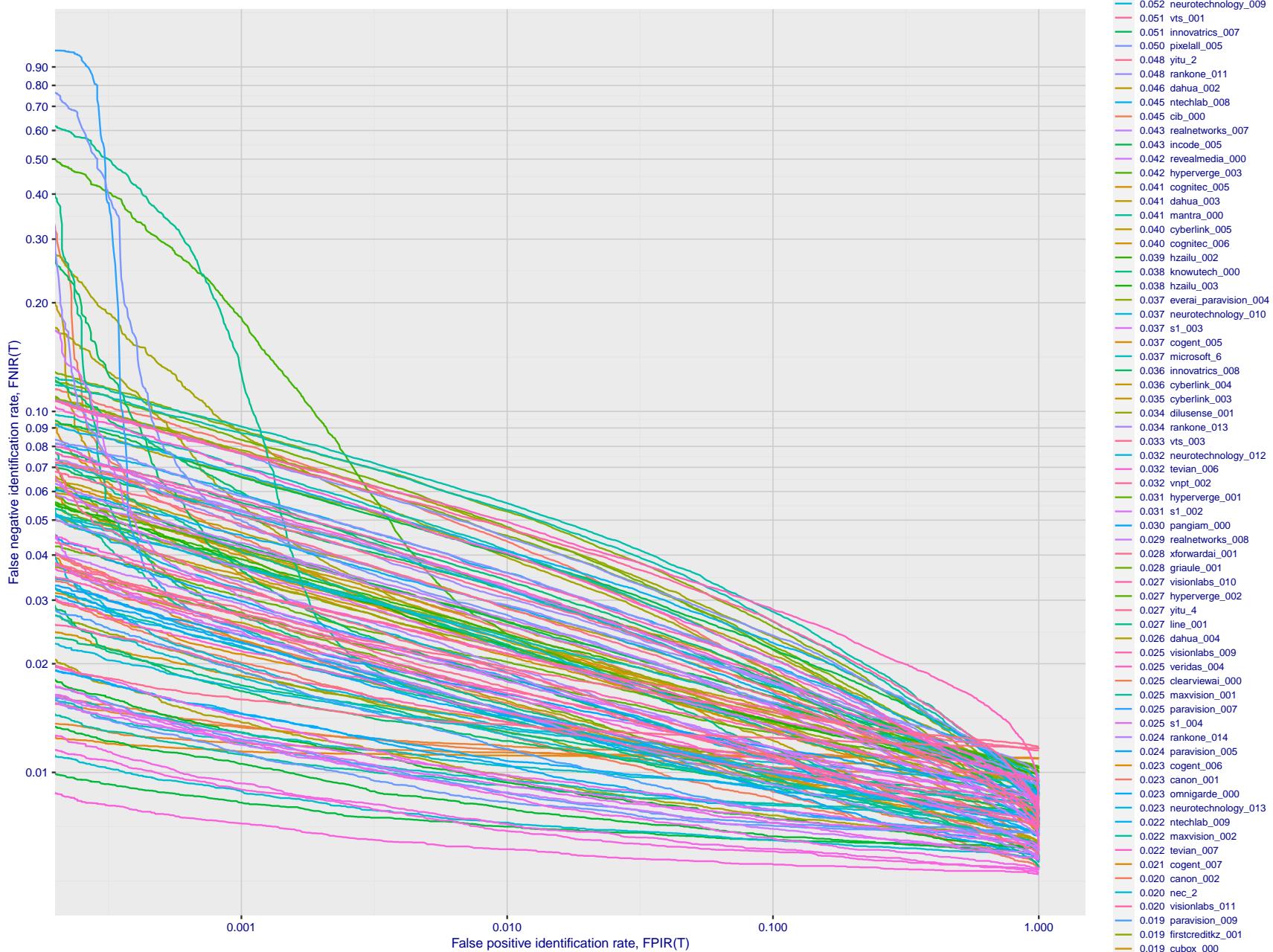
T = 0 → Investigation
T > 0 → Identification

Figure 305: [Webcam Dataset] Identification miss rates vs. false positive rates. The results apply to cross-domain recognition in which webcams are searched against enrolled mugshots. The FNIR values are higher than those for mugshot-mugshot identification due to low image resolution, lighting and less constrained subject pose in webcam images - see Figure 6.

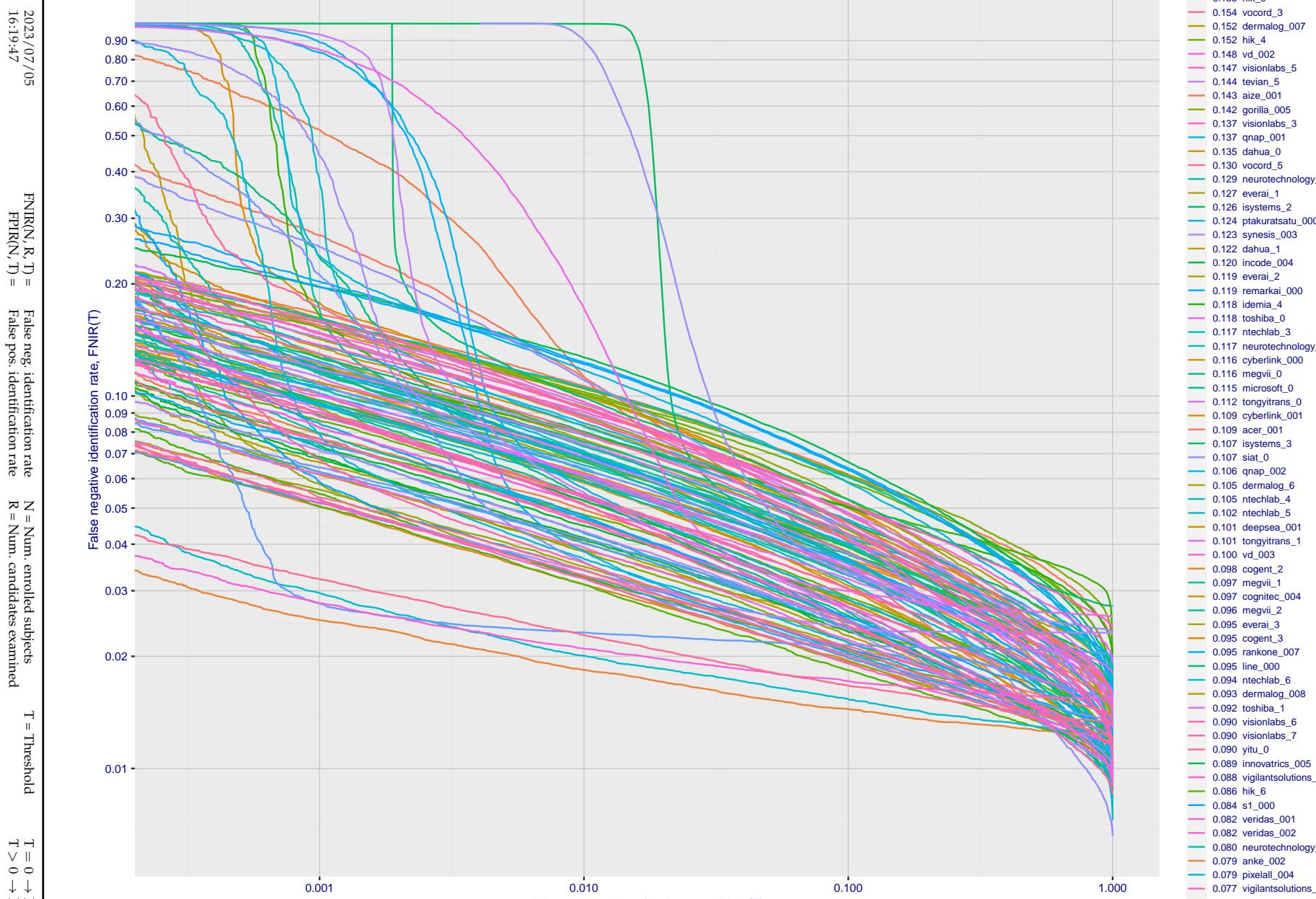


Figure 306: [Webcam Dataset] Identification miss rates vs. false positive rates. The results apply to cross-domain recognition in which webcams are searched against enrolled mugshots. The FNIR values are higher than those for mugshot-mugshot identification due to low image resolution, lighting and less constrained subject pose in webcam images - see Figure 6.

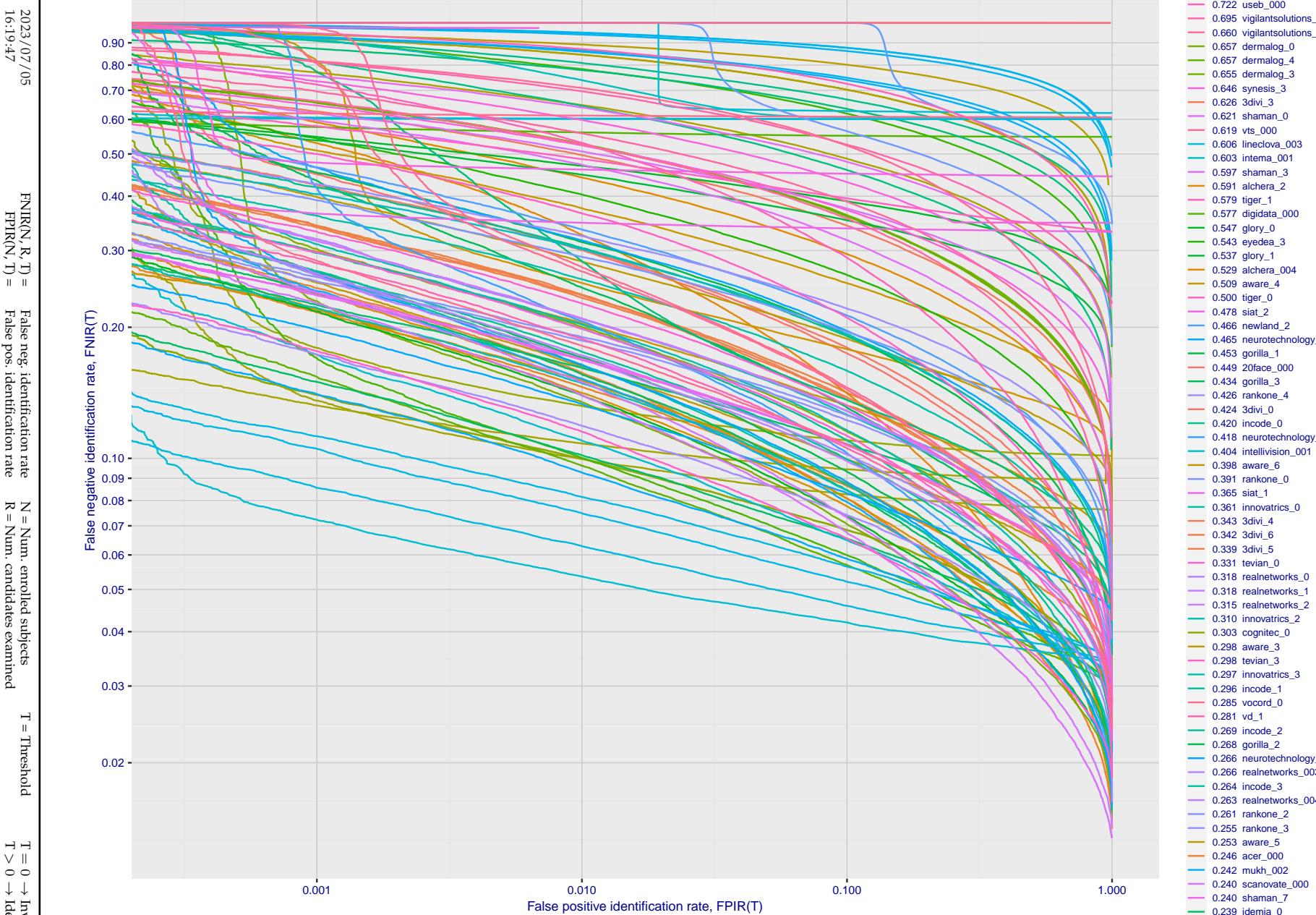


Figure 307: [Webcam Dataset] Identification miss rates vs. false positive rates. The results apply to cross-domain recognition in which webcams are searched against enrolled mugshots. The FNIR values are higher than those for mugshot-mugshot identification due to low image resolution, lighting and less constrained subject pose in webcam images - see Figure 6.

Appendix E Accuracy for profile-view to frontal recognition

Figures 308 - 310 gives accuracy results for searching 100 000 mated and 100 000 non-mated profile-view images against the same FRVT 2018 frontal enrollment dataset, $N = 1\,600\,000$, used in the main mugshot trials. This experiment corresponds to row-13 of Table 1. An example of profile-view image is given in Figure 7.

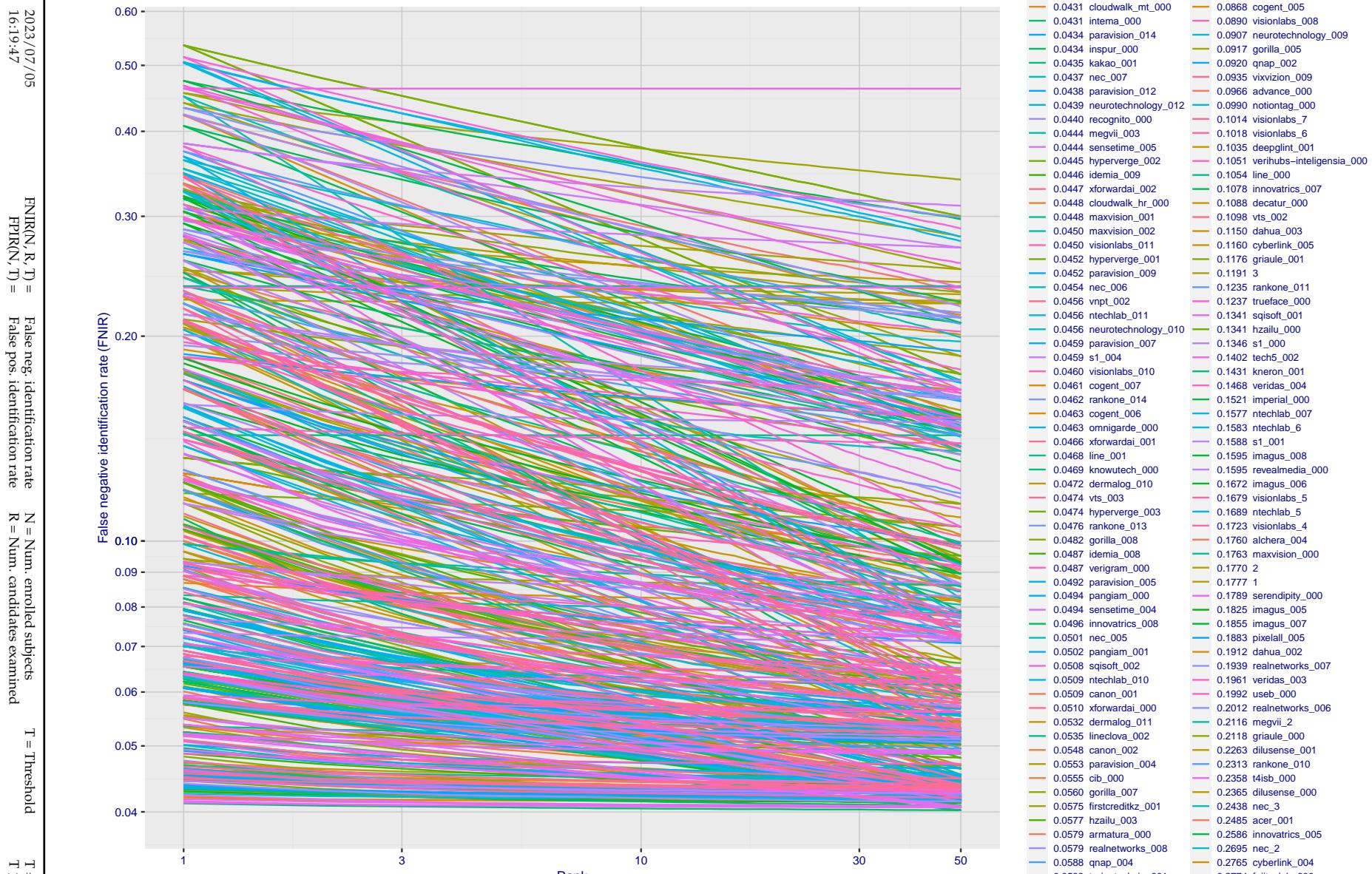


Figure 308: [Mugshot and profile-view dataset] Rank-based accuracy. For some of the more accurate Phase 3 algorithms the figure plots error tradeoff characteristics for frontal and profile-view searches into an enrolled set of $N = 1\,600\,000$ frontal images. Note that some algorithms fail on profile-view images with $\text{FNIR} \rightarrow 1$ - this evaluation did not ask developers to provide profile-view capability. Some algorithms, on the other hand, give FNIR approaching that for frontal-view searches using c. 2010 algorithms. The best result is that 91% of profile-view searches yield the correct mate at rank 1, and better than 94% in the top-50 candidates.

2023/07/05
16:19:47FNIR(N, R, T) = False neg. identification rate
FPIR(N, T) = False pos. identification rateN = Num. enrolled subjects
R = Num. candidates examined

T = Threshold

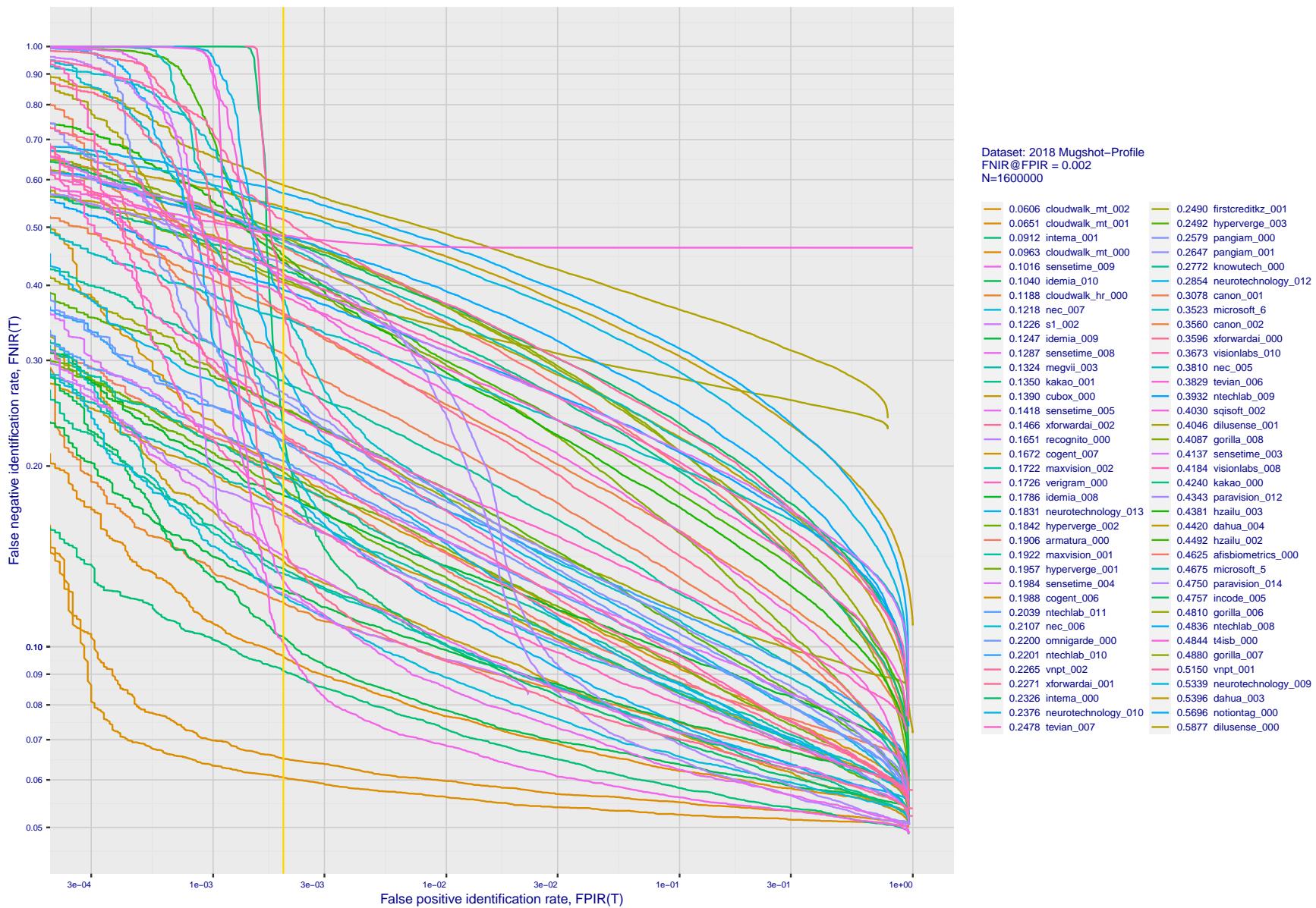
T = 0 → Investigation
T > 0 → Identification

Figure 309: [Mugshot and profile-view dataset] Threshold-based accuracy. For some of the more accurate Phase 3 algorithms the figure plots error tradeoff characteristics for frontal and profile-view searches into an enrolled set of $N = 1\,600\,000$ frontal images. Note that some algorithms fail on profile-view images with $\text{FNIR} \rightarrow 1$ - this evaluation did not ask developers to provide profile-view capability. Some algorithms, on the other hand, give FNIR approaching that for frontal-view searches using c. 2010 algorithms.

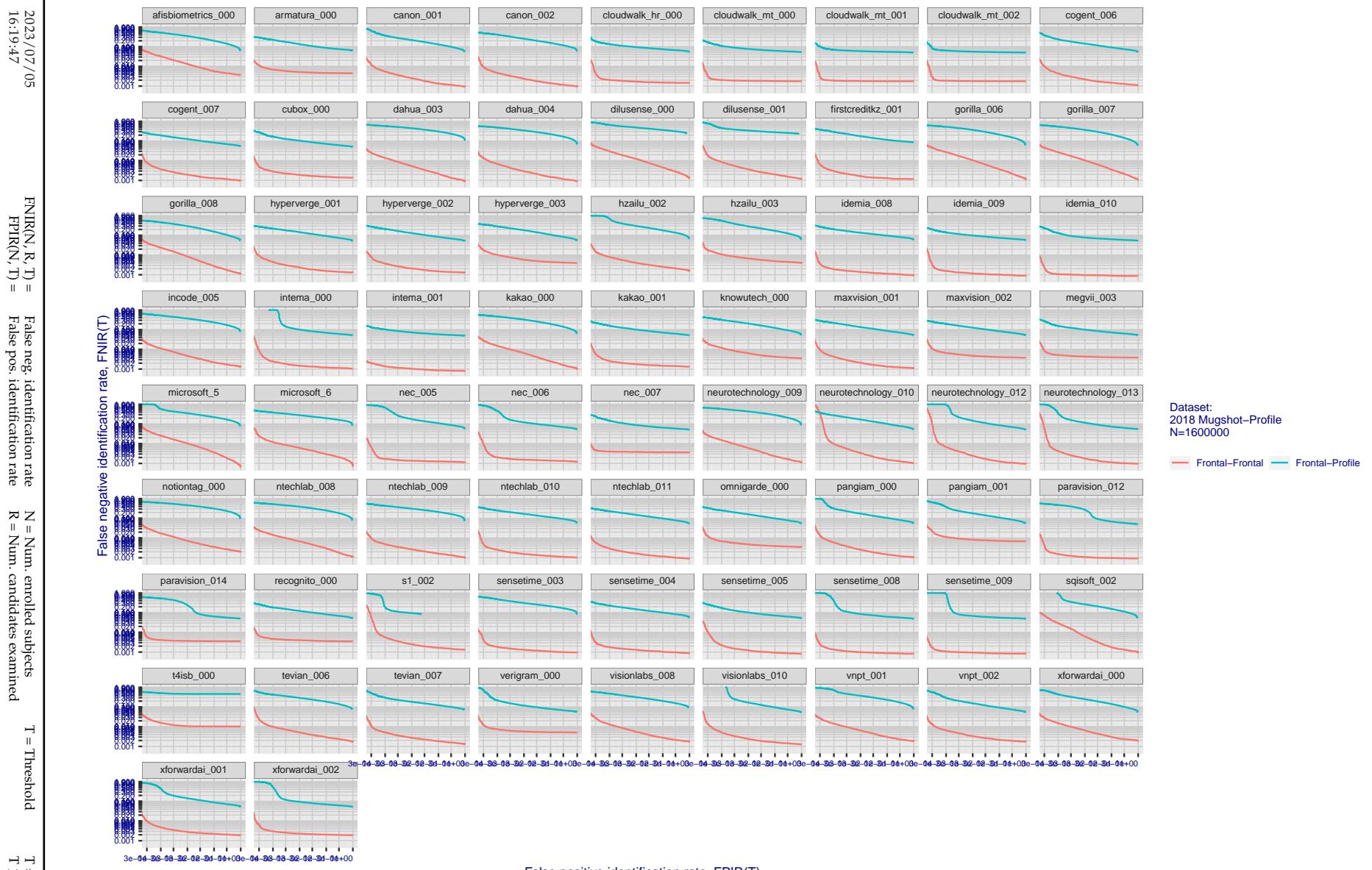


Figure 310: [Mugshot and profile-view dataset] Speed-accuracy tradeoff. For some of the more accurate Phase 3 algorithms the figure plots error tradeoff characteristics for frontal and profile-view searches into an enrolled set of $N = 1\,600\,000$ frontal images. Some algorithms fail on profile-view images with $\text{FNIR} \rightarrow 1$ - this evaluation did not ask developers to provide profile-view capability. Some algorithms, on the other hand, give FNIR approaching that for frontal-view searches using c. 2010 algorithms. Blue lines connect points of equal threshold from which it is evident that some algorithms would give markedly higher false positive outcomes if profile-view images were searched in a system configured for frontal searches. This would be a vulnerability in an access control system.

Appendix F Search duration

As in and prior tests, this section documents search speeds spanning three orders of magnitude. In applications where search volumes are high enough, this will have implications for hardware requirements especially for large N or when search duration is appreciably larger than the time it takes to prepare a template from the search image(s). Further, given very large (and growing) operational databases, the scalability of algorithms is important. It has been reported previously [8] that search duration can scale sublinearly with enrolled population size N. Further there has been considerable recent research on indexing, exact [13] and approximate nearest neighbor search [1,13] and fast-search [14,16].

Figure 311 charts the search duration measurements presented earlier in Tables 2 - 4.

- ▷ Most algorithms scale linearly. For those in that category, there is a wide range in speed with search durations ranging from 82 milliseconds for a 12 million gallery (for NEC-3) to more than 40 seconds (for Yitu-3, Toshiba-2) and even higher for less accurate algorithms.
- ▷ Some developers (Camvi, Dermalog, EverAI, Innovatrics, and Visionlabs) provide algorithms whose template search durations grow approximately logarithmically i.e. $T(N) \sim \log N$ with the constant a varying between implementations. In the figure this model is fit using the point $T(1) = 0$, and $T(640\,000)$. This very sublinear behaviour affords extremely fast search times in very large galleries. One caveat for the sublinear algorithms is that their fast-search data structures can require considerable computation time - on the order of hours - for N in the millions, and this scales mildly super-linearly, i.e. $O(N^b)$, $b > 1$. There are exceptions: the Camvi algorithms take minutes; and Innovatrics' scale sublinearly.

2023/07/05
16:19:47

FNIR(N, R, T) = False neg. identification rate
FPTR(N, T) = False pos. identification rate

N = Num. enrolled subjects
R = Num. candidates examined

T = Threshold
T > 0 → Identification

2023/07/05
16:19:47FNIR(N, R, T) = False neg. identification rate
FPTR(N, T) = False pos. identification rateN = Num. enrolled subjects
R = Num. candidates examinedT = Threshold
T = 0 → Investigation

T > 0 → Identification

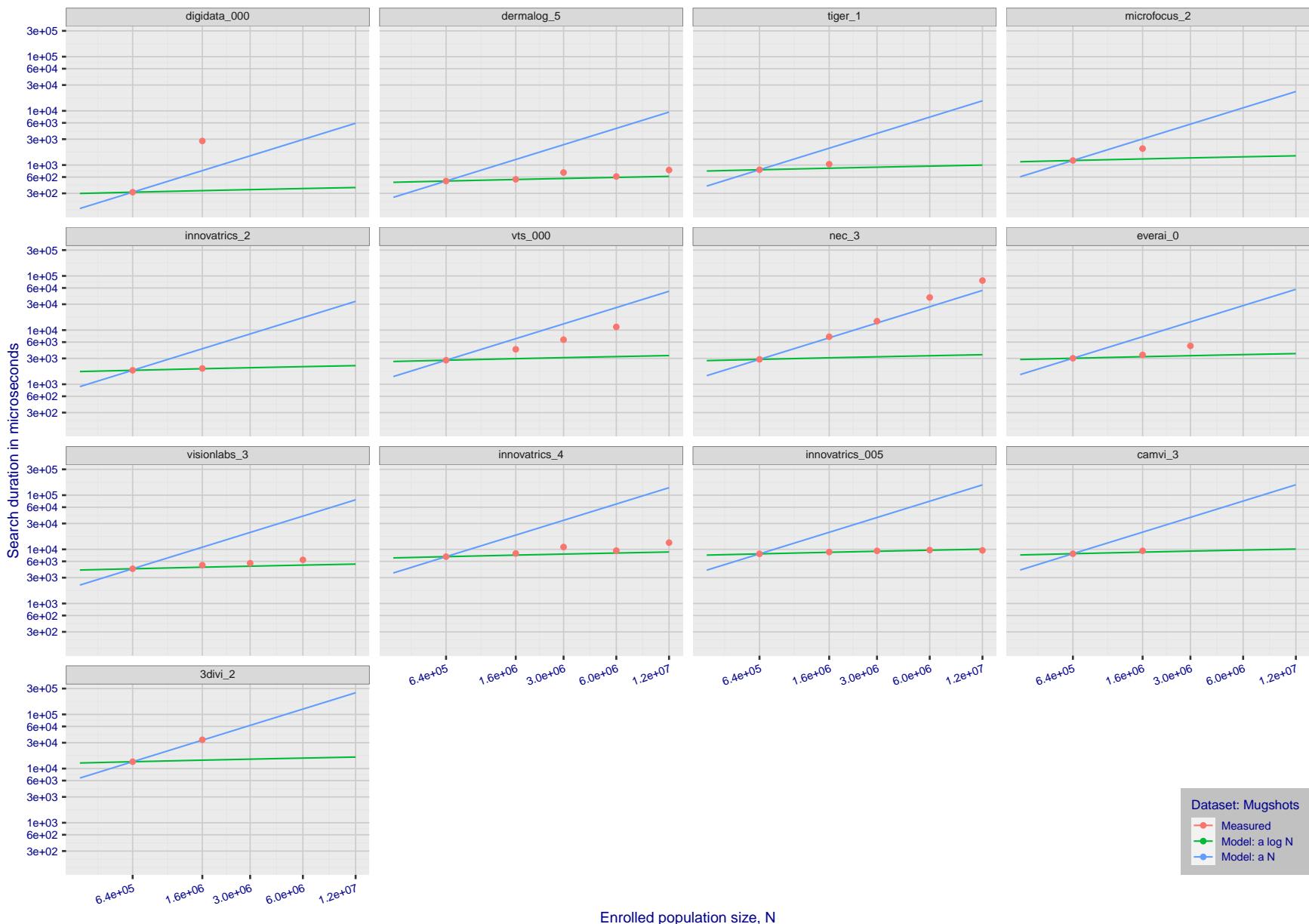


Figure 311: [Mugshot Dataset] Search duration vs. enrolled population size. In red are the actual point durations measured on a single c. 2016 core. The blue shows linear growth from $N = 640\,000$. The green line shows logarithmic growth from that point to $N = 1\,600\,000$. Note the sublinear growth from algorithms from Camvi, Dermalog, EverAI, Innovatrics, and Visionlabs. The tiger_1 algorithm is also sublinear, but inaccurate and inoperable at $N \geq 3000000$. This capability sometimes comes at the additional expense of converting a linear gallery data structure into whatever fast-search data structure is used. Note that search times are sometimes dominated by the template generation times shown in Table 29.

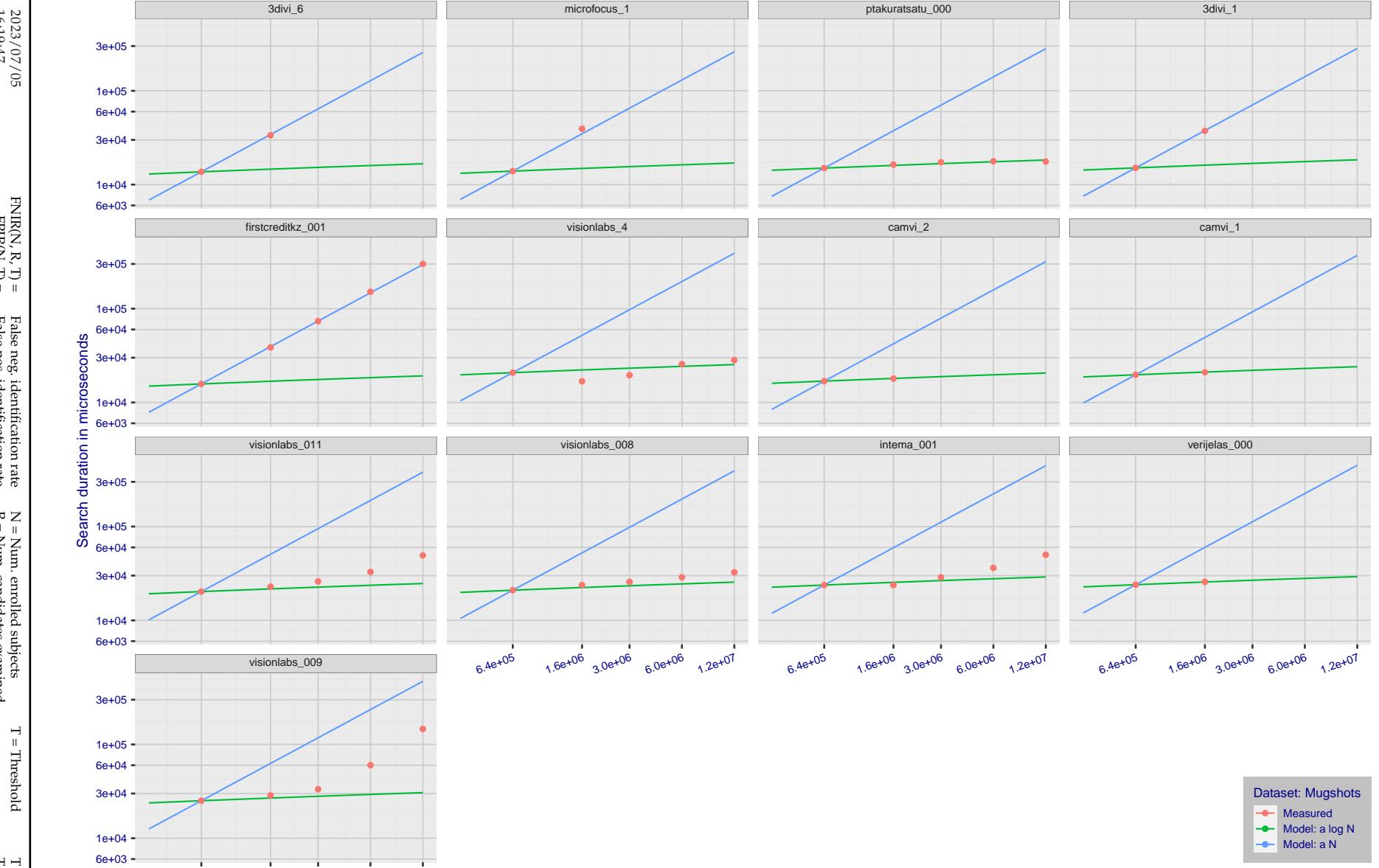


Figure 312: [Mugshot Dataset] Search duration vs. enrolled population size. In red are the actual point durations measured on a single c. 2016 core. The blue shows linear growth from $N = 640\,000$. The green line shows logarithmic growth from that point to $N = 1\,600\,000$. Note the sublinear growth from algorithms from Camvi, Dermalog, EverAI, Innovatrics, and Visionlabs. The tiger_1 algorithm is also sublinear, but inaccurate and inoperable at $N \geq 3000000$. This capability sometimes comes at the additional expense of converting a linear gallery data structure into whatever fast-search data structure is used. Note that search times are sometimes dominated by the template generation times shown in Table 29.

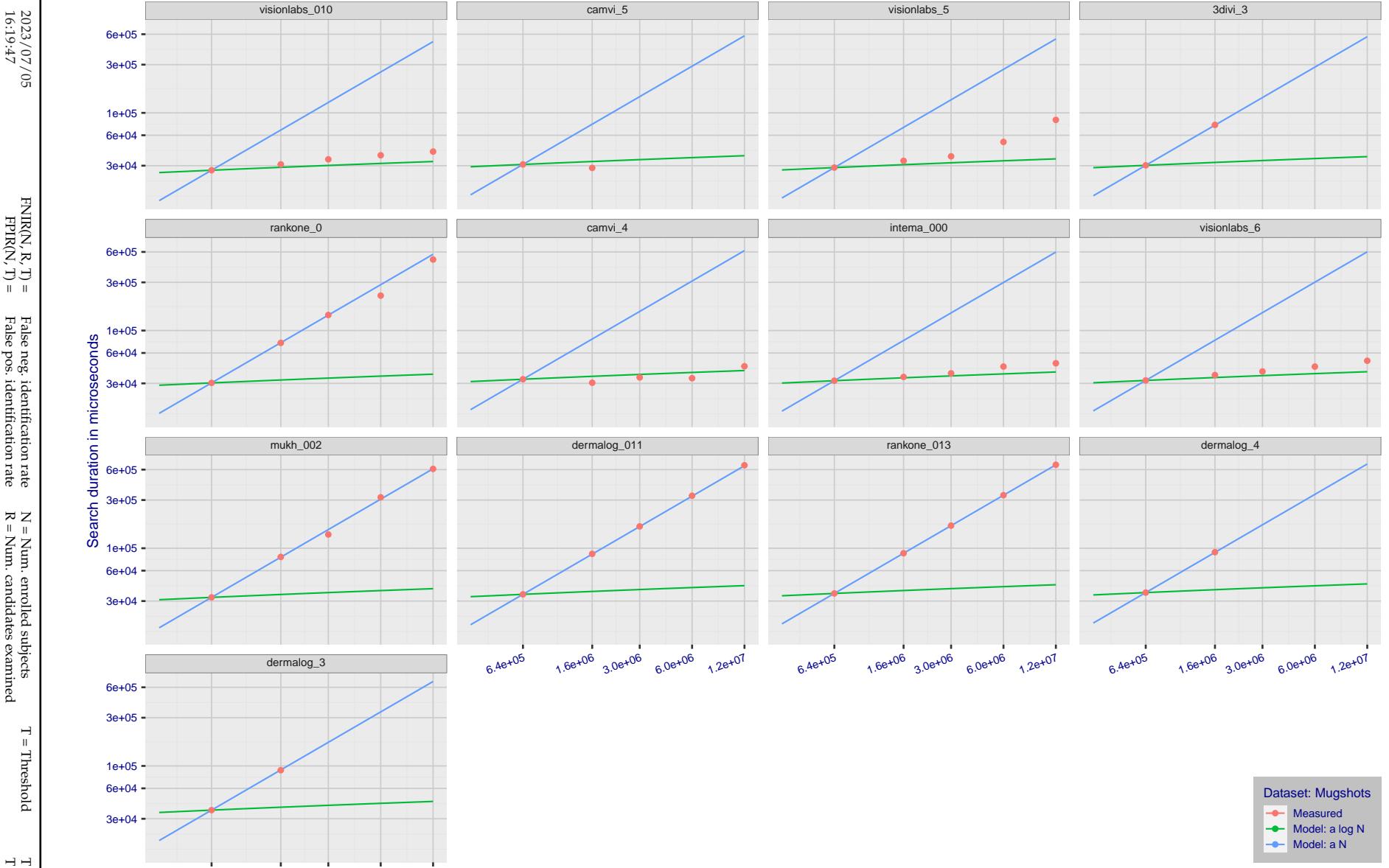


Figure 313: [Mugshot Dataset] Search duration vs. enrolled population size. In red are the actual point durations measured on a single c. 2016 core. The blue shows linear growth from $N = 640\,000$. The green line shows logarithmic growth from that point to $N = 1\,600\,000$. Note the sublinear growth from algorithms from Camvi, Dermalog, EverAI, Innovatrics, and Visionlabs. The tiger_1 algorithm is also sublinear, but inaccurate and inoperable at $N \geq 3000000$. This capability sometimes comes at the additional expense of converting a linear gallery data structure into whatever fast-search data structure is used. Note that search times are sometimes dominated by the template generation times shown in Table 29.

2023/07/05
16:19:47FNIR(N, R, T) = False neg. identification rate
FPIR(N, T) = False pos. identification rateN = Num. enrolled subjects
R = Num. candidates examinedT = Threshold
T = 0 → Investigation

T > 0 → Identification

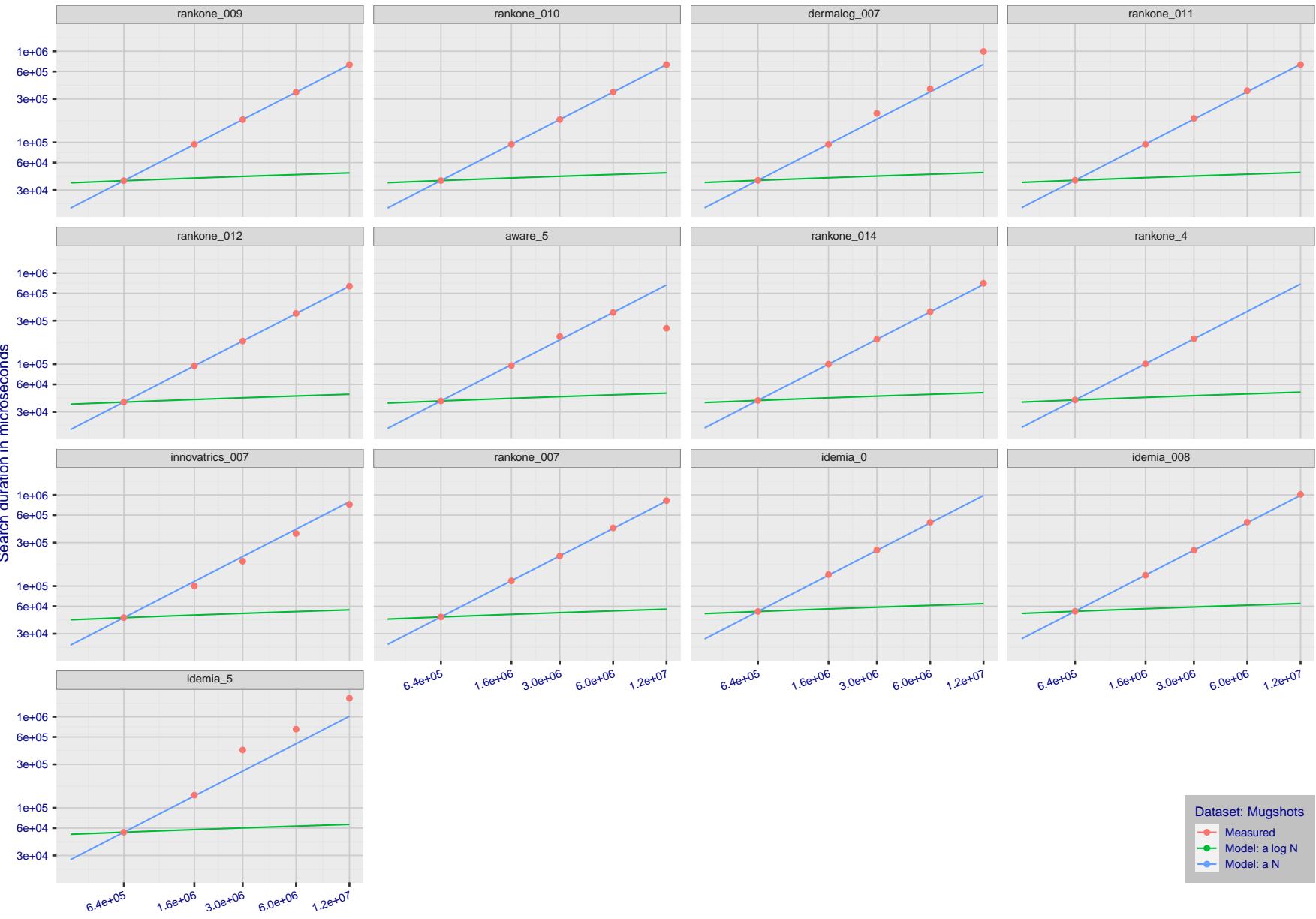


Figure 314: [Mugshot Dataset] Search duration vs. enrolled population size. In red are the actual point durations measured on a single c. 2016 core. The blue shows linear growth from $N = 640\,000$. The green line shows logarithmic growth from that point to $N = 1\,600\,000$. Note the sublinear growth from algorithms from Camvi, Dermalog, EverAI, Innovatrics, and Visionlabs. The tiger_1 algorithm is also sublinear, but inaccurate and inoperable at $N \geq 3000000$. This capability sometimes comes at the additional expense of converting a linear gallery data structure into whatever fast-search data structure is used. Note that search times are sometimes dominated by the template generation times shown in Table 29.

2023/07/05
16:19:47FNIR(N, R, T) = False neg. identification rate
FPFR(N, T) = False pos. identification rateN = Num. enrolled subjects
R = Num. candidates examined

T = Threshold

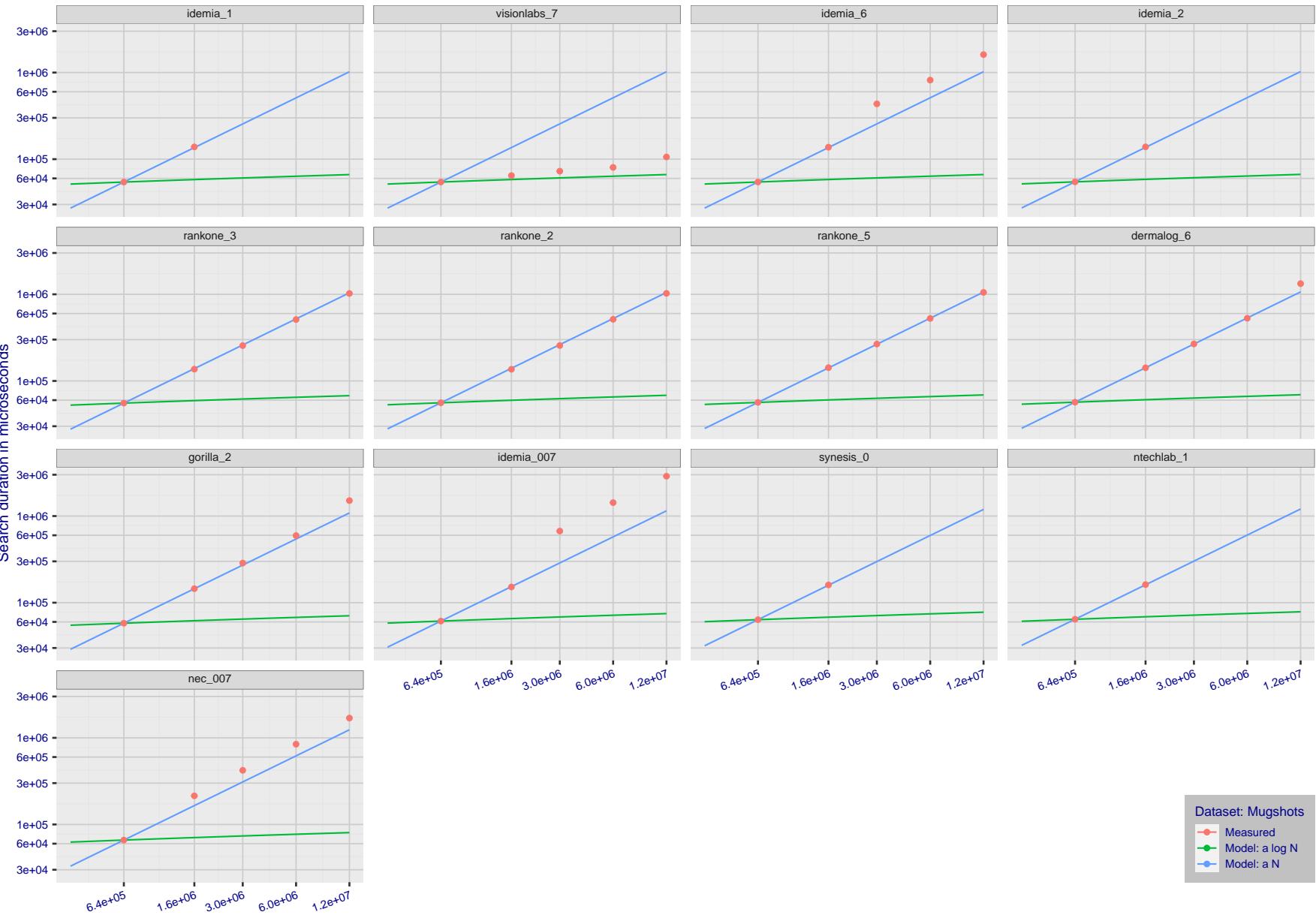
T = 0 → Investigation
T > 0 → Identification

Figure 315: [Mugshot Dataset] Search duration vs. enrolled population size. In red are the actual point durations measured on a single c. 2016 core. The blue shows linear growth from $N = 640\,000$. The green line shows logarithmic growth from that point to $N = 1\,600\,000$. Note the sublinear growth from algorithms from Camvi, Dermalog, EverAI, Innovatrics, and Visionlabs. The tiger_1 algorithm is also sublinear, but inaccurate and inoperable at $N \geq 3000000$. This capability sometimes comes at the additional expense of converting a linear gallery data structure into whatever fast-search data structure is used. Note that search times are sometimes dominated by the template generation times shown in Table 29.

2023/07/05
16:19:47FNIR(N, R, T) = False neg. identification rate
FPIR(N, T) = False pos. identification rateN = Num. enrolled subjects
R = Num. candidates examined

T = Threshold

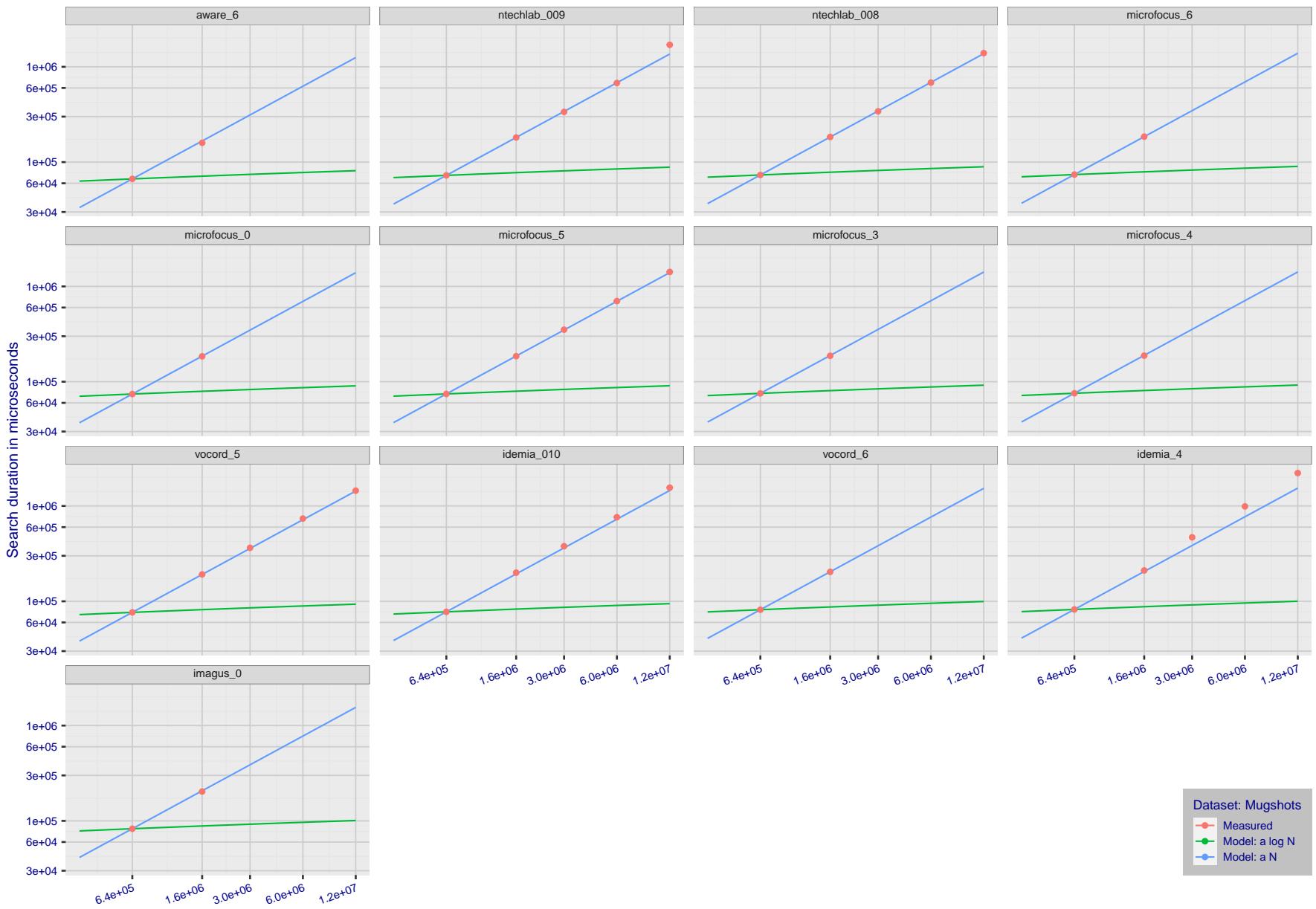
T = 0 → Investigation
T > 0 → Identification

Figure 316: [Mugshot Dataset] Search duration vs. enrolled population size. In red are the actual point durations measured on a single c. 2016 core. The blue shows linear growth from $N = 640\,000$. The green line shows logarithmic growth from that point to $N = 1\,600\,000$. Note the sublinear growth from algorithms from Camvi, Dermalog, EverAI, Innovatrics, and Visionlabs. The tiger_1 algorithm is also sublinear, but inaccurate and inoperable at $N \geq 3000000$. This capability sometimes comes at the additional expense of converting a linear gallery data structure into whatever fast-search data structure is used. Note that search times are sometimes dominated by the template generation times shown in Table 29.

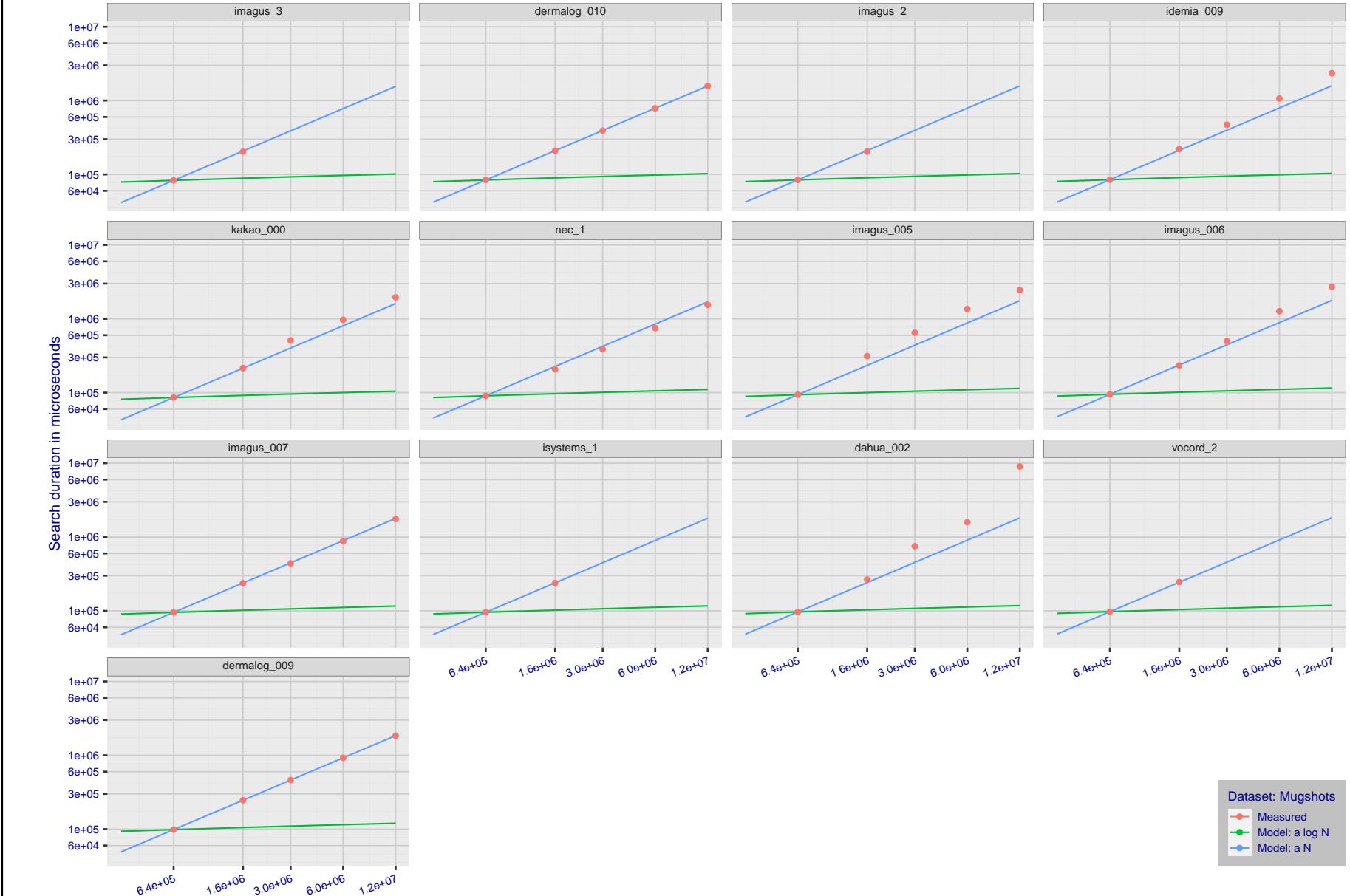


Figure 317: [Mugshot Dataset] Search duration vs. enrolled population size. In red are the actual point durations measured on a single c. 2016 core. The blue shows linear growth from $N = 640\,000$. The green line shows logarithmic growth from that point to $N = 1\,600\,000$. Note the sublinear growth from algorithms from Camvi, Dermalog, EverAI, Innovatrics, and Visionlabs. The tiger_1 algorithm is also sublinear, but inaccurate and inoperable at $N \geq 3000000$. This capability sometimes comes at the additional expense of converting a linear gallery data structure into whatever fast-search data structure is used. Note that search times are sometimes dominated by the template generation times shown in Table 29.

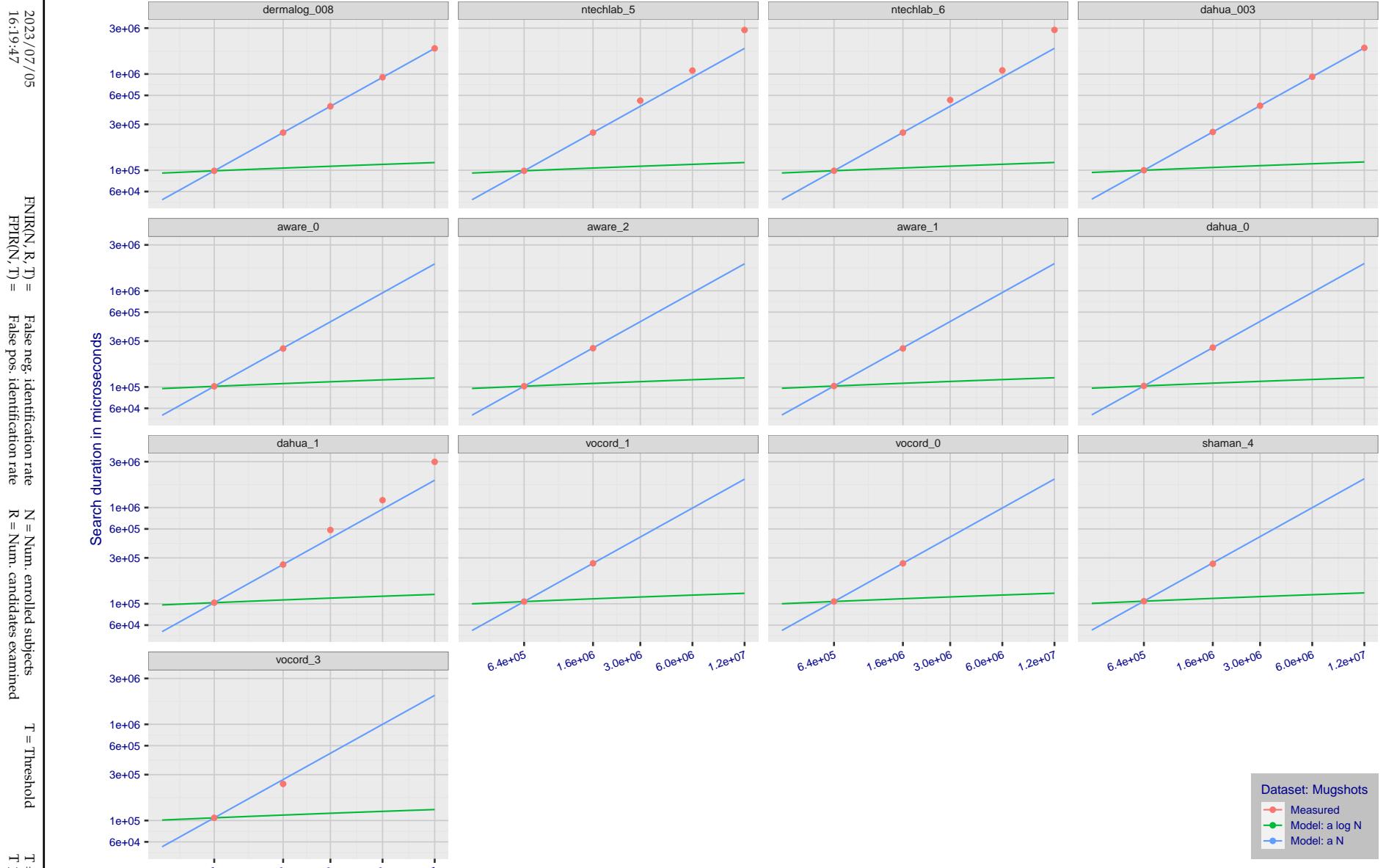


Figure 318: [Mugshot Dataset] Search duration vs. enrolled population size. In red are the actual point durations measured on a single c. 2016 core. The blue shows linear growth from $N = 640\,000$. The green line shows logarithmic growth from that point to $N = 1\,600\,000$. Note the sublinear growth from algorithms from Camvi, Dermalog, EverAI, Innovatrics, and Visionlabs. The tiger_1 algorithm is also sublinear, but inaccurate and inoperable at $N \geq 3000000$. This capability sometimes comes at the additional expense of converting a linear gallery data structure into whatever fast-search data structure is used. Note that search times are sometimes dominated by the template generation times shown in Table 29.

2023/07/05
16:19:47FNIR(N, R, T) = False neg. identification rate
FPTR(N, T) = False pos. identification rateN = Num. enrolled subjects
R = Num. candidates examined

T = Threshold

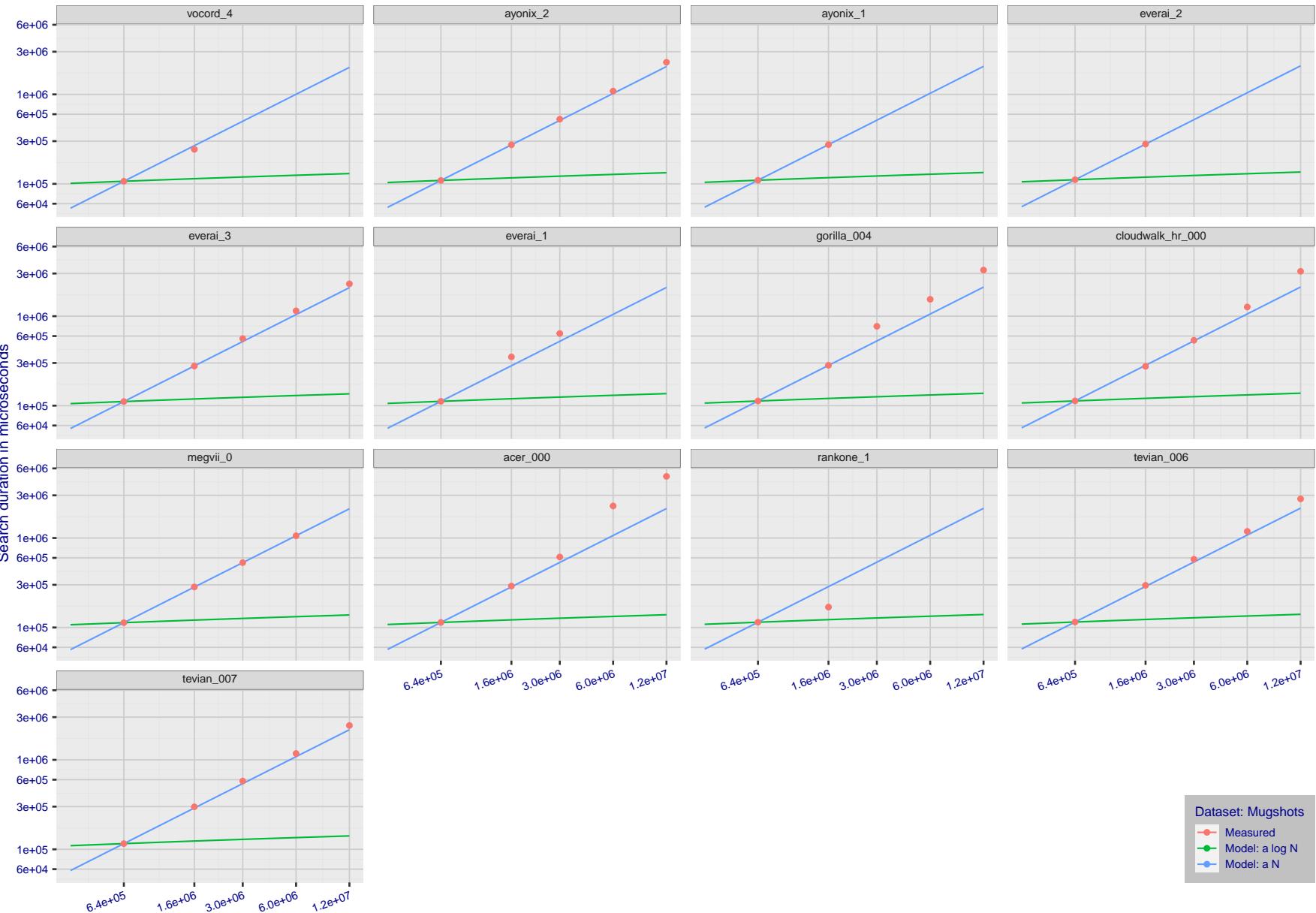
T = 0 → Investigation
T > 0 → Identification

Figure 319: [Mugshot Dataset] Search duration vs. enrolled population size. In red are the actual point durations measured on a single c. 2016 core. The blue shows linear growth from $N = 640\,000$. The green line shows logarithmic growth from that point to $N = 1\,600\,000$. Note the sublinear growth from algorithms from Camvi, Dermalog, EverAI, Innovatrics, and Visionlabs. The tiger_1 algorithm is also sublinear, but inaccurate and inoperable at $N \geq 3000000$. This capability sometimes comes at the additional expense of converting a linear gallery data structure into whatever fast-search data structure is used. Note that search times are sometimes dominated by the template generation times shown in Table 29.

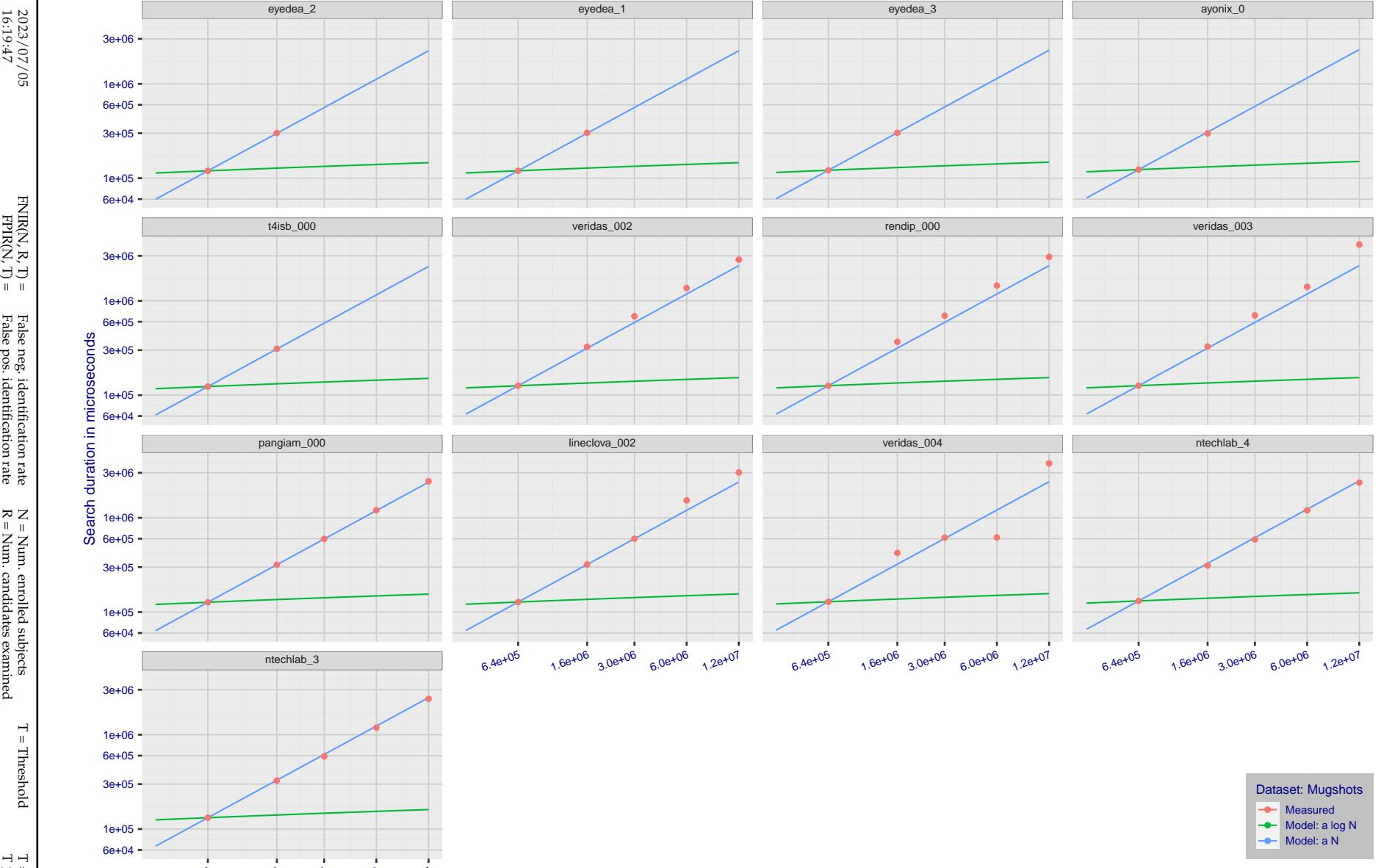


Figure 320: [Mugshot Dataset] Search duration vs. enrolled population size. In red are the actual point durations measured on a single c. 2016 core. The blue shows linear growth from $N = 640\,000$. The green line shows logarithmic growth from that point to $N = 1\,600\,000$. Note the sublinear growth from algorithms from Camvi, Dermalog, EverAI, Innovatrics, and Visionlabs. The tiger_1 algorithm is also sublinear, but inaccurate and inoperable at $N \geq 3000000$. This capability sometimes comes at the additional expense of converting a linear gallery data structure into whatever fast-search data structure is used. Note that search times are sometimes dominated by the template generation times shown in Table 29.

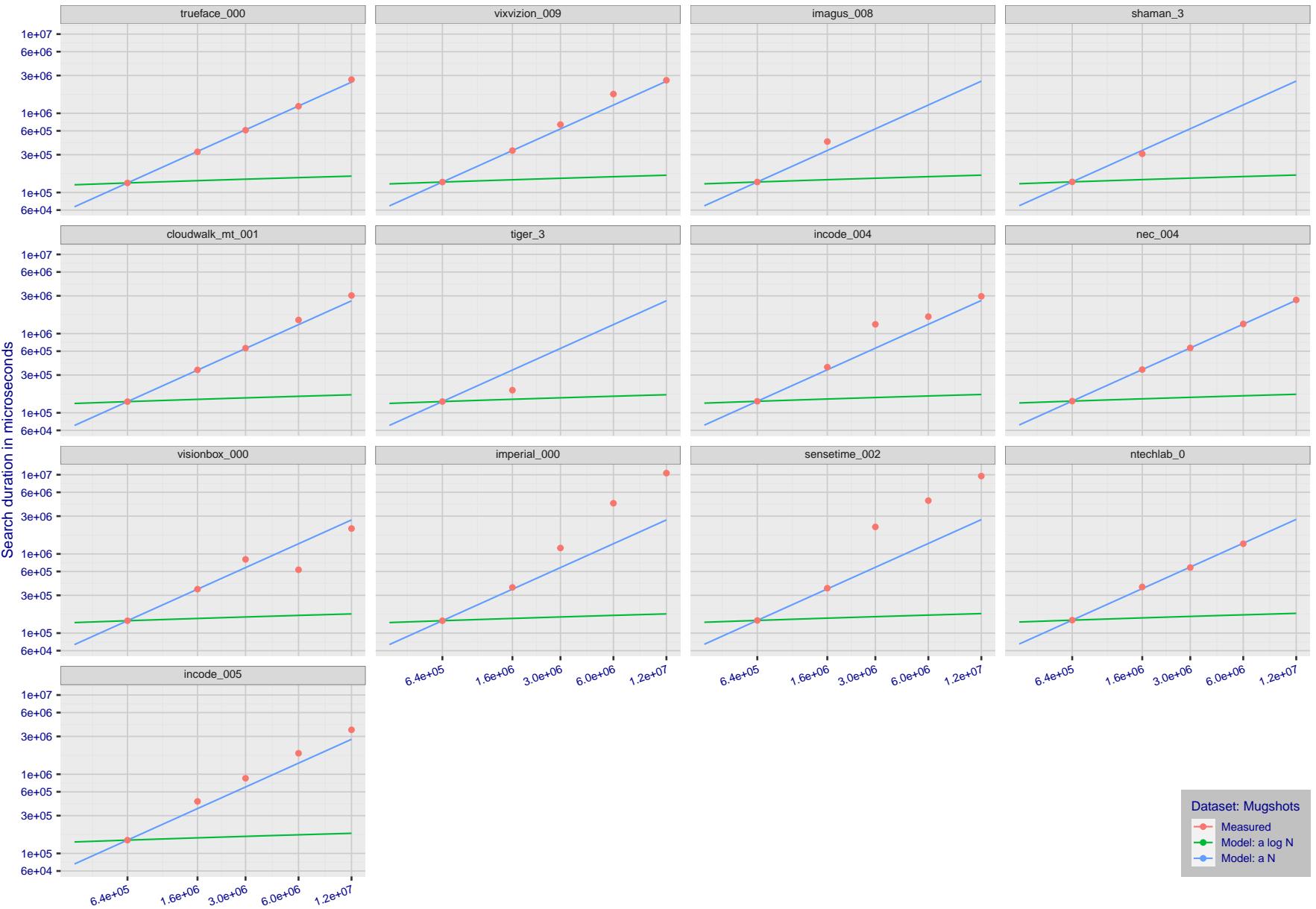


Figure 321: [Mugshot Dataset] Search duration vs. enrolled population size. In red are the actual point durations measured on a single c. 2016 core. The blue shows linear growth from $N = 640\,000$. The green line shows logarithmic growth from that point to $N = 1\,600\,000$. Note the sublinear growth from algorithms from Camvi, Dermalog, EverAI, Innovatrics, and Visionlabs. The tiger_1 algorithm is also sublinear, but inaccurate and inoperable at $N \geq 3000000$. This capability sometimes comes at the additional expense of converting a linear gallery data structure into whatever fast-search data structure is used. Note that search times are sometimes dominated by the template generation times shown in Table 29.

2023/07/05
16:19:47FNIR(N, R, T) = False neg. identification rate
FPIR(N, T) = False pos. identification rateN = Num. enrolled subjects
R = Num. candidates examined

T = Threshold

T = 0 → Investigation
 $T > 0 \rightarrow$ Identification

2023/07/05
16:19:47FNIR(N, R, T) = False neg. identification rate
FPIR(N, T) = False pos. identification rateN = Num. enrolled subjects
R = Num. candidates examined

T = Threshold

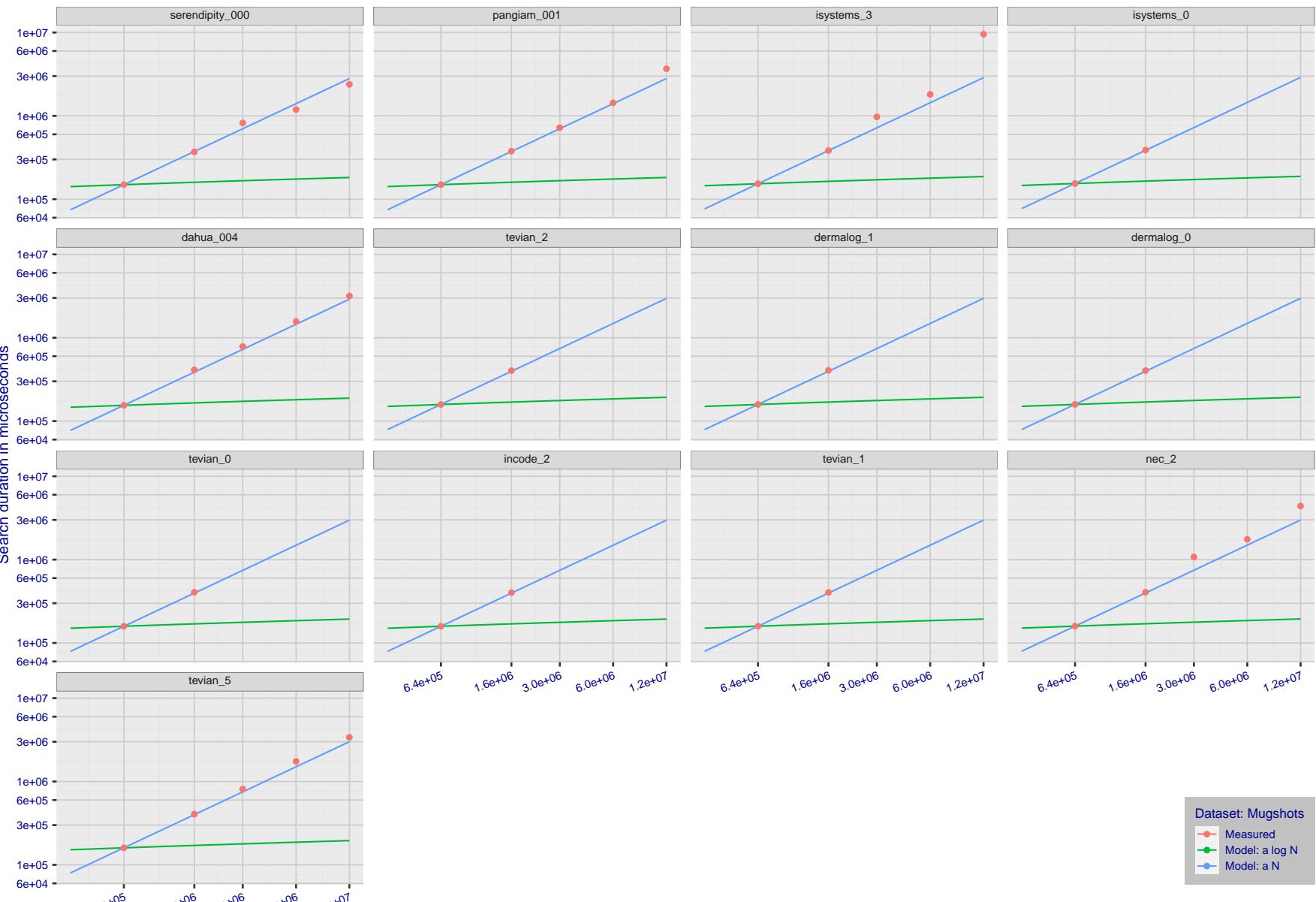
T = 0 → Investigation
T > 0 → Identification

Figure 322: [Mugshot Dataset] Search duration vs. enrolled population size. In red are the actual point durations measured on a single c. 2016 core. The blue shows linear growth from $N = 640\,000$. The green line shows logarithmic growth from that point to $N = 1\,600\,000$. Note the sublinear growth from algorithms from Camvi, Dermalog, EverAI, Innovatrics, and Visionlabs. The tiger_1 algorithm is also sublinear, but inaccurate and inoperable at $N \geq 3000000$. This capability sometimes comes at the additional expense of converting a linear gallery data structure into whatever fast-search data structure is used. Note that search times are sometimes dominated by the template generation times shown in Table 29.

2023/07/05
16:19:47FNIR(N, R, T) = False neg. identification rate
FPFR(N, T) = False pos. identification rateN = Num. enrolled subjects
R = Num. candidates examined

T = Threshold

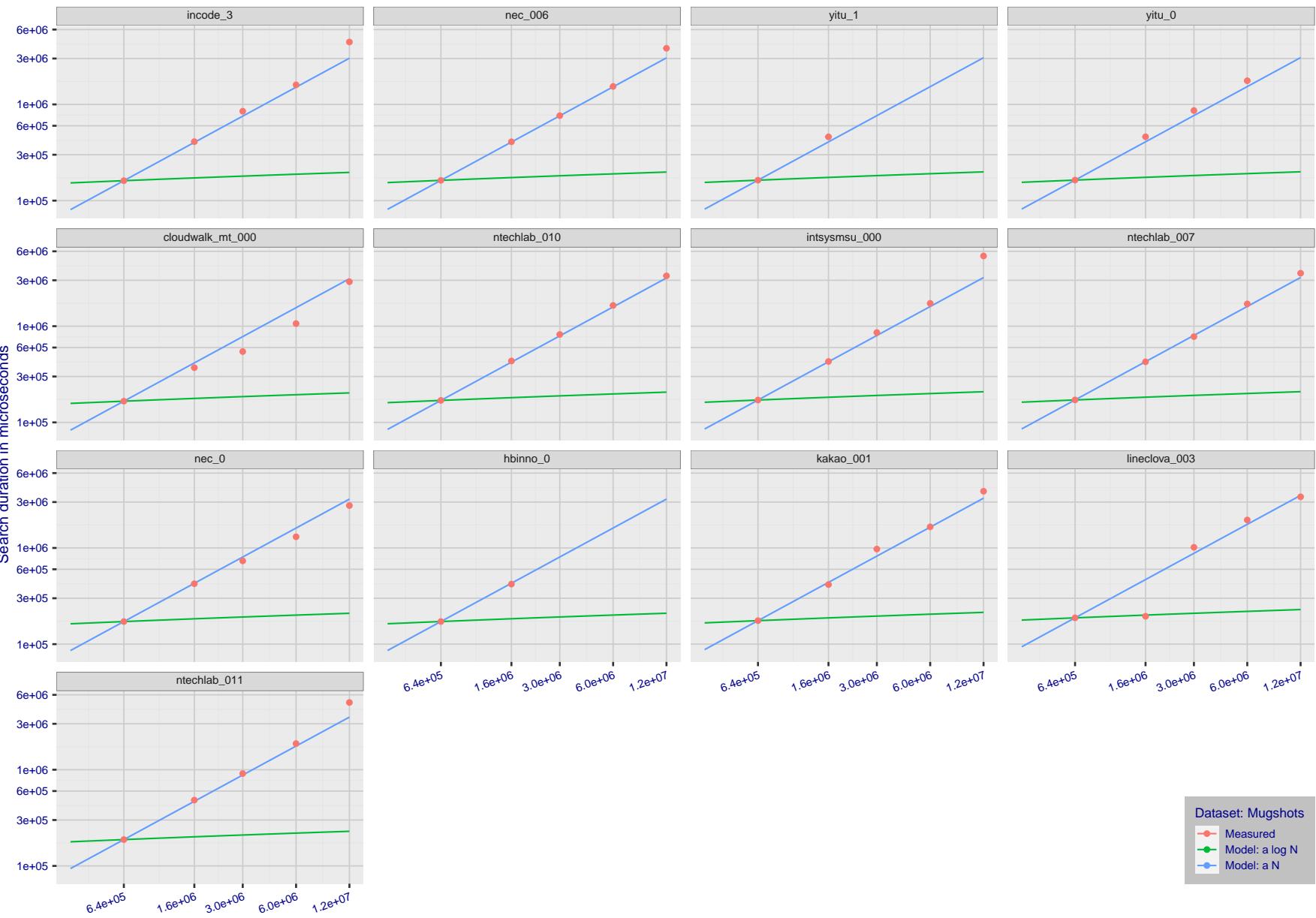
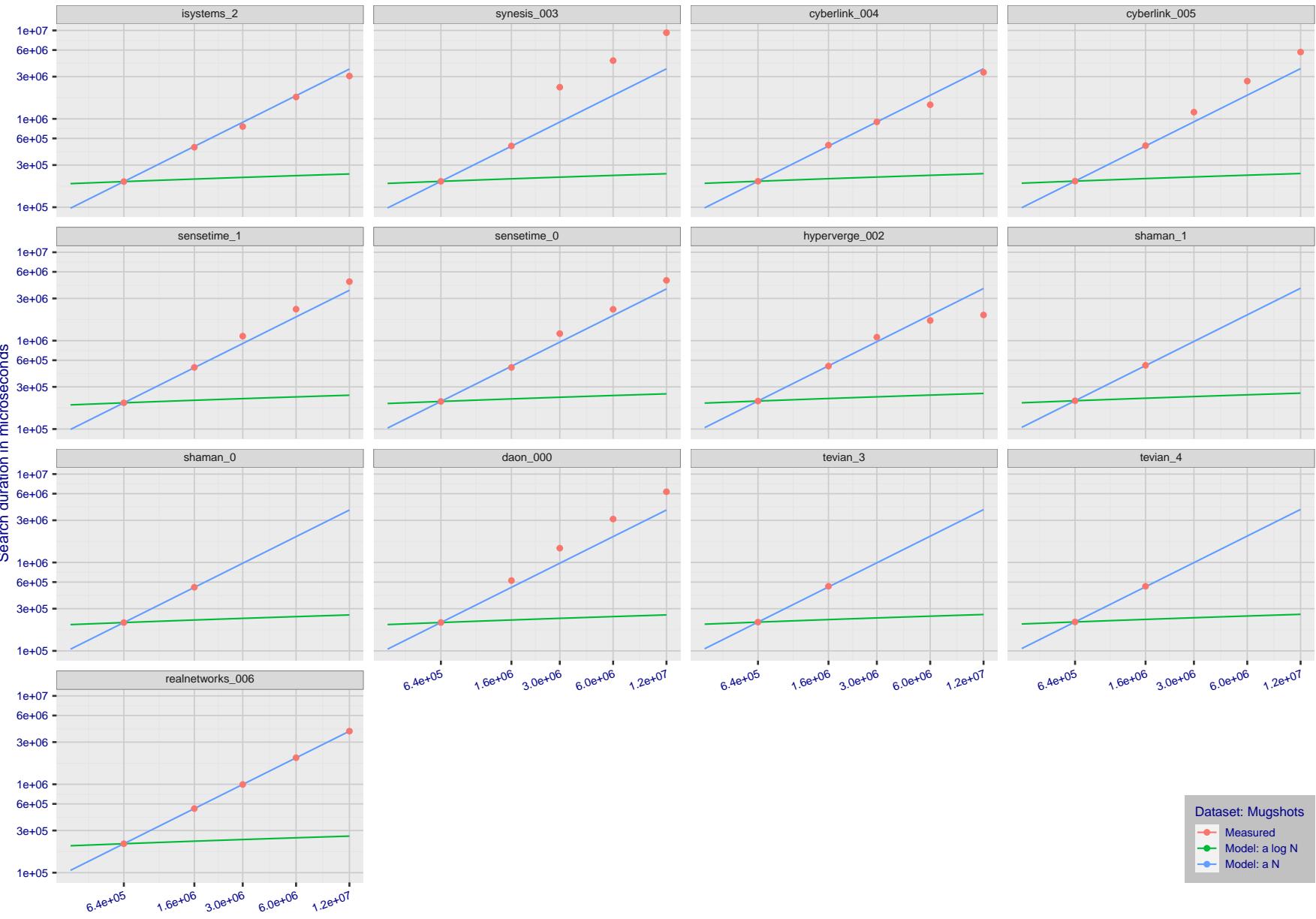
T = 0 → Investigation
 $T > 0 \rightarrow$ Identification

Figure 323: [Mugshot Dataset] Search duration vs. enrolled population size. In red are the actual point durations measured on a single c. 2016 core. The blue shows linear growth from $N = 640\,000$. The green line shows logarithmic growth from that point to $N = 1\,600\,000$. Note the sublinear growth from algorithms from Camvi, Dermalog, EverAI, Innovatrics, and Visionlabs. The tiger_1 algorithm is also sublinear, but inaccurate and inoperable at $N \geq 3000000$. This capability sometimes comes at the additional expense of converting a linear gallery data structure into whatever fast-search data structure is used. Note that search times are sometimes dominated by the template generation times shown in Table 29.

2023/07/05
16:19:47FNIR(N, R, T) = False neg. identification rate
FPIR(N, T) = False pos. identification rateN = Num. enrolled subjects
R = Num. candidates examined

T = Threshold

T = 0 → Investigation
T > 0 → Identification

Dataset: Mugshots
● Measured
● Model: a log N
● Model: a N

Figure 324: [Mugshot Dataset] Search duration vs. enrolled population size. In red are the actual point durations measured on a single c. 2016 core. The blue shows linear growth from $N = 640\,000$. The green line shows logarithmic growth from that point to $N = 1\,600\,000$. Note the sublinear growth from algorithms from Camvi, Dermalog, EverAI, Innovatrics, and Visionlabs. The tiger_1 algorithm is also sublinear, but inaccurate and inoperable at $N \geq 3000000$. This capability sometimes comes at the additional expense of converting a linear gallery data structure into whatever fast-search data structure is used. Note that search times are sometimes dominated by the template generation times shown in Table 29.

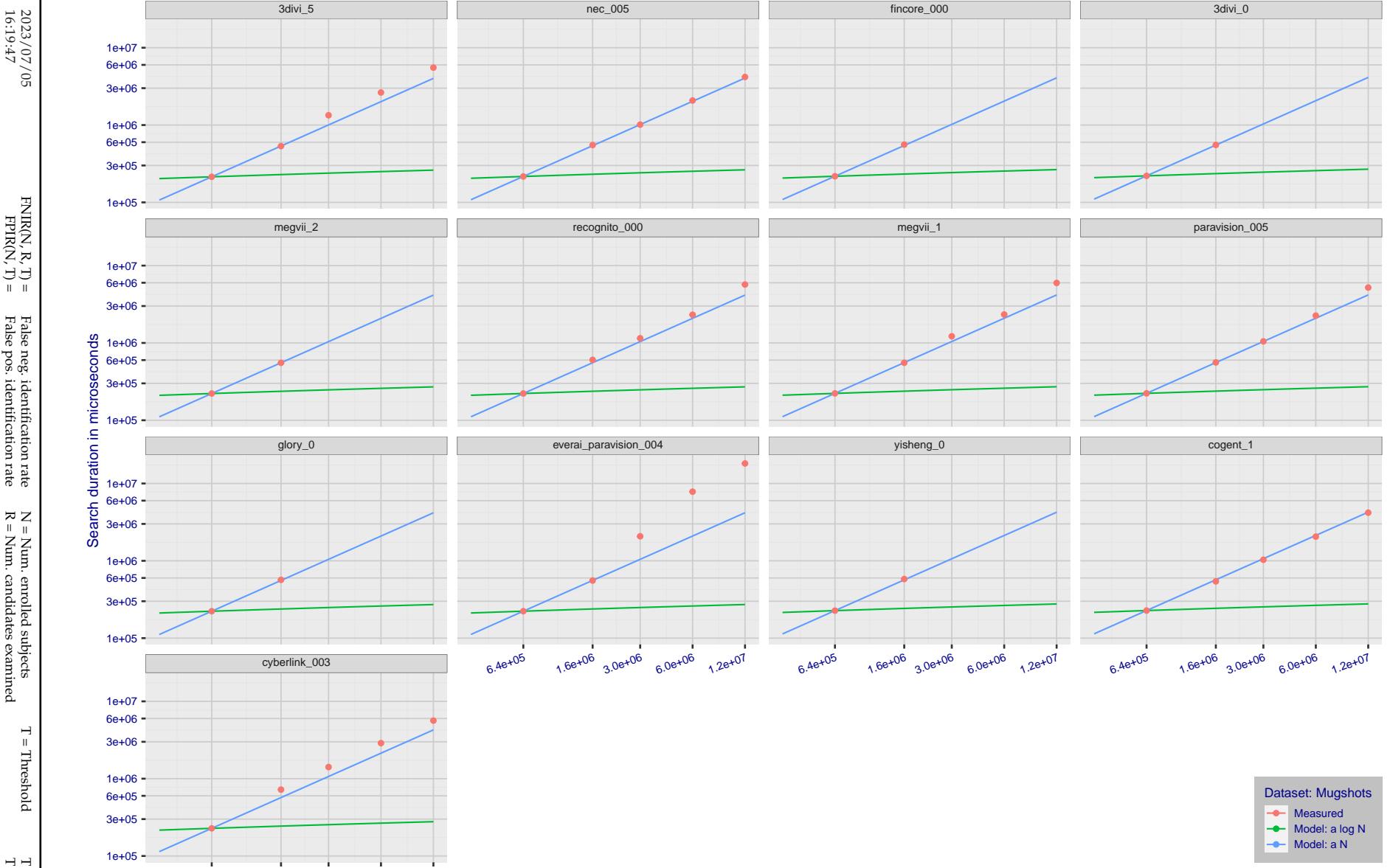


Figure 325: [Mugshot Dataset] Search duration vs. enrolled population size. In red are the actual point durations measured on a single c. 2016 core. The blue shows linear growth from $N = 640\,000$. The green line shows logarithmic growth from that point to $N = 1\,600\,000$. Note the sublinear growth from algorithms from Camvi, Dermalog, EverAI, Innovatrics, and Visionlabs. The tiger_1 algorithm is also sublinear, but inaccurate and inoperable at $N \geq 3000000$. This capability sometimes comes at the additional expense of converting a linear gallery data structure into whatever fast-search data structure is used. Note that search times are sometimes dominated by the template generation times shown in Table 29.

2023/07/05
16:19:47FNIR(N, R, T) = False neg. identification rate
FPIR(N, T) = False pos. identification rateN = Num. enrolled subjects
R = Num. candidates examined

T = Threshold

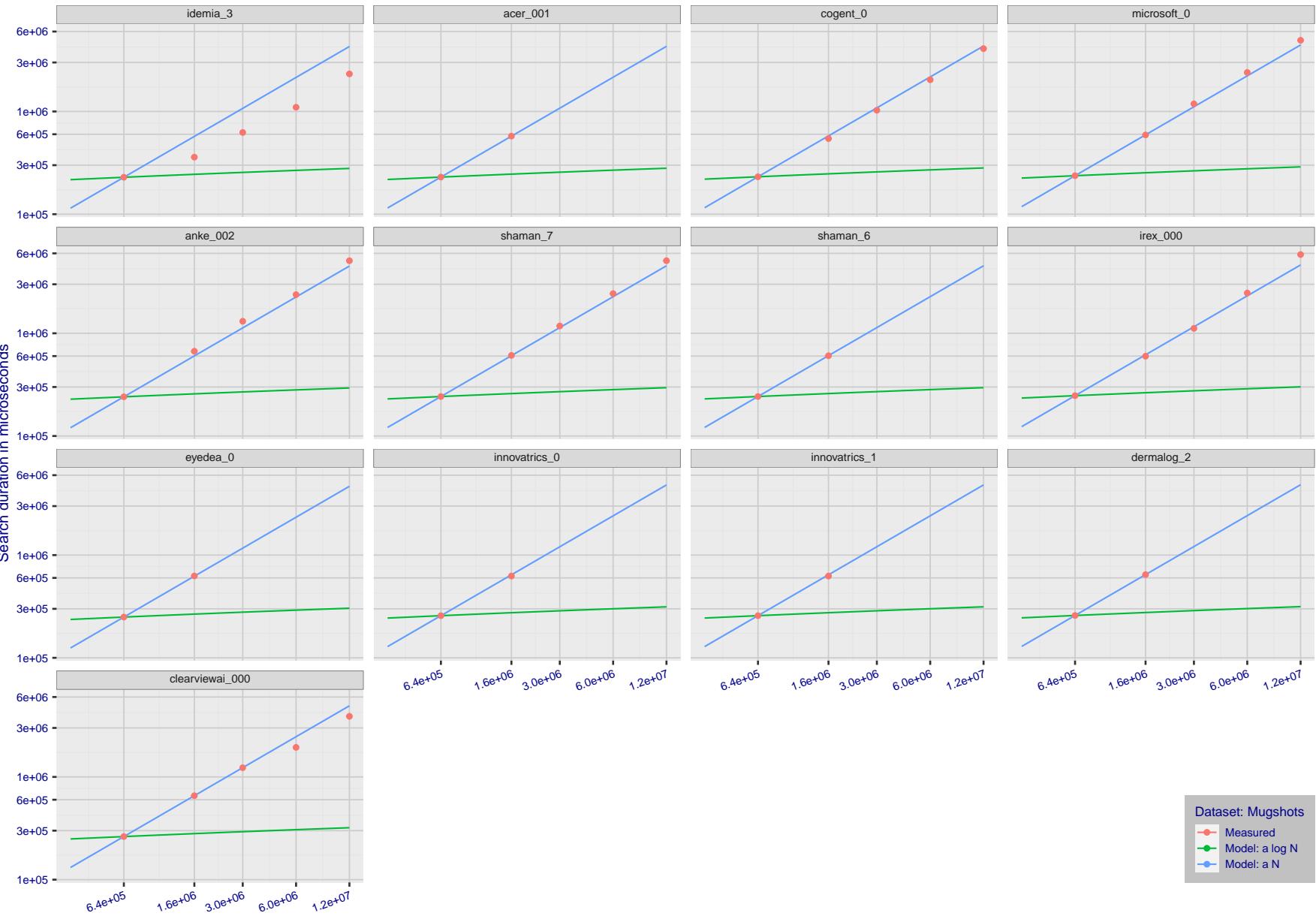
T = 0 → Investigation
T > 0 → Identification

Figure 326: [Mugshot Dataset] Search duration vs. enrolled population size. In red are the actual point durations measured on a single c. 2016 core. The blue shows linear growth from $N = 640\,000$. The green line shows logarithmic growth from that point to $N = 1\,600\,000$. Note the sublinear growth from algorithms from Camvi, Dermalog, EverAI, Innovatrics, and Visionlabs. The tiger_1 algorithm is also sublinear, but inaccurate and inoperable at $N \geq 3000000$. This capability sometimes comes at the additional expense of converting a linear gallery data structure into whatever fast-search data structure is used. Note that search times are sometimes dominated by the template generation times shown in Table 29.

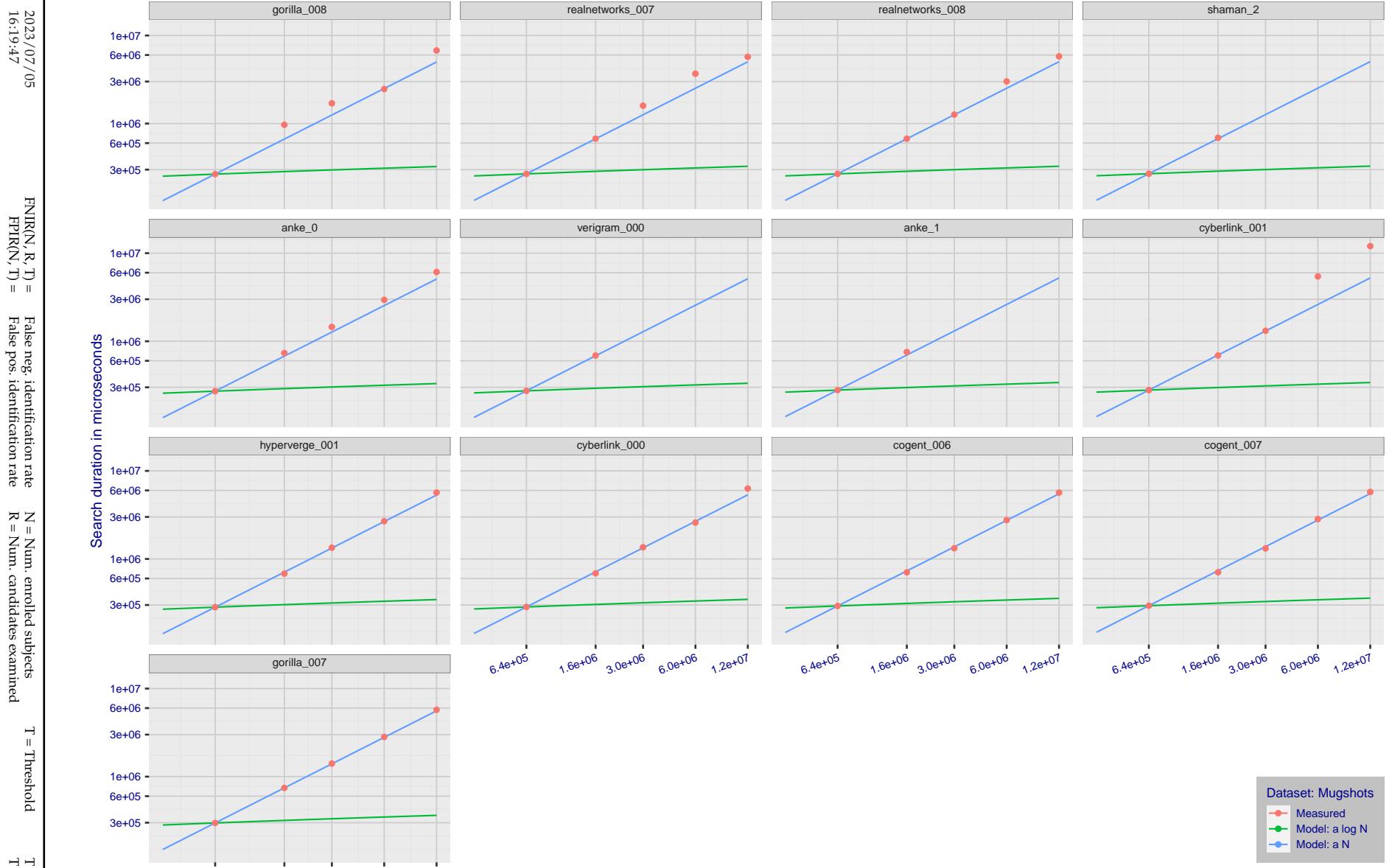


Figure 327: [Mugshot Dataset] Search duration vs. enrolled population size. In red are the actual point durations measured on a single c. 2016 core. The blue shows linear growth from $N = 640\,000$. The green line shows logarithmic growth from that point to $N = 1\,600\,000$. Note the sublinear growth from algorithms from Camvi, Dermalog, EverAI, Innovatrics, and Visionlabs. The tiger_1 algorithm is also sublinear, but inaccurate and inoperable at $N \geq 3000000$. This capability sometimes comes at the additional expense of converting a linear gallery data structure into whatever fast-search data structure is used. Note that search times are sometimes dominated by the template generation times shown in Table 29.

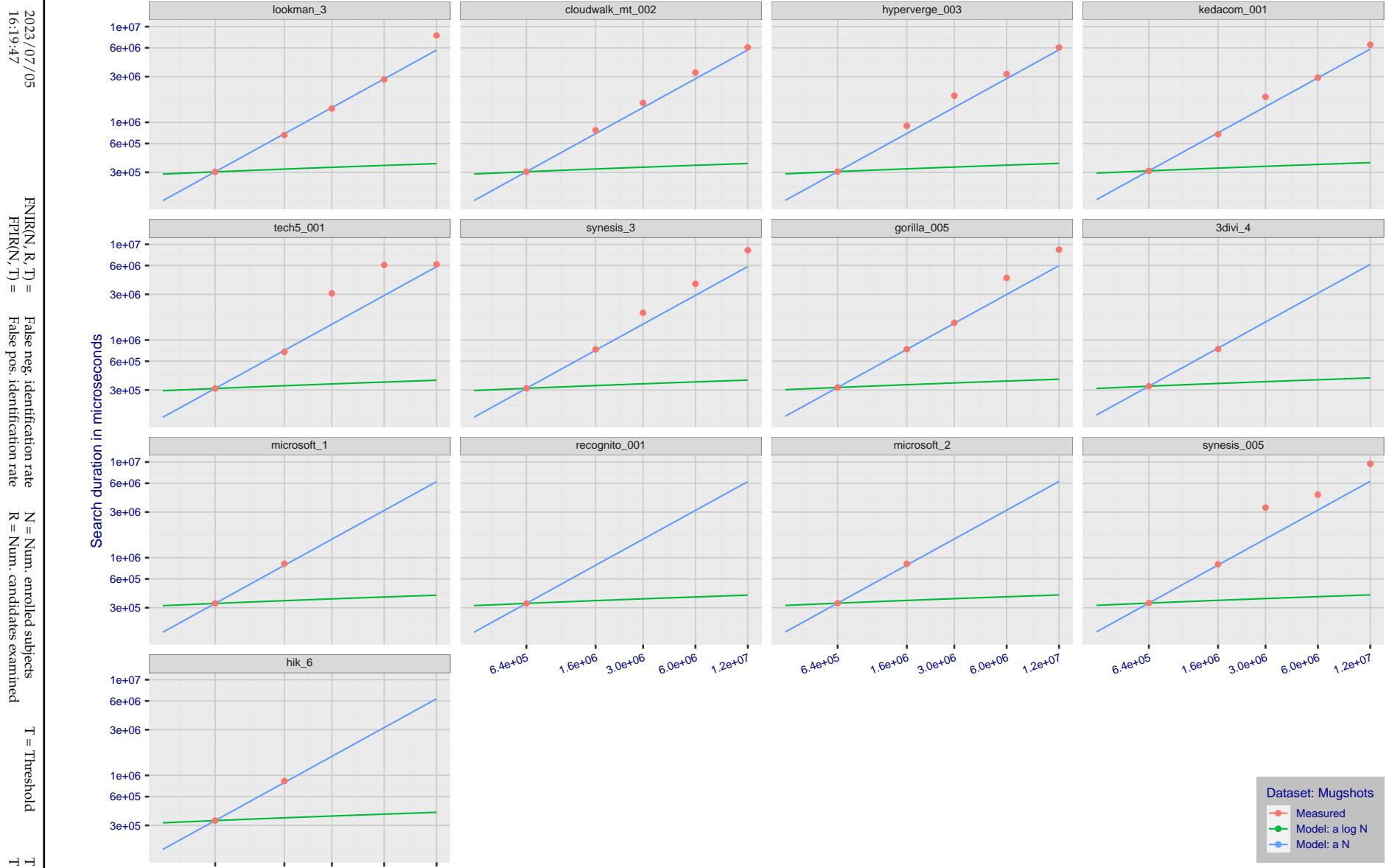


Figure 328: [Mugshot Dataset] Search duration vs. enrolled population size. In red are the actual point durations measured on a single c. 2016 core. The blue shows linear growth from $N = 640\,000$. The green line shows logarithmic growth from that point to $N = 1\,600\,000$. Note the sublinear growth from algorithms from Camvi, Dermalog, EverAI, Innovatrics, and Visionlabs. The tiger_1 algorithm is also sublinear, but inaccurate and inoperable at $N \geq 3000000$. This capability sometimes comes at the additional expense of converting a linear gallery data structure into whatever fast-search data structure is used. Note that search times are sometimes dominated by the template generation times shown in Table 29.

2023/07/05
16:19:47FNIR(N, R, T) = False neg. identification rate
FPIR(N, T) = False pos. identification rateN = Num. enrolled subjects
R = Num. candidates examined

T = Threshold

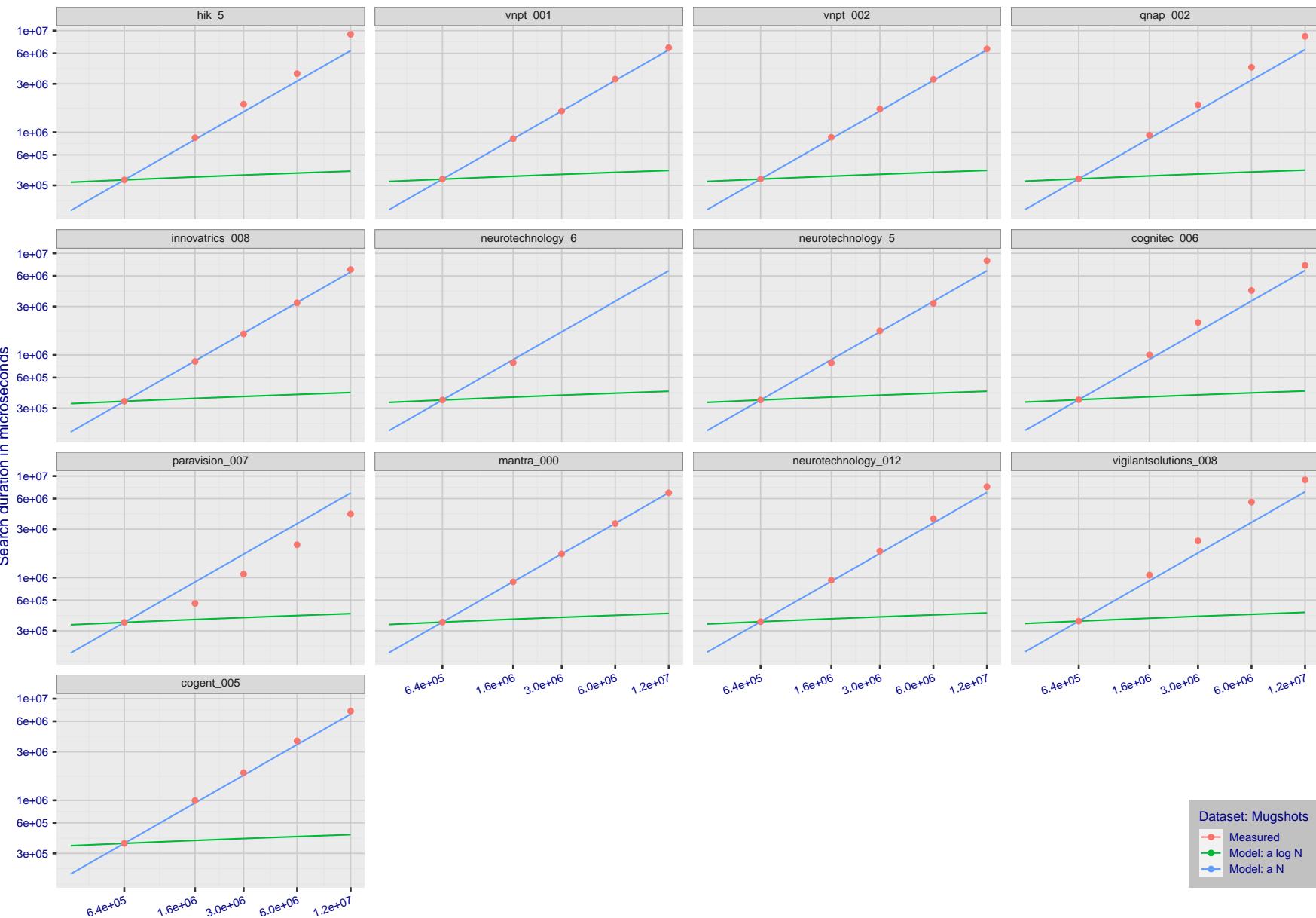
T = 0 → Investigation
 $T > 0 \rightarrow$ Identification

Figure 329: [Mugshot Dataset] Search duration vs. enrolled population size. In red are the actual point durations measured on a single c. 2016 core. The blue shows linear growth from $N = 640\,000$. The green line shows logarithmic growth from that point to $N = 1\,600\,000$. Note the sublinear growth from algorithms from Camvi, Dermalog, EverAI, Innovatrics, and Visionlabs. The tiger_1 algorithm is also sublinear, but inaccurate and inoperable at $N \geq 3000000$. This capability sometimes comes at the additional expense of converting a linear gallery data structure into whatever fast-search data structure is used. Note that search times are sometimes dominated by the template generation times shown in Table 29.

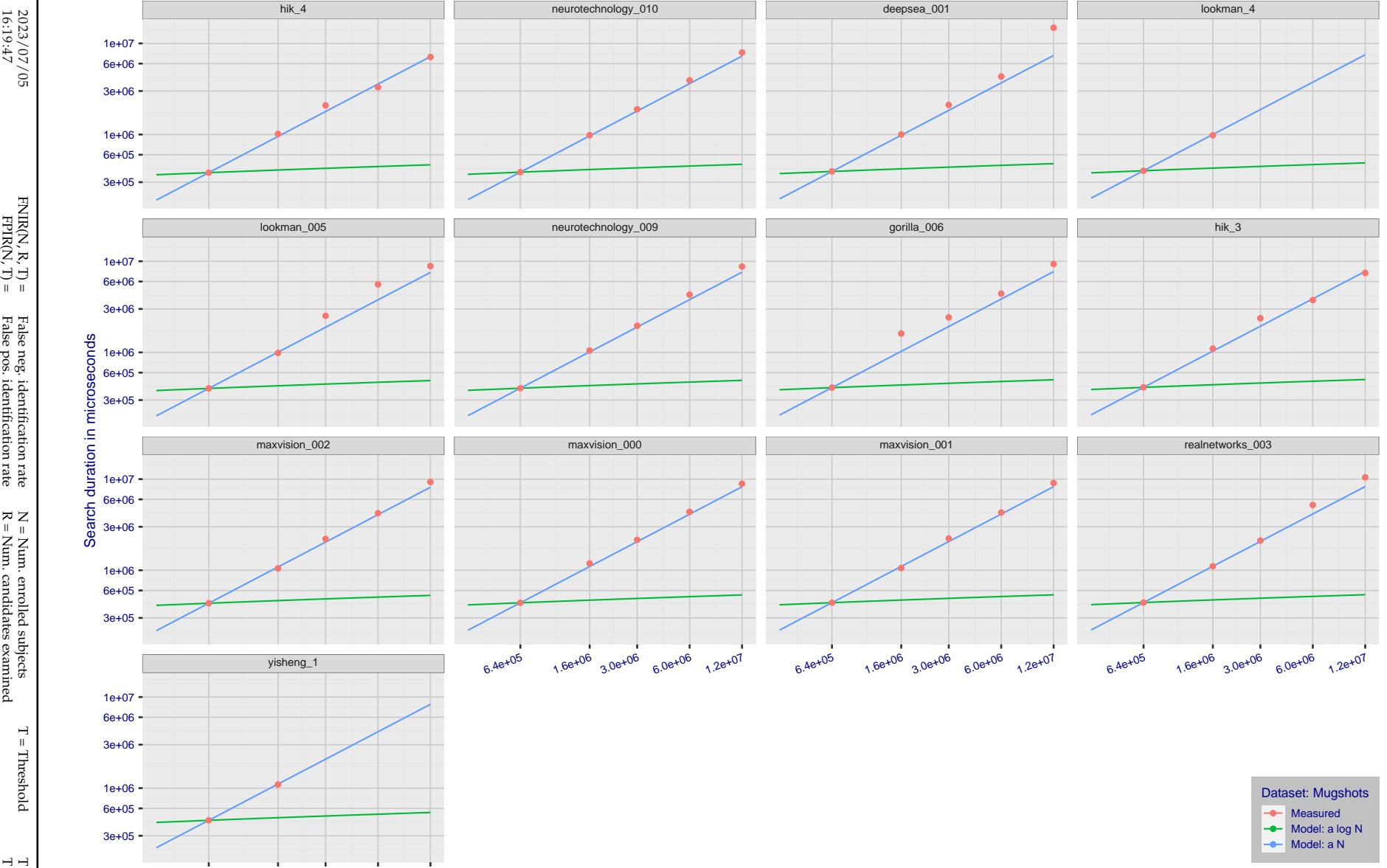


Figure 330: [Mugshot Dataset] Search duration vs. enrolled population size. In red are the actual point durations measured on a single c. 2016 core. The blue shows linear growth from $N = 640\,000$. The green line shows logarithmic growth from that point to $N = 1\,600\,000$. Note the sublinear growth from algorithms from Camvi, Dermalog, EverAI, Innovatrics, and Visionlabs. The tiger_1 algorithm is also sublinear, but inaccurate and inoperable at $N \geq 3000000$. This capability sometimes comes at the additional expense of converting a linear gallery data structure into whatever fast-search data structure is used. Note that search times are sometimes dominated by the template generation times shown in Table 29.

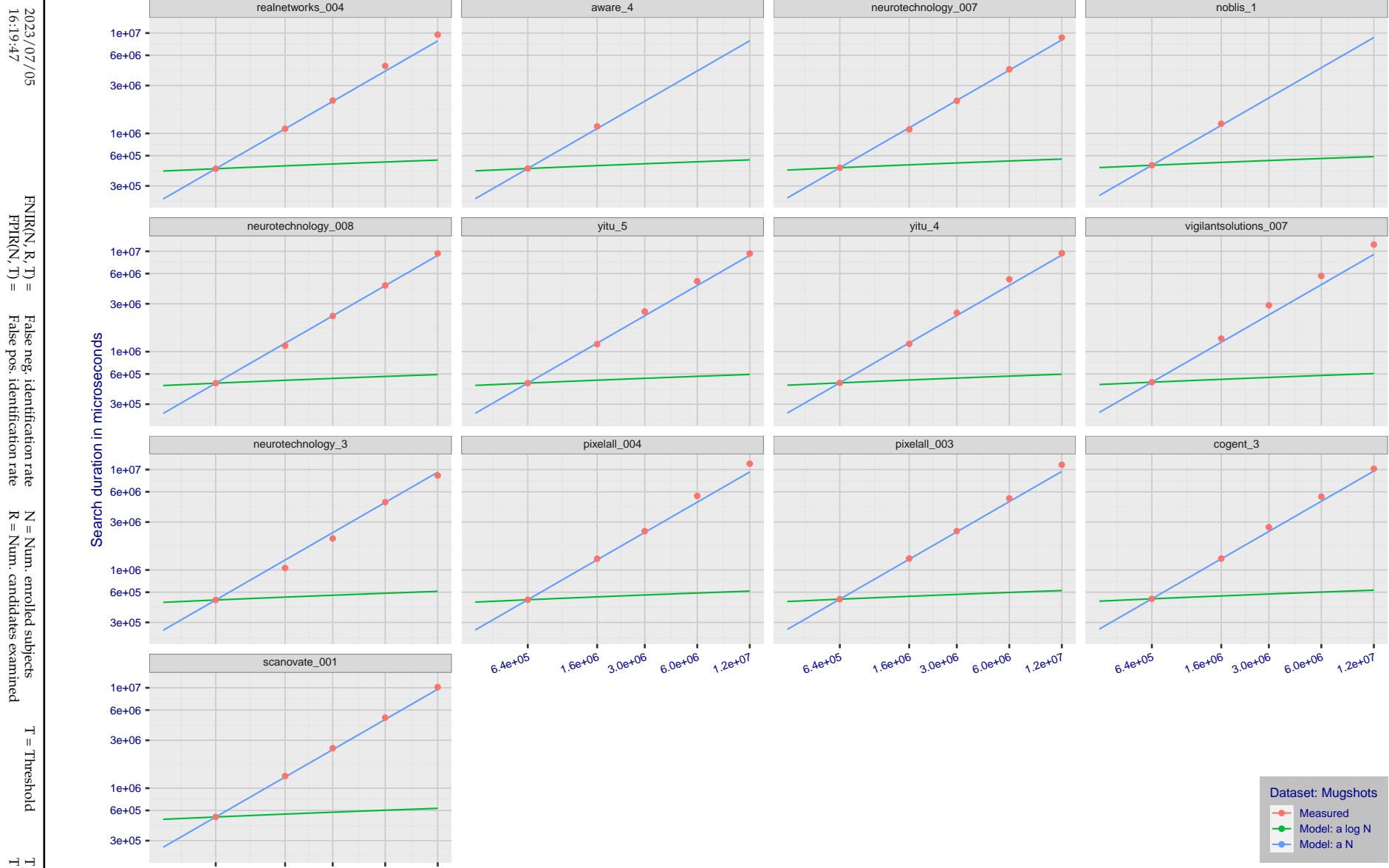


Figure 331: [Mugshot Dataset] Search duration vs. enrolled population size. In red are the actual point durations measured on a single c. 2016 core. The blue shows linear growth from $N = 640\,000$. The green line shows logarithmic growth from that point to $N = 1\,600\,000$. Note the sublinear growth from algorithms from Camvi, Dermalog, EverAI, Innovatrics, and Visionlabs. The tiger_1 algorithm is also sublinear, but inaccurate and inoperable at $N \geq 3000000$. This capability sometimes comes at the additional expense of converting a linear gallery data structure into whatever fast-search data structure is used. Note that search times are sometimes dominated by the template generation times shown in Table 29.

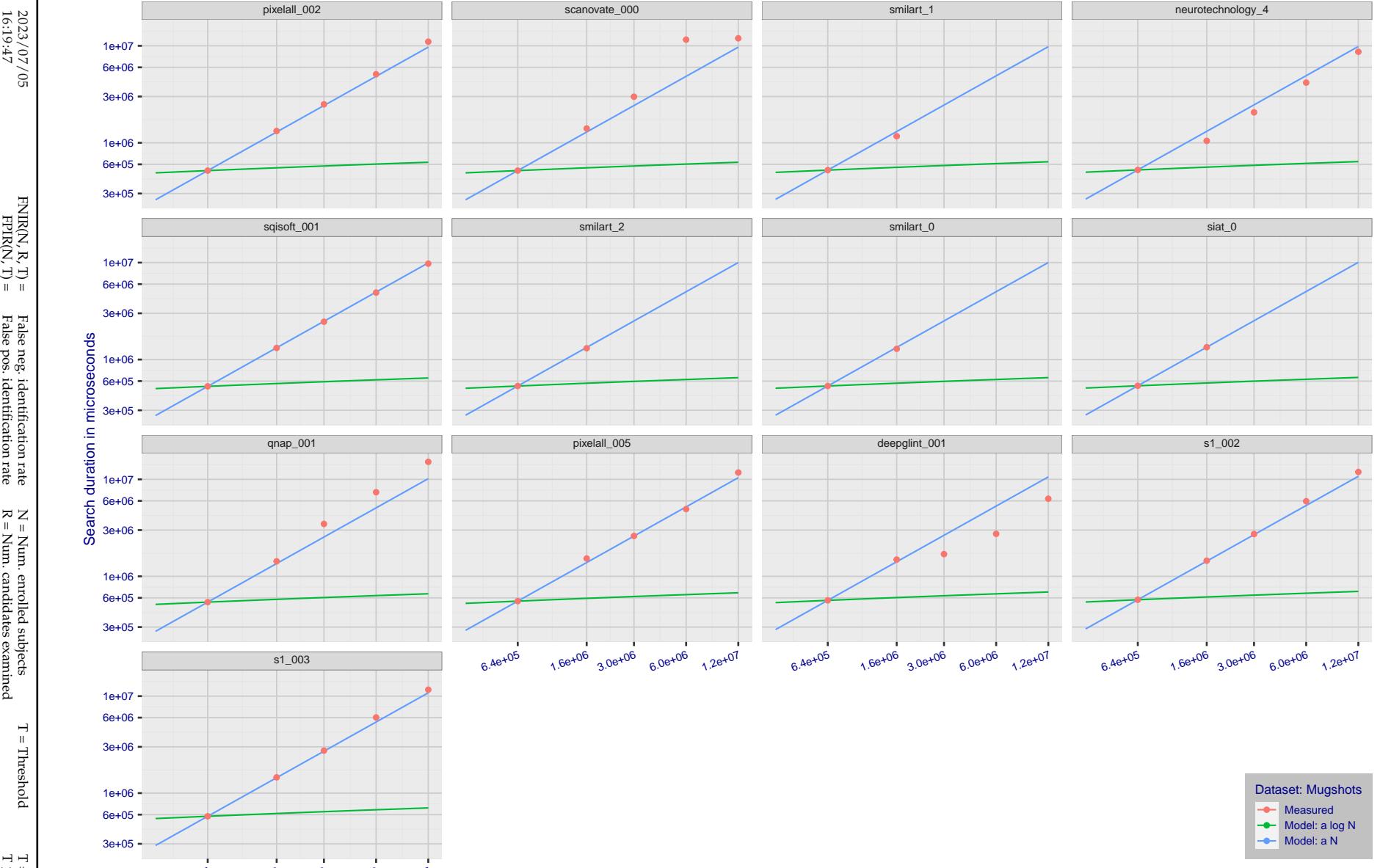


Figure 332: [Mugshot Dataset] Search duration vs. enrolled population size. In red are the actual point durations measured on a single c. 2016 core. The blue shows linear growth from $N = 640\,000$. The green line shows logarithmic growth from that point to $N = 1\,600\,000$. Note the sublinear growth from algorithms from Camvi, Dermalog, EverAI, Innovatrics, and Visionlabs. The tiger_1 algorithm is also sublinear, but inaccurate and inoperable at $N \geq 3000000$. This capability sometimes comes at the additional expense of converting a linear gallery data structure into whatever fast-search data structure is used. Note that search times are sometimes dominated by the template generation times shown in Table 29.

2023/07/05
16:19:47FNIR(N, R, T) = False neg. identification rate
FPIR(N, T) = False pos. identification rateN = Num. enrolled subjects
R = Num. candidates examined

T = Threshold

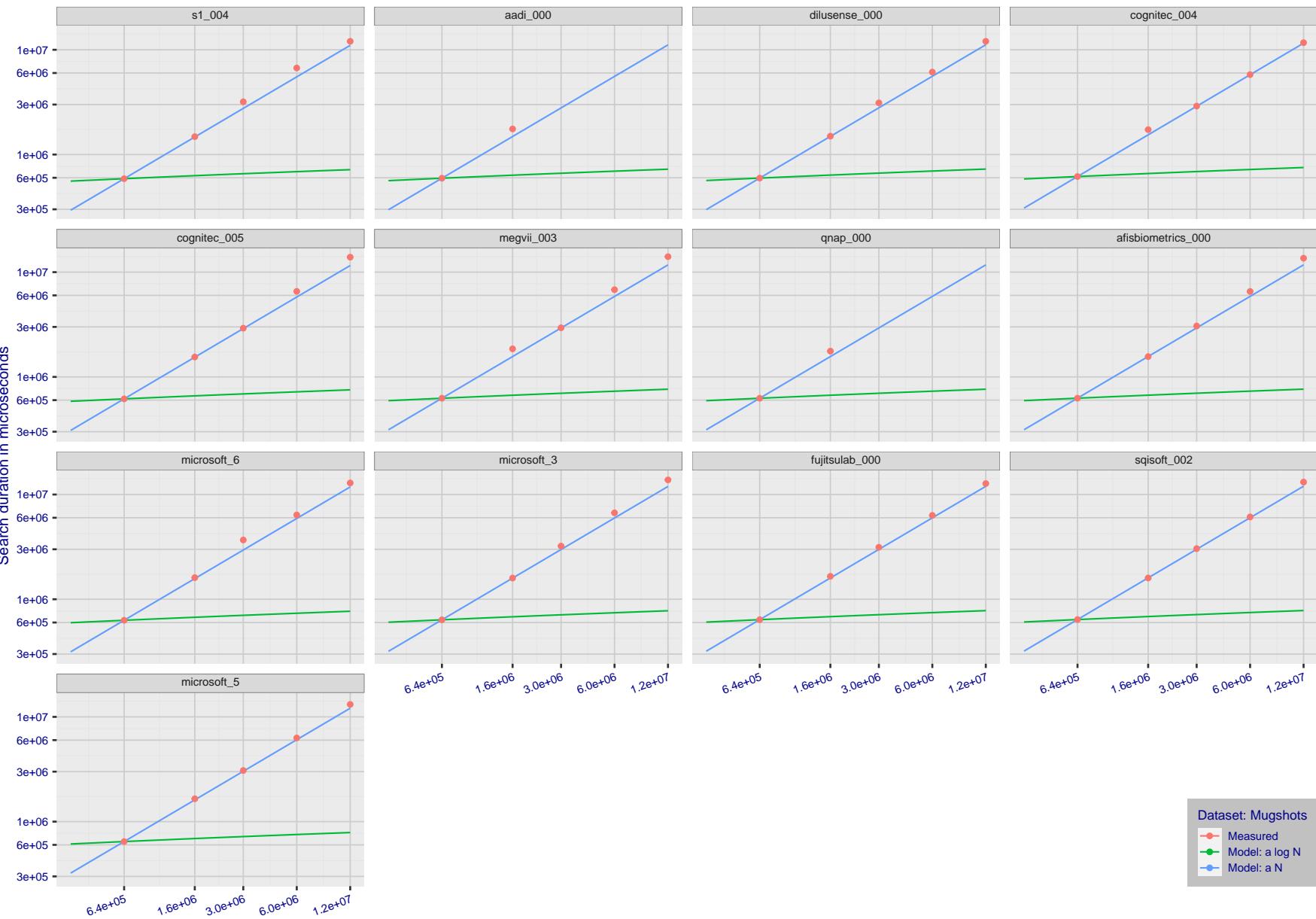
T = 0 → Investigation
T > 0 → Identification

Figure 333: [Mugshot Dataset] Search duration vs. enrolled population size. In red are the actual point durations measured on a single c. 2016 core. The blue shows linear growth from $N = 640\,000$. The green line shows logarithmic growth from that point to $N = 1\,600\,000$. Note the sublinear growth from algorithms from Camvi, Dermalog, EverAI, Innovatrics, and Visionlabs. The tiger_1 algorithm is also sublinear, but inaccurate and inoperable at $N \geq 3000000$. This capability sometimes comes at the additional expense of converting a linear gallery data structure into whatever fast-search data structure is used. Note that search times are sometimes dominated by the template generation times shown in Table 29.

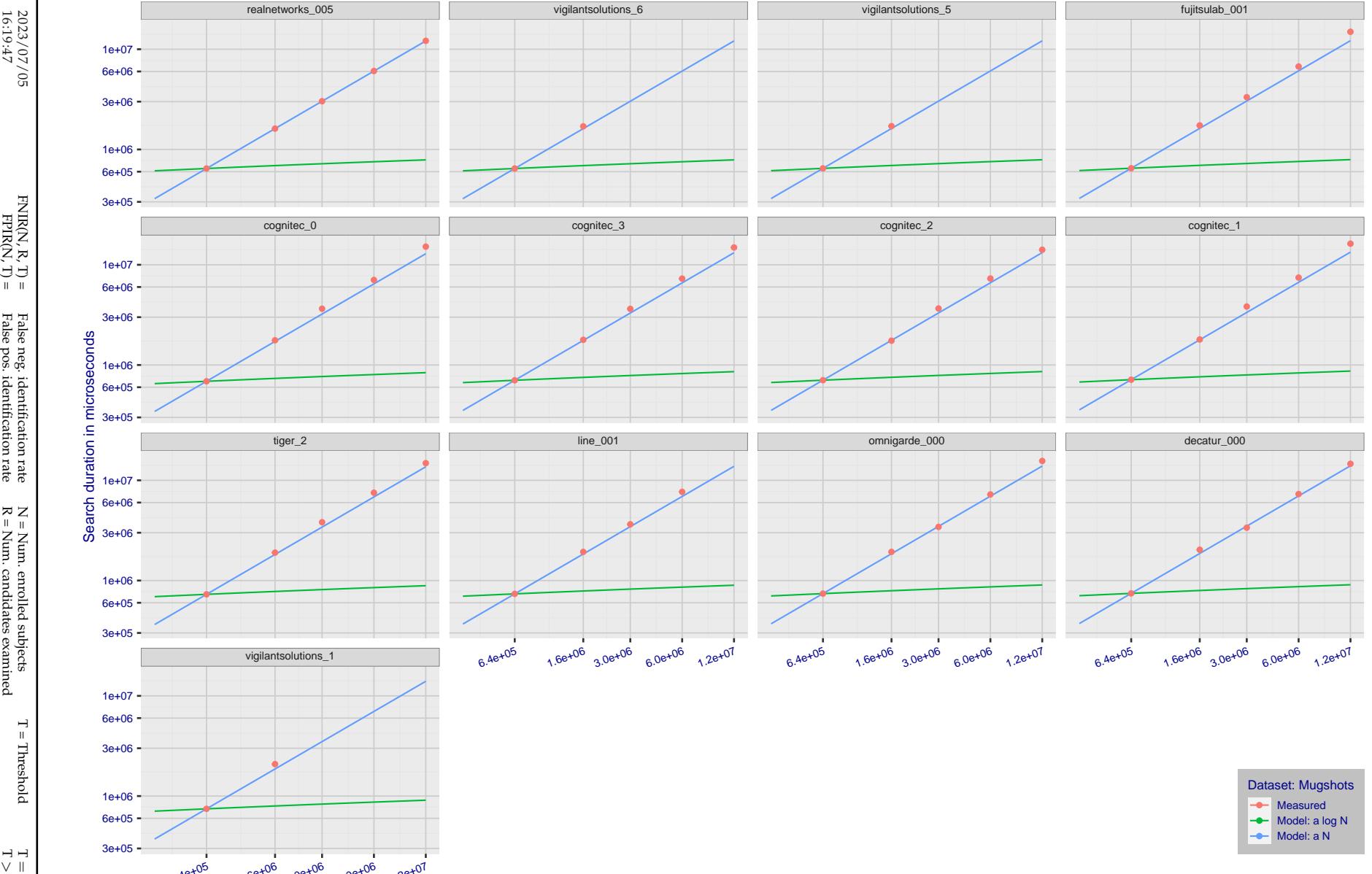


Figure 334: [Mugshot Dataset] Search duration vs. enrolled population size. In red are the actual point durations measured on a single c. 2016 core. The blue shows linear growth from $N = 640\,000$. The green line shows logarithmic growth from that point to $N = 1\,600\,000$. Note the sublinear growth from algorithms from Camvi, Dermalog, EverAI, Innovatrics, and Visionlabs. The tiger_1 algorithm is also sublinear, but inaccurate and inoperable at $N \geq 3000000$. This capability sometimes comes at the additional expense of converting a linear gallery data structure into whatever fast-search data structure is used. Note that search times are sometimes dominated by the template generation times shown in Table 29.

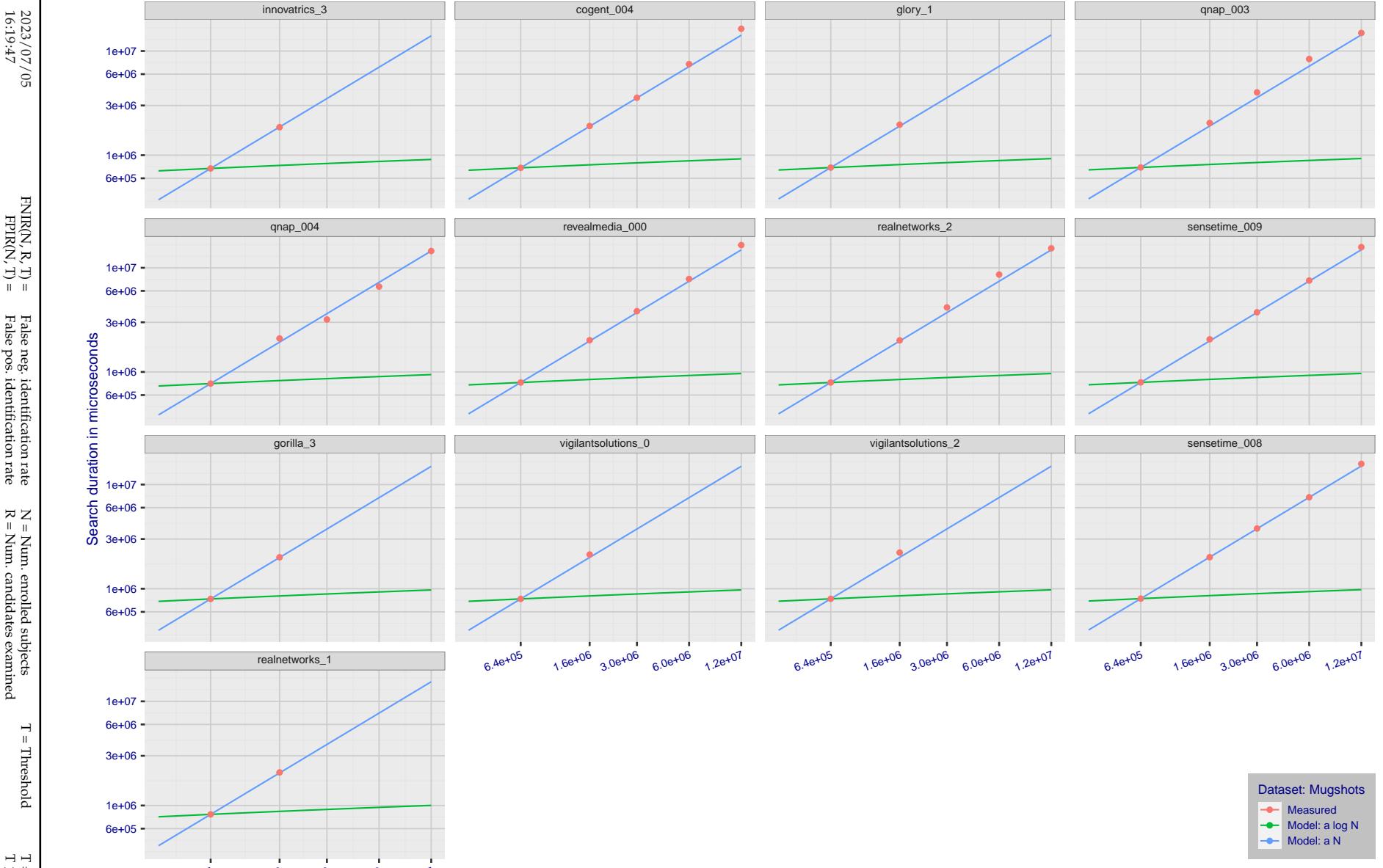


Figure 335: [Mugshot Dataset] Search duration vs. enrolled population size. In red are the actual point durations measured on a single c. 2016 core. The blue shows linear growth from $N = 640\,000$. The green line shows logarithmic growth from that point to $N = 1\,600\,000$. Note the sublinear growth from algorithms from Camvi, Dermalog, EverAI, Innovatrics, and Visionlabs. The tiger_1 algorithm is also sublinear, but inaccurate and inoperable at $N \geq 3000000$. This capability sometimes comes at the additional expense of converting a linear gallery data structure into whatever fast-search data structure is used. Note that search times are sometimes dominated by the template generation times shown in Table 29.

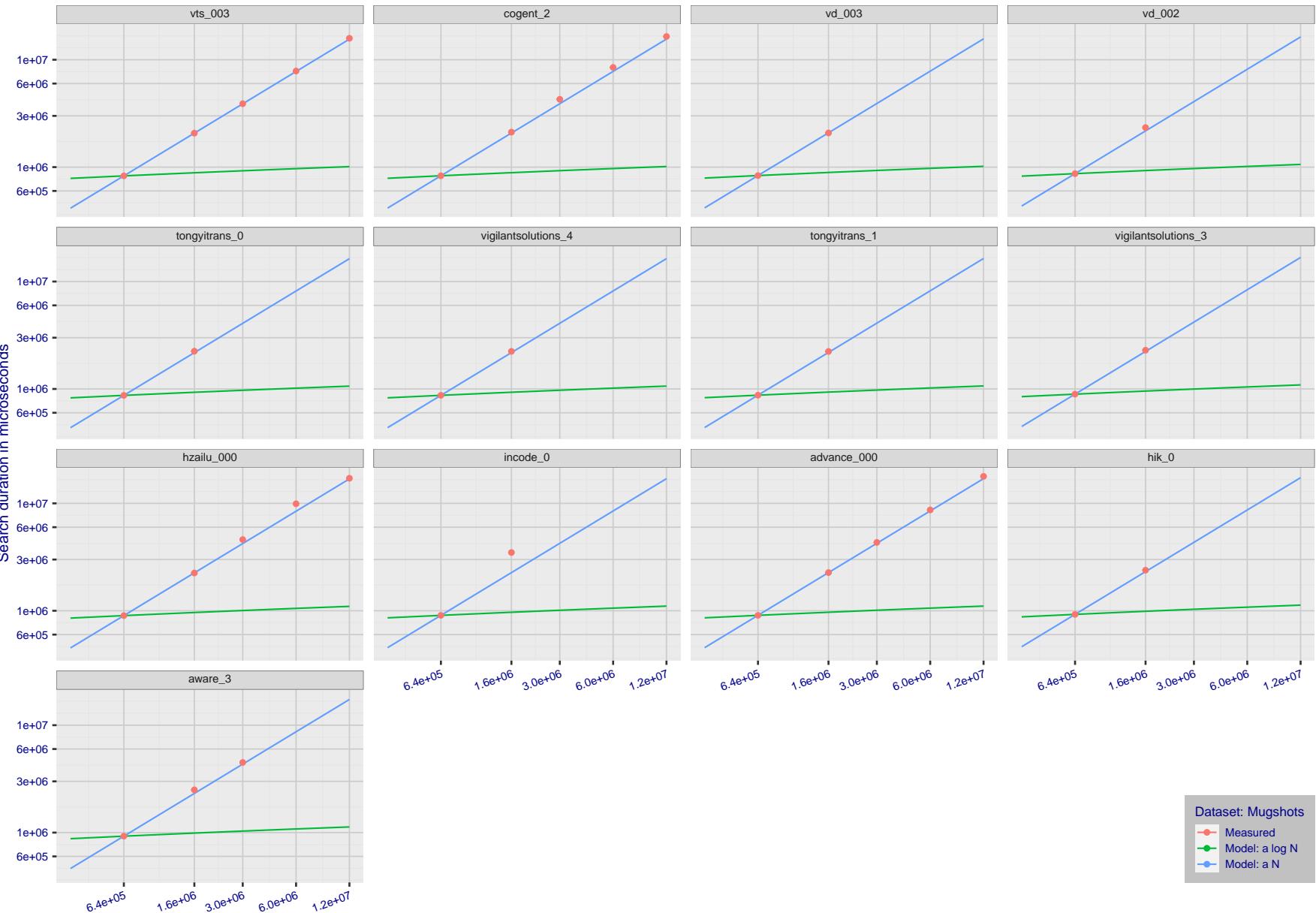
2023/07/05
16:19:47FNIR(N, R, T) = False neg. identification rate
FPIR(N, T) = False pos. identification rateN = Num. enrolled subjects
R = Num. candidates examined

T = Threshold

T = 0 → Investigation
 $T > 0 \rightarrow$ Identification

2023/07/05
16:19:47FNIR(N, R, T) = False neg. identification rate
FPIR(N, T) = False pos. identification rateN = Num. enrolled subjects
R = Num. candidates examined

T = Threshold

T = 0 → Investigation
T > 0 → Identification

Dataset: Mugshots
● Measured
● Model: a log N
● Model: a N

Figure 336: [Mugshot Dataset] Search duration vs. enrolled population size. In red are the actual point durations measured on a single c. 2016 core. The blue shows linear growth from $N = 640\,000$. The green line shows logarithmic growth from that point to $N = 1\,600\,000$. Note the sublinear growth from algorithms from Camvi, Dermalog, EverAI, Innovatrics, and Visionlabs. The tiger_1 algorithm is also sublinear, but inaccurate and inoperable at $N \geq 3000000$. This capability sometimes comes at the additional expense of converting a linear gallery data structure into whatever fast-search data structure is used. Note that search times are sometimes dominated by the template generation times shown in Table 29.

2023/07/05
16:19:47FNIR(N, R, T) = False neg. identification rate
FPTR(N, T) = False pos. identification rateN = Num. enrolled subjects
R = Num. candidates examined

T = Threshold

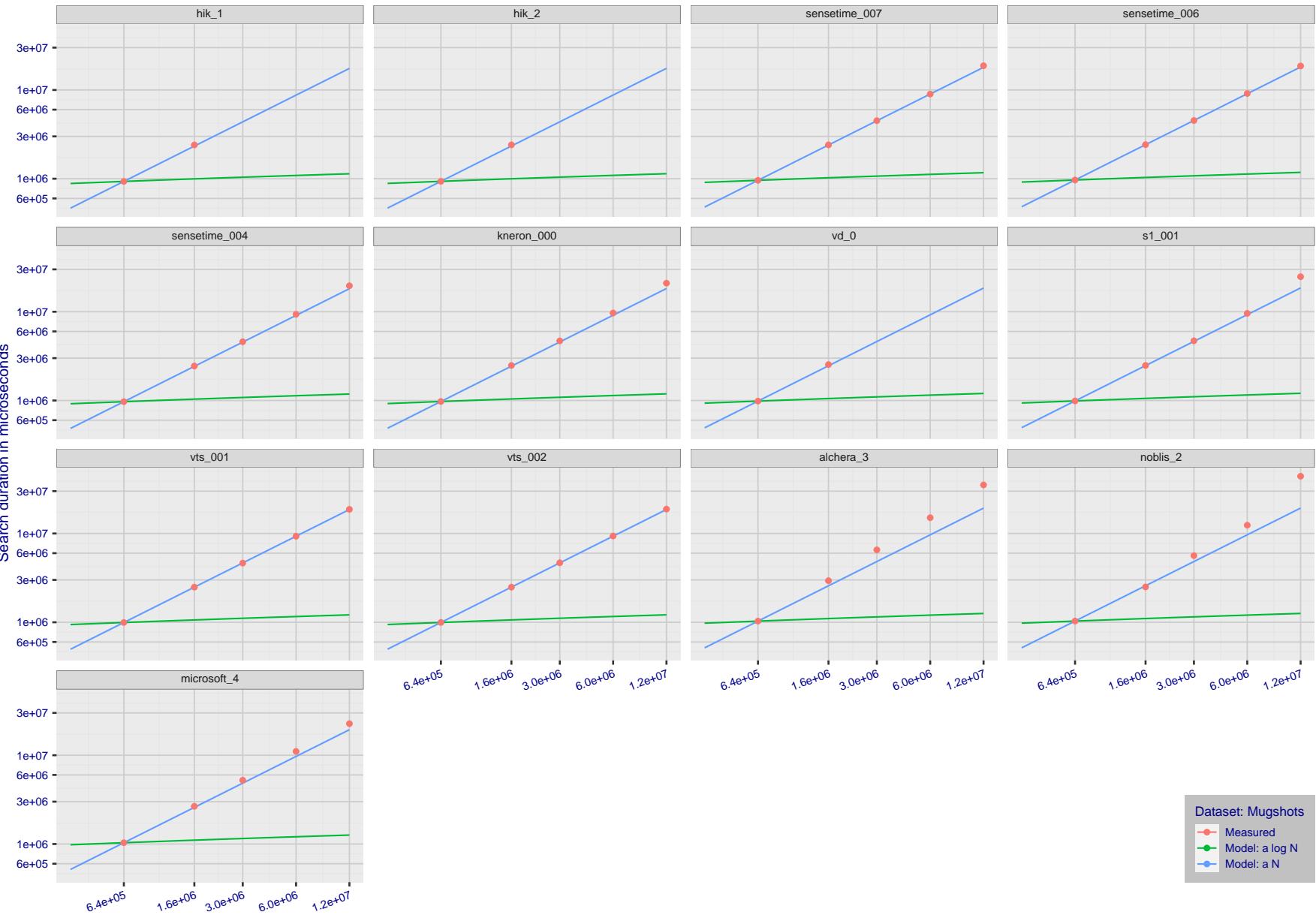
T = 0 → Investigation
T > 0 → Identification

Figure 337: [Mugshot Dataset] Search duration vs. enrolled population size. In red are the actual point durations measured on a single c. 2016 core. The blue shows linear growth from $N = 640\,000$. The green line shows logarithmic growth from that point to $N = 1\,600\,000$. Note the sublinear growth from algorithms from Camvi, Dermalog, EverAI, Innovatrics, and Visionlabs. The tiger_1 algorithm is also sublinear, but inaccurate and inoperable at $N \geq 3000000$. This capability sometimes comes at the additional expense of converting a linear gallery data structure into whatever fast-search data structure is used. Note that search times are sometimes dominated by the template generation times shown in Table 29.

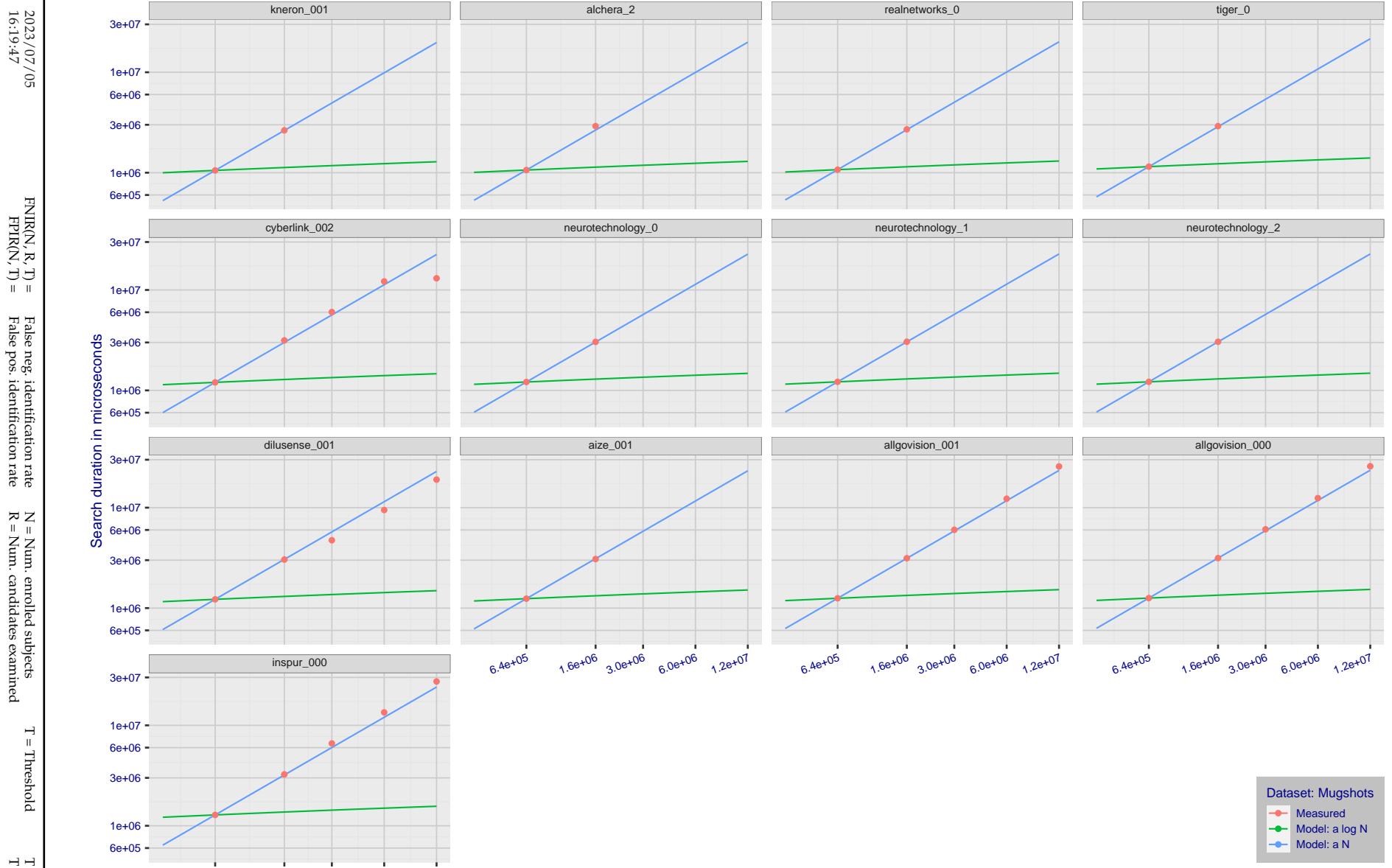


Figure 338: [Mugshot Dataset] Search duration vs. enrolled population size. In red are the actual point durations measured on a single c. 2016 core. The blue shows linear growth from $N = 640\,000$. The green line shows logarithmic growth from that point to $N = 1\,600\,000$. Note the sublinear growth from algorithms from Camvi, Dermalog, EverAI, Innovatrics, and Visionlabs. The tiger_1 algorithm is also sublinear, but inaccurate and inoperable at $N \geq 3000000$. This capability sometimes comes at the additional expense of converting a linear gallery data structure into whatever fast-search data structure is used. Note that search times are sometimes dominated by the template generation times shown in Table 29.

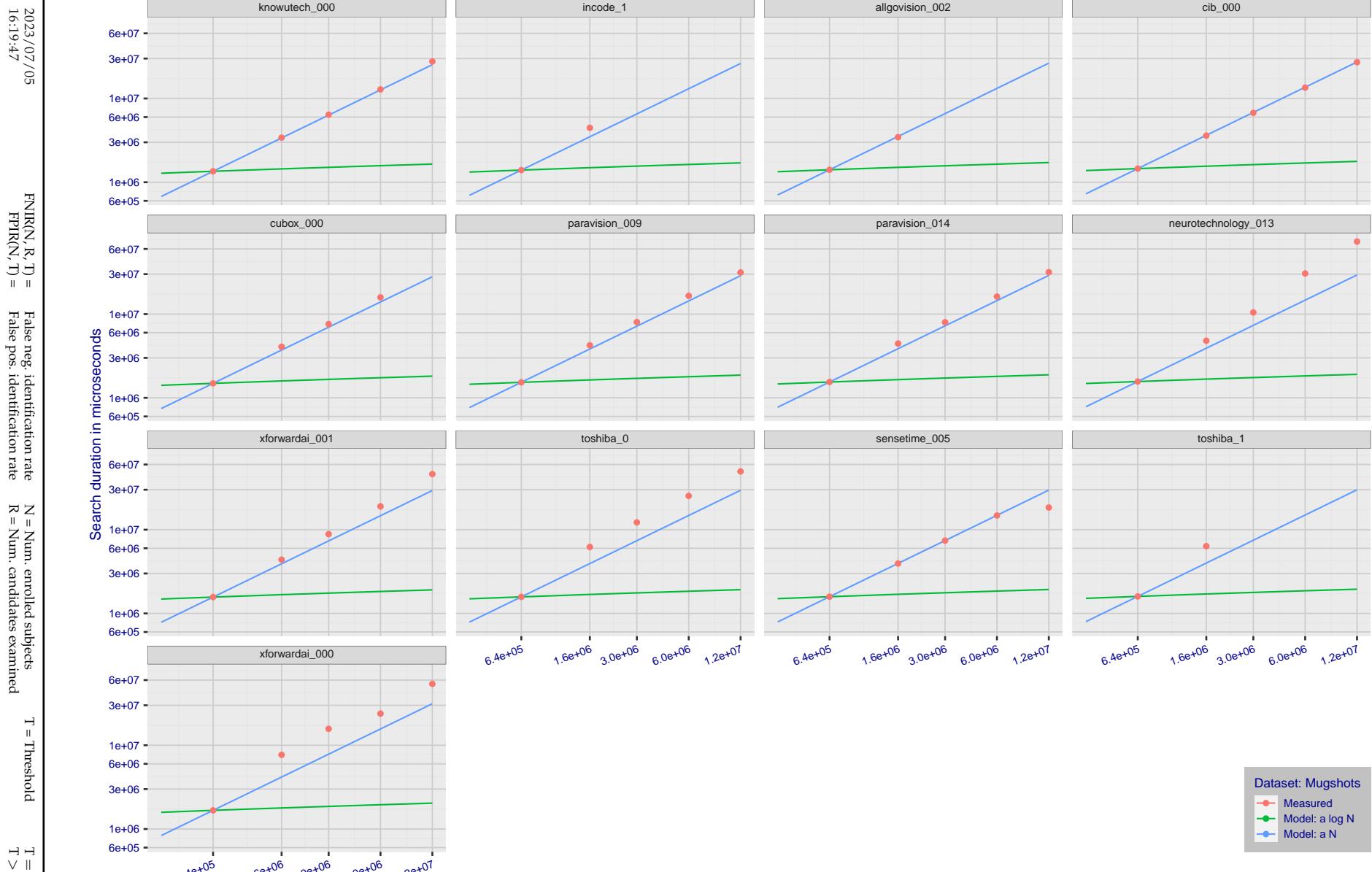


Figure 339: [Mugshot Dataset] Search duration vs. enrolled population size. In red are the actual point durations measured on a single c. 2016 core. The blue shows linear growth from $N = 640\,000$. The green line shows logarithmic growth from that point to $N = 1\,600\,000$. Note the sublinear growth from algorithms from Camvi, Dermalog, EverAI, Innovatrics, and Visionlabs. The tiger_1 algorithm is also sublinear, but inaccurate and inoperable at $N \geq 3000000$. This capability sometimes comes at the additional expense of converting a linear gallery data structure into whatever fast-search data structure is used. Note that search times are sometimes dominated by the template generation times shown in Table 29.

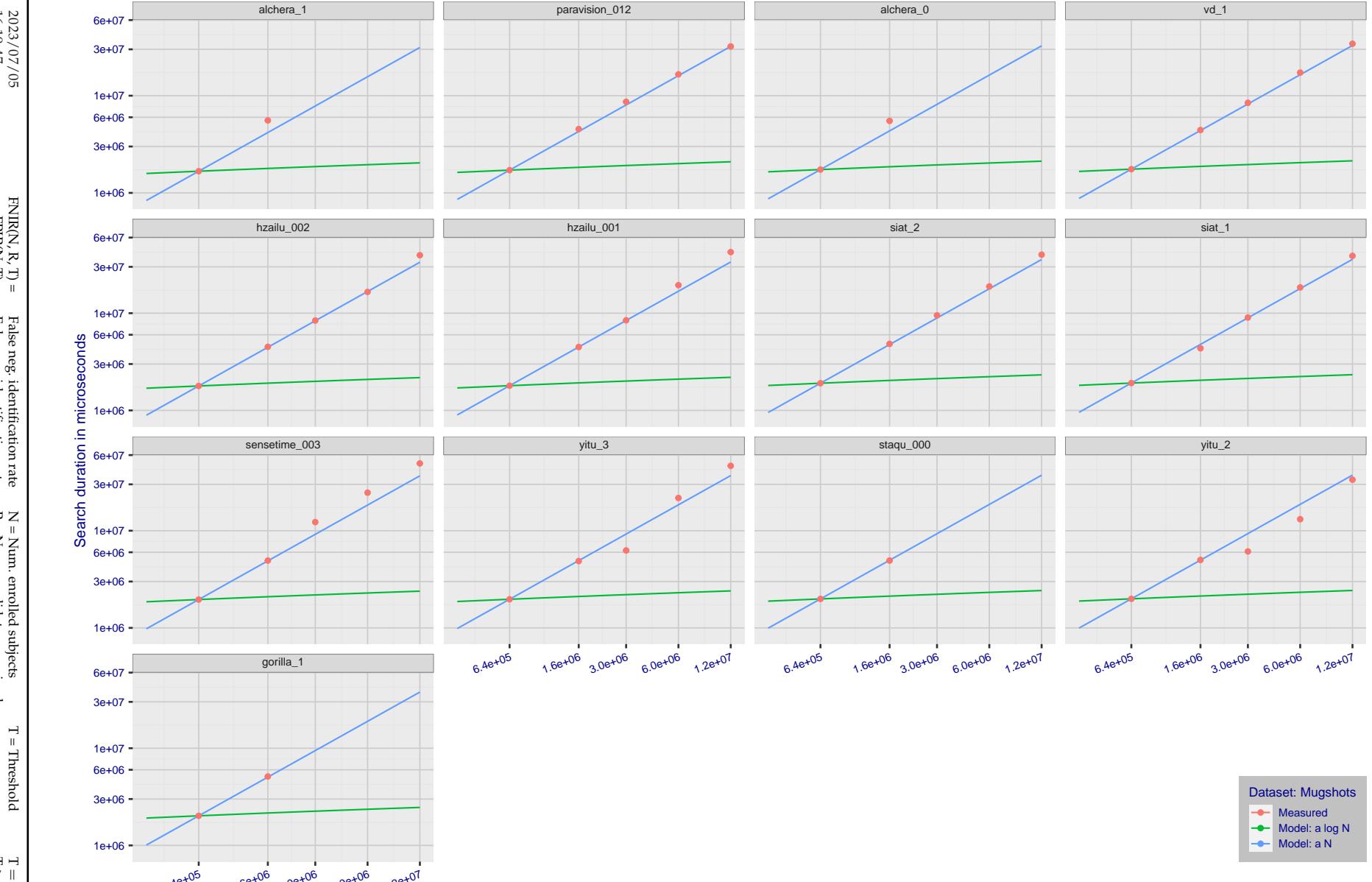


Figure 340: [Mugshot Dataset] Search duration vs. enrolled population size. In red are the actual point durations measured on a single c. 2016 core. The blue shows linear growth from $N = 640\,000$. The green line shows logarithmic growth from that point to $N = 1\,600\,000$. Note the sublinear growth from algorithms from Camvi, Dermalog, EverAI, Innovatrics, and Visionlabs. The tiger_1 algorithm is also sublinear, but inaccurate and inoperable at $N \geq 3000000$. This capability sometimes comes at the additional expense of converting a linear gallery data structure into whatever fast-search data structure is used. Note that search times are sometimes dominated by the template generation times shown in Table 29.

2023/07/05
16:19:47FNIR(N, R, T) = False neg. identification rate
FPIR(N, T) = False pos. identification rateN = Num. enrolled subjects
R = Num. candidates examined

T = Threshold

T = 0 → Investigation
 $T > 0 \rightarrow$ Identification

2023/07/05
16:19:47FNIR(N, R, T) = False neg. identification rate
FPIR(N, T) = False pos. identification rateN = Num. enrolled subjects
R = Num. candidates examined

T = Threshold

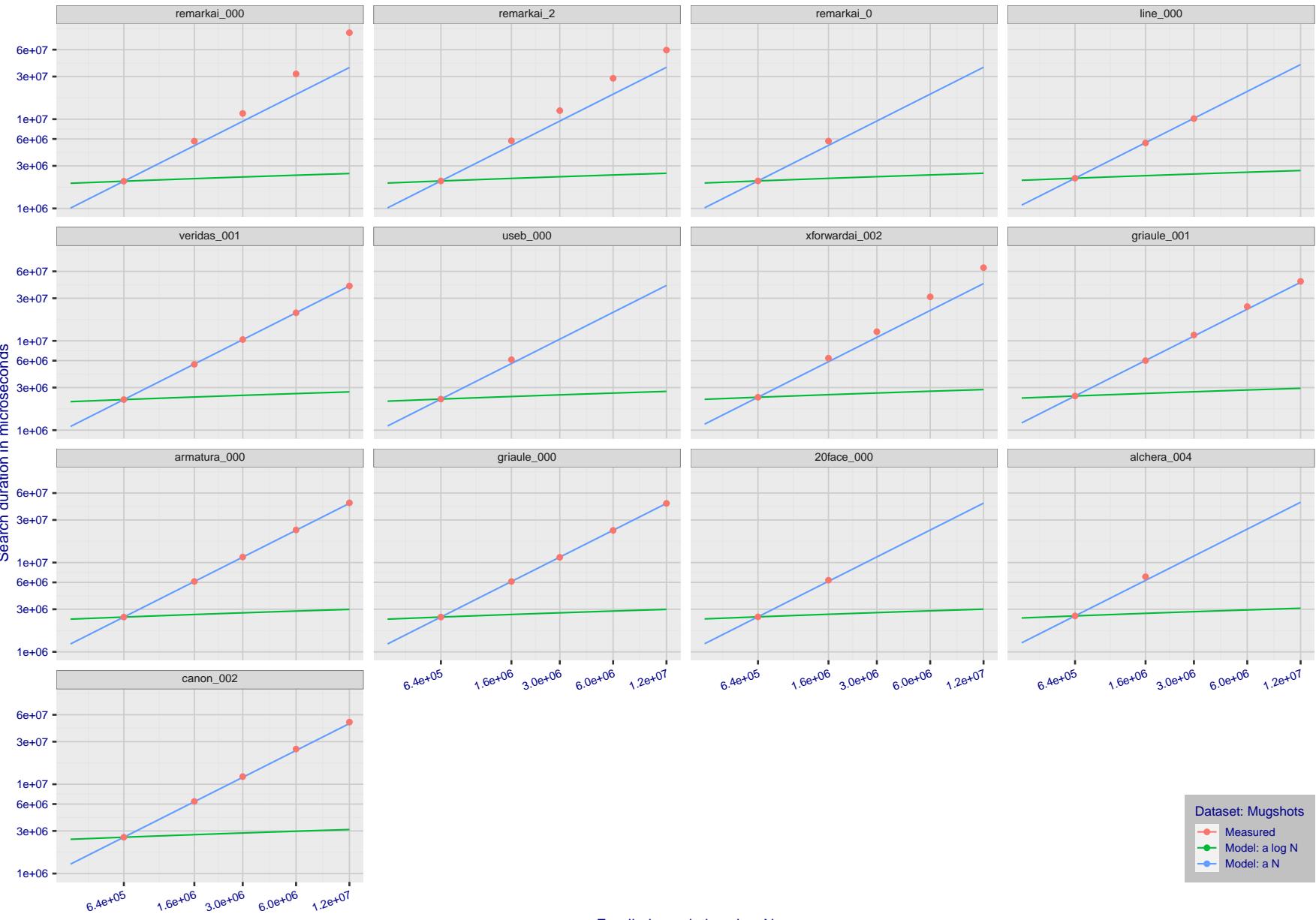
T = 0 → Investigation
T > 0 → Identification

Figure 341: [Mugshot Dataset] Search duration vs. enrolled population size. In red are the actual point durations measured on a single c. 2016 core. The blue shows linear growth from $N = 640\,000$. The green line shows logarithmic growth from that point to $N = 1\,600\,000$. Note the sublinear growth from algorithms from Camvi, Dermalog, EverAI, Innovatrics, and Visionlabs. The tiger_1 algorithm is also sublinear, but inaccurate and inoperable at $N \geq 3000000$. This capability sometimes comes at the additional expense of converting a linear gallery data structure into whatever fast-search data structure is used. Note that search times are sometimes dominated by the template generation times shown in Table 29.

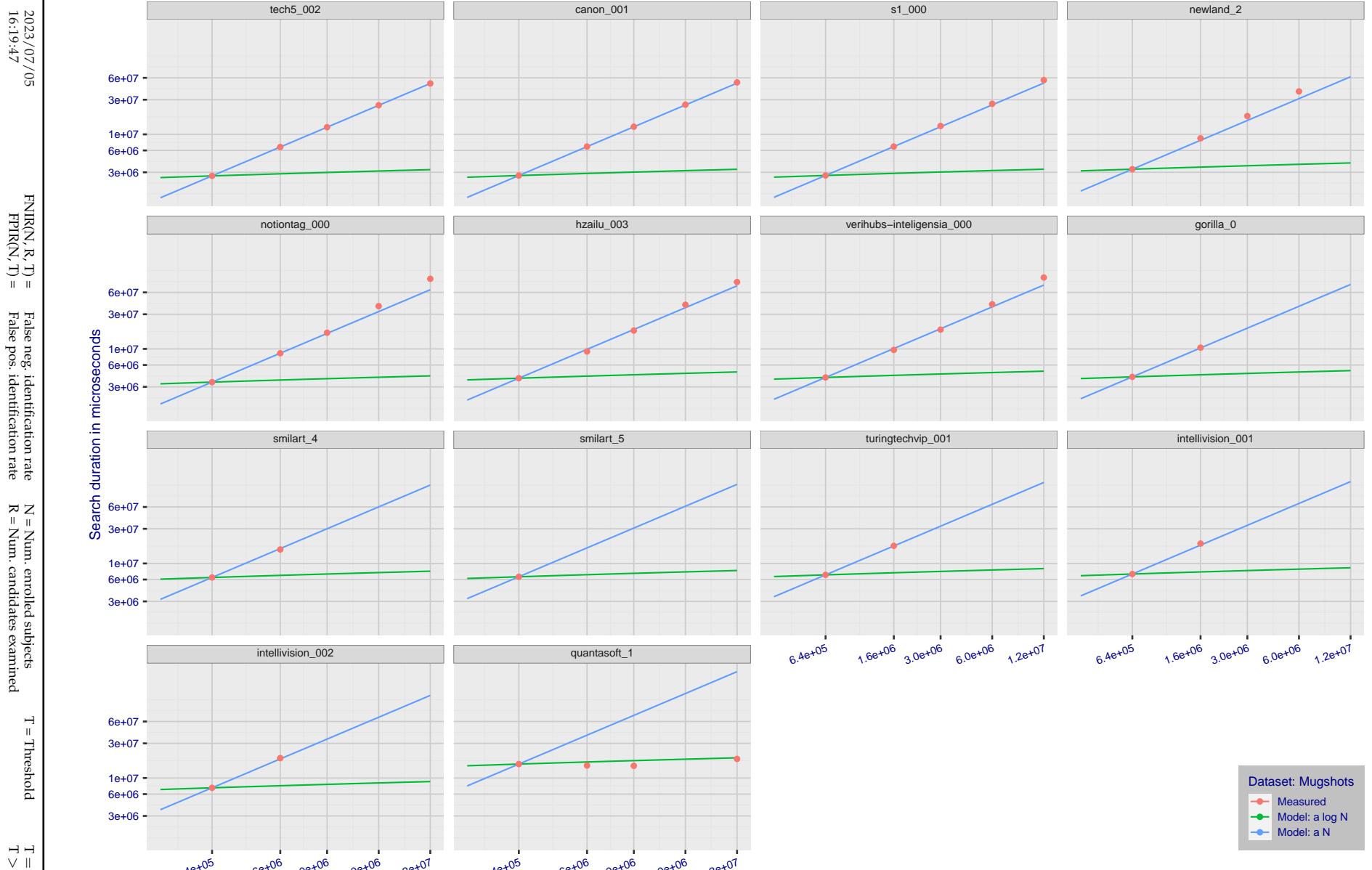


Figure 342: [Mugshot Dataset] Search duration vs. enrolled population size. In red are the actual point durations measured on a single c. 2016 core. The blue shows linear growth from $N = 640\,000$. The green line shows logarithmic growth from that point to $N = 1\,600\,000$. Note the sublinear growth from algorithms from Camvi, Dermalog, EverAI, Innovatrics, and Visionlabs. The tiger_1 algorithm is also sublinear, but inaccurate and inoperable at $N \geq 3000000$. This capability sometimes comes at the additional expense of converting a linear gallery data structure into whatever fast-search data structure is used. Note that search times are sometimes dominated by the template generation times shown in Table 29.

Appendix G Gallery Insertion Timing

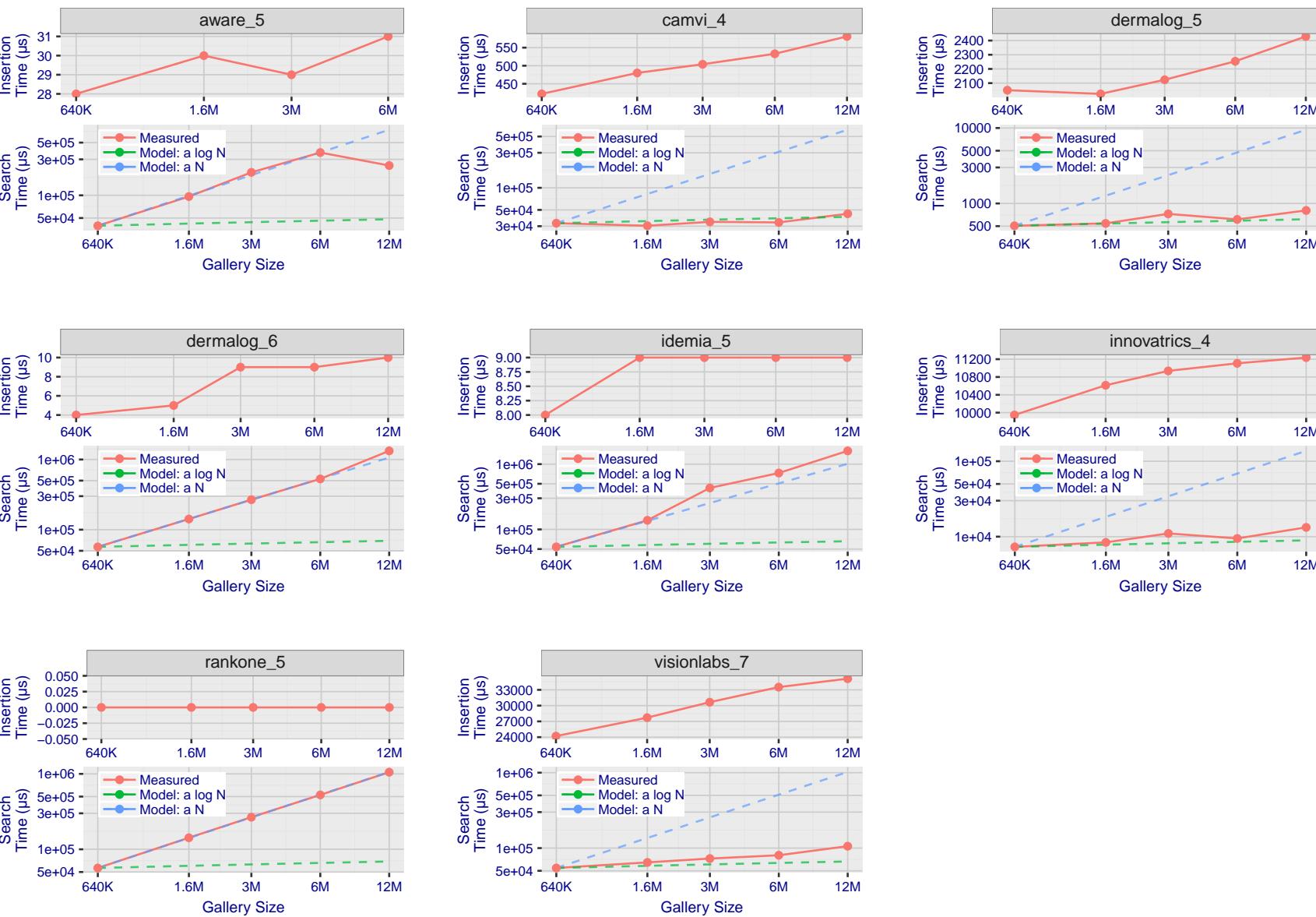
2023/07/05
16:19:47FNIR(N, R, T) = False neg. identification rate
FPIR(N, T) = False pos. identification rate
R = Num. candidates examinedN = Num. enrolled subjects
T = ThresholdT = 0 → Investigation
T > 0 → Identification

Figure 343: [Mugshot Dataset] Gallery insertion duration vs. enrolled population size. This chart plots the time it takes to insert a single template into a finalized gallery, illustrated over increasing gallery sizes. For reference, search times on finalized galleries of corresponding sizes are plotted right underneath. Gallery insertion time plots were generated on algorithms that 1) successfully implemented gallery insertion with no errors and 2) that were run on galleries with N up to 12 000 000. Generally, only the more accurate algorithms were run on galleries with N up to 12 000 000.

2023/07/05
16:19:47FNIR(N, R, T) = False neg. identification rate
FPFR(N, T) = False pos. identification rateN = Num. enrolled subjects
R = Num. candidates examinedT = Threshold
T = 0 → Investigation

T > 0 → Identification

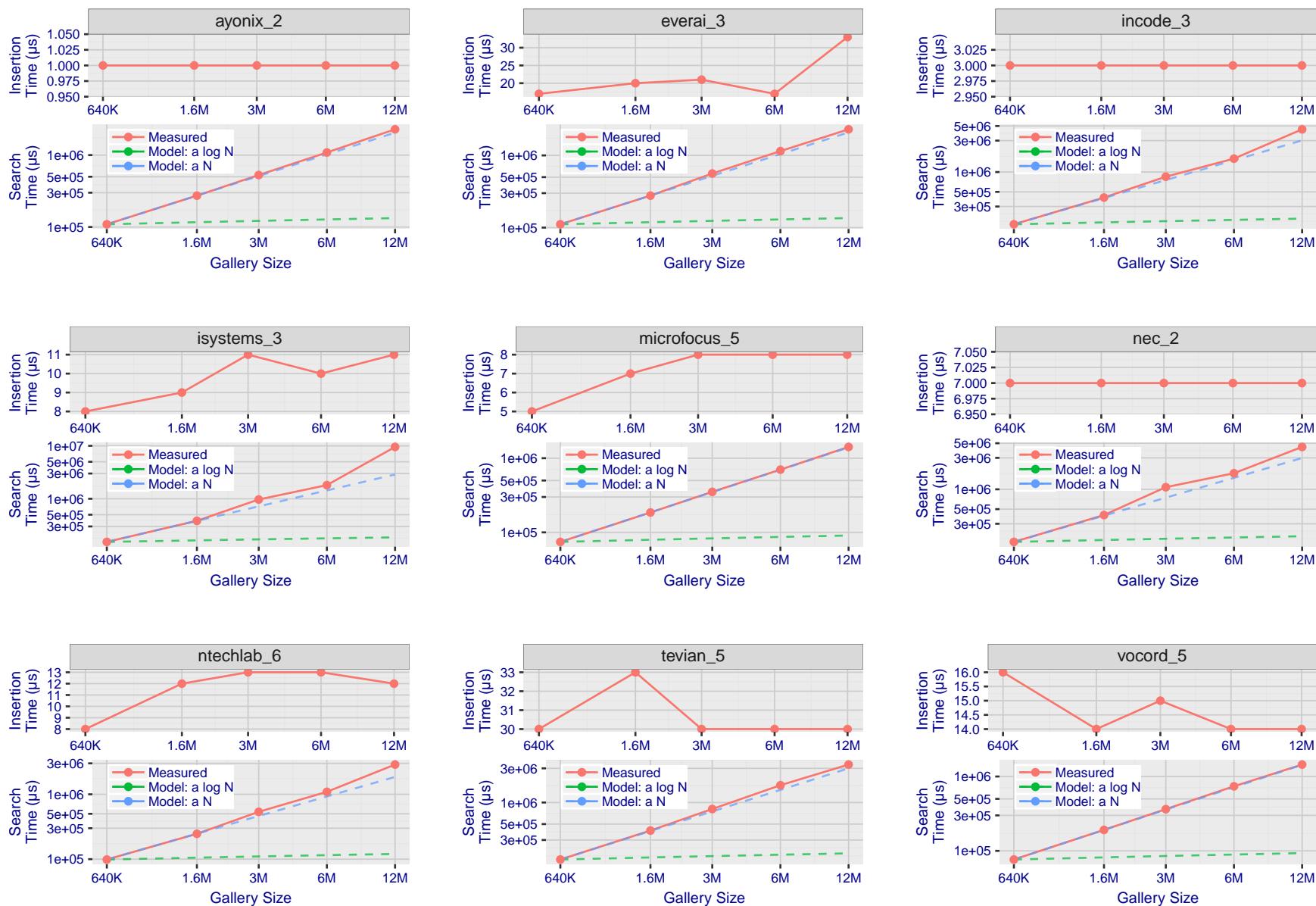


Figure 344: [Mugshot Dataset] Gallery insertion duration vs. enrolled population size. This chart plots the time it takes to insert a single template into a finalized gallery, illustrated over increasing gallery sizes. For reference, search times on finalized galleries of corresponding sizes are plotted right underneath. Gallery insertion time plots were generated on algorithms that 1) successfully implemented gallery insertion with no errors and 2) that were run on galleries with N up to 12 000 000. Generally, only the more accurate algorithms were run on galleries with N up to 12 000 000.

2023/07/05
16:19:47FNIR(N, R, T) = False neg. identification rate
FPTR(N, T) = False pos. identification rateN = Num. enrolled subjects
R = Num. candidates examined

T = Threshold

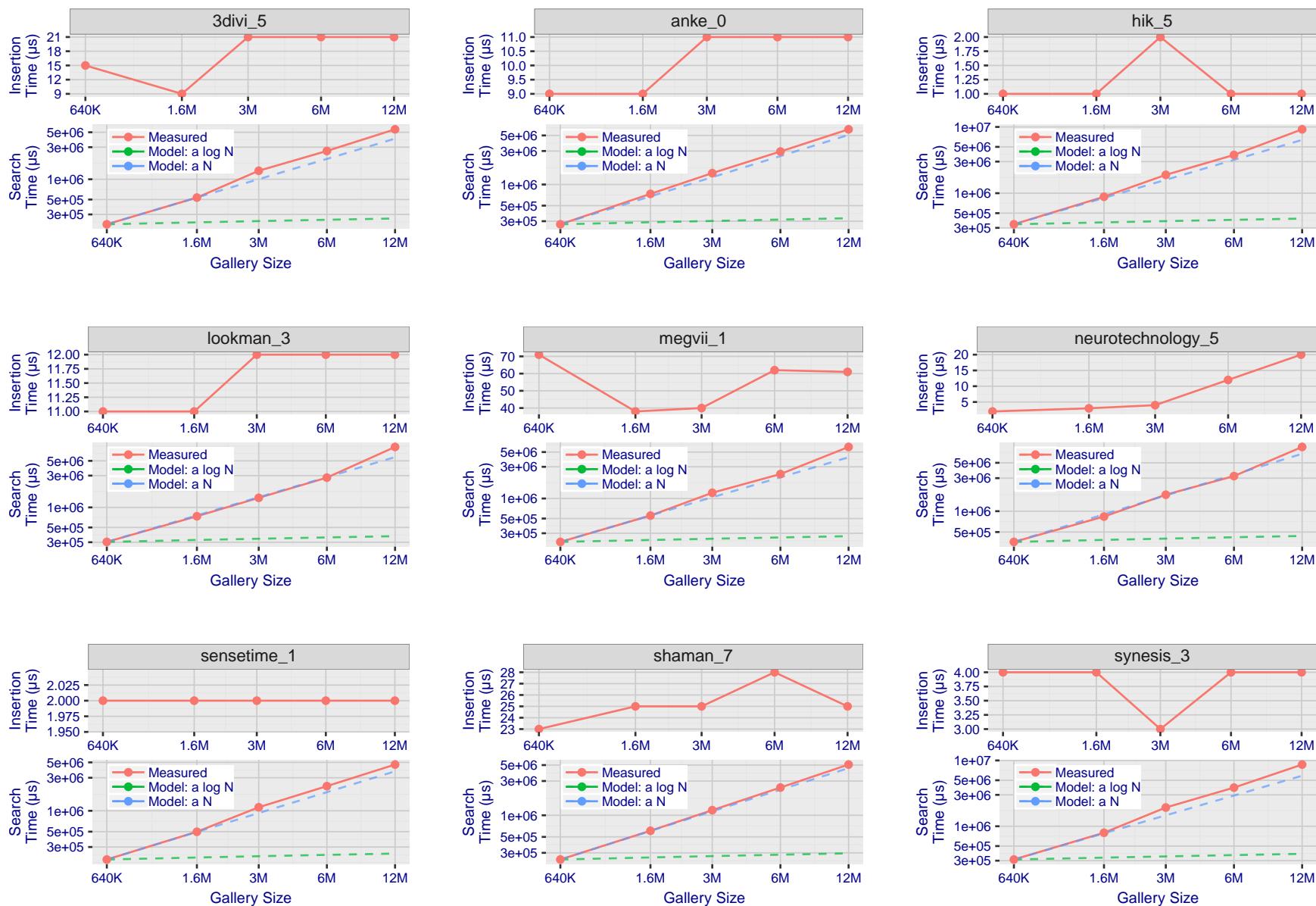
T = 0 → Investigation
 $T > 0 \rightarrow$ Identification

Figure 345: [Mugshot Dataset] Gallery insertion duration vs. enrolled population size. This chart plots the time it takes to insert a single template into a finalized gallery, illustrated over increasing gallery sizes. For reference, search times on finalized galleries of corresponding sizes are plotted right underneath. Gallery insertion time plots were generated on algorithms that 1) successfully implemented gallery insertion with no errors and 2) that were run on galleries with N up to 12 000 000. Generally, only the more accurate algorithms were run on galleries with N up to 12 000 000.

2023/07/05
16:19:47FNIR(N, R, T) = False neg. identification rate
FPTR(N, T) = False pos. identification rateN = Num. enrolled subjects
R = Num. candidates examinedT = Threshold
T = 0 → Investigation

T > 0 → Identification

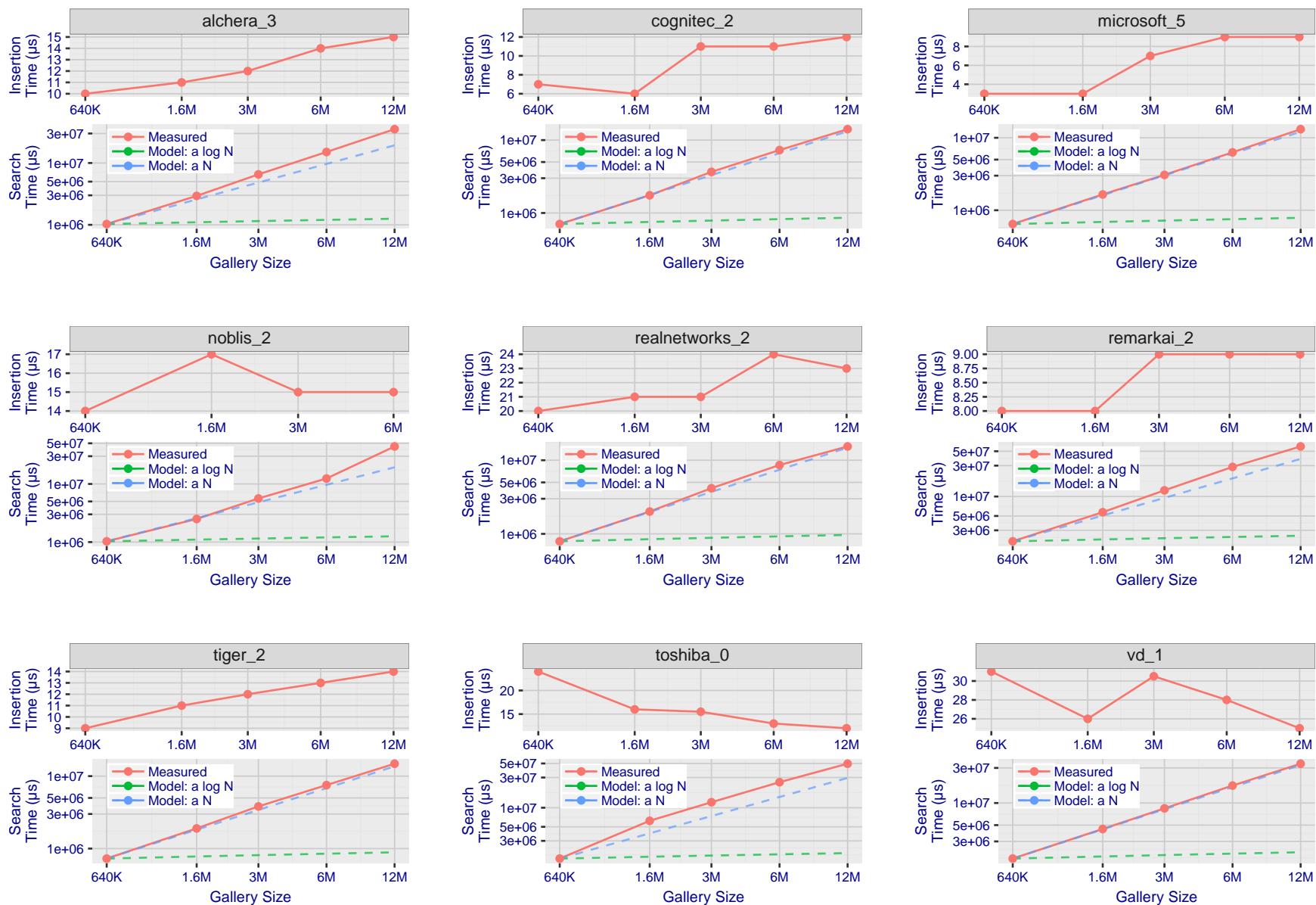


Figure 346: [Mugshot Dataset] Gallery insertion duration vs. enrolled population size. This chart plots the time it takes to insert a single template into a finalized gallery, illustrated over increasing gallery sizes. For reference, search times on finalized galleries of corresponding sizes are plotted right underneath. Gallery insertion time plots were generated on algorithms that 1) successfully implemented gallery insertion with no errors and 2) that were run on galleries with N up to 12 000 000. Generally, only the more accurate algorithms were run on galleries with N up to 12 000 000.

References

- [1] Artem Babenko and Victor Lempitsky. Efficient indexing of billion-scale datasets of deep descriptors. In *The IEEE Conference on Computer Vision and Pattern Recognition (CVPR)*, June 2016.
- [2] L. Best-Rowden and A. K. Jain. Longitudinal study of automatic face recognition. *IEEE Transactions on Pattern Analysis and Machine Intelligence*, 40(1):148–162, Jan 2018.
- [3] Blumstein, Cohen, Roth, and Visher, editors. *Random parameter stochastic models of criminal careers*. National Academy of Sciences Press, 1986.
- [4] Thomas P. Bonczar and Lauren E. Glaze. Probation and parole in the united statesm 2007, statistical tables. Technical report, Bureau of Justice Statistics, December 2008.
- [5] White D., Kemp R. I., Jenkins R., Matheson M, and Burton A. M. Passport officers' errors in face matching. *PLoS ONE*, 9(8), 2014. e103510. doi:10.1371/journal.pone.0103510.
- [6] P. Grother, G. W. Quinn, and P. J. Phillips. Evaluation of 2d still-image face recognition algorithms. NIST Interagency Report 7709, National Institute of Standards and Technology, 8 2010. <http://face.nist.gov/mbe> as MBE2010 FRVT2010.
- [7] P. J. Grother, R. J. Micheals, and P. J. Phillips. Performance metrics for the frvt 2002 evaluation. In *Proceedings of Audio and Video Based Person Authentication Conference (AVBPA)*, June 2003.
- [8] Patrick Grother and Mei Ngan. Interagency report 8009, performance of face identification algorithms. *Face Recognition Vendor Test (FRVT)*, May 2014.
- [9] Patrick Grother, George Quinn, and Mei Ngan. Face in video evaluation (five) face recognition of non-cooperative subjects. Interagency Report 8173, National Institute of Standards and Technology, March 2017. <https://doi.org/10.6028/NIST.IR.8173>.
- [10] Patrick Grother, George W. Quinn, and Mei Ngan. Face recognition vendor test - still face image and video concept, evaluation plan and api. Technical report, National Institute of Standards and Technology, 7 2013. http://biometrics.nist.gov/cs.links/face/frvt/frvt2012/NIST_FRVT2012.api_Aug15.pdf.
- [11] K. He, X. Zhang, S. Ren, and J. Sun. Deep residual learning for image recognition. In *2016 IEEE Conference on Computer Vision and Pattern Recognition (CVPR)*, pages 770–778, June 2016.
- [12] Gary B. Huang, Manu Ramesh, Tamara Berg, and Erik Learned-Miller. Labeled faces in the wild: A database for studying face recognition in unconstrained environments. Technical Report 07-49, University of Massachusetts, Amherst, October 2007.
- [13] Masato Ishii, Hitoshi Imaoka, and Atsushi Sato. Fast k-nearest neighbor search for face identification using bounds of residual score. In *2017 12th IEEE International Conference on Automatic Face & Gesture Recognition (FG 2017)*, pages 194–199, Los Alamitos, CA, USA, May 2017. IEEE Computer Society.
- [14] Jeff Johnson, Matthijs Douze, and Hervé Jégou. Billion-scale similarity search with gpus. *CoRR*, abs/1702.08734, 2017.

- [15] Ira Kemelmacher-Shlizerman, Steven M. Seitz, Daniel Miller, and Evan Brossard. The megaface benchmark: 1 million faces for recognition at scale. *CoRR*, abs/1512.00596, 2015.
- [16] Yury A. Malkov and D. A. Yashunin. Efficient and robust approximate nearest neighbor search using hierarchical navigable small world graphs. *CoRR*, abs/1603.09320, 2016.
- [17] Joyce A. Martin, Brady E. Hamilton, Michelle J.K. Osterman, Anne K. Driscoll, , and Patrick Drake. National vital statistics reports. Technical Report 8, Centers for Disease Control and Prevention, National Center for Health Statistics, National Vital Statistics System, Division of Vital Statistics, November 2018.
- [18] O. M. Parkhi, A. Vedaldi, and A. Zisserman. Deep face recognition. In *British Machine Vision Conference*, 2015.
- [19] P. Jonathon Phillips, Amy N. Yates, Ying Hu, Carina A. Hahn, Eilidh Noyes, Kelsey Jackson, Jacqueline G. Cava-zos, Géraldine Jeckeln, Rajeev Ranjan, Swami Sankaranarayanan, Jun-Cheng Chen, Carlos D. Castillo, Rama Chellappa, David White, and Alice J. O'Toole. Face recognition accuracy of forensic examiners, superrecognitioners, and face recognition algorithms. *Proceedings of the National Academy of Sciences*, 115(24):6171–6176, 2018.
- [20] Florian Schroff, Dmitry Kalenichenko, and James Philbin. Facenet: A unified embedding for face recognition and clustering. *CoRR*, abs/1503.03832, 2015.
- [21] Jeroen Smits and Christiaan Monden. Twinning across the developing world. *PLOS ONE*, 6(9):1–5, 09 2011.
- [22] Yaniv Taigman, Ming Yang, Marc'Aurelio Ranzato, and Lior Wolf. Deepface: Closing the gap to human-level performance in face verification. In *Proceedings of the 2014 IEEE Conference on Computer Vision and Pattern Recognition, CVPR '14*, pages 1701–1708, Washington, DC, USA, 2014. IEEE Computer Society.
- [23] A. Towler, R. I. Kemp, and D White. *Unfamiliar face matching systems in applied settings*. Nova Science, 2017.
- [24] Working Group 3. Ed. M. Werner. *ISO/IEC 19794-5 Information Technology - Biometric Data Interchange Formats - Part 5: Face image data*. JTC1 :: SC37, 2 edition, 2011. <http://webstore.ansi.org>.
- [25] David White, James D. Dunn, Alexandra C. Schmid, and Richard I. Kemp. Error rates in users of automatic face recognition software. *PLoS ONE*, 10:1–14, October 2015.
- [26] Bradford Wing and R. Michael McCabe. Special publication 500-271: American national standard for information systems data format for the interchange of fingerprint, facial, and other biometric information part 1. Technical report, NIST, September 2015. ANSI/NIST ITL 1-2015.
- [27] Andreas Wolf. Portrait quality - (reference facial images for mrtd). Technical report, ICAO, April 2018.
- [28] D. Yadav, N. Kohli, P. Pandey, R. Singh, M. Vatsa, and A. Noore. Effect of illicit drug abuse on face recognition. In *2016 IEEE Winter Conference on Applications of Computer Vision (WACV)*, pages 1–7, Los Alamitos, CA, USA, mar 2016. IEEE Computer Society.